UNIVERSITY OF CALIFORNIA

Los Angeles

Prodiginines, JBIR-141 and Surveying the Computational Landscape of OFCP-Derived Macrobicycles

A dissertation submitted in partial satisfaction of the

requirements for the degree Doctor of Philosophy

in Chemistry

by

Morris Joseph Dweck

2023

ABSTRACT OF THE DISSERTATION

Prodiginines, JBIR-141 and Surveying the Computational Landscape of OFCP-Derived Macrobicycles

by

Morris Joseph Dweck

Doctor of Philosophy in Chemistry

University of California, Los Angeles, 2023

Professor Patrick G. Harran, Chair

Chapter one outlines my work surrounding the investigation of the reaction pathways operative upon the photoirradiation of [8]-(2,6)-pyridinophane N-oxide. Herein, I describe the isolation and characterization of two previously undiscovered heterocyclophanes identified as photolabile intermediates in the production of a ketopyrrolophane compound central to our synthetic approach to the natural product (+)-marineosin A. In addition, I outline a unified and computationally supported mechanistic framework developed in collaboration with Janice B. Lin and Selbi Nuryyeva under the guidance of Professor Ken Houk. This framework describes the formation and interconversion of all isolated products and intermediates. This framework greatly adds to our overall understanding of the photochemistry of pyridine N-oxides.

Chapter two details my work surrounding the exploration of an unprecedented alkyl chain migration observed in the assembly of the tripyrrolic core of the prodiginine natural product (+)-

marineosin A. Various experiments demonstrating the generality of this reaction are shown through the utilization of electronically perturbed heterobiaryl systems. Further detailed is an in-depth examination of my efforts to elucidate the mechanism of this unique migration which is complimented by computational analysis carried out in collaboration by Mark A. Maskeri formerly of the Houk Group.

Chapter three outlines my progress towards establishing the first total synthesis of the natural product JBIR-141. Further detailed is our plan towards completion of the route as well as a set of proposed analogs, all of which are easily accessed due to the modularity of our synthetic pathway. These analogs will play a crucial role in identifying the natural product's active pharmacophore, elucidating its mechanism of action, and maximizing its potential as a chemotherapeutic agent.

Chapter four details my work surrounding the development of peptide macrocyclization methodology utilizing commercial octafluorocyclopentene (OFCP). Herein, I showcase the ability of OFCP to engage linear, unprotected peptides in polysubstitution cascade reactions to generate complex fluorinated polycycles. In addition, I show that intermediates of these cascades can be intercepted by exogenous nucleophiles, enabling access to a diverse range of hybrid compounds composed of peptides, sugars, lipids, and heterocyclic components. Further detailed is the use of small molecular inserts which greatly expands the diversity of polycyclic structures accessible using this methodology. Lastly, I delve into my work in the field of computational analysis where I discuss the capability of polycycles generated using this methodology to structurally mimic protein surface loops central to mediating a wide variety of protein-protein interactions.

The dissertation of Morris Joseph Dweck is approved.

Ohyun Kwon

Neil K. Garg

Kendall N. Houk

Patrick G. Harran, Committee Chair

University of California, Los Angeles

2023

This work is dedicated to my wife Sharon,

my greatest love and truest guiding inspiration

TABLE OF CONTENTS

LIST OF FIGURES, SCHEMES, TABLES AND SPECTRA

Figures

Schemes

Tables

Spectra

LIST OF ABBREVIATIONS AND ACRONYMS

Ac	acetyl
Acac	acetylacetonate
Akt	protein kinase B
Ala	alanine
APT	attached proton test
aq	aqueous
Ar	aryl group
BCR-ABL	break point cluster region-abelson fusion oncogene
Bn	benzyl
Boc	tert-butoxycarbonyl
br	broad
c-Hex	cyclohexyl
cat.	catalytic
Cbz	benzyloxycarbonyl
CML	chronic myeloid leukemia
COSY	correlation spectroscopy
CSA	camphorsulfonic acid
d	doublet
d.r	diastereomeric ratio
DBU	1,8-diazabicyclo[5.4. 0]undec-7-ene
DCC	N,N'-dicyclohexylcarbodiimide
DCE	1,2-dichloroethane

DCM	dichloromethane
Deoxo-Fluor®	1-bis(2-methoxyethyl)aminosulfur trifluoride
DFT	density-functional theory
DIBAL-H	diisobutylaluminum hydride
DIPEA	diisopropylethylamine
DMAP	4-dimethylaminopyridine
DME	1,2-dimethoxyethane
DMF	dimethylformamide
DMSO	dimethylsulfoxide
dr, d.r.	diastereomeric ratio
EDC•HCl	N-(3-dimethylaminopropyl)-N′-ethylcarbodiimide hydrochloride
ee, e.e.	enantiomeric excess
EI	electron ionization
eq., equiv	equivalent(s)
ESI	electrospray ionization
Et	ethyl
Et_2O	diethyl ether
Et_3N	triethylamine
EtOAc	ethyl acetate
FCC	flash column chromatography
FEP	fluorinated ethylene-propylene
Fmoc	fluorenylmethoxycarbonyl
FOXO3a	forkhead box subclass O member 3a
GC	gas chromatography

h	hour
HATU	hexafluorophosphate azabenzotriazole tetramethyl uranium
HBTU	2-(1H- benzotriazol1-yl)-1,1,3,3-tetramethyluronium
HCT116	human colorectal carcinoma
HMBC	heteronuclear multiple bond correlation
HPLC	high-performance liquid chromatography
HRMS	high-resolution mass spectroscopy
HSC	hematopoietic stem cells
HSQC	heteronuclear single quantum correlation spectroscopy
hv	light
Hz	hertz
IC_{50}	half maximal inhibitory concentration
IR	infrared spectroscopy
KHMDS	potassium bis(trimethylsilyl)amide/ potassium hexamethyldisilazide
LAH	lithium aluminum hydride
LD_{50}	lethal dosage to kill 50% of test population
LDA	lithium diisopropylamide
LIC	leukemia inducing cell
LiHMDS	lithium bis(trimethylsilyl)amide/ lithium hexamethyldisilazide
LLC	longest linear sequence
M	molar
m	multiplet
m/z	mass to charge ratio
mCPBA	meta-chloroperoxybenzoic acid

Me	methyl
$Me_2C(OMe)_2$	2,2-dimethoxypropane
Me_2CO	acetone
MeCN	acetonitrile
$MeNO_2$	nitromethane
MeOH	methanol
MESO-1	human malignant mesothelioma
MIC	minimal inhibitory concentration
min	minute(s)
MNBA	2-methyl-6-nitrobenzoic anhydride
mol	mole(s)
mol%	percentage used based on moles
MS	mass spectrometer/spectrometry/spectrum
N	normal
N/R	no reaction
nBuLi	n-butyl lithium
NCI	National Cancer Institute
NCS	N-chlorosuccinimide
nd, n.d.	not determined
NMR	nuclear magnetic resonance
NO	nitric oxide
NOESY	nuclear Overhauser effect spectroscopy
ORTEP	Oak Ridge thermal ellipsoid plot
PDB	Protein Data Bank

PG	protecting group
Ph	phenyl
pH	hydrogen ion concentration in aqueous solution
PhH	benzene
PhMe	toluene
PI3K	phosphatidylinositol 3-kinase
PPI	protein-protein interaction
ppm	parts per million
PTLC	preparative thin-layer chromatography
pTsOH	para-toluenesulfonic acid
q	quartet
qTOF	quadrupole time-of-flight
R	alkyl group
RT, rt, r.t.	room temperature
s	singlet
SAR	structure-activity relationship
sat.	saturated
SKOV-3	human ovarian adenocarcinoma
Su	succinimide
t	triplet
t-Bu	tert-butyl
TBS	tert-butyldimethylsilyl
TD-DFT	time-dependent density-functional theory

TEA	triethylamine
temp.	temperature
Teoc	2-(trimethylsilyl)ethoxycarbonyl
TFA	trifluoroacetic acid
THF	tetrahydrofuran
TIPS	triisopropylsilane
TKI	tyrosine kinase inhibitor
TLC	thin-layer chromatography
TMS	trimethylsilyl
TNF	tumor necrosis factor
UV	ultraviolet
UV-Vis	ultraviolet visual
UV-Vis-NIR	ultraviolet visual near-infrared
w/v	weight per volume
wt%	percent by weight
X	halide or trifluoromethanesulfonate
XRD	X-ray diffraction
δ	chemical shift in parts per million
λ	wavelength
μ	micro

ACKNOWLEDGEMENTS

I would like to begin by expressing my gratitude to all the individuals with whom I have had the privilege of co-authoring a publication. The essence of science lies not only in making groundbreaking discoveries but also in sharing those findings with world at large. I am truly honored to have had the opportunity to contribute to mankind's understanding of chemistry, an achievement which would not have been possible without the time, dedication, and passion invested by all of my co-authors.

It goes without saying that my accomplishments over the past five years would not have been possible without the time, dedication, and most of all, patience of Professor Patrick Harran. His passion for chemistry is infectious and his desire to continually push the boundaries of what is possible in the field of organic synthesis serves as a constant source of inspiration to both myself as well as his entire group. His emphasis on expanding the horizons of knowledge and the significance of understanding the fundamentals of our art are invaluable lessons that I will carry with me throughout my career.

Among all the chemists I've had the pleasure of working with over the past five years, several stand out as figures of particular importance, but none more so than my mentor and closest friend, Doctor Evan Hurlow. Of all Evan's gifts, perhaps the one I cherish most is his ability to understand what I'm trying to convey when words fail me. Evan, please recognize this as one of those times where I fail to find the words which accurately describe the profound impact you've had on me as a chemist, mentor, and person during our brief time together. In addition to my mentor, I want to express profound gratitude to Gilbert L. Walker, my first and only true mentee. Mentoring such a talented individual was often intimidating but witnessing Gilbert's growth as a chemist and leader was one of the most rewarding experiences I have had in graduate school.

Gilbert, you are unquestionably one of the most talented chemists I've ever had the pleasure of working with and trust that you know that there is not a single person on this earth I would have rather had as a mentee. I'd also like to make a special acknowledgement of Angel Mendoza and Salvador Bernardino, two of the most supportive friends I've ever had. Sharing a lab with both of you has made graduate school one of the most enjoyable times in my life and for that, I can't thank you both enough.

In addition to those named above, I also want to extend my heartfelt gratitude to both the current and past members of the Harran group with whom I have worked including Hui Ding, Zhengao Fang, Tomoyuki Tsunemi, Emily Murzinski, Luke Sisto, Liubo (Rupert) Li, Anton El Khoury (my favorite movie critic), Ishika Saha (my fellow computational chemist), Darsheed 'Ani' Mustafa, Brennan Clement, Alek Lotuzas (my editor in chief), Gabriella Cooper, Emma Greene, Jacqueline Bustamante, Nathan Incandela, Marcelo Mazariego, Jerry Hsu, Melinda Cheng, Kyle Nagasawa, Vanlinh Nguyen, Ashley Michel, and numerous other rotation and undergraduate students. It has been a pleasure working with each-and-every one of you and I am grateful for the fond memories we've created. You are like family to me and I thank you all from the bottom of my heart.

In addition to my lab colleagues, I would also like to express my gratitude to my thesis committee; Professor Kendall Houk, Professor Neil Garg, Professor Ohyun Kwon, and formerly, Professor Hosea Nelson. Each of you have instilled in me lessons which I will forever remember and use moving forward, and for that, I thank you all. Special thanks go to my high school chemistry teachers, Anne Lander and Anat Firnberg both of whom were instrumental in igniting not only my love for chemistry but also my passion for teaching. I would also like to acknowledge my undergraduate research advisor, Elena Galoppini, for introducing me to the world of

experimental synthetic organic chemistry by letting me conduct research in her lab as an ambitious undergraduate student.

In closing, I would like to thank my family—my mother (who has always taken the greatest pride in my achievements), father, brother Alan, and sisters Millie and Amy—for their unwavering support throughout my life. Their love has been a constant source of strength which has enabled me to overcome the many challenges I have faced to reach this point.

Finally, I would like to give my greatest thanks and acknowledgment to my best friend, life-partner, forever teammate and wife, Sharon. Words can't describe how much your love and support has helped me over the past five years and beyond. While my passion for chemistry is boundless, you will forever be my first love and priority. While I have many fond memories over the past five years in graduate school, none do I cherish more than the memories I have created with you. You are and will forever be my one true love and greatest source of inspiration.

CURRICULUM VITAE

Morris Dweck *Curriculum Vitae*

EDUCATION

University of California, Los Angeles *September 2018 – Present*
M.S. in Chemistry – Organic Concentration *March 2020*

Touro College of Osteopathic Medicine (Middletown Campus) *August 2015 – January 2017*

Rutgers, The State University of New Jersey (Newark Campus)
Bachelor of Arts (B.A.) in Chemistry *May 2014*

Bergen Community College
Associate Degree (A.S.) *December 2011*

RESEARCH EXPERIENCE

University of California, Los Angeles, CA *July 2018 – Present*
Graduate Student Researcher, Department of Chemistry & Biochemistry
Advisor: Professor Patrick G. Harran

- Synthesized (+)-marineosin A as well as novel prodiginine compounds used for mechanistic studies and comparative biological testing.
- Investigated the mechanism of the photorearrangement of [8]-2,6-pyridinophane N-oxide.
- Developed generalized conditions and expanded the substrate scope for the macrobicyclization of unfunctionalized peptides using octafluorocyclopentene (OFCP) as a scaffold.
- Computationally demonstrated the ability of our macrobicycles to mimic protein-protein mediating loop types.
- Working to experimentally validate loop mimicry computational predictions.
- Leading a team to complete the first laboratory synthesis of the natural product JBIR-141.

Rutgers, The State University of New Jersey, Newark, NJ
Research Assistant, Department of Chemistry *May 2014 – June 2015*
Undergraduate Researcher, Department of Chemistry *January 2013 – May 2014*
Advisor: Professor Elena Galoppini

- Synthesized molecular anchors incorporated into ruthenium polypyridyl "star" complexes used for the functionalization of TiO_2 semiconductor nanoparticles in dye-sensitized solar cells.

PUBLICATIONS, PATENTS & PRESENTATIONS

1. Mendoza, A.[†]; Bernardino, S. J.[†]; **Dweck, M. J.**; Valencia, I.; Evans, D.; Tian, H.; Lee, W.; Li, Y.; Houk, K. N.; Harran, P. G. "Cascade Synthesis of Fluorinated Spiroheterocyclic Scaffolding for Peptidic Macrobicycles." *J. Am. Chem. Soc.* **2023**, *145*, 29, 15888–15895.

2. **Dweck, M. J.**; Mendoza, A.; Hurlow, E. E.; Harran, P. G. "Atypical Chain-Migration of Ansa-Bridged Prodiginine Chromophores." (*Manuscript in Progress*)

3. Patrick G. Harran, Angel Mendoza, Salvador J. Bernardino, **Morris J. Dweck**. (**2023**). Methods to Generate Constrained Fluorinated Macrocycles. Provisional Patent Application U.S. 63/489,603. Filed *March 10, 2023*.

4. **Dweck, M. J.**, Computational Study of PPI Mediating Loop Mimicry using OFCP-Derived Macrobicycles. *University of California Chemical Symposium*, Los Angeles CA, April **2023**. (*Poster Presentation*)

5. Hurlow, E. E.; Lin, J. B.; **Dweck, M. J.**; Nuryyeva, S.; Feng, Z.; Allred, T. K.; Houk, K. N.; Harran, P. G. "Photorearrangement of [8]-2,6-Pyridinophane N-Oxide." *J. Am. Chem. Soc.* **2020**, *142,* 49, 20717–20724.

HONORS & AWARDS

Majeti-Alapati Dissertation Award – University of California, Los Angeles *June 2023*
Ralph and Charlene Bauer Award – University of California, Los Angeles *May 2022*
Hugh W. Thompson Memorial Award – Rutgers University *May 2014*
Tau Sigma Honor Society Award – Rutgers University *October 2013*
Undergraduate Chemistry Merit Award – Rutgers University *May 2013*
Dean's List – Rutgers University *September 2012 – May 2014*
Dean's List – Bergen Community College *September 2010 – December 2011*

SKILLS

- Structural determination and characterization of small molecules and peptides using NMR spectroscopy (1D-, 2D- and VT-NMR), mass spectroscopy (QMA, TOF and DART) and chromatographic instrumentation (GC, HPLC, UPLC).
- Computational ligand and scaffold-based drug design utilizing various molecular modeling programs (Schrödinger Maestro/MacroModel, Spartan), molecular docking applications (AutoDock suite) and molecular visualization software (PyMOL, Chimera, CYLview).
- Mentoring, training, and teaching both graduate and undergraduate students as a senior lab member and as a departmental TA (Chemistry and Biochemistry [Discussion/Lab] – 19 quarters).

Chapter One: The Photochemistry of [8]-Pyridinophane N-Oxide

1.1 Introduction

1.1.1 History of the Photochemistry of Pyridinophane N-Oxides

The photochemistry of heterocyclic N-oxides is a rich and interesting field of study as many of these compounds exhibit diverse photoreactivity, undergoing a wide variety of transformations to form a plethora of unique products.[1-3] Despite being one of the simplest in this class of compounds, pyridine *N*-oxide exhibits exceptionally diverse photoreactivity. The photochemistry of pyridine N-oxide (**1**) was first investigated in the 1950s with studies that probed its electronic structure and described its photodeoxygenation.[4-5] In 1966, Streith and Sigwalt described the photorearrangement of pyridine N-oxide (**1**) to 2-formylpyrrole (**2**) (**Scheme 1.1.1**).[6] Drawing an analogy to nitrone chemistry[7], they postulated an oxaziridine as the first ground state intermediate in these reactions with subsequent norcaradiene-type electrocyclic ring expansion leading to the generation of a 1,2-oxazepine en route to the formylpyrrole. In 1975, the same group discovered that performing the reaction in aqueous $CuSO_4$ markedly improved yields of formylpyrrole products.[8] Compared to previous conditions, this new procedure was scalable[9-11] and minimized tar formation typically observed in metal-free variants of the reaction. To explain this increased efficiency, the authors proposed the formation of a nitrene intermediate, derived from their previously hypothesized 1,2-oxazepine, and rationalized that stabilization of this nitrene via metal complexation allowed for electrocyclic ring closure to the formylpyrrole to proceed more efficiently.

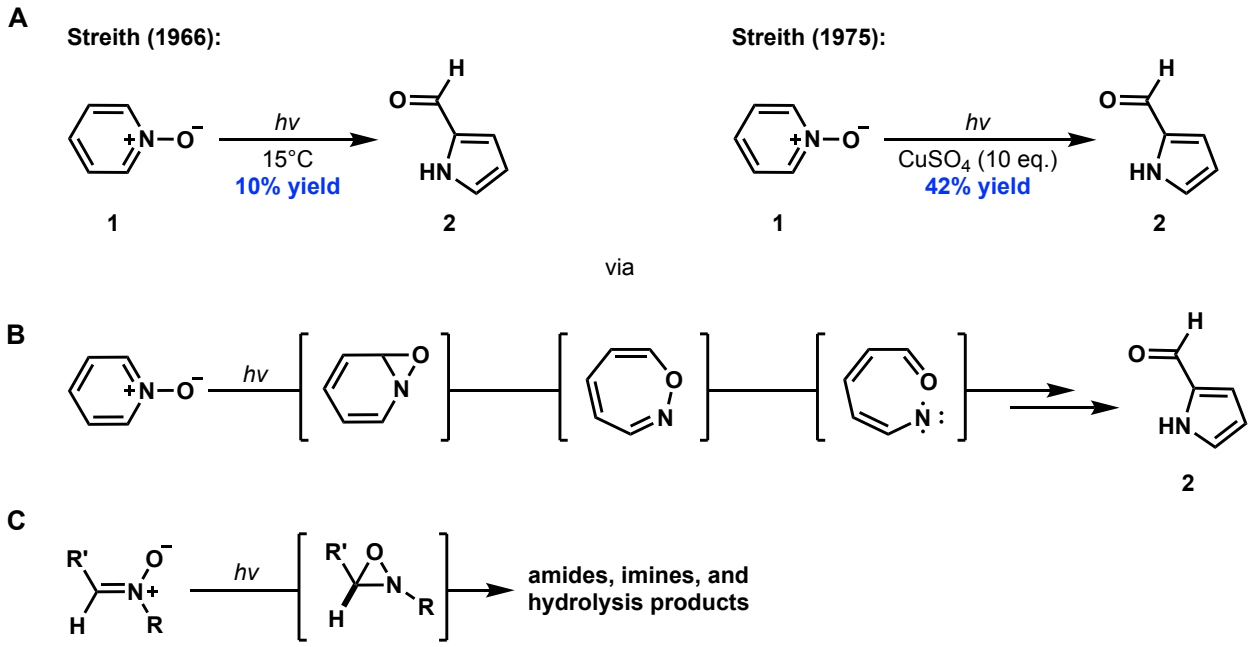

Scheme 1.1.1 Photorearrangement of pyridine N-oxide. (**A**) Early findings and optimizations surrounding the photorearrangement of pyridine N-oxide to 2-formylpyrrole. (**B**) Early mechanistic hypothesis for the photorearrangement of pyridine N-oxide to 2-formylpyrrole. (**C**) The photorearrangement of pyridine N-oxide was proposed to proceed through an oxaziridine intermediate analogous to that produced by irritation of nitrones.

Additional support for a nitrene intermediate came from flash photolysis studies carried out by Lohse and co-workers.[12] In these studies, it was observed that irradiation of pyridine N-oxide in the presence of base rapidly formed dienyl nitriles and that *N*-oxide decomposition quantum yield was insensitive to base concentration and dissolved oxygen (**Scheme 1.1.2**). Reactivity of an unknown intermediate (lifetime in $H_2O \sim 63$ ms) toward amines was inconsistent with ground state chemistry of oxaziridines and oxazepines and product formation was thought too slow to involve an excited state. Instead, they postulated this unknown intermediate to be a vinyl nitrene, deprotonation of which was the source of the observed nitrile. This helped to explain why tars formed in many pyridine N-oxide photolysis reactions contain nitrile functional groups.[12]

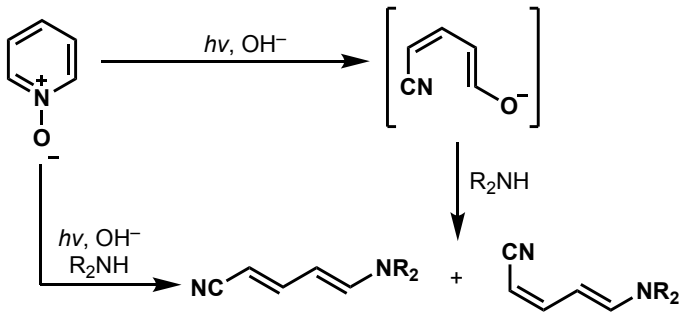

Scheme 1.1.2 Results of photolysis experiments carried out by Lohse and coworkers.

Weber (1989):

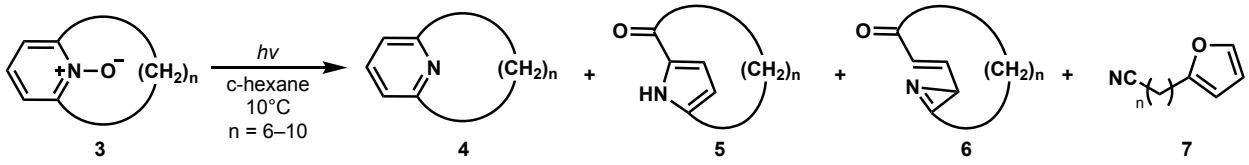

n	Time (h)	% Yield				
		4	**5**	**6**	**7**	**3** (recovered)
6	3	1.0	0.4	–	4.2	–
7	5	4.6	1.3	4.0	0.7	20.0
8	5	5.3	0.6	5.2	–	25.0
9	15	–	1.7	1.0	–	9.4
10	20	5.8	11.9	0.4	3.1	7.6

Table 1.1.1 Results from Weber's study of pyridinophane N-oxide photorearrangement.

In 1989, Weber reported syntheses of pyridine *N*-oxides with carbons 2 and 6 bridged by hydrocarbon chains of varying length.[13] Photolyses of these pyridinophane N-oxides gave product mixtures containing ketopyrrolophanes, macrocyclic azirenes and furanylalkyl nitriles (**Table 1.1.1**). Based on the mechanistic hypotheses previously proposed by Streith and Sigwalt, Weber proposed that photoexcitation of his pyridinophane N-oxide substrates generate oxaziridines i as primary photointermediates with valence bond isomerism analogous to norcaradiene-type walking rearrangements[14] allowing for the interconversion between oxaziridines i and epoxides ii (**Scheme 1.1.3**). From these two interconvertible species, it was hypothesized that intermediate 1,2-oxazepine iii and 1,3-oxazepine iv could be derived via electrocyclic ring expansions of oxaziridine

i and epoxide ii respectively. While the latter of these oxazepines was postulated to fragment to form furanylalkyl nitriles **7**, the former were thought to proceed to vinyl nitrenes v which could then undergo competing 1,5- or 1,3- electrocyclic ring closure to form ketopyrrolophanes **5** or azirenes **6** respectively.

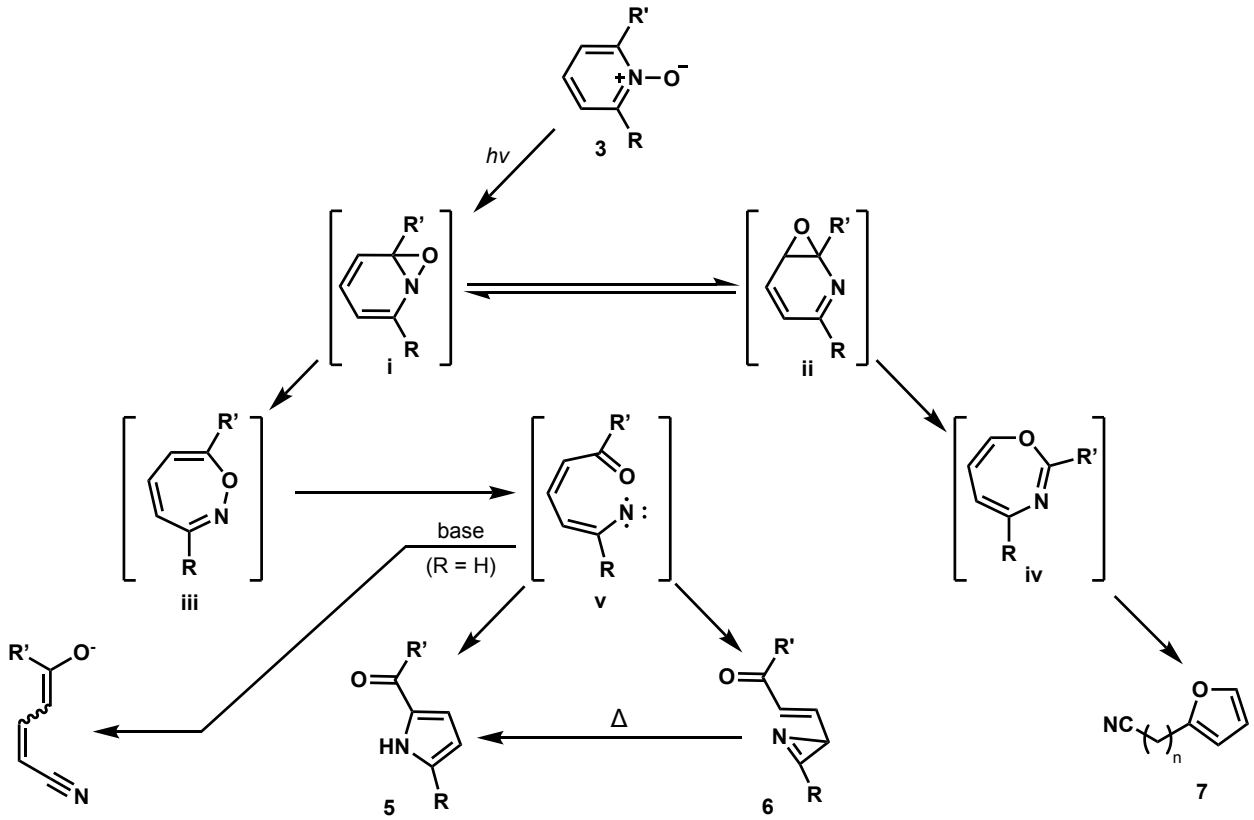

Scheme 1.1.3 Mechanistic framework for the photorearrangement of pyridinophane N-oxides put forth by Weber circa 1989.

In his report, Weber found that the amount of ketopyrrolophane versus azirine formed in a reaction was directly correlated with the length of the pyridinophane N-oxide hydrocarbon bridge; with longer aliphatic chains (n > 8) generally favoring the formation of the ketopyrrolophane over the azirine. In addition, Weber demonstrated that while thermolysis of isolated azirines resulted in their conversion to corresponding ketopyrrolophanes, their re-exposure to irradiation resulted in decomposition to intractable mixtures.

1.1.2 Relevance to Our 2019 Total Synthesis of (+)-Marineosin A

The prodiginine alkaloids are a family of natural products which have fascinated chemists for decades, holding a unique and privileged position in terms of their historical and chemical significance. Produced as secondary metabolites by several members of the *Streptomyces* actinomycetes and *Serratia* enterobacteriaceae bacterial families, the prodiginines are most often characterized by their brilliant red/pink color; a consequence of their prototypical tripyrrolic core.[15] Many of these bacterial lipochromophores have been shown to possess a range of interesting biological activities[16] with one synthetic variant, Obatoclax (**8**) (**Figure 1.1.1**), having advanced to clinical trials as a chemotherapeutic.[17-18] Of the prodiginines, the ansa-bridged members of the family have long been coveted synthetic targets due to both their challenging structure and promising cytotoxicity towards a variety of cancer cell lines.[15]

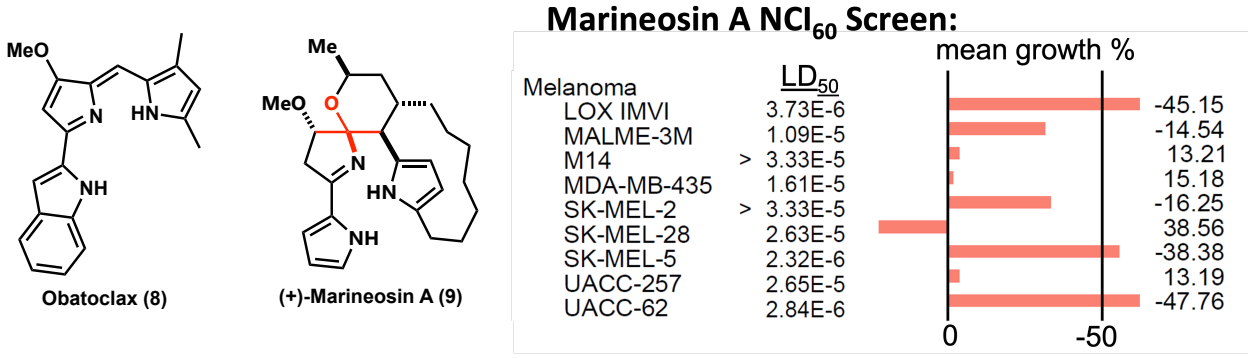

Figure 1.1.1 Prodiginines with clinical chemotherapeutic potential. Structure of phase II clinical trial chemotherapeutic Obatoclax (**8**) and (+)-maineosin A (**9**) along with results of (+)-marineosin A NCI-60 cell screening panel showing potent cytotoxicity against a range of melanoma derived cell lines.

In 2019, our lab published the first laboratory synthesis of (+)-marineosin A (**9**)[19], an ansa-bridged prodiginine natural product first isolated in 2008 by Fenical and coworkers from the culture broth of a marine-derived *Streptomyces*-related actinomycete (strain CNQ-617).[20] Unlike

many prodiginines, marineosin-A is unique in that it is completely colorless. This is due to the presence of a spiroiminal motif which interrupts its chromaphoric tripyrrolic system, a feature which makes marineosin-A one of the most structurally complex members of the prodiginine family. In addition to its complex structure, marineosin-A also exhibits a wide range of useful biological activity, showing significant inhibition of human colon carcinoma (HCT-116) cells (IC_{50} 0.5 μM) as well as selective activities against a variety of melanoma cell lines (as shown in **Figure 1.1.1**).[20,21]

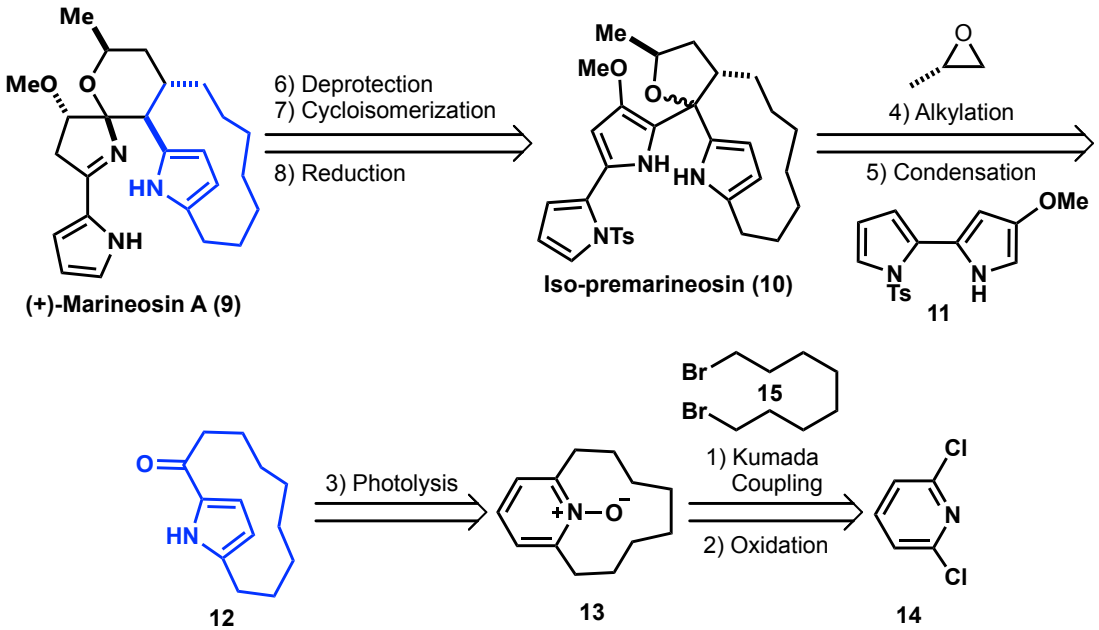

Scheme 1.1.4 Our published retrosynthetic analysis of (+)-marineosin A.

As shown in our retrosynthetic analysis of (+)-marineosin A (**Scheme 1.1.4**), we were able to access the natural product in just 8-steps with assembly of the tripyrrolic core achieved via the condensation of fragments of reversed polarity relative to conventional prodiginine construction.[15,18,22] A highlight of our strategy was its convergent nature, which allows for the facile design and synthesis of diastereomers, congeners and synthetic analogs biosynthetically inaccessible. A key transformation exploited in this route was the photochemical rearrangement

of [8]-(2,6)-pyridinophane N-oxide **13** to ketopyrrolophane **12**, an integral building block which maps directly onto the ansa-bridged pyrrolic unit present in the natural product. While this exact transformation was first published by Weber and coworkers in the late 1980's, reported yields of desired ketopyrrolophane **12** were low (0.6%) (**Table 1.1.1**, n = 8) with no definitive evidence provided for its mechanistic formation.[13] Despite this challenging starting point, we decided to pursue optimization of this photorearrangement. This decision was largely driven by the convenience by which the reaction's starting material, pyridinophane N-oxide **13**, could be prepared from commercial 2,6-dichloropyridine (**14**) and 1,8-dibromoctane (**15**) via successive nickel-catalyzed Kumada cross-couplings[23] followed by oxidation of the resulting pyridinophane with *m*CPBA.

Optimization of this reaction carried out via batch photolysis, done by screening various reaction solvents and temperatures (**Table 1.1.2**), resulted in dramatically improved isolated yield of **12** with the use of THF at –78°C providing the best results (**Entry 7**, 19%). While this optimization represents an over 30-fold yield improvement upon Weber's reported yield, control experiments showed that desired ketopyrrolophane **12** was photolabile and degraded during the time frame of the batch process. This finding, coupled with our relatively limited throughput using batch photolyses, prompted us to redesign our experimental setup to a continuous flow system (i.e flow photolysis). In this system, a cold THF solution (–78°C, 0.01M) of **13** was pumped through small-bore FEP tubing which was wrapped around an insulated jacketed mercury lamp. By controlling the rate at which the solution was propelled through the tubing, we were able to control the residence time of the reaction mixture. Optimization of this residence time to 5 min resulted in our highest isolated yields of the desire ketopyrrolophane (**Entry 10**, 25%) and allowed for its isolation on gram scale in short order.

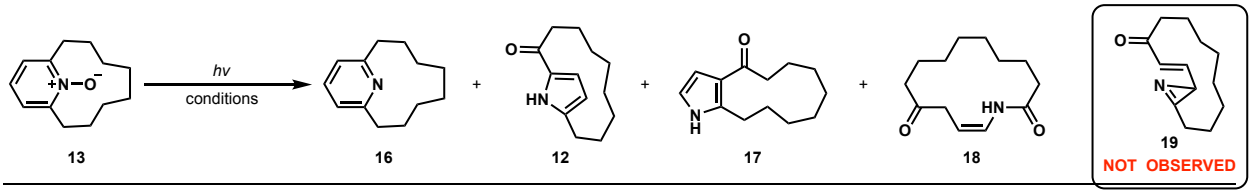

Entry	Solvent	Temp (°C)	% Yield			
			16	**17**	**12**	**18**
1	c-hexane	r.t.	17	3	3	4
2	DME	r.t.	12	6	4	10
3	EtOH	r.t.	7	3	6	7
4	MeCN	r.t.	8	4	5	7
5	THF	r.t.	11	9	7	14
6	THF	–40	19	5	18	12
7	THF	–78	10	2	19	10
8	DME	–30	14	5	10	15
9[a]	THF	–75	9	3	19	17
10[b]	**THF**	**–75**	**15**	**5**	**25**	**18**

Table 1.1.2 Optimization of the photorearrangement towards ketopyrrolophane **12**.[a]Experiment performed in flow format (residence time = 2 min) with one layer of FEP tubing wrapped around the immersion well. [b]Experiment performed in flow format (residence time = 5 min) with three layers of FEP tubing wrapped around immersion well.

While these optimizations and the implementation of flow chemistry were significant breakthroughs in removing the bottleneck towards pushing material through our synthetic route, we couldn't help but notice major differences between Weber's experimental results and our own. During the course of these reaction optimizations and experimental redesigns, we were surprised to have consistently isolated substantial amounts of two macrocyclic products, fused bicyclic pyrrole **17** and macrolactam **18**, not mentioned in Weber's publication. Additionally, we were perplexed by the conspicuous absence of azirine **19**, which Weber isolated as the predominant product of the reaction, from essentially all optimization product mixtures. Intrigued by these experimental inconsistencies, we decided to further investigate the mechanism of this photoinduced transformation with the goal of further optimizing the reaction by eliminating and/or

suppressing the formation of undesired side products (i.e **17** and **18**).

1.2 The Photorearrangement of [8]-(2,6)-Pyridinophane N-Oxide

Our interest in the photochemistry of pyridinophane *N*-oxide **13** persisted following the publication of our total synthesis of (+)-marineosin A.[19] By optimizing reaction parameters and adapting the experimental setup to a flow format, we increased the yield of key building block ketopyrrolophane **12** 40-fold compared to previous literature reports.[13] This ultimately facilitated a synthesis of (+)-marineosin A. Interestingly, the optimized photolysis of **13** on gram scales did not produce appreciable amounts of azirene **19,** the major product reported by Weber. Rather, two novel side products, fused bicyclic pyrrole **17** and macrolactam **18** were isolated, the formation of which we were unable to rationalize within the existing mechanistic framework put forth by Streith, Sigwalt and Weber.[6,8,13] In an attempt to rationalize these findings, we used computations to guide further experiments towards the goal of developing a comprehensive mechanistic framework which describes the formation of all isolated products. Herein, we describe a more detailed view of the reaction aided by the identification of novel heterocyclic intermediates coupled with computational analysis carried out in collaboration with the Houk group.

To begin constructing a mechanistic framework which describes the formation of all isolated products resulting from the photolysis of pyridinophane N-oxide **13**, we probed relative energies of postulated photolytic intermediates in **Scheme 1.1.3** using density functional theory (DFT). We included electronic energies, appropriate in describing electronic excitations, and free energies, appropriate for energetics on the ground state. The calculations supported a pathway from **13** to **12** and **19** *via* common intermediate nitrene **22**. As shown in **Figure 1.2.1**, the first excited state of N-oxide **13** is calculated to relax to a geometry with increased C-O bonding and pass

through a funnel onto the ground state surface of oxaziridine **20**. Cleavage of the C-N bond (**20→21 TS**, via electrocyclic ring expansion) in **20** is calculated to proceed with a low barrier of 4.5 kcal/mol to generate 1,2-oxazepine **21**. Photoexcitation of **21** (vide infra) would then lead to lengthening of its N-O bond and the formation of nitrene **22**. Both singlet and triplet states of **22** were probed, and the triplet state was calculated to be significantly more stable. Triplet nitrene **22** is a key intermediate in the overall photorearrangement.

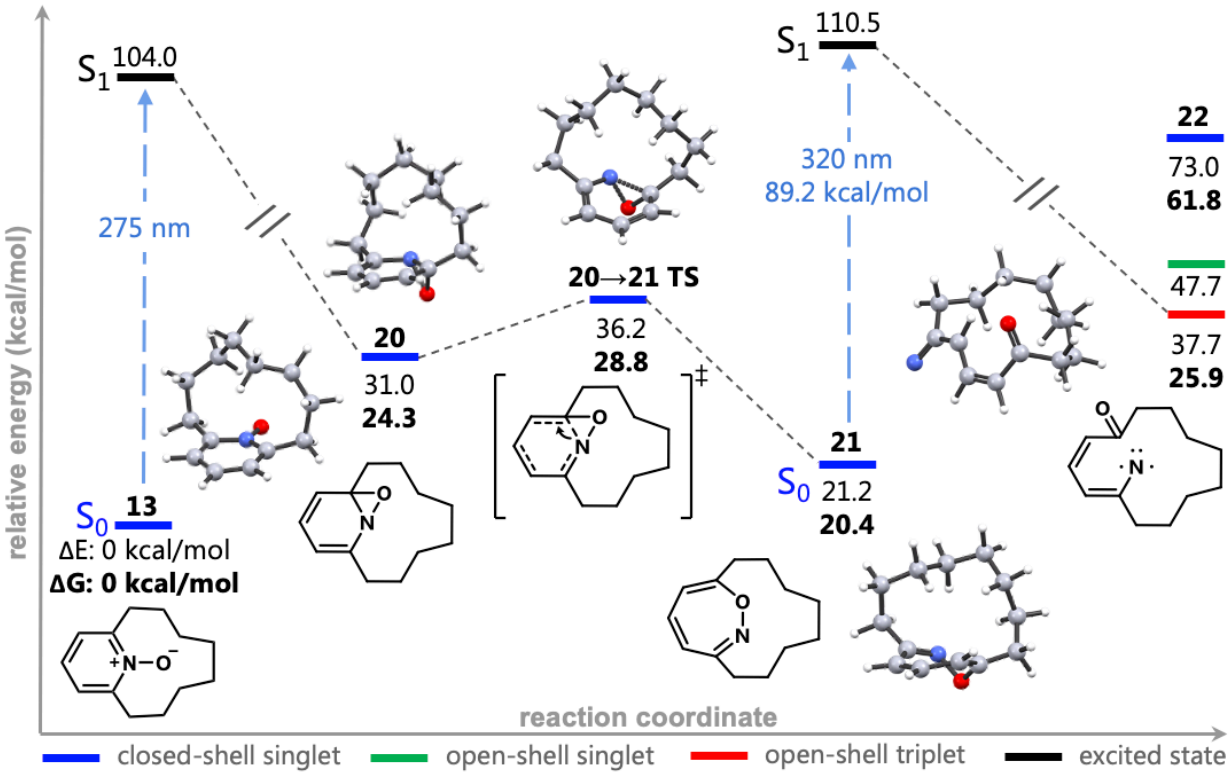

Figure 1.2.1 Calculated energies for proposed intermediates en route to nitrene **22**. Unless indicated otherwise, all geometries were optimized using B3LYP/6-31G(d) in the gas phase as a closed shell singlet.[24-27] **22** was optimized as an open shell triplet using UB3LYP/6-31G(d) in the gas phase. Subsequent single-point energy calculations on each of the optimized structures were performed using (U)M06-2X/6-311+G(d,p) with the polarizable continuum model IEF-PCM for solvation by cyclohexane as either a closed shell singlet (blue) or open-shell triplet (red).[28] For **13** and **21**, a TD-DFT energy calculation was used to compute its lowest energy excitation using M06-2X/6-311+G(d,p) with the same solvation model as single-point calculations (black). Images of optimized structures were generated with Mercury 4.3.1.[29]

Figure 1.2.2 depicts the pathway for conversion of **22** to azirene **19** and ketopyrrolophane **12**. The c*is* geometric isomer of **19** is calculated to be 1.2 kcal/mol higher in energy than its *trans* counterpart and has not been observed experimentally. Thus, *trans*-**19** is referred to simply as **19** from here on. Reversion of **19** to **22** is unfavorable, as cleavage of the newly formed C-N bond would require temperatures of ~200°C.[30, 31] Triplet **22** could also electrocyclize to 2H-pyrrole **23.** Isomerization of **23** to its 1H form **12** may occur via thermal 1,5 hydrogen shift (activation barrier = 19 kcal/mol) or via bimolecular proton transfers.

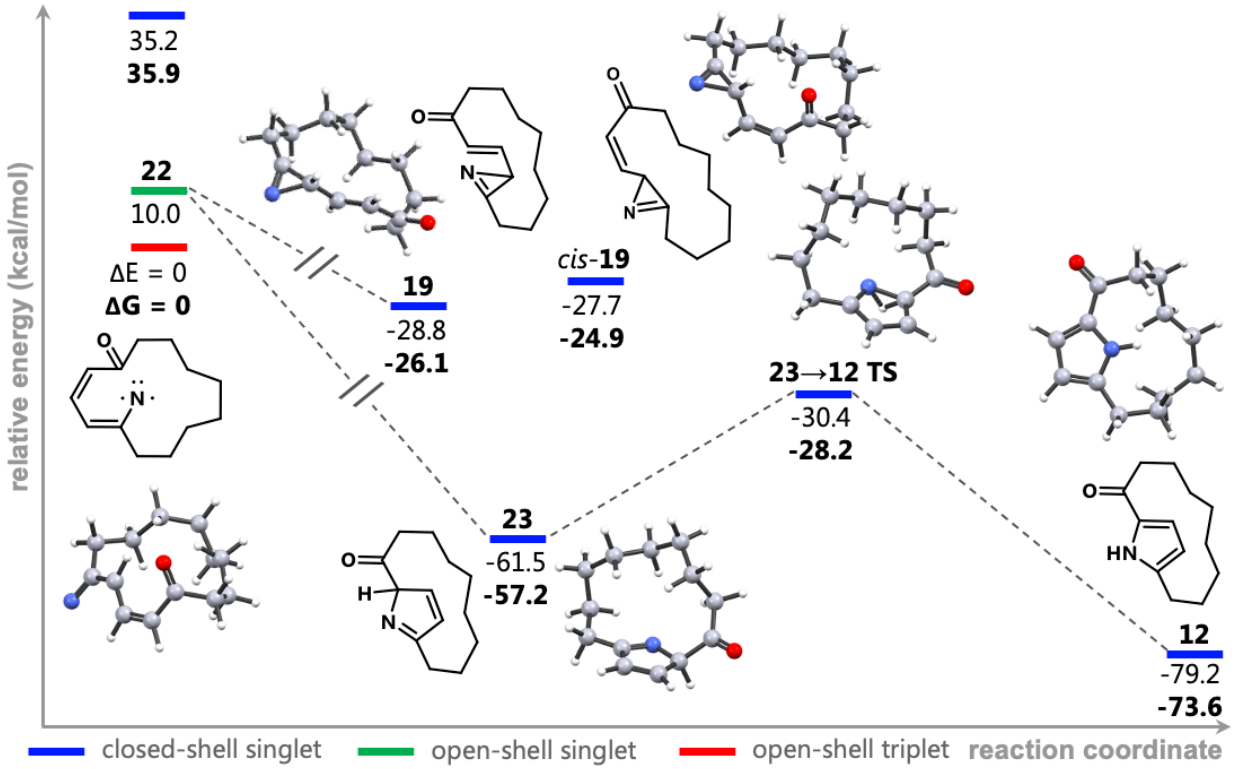

Figure 1.2.2 Calculated relative energies of intermediates in the formation of acylpyrrolophane **12** from nitrene **22**. See **Figure 1.2.1** for computational details.

Regarding the origin of fused bicyclic pyrrole **17**, Padwa had reported that photolysis of vinyl azirenes of type **24** gave 3-formylpyrroles,[30] with subsequent mechanistic studies implicating a nitrile ylide intermediate (e.g. **25**[32], **Figure 1.2.3**, inset). Though these findings seemed at odds

with Weber's account of unproductive azirine photolysis, DFT calculations suggested this to be a feasible pathway to **17**. As depicted in **Figure 1.2.3**, photoexcitation of **19** could cleave the azirene C-C bond to generate nitrile ylide **27**. Ring closure in **27** to afford 2H pyrrole **28** is calculated to be facile (**27→28 TS**), whereupon prototropy in **28** would generate fused bicyclic 1H-pyrrole **17**.

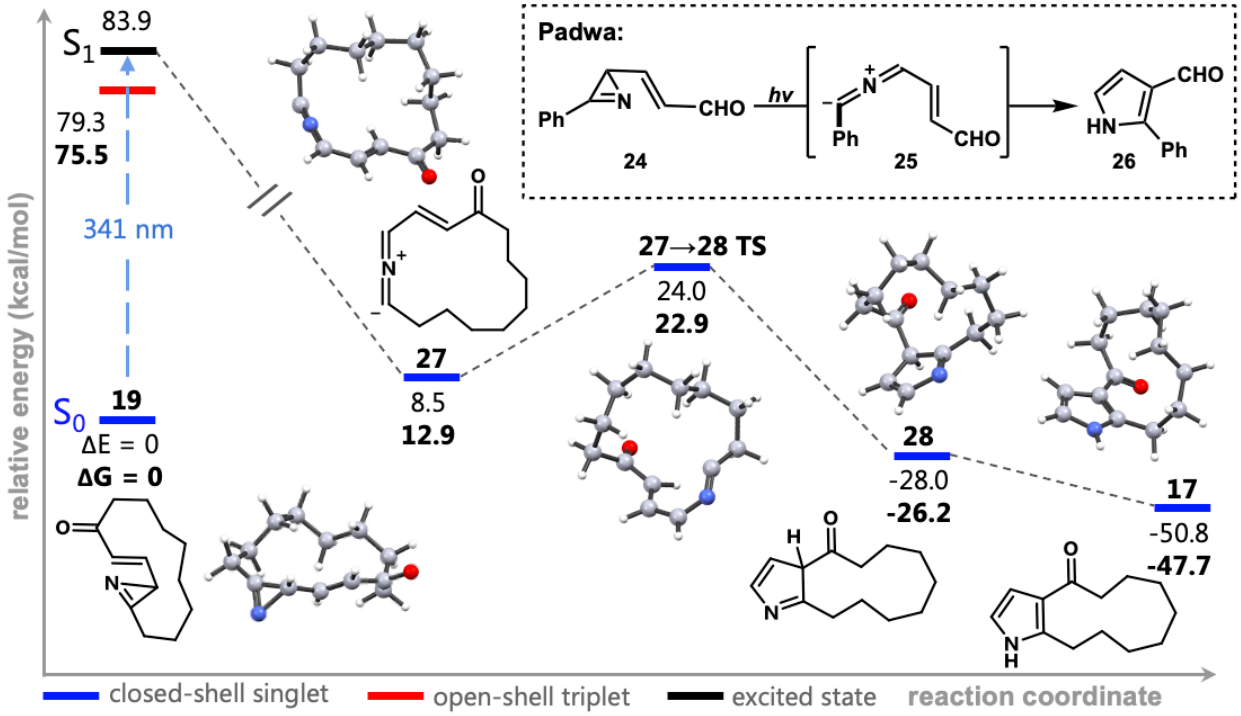

Figure 1.2.3 Calculated pathway from azirine **19** to fused bicyclic pyrrole **17**. Photoexcitation of vinyl azirene **19** is thought to generate nitrile ylide **27** en route to bicyclic pyrrole **7**. Precedent for this proposal is found in Padwa's synthesis of formyl pyrroles from vinyl azirenes (inset). See **Figure 1.2.1** for computational details.

The above calculations provided a framework to design new experiments. If fused bicyclic pyrrole **17** derived from photorearrangement of azirene **19**, blocking that process could be useful. We simulated the UV-Vis spectrum of **19** (TD-DFT) and compared it to experimental spectra for N-oxide **13** and ketopyrrolophane **12** (**Figure 1.2.4**). All three absorbed maximally near 280 nm. However, the spectrum of **13** showed a second absorbance maxima near 235 nm. We speculated that selective irradiation in that region might allow the photorearrangement of **13** to proceed to **12**

while minimizing secondary photochemistry of azirene **19**. In that case **19** would accumulate in the reaction, allowing it to be isolated and subsequently converted to **12** by thermolysis.[13]

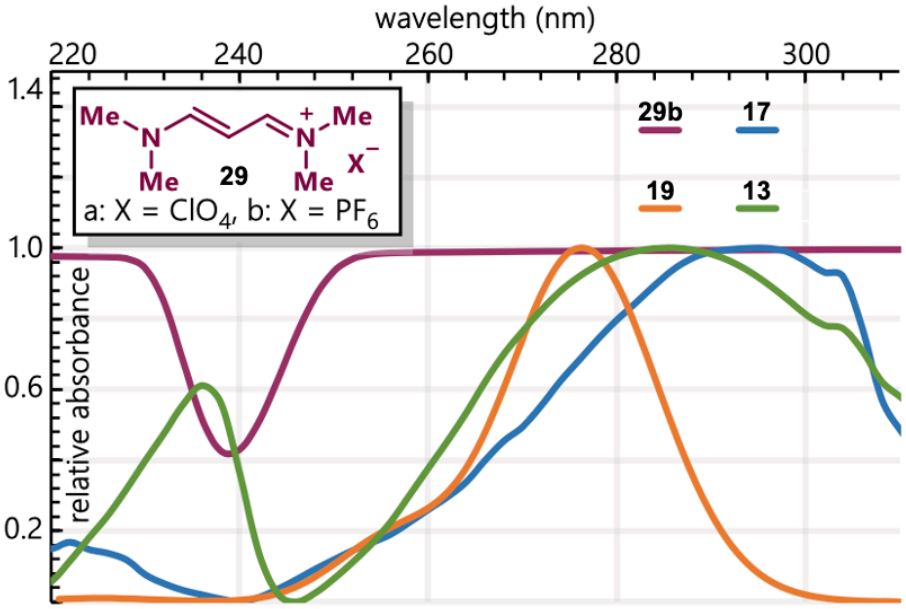

Figure 1.2.4 Experimental and calculated UV-vis spectra. Overlay of UV-vis spectra of **29b** (15 mM 70% aq. ethylene glycol), pyrrolophane **12** (0.1 mM THF), N-oxide **13** (0.005 mM THF), and the simulated spectrum of azirene **19** (computed using TD-B3LYP/-@31+G(d,p)/IEFPCMcyclo-hexane).

We considered laser excitation and the use of band pass filters to achieve selective excitation at 235 nm, but neither was practical in our experimental format. Fortunately, published spectra of vinamidinium perchlorate (**29a**) suggested it could serve as a solution filter with transmissive character in the region around 240 nm.[33] Both the perchlorate and hexafluorophosphate salts of compound **29** were readily synthesized and isolated as light yellow crystals.[34] Screening counter ion, solvent, and concentration revealed that a 15 mM solution of hexafluorophosphate salt **29b** in 70% aqueous ethylene glycol possessed a UV spectrum aligned with our needs (**Figure 1.2.4**). To filter light in our flow apparatus, the glycol solution of **29b** was pumped through the inner lamp-jacket of the Hanovia apparatus (see Experimental Section for

details) from an external reservoir pre-cooled to –78˚C. Control experiments showed the filter solution lost transmittance in the 240 nm region within 1 hour, necessitating its replacement every 45 minutes. Even in that case, however, product mixtures from solution filtered photolyses were little changed relative to those run in Pyrex. Because the experiments were premised on the simulated UV-Vis spectrum of azirene **19** being accurate and the absence of overlapping absorption from other intermediates, we were hesitant to interpret the results.

Instead, to test the validity of **Figure 1.2.3**, we sought to isolate **19**, which Weber had characterized previously. Analytical GC/MS was used to monitor products formed in the photolysis of **13** over time. This was best achieved by sampling solutions of **13** (10 mM in THF) during irradiation at ambient temperature in a Rayonet carousel. Preparative-scale batch reactions require several hours to complete. The GC/MS trace after 1 hour was surprising (**Figure 1.2.5A**). While expected products **16, 12,** and **17** were present, lactam **18** was absent, and the major products were three unknown molecules. The mass spectrum of each unknown showed a parent ion with m/z = 205, indicating they were isomers of starting material **13**. Sampling the photolysis every 15 minutes and plotting relative peak areas versus time showed that unknowns **I-III** predominated at early time points (**Figure 1.2.5B**). The concentration of **II** plateaued at 45 min and remained stable thereafter, whereas amounts of **I** and **III** decreased significantly. The concentration of target pyrrolophane **12** continued to increase after starting material **13** was consumed, indicating it derived from either **I** or **III**. The time course experiment was repeated in 1:1 DME:H_2O solvent. This resulted in rapid consumption of **13** (<1 h) and a correspondingly fast appearance of **I**, yet neither **II** nor **III** were detected (**Figure 1.2.5C**). In the context of prior observations, this pointed towards **I** as the source of pyrrolophane **12**.

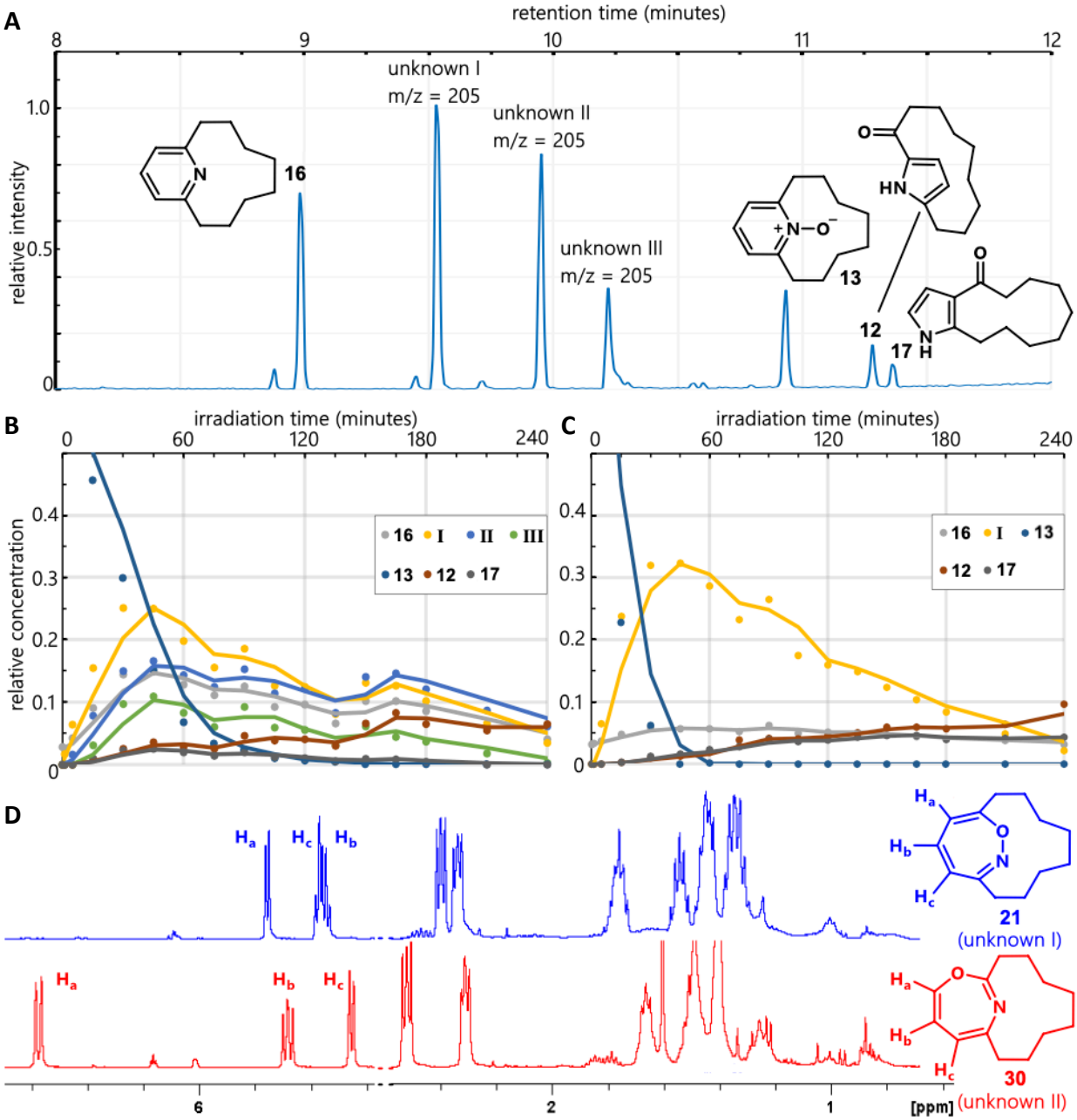

Figure 1.2.5 Data towards identification, isolation and charterization of photolabile intermediates. (**A**) Analytical gas chromatograph of crude mixture derived from batch photolysis of **13** (254 nm, 0.01 M THF, rt) after 60 minutes. (**B**) Relative concentrations of species in panel a plotted vs time during photolysis of **13** (254 nm, 0.01 M THF, rt). For SI for details. (**C**) Same as panel (**B**) except photolysis reaction solvent was 1:1 DME:H_2O. Trend lines are two-period moving averages. (**D**) ^{1}H NMR spectra ($CDCl_3$, 400 MHz) of isolated unknowns I and II from panel A), eventually assigned as structures **21** and **30**, respectively.

To verify this hypothesis, it was necessary to isolate and photolyze **I**. This substance was acid-labile and unstable to chromatography. However, we were able to enrich crude samples in the molecule. Pyridinophane N-oxide **13** was photolyzed for 1 hour in 1:1 DME:H_2O (wherein **II** and **III** were not formed) and the reaction mixture was extracted with ethyl acetate. Concentration of the organic layer provided a residue that was triturated with hexanes to leave behind insoluble pyrroles **12** and **17**. The resultant hexanes solution contained ~75% **I** (GC/MS). ^{13}C-NMR analysis indicated the main component of the mixture had an intact ansa bridge and the three vinylic resonances observed by ^{1}H-NMR were consistent with 1,2–oxazepinophane **21** (**Figure 1.2.5D**). To our knowledge, this was the first direct evidence for a 1,2-oxazepine intermediate in the photorearrangement of pyridine N-oxides.[35] Moreover, structure **21** is the first 1,2-oxazepine isolated lacking electron withdrawing substitution.[36] Re-photolyzing **21** in DME:H_2O resulted in its conversion to keto pyrrolophane **12** and unknown **II**, confirming **21** as an intermediate in the photolysis of **13**. This is supported by several additional experiments: Irradiation of a 0.1 M THF solution of **13** produced a dark orange mixture in which **21** accumulated quickly, but **12** and **II** were produced in trace quantities (**Figure 1.4.5**). Strongly absorbing orange tars likely slowed photoreaction of **21**. Similar results were observed when the photolysis was carried out using a 312 nm light source, a wavelength at which **21** has minimal absorbance (**Figure 1.4.7**). The instability of **21** accounts for it not being observed in prior studies.[13]

GC/MS analysis of an optimized flow photolysis reaction showed substantial production of **II** (**Figure 1.4.4**). **II** proved to be quite sensitive, but careful chromatography using dry, triethylamine-neutralized silica gel afforded small quantities of the compound (~85% purity by GCMS). Its ^{1}H NMR spectrum was similar to that obtained for 1,2-oxazepine **21**, but a downfield resonance was indicative of a vinyl ether, suggesting **II** to be 1,3-oxazepinophane **30** (**Figure**

1.2.5D). Precedent for this assignment was found in prior photolyses of pyridine N-oxides bearing one or more phenyl substituents, which were reported to afford the corresponding 1,3-oxazepins in high yields.[37] Photolysis of **30** did not lead to discernible products, only slow decomposition (**Figure 1.4.8**) This result was consistent with the reported photostability of 1,3-oxazepin-2,4-dicarbonitrile.[38] To our knowledge, **30** represents the first 1,3-oxazepinophane and indeed the first 1,3-oxazepine to be isolated without the aid of aryl and cyano substitutions.[39] Unknown **III**, despite numerous attempts, has yet to be isolated. Merely concentrating crude solutions containing **III** resulted in its degradation.

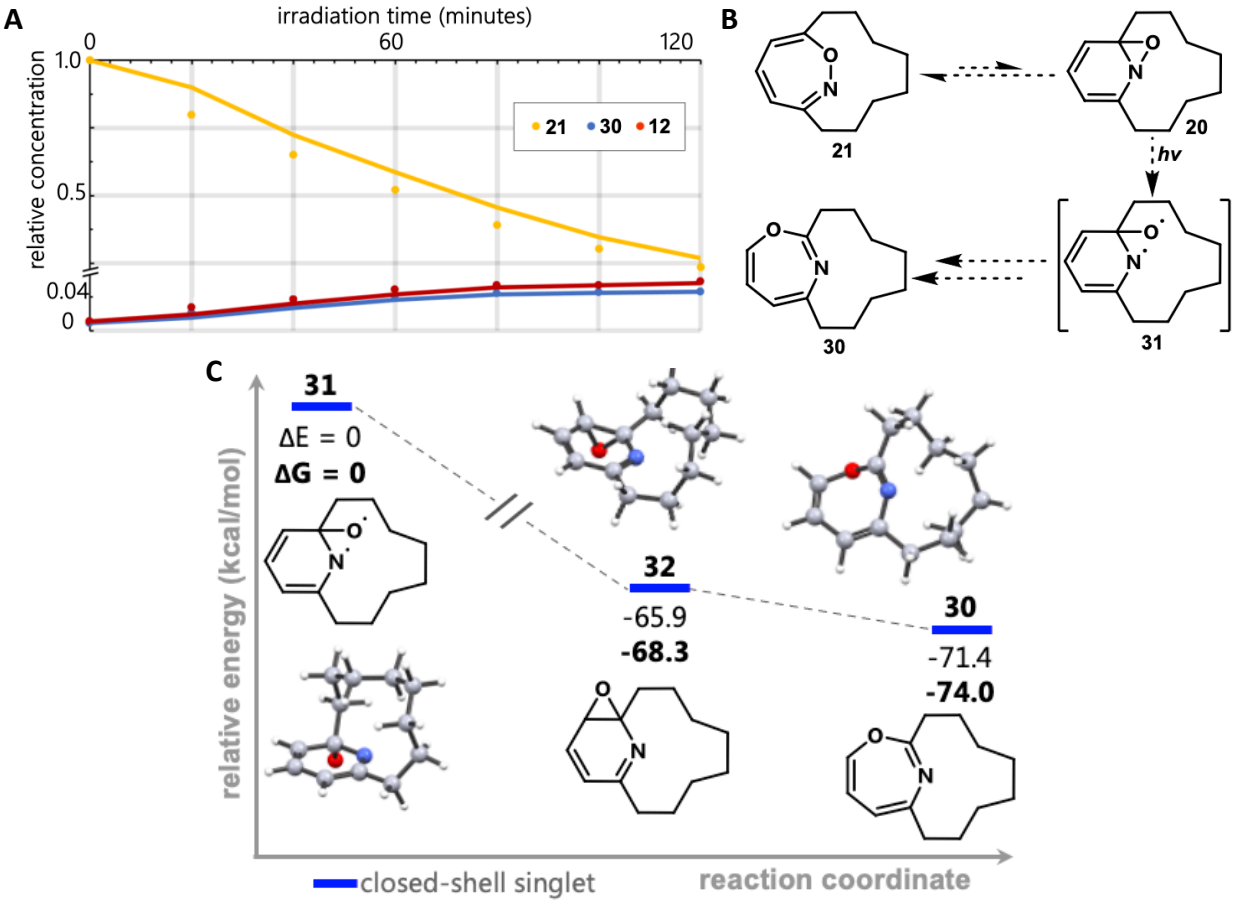

Figure 1.2.6 Experimental and computational evidence for formation of 1,3-oxazepine **30**. (**A**) Time dependent concentrations of major species observed during the photolysis of isolated **21** (254 nm, 0.01 M THF, rt). (**B**) A possible path to 30 during the photolysis of **21** (**C**) If formed, calculations indicate aminyl diyl **31** could proceed readily to **30** by way of intermediate epoxypyridine **32**. See **Figure 1.2.1** and Experimental Section for computational details.

Mechanistically, it is not clear how the excited state of **21** leads to **30** in addition to products **12** and **17**. One possibility is that a ground state equilibrium between **21** and its electrocyclized counterpart **20** (calculated to be ~1000:1 at 25˚C) is perturbed towards **20** in the excited state, such that N-O bond homolysis to afford aminyl diyl **31** (**Figure 1.2.6B**) becomes competitive with nitrene formation. If so, calculations predict cyclization to epoxypyridine **32** and subsequent electrocyclic ring-opening to **30** to be facile (**Figure 1.2.6C**).

In the photolysis of **21**, azirene **19** was isolated alongside **30.** Interestingly, **19** co-eluted with macrolactam **18** during silica gel chromatography, despite the two having significantly different R_f values on TLC. A 2D-TLC experiment was performed, drying the plate between runs. In that case, the spot for **19** cleanly converted into the spot for **18**. GC/MS analyses of samples of **19** that had been adsorbed onto silica gel and allowed to stand at ambient atmosphere overnight also showed full conversion of **19** into **18** (**Figure 1.2.7A**). Calculations depicted in **Scheme 1.2.7B** indicate hydration of **19** and ring opening of the resulting hemiaminal **33** should be facile. We conclude that macrolactam **18** is not a primary photoproduct. It forms only through hydrolysis of residual azirine **19** during chromatographic purification of crude reaction mixtures.

When protected from hydrolysis, **19** was found to convert to fused bicyclic pyrrole **17** within minutes of exposure to 254 nm light (**Figure 1.2.7C**), confirming the prediction outlined in **Figure 1.2.3**. Continued irradiation resulted in near-complete degradation of **17** within an additional 45 minutes. Such photoinstability is perhaps why this molecule escaped Weber's careful analyses, as their irradiations were conducted over a period of hours. Additionally, we obtained a UV-Vis spectrum of **19** (**Figure 1.4.12**). Although our calculations accurately predicted its absorbance maxima at 269 nm, they markedly overestimated absorbance at 235 nm (see

Experimental Section for additional discussion). This likely contributed to ineffectual attempts at solution filtering described earlier.

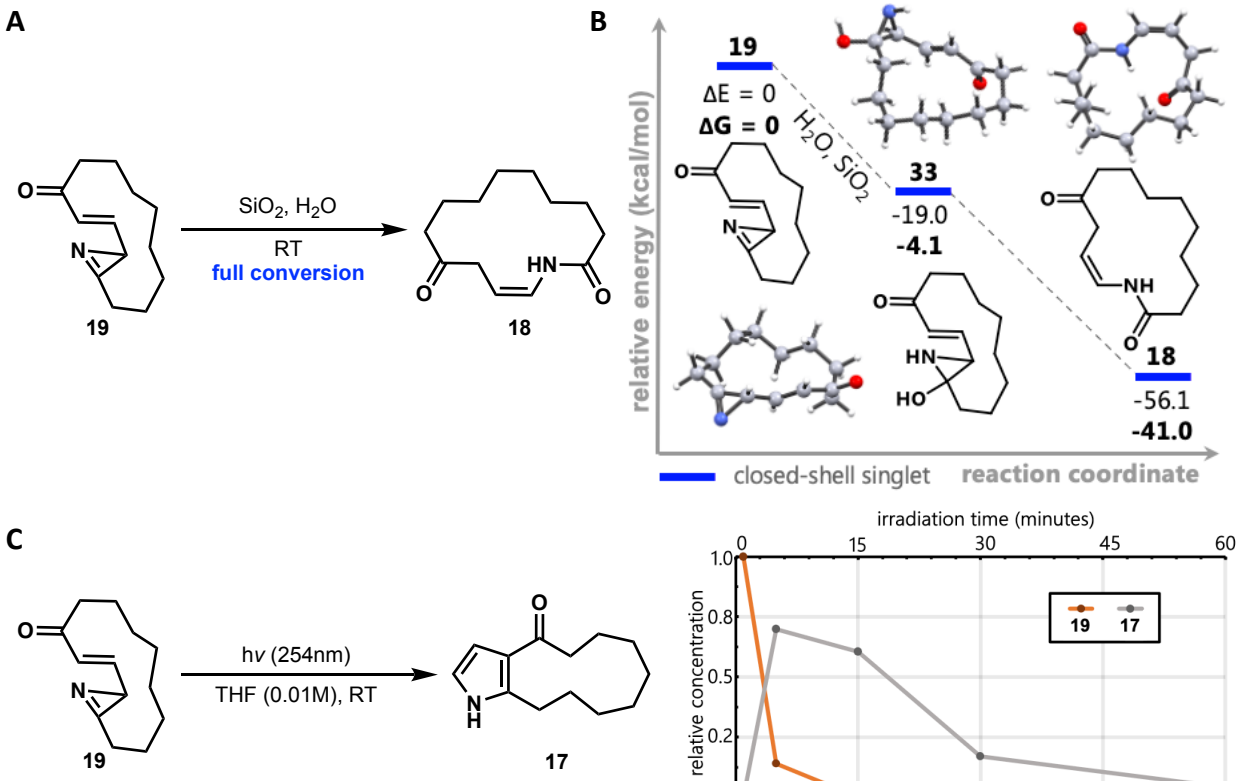

Figure 1.2.7 Experimental and computational evide hydrolyzes to lactam **18** during silica gel chromatography (see **Figure 1.4.9**). (**B**) Computations which indicate the hydrolysis of **19** to **18** is energetically favorable. See **Figure 1.2.1** and Experimental Section for computational details. (**C**) GC/MS analysis reveals that photolysis of **19** (254 nm, 0.01 M THF, rt) forms bicyclic pyrrole **17** and that **17** is unstable to the reaction conditions.

On a related note, we did not detect formation of furanonitrile **7** (**Table 1.1.1**) in any photolysis. This was consistent with Weber's findings, wherein furanonitriles (postulated to be derived from 1,3-oxazepine intermediates) were detected only in photorearrangement of the shortest and longest ansa bridge lengths examined (**Table 1.1.1**, n = 6, 4.2%; n = 7, 0.7%; n = 10, 3.1%). Lastly, we speculate reduction of **20** is the source of pyridinophane **16** (**Table 1.1.2**). **16** is

observed in all photoreactions of **13**. However, we have not yet identified the species that is concomitantly oxidized.[40]

1.3 Conclusion

The photorearrangement of [8]-2,6-pyridinophane N-oxide has been studied using a combination of experiments and calculations. Weber had originally isolated 0.6% yield of keto pyrrolophane **12** from the reaction. We modified the photolysis solvent and temperature and adapted the reaction to a flow format to maximize pyrrolophane formation. The yield of product **12** increased 40-fold under those conditions, but previously undetected by-products were formed. Density functional theory was used to calculate energies of putative oxaziridine, oxazepine and nitrene intermediates consistent with early mechanistic studies of pyridine N-oxide photorearrangements. By carefully analyzing the time course of batch photolyses using analytical GC/MS, we were able to show that ansa-bridged 1,2- and 1,3-oxazepins were isolable species that formed rapidly in the reaction. Control experiments established that both pyrrolophane **12** and bicyclic pyrrole **17** in our optimized photolysis were actually derived from secondary photoexcitation of 1,2-oxazepine **21**. We speculate that the excited state of **21** diverges to either nitrene or walking-type rearrangement pathways leading to ketopyrrolophane **12** and azirene **19** or 1,3-oxazepinophane **30**, respectively. We isolated trace amounts of macrocyclic vinyl azirene **19** first identified by Weber and showed it converted to **17** within minutes upon UV photolysis at room temperature.

The data show that the formation of **12** is the result of two successive photoexcitations starting from **13**, wherein the second photoexcitation is the origin of competing pathways that result in multiple end products. This suggests optimizing the photosynthesis of 1,2-oxazepine **21**

may be the most the effective means to access **12** on scale, wherein a non-photochemical method to rearrange **21** would be required. Studies and results to identify such a method are outlined in the thesis of lab member Dr. Evan E. Hurlow.[41]

1.4 Experimental Section

General Methods and Materials

Unless otherwise specified, reactions were performed in flame-dried glassware under an atmosphere of argon. Reagents were purchased from commercial vendors and used as received unless otherwise stated. Diethyl ether (Et_2O), chloroform ($CHCl_3$), tetrahydrofuran (THF) and 1,2-dimethoxy ethane (DME) were passed through a Glass Contour solvent drying system. Magnesium turnings were polished by sequential rinsing with aqueous 1M HCl, absolute ethanol, and Et_2O. The washed turnings were placed under vacuum for several hours then stored under an atmosphere of argon. Yields refer to chromatographically and spectroscopically (^{1}H-NMR) homogeneous materials, unless otherwise stated. Thin-layer chromatography (TLC) was conducted on precoated plates (Sorbent Technologies, silica gel 60 PF254, 0.25 mm) visualized with UV 254 nm. For acid-sensitive compounds, TLC plates were neutralized with TEA/Hexane (1%) before use. Column chromatography was performed on silica gel 60 (SiliCycle, 240−400 mesh). For acid-sensitive compounds, silica gel was premixed with TEA/Hexane (1%) before being loaded into the column. NMR spectra were recorded on Bruker Avance spectrometers (400/100 MHz, 500/125 MHz, and 600/100 MHz). Chemical shifts are reported in ppm and referenced to residual internal $CHCl_3$ for ^{1}H (δ 7.26) and ^{13}C (δ 77.2) spectra. Deuterated chloroform used in NMR experiments was neutralized prior to sample dissolution via passage through a plug of neutral alumina. UV-Vis spectra were obtained using a Shimadzu UV3101PC UV-VIS-NIR Scanning Spectrophotometer unless otherwise noted. GC/MS analyses were run on an Agilent 7250 Q-TOF GC/MS using an Agilent 19091S-433 HP-5MS capillary column. High resolution mass spectra were recorded using Thermo Fisher Scientific Exactive Plus with IonSense ID-CUBE DART source and Orbitrap

analyzer.

Batch photoreactions were carried out in either a standard Ace Glass immersion well photoreactor or an Ace Glass low temperature immersion well photoreactor using a Hanovia 450W mercury arc lamp. Flow photoreactions were carried out using 1/16" ID x 1/8" OD x 1/32" Wall Versilon™ FEP Tubing coiled around an Ace Glass 7858 triple-walled quartz immersion well in either one or three layers. The reaction solution was propelled by a peristaltic pump (Binaca model 1001) through the FEP tubing under irradiation by a Hanovia 450W mercury arc lamp. Time course experiments were conducted inside of a Rayonet Reactor (Southern New England Ultraviolet Co.) utilizing a 254 nm bulb set using quartz test tubes unless otherwise stated.

Experimental Procedures and Product Characterization

[8]-(2,6)-pyridinophane (**16**)

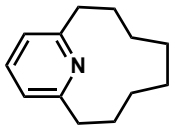

To a flame-dried 500 mL 3-neck round bottom flask, equipped with an addition funnel, condenser, and stir bar, were added polished magnesium tunings (4.86 g, 0.2 mol, 2.0 eq.) and a single iodine crystal in anhydrous Et_2O (200 ml) under Ar. With vigorous stirring, from the addition funnel was added 1,8-dibromooctane (1 mL). The mixture was heated using a heat gun until the brown color dissipated. The remaining 1,8-dibromooctane (27.6 g in total, 0.1 mol, 1.0 eq.) was added dropwise into the flask at a rate such that the solution was maintained at a gentle reflux. After addition was complete, the addition funnel was rinsed with anhydrous diethyl ether (10 mL) into the reaction mixture. The resulting mixture was refluxed for another hour. (When stirring was stopped, the mixture separated into two layers; the top a translucent light gray and the bottom a viscous, opaque gray).

During the reflux, to a separate flame-dried 2 L 3-necked round bottom flask equipped with a thermometer was added 2,6-dichloropyridine (14.8 g, 0.1 mol, 1.0 eq.) and $NiCl_2$(dppp) (0.43 g, 0.75 mmol, 0.8 mol %) in anhydrous Et_2O (1 L) under Ar. The mixture was cooled in an ice-water batch to 10 °C, followed by addition of the newly formed di-Grignard solution in Et_2O via syringe pump over 6 h. During the addition, the reaction solution was kept at 10 °C with vigorous stirring. When TLC monitoring (5% EtOAc/Hexane) confirmed that 2,6-dichloropyridine was fully consumed, the reaction mixture was carefully poured into ice water then filtered through celite. The organic layer was separated and the aqueous layer was extracted with EtOAc (100 mL X 3).

The organic layers were combined, washed with brine, dried over Na_2SO_4, filtered, and concentrated to an orange oil. The resulting 23 g of crude product was dry-loaded onto silica gel (30 g) and purified by flash column chromatography (EtOAc in Hexane: 3%) to yield compound **16** (9.48 g, 50 mmol, 50%) as a colorless oil. ^{1}H-NMR (400 MHz, $CDCl_3$) δ 7.46 (t, *J* = 7.6 Hz, 1H), 6.89 (d, *J* = 7.6 Hz, 2H), 2.84 (t, *J* = 6.38 Hz, 4H), 1.83 – 1.77 (m, 4H), 1.42 – 1.36 (m, 4H), 1.06 – 0.98 (m, 4H); ^{13}C-NMR (100 MHz, $CDCl_3$) δ 160.6, 136.6, 120.0, 35.7, 26.3, 25.1, 23.2; HRMS (EI) calculated for $C_{13}H_{20}N$ $[M+H]^+$: 190.1590, found 190.1583.

[8]-(2,6)-pyridinophane *N*-oxide (**13**)

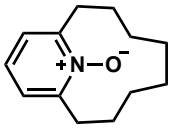

To a stirred solution of **16** (34.4 g, 182 mmol, 1.0 eq.) in $CHCl_3$ (182 mL) in a 3 L flask submerged in a room temperature water bath was added mCPBA (62.8 g, 75% purity, 273 mmol, 1.5 eq.) in several portions. After 30 min, the reaction turned too thick to stir and another 100 mL of $CHCl_3$ was added. The resulting mixture was then stirred at r.t. for 16 h, and then diluted with $CHCl_3$ (2 L), followed by addition of K_2CO_3. The resulting white slurry was stirred at r.t. for 2 h then mixed with celite (200 g) and filtered through a layer of celite. The filter cake was rinsed with $CHCl_3$ until no product could be detected by TLC. The filtrate was then concentrated and purified by flash column chromatography (EtOAc in Hexane:10%-40%) to yield compound **13** (30.6 g, 149 mmol, 82%) as pale yellow crystalline solid, and recovered compound **16** (2.64 g, 14 mmol, 8%). Alternatively, desired compound **13** can be isolated from the crude product via recrystallization from hot pentanes. ^{1}H-NMR (400 MHz, $CDCl_3$) δ 7.46 (t, *J* = 7.6 Hz, 1H), 6.89 (d, *J* = 7.6 Hz, 2H), 2.84 (t, *J* = 6.38 Hz, 4H), 1.82 – 1.76 (m, 4H), 1.42 – 1.36 (m, 4H), 1.04 – 0.98 (m, 4H); ^{13}C-

NMR (100 MHz, $CDCl_3$) δ 160.6, 136.6, 120.0, 35.7, 26.3, 25.1, 23.2; HRMS (EI) calculated for $C_{13}H_{20}NO$ $[M + H]^+$: 206.1539, found 206.1534.

General Procedures for the Photolysis of **13**

Batch Irradiation Conditions (**Table 1.1.2**, Entry 7):

A 1 L immersion well photoreactor was charged with a solution of **13** (3.9 g, 19.18 mmol) in THF (1 L, 0.02M). The solution was cooled to -78 °C and then irradiated with a 450 W Hanovia Mercury Arc lamp for 3h with stirring. The mixture was monitored by ^{1}H-NMR spectrum analysis of aliquots. The lamp was removed and the mixture was warmed to room temperature and concentrated. The residue was then purified by flash column chromatography (EtOAc in Hexane: 10% - 20% - 22% - 30% - 40%).

Flow Irradiation Conditions (**Table 1.1.2**, Entry 10):

A quartz immersion well wrapped with 3 layers of FEP tubing was placed in a dewar and cooled to -75 °C with isopropanol and dry ice. The solution of **13** (6.32 g, 30.8 mmol) in anhydrous THF (0.01 M) was pumped through the FEP tubing with a residence time of 5 minutes. The resulting light-yellow solution was concentrated, purified by flash column chromatography (EtOAc in Hexane: 10% - 20% - 22% - 30% - 40%). This resulted in **12** (1.56 g, 7.6 mmol, 25%), **17** (292 mg, 1.42 mmol, 5%), **18** (1.185 g, 5.3 mmol, 18%) and **16** (866 mg, 4.6 mmol, 15%).

1*1H*-1(2,5)-pyrrolacyclodecaphan-2-one (**12**)

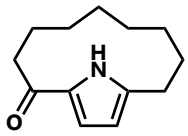

White solid. M.P.: 198 °C. ^{1}H-NMR (500 MHz, $CDCl_3$) δ 8.73 (s, 1H), 6.98 (t, *J* = 3.2 Hz, 1H), 6.09 (t, *J* = 3.2 Hz, 1H), 2.78 – 2.73 (m, 2H), 2.68 (t, *J* = 6.3 Hz, 2H), 1.79 (tq, *J* = 13.6, 6.8, 6.1 Hz, 4H), 1.60 – 1.49 (m, 2H), 1.37 (p, *J* = 6.0 Hz, 2H), 1.21 (p, *J* = 6.9 Hz, 2H), 1.08 (ddt, *J* = 12.3, 8.9, 5.4 Hz, 2H); ^{13}C-NMR (125 MHz, $CDCl_3$): 190.3, 137.9, 132.3, 115.9, 111.5, 36.1, 27.0, 26.7, 26.2, 23.5, 23.4, 23.3, 21.7; HRMS (EI) calculated for $C_{13}H_{20}NO$ $[M + H]^+$: 206.1545, found 206.1533.

5,6,7,8,9,10,11,12-octahydrocycloundeca[*b*]pyrrol-4(1*H*)-one (**17**)

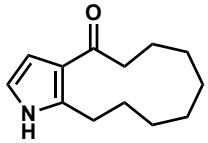

White solid. M.P.: 154 °C. ^{1}H-NMR (500 MHz, $CDCl_3$) δ 8.14 (s, 1H), 6.63 (t, *J* = 2.7 Hz, 1H), 6.44 (t, *J* = 2.9 Hz, 1H), 3.09 (t, *J* = 6.35 Hz, 1H), 2.68 (t, *J* = 6.35 Hz, 1H), 1.75 (p, *J* = 6.2 Hz, 2H), 1.64 – 1.58 (m, 2H), 1.37 (p, *J* = 6.1 Hz, 2H), 1.23 (tt, *J* = 8.9, 4.6 Hz, 2H), 1.12 (ddt, *J* = 10.3, 7.7, 4.6 Hz, 2H), 1.09 – 1.01 (m, 2H); ^{13}C-NMR (125 MHz, $CDCl_3$) δ 202.3, 136.9, 124.3, 116.6, 110.1, 41.7, 28.1, 27.8, 25.4, 25.1, 24.6, 24.5, 22.8; HRMS (EI) calculated for $C_{13}H_{20}NO$ $[M + H]^+$: 206.1545, found 206.1532.

(*Z*)-azacyclotetradec-13-ene-2,11-dione (**18**)

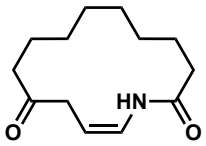

White solid. M.P.: 119 °C. ^{1}H-NMR (500 MHz, $CDCl_3$) δ 7.63 (d, *J* = 10.1 Hz, 1H), 6.90 (ddt, *J* = 10.4, 9.0, 1.3 Hz, 1H), 4.80 (dt, *J* = 9.1, 7.7 Hz, 1H), 3.15 (dd, *J* = 7.7, 1.2 Hz, 2H), 2.45 (t, *J* = 6.7 Hz, 2H), 2.36 – 2.33 (m, 2H), 1.69 – 1.61 (m, 4H), 1.35 (tt, *J* = 7.1, 3.0 Hz, 4H), 1.27 (q, *J* = 7.3 Hz, 2H), 1.17 (dq, *J* = 8.4, 6.5 Hz, 2H); ^{13}C-NMR (126 MHz, $CDCl_3$) δ 210.7, 170.9, 125.4, 101.0, 41.9, 40.7, 36.0, 26.8, 26.0, 25.3, 25.3, 24.3, 23.3; HRMS (EI) calculated for $C_{13}H_{21}NO_2$ $[M + H]^+$: 224.1651, found 224.1637.

(E)-14-azabicyclo[11.1.0]tetradeca-2,13-dien-4-one (**19**)

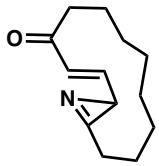

A quartz immersion well enclosing a medium pressure mercury arc lamp and wrapped with FEP tubing was placed in a dewar and cooled to -75 °C with isopropanol and dry ice. The lamp was turned on and allowed to warm up for 15 minutes. A peristaltic pump was then used to drive a solution of **13** (4.1 g, 20 mmol) in anhydrous THF (0.01 M) through the FEP tubing at a rate corresponding to a residence time of 2 minutes. The resulting light yellow solution was concentrated and purified by flash column chromatography using neutralized silica gel (EtOAc in Hexane: 15%) to afford **19** as a light yellow oil. The product's NMR spectra matched those reported by Weber.[13] UV-VIS: (0.01 mM THF) λ_{max1} = 238 nm, λ_{max2} = 269 nm.

(*Z*)-14-oxa-15-azabicyclo[8.3.2]pentadeca-1(13),10(15),11-triene (**21**)

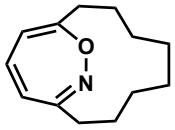

To a 20 ml quartz test tube containing a stir bar was added 21 mg (0.1 mmol) [8]-2,6-pyridinophane N-oxide **13**. 5 ml DME then 5 ml water were added and the tube capped with a septum and pierced with a needle. The solution was degassed in a bath sonicator for 5 minutes, after which the tube was suspended in a Rayonet photoreactor equipped with a stir plate and irradiated at 254 nm for 60 minutes. The resulting light-yellow solution was washed with water and the aqueous fraction extracted with EtOAc. The organic layer was dried with Na_2SO_4 and concentrated under reduced pressure. 0.5 ml hexanes were added to the residue resulting in precipitation of compounds **12** and **17**. The hexanes were carefully pipetted away and concentrated to afford 12 mg of a light-yellow oil containing ~75% **21** (GC/MS) with **16** as the major contaminant. ^{1}H-NMR (600 MHz, $CDCl_3$): δ 5.76 (d, *J*= 4.9 Hz, 1H), 5.58 (d, *J*= 5.5 Hz, 1H), δ 5.55 (t, *J*= 5.2 Hz, 1H), 2.40 (dd, *J*= 6.1, 6.5 Hz, 2H), 2.34 (dd, *J*= 6.0, 6.2 Hz, 2H), 1.76 (m, 2H), 1.55 (m, 2H), 1.45 (m, 4H), 1.34 (m, 4H). ^{13}C-NMR (100 MHz, $CDCl_3$): δ 160.5, 154.2, 138.1, 116.7, 113.4, 35.2, 34.0, 25.9, 25.0, 24.9, 24.8, 23.9, 22.6. UV-VIS: (0.07 mM THF) λ_{max1} = 234 nm, λ_{max2} = 288 nm.

(Z)-11-oxa-15-azabicyclo[8.4.1]pentadeca-1(14),10(15),12-triene (**30**)

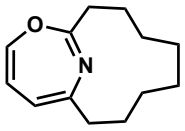

A quartz immersion well enclosing a medium pressure mercury arc lamp and wrapped with FEP tubing was placed in a dewar and cooled to -75 °C with isopropanol and dry ice. The lamp was turned on and allowed to warm up for 15 minutes. A peristaltic pump was then used to drive a

solution of **13** (4.1 g, 20 mmol) in anhydrous THF (0.01 M) through the FEP tubing at a rate corresponding to a residence time of 2 minutes. The resulting light yellow solution was concentrated and purified by flash column chromatography using neutralized silica gel (EtOAc in Hexane: 10%) to afford 5 mg of a clear oil containing ~85% **30**. ^{1}H-NMR (400 MHz, $CDCl_3$): δ 6.58 (d, *J*= 8.0 Hz, 1H), 5.68 (dd, *J*= 8.0, 8.0 Hz, 1H), δ 5.46 (dd, *J*= 5.9, 0.8 Hz, 1H), 2.52 (t, *J*= 6.3 Hz, 2H), 2.31 (t, *J*= 6.2 Hz, 2H), 1.67 (m, 2H), 1.49 (m, 4H), 1.41 (s, 6H). ^{13}C-NMR (100 MHz, $CDCl_3$): δ 155.5, 154.1, 138.0, 118.4, 112.1, 33.5, 33.4, 24.4, 24.3, 23.3, 22.4, 21.6, 21.4. UV-VIS: (0.07 mM THF) λ_{max1} = 238 nm, λ_{max2} = 304 nm.

Photolysis Reactor Experimental Setups

Flow photolyses were carried out using a flow reactor setup as depicted in **Figures 1.4.1**, **Figure 1.4.2** and **Figure 1.4.3**.

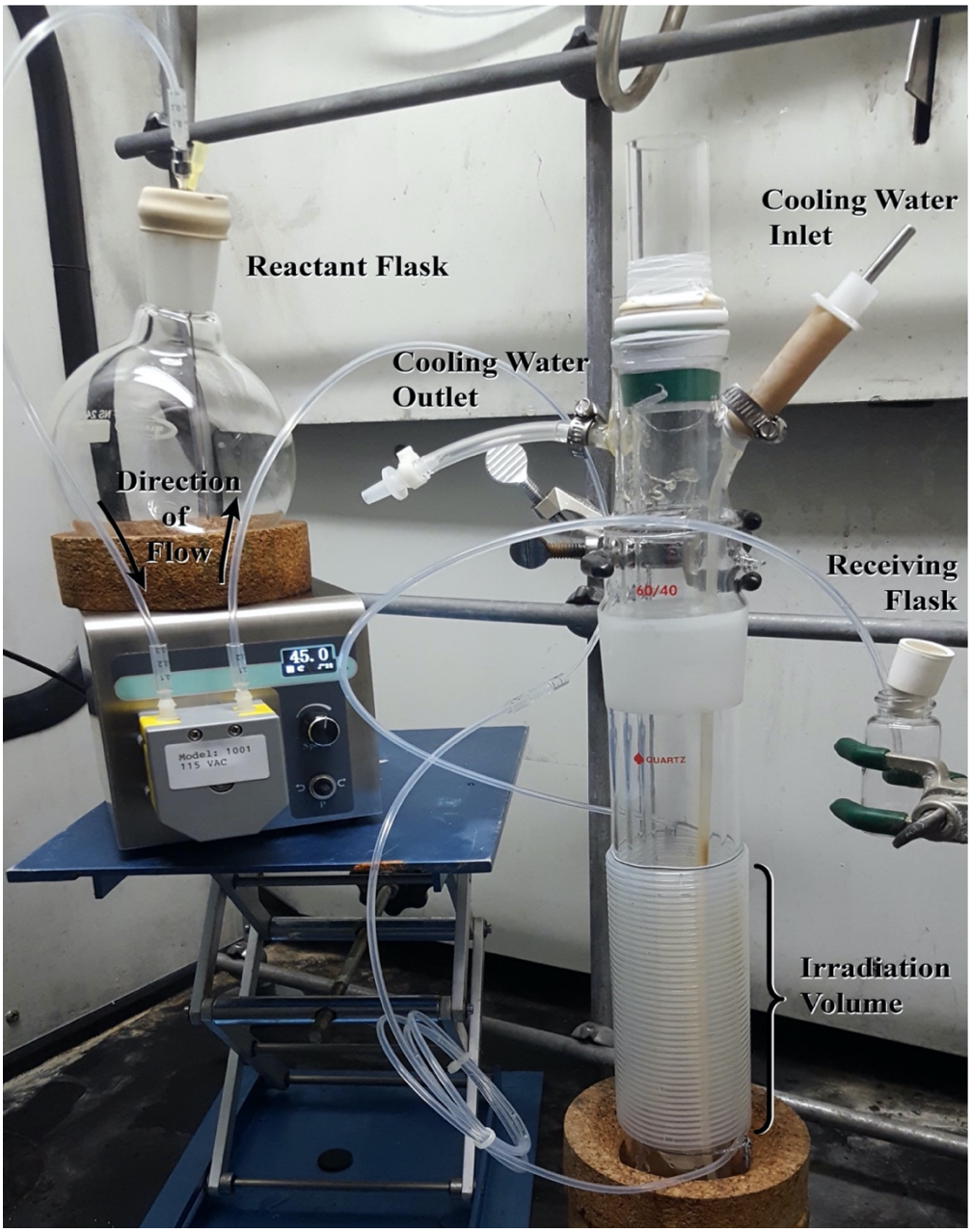

Figure 1.4.1 Flow Reactor Setup. Arrows indicate direction of flow.

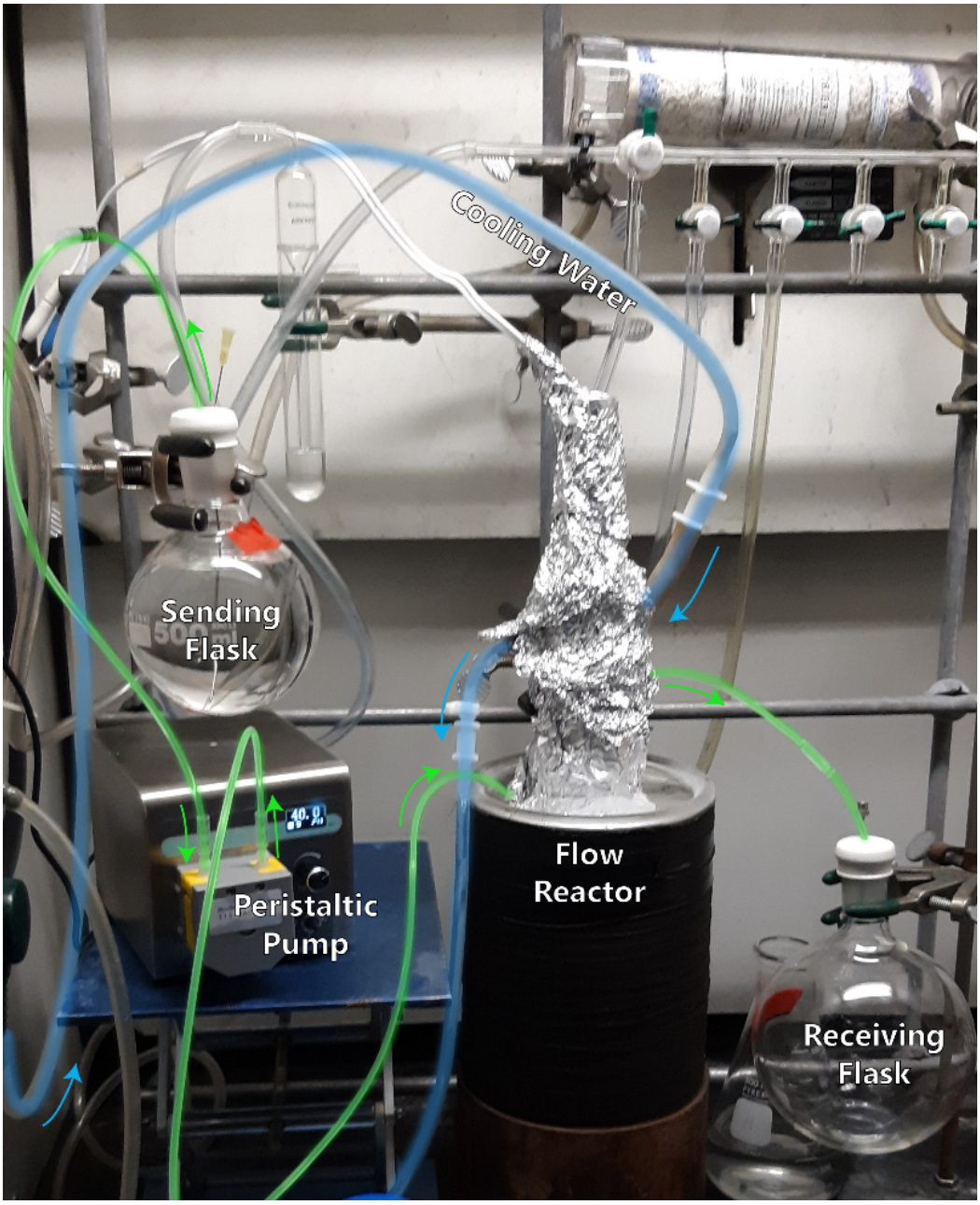

Figure 1.4.2 Experimental setup for flow photolysis. Arrows indicate direction of flow of solution of **13** (green) and water (blue).

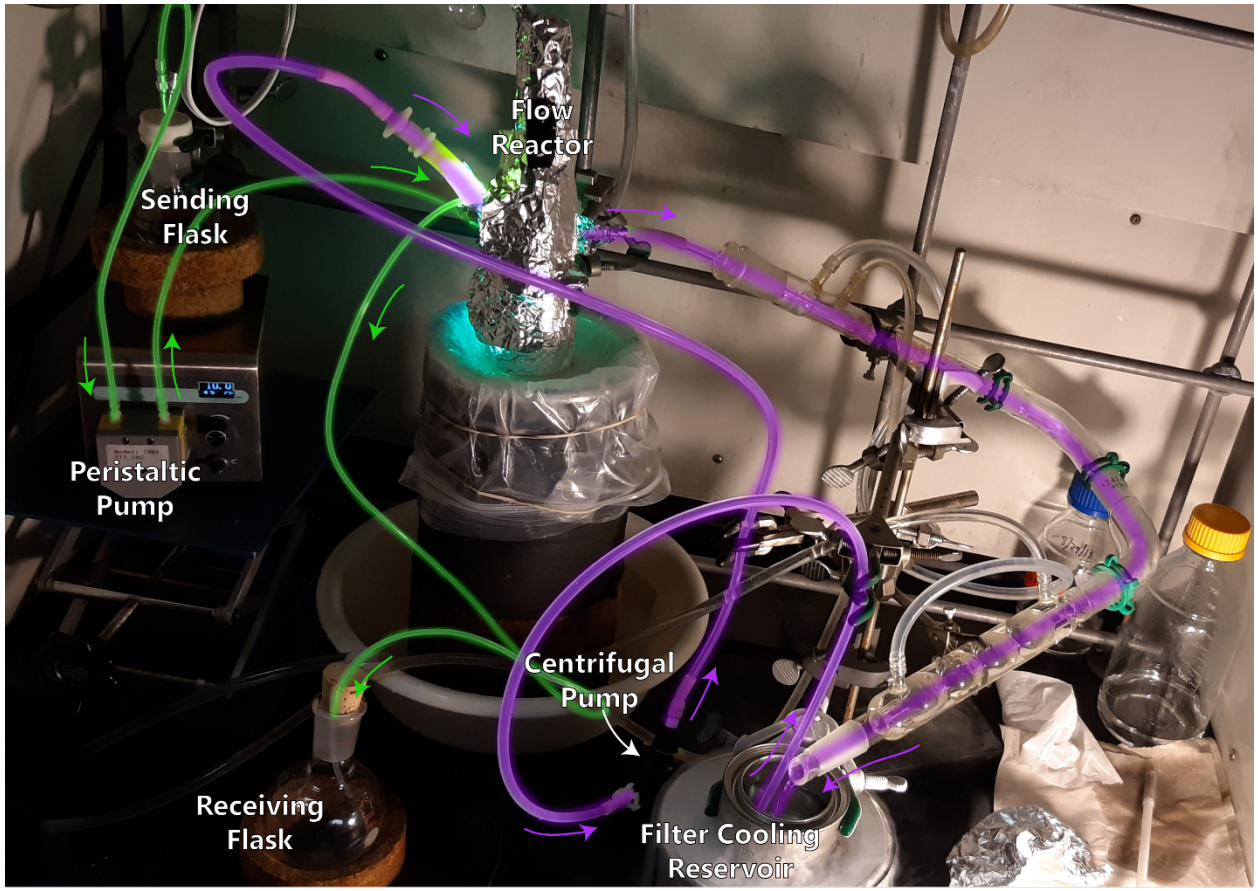

Figure 1.4.3 Experimental setup for filtered flow photolysis. Arrows indicate direction of flow of solution of **13** (green) and cooled filtration solution (purple).

Time Course Experiment Procedures and Additional GC/MS Data

General Procedure:

To a 20 ml quartz test tube was added 0.1 mmol **13** and a stir bar. The appropriate solvent was then added and the tube capped with a rubber septum. The septum was pierced with a needle and the vessel was degassed using a bath sonicator for 5 minutes. The tube was then suspended in the center of a Rayonet photoreactor with stirring. The reactor was covered with a light-blocking cloth and powered on. To sample the reaction, the reactor was powered-off, the reaction vessel was removed and uncapped, and the desired volume of reaction media was removed using a micropipette.

GC/MS Sample Preparation:

To a GC/MS vial containing a low-volume insert was added 50 µl of reaction media, 200 µl of cyclohexane, and 10 µl of a 10 mg/ml cyclohexane solution of [6]-2,6-pyridinophane as an internal standard.

GC/MS Method:

For all samples, oven temperature was held at 70 °C for 1 minute, then ramped up to 300 °C at a rate of 20 °C/min, then held at 300 °C for 4 minutes.

Data Workup:

Peak identity was verified using authentic samples of **12**, **13**, **16**, **17**, and **18** isolated previously by column chromatography. Peaks of interest for a given sample were integrated manually using

Agilent ChemStation software and peak areas were exported as a Microsoft Excel spreadsheet. Spreadsheets of a given time course were then compiled into a single file using Microsoft Excel and peak areas were normalized with respect to the internal standard's peak area for each time point. The data was then normalized with respect to the largest area observed and plotted. Trend lines are two-period moving averages.

Figure 1.4.4 GC/MS trace of a flow photolysis reaction from which azirine **19** and 1,3-oxazepine **30** were isolated.

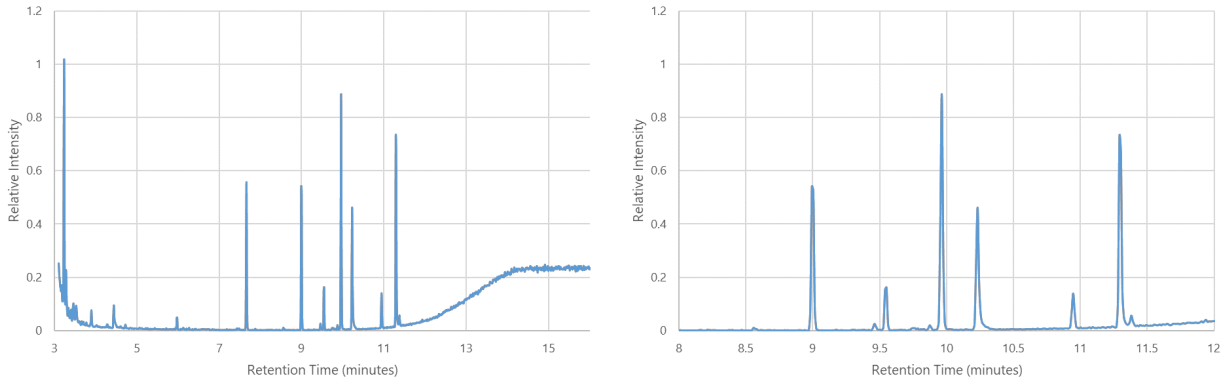

Figure 1.4.5 Time Course Irradiation of a 0.1 M solution of **13**.

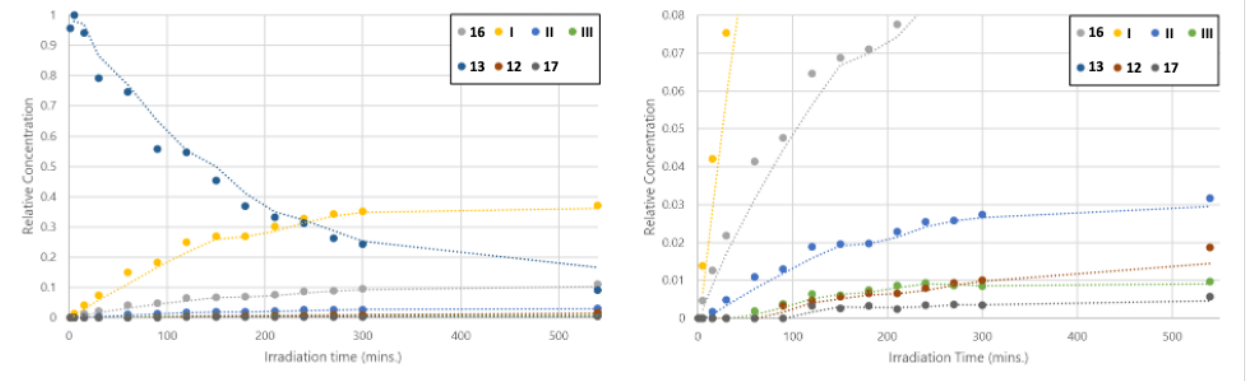

Figure 1.4.6 Time Course Irradiation of **13** filtered by **29b** (15 mM in 70% aq. glycol).

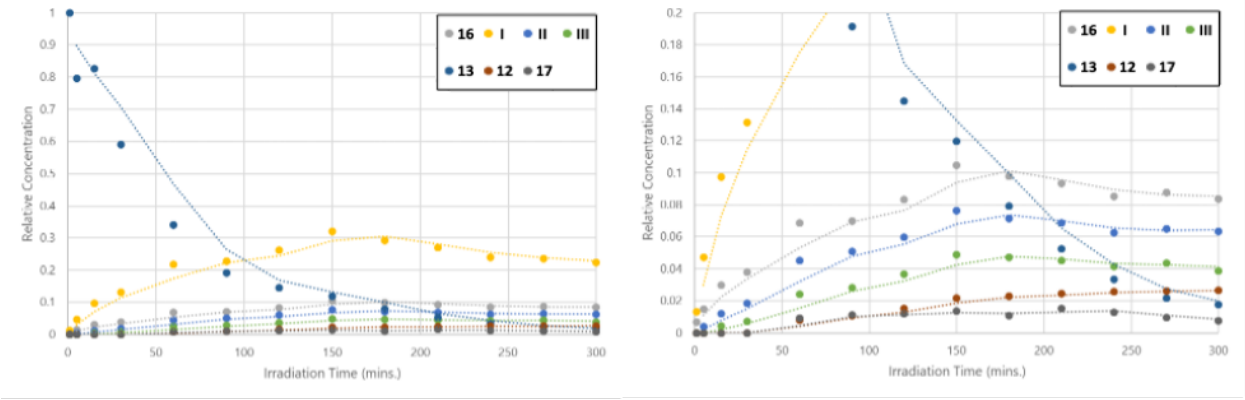

Filtration was affected by immersion of a stoppered quartz test tube containing the reaction mixture within a larger quartz test tube containing the filter solution. Resultant filtration path length was approximately 1 cm.

Figure 1.4.7 Time Course Irradiation of **13** at 312 nm.

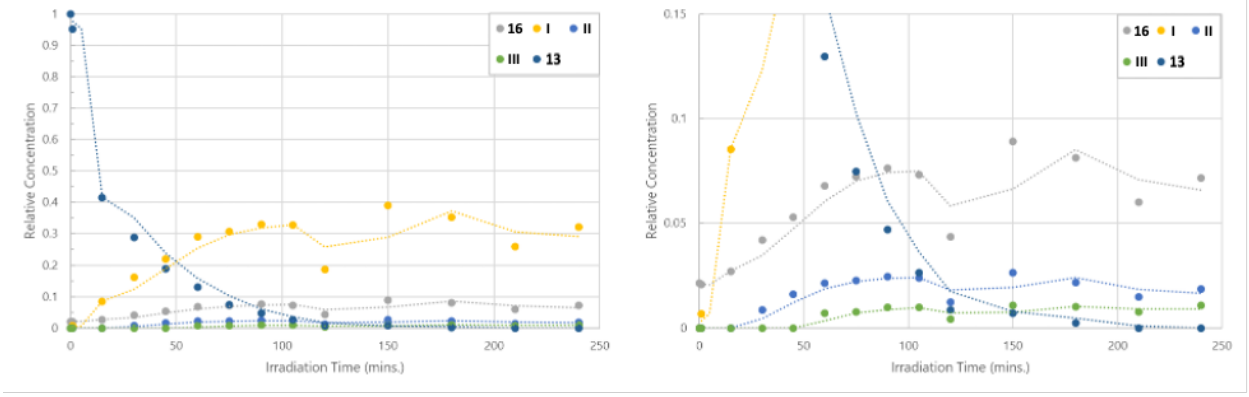

Figure 1.4.8 Time Course Irradiation of **30** (254 nm, 0.01 M THF).

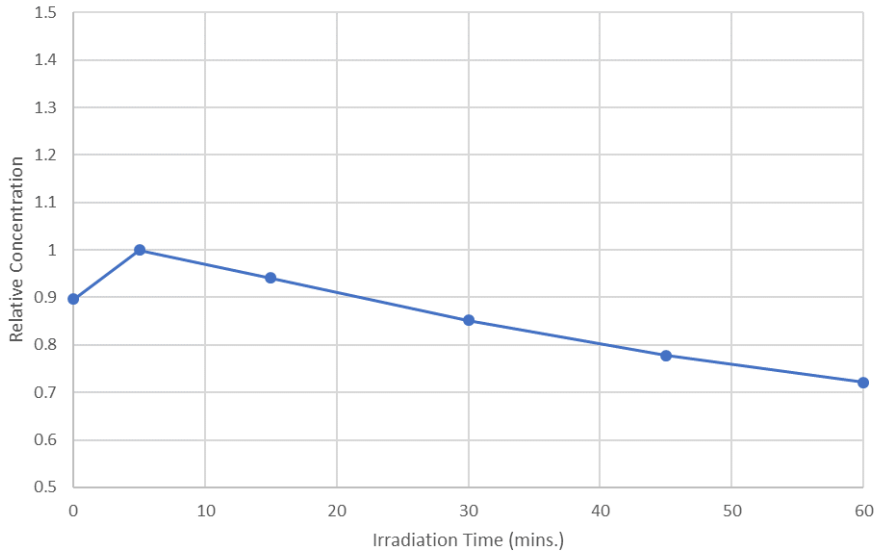

*No products resulting from the photolysis of **30** were detected.*

Figure 1.4.9 GC/MS chromatograms of **19** before and after hydrolysis on SiO_2.

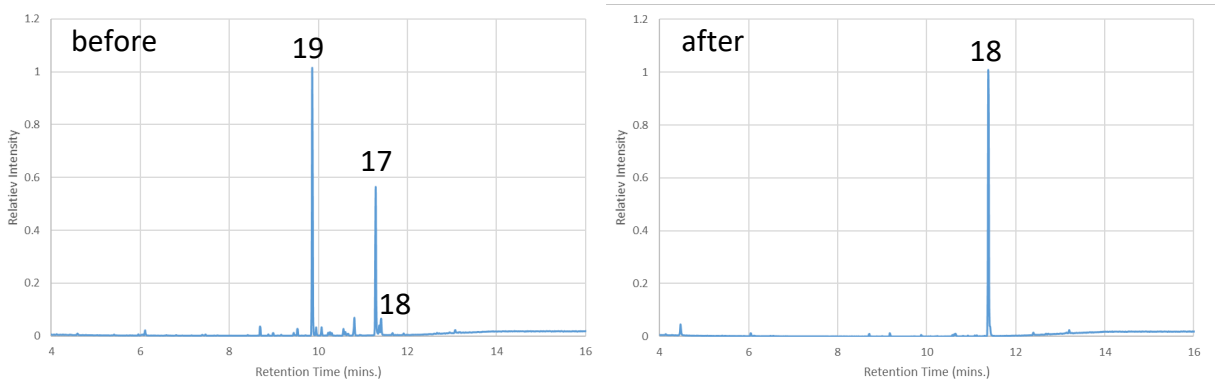

UV-Vis Spectra

Figure 1.4.10 UV-Vis spectrum of **21** (0.07 mM in THF).

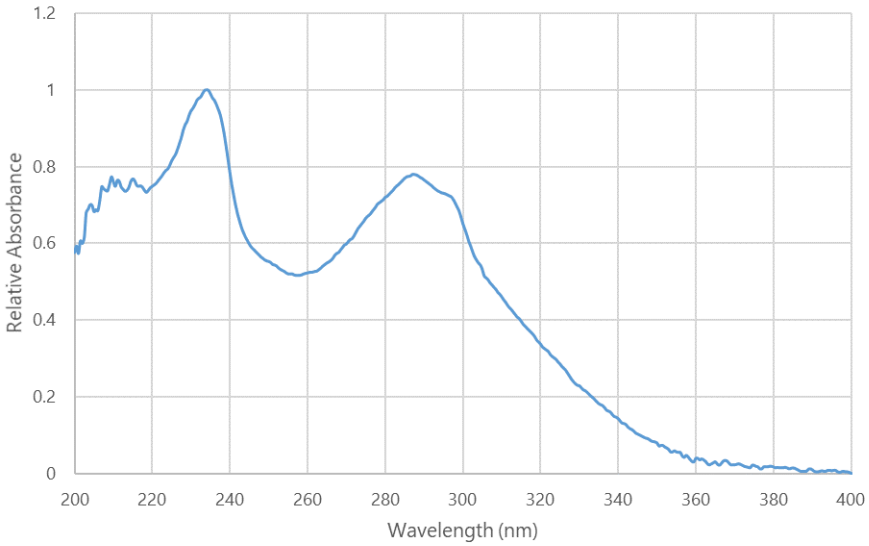

Figure 1.4.11 UV-Vis spectrum of **30** (0.07 mM in THF).

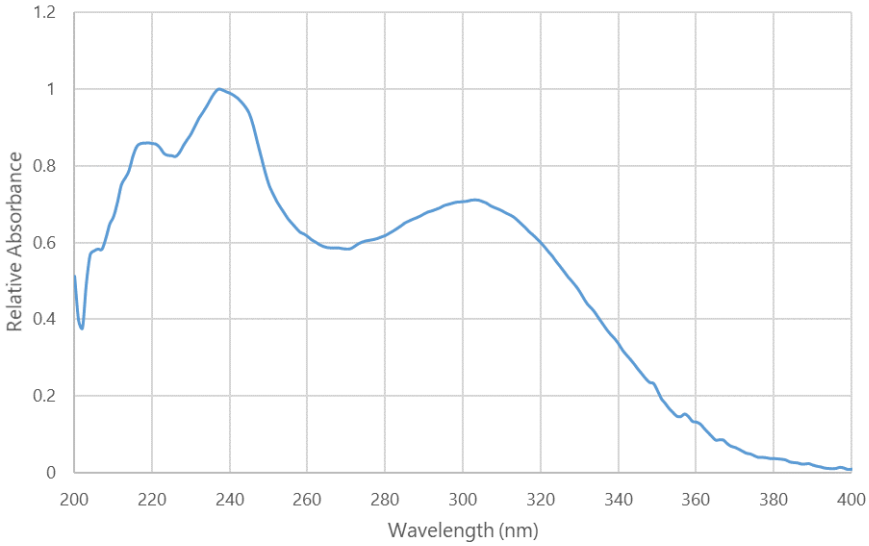

Figure 1.4.12 UV-Vis spectrum of **19** (0.1 mM in THF).

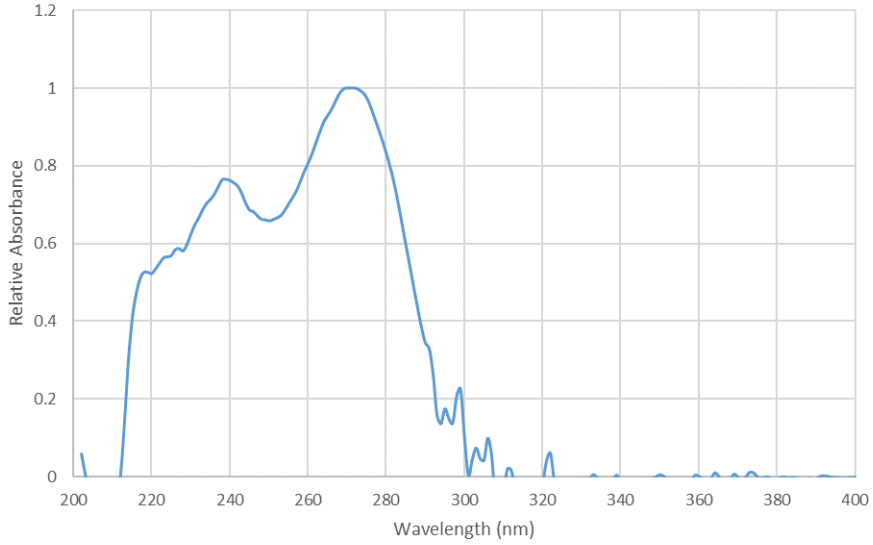

Figure 1.4.13 UV-Vis spectrum of **13** (0.005 mM in THF).

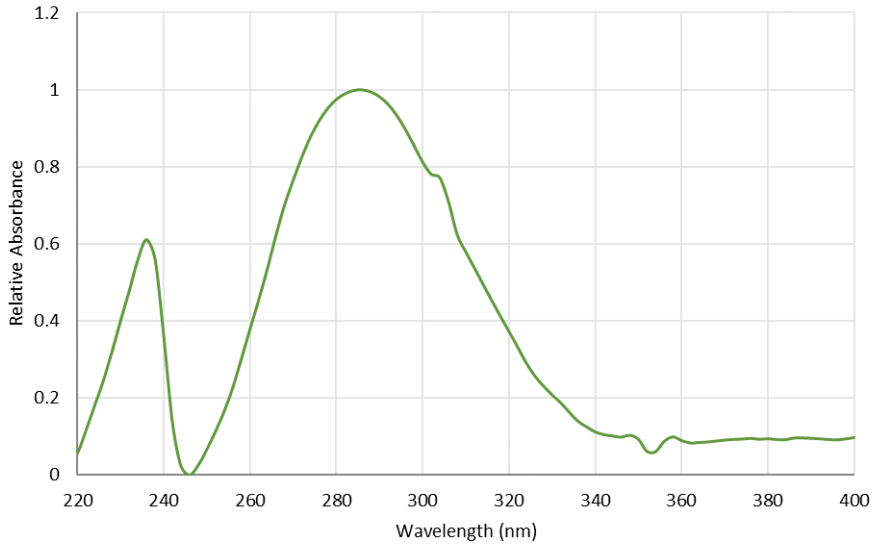

Figure 1.4.14 UV-Vis spectrum of **12** (0.1 mM in THF).

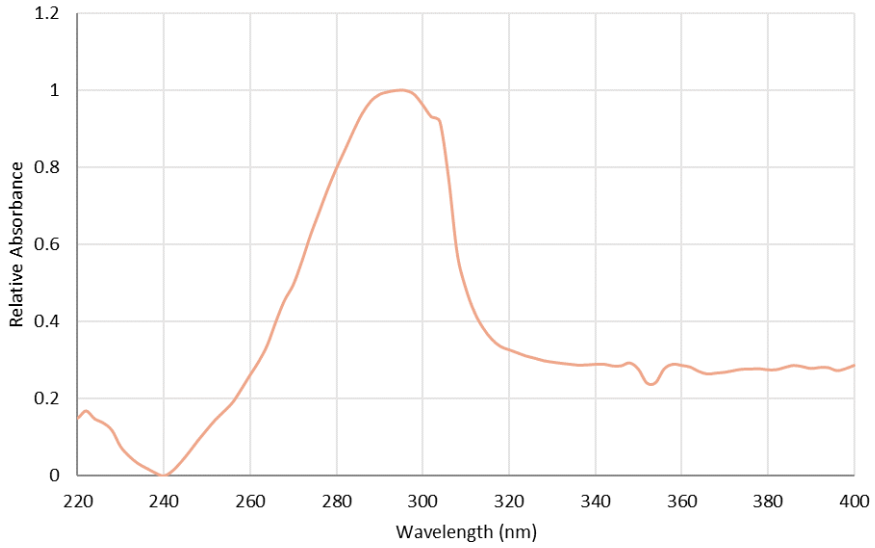

Figure 1.4.15 UV-Vis of **29b** (15 mM in 70% aqueous glycol) before and after 1 hour of irradiation.

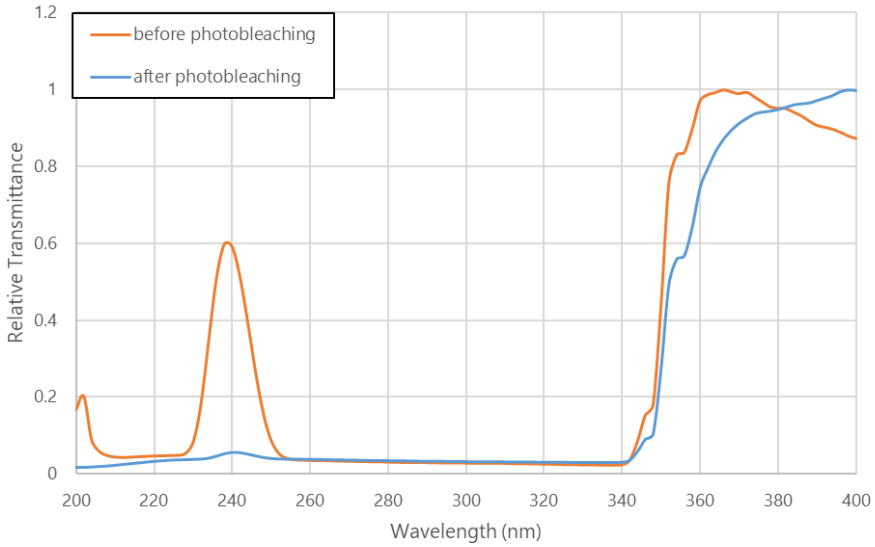

Figure 1.4.16 UV-Vis spectra of **29b** (15 mM) in glycol solutions of varying aqueous content.

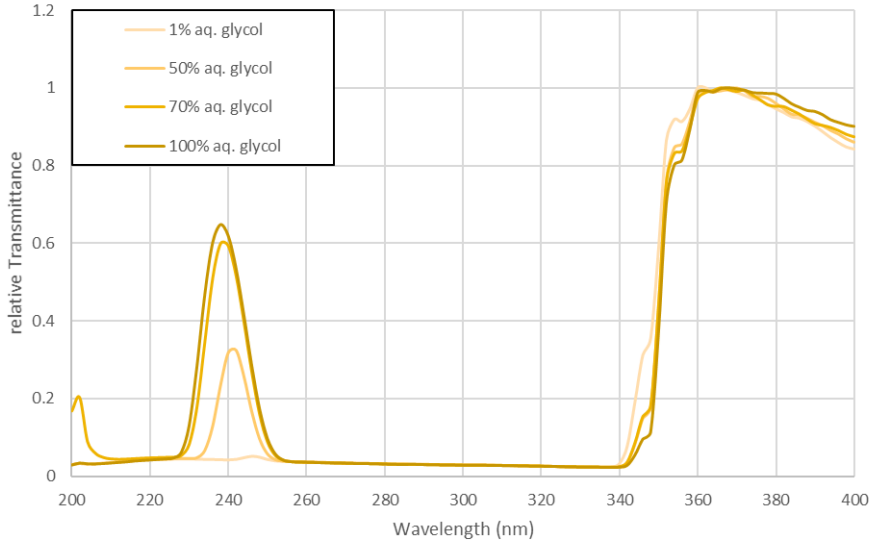

Figure 1.4.17 UV-Vis spectra of **S1** in various solvents at 60 mM.

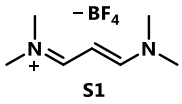

S1

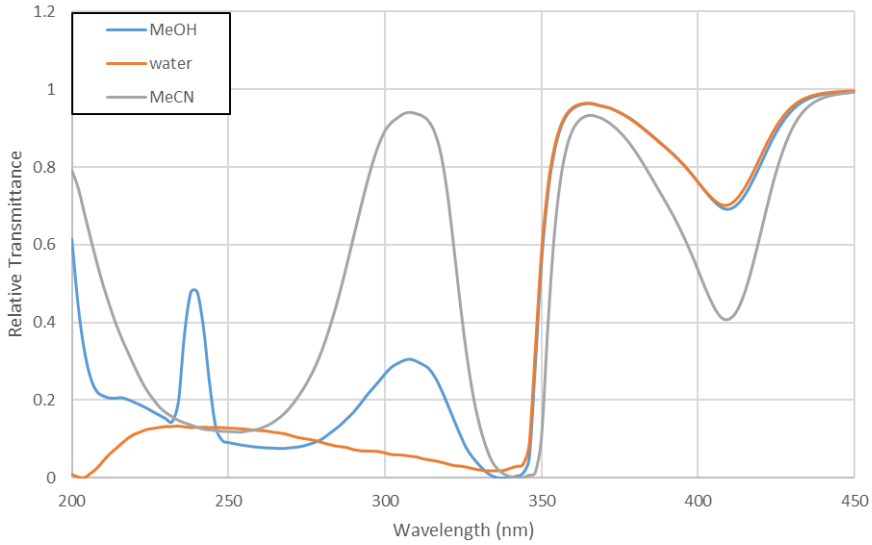

*Spectra in **Figure 1.5.17** were collected using a JASCO V-770 UV-Vis spectrophotometer*

Computational Methods

Using density functional theory (DFT), we optimized the geometries of each of the structures discussed in the main text, either as a closed-shell singlet or open-shell triplet in the gas phase (See **Table 1.4.1**).[24-27] Subsequent single-point energy calculations on each of the optimized structures were performed using (U)M06-2X/6-311+G(d,p) with the polarizable continuum model IEF-PCM for solvation by cyclohexane as either a closed shell singlet or open-shell triplet.[28] The energy of the pure open shell singlet **22** was determined using the sum method based on the total spin operator (S^2) derived from the single-point entry calculations shown in **Table 1.4.1**.[42-44] All optimized geometries were verified by frequency computations at the higher level of theory as minima (no imaginary frequencies) or transition structures (one imaginary frequency). Frequency analysis was performed at 298.15 K. Free energies were corrected using GoodVibes program[45] based on Truhlar's quasiharmonic approximation, which sets all the real vibrational frequencies that are lower than 100 cm^{-1} to correct entropies for the breakdown of the harmonic oscillator approximation.[46,47] TD-DFT was used to compute the lowest energy excited state for **13**, **19-trans**, and **21** using M06-2X/6-311+G(d,p) with the polarizable continuum model IEF-PCM for solvation by cyclohexane (see **Table 1.4.1**). TD-DFT was also used to compute the lowest 100 excitations for **19-trans** in order to obtain absorption spectra for the molecule based on the ground state geometry. All quantum chemical computations were performed using either Gaussian 09 or Gaussian 16.[48,49]

A conformational search for each of the structures was carried out with one of two methods: (1) *MacroModel* from *Schrödinger* using OPLS_2005 and an energy window of 10.0 kcal mol.[50,51] (2) Metadynamic sampling in extended tight binding Conformer–Rotamer Ensemble Sampling Tool (xtb CREST) program package (version 6.2).[52] Redundant conformer eliminations were

performed using an energy window of 10.0 kcal mol^{-1} and a maximum atom deviation cutoff of 0.5 Å. The lowest energy conformers were optimized with B3LYP/6-31G(d) to locate the global minimum for each structure.

Table 1.4.1 Relative electronic energy and total spin operator (S^2) for **22**.

		Relative Electronic Energies (kcal/mol)	**S^2**
triplet	open-shell	0.00	2.0714
singlet	open-shell	5.03	1.0308
singlet	closed-shell	35.22	

Table 1.4.2 Summary of DFT calculations and energies for each structure

	Optimization (U)B3LYP/6-31G(d)		Frequency (U)M06-2X/6-311+G(d,p) IEFPCM$_{cyclohexane}$								Single-point (U)M06-2X/6-311+G(d,p) IEFPCM$_{cyclohexane}$	
Structure	**R1/U3 ***	**Electronic Energy**	**R1/U3 ***	**Zero Point Energy Correction**	**Energy Correction**	**Enthalpy Correction**	**Quasiharmonic Free Energy Correction**	**Enthalpy**	**Quasiharmonic Free energy**	**Negative Frequency**	**Electronic Energy R1 ***	**Electronic Energy U3 ***
4	R1	-636.74927	R1	0.302079	0.314853	0.315798	0.255260	-636.320498	-636.381035	-	-636.6362955	-
5	R1	-636.80393	R1	0.302142	0.315355	0.316299	0.254697	-636.386034	-636.447636	-	-636.7023332	-
6-trans	R1	-636.7278	R1	0.298761	0.313041	0.313985	0.249973	-636.308043	-636.372055	-	-636.6220281	-636.495592
6-cis	R1	-636.72683	R1	0.298763	0.312955	0.313899	0.250203	-636.306354	-636.370051	-	-636.6202536	-
7	R1	-636.80288	R1	0.302376	0.315657	0.316602	0.254892	-636.386312	-636.448022	-	-636.7029138	-
8	R1	-713.24229	R1	0.328265	0.343763	0.344707	0.277438	-712.790526	-712.857795	-	-713.1352327	-
14	R1	-636.69294	R1	0.300608	0.313365	0.314309	0.253940	-636.272524	-636.332893	-	-636.5868331	-
14→15TS	R1	-636.68702	R1	0.299255	0.311736	0.31268	0.252850	-636.2659	-636.32573	-458.768	-636.5785803	-
15	R1	-636.71204	R1	0.30088	0.313798	0.314743	0.254044	-636.287735	-636.348434	-	-636.6024777	-
16	U3	-636.69486	U3	0.295761	0.310477	0.311421	0.189603	-636.264734	-636.330423	-	-636.5200259	-636.5761551
17	R1	-636.77865	R1	0.300338	0.313755	0.314699	0.252568	-636.359442	-636.421573	-	-636.6741409	-
17→5TS	R1	-636.72602	R1	0.296489	0.309572	0.310516	0.249243	-636.314032	-636.375305	-1438.813	-636.6245479	-
21	R1	-636.72429	R1	0.297517	0.312099	0.313043	0.248522	-636.295385	-636.359906	-	-636.6084279	-
21→22TS	R1	-636.69892	R1	0.296329	0.310229	0.311173	0.248206	-636.272666	-636.335633	-290.545	-636.5838392	-
22	R1	-636.76971	R1	0.300446	0.313861	0.314806	0.252802	-636.351838	-636.413842	-	-636.6666437	-
25	R1	-636.75649	R1	0.301126	0.314196	0.31514	0.270255	-636.335217	-636.396389	-	-636.6666437	-
26	U3	-636.68084	U3	0.298026	0.311279	0.312224	0.217876	-636.256282	-636.318578	-	-636.5364544	-636.5685054
27	R1	-636.74615	R1	0.301152	0.313888	0.314832	0.254360	-636.32676	-636.387232	-	-636.6415921	-
28	R1	-713.17022	R1	0.327703	0.343082	0.344026	0.277054	-712.732095	-712.799067	-	-713.0761213	-

* R1 indicates closed-shell singlet; U3 indicates open-shell triplet

Calculated XYZ Coordinate Geometries

13

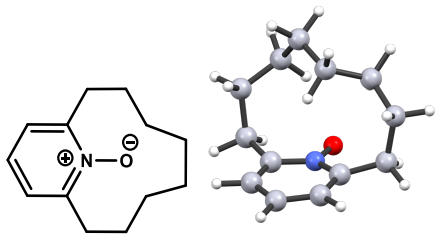

C	-2.31485	-1.05476	-0.66027
C	-1.72733	-0.25800	0.31414
N	-0.51033	-0.63151	0.85267
C	0.21295	-1.66119	0.28611
C	-0.37954	-2.45025	-0.69313
C	-1.66587	-2.18334	-1.15576
H	-2.13120	-2.81142	-1.90831
H	0.19997	-3.27340	-1.10051
C	1.65096	-1.79283	0.70056
H	1.95189	-2.83496	0.54065
H	1.74579	-1.57305	1.76694
C	2.61275	-0.88274	-0.11858
H	3.62224	-1.27580	0.05687
C	2.60999	0.64243	0.20140
H	3.64265	0.93805	0.42679
C	2.11193	1.57299	-0.92866
H	2.47206	2.59086	-0.71879
H	2.59982	1.27413	-1.86799
C	0.58838	1.63887	-1.15697
H	0.40042	2.10672	-2.13433
H	0.18994	0.62266	-1.24452
C	-0.17439	2.44586	-0.08240
H	0.20630	2.20195	0.91290
H	0.04446	3.50947	-0.25160
C	-1.71052	2.26128	-0.08367
H	-2.18039	3.16708	0.32146
H	-2.06912	2.16991	-1.11938
C	-2.27025	1.07208	0.74999
H	-2.03479	1.22277	1.80609
H	-3.36101	1.05773	0.64075
H	2.03372	0.82070	1.11276
H	2.41517	-1.04416	-1.18769
O	-0.01936	0.02555	1.84823
H	-3.28600	-0.75547	-1.04328

12

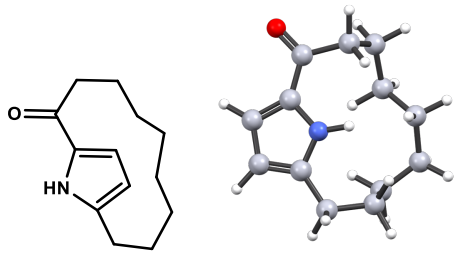

C	0.82504	-1.88690	0.18046
C	0.10508	-2.77232	-0.61990
C	-1.23509	-2.33120	-0.65888
C	-1.32645	-1.17476	0.11236
N	-0.06022	-0.95168	0.62900
H	0.19175	-0.16211	1.20059
H	0.52206	-3.63048	-1.13066
H	-2.05828	-2.76314	-1.21034
C	-2.41964	-0.21410	0.23737
O	-3.52517	-0.43883	-0.24619
C	2.28992	-1.78270	0.50474
H	2.51964	-2.30318	1.44634
H	2.85040	-2.30998	-0.27673
C	2.77969	-0.31964	0.61148
H	2.28254	0.15637	1.46895
H	3.84381	-0.32631	0.87690
C	2.56133	0.52406	-0.66722
H	1.74674	0.09179	-1.25966
H	3.45626	0.44815	-1.29786
C	2.26452	2.01678	-0.41042
H	2.35685	2.56003	-1.36103
H	3.04228	2.42782	0.24871
C	0.88077	2.33474	0.19645
H	0.86364	3.39427	0.48706
H	0.75983	1.78773	1.14368
C	-0.31104	2.06925	-0.74235
H	-0.24189	2.77607	-1.58076
H	-0.23398	1.07177	-1.18971
C	-1.70117	2.23237	-0.09432
H	-1.74689	3.20239	0.41969
H	-2.45973	2.26704	-0.88583
C	-2.14115	1.13623	0.91215
H	-3.08806	1.44706	1.36445
H	-1.41491	1.04615	1.73115

19-trans

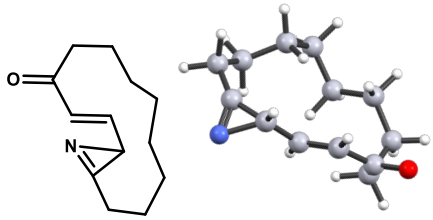

C	-2.41111	-1.30957	-0.11532
O	-3.39643	-1.62823	-0.77216
C	-1.08885	-1.86542	-0.47401
C	0.06961	-1.63953	0.17562
C	1.38872	-2.08208	-0.28402
C	2.59286	-1.32162	0.08052
N	2.49671	-2.35417	0.78765
C	3.41155	-0.08993	-0.07263
H	3.77723	-0.02752	-1.10638
H	4.28472	-0.18863	0.58310
C	2.61373	1.19115	0.27606
C	1.61325	1.63663	-0.80343
C	0.68215	2.76957	-0.32453
H	1.27236	3.48616	0.26360
C	-0.52765	2.28778	0.50297
H	-0.20106	1.51608	1.21435
H	-0.90319	3.11689	1.11803
C	-1.68488	1.76232	-0.36397
H	-1.30549	1.04196	-1.10087
H	-2.07983	2.60490	-0.94823
C	-2.84687	1.12604	0.42072
H	-3.14244	1.79420	1.24096
H	-3.71818	1.03085	-0.23761
C	-2.56169	-0.27830	1.00423
H	-3.42625	-0.58939	1.60114
H	-1.69691	-0.25294	1.67370
H	0.31138	3.32880	-1.19399
H	1.01095	0.78229	-1.13688
H	2.18043	1.96917	-1.68339
H	2.10230	1.03753	1.23513
H	3.33655	1.99930	0.44571
H	1.41307	-2.73663	-1.15530
H	0.07692	-1.05064	1.09072
H	-1.10303	-2.47963	-1.37326

19-cis

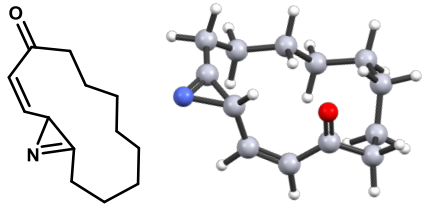

C	-1.07126	-1.91458	-0.20579
O	-0.69106	-1.90932	-1.37361
C	-0.13998	-1.98658	0.94458
C	1.17957	-1.69859	0.89243
C	1.97211	-1.31851	-0.28619
C	2.80688	-0.10589	-0.23482
N	3.50930	-1.12997	-0.06232
C	2.86065	1.38006	-0.29320
H	2.86098	1.67669	-1.35218
H	3.82053	1.70240	0.12857
C	1.67279	2.05331	0.42903
H	1.59050	1.63818	1.44270
H	1.90604	3.11843	0.55342
C	0.33416	1.89388	-0.30794
C	-0.87014	2.35537	0.52601
C	-2.23582	2.19544	-0.17191
H	-3.01743	2.58121	0.49816
C	-2.59492	0.76205	-0.60820
H	-1.82547	0.38711	-1.29185
C	-2.78683	-0.23665	0.55109
H	-2.10714	0.00270	1.37858
H	-3.80170	-0.14397	0.95836
C	-2.54332	-1.71117	0.13635
H	-2.83821	-2.37445	0.95961
H	-3.13954	-1.96484	-0.74599
H	-3.51863	0.79456	-1.20118
H	-2.25450	2.84106	-1.06119
H	-0.74031	3.41287	0.79697
H	-0.87133	1.80449	1.47699
H	0.20692	0.84384	-0.59056
H	0.37072	2.45989	-1.25072
H	1.66278	-1.70915	-1.24914
H	1.73741	-1.69445	1.83024
H	-0.58145	-2.20100	1.91561

17

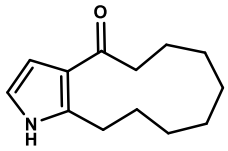

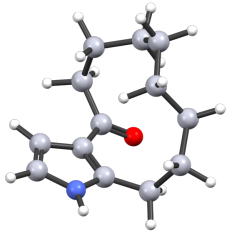

C	-2.58103	-1.27876	-1.31112
C	-1.78252	0.13755	0.26878
C	-0.99089	-1.01622	0.28253
H	-3.26242	-1.60608	-2.08274
H	-3.43703	0.63300	-0.93656
C	0.19764	-1.21316	1.13020
O	0.37489	-0.57984	2.17002
C	1.28497	-2.14962	0.61660
H	1.95032	-2.36999	1.45750
H	0.85279	-3.09481	0.26484
C	2.07942	-1.49108	-0.54146
H	1.39029	-1.31707	-1.37658
H	2.81303	-2.22106	-0.90502
C	2.79411	-0.16850	-0.15442
H	2.51362	0.11687	0.86575
H	3.87761	-0.33932	-0.12410
C	2.51573	1.00855	-1.11231
H	2.78349	0.70238	-2.13387
H	3.19126	1.83845	-0.85888
C	1.06414	1.52644	-1.11415
H	0.38030	0.68899	-1.28935
H	0.93177	2.20366	-1.97026
C	0.65954	2.27871	0.16830
H	0.99683	1.73098	1.05506
H	1.19575	3.23784	0.18220
C	-0.85371	2.55423	0.31141
H	-1.28874	2.77493	-0.67456
H	-0.99414	3.46126	0.91374
C	-1.67316	1.43638	1.01215
H	-2.68747	1.81968	1.19666
H	-1.22732	1.22656	1.98674
N	-2.72954	-0.04816	-0.70103
C	-1.50363	-1.89584	-0.73095
H	-1.13601	-2.88243	-0.97688

18

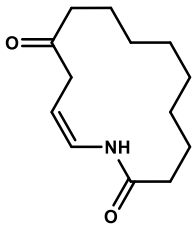

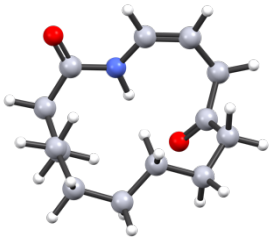

O	-1.92478	-2.65146	-0.97784
O	1.44263	0.22715	1.50593
N	-0.11967	-1.88533	0.19600
H	0.19512	-1.32724	0.98420
C	-1.48530	-2.03836	-0.01695
C	-2.37494	-1.34299	1.00702
H	-2.13576	-1.71158	2.01383
H	-3.39995	-1.64557	0.77550
C	-2.23650	0.19728	0.98048
H	-2.92854	0.61723	1.72296
H	-1.23037	0.47112	1.31768
C	-2.51624	0.81752	-0.39804
H	-1.90857	0.30736	-1.15617
H	-3.55887	0.61481	-0.67824
C	-2.26772	2.33736	-0.48428
H	-3.01013	2.86100	0.13460
H	-2.45811	2.65574	-1.51882
C	-0.86433	2.80807	-0.05402
H	-0.79602	3.89514	-0.20122
H	-0.74327	2.64518	1.02504
C	0.29904	2.11258	-0.77637
H	0.14601	1.03002	-0.72088
H	0.28190	2.36162	-1.84681
C	1.68275	2.44826	-0.17716
H	1.56809	2.70586	0.88175
H	2.11375	3.32769	-0.67064
C	2.66974	1.27757	-0.27101
H	2.77003	0.90897	-1.30112
H	3.68268	1.58739	0.03167
C	2.27785	0.10586	0.61884
C	2.90049	-1.26108	0.34229
H	3.94439	-1.14477	0.03128
H	2.88916	-1.82235	1.28554
C	2.13420	-1.98697	-0.75118
H	2.70775	-2.33012	-1.60638
C	0.81484	-2.24784	-0.76971
H	0.36220	-2.77923	-1.59989

20

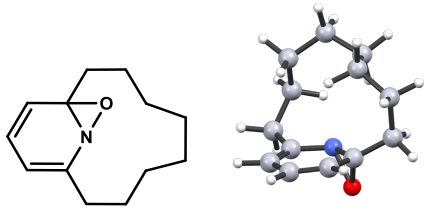

C	2.36418	0.08503	0.78778
C	2.17441	-1.09903	1.40505
C	1.13861	-2.00534	0.95254
C	0.33664	-1.68720	-0.09000
N	0.55245	-0.51771	-0.88424
C	1.63760	0.39003	-0.46438
O	1.90623	-0.50011	-1.53994
C	1.40254	1.83891	-0.84640
H	2.37321	2.31619	-1.03940
H	0.86000	1.82900	-1.79604
C	0.63804	2.65448	0.22259
H	0.38826	3.63068	-0.21488
H	1.31490	2.86686	1.06137
C	-0.63318	1.99501	0.79419
H	-0.34320	1.05839	1.28533
H	-1.02170	2.63891	1.59608
C	-1.75925	1.72638	-0.21846
H	-1.34065	1.26331	-1.11797
H	-2.18894	2.68686	-0.53686
C	-2.89298	0.83324	0.32896
H	-3.29006	1.28262	1.25085
C	-2.49591	-0.62923	0.62340
H	-3.31952	-1.11298	1.16459
H	-1.64824	-0.63667	1.31951
C	-2.14472	-1.46341	-0.63261
H	-1.92542	-0.79921	-1.47347
H	-3.00911	-2.06698	-0.93592
C	-0.93376	-2.41273	-0.46025
H	-0.78251	-2.94572	-1.41060
H	-1.14437	-3.17346	0.30162
H	-3.72354	0.83718	-0.39123
H	0.92931	-2.89838	1.53564
H	2.72771	-1.34892	2.30655
H	3.03363	0.84030	1.18954

20→21 TS

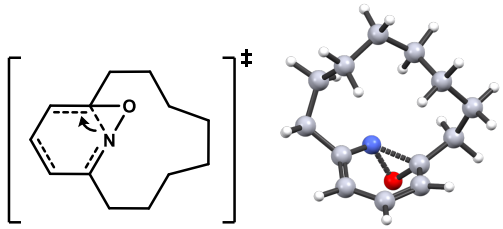

C	2.13234	0.42384	0.92185
C	2.24777	-0.86870	1.38194
C	1.52665	-1.94153	0.79967
C	0.61083	-1.71184	-0.20917
N	0.63136	-0.60063	-1.02182
C	1.61227	0.68163	-0.37892
O	2.00239	-0.20864	-1.36627
C	1.13582	2.03456	-0.85139
H	2.01800	2.64564	-1.09378
H	0.61385	1.86695	-1.79771
C	0.24194	2.80678	0.14410
H	-0.13470	3.69991	-0.37278
H	0.86204	3.18138	0.96998
C	-0.93396	2.01441	0.74644
H	-0.52381	1.17519	1.31959
H	-1.44109	2.65683	1.48020
C	-1.97215	1.49267	-0.26134
H	-1.46075	1.04710	-1.12129
H	-2.55101	2.34157	-0.65175
C	-2.94253	0.45442	0.34047
H	-3.38810	0.86902	1.25627
C	-2.29964	-0.90943	0.66749
H	-2.98937	-1.48833	1.29572
H	-1.40829	-0.74697	1.28578
C	-1.92049	-1.74351	-0.57798
H	-1.79448	-1.08854	-1.44521
H	-2.73786	-2.43110	-0.82883
C	-0.62518	-2.57103	-0.41948
H	-0.49004	-3.17646	-1.32702
H	-0.72031	-3.27034	0.41967
H	-3.77702	0.29617	-0.35732
H	1.50040	-2.89240	1.32524
H	2.74207	-1.05077	2.33356
H	2.35981	1.26501	1.57053

21

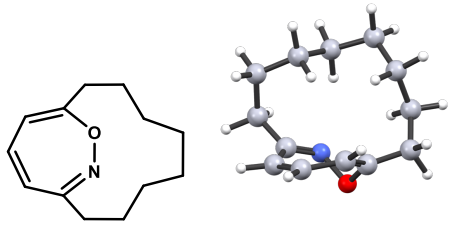

C	0.70562	-1.85801	-0.00181
C	0.05744	-2.00173	1.17814
C	-1.38435	-1.94910	1.27809
C	-2.18847	-1.25612	0.42874
C	-1.68568	-0.38733	-0.63210
N	-0.64182	-0.57545	-1.36885
O	-0.05052	-1.89968	-1.16246
C	-2.33061	0.97175	-0.84758
H	-1.96169	1.36532	-1.79854
H	-3.41614	0.84123	-0.95137
C	-2.04883	1.97945	0.29707
H	-2.36688	2.97235	-0.04898
H	-2.68993	1.73338	1.15392
C	-0.59099	2.02918	0.79364
H	-0.53420	2.75712	1.61574
C	0.47283	2.37868	-0.26111
H	0.32191	3.41582	-0.59368
H	0.33568	1.74781	-1.14513
C	1.92344	2.23071	0.24716
H	2.60759	2.61994	-0.52023
H	2.05930	2.87552	1.12766
C	2.35101	0.79629	0.62362
H	3.30295	0.84500	1.16947
H	1.62617	0.38714	1.33739
C	2.50612	-0.17898	-0.56374
H	1.85315	0.11092	-1.39294
H	3.53352	-0.13490	-0.94689
C	2.17956	-1.65490	-0.19913
H	2.51584	-2.30853	-1.01355
H	2.72140	-1.94520	0.70991
H	-0.35688	1.05692	1.24151
H	-3.25073	-1.18112	0.65034
H	-1.84301	-2.41396	2.14980
H	0.63624	-2.11848	2.09120

22

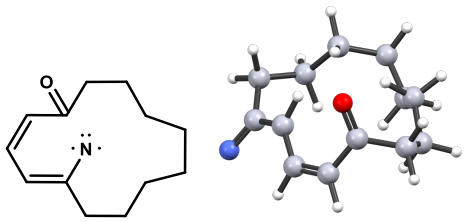

C	2.15748	-1.20770	0.54958
O	1.78160	-1.10416	1.71263
C	1.48834	-2.11261	-0.41845
C	0.11738	-2.25046	-0.52332
C	-0.82505	-1.55932	0.25810
C	-2.23149	-1.46126	-0.08792
N	-2.80320	-2.27841	-0.88842
C	-3.04023	-0.27373	0.45714
H	-4.08814	-0.44223	0.19377
C	-2.54957	1.08482	-0.11748
C	-1.54366	1.83928	0.77631
H	-0.86861	1.12932	1.26705
C	-0.70499	2.89880	0.03146
C	0.42758	2.31672	-0.83987
C	1.59210	1.72451	-0.02508
C	2.55025	0.83781	-0.84976
C	3.22959	-0.28633	-0.01840
H	3.79399	0.13704	0.81870
H	3.92131	-0.84420	-0.66268
H	1.99585	0.36619	-1.67203
H	3.33157	1.44718	-1.32034
H	1.18468	1.13253	0.80044
H	2.15800	2.53591	0.45273
H	0.01511	1.53510	-1.49370
H	0.80648	3.09814	-1.51244
H	-1.37131	3.50593	-0.59724
H	-0.26863	3.59034	0.76533
H	-2.09894	2.32210	1.59155
H	-2.12064	0.90903	-1.11167
H	-3.42151	1.73023	-0.28243
H	-2.97804	-0.27245	1.55346
H	-0.47384	-0.98450	1.10611
H	-0.26687	-2.84722	-1.34886
H	2.11272	-2.56940	-1.18372

23

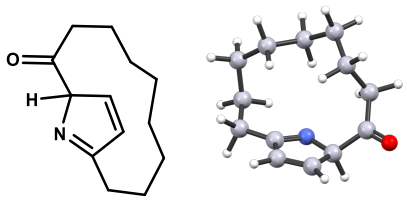

C	1.77435	-1.02259	-0.51757
N	0.35508	-0.99713	-0.85481
C	-0.24930	-1.75525	0.00574
C	0.67086	-2.32991	1.00844
C	1.90352	-1.88030	0.71280
H	2.83855	-2.06645	1.22607
H	0.38004	-2.97980	1.82662
C	-1.72417	-2.07035	-0.04344
H	-2.09442	-2.18845	0.98508
C	-2.61216	-1.08033	-0.82538
H	-2.02615	-0.65687	-1.64744
H	-3.43252	-1.64357	-1.28716
C	-3.24053	0.03375	0.03472
H	-3.85519	-0.44016	0.81391
H	-3.93948	0.60546	-0.59272
C	-2.25938	1.00912	0.70653
C	-1.56883	1.97905	-0.26552
C	-0.42373	2.78618	0.37413
C	0.84053	1.95678	0.66209
H	1.50702	2.50363	1.33922
H	0.55759	1.04061	1.19388
C	1.63959	1.59656	-0.61888
C	2.47496	0.35861	-0.38592
O	3.65312	0.38563	-0.09335
H	0.94987	1.40127	-1.44496
H	2.30841	2.41891	-0.89119
H	-0.77851	3.23100	1.31470
H	-0.15655	3.62817	-0.27942
H	-2.32236	2.67453	-0.66064
H	-1.18409	1.42257	-1.12819
H	-1.50848	0.43500	1.26482
H	-2.80410	1.59595	1.45984
H	-1.80979	-3.07188	-0.49197
H	2.30551	-1.50291	-1.35635

23→12 TS

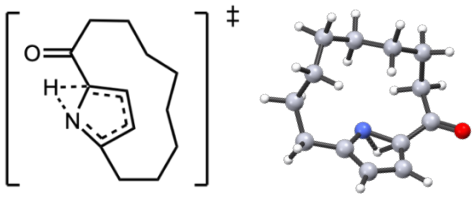

C	0.73467	-1.84857	0.15606
C	-0.01580	-2.70020	-0.68366
C	-1.34268	-2.29190	-0.64251
C	-1.39907	-1.16400	0.20916
N	-0.04366	-0.88176	0.69315
H	0.38434	-3.53182	-1.25297
H	-2.18677	-2.70551	-1.17777
C	-2.43743	-0.09502	0.23519
O	-3.52170	-0.29210	-0.29088
C	2.21461	-1.85740	0.44166
H	2.42213	-2.44250	1.34991
H	2.72363	-2.38029	-0.37880
C	2.78184	-0.43272	0.61219
H	2.26517	0.03268	1.45784
H	3.83848	-0.50407	0.89935
C	2.63646	0.45334	-0.64744
H	1.83069	0.06364	-1.28055
H	3.55054	0.37396	-1.25073
C	2.36271	1.94197	-0.35196
H	2.49608	2.51670	-1.27981
H	3.12895	2.31232	0.34432
C	0.96921	2.25504	0.23216
H	0.96163	3.30117	0.57112
H	0.80378	1.64058	1.12368
C	-0.19562	2.05543	-0.75215
H	-0.07080	2.75689	-1.58963
H	-0.15178	1.05208	-1.19223
C	-1.59253	2.28916	-0.14430
H	-1.60659	3.26905	0.35218
H	-2.33603	2.34220	-0.94963
C	-2.08900	1.23850	0.88534
H	-3.01521	1.61094	1.33573
H	-1.34552	1.10466	1.67691
H	-0.97772	-1.36541	1.41758

27

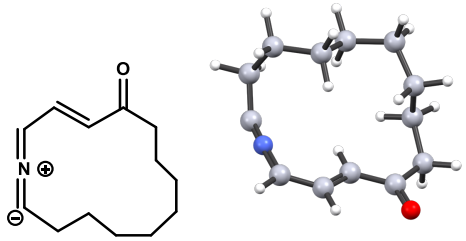

C	0.72314	-2.81678	-0.38922
N	1.63705	-2.11031	0.22905
C	2.32964	-1.44214	0.94817
C	3.18476	-0.22897	0.79466
C	3.08332	0.53127	-0.54716
C	1.70461	1.12447	-0.88283
H	1.76735	1.56216	-1.88905
H	0.96810	0.31537	-0.95549
C	1.20692	2.20383	0.09314
H	1.99603	2.95961	0.21899
H	1.05068	1.76753	1.08936
C	-0.07926	2.92270	-0.36457
H	-0.28398	3.75047	0.32940
H	0.11563	3.38797	-1.34116
C	-1.33765	2.04149	-0.48067
C	-1.89876	1.55209	0.86579
C	-2.96393	0.44792	0.73320
H	-3.32324	0.17343	1.73683
H	-3.83939	0.81123	0.18333
C	-2.53009	-0.85291	0.03994
O	-3.33975	-1.47875	-0.64124
C	-1.14400	-1.29773	0.22727
C	-0.63892	-2.38469	-0.41914
H	-1.31896	-2.96465	-1.03957
H	-0.49774	-0.70978	0.87072
H	-1.08410	1.19808	1.50962
H	-2.34115	2.40354	1.40097
H	-1.12232	1.18026	-1.12508
H	-2.12076	2.61055	-0.99992
H	3.38800	-0.14721	-1.35393
H	3.82983	1.33750	-0.51777
H	2.96176	0.43080	1.64188
H	4.21842	-0.55971	0.96477
H	1.05597	-3.70832	-0.90894

27→28 TS

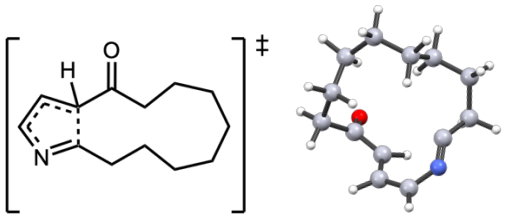

C	-2.03502	-2.15767	-1.13225
C	-2.12309	0.01128	-0.22026
C	-0.36943	-1.70582	0.57825
H	-2.48265	-2.71597	-1.94290
C	1.00861	-1.52540	1.03250
O	1.23548	-1.05943	2.15263
C	2.15104	-1.73369	0.04415
H	3.07537	-1.83880	0.62139
H	2.00766	-2.64871	-0.54529
C	2.24700	-0.52144	-0.91927
H	1.30716	-0.46269	-1.48015
H	3.03174	-0.72122	-1.66058
C	2.52743	0.82150	-0.20846
H	2.16997	0.77303	0.82548
H	3.61344	0.96637	-0.13508
C	1.91087	2.04806	-0.90929
H	2.23900	2.06649	-1.95866
H	2.32022	2.95903	-0.44926
C	0.37147	2.12881	-0.87939
H	-0.05875	1.21789	-1.31303
H	0.05510	2.95347	-1.53465
C	-0.23699	2.36216	0.51532
H	0.09553	1.58351	1.21339
H	0.15366	3.31001	0.91004
C	-1.78083	2.42711	0.52287
H	-2.14003	2.87968	-0.41067
H	-2.12146	3.08452	1.33215
C	-2.49782	1.07367	0.73644
H	-3.59034	1.20477	0.70984
H	-2.25466	0.69122	1.73763
N	-2.57478	-0.96987	-0.78875
C	-0.83310	-2.46935	-0.49246
H	-0.22896	-3.26535	-0.92392
H	-1.09332	-1.32795	1.29571

28

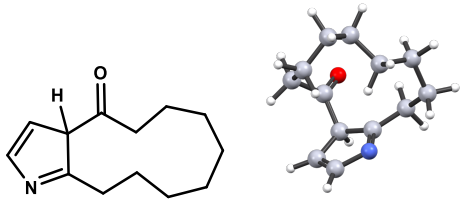

C	1.89050	-1.25092	-1.73499
C	0.72904	-1.36099	0.11357
C	1.92193	-0.43468	0.40601
H	2.08855	-1.51256	-2.76844
C	1.48590	0.92387	1.01200
O	1.24003	0.98433	2.20205
C	1.31820	2.12409	0.09476
H	1.24563	3.01157	0.73208
H	2.20509	2.22269	-0.54233
C	0.06172	1.99422	-0.79994
H	0.13324	1.06252	-1.37023
H	0.08548	2.80175	-1.54263
C	-1.26215	2.05254	-0.01571
H	-1.14211	1.55048	0.95263
H	-1.48494	3.10030	0.22615
C	-2.45406	1.43017	-0.76656
H	-2.51522	1.86947	-1.77260
H	-3.38507	1.71277	-0.25540
C	-2.38669	-0.10473	-0.88372
H	-1.43170	-0.39922	-1.32872
H	-3.15117	-0.43900	-1.59694
C	-2.59025	-0.85219	0.45833
H	-2.42784	-0.16705	1.30184
H	-3.64133	-1.15934	0.53474
C	-1.70022	-2.09362	0.67180
H	-1.65155	-2.69353	-0.24456
H	-2.16818	-2.72589	1.43688
C	-0.26547	-1.79027	1.15771
H	0.14587	-2.70301	1.61717
H	-0.28308	-1.04652	1.96331
N	0.74811	-1.80549	-1.10122
C	2.61173	-0.45203	-0.92606
H	3.52890	0.07202	-1.16423
H	2.53118	-0.90649	1.19033

30

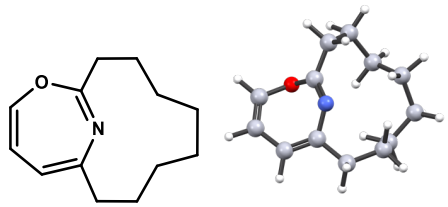

C	2.46091	1.30052	-0.26863
C	3.27674	0.11231	-0.44375
C	2.76996	-1.12073	-0.58310
C	0.73074	-0.99703	0.51093
C	1.24021	1.30529	0.32398
H	2.88217	2.25295	-0.58485
H	4.35982	0.21519	-0.46401
H	3.36917	-2.02433	-0.65828
N	0.66458	0.19193	0.94824
C	0.42163	2.57568	0.49579
H	0.71024	3.28743	-0.28755
H	0.68784	3.04351	1.45564
C	-0.06710	-2.12147	1.10683
H	-0.51838	-1.75015	2.02961
H	0.59389	-2.95732	1.36749
O	1.39774	-1.35943	-0.67137
C	-1.15399	-2.63254	0.11781
H	-0.67831	-3.30746	-0.60282
H	-1.86807	-3.23757	0.69195
C	-1.88960	-1.53242	-0.67078
H	-1.15343	-1.02727	-1.30749
H	-2.59154	-2.01536	-1.36425
C	-2.65138	-0.49106	0.17237
H	-2.09590	-0.27284	1.09125
H	-3.61025	-0.92004	0.49420
C	-2.91238	0.83282	-0.57781
H	-3.65530	1.42092	-0.02032
H	-3.37256	0.60741	-1.55055
C	-1.65522	1.70030	-0.80186
C	-1.10177	2.34030	0.48933
H	-1.33704	1.70382	1.34790
H	-1.60443	3.29915	0.67169
H	-1.88969	2.49031	-1.52791
H	-0.87472	1.09166	-1.27512

31

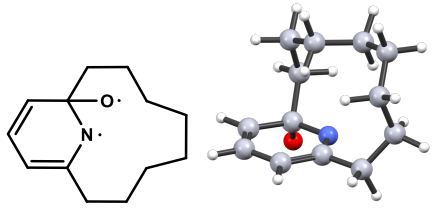

C	-0.10934	-1.54270	-0.09096
C	-0.77765	-1.93032	1.12111
C	-1.95996	-1.26976	1.50634
C	-2.46710	-0.27301	0.71668
C	-1.79246	0.08758	-0.58529
N	-0.55049	-0.60666	-0.88434
H	-2.46784	-1.55599	2.42444
H	-0.36882	-2.73314	1.72640
H	-3.38822	0.24882	0.95733
C	1.18307	-2.24237	-0.49529
H	1.49249	-2.92939	0.30271
H	0.97516	-2.85942	-1.37961
C	-1.52045	1.66895	-0.67252
H	-2.50154	2.13902	-0.79464
H	-0.96501	1.80654	-1.60313
C	2.32363	-1.25972	-0.82207
H	1.96871	-0.59823	-1.61843
H	3.16271	-1.82646	-1.24399
C	-0.80421	2.31962	0.52502
H	-1.45972	2.26816	1.40399
H	-0.72308	3.38736	0.27127
C	2.80533	-0.43351	0.39904
H	2.12143	-0.59131	1.24309
H	3.77554	-0.81718	0.74007
O	-2.69452	-0.07860	-1.60892
C	0.58286	1.78382	0.91726
H	0.46740	0.76546	1.29940
H	0.94632	2.38054	1.76651
C	2.94487	1.08085	0.14533
H	3.39166	1.54566	1.03633
H	3.66246	1.24028	-0.67203
C	1.63291	1.80907	-0.20363
H	1.86424	2.85367	-0.45720
H	1.20667	1.35995	-1.10686

32

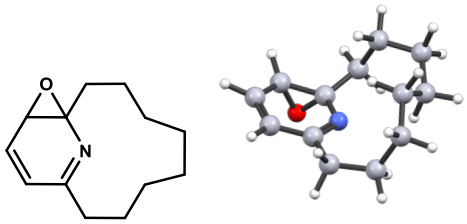

C	-2.68118	0.40174	0.31326
C	-2.77066	-0.92542	0.92766
C	-1.82891	-1.85556	0.65683
C	-0.61525	-1.48099	-0.06845
N	-0.38828	-0.28544	-0.49832
C	-1.38127	0.71112	-0.41951
C	-0.83982	2.12646	-0.49851
H	-0.38770	2.26243	-1.48981
H	-1.69417	2.81058	-0.45081
C	0.18579	2.46524	0.61776
H	-0.05480	3.46068	1.01233
H	0.04402	1.77606	1.46004
C	1.67426	2.49244	0.20687
H	2.24948	2.86463	1.06764
H	1.79544	3.24850	-0.58256
C	2.30181	1.17472	-0.28428
H	1.73632	0.81306	-1.14672
H	3.31926	1.39333	-0.64121
C	2.38040	0.06391	0.77542
H	1.42257	-0.02482	1.29732
C	2.78857	-1.31575	0.22181
H	3.75975	-1.21204	-0.28424
C	1.82966	-2.02101	-0.76312
H	2.36022	-2.90163	-1.14866
H	1.62994	-1.37920	-1.62729
C	0.48794	-2.51600	-0.19306
H	0.64199	-2.98039	0.79335
H	0.09856	-3.32643	-0.82859
H	2.96765	-1.99303	1.07040
H	3.11667	0.35425	1.53990
O	-2.59494	0.45807	-1.12351
H	-1.87984	-2.84680	1.10007
H	-3.57439	-1.12632	1.63228
H	-3.26151	1.21534	0.74683

33

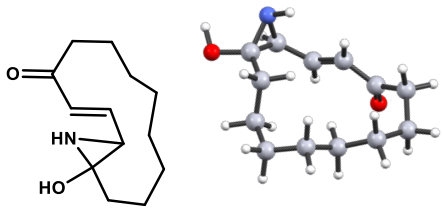

C	-1.82699	0.89695	-0.51522
C	-2.69442	-0.32127	-0.26891
N	-2.67098	-1.47508	-1.14162
H	-1.93617	-1.41556	-1.84746
C	-2.11322	-1.64498	0.22523
C	-0.68731	-1.82308	0.53193
C	0.37149	-1.73137	-0.29420
C	1.75548	-1.75950	0.25280
O	1.98400	-2.05119	1.42002
C	2.90267	-1.35439	-0.67113
H	3.63990	-2.16517	-0.61873
H	2.56688	-1.28154	-1.71326
C	3.60292	-0.03766	-0.24822
C	2.84022	1.25575	-0.59491
C	1.63594	1.57522	0.30730
H	1.99281	1.87357	1.30348
H	1.04886	0.66641	0.46331
C	0.71790	2.66352	-0.26938
H	0.46259	2.39531	-1.30483
H	1.26886	3.61184	-0.34046
C	-0.58037	2.90801	0.52580
H	-1.16768	3.67355	-0.00065
H	-0.32987	3.33931	1.50479
C	-1.46637	1.66860	0.76446
H	-2.39031	1.98076	1.26521
H	-0.96215	0.98159	1.45599
H	2.50297	1.19229	-1.64105
H	3.54345	2.09942	-0.56224
H	4.57761	-0.01048	-0.75113
H	3.80860	-0.08745	0.82850
H	0.25632	-1.55103	-1.36136
H	-0.46166	-2.01435	1.58123
H	-2.77891	-2.21158	0.87516
O	-3.96368	0.05136	0.17066
H	-4.56867	-0.65592	-0.10962
H	-0.91364	0.57949	-1.02452
H	-2.37316	1.54889	-1.20974

TD-DFT Calculations

The lowest excited state for each of the structures in below in **Table 1.4.3** were calculated using TD-M06-2X/6-311+G(d,p) with the IEFPCM solvation model with cyclohexane and are discussed in the main text.

Table 1.4.3 Lowest excited state for **13**, **19-trans**, and **21**.

Structure	Excitation (*n*)	Energy (eV)	Energy (nm)	Oscillator Strength (*f*)
13	1	4.5096	274.94	0.0025
19-trans	1	3.6393	340.68	0.0002
21	1	3.8699	320.38	0.0378

In previous work, we had successfully used B3LYP with 6-31+G(d,p) to simulate absorption spectra of conjugated aromatic rings; however, we found, as described in the main text, this method was unsuccessful in predicting accurate absorption of **19-trans**. Therefore, we performed a benchmark of other DFT methods (CAM-B3LYP, M06-2X, and ωB97XD with a larger basis set 6-311+G(d,p)) for **19-trans** and compare to the spectrum calculated at the B3LYP/6-31+G(d,p) level of theory (Figure S9). The 100 lowest excited states were calculated using each method and basis set with the IEFPCM solvation model with cyclohexane. The calculated spectrum shown in Figure 1 of the main text, which was used to guide experiments initially, was plotted with a peak half-width at half height of 0.33 eV. However, computed spectra below were plotted with peak half-width at half height of 0.1 eV to provide more insight to the simulated band shapes.

We find that although all methods are able to predict the general band shape (peaks), the excited state energies deviate between methods. Compared to experimental results, B3LYP energies are significantly red-shifted, while CAM-B3LYP and ωB97XD energies match well for the higher peak (~240 nm) but are slightly overestimated for the lowest energy peak. On the other

hand, M06-2X predicts the lowest energy peak fairly accurately, but the second peak at 248 nm is slightly red-shifted. Across all the methods, oscillator strengths, which are known to be unreliable for TD-DFT, agree only moderately with experiment.

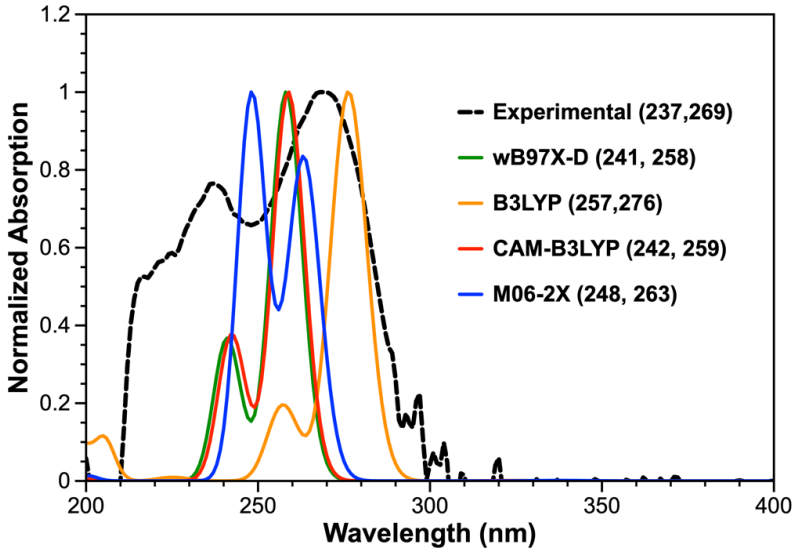

Figure 1.4.18 Experimental absorption spectrum (black dashed line) plotted against computed absorption spectra of **19-trans** calculated using B3LYP/6-31+G(d,p), CAM-B3LYP/6-311+G(d,p), M06-2X/6-311+G(d,p) and ωB97X-D/6-311+G(d,p) in cyclohexane (IEFPCM solvation model). The excitation energies of absorption peaks in nm are indicated in parentheses. Computed spectra were plotted with peak half-width at half height of 0.1 eV (or 806.6 cm^{-1}).

The lowest 100 excited states calculated using each method can be found below (energy in eV, energy in nm, oscillator strength):

B3LYP/6-31+G(d,p)

3.5866 eV 345.69 nm 0.0002
4.4873 eV 276.30 nm 0.3301
4.8197 eV 257.25 nm 0.0645
5.4524 eV 227.39 nm 0.0021
5.5705 eV 222.57 nm 0.0018
6.0339 eV 205.48 nm 0.0317
6.0744 eV 204.11 nm 0.0046
6.2132 eV 199.55 nm 0.0085
6.2305 eV 199.00 nm 0.0102
6.2571 eV 198.15 nm 0.0031
6.2689 eV 197.78 nm 0.0049
6.3313 eV 195.83 nm 0.0061
6.4527 eV 192.14 nm 0.0065
6.4820 eV 191.27 nm 0.0334
6.5123 eV 190.39 nm 0.0064
6.6052 eV 187.71 nm 0.0148
6.6377 eV 186.79 nm 0.0169
6.6515 eV 186.40 nm 0.0110
6.6686 eV 185.92 nm 0.0082
6.7064 eV 184.87 nm 0.0213
6.7590 eV 183.43 nm 0.0185
6.8436 eV 181.17 nm 0.0195
6.8920 eV 179.90 nm 0.0426
6.9791 eV 177.65 nm 0.0223
7.0262 eV 176.46 nm 0.0125
7.0388 eV 176.14 nm 0.0146
7.0415 eV 176.08 nm 0.0069
7.0807 eV 175.10 nm 0.0071
7.1057 eV 174.49 nm 0.0029
7.2072 eV 172.03 nm 0.0082
7.2388 eV 171.28 nm 0.0022
7.3124 eV 169.55 nm 0.0033
7.3183 eV 169.42 nm 0.0100
7.3305 eV 169.14 nm 0.0009
7.3644 eV 168.36 nm 0.0063
7.3775 eV 168.06 nm 0.0027
7.3897 eV 167.78 nm 0.0056
7.4119 eV 167.28 nm 0.0066
7.4512 eV 166.39 nm 0.0001
7.4870 eV 165.60 nm 0.0004
7.5108 eV 165.07 nm 0.0349
7.6657 eV 161.74 nm 0.0134
7.7418 eV 160.15 nm 0.0169
7.7609 eV 159.75 nm 0.0016
7.7969 eV 159.02 nm 0.0000
7.8105 eV 158.74 nm 0.0078
7.8276 eV 158.39 nm 0.0343
7.8468 eV 158.01 nm 0.0203
7.8730 eV 157.48 nm 0.0082
7.8944 eV 157.05 nm 0.0081
7.9030 eV 156.88 nm 0.0089
7.9353 eV 156.24 nm 0.0095
7.9595 eV 155.77 nm 0.0124
7.9729 eV 155.51 nm 0.0060
7.9992 eV 155.00 nm 0.0173
8.0163 eV 154.67 nm 0.0097
8.0354 eV 154.30 nm 0.0167
8.0669 eV 153.69 nm 0.0025
8.0869 eV 153.31 nm 0.0149
8.0920 eV 153.22 nm 0.0002
8.1031 eV 153.01 nm 0.0169
8.1078 eV 152.92 nm 0.0182
8.1215 eV 152.66 nm 0.0283
8.1361 eV 152.39 nm 0.0203
8.1402 eV 152.31 nm 0.0134
8.1711 eV 151.74 nm 0.0265
8.1903 eV 151.38 nm 0.0014
8.2184 eV 150.86 nm 0.0017
8.2398 eV 150.47 nm 0.0146
8.2556 eV 150.18 nm 0.0312
8.2604 eV 150.09 nm 0.0061
8.2747 eV 149.84 nm 0.0156
8.2922 eV 149.52 nm 0.0123
8.3151 eV 149.11 nm 0.0106
8.3536 eV 148.42 nm 0.0009
8.3604 eV 148.30 nm 0.0041
8.3747 eV 148.05 nm 0.0204
8.3908 eV 147.76 nm 0.0230
8.3995 eV 147.61 nm 0.0151
8.4346 eV 146.99 nm 0.0019
8.4805 eV 146.20 nm 0.0059
8.4854 eV 146.11 nm 0.0176
8.4885 eV 146.06 nm 0.0092
8.5162 eV 145.59 nm 0.0255
8.5450 eV 145.10 nm 0.0069
8.5565 eV 144.90 nm 0.0275
8.5661 eV 144.74 nm 0.0065
8.5743 eV 144.60 nm 0.0304
8.5948 eV 144.26 nm 0.0147
8.6046 eV 144.09 nm 0.0131
8.6124 eV 143.96 nm 0.0025
8.6362 eV 143.56 nm 0.0220
8.6519 eV 143.30 nm 0.0054
8.6608 eV 143.16 nm 0.0258
8.7128 eV 142.30 nm 0.0022
8.7189 eV 142.20 nm 0.0028
8.7435 eV 141.80 nm 0.0020
8.7567 eV 141.59 nm 0.0223
8.7642 eV 141.47 nm 0.0022
8.7851 eV 141.13 nm 0.0114

CAM-B3LYP/6-311+G(d,p)

3.8282 eV 323.87 nm 0.0003
4.7908 eV 258.80 nm 0.3105
5.1157 eV 242.36 nm 0.1170
6.2625 eV 197.98 nm 0.0041
6.7152 eV 184.63 nm 0.0316
6.7992 eV 182.35 nm 0.0150
6.9153 eV 179.29 nm 0.0112
7.0023 eV 177.06 nm 0.0239
7.0624 eV 175.55 nm 0.0167
7.1010 eV 174.60 nm 0.0293
7.2031 eV 172.13 nm 0.0777
7.2469 eV 171.09 nm 0.0215
7.2868 eV 170.15 nm 0.0131
7.3283 eV 169.19 nm 0.0382
7.3776 eV 168.05 nm 0.0053
7.4293 eV 166.89 nm 0.0018
7.4556 eV 166.30 nm 0.0136
7.5134 eV 165.02 nm 0.0246
7.5257 eV 164.75 nm 0.0381
7.6501 eV 162.07 nm 0.0121
7.7324 eV 160.34 nm 0.0066
7.7456 eV 160.07 nm 0.0107
7.8443 eV 158.06 nm 0.0146
7.9091 eV 156.76 nm 0.0004
7.9584 eV 155.79 nm 0.0023
7.9849 eV 155.27 nm 0.0051
8.0403 eV 154.20 nm 0.0079
8.0825 eV 153.40 nm 0.0112
8.1303 eV 152.50 nm 0.0074
8.1453 eV 152.22 nm 0.0072
8.1532 eV 152.07 nm 0.0325
8.1866 eV 151.45 nm 0.0006
8.2318 eV 150.62 nm 0.0095
8.3082 eV 149.23 nm 0.0039
8.3699 eV 148.13 nm 0.0074
8.3982 eV 147.63 nm 0.0091
8.4181 eV 147.28 nm 0.0369
8.4361 eV 146.97 nm 0.0021
8.4704 eV 146.37 nm 0.0182
8.4933 eV 145.98 nm 0.0196
8.5489 eV 145.03 nm 0.0050
8.5715 eV 144.65 nm 0.0914
8.6071 eV 144.05 nm 0.0061
8.6268 eV 143.72 nm 0.0026
8.6354 eV 143.58 nm 0.0046
8.6576 eV 143.21 nm 0.0242
8.6814 eV 142.82 nm 0.0249
8.6884 eV 142.70 nm 0.0186
8.7160 eV 142.25 nm 0.0490
8.7532 eV 141.64 nm 0.0514
8.7620 eV 141.50 nm 0.0213
8.7812 eV 141.19 nm 0.0071
8.8419 eV 140.22 nm 0.0192
8.8633 eV 139.88 nm 0.0152
8.8889 eV 139.48 nm 0.0152
8.9012 eV 139.29 nm 0.0017
8.9375 eV 138.72 nm 0.0143
8.9379 eV 138.72 nm 0.0098
8.9528 eV 138.49 nm 0.0276
8.9762 eV 138.12 nm 0.0568
8.9972 eV 137.80 nm 0.0066
9.0101 eV 137.61 nm 0.0030
9.0423 eV 137.12 nm 0.0016
9.0514 eV 136.98 nm 0.0230
9.0721 eV 136.66 nm 0.0109
9.0823 eV 136.51 nm 0.0219
9.1162 eV 136.00 nm 0.0041
9.1449 eV 135.58 nm 0.0163
9.1570 eV 135.40 nm 0.0056
9.1754 eV 135.13 nm 0.0112
9.1927 eV 134.87 nm 0.0488
9.2078 eV 134.65 nm 0.0182
9.2189 eV 134.49 nm 0.0140
9.2578 eV 133.92 nm 0.0138
9.2885 eV 133.48 nm 0.0205
9.3076 eV 133.21 nm 0.0144
9.3149 eV 133.10 nm 0.0112
9.3325 eV 132.85 nm 0.0094
9.3566 eV 132.51 nm 0.0314
9.3779 eV 132.21 nm 0.0130
9.3895 eV 132.05 nm 0.0246
9.4110 eV 131.74 nm 0.0092
9.4411 eV 131.32 nm 0.0283
9.4525 eV 131.17 nm 0.0305
9.4739 eV 130.87 nm 0.0136
9.4919 eV 130.62 nm 0.0153
9.5136 eV 130.32 nm 0.0119
9.5321 eV 130.07 nm 0.0103
9.5410 eV 129.95 nm 0.0068
9.5863 eV 129.34 nm 0.0767
9.5911 eV 129.27 nm 0.0562
9.6145 eV 128.96 nm 0.0081
9.6237 eV 128.83 nm 0.0178
9.6308 eV 128.74 nm 0.0121
9.6457 eV 128.54 nm 0.0226
9.6643 eV 128.29 nm 0.0112
9.6767 eV 128.13 nm 0.1882
9.6863 eV 128.00 nm 0.0051
9.7088 eV 127.70 nm 0.0542
9.7188 eV 127.57 nm 0.0511

M06-2X/6-311+G(d,p)

3.6655 eV 338.24 nm 0.0003
4.7097 eV 263.25 nm 0.1886
4.9959 eV 248.17 nm 0.2263
6.1850 eV 200.46 nm 0.0031
6.5782 eV 188.48 nm 0.0056
6.7353 eV 184.08 nm 0.0372
6.7785 eV 182.91 nm 0.0179
6.9621 eV 178.08 nm 0.0060
7.0076 eV 176.93 nm 0.0077
7.0686 eV 175.40 nm 0.0119
7.1156 eV 174.24 nm 0.0578
7.1697 eV 172.93 nm 0.0123
7.1885 eV 172.48 nm 0.0111
7.2463 eV 171.10 nm 0.0635
7.3178 eV 169.43 nm 0.0126
7.3800 eV 168.00 nm 0.0011
7.4282 eV 166.91 nm 0.0278
7.4554 eV 166.30 nm 0.0133
7.4991 eV 165.33 nm 0.0286
7.5342 eV 164.56 nm 0.0106
7.5513 eV 164.19 nm 0.0125
7.6366 eV 162.36 nm 0.0239
7.6437 eV 162.20 nm 0.0008
7.7352 eV 160.29 nm 0.0092
7.7659 eV 159.65 nm 0.0095
7.8222 eV 158.50 nm 0.0025
7.8464 eV 158.01 nm 0.0028
7.8913 eV 157.12 nm 0.0260
7.9720 eV 155.52 nm 0.0038
8.0532 eV 153.96 nm 0.0024
8.0908 eV 153.24 nm 0.0207
8.1097 eV 152.88 nm 0.0081
8.1281 eV 152.54 nm 0.0022
8.2231 eV 150.77 nm 0.0022
8.2569 eV 150.16 nm 0.0072
8.2845 eV 149.66 nm 0.0080
8.3105 eV 149.19 nm 0.0069
8.3255 eV 148.92 nm 0.0113
8.3455 eV 148.56 nm 0.0056
8.3636 eV 148.24 nm 0.0093
8.3982 eV 147.63 nm 0.0124
8.4178 eV 147.29 nm 0.0110
8.4253 eV 147.16 nm 0.0080
8.4414 eV 146.88 nm 0.0107
8.4694 eV 146.39 nm 0.0090
8.5266 eV 145.41 nm 0.0101
8.5296 eV 145.36 nm 0.0366
8.5521 eV 144.98 nm 0.0170
8.5650 eV 144.76 nm 0.0085
8.5809 eV 144.49 nm 0.0010
8.5863 eV 144.40 nm 0.0033
8.5956 eV 144.24 nm 0.0217
8.6296 eV 143.67 nm 0.0706
8.6619 eV 143.14 nm 0.0942
8.7044 eV 142.44 nm 0.0168
8.7243 eV 142.11 nm 0.0176
8.7680 eV 141.40 nm 0.0186
8.7839 eV 141.15 nm 0.0086
8.8153 eV 140.65 nm 0.0151
8.8402 eV 140.25 nm 0.0058
8.8739 eV 139.72 nm 0.0093
8.8771 eV 139.67 nm 0.0081
8.9003 eV 139.30 nm 0.0032
8.9122 eV 139.12 nm 0.0245
8.9343 eV 138.77 nm 0.0045
8.9477 eV 138.56 nm 0.0328
8.9536 eV 138.47 nm 0.0088
8.9706 eV 138.21 nm 0.0077
8.9750 eV 138.14 nm 0.0206
8.9867 eV 137.96 nm 0.0194
9.0191 eV 137.47 nm 0.0297
9.0423 eV 137.12 nm 0.0092
9.0690 eV 136.71 nm 0.0131
9.0694 eV 136.71 nm 0.0186
9.0936 eV 136.34 nm 0.0110
9.1324 eV 135.76 nm 0.0140
9.1399 eV 135.65 nm 0.0151
9.1749 eV 135.13 nm 0.0061
9.1909 eV 134.90 nm 0.0103
9.2184 eV 134.50 nm 0.0024
9.2213 eV 134.45 nm 0.0142
9.2422 eV 134.15 nm 0.0108
9.2486 eV 134.06 nm 0.0101
9.2633 eV 133.84 nm 0.0042
9.2813 eV 133.59 nm 0.0304
9.3056 eV 133.24 nm 0.0108
9.3135 eV 133.12 nm 0.0200
9.3225 eV 132.99 nm 0.0193
9.3374 eV 132.78 nm 0.0339
9.3592 eV 132.47 nm 0.0439
9.3720 eV 132.29 nm 0.0085
9.4025 eV 131.86 nm 0.0238
9.4091 eV 131.77 nm 0.0043
9.4281 eV 131.51 nm 0.0246
9.4374 eV 131.37 nm 0.0289
9.4517 eV 131.18 nm 0.0493
9.4719 eV 130.90 nm 0.0169
9.4748 eV 130.86 nm 0.0118
9.4919 eV 130.62 nm 0.0033
9.5179 eV 130.26 nm 0.0485

ωB97XD/6-311+G(d,p)

3.8077 eV 325.61 nm 0.0003
4.8022 eV 258.18 nm 0.3170
5.1442 eV 241.02 nm 0.1163
6.2590 eV 198.09 nm 0.0042
6.7233 eV 184.41 nm 0.0342
6.9832 eV 177.55 nm 0.0062
7.0304 eV 176.35 nm 0.0400
7.0993 eV 174.64 nm 0.0086
7.1787 eV 172.71 nm 0.0449
7.2438 eV 171.16 nm 0.0230
7.2738 eV 170.45 nm 0.0743
7.3164 eV 169.46 nm 0.0220
7.3933 eV 167.70 nm 0.0051
7.4135 eV 167.24 nm 0.0074
7.4512 eV 166.40 nm 0.0197
7.5452 eV 164.32 nm 0.0441
7.5592 eV 164.02 nm 0.0244
7.7011 eV 160.99 nm 0.0193
7.7185 eV 160.63 nm 0.0059
7.7583 eV 159.81 nm 0.0044
7.9235 eV 156.48 nm 0.0184
7.9935 eV 155.11 nm 0.0163
8.0387 eV 154.23 nm 0.0045
8.1519 eV 152.09 nm 0.0162
8.1914 eV 151.36 nm 0.0132
8.1947 eV 151.30 nm 0.0066
8.2261 eV 150.72 nm 0.0121
8.3589 eV 148.33 nm 0.0054
8.3829 eV 147.90 nm 0.0012
8.4206 eV 147.24 nm 0.0155
8.4315 eV 147.05 nm 0.0183
8.4587 eV 146.58 nm 0.0030
8.4796 eV 146.21 nm 0.0077
8.5369 eV 145.23 nm 0.0204
8.5694 eV 144.68 nm 0.0529
8.5771 eV 144.55 nm 0.0400
8.6301 eV 143.66 nm 0.0091
8.6632 eV 143.12 nm 0.0201
8.6786 eV 142.86 nm 0.0159
8.7141 eV 142.28 nm 0.0674
8.7175 eV 142.22 nm 0.0023
8.7803 eV 141.21 nm 0.0012
8.7904 eV 141.04 nm 0.0454
8.8335 eV 140.36 nm 0.0254
8.8641 eV 139.87 nm 0.0043
8.9043 eV 139.24 nm 0.0193
8.9270 eV 138.89 nm 0.0225
8.9403 eV 138.68 nm 0.0528
8.9638 eV 138.32 nm 0.0257
8.9895 eV 137.92 nm 0.0177
8.9932 eV 137.86 nm 0.0016
9.0621 eV 136.82 nm 0.0153
9.0898 eV 136.40 nm 0.0194
9.1086 eV 136.12 nm 0.0074
9.1280 eV 135.83 nm 0.0042
9.1512 eV 135.48 nm 0.0008
9.1782 eV 135.09 nm 0.0552
9.1918 eV 134.89 nm 0.0680
9.2171 eV 134.52 nm 0.0140
9.2456 eV 134.10 nm 0.0393
9.2766 eV 133.65 nm 0.0020
9.2946 eV 133.39 nm 0.0160
9.3023 eV 133.28 nm 0.0039
9.3263 eV 132.94 nm 0.0020
9.3641 eV 132.40 nm 0.0016
9.3699 eV 132.32 nm 0.0204
9.3890 eV 132.05 nm 0.0314
9.3940 eV 131.98 nm 0.0109
9.4022 eV 131.87 nm 0.0135
9.4355 eV 131.40 nm 0.0275
9.4466 eV 131.25 nm 0.0016
9.4564 eV 131.11 nm 0.0412
9.4967 eV 130.55 nm 0.0150
9.5071 eV 130.41 nm 0.0243
9.5115 eV 130.35 nm 0.0425
9.5398 eV 129.96 nm 0.0090
9.5870 eV 129.33 nm 0.0134
9.6097 eV 129.02 nm 0.0907
9.6453 eV 128.54 nm 0.0786
9.6530 eV 128.44 nm 0.0373
9.6742 eV 128.16 nm 0.0154
9.6930 eV 127.91 nm 0.0079
9.7144 eV 127.63 nm 0.0105
9.7356 eV 127.35 nm 0.0025
9.7417 eV 127.27 nm 0.0224
9.7577 eV 127.06 nm 0.0181
9.7758 eV 126.83 nm 0.0226
9.7861 eV 126.69 nm 0.0024
9.7987 eV 126.53 nm 0.0050
9.8229 eV 126.22 nm 0.0624
9.8364 eV 126.05 nm 0.0310
9.8632 eV 125.70 nm 0.0376
9.8816 eV 125.47 nm 0.0544
9.9040 eV 125.19 nm 0.2617
9.9075 eV 125.14 nm 0.0279
9.9284 eV 124.88 nm 0.0193
9.9506 eV 124.60 nm 0.0034
9.9613 eV 124.47 nm 0.1327
9.9773 eV 124.27 nm 0.0065
9.9886 eV 124.13 nm 0.0129

Crystallographic Data

Crystals suitable for X-ray analysis were grown by slow diffusion of the samples in EtOAc into Hexane at room temperature. The diffraction data were measured 100K(2) on a Bruker Smart Apex2 CCD-based X-ray diffractometer system equipped with a Mo-Kα radiation (λ = 0.71073 Å). The frames were integrated with the Bruker Saint software package using a narrow-frame integration algorithm. The structure was solved and refined using the Bruker SHELXTL Software Package. All atoms were refined anisotropically, and hydrogen atoms were removed for clarity.

ORTEP of 12 (50% probability ellipsoids)

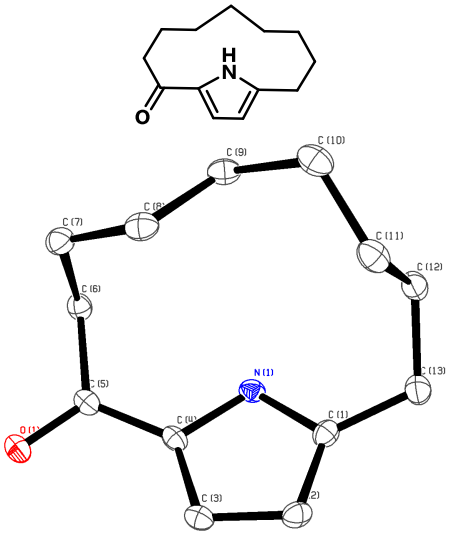

Crystal data and structure refinement for Compound **12**.

Identification code	cu_har1702s_a	
Empirical formula	C13 H19 N O	
Formula weight	205.29	
Temperature	0(2) K	
Wavelength	1.54178 Å	
Crystal system	Monoclinic	
Space group	$P2_1/n$	
Unit cell dimensions	a = 7.7866(3) Å	a= 90°.
	b = 15.2172(7) Å	b= 112.279(3)°.
	c = 10.1883(5) Å	g = 90°.
Volume	1117.09(9) $Å^3$	
Z	4	
Density (calculated)	1.221 Mg/m^3	
Absorption coefficient	0.594 mm^{-1}	
F(000)	448	
Crystal size	? x ? x ? mm^3	
Theta range for data collection	5.520 to 69.358°.	
Index ranges	-8<=h<=9, -18<=k<=15, -11<=l<=11	
Reflections collected	8118	
Independent reflections	2005 [R(int) = 0.0742]	
Completeness to theta = 67.679°	98.0 %	
Refinement method	Full-matrix least-squares on F^2	
Data / restraints / parameters	2005 / 0 / 145	
Goodness-of-fit on F^2	0.958	
Final R indices [I>2sigma(I)]	R1 = 0.0400, wR2 = 0.0984	
R indices (all data)	R1 = 0.0492, wR2 = 0.1006	
Extinction coefficient	n/a	

Largest diff. peak and hole	0.218 and -0.229 e.Å^{-3}

ORTEP of 17 (50% probability ellipsoids)

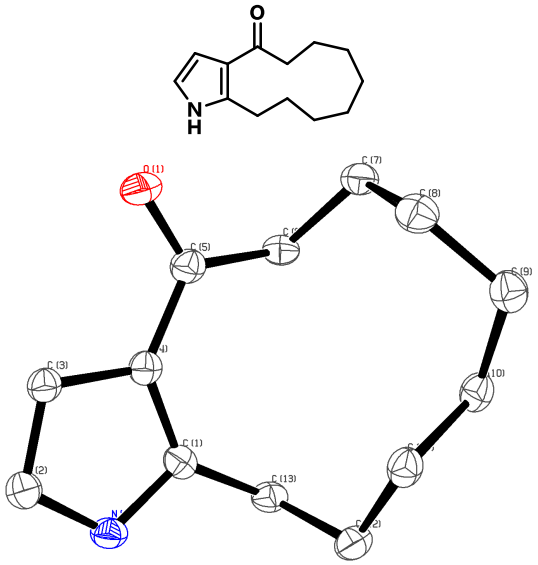

Crystal data and structure refinement for Compound **17**.

Identification code	cu_har1703s_a	
Empirical formula	C13 H19 N O	
Formula weight	205.29	
Temperature	100(2) K	
Wavelength	1.54178 Å	
Crystal system	Monoclinic	
Space group	$P2_1/n$	
Unit cell dimensions	a = 9.4220(3) Å	a= 90°.
	b = 9.3471(3) Å	b= 99.966(2)°.
	c = 12.8767(5) Å	g = 90°.
Volume	1116.92(7) Å^3	
Z	4	
Density (calculated)	1.221 Mg/m^3	
Absorption coefficient	0.594 mm^{-1}	
F(000)	448	
Crystal size	.4 x .3 x .1 mm^3	
Theta range for data collection	5.397 to 69.880°.	
Index ranges	-11<=h<=11, -11<=k<=11, -15<=l<=12	
Reflections collected	8386	
Independent reflections	2062 [R(int) = 0.0213]	
Completeness to theta = 67.679°	99.2 %	
Absorption correction	Semi-empirical from equivalents	
Max. and min. transmission	0.75 and 0.68	

Refinement method	Full-matrix least-squares on F^2
Data / restraints / parameters	2062 / 0 / 145
Goodness-of-fit on F^2	1.098
Final R indices [I>2sigma(I)]	R1 = 0.0389, wR2 = 0.0921
R indices (all data)	R1 = 0.0420, wR2 = 0.0934
Extinction coefficient	n/a
Largest diff. peak and hole	0.330 and -0.198 e.Å^{-3}

ORTEP of 18 (50% probability ellipsoids)

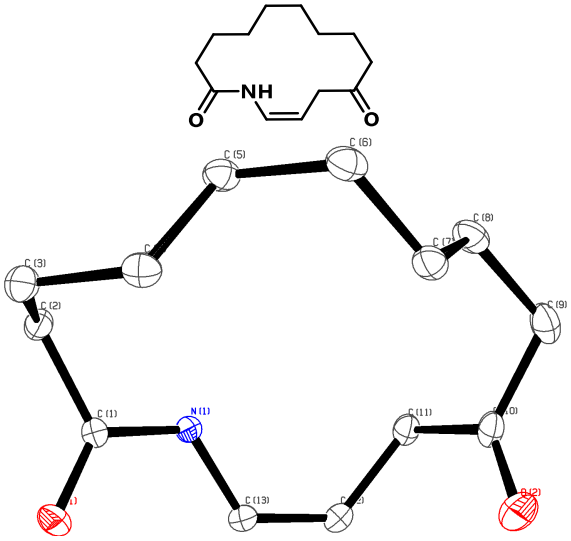

Crystal data and structure refinement for Compound **18**.

Identification code	mo_har1704s_a	
Empirical formula	C13 H21 N O2	
Formula weight	223.31	
Temperature	100(2) K	
Wavelength	0.71073 Å	
Crystal system	Monoclinic	
Space group	$P2_1/n$	
Unit cell dimensions	a = 9.7653(9) Å	a= 90°.
	b = 9.7181(9) Å	b= 98.8330(10)°.
	c = 13.3075(12) Å	g = 90°.
Volume	1247.9(2) Å^3	
Z	4	
Density (calculated)	1.189 Mg/m^3	
Absorption coefficient	0.079 mm^{-1}	
F(000)	488	
Crystal size	0.400 x 0.300 x 0.200 mm^3	
Theta range for data collection	2.419 to 30.916°.	

Index ranges	-13<=h<=13, -13<=k<=13, -18<=l<=19
Reflections collected	18951
Independent reflections	3718 [R(int) = 0.0224]
Completeness to theta = 25.242°	100.0 %
Absorption correction	Semi-empirical from equivalents
Max. and min. transmission	0.75 and 0.70
Refinement method	Full-matrix least-squares on F^2
Data / restraints / parameters	3718 / 0 / 145
Goodness-of-fit on F^2	1.072
Final R indices [I>2sigma(I)]	R1 = 0.0433, wR2 = 0.1111
R indices (all data)	R1 = 0.0454, wR2 = 0.1133
Extinction coefficient	n/a
Largest diff. peak and hole	0.360 and -0.341 e.$Å^{-3}$

NMR Spectra

Spectrum 1.4.1 ^{1}H-NMR spectrum of compound **12** ($CDCl_3$, 500 MHz)

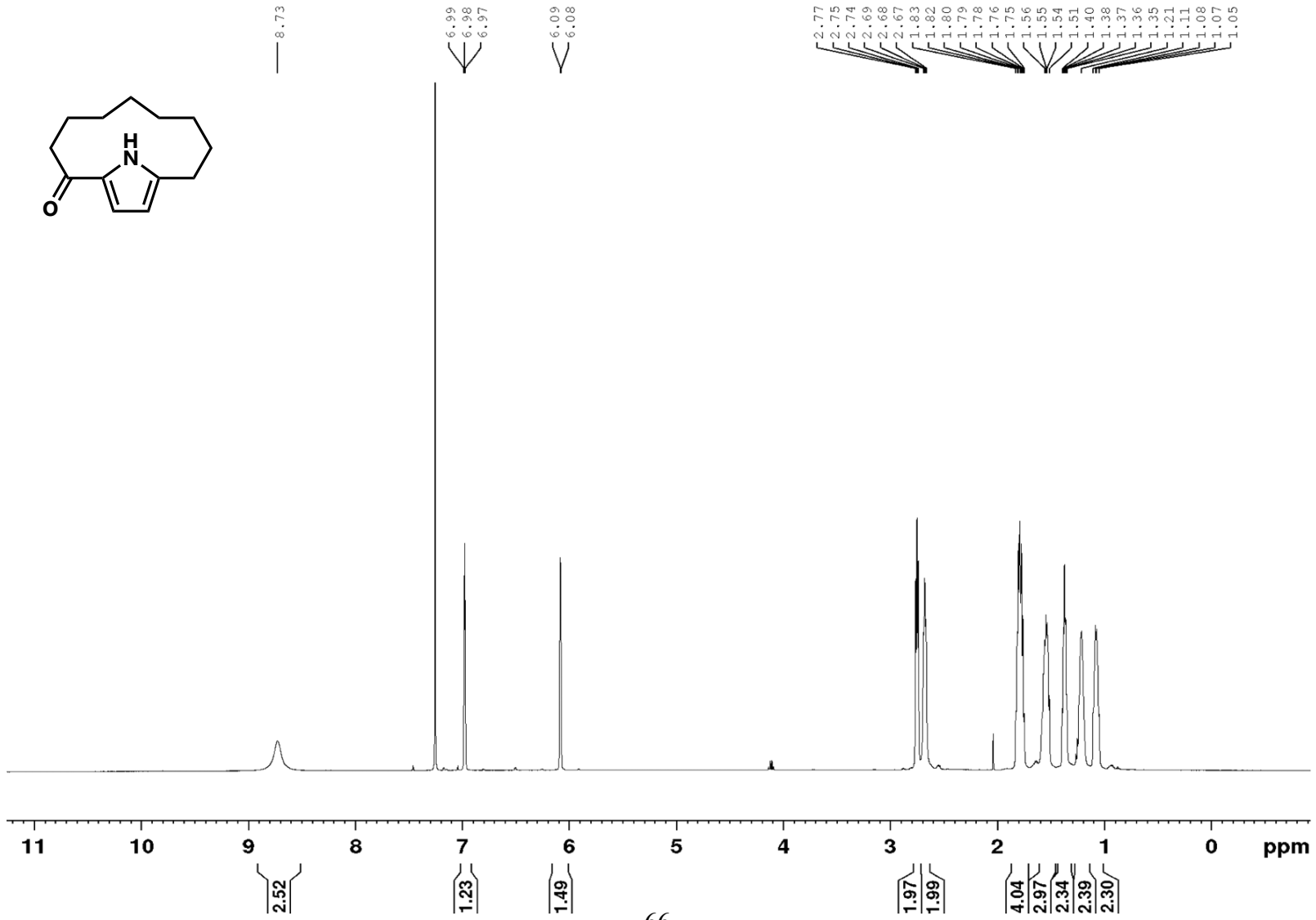

Spectrum 1.4.2 ^{13}C-NMR spectrum of compound **12** ($CDCl_3$, 125 MHz)

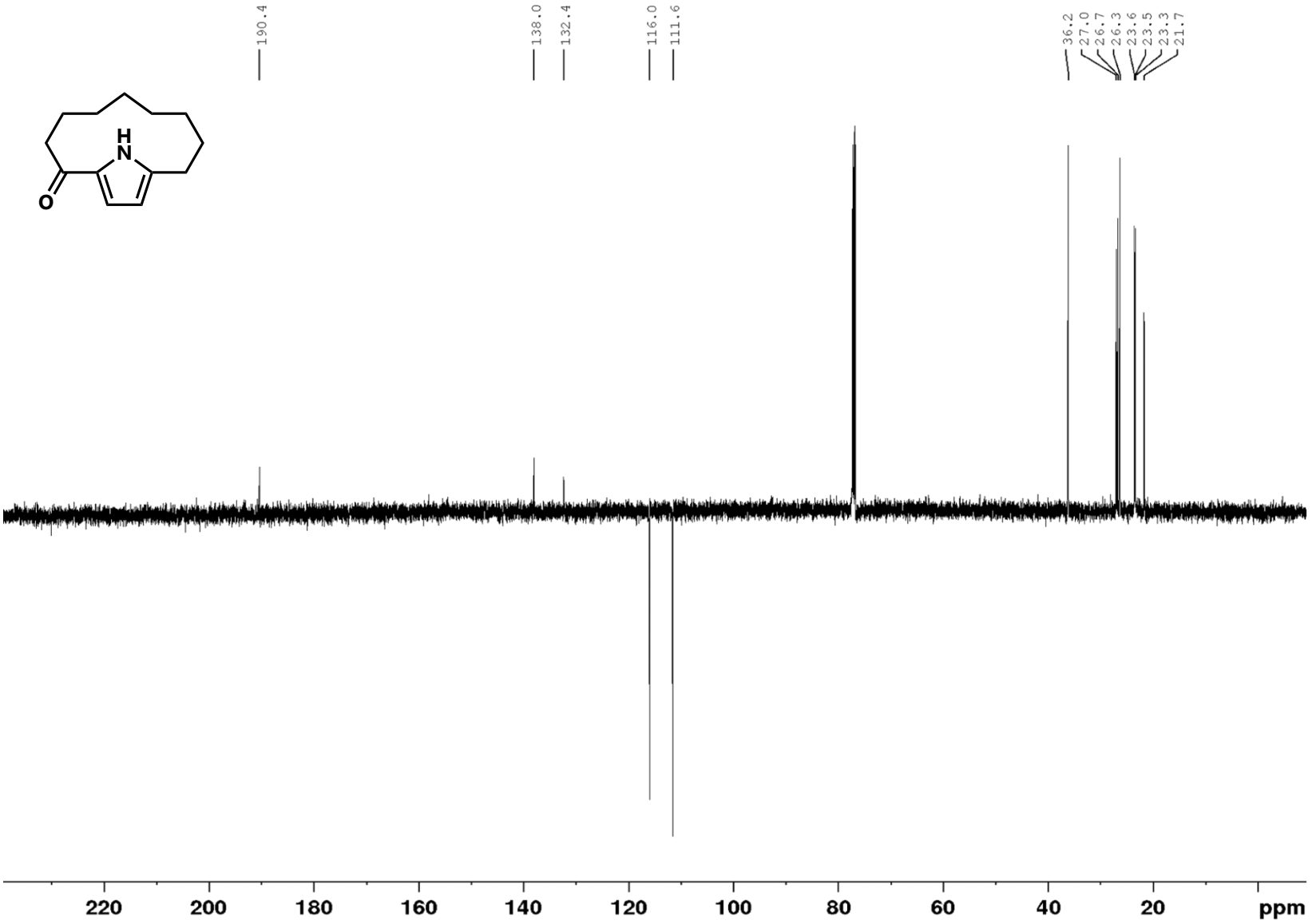

Spectrum 1.4.3 ^{1}H-NMR spectrum of compound **17** ($CDCl_3$, 500 MHz)

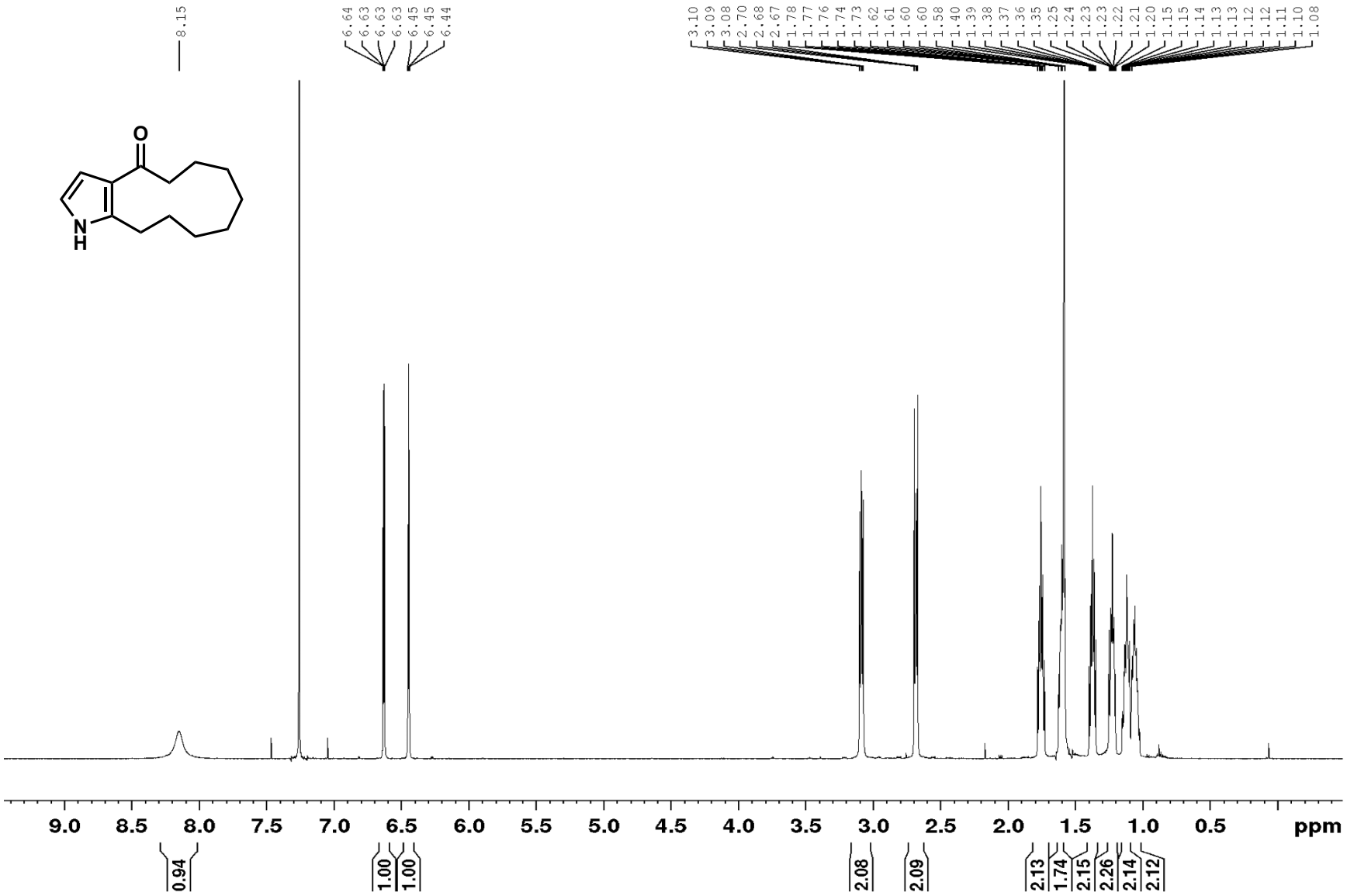

Spectrum 1.4.4 ^{13}C-NMR spectrum of compound **17** ($CDCl_3$, 125 MHz)

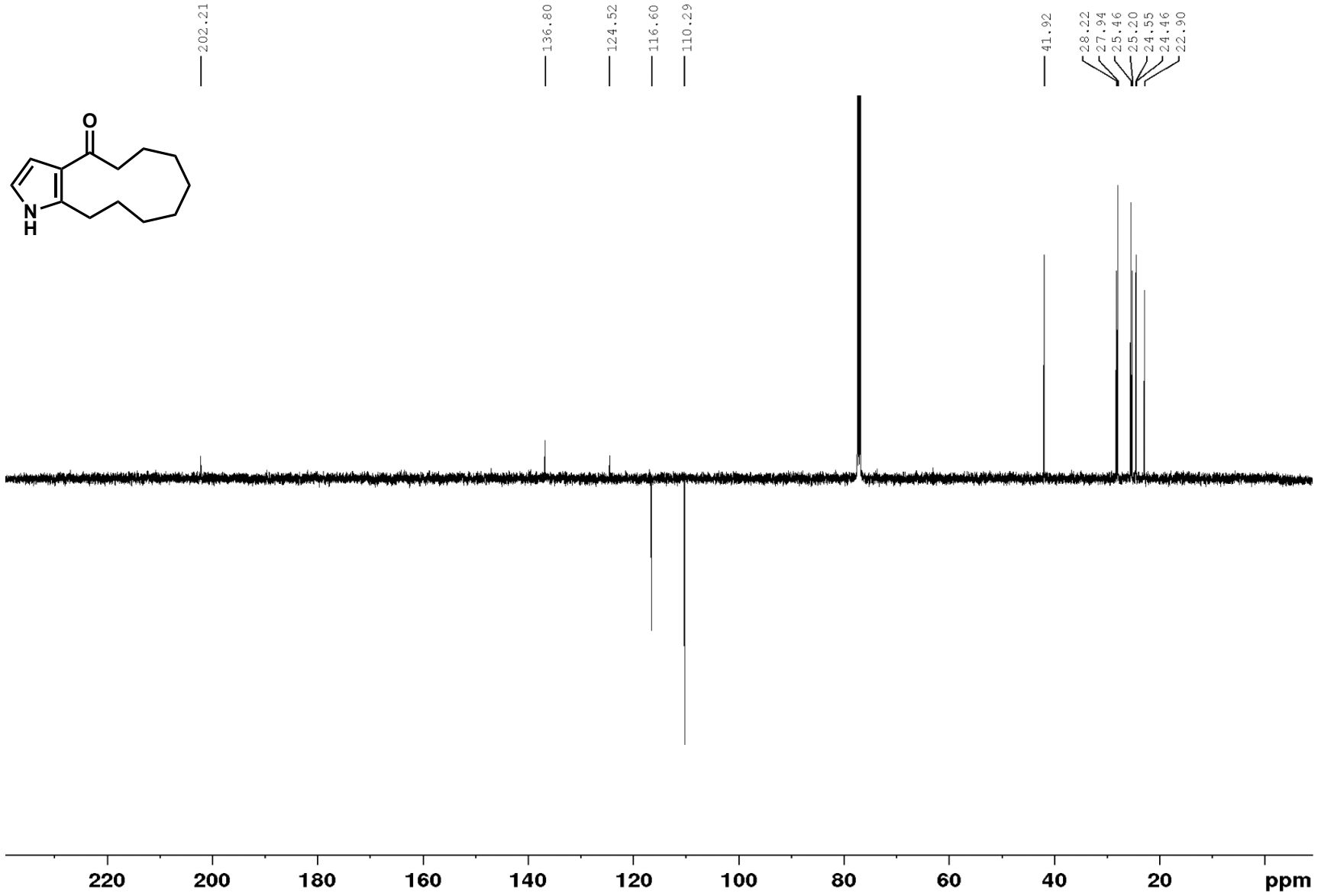

Spectrum 1.4.5 ^{1}H-NMR spectrum of compound **18** ($CDCl_3$, 500 MHz)

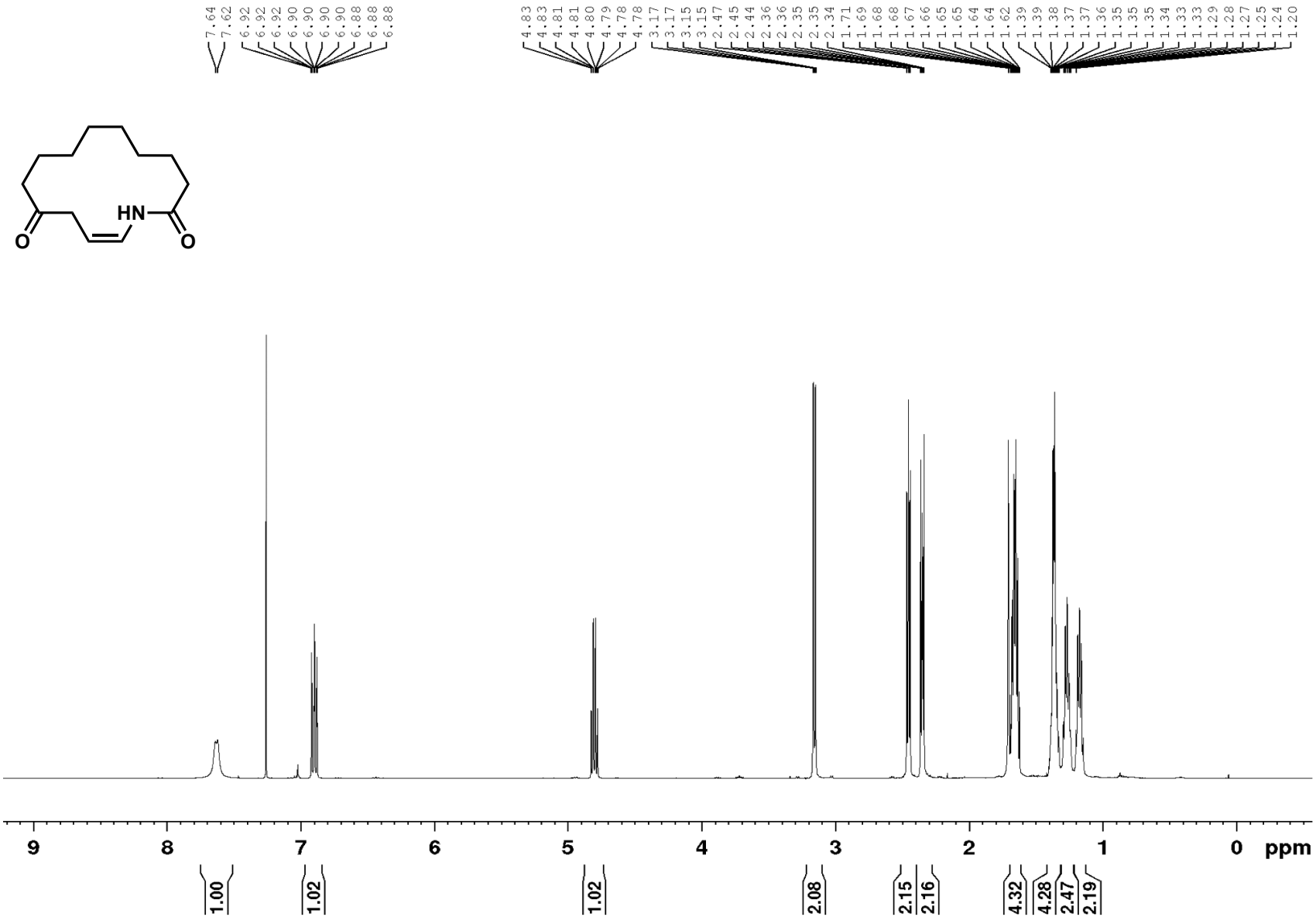

Spectrum 1.4.6 ^{13}C-NMR spectrum of compound **18** ($CDCl_3$, 125 MHz)

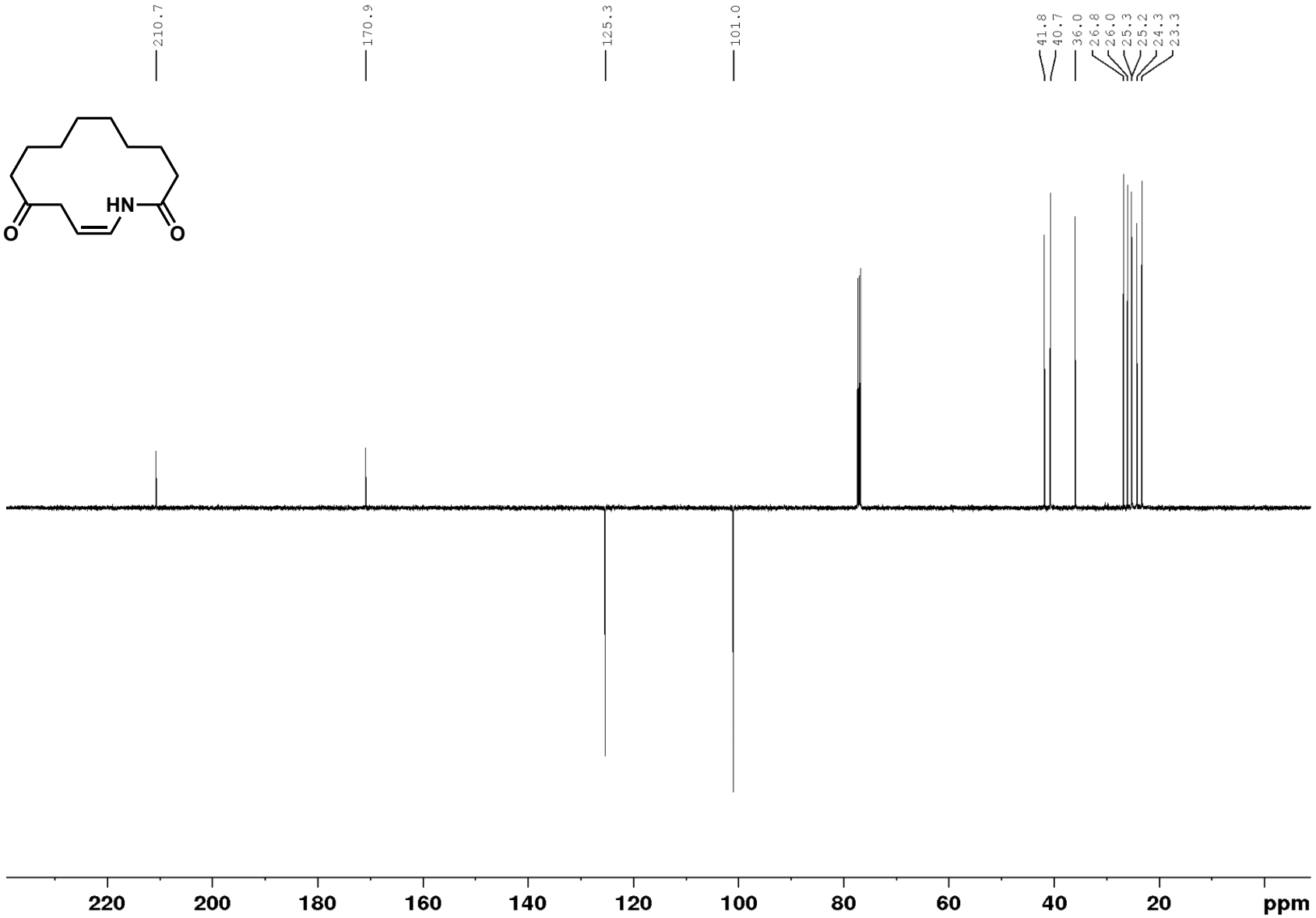

Spectrum 1.4.7 ^{1}H-NMR spectrum of compound **19** ($CDCl_3$, 500 MHz)

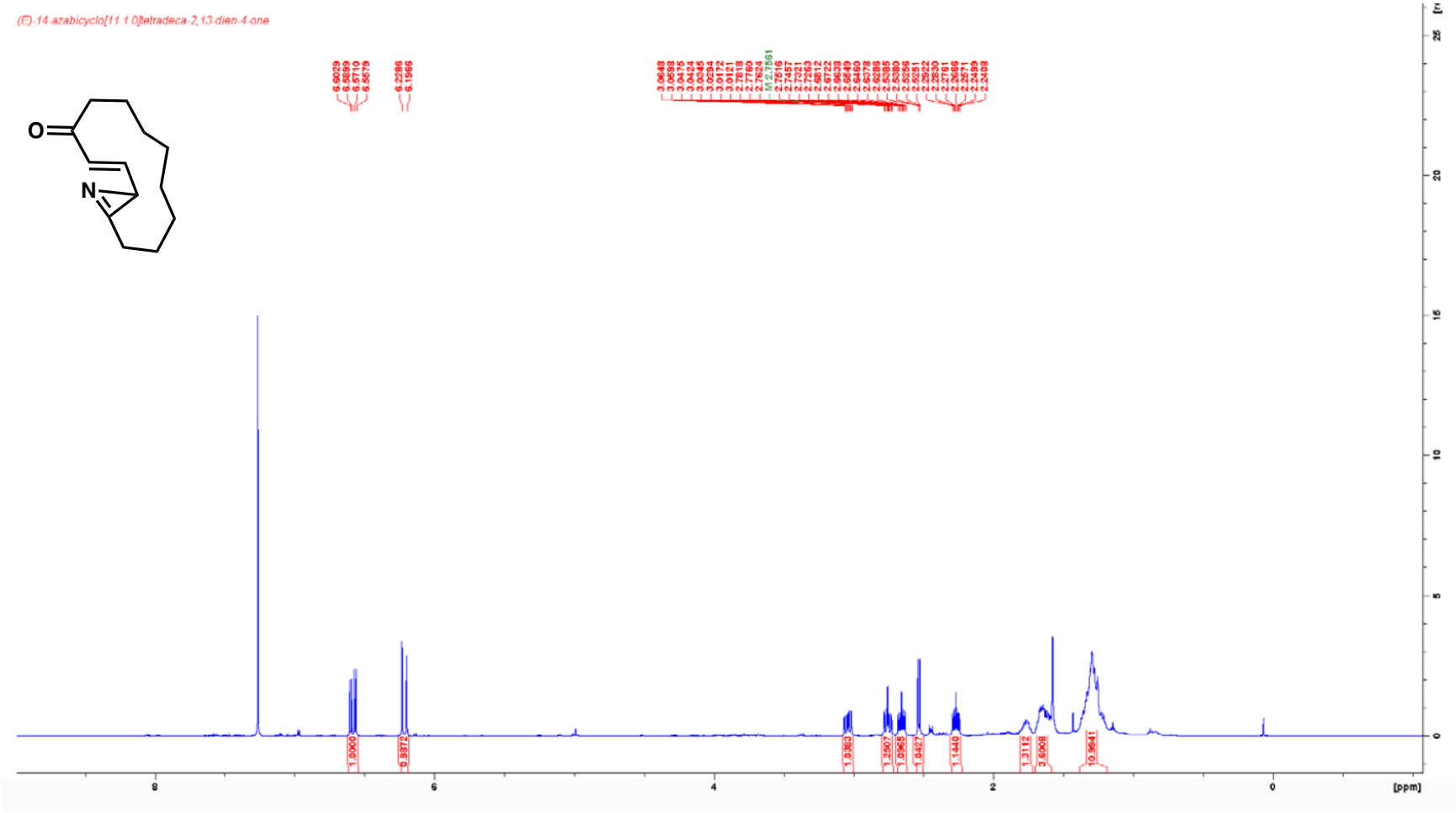

Spectrum 1.4.8 ^{13}C-NMR spectrum of compound **19** ($CDCl_3$, 125 MHz)

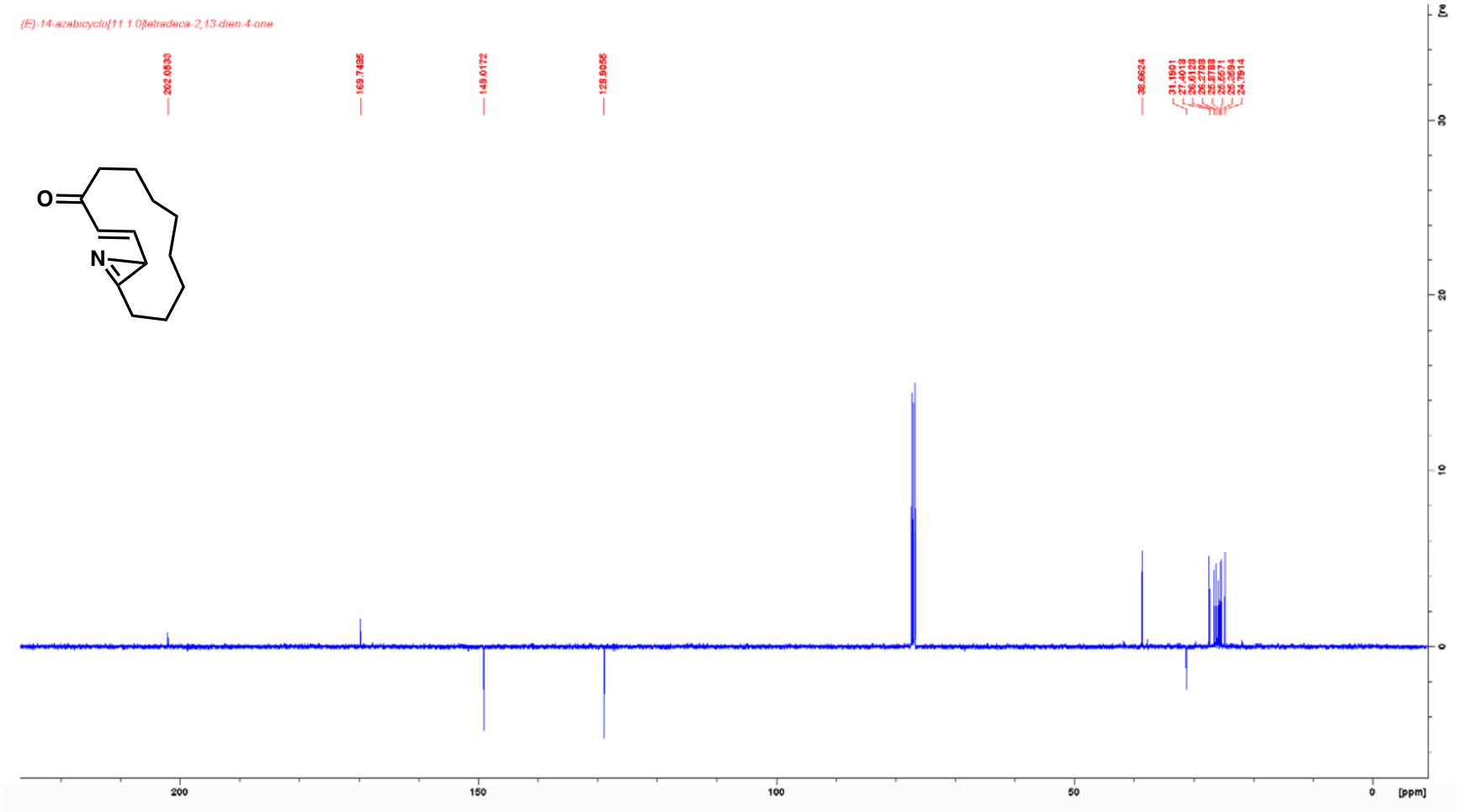

Spectrum 1.4.9 ^{1}H-NMR spectrum of compound **21** ($CDCl_3$, 600 MHz)

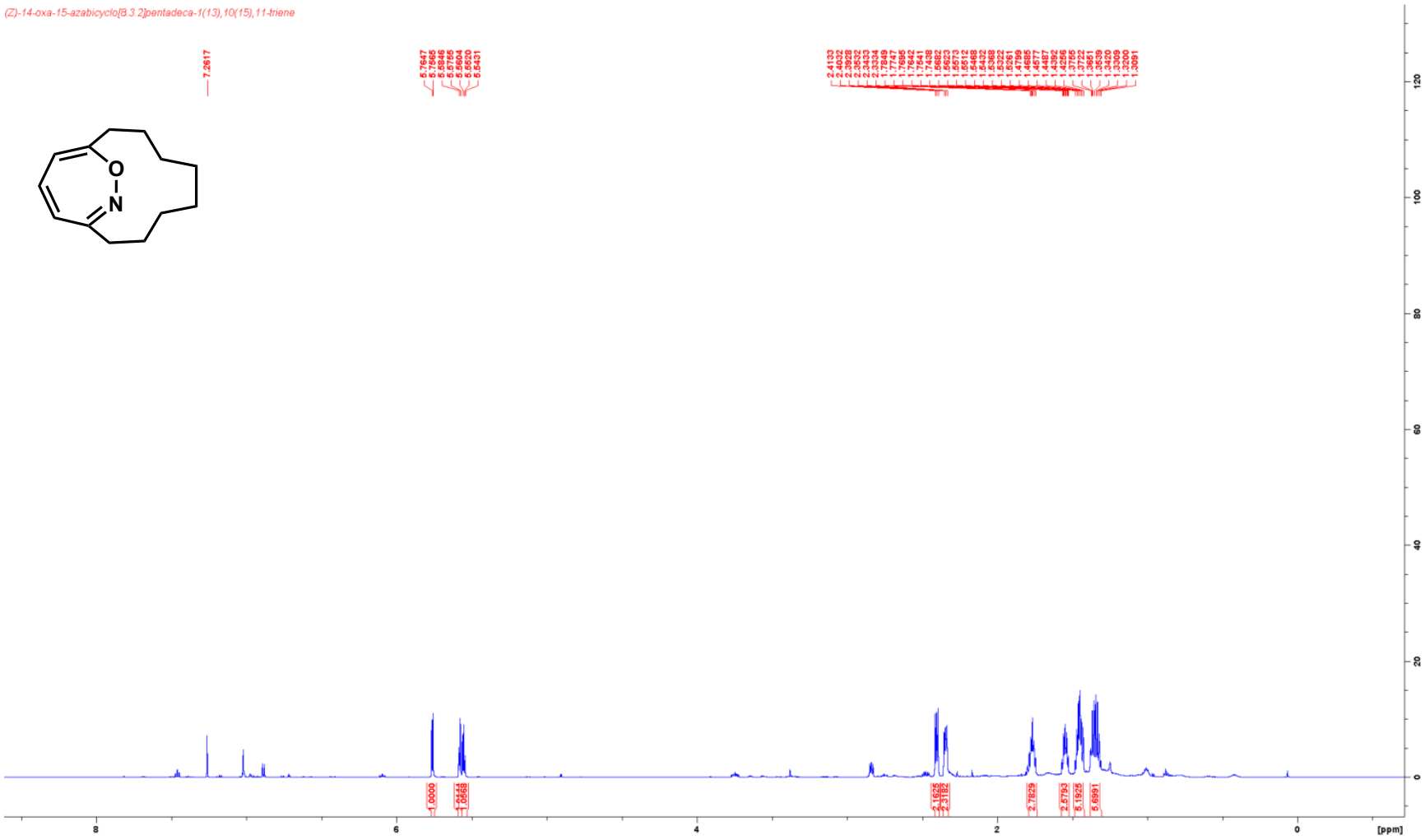

Spectrum 1.4.10 ^{13}C-NMR spectrum of compound **21** ($CDCl_3$, 100 MHz)

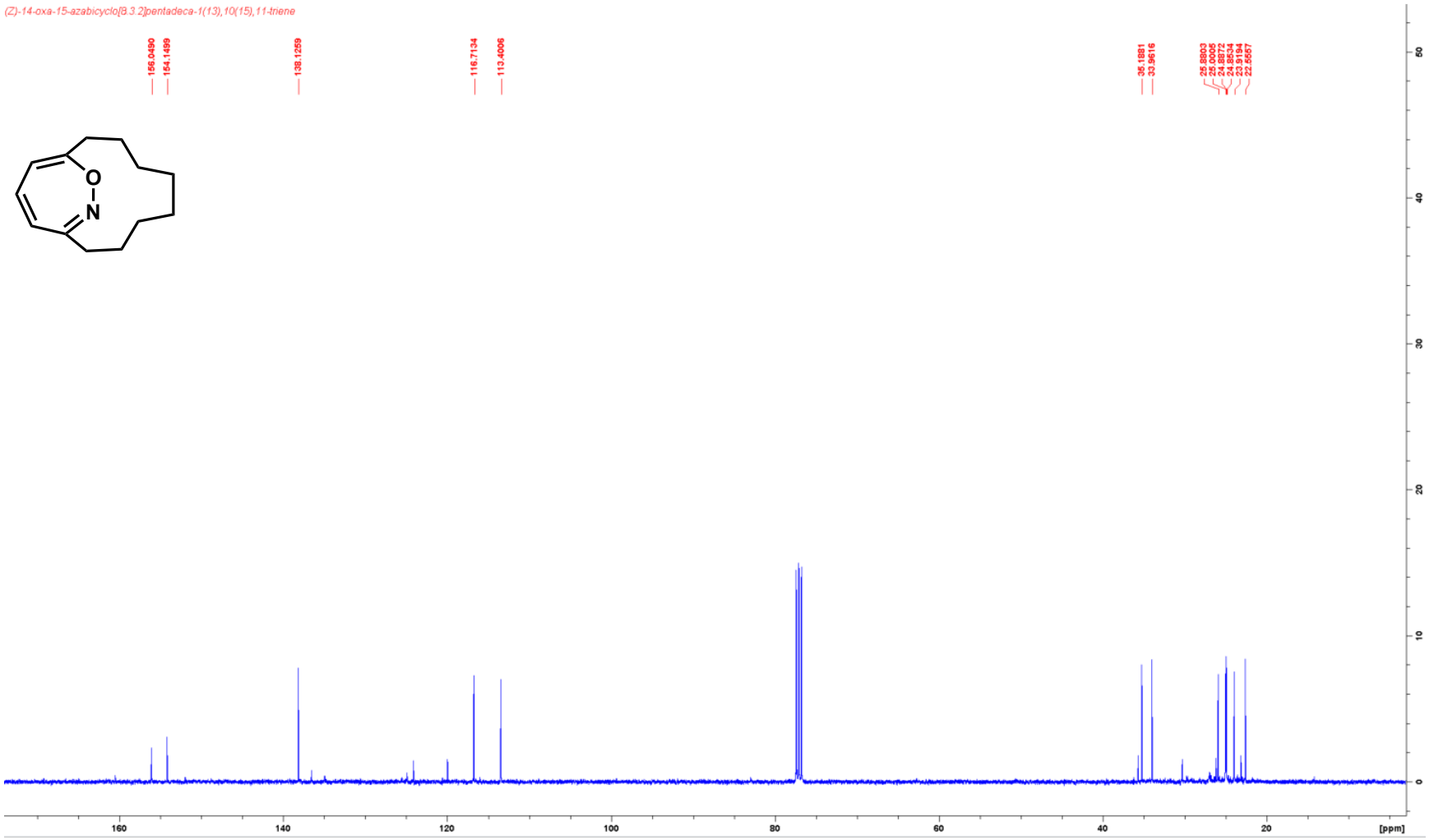

Spectrum 1.4.11 HSQC spectrum of compound **21** ($CDCl_3$, 400 MHz)

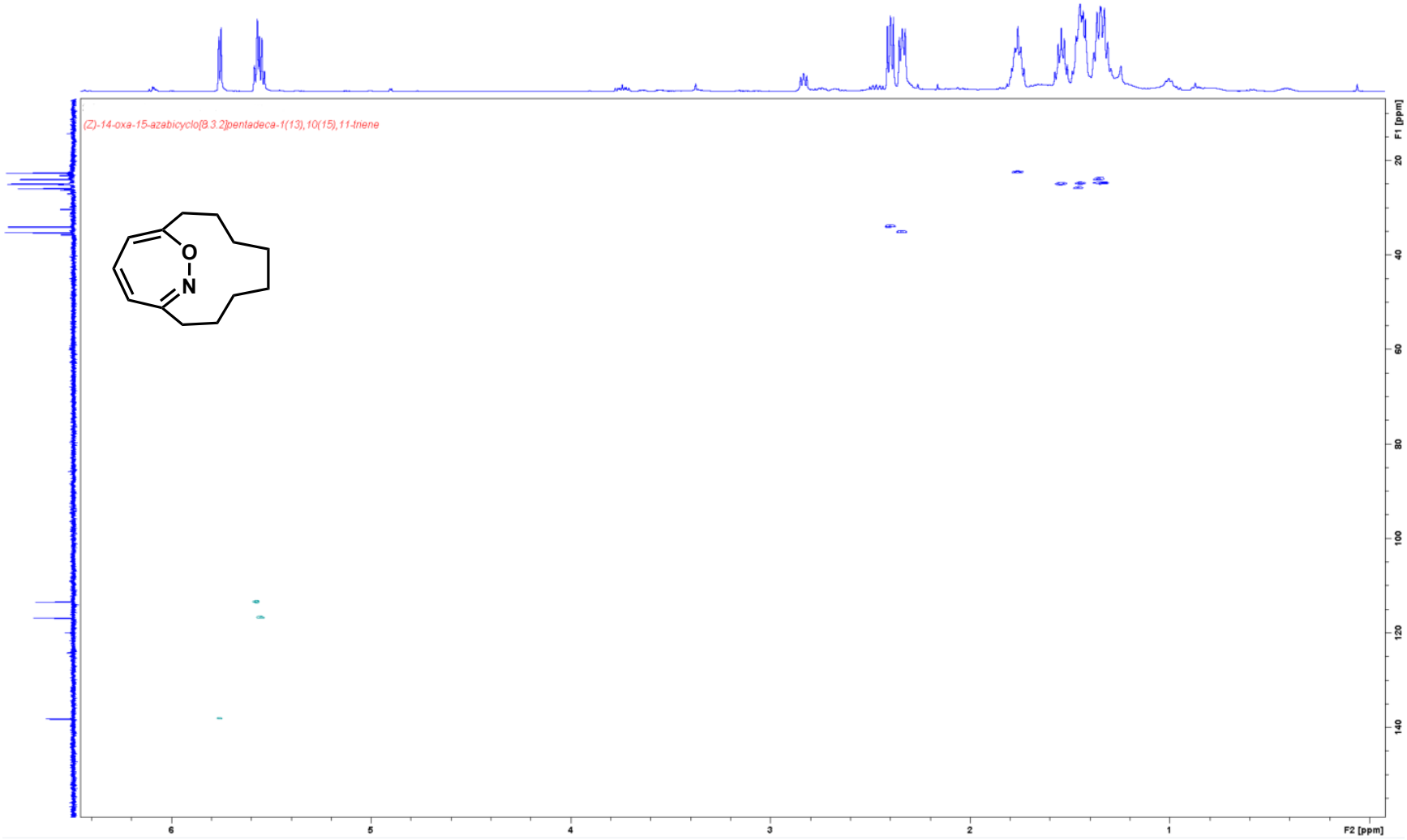

Spectrum 1.4.12 HMBC spectrum of compound **21** ($CDCl_3$, 400 MHz)

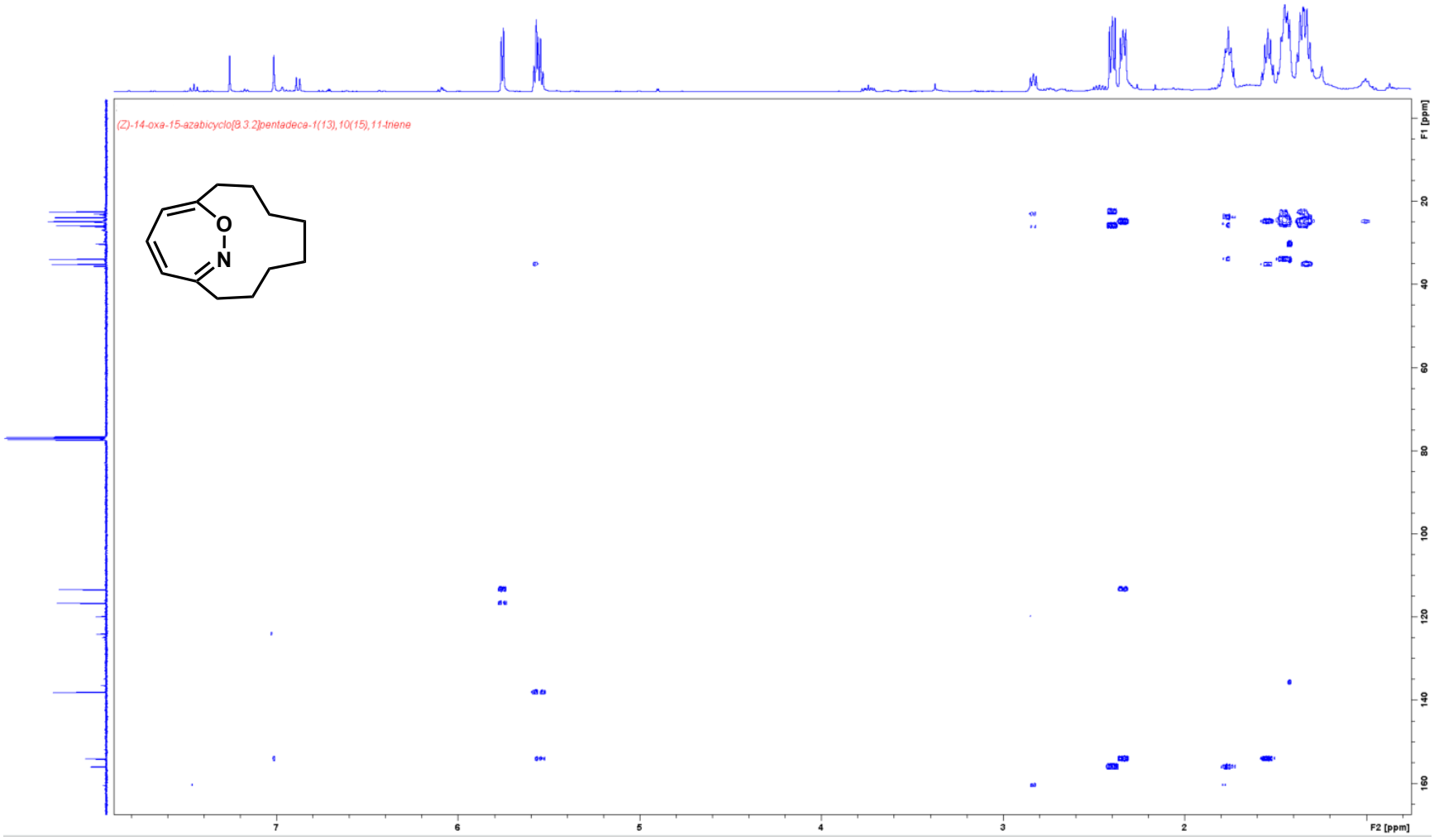

Spectrum 1.4.13 ^{1}H-NMR spectrum of compound **30** ($CDCl_3$, 400 MHz)

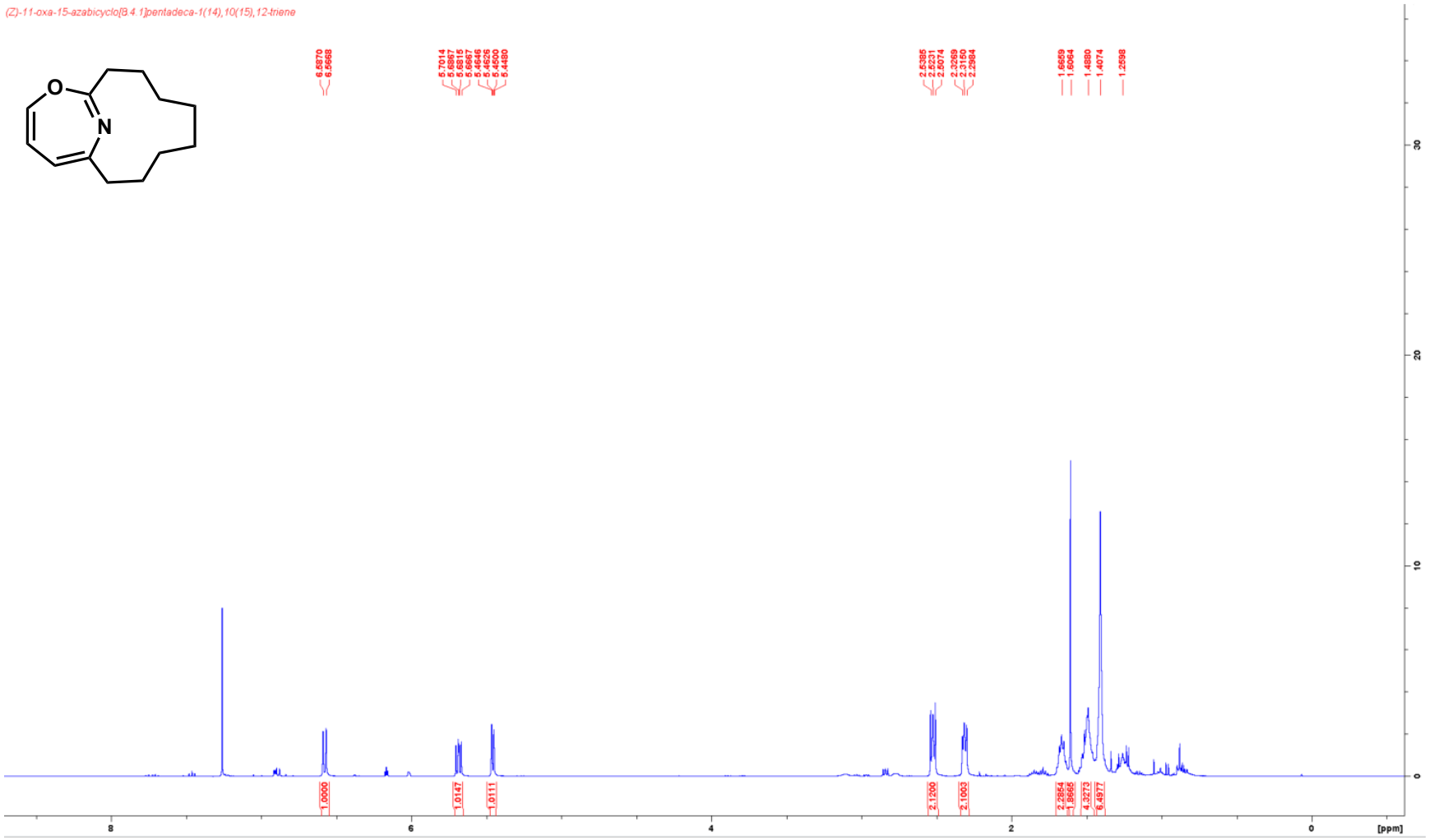

Spectrum 1.4.14 ^{13}C-NMR spectrum of compound **30** ($CDCl_3$, 100 MHz)

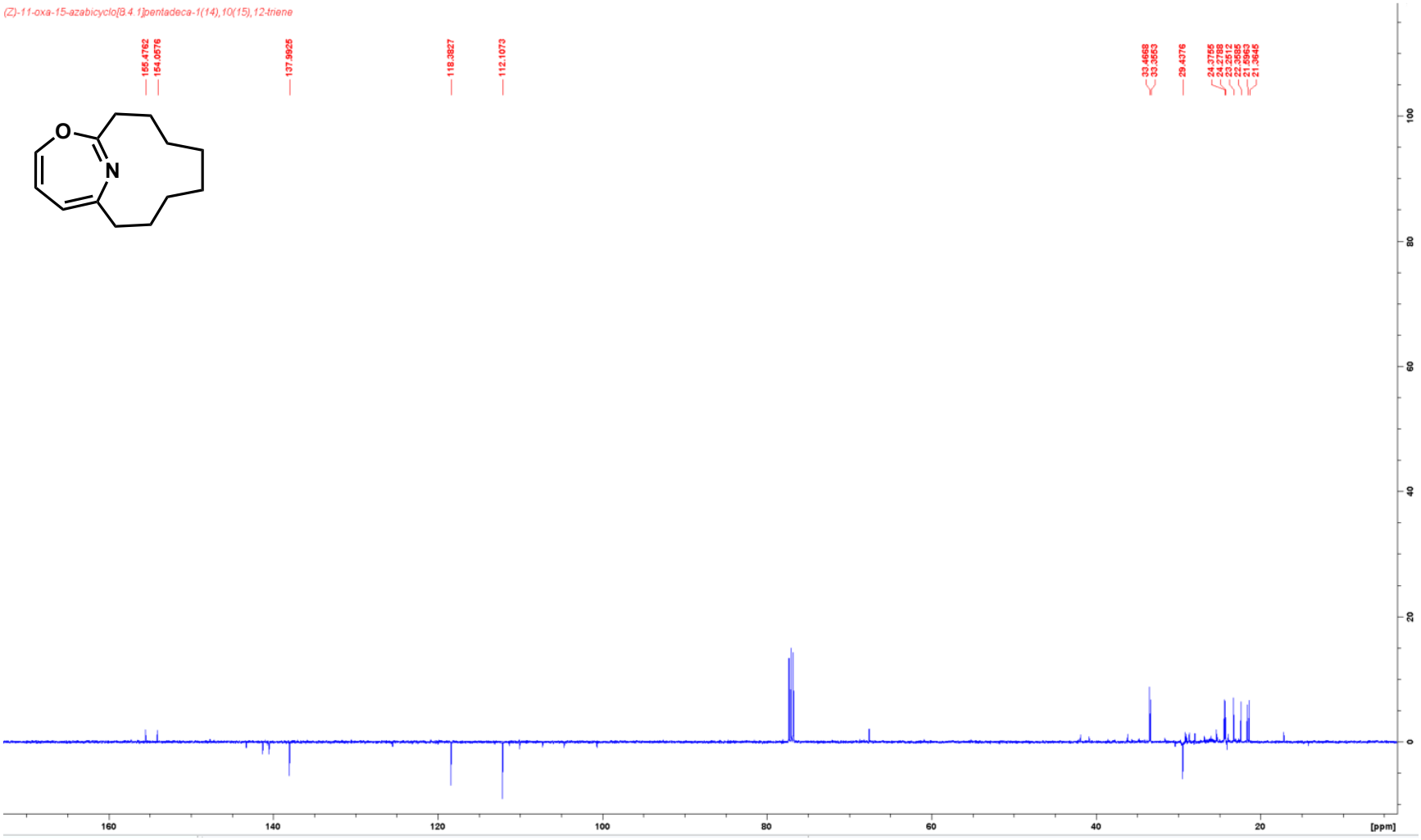

Spectrum 1.4.15 HSQC spectrum of compound **30** ($CDCl_3$, 400 MHz)

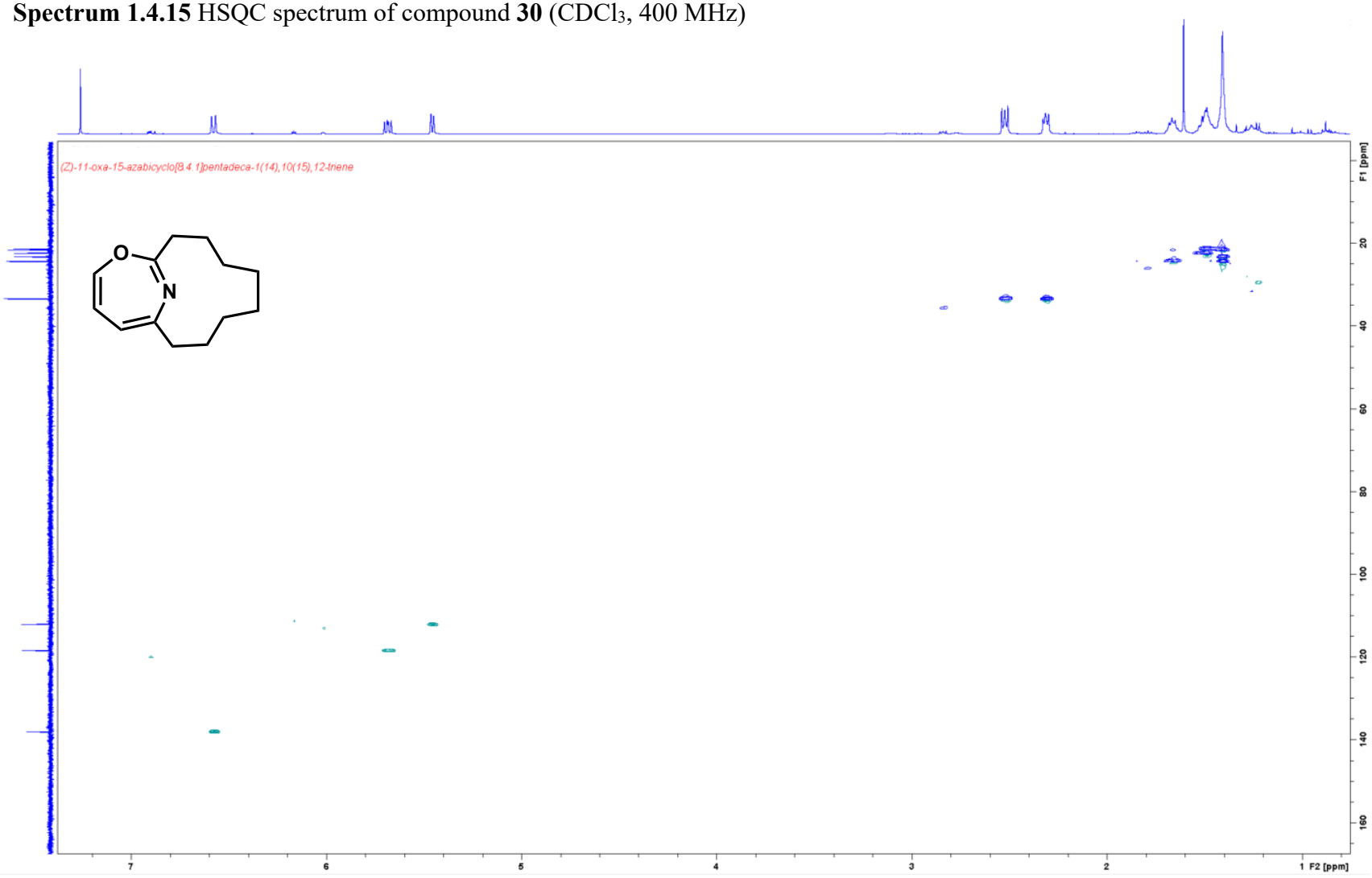

Spectrum 1.4.16 HMBC spectrum of compound **30** ($CDCl_3$, 400 MHz)

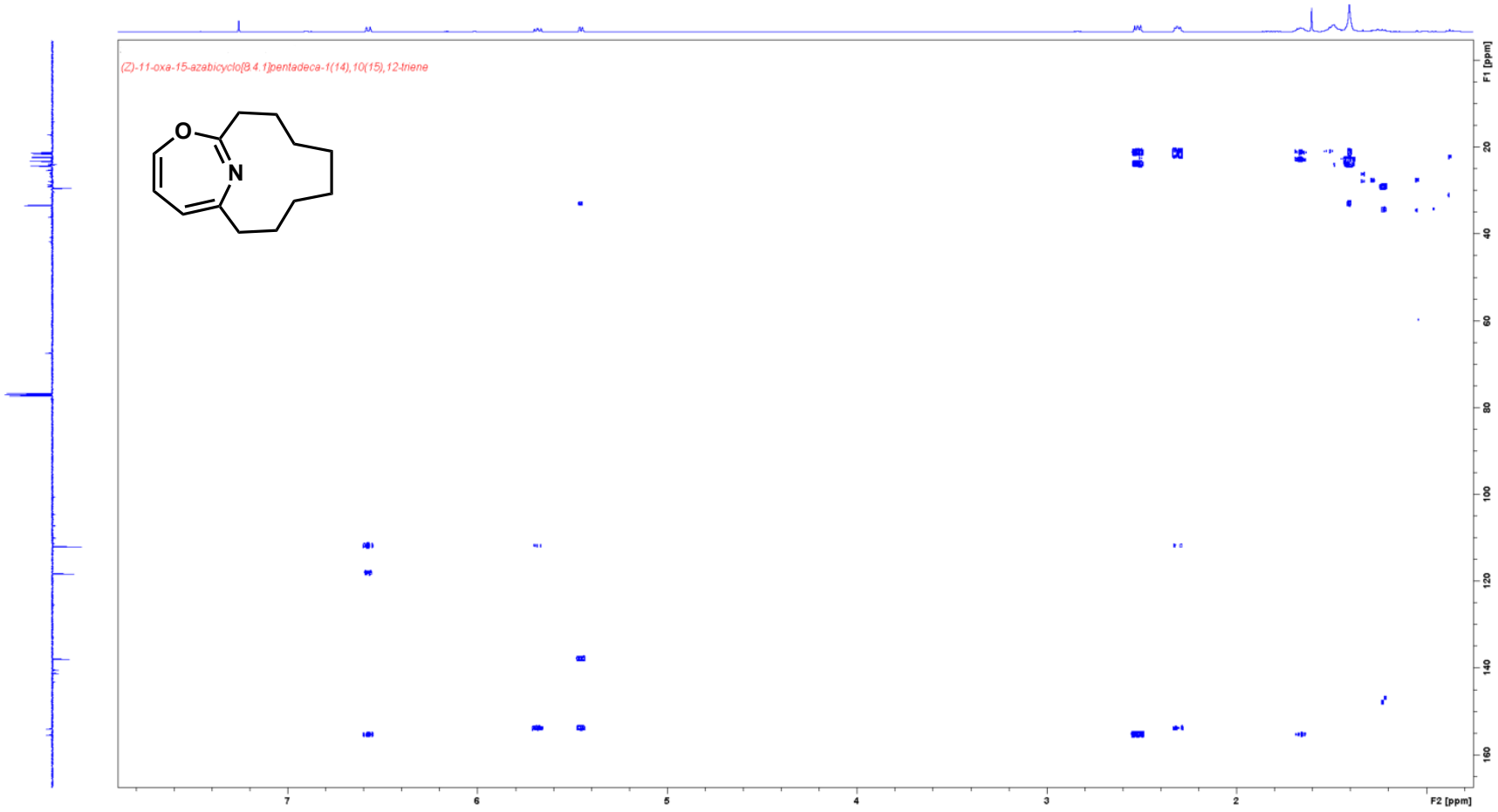

1.5 References

1. Spence, G. G.; Taylor, E. C.; Buchardt, O., Photochemical reactions of azoxy compounds, nitrones, and aromatic amine N-oxides. *Chem. Rev.* **1970**, *70* (2), 231–265.

2. Albini, A.; Alpegiani, M., The photochemistry of the N-oxide function. *Chem. Rev.* **1984**, *84* (1), 43–71.

3. Poole, J. S., Recent Advances in the Photochemistry of Heterocyclic N-Oxides and Their Derivatives. In *Heterocyclic N-Oxides*, Larionov, O. V., Ed. Springer International Publishing: Cham, **2017**, 111–151.

4. Ito, M.; Hata, N., The Ultra-violet Absorption Spectrum of Pyridine N-oxide. *Bull. Chem. Soc. Jpn.* **1955**, *28* (4), 260–263.

5. Hata, N.; Tanaka, I., Chemical Processes Subsequent to n—π* and π—π* Transitions of Pyridine N-oxide and 2-Picoline N-oxide. *J. Chem. Phys.* **1962**, *36* (8), 2072–2077.

6. Streith, J.; Sigwalt, C., Contraction d'heterocycles aromatiques par voie photocmique. *Tetrahedron Lett.* **1966**, *7* (13), 1347–1350.

7. Splitter, J. S.; Calvin, M., Oxaziridines. I. The Irradiation Products of Several Nitrones 1. *The J. Org. Chem.* **1965**, *30* (10), 3427–3436.

8. Bellamy, F.; Martz, P.; Streith, L., An Intriguing Copper Salt Effect upon the Photochemistry of Pyridine-N-oxides. Specific Photoinduced Syntheses of 3-Substituted 2-Formylpyrroles. *Heterocycles* **1975**, *3* (5), 395–400.

9. Brüggemann, M.; McDonald, A. I.; Overman, L. E.; Rosen, M. D.; Schwink, L.; Scott, J. P., Total Synthesis of (±)-Didehydrostemofoline (Asparagamine A) and (±)-Isodidehydrostemofoline. *J. Am. Chem. Soc.* **2003**, *125* (50), 15284–15285.

10. Hunter, G. A.; McNab, H.; Withell, K., The Meldrum's Acid Route to Prodigiosin Analogues. *Synth.* **2010**, *2010* (10), 1707–1711.

11. Boudif, A.; Momenteau, M., A new convergent method for porphyrin synthesis based on a '3 + 1' condensation. *J. Chem. Soc. Perkin Trans. 1* **1996**, *11*, 1235–1242.

12. Lohse, C.; Hagedorn, L.; Albini, A.; Fasani, E., Photochemistry of pyridine n-oxides. *Tetrahedron* **1988**, *44* (9), 2591–2600.

13. Weber, H.; Rohn, T., 2H-Azirine und 2-(ω-Cyanalkyl)furane als neuartige Photoprodukte aus [n](2,6)Pyridinophan-N-oxiden und ihre Bedeutung für den Reaktionsverlauf. *Chem. Ber.* **1989**, *122* (5), 945–950.

14. Berson, J. A.; Willcott, M. R., New Thermal Rearrangements of Tropilidenes1. *J. Am. Chem. Soc.* **1965**, *87* (12), 2751–2752.

15. Hu, D. X.; Withall, D. M.; Challis, G. L.; Thomson, R. J., Structure, Chemical Synthesis, and Biosynthesis of Prodiginine Natural Products. *Chem. Rev.* **2016**, *116* (14), 7818–7853.

16. Fürstner, A., Chemistry and biology of roseophilin and the prodigiosin alkaloids: a survey of the last 2500 years. *Angew. Chem., Int. Ed. Engl.* **2003,** *42* (31), 3582–3603.

17. Obatoclax at https://clinicaltrials.gov

18. Nguyen, M.; Marcellus, R. C.; Roulston, A.; Watson, M.; Serfass, L.; Murthy Madiraju, S. R.; Goulet, D.; Viallet, J.; Belec, L.; Billot, X.; Acoca, S.; Purisima, E.; Wiegmans, A.; Cluse, L.; Johnstone, R. W.; Beauparlant, P.; Shore, G. C., Small molecule obatoclax (GX15-070) antagonizes MCL-1 and overcomes MCL-1-mediated resistance to apoptosis. *PNAS.* **2007,** *104* (49), 19512–19517.

19. Feng, Z.; Allred, T. K.; Hurlow, E. E.; Harran, P. G. Anomalous Chromophore Disruption Enables an Eight-Step Synthesis and Stereochemical Reassignment of (+)-Marineosin A. *J. Am. Chem. Soc.* **2019**, *141* (6), 2274–2278.

20. Boonlarppradab, C.; Kauffman, C. A.; Jensen, P. R.; Fenical, W., Marineosins A and B, Cytotoxic Spiroaminals from a Marine-Derived Actinomycete. *Org. Lett.* **2008,** *10* (24), 5505–5508.

21. Information concerning the cytotoxic properties of **1.6** and **1.1** and the prodigiosins assayed in the standard 60-xell line panel are available at the home page of the National Cancer Institute (NCI), Bethesda, at http://www.dtp.nci.nih.gov.

22. Sydor, P. K.; Barry, S. M.; Odulate, O. M.; Barona-Gomez, F.; Haynes, S. W.; Corre, C.; Song, L.; Challis, G. L., Regio- and stereodivergent antibiotic oxidative carbocyclizations catalysed by Rieske oxygenase-like enzymes. *Nat. Chem.* **2011**, *3* (5), 388–392.

23. Weber, H.; Pant, J.; Wunderlich, H., Sterisch gehinderte Pyridiniumsalze, III. Darstellung und Eigenschaften von N-Methyl-[n](2, 6) pyridinophaniumsalzen. *Chem. Ber.* **1985**, *118* (10), 4259–4270.

24. Becke, A. D., Density-functional thermochemistry. III. The role of exact exchange. *J. Chem. Phys.* **1993**, *98* (7), 5648–5652.

25. Lee, C.; Yang, W.; Parr, R. G., Development of the Colle-Salvetti correlation-energy formula into a functional of the electron density. *Phys. Rev. B Condens.* **1988**, *37* (2), 785–789.

26. Stephens, P. J.; Devlin, F. J.; Chabalowski, C. F.; Frisch, M. J., Ab Initio Calculation of Vibrational Absorption and Circular Dichroism Spectra Using Density Functional Force Fields. *J. Phys. Chem.* **1994**, *98* (45), 11623–11627.

27. Vosko, S. H.; Wilk, L.; Nusair, M., Accurate spin-dependent electron liquid correlation energies for local spin density calculations: a critical analysis. *Can. J. Phys.* **1980**, *58* (8), 1200–1211.

28. Zhao, Y.; Truhlar, D. G., The M06 suite of density functionals for main group thermochemistry, thermochemical kinetics, noncovalent interactions, excited states, and transition elements: two new functionals and systematic testing of four M06-class functionals and 12 other functionals. *Theor. Chem. Acc.* **2008**, *120* (1), 215–241.

29. Macrae, C. F.; Sovago, I.; Cottrell, S. J.; Galek, P. T. A.; McCabe, P.; Pidcock, E.; Platings, M.; Shields, G. P.; Stevens, J. S.; Towler, M.; Wood, P. A., Mercury 4.0: from visualization to analysis, design and prediction. *J. Appl. Crystallogr.* **2020**, *53* (1), 226–235.

30. Padwa, A.; Smolanoff, J.; Tremper, A., Intramolecular photochemical and thermal cyclization reactions of 2-vinyl substituted 2H-azirines. *Tetrahedron Lett.* **1974**, *15* (1), 29–32.

31. Padwa, A.; Smolanoff, J.; Tremper, A., Photochemical transformations of small ring heterocyclic systems. LXV. Intramolecular cycloaddition reactions of vinyl-substituted 2H-azirines. *J. Am. Chem. Soc.* **1975**, *97* (16), 4682–4691.

32. Padwa, A., Azirine photochemistry. *Acc. Chem. Res.* **1976**, *9* (10), 371–378.

33. *UV Atlas of Organic Compounds*. Springer Science+Business Media: New York, 1967; Vol. III, p. 183.

34. Arnold, Z.; Dvořák, D.; Havránek, M., Convenient Preparation of 1,3-Bis(dimethylamino)trimethinium Perchlorate, Tetrafluoroborate and Hexafluorophosphate. *Collect. Czech. Chem. Commun.* **1996**, *61* (11), 1637–1641.

35. Yamada, S.; Kaneko, C., Studies on the n-oxides of π-deficient n-heteroaromatics—XXX11Part XXIX. C. Kaneko, M. Yamamori, A. Yamamoto and R. Hayashi, Tetrahedron Letters 2799 (1978). This paper also forms Part VII of Studies on the Oxazepine Derivatives—VI: C. Kaneko, S. Kawai and M. Somei, Chemistry Letters submitted.: Photochemistry of acridine 10-oxides (2):2 synthesis and reaction of dibenz[c,f]-1,2-oxazepines. *Tetrahedron* **1979**, *35* (10), 1273–1278.

36. Kurihara, T.; Nasu, K.; Mizuhara, Y.; Hayashi, K., Reaction of 3-[3-(2-Nitrophenyl)-2-propenylidene]-2, 4-pentanedione with Hydroxylamine Hydrochloride. Formation of a 2-Chloromethyleneindolin-3-one. *Chem. Pharm. Bull.* **1982**, *30* (8), 2742–2746.

37. Bellamy, F.; Streith, J., The Photochemistry of Aromatic N-Oxides. A Crystal Review. *Heterocycles* **1976**, *4* (8), 1391–1447.

38. Ishikawa, M.; Kaneko, C.; Yokoe, I.; Yamada, S., Photolysis of 2,6-dicyanopyridine 1-oxides. *Tetrahedron* **1969,** *25* (2), 295–300.

39. For previous syntheses of 1,3-oxazepines, see: (a) Kumagai, T.; Sawaura, M.; Kabuto, C.; Mukai, T., Organic photochemistry. 66. Photochemical reaction of 2-oxa-3-azabicyclo[3.2.0]hepta-3,6-diene derivatives. *Nippon Kagaku Kaishi* **1984**, *1*, 158–164. (b) Kobayashi, T.; Nitta, M., The Reaction of (Z)-2-(3-Oxo-1-propenyl)-2H-azirine Derivative with Molybdenum Carbonyl Complexes. *Bull. Chem. Soc. Jpn.* **1985**, *58* (3), 1057–1058. (c) Kurita, J.; Iwata, K.; Tsuchiya, T., Synthesis of the first examples of fully unsaturated monocyclic 1,4-oxazepines. *J. Chem. Soc. Chem. Commun.* **1986**, (15), 1188–1189.

40. Scaiano has postulated deoxygenation of pyridine N-oxide can occur via N-O homolysis to afford atomic oxygen. See Bucher, G.; Scaiano, J. C., Laser Flash Photolysis of Pyridine N-Oxide: Kinetic Studies of Atomic Oxygen [O(3P)] in Solution. *J. Phys. Chem.* **1994**, *98* (48), 12471–12473.

41. Hurlow E. E. The Photochemistry of [8]-Pyridinophane N-Oxide and Characterization of Prodiginine–microRNA Binding Interactions. Ph.D. Dissertation, University of California, Los Angeles, CA, 2022.

42. Johnson, W. T. G.; Sullivan, M. B.; Cramer, C. J., meta and para substitution effects on the electronic state energies and ring-expansion reactivities of phenylnitrenes. *Int. J. Quantum Chem.* **2001,** *85* (4-5), 492–508.

43. Yamaguchi, K.; Jensen, F.; Dorigo, A.; Houk, K. N., A spin correction procedure for unrestricted Hartree-Fock and Møller-Plesset wavefunctions for singlet diradicals and polyradicals. *Chem. Phys. Lett.* **1988,** *149* (5), 537–542.

44. Noodleman, L., Valence bond description of antiferromagnetic coupling in transition metal dimers. *J. Chem. Phys.* **1981,** *74* (10), 5737–5743.

45. Luchini, G.; Alegre-Requena, J.; Funes-Ardoiz, I.; Paton, R., GoodVibes: automated thermochemistry for heterogeneous computational chemistry data [version 1; peer review: 2 approved with reservations]. *F1000Research* **2020**, *9* (291).

46. Zhao, Y.; Truhlar, D. G., Computational characterization and modeling of buckyball tweezers: density functional study of concave–convex π···π interactions. ***Phys. Chem. Chem. Phys.*** **2008**, *10* (19), 2813–2818.

47. Ribeiro, R. F.; Marenich, A. V.; Cramer, C. J.; Truhlar, D. G., Use of Solution-Phase Vibrational Frequencies in Continuum Models for the Free Energy of Solvation. *J. Phys. Chem. B.* **2011**, *115* (49), 14556–14562.

48. M. J. Frisch *et al., Gaussian 16*, Revision C.01; Gaussian, Inc.: Wallingford CT, **2009**.

49. M. J. Frisch *et al., Gaussian 16*, Revision C.01; Gaussian, Inc.: Wallingford CT, **2016**.

50. Watts, K. S.; Dalal, P.; Tebben, A. J.; Cheney, D. L.; Shelley, J. C., Macrocycle Conformational Sampling with MacroModel. *J. Chem. Inf. Model.* **2014**, *54* (10), 2680–2696.

51. **Schrödinger Release 2023-3**: MacroModel, Schrödinger, LLC, New York, NY, 2023.

52. Grimme, S., Exploration of Chemical Compound, Conformer, and Reaction Space with Meta-Dynamics Simulations Based on Tight-Binding Quantum Chemical Calculations. *J. Chem. Theory Comput.* **2019,** *15* (5), 2847–2862.

Chapter Two: An Atypical Chain-Migration in Ansa-Bridged Prodiginine Chromophores

2.1 Introduction

In our 2019 synthesis of the natural product (+)-marineosin A[1], we elected to forge the prototypical tripyrrolic prodiginine core from fragments of reversed polarity relative to their biosynthesis as well as conventional construction methodologies detailed in previous publications (**Scheme 2.1.1**).[2-4] This was done via the condensation of nucleophilic methoxy-bispyrrole **3** with α-branched 2-hydroxypropyl ketopyrrolophane **2**, the latter of which was the product of alkylation of ketopyrrolophane **1** with (S)-propylene oxide (**Scheme 2.1.2**).

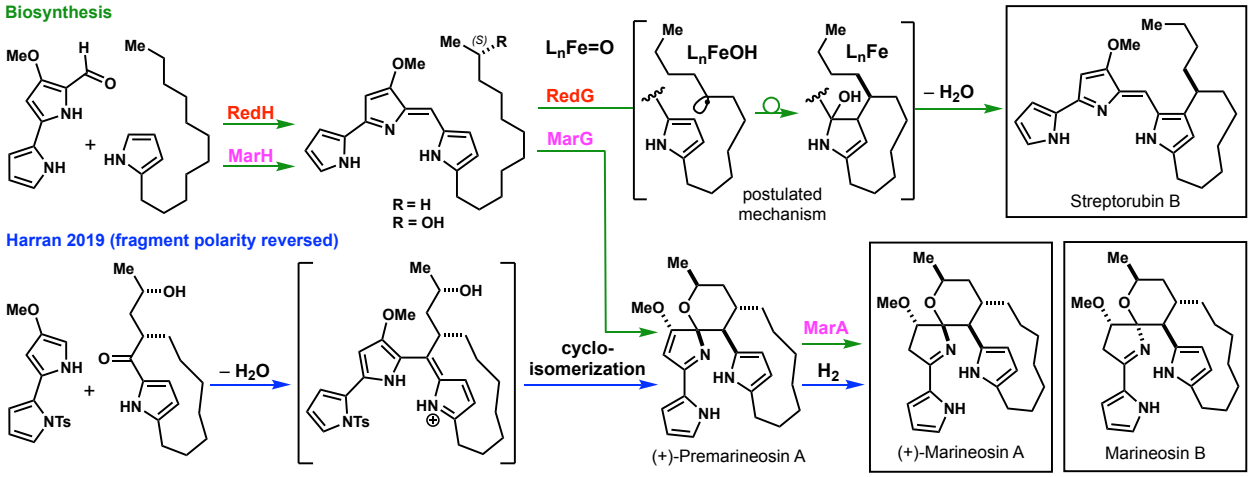

Scheme 2.1.1 Biosynthesis of prodiginines Marineosin A and Streptorubin B along with our approach for the construction of the tripyrrolic prodiginine core.

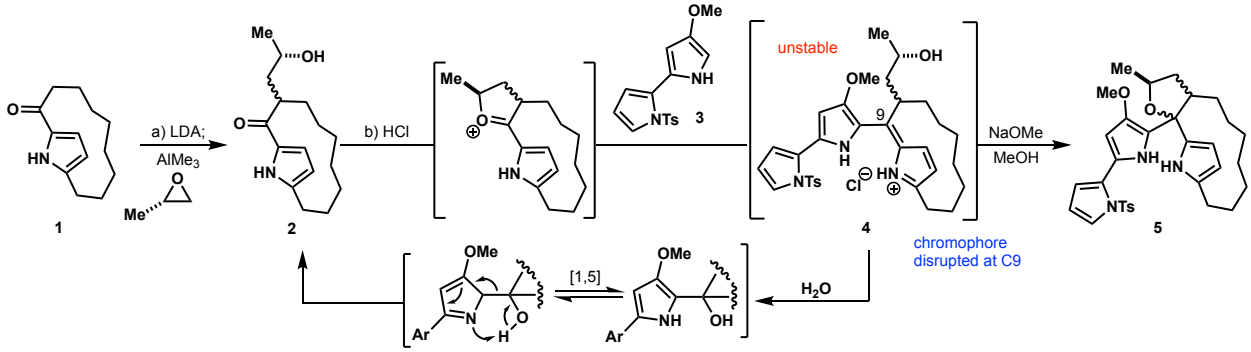

Scheme 2.1.2 Our published route to tetrahydrofuran containing iso-premarineosins **5**. Reagents and conditions: a) LDA (3.1 eq.), 0 °C, 0.5 h; (S)-propylene oxide (5.0 eq.), $AlMe_3$ (1.1 eq.), –

78°C to rt, 12 h, 71%, d.r = 2:1; b) **2** (1.0 eq.), **3** (1.0 eq.), 1.5 eq. HCl (1M in MeOH), Na_2SO_4, toluene, 0°C, 0.5 h; 1M NaOMe/MeOH, 87%, d.r = 1:1.

When a solution of fragments **2** and **3** was treated with dry HCl, the solution turned deep red within seconds, indicating the formation condensation product **4**. Despite repeated attempts, **4** could not be isolated from the reaction as predominantly starting materials were recovered following aqueous workup of the reaction. From this, we concluded that while prodiginines bearing a hydrogen at C9 position (e.g. Streptorubin B in **Scheme 2.1.1**) are isolable species[5], branched ansa-bridge connectivity at C9 destabilizes the resulting extended conjugated system making it prone to hydrolysis (as depicted). To stabilize **4** in situ, we quenched the reaction with dry NaOMe. This gave novel structural variants of iso-premarineosin (**5**) in good yield. These tetrahydrofuran products derive from the chromophore of charged azafulvene **4** being internally disrupted at C9, the same position attacked by water during hydrolysis. While compounds **5** were found to be air-sensitive, they were sufficiently stable to be purified by flash column chromatography and isolated in high yield (87%, 1:1 d.r).

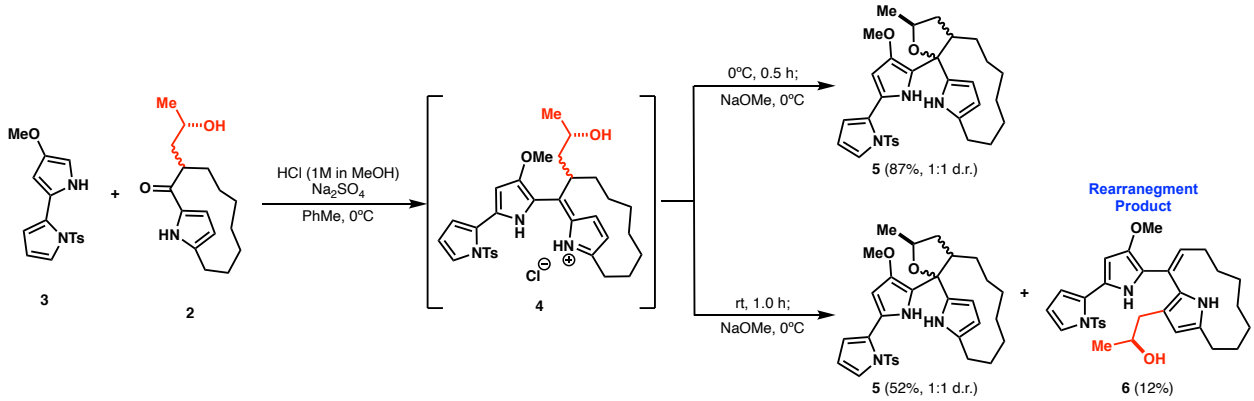

Scheme 2.1.3 Discovery of an unprecedented alkyl chain migration in the assembly of ansa-bridged prodiginine tripyrrolic core.

During the course of optimizing this reaction, we found that allowing the reaction to stir for an additional hour at room temperature before quenching resulted in the diminished isolation

of desired **5** (52%, 1:1 d.r) and the isolation of a structurally distinct unknown compound having an identical mass to that of the desired product in 12% yield. Extensive characterization of this unknown via 2D-NMR suggests it to have a structure consistent with that of **6**, a product which appears to be the resultant of 2-hydroxypropyl side chain migration onto the proximal pyrrole ring (**Scheme 2.1.3**). Realizing this rearrangement to be unprecedented in the literature and of great value towards the design and synthesis of synthetic prodiginines, we decided to explore the generality of this rare migration as well as better understand the operative mechanism by which is proceeds. The latter of these goals was done with the assistance of DFT calculations carried out in collaboration with the Houk Group.

2.2 Exploration of the Generality and Mechanism of Observed Rearrangement

2.2.1 Exploration of Observed Rearrangement Generality

The exploration of this unpresented chain migration began with a brief analysis of the kinetics governing the condensation between bispyrrole **3** and 2-hydroxypropyl ketopyrrolophane **2**. Because tetrahydrofurans **5** proved to be unstable to LCMS analysis, optimal time points for isolating maximal yields of **5** and **6** were determined via isolated yields of reactions run in parallel. From this data, we found that while the highest isolated yield of **5** was achieved by quenching the reaction after 0.5 h at 0°C (87%), the highest isolated yield of rearrangement product **6** (16%) was obtained by allowing the reaction to stir at room temperature for an addition 2 h before quenching (total reaction time = 2.5 h). These findings suggests that the rate of formation of **6** is slower than **5** which adds credence to our hypothesis that the former comes from the latter.

With an optimal timepoint for the isolation of the rearrangement product established, we next turned our attention towards investigating how altering the electronics of the bispyrrole system affected the propensity for the observed rearrangement. To probe how altering the electronics in the pyrrole ring bearing the methoxy group (B-ring) effects the results of the condensation reaction, known dess-methoxy bispyrrole **7**[6] was condensed with **2** and left to stir at room temperature for various extended periods of time before quenching (**Scheme 2.2.1**). While this resulted in the isolation of tetrahydrofuran product **8**, no product resulting from chain migration was observed. This suggests that while the electron density of the dess-methoxy bispyrrole B-ring is sufficient for condensation to occur, it is not electron rich enough to promote chain migration.

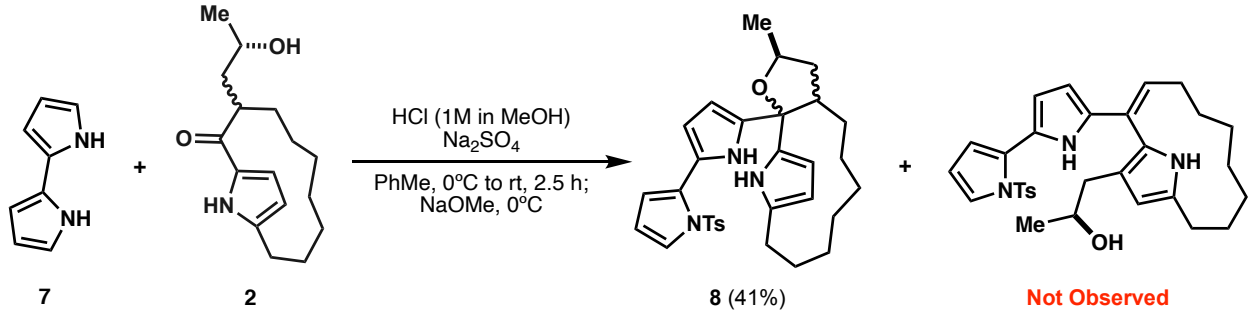

Scheme 2.2.1 Results of condensation of dess-methoxy bipyrrole **7** with alkyl ketopyrrolophane **2**.

We next decided to investigate how altering the electronics of the pyrrole ring not bearing the methoxy group (A-ring) effected the reaction. Towards this goal, a series of methoxy-pyrrole heterobiaryls were synthesized (shown in **Figure 2.2.1**) using the sequence shown in **Scheme 2.2.2**, the same sequence used to synthesize methoxy bispyrrole **3**.

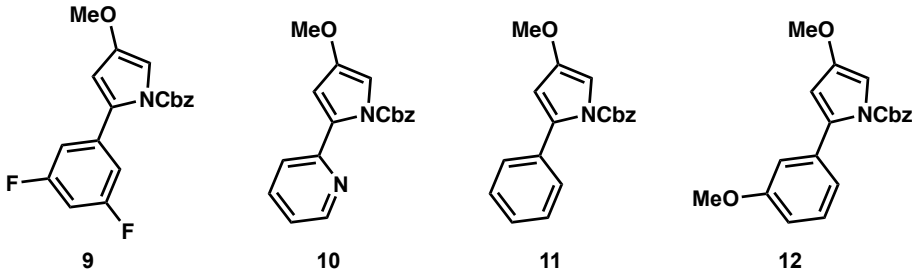

Figure 2.2.1 Synthesized heterobiaryls used to study how altered electronics of the A-ring pyrrole effects rearrangement behavior.

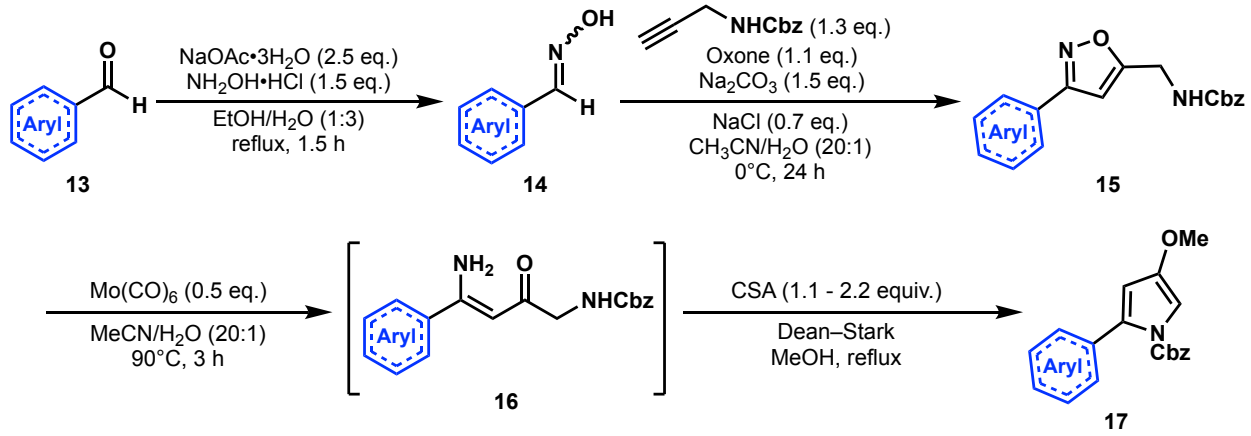

Scheme 2.2.2 General synthetic scheme used to synthesize the heterobiaryls shown in **Figure 2.2.1**.

While this preparation closely mirrors our 2013 published route to substituted 2,2-bipyrroles and pyrrolylfurans[7], it differs only in the procedure of the cycloaddition reaction used to afford heterobiaryl isoxazoles **15**[8] as well as the incorporation of a Cbz protecting group on the A-ring nitrogen. While not explicitly shown in any of the schemes in this chapter, the Cbz protecting group of these methoxy heterobiaryls (as well as the Cbz group of **3**) were removed prior to their use in condensation reactions. This was done using typical hydrogenolysis conditions using Pd/C under an atmosphere of hydrogen gas (See Experimental Section for details). It is worth noting that these Cbz-deprotected products were found to be quite unstable, often turning black in color when exposed to air for mere seconds. For this reason, we decided to minimize handling of

these compounds by telescoping them directly to condensation reactions after their isolation from the hydrogenolysis procedure.

Once prepared, these heterobiaryls were condensed with **2** using conditions aimed to maximize the yield of rearrangement product (outlined above).These reactions resulted in the isolation of iso-premarineosin analogs as well as products resulting from rearrangement in various yields as shown in **Scheme 2.2.3**.

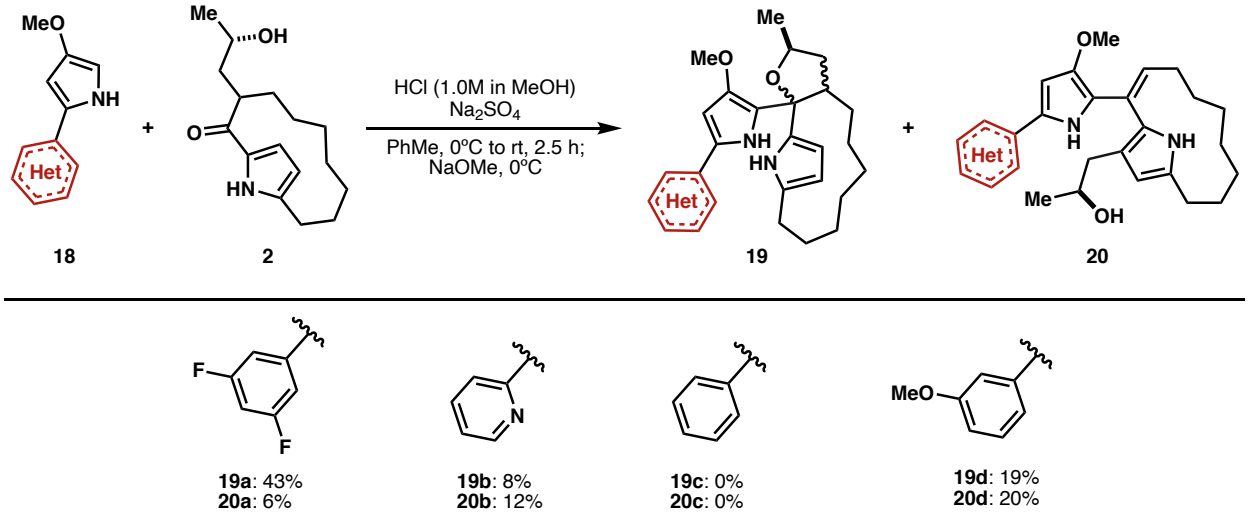

Scheme 2.2.3 Results of the condensation of 2-hydroxypropyl ketopyrrolophane **2** with heterobiaryls.

Condensation of heterobiaryls **9** and **10** (**Figure 2.2.1**), derived from 3,5-difluorobenzaldehyde and pyridine-2-carboxaldehyde respectively, with **2** resulted in the isolation of rearrangement products **20a** and **20b** along with corresponding iso-premarineosin analogs **19a** and **19b** respectively. Comparing the isolated yields of these rearrangements products (6% for **20a** and 12% for **20b**) to that obtained for the parent methoxy bispyrrole system (16%), we postulated that the electron donating capability of the A-ring might be directly responsible for this observed trend in isolated yields. More specifically, we hypothesized that lowering the electron density in the A-ring of the heterobiaryl lowered the propensity for chain migration. In this way, we reasoned

that increasing the electron density in the heterobiaryl A-ring would have the opposite effect. Evidence for this hypothesis was provided by the results of condensing **12**, derived from 3-methoxybenzaldehyde, with **2** which yielded rearrangement product **20d** in 20% yield and tetrahydrofuran product **19d** in 19% yield. It should be noted that while attempts were made to further support this hypothesis through the utilization of electronically-neutral heterobiaryl **11** (derived from benzaldehyde) these condensation reactions failed to yield any definitively characterizable products. This is thought to be a result of the instability of reaction intermediates form during the condensation. It should also be noted that the lack of any observed trend in the isolated yields of tetrahydrofuran products **19a** –**19d** did not go unnoticed and it is thought to the result of the varying hydrolytic instability of these products.

The results of the above two studies suggest that while sufficient electron density in the B-ring is necessary for the observed rearrangement to occur, the efficiency of this migration is greatly affected by the electron density of the aromatic A-ring; with increasing A-ring electron density resulting in a greater propensity for rearrangement as summarized in **Figure 2.2.2**. While the reason for this observed trend is not currently known, we feel this observation to be quite valuable as it can be leveraged to access new prodiginine scaffolds as well as analogs of (+)-marineosin A for structure-activity relationship (SAR) studies.

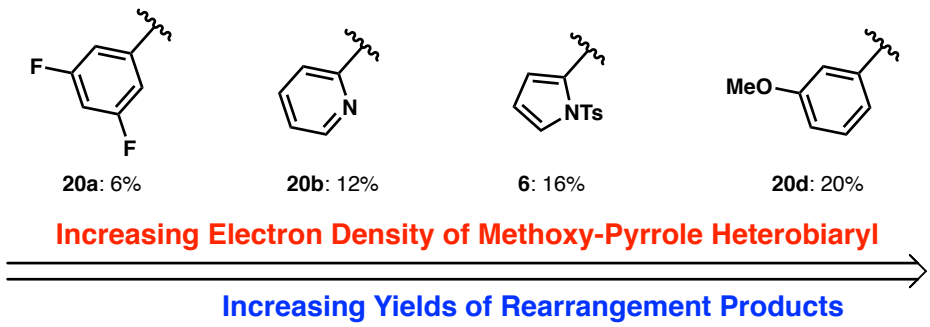

Figure 2.2.2 Observed trend in the electron density of the pyrrole A-ring and the isolated yield of rearrangement products.

To further assess the generality of this rearrangement, we then turned our attention to see if sidechains other than 2-hydroxypropyl groups would undergo the observe rearrangement. Towards this goal, we synthesized butyl and allyl alkylated ketopyrrolophane analogs **21** and **22,** done by simply changing the electrophile used in the ketopyrrolophane alkylation reaction, and condensed them with methoxy bispyrrole **3** (**Scheme 2.2.4**).

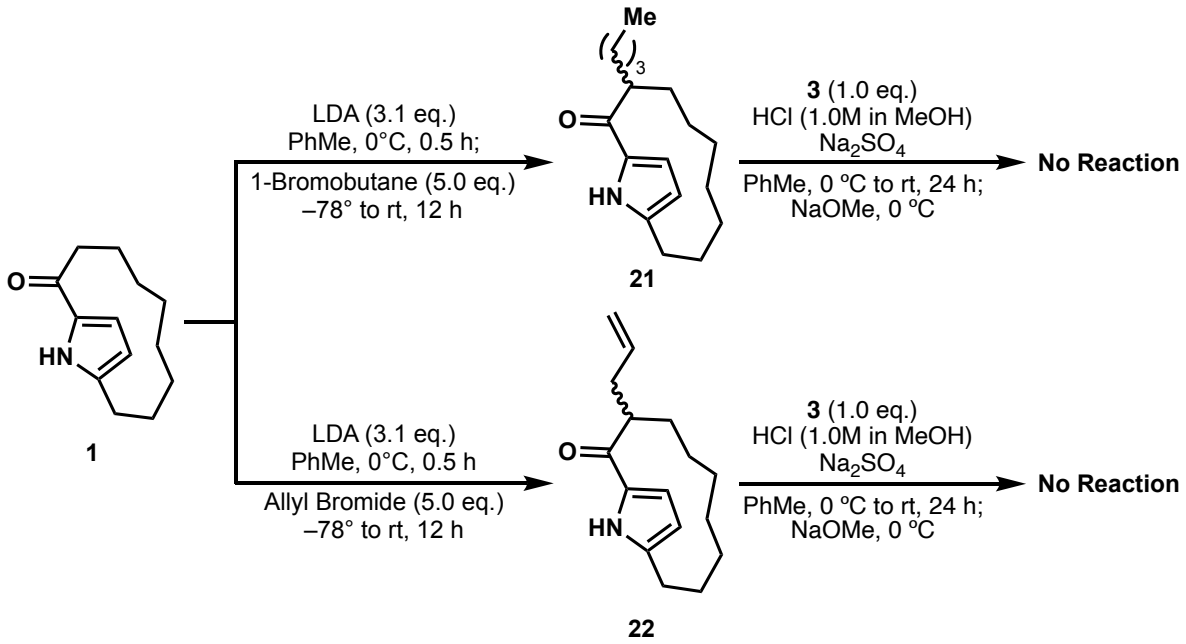

Scheme 2.2.4 Condensation of differentially alkylated ketopyrrolophane analogs **21** and **22** with methoxy bispyrrole **3.**

To our surprise, these reactions failed to yield any products resulting from condensation and returned only starting materials, even when left for extended periods of time. As a control, we condensed non-alkylated ketopyrrolophane **1** with methoxy-bispyrrole **3** in a similar manner which resulted in the isolation of condensation product **23** in 48% isolated yield (**Scheme 2.2.5**). From these experiments, we concluded that α-substitution of ketopyrrolophane **1** creates steric interference which prevents effective condensation with the ketopyrrolophane ketone. In the case of 2-hydroxypropyl alkylated **2**, we hypothesize that the steric bulk created by α-substitution is

mitigated by activation of the ketone via the formation of an oxonium containing tetrahydrofuran intermediate under the acidic condition of the reaction as shown in **Scheme 2.1.2**.

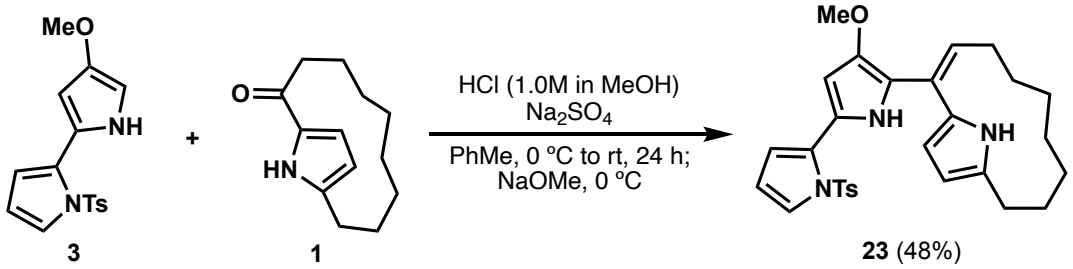

Scheme 2.2.5 Control condensation reaction between methoxy bispyrrole **3** and ketopyrrolophane **1**.

To test this hypothesis, we synthesized 2-hydroxybutyl alkylated ketopyrrolophane **24**, utilizing (S)-butylene oxide in a manner analogous to the synthesis of **2**, and condensed it with methoxy bispyrrole **3** (**Scheme 2.2.6A**). To our satisfaction, this resulted in the isolation of tetrahydrofuran product **25** in 37% yield but to our surprise, failed to produce any product resulting from migration of the hydroxylbutyl sidechain. To further verify this hypothesis, we synthesized alkylated ketopyrrolophane analog **26**, via the acylation of **3** with pivalic anhydride, and attempted condensation with **3** (**Scheme 2.2.6B**). As expected, this failed to yield any condensation products, returning only alkylated starting material **26**.

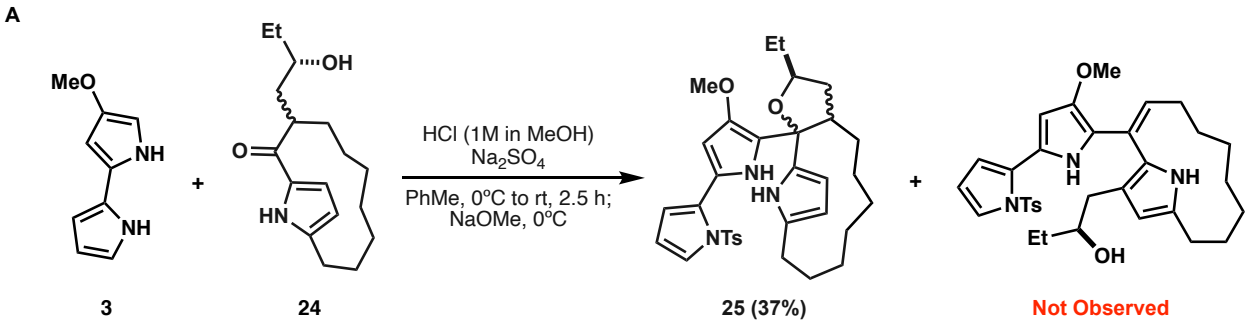

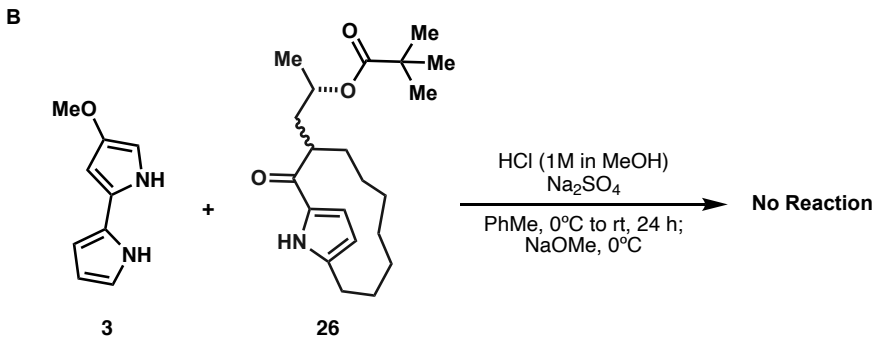

Scheme 2.2.6 Reactions designed to test oxonium intermediate hypothesis. (**A**) Condensation of 2-hydroxybutyl alkylated ketopyrrolophane **24** with methoxy bispyrrole **3**. (**B**) Condensation of alkylated ketopyrrolophane analog **26** with methoxy bispyrrole **3**.

While these findings supported our hypothesis as to the importance of a hydroxylated sidechain in condensation reactions utilizing α-alkylated ketopyrrolophanes, the lack of any observed rearrangement product in the reaction using **24** confounded us. For this reason, we decided to further explore the mechanism by which this perceived rearrangement occurred.

2.2.2 Exploration of Observed Rearrangement Mechanism

Upon the initial isolation and characterization of **6**, we attributed its formation to the result of a rare alkyl [1,7]-sigmatropic shift. While a plethora of examples exist for the [1,7]-sigmatropic hydrogen shifts[9-13], corresponding alkyl shifts are considerably rarer with far fewer examples cited in literature. Of the cited examples, the vast majority have been observed in high energy and/or strained systems.[14-15] Considering this observed trend, we felt that the instability of azafulvene intermediate **4** (**Scheme 2.1.2**), the direct product resultant from condensation between **2** and **3**, would be sufficiently high in energy to undergo such an alkyl chain migration. Mechanistically, we envisioned that this shift would proceed via migration of the 2-hydroxypropyl sidechain to the

C7 position of the ansa-bridged pyrrole ring (C-ring) with concomitant reorganization of the π-system followed by re-aromatization of the resulting 3H-pyrrole resulting in **6** (**Scheme 2.2.7**).

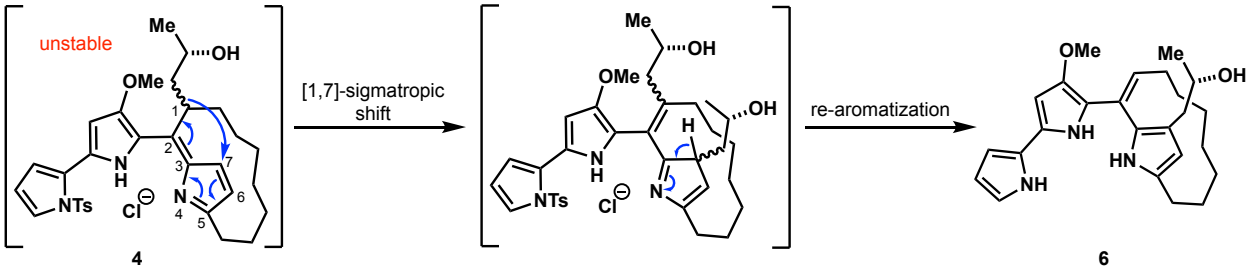

Scheme 2.2.7 Mechanistic hypothesis for a [1,7]-sigmatropic rearrangement leading to the formation of **6**.

To test this hypothesis, we began by re-acidifying a solution of iso-premarineosin **5** to see if it would undergo rearrangement. While reacidification of **5** did result in the successful formation of azafulvene intermediate **4**, as indicated by the appearance of a prototypical bright red color consistent with presence of a prodiginine chromophore, allowing the resulting solution to stir at room temperature overnight failed to yield any product resulting from rearrangement. This same experiment was done using iso-premarineosin analogs **19a**, **19b** and **19d** all of which failed to produce products resulting from rearrangement (**Scheme 2.2.8A**). To ensure that migration of the 2-hydroxypropyl side chain was not occurring prior to condensation of the two fragments, albeit how unlikely that might seem, a solution of alkylated ketopyrrolophane **3** was acidified and allowed to stir at room temperature overnight, resulting in the isolation of only starting material (**Scheme 2.2.7B**).

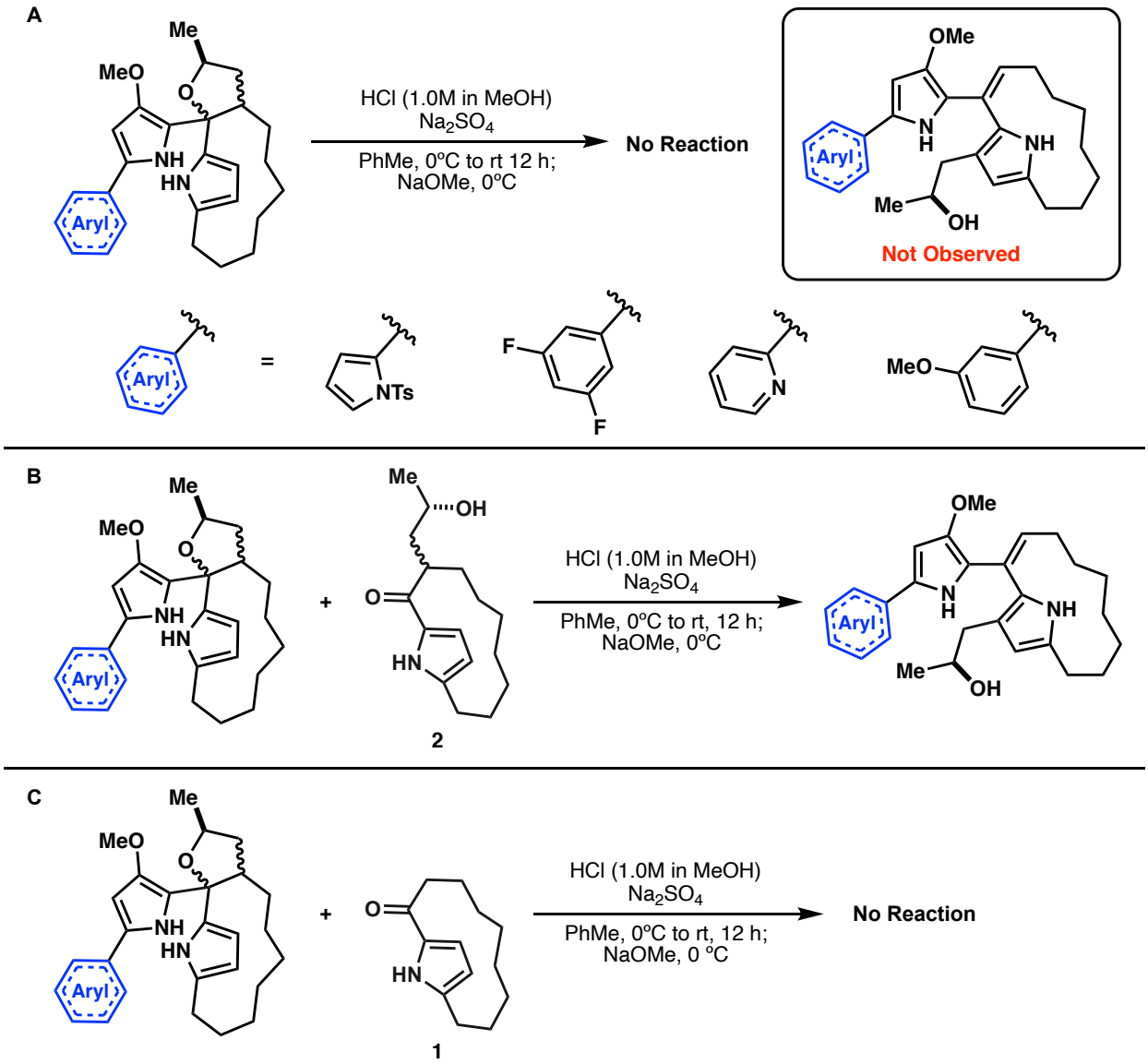

Scheme 2.2.8 (**A**) Re-acidification of iso-premarineosin **6** and related analogs failed to yield any products resulting from rearrangement indicating the mechanism of this migration to be inconsistent with a unimolecular [1,7]-sigmatropic rearrangement. (**B**) Acidification of the same compounds used in panel (**A**) in the presence of 1.0 eq. of **2** yielded rearrangements products with greater yield than ever observed indicating the operative mechanism to be bimolecular in nature. (**C**) Repeating the experiments depicted in panel (**B**) using ketopyrrolophane **1** failed to yield rearrangement products indicating the likelihood of some chain transfer process as shown in **Scheme 2.2.9**.

Realizing that these experimental results pointed to a mechanism other than a [1,7]-sigmatropic shift, we decided to re-attempt acidification of tetrahydrofuran **5** in the presence of an additional equivalent of 2-hydroxypropyl alkylated ketopyrrolophane **3**. To our utter

astonishment, this resulted in the isolation of **6** in yields higher than observed previously (39%). This same experiment was also carried out using iso-premarineosin analogs **19a**, **19b** and **19d** which yielded similar behavior, resulting in the isolation of rearrangement products **20a**, **20b** and **20d** in 22%, 31% and 43% yield respectively (**Scheme 2.2.8B**). Interestingly, control experiments done by reacidifying iso-premarineosin **5** as well as related analogs **19a**, **19b** and **19d** in the presence of ketopyrrolophane **1** (lacking the 2-hydroxypropyl side chain) failed to result in the formation of any products resulting from rearrangement (**Scheme 2.2.8C**). These results greatly indicate that the observed chain migration likely proceeds via a bimolecular reaction and not unimolecular [1,7]-sigmatropic rearrangement as originally postulated. Furthermore, these results also strongly suggests that alkyl chain's "migration" onto the B-ring pyrrole might actually be the resultant of an intermolecular transfer as opposed to an intramolecular migration as shown in **Scheme 2.2.9**.

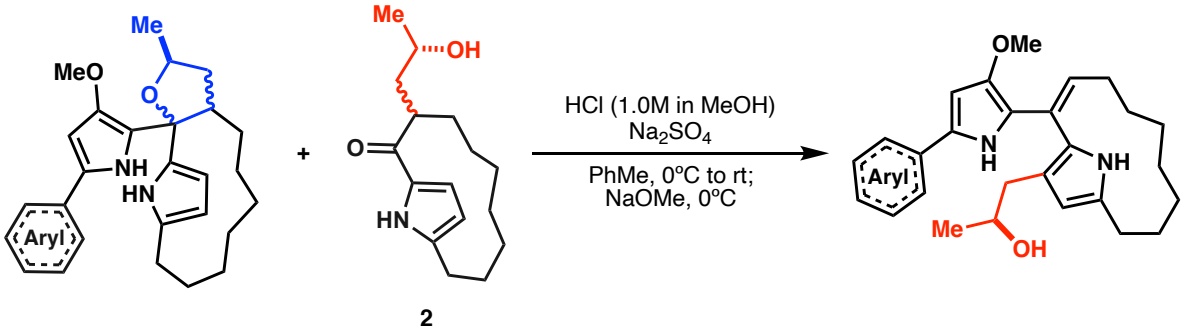

Scheme 2.2.9 Reaction depicting the idea that the "migrated" alkyl chain on the pyrrole B-ring might result from intermolecular transfer as opposed to intramolecular migration.

Lacking appropriate experimental evidence for this hypothesis and challenged to devise an alternative mechanism that might account for the formation of these rearranged products, we turned to collaboration with Professor Houk to see if computations might be able to narrow our mechanistic focus. These computations, conducted by Dr. Mark Maskeri, attempted to answer three guiding questions we felt were central to understanding the mechanism of this migration.

The first of these questions was, is the observed migrations truly bimolecular in nature? While logic suggests that the simplest mechanism for this observed rearrangement is unimolecular, experimental evidence supported a bimolecular mechanism to be operative. Secondly, if we are to assume that the isolated rearrangement products are the resultants of bimolecular processes, how does the 2-hydroxypropyl ketopyrrolophane facilitate this rearrangement in bimolecular manner? Lastly, we asked ourselves, if the observed rearrangement is the result of intermolecular chain transfer as opposed to intramolecular migration (as shown in **Scheme 2.2.9**), how is the migrating chain activated?

To answer the first of these guiding questions, DFT calculations were carried out on a model system to determine the energetic feasibility of a unimolecular [1,7]-sigmatropic rearrangement. These calculations (shown in **Figure 2.2.3**) show that the energy required for such a suprafacial rearrangement are prohibitively high from both the neutral and charged chromophore systems ($\Delta G^{\ddagger}$ 77.5 and 69.0 kcal/mol respectively). Realizing that the inherit topology of the molecule would not allow for such a rearrangement to occur in an antarafacially fashion, calculations for such pathway were not explored.

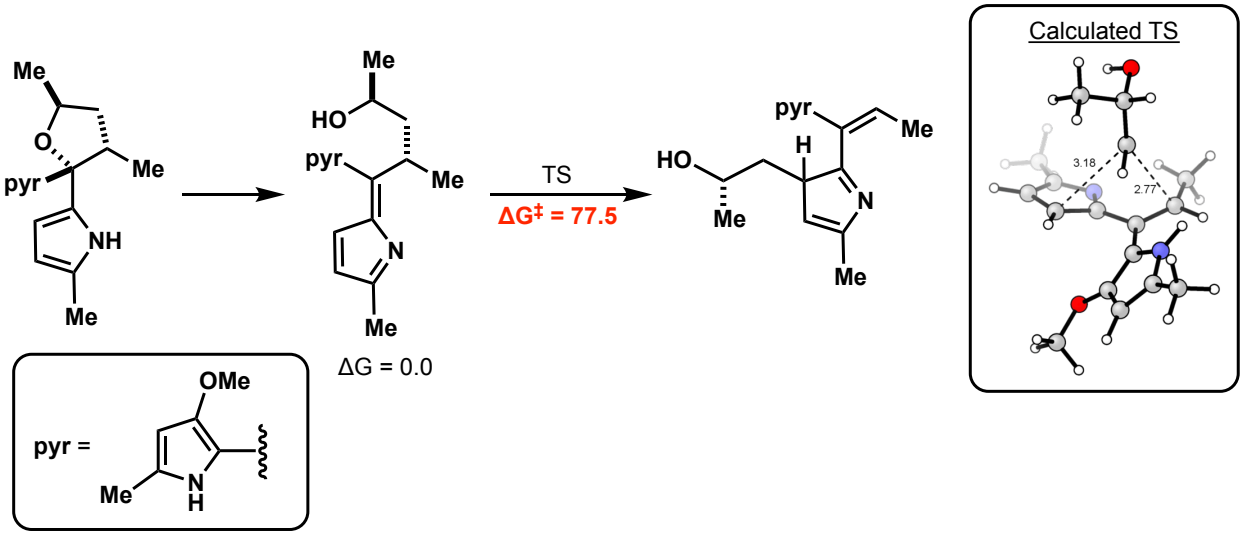

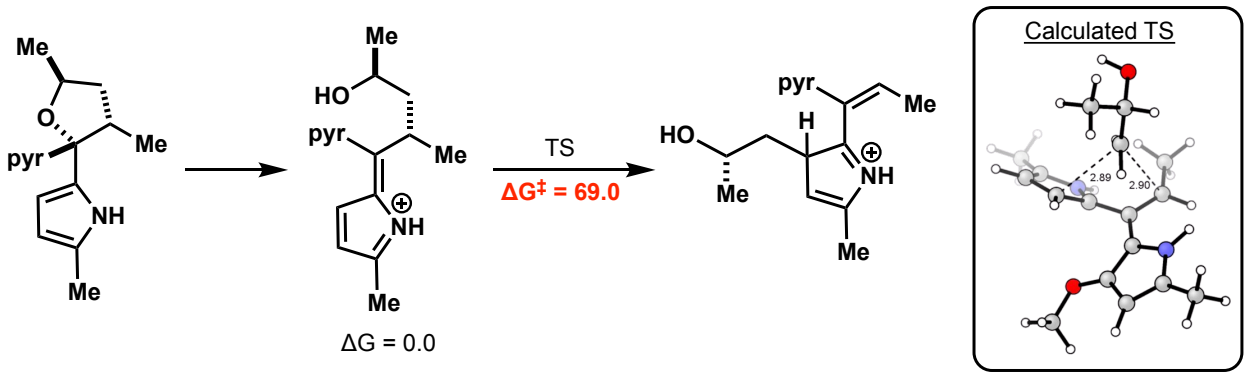

Figure 2.2.3 DFT calculations to determine the feasibility of a unimolecular, superficial [1,7]-sigmatropic rearrangement as the operative migration mechanism from both a neutral and charged chromophoric system. These calculations were carried out using the following parameters: ωB97X-D/def2-TZVPP/SMD(PhMe)//ωB97X-D/def2-SVP/SMD(PhMe), QH corrections (@298.15 K). Displayed energies are in kcal/mol (see Experimental Section for details).

Confident that the observed migration likely proceeds via some bimolecular pathway, a potential mechanism was proposed (**Scheme 2.2.10**). The proposed mechanism proceeds via the nucleophilic attack of the sidechain chiral center in **2**, activated as an oxonium ion under the acidic conditions of the reaction, by the C7 position of the C-ring pyrrole of **5**. Rearomatization of the C-ring followed by rebound nucleophilic attack of the sidechain C1 carbon results in a proposed strained cyclopropane containing system via phenonium-ion type elimination of enol-ketopyrrolophane **1**. Cyclopropane ring opening by water, released during the condensation reaction, is then thought to yield the 2-hydroxypropyl sidechain at the pyrrole C7 position with stereoinversion at the chiral center.

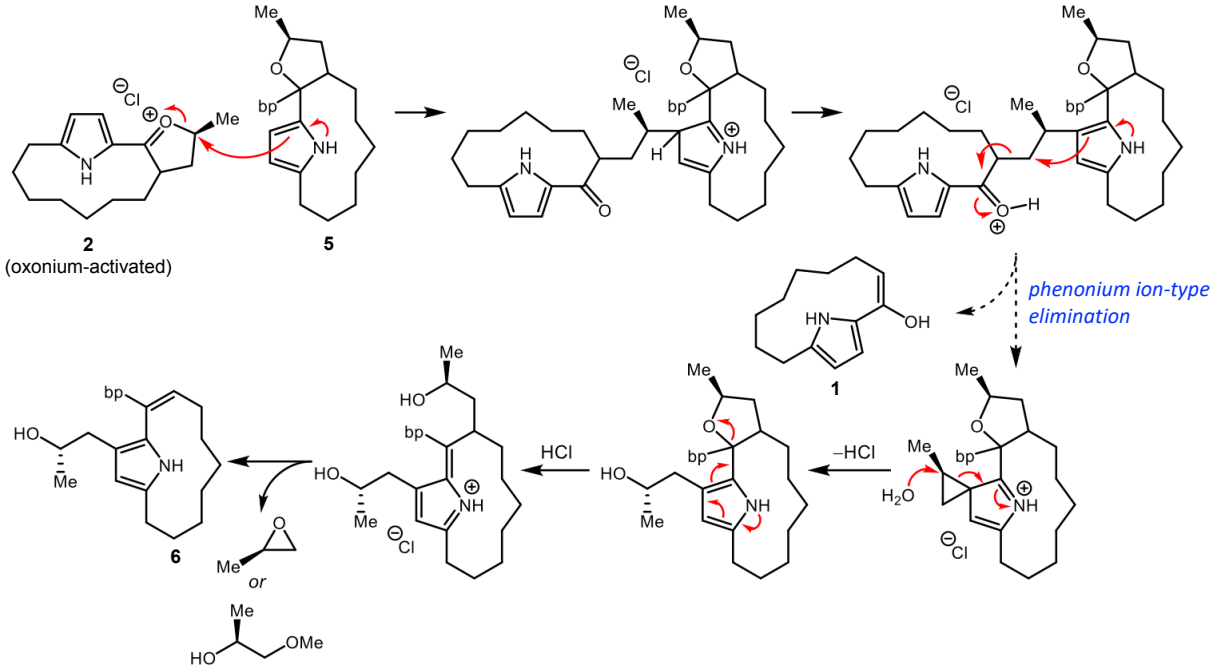

Scheme 2.2.10 Proposed bimolecular mechanism for the observed alkyl chain migration.

With the 2-hydroxypropyl sidechain from **2** successfully transferred to the condensation product, the system is then proposed to undergo acid promoted tetrahydrofuran ring opening followed by elimination of either propylene oxide or 1-methoxy-2-propanol via some unknown mechanism. Calculation of the energetics of this pathway is shown in **Figure 2.2.4** – **2.2.6**. Unfortunately, these calculations suggest that the phenonium ion-type elimination of **1** to be prohibitively high in energy ($\Delta G^{\ddagger}$ = 47 kcal/mol). In addition, a plausible transition state for the elimination of the "un-migrated" 2-hydroxypropyl sidechain, as either propylene oxide or 1-methoxypropan-2-ol, could not be ascertained. For these reasons, we have severe reservations about the validity of this mechanism but do feel it contains components which speaks to the feasibility of other predicated steps.

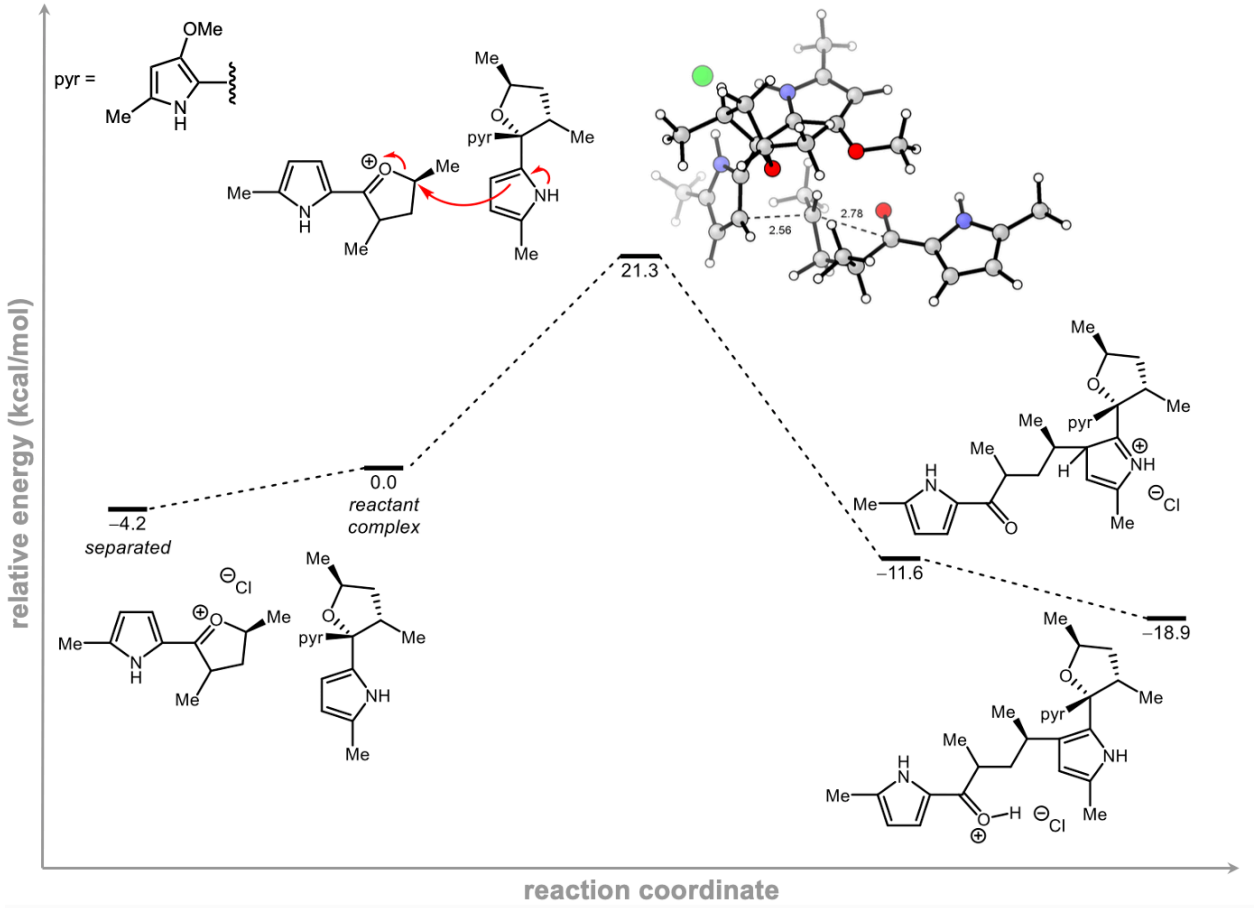

Figure 2.2.4 DFT calculations related to the nucleophilic attack of the sidechain chiral center in **2** by the C7 position of the C-ring pyrrole of **5** followed by rearomatization of the C-ring pyrrole as shown in **Figure 2.2.3**. To simplify calculations, the ansa-bridge of both 2-hydroxypropyl alkylated ketopyrrolophane **2** and condensation product **5** were removed. These calculations were carried out using the following parameters: ωB97X-D/def2-TZVPP/SMD(PhMe)//ωB97X-D/def2-SVP/SMD(PhMe), QH corrections (@298.15 K) (see Experimental Section for details).

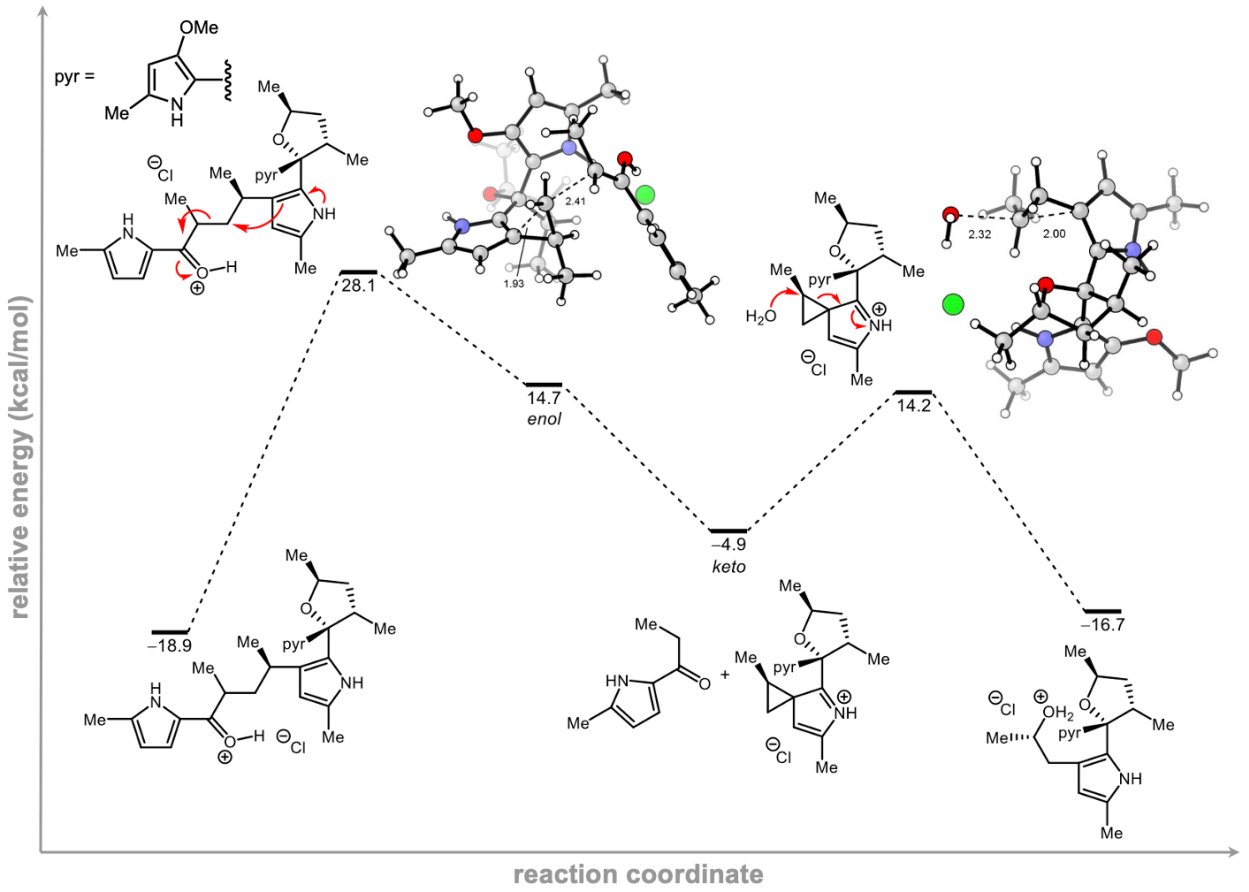

Figure 2.2.5 DFT calculations related to the rebound nucleophilic attack of the 2-hydroxypropyl sidechain C1 carbon resulting in the formation of a cyclopropane ring via phenonium-ion type elimination followed by opening of the cyclopropane ring by water as shown in **Figure 2.2.3**. See **Figure 2.2.4** and Experimental Section for computational details.

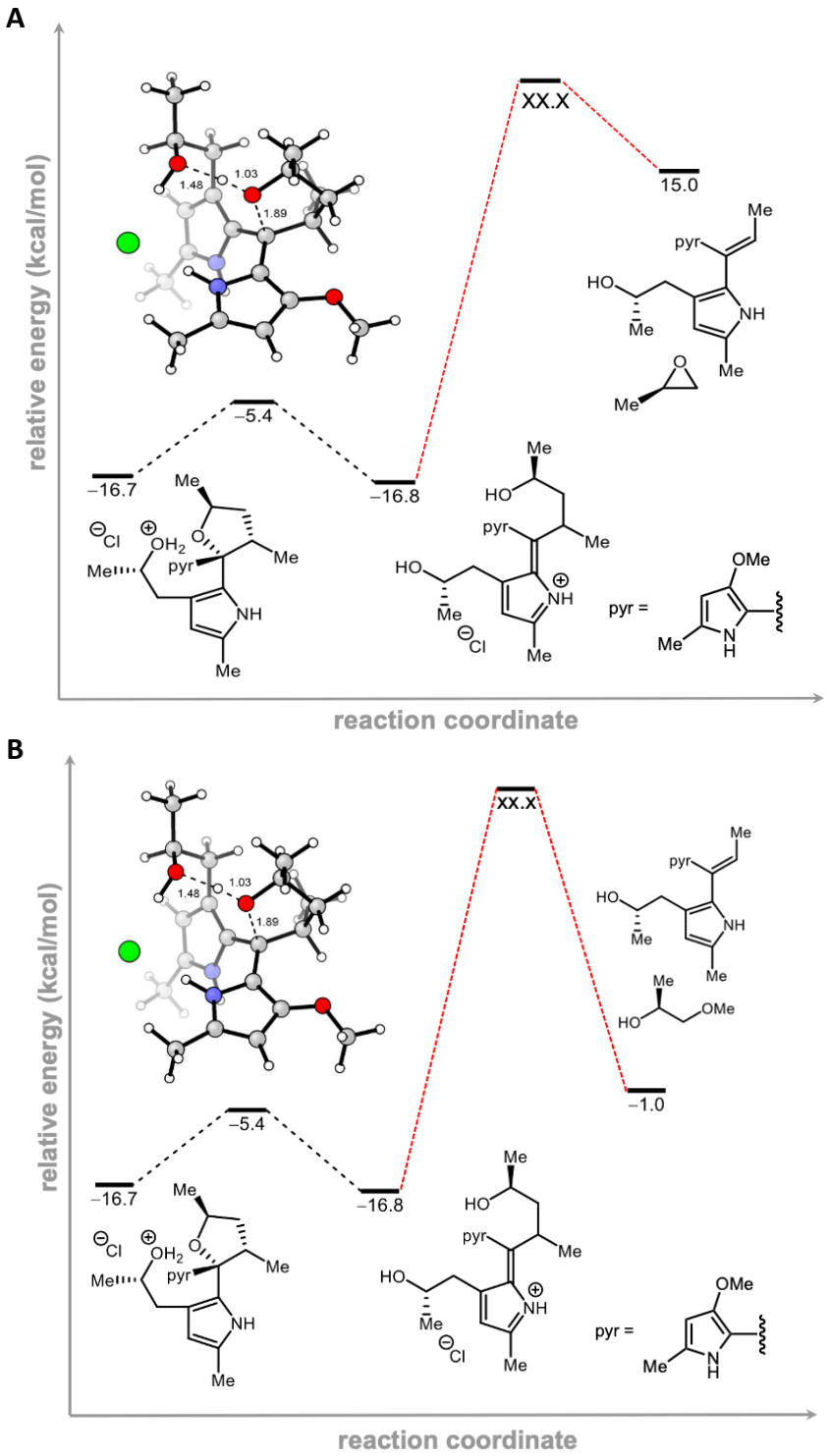

Figure 2.2.6 (**A**) DFT calculations related to the opening of the tetrahydrofuran ring under acidic conditions followed by the elimination of the 2-hydroxylpropyl sidechain as propylene oxide as shown in **Figure 2.2.3**. (**B**) DFT calculations related to the opening of the tetrahydrofuran ring under acidic conditions followed by the elimination of the 2-hydroxylpropyl sidechain as 1-methoxypropan-2-ol as shown in **Figure 2.2.3**. See **Figure 2.2.4** and Experimental Section for computational details.

While the calculations outlined above cast great doubt towards an operative mechanism which proceeds via the release of the propylene oxide, we decided to further explore this potential reaction pathway via experimentation. This was done by conducting condensation reactions between **2** and **3** under previously described conditions monitoring both the reaction mixture as well as the head space above the reaction via GCMS for any trace of propylene oxide. To our dismay, no propylene oxide, or related products thereof, were detected at any point during the progress of the reaction. While this finding does not definitively eliminate the possibility of a mechanism which proceeds via the release of propylene oxide, it does cast doubt on that hypothesis.

To entertain the possibility that our structural assignment for these migration products might be incorrect, we attempted to grow crystals of all isolated rearrangements products which showed the potential to be crystalline so that their structure could be verified via x-ray crystallography and/or MicroED. From these attempts, no analyzable crystals were isolated. For this reason, we derivatized the migrated sidechain of **6** hoping that these products would be more crystalline. These derivatives, as well as the rearrangement products we attempted to recrystallize, are shown in **Figure 2.2.7**. Unfortunately, all attempts to recrystallize these derivatives failed despite having screen a great number of conditions. To date, we are still working to grow crystals of these products as well as related analogs so that our structural assignment of these unique products can be definitively verified.

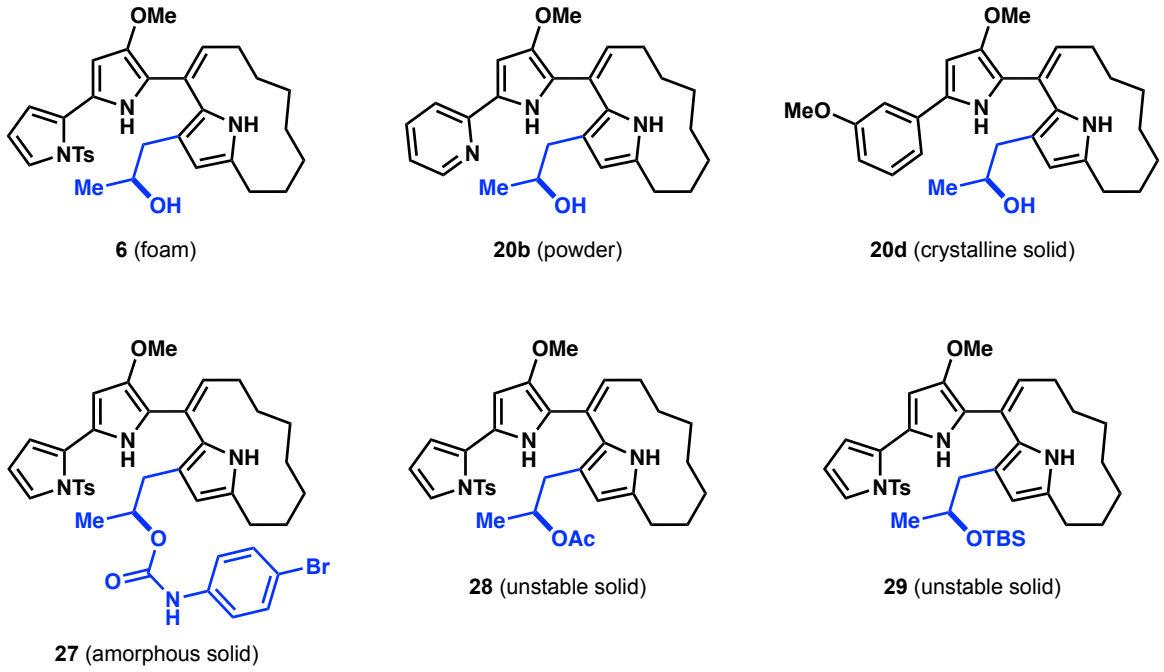

Figure 2.2.7 Rearrangement compounds and analogs thereof used for recrystallization attempts for structure verification.

2.3 Conclusion

In our 2019 published route to (+)-marineosin A, the prototypical tripyrrolic prodiginine core was established via the condensation of a nucleophilic methoxy-bispyrrole fragment with an α-branched 2-hydroxypropyl ketopyrrolophane. Allowing this condensation reaction to stir for extended periods of time at room temperature before quenching resulted in diminished yields of the desired condensation product along with the isolation of a product appearing to result from the migration of the 2-hydroypropyl sidechain onto the proximal C3 pyrrole position. To better understand the nature of this unprecedented rearrangement, the propensity for the observed migration was probed via the utilization of electronically perturbed analogs of the methoxy-bispyrrole system as well as differentially alkylated α-branched ketopyrrolophanes. From these experiments, we found that while the presence of the methoxy group on the bispyrrole B-ring is

not necessary for condensation to occur, it is necessary for the observed migration and that increasing electron density in the pyrrole A-ring results in higher isolated yields of the rearrangement product. In addition, we observed that the use of non-hydroxyl containing α-branched ketopyrrolophanes in these reactions failed to yield any condensation products. This led us to hypothesize that the presence of the sidechain C2 hydroxyl group is necessary when using α-branched ketopyrrolophanes as it allows for the formation of an activated oxonium ion which counteracts the steric encumbrance created by the α-branching.

Towards elucidation of an operative mechanism for this migration, we explored the potential that the isolated rearrangement product might be the result of a rare alkyl [1,7]-sigmatropic shift. While this explanation seemed the most likely, both experimentation and DFT calculations carried out in collaboration with the Houk group, showed this scenario to be unlikely. To our surprise, continued experimentation eventually provided evidence that this migration might actually be the result of a bimolecular process. While this finding was supported by further experimentations, DFT calculations were unable to provide a computationally supported bimolecular mechanism for the formation of the rearrangement products.

Finally, attempts to confirm the absolute structure of the rearrangement products using x-ray crystallography and/or MicroED were undertaken via attempted recrystallization of isolated products as well as derivatives thereof. To date, the operative mechanism for this alkyl chain migration is unknown and the absolute structure of these rearrangement products await definitive characterization via crystal analysis methods. Despite this, we feel that our current understanding of this rare migration, albeit limited, is of great value as it allows for the design and synthesis of unique prodiginine analogs which have the potential for a wide variety of interesting and impact biological activities.

2.4 Experimental Section

General Methods and Materials

Unless otherwise specified, reactions were performed in flame-dried glassware under an atmosphere of argon using anhydrous solvents. Reagents were purchased from commercial vendors and used as received unless otherwise stated. Tetrahydrofuran (THF), diethyl ether (Et_2O), acetonitrile (MeCN) and toluene (PhMe) were passed through a Glass Contour solvent drying system. Anhydrous N,N dimethylformamide (DMF) was purchased from Supelco, Inc – Sigma Aldrich. Yields refer to chromatographically and spectroscopically (^{1}H-NMR) homogeneous materials, unless otherwise stated. Thin-layer chromatography (TLC) was conducted on precoated plates (Sorbent Technologies, silica gel 60 PF254, 0.25 mm) visualized with UV 254 nm. For acid-sensitive compounds, TLC plates were neutralized with TEA/Hexane (1%) before use. Column chromatography was performed on silica gel 60 (SiliCycle, 240−400 mesh). Purification of peptides was performed using an Agilent 1200 HPLC system equipped with G1361A preparative pumps, a G1314A auto sampler, a G1314A VWD, a G1364B automated fraction collector, and a Waters Sunfire C18 column (5 μm, 19 mm × 250 mm), unless otherwise noted. 0.1% TFA in MeCN/H_2O solvent system. Analytical HPLC was performed using the same system, but with a G1312A binary pump. 0.1% TFA in MeCN/H_2O solvent system. Mass spectra were recorded using an Agilent 6130 LC/MS system equipped with an ESI source. High-resolution mass spectra were recorded on Thermo Scientific Exactive® Mass Spectrometer with DART ID-CUBE Waters GST Premier, Waters LCT Premier, and Agilent 6545 LC-QTOF. NMR spectra were recorded on Bruker Avance spectrometers (400/100 MHz, 500/125 MHz, and 600/150 MHz). NMR spectra were recorded on Bruker Advance (300, 400, 500, or 600 MHz) spectrometers. HSQC, HMBC,

and COSY NMR experiments were used to aid assignment of NMR peaks when required. All ^{19}F NMR spectrums used $CFCl_3$ as a calibration standard.

General Experimental Procedures

General Procedure for the Alkylation of Ketopyrrolophane **1**

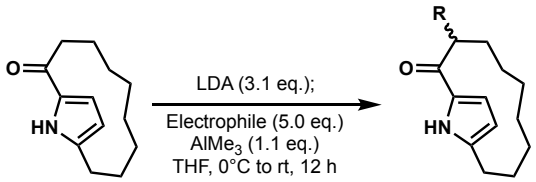

1

To a flame-dried 3-neck 100 mL round bottom flask, equipped with a low-temperature thermometer and a stir bar, was added anhydrous THF (10 mL) and *i*Pr_2NH (0.9 mL, 6.2 mmol, 3.2 eq.) after which, the resulting solution was then cooled to –78°C. To this solution was added n-BuLi (2.5 M in hexane, 2.5 mL, 6.2 mmol, 3.1 eq.) dropwise. Once done, the resulting colorless solution was stirred for 10 min at –78°C and then warmed up to 0°C. The solution of **1** (410 mg, 2 mmol, 1.0 eq.) in anhydrous THF (30 mL) was added into the formed LDA solution via syringe pump over 3 h while maintaining the LDA solution at 0°C. The resulting light yellow solution was then stirred for another 30 min at 0°C, and then cooled to –78°C. Once done, the appropriate electrophile (5.0 eq.) was added followed by a $AlMe_3$ solution (2.0 M in hexane, 1.1 mL, 2.2 mmol, 1.1 eq.) if appropriate. The reaction mixture was stirred at –78°C for another 30 min, slowly warmed up to rt over 1 h, and then allowed to stir at rt overnight. To quench the reaction, the mixture was carefully added into a stirred solution of potassium sodium tartrate and ice which was then extracted with EtOAc (process repeated 3x). The organic layers were then combined, washed with brine, dried over Na_2SO_4, filtered, concentrated, and purified by flash column chromatography using TEA neutralized silica gel using a EtOAc in Hexane eluding system.

General Procedures for the Synthesis of Methoxy-Pyrrole Aryls

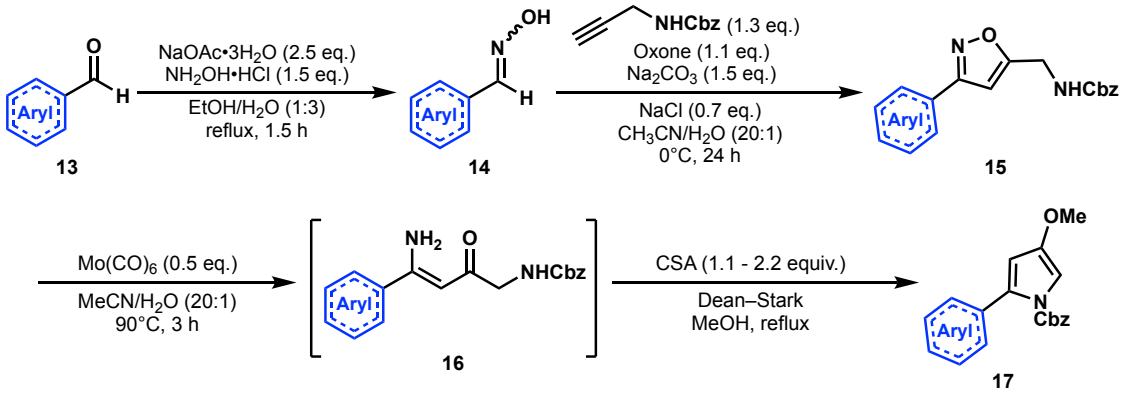

Scheme 2.2.11 General route for the synthesis of methoxy-pyrrole aryl nucleophiles.

Methoxy pyrrole-aryl compounds were synthesized using modified procedures based on references 7 and 8.

General Procedure for the Synthesis of Aryl-Oximes **14**

To a 500mL round bottom flask, equipped with a stir bar, was added Aryl-Aldehydes **13** (110 mmol, 1.0 eq), sodium acetate trihydrate (275 mmol, 2.5 eq.) and hydroxylamine hydrochloride (165 mmol, 1.5 eq.) followed by a 1:3 Ethanol/Water solution (180 mL). The reaction vessel was then equipped with a water jacketed condenser and heated to reflux. Once done, the reaction mixture was left to reflux while stirring under an atmosphere of argon gas for 1.5 h. After this time, the reaction was cooled to room temperature and extracted with DCM (process repeated 3x). The isolated organic layers were then combined, washed with brine, dried over $MgSO_4$, filtered and concentrated. The isolated crude products from these reactions were carried directly forward to the next reaction without any further purification.

General Procedure for the Synthesis of Aryl-Isoxazoles **15**

To a 1000mL round bottom flask, equipped with a stir bar, was added Aryl-Oximes **14** (80 mmol, 1.0 eq), Cbz-protected propargylamine (104 mmol, 1.3 eq.), sodium chloride (56 mmol, 0.7 eq.) and sodium carbonate (120mmol, 1.5 eq.) followed by 20:1 MeCN/H_2O solution (350 mL). The resulting reaction mixture was then sparged with argon gas for 30 min after which, Oxone® (88 mmol, 1.1 eq.) was added. Once done, the reaction was stirred at 0°C for 24 h under an atmosphere of argon gas. After this time, the mixture was filtered through celite and the resulting filtrate washed with a sat. $NaHCO_3$ solution, a sat. $Na_2S_2O_3$ solution, brine, dried over Na_2SO_4, filtered, concentrated and purified via flask column chromatography using a EtOAc in Hexane eluding system.

General Procedure for the Synthesis β-Keto Enamine **16**

To a 500mL round bottom flask, equipped with a stir bar, containing an argon sparged 20:1 MeCN/H_2O solution (200mL) was added molybdenum hexacarbonyl (10 mmol, 1.0 eq.). The resulting suspension was then heated to 90°C until all solids dissolved (~15 min) after which, the transparent light-yellow solution was cooled to rt. To this solution was added a solution of Aryl-Isoxazoles **15** (10 mmol, 1.0 eq.) dissolved in a 20:1 MeCN/H_2O solution (40 mL) dropwise over 1 h. Once complete, the reaction vessel was equipped with a water jacketed reflux condenser and heated to reflux where it was left to stir under an atmosphere of argon gas for 3 h. After this time, the product mixture was concentrated and to the resulting brown solid was added 50 mL of EtOAc followed by 11.0 g of silica gel after which, the resulting mixture was vigorously stirred while air was bubble through it for 1 h. Once done, the resulting slurry was filtered through celite and the resulting filtrate concentrated. The isolated crude products from these reactions were carried directly forward to the next reaction without any further purification.

General Procedure for the Synthesis of Methoxy Pyrrole-Aryls **17**

To a flame-dried 250mL round bottom flask, equipped with a stir bar, containing β-Keto Enamines **16** (10 mmol, 1.0 eq.) was added camphorsulfonic acid (11 mmol, 1.1 eq.) followed by anhydrous MeOH (66 mL). Note: Synthesis of the methoxy-pyrrole pyridyl heterobiaryl system required the use of 2.2 eq. of camphorsulfonic acid . Once done, the reaction vessel was equipped with a Deak–Stark apparatus (the collection arm of which was filled with activated 3Å molecular sieves) and the reaction was heated to reflux where it was left to stir under an atmosphere of argon gas until TLC analysis indicated complete consumption of the starting material. After this time, the reaction was concentrated and the resulting solids diluted with EtOAc. The resulting solution was then washed with sat. $NaHCO_3$ solution, brine, dried over $MgSO_4$, filtered, concentrated and purified via flask column chromatography using a EtOAc in Hexane eluding system.

General Procedure for the Cbz-Deprotected of Methoxy Pyrrole-Aryls

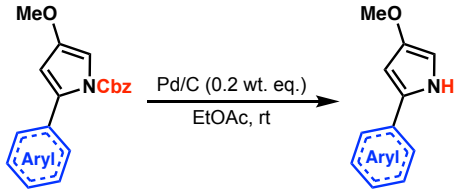

Before their use in condensation reactions, all Cbz-protected methoxy-pyrrole aryls were Cbz-deprotected using the procedure outlined below. Due to their instability in air, these deprotected products were not subjected to characterization:

To a 50 mL round bottom flask, equipped with a stir bar, was added Cbz-protected methoxy-pyrrole aryls (0.7 mmol, 1.0 eq.) and Pd/C (0.2 wt. eq.) followed by EtOAc (7 mL). Once done, the reaction vessel was evacuated of air and the atmosphere replaced with hydrogen gas after which, the reaction was left to stir at rt until TLC indicated complete conversion of the starting material. After this time, the reaction mixture was filtered through celite and the resulting filtrate

concentrated via rotary evaporation (making sure to back fill the rotary evaporation apparatus with argon gas). The isolated crude products from these reactions were then carried directly forward to the next reaction without any further purification. Note: Because nearly all of the products isolated from these reactions were found to be air sensitive, handling of the concentrated products were minimized to prevent further degradation.

General Procedure for the Condensation of Methoxy Pyrrole-Aryls with Ketopyrrolophanes

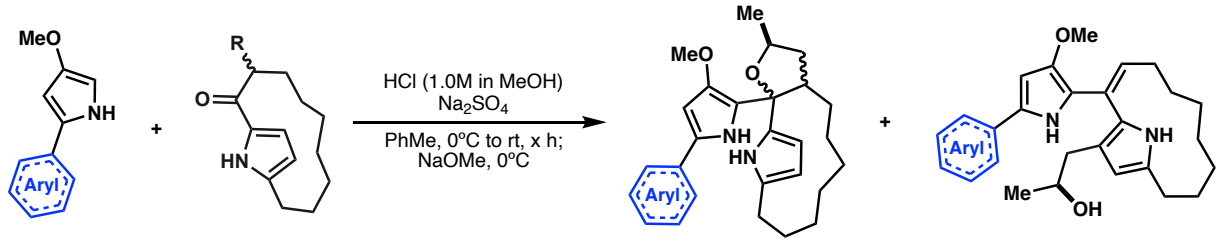

To a flame-dried 50 mL round bottom flask, equipped with a stir bar, was added ketopyrrolophanes (2.6 mmol, 1.0 eq.) and Na_2SO_4 (2.6 g) followed by of PhMe (26 mL, 0.1M) after which, the resulting solution was cooled to 0°C. To the reaction mixture was added a solution of Cbz-deprotected methoxy pyrrole-aryls (2.6 mmol, 1.0 eq.) dissolved in PhMe (26 mL, 0.1M) dropwise over 30 min. Upon the first drop of this solution being added to the reaction mixture, HCl (3.9 mL, 1M in MeOH, 1.5 eq.) was rapidly added, causing the reaction mixture to turn bright pink to dark purple in color. To quench the reaction, a freshly prepared solution of NaOMe in MeOH (10 mL 3.85 eq.) was added to the reaction mixture at 0°C after which, the resulting solution was added dropwise into ice-water which was then extracted with EtOAc (process repeated 3x). The organic layers were then combined, washed with brine, dried over Na2SO4, filtered, and concentrated. The resulting crude product was immediately purified via flash column chromatography using a EtOAc in Hexane eluding system.

Experimental Procedures and Product Characterization

1[1]*H*-1(2,5)-pyrrolacyclodecaphan-2-one (**1**)

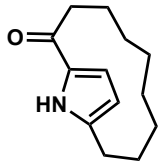

The experimental procedure for the synthesis of **1** can be found in our 2019 publication of the total synthesis of (+)-Marineosin A.[1] **1** was isolated as a white solid. **^{1}H-NMR** ($CDCl_3$, 500 MHz,) δ 8.73 (s, 1H), 6.98 (t, *J* = 3.2 Hz, 1H), 6.09 (t, *J* = 3.2 Hz, 1H), 2.78 – 2.73 (m, 2H), 2.68 (t, *J* = 6.3 Hz, 2H), 1.79 (tq, *J* = 13.6, 6.8, 6.1 Hz, 4H), 1.60 – 1.49 (m, 2H), 1.37 (p, *J* = 6.0 Hz, 2H), 1.21 (p, *J* = 6.9 Hz, 2H), 1.08 (ddt, *J* = 12.3, 8.9, 5.4 Hz, 2H); **^{13}C-NMR** ($CDCl_3$, 126 MHz): 190.3, 137.9, 132.3, 115.9, 111.5, 36.1, 27.0, 26.7, 26.2, 23.5, 23.4, 23.3, 21.7; **HRMS** (EI) calculated for $C_{13}H_{20}NO$ $[M + H]^+$: 206.1545, found 206.1541 (1.9 ppm mass defect)

3-((*S*)-2-hydroxypropyl)-1[1]*H*-1(2,5)-pyrrolacyclodecaphan-2-ones (**2**)

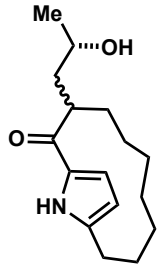

Synthesized following the general procedure for the alkylation of ketopyrrolophane **1** (outlined above) using (S)-propylene oxide as the electrophile along with the use of $AlMe_3$. **2** was isolated as a mixture of diastereomers as a light-yellow foam (71% yield, 2:1 d.r). (*S*)-3-((*S*)-2-hydroxypropyl)-11*H*-1(2,5)-pyrrolacyclodecaphan-2-one (**2S**): **^{1}H-NMR** (C_6D_6, 500 MHz,) δ 9.23 (s, 1H), 7,22 (dd, *J* = 2.7, 3.7 Hz, 1H), 5.94 (t, *J* = 2.7 Hz, 1H), 3.70 – 3.80 (m, 1H), 3.25 – 3.32 (m,1H), 2.49 (td, *J* = 3.9, 15.5 Hz, 1H), 2.15 – 2.32 (m, 3H), 1.63 – 1.72 (m, 1H), 1.50 – 1.61 (m, 2H), 1.40 − 1.11 (m, 5H), 1.09 (d, *J* = 6.2 Hz, 3H), 0.99 − 0.80 (m, 5H); **^{13}C-NMR** (C_6D_6, 126

MHz) δ 193.0, 138.1, 133.8, 116.2, 111.6, 67.0, 41.52, 41.50, 35.2, 27.2, 27.0, 24.5, 24.3, 24.1, 24.0, 22.5; **HRMS** (EI) calculated for $C_{16}H_{25}NO_2$ $[M]^+$: 263.1885, found: 263.1876 (3.4 ppm mass defect). (R)-3-((S)-2-hydroxypropyl)-11H-1(2,5)-pyrrolacyclodecaphan-2-one (**2R**): **^{1}H-NMR** (C_6D_6, 500 MHz,) δ 9.14 (s, 1H), 7,25 (t, *J* = 3.0 Hz, 1H), 5.94 (t, *J* = 3.0 Hz, 1H), 3.81 – 3.79 (m, 1H), 3.47 – 3.43 (m, 1H), 2.45 – 2.40 (m, 1H), 2.38 – 2.35 (m, 1H), 2.23 – 2.16 (m, 1H), 1.77 – 1.75 (m, 1H), 1.65 – 1.60 (m, 1H), 1.51 – 1.49 (m, 1H), 1.40-1.03 (m, 7H), 1.00 (d, *J* = 6.2 Hz, 3H), 0.98 – 0.75 (m, 4H); **^{13}C-NMR** (C_6D_6, 126 MHz,) δ 192.0, 137.9, 134.3, 115.9, 111.6, 66.4, 42.1, 41.1, 35.7, 27.2, 26.9, 24.9, 24.4, 24.1, 24.0, 22.3; **HRMS** (ESI) calculated for $C_{16}H_{25}NO_2$ $[M]^+$: 263.1885, found: 263.1874 (4.2 ppm mass defect).

Benzyl 4-methoxy-1'-tosyl-1*H*,1'*H*-[2,2'-bipyrrole]-1-carboxylate (Cbz-Protected **3**)

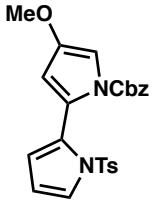

Synthesized following the general route for the synthesis of methoxy-pyrrole aryl nucleophiles (shown in **Scheme 2.2.8**). **3** was isolated as a white solid. **^{1}H-NMR** ($CDCl_3$, 500 MHz) δ 7.42 (d, J = 8.2 Hz, 2H), 7.34-7.31 (m, 3H), 7.28-7.23 (m, 3H), 7.18 (d, J = 8.1 Hz, 2H), 6.94 (d, J = 2.0 Hz, 1H), 6.18-6.16 (m, 2H), 5.68 (d, J = 2.1 Hz, 1H), 5.16 (bs, 2H), 3.74 (s, 3H), 2.36 (s, 3H); **^{13}C-NMR** ($CDCl_3$, 126 MHz) δ 150.0, 148.9, 144.7, 135.8, 134.7, 129.5, 128.5, 128.46, 128.4, 127.2, 125.5, 123.3, 121.5, 116.8, 111.3, 110.2, 102.4, 68.8, 57.5, 21.6; **HRMS** (ESI) calculated for $C_{24}H_{23}N_2O_5S$ $[M+H]^+$: 451.1328, found 451.1324 (0.9 ppm mass defect).

(2^5S)-2^2-(4-methoxy-1'-tosyl-1*H*,1'*H*-[2,2'-bipyrrol]-5-yl)-2^5-methyl-2^2,2^3,2^4,2^5-tetrahydro-1^1H-1(2,5)-pyrrola-2(2,3)-furanacyclononaphane (**5**)

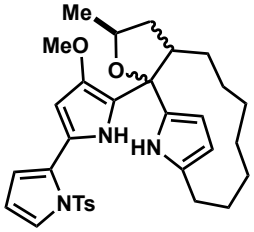

Synthesized following the general procedure for the condensation of methoxy pyrrole-aryls with ketopyrrolophanes quenching the reaction immediately after addition of the methoxy pyrrole-aryl solution was complete. **5** was isolated as a mixture of diastereomers as a tan foam (87% yield, 1:1 d.r) **^{1}H-NMR** ($CDCl_3$, 500 MHz,) δ 8.96 (s, 1H), 8.84 (s, 1H), 8.76 (s, 1H), 8.69 (s, 1H), 7.39 – 7.36 (m, 2H), 7.26 (d, *J* = 3.0 Hz, 2H), 7.25 (d, *J* = 3.0 Hz, 2H), 6.92 (d, *J* = 8.0 Hz, 2H), 6.83 (d, *J* = 8.0 Hz, 2H), 6.23 (t, *J* = 3.3 Hz, 2H), 6.18 (ddd, *J* = 3.3, 1.8, 9.1Hz, 2H), 6.01 (dq, *J* = 3.1, 2.8Hz, 2H), 6.01 (dd, *J* = 3.2, 7.4 Hz, 2H), 5.82 (dt, *J* = 14.8, 2.8 Hz, 2H), 4.45 – 4.38 (m, 1H), 4.20 – 4.14 (m, 1H), 3.83 (s, 3H), 3.8o (s, 3H), 2.87 (q, *J* = 7.5 Hz, 1H), 2.76 (t, *J* = 6.1 Hz, 1H), 2.72-2.51 (m, 4H), 2.28 (s, 3H), 2.24 (s, 3H), 2.22 – 2.16 (m, 1H), 1.88 – 1.83 (m, 1H), 1.79 – 1.72 (m, 1H), 1.69 – 1.58 (m, 2H), 1.57 – 1.42 (m, 6H), 1.39 (d, *J* = 6.2 Hz, 3H), 1.35 (d, *J* = 6.2 Hz, 3H), 1.32 – 0.84 (m, 15H), 0.82 – 0.75 (m, 1H), 0.74 – 0.65 (m, 1H); **^{13}C-NMR** ($CDCl_3$, 126 MHz) δ 144.7, 144.6, 141.6, 139.7, 134.7, 134.5, 133.4, 132.2, 131.3 130.9, 129.5, 129.4, 127.60, 127.56, 127.52, 127.4, 123.3, 123.11, 123.08, 121.6, 115.3, 114.9, 114.5, 114.1, 111.3, 111.1, 106.2, 105.3, 105.0, 104.9, 100.0, 99.9, 85.2, 84.5, 75.5, 73.7, 58.82, 58.80, 48.1, 48.0, 42.1, 41.0, 31.6, 31.5, 29.5, 28.2, 27.8, 27.3, 26.8, 26.7, 25.8, 25.5, 25.4, 23.8, 22.7, 21.6, 21.5, 21.3, 14.2, 14.1; **HRMS** (ESI) calculated for $C_{32}H_{40}N_3O_4S$ $[M + H]^+$: 562.2734, found: 562.2723 (2.0 ppm mass defect).

(*S*,*E*)-1-(2-(4-methoxy-1'-tosyl-1*H*,1'*H*-[2,2'-bipyrrol]-5-yl)-1^{1}*H*-1(2,5)-pyrrolacyclodecaphan-2-en-1^{3}-yl)propan-2-ol (**6**)

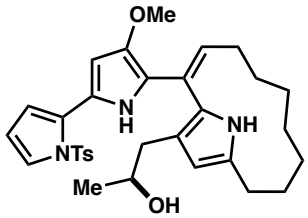

Synthesized following the general procedure for the condensation of methoxy pyrrole-aryls with ketopyrrolophanes allowing the reaction mixture to warm to rt and stir for 2 h after addition of the methoxy pyrrole-aryl solution was complete before quenching. **6** was isolated as a purple foam (16% yield) alongside **5** (48% yield). **^{1}H-NMR** (acetone-d6, 500 MHz) δ 9.30 (s, 1H), 9.11 (s, 1H), 7.38 (d, *J* = 8.4 Hz, 2H), 7.32 (dd, *J* = 3.2, 1.9 Hz, 1H), 7.30 (d, *J* = 8.4 Hz, 2H), 6.47 (t, *J* = 8.4 Hz, 1H), 6,26 (m, 2H), 6.08 (s, 1H), 5.79 (d, *J* = 2.8 Hz, 1H), 3.89 (q, *J* = 6.4 Hz, 1H), 3.75 (s, 3H), 2.64 (m, 2H), 2.44 (d, *J* = 7.3 Hz, 1H), 2.42 (d, *J* = 5.9 Hz, 1H), 2.36 (s, 3H), 1.92 (m, 2H), 1.60 (m, 2H), 1.53-1.13 (m, 7H), 1.11 (d, *J* = 6.2 Hz, 3H), 0.61 (m, 1H), 0.54 (m, 1H); **^{13}C-NMR** (acetone-d6, 126 MHz) δ 146.1, 146.0, 136.2, 132.9, 130.7, 129.8, 129.2, 129.2, 127.9, 127.4, 127.4, 124.2, 123.9, 119.4, 118.5, 118.3, 117.3, 117.2, 115.2, 112.9, 106.3, 99.9, 99.8, 68.6, 58.1, 37.4, 30.1, 29.0, 28.5, 28.4, 27.7, 27.4, 26.3, 23.6, 21.5; **HRMS** (ESI) calculated for $C_{32}H_{40}N_3O_4S$ $[M + H]^+$: 562.2734, found: 562.2725 (1.6 ppm mass defect).

1*H*,1'*H*-2,2'-bipyrrole (**7**)

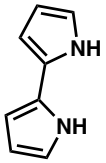

To a flame-dried 500-mL round bottom flask ,equipped with a stir bar, was added 1H-pyrrole (1.0 g, 1.0 mL, 1.0 eq., 15 mmol) followed by DCM (248 mL, 0.06 M) after which, .the resulting solution was cooled to –78°C. To the cooled solution was then added bis(trifluoroacetoxy)iodo]benzene (2.2 g, 0.33 eq., 4.9 mmol, 98% wt.) and bromotrimethylsilane

(1.6 g, 1.3 mL, 0.67 eq., 10 mmol, 97% wt.) under argon. The reaction mixture was then allowed to stir for 1 h at –78 °C. After this time, the reaction mixture was warmed to 0°C and quenched via the addition of 50 mL of sat. $NaHCO_3$ after which, it was warmed to rt and stirred for 10 min. The reaction was then extracted with DCM (process repeated 3x). Then organic layers were then combined, dried over Na_2SO_4, filtered, concentrated and purified via flask column chromatography using silica gel (EtOAc in Hexane: 0% - 10% - 20%). **7** was isolated as a dark-purple powder (349 mg, 35% yield). **7** was found to be very unstable to air and had to be stored under argon in the freezer. **^{1}H-NMR** ($CDCl_3$, 500 MHz) δ 8.27 (s, 2H), 6.79–6.76 (m, 2H), 6.25 (q, J = 2.9 Hz, 2H), 6.23–6.20 (m, 2H); **^{13}C-NMR** ($CDCl_3$, 126 MHz) δ 126.1, 117.7, 109.6, 103.7; **HRMS** (ESI) calculated for $C_8H_8N_2$ $[M+H]^+$: 133.0766, found 133.0768 (1.5 ppm mass defect).

(2^5S)-2^5-methyl-2^2-(1'-tosyl-1*H*,1'*H*-[2,2'-bipyrrol]-5-yl)-2^2,2^3,2^4,2^5-tetrahydro-1^1*H*-1(2,5)-pyrrola-2(2,3)-furanacyclononaphane (**8**)

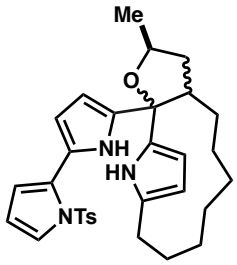

Synthesized following the general procedure for the condensation of methoxy pyrrole-aryls with ketopyrrolophanes quenching the reaction immediately after addition of the bispyrrole (**7**) solution was complete. **8** was isolated as a mixture of diastereomers as a tan foam (41% yield). **^{1}H-NMR** ($CDCl_3$, 500 MHz) δ 8.57 (s, 1H), 8.50 (s, 1H), 7.75 (s, 1H), 7.44 (s, 1H), 6.78–6.71 (m, 2H), 6.28 (t, J = 3.0 Hz, 1H), 6.22–6.19 (m, 3H), 6.19–6.16 (m, 3H), 6.15 (t, J = 6.2 Hz, 1H), 6.04 (t, J = 2.9 Hz, 1H), 5.86 (t, J = 3.0 Hz, 1H), 5.83 (t, J = 2.8 Hz, 1H), 5.80 (t, J = 3.0 Hz, 1H), 4.48 (s, J = 6.3 Hz, 1H), 3.96–3.87 (m, 1H), 2.82–2.74 (m, 2H), 2.73–2.67 (m, 1H), 2.64–2.57 (m, 1H), 2.54–2.47 (m, 1H), 2.33–2.24 (m, 1H), 2.15–2.08 (m, 1H), 1.99–1.83 (m, 3H), 1.76–1.68 (m, 3H), 1.53–1.49

(m, 2H), 1.45–1.40 (m, 3H), 1.39–1.35 (m, 2H), 1.35–1.33 (m, 3H), 1.13 (d, J = 6.3 Hz, 3H), 1.08–0.99 (m, 6H), 0.97 (d, J = 6.6 Hz, 3H), 0.86–0.83 (m, 3H); **HRMS** (ESI) calculated for $C_{24}H_{31}N_3O$ $[M+H]^+$: 378.2545, found 378.2552 (1.9 ppm mass defect).

Benzyl 2-(3,5-difluorophenyl)-4-methoxy-1*H*-pyrrole-1-carboxylate (**9**)

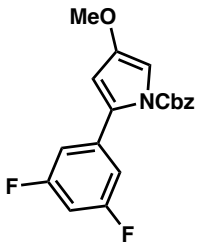

Synthesized following the general route for the synthesis of methoxy-pyrrole aryl nucleophiles (shown in **Scheme 2.2.8**). **9** was isolated as a white powder. **^{1}H-NMR** ($CDCl_3$, 400MHz) δ 7.35 (t, J = 3.26 Hz, 3H), 7.26-7.23 (m, 1H), 6.84 (d, J = 2.15 Hz, 2H), 6.82 (d, J = 2.35 Hz, 1H), 6.71 (tt, J = 9.01, 2.35 Hz, 2.35 Hz, 1H), 6.03 (d, J = 2.15, 1H), 5.21 (s, 2H), 3.74 (s, 3H); **HRMS** (ESI) calculated for $C_{19}H_{15}F_2NO_3$ $[M+H]^+$;344.1098, found 344.1107 (2.6 ppm mass defect).

Benzyl 4-methoxy-2-(pyridin-2-yl)-1*H*-pyrrole-1-carboxylate (**10**)

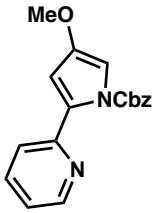

Synthesized following the general route for the synthesis of methoxy-pyrrole aryl nucleophiles (shown in **Scheme 2.2.8**). **10** was isolated as a green solid as a suspected pyridinium salt. **^{1}H-NMR** ($CDCl_3$, 500MHz) δ 9.23 (s, 1H), 8.32 (ddd, J = 4.9, 1.7, 1.0 Hz, 1H), 7.61 (td, J = 7.3, 1.8 Hz, 1H), 7.55 (dt, J = 8.0, 1.0 Hz, 1H), 7.39–7.34 (m, 3H), 7.33–7.27 (m, 1H), 7.03 (ddd, J = 7.4, 4.9, 1.1 Hz, 1H), 6.48 (dd, J = 2.7, 1.8 Hz 1H), 6.38 (dd, J = 2.8, 1.8 Hz, 1H), 4.71 (s, 2H), 3.78 (s, 3H); **^{13}C NMR** ($CDCl_3$, 126 MHz) δ 171.3, 150.4, 150.3, 148.9, 141.0, 136.7, 128.9, 128.7, 127.8,

127.1, 120.7, 118.1, 102.2, 95.8, 65.5, 58.1; **HRMS** (ESI) calculated for $C_{18}H_{16}N_2O_3$ $[M+H]^+$: 309.1239, found 309.1243 (1.3 ppm mass defect).

Benzyl 4-methoxy-2-phenyl-1*H*-pyrrole-1-carboxylate (**11**)

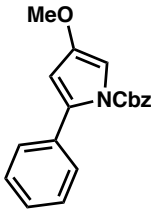

Synthesized following the general route for the synthesis of methoxy-pyrrole aryl nucleophiles (shown in **Scheme 2.2.8**). **11** was isolated as a pale-yellow oil. **^{1}H-NMR** ($CDCl_3$, 400 HMz) δ 7.97 (dd, J = 8.4, 1.3 Hz, 1H), 7.47 (tt, J = 7.3, 1.5 Hz, 1H), 7.36-7.28 (m, 6H), 7.21-7.15 (m, 2H), 6.83 (d, J = 2.1 Hz, 1H), 6.00 (d, J = 2.1 Hz, 1H). 5.19 (s, 2H), 3.74 (s, 3H); **^{13}C-NMR** ($CDCl_3$, 101 HMz) δ 150.6, 149.9, 134.8, 134.6, 133.5, 133.1, 129.3, 128.5, 128.3, 127.7, 127.6, 107.7, 101.4, 68.6, 57.6; **HRMS** (ESI) calculated for $C_{19}H_{17}NO_3$ $[M+H]^+$: 308.1281, found 308.1275 (1.9 ppm mass defect).

Benzyl 4-methoxy-2-(3-methoxyphenyl)-1*H*-pyrrole-1-carboxylate (**12**)

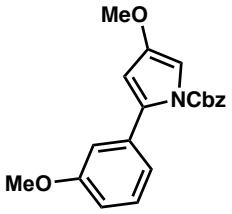

Synthesized following the general route for the synthesis of methoxy-pyrrole aryl nucleophiles (shown in **Scheme 2.2.8**). **12** was isolated as a tan powder. **^{1}H-NMR** ($CDCl_3$, 500MHz) δ 7.54 (d, J = 8.18 Hz, 1H), 7.51-7.46 (m, 1H), 7.38 (t, J = 8.18 Hz, 1H), 7.34-7.28 (m, 2H), 7.23-7.16 (m, 2H), 7.11 (dd, J = 8.18, 2.56 Hz, 1H), 6.94-6.80 (m, 2H), 5.19 (s, 1H), 3.86 (s, 3H), 3.75 (d, J = 2.56 Hz, 2H), 2.60 (s, 3H); **^{13}C-NMR** ($CDCl_3$, 126MHz) δ 159.8, 149.8, 138.5, 129.6, 128.5,

128.3, 121.9, 121.1, 119.7, 114.9, 113.4, 112.3, 107.7, 101.4, 68.6, 57.6, 55.5, 55.2. **HRMS** (ESI) calculated for $C_{20}H_{19}NO_4$ $[M+H]^+$: 338.1392, found 338.1399 (2.1 ppm mass defect).

(2^5S)-2^2-(5-(3,5-difluorophenyl)-1*H*-pyrrol-2-yl)-2^5-methyl-2^2,2^3,2^4,2^5-tetrahydro-1^1H-1(2,5)-pyrrola-2(2,3)-furanacyclononaphane (**19a**)

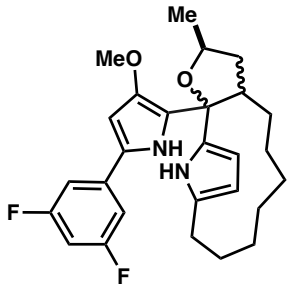

Synthesized following the general procedure for the condensation of methoxy pyrrole-aryls with ketopyrrolophanes allowing the reaction mixture to warm to rt and stir for 2 h after addition of the methoxy pyrrole-aryl solution was complete before quenching. **19a** was isolated as a light-pink film (43% yield). **^{1}H-NMR** ($CDCl_3$, 500 MHz) δ 8.89 (s, 1H), 8.53 (s, 1H), 8.46 (s, 1H), 8.39 (s, 1H), 6.92–6.80 (m, 4H), 6.62–6.52 (m, 2H), 6.33–6.28 (m, 2H), 6.00–5.96 (m, 1H), 5.95 (t, J = 2.8 Hz, 1H), 5.80 (t, J = 2.80 Hz, 1H), 5.76 (t, J = 2.80 Hz, 1H), 4.51–4.40 (m, 1H), 4.20–4.09 (m, 1H), 3.93 (s, 3H), 3.90 (s, 3H), 2.93–2.88 (m, 3H), 2.83–2.76 (m, 1H), 2.69–2.61 (m, 1H), 2.61–2.56 (m, 2H), 2.56–2.48 (m, 1H), 2.22–2.14 (m, 1H), 1.91–1.83 (m, 1H), 1.79–1.71 (m, 1H), 1.55–1.45 (m, 5H), 1.42 (d, J = 6.1 Hz, 3H), 1.41–1.38 (m, 5H), 1.33–1.25 (m, 4 H), 1.20–1.13 (m, 4H), 1.11–1.02 (m, 4H), 1.01–0.92 (m, 2H), 0.91–0.87 (m, 1H), 0.86–0.77 (m, 2H), 0.76–0.66 (m, 1H). **^{13}C-NMR** ($CDCl_3$, 126 MHz) δ 150.3, 150.2, 149.1, 148.9, 143.2, 141.1, 136.2, 136.1, 132.8, 131.9, 131.5, 131.0, 128.6, 127.7, 127.5, 127.0, 125.5, 125.0, 124.2, 122.6, 120.1, 119.9, 117.3, 117.0, 106.2, 105.4, 105.0, 104.8, 95.5, 95.3, 85.2, 84.6, 75.5, 73.7, 65.4, 58.7, 58.6, 47.9, 47.5, 42.1, 40.7, 29.7, 28.0, 27.6, 27.0, 26.7, 26.6, 25.8, 25.3, 23.5, 22.7, 21.9, 21.4; **HRMS** (ESI) calculated for $C_{27}H_{32}F_2N_2O_2$ $[M+H]^+$: 455.2110, found 455.2122 (2.6 ppm mass defect).

(2^5S)-2^5-methyl-2^2-(5-(pyridin-2-yl)-1*H*-pyrrol-2-yl)-2^2,2^3,2^4,2^5-tetrahydro-1^1H-1(2,5)-pyrrola-2(2,3)-furanacyclononaphane (**19b**)

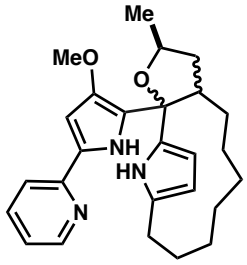

Synthesized following the general procedure for the condensation of methoxy pyrrole-aryls with ketopyrrolophanes allowing the reaction mixture to warm to rt and stir for 2 h after addition of the methoxy pyrrole-aryl solution was complete before quenching. **19b** was isolated as a light-red film (8% yield) as a suspected hydrochloride salt. **^{1}H-NMR** ($CDCl_3$, 500 MHz) δ 9.44 (s, 1H), 9.31 (s, 1H), 8.96 (s, 1H), 8.62 (s, 1H), 8.41–8.37 (m, 2H), 7.59–7.50 (m, 2H), 7.39–7.34 (m, 4H), 6.98–6.91 (m, 2H), 6.48–6.43 (m, 2H), 5.99–5.94 (m, 2H), 5.78 (t, J = 2.6 Hz, 1H), 5.74 (t, J = 2.9 Hz, 1H), 4.49–4.40 (m, 1H), 4.24–4.15 (m, 1H), 3.95 (s, 3H), 3.91 (s, 3H), 2.94–2.88 (m, 1H), 2.82–2.76 (m, 1H), 2.66–2.60 (m, 1H), 2.60–2.56 (m, 2H), 2.56–2.48 (m, 1H), 2.21–2.14 (m, 1H), 1.86–1.81 (m, 1H), 1.78–1.70 (m, 1H), 1.67–1.58 (m, 3H), 1.55–1.44 (m, 6H), 1.42–1.40 (m, 6H), 1.36–1.29 (m, 3H), 1.19–1.13 (m, 3H), 1.09–1.03 (m, 2H), 0.99–0.93 (m, 2H), 0.86–0.78 (m, 3H), 0.75–0.69 (m, 1H); **^{13}C-NMR** ($CDCl_3$, 126 MHz) δ 150.3, 150.2, 149.1, 148.9, 143.2, 141.1, 136.2, 136.1, 132.8, 131.9, 131.5, 131.0, 128.6, 127.7, 127.5, 127.0, 125.5, 125.0, 124.2, 122.6, 120.1, 119.9, 117.3, 117.0, 106.2, 105.4, 105.0, 104.8, 95.5, 95.4 85.2, 84.6, 75.5, 73.7, 65.4, 58.7, 58.6, 47.9, 47.6, 42.1, 40.7, 29.7, 29.5, 28.0, 27.6, 27.0, 26.7, 26.6, 25.8, 25.3, 23.5, 22.7, 21.9, 21.4; **HRMS** (ESI) calculated for $C_{26}H_{33}N_2O_2$ $[M+H]^+$: 420.2651, found 420.2659 (1.9 ppm mass defect).

(2^5S)-2^2-(5-(3-methoxyphenyl)-1*H*-pyrrol-2-yl)-2^5-methyl-2^2,2^3,2^4,2^5-tetrahydro-1^1H-1(2,5)-pyrrola-2(2,3)-furanacyclononaphane (**19d**)

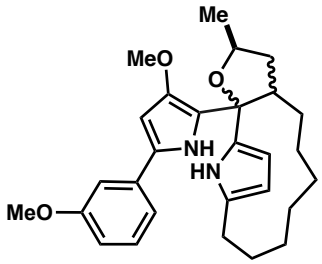

Synthesized following the general procedure for the condensation of methoxy pyrrole-aryls with ketopyrrolophanes allowing the reaction mixture to warm to rt and stir for 2 h after addition of the methoxy pyrrole-aryl solution was complete before quenching. **19d** was isolated as a dark-purple film (19% yield). **^{1}H-NMR** ($CDCl_3$, 400 MHz) δ 8.96 (s, 1H), 8.52 (s, 1H), 8.45 (s, 1H), 8.35 (s, 1H), 7.23 (t, J = 7.9 Hz, 2H), 6.99–6.97 (m, 1H), 6.97–6.95 (m, 1H), 6.92 (t, J = 1.9 Hz, 1H), 6.91 (t, J = 1.7 Hz, 1H), 6.73–6.67 (m, 2H), 6.31–6.26 (m, 2H), 5.99 (t, J = 2.8 Hz, 1H), 5.96 (t, J = 2.8 Hz, 1H), 5.80 (t, J = 2.9 Hz, 1H), 5.75 (t, J = 2.9 Hz, 1H), 4.50–4.41 (m, 1H), 4.18–4.09 (m, 1H), 3.94 (s, 3H), 3.90 (s, 3H), 3.82 (s, 6H), 3.01–2.91 (m, 1H), 2.85–2.77 (m, 1H), 2.69–2.61 (m, 1H), 2.58 (t, J = 5.8 Hz, 2H), 2.55–2.46 (m, 1H), 2.23–2.13 (m, 1H), 1.89–1.82 (m, 2H), 1.80–1.71 (m, 3H), 1.66–1.60 (m, 2H), 1.56–1.50 (m, 2H), 1.48–1.44 (m, 2H), 1.42 (d, J = 6.6 Hz, 3H), 1.41–1.38 (m, 5H), 1.23–1.20 (m, 2H), 1.18–1.14 (m, 2H), 1.10–1.05 (m, 2H), 0.97 (d, J = 6.7 Hz, 2H), 0.89–0.87 (m, 3H), 0.85–0.81 (m, 2H), 0.76–0.67 (m, 1H); **^{13}C-NMR** ($CDCl_3$, 101 MHz) δ 160.2, 160.1, 134.3, 134.2, 133.0, 132.1, 131.8, 131.3, 130.0, 129.9, 126.6, 125.8, 125.6, 125.1, 122.6, 116.4, 116.2, 115.8, 111.8, 111.6, 111.4, 109.2, 109.0 106.5, 106.4, 105.5, 105.0, 105.0, 95.2, 95.1, 85.4, 84.8, 75.7, 73.9, 58.8, 55.4, 55.4, 48.1, 47.5, 34.8, 31.7, 29.8, 28.1, 27.8, 26.9, 26.8, 26.6, 25.9, 25.6, 25.5, 25.4, 22.8, 22.1, 21.4, 14.3, 14.3; **HRMS** (ESI) calculated for $C_{28}H_{36}N_2O_3$ $[M+H]^+$: 449.2804, found 449.2818 (3.1 ppm mass defect).

(*S*,*E*)-1-(2-(5-(3,5-difluorophenyl)-3-methoxy-1*H*-pyrrol-2-yl)-1^{1}*H*-1(2,5)-pyrrolacyclodecaphan-2-en-1^{3}-yl)propan-2-ol (**20a**)

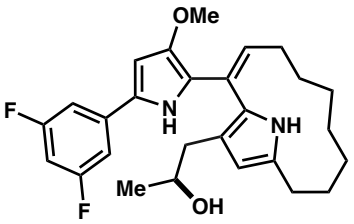

Synthesized following the general procedure for the condensation of methoxy pyrrole-aryls with ketopyrrolophanes allowing the reaction mixture to warm to rt and stir for 2 h after addition of the methoxy pyrrole-aryl solution was complete before quenching. **20a** was isolated as a light-purple film (6% yield). **^{1}H-NMR** ($CDCl_3$, 500 MHz) δ 8.79 (s, 1H), 7.68 (s, 1H), 6.93–6.87 (m, 2H), 6.59 (t, J = 7.9 Hz, 1H), 6.51 (tt, J = 8.9, 2.1 Hz, 1H), 6.31 (d, J = 3.0 Hz, 1H), 5.85 (d, J = 2.8 Hz, 1H), 4.08–3.99 (m, 1H), 3.88 (s, 3H), 2.73–2.64 (m, 1H), 2.59 (dd, J = 14.3, 3.8 Hz, 1H), 2.56–2.47 (m, 1H), 2.37 (dd, J = 14.4, 9.4 Hz), 1.99–1.84 (m, 2H), 1.74–1.60 (m, 4H), 1.51–1.45 (2 H), 1.23 (d, J = 6.2 Hz, 3H), 0.98–0.95 (m, 1H), 0.86–0.83 (m, 1H), 0.80–0.72 (m, 1H), 0.65–0.51 (m, 1H); **^{13}C-NMR** ($CDCl_3$, 126 MHz) δ 164.6, 164.5, 162.7, 162.6, 146.4, 133.1, 132.2, 125.5, 123.7, 118.5, 106.0, 105.8, 100.6, 96.0, 68.8, 58.1, 35.9, 34.8, 31.7, 29.9, 28.7, 28.6, 28.6, 28.1, 27.2, 27.0, 25.6, 25.4, 23.5, 14.3; **HRMS** (ESI) calculated for $C_{27}H_{32}F_2N_2O_2$ $[M+H]^+$: 455.2510, found 455.2515 (1.1 ppm mass defect).

(*S*,*E*)-1-(2-(3-methoxy-5-(pyridin-2-yl)-1*H*-pyrrol-2-yl)-1^{1}*H*-1(2,5)-pyrrolacyclodecaphan-2-en-1^{3}-yl)propan-2-ol (**20b**)

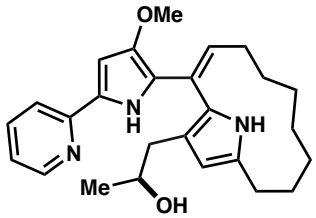

Synthesized following the general procedure for the condensation of methoxy pyrrole-aryls with ketopyrrolophanes allowing the reaction mixture to warm to rt and stir for 2 h after addition of the

methoxy pyrrole-aryl solution was complete before quenching. **20b** was isolated as a light-pink film (12% yield). **^{1}H-NMR** ($CDCl_3$, 500 MHz) δ 9.32 (s, 1H), 8.35 (m, 1H), 7.70 (s, 1H), 7.55 (t, J = 7.4 Hz, 1H), 7.39 (d, J = 8.1 Hz, 1H), 6.94 (m, 1H), 6.58 (t, J = 8.5 Hz, 1H), 6.45 (s, 1H), 5.88 (d, J = 2.4 Hz, 1H), 4.01–3.92 (m, 1H), 3.87 (s, 1H), 2.71–2.61 (m, 1H), 2.60–2.51 (m, 1H), 2.39 (dd, J = 14.2, 9.2 Hz, 1H), 2.01–1.91 (m, 1H), 1.78–1.66 (m, 2H), 1.64–1.56 (m, 2H), 1.53–1.45 (m, 2H), 1.44–1.35 (m, 2H), 1.19 (d, J = 6.2 Hz, 3H), 0.79–0.71 (m, 1H), 0.70–0.59 (m, 1H); **^{13}C-NMR** ($CDCl_3$, 126 MHz) δ 150.2, 148.9, 146.6, 136.6, 132.8, 130.8, 126.0, 123.3, 120.1, 119.0, 118.6, 117.9, 106.2, 95.8, 68.3, 58.1, 36.4, 29.8, 28.7, 28.6, 28.5, 28.1, 25.6, 23.3; **HRMS** (ESI) calculated for $C_{26}H_{33}N_3O_2$ $[M+H]^+$: 420.2651, 420.2653 (0.5 ppm mass defect).

(*S*,*E*)-1-(2-(3-methoxy-5-(3-methoxyphenyl)-1*H*-pyrrol-2-yl)-1^1*H*-1(2,5)-pyrrolacyclodecaphan-2-en-1^3-yl)propan-2-ol (**20d**)

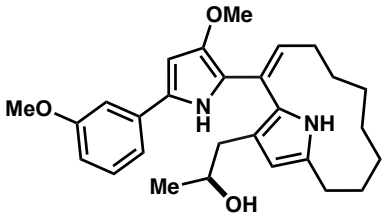

Synthesized following the general procedure for the condensation of methoxy pyrrole-aryls with ketopyrrolophanes allowing the reaction mixture to warm to rt and stir for 2 h after addition of the methoxy pyrrole-aryl solution was complete before quenching. **20d** was isolated as a light-purple film (20% yield). **^{1}H-NMR** ($CDCl_3$, 400 MHz) δ 8.50 (s, 1H), 7.73 (s, 1H), 7.19 (t, J = 7.1 Hz, 1H), 6.97 (d, J = 7.7 Hz, 1H), 6.94 (t, J = 1.8 Hz, 1H), 6.73–6.62 (m, 1H), 6.52 (t, J = 8.5, 1H), 6.30 (d, J = 3.0, 1H), 5.84 (d, J = 2.9 Hz, 1 H), 4.03–3.94 (m, 1H), 3.88 (s, 3H), 3.80 (s, 3H), 2.69–2.61 (m, 1H), 2.60–2.49 (m, 2H), 2.44–2.35 (m, 1H), 1.98–1.90 (m, 1H), 1.90–1.82 (m, 2H), 1.76–1.68 (m, 1H), 1.66–1.57 (m, 2H), 1.55–1.46 (m, 2H), 1.42–1.38 (m, 2H), 1.20 (t, J = 6.2, 3H), 0.78–0.65 (m, 1H), 0.65–0.52 (m, 1H); **^{13}C-NMR** ($CDCl_3$, 101 MHz) δ 160.1, 146.4, 134.1, 132.9, 130.5, 129.8, 127.2, 125.7, 123.9, 118.5, 117.2, 116.2, 111.3, 109.3, 105.6, 95.1, 68.7, 58.1, 55.4,

36.1, 31.7, 28.1, 27.2, 26.9, 25.6, 25.4, 23.2, 22.8; **HRMS** (ESI) calculated for $C_{28}H_{36}N_2O_3$ $[M+H]^+$: 449.2804, found 449.2807 (0.7 ppm mass defect).

3-butyl-1^1*H*-1(2,5)-pyrrolacyclodecaphan-2-one (**21**)

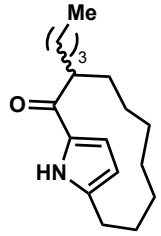

Synthesized following the general procedure for the alkylation of ketopyrrolophane **1** (outlined above) using 1-bromobutne as the electrophile. **21** was isolated as a white film (32% yield). **^{1}H-NMR** ($CDCl_3$, 400 MHz) δ 8.77 (s, 1H), 6.98 (dd, J = 3.5, 2.8 Hz, 1H), 6.10–6.08 (m, 1H), 2.97–2.83 (m, 2H), 2.69–2.57 (m, 1H), 2.02–1.92 (m, 1H), 1.92–1.8 1(m, 1H), 1.74–1.63 (m, 2H), 1.62–1.57 (m, 2H), 1.50–1.38 (m, 3H), 1.35–1.28 (m, 3H), 1.26–1.19 (m, 3H), 1.17–1.09 (m, 1H), 0.88 (t, J = 7.1 Hz, 3H); **^{13}C-NMR** ($CDCl_3$, 101 MHz) δ 191.5, 137.9, 133.2, 116.0, 111.6, 44.7, 35.0, 32.1, 30.6, 26.8, 26.6, 24.6, 23.8, 23.7, 23.1, 22.2, 14.2. **HRMS** (ESI) calculated for $C_{17}H_{27}NO$ $[M+H]^+$: 262.2171, found 262.2179 (3.1 ppm mass defect).

3-allyl-1^1*H*-1(2,5)-pyrrolacyclodecaphan-2-one (**22**)

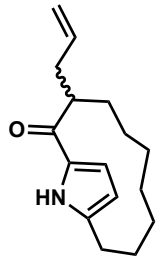

Synthesized following the general procedure for the alkylation of ketopyrrolophane **1** (outlined above) using allyl bromide as the electrophile. **21** was isolated as a white film (40% yield). ^{1}H-NMR ($CDCl_3$, 400 MHz) δ 6.79 (d, J = 4.9 Hz, 1H), 5.61-5.47 (m, 1H), 5.13-4.90 (m, 2H), 3.56 (sept, J = 4.0 Hz, 1H), 2.65 (dd, J = 13.3, 7.5 Hz, 1H), 4.90-2.28 (m, 2H), 2.16-1.99 (m, 2H), 1.84-

1.67 (m, 1H), 1.67-1.54 (m, 2H), 1.53-1.37 (m, 3H), 1.37-1.11 (m, 4H), 1.09-0.86 (m, 2H), 0.79-0.63 (m, 1H); **HRMS** (ESI) calculated for $C_{29}H_{33}N_3O_3S$ $[M+H]^+$: 504.2321, found 504.2330 (1.8 ppm mass defect).

(*E*)-2-(4-methoxy-1'-tosyl-1*H*,1'*H*-[2,2'-bipyrrol]-5-yl)-1[1]*H*-1(2,5)-pyrrolacyclodecaphan-2-ene (**23**)

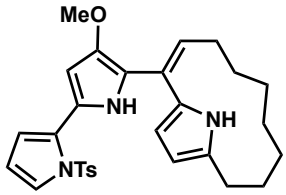

Synthesized following the general procedure for the condensation of methoxy pyrrole-aryls with ketopyrrolophanes allowing the reaction mixture to warm to rt and stir for 24 h after addition of the methoxy pyrrole-aryl solution was complete before quenching. **23** was isolated as a red oil (48% yield). **^{1}H-NMR** ($CDCl_3$, 500 MHz) δ (ppm) 8.45 (bs, 1H), 8.00 (bs, 1H), 7.33-7.29 (m, 3H), 7.14 (d, J = 8.0 Hz, 2H), 6.53 (t, J = 8.4 Hz, 1H), 6.21 (t, J = 3.3 Hz, 1H), 6.17 (dd, J = 1.8, 3.4 Hz, 1H), 6.07 (t, J = 2.9 Hz, 1H), 5.95 (t, J = 2.9 Hz, 1H), 5.93 (d, J = 3.0 Hz, 1H), 3.79 (s, 3H), 2.65 (t, J = 6.1 Hz, 2H), 2.35 (s, 3H), 2.04 (q, J = 7.7 Hz, 2H), 1.58 (p, J = 5.4 Hz, 2H), 1.48-1.40 (m, 2H), 1.40-1.32 (m, 2H), 1.30-1.15 (m, 4H), 0.88-0.76 (m, 2H); **^{13}C-NMR** ($CDCl_3$, 126 MHz,) δ 145.2, 144.7, 135.0, 132.4, 129.5, 128.4, 127.6, 127.2, 126.6, 125.3, 123.4, 116.9, 116.3, 114.7, 111.79, 108.5, 105.5, 99.2, 58.0, 28.7, 28.0, 27.9, 27.8, 27.3, 26.9, 25.3, 21.6; **HRMS** (ESI) calculated for $C_{29}H_{33}N_3O_3S$ $[M+H]^+$: 504.2321, found 504.2330 (1.8 ppm mass defect).

3-((*S*)-2-hydroxybutyl)-1^1*H*-1(2,5)-pyrrolacyclodecaphan-2-one (**24**)

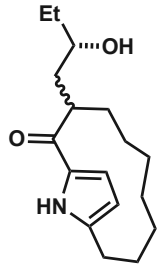

Synthesized following the general procedure for the alkylation of ketopyrrolophane **1** (outlined above) using (S)-butylene oxide as the electrophile along with the use of $AlMe_3$. **24** was isolated as a mixture of diastereomers as a light-yellow foam (32% yield). **^{1}H-NMR** ($CDCl_3$, 500 MHz) δ 9.37 (s, 1H), 6.94 (s, 1H), 6.05 (s, 1H), 3.58-3.36 (m, 2H), 2.89-2.74 (m, 1H) , 2.74-2.54 (m, 2H), 2.21 (t, J = 11.7 Hz, 1H), 1.88-1.57 (m, 6H), 1.57-1.29 (m, 9H), 1.15-1.04 (m, 3H); **^{13}C-NMR** ($CDCl_3$, 126 MHz) δ 193.5, 102.8, 171.2, 138.8, 133.4, 116.1, 111.6, 72.7, 71.6, 40.6, 39.4, 31.3, 26.7, 24.1, 23.9, 23.7, 9.9; **HRMS** (ESI) calculated for $C_{17}H_{27}NO_2$ $[M+H]^+$: 278.2115, found: 278.2111 (1.4 ppm mass defect)

(2^5*S*)-2^5-ethyl-2^2-(4-methoxy-1'-tosyl-1*H*,1'*H*-[2,2'-bipyrrol]-5-yl)-2^2,2^3,2^4,2^5-tetrahydro-1^1*H*-1(2,5)-pyrrola-2(2,3)-furanacyclononaphane (**25**)

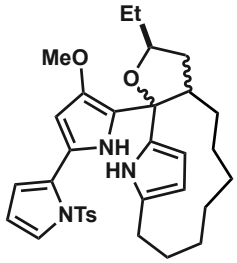

Synthesized following the general procedure for the condensation of methoxy pyrrole-aryls with ketopyrrolophanes allowing the reaction mixture to warm to rt and stir for 2 h after addition of the methoxy pyrrole-aryl solution was complete before quenching. **25** was isolated as a purple film (37% yield). **^{1}H-NMR** ($CDCl_3$, 500 MHz) δ 8.90 (s, 2H), 8.54 (s, 1H), 8.69 (s, 1H), 7.38 (m, 2H), 7.27 (m, 2H), 7.25 (m, 2H), 6.90 (d, J = 8.2 Hz, 2H), 6.80 (d, J = 8.2 Hz, 2 H), 6.23 (t, J = 3.1 Hz,

2H), 6.19 (dd, J = 3.3, 1.8 Hz, 1H), 6.17 (dd, J = 3.3, 1.8 Hz, 1H), 6.02 (t, J = 2.8 Hz, 1H), 6.00 (t, J = 2.8 Hz, 1H), 5.88 (dd, J = 3.2, 1 Hz, 2H), 5.83 (t, J = 2.9 Hz, 1 H), 5.81 (t, J = 2.9 Hz, 1 H), 4.17 (m, 1H), 3.94 (m, 1H), 3.82 (s, 3H), 3.80 (s, 3H), 2.84 (q, J = 7.2 Hz, 1 H), 2.76 (m, 1H), 2.73–2.66 (m, 1H), 2.66–2.61 (m, 1H), 2.61–2.57 (m, 1H), 2.57–2.49 (m, 1H), 2.27 (s, 3H), 2.24 (s, 3H), 2.19–2.13 (m, 1H), 1.90–1.80 (m, 3 H), 1.80–1.69 (m, 2H), 1.68–1.60 (m, 4H), 1.53–1.43 (m, 6H), 1.18–1.12 (m, 4H), 1.11–1.06 (m, 2H), 1.02 (t, J = 7.5 Hz, 3H), 1.00–0.94 (m, 6H), 0.91–0.82 (m, 5H), 0.81–0.67 (m, 2H); **^{13}C-NMR** ($CDCl_3$, 126 MHz) δ 144.7, 144.6, 141.6, 139.9, 136.4, 134.7, 134.5, 133.5, 132.5, 131.2, 130.9, 129.6, 129.5, 129.0, 128.2, 127.7, 127.7, 127.6, 126.8, 126.5, 123.3, 123.2, 123.1, 121.9, 115.4, 115.1, 114.5, 114.0, 111.3, 111.2, 106.2, 105.3, 105.2, 105.1, 99.9, 99.9, 84.9, 84.3, 81.3, 79.4, 59.0, 58.9, 47.9, 47.7, 40.3, 39.1, 34.8, 31.7, 30.1, 29.6, 28.9, 28.2, 27.9, 27.5, 26.9, 26.0, 26.0, 25.5, 25.4, 23.9, 22.8, 21.7, 14.3, 11.6, 11.0, 10.9; **HRMS** (ESI) calculated for $C_{33}H_{40}N_3O_4S$ $[M+H]^+$: 576.2891, found 576.2879 (2.1 ppm mass defect).

(2*S*)-1-(2-oxo-1^1*H*-1(2,5)-pyrrolacyclodecaphane-3-yl)propan-2-yl pivalate (**26**)

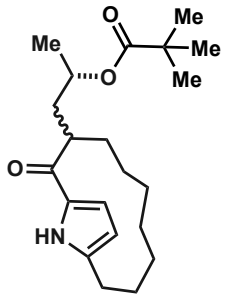

To a flame-dried dram vial, equipped with a stir bar, was added **2** (34 mg, 0.13 mmol, 1.0 eq) and DMAP (16 mg, 0.13 eq., 1.0 eq) followed by DCM (0.7mL, 0.2M) after which, the resulting solution was cooled to –78°C. To the reaction mixture was added trimethylacetic anhydride (27.0 µL, 0.13 mmol, 1.0 eq). Once done, the reaction was allowed to warm to rt and was stirred at rt for 16 h. After this time, the reaction was quenched via the addition of de-ionized water and the

resulting biphasic mixture extracted with DCM (process repeated 3x). The organic layers were then combined, washed with a sat. NH_4Cl solution, brine, dried over Na_2SO_4, filter, concentrated and purified via flask column flash column chromatography using TEA neutralized silica gel (EtOAc in Hexane: 0% - 10% - 15% - 20%). **26** was isolated as a mixture of diastereomers as a yellow oil (37% yield). **^{1}H-NMR** ($CDCl_3$, 400 MHz) δ 8.81 (s, 1H), 6.93 (q, J = 3.6 Hz, 1H), 6.06 (t, J = 2.8 Hz, 1H), 5.25-4.64 (m, 1H), 3.22-3.02 (m, 1H), 2.85 (dq, J = 15.8, 3.6 Hz, 1H), 2.67-2.53 (m, 1H), 2.42-2.31 (m, 1H), 2.03 (s, 1H), 1.94-1.74 (m, 2H), 1.70-1.18 (m, 22H); **^{13}C-NMR** ($CDCl_3$, 101 MHz) δ 191.7, 178.7, 138.4, 133.0, 116.2, 111.4, 70.5, 69.9, 41.3, 41.1, 39.0, 38.8, 38.2, 34.9, 34.8, 24.2, 24.1,23.8, 23.6, 22.8, 20.7; **HRMS** (ESI) calculated for $C_{21}H_{33}NO_3$ [M + H]$^+$: 348.2538, found: 348.2526 (3.4 ppm mass defect).

(*S*,*E*)-1-(2-(4-methoxy-1'-tosyl-1*H*,1'*H*-[2,2'-bipyrrol]-5-yl)-1^1*H*-1(2,5)-pyrrolacyclodecaphan-2-en-1^3-yl)propan-2-yl (4-bromophenyl)carbamate (**27**)

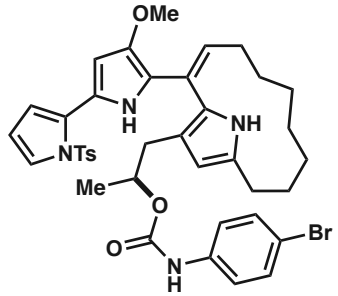

To a flame-dried dram vial, equipped with a stir bar, was added **6** (31.4 mg, 1.0 eq., 55.9 μmol) and 1-bromo-4-isocyanatobenzene (22.1 mg, 2.0 eq., 112 μmol) followed by DCE (559 μL, 0.1M). To the resulting stirred solution was then added NEt_3 (31.2 μL, 2.0 eq., 224 μmol) after which, the reaction was left to stir at rt under an atmosphere of argon gas for 3h. After this time, the reaction was diluted with deionized water and extracted with EtOAc (process repeated 3x). The organic layers were then combined, washed with brine, dried over Na_2SO_4, filtered, concentrated, and purified via flash column chromatography using TEA neutralized silica gel (EtOAc in Hexane:

0% - 10%). **27** was isolated as a dark-red film (14.8mg, 34% yield). **^{1}H-NMR** ($CDCl_3$, 500 MHz) δ 8.50 (s, 1H), 7.67 (s, 1H), 7.35–7.31 (m, 4H), 7.19 (d, J = 8.8 Hz, 2H), 7.12 (d, J = 8.2 Hz, 2H), 6.52 (t, J = 8.4 Hz, 1H), 6.46 (s, 1H), 6.22 (t, J = 3.3 Hz, 1H), 6.18 (dd, J = 3.3, 1.7 Hz, 1H), 5.93 (d, J = 2.9 Hz, 1H), 5.83 (d, J = 2.6 Hz, 1H), 5.08 (sext, J = 6.2 Hz, 1H), 3.77 (s, 3H), 3.41 (q, J = 7.2 Hz, 1H), 2.96 (q, J = 7.2 Hz, 1H), 2.64 (d, J = 6.2 Hz, 2H), 2.61–2.52 (m, 2H), 2.32 (s, 3H), 2.01–1.93 (m, 2H), 1.56–1.45 (m, 2H), 1.43–1.36 (m, 2H), 1.19–1.12 (m, 3H), 0.86–0.80 (m, 2H), 0.64–0.55 (m, 1H), 0.55–0.45 (m, 1H); **HRMS** (ESI) calculated for $C_{39}H_{43}BrN_4O_5S$ $[M+H]^+$: 759.2216, found 759.2223 (0.9 ppm mass defect).

(*S*,*E*)-1-(2-(4-methoxy-1'-tosyl-1*H*,1'*H*-[2,2'-bipyrrol]-5-yl)-1^1*H*-1(2,5)-pyrrolacyclodecaphan-2-en-1^3-yl)propan-2-yl acetate (**28**)

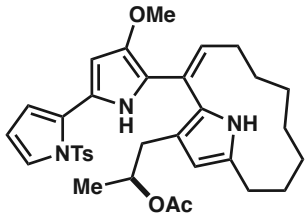

To a flame-dried dram vial equipped, equipped with a stir bar, was added **6** (10.6 mg, 1.0 eq., 18.9 µmol) followed by DCM (78.9 µL, 0.24 M) after which, the resulting solution was cooled to 0ºC. To the cold reaction mixture was then added NEt_3 (5.31 µL, 2.0 eq., 37.7 µmol), DMAP (233 µg, 0.1 eq., 1.89 µmol) and Ac_2O (2.31 µL, 1.3 eq., 24.5 µmol). Once done, the reaction was allowed to warm to rt and then stirred at rt under an atmosphere of argon gas for 16 h. After this time, the reaction mixture was quenched via the addition of a sat. NH_4Cl solution after which, it was extracted with DCM (process repeated 3x). The organic layers were then combined, washed with a sat. $NaHCO_3$ solution, brine, dried over Na_2SO_4, filtered, concentrated, and purified via flash column chromatography using TEA neutralized silica gel (EtOAc in Hexane: 0% - 15%). **28** was isolated as a dark red-oil (4.3 mg, 38% yield). **28** was found to be very unstable and notable

degradation was observed via ^{1}H-NMR over hours at rt in solution with $CDCl_3$ and acetone-d_6. **^{1}H-NMR** (acetone-d_6, 500 MHz) δ 9.53 (s, 1H), 7.75 (d, J = 8.3 Hz, 2H), 7.68 (dd, J = 3.2, 1.8 Hz, 1H), 7.08 (d, J = 8.0 Hz, 2H), 6.93 (dd, J = 3.6, 1.8 Hz, 1H), 6.43 (t, J = 4.2 Hz, 1H), 6.14 (s, 1H), 6.08 (s, 1H), 5.02–4.94 (m, 1H), 3.79 (s, 3H), 3.15–3.07 (m, 1H), 2.77–2.71 (m, 2H), 2.67–2.62 (m, 1H), 2.58–2.49 (m, 1H), 2.46–2.40 (m, 1H), 2.31 (s, 3H), 1.86 (s, 3H), 1.83–1.78 (m, 2H), 1.45–1.35 (m, 3H), 1.05 (d, J = 6.4 Hz, 3H), 0.77–0.70 (m, 2H); **HRMS** (ESI) calculated for $C_{34}H_{41}N_3O_5S$ $\{M+H\}^+$: 604.2845, found 604.2851 (1.0 ppm mass defect).

(*S*,*E*)-1^3-(2-((*tert*-butyldimethylsilyl)oxy)propyl)-2-(4-methoxy-1'-tosyl-1*H*,1'*H*-[2,2'-bipyrrol]-5-yl)-1^1*H*-1(2,5)-pyrrolacyclodecaphan-2-ene (**29**)

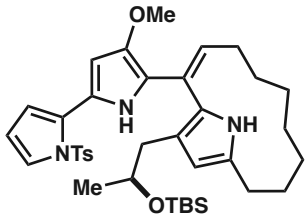

To a flame-dried dram vial, equipped with a stir bar, was added **6** (7.1 mg, 1.0 eq., 13 μmol) and imidazole (1.7 mg, 2.0 eq., 25 μmol) followed by DCM (97 μL, 0.13 M) after which the reaction mixture was cooled to 0ºC. To the cold reaction mixture was then added TBSCl (2.3 mg, 1.2 eq., 15 μmol). Once done, the reaction was allowed to warm to rt and then stirred at rt under an atmosphere of argon gas for 16 h. After this time, the reaction mixture was added to ice water and the resulting biphasic mixture extracted with EtOAc (process repeated 3x). The organic layers were then combined, dried over Na_2SO_4, filtered, concentrated and purified via flash column chromatography using TEA neutralized silica gel (EtOAc in Hexane: 0% - 10%). **29** was isolated as a dark-red film (2.6 mg, 30% yield). as a dark-red film. 28 was found to be very unstable and notable degradation was observed via ^{1}H-NMR over hours at rt in acetone-d_6. **^{1}H-NMR** (acetone-d_6, 500 MHz) δ 9.30 (s, 1H), 8.83 (s, 1H), 7.35 (d, J = 8.4 Hz, 2H), 7.31–7.27 (m, 3H), 6.50 (t, J =

8.4 Hz, 1H), 6.28–6.23 (m, 2H), 6.05 (d, J = 2.9 Hz, 1H), 5.77 (d, J = 2.7 Hz, 1H), 4.28–4.21 (m, 1H), 4.21–4.15 (m, 1H), 4.07–4.0 (m, 1H), 3.97–3.91 (m, 1H), 3.74 (s, 3H), 2.66–2.61 (m, 2H), 2.34 (s, 3H), 2.31–2.26 (m, 2H), 1.56–1.53 (m, 2H), 1.42–1.39 (m, 3H), 1.15–1.10 (m, 3H), 1.05–1.02 (m, 2H), 0.65–0.59 (m, 2H), 0.11 (s, 9H), -0.04 (s, 6H); **HRMS** (ESI) calculated for $C_{38}H_{53}N_3O_4SSi$ $[M+H]^+$: 676.3604, 676.3609 (0.7 ppm mass defect).

Computational Methods

Quantum mechanical investigations of the putative intramolecular rearrangement were conducted with density functional theory (DFT) calculations using Gaussian 16.[16]

Geometries were prepared and conformationally sampled with Grimme's xTB/CREST[17,18] and Zimmerman's GSM[19] codes. Semiempirical quantum mechanics optimizations with xTB were conducted at the GFN-XTB-2[20] level of theory with the analytical linearized Poisson-Boltzmann (ALPB) model for toluene implicit solvation. Conformational sampling with CREST was conducted at the GFN-XTB-2 level of theory with ALPB toluene implicit solvation, confining any relevant ion pairs with ellipsoidal potentials.

Initial DFT geometry optimizations were completed at the ωB97X-D/def2-SVrP[21,22] level with the solvation model based on density (SMD) for toluene.[23] Single-point corrections to energy were made at the ωB97X-D/def2-TZVPP level with the SMD for toluene.

Ensembles for the calculation of candidate structure NMR spectra were prepared with xTB/CREST. Structures contributing >1% of the overall Boltzmann population at 298.15 K were subjected to further geometry optimization using B3LYP/6-31+G(d,p)[24-26]. Degenerate structures were rejected and NMR spectra were computed with using Hoye's protocol[27], estimated RMSD 2.1 ppm, at the mPW1PW91/6-311+G(2d,p)[28] with the polarizable continuum model (PCM) solvation for acetone.[29] The resulting ensembles were subsequently re-weighted by Boltzmann contribution to total population.

Quasiharmonic corrections to enthalpy (Head-Gordon) and entropy (Grimme) were applied to optimized structure energies using Paton's GoodVibes software[30] at 298.15 K unless otherwise specified. Visualizations were prepared with Legault's CYLview20.[31]

NMR Spectra

Spectrum 2.4.1 ^{1}H-NMR of Compound **1** ($CDCl_3$, 500 MHz)

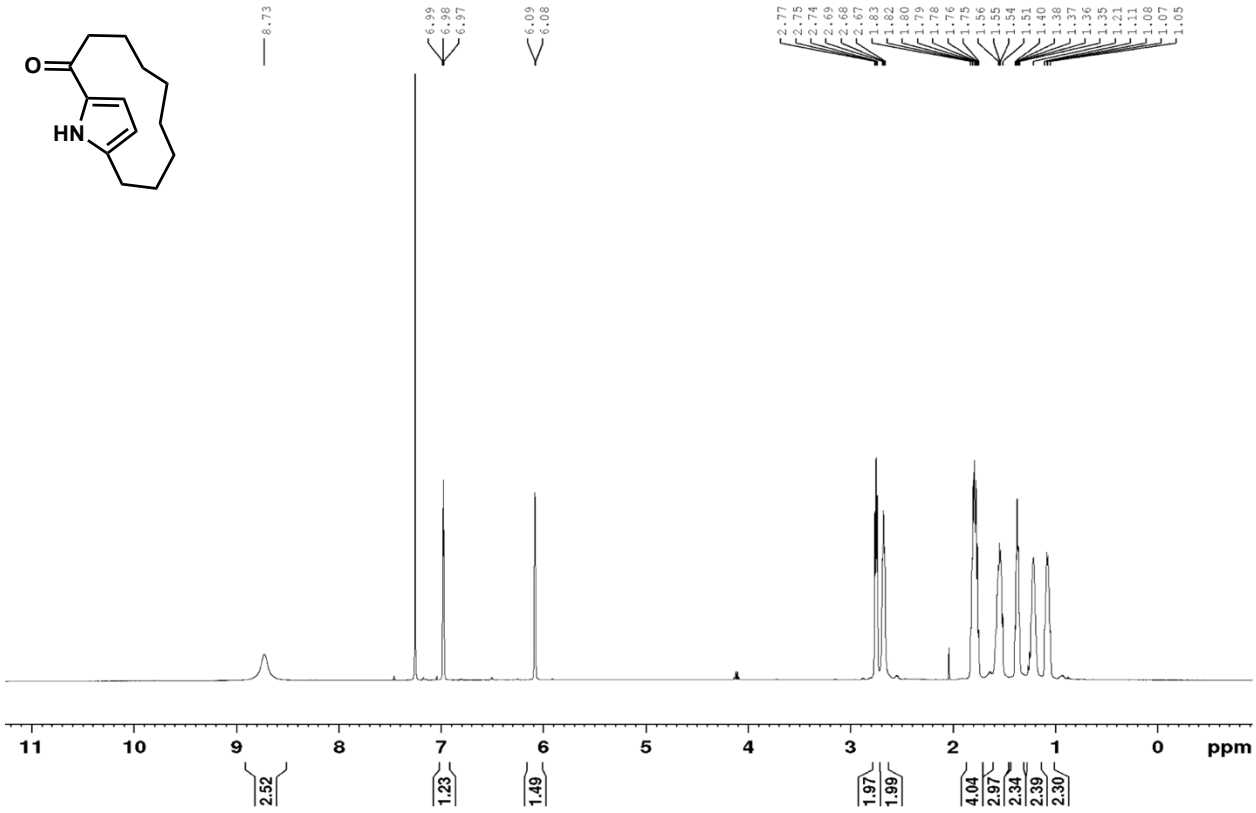

Spectrum 2.4.2 ^{13}C-NMR spectrum of compound **1** ($CDCl_3$, 126 MHz)

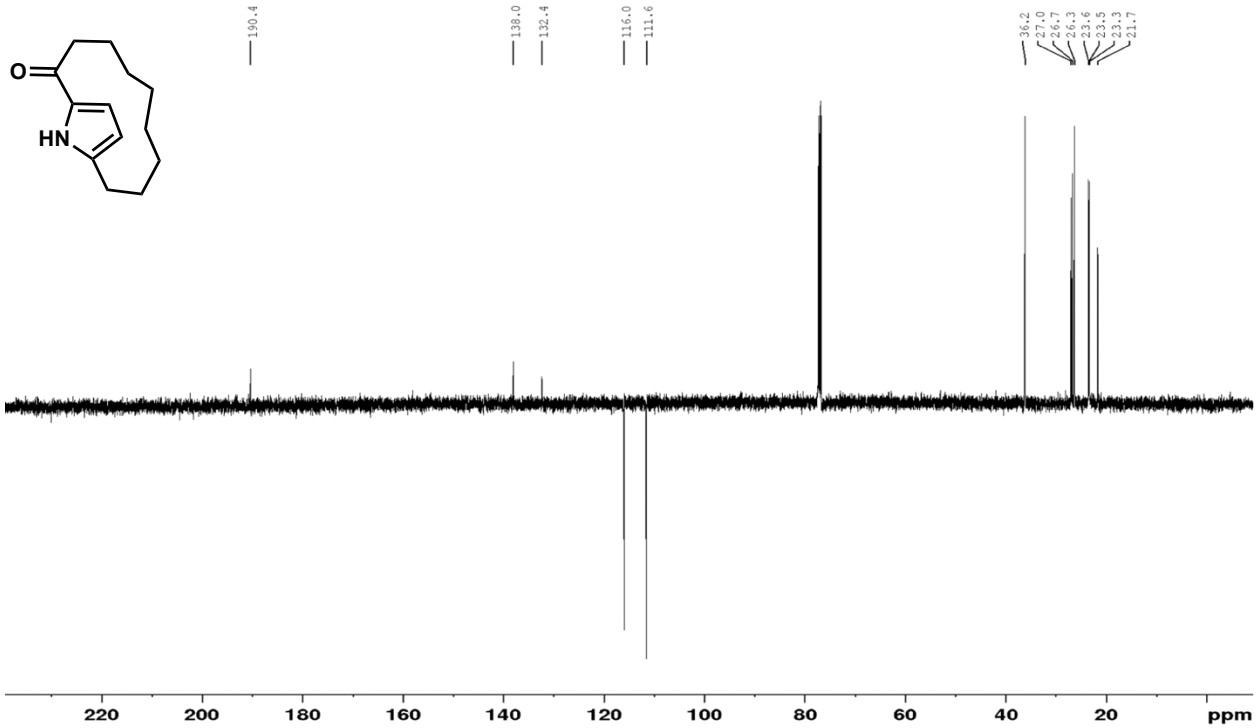

Spectrum 2.4.3 ^{1}H-NMR of compound **2S** (C_6D_6, 500 MHz)

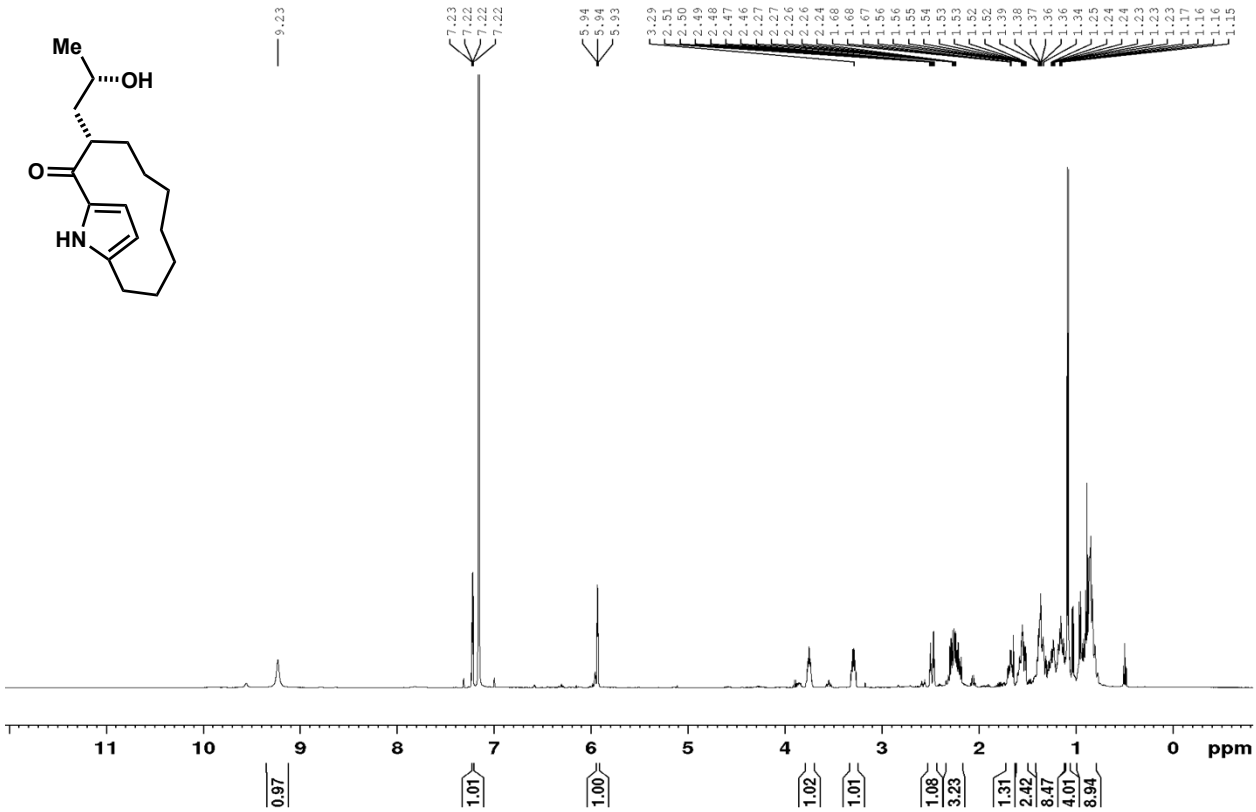

Spectrum 2.4.4 ^{13}C-NMR of compound **2S** (C_6D_6, 126 MHz)

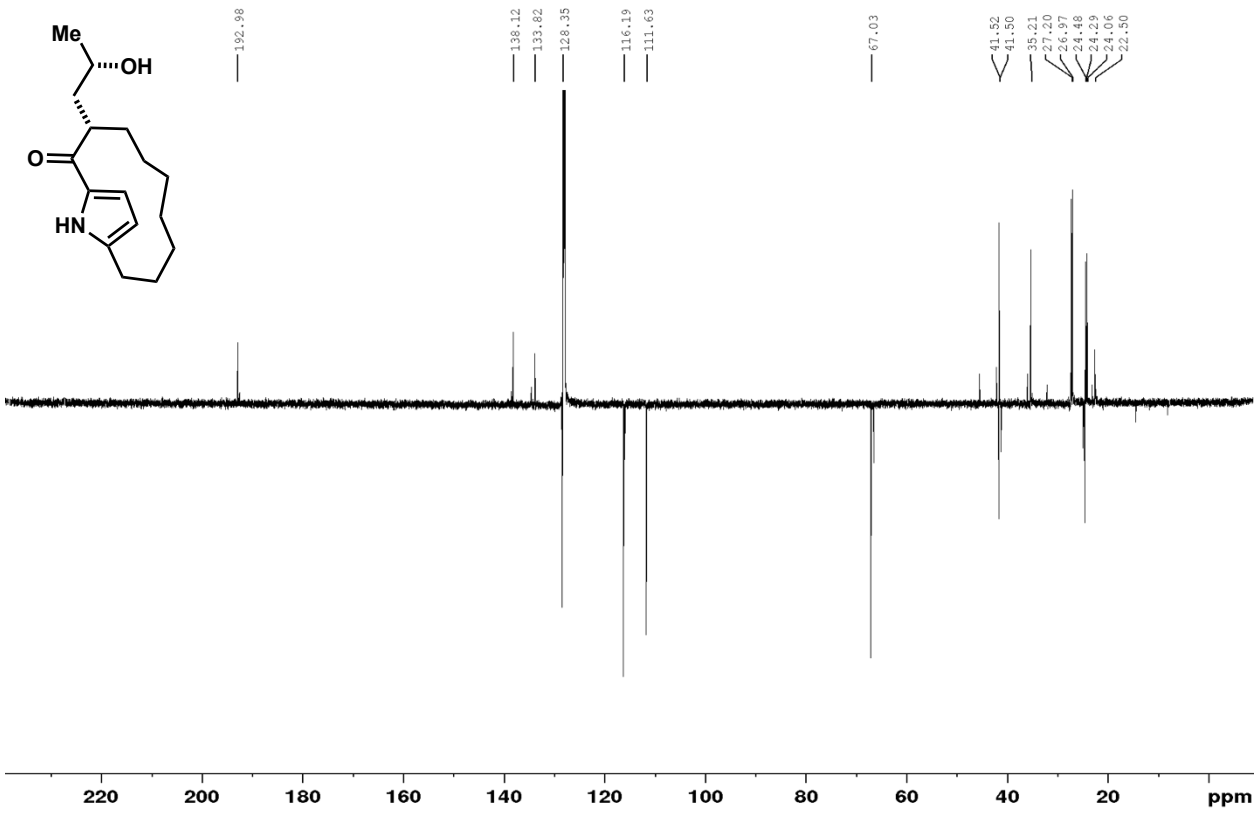

Spectrum 2.4.5 ^{1}H-NMR of compound **2R** (C_6D_6, 500 MHz)

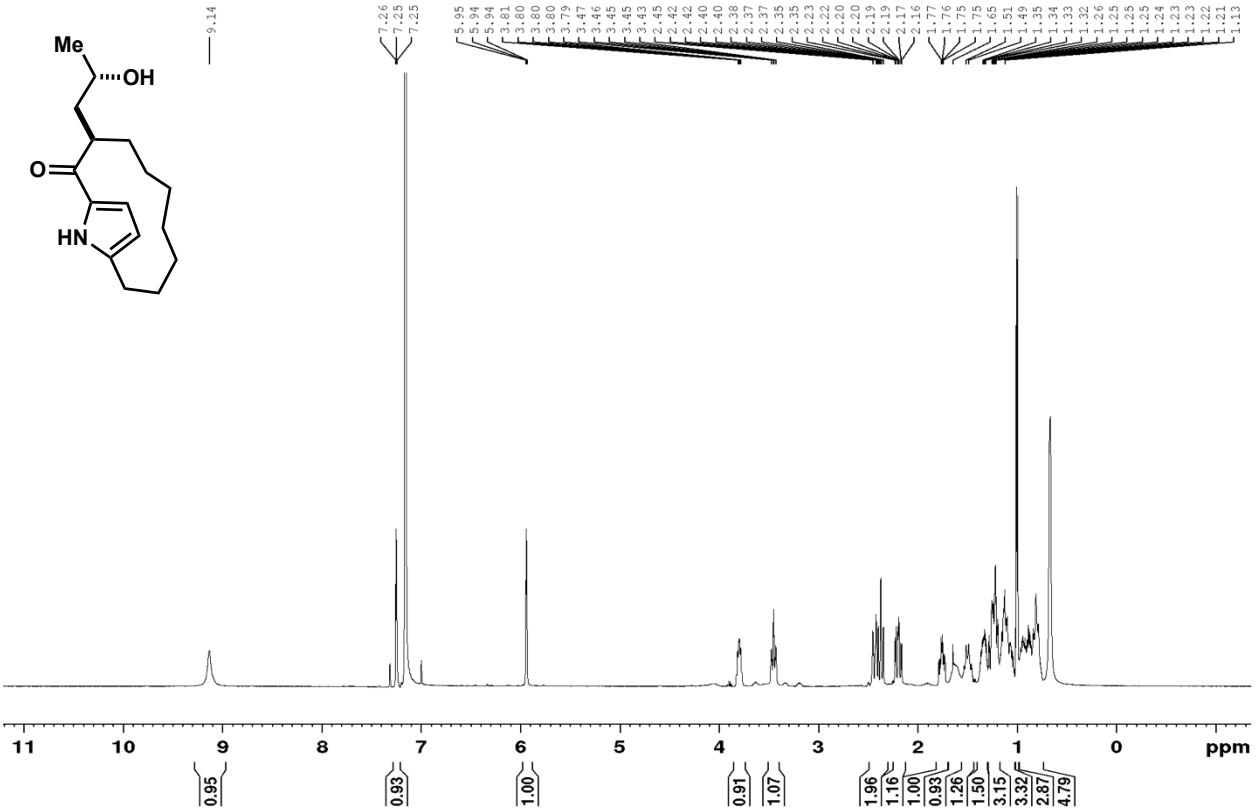

Spectrum 2.4.6 ^{13}C-NMR of compound **2R** (C_6D_6, 126 MHz)

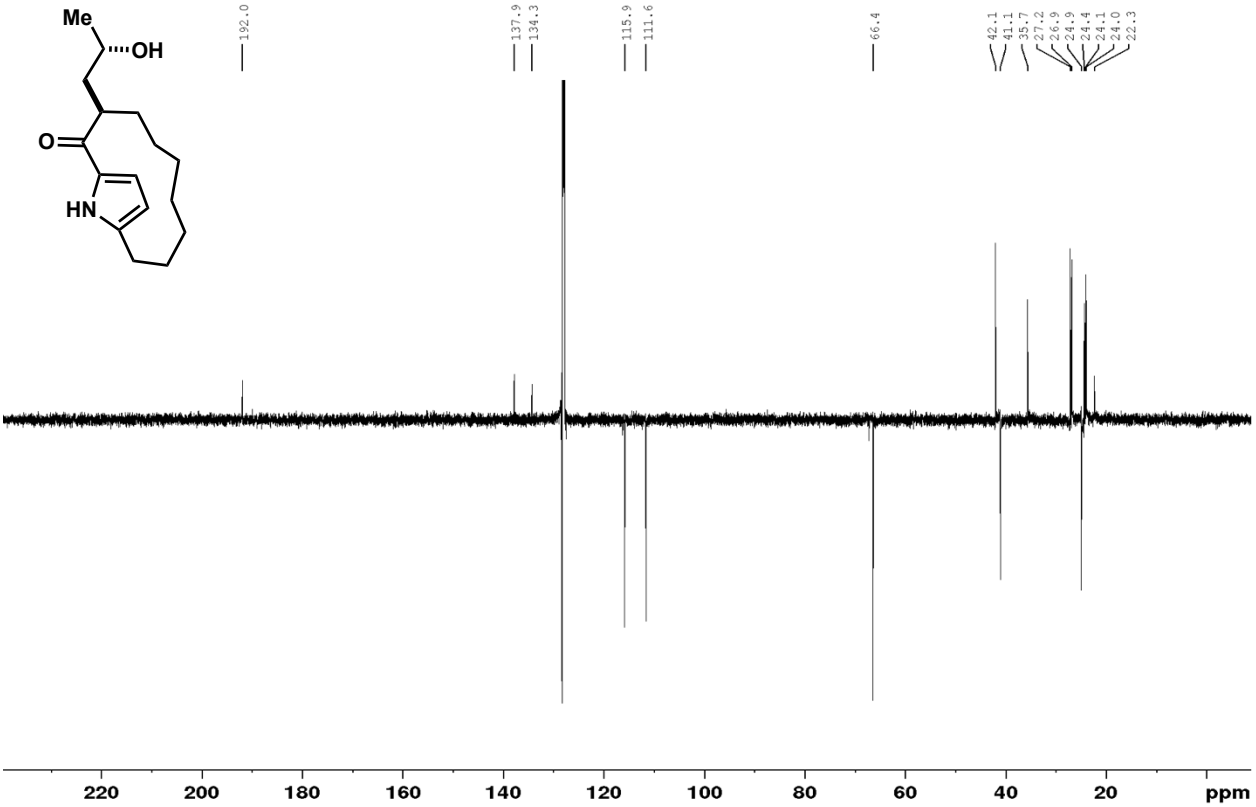

Spectrum 2.4.7 ^{1}H-NMR of compound Cbz-Protected **3** ($CDCl_3$, 500 MHz)

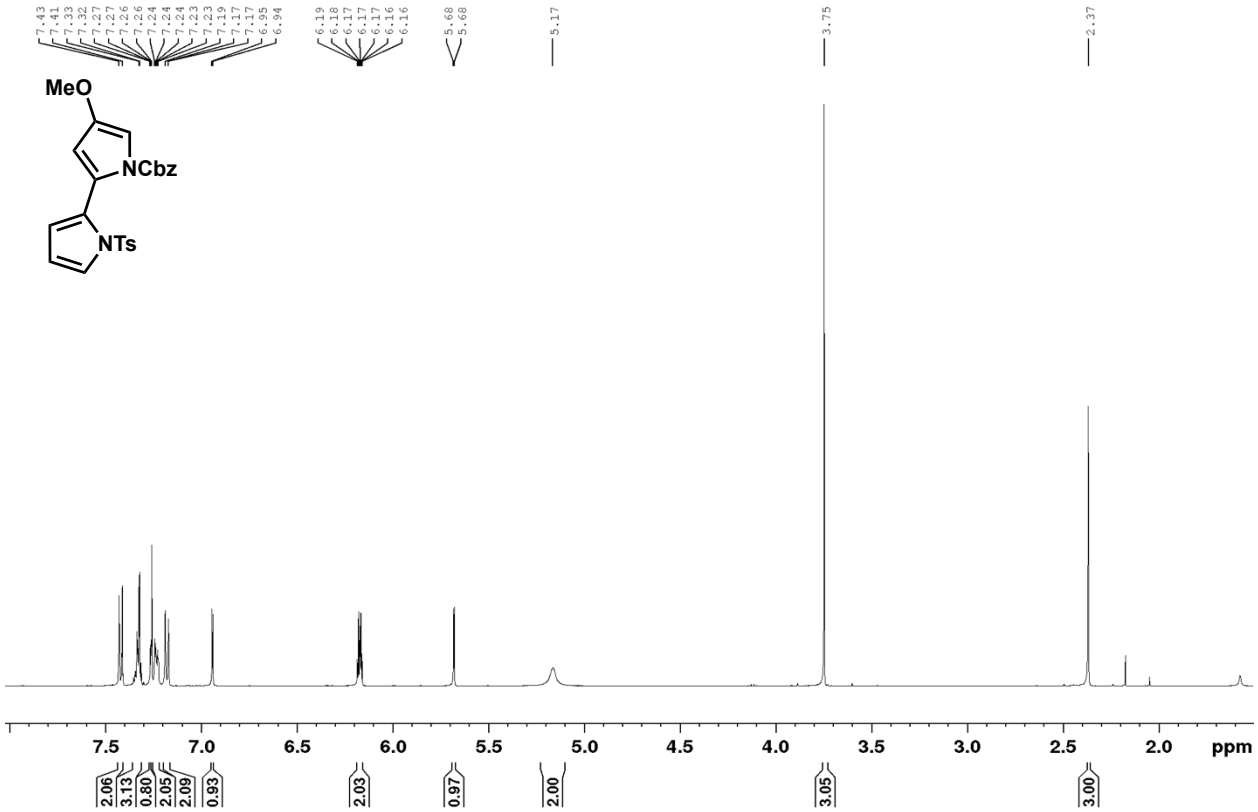

Spectrum 2.4.8 ^{13}C-NMR of compound Cbz-Protected **3** ($CDCl_3$, 126 MHz)

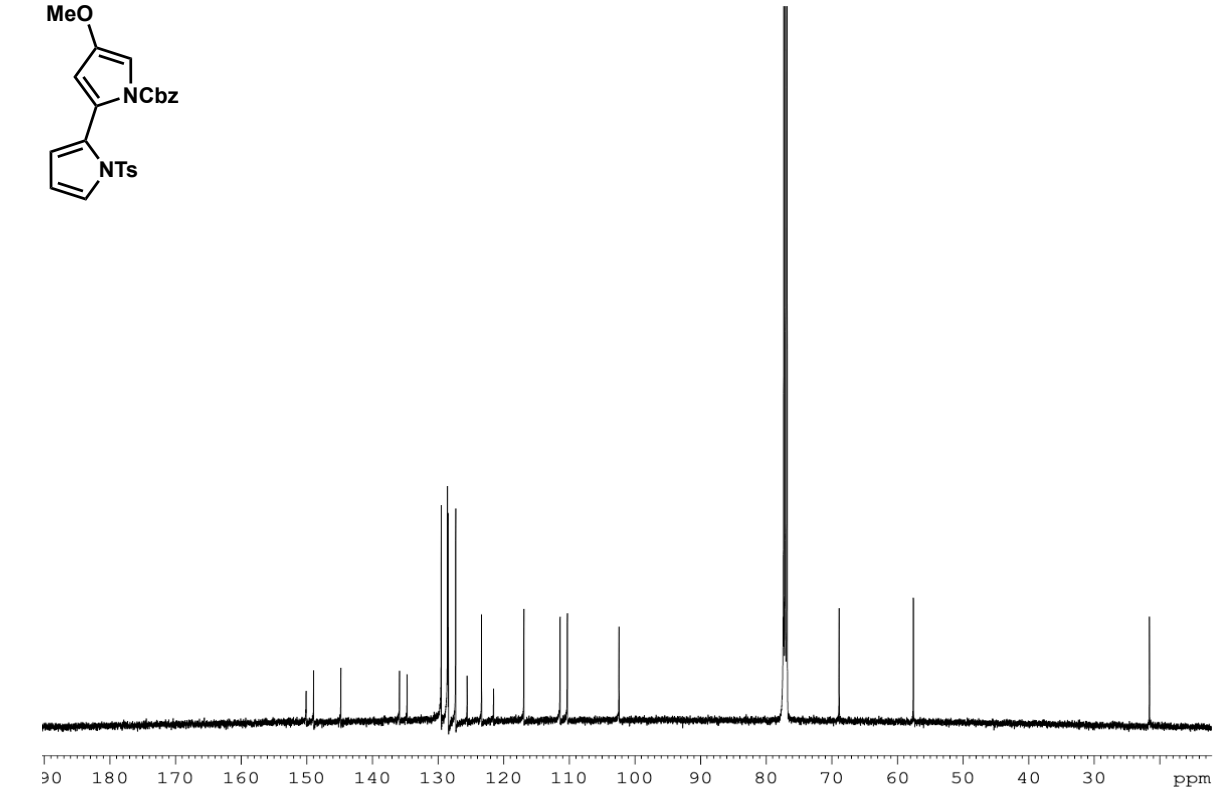

Spectrum 2.4.9 ^{1}H-NMR of compound **5** ($CDCl_3$, 500 MHz)

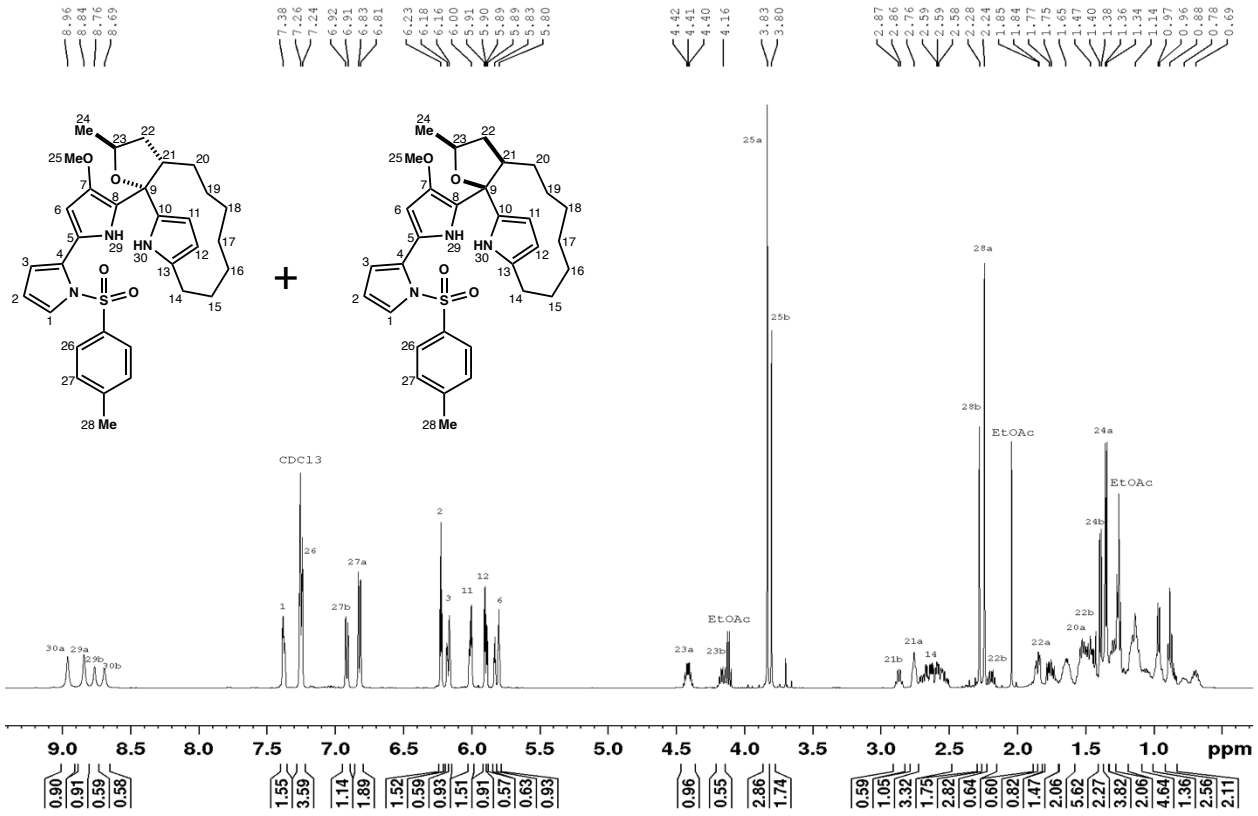

Spectrum 2.4.10 ^{13}C-NMR of compound **5** ($CDCl_3$, 126 MHz)

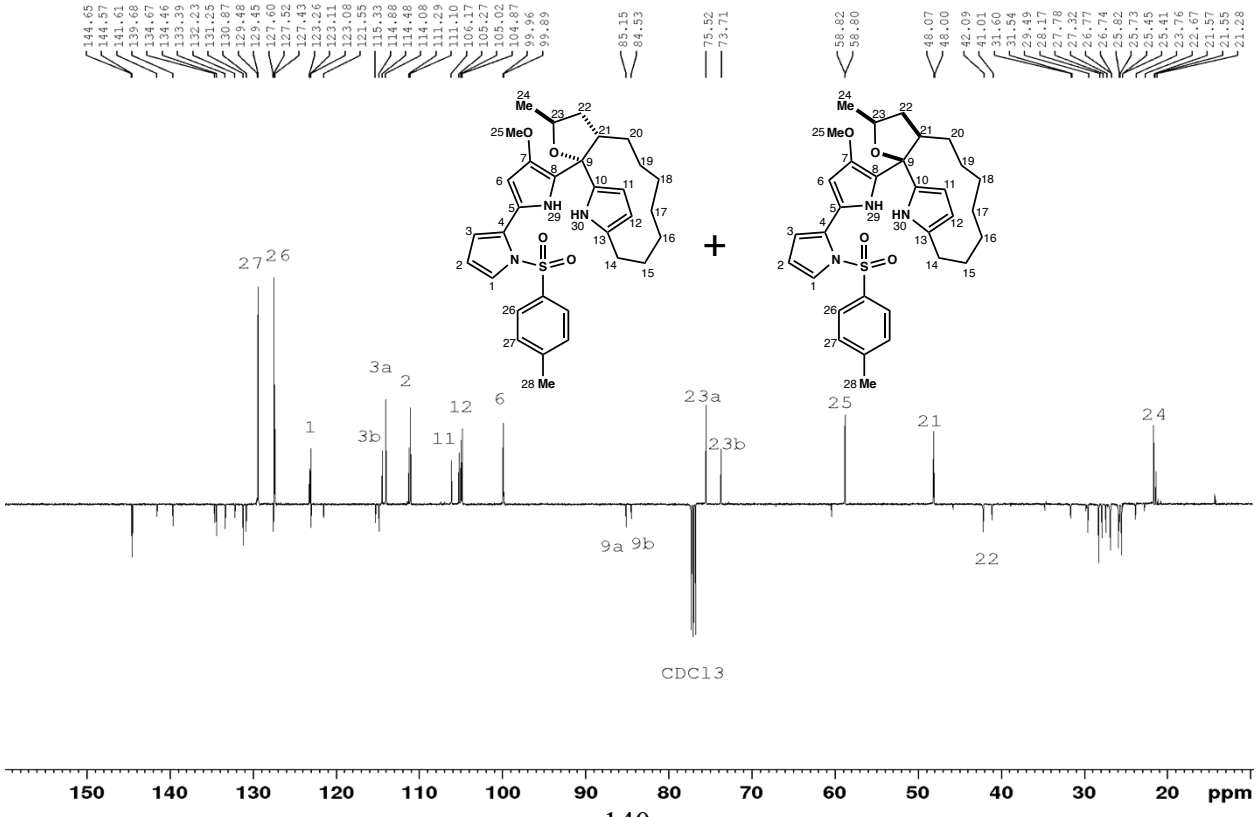

Spectrum 2.4.11 HSQC of compound **5** ($CDCl_3$, 126 MHz)

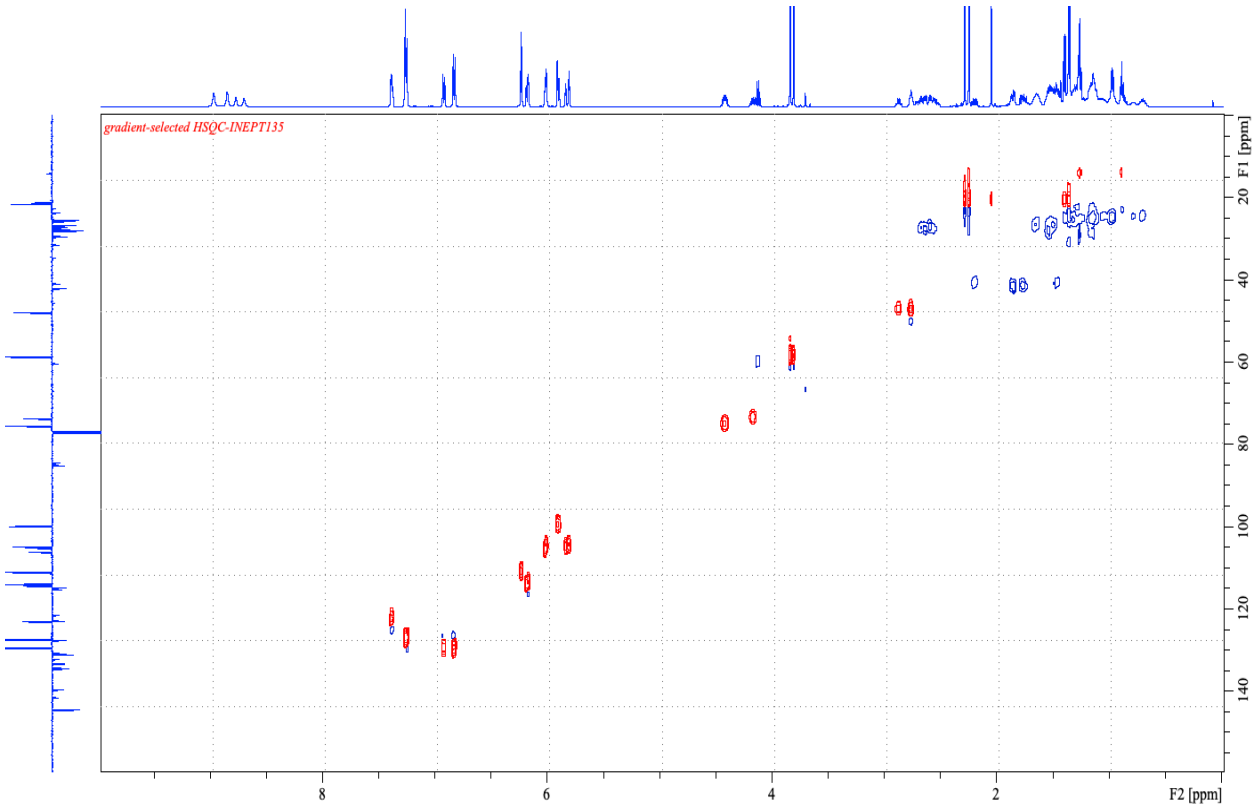

Spectrum 2.4.12 HMBC of compound **5** ($CDCl_3$, 126 MHz)

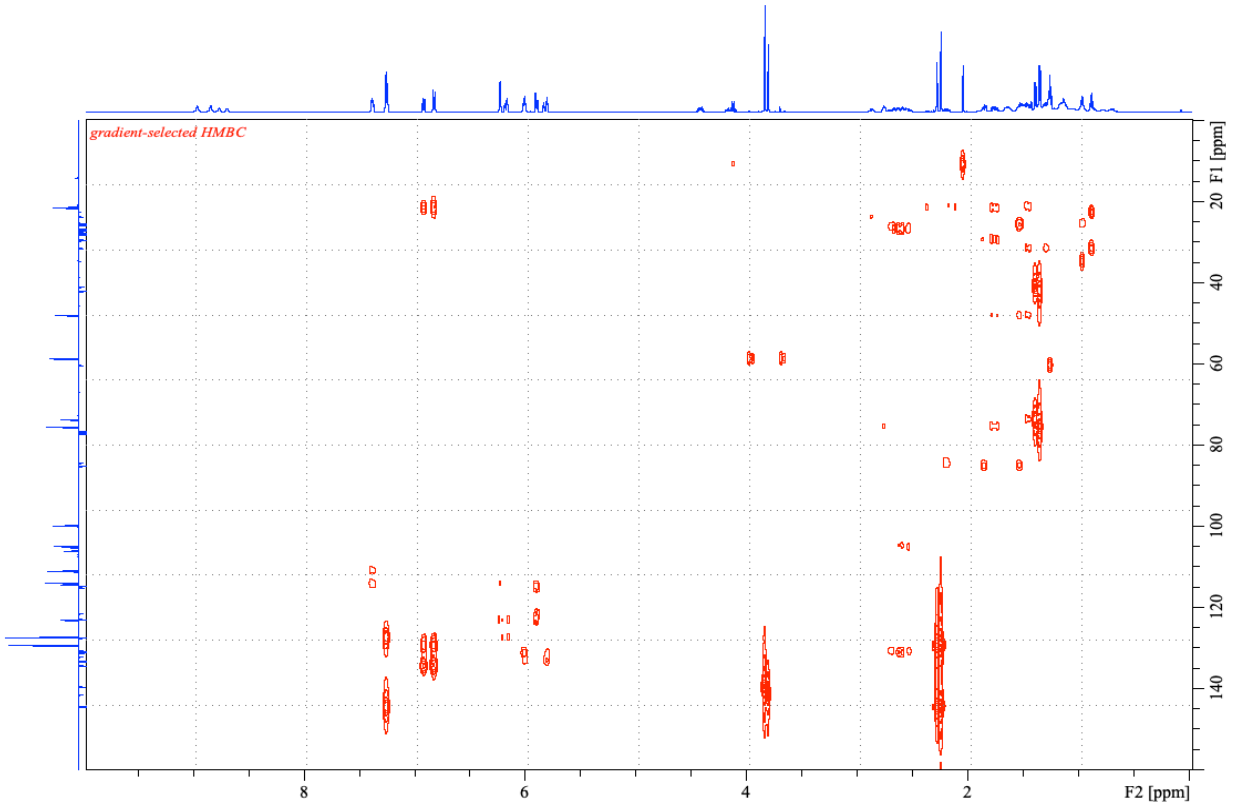

Spectrum 2.4.13 COSY of compound **5** ($CDCl_3$, 500 MHz)

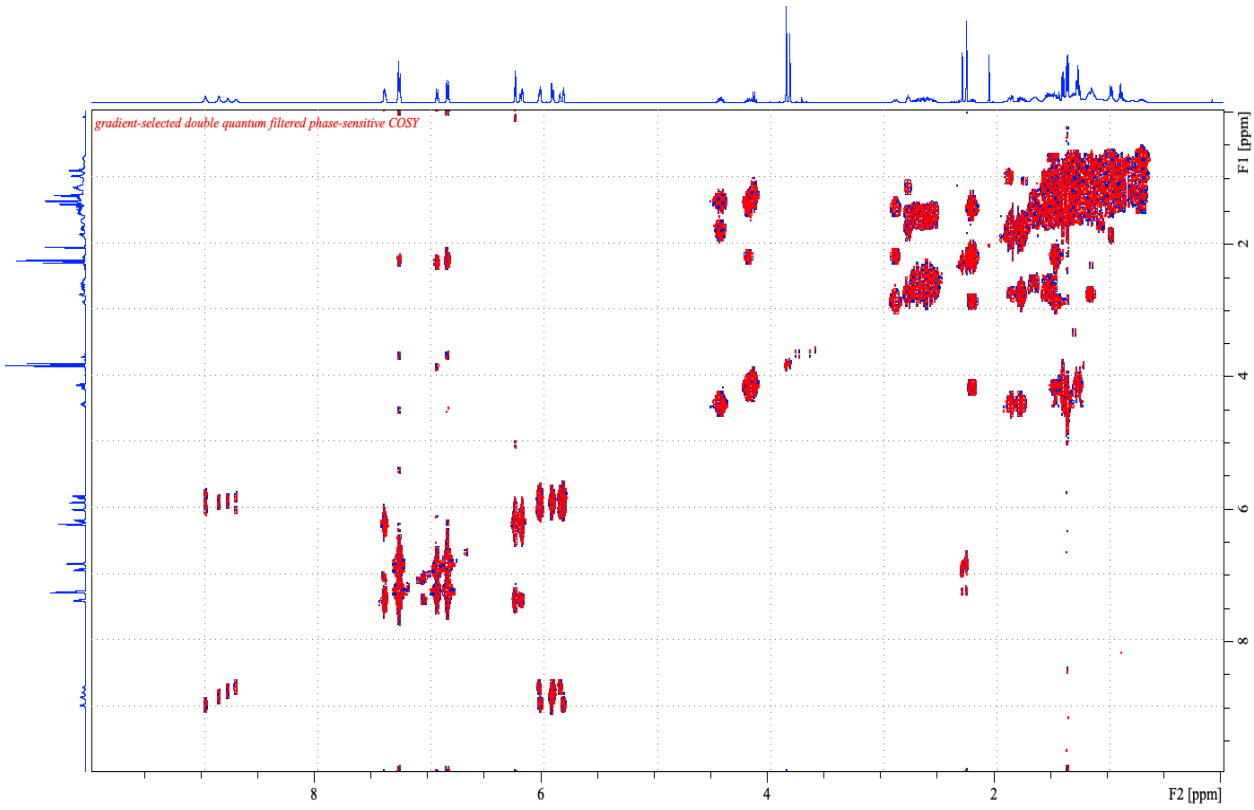

Spectrum 2.4.14 NOSEY of compound **5** ($CDCl_3$, 500 MHz)

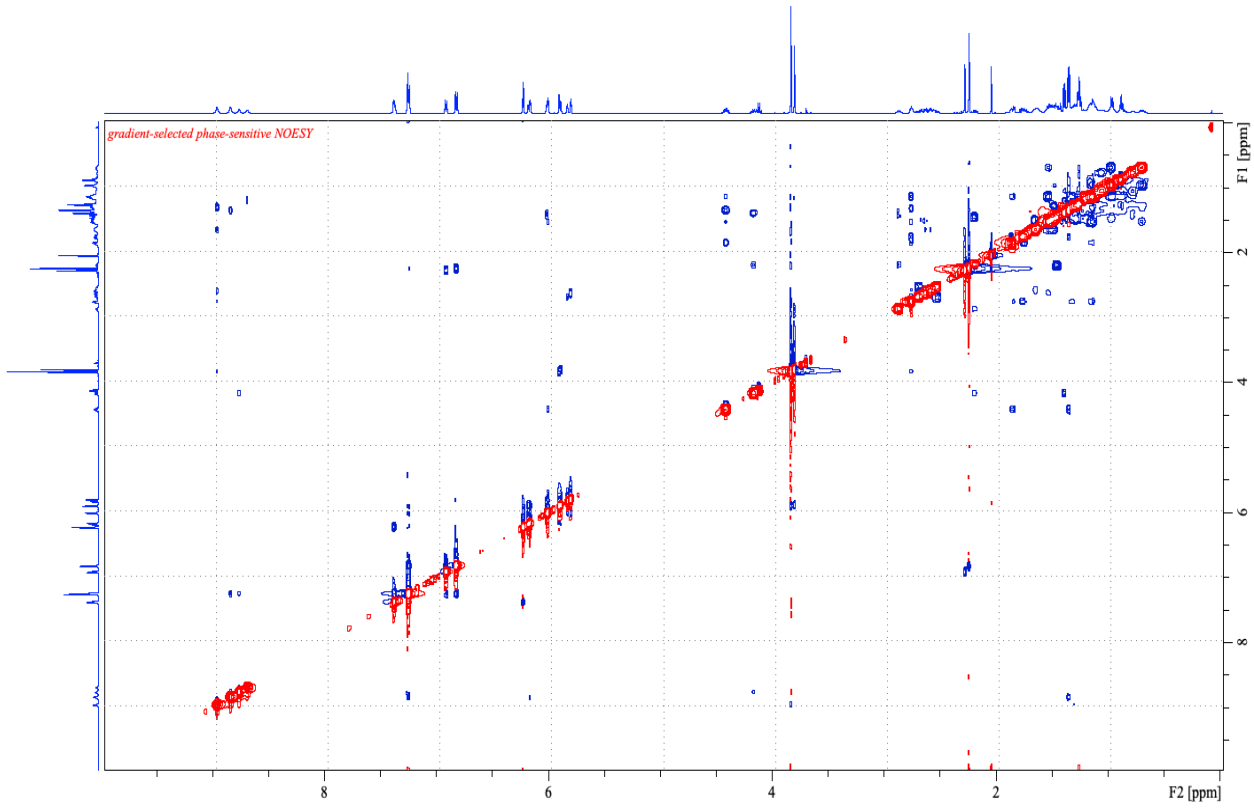

Spectrum 2.4.15 ^{1}H-NMR of compound **6** (acetone-d6, 500 MHz)

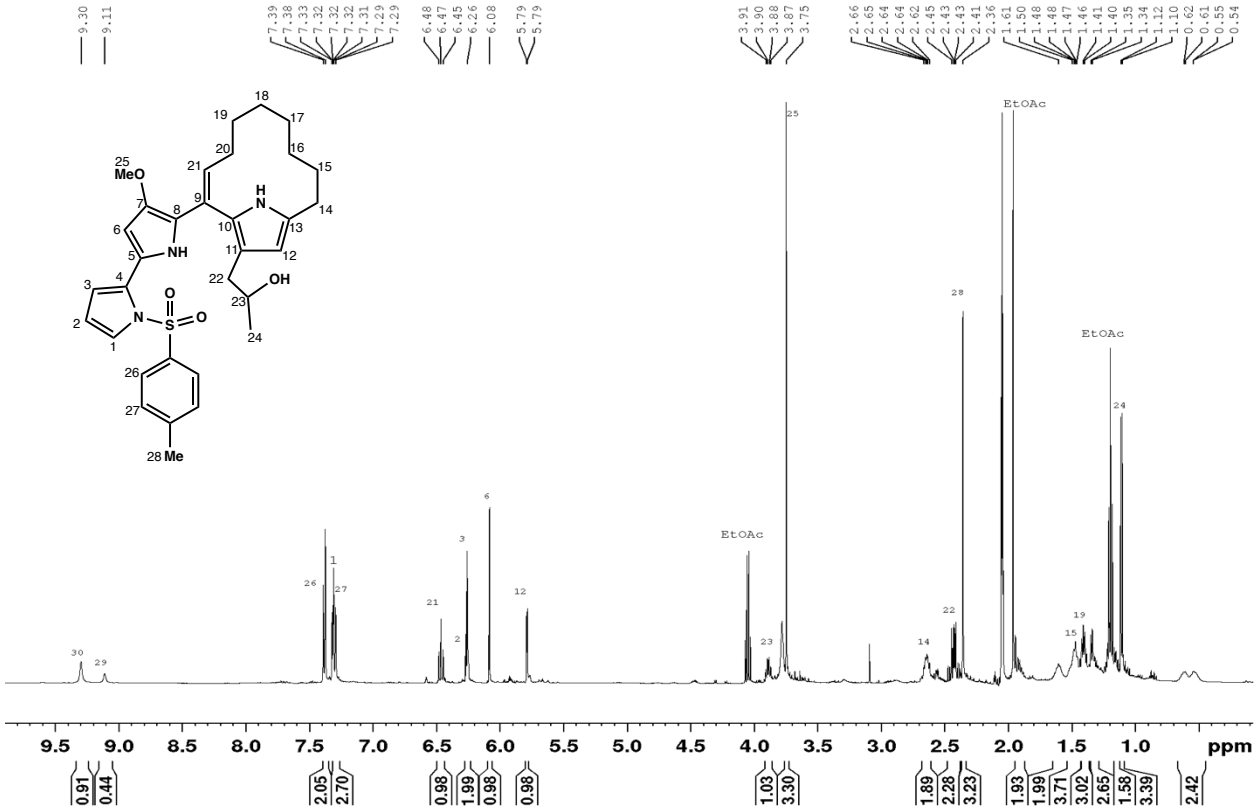

Spectrum 2.4.16 ^{13}C-NMR of compound **6** (acetone-d6, 126 MHz)

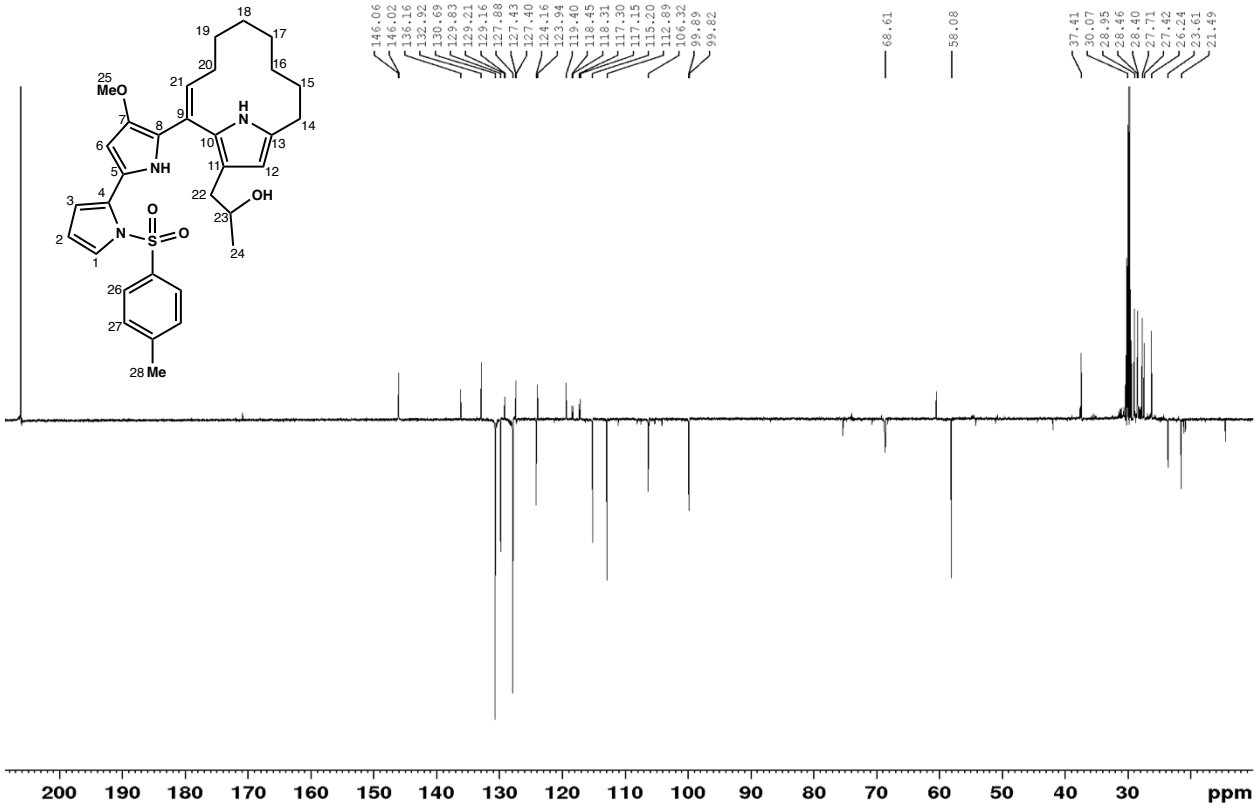

Spectrum 2.4.17 HSQC of compound **6** (acetone-d6, 126 MHz)

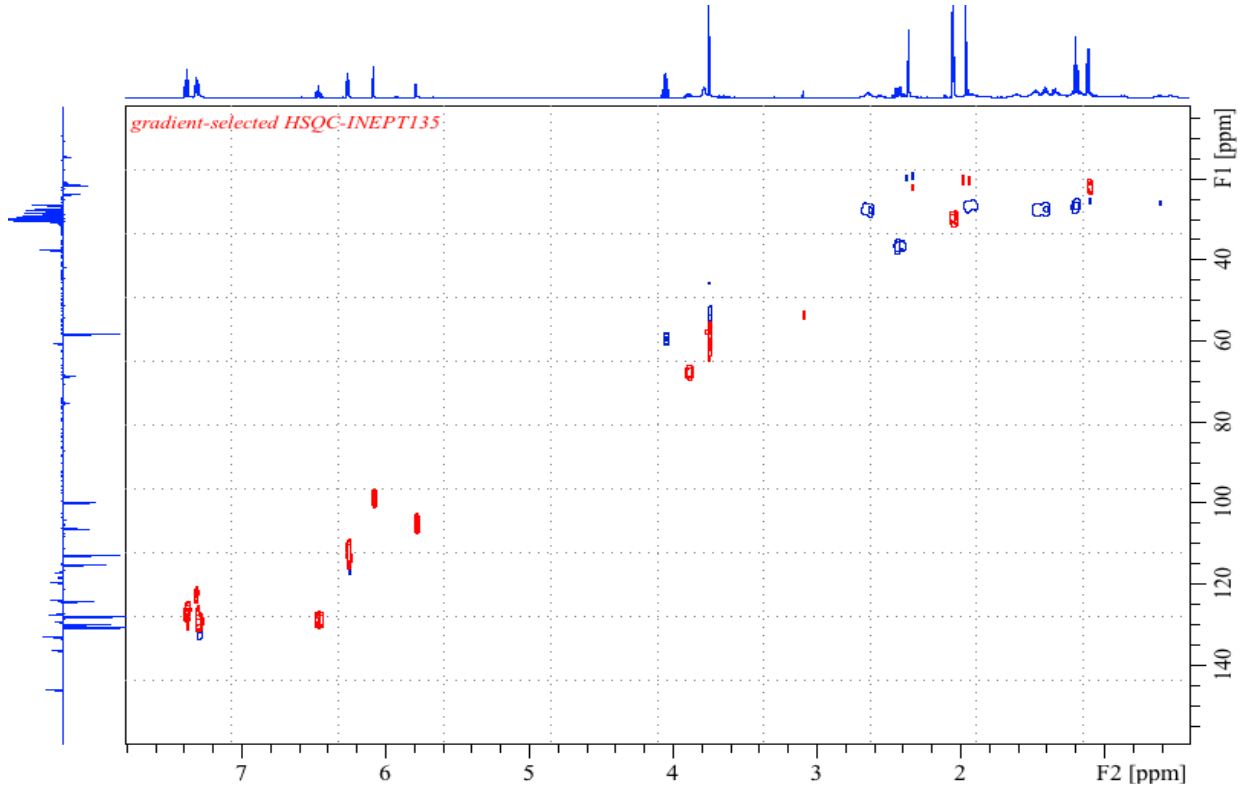

Spectrum 2.4.18 HMBC of compound **6** (acetone-d6, 126 MHz)

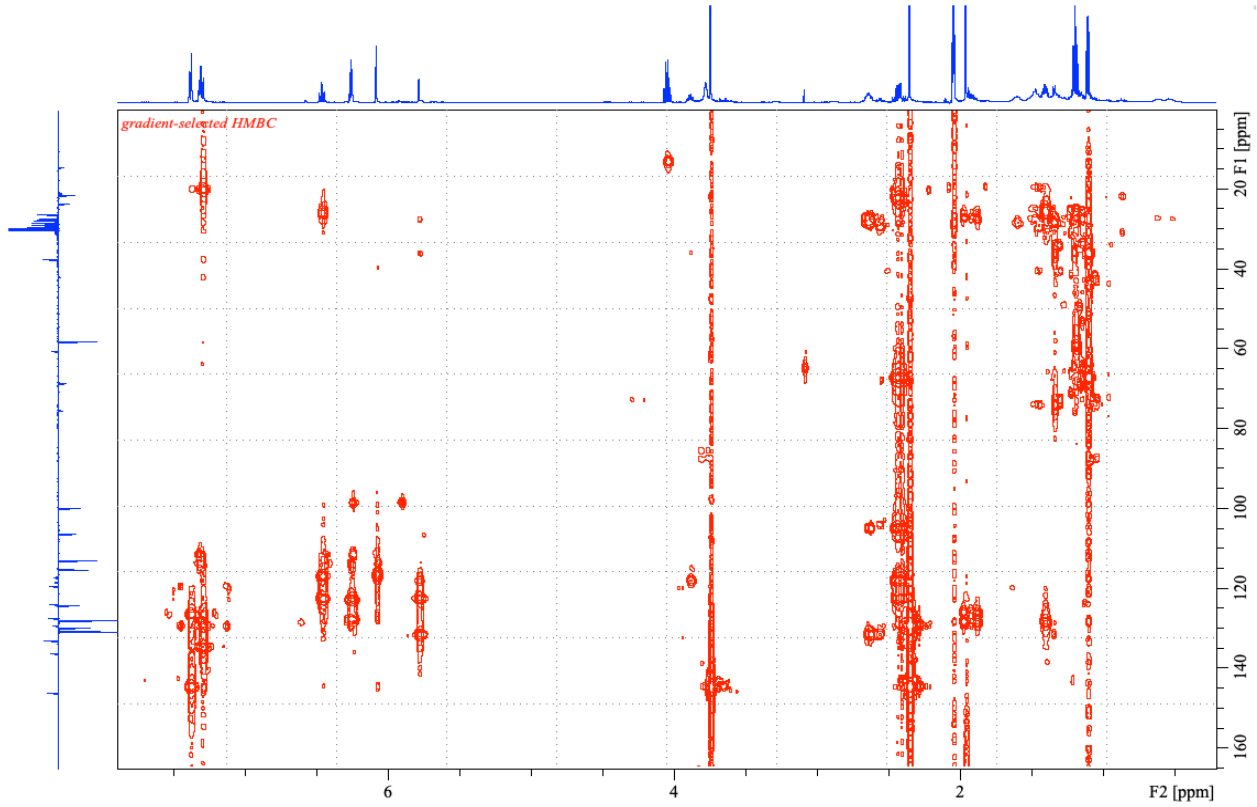

Spectrum 2.4.19 COSY of compound **6** (acetone-d6, 500 MHz)

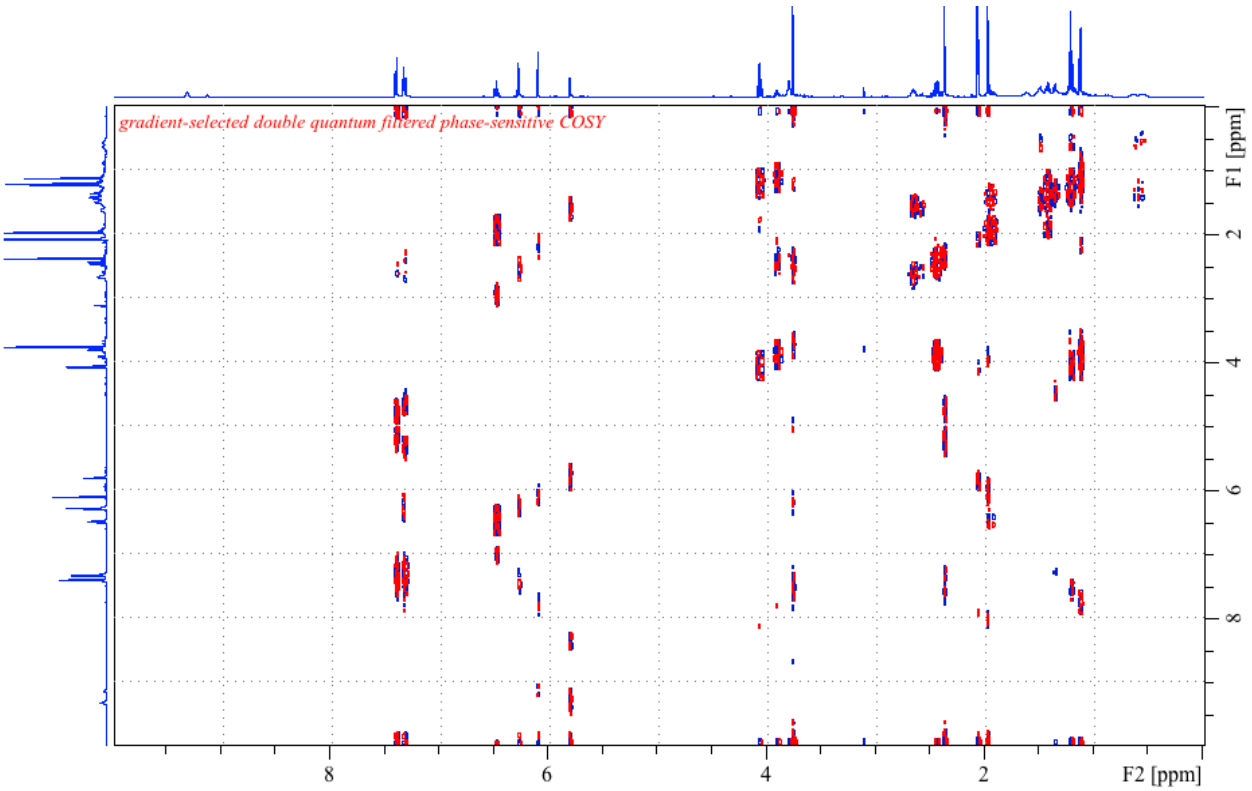

Spectrum 2.4.20 NOSEY of compound **6** (acetone-d6, 500 MHz)

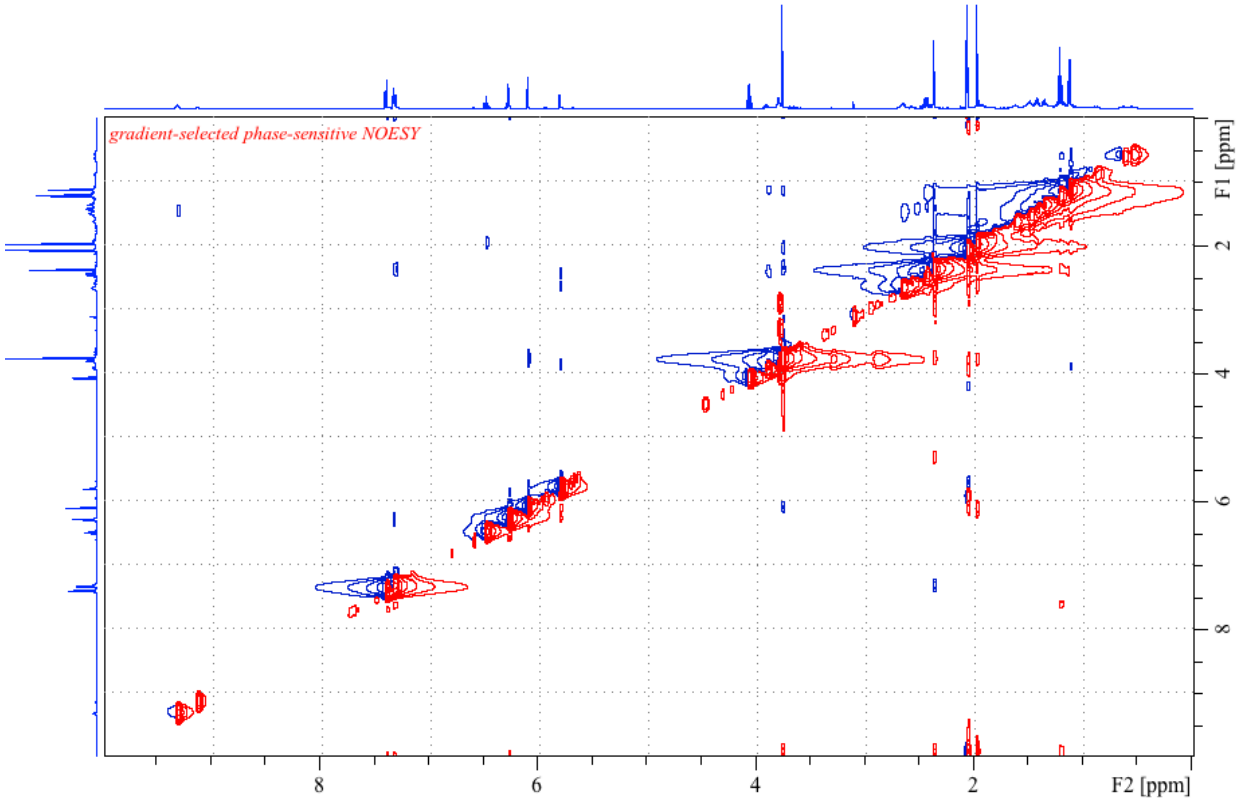

Spectrum 2.4.21 ^{1}H-NMR of compound **7** ($CDCl_3$, 500 MHz)

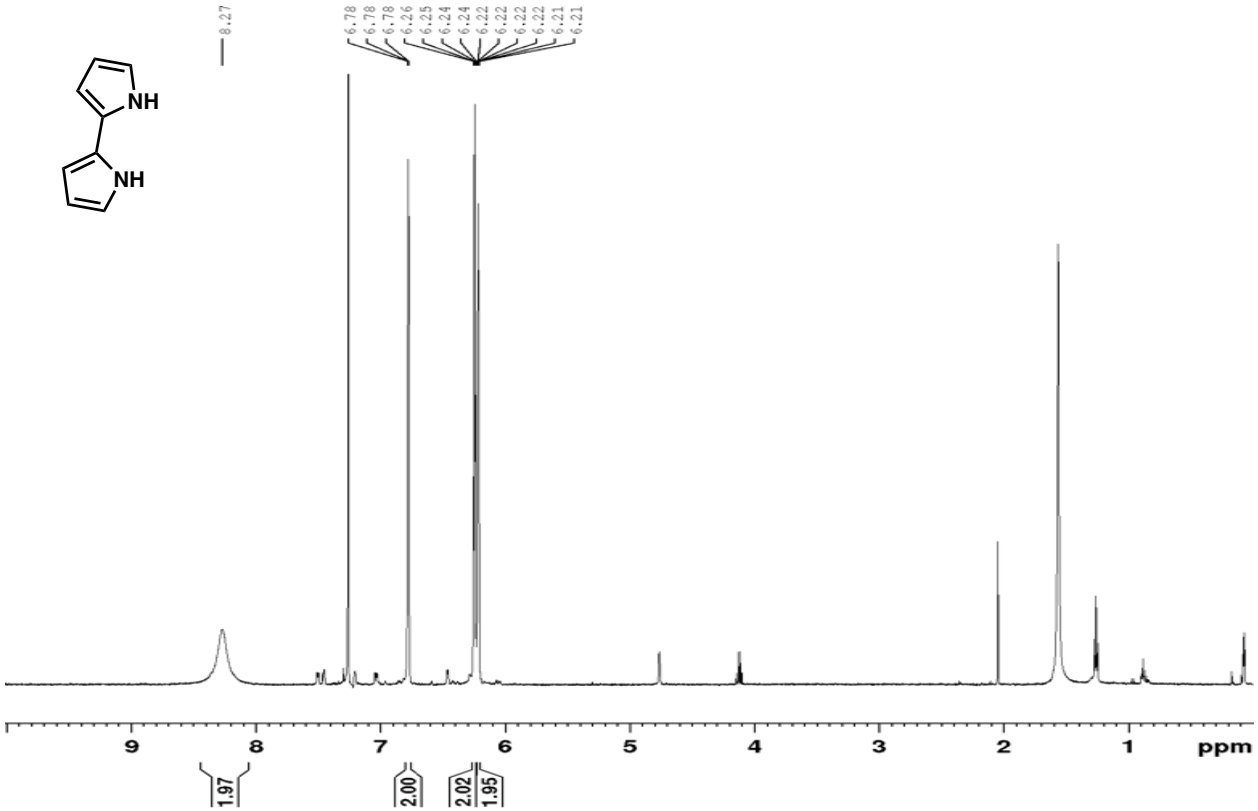

Spectrum 2.4.22 ^{1}H-NMR of compound **8** ($CDCl_3$, 500 MHz)

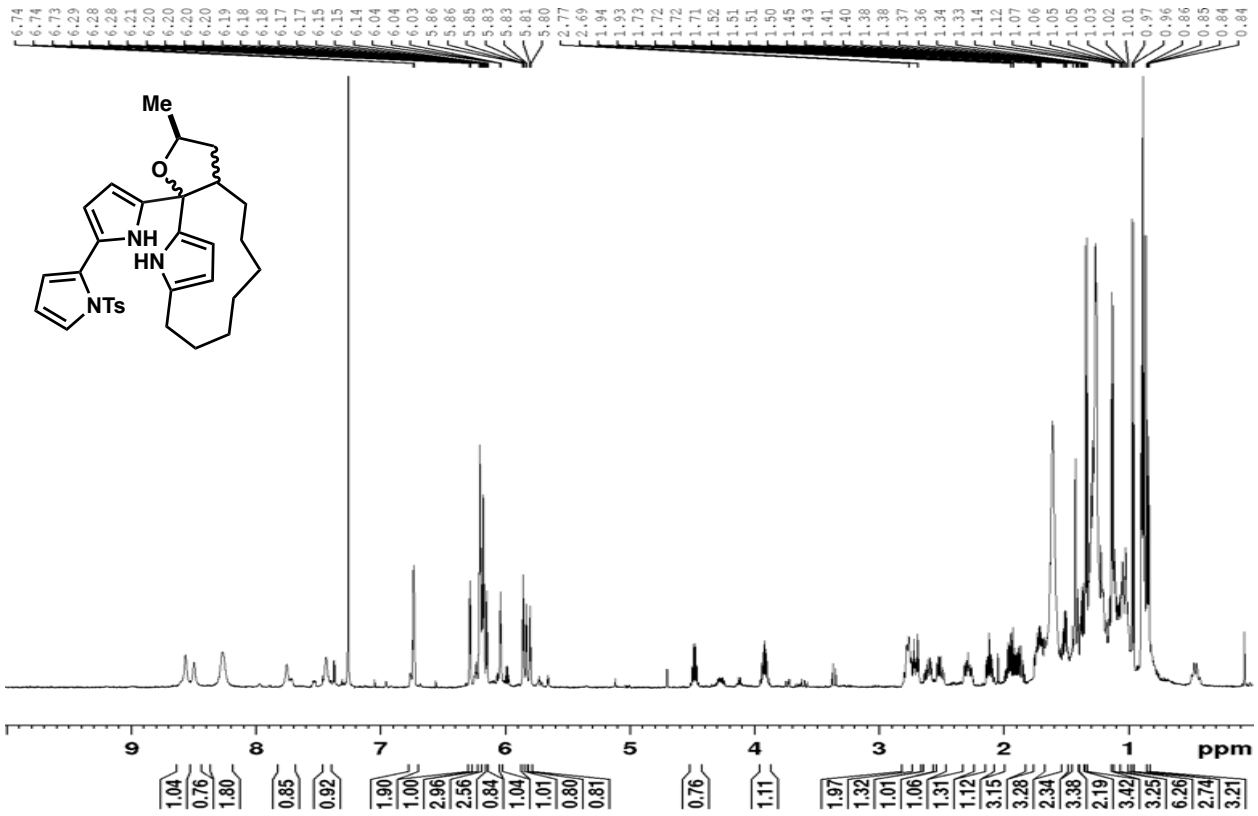

Spectrum 2.4.23 ^{1}H-NMR of compound **9** ($CDCl_3$, 400 MHz)

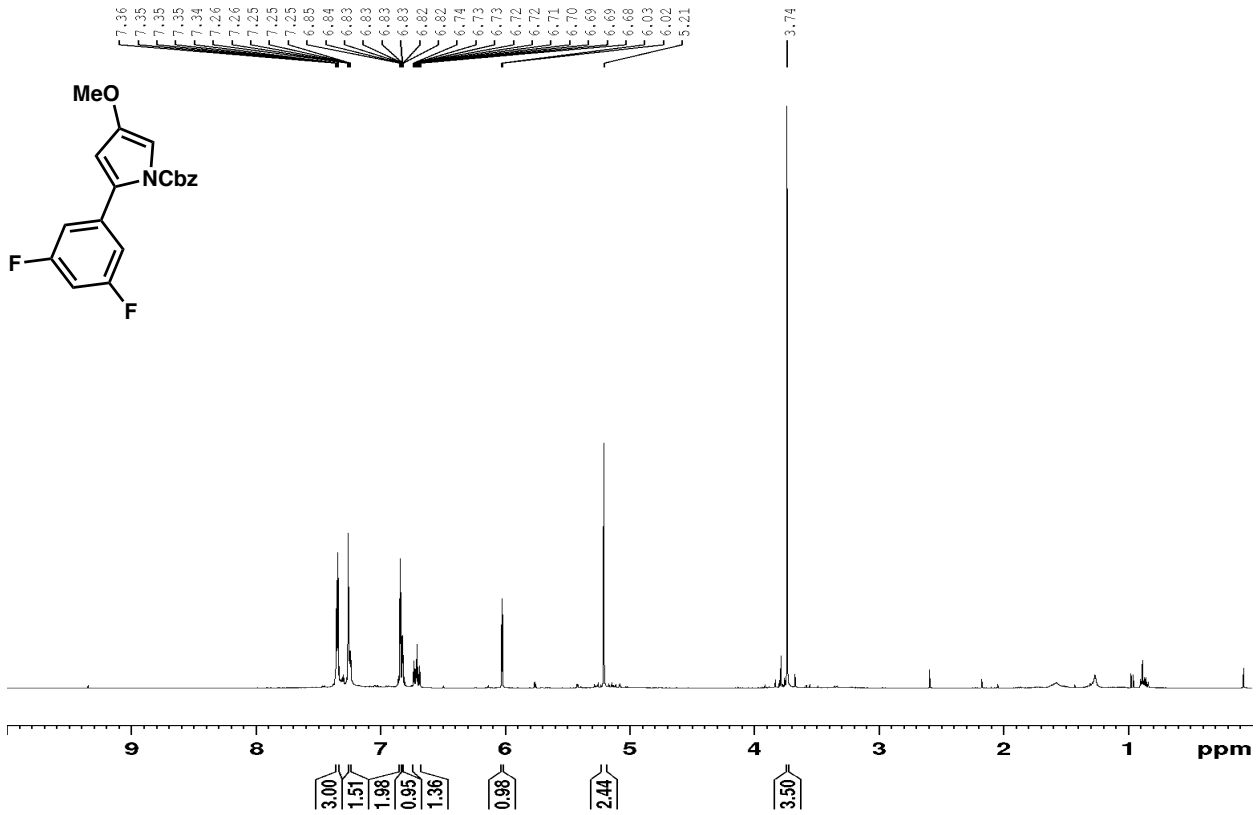

Spectrum 2.4.24 ^{1}H-NMR of compound **10** ($CDCl_3$, 500 MHz)

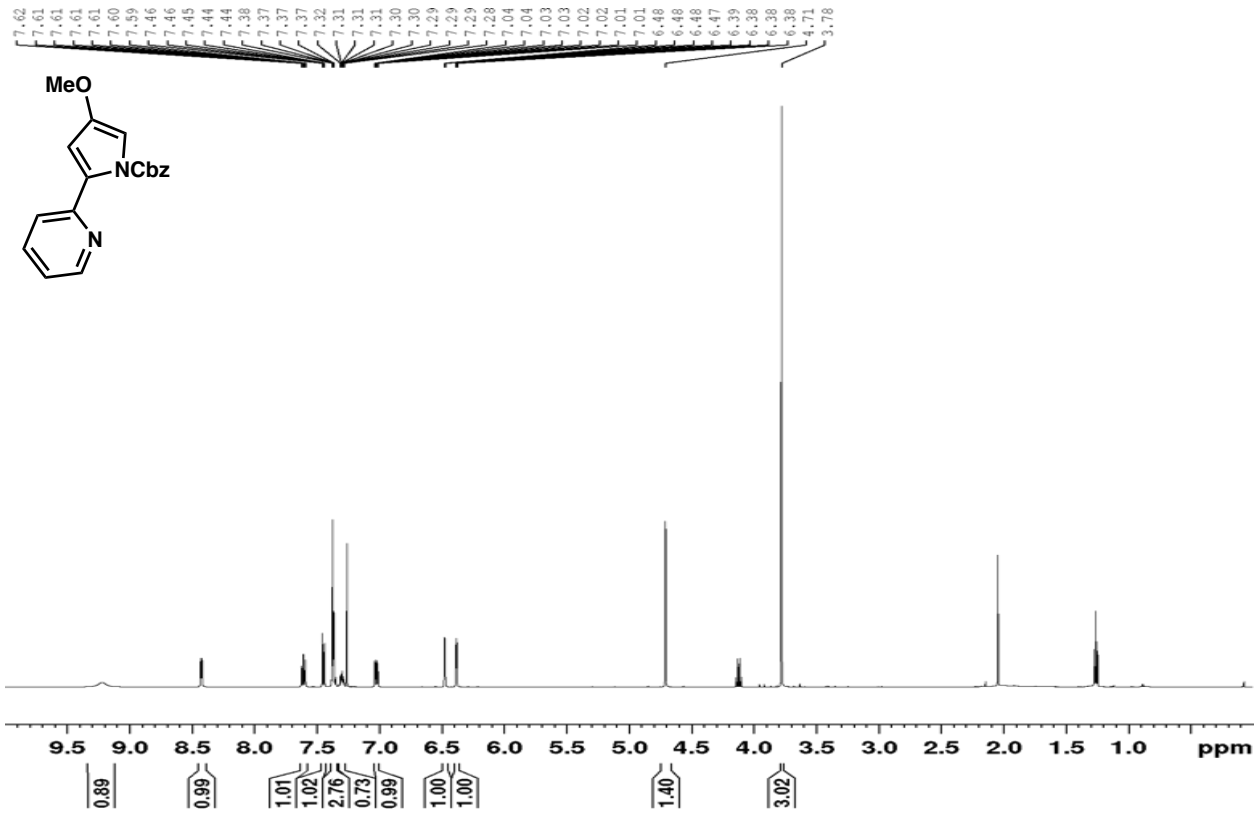

Spectrum 2.4.25 ^{13}C-NMR of compound **10** ($CDCl_3$, 126 MHz)

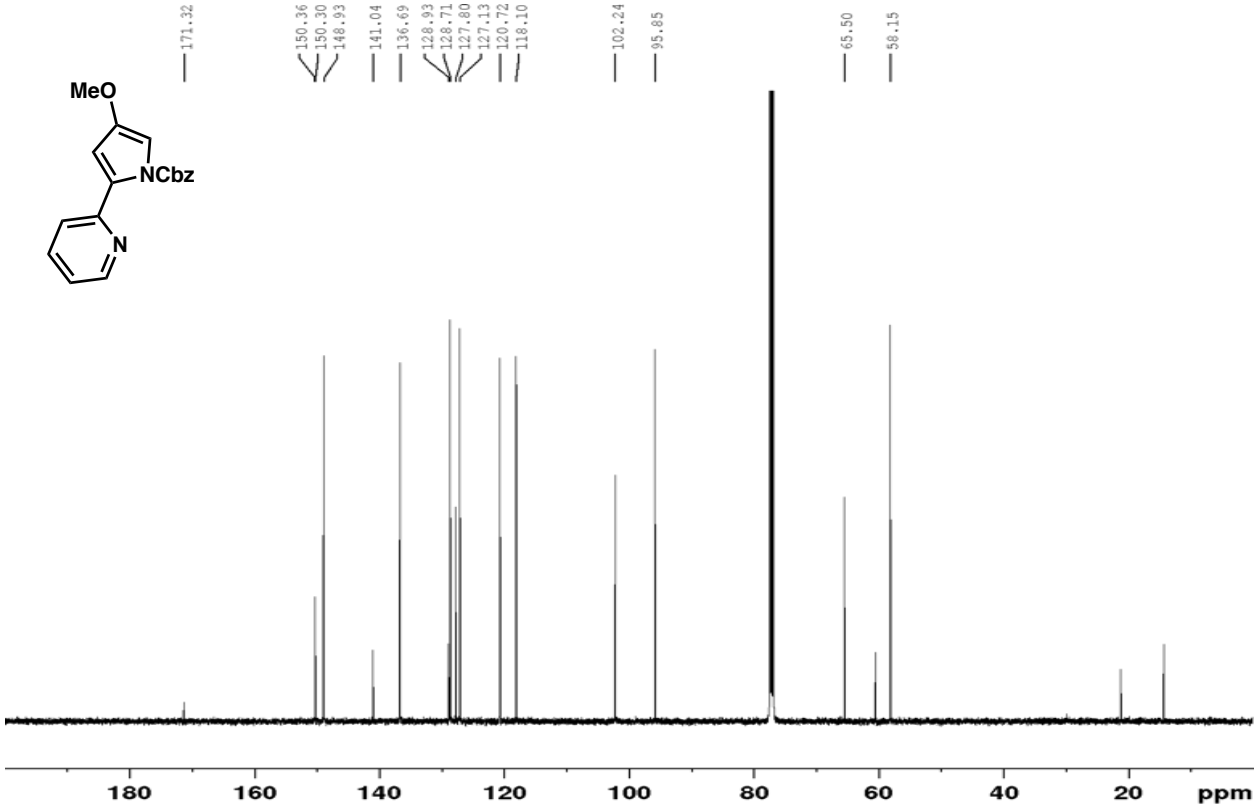

Spectrum 2.4.26 ^{1}H-NMR of compound **11** ($CDCl_3$, 400 HMz)

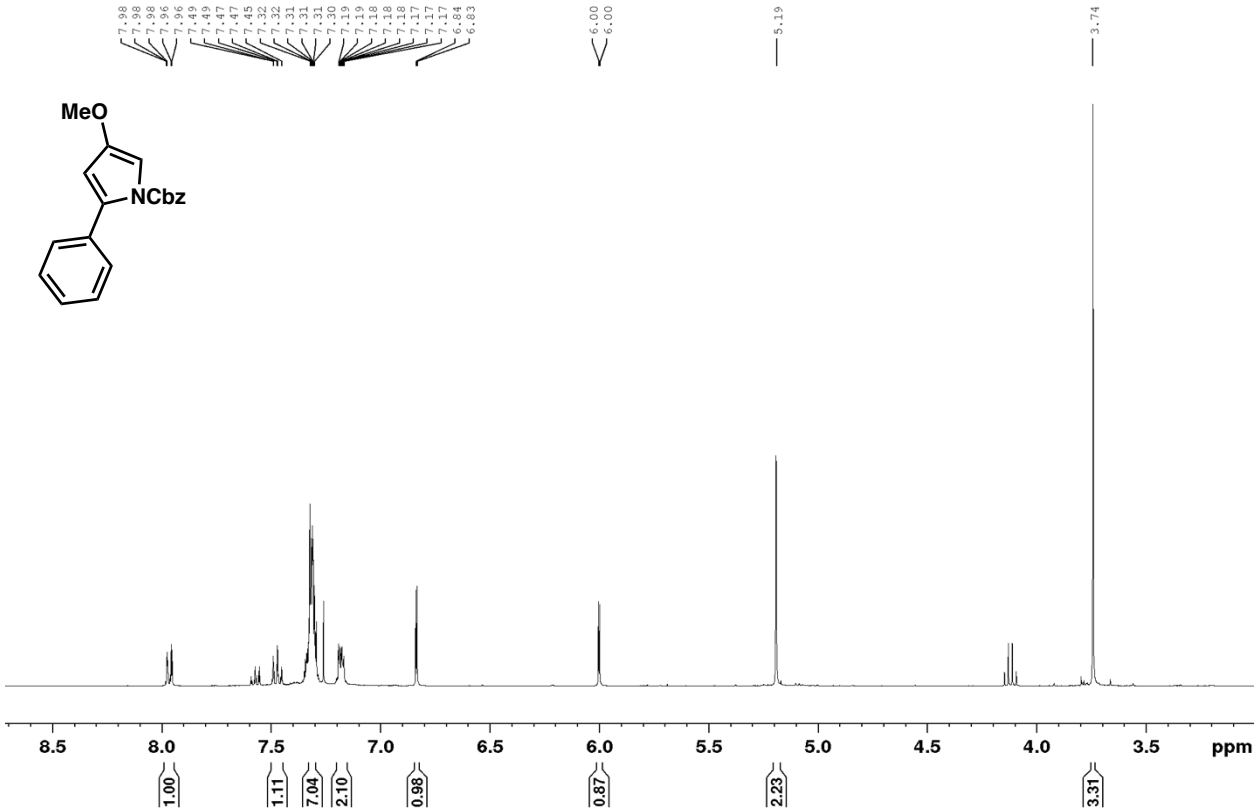

Spectrum 2.4.27 ^{13}C-NMR of compound **11** ($CDCl_3$, 101 HMz)

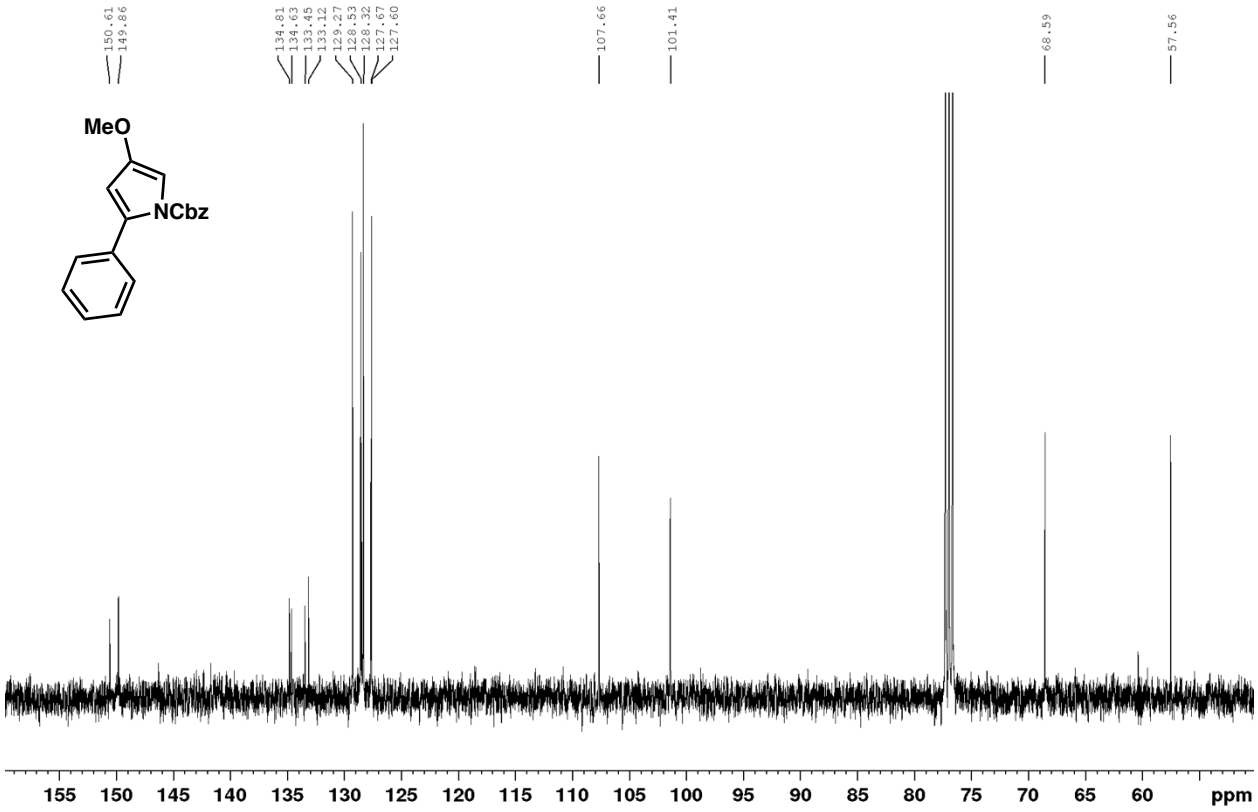

Spectrum 2.4.28 ^{1}H-NMR of compound **12** ($CDCl_3$, 500 MHz)

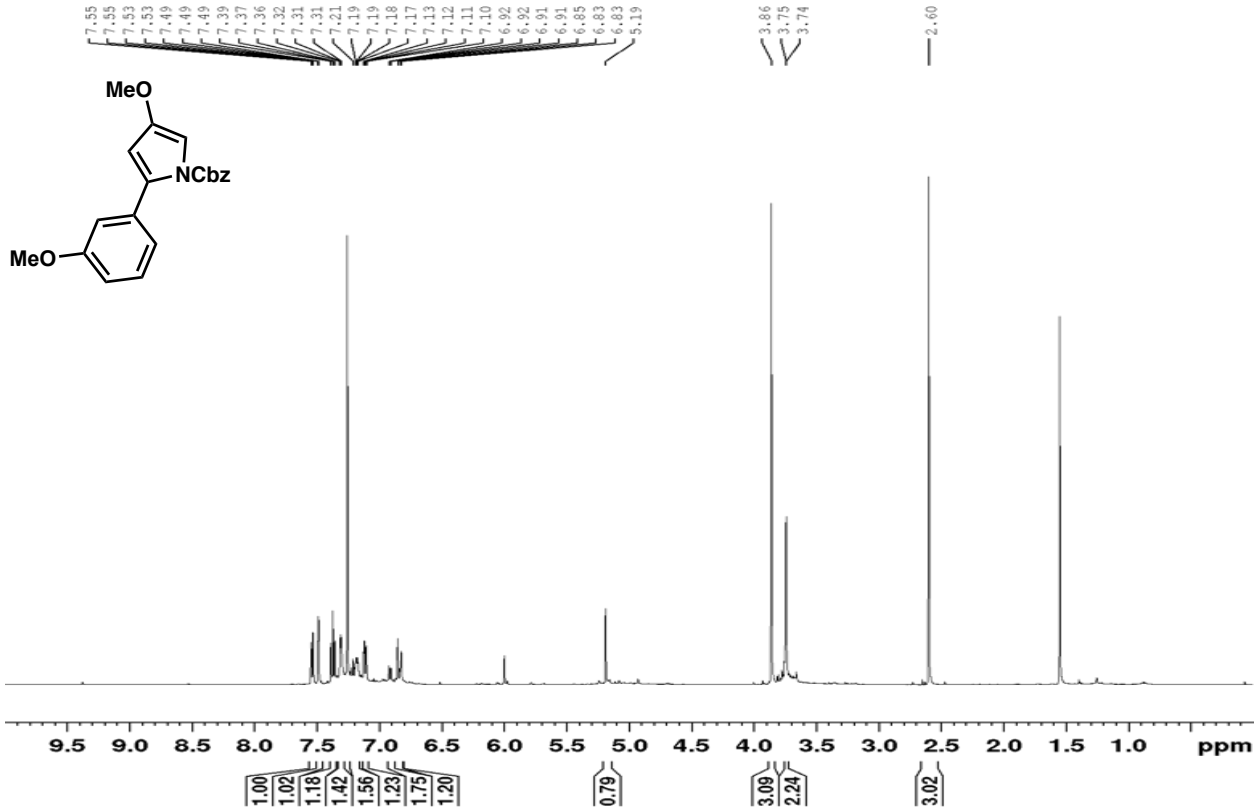

Spectrum 2.4.29 ^{13}C-NMR of compound **12** ($CDCl_3$, 126 MHz)

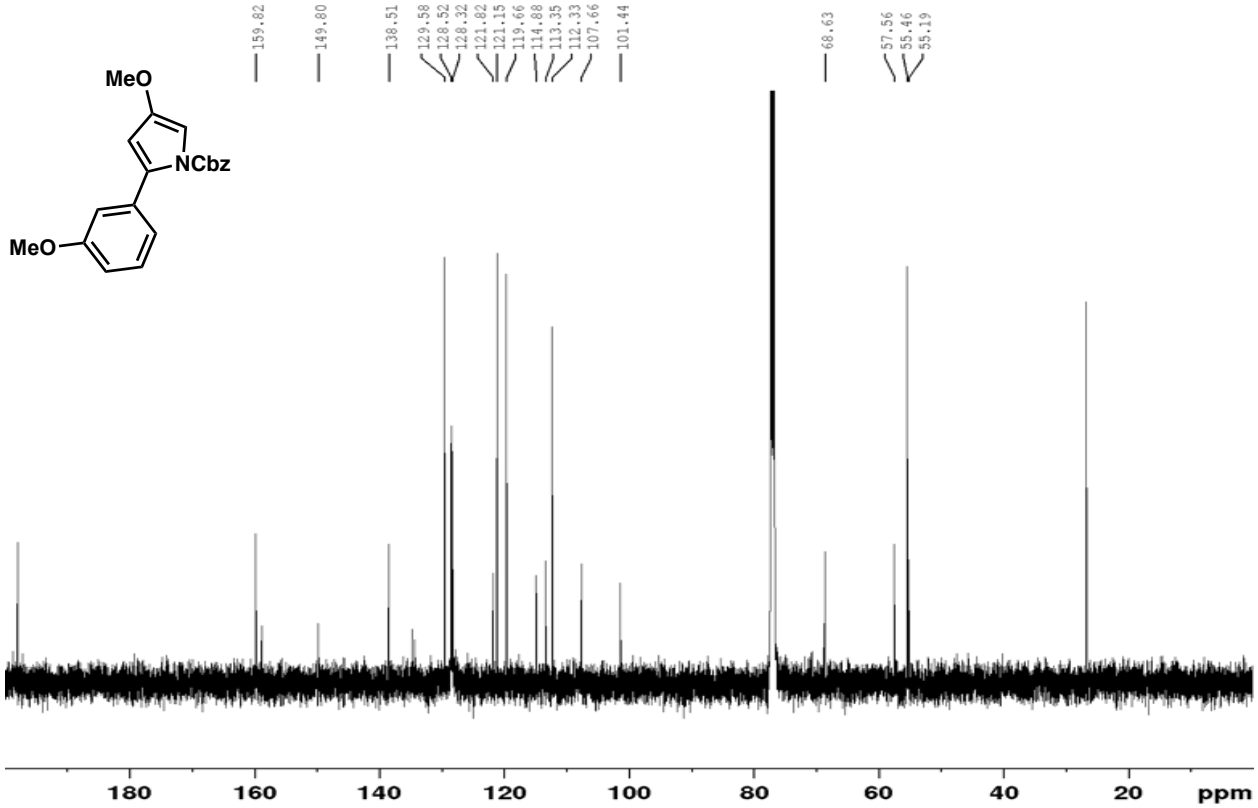

Spectrum 2.4.30 ^{1}H-NMR of compound **19a** ($CDCl_3$, 500 MHz)

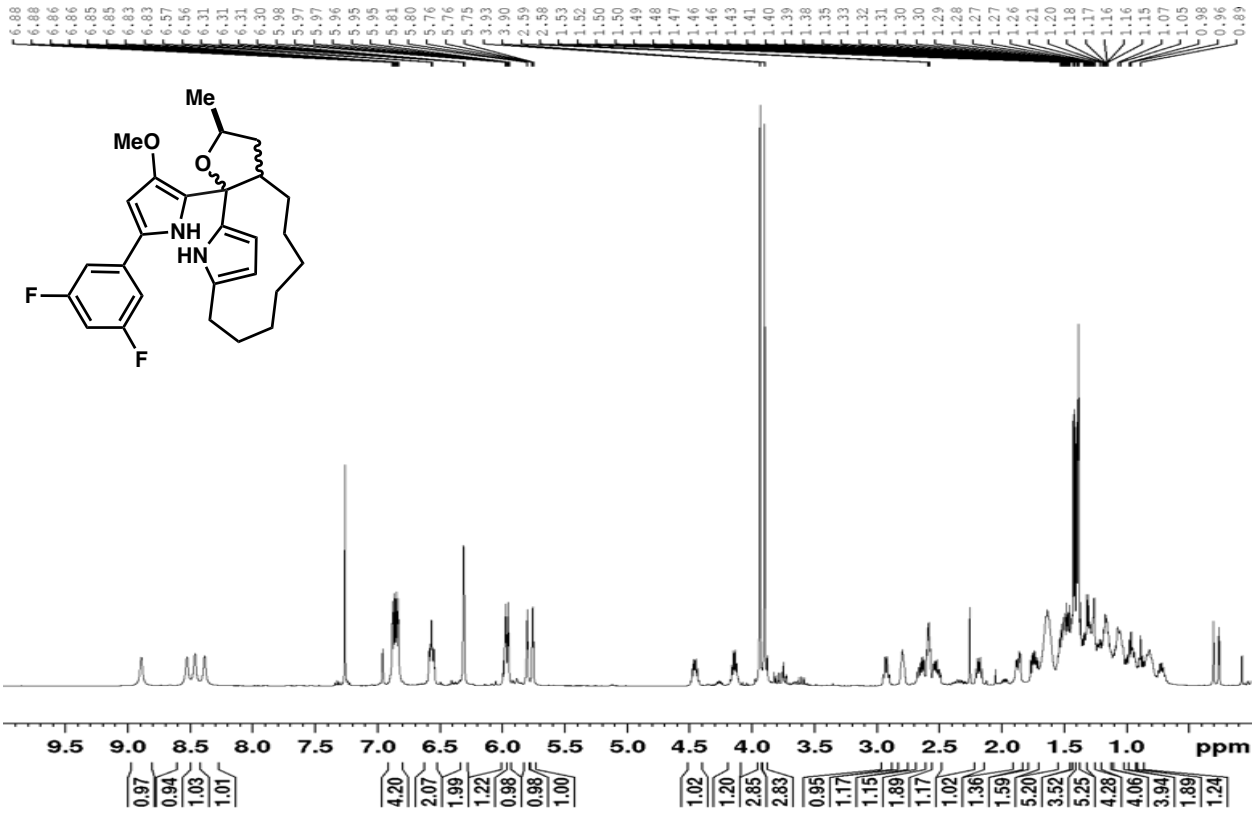

Spectrum 2.4.31 ^{13}C-NMR of compound **19a** ($CDCl_3$, 126 MHz)

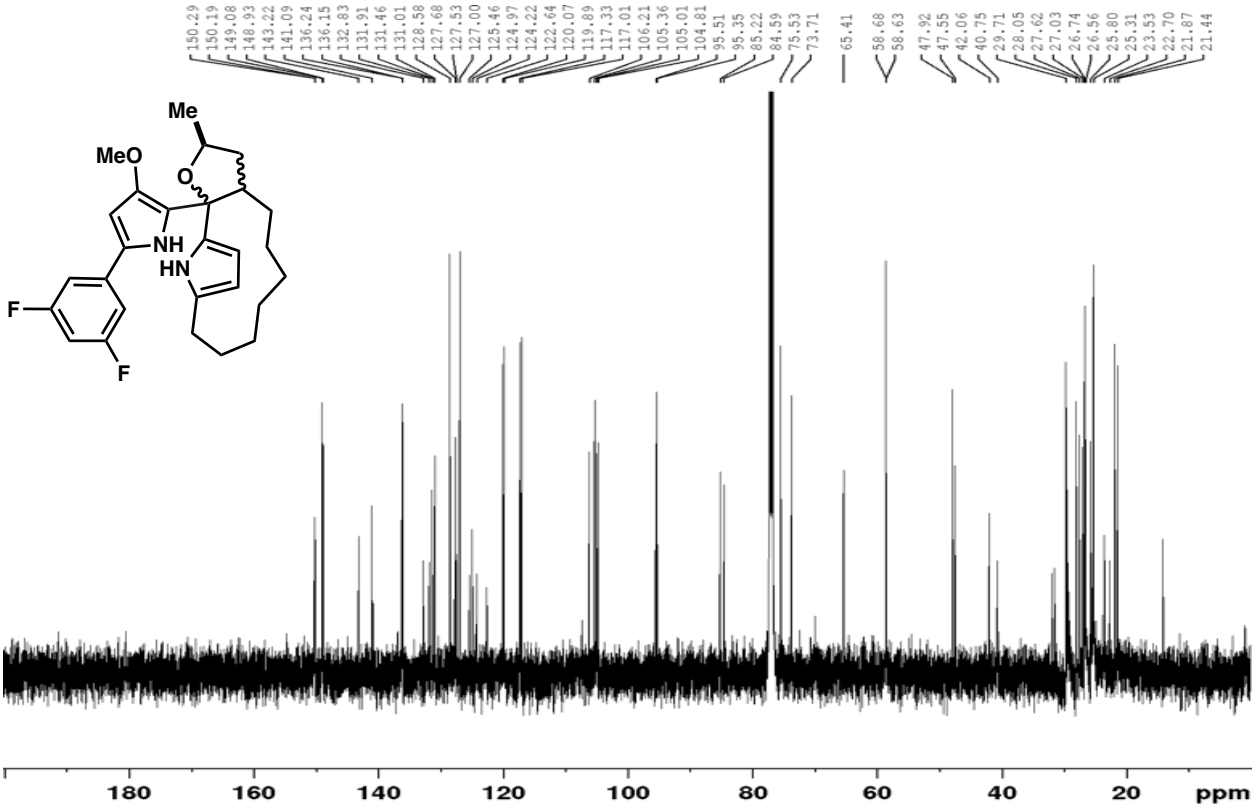

Spectrum 2.4.32 ^{1}H-NMR of compound **19b** ($CDCl_3$, 500 MHz)

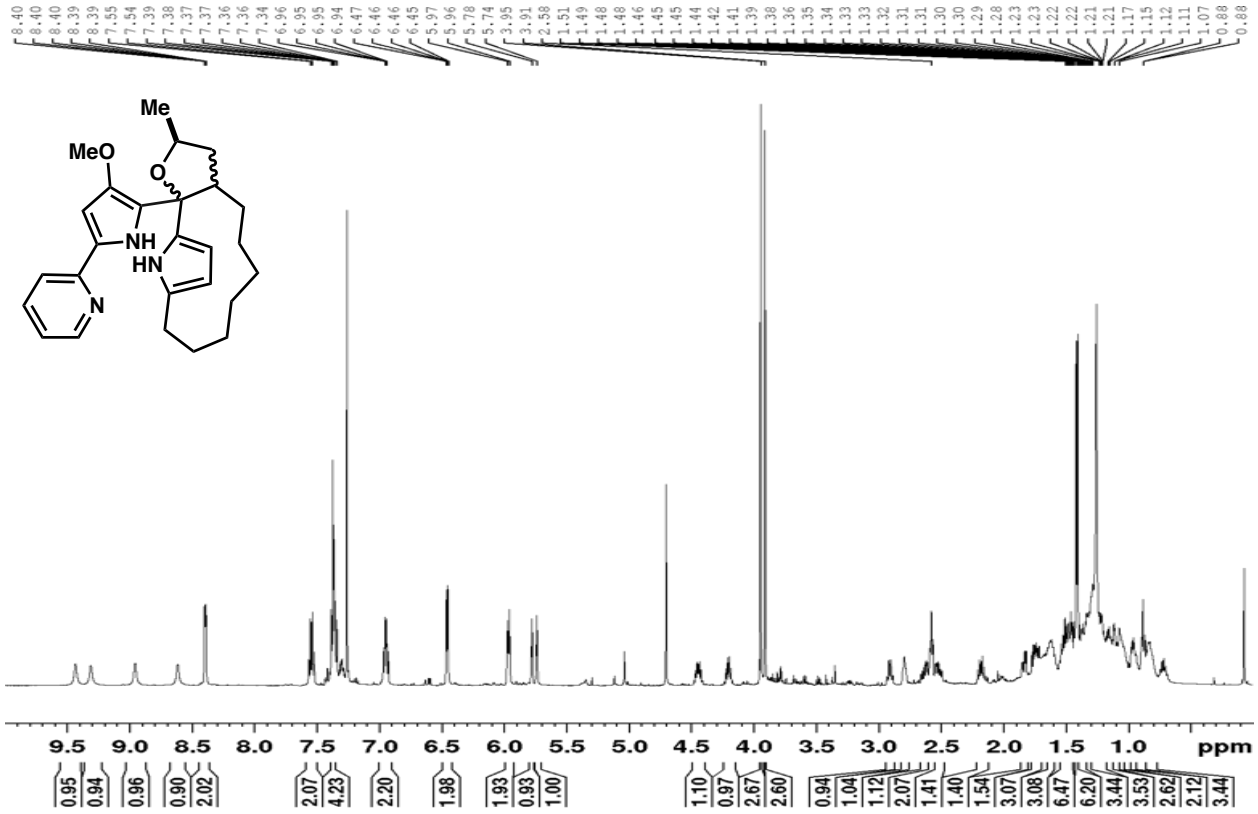

Spectrum 2.4.33 ^{13}C-NMR of compound **19b** ($CDCl_3$, 126 MHz)

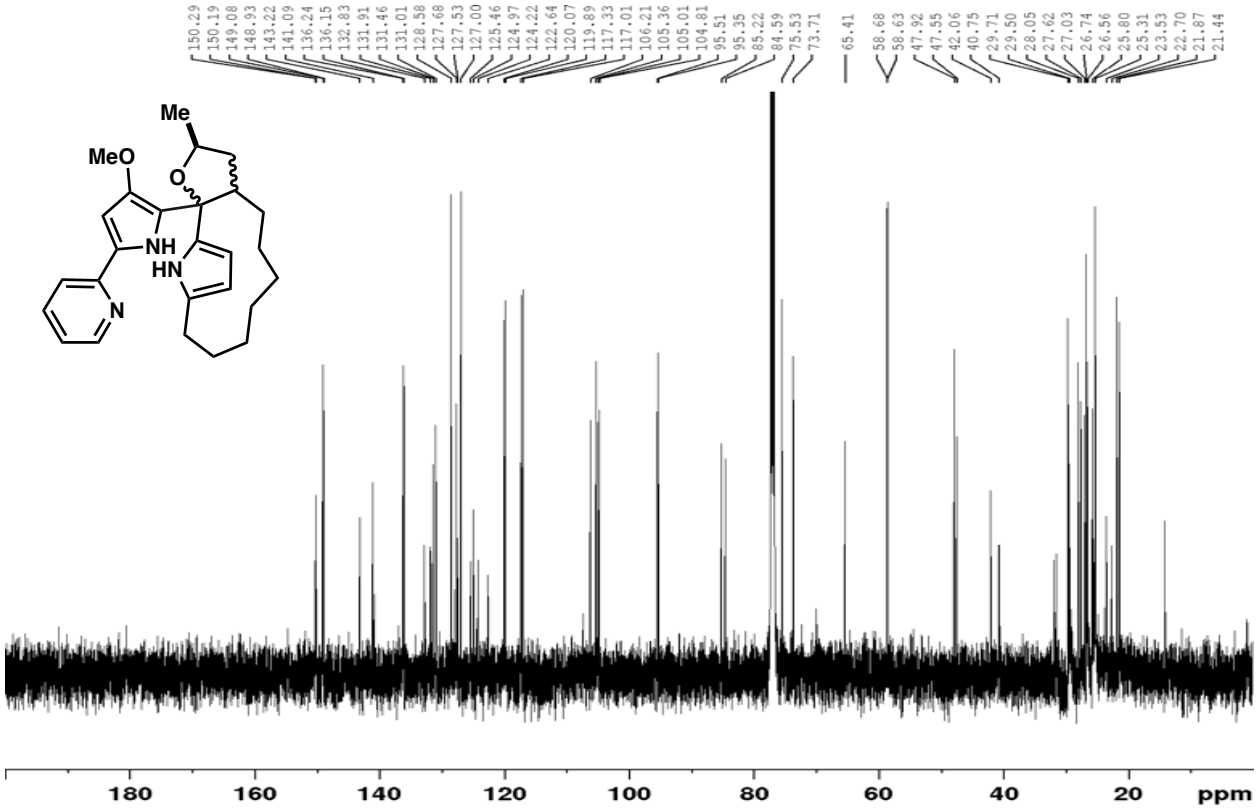

Spectrum 2.4.34 ^{1}H-NMR of compound **19d** ($CDCl_3$, 400 MHz)

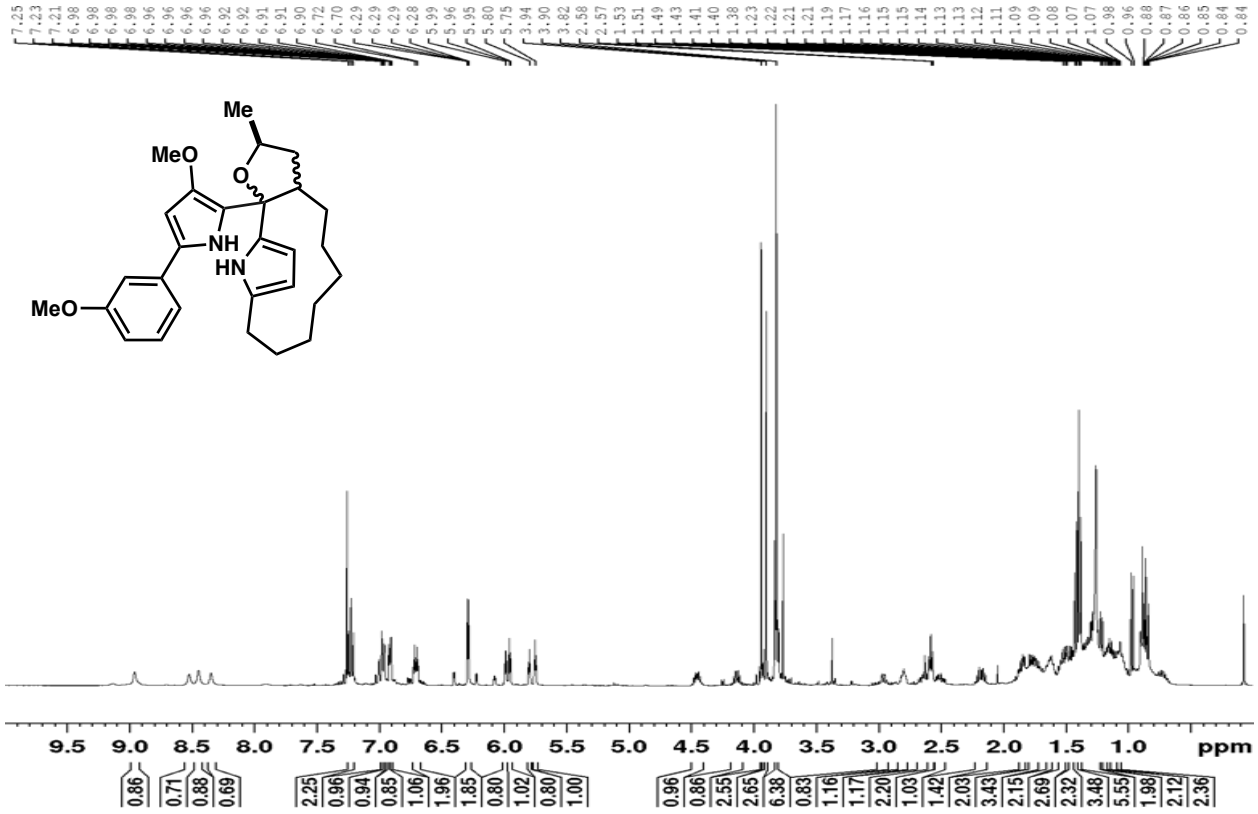

Spectrum 2.4.35 ^{13}C-NMR of compound **19d** ($CDCl_3$, 101 MHz)

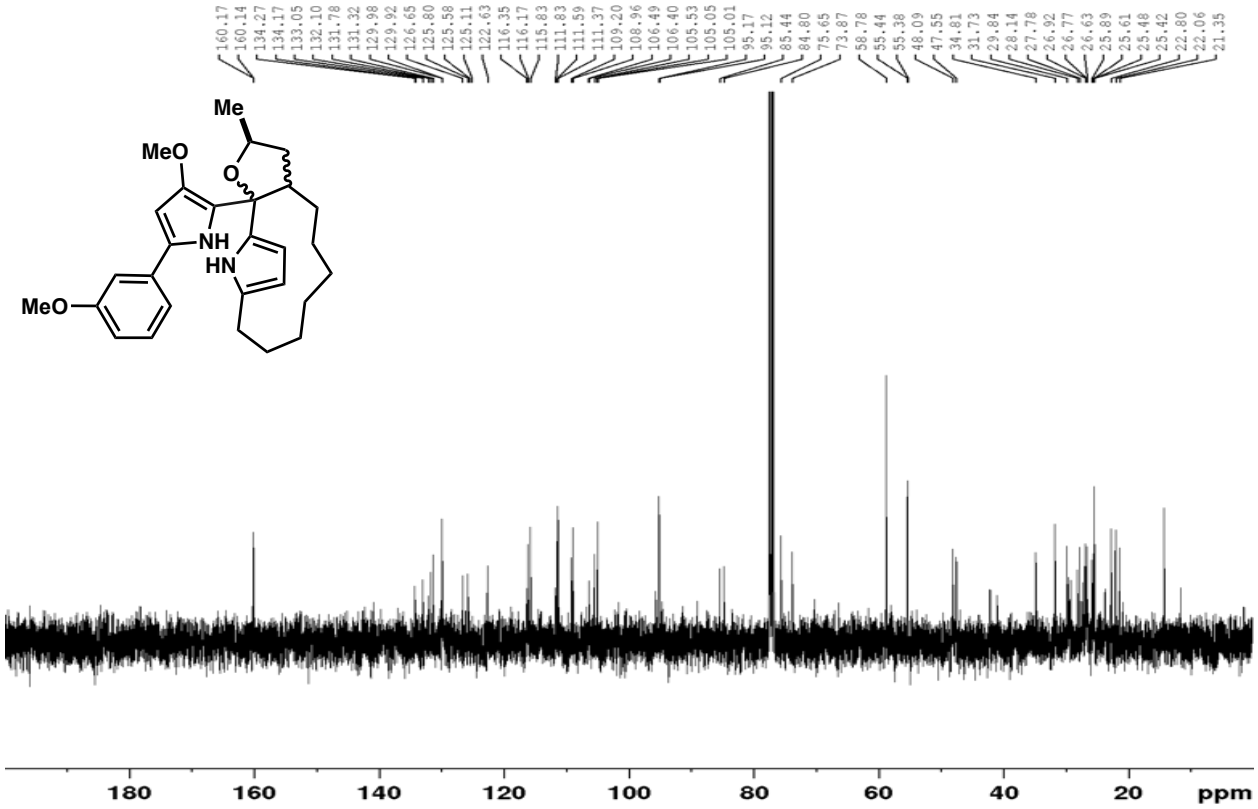

Spectrum 2.4.36 ^{1}H-NMR of compound **20a** ($CDCl_3$, 500 MHz)

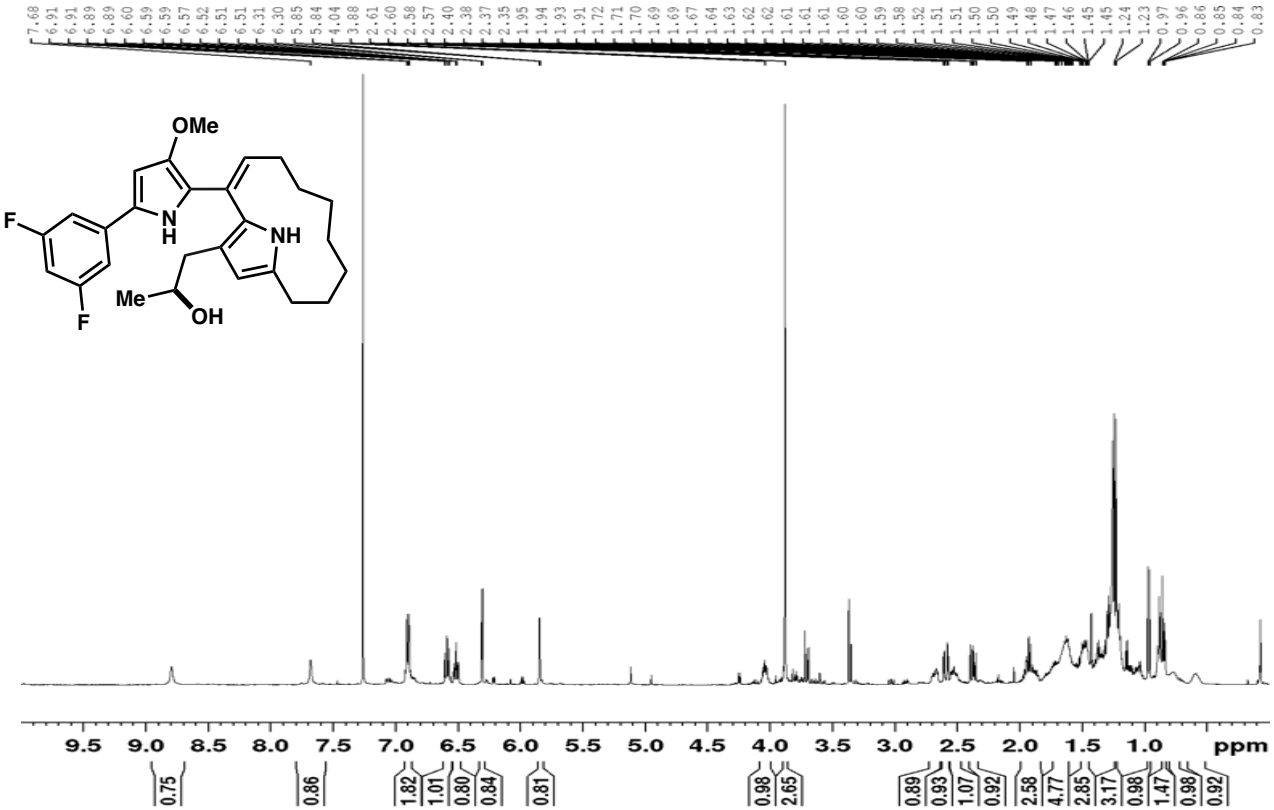

Spectrum 2.4.37 ^{13}C-NMR of compound **20a** ($CDCl_3$, 126 MHz)

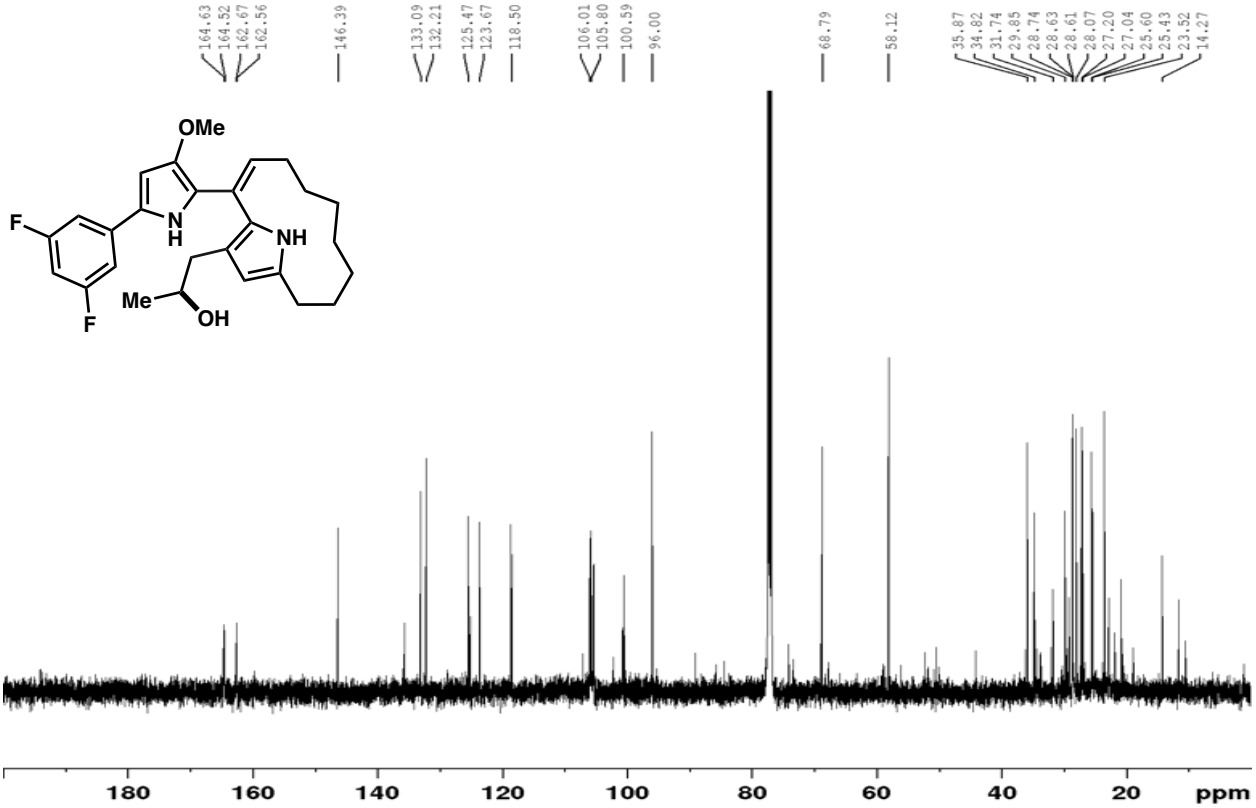

Spectrum 2.4.38 HSQC of compound **20a** ($CDCl_3$, 126 MHz)

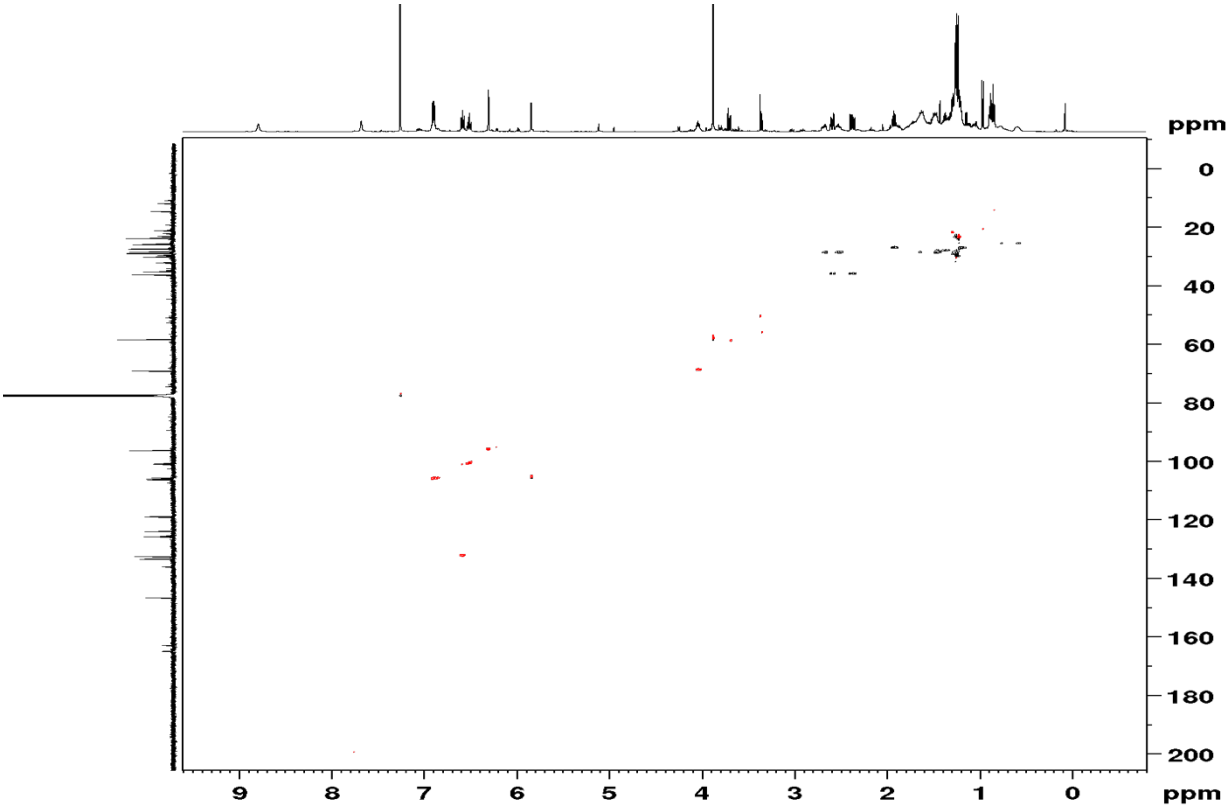

Spectrum 2.4.39 HMBC of compound **20a** ($CDCl_3$, 126 MHz)

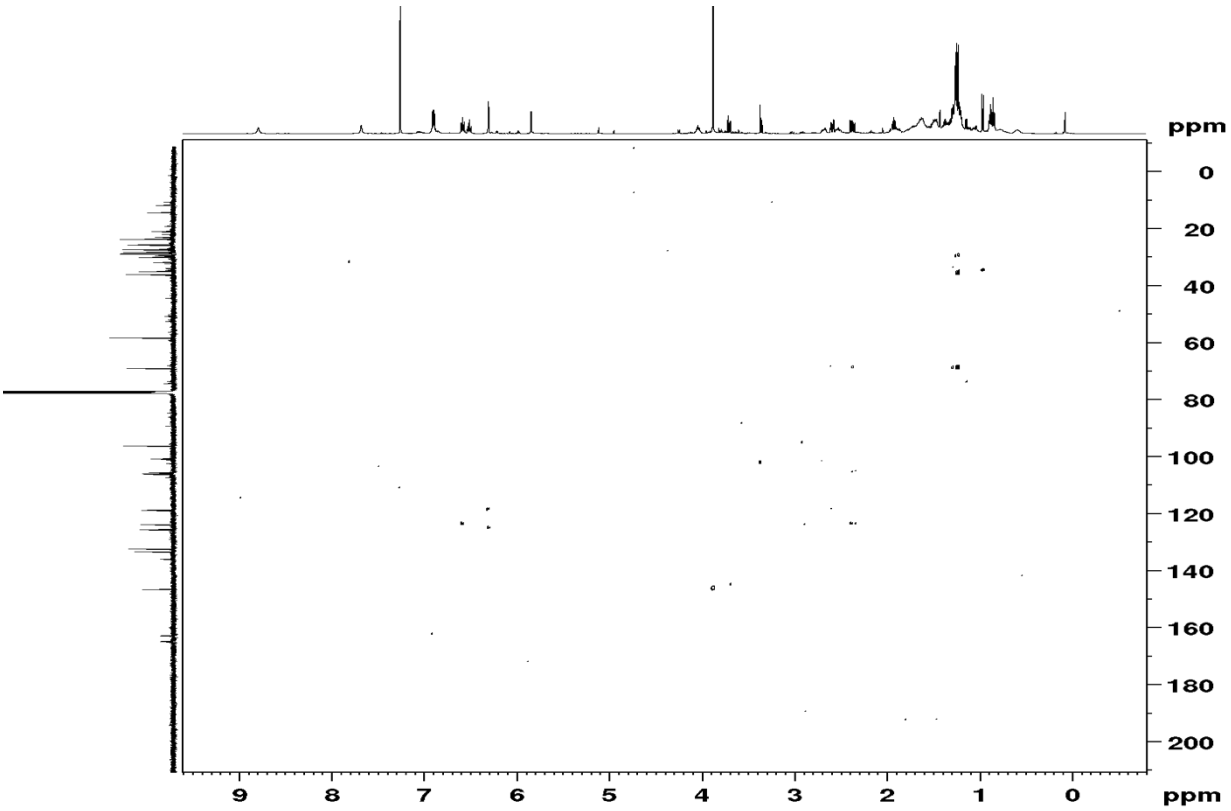

Spectrum 2.4.40 COSY of compound **20a** ($CDCl_3$, 126 MHz)

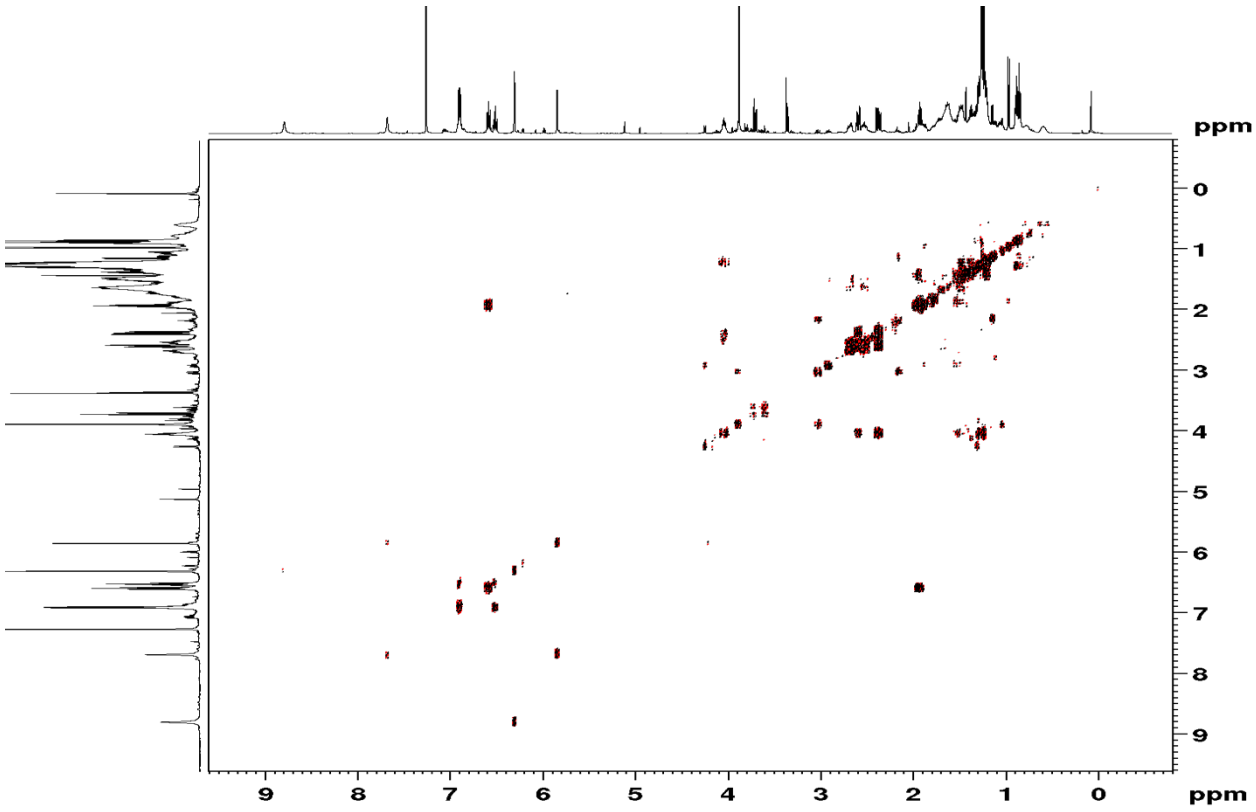

Spectrum 2.4.41 ^{1}H-NMR of compound **20b** ($CDCl_3$, 500 MHz)

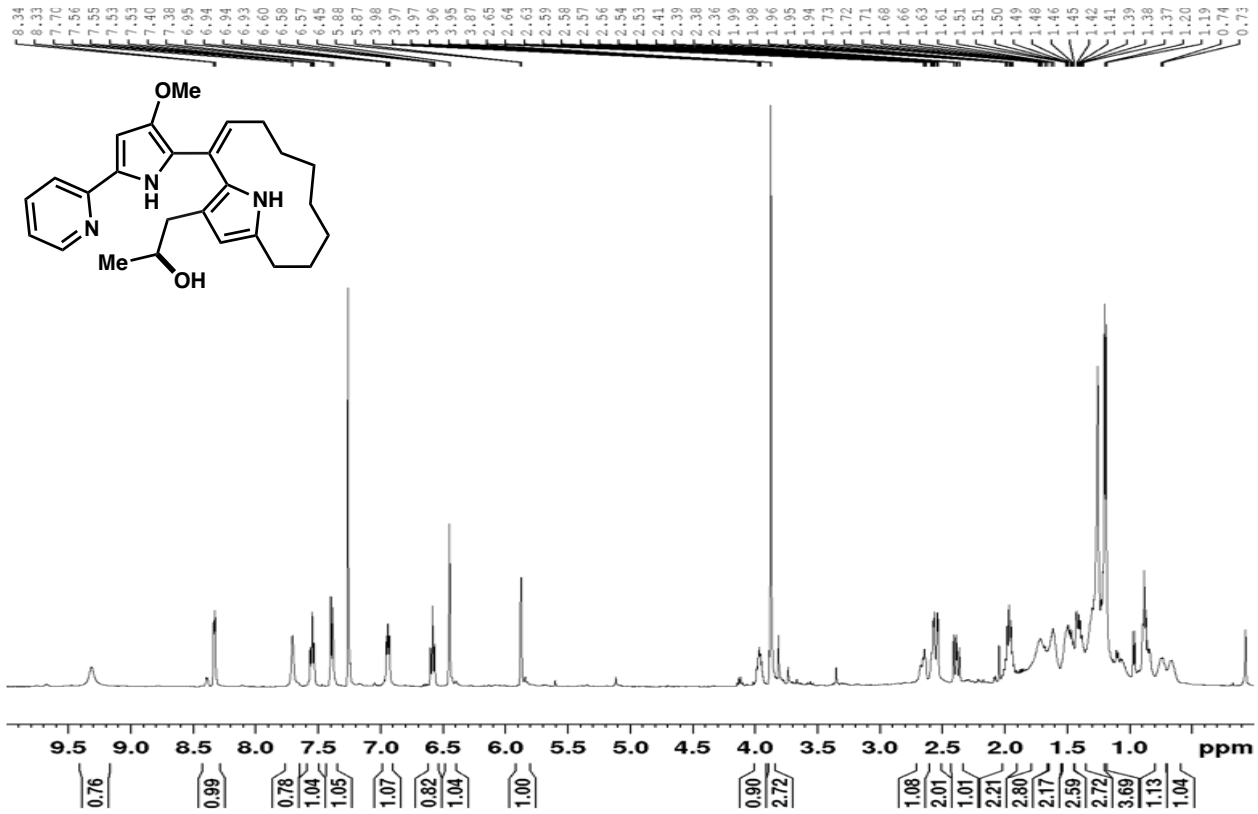

Spectrum 2.4.42 ^{13}C-NMR of compound **20b** ($CDCl_3$, 126 MHz)

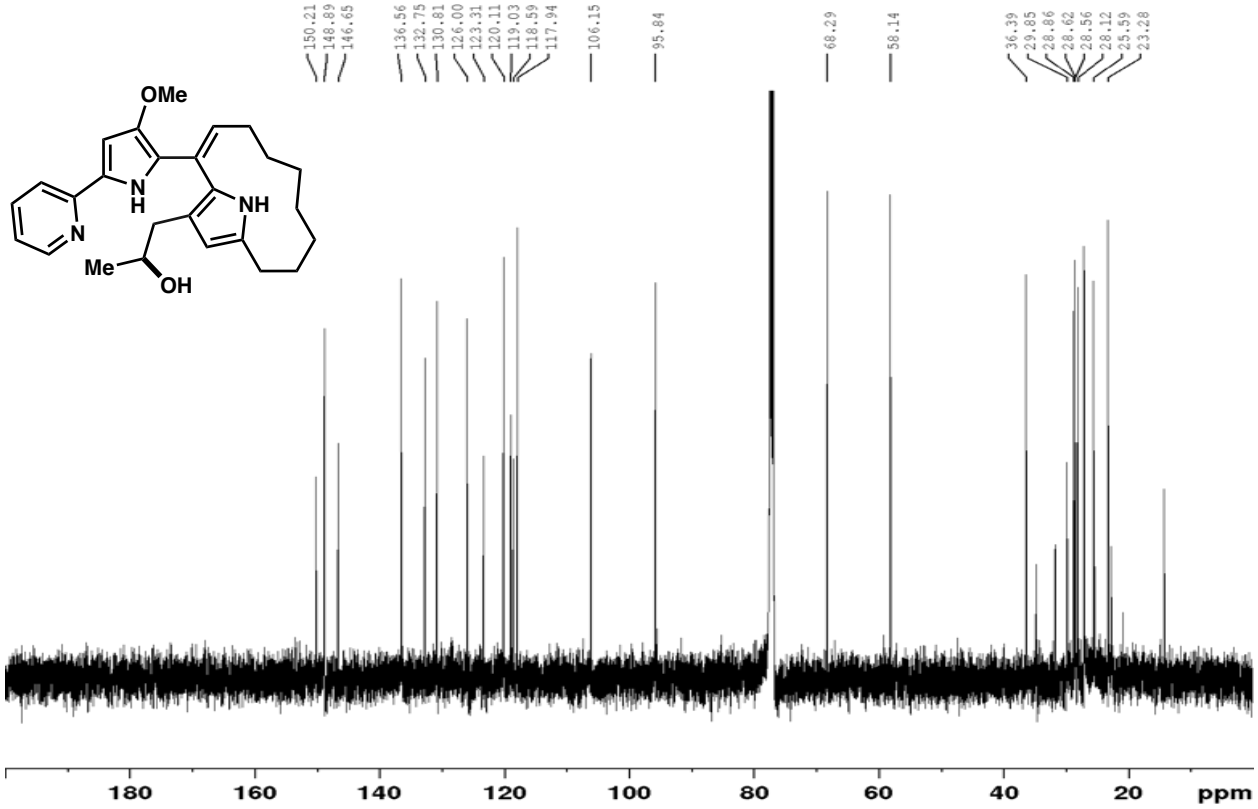

Spectrum 2.4.43 HSQC of compound **20b** ($CDCl_3$, 126 MHz)

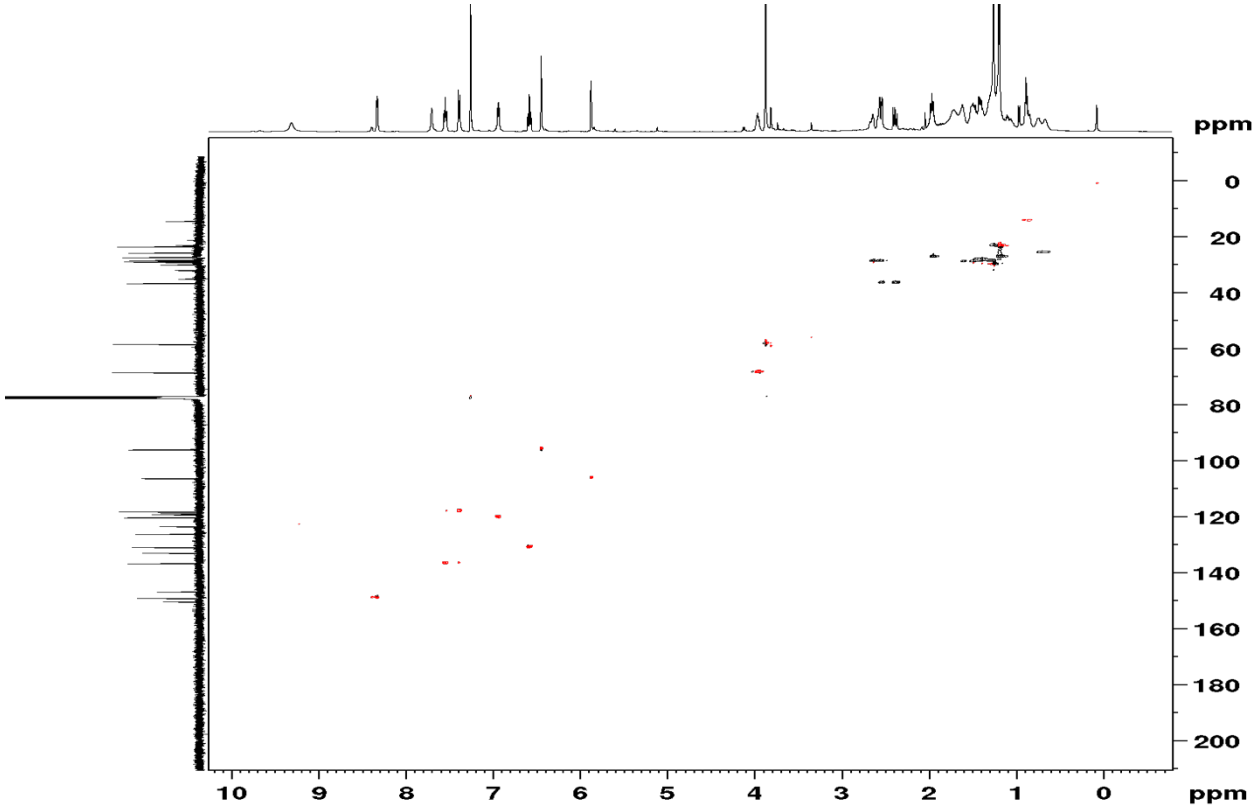

Spectrum 2.4.44 HMBC of compound **20b** ($CDCl_3$, 126 MHz)

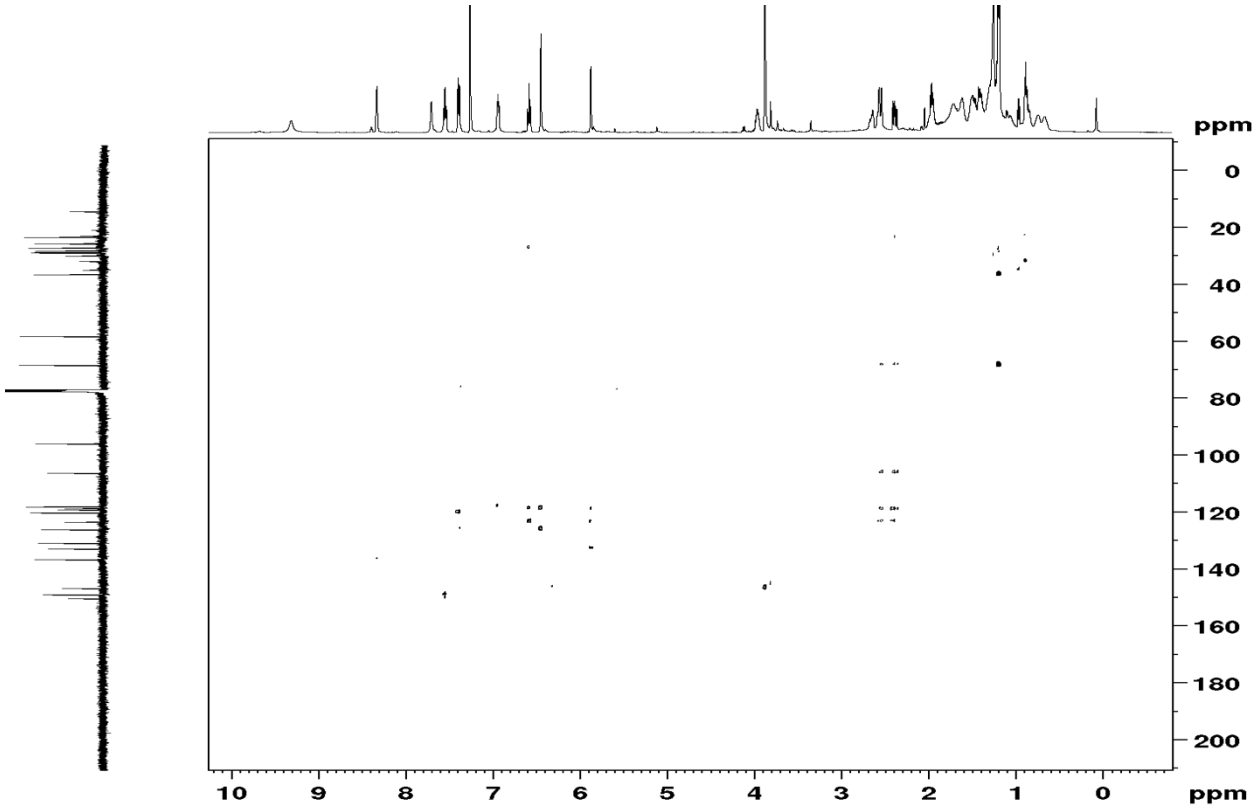

Spectrum 2.4.45 COSY of compound **20a** ($CDCl_3$, 500 MHz)

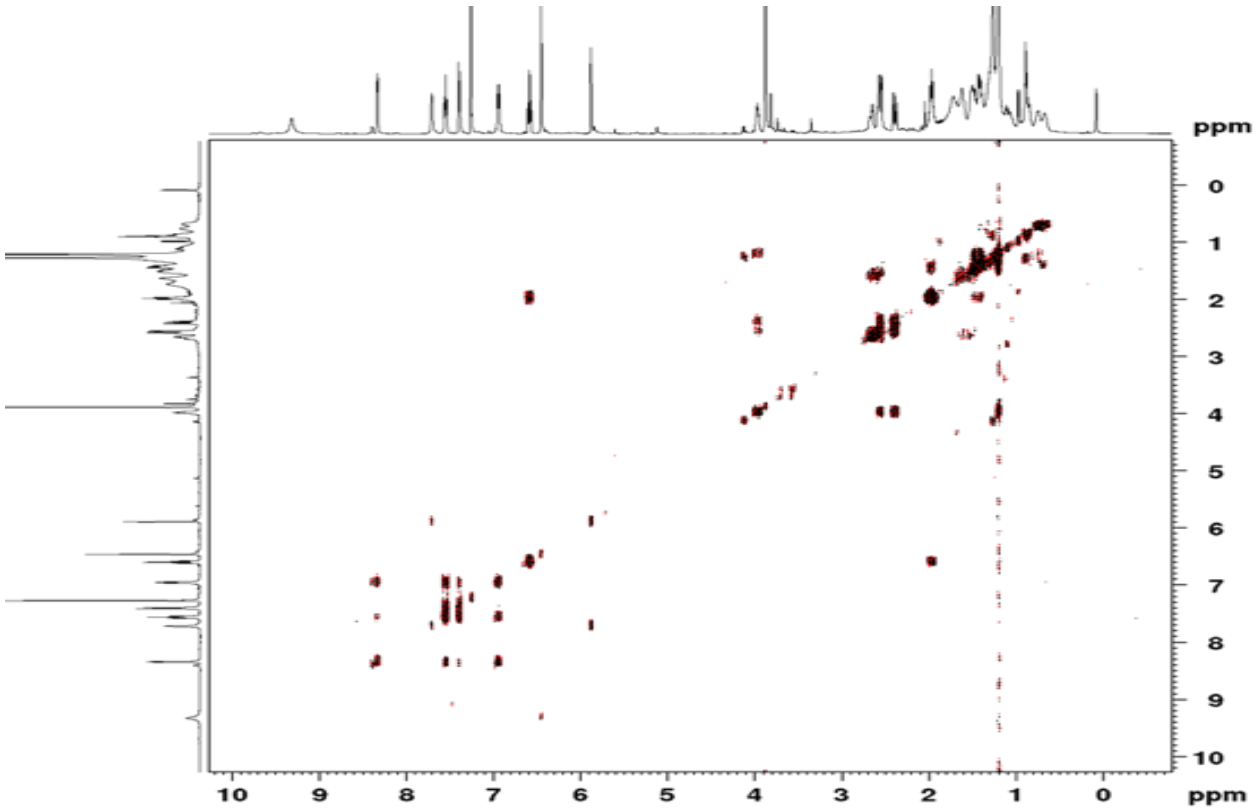

Spectrum 2.4.46 ^{1}H-NMR of compound **20d** ($CDCl_3$, 400 MHz)

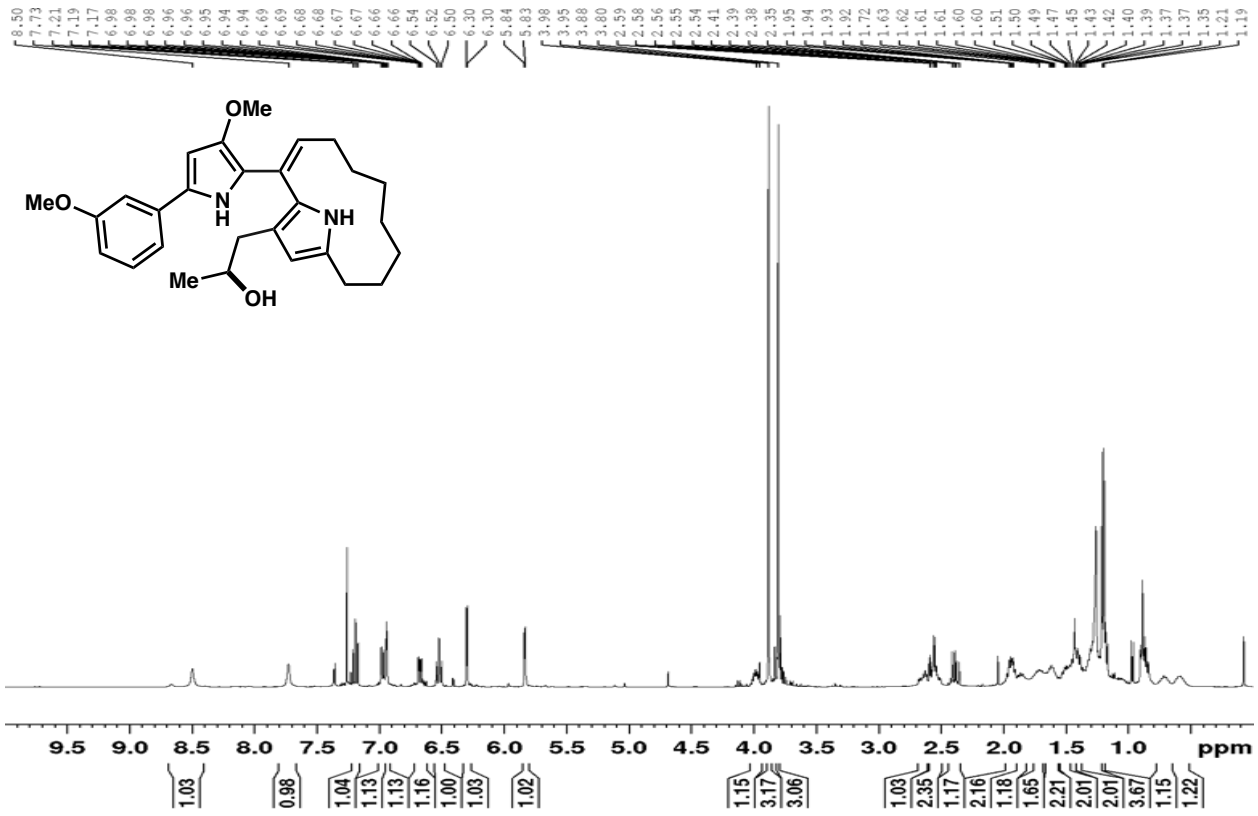

Spectrum 2.4.47 ^{13}C-NMR of compound **20d** ($CDCl_3$, 101 MHz)

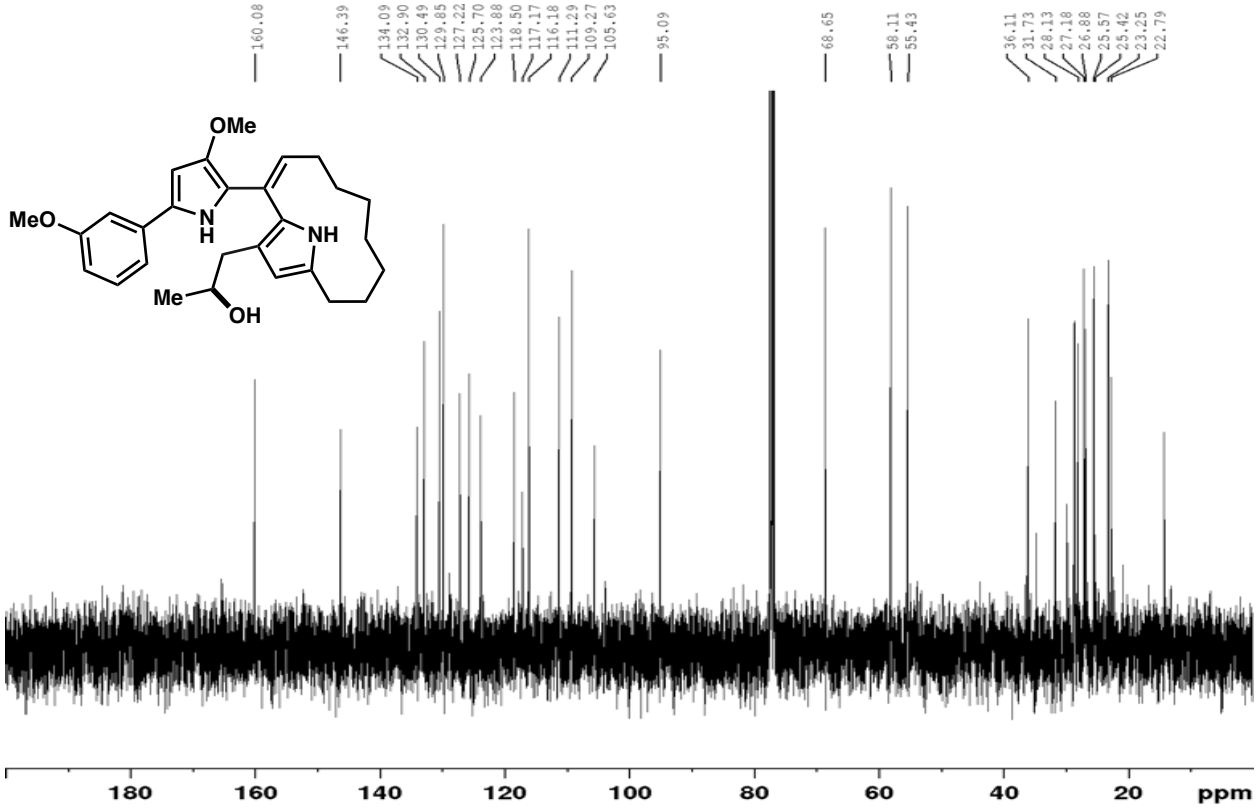

Spectrum 2.4.48 HSQC of compound **20d** ($CDCl_3$, 101 MHz)

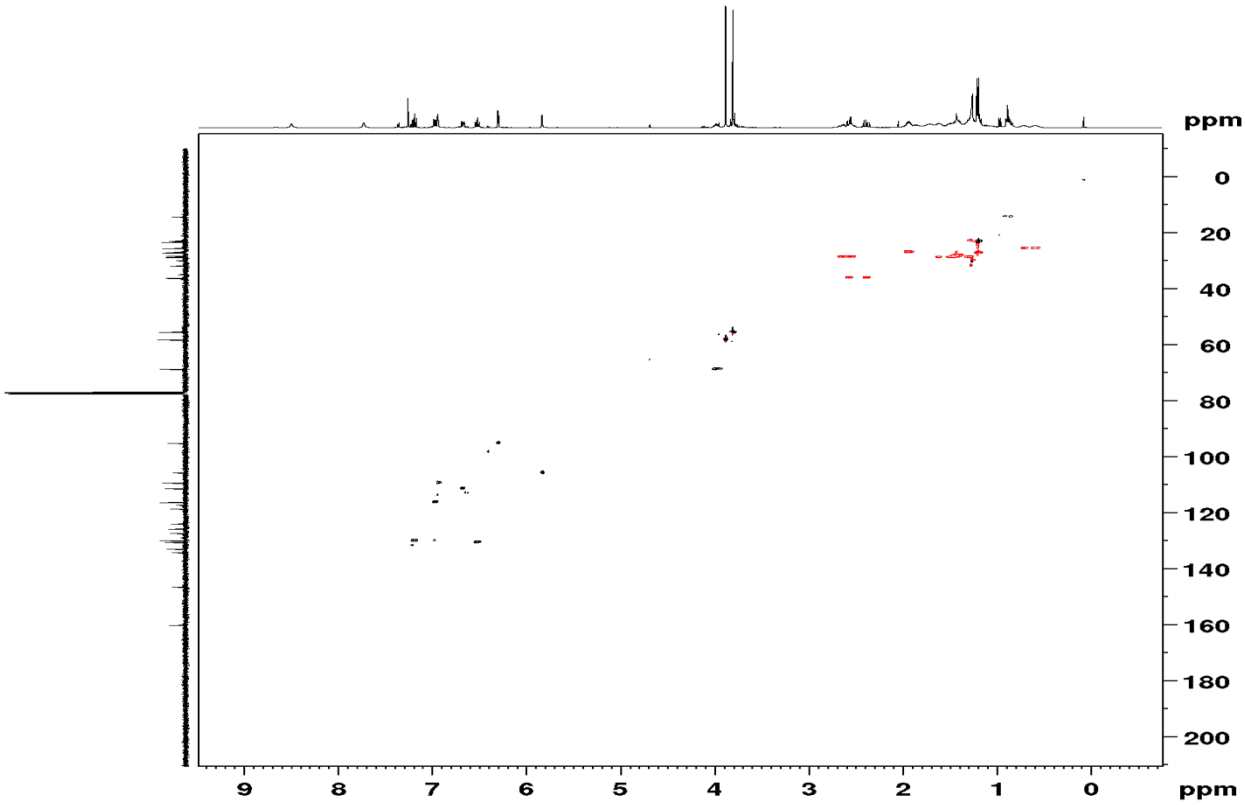

Spectrum 2.4.49 HMBC of compound **20d** ($CDCl_3$, 101 MHz)

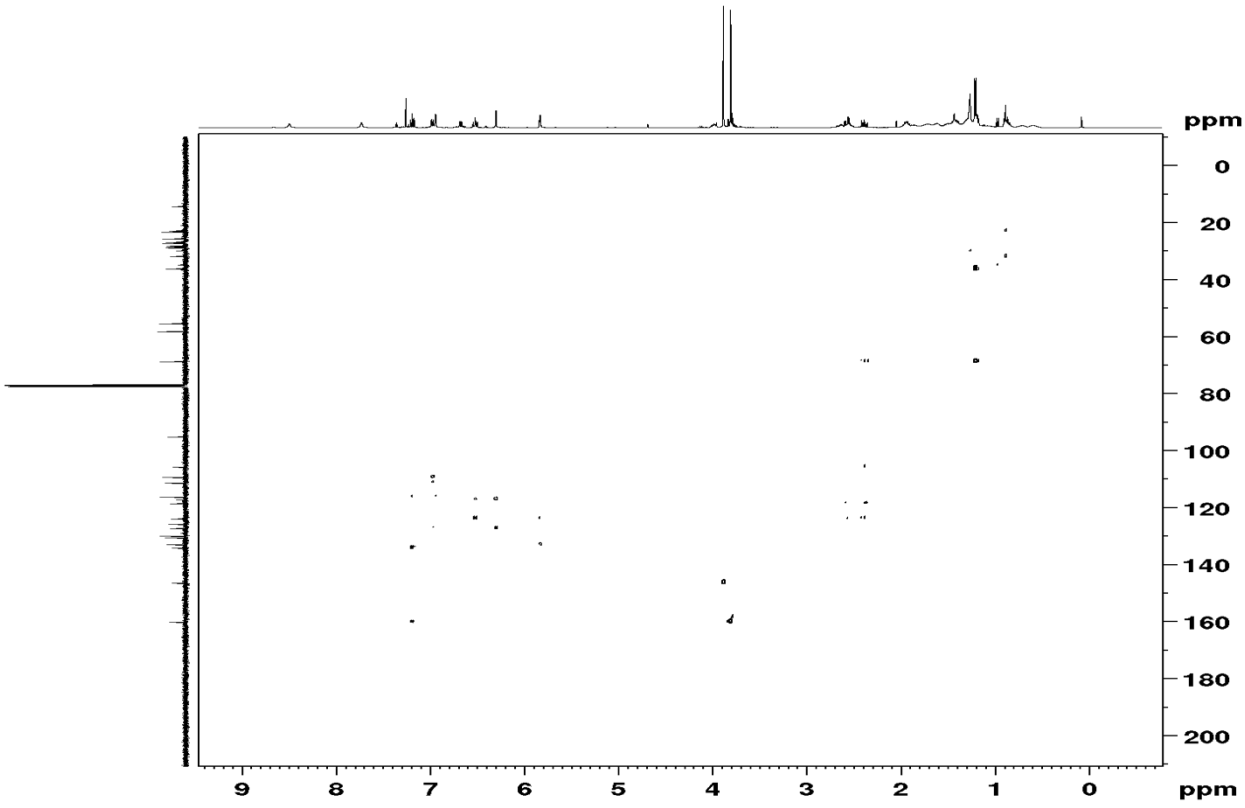

Spectrum 2.4.50 COSY of compound **20d** ($CDCl_3$, 400 MHz)

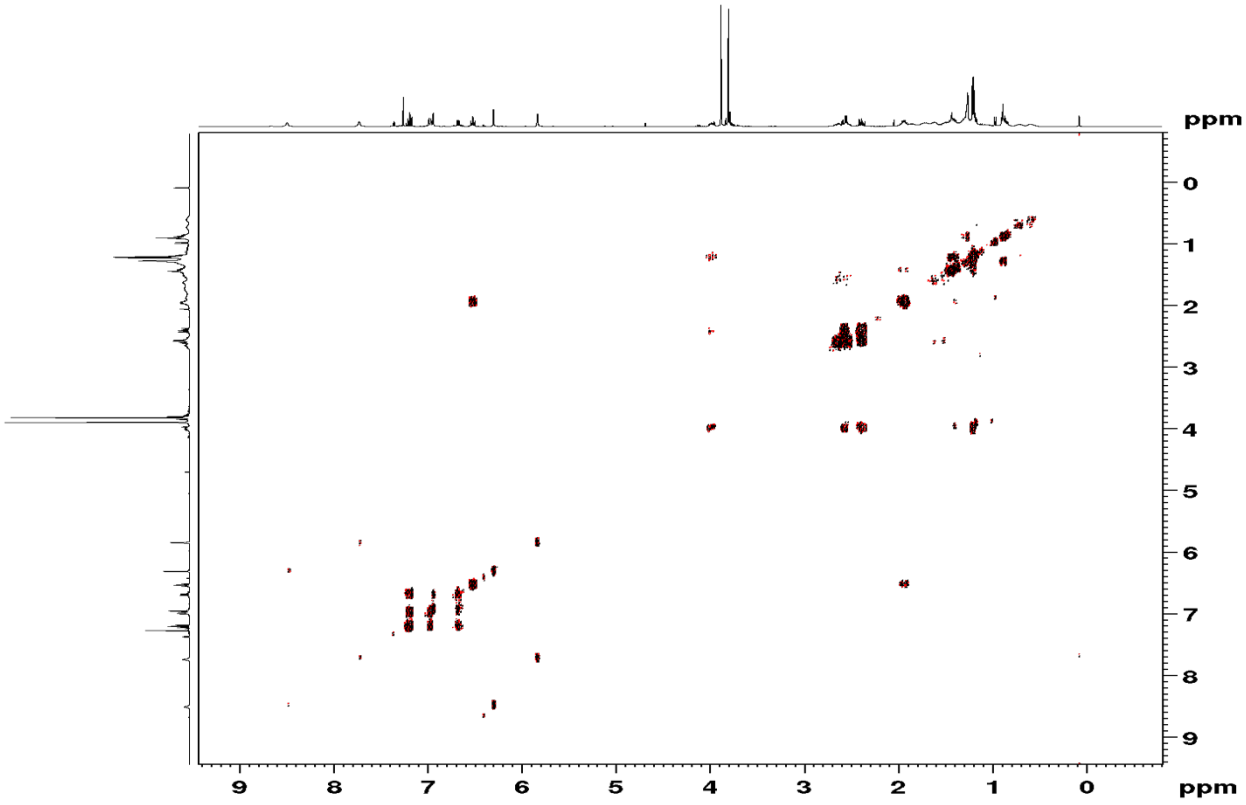

Spectrum 2.4.51 ^{1}H-NMR of compound **21** ($CDCl_3$, 400 MHz)

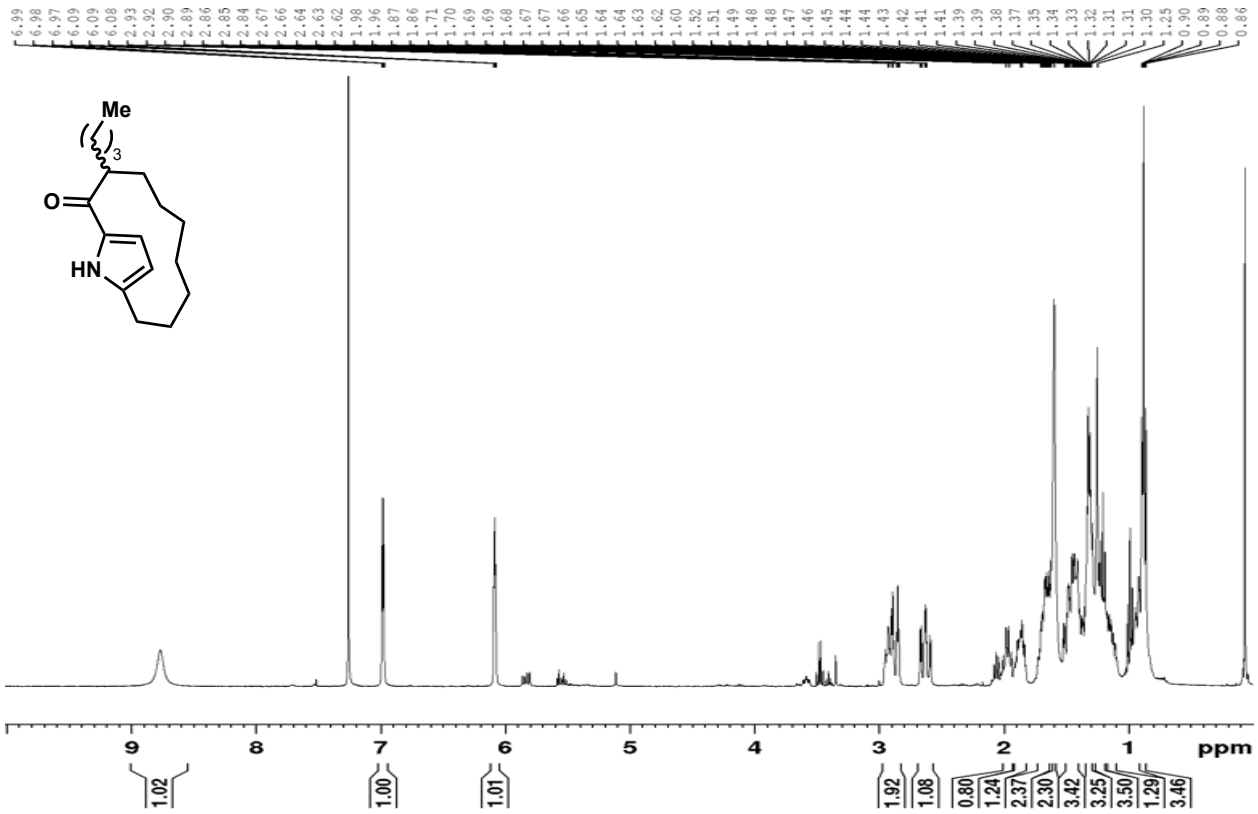

Spectrum 2.4.52 ^{13}C-NMR of compound **21** ($CDCl_3$, 101 MHz)

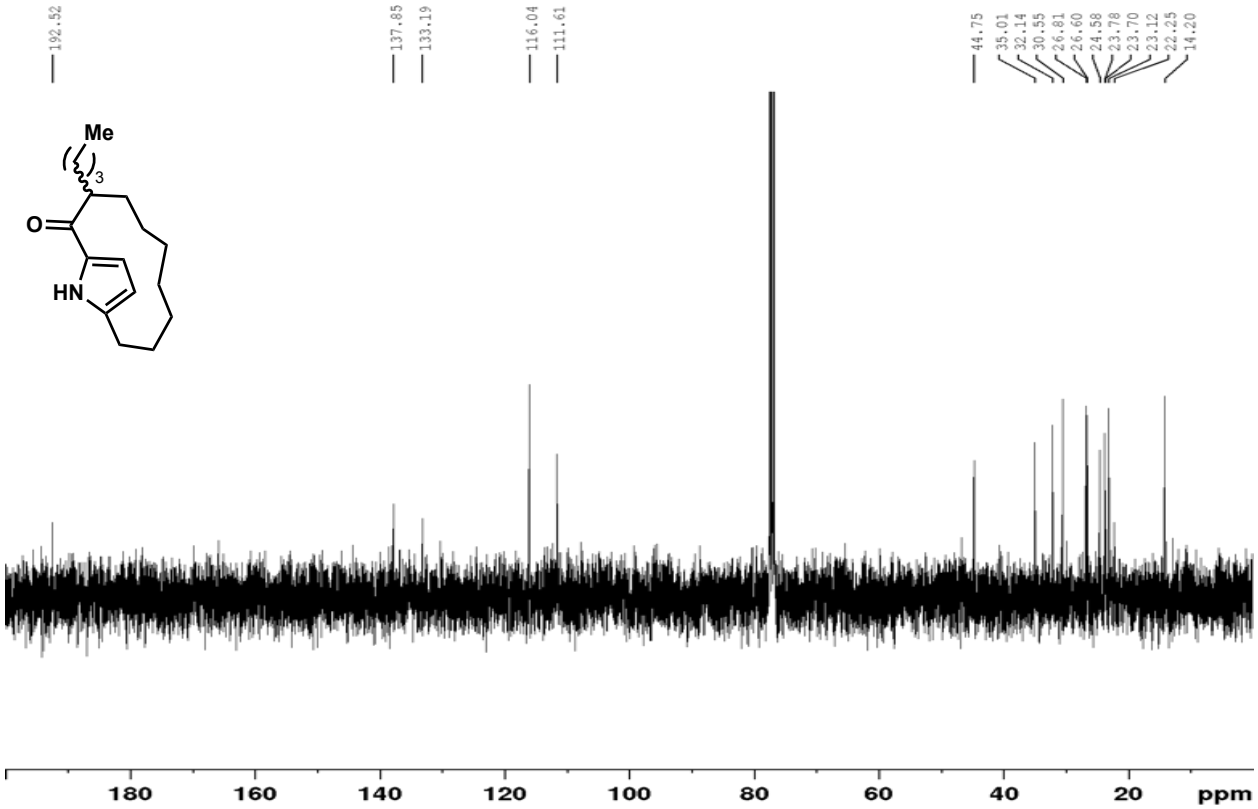

Spectrum 2.4.53 ^{1}H-NMR of compound **22** ($CDCl_3$, 400 MHz)

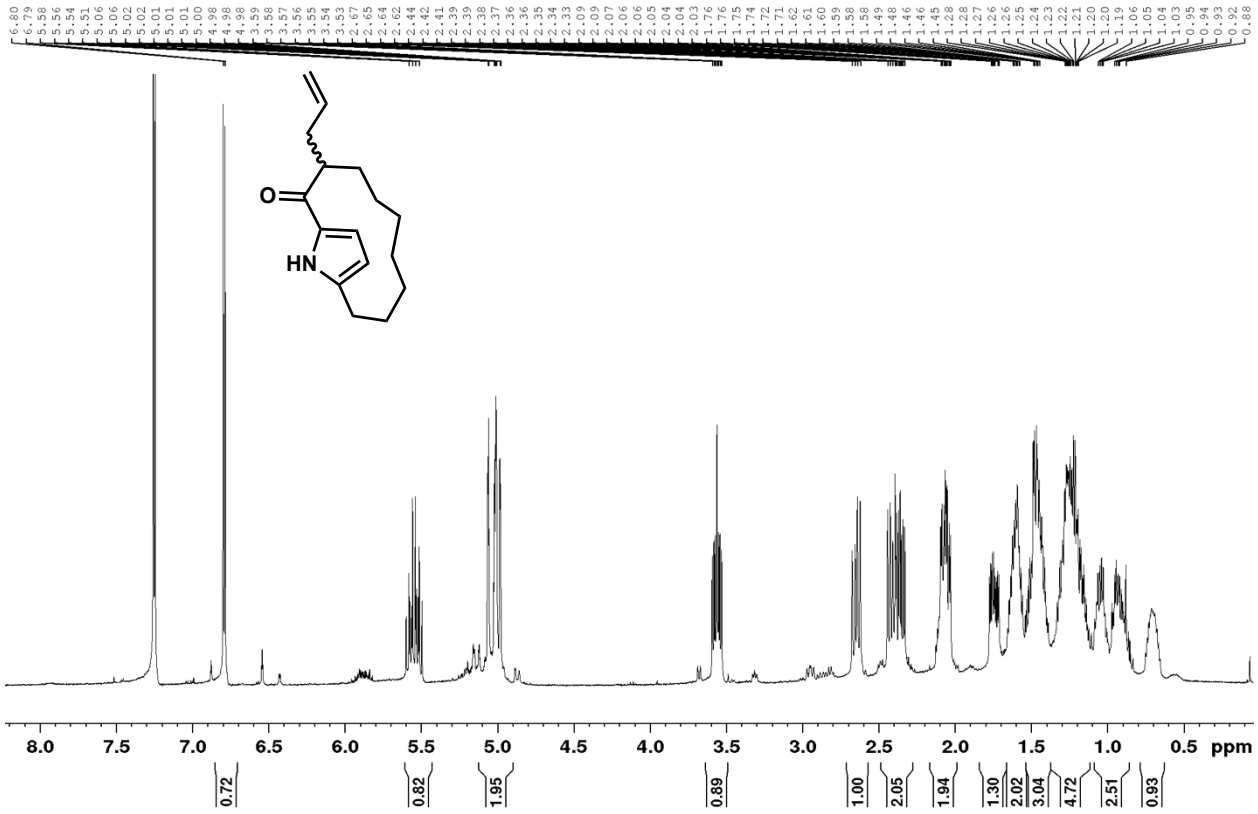

Spectrum 2.4.54 ^{1}H-NMR of compound **23** ($CDCl_3$, 500 MHz)

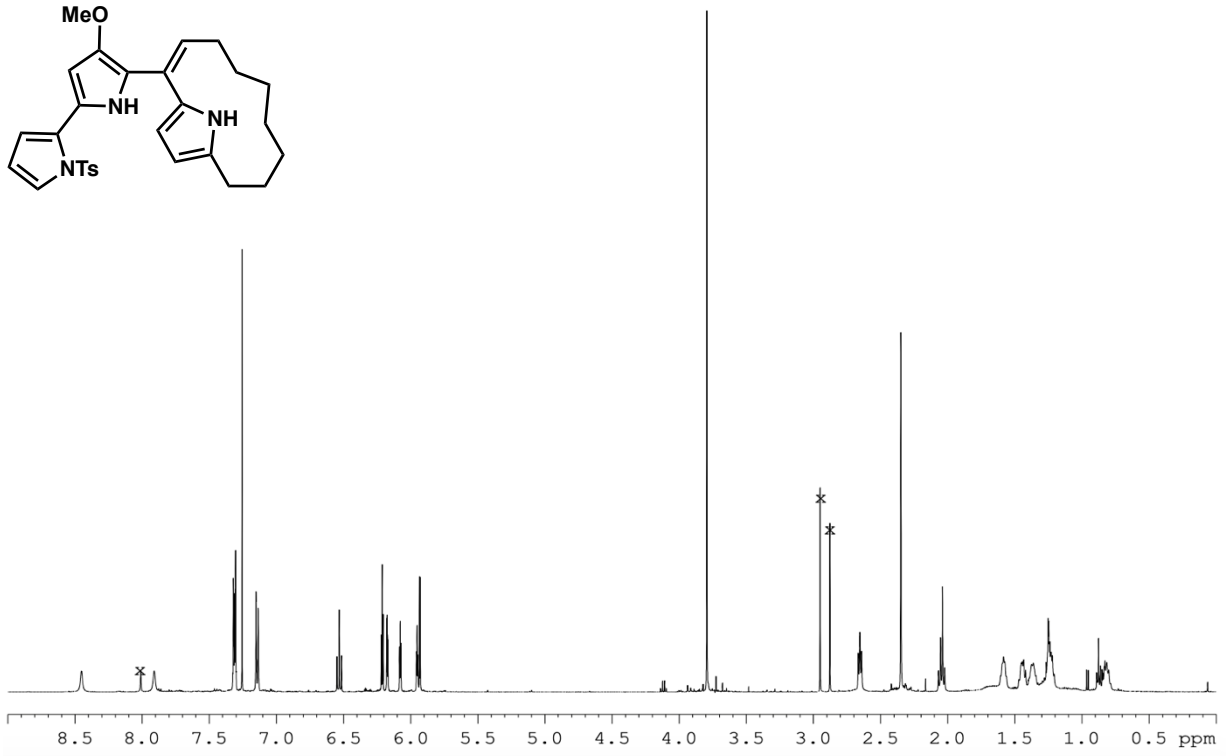

Spectrum 2.4.55 ^{13}C-NMR of compound **23** ($CDCl_3$, 126 MHz)

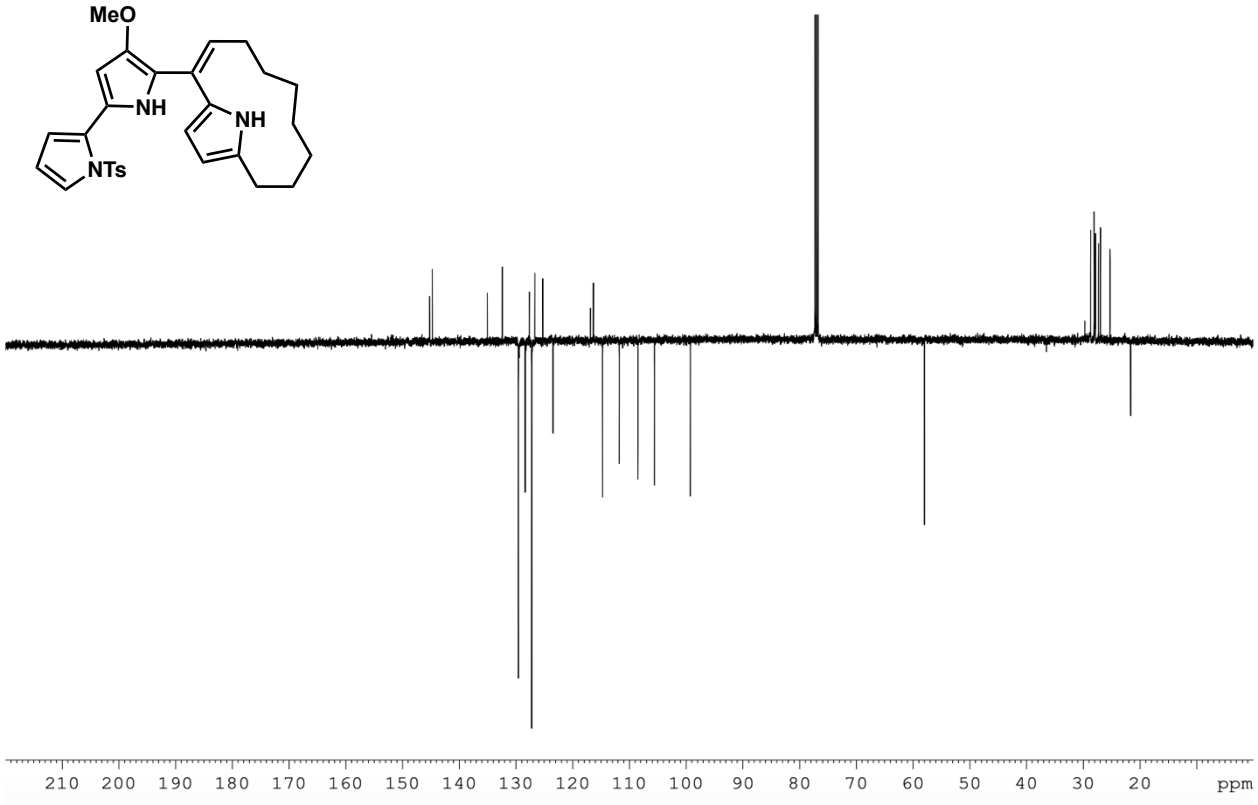

Spectrum 2.4.56 ^{1}H-NMR of compound **24** ($CDCl_3$, 500 MHz)

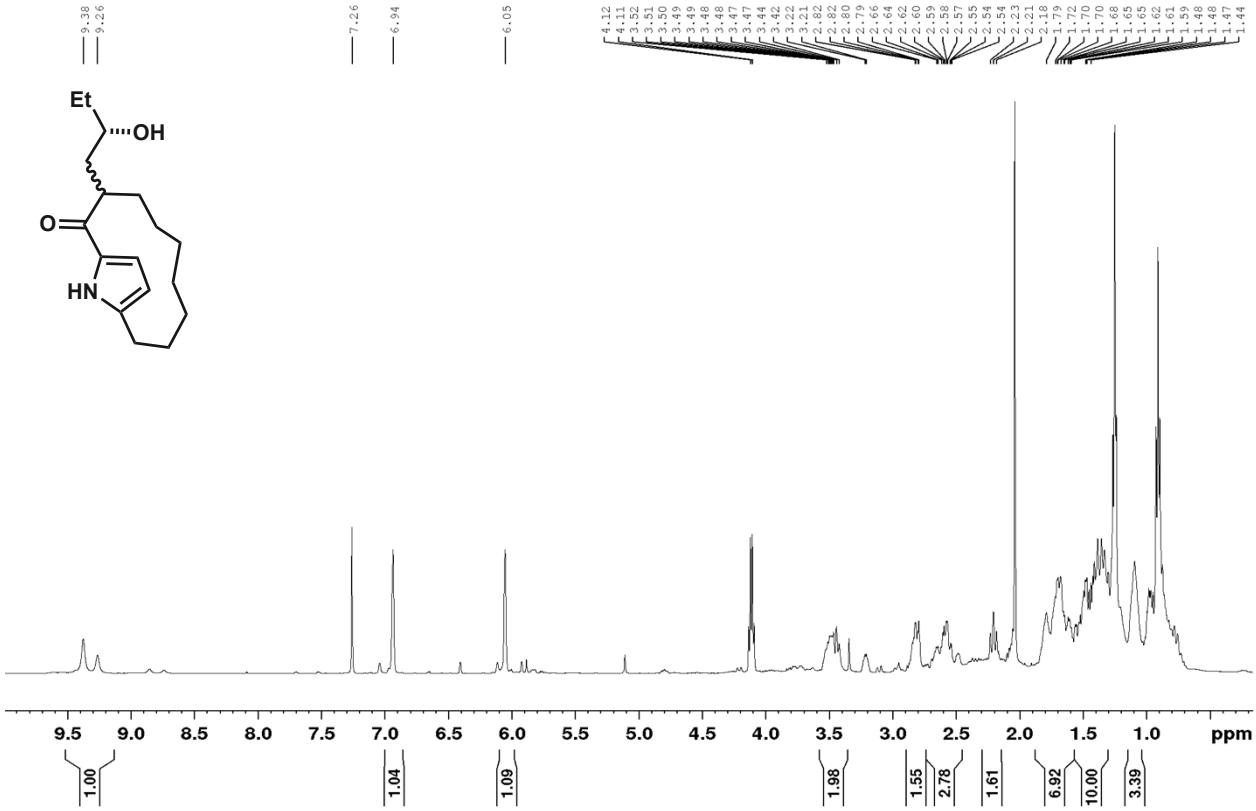

Spectrum 2.4.57 ^{13}C-NMR of compound **24** ($CDCl_3$, 126 MHz)

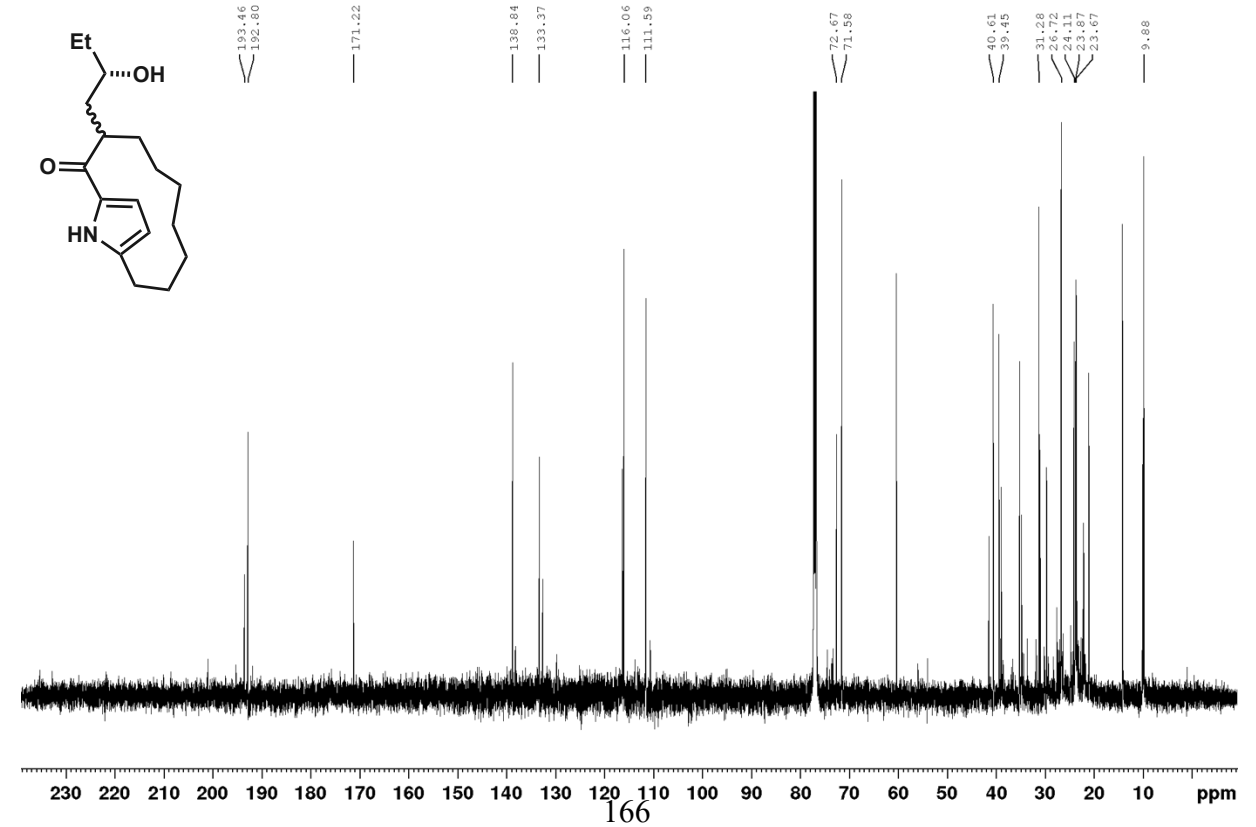

Spectrum 2.4.58 ^{1}H-NMR of compound **25** ($CDCl_3$, 500 MHz)

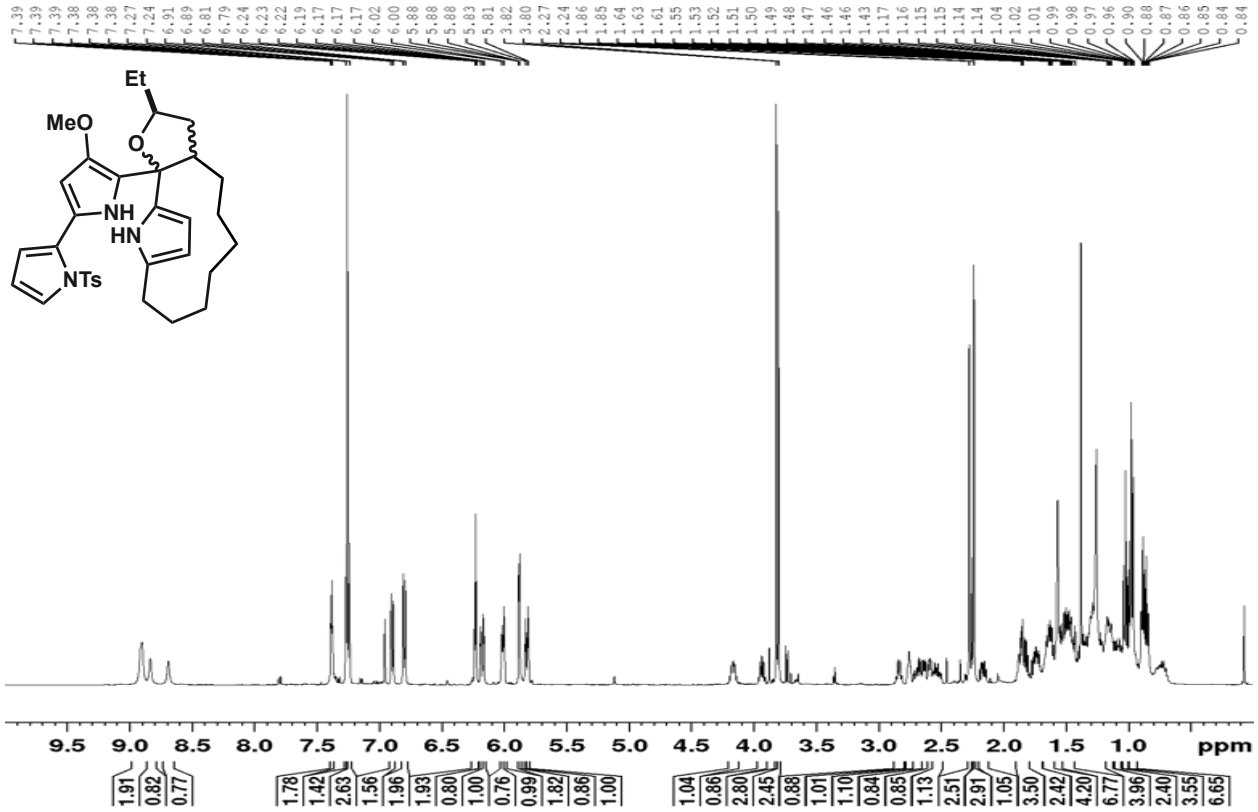

Spectrum 2.4.59 ^{13}C-NMR of compound **25** ($CDCl_3$, 126 MHz)

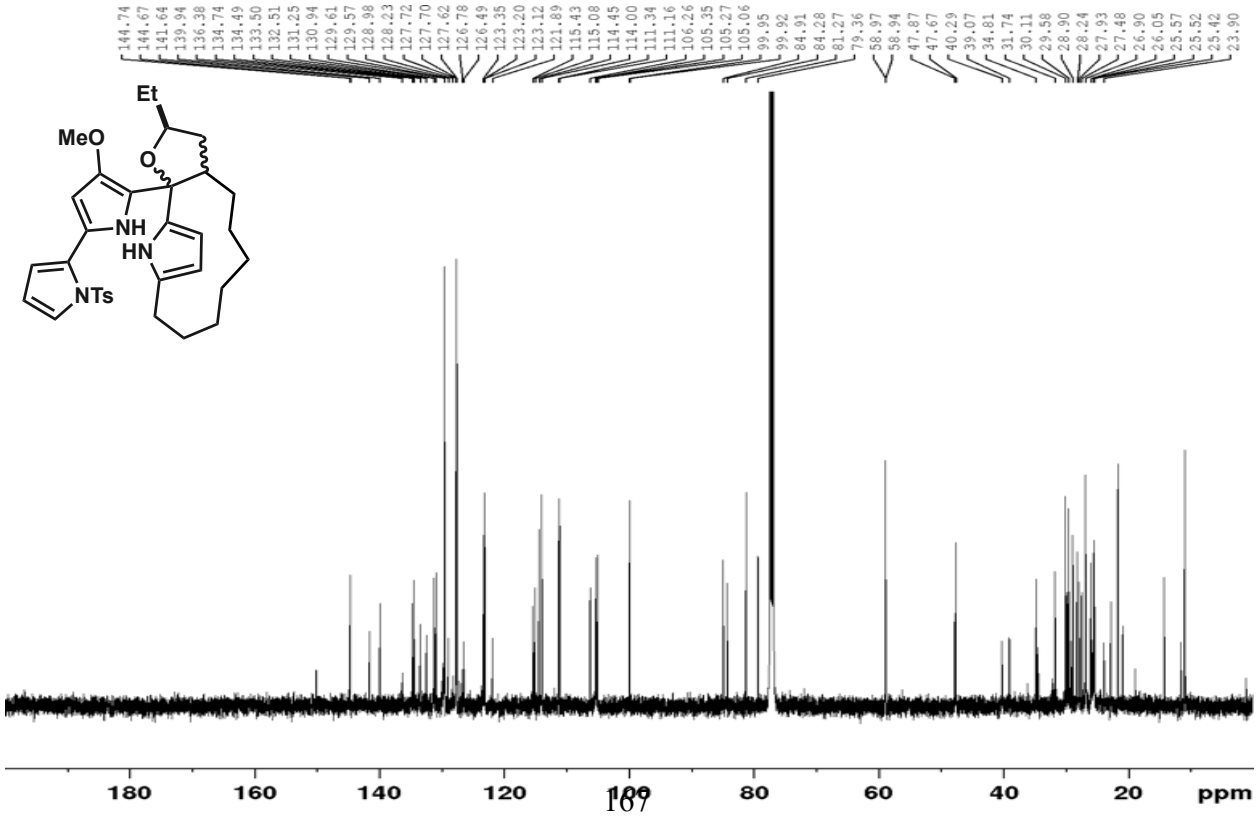

Spectrum 2.4.60 ^{1}H-NMR of compound **26** ($CDCl_3$, 400 MHz)

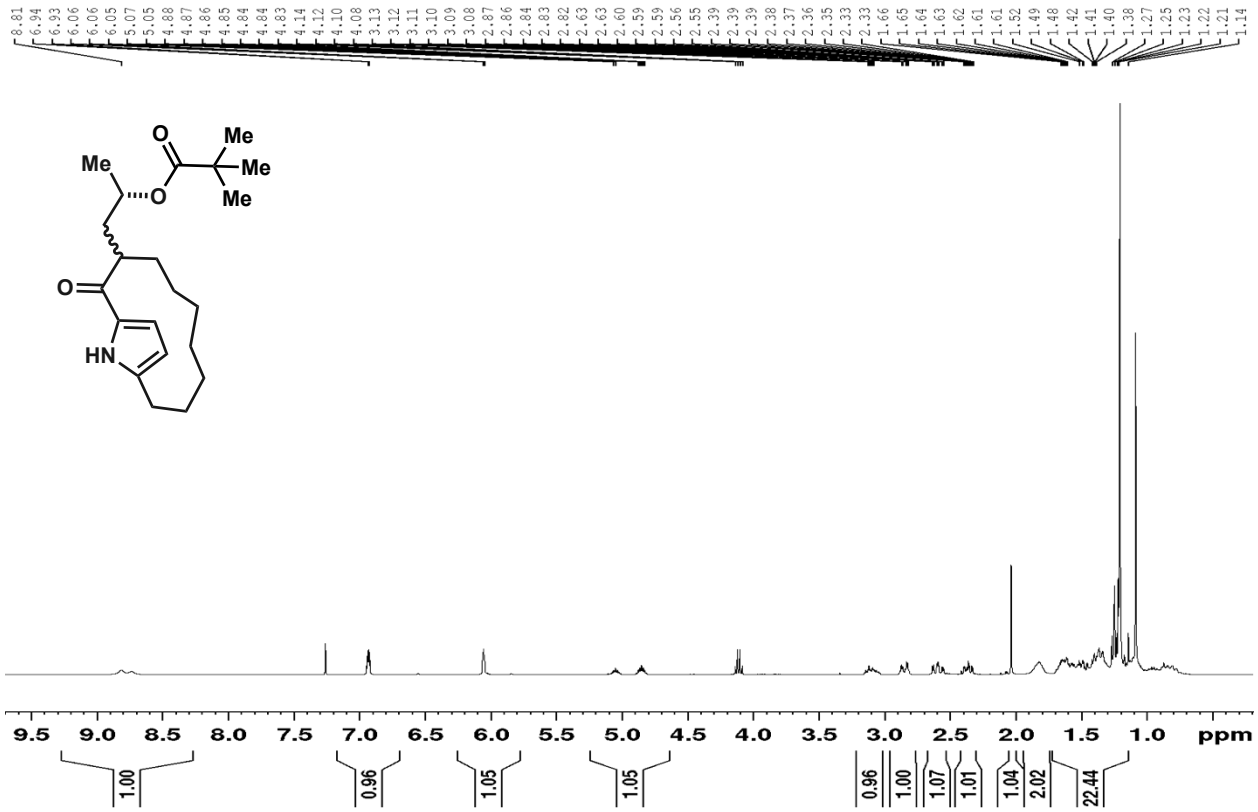

Spectrum 2.4.61 ^{13}C-NMR of compound **26** ($CDCl_3$, 101 MHz)

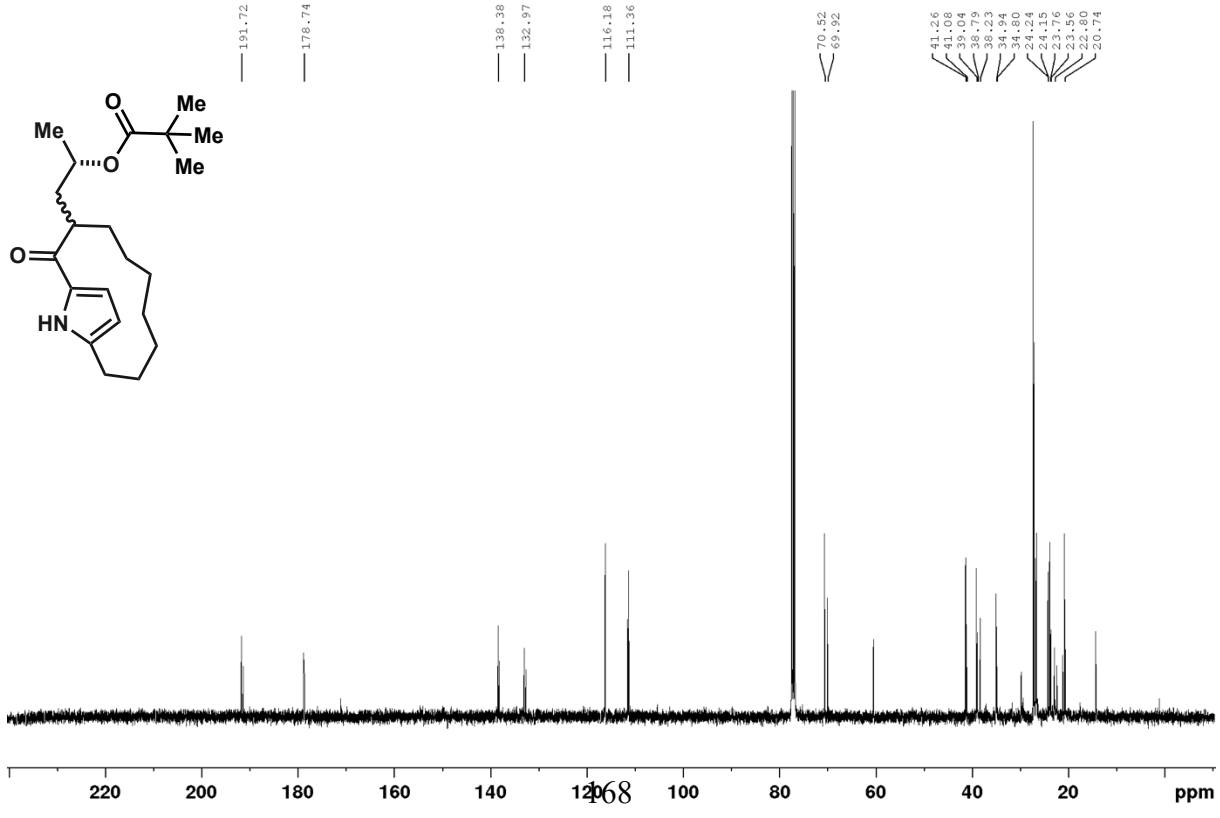

Spectrum 2.4.62 ^{1}H-NMR of compound **27** ($CDCl_3$,500 MHz)

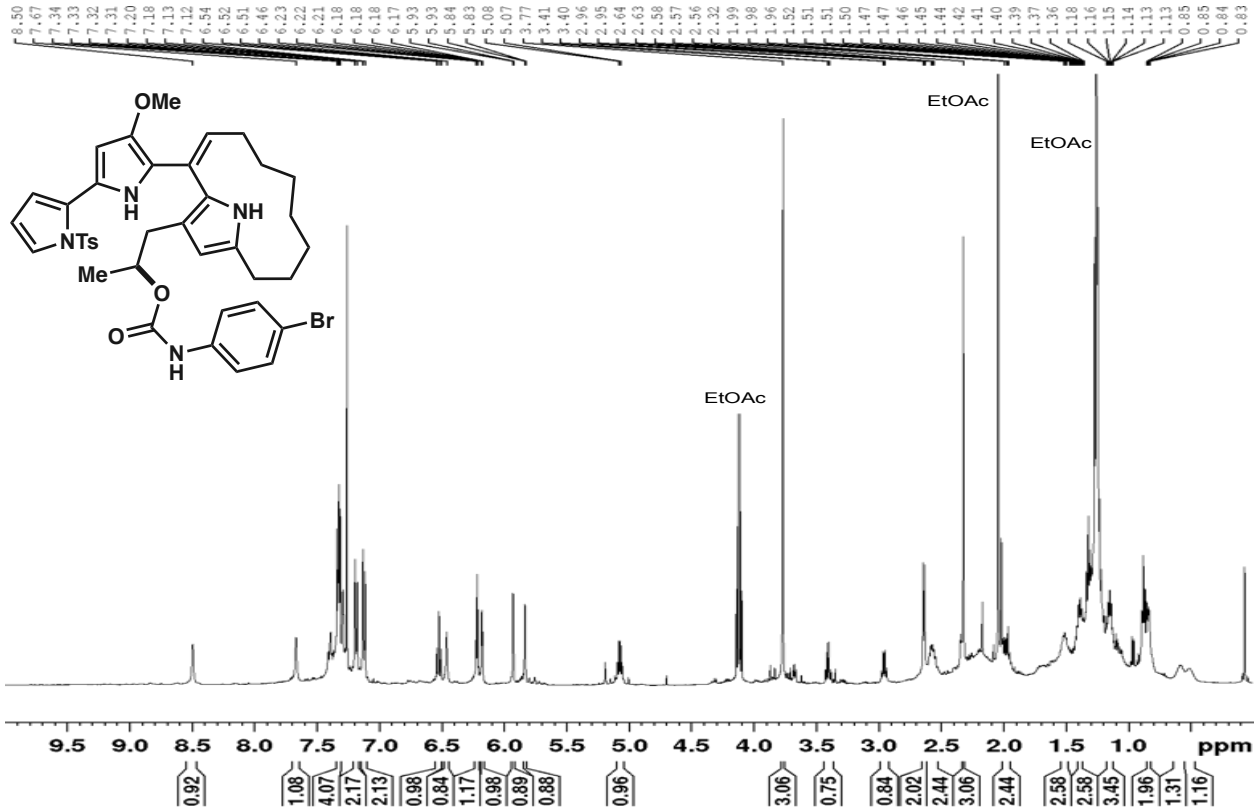

Spectrum 2.4.63 ^{1}H-NMR of compound **28** (acetone-d6, 500 MHz)

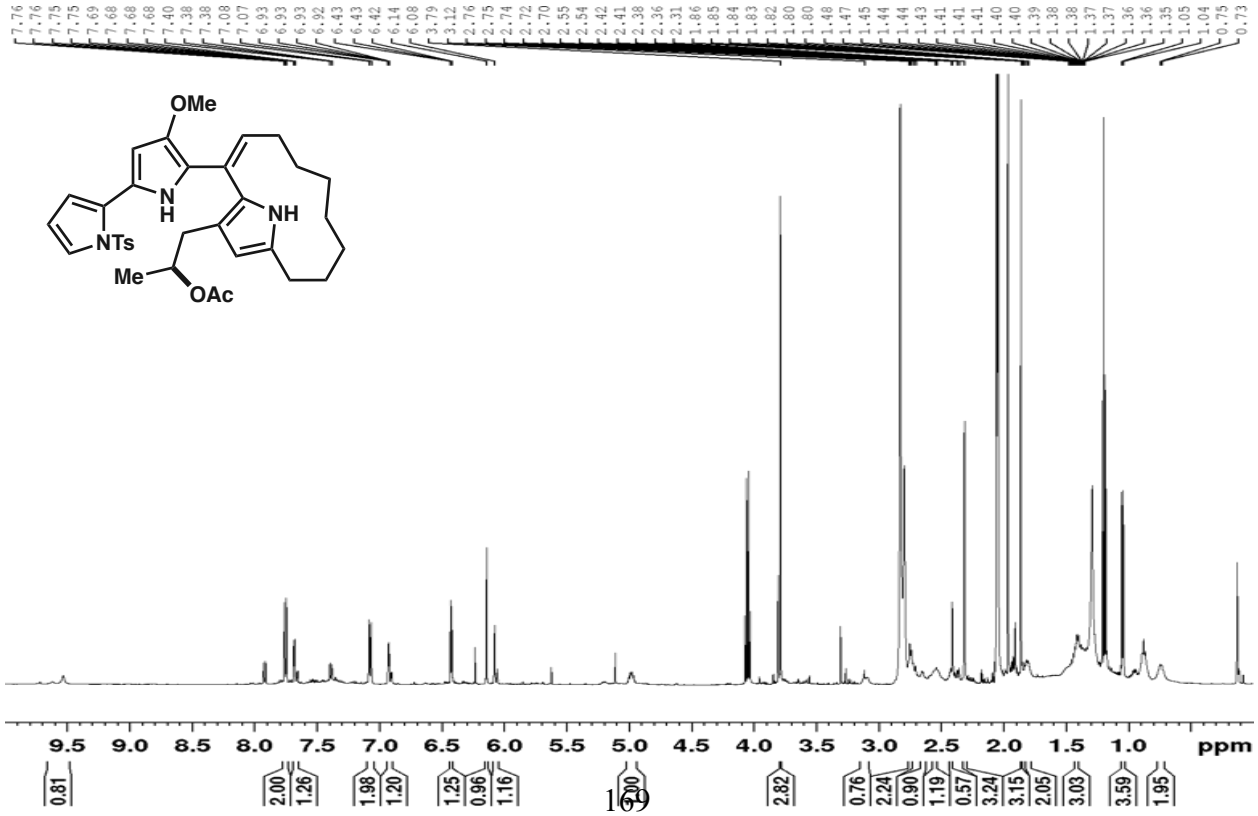

Spectrum 2.4.64 ^{1}H-NMR of compound **29** (acetone-d6, 500 MHz)

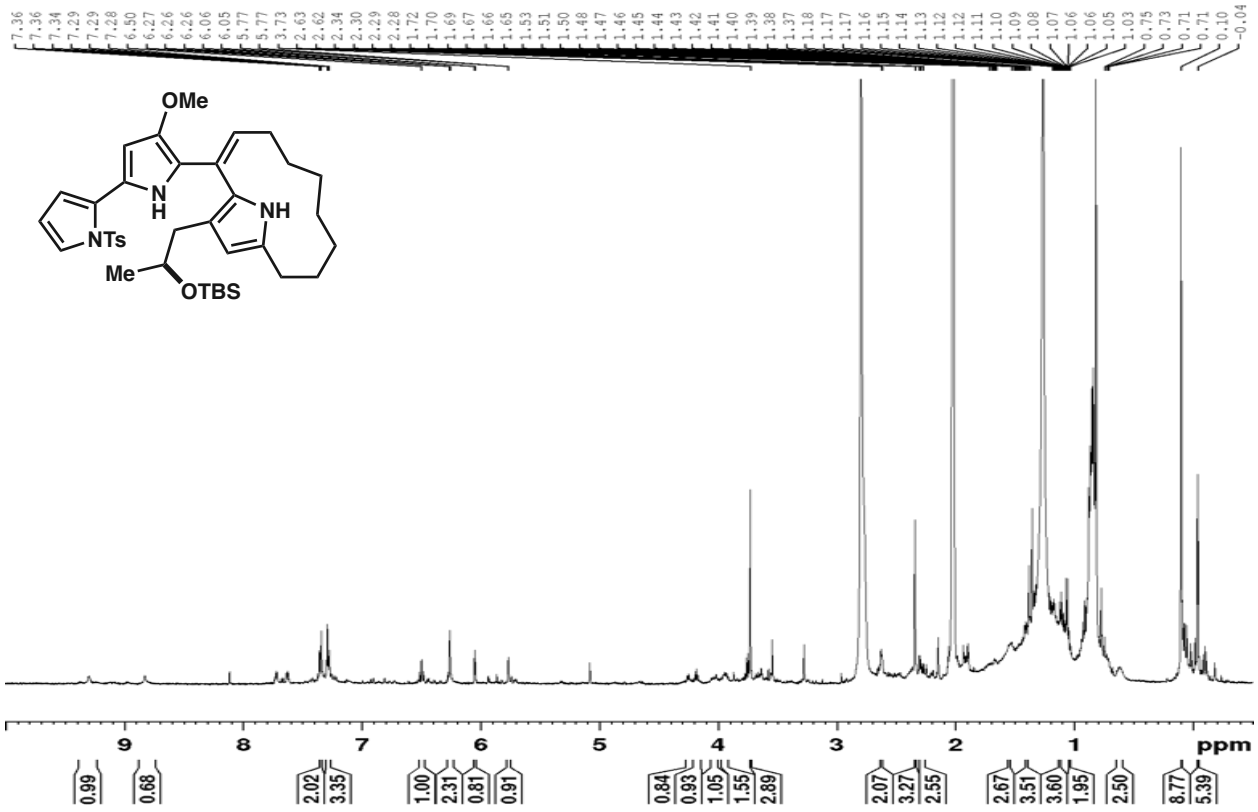

2.5 References

1. Feng, Z.; Allred, T. K.; Hurlow, E. E.; Harran, P. G. Anomalous Chromophore Disruption Enables an Eight-Step Synthesis and Stereochemical Reassignment of (+)-Marineosin A. *J. Am. Chem. Soc.* **2019**, *141* (6), 2274–2278.

2. Fürstner, A. Chemistry and Biology of Roseophilin and the Prodigiosin Alkaloids: A Survey of the Last 2500 Years. *Angew. Chem., Int. Ed*. **2003**, *42* (31), 3582−3603.

3. Hu, D. X.; Withall, D. M.; Challis, G. L.; Thomson, R. J. Structure, Chemical Synthesis, and Biosynthesis of Prodiginine Natural Products. *Chem. Rev.* **2016**, *116* (14), 7818−7853.

4. Sydor, P. K.; Barry, S. M.; Odulate, O. M.; Barona-Gomez, F.; Haynes, S. W.; Corre, C.; Song, L.; Challis, G. L. Regio- and Stereodivergent Antibiotic Oxidative Carbocyclizations Catalysed by Rieske Oxygenase-like Enzymes. *Nat. Chem.* **2011**, *3* (5), 388−392.

5. Hu, D. X.; Clift, M. D.; Lazarski, K. E.; Thomson, R. J. Enantioselective Total Synthesis and Confirmation of the Absolute and Relative Stereochemistry of Streptorubin B. *J. Am. Chem. Soc.* **2011**, *133* (6), 1799−1804.

6. Dohi, T.; Morimoto, K.; Maruyama, A.; Kita Y. Direct Direct Synthesis of Bipyrroles Using Phenyliodine Bis(trifluoroacetate) with Bromotrimethylsilane. *Org. Lett.*, 2006, 8 (10), 2007−2010.

7. Frederich, J. H.; Matsui, J. K.; Chang, R. O.; Harran, P. G. Substituted 2,2'-bipyrroles and pyrrolylfurans via intermediate isoxazolylpyrroles. *Tetrahedron Lett.* **2013**, *54* (21), 2645−2647.

8. Zhao, G.; Liang, L.; Wen, C. H. E.; Tong, R., In Situ Generation of Nitrile Oxides from NaCl–Oxone Oxidation of Various Aldoximes and Their 1,3-Dipolar Cycloaddition. *Org. Lett.* **2019,** *21* (1), 315−319.

9. Jiao, H.; Schleyer, P. R., A Detailed Theoretical Analysis of the 1,7-Sigmatropic Hydrogen Shift: The Möbius Character of the Eight-Electron Transition Structure. *Angew. Chem., Int. Ed. Engl.*, **1993,** *32* (12), 1763−1765.

10. Havinga, E.; Schlatmann, J. L. M. A., Remarks on the specificities of the photochemical and thermal transformations in the vitamin D field. *Tetrahedron* **1961,** *16* (1), 146−152.

11. Schiess, P.; Dinkel, R., Thermal isomerization of 1,1-disubstituted cyclohexa-2,4-dienes. *Tet. Lett.*, **1975,** *16* (29), 2503−2506.

12. Gurskii, M. E.; Gridnev, I. D.; Il'ichev, Y. V.; Ignatenko, A. V.; Bubnov, Y. N., Investigation of the (1,7) Sigmatropic Hydrogen Shift in a Parent Compound (Z,Z)-1,3,5-Heptatriene and Its Monodeuterium Analogue. *ChemInform* **1992,** *23* (39), 762−764.

13. Lim, H. N.; Parker, K. A., Total Synthesis of the Potent Androgen Receptor Antagonist (−)-Arabilin: A Strategic, Biomimetic [1,7]-Hydrogen Shift. *J. Am. Chem. Soc.*, **2011,** *133* (50), 20149−20151.

14. Clarke, J.; Fowler, P. W.; Gronert, S.; Keeffe, J. R., Effect of Ring Size and Migratory Groups on [1,n] Suprafacial Shift Reactions. Confirmation of Aromatic and Antiaromatic Transition-State Character by Ring-Current Analysis. *J. Org. Chem.*, **2016,** *81* (19), 8777−8788.

15. Klärner, F. G., A Degenerate Rearrangement of cis-Bicyclo [6.1.0]nona-2,4,6-triene. *Angew. Chem., Int. Ed. Engl.*, **1972,** *11* (9), 832−833.

16. M. J. Frisch *et al., Gaussian 16*, Revision C.01; Gaussian, Inc.: Wallingford CT, **2016**.

17. Bannwarth, C.; Caldeweyher, E.; Ehlert, S.; Hansen, A.; Pracht, P.; Seibert, J.; Spicher, S.; Grimme, S., Extended tight-binding quantum chemistry methods. *Wiley Interdiscip. Rev.: Comput. Mol. Sci.* **2020,** *11* (2), 1493–1541.

18. Pracht, P.; Bohle, F.; Grimme, S., Automated exploration of the low-energy chemical space with fast quantum chemical methods. *Phys. Chem. Chem. Phys.* **2020,** *22* (14), 7169 –7192.

19. Zimmerman, P. M., Growing string method with interpolation and optimization in internal coordinates: method and examples. *J. Chem. Phys.* **2013,** *138* (18), 184102–18411.

20. Bannwarth, C.; Ehlert, S.; Grimme, S., GFN2-xTB-An Accurate and Broadly Parametrized Self-Consistent Tight-Binding Quantum Chemical Method with Multipole Electrostatics and Density-Dependent Dispersion Contributions. *J. Chem. Theory. Comput.* **2019,** *15* (3), 1652–1671.

21. Chai, J. D.; Head-Gordon, M., Long-range corrected hybrid density functionals with damped atom-atom dispersion corrections. *Phys. Chem. Chem. Phys.* **2008,** *10* (44), 6615 –6620.

22. Weigend, F.; Ahlrichs, R., Balanced basis sets of split valence, triple zeta valence and quadruple zeta valence quality for H to Rn: Design and assessment of accuracy. *Phys. Chem. Chem. Phys.* **2005,** *7* (18), 3297–3305.

23. Marenich, A. V.; Cramer, C. J.; Truhlar, D. G., Universal solvation model based on solute electron density and on a continuum model of the solvent defined by the bulk dielectric constant and atomic surface tensions. *J. Phys. Chem. B* **2009,** *113* (18), 6378 –6396.

24. Becke, A. D., Density-functional thermochemistry. III. The role of exact exchange. *J. Chem. Phys.* **1993,** *98* (7), 5648–5652.

25. Hehre, W. J.; Ditchfield, R.; Pople, J. A., Self—Consistent Molecular Orbital Methods. XII. Further Extensions of Gaussian—Type Basis Sets for Use in Molecular Orbital Studies of Organic Molecules. *J. Chem. Phys.* **1972,** *56* (5), 2257–2261.

26. Krishnan, R.; Binkley, J. S.; Seeger, R.; Pople, J. A., Self-consistent molecular orbital methods. XX. A basis set for correlated wave functions. *J. Chem. Phys.* **1980,** *72* (1), 650 – 654.

27. Willoughby, P. H.; Jansma, M. J.; Hoye, T. R., A guide to small-molecule structure assignment through computation of 1H and 13C NMR chemical shifts. *Nat. Protoc.* **2014,** *9* (3), 643–660.

28. Adamo, C.; Barone, V., Exchange functionals with improved long-range behavior and adiabatic connection methods without adjustable parameters: The mPW and mPW1PW models. *J. Chem. Phys.* **1998,** *108* (2), 664–675.

29. Tomasi, J.; Mennucci, B.; Cammi, R., Quantum mechanical continuum solvation models. *Chem. Rev.* **2005,** *105* (8), 2999–3093.

30. Luchini, G.; Alegre-Requena, J. V.; Funes-Ardoiz, I.; Paton, R. S., GoodVibes: automated thermochemistry for heterogeneous computational chemistry data. *F1000Research* **2020,** *9*.

31. CYLview20; Legault, C. Y., Université de Sherbrooke, **2020** (http://www.cylview.org).

Chapter Three: Progress Towards the Total Synthesis of JBIR-141

3.1 Introduction

Transcription factors are proteins that regulate the expression of genes by binding to replication complexes and modulating the activity of DNA polymerase. They control a myriad of processes ranging from cellular nutrient utilization to cell cycle progression, mitosis, and apoptosis. Despite their central role in the life cycle of "normal" cells, the activity of certain transcription factors has been associated with cancer progression as drivers of metastases, angiogenesis, and drug resistance.[1] For this reason, transcription factors have long been coveted as potential targets of chemotherapeutic small-molecule drugs. Frustratingly, the identification and development of specific transcription factor inhibitors that function effectively within cells has been a mountainous challenge, with the utilization of large screening libraries composed of drug-like heterocycles yielding limited success.[2]

While many of the over 1,500 known transcription factors have been well studied for their role in the orchestration of numerous biological processes, the FoxO (forkhead box subclass O) family has garnered particular attention due to their association as regulators of cellular longevity. In addition, they have also been well acknowledged for their role as tumor suppressors by inducing cell cycle arrest and apoptosis. The FoxO family of transcription factors consists of four members; FoxO1, FoxO3, FoxO4 and FoxO6. Among them, FoxO3a, a subtype of FoxO3, is unique in that it is a disordered protein which, in addition to its normal function as a tumor suppressor, has been found to induce cancer cell invasion, metastases, and drug resistance.[3-8]

When carrying out its typical function as a tumor suppressor, FoxO3a functions within the nucleus, transcribing genes involved in cell cycle arrest and apoptosis. Like many members of the FoxO family, the transcriptional activity of FoxO3a is tightly regulated, via mechanisms which controls its nuclear concentration, though modulation of the phosphatidylinositol 3-kinase (PI3K)-protein kinase B (Akt) signaling pathway. In cells not designated for programmed cell death, this pathway proceeds via the activation of Akt by PI3K, the former of which is responsible for the direct phosphorylation of FoxO3a. This causes FoxO3a's expulsion from the nucleus and its subsequent degradation in the cytoplasm, thus down regulating the transcription of its target apoptotic genes.[9] Dysregulation or improper functioning of this PI3K-Akt regulatory pathway has been shown to lead to unfettered cell proliferation and the development of cancers such as chronic myeloid leukemia (CML). This was confirmed though the finding that CML cells carry an abnormal BCR-ABL gene absent in normal cells; a genetic abnormality which has been associated with the increased production of BCR-ABL proteins, which, by activating the PI3K-Akt signaling pathway, leads to the translocation of FoxO3a out of the nucleus and the downregulation of apoptosis, enabling unchecked growth and proliferation of CML cells (**Figure 3.1.1A**).[10]

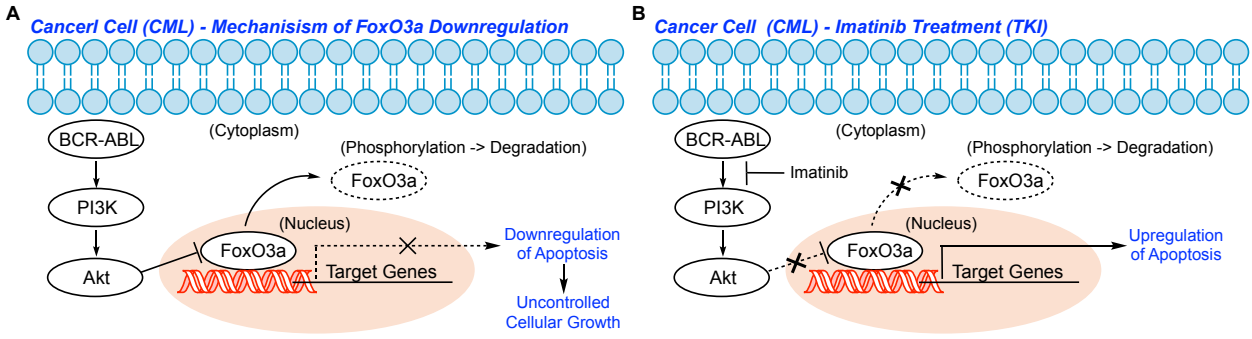

Figure 3.1.1 Cellular Regulation of FoxO3a transcriptional activity (**A**) Regulation of FoxO3a transcriptional activity in cancer (CML) cells (**B**) Regulation of FoxO3a transcriptional activity during treatment with Imatinib.

Today, the most common treatment for CML employs developed tyrosine kinase inhibitors (TKIs). Imatinib (aka Gleevec or Glivec), one of the most widely used of these TKIs since its introduction to the market in late 2001, has been shown to operate upstream of PI3K and successfully treats CML by acting as an inhibitor of BCR-ABL proteins, downregulating the anti-apoptotic PI3K-Akt pathway (**Figure 3.1.1B**).[11] While the advent of these TKIs was once hailed as a "magic bullet" in the fight against chronic myeloid leukemia, their continued use was found to lead to cancer recurrence via the formation of drug resistant stem cells whose growth was promoted by the accumulation of nuclear FoxO3a driven by TGF-β signaling.[12] Further studies have also show FoxO3a to be critical for the maintenance and self-renewal of hematopoietic stem cells (HSCs) as well as leukemia initiating cells (LICs), factors which also contribute to drug resistance and cancer recurrence.[12-15]

This paradoxical role of FoxO3a as a pro-apoptotic transcription factor in non-cancerous cells and an anti-apoptotic promoter in cancer stem cells is attributed to increased concentrations of intranuclear β-catenin found in the latter; a protein which binds to FoxO3a and diverts its function to stem cell maintenance without inducing apoptosis.[4] As a result of these findings, it has been posited that small molecules capable of selectively inhibiting FoxO3a transcriptional would be highly valuable towards the elimination of CML stem cells not targeted by TKIs. In 2015, a Japanese laboratory, led by Kazuo Shin-ya and coworkers, screened over 250,000 natural products in search of inhibitors of FoxO3a mediated transcription.[16] From this screen, JBIR-141 (**1**, **Figure 3.1.2**) and JBIR-142 (**2**) were identified as a potent inhibitor of FoxO3a transcriptional activity.[17]

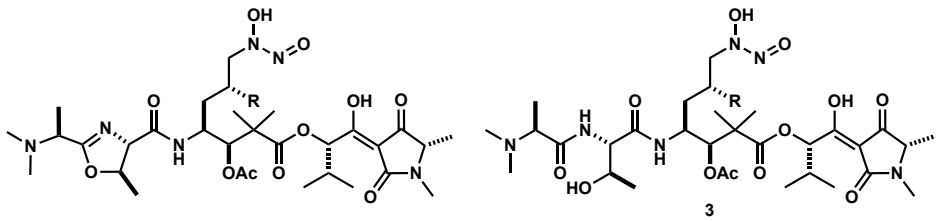

Figure 3.1.2 Structures of JBIR-141 (**1**), JBIR-142 (**2**) and co-isolated **3.**

JBIR-141 (**1**) and JBIR-142 (**2**) are peptidomimetic natural products extracted from the culture broth of *Streptomyces* sp. 4587H4S, a soil-derived actinomycete bacterial strain isolated from samples collected at Ishigaki island, Japan. Their structure was elucidated utilizing mass spectroscopy (HRESIMS) and UV/IR absorption data in conjunction with extensive 1D- and 2D-NMR analysis (i.e DQF-COSY, HSQC, CT-HMBC[18]). For further structural elucidation, literature protocols for degradation studies[19,20] were carried out on **3** (**Figure 3.1.2**); a product co-isolated with **1** and **2** resulting from hydrolysis of the N-terminal oxazoline of the latter. The products isolated from these studies were further analyzed using the methods outlined above with absolute stereochemical elucidation provided via the utilization of Marfey's method.[21,22]

Using cell-based luciferase reporter assays conducted on HEK293 cells, both JBIR-141 (**1**) and JBIR-142 (**2**) were identified as potent inhibitors of FoxO3a transcriptional activity with cellular IC_{50} values of 23.1 nm and 166.1 nm, respectively.[17] Moreover, both compounds show notable selectivity against FoxO3a over other transcription factors such as NF-κB, p53, and notch (**Figure 3.1.3A/B**). Interestingly, this data also indicates the concomitant effect of these compounds to up-regulate NF-κB transcriptional activity, an unexpected finding. It should also be noted that cell viabilities during the 24 h incubation period remained relatively unchanged, indicating the low cytotoxicity of **1** and **2** in these studies.

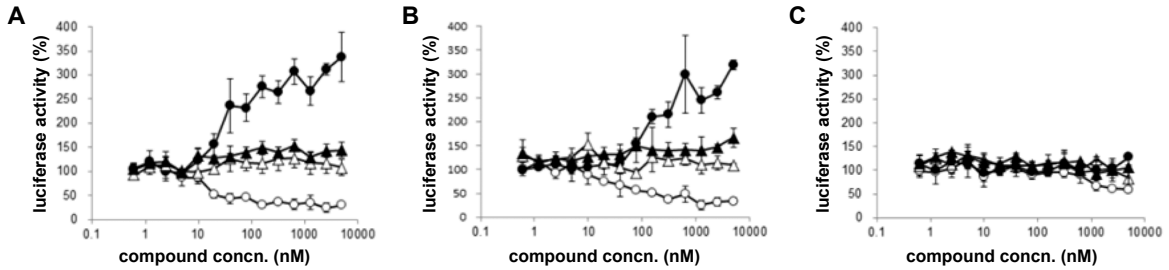

Figure 3.1.3 Data obtained from cell-based luciferous assays measuring the inhibition of transcription factor activity by (**A**) JBIR-141 (**1**), (**B**) JBIR-142 (**2**) and (**C**) compound **3**. (○) Foxo3a, (●) NF-kB, (Δ) p53, (▲) notch.

In addition to their potent inhibition of FoxO3a transcriptional activity, further biological testing showed both **1** and **2** to exhibit strong cytotoxic activity against a variety of human cancer cell lines including, SKOV-3 (human ovarian adenocarcinoma), MESO-1 (human malignant mesothelioma), and Jurkat (human T-lymphoma): IC_{50} values 11.7 and 101 nm against SKOV-3, 89.8 and 66.5 nm against MESO-1, 4.4 and 30.6 nm against Jurkat for **1** and **2**, respectively. Interestingly, parallel testing of these compounds alongside **3** showed the latter to be almost completely inactive towards FoxO3a inhibition (**Figure 3.13C**) as well as dramatically less cytotoxic against SKOV-3, MESO-1 and Jurkat cell lines (IC_{50} = 1094, 3353 and 836 nm, respectively). These findings underscore the significance of the N-terminal oxazoline functionality in compounds **1** and **2** with respect to their biological activity. A summary of cytotoxicity IC_{50} values against these various cell lines is shown in **Table 3.1.1**.

	IC_{50} [nM]		
	JBIR-141 (**1**)	JBIR-142 (**2**)	**3**
SKOV-3	11.7	101	1094
MESO-1	89.8	66.5	3353
JURKAT	4.41	30.6	836

Table 3.1.1 Summary of IC_{50} values for **1**, **2** and **3** against SKOV-3, MESO-1 and Jurkat cell lines.

In a 2022 patent, Sir Paul Nurse and colleagues at the Francis Crick Institute in London reported the isolation and characterization of a stable JBIR-141 Zn^{2+} complex from extracts of actinomycete strain DEM21859.[23] Bioassays of this isolated zinc-complex ran in parallel with the apo-natural product showed the former to be significantly more active against unicellular fission yeast *S. Pombe* as well as other bacterial strains. In addition, Zinc-bound **1** was also found to display potent cytotoxicity against a variety of acute myeloid leukemia (AML) cell lines (Kasumi-I, SKNO-I, THP-I, MV-4-11 , HL-60 and OCI-AML3) as well as burkitts lymphoma (i.e non-

hodgkins lymphoma) cell lines (Ramos and BL-41) with EC_{50} values ranging from 10 to 200 nm (see **Table 3.1.2** for EC_{50} values). In addition to these results, the isolated complex was found to be 10^2-20^3 less cytotoxic towards the negative control mesenchymal stromal cells (MSC).

Cell Line	EC_{50} (nM)
MSC	20,000
Kasumi-1	80
SKNO-1	30
MD-4-11	60
BL-41	10
HL-60	50
OCI-AML3	200
THP-1	60
Ramos	50

Table 3.1.2 Summary of EC_{50} values of JBIR-141(**1**) Zn^{2+} complex against a variety of acute myeloid leukemia (AML) cell lines and burkitts lymphoma (i.e non-hodgkins lymphoma) cell lines.

While no structure for the isolated complex was reported, we hypothesize that JBIR-141 binds Zn^{2+} in a manner analogous to the binding of Cu^{2+} in chalkophomycin[24] (**Figure 3.1.4A**) wherein the deprotonated N-nitrosohydroxylamine (aka diazeniumdiolate) and acyl tetramate motifs coordinate to the metal as planar LX type ligands (e.g acetylacetonate, aka 'acac'). A computationally supported and refined model of our purported structure for this coordination complex, created in collaboration with the group of Professor Ken Houk, is shown be below in **Figure 3.1.4B**.

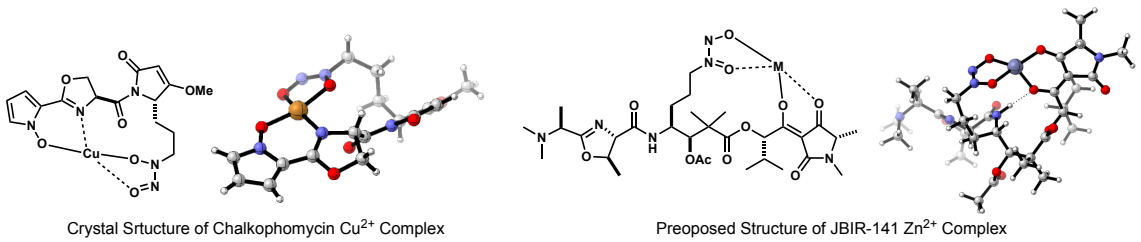

Figure 3.1.4 X-ray crystal structure of chalkophomycin Cu^{2+} complex and proposed coordination complex of JBIR-141 Zn^{2+} complex. (**A**) Single crystal X-ray structure of Chalkophomycin Cu^{2+} complex (CCDC database ID# 2019562). (**B**) Proposed structure of JBIR-141 Zn^{2+} complex. This

structure was determined via conformation sampling of the deprotonated parent compound (**1**) using Conformer–Rotamer Ensemble Sampling Tool (CREST)[25]. To the lowest energy conformation of anionic ligand **1** was then manually added a Zn^{2+} ion (shown in purple) at close proximity to the anionic acyl tetramate. Free rotation of the sigma bonds allows the anionic N-nitrosohydroxylamine group to coordinate the Zn^{2+} center in a 4-coordinate tetrahedral geometry. The geometry of this complex was subsequently optimized using DFT calculations using the B3LYP-D3[26,27] functional and def2SVP[28] basis set.

While both JBIR-141 (**1**) and JBIR-142(**2**) display a wide variety of promising biological activities which makes them well positioned for development into chemotherapeutic agents, particularly as a TKI-compliments in the treatment of CML, more research is needed as essentially nothing is known about their biological mechanisms of action or their molecular target(s).[17] Moreover, because these products encompass a diverse range of biologically active structural motifs, numerous potential hypotheses can be posited to explain their mechanism of action as a FoxO3a inhibitor.

Several of these hypotheses stem from the potential for these compounds to bind metals via their N-nitrosohydroxylamine functionality, a finding well reported in the literature[29,30], working in concert with either their amino oxazoline and/or acyl tetramate motifs. While fluctuating intracellular concentrations of Cu^{2+} and Zn^{2+} ions has been shown to modulate FoxO signaling in human hepatoma cells via activation of the PI3K-Akt pathway[31] and be instrumental in the ability of β-thujaplicin (aka hinokitiol) to down regulate the activity of FOXOla[32], we feel it is unlikely that metal ion sequestration is responsible for the inhibition of FoxO3a activity by these compounds. This doubt is supported by the high cellular potency of the aforementioned JBIR-141 Zn^{2+} complex (EC_{50} 10-200 nM) which, at such low concentrations, is unlikely to significantly perturb intracellular zinc concentrations. An alternative theory to metal sequestration proposes that these compounds may operate through the release of nitric oxide (NO). This hypothesis is grounded in findings which show NO signaling to be correlated with inhibited

FoxO3a activity.[33] While the N-nitrosohydroxylamine moiety found in these structures do not typically function as NO donors[34], its conjugate base has been shown to release NO upon one electron enzymatic oxidation.[35] Finally, it has also been proposed that these structure function as a pro-drug wherein their acetate group is cleaved by esterase activity upon entry into the cell, revealing an amido ethanol motif reminiscent of transition state isosteres used for protease inhibition.[36]

Because the isolated yields of these two compounds were extremely low (14 mg and 17 mg for **1** and **2**, respectively) and to date, neither have been synthesized in a laboratory, we set out to establish the first laboratory synthesis of JBIR-141 and JBIR-142. In doing so, we plan to establish the means to procure sufficient material, as well as analogs thereof, to facilitate structure-activity relationship (SAR) and expanded biological studies to better understand their mechanism of action as a FoxO3a inhibitor towards the ultimate goal of maximizing their therapeutic potential as a complimentary CML treatment. Towards these efforts, we quickly narrowed our focus to the synthesis of JBIR-141 alone as it shows superior cytotoxicity against a majority of tested cell lines as well as 7-fold greater inhibition of FoxO3a transcriptional activity compared to JBIR-142 (23.1 vs. 166.1 nm).

3.2 Overview of Relevant Literature

JBIR-141's potential utility as a selective inhibitor of FoxO3a transcriptional activity coupled with its potent cytotoxicity against several human cancer cell lines has garnered considerable attention from researchers worldwide. This has resulted in the concerted effort of several labs to actively pursue the development of a synthetic route to the natural product. Despite these efforts, to date, none have succeeded.

One research group who has so far made notable progress towards developing a route to JBIR-141 is the group of Takayuki Doi at Tohoku University in Japan. In late 2022, Doi and coworkers published work describing the 14-step synthesis of the central N-nitrosohydroxylamine containing γ-amino acid segment of JBIR-141 derived from allyl (S)-N-Boc-pyroglutamate.[37] This route is shown in **Scheme 3.2.1** below. While this same laboratory has reported elaborations of this central fragment in conference proccedings[38], to our knowledge these efforts have not yet generated JBIR-141.

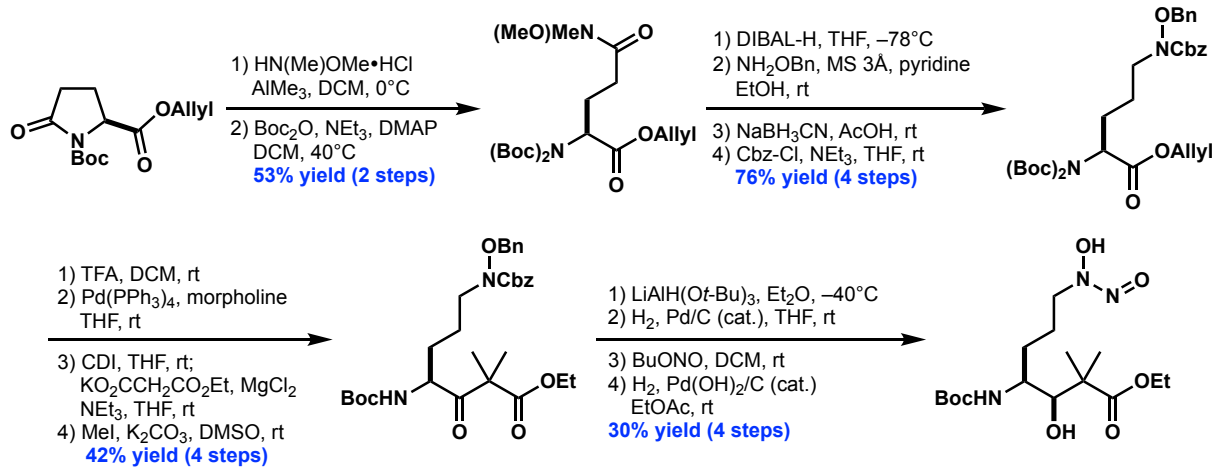

Scheme 3.2.1 Synthetic route to the N-nitrosohydroxylamine containing central fragment of JBIR-141 (**1**) developed by the laboratory of Takayuki Doi at Tohoku University, Japan.

In addition to these efforts led by Doi and colleagues, the laboratory of Rainer Schobert at the University of Bayreuth in Germany has also made significant contributions towards establishing the first total synthesis of JBIR-141 through his publication of a related synthetic analog (**4**, **Figure 3.2.1**)[39] While this analog contains all three key functionalities present in JBIR-141 (**1**), including the N-terminal oxazoline, N-nitrosohydroxylamine and C-terminal acyl tetramate as well as six of the seven chiral centers, it differs from the natural product only via the omission of a centrally located isobutyl acetate spacer (highlighted in red). In this work, the authors make clear that their goal was the development of a "flexible synthetic approach to these [JBIR-

141 and JBIR-142] compounds" and to "fathom the compatibility of the *N*-nitrosohydroxylamine group with reactions and conditions typical of heterocyclic and tetramate chemistry and its amenability to standard protecting/deprotecting protocols." As shown in their retrosynthetic analysis of analog **4** (**Scheme 3.2.2**), Schobert and workers utilized a fragment assembly approach to arrive at the backbone of the natural product with final tailoring of the N-nitrohydroxylamine greatly mirroring that employed by Doi and coworkers.[37]

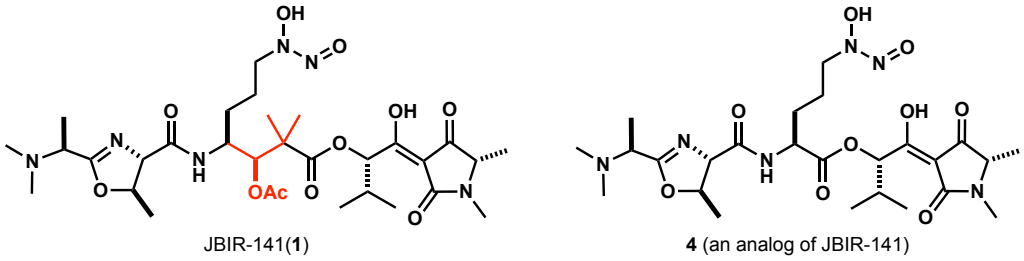

Figure 3.2.1 The natural product JBIR-141(**1**) alongside analog **4** (synthesized by Schobert and coworkers) which is missing the central isobutyl acetate linker (shown in red) of the natural product.

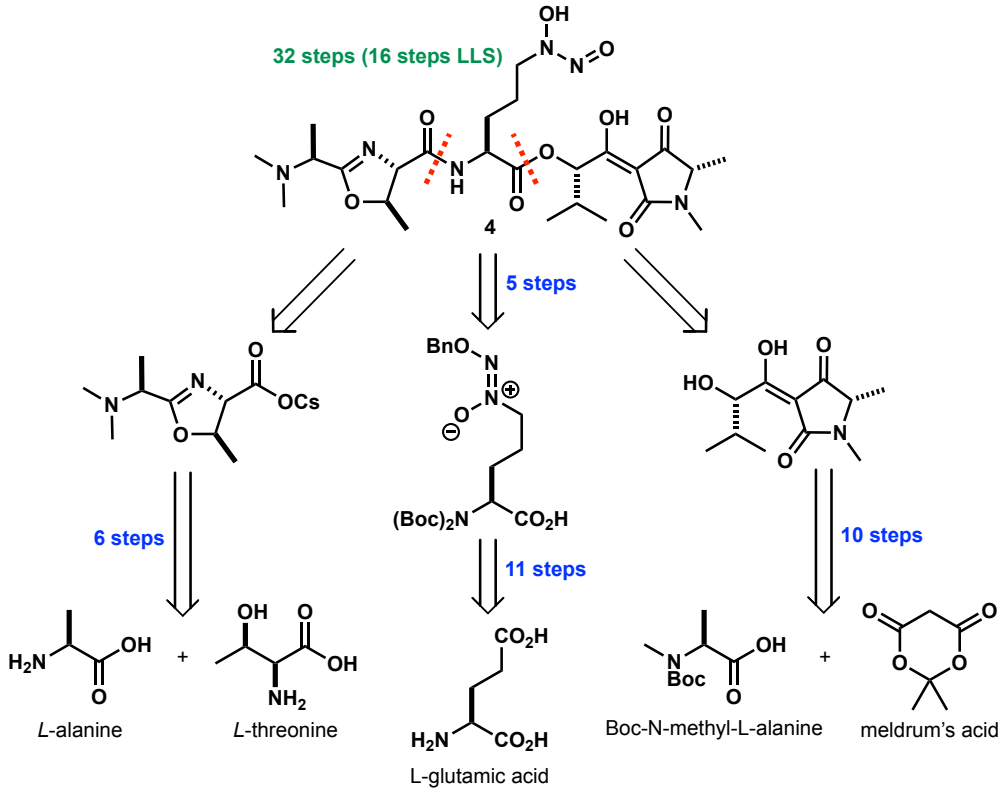

Scheme 3.2.2 Retrosynthetic analysis of **4**, an analog of JBIR-141(**1**) synthesized by Rainer Schobert of University of Bayreuth, Germany.

Upon its completion, **4**, along with numerous route intermediates (**Figure 3.2.2**), were tested for their cytotoxic and antimicrobial activities against KB-3-1 (cervix carcinoma) and L-929 (mouse fibroblast) cell lines as well as a panel of a dozen microorganisms. To the authors great surprise, none of the tested compounds showed any noticeable inhibitory effect on the proliferation or viability against any of the tested cancel cancer cell lines (**Table 3.2.1**). This inactivity greatly suggests that the central isobutyl acetate linker missing from **4** is essential for the cytotoxicity against cancer cell lines observed in previous studies.[17] Even more surprising was the inactivity of compounds **4**, **6** and **8** against the entire panel of tested bacteria and fungi (**Table 3.2.2**). Such inactivity amongst C3-acyltetramate containing compounds is rare as a wealth of literature indicates that a substantial amount of bacterially derived tetramic acids show strong antimicrobial activity.[40-42]

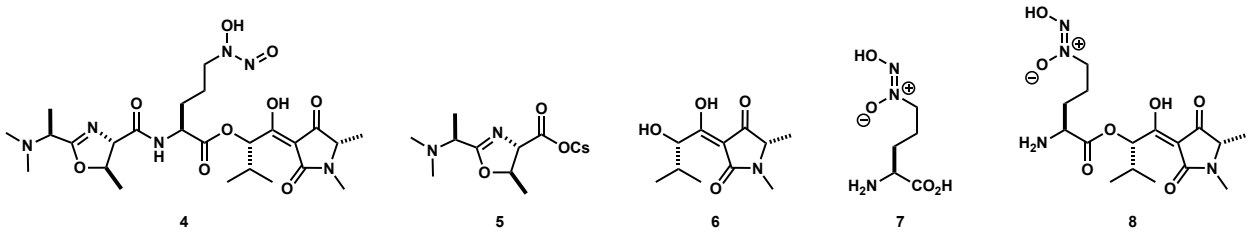

Figure 3.2.2 Compounds tested for cytotoxicity and antimicrobial activity against KB-3-1 (cervix carcinoma) and L-929 (mouse fibroblast) cell lines as well as a panel of a dozen microorganism by Schobert lab.

IC_{50} [µg/L]				
Compound	L-929 [ACC2]	Tox. Nr.	KB-3-1 [ACC158]	Tox.Nr.
4	–	3847	–	3848
5	–	3845	–	3846
6	–	3845	–	3846
7	–	3849	–	2850
8	–	3847	–	3848
Epo B	0.00022	3807	0.000023	3808

Reference: Epo B: epothilone B; –: not active

Table 3.2.1 Results of cytotoxicity studies of **Figure 3.2.2** compounds against KB-3-1 (cervix carcinoma) and L-929 (mouse fibroblast) cell lines. Epo B: epothilone B; – : not active.

MIC [µg/mL]							
Tested Organisms	**Strain No.**	**4**	**5**	**6**	**7**	**8**	**Reference**
Bacteria							
Bacillus subtilis	DSM 10	–	–	–	–	–	8.3[a]
Staphylococcus aureus	DSM 346	–	–	–	–	–	0.2[d]
Mycobacterium smegmatis	ATCC 700084	–	–	–	–	–	1.7b
Acinetobacter baumannii	DSM 30008	–	–	–	–	–	0.3[c]
Chromobacterium violaceum	DSM 30191	–	–	–	–	–	0.8[a]
Escherichia coli	DSM 1116	–	–	–	–	–	0.8[d]
Pseudomonas aeruginosa	PA14	–	–	–	–	–	0.2[d]
Fungi							
Mucor hiemalis	DSM 2656	–	–	–	–	–	8.3[e]
Pichia anomala	DSM 6766	–	–	–	–	–	8.3[e]
Rhodoturula glutinis	DSM 10134	–	–	–	–	–	4.2[e]
Candida albicans	DSM 1665	–	–	–	–	–	16.6[e]
Schizosaccharomyces pombe	DSM 70572	–	–	–	–	–	4.2[e]

References: [a]oxytetracycline; [b]kanamycin; [c]ciprobay; [d]gentamicin; [e]nystatin; –: not active

Table 3.2.2 Results of antimicrobial studies of **Figure 3.2.2** compounds against a panel of a bacteria and fungi. [a]oxytetracycline; [b]kanamycin; [c]ciprobay; [d]gentamicin; [e]nystatin; – : not active.

3.3 Initial Retrosynthetic Analysis of JBIR-141

Looking at the structure of JBIR-141 (**1**, **Figure 3.3.1**) one can readily see that it is comprised of three major functionalities: an N-terminal oxazoline (boxed in blue), a centrally located N-nitrosohydroxylamine (boxed in red) and a C-terminal C3-acylated tetramic acid (boxed in green). While a wealth of literature exists surrounding the synthesis and general stability of both oxazolines[43] and tetramic acids[44], the synthesis, reactivity, and general stability of N-nitrosohydroxylamines is far less researched as these chemical entities are generally rare in nature.[24, 45,46] In fact, both JBIR-141 and JBIR-142 represent the first isolated complex natural products that feature this delicate moiety. In our eyes, it is the presence of all three of these functionalities in a single structure which makes JBIR-141 such a synthetic challenge.

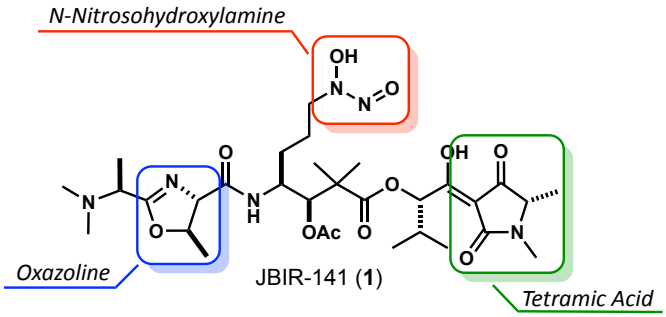

Figure 3.3.1 Structure of JBIR-141 (**1**) with its three major structural functionalities highlighted.

Retrosynthetically, we envision disconnection and the indicated amide and ester bonds (**Scheme 3.3.1**) to afford three fragments of comparable complexity (**9**, **10** and **6**) with the oxazoline and C3-acyated tetramic acid motifs already established is fragments **9** and **6**, respectively. In line with the putative biosynthesis of the natural product, we view these segments as derivable from common amino acids and commodity chemicals. This provides an inexpensive chiral pool source for all but one of the stereocenters in **1**. Fragment assembly followed by installation of the N-nitrosohydroxylamine, which we planned to execute late-stage due to its delicate nature, will provide JBIR-141 (**1**).

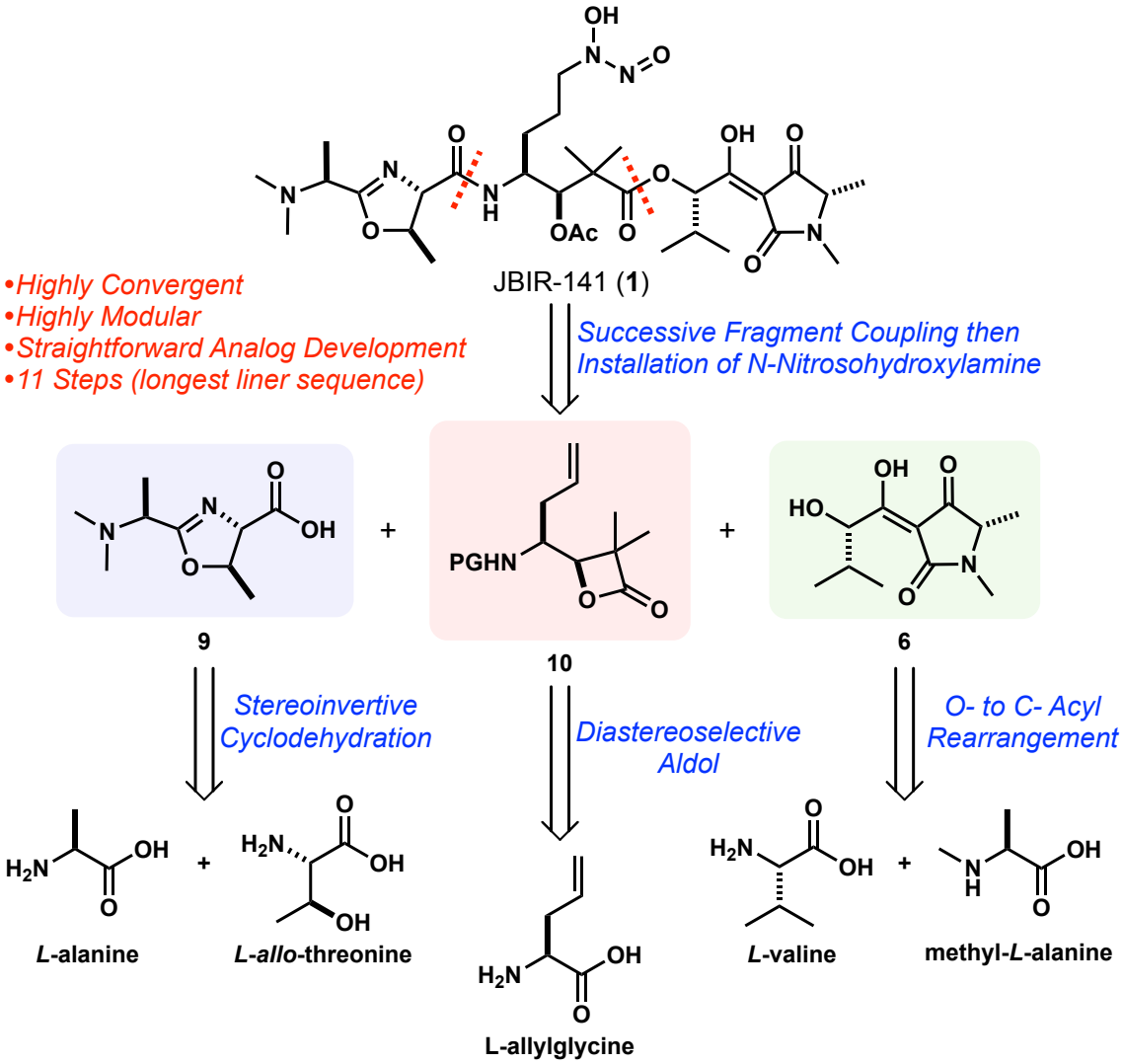

Scheme 3.3.1 Our initial retrosynthetic analysis of JBIR-141 (**1**).

Unlike the approaches of Doi[37] and Schobert[39], we decided to install this functionality via elaboration of a centrally located allyl functional handle as opposed to a benzylated hydroxylamine; a strategic decision which will be discussed later. One of the key advantages of this proposed route is its highly convergent and modular nature which easily accommodates substituent variations as well as fragment deletions and is well suited for the design and synthesis of structural analogs which will be used in future structure-activity relationship (SAR) studies. It

should be noted that since the development of this proposed route, a great number of strategy level changes have been made and the proposed fragments shown above represent only our initial plan.

3.4 Synthetic Studies Towards JBIR-141

3.4.1 Synthetic Studies Towards N-Terminal Oxazoline Fragment 9

Due to the abundance of oxazoline heterocycles found in natural products[47,48] and their extensive use in ligand systems for asymmetric catalysis[49], numerous methods for their syntheses have been published.[43] One widely employed approach is the stereoinvertive cyclodehydration of β-hydroxyamides, functionalities found in serine and threonine containing peptides. In contrast to their biosynthesis[50], this strategy involves the activation and subsequent displacement of the β-hydroxyl group, a process that literature shows can be facilitated by a variety of different reagents.[51]Notably, the use of DeoxoFluor® and DAST, compounds originally developed for deoxofluorination, have been utilized for such purposes.[52-54] This greatly shaped how we envisioned forging the key oxazoline functionality of fragment **9**.

Our initial plan for the synthesis of fragment **9** is shown below in **Scheme 3.4.1**. This route commenced with the synthesis of known N,N-dimethyl-L-alanine (**11**)[55] and L-*allo*-threonine methyl ester hydrochloride (**12**)[56] from commercially available L-alanine and L-*allo*-threonine, respectively. It should be noted that while L-*allo*-threonine is available for purchase from a variety of commercial sources, as of current date, its cost exceeds >$10/gram. For this reason, we elected to prepare it in house from L-threonine in just 4 steps.[57] With both of these components in hand, we envisioned that treating an equimolar mixture of **11** and **12** with an excess of Deoxo-Fluor® would result in direct formation of the desired oxazoline functionality.

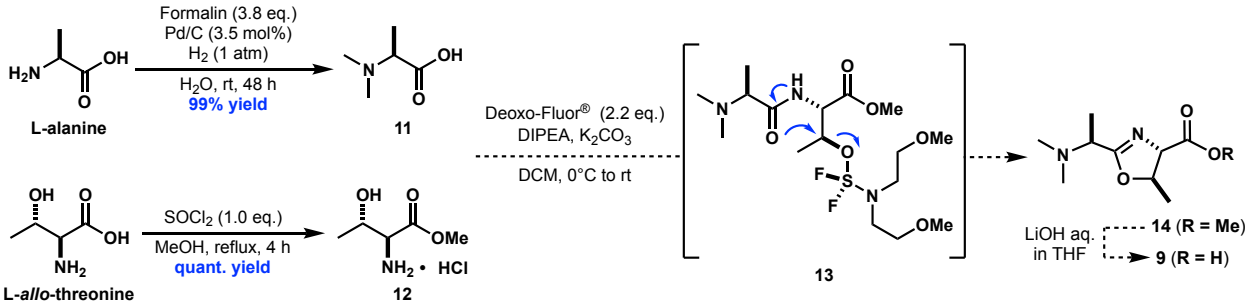

Scheme 3.4.1 Initial plan for the synthesis of N-terminal oxazoline fragment **9**.

We postulated that this 2-step process would proceed via the formation of an amide bond between **12** and an acyl fluoride derived from alanine component **11** followed by activation of the secondary alcohol of the in-situ generated dipeptide. This would initiate a stereoinvertive cyclodehydration as shown in rendering **13**.[58,59] To screen condition for this reaction, we began by adopting procedures put forth by Kangani and workers who published a series of papers outlining the one- pot synthesis of oxazolines from carboxylic acids using Deoxo-Fluor®.[52,53] While none of these publications described the use of two amino acids as the components for this cascade, this did not deter us from pursuing this avenue. Unfortunately, despite extensive screening of reagent equivalents, reaction temperature, reaction solvent, and reagent order of addition, we observed no detectable formation of desired **14** and only minor traces of its antecedent dipeptide. It was the latter of these findings that prompted us to explore a stepwise approach for this sequence.

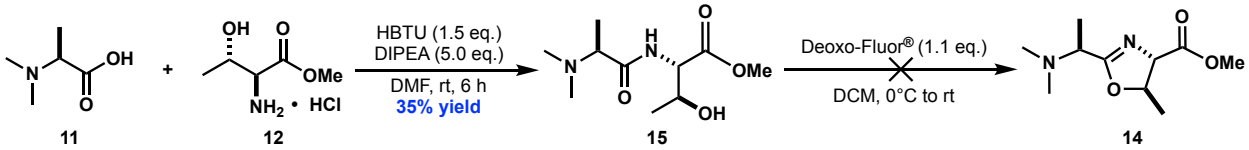

Scheme 3.4.2 Stepwise approach for the synthesis of oxazoline fragment **14** using Deoxo-Fluor®

As shown above in **Scheme 3.4.2**, the coupling of **11** and **12** using conventional methods produced desired dipeptide **15**. The modest yield of this straightforward reaction was attributed to the product's high solubility in both water and brine. This was confirmed by LCMS analysis of

the aqueous layers produced from the workup of the reaction. Consequently, we opted to avoid unnecessary aqueous washes prior to purification of the product via flash column chromatography. To our dismay, both NMR and LCMS analysis of the crude product resulting from treatment of **15** with Deoxo-Fluor® revealed a complex mixture of species, with the desired product appearing to be only a minor component. To exacerbate our frustrations, subsequent attempts to find suitable conditions for this transformation using alternative fluorinating agents, such as DAST and XtalFluor-E, also yielded complex mixtures of products with no appreciable formation of the desired oxazoline. While a cursory survey of the literature revealed numerous unexplored methodologies for achieving the desired stereoinvertive cyclodehydration from **15**, such as the use of Ph_2SO-Tf_2O[60], Martin's sulfurane[61], Burgess reagent[62], and various Mitsunobu protocols[63], we decided to turn our attention towards alternative cyclization approaches.

In 2005, Ishihara and coworkers at Nagoya University published work which demonstrated the ability of various molybdenum oxides to efficiently catalyze dehydrative cyclization reactions of N-acylserines and N-acylthreonines to form oxazolines.[64] While we were initially attracted to this method due to its use of sub-stoichiometric (i.e catalytic) quantities of dehydrating agent, we quickly realized that it most appealing aspect was its ability to proceed with high stereochemical retention at the oxazoline C5 position (the one adjacent to the oxazoline oxygen). While the authors never carried out studies to determine the operative mechanism of these reported reactions, they attributed this stereochemical retention to be the result of a biomimetic-like cyclization, a plausible mechanism for which is shown in **Figure 3.4.1A**.[65,66] This stands in stark contrast to the mechanistic pathway employed by conventional stoichiometric dehydrating agents, which involve the activation and subsequent displacement of the β-hydroxyl group (**Figure 3.4.1B**). The ability to achieve cyclodehydration with stereochemical retention at the C5 center was significant because

it allowed for the substitution of L-*allo*-threonine with L-threonine in our envisioned, the latter of which is dramatically more cost-effective.

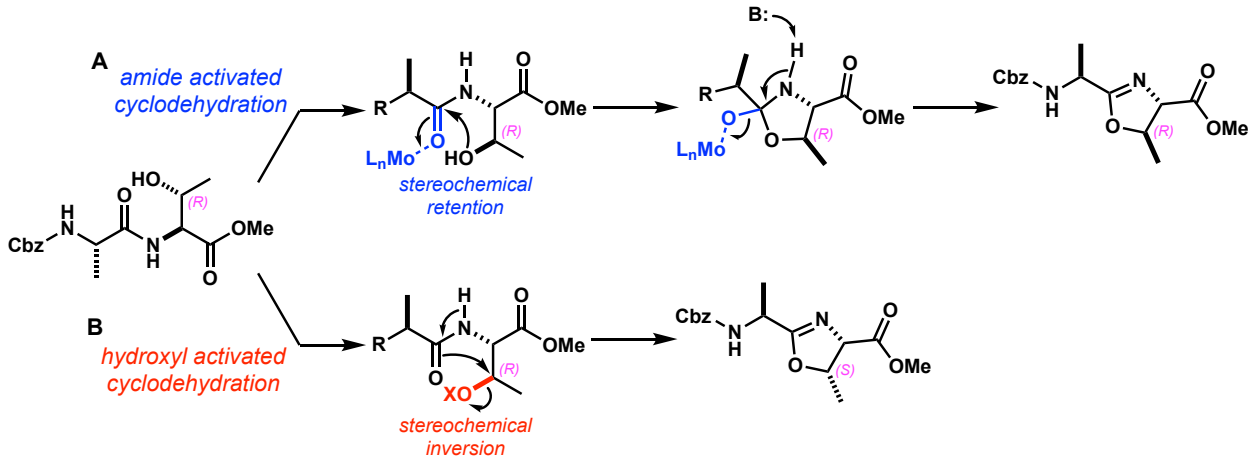

Figure 3.4.1 Comparison of oxazoline forming cyclodehydration mechanisms. (**A**) Biomimetic like amide activated cyclodehydration mechanism. (**B**) Hydroxyl activated cyclodehydration mechanism.

Inspired by this newly found methodology, we quickly revised our approach to fragment **9**, implementing several notable changes to our previously envisioned plan. This revised route commenced with the quantitative conversion of L-threonine to its corresponding ammonium ester salt (**16**) through reflux in dry, acidic methanol[67] (**Scheme 3.4.3**). Coupling of **16** with commercially available Cbz-protected L-alanine, employing HATU and DIPEA, yielded dipeptide **17**, which necessitated no further purification beyond routine acidic followed by basic aqueous washes. While Ishihara and coworkers showed that their developed cyclodehydration methodology can be executed using a variety of molybdenum (IV or VI) oxide catalysts[64], they noted that the use of $(NH_4)_6Mo_7O_{24}x4H_2O$ resulted in the highest yield of the desired trans-oxazolines with the least amount of epimerization at the C2-exomethine position.[65] For this reason, dehydrative cyclization of dipeptide **17** was carried out in the presence of the aforementioned ammonium heptamolybdate catalyst in toluene under azeotropic removal of water using a Dean–

Stark apparatus. ^{1}H-NMR analysis of the reaction mixture after 3 h showed complete consumption of the dipeptide starting material and successful formation to the desired oxazoline with little to no epimerization at the C2-exomethine position. While the reason for this reduced epimerization is not definitively known, we attribute it to doubling the catalyst loading compared to the amount outlined by Ishihara and coworkers. Because amino acid derived oxazolines have been shown to be hydrolytically unstable[43], oxazoline **18** was purified via flash column chromatography using rigorously dried, deactivated silica gel. While we recognize that replacing Cbz-protected L-alanine with N,N-dimethyl-L-alanine **11** would enhance the efficiency of this route, we noticed that all oxazoline synthesized from comparable polypeptides using this methodology featured an aromatic residue in the N-acyl side chain[64,66] which, we speculated to be necessary for effective cyclization. In addition, we felt that the ease with which dipeptide **17** was prepared compared to dipeptide **15** justified this slight reduction in step efficiency.

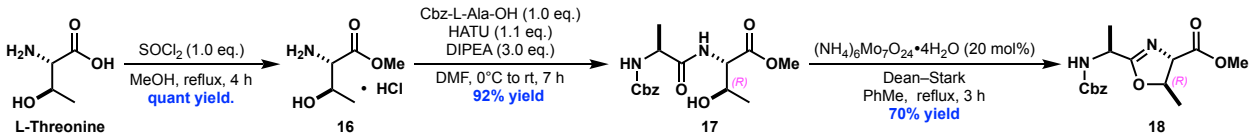

Scheme 3.4.3 Synthesis of 2,4-disubstituted oxazoline methyl ester **18** from L-threonine.

With the key oxazoline functionality of the fragment forged, one-pot Cbz-deprotection followed by successive reductive aminations of the liberated amine, done using Pd/C in the presence of formaldehyde, afforded dimethyl amino-2,4-disubstituted oxazoline **14** (**Scheme 3.4.4**). Purification of this isolated crude product, obtained through filtration of the reaction mixture through celite followed by washing the filter cake with boiling methanol, was not deemed essential for achieving acceptably clean **14**. However, if desired, analytically pure product can be isolated via flash column chromatography using deactivated silica gel, albeit with a notable loss

of material (84% yield compared to 96% yield). While we had Initially anticipated the hydrolytic instability of the oxazoline motif to require neutral, anhydrous conditions for the conversion of **14** to **9,** such as the use of Me_3SnOH[68] or MgI_2[69], methodologies developed by Nicolaou and Parrot, respectively. To our delight, we were pleased to find that traditional saponification conditions using CsOH yielded desired N-terminal oxazoline fragment **9** in near quantitative yield.

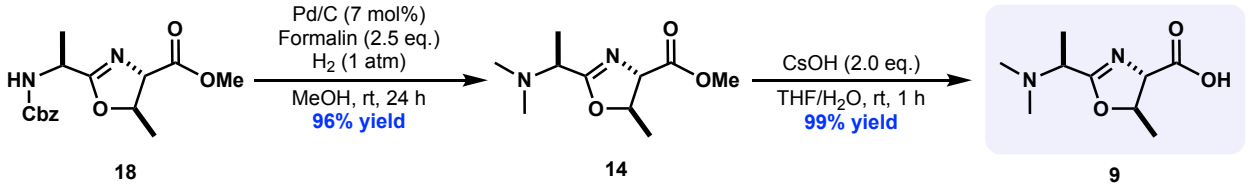

Scheme 3.4.4 Completion of the synthesis of N-terminal oxazoline fragment **9**.

While the route to fragment **9** outlined above is both short and efficient, one of its greatest attributes is its inherent flexibility. As demonstrated in **Scheme 3.4.5**, the ability to alter the amino acid inputs within this sequence offers a straightforward means of varying both the C3 and C5 substituents. This provides facile access to a diverse range of structural analogs which, in turn, will be used in structure-activity relationship (SAR) studies.

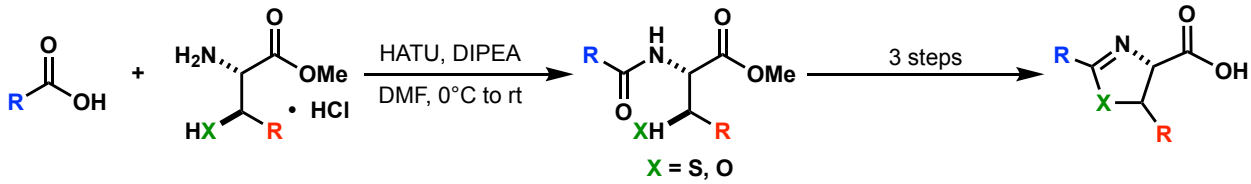

Scheme 3.4.5 Illustration of the inherent flexibility of our route towards the design and synthesis of structural analogs.

3.4.2 Synthetic Studies Towards Central β-Lactone Fragment 10

Initially, we envisioned the central fragment of JBIR-141 would derive from some protected form of L-ornithine methyl ester (**19**, **Scheme 3.4.6A**), which could be easily prepared from its corresponding free acid. Controlled oxidation of **19**'s primary amine was to be achieved using Bode's sulfonyloxaziridine **20**.[70,71] Condensing **19** with **20** would result in Schiff base **21b** which is internally oxygenated as shown in **Scheme 3.4.6B** to give nitrone **21c**. Subsequent exchange aminolysis with hydroxylamine would then liberate **22**.[70] Given the potential instability of a free hydroxylamine functionality moving forward in this route, we planned to carry it forward in protected form (**23**). While numerous protecting groups could have been employed in this context, our preference leaned toward N-allyloxycarbonyl (Alloc) due to its compatibility with subsequent reactions in our planned route. From **23**, partial reduction of it ester using DIBAL-H would yield protected α-amino aldehyde **24** which, we envisioned could be quickly elaborated to the desired β-lactone in a straightforward manner.

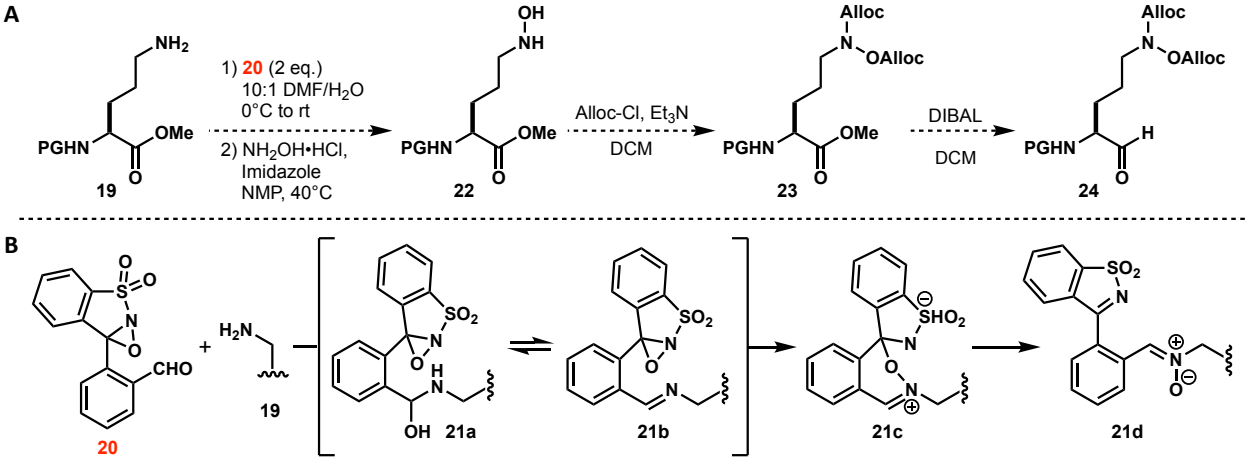

Scheme 3.4.6 Plan for the synthesis of JBIR-141's central fragment. (**A**) Initial plan for the synthesis of the central fragment derived from L-ornithine. (**B**) Mechanism of amine hydroxylation using sulfonyloxaziridine **20**.

Seeking a route more conducive to the design and synthesis of structural analogs, we reevaluated this strategy and determined that the central β-lactone fragment should instead be derived from allylglycine (as opposed to L-ornithine). This approach offers a broader range of potential analogs thanks to the allyl group's ability to serve as a versatile handle for the late-stage installation of the N-nitrosohydroxylamine as well as a wide variety of alternative functionalities. These analogs will be vital towards assessing the importance of this central functionality in the natural product's biological activity. Among various protecting groups considered for this modified route, we chose 2-(Trimethylsilyl)ethoxycarbonyl (Teoc) due to its compatibility with future planned reactions.

The synthesis of Teoc-protected β-Lactone **10** (further referred to as simply **10**) commenced with the conversion of L-allylglycine to it its corresponding methyl ester hydrochloride salt (**25**) using literature outlined conditions (**Scheme 3.4.7**).[72] Teoc protection of crude **25**'s free amine gave **26** in high yield (91%) which was subsequently purified via passage through a short silica gel plug. Although Teoc-OSu is commercially available, we opted to synthesize it in-house from 2-trimethylsilylethanol following a two-step procedure detailed in the literature.[73] DIBAL-H reduction of methyl ester **25** yielded **26**, setting the stage for formation of the β-lactone functionality.

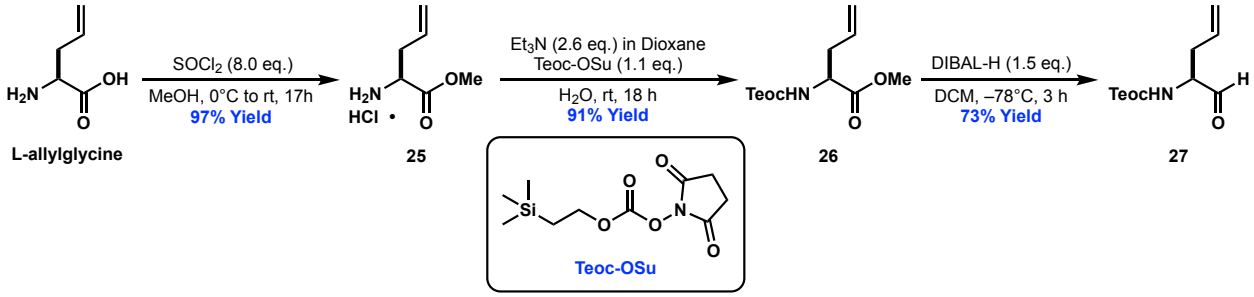

Scheme 3.4.7 Synthesis of Teoc-protected α-amino aldehyde **27** from L-allylglycine.

Our construction of the β-lactone functionality of **10** was inspired by the work of Cossìoa and coworkers at the University of the Basque Country, who, in 1996, published work demonstrating the stereocontrolled synthesis of β-*Propiolactones from achiral lithium enolates and homochiral aldehydes.*[74] *This work, which elaborates on methodology published several years earlier by the laboratory of Rick Danheiser*[75,76]*, outlines the synthesis of* β-lactones via the condensation of achiral thiol ester enolates with chiral aldehydes to form a β-hydroxyl thiol ester alkoxide intermediates which, upon warming, cyclizes to β-lactones (**Scheme 3.4.8**). The authors attribute the high diastereoselectivity of these reactions to be the result of attack of the aldehyde by the lithium enolate in open transition state consistent with the Felkin-Ahn model.[77,78]

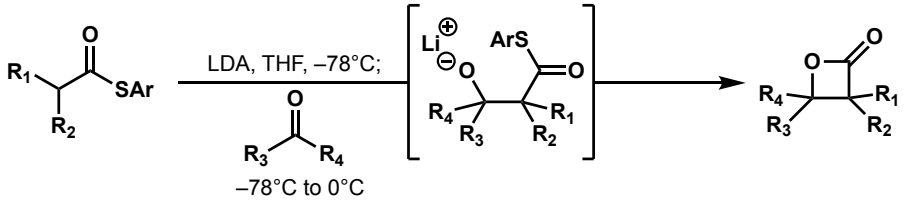

Scheme 3.4.8 Methodology developed by Danheiser et al. and further elaborated on by Cossìoa and workers for the synthesis of β-lactones from achiral lithium enolates and homochiral aldehydes.

For our system, we envisioned that the stereocontrolled addition of lithiated phenylthiol-isobutyrate to protected α-amino aldehyde **27** followed by mild acidic workup would provide desired β-lactone **10**. The execution of this reaction was carried out via the dropwise addition of known S-phenyl 2-methylpropanethioate (**28**)[79], derived from isobutyryl chloride and thiophenol in a single step, to a cold solution of LDA (–78°C), followed by the dropwise addition of **27** (**Scheme 3.4.9**). Slow warming of the resulting reaction mixture to 0°C and then to rt, followed by quenching with a saturated solution of ammonium chloride, yielded β -lactone **10** (60%, d.r 4:1) after purification via flash column chromatography.

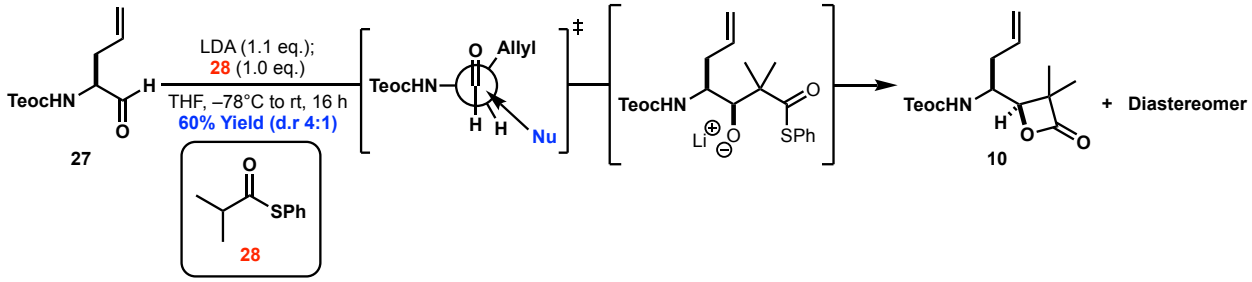

Scheme 3.4.9 Synthesis of β-lactone **10** from Teoc-protected allylglycine derived aldehyde **27** and S-phenyl 2-methylpropanethioate (**28**) using methodology developed by Cossìoa and Danheiser.

Having established a synthetic route to the central fragment, we anticipated that the ester linkage between the central and C-terminal fragments could be formed via the nucleophilic opening of the β-lactone of **10** by the hydroxyl group of C3-acylated tetramic acid **6** (**Scheme 3.4.10A**). To model this reaction, we attempted to open the β-lactone of **10** with α-hydroxyisovaleric acid ethyl ester (**30**) which we viewed as a good surrogate for C3-acylated tetramic acid **6**. Stirring these two compounds in DCM at various temperatures (ranging from 0°C to 60°C) failed to forge the desired ester linkage and instead show no reaction (**Scheme 3.4.10B**). Subsequent efforts done with the inclusion of DMAP as an additive yielded analogous results.

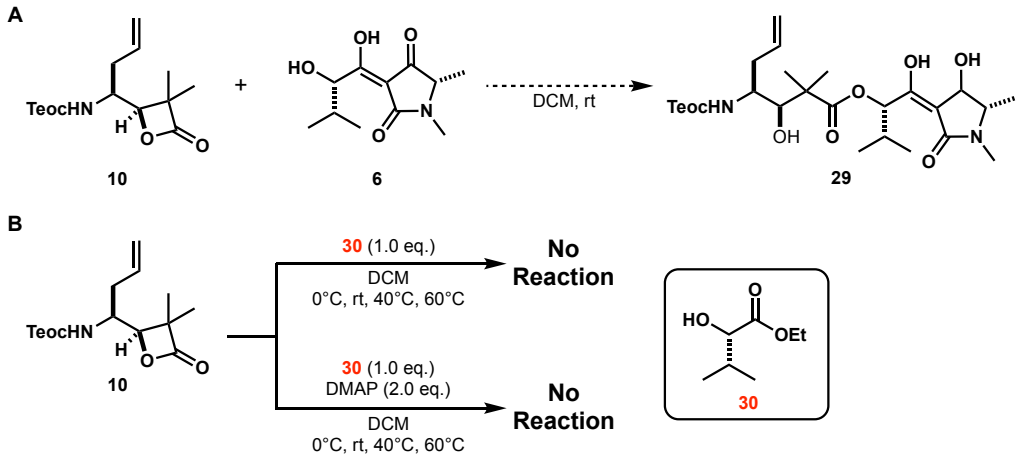

Scheme 3.4.10 Plans and model system for the coupling of the central and C-terminal fragments of JBIR-141. (**A**) Planned approach for the formation of ester linkage between the central and C-terminal fragments of JBIR-141. **(B)** Model system used to explore the formation of the aforementioned ester linkage.

Speculating this lack of reactivity to be the result of steric interference, created by the neopentyl center adjacent to the ester carbonyl of **10** as well as the isopropyl group of **30**, we decided to explore the hydrolysis of β-lactone **10**. We believed that the resulting carboxylic acid product (**31**, **Scheme 3.4.11A**) would be more electrophilic than the β-lactone, particularly after activation with traditional coupling reagents (e.g EDC, HBTU, HATU, etc.). Frustratingly, attempts to hydrolyze the β-lactone of **10** using LiOH, NaOH and KOH at temperatures ranging from 0°C to 60°C yielded mixtures of unreacted starting material and the product resulting from Teoc deprotection (**Scheme 3.4.11B**). Similar results were obtained when hydrolysis was attempted using H_2O_2 and LiOH, conditions shown to be effective for the hydrolysis of sterically hindered amide bonds.[80] Suspecting that carboxylic acid **31** is prone reclosure upon hydrolysis due to the Thorpe–Ingold effect[81,82], we decided to test this hypothesis by attempting ring opening with $NaBH_4$ as the resulting aldehyde could not reclose to the β-lactone. To our surprise, treatment of **10** with 1.1 eq. of $NaBH_4$ yielded no reaction. In an ambitious endeavor to both hydrolyze the β-lactone ring and install the acylated secondary alcohol of the central fragment, acidic ring opening was attempted using sodium acetate (NaOAc) in boiling acetic acid (AcOH). Mass analysis of crude product isolated from this reaction showed it to contain a major mass consistent with that of γ-lactam **33**, the product resulting from internal lactamization of Teoc deprotected **31**.

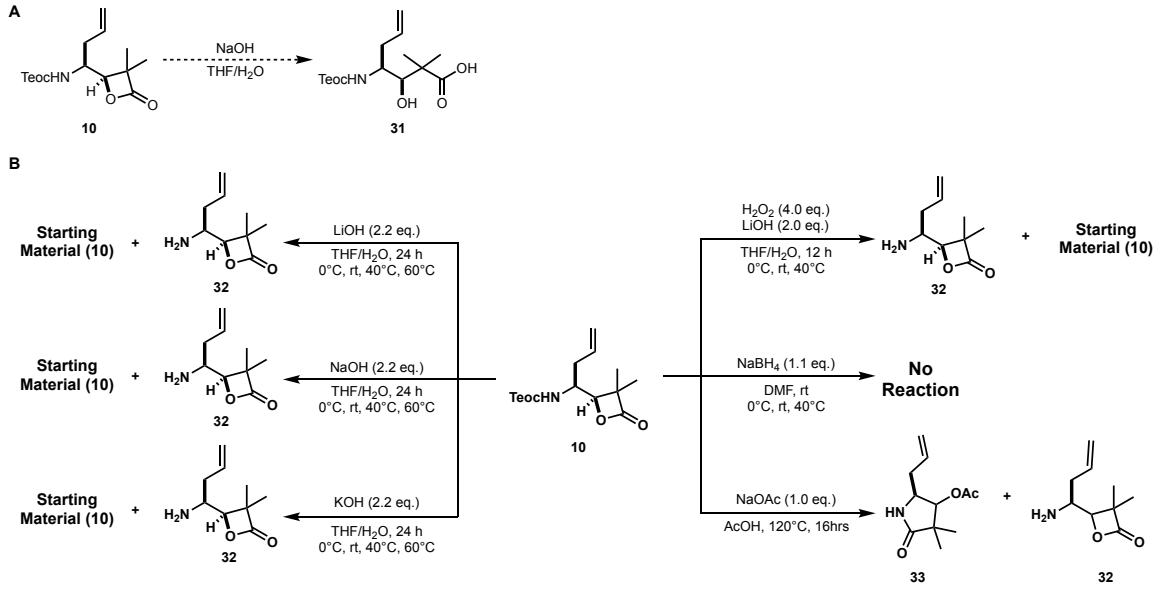

Scheme 3.4.11 Opening of central fragment **10**'s β-lactone via hydrolysis. (**A**) Envisioned hydrolysis of β-lactone **10** to yield desired carboxylic acid **31**. (**B**) Exploration of the hydrolysis of β-lactone **10** under both basic and acidic conditions.

Disheartened by our inability to open the β-lactone of **10** without deprotection of the amine, we decided to alter our approach towards the central fragment in pursuit of one more akin to carboxylic acid **31**. While we deemed this strategy to be the most straightforward, we did anticipate some difficulties in coupling to the carboxylic acid due to the presence of the adjacent neopentyl center. These concerns were underscored by the fact that Schobert and coworkers chose to omit this neopentyl-containing portion in their synthesis of JBIR-141 analog **4** (**Figure 3.2.1**).[39]

Further planning led us to conclude that structure **34** (**Figure 3.4.2**) would serve as the optimal central fragment for construction of the desired natural product. This fragment differs from previously envisioned **31** in two significant aspects. To prevent internal lactamization when coupling to the C-terminal fragment, we decided to protect the vicinal hydroxy carbamate of **31** as an oxazolidine. In addition, the amino protecting group was switched from Teoc to Boc as the latter enables simultaneous deprotection of both protecting groups under acidic conditions.

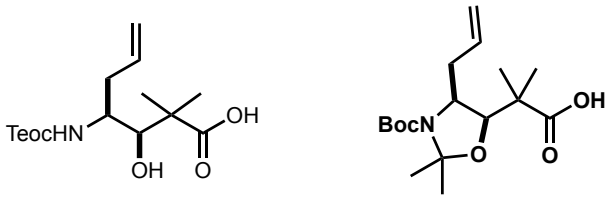

31 34

Figure 3.4.2 New target for the central fragment to be used towards the synthesis of JBIR-141(**1**).

The synthesis of central fragment **34** began with the conversion of Boc-L-allylglycine, purchased as the dicyclohexylammonium salt, into its corresponding Boc-protected α-amino aldehyde (**36**, **Scheme 3.4.12**). This commenced via methyl esterification, carried out using methyl iodide (MeI) and potassium carbonate (K_2CO_3), followed by reduction of the resulting crude methyl ester (**35**) with DIBAL-H. From **36**, BF_3 mediated Mukaiyama aldol addition of trimethylsilylketene[83], derived from methyl isobutyrate, yielded β-hydroxy ester **37** in good yield (72%) with high diastereoselectivity (10:1). The observed diastereoselectivity of this reaction is consistent with an open transition state and nucleophilic attack of the aldehyde rotamer having the carbamate substituent perpendicular to the carbonyl group (i.e Felkin geometry).[84]

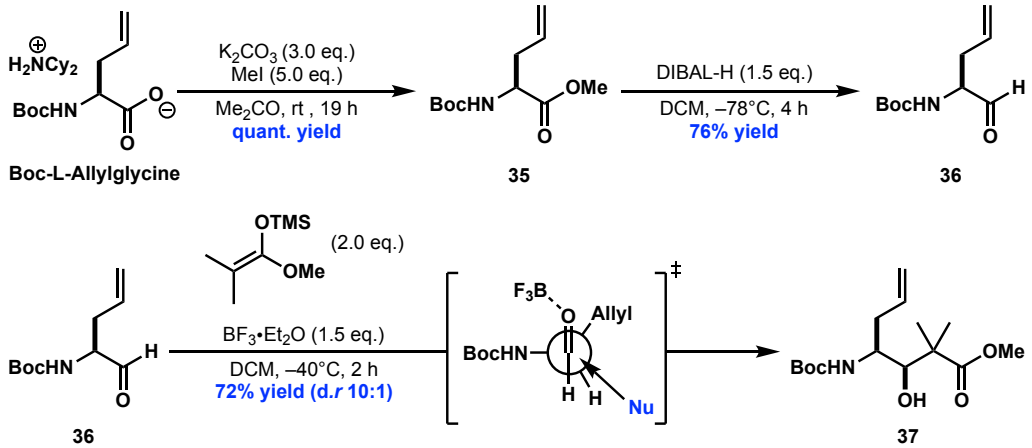

Boc-L-Allylglycine 35 36

36 37

Scheme 3.4.12 Synthesis of central fragment intermediate β-hydroxy ester **37** from Boc-L-allylglycine.

Installation of the central fragments oxazolidine component, the protection scheme selected to prevent internal lactamization during activation of **34** when coupling to **6**, was accomplished using 2,2-dimethoxypropane in the presence of catalytic p-toluenesulfonic acid (pTsOH) (**Scheme 3.4.13**). Best yields for this reaction were obtained when a drying agent (Na_2SO_4) was added to the reaction mixture. Finally, saponification of oxazolidine **38** yielded desired central fragment **34** in quantitative yield.

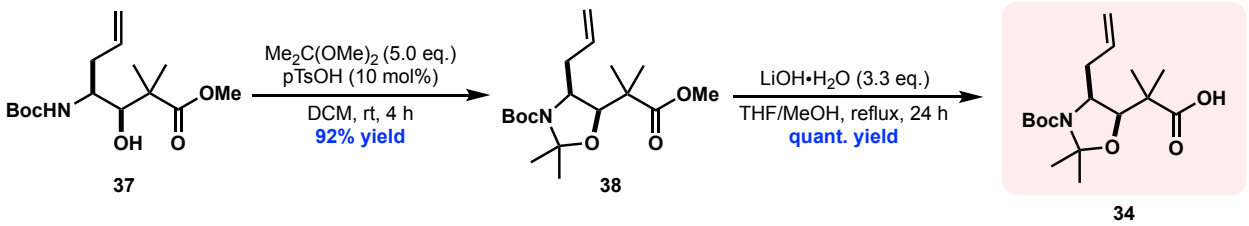

Scheme 3.4.13 Completion of the synthesis of central fragment **34.**

3.4.3 Synthetic Studies Towards C-Terminal C3-Acylated Tetramic Acid 6

Among the three fragments selected to construct the backbone of JBIR-141, we anticipated the synthesis of C-terminal C3-acylated tetramic acid **6** would present the greatest challenge. Retorosynthetically, we envisioned that this fragment would be formed via the C3-acylation of tetramic acid **39** with a protected form of (S)-α-hydroxy isovaleric acid (**40**, **Scheme 3.4.14**). For the latter of these components, we opted for a benzyl protecting group due to its straightforward removal via hydrogenolysis.

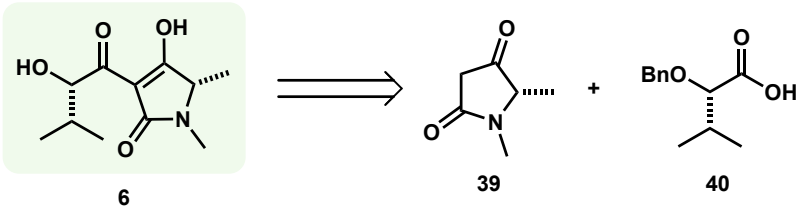

Scheme 3.4.14 Retrosynthetic analysis of C-terminal C3-acylated tetramic acid **6**.

Initially, we envisioned construction of tetramic acid **39** would be accomplished using an adapted protocol develop by Jouin and coworkers.[85] This protocol was made to proceed via the condensation of Boc-N-methyl-L-alanine with commercial Meldrum's acid (**41, Scheme 3.4.15**). Exposing the product of this reaction (**42**) to dry HCl in dioxane would cleave its tert-butyl carbamate (Boc) protecting group with mild thermolysis of the resultant amine hydrochloride salt expected to initiate lactam formation via ensuing loss of acetone followed by in-situ decarboxylation, resulting in tetramic acid **39**. Unfortunately, we found that this methodology was not efficient using systems containing N-methylated amino acids. This led us to explore a number of alternative potential routes which eventually led to the successful synthesis of **39** utilizing a strategy centering around Dieckmann cyclization.

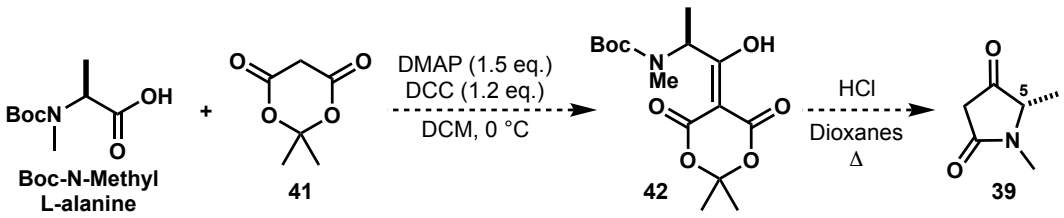

Scheme 3.4.15 Initially envision route to tetramic acid **39** utilizing methodology develop by Jouin et al.

Our first developed route to tetramic acid **39** commenced with the ethyl esterification of N-methyl-L-alanine[86], resulting in the quantitative isolation of **43** which was carried forward without purification (**Scheme 3.4.16A**). Subsequent N-acylation of **43** with acetyl chloride yielded **44**, which was isolated in 92% yield via vacuum distillation. A thorough screening of bases and additives revealed that a combination of KHMDS and 18-crown-6-ether provided the highest yields of tetramic acid **39** via Dieckmann cyclization (**Scheme 3.4.15B**). Although purification of **39** via flash column chromatography was effective, it was found that acid/base extraction could be employed as an alternative albeit with some loss of material (88% recovery).

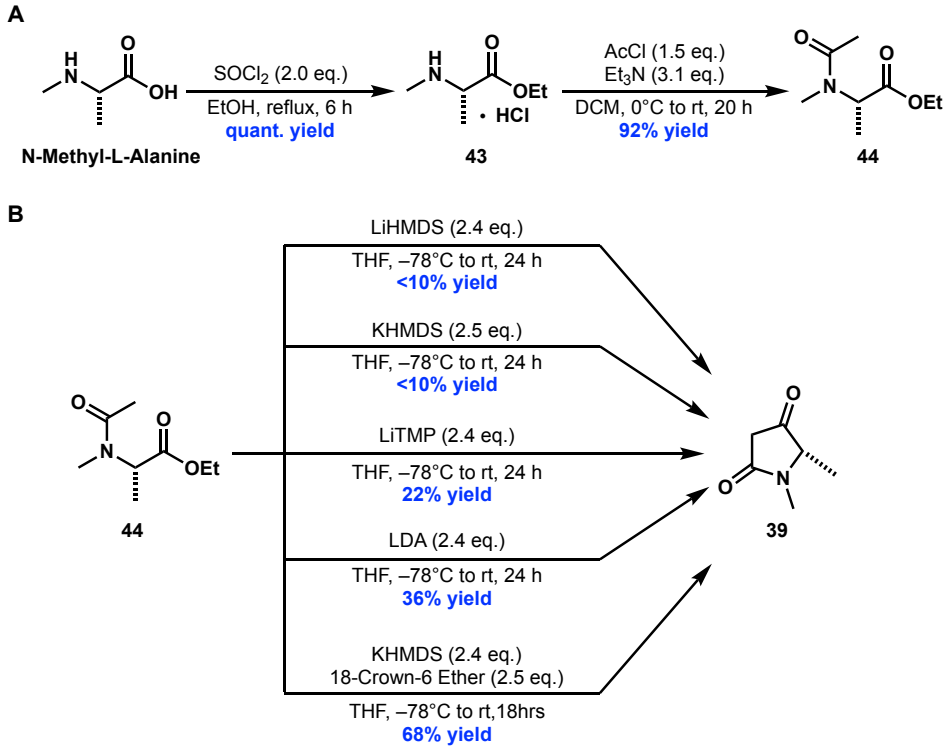

Scheme 3.4.16 Our first developed route to tetramic acid **39**. (**A**) Synthesis of **44** from N-methyl-L-alanine. (**B**) Screened conditions for the Dieckmann cyclization of **44**.

Shortly after establishing this route to **39**, we discovered an optimized protocol for the synthesis of C5-substituted chiral tetramic acids which appeared to have several advantages over our initial route (outlined above). This procedure, developed by Wood and coworkers[87]at Baylor University, exhibited high yields, great scalability as well as close to no epimerization at the chiral center adjacent to the nitrogen. Utilization of this route towards **39** began with the methyl esterification of N-methyl-L-alanine[88], the crude product of which was acylated with methyl malonyl chloride (**45**). The resultant crude amidyl diester (**46**) was subsequently treated with a slight excess of freshly prepared sodium methoxide (NaOMe) which resulted in the formation of **47** via Dieckmann cyclization. For this step, Wood and coworkers stress the importance of running this reaction at low temperatures for short durations of time, as failing to do so often results in

significant epimerization of the tetramic acid C5 center. Heating of **47**, which if needed can be efficiently purified via acid/base extraction, with slightly less than one equivalent of water efficiently initiated decarboxylation, resulting in the isolation of optically active tetramic acid **39** which did not necessitate further purification after workup. One of the things which attracted us to this approach is its ability to provide facile access to various analogs of **39** such as its non-methylated congener as well as higher alkyl homologs.[89]

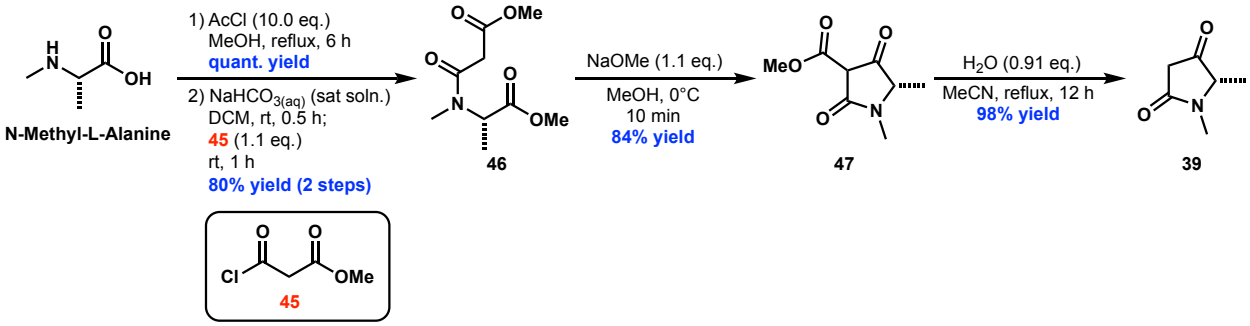

Scheme 3.4.17 Improved synthesis of tetramic acid **39** utilizing a protocol develop by Wood et al.

The preparation of benzyl-protected (S)-α-hydroxy isovaleric acid (**40**) began with the methyl esterification of (S)-α-hydroxy isovaleric acid (**48**) using catalytic sulfuric acid in boiling methanol (**Scheme 3.4.18)**. While commercially available, (S)-α-hydroxy isovaleric acid can be readily prepared from L-valine in high yield via a Sandmeyer reaction using established conditions as a cheaper alternative.[90] It should be noted that the product of this methyl esterification (**49**) was found to be quite volatile. For this reason, the crude product of this reaction was not put under powerful vacuum and evaporation of the reaction solvent was done at room temperature. Benzyl protection of the α-hydroxyl group was accomplished using benzyl 2,2,2-trichloroacetimidate[91] (**50**), prepared in a single step from benzyl alcohol and trichloroacetonitrile using procedures outlined by Yamada et al[92], and catalytic trifluoromethanesulfonic acid (i.e triflic acid). The resultant purified product (**51**) was then subjected to saponification conditions leading to the

isolation of desired **40**. While the product of this reaction was most often spectroscopically pure via ^{1}H-NMR analysis, it was found that isolated **40** can be further purified via acid/base extraction if desired.

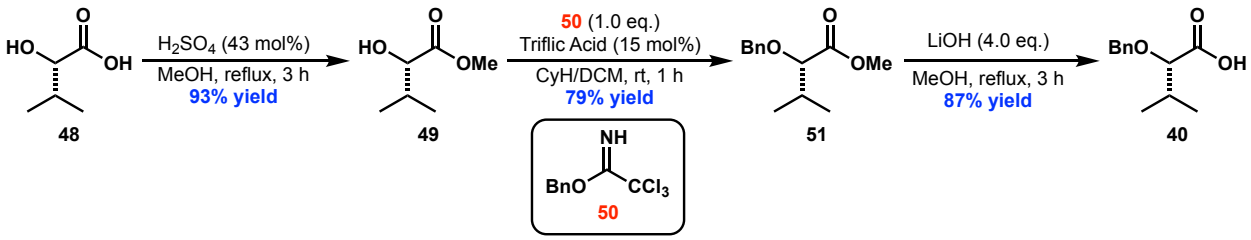

Scheme 3.4.18 Synthesis of benzyl-protected (S)-α-hydroxyisovaleric acid **40**.

With both tetramic acid **39** and acylation partner **40** in hand, final steps towards the synthesis of C3-acyalted tetramic acid **6** began. While several methodologies have been outlined for the direct C3-acylation of unsubstituted tetramic acids, such reactions usually require harsh conditions which we felt would likely epimerize the tetramic acid C5 center. For this reason, we chose to pursue an alternative strategy by which the C3-acyaltion is accomplished via O- acylation followed by O- to C- acyl transfer. This strategy, originally outlined by Yoshii and coworkers[93] in the late 1980's, was later modified by Yoda et al.[94,95] who noted that the addition of super-stoichiometric $CaCl_2$ was found to suppress tetramic acid epimerization and enhance product formation when using branched carboxylic acid derivatives (such as **40)**. Furthermore, he found that the use of 4-dimethylaminopyridine (DMAP) as a catalyst shortened reaction times and increased yields. While Yoda provided no precise explanation for the role $CaCl_2$ plays in this transfer process, we speculate that Lewis acidic $CaCl_2$ likely accelerates DMAP addition to the enol ester carbonyl to give an intermediate pyridinium ion pair that collapses to form a thermodynamically more stable carbon-carbon bond.

Towards the utilization of this outlined strategy, O-acylation of tetramic acid **39** with **40** was first accomplished using DCC in the present of base, resulting in the in-situ generation of **52** (**Scheme 3.4.19**). To our frustration, O- to C- acyl transfer conditions outlined by Yoda et al. failed to yield **53** in appreciable quantities (**Table 3.4.1** entry 1). In addition, attempts to optimize both the formation of intermediate **52** as well as the efficiency of the O- to C- acyl transfer were met with limited success (**Table 3.4.1** entries 2–7). Inspired by recent work published by Li and coworkers in their total synthesis of the natural product Kibdelomycin[96], we decided to explore the use of cyanide as a potential O- to C- acyl transfer promoter. After several rounds of optimization (entries 8–11), highest yields of **53** were isolated using 35 mol% of potassium cyanide (KCN) at rt for 48 h (entry 12).

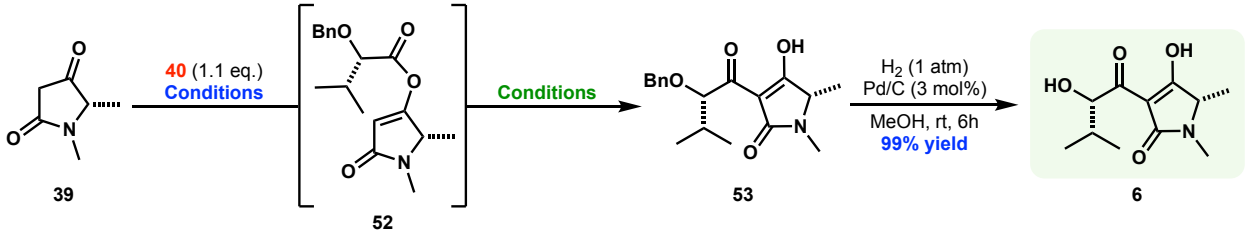

Scheme 3.4.19 Final steps towards the synthesis of C3-acyated tetramic acid **6**.

	O-Acylation Conditions					O- to C- Acyl Transfer Conditions				
entry	Coupling Reagent	Base	Solvent	Temp.(°C)	Time (h)	Base	Additives	Temp. (°C)	Time (h)	Yield of **53**
1	DCC (1.2 eq.)	DMAP (0.2 eq.)	DCM	0°C to rt	6 h	Et_3N (1.3 eq.)	$CaCl_2$ (1.5 eq.)/DMAP (0.1 eq.)	rt	44 h	14%
2	DCC (1.2 eq.)	DMAP (0.3 eq.)	DCM	0°C to rt	5 h	Et_3N (1.3 eq.)	$CaCl_2$ (1.5 eq.)/DMAP (0.2 eq.)	rt	36 h	17%
3	DCC (1.2 eq.)	DMAP (0.3 eq.)	DCM	0°C to rt	5 h	Et_3N (1.3 eq.)	$CaCl_2$ (1.5 eq.)/ DMAP (0.3 eq.)	rt	24 h	26%
4	DCC (1.2 eq.)	DMAP (0.3 eq.)	DCM	0°C to rt	5 h	Et_3N (1.5 eq.)	$CaCl_2$ (1.5 eq.)/DMAP (0.3 eq.)	30°C	8 h	12%
5	DCC (1.2 eq.)	DMAP (0.3 eq.)	DCM	0°C to rt	5 h	Et_3N (1.5 eq.)	$CaCl_2$ (1.5 eq.)/DMAP (0.3 eq.)	40°C	6 h	10%
6	DCC (1.2 eq.)	DMAP (0.3 eq.)	DCM	0°C to rt	5 h	Et_3N (1.5 eq.)	$CaCl_2$ (1.5 eq.)/DMAP (0.3 eq.)	50°C	6 h	<5%
7	HATU (1.2 eq.)	DMAP (0.3 eq.)	DCM	0°C to rt	9 h	Et_3N (1.5 eq.)	$CaCl_2$ (1.5 eq.)/DMAP (0.3 eq.)	rt	24 h	28%
8	HATU (1.2 eq.)	DMAP (0.3 eq.)	DCM	0°C to rt	9 h	Et_3N (1.5 eq.)	KCN (0.10 eq.)	rt	24 h	36%
9	HATU (1.2 eq.)	DMAP (0.3 eq.)	DCE	0°C to rt	7 h	Et_3N (1.5 eq.)	KCN (0.15 eq.)	rt	24 h	44%
10	HATU (1.2 eq.)	DMAP (0.3 eq.)	DCE	0°C to rt	7 h	Et_3N (1.5 eq.)	KCN (0.25 eq.)	rt	24 h	47%
11	HATU (1.2 eq.)	DMAP (0.3 eq.)	DCE	0°C to rt	7 h	Et_3N (1.5 eq.)	KCN (0.35 eq.)	rt	24 h	51%
12	HATU (1.2 eq.)	DMAP (0.3 eq.)	DCE	0°C to rt	7 h	Et_3N (1.5 eq.)	KCN (0.35 eq.)	rt	48 h	67%

Table 3.4.1 Attempts at optimization of O- to C- acyl transfer towards the synthesis of **53**.

From **53**, debenzylation using typical hydrogenolysis conditions (Pd/C under H_2) afforded desired C3-acyalted tetramic acid **6**. While this route allows for facile analog synthesis via the utilization of numerous lactic acid variant (i.e analogs of **40**) as a means to vary the isopropyl unit, we were continually frustrated by our inability to definitively characterize as well as efficiently purify both **53** and **6**. While these difficulties in characterization stem from the known propensity of C3-acylated tetramic acids to exist in a variety of tautomeric states[87,97-98] (**Figure 3.4.3A**), difficulties in their purification is ascribed to their known ability to bind metals from diverse sources, such as drying agents (e.g Na_2SO_4 and $MgSO_4$) as well as silica gel, in a manner akin to acetylacetonate ligands (**Figure 3.4.3B**).[87,99-100] Recognizing that these inherent properties would present significant challenges when it came to the characterization and purification of subsequent compounds, we decided to reconsider our approach towards construction of the backbone of JBIR-141.

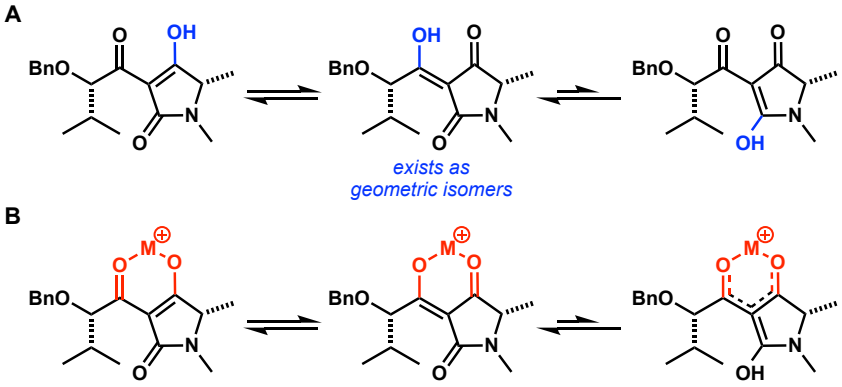

Figure 3.4.3 Difficulties encountered due to the presence of the C3-acylated tetramic acid moiety. (**A**) Depiction of multiple potential tautomers of **6** which causes difficulties in definitive characterization. (**B**) Depiction of the ability of **6** to bind metals akin to acetylacetonate (acac) ligands.

As shown in **Scheme 3.4.20A**, our initial plan was to construct the backbone of the natural product with the tetramic acid functionality present prior to fragment coupling and installation of the N-nitrosohydroxylamine. In light of these recent findings however, we instead opted to

construct the backbone of the natural product using β-ketoamide acyl tetramate linear precursor **6'**, which would be used to form the tetramic acid functionality via Dieckmann cyclization after installation of the N-nitrosohydroxylamine amine (**Scheme 3.4.20B**). We reasoned that while **6'** could still exist in a variety of different tautomeric states, it would be significantly easier to purify than the corresponding C3-acyalted tetramic acids.

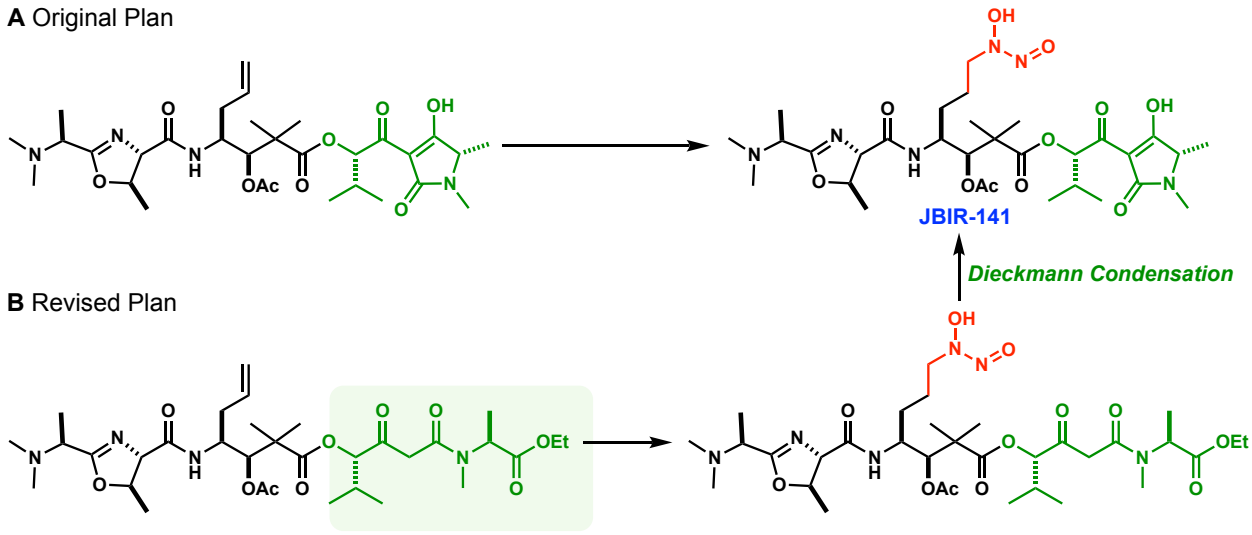

Scheme 3.4.20 Envisioned routes towards the completion of JBIR-141. (**A**) Originally planned route to JBIR-141 with tetramic acid present before installation of the N-nitrosohydroxylamine. (**B**) Revised plan to JBIR-141with with tetramic acid formation after installation of the N-nitrosohydroxylamine.

Confident in this new plan, the synthesis of β-ketoamide acyl tetramate linear precursor **6'** began with the condensation of known **40** with Meldrum's acid (**41**) using EDC and DMAP (**Scheme 3.4.21**). Because the isolated product from this reaction (**54**) was found to be unstable towards purification via flash column chromatography, it was carried directly forward to the next reaction without any further purification besides conventional aqueous workup. **54** was then converted, in a single step, to β-ketoamide **56** via exposure to an amino acid nucleophile and base in boiling toluene. This reaction, inspired by the process route towards Sitagliptin[101], a drug developed by Merck & Co. Inc. for the treatment of type II diabetes, proceeds via the thermal

decomposition of the Meldrum's acid portion of the molecule, which, after releasing acetone and carbon dioxide (CO_2) results in the in-situ generation of acyl ketene intermediate **55**.[102] Nucleophilic attack of this intermediate by N-methyl-L-alanine methyl ester followed by tautomerization results in desired β-ketoamide **56**. To access **6'**, debenzylation of **54** was carried out using typical hydrogenolysis conditions (i.e Pd/C, H_2) which proceeded in high yield and did not require purification after isolation of the crude. With all of the fragments needed to assemble the backbone of JBIR-141 in hand, fragment assembly could finally begin.

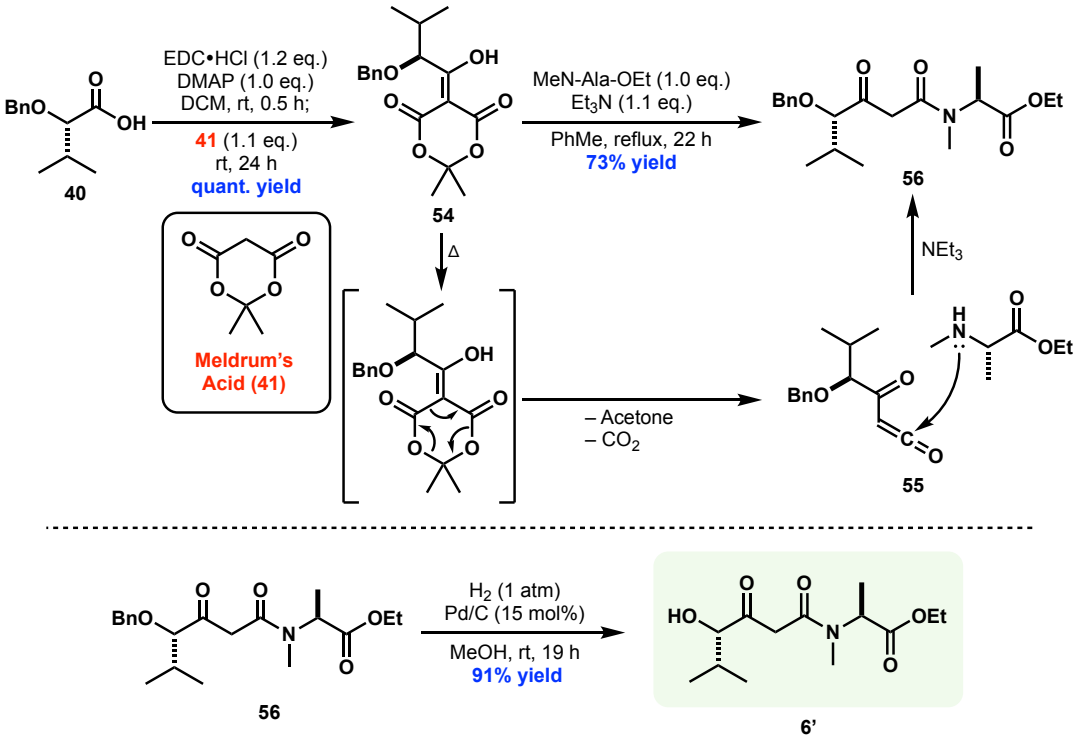

Scheme 3.4.21 Synthetic route towards β-ketoamide acyl tetramate linear precursor **6'**.

3.4.4 Synthetic Studies Towards Backbone Assembly of JBIR-141

With all of the fragments needed to assemble the core of JBIR-141 (**1**) in hand, backbone assembly commenced with the coupling of central fragment **34** and C-terminal fragment **6'** (**Scheme 3.4.22**). While traditional coupling reagents such as EDC, HBTU, and HATU failed to form the desired ester linkage, we discovered that 2-methyl-6-nitrobenzoic anhydride[103] (MNBA, i.e Shinna's reagent) was effective, yielding the desired product (**57**) in 58% yield. It should be noted that while ^{1}H-NMR characterization of this product was relatively challenging, due to the presence of equilibrating tautomers, both its characterization and purification were markedly easier than what was observed with previous C3-acylated tetramic acids. From this intermediate, concurrent Boc deprotection and oxazolidine removal were achieved by refluxing **57** in a 2:2:1 mixture of formic acid/H_2O/THF, leading to the isolation of **58** in nearly quantitative yield. While compound **58** represents the furthest intermediate we have achieved to date towards establishing the first total synthesis of JBIR-141 (**1**), we are optimistic in our ability to complete the synthesis in the near future.

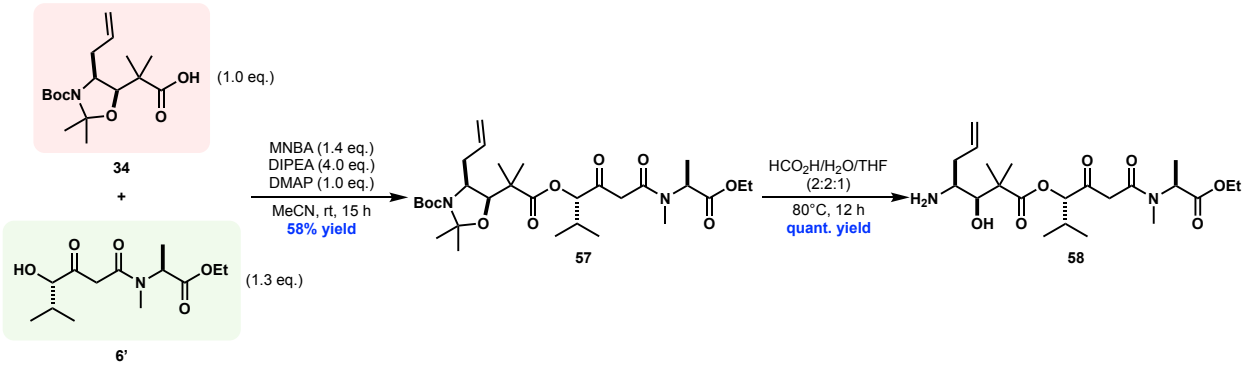

Scheme 3.4.22 Progress towards backbone assembly towards JBIR-141 (**1**).

3.5 Plans Towards the Completion of JBIR-141

Scheme 3.5.1 below shows our envisioned plan towards completing the first total synthesis of JBIR-141 (**1**). This plan begins with the coupling of N-terminal fragment **9** with **58** (our furthest intermediate to date) to establish the backbone of the natural product. While we show the use of TBTU-mediated amidation as the expected method for this purpose, many alternative coupling reagents exist and will be explored. From **59**, we expect acylation of the central fragment's secondary alcohol to be relatively straightforward with the upcoming installation of the N-nitrosohydroxylamine being our greatest challenge.

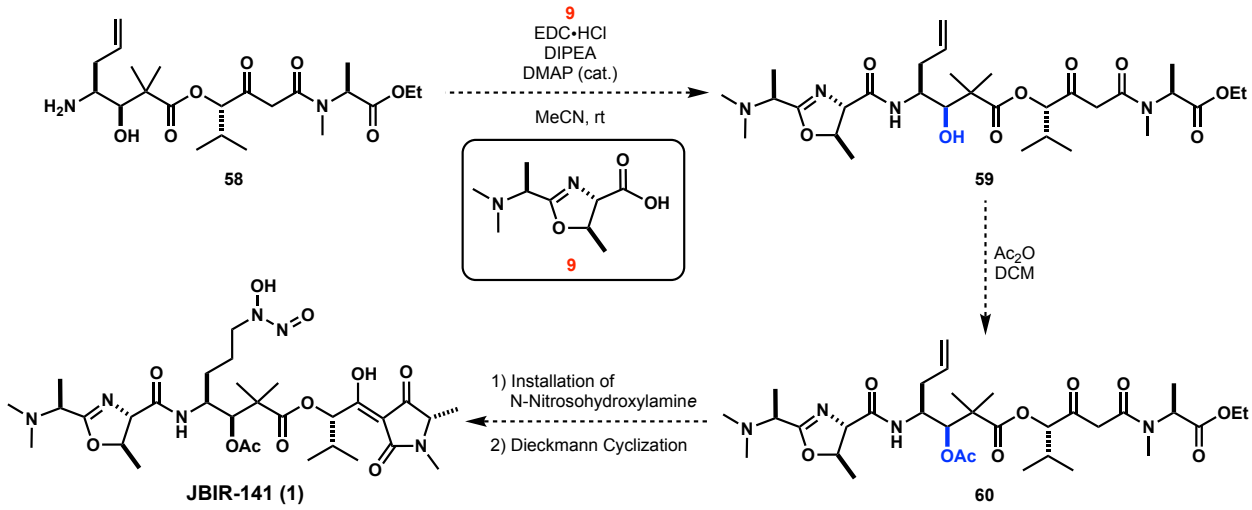

Scheme 3.5.1 Our envisioned plan towards completing the first total synthesis of JBIR-141 (**1**).

Literature on the synthesis of N-nitrosohydroxylamines suggests nitrosoylating a hydroxylamine to be the most effective and straight forward path to this functionality. **Scheme 3.5.2** below shows two proposed routes for conversion of the allyl functional handle in **60** to the requisite hydroxylamine. The first of these pathways (shown on right) uses a nitrite Co-catalyzed Tsuji-Wacker oxidation, originally developed by Grubbs, to convert **60** to aldehyde **61**.[104,105] This aldehyde could then be condensed with H_2NOH and the resultant oxime reduced with $NaCNBH_3$,

under acidic conditions, to yield a hydroxylamine.[106] Subsequent exposure of the resultant product to *t*-butyl nitrite should generate the desired N-nitrosohydroxylamine.[107] While this is currently our favored plan, we do have concerns that the oxazoline ring in **61** may not survive oxime reduction conditions. For this reason, we propose an alternative route (shown on left). This alternative route begins with the conversion of alkene **60** to its corresponding primary iodide via Brown's hydroboration / iodination sequence.[108] Subsequent treatment with $NaNO_2$ should give nitroalkane **62**, from which, the hydroxylamine could derive from partial reduction using Zn(0).[109-111] As postulated previously, treatment of the resulting hydroxylamine with *t*-butyl nitrite should generate the desired N-nitrosohydroxylamine.[107]

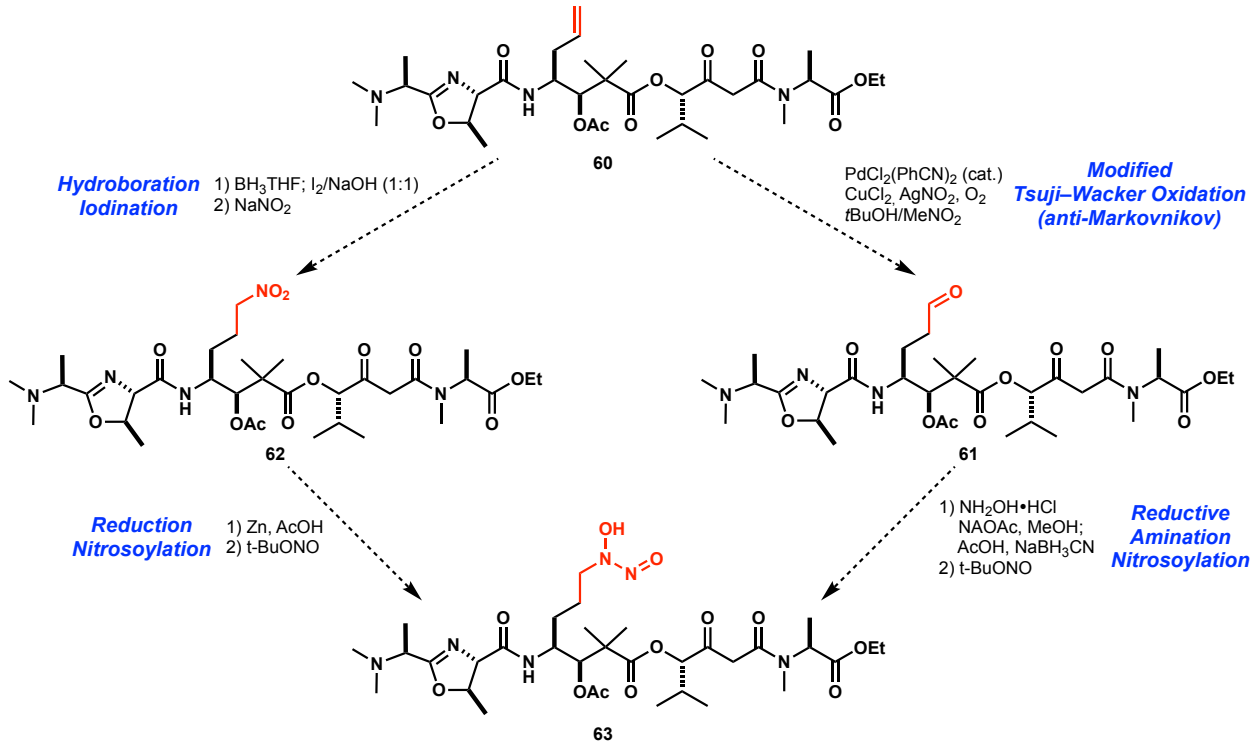

Scheme 3.5.2 Two proposed routes for installation of the N-nitrosohydroxylamine motif.

With the key N-nitrosohydroxylamine functionality of the natural product installed, we plan to access JBIR-141 (**1**) via Dieckmann cyclization of the C-terminal acyl tetramate linear precursor (**Scheme 3.5.3**) . To affect this reaction, multiple options exist but we postulate the use

of TBAF/THF to be the most appropriate as it should not interfere with any of the other existing functionalities.[112] By executing the synthetic route proposed herein, the first laboratory synthesis of JBIR-141 (**1**) will be completed in 13/14 steps as the longest linear sequence depending on pathway utilized for installation of the N-nitrosohydroxylamine.

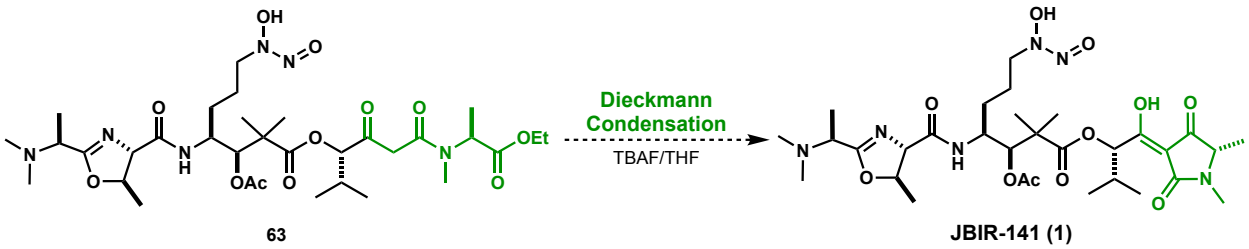

Scheme 3.5.3 Tetramic acid formation via Dieckmann cyclization affording JBIR-141 (**1**).

3.6 Proposed Analog Synthesis for Structure-Activity Relationship Studies

With a synthetic route to JBIR-141 (**1**) established, our next step will be to utilize said route to synthesize structural analogs which will be used to help us address numerous questions we have concerning both the structure of the natural product as well as its mechanism of action as an inhibitor of FoxO3a transcriptional activity. These questions include: Is the N-terminal threonine derived oxazoline segment stable at/below pH 7.4? Would an oxazole or thiazole, both common in natural products, be a more stable and tolerated surrogate? Is the acetate group of the central fragment esterase sensitive? Is the N-nitrosohydroxylamine functionality a source of nitric oxide in biological settings? If so, is controlled NO release responsible, in part or in full, for its effects on FoxO3a transcriptional activity? Is the C-terminal acyl tetramate configurationally stable? Do segments of JBIR-141 internally cooperate to bind metals? If so, which ones and with what affinity? How does the positioning of peripheral functionality relative to main chain elements effect its biological activity? And finally, what is the active pharmacophore of JBIR-141 (**1**) and

how can we increase its potency as a FoxO3a inhibitor. Addressing these questions will enhance our understanding of JBIR-141 (**1**) as well as its potential applications.

Towards the design and synthesis of structural analogs, we will begin by generating a focused library of truncation variants in hopes of identifying segments of the natural product that can be simplified or eliminated while retaining its biological functions. **Figure 3.6.1** below outlines five initial targets towards this effort. Hydrogenation of **60** followed by Dieckmann cyclization will afford **64** wherein the effect of eliminating the N-nitrosohydroxylamine will be ascertained. Likewise, the effect of eliminating the C-terminate tetramate will be examined using structure **65**. This molecule will be prepared by esterifying **34** with isobutanol (instead of coupling with **6'**) and then carrying that product through the remaining steps of our proposed route. By directly coupling **9** with **6**, we will generate compound **66**, wherein the entire central fragment is missing. Lastly, vicinal amino alcohol **58** will be coupled to butyric acid and N,N-dimethyl-L-alanine. Those two products will be advanced to structures **67** and **68**, respectively, via continuation of our proposed route. Relative to **1**, **68** has the methyloxazoline ring excised yet retains a basic N-terminus whereas **67** has both the heterocycle as well as its basic appendage removed.

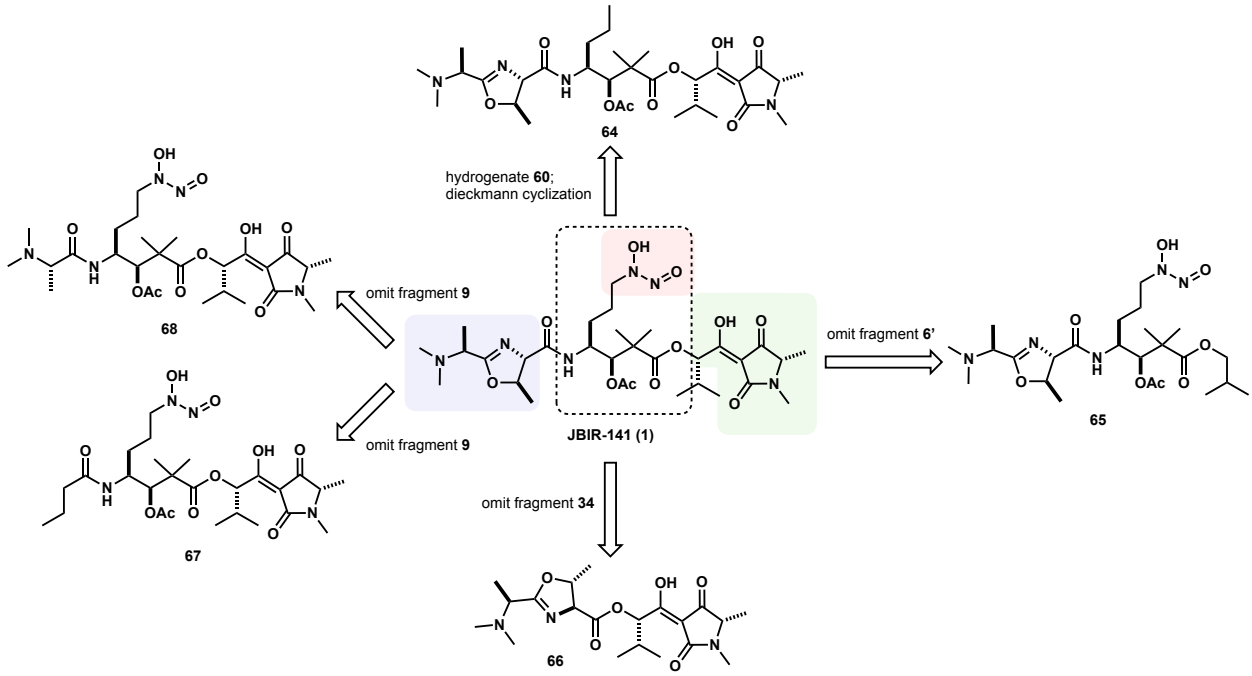

Figure 3.6.1 Proposed truncation analogs of JBIR-141 (**1**) for structure-activity relationship studies.

Screening compounds **64**–**68** for cellular cytotoxicity and examining their effects on FoxO3a mediated transcription will give us key information on which motifs / functional groups (if any) in **1** can be eliminated. This will focus and accelerate subsequent analog syntheses. In addition to this proposed set of truncation analogs, we plan to analog each domain of the structure. Most pressing is determining the role of the N-nitrosohydroxylamine. Acting in concert with both the amino oxazoline and acyl tetramate motifs, the N-nitrosohydroxylamine may allow JBIR-141 (**1**) to function as a zinc or iron siderophore for its producing organism. Despite this, zinc or iron sequestration is likely not responsible for its effects on FoxO3a transcriptional activity as Nurse and coworkers point out that the high cellular potency of the JBIR-141 Zn complex (EC_{50} 10-200 nM) makes it unlikely that the molecule perturbs intracellular zinc concentrations significantly.[23] Instead, they hypothesize the zinc complex has a defined receptor.

To investigate the impact modifications to the N-nitrosohydroxylamine functionality will

have on JBIR-141's biological activity, analogs having the N-nitrosohydroxylamine replaced with a hydroxamic acid and an alkyl imidazole will be prepared from aldehyde **61** (via oxidation / hydroxylamine coupling or tosylmethylisocyanide / Schiff base cycloaddition, respectively) (**Figure 3.6.2**) . There is also potential for JBIR-141 to release nitric oxide (NO). NO signaling has been correlated with inhibited FoxO3a activity.[33] While N-nitrosohydroxylamines are not typically used as NO donors[34], their conjugate bases do release NO upon one electron enzymatic oxidation.[35] We will test if JBIR-141 has this activity and whether N-alkoxy nitrosamine variants of **1** do as well. The latter compounds should be less susceptible to oxidation and thus poorer NO donors. Similar perturbations will be made to structures like **70**, wherein the alkyl chain displaying the N-nitrosohydroxylamine has been replaced by a phenyl group, rigidifying the system, and likely lowering its pKa. Lastly, JBIR-141 is possibly a pro-drug, wherein its acetate group is cleaved by esterase activity upon entry into the cell, revealing an amido ethanol motif reminiscent of transition state isosteres used for protease inhibition.[36] Elaborating from **59**, analogs of JBIR-141 having esterase stable functional groups (e.g carbonate and urethane) in place of the acetate will be synthesized and their activities tested. Kawahara has reported the threonine form of JBIR-141 (**3**, **Figure 3.1.2**) was devoid of activity.[17] We will synthesize planar oxazole and thiazole congeners of **1** (i.e **71**) anticipating greater hydrolytic stability and, if activity is retained, better pharmacological performance. Lastly, regarding the C-terminus, we note that by using achiral or symmetric variants of **39** (i.e **72** and **73**) in the synthesis of analogs of **6**, we can streamline the overall route and further improve scalability. These analogs, as well as ones resultant from further design and exploration, will prove to be instrumental towards establishing structure-activity relationships of JBIR-141.

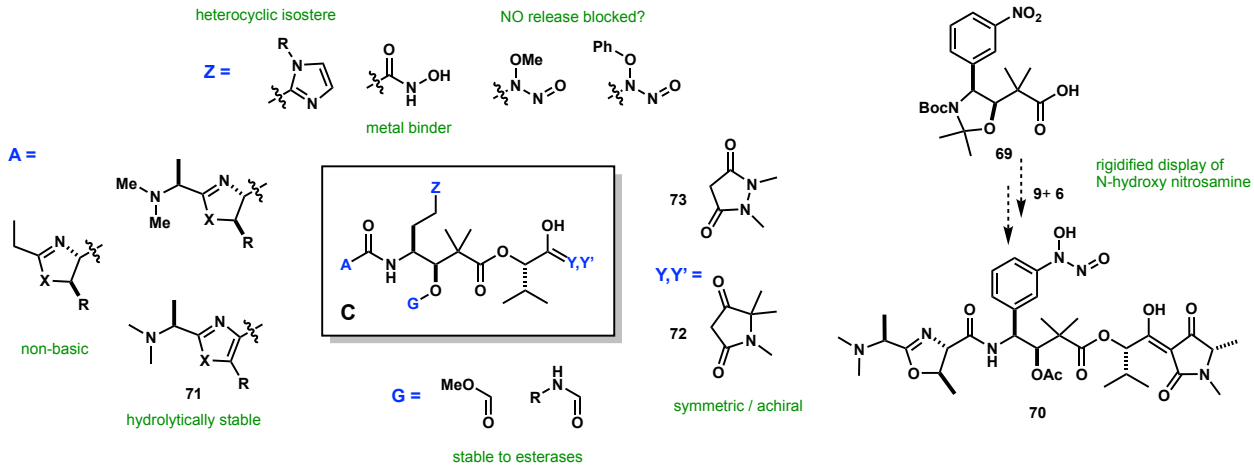

Figure 3.6.2 Proposed functional group analogs of JBIR-141 (**1**) for structure-activity relationship studies.

3.7 Conclusion

JBIR-141, a recently isolated peptidomimetic natural product, shows impressive cytotoxicity towards SKOV-3, MESO-1 and Jurkat cancer cell lines in vitro as well as a potent inhibition of FoxO3a transcriptional activity. The transcription factor FoxO3a has been shown to confer drug resistance and promote the metastasis and growth of leukemia initiating cells and drug resistant stem cells which are responsible for the downstream development of diseases such as chronic myeloid leukemia. For this reason, inhibitors of FoxO3a transcriptional activity are well poised to become a new type of targeted cancer therapeutic. To date, no synthesis of JBIR-141 has been reported and its mechanism of action as an inhibitor of FoxO3a transcriptional activity is unknown.

Selective and potent small molecule inhibitors of gene expression attributed to individual transcription factors are rare, making JBIR-141 a highly valuable synthetic target. Outlined in this chapter is our progress towards and proposed completion of the natural product JBIR-141 (**1**). This route is both efficient and highly modular, making it conducive to the facile design and synthesis

of a wide variety of structural analogs. These analogs will be used to probe structure-activity relationships which will be used to identify the active pharmacophore of the natural product. This will prove to be vital towards achieving our ultimate goal, maximizing its therapeutic potential as an inhibitor of FoxO3a transcriptional activity towards the development of a complimentary chemotherapeutic agent to be used to treat chromic myeloid leukemia.

3.8 Experimental Section

General Methods and Materials

Unless otherwise specified, reactions were performed in flame-dried glassware under an atmosphere of argon using anhydrous solvents. Reagents were purchased from commercial vendors and used as received unless otherwise stated. Tetrahydrofuran (THF), diethyl ether (Et_2O), acetonitrile (MeCN), dichloromethane (DCM), chloroform ($CHCl_3$) and toluene (PhMe) were passed through a Glass Contour solvent drying system. Methanol (MeOH) was distilled from $Mg(OMe)_2$, which was generated by refluxing methanol over magnesium turnings until all the turnings had converted into a white precipitate. The distilled MeOH was stored in a flame-dried flask over activated 3Å molecular sieves under argon. Anhydrous N,N dimethylformamide (DMF) was purchased from Supelco, Inc – Sigma Aldrich. Yields refer to chromatographically and spectroscopically (^{1}H-NMR) homogeneous materials, unless otherwise stated. Thin-layer chromatography (TLC) was conducted on precoated plates (Sorbent Technologies, silica gel 60 PF254, 0.25 mm) visualized with UV 254 nm. For acid-sensitive compounds, TLC plates were neutralized/deactivated with TEA/Hexane (1%) before use. Column chromatography was performed on silica gel 60 (SiliCycle, 240−400 mesh). Purification of compounds via preparative HPLC was performed using an Agilent 1200 HPLC system equipped with G1361A preparative pumps, a G1314A auto sampler, a G1314A VWD, a G1364B automated fraction collector, and a Waters Sunfire C18 column (5 μm, 19 mm × 250 mm), unless otherwise noted. 0.1% TFA in MeCN/H_2O solvent system. Analytical HPLC was performed using the same system, but with a G1312A binary pump. 0.1% TFA in MeCN/H_2O solvent system. Mass spectra were recorded using an Agilent 6130 LC/MS system equipped with an ESI source. High-resolution mass spectra were

recorded on Thermo Scientific Exactive® Mass Spectrometer with DART ID-CUBE Waters GST Premier, Waters LCT Premier, and Agilent 6545 LC-QTOF. NMR spectra were recorded on Bruker Avance spectrometers (400/100 MHz, 500/125 MHz, and 600/150 MHz). NMR spectra were recorded on Bruker Advance (300, 400, 500, or 600 MHz) spectrometers. HSQC, HMBC, and COSY NMR experiments were used to aid assignment of NMR peaks when required.

Experimental Procedures and Product Characterization

(S)-N,N-dimethyl-L-alanine (**11**)[55]

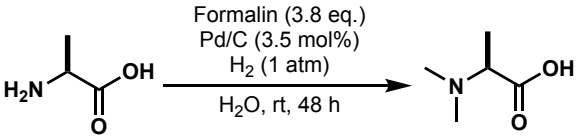

L-alanine **11**

To a 250 mL round-bottom flask (equipped with a stir bar) was added L-alanine (6.0 g, 67.3 mmol. 1.0 eq), a 37% aqueous solution of formaldehyde (20.8 mL, 255.9 mmol, 3.8 eq.) and water (127 mL) followed by Pd/C (10 wt. % Pd) (2.52 g, 2.4 mol, 3.5 mol%). Once done, the reaction flask was evacuated of air and backfilled with H_2 after which, the reaction mixture was left to stir at rt under an atmosphere of H_2 gas for 48 h. After this time, the reaction mixture was heated to reflux and left to stir for 0.5 h. Once done, the reaction vessel was purged with argon gas, and the hot reaction mixture filtered through a plug of Celite®. The isolated filtrate was then concentrated under reduced pressure and then repeatedly azeotroped with toluene (3x) to afford (*S*)-*N*,*N*-dimethyl-L-alanine (**11**) (7.8 g, 99% yield) as a white solid. All characterization data obtained for the isolated product was in accordance with literature reported data.[55]

L-*allo*-threonine methyl ester hydrochloride (**12**)[56]

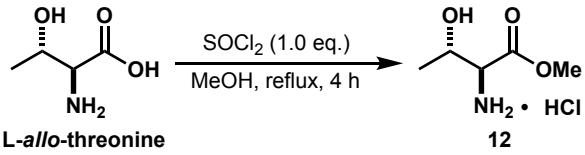

L-*allo*-threonine **12**

To a 250 mL round-bottom flash (equipped with a stir bar) containing MeOH (150 mL) at 0 °C was slowly added $SOCl_2$ (2.2 mL, 30.3 mmol, 1.0 eq.). After stirring for several minutes, L-*allo*-threonine (3.6 g, 30.2 mmol, 1.0 eq) was added to the acidic MeOH solution after which, the reaction mixture was heated to reflux and left to stir under an atmosphere of argon gas for 4 h. After this time, the reaction mixture was cooled to rt and then directly concentrated under reduced

pressure. The resulting solid was then stripped with Et_2O (2x) to afford L-*allo*-threonine methyl ester hydrochloride (**12**) (5.1 g, 100% yield) as a white solid. All characterization data obtained for the isolated product was in accordance with literature reported data.[56]

Methyl dimethyl-*L*-alanyl-*L*-allothreoninate (**15**)

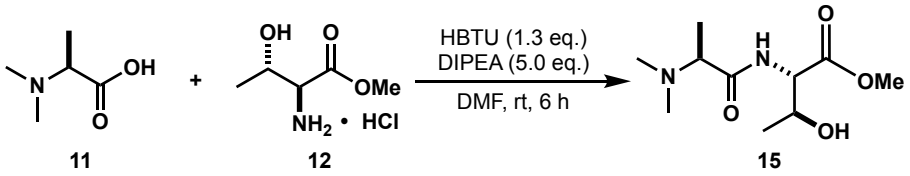

11 12 15

To a 25 mL round-bottom flask (equipped with a stir bar) was added N,N-dimethyl-L-alanine (300 mg, 2.6 mmol 1.0 eq.) and L-*allo*-threonine methyl ester hydrochloride (521 mg, 3.1 mmol, 1.2 eq.) followed by DMF (5.0 mL). To the resulting stirred solution was then added HBTU (1.5 g, 3.8 mmol, 1.5 eq.) followed by DIPEA (2.2 mL, 12.8 mmol, 5.0 eq.). Once done, the reaction mixture was then left to stir at rt under an atmosphere of argon gas for 6 h. After this time, the reaction mixture was diluted with EtOAc, washed with sat. $NaHCO_{3(aq)}$ followed by brine, dried over Na_2SO_4, filtered, concentrated under reduced pressure, and purified via flash column chromatography (silica gel, MeOH/DCM: 0%→5%→10%) to yield **15** (208 mg, 35% yield) as a yellow oil. **^{1}H-NMR** (methanol-d4, 400 MHz): δ 4.61 (br, 2H), 4.56 (d, J = 5.3 Hz, 1H), 4.14-4.02 (m, 1H), 3.75 (s, 3H), 3.35 (s, 2H), 3.18 (q, J = 6.9 Hz, 1H), 2.40 (s, 4H), 1.30 (d, J = 6.7 Hz, 3H), 1.24 (d, J = 6.7 Hz, 3H); **HRMS** (EI) m/z calculated for $C_{10}H_{20}N_2O_4$ $[M+H]^+$: 233.1496, found 233.1498.

L-threonine methyl ester hydrochloride (**16**)[67]

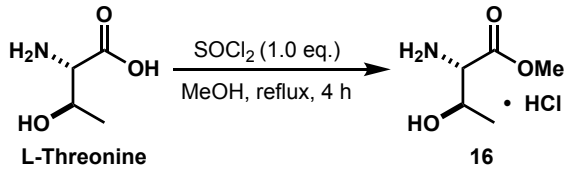

L-Threonine **16**

To a 250 mL round-bottom flash (equipped with a stir bar) containing MeOH (84 mL) at 0 °C was slowly added $SOCl_2$ (6.1 mL, 83.9 mmol, 1.0 eq.). After stirring for several minutes, L-threonine (10.0 g, 83.9 mmol, 1.0 eq) was added to the acidic MeOH solution after which, the reaction mixture was heated to reflux and left to stir under an atmosphere of argon gas for 4 h. After this time, the reaction mixture was cooled to rt and then directly concentrated under reduced pressure. The resulting solid was then stripped with Et_2O (2x) to afford L-Threonine methyl ester hydrochloride (**16**) (14.2 g, 100% yield) as a white solid. All characterization data obtained for the isolated product was in accordance with literature reported data.[67]

Methyl ((benzyloxy)carbonyl)-*L*-alanyl-*L*-threoninate (**17**)

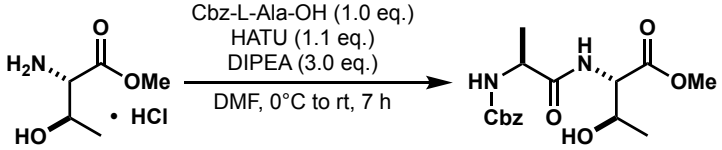

16 **17**

To a 100 mL round-bottom flask (equipped with as stir bar) was added **16** (5.0 g, 29.5 mmol, 1.0 eq.), Cbz-L-alanine (6.6 g, 29.5 mmol, 1.0eq) and HATU (12.3 g, 32.4 mmol, 1.1 eq) followed by DMF (59 mL), after which, the resulting solution was cooled to 0 °C. To the resulting stirred cold solution was then added DIPEA (15.4 mL, 88.4 mmol, 3.0 eq.) dropwise; causing the reaction mixture to turn bright yellow. Once done, the reaction was then left to stir at 0°C for 0.5 h after which, it was warmed to rt and left to stir under an atmosphere of argon gas for 7 h. After this time, the reaction was quenched via the addition of 1M $HCl_{(aq)}$ (60 mL) and extracted with EtOAc (3x). The isolated organic layers were then combined, washed with sat. $NaHCO_{3\,(aq)}$ followed by brine,

dried over Na_2SO_4, filtered, and concentrated under reduced pressure to yield **17** (9.2 g, 92 % yield) as a white solid. Crude **17** was carried forward to the next reaction without purification. **^{1}H-NMR** (methanol-d4, 500MHz): δ 7.41-7.21 (m,5H), 5.10 (s,2H), 4.45 (d, J = 2.6 Hz, 1 H), 4.29 (dd, J = 6.7, 2.9 Hz, 1 H), 4.25 (q, J = 6.9 Hz, 1 H), 3.73 (s, 3 H), 2.80 (s, 3H), 1.37 (d, J = 7.6 Hz, 3H), 1.17 (d, J = 6.8 Hz, 3 H); **HRMS** (ESI) *m/z* calculated for $C_{16}H_{22}O_6N_2$ $[M+H]^+$: 339.1551; found 339.1549.

Methyl (4*S*,5*R*)-2-((*S*)-1-(((benzyloxy)carbonyl)amino)ethyl)-5-methyl-4,5-dihydrooxazole-4-carboxylate (**18**)

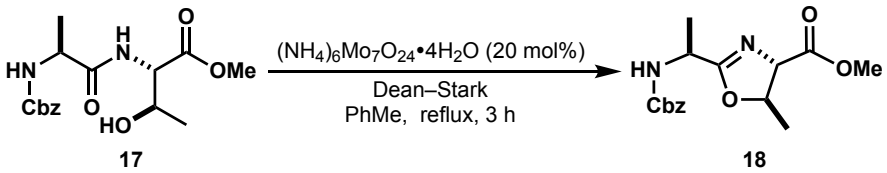

To a 500 mL round-bottom flask (equipped with a stir bar) was added **17** (4.5 g, 13.3 mmol, 1.0 eq.) followed by toluene (226 mL). To the resulting stirred solution was then added $(NH_4)_6Mo_7O_{24}•4H_2O$ (3.3 g, 2.7 mmol, 0.2 eq.) after which, the reaction vessel was equipped with a Dean–Stark apparatus and a reflux condenser. Once done, the reaction mixture was then heated to reflux and left to stir under an atmosphere of argon gas (with azeotropic removal of water) for 3 h. After this time, the reaction mixture was cooled to rt, directly concentrated under reduced pressure, and purified via flash column chromatography (deactivated silica gel, EtOAc/Hex: 0%→15%→35%) to yield **18** (3.0 g, 70% yield) as a colorless oil. **^{1}H-NMR** ($CDCl_3$, 500 MHz): δ 7.38-7.28 (m, 5 H), 5.50 (dd, J = 15.9, 6.9 Hz, 1H), 5.15-5.06 (m, 2H), 4.91-4.82 (m, 1H), 4.57-4.45 (m, 1H), 4.25 (t, J = 6.2 Hz, 1H), 3.77 (d, 3.5 Hz, 3H), 1.43 (d, J = 6.9 Hz, 6H) ppm; **^{13}C-NMR** ($CDCl_3$, 125 MHz): δ 171.3, 170.0, 155.6, 136.5, 128.6, 128.2, 128.2, 80.0, 74.3, 67.0, 52.8, 45.5, 21.0, 19.7 ppm; **HRMS** (ESI) *m/z* calculated for $C_{16}H_{20}N_2O_5$ $[M+H]^+$: 321.1445, found 321.1442.

Methyl (4*S*,5*R*)-2-((*S*)-1-(dimethylamino)ethyl)-5-methyl-4,5-dihydrooxazole-4-carboxylate (**14**)

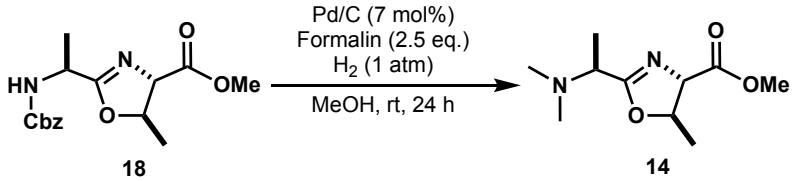

To a 250 mL round-bottom flask (equipped with a stir bar) was added **18** (320 mg, 1.0 mmol, 1.0 eq.), a 37% aqueous solution of formaldehyde (0.19 mL, 2.5 mmol, 2.5 eq.) and MeOH (100 mL) followed by Pd/C (10 wt. % Pd) (74 mg, 0.07 mol, 7.0 mol%). Once done, the reaction flask was evacuated of air and backfilled with H_2 after which, the reaction mixture was left to stir at rt under an atmosphere of H_2 gas for 24 h. After this time, the reaction vessel was purged with argon gas, and the reaction mixture filtered through a plug of Celite®. The isolated filtrate was then concentrated under reduced pressure to yield **14** (205 mg, 96% yield) as a colorless oil. While crude **14** was often carried forward to the next reaction without purification, an analytically pure sample can be isolated via flash column chromatography (deactivated silica gel, MeOH/DCM: 0%→1%→2%). **^{1}H-NMR** ($CDCl_3$, 500 MHz): δ 4.88-4.79 (m, 1H), 4.25 (d, J = 6.9 H, 1H), 3.76 (s, 3H), 3.43-3.29 (m, 1H), 2.32 (s, 6H), 1.42 (d, J = 6.9 Hz, 3H), 1.32 (d, J = 6.9 Hz, 3H); **HRMS** (ESI) *m/z* calculated for $C_{10}H_{18}N_2O_3$ $[M+H]^+$: 215.1390, found 215.1394.

(4*S*,5*R*)-2-((*S*)-1-(dimethylamino)ethyl)-5-methyl-4,5-dihydrooxazole-4-carboxylic acid (**9**)

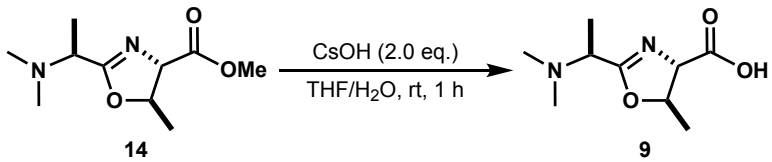

To a 100 mL round-bottom flask (equipped with a stir bar) was added **14** (650 mg, 3.0 mmol, 1.0 eq.) followed by a solution of THF/H_2O (100:1) (30 mL). To the resulting stirred solution was then added CsOH (909 mg, 6.1 mmol, 2.0 eq.) after which, the resulting reaction mixture was left stir at rt under an atmosphere of argon has for 1 h. After this time, the reaction mixture was directly

concentrated under reduced pressure and then repeatedly azeotroped with toluene (3x). The isolated crude product was then dissolved in DCM and then filtered through a short plug of Celite® (to remove any insoluble impurities) after which, the isolated filtrate was concentrated under reduced pressure to yield **9** (601 mg, 99% yield) as a white solid. Because the ^{1}H-NMR spectrum of the isolated crude product showed it to be free of impurities, it was not subjected to any further purification. **^{1}H-NMR** (methanol-d4, 500 MHz): δ 4.80-4.67 (m, 1H), 4.01 (d, 6.8 Hz, 1H), 3.39-3.31 (m, 1H), 2.30 (s, 6H), 1.38 (d, J = 6.8 Hz, 3H), 1.30 (d, J = 6.8 Hz, 3H); **HRMS** (ESI) *m/z* calculated for $C_9H_{16}N_2O_3$ $[M+H]^+$: 201.1234, found 201.1232.

L-allylglycine methyl ester hydrochloride (**25**)[72]

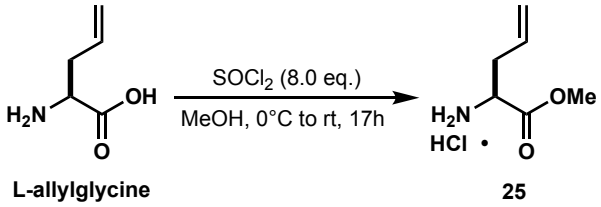

To a 250 mL round-bottom flash (equipped with a stir bar) containing MeOH (145 mL) at 0 °C was slowly added $SOCl_2$ (25.2 mL, 347.4 mmol, 8.0 eq.). After stirring for several minutes, L-allylglycine (5.0 g, 43.4 mmol, 1.0 eq) was added to the acidic MeOH solution after which, the reaction mixture was warmed to rt and left to stir under an atmosphere of argon gas for 17 h. After this time, the reaction mixture was directly concentrated under reduced pressure and stripped with Et_2O (2x) to yield **25** (7.0 g, 97% yield) as a white solid. Crude **25** was carried forward to the next reaction without purification. All characterization data obtained for the isolated product was in accordance with literature reported data.[72]

Methyl (*S*)-2-(((2-(trimethylsilyl)ethoxy)carbonyl)amino)pent-4-enoate (**26**)

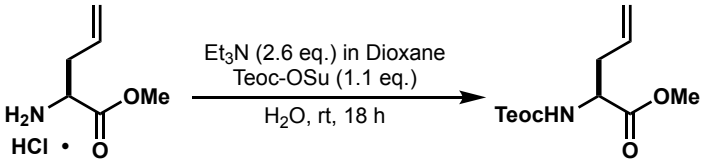

25 **26**

To a 10 mL conical flask (equipped with a stir bar) was added **25** (1.0 g, 15.7 mmol, 1.0 eq) and Teoc-OSu (1.7 g, 6.6 mmol, 1.1 eq.) followed by H_2O (6 mL). To the resulting stirred solution was then added Et_3N (2.2 mL, 15.7 mmol, 2.6 eq.) dissolved in dioxanes (6 mL), after which, the resulting reaction mixture was left to stir at rt under an atmosphere of argon gas for 18 h. After this time, the reaction was diluted with H_2O (20 mL) and extracted with Et_2O (3x). The isolated organic layers were then combined, washed with 1M $KHSO_{4(aq)}$, dried over $MgSO_4$, filtered, concentrated under reduced pressure, and purified via flask column chromatography (silica gel, EtOAc, Hex: 20%) to yield **26** (1.5 g, 91% yield) as a colorless oil. **^{1}H-NMR** ($CDCl_3$, 400 MHz): δ 5.78-5.59 (m, 1H), 5.21-5.04 (m, 3H), 4.44 (q, J = 6.09 Hz, 1H), 4.16 (t, J = 9.4 Hz, 2H), 3.75 (s, 3H), 2.62-2.42 (m, 2H), 1.03- 0.94 (m, 2H), 0.03 (s, 9); **HRMS** (ESI) *m/* calculated for $C_{12}H_{23}NO_4Si$ $[M+H]^+$: 274.1469, found 274.1466.

2-(trimethylsilyl)ethyl (*S*)-(1-oxopent-4-en-2-yl)carbamate (**27**)

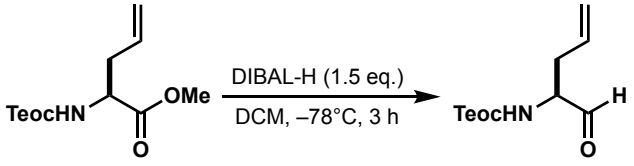

26 **27**

To a 100 mL round-bottom flask (equipped with a stir bar) was added **26** (1.5 g, 5.5 mmol. 1.0 eq.) followed by DCM (55 mL) after which, the resulting solution was cooled to –78°C. To the resulting stirred cold solution was then added DIBAL-H (1.0 M in in Hex, 8.2 mL, 8.2 mmol, 1.5 eq.) over a period of 1 h. After addition of the DIBAL-H solution was complete, the resulting

reaction mixture was left to stir at –78°C under an atmosphere of argon gas for 2 h. After this time, the reaction was quenched via the dropwise addition of 1M $HCl_{(aq)}$ (50 mL) and then allowed to warm to rt. The reaction mixture was then extracted with DCM (3x) and the isolated organic layers combined, washed with 1M $HCl_{(aq)}$ followed by H_2O, dried over $MgSO_4$, filtered, concentrated under reduced pressure, and purified via flash column chromatography (silica gel, EtOAc/Hex: 0%→5%→10%→15%) to yield **27** (975 mg, 73% yield) as a colorless oil. **^{1}H-NMR** ($CDCl_3$, 400 MHz): δ 9.58 (s, 1H), 5.78-5.58 (m, 1H), 5.22-5.08 (m, 3H), 4.31 (q, J = 5.8, Hz, 1H), 4.14 (t, J = 9.2 Hz, 2H), 2.68-2.39 (m, 2H), 1.03-0.90 (m, 2H), 0.01 (s, 9H); **HRMS** (ESI) *m/* calculated for $C_{11}H_{21}NO_3Si$ $[M+H]^+$: 244.1364, found 244.1367.

S-phenyl 2-methylpropanethioate (**28**)[79]

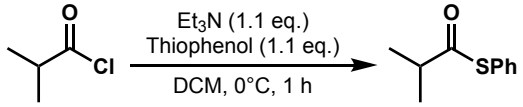

Isobutyryl chloride **28**

To a 500 mL round-bottom flask was added Thiophenol (5.2 mL, 49.5 mmol, 1.1 eq., 97%) followed by DCM (247 mL). To the resulting stirred solution was then added Et_3N (6.9 mL, 49.5 mmol, 1.1 eq.) after which, the resulting solution was cooled to 0°C. To the resulting stirred cold solution was then added isobutyryl chloride (4.8 mL, 45.0 mmol, 1.0 eq.) dropwise over 1 h. After addition of the isobutyryl chloride was complete, the resulting reaction mixture was left stir at 0°C under an atmosphere of argon gas for 1 h. After this time, the reaction was quenched via the addition of water and extracted with DCM (3x). The isolated organic layers were then combined, washed with brine, dried over $MgSO_4$, filtered, concentrated under reduced pressure, and purified via flask column chromatography (silica gel, DCM/Hex: 10%→20%→50%) to yield **28** (6.5g 80%

yield) as a colorless oil. All characterization data obtained for the isolated product was in accordance with literature reported data.[79]

2-(trimethylsilyl)ethyl ((*S*)-1-((*R*)-3,3-dimethyl-4-oxooxetan-2-yl)but-3-en-1-yl)carbamate (**10**)

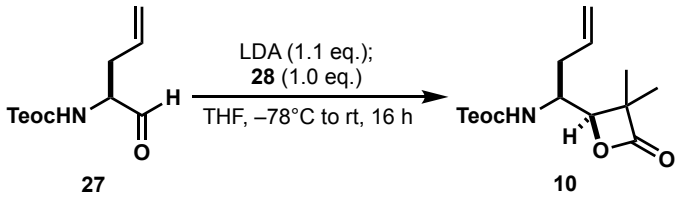

27 **10**

To a 250 mL round-bottom flask (equipped with a stir bar) was added THF (60 mL) followed by diisopropylethylamine (1.9 mL, 13.6 mmol, 1.1 eq.) after which, the resulting solution was cooled to –78°C. To the resulting stirred cold solution was then added *n*BuLi (2.21M in Hex, 5.9 mL, 12.9 mmol, 1.05 eq.) dropwise with the resultant solution of LDA being left to stir at –78°C under an atmosphere of argon gas for 10 min. To this cold solution of LDA was then added a solution of **28** (2.2 g, 12.3 mmol, 1.0 eq.) dissolved in THF (15 mL) after which, the resulting reaction mixture was left to stir at –78°C under an atmosphere of argon gas for 1 hr. After this time, a solution of **27** (3.0 g, 12.3 mmol, 1.0 eq.) dissolved in THF (15 mL) was added to the reaction mixture over a period of 0.5 h. After addition of the solution of **27** was complete, the resulting reaction mixture was left to stir at –78°C under an atmosphere of argon gas for 0.5 h after which, it was allowed to gradually warm to rt where it was left to stir under an atmosphere of argon gas for 16 h. After this time, the reaction was quenched via the dropwise addition of $NH_4Cl_{(aq)}$ (50 mL) and then extracted with EtOAc (3x). The isolated organic layers were then combined, washed with $K_2CO_{3(aq)}$ (10% w/v) followed by brine, dried over $MgSO_4$, filtered, concentrated under reduced pressure, and purified via flask column chromatography (silica gel, EtOAc/Hex: 0%→15%→30%→45%) to yield **10** (1.86g, 48% yield) as well as its corresponding diastereomer (**10'**) (464mg, 12%) (d.r 4:1) both as yellow oils. **10**: ^{1}H-NMR ($CDCl_3$, 400 MHz): δ 5.82-5.63 (m, 2H), 5.19 (d, J = 3.9 Hz,

1H), 5.15 (s, 1H), 4.76 (d, J = 6.1 Hz, 1H), 4.31-4.22 (m, 2H), 3.62-3.54 (m, 1H), 2.61-2.51 (m, 1H), 2.26-2.14 (m, 1H), 1.27 (s, 3H), 1.14 (s, 3H), 1.12-1.04 (m, 2H), 0.06 (s, 9H); **^{13}C-NMR** ($CDCl_3$, 125 MHz): δ 179.3, 154.8, 132.8, 129.0, 119.2, 83.7, 67.1, 55.6, 44.3, 38.4, 29.7, 23.7, 18.7, 17.5, 1.53; **HRMS** (ESI) *m/* calculated for $C_{15}H_{27}NO_4Si$ $[M+H]^+$: 314.1782, found 314.1786. **10'**: **^{1}H-NMR** ($CDCl_3$, 400 MHz): δ 5.97 (s, 1H), 5.80-5.68 (m, 1H), 5.18 (q, J = 1.4 Hz, 1H), 5.16-5.12 (m, 1H), 5.01 (d, J = 4.7 Hz, 1H), 4.24 (ddd, J = 8.3 Hz, 5.8 Hz, 2.1 Hz, 2H), 3.92-3.85 (dt, J = 8.9 Hz, 5.3 Hz, 1H), 2.43-2.33 (m, 1H), 2.32-2.22 (m, 1H), 1.24 (s, 3H), 1.13 (s, 3H), 1.05 (m, 2H) , 0.05 (s, 9H); **^{13}C-NMR** ($CDCl_3$, 125 MHz): δ 179.9, 155.0, 133.4, 118.7, 81.2, 67.0, 54.0, 45.2, 33.8, 29.7, 23.0, 19.1, 17.6, 17.4, 1.54; **HRMS** (ESI) m/z calculated for $C_{15}H_{27}NO_4Si$ $[M+H]^+$: 314.1782, found 314.1784.

Ethyl (*S*)-2-hydroxy-3-methylbutanoate (**30**)[39]

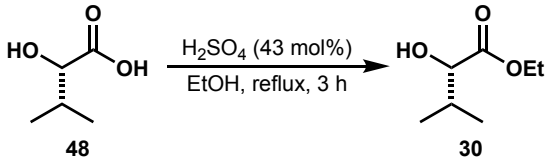

48 **30**

To a 25 mL round-bottom flask (equipped with a stir bar) was added **48** (1.0 g, 8.5 mmol, 1.0 eq.) followed by EtOH (10 mL). To the resulting stirred solution was then added conc. H_2SO_4 (0.2 mL, 3.6 mmol, 43 mol%) after which, the resulting reaction mixture was heated to reflux and then left to stir under an atmosphere of argon gas for 3 h. After this time, the reaction mixture was cooled to rt and extracted with EtOAc (3x). The isolated organic layers were then combined, washed with sat. $NaHCO_{3(aq)}$ followed by brine, dried over Na_2SO_4, filtered, and concentrated under reduced pressure to yield **30** (1.1 g, 80% yield) as a colorless oil. Crude **30** was carried forward to the next reaction without purification. All characterization data obtained for the isolated product was in accordance with literature reported data.[39]

Methyl (*S*)-2-((*tert*-butoxycarbonyl)amino)pent-4-enoate (**35**)[113]

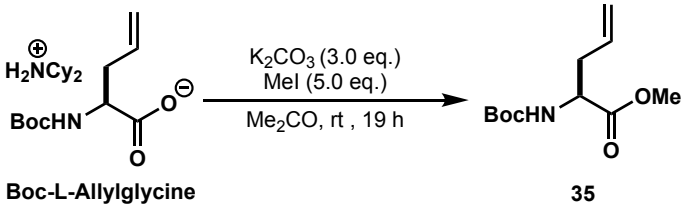

Boc-L-Allylglycine **35**

To a 250 mL round-bottom flask (equipped with a stir bar) was added Boc-L-allyglycine cyclohexylammonium salt (12.0 g, 30.3 mmol, 1.0 eq.) followed by Me_2CO (138 mL). To the resulting stirred solution was then added K_2CO_3 (12.5 g, 90.8 mmol, 3.0 eq.) followed by MeI (9.4 mL, 151.3 mmol, 5.0 eq.) after which, the resulting reaction mixture was left to stir at rt under an atmosphere of argon gas for 19 h. Note: During this time, the reaction mixture thickened and became hard to stir. For this reason, more Me_2CO (50 mL) was added. After this time, the reaction was quenched via the dropwise addition of 1M $HCl_{(aq)}$ (to a pH of 1) after which, it was extracted with EtOAc (3x). The isolated organic layers were then combined, washed with brine, dried over $MgSO_4$, filtered, concentrated under reduced pressure, and purified by filtration through a plug of silica gel using a 20% EtOAc/Hex solution to yield **35** (6.9 g, 100% yield) as a yellow oil. All characterization data obtained for the isolated product was in accordance with literature reported data.[113]

Tert-butyl (*S*)-(1-oxopent-4-en-2-yl)carbamate (**36**)

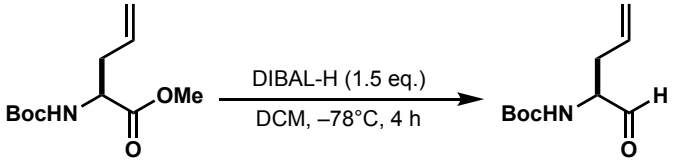

35 **36**

To a 250 mL round-bottom flask (equipped with a stir bar) was added **35** (3.0 g, 13.1 mmol, 1.0 eq.) followed by DCM (130 mL) after which, the resulting solution was cooled to –78°C. To the resulting stirred cold solution was then added DIBAL-H (1.0 M in in Hex, 19.6 mL, 19.6 mmol,

1.5 eq.) over a period of 1 h. After addition of the DIBAL-H solution was complete, the resulting reaction mixture was left to stir at –78°C under an atmosphere of argon gas for 4 h. After this time, the reaction was quenched via the dropwise addition of 1M $HCl_{(aq)}$ (50 mL) and then allowed to warm to rt. The reaction was then extracted with EtOAc (3x) and the isolated organic layers combined, washed with 1M $HCl_{(aq)}$ followed by H_2O, dried over Na_2SO_4, filtered, concentrated under reduced pressure, and purified via flash column chromatography (silica gel, EtOAc/Hex: 0%→10%→15%) to yield **36** (2.0 g, 76% yield) as a colorless oil. **^{1}H-NMR** ($CDCl_3$, 500 MHz): δ 9.60 (s, 1H), 5.76-5.67 (m, 1H), 5.18- 5.15 (m, 2H), 5.08-5.06 (m, 1H), 4.27 (q, J = 7.1 Hz, 1H), 2.62-2.55 (m, 1H), 2.52-2.49 (m, 1H), 1.45 (s, 9H); **HRMS** (ESI) m/z calculated for $C_{10}H_{17}NO_3$ $[M+H]^+$: 200.1281, found 200.1279.

Methyl (3*R*,4*S*)-4-((*tert*-butoxycarbonyl)amino)-3-hydroxy-2,2-dimethylhept-6-enoate (**37**)

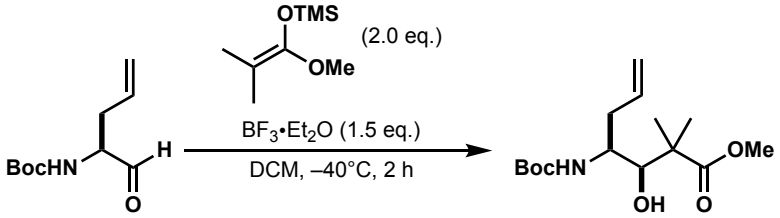

36 **37**

To a 10 mL conical flask (equipped with a stir bar) was added **36** (100 mg, 0.50 mmol, 1.0 eq.) followed by DCM (5 mL) after which, the resulting solution was cooled to –40°C. To the resulting stirred cold solution was then added BF_3•Et_2O (0.1 mL, 0.75 mmol , 1.5 eq.) followed by 1-methoxy-2-methyl-1-(trimethylsiloxy)propene (0.2 mL, 1.0 mmol, 2.0 eq.) after which, the resulting reaction mixture was left to stir a –40°C under an atmosphere of argon gas for 2 h. After this time, the reached was quenched via the dropwise addition of sat. $NH_4Cl_{(aq)}$ and then allowed to warm to rt. The quenched reaction was then extracted with EtOAc (3x) and the isolated organic layers combined, washed with brine, dried over $MgSO_4$, filtered, concentrated under reduced

pressure, and purified via flash column chromatography (silica gel, EtOAc/Hex: 0%→10%→15%→20%) to yield **37** (99 mg, 65% yield) as a white solid as well as its corresponding diastereomer (**37'**) (10 mg, 7%) (d.r 10:1) as a colorless oil. **37**: **^{1}H-NMR** ($CDCl_3$, 500 MHz): δ 5.83-5.71 (m, 1H), 5.07 (dd, J = 18.6 Hz, 9.7 Hz, 2D), 4.62 (d, J = 9.7 Hz, 1H) , 3.85 (q, 7.6 Hz, 1H), 3.78 (s, 1H), 3.69 (s, 3H), 3.54 (s, 1H), 2.31 (t, J = 6.9 Hz, 2H), 1.40 (s, 9H), 1.29 (s, 3H), 1.19 (s, 3H); **^{13}C-NMR** ($CDCl_3$, 125 MHz): δ 179.1, 155.4, 134.8, 117.7, 79.2, 77.9, 52.3, 50.1, 45.0, 39.0, 28.4, 24.6, 20.6; HRMS (EI); **HRMS** (ESI) m/ calculated for $C_{15}H_{27}NO_5$ $[M+H]^+$: 302.1962, found 302.1968. **37'**: **^{1}H-NMR** ($CDCl_3$, 500 MHz): 5.86-5.72 (m, 1H), 5.15-5.00 (m, 2H), 4.55 (d, J = 9.7 Hz, 1H), 3.81-3.73 (m, 1H), 3.71 9s, 3H), 3.04-2.90 (br, 1H), 2.32-2.22 (m, 1H), 2.22-2.10 (m, 1H), 1.57 (d, J = 3.5 Hz, 1H), 1.41 (s, 9H), 1.25 (d, J = 8.3 hz, 6H); **^{13}C-NMR** ($CDCl_3$, 125 MHz): 178.6, 155.3, 134.5, 117.8, 79.3, 78.9, 52.2, 51.6, 45.1, 35.7, 28.4, 23.0, 21.4; **HRMS** (ESI) m/ calculated for $C_{15}H_{27}NO_5$ $[M+H]^+$: 302.1962, found 302.1959.

Tert-butyl (4*S*,5*R*)-4-allyl-5-(1-methoxy-2-methyl-1-oxopropan-2-yl)-2,2-dimethyloxazo-lidine-3-carboxylate (**38**)

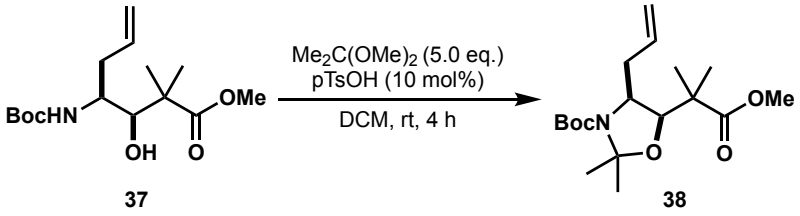

37 **38**

To a 100 mL round-bottom flask (equipped with a stir bar) was added **37** (1.3 g, 4.2 mmol, 1.0 eq.) followed by DCM (35 mL). To the resulting stirred solution was then added 2,2,-dimethoxypropane ($Me_2C(OMe)_2$) (2.6 mL, 20.9 mmol, 5.0 eq.) followed by p-Toluenesulfonic acid (pTsOH) (72 mg, 0.4 mmol, 10 mol%) along with Na_2SO_4 (500 mg) after which, the resulting reaction mixture was left to stir at rt under an atmosphere of argon gas for 4 h. After this time, the reaction was quenched via the addition of sat. $NaHCO_{3(aq)}$ and then extracted with DCM (3x). The

isolated organic layers were then combined, washed with brine, dried over Na_2SO_4, filtered, concentrated under reduced pressure, and then purified via flash column chromatography (silica gel, EtOAc/Hex: 0%→5%→10%→15%) to yield **38** (1.3 g, 92% yield) as a colorless oil. **^{1}H-NMR** (methanol-d4, 500 MHz): δ 5.82-5.68 (m, 1H), 5.14 (d, J = 5.1 Hz, 1H), 4.10 (d, J = 5.5 Hz, 1H), 4.01 (br, 1H), 3.96 (br, 1H), 3.67 (s, 3H), 2.68 (br, 1H), 2.30 (br, 1H), 1.54 (s, 3H), 1.48 (s, 9H), 1.43 (s, 3H) 1.19 (s, 3H), 1.16 (s, 3H); **^{13}C-NMR** (methanol-d4, 125 MHz): 176.1, 133.7, 117.7, 82.9, 82.8, 80.4, 57.4, 51.1, 45.5, 38.2, 36.2, 27.3, 26.2, 20.4; **HRMS** (ESI) m/ calculated for $C_{18}H_{31}NO_5$ $[M+H]^+$: 342.2275, found 342.2278.

2-((4*S*,5*R*)-4-allyl-3-(*tert*-butoxycarbonyl)-2,2-dimethyloxazolidin-5-yl)-2-methylpropanoic acid (**34**)

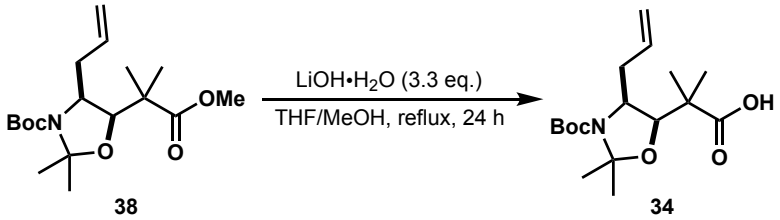

38 **34**

To a 100mL round-bottom flask (equipped with a stir bar) was added **38** (1.2 g, 3.5 mmol, 1.0 eq.) followed by a solution of THF/MeOH (4:1) (35 mL). To the resulting stirred solution was then added lithium hydroxide monohydrate ($LiOH•H_2O$) (487 mg, 11.6 mmol, 3.3 eq.) after which, the resulting reach mixture was heated to reflux and left to stir under an atmosphere of argon gas for 24 h. After this time, the reaction mixture was directly concentrated under reduced pressure. Once done, the resulting material was dissolved in EtOAc, washed with 1M $HCl_{(aq)}$ followed by brine, dried over Na_2SO_4, filtered and concentrated to yield **34** (1.2 g, 100% yield) as a colorless oil which solidified into a white solid when stored in the freezer. While crude **34** was often carried forward to the next reaction without purification, an analytically pure sample can be isolated via flash column chromatography (silica gel, EtOAc/Hex: 0%→10%→20%) albeit with the loss of

some material (1.1 g, 91% yield). **^{1}H-NMR** (DMSO-d6, 500 MHz): δ 5.76-5.60 (m, 1H), 5.09 (d, J = 9.7 Hz, 2H), 4.02 (d, J = 5.5 Hz, 1H), 3.81 (br, 1H), 2.78-2.53 (m, 1H), 2.21 (br, 1H), 1.46 (s, 3H), 1.40 (s, 9H), 1.34 (s, 3H), 1.06 (s, 3H), 1.03(s, 3H); **^{13}C-NMR** (DMSO-d6, 125 MHz): δ 177.1, 151.2, 134.3, 119.0, 79.7, 57.3, 45.1, 40.6, 28.5, 21.6; **HRMS** (ESI) m/ calculated for $C_{17}H_{39}NO_5$ $[M+H]^+$: 328.2119, found 328.2122.

N-methyl-L-alanine ethyl ester hydrochloride (**43**)[86]

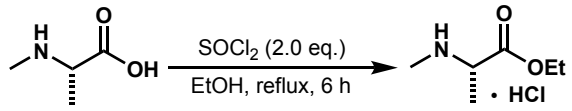

N-Methyl-L-Alanine **43**

To a 250 mL round-bottom flash (equipped with a stir bar) containing EtOH (110 mL) at 0 °C was slowly added $SOCl_2$ (7.0 mL, 97.0 mmol, 2.0 eq.). After stirring for several minutes, N-methyl-L-alanine (5.0 g, 48.5 mmol, 1.0 eq) was added to the acidic EtOH solution after which, the reaction mixture was heated to reflux and left to stir under an atmosphere of argon gas for 6 h. After this time, the reaction mixture was cooled to rt and then directly concentrated under reduced pressure. The resulting solid was then stripped with Et_2O (2x) to afford **43** (8.1 g, 100% yield) as a white solid. All characterization data obtained for the isolated product was in accordance with literature reported data.[86]

Ethyl *N*-acetyl-*N*-methyl-*L*-alaninate (**44**)

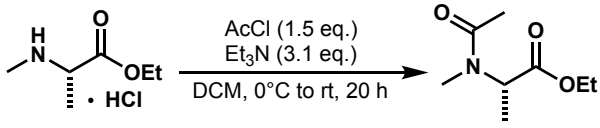

43 **44**

To a 1000 mL round-bottom flask (equipped with a stir bar) was added **43** (7.9 g, 47.1 mmol, 1.0 eq.) followed by DCM (490 mL) after which, the resulting solution was cooled to 0°C. To the

resulting stirred cold solution was then added acetyl chloride (AcCl) (5.1 mL, 70.7 mmol, 1.5 eq. 98%) followed by Et_3N (20.4 mL, 146.1 mmol, 3.1 eq.) dropwise. Once done, the reaction was then left to stir at 0 °C for 0.5 h after which, it was warmed to rt and left to stir under an atmosphere of argon gas for 20 h. After this time, the reaction was quenched via the addition of sat. $NH_4Cl_{(aq)}$ (300mL) and extracted with DCM (3x). The isolated organic layers were then combined, washed with brine, dried over $MgSO_4$, filtered, concentrated under reduced pressure, and purified via short path vacuum distillation at 116°C–120°C to yield **44** (7.5 g, 92%) was a yellow oil. **^{1}H-NMR** ($CDCl_3$, 400 MHz): δ 5.23 (q, J = 7.2 Hz, 1H), 4.30-4.00 (m, 2H), 2.94 (s, 3H), 2.12 (s, 3H), 1.38 (d, J = 7.2 Hz, 3H), 1.26 (t, 6.9 Hz, 3H); **HRMS** (ESI) m/ calculated for $C_8H_{15}NO_3$ $[M+H]^+$: 174.1125, found 174.1129.

(*S*)-1,5-dimethylpyrrolidine-2,4-dione (**39**) (Initial Synthesis)

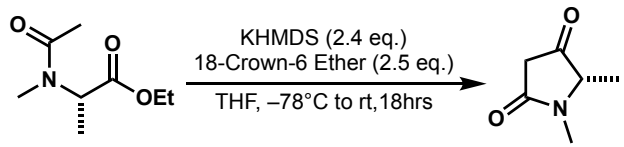

44 **39**

To a 500 mL round-bottom flask (equipped with a stir bar) was added THF (67 mL) followed by potassium bis(trimethylsilyl)amide (KHMDS) (0.7M in toluene, 79.0 mL, 55.4 mmol, 2.4 eq.) after which, the resulting solution was cooled to –78°C. To the resulting stirred solution cold was then added a solution of **44** (4.0 g, 23.1 mmol, 1.0 eq.) and 18-Crown-6 Ether (15.3 g, 57.7 mmol, 2.5 eq.) dissolved in THF (144 mL) over a period of 2 h. After addition of this solution was complete, the reaction was then left to stir at –78°C for 2 h, after which, it was warmed to rt and left to stir under an atmosphere of argon gas for 18 h. After this time, the reaction was quenched via the dropwise addition of 1M $HCl_{(aq)}$ (to a pH of 1) and extracted with EtOAc (3x). The isolated organic layers were then combined, washed with brine, dried over Na_2SO_4, filtered, concentrated

under reduced pressure, and purified via flash column chromatography (silica gel, EtOAc/Hex: 25%→50%→75%→100%) to yield **39** (2.0 g, 68% yield) as an orange oil. **^{1}H-NMR** ($CDCl_3$, 500 MHz): δ 3.91 (q, J = 6.9 Hz, 1H), 3.04 (S, 2H), 2.9 (s, 3H), 1.38 (d, J = 6.9 Hz, 3H); **^{13}C-NMR** ($CDCl_3$, 125 MHz); δ 206.8, 168.4, 64.4, 40.3, 27.2, 15.1; **HRMS** (ESI) m/ calculated for $C_6H_9NO_2$ $[M+H]^+$: 18.0706, found 128.0707.

N-methyl-L-alanine methyl ester hydrochloride (**SI1**)[88]

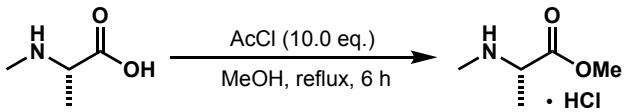

N-Methyl-L-Alanine **S1**

To a 500 mL round-bottom flask (equipped with a stir bar) was added N-methyl-L-alanine (3.0g, 29.1 mmol, 1.0 eq.) followed by MeOH (242 mL) after which, the resulting solution was cooled to 0°C. To the resulting stirred cold solution was then added acetyl chloride (AcCl) (20.7 mL, 290.9 mmol, 10.0 eq.) dropwise. Once done, the resulting reaction mixture was gradually warmed to rt and then heated to reflux where it was left to stir under an atmosphere of argon gas for 6 h. After this time, the reaction was cooled to rt, directly concentrated under reduced pressure, and stripped with Et_2O (3x) to yield **S1** (4.5 g, 100% yield) as an opaque yellow oil. All characterization data obtained for the isolated product was in accordance with literature reported data.[88]

Methyl (*S*)-3-((1-methoxy-1-oxopropan-2-yl)(methyl)amino)-3-oxopropanoate (**46**)

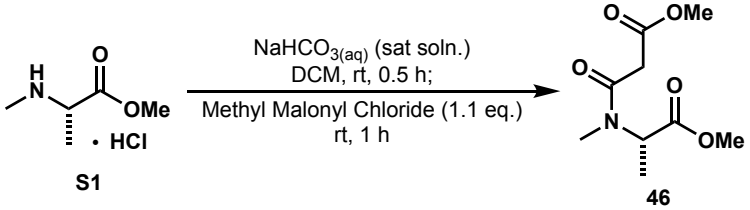

S1 **46**

To a 500 mL round-bottom flask (equipped with as stir bar) was added **S1** (4.7 g, 30.6 mmol, 1.0 eq.) followed by DCM (92 mL). To the resulting stirred solution was then added sat. $NaHCO_{3(aq)}$

(153 mL) after which, the resulting mixture was vigorously stirred at rt under an atmosphere of argon gas for 0.5 h. After this time methyl malonyl chloride (3.8 mL, 33.7mmol, 1.1 eq., 95%) was added dropwise over 5 min. After addition of the methyl malonyl chloride was complete, the reaction was then left to stir at rt under an atmosphere of argon gas for 1 h. After this time, the reaction mixture was transferred to a separatory funnel, organic layer (DCM) isolated and the aqueous layer back extracted with DCM (3x). The isolated organic layers were then combined, dried over Na_2SO_4, filtered, and concentrated under reduced pressure to yield **46** (5.3 g, 80% yield) as a dark yellow oil. Crude **46** was carried forward to the next reaction without purification. **^{1}H-NMR** ($CDCl_3$, 500 MHz): δ 5.25 (q, J = 6.9 Hz, 1H), 3.75 (s, 3H), 3.71 (s, 3H), 3.50 (d, J = 6.2 Hz, 2H), 2.95 (s, 3H), 1.41 (d, J= 6.9 Hz, 3H); **^{13}C-NMR** ($CDCl_3$, 500 MHz) 171.8, 168.1, 167.7, 53.5, 51.4, 40.4, 32.1, 14.16. 12.9; **HRMS** (EI) m/z calculated for $C_9H_{15}NO_5$ $[M+H]^+$: 218.1023, found 218.1020.

Methyl (5*S*)-1,5-dimethyl-2,4-dioxopyrrolidine-3-carboxylate (**47**)

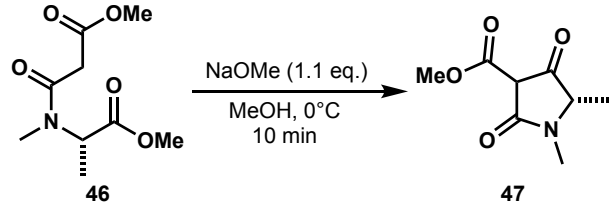

To a 250 mL round-bottom flask (equipped with a stir bar) was added **46** (4.9 g, 22.6 mmol, 1.0 eq) followed by MeOH (114 mL) after which, the resulting solution was cooled to 0°C. To the resulting stirred cold solution was then added freshly prepared NaOMe (1.0M in MeOH, 24.8 mL, 24.8 mmol, 1.1 eq.) dropwise. Once done, the resulting reaction mixture was then left to stir at 0°C under an atmosphere of an argon gas for 10 min. After this time, the reaction was directly concentrated under reduced pressure and the isolated crude material dissolved in H_2O, which was subsequently extracted with EtOAc (3x). To the isolated AQUEOUS layer was then added 1M

$HCl_{(aq)}$ (to a pH of 1) which was then extracted with DCM (3x). The isolated organic layers were then combined, dried over Na_2SO_4, filtered, and concentrated under reduce pressure to yield **47** (3.5 g, 84% yield) as an off-white solid. **^{1}H-NMR** ($CDCl_3$, 500 MHz): δ 11.20 (br, 1H), 4.01 (q, J = 6.6 Hz, 1H) 3.92 (s, 3H), 2.93 (S, 3H), 1.42 (d, J = 6.6 Hz, 3H); **HRMS** (EI) m/z calculated for $C_8H_{11}NO_4$ $[M+H]^+$: 186.0761, found 186.0766.

(*S*)-1,5-dimethylpyrrolidine-2,4-dione (**39**) (Second Synthesis)

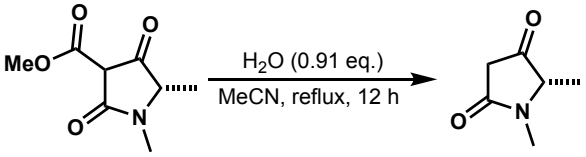

47 **39**

To a 500 mL round-bottom flask (equipped with a stir bar) was added **47** (3.5 g, 18.9 mmol, 1.0 eq.) followed by H_2O (0.31 mL, 17.2 mmol, 0.91 eq.) followed by MeCN (250 mL) after which, the reaction flask was heated to reflux and then left to stir under an atmosphere of argon gas for 12 h. After this time, the reaction mixture was then directly concentrated under reduced pressure and then repeatedly azeotroped with toluene (3x) to yield **39** (2.4 g, 98% yield) as an orange oil. **^{1}H-NMR** ($CDCl_3$, 500 MHz): δ 3.91 (q, J = 6.9 Hz, 1H), 3.04 (S, 2H), 2.9 (s, 3H), 1.38 (d, J = 6.9 Hz, 3H); **^{13}C-NMR** ($CDCl_3$, 125 MHz); δ 206.8, 168.4, 64.4, 40.3, 27.2, 15.1; **HRMS** (ESI) m/ calculated for $C_6H_9NO_2$ $[M+H]^+$: 18.0706, found 128.0707.

Methyl (*S*)-2-hydroxy-3-methylbutanoate (**49**)[90]

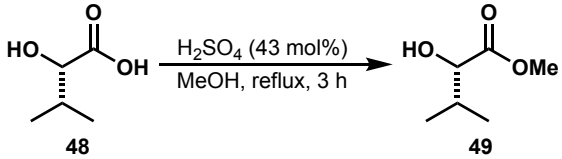

48 **49**

To a 100 mL round-bottom flask (equipped with a stir bar) was added **48** (5.0 g, 42.3 mmol, 1.0 eq.) followed by MeOH (50 mL). To the resulting stirred solution was then added conc. H_2SO_4

(1.0 mL, 18.2 mmol, 43 mol%) after which, the resulting reaction mixture was heated to reflux and then left to stir under an atmosphere of argon gas for 3 h. After this time, the reaction mixture was cooled to rt and extracted with EtOAc (3x). The isolated organic layers were then combined, washed with sat. $NaHCO_{3(aq)}$ followed by brine, dried over Na_2SO_4, filtered, and concentrated under reduced pressure (at rt) to yield **49** (5.2 g, 93% yield) as a colorless oil. Crude **49** was carried forward to the next reaction without purification. All characterization data obtained for the isolated product was in accordance with literature reported data.[90] Note: Due to the volatility of this compound, at no point was it placed under strong vacuum.

Benzyl 2,2,2-Trichloroacetimidate (**50**)[92]

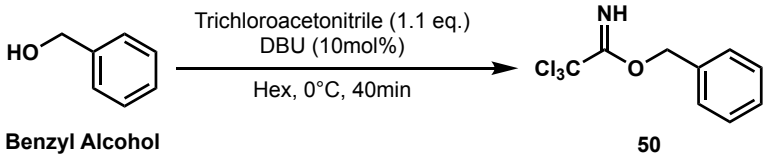

Benzyl Alcohol **50**

To a 2000 mL round-bottom flask (equipped with a stir bar) was added benzyl alcohol (15.0 mL, 144.8 mmol, 1.0 eq.) and trichloroacetonitrile (16.0 mL, 159.3 mmol, 1.1 eq.) followed by Hexanes (360 mL) after which, the resulting reaction mixture was cooled to 0°C. To the resulting stirred cold solution was then added DBU (2.2 mL, 14.5 mmol, 10 mol%) after which, the reaction was left to stir at 0°C under an atmosphere of argon gas for 40 min. After this time, the reaction was diluted with hexanes (360 mL) followed by sat. $NH_4Cl_{(aq)}$ (720 mL). Once done, the organic layer was isolated and the aqueous layer back extracted with hexanes (3x). The isolated organic layers were then combined, dried over Na_2SO_4, filtered, and concentrated under reduced pressure to yield **50** (35.1 g, 96% yield) as a colorless oil. Crude **50** was carried forward to the next reaction without purification. All characterization data obtained for the isolated product was in accordance with literature reported data.[92]

Methyl (*S*)-2-(benzyloxy)-3-methylbutanoate (**51**)[91]

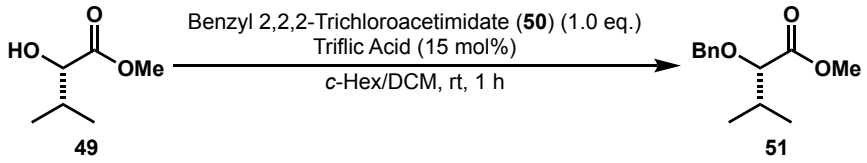

To a 250 mL round-bottom flask (equipped with as stir bar) was added **49** (9.4 g, 71.1 mmol, 1.0 eq.) followed by a solution of *c*-Hex/DCM (2:1) (104 mL). To the resulting stirred solution was then added Benzyl 2,2,2-Trichloroacetimidate (**50**) (14.5 mL, 78.2 mmol, 1.1 eq.) followed by triflic acid (0.94 mL, 10.7 mmol, 15 mol%) after which, the resulting reaction mixture was left to stir at rt under an atmosphere of argon gas for 1 h. Note: During this time the reaction transitioned from milky white to milky red in color. After this time, the reaction was filtered (to remove the white precipitate formed during the reaction) after which, the isolated filtrate was washed with sat. $NaHCO_{3(aq)}$ followed by brine, dried with Na_2SO_4, filtered, concentrated under reduced pressure, and purified via flash column chromatography (silica gel, EtOAc/Hex:0%→5%) to yield **51** (12.5 g, 79% yield) as a colorless oil. All characterization data obtained for the isolated product was in accordance with literature reported data.[91]

(*S*)-2-(benzyloxy)-3-methylbutanoic acid (**51**)[91]

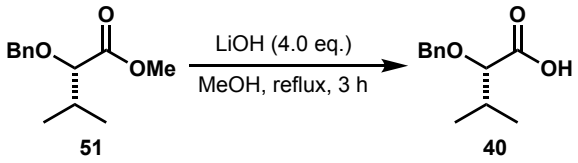

To a 250 mL round-bottom flask (equipped with a stir bar) was added **51** (11.0 g, 49.5 mmol, 1.0 eq.) followed by MeOH (100 mL). To the resulting stirred solution was then added a solution of lithium hydroxide (LiOH) (4.7 g, 197.9 mmol, 4.0 eq.) dissolved in H_2O (34 mL). Once done, the resulting reaction mixture was heated to reflux and left to stir under an atmosphere of argon gas for 3 h. After this time, the reaction was cooled to rt and then diluted with 1 M $NaOH_{(aq)}$ (to a pH

of 14 after which, the resulting basic solution was extracted with DCM (3x). To the isolated AQUEOUS layer was then added 2M $HCl_{(aq)}$ (to a pH of 1) which was then extracted with DCM (3x). The isolated organic layers were then combined, dried over $MgSO_4$, filtered, and concentrated under reduce pressure to yield **50** (9.0 g, 87% yield) as a colorless oil which solidified into a white solid when stored in the freezer. All characterization data obtained for the isolated product was in accordance with literature reported data.[91]

(*S*)-3-((*S*)-2-(benzyloxy)-3-methylbutanoyl)-4-hydroxy-1,5-dimethyl-1,5-dihydro-2*H*-pyrrol-2-one (53)

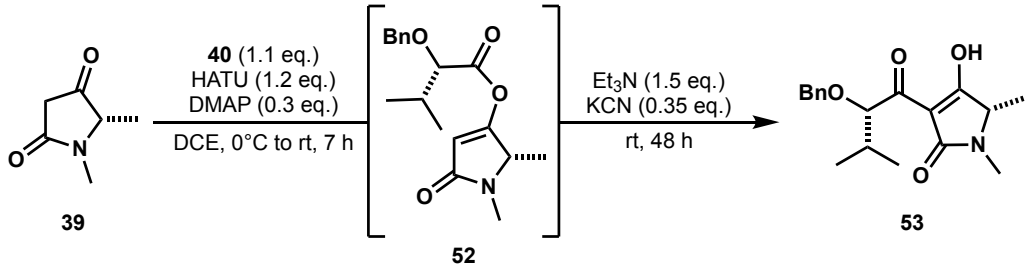

To a 100 mL round-bottom flask (equipped with as stir bar) was added **39** (2.0 g, 15.7 mmol, 1.0 eq.) followed by DCE (79 mL) after which, the resulting solution was cooled to 0°C. To the resulting stirred cold solution was then added HATU (7.2 g, 18.9 mmol, 1.2 eq.) followed by DMAP (576 mg, 4.7 mmol. 0.3 eq.) after which, the resulting reaction mixture was warmed to rt and left to stir under an atmosphere of argon gas for 7 h. After this time, KCN (358 mg, 5.5 mmol, 35 mol%) was added to the reaction mixture followed by Et_3N (3.3 mL, 23.6 mmol, 1.5 eq.). Once done, the resulting reaction mixture was left to stir at rt under an atmosphere of argon gas for 48 h. After this time, the reaction was diluted with DCM (50 mL) and washed with brine, which was back extracted with DCM (3x). The isolated organic layers were then combined, dried over Na_2SO_4, filtered, concentrated under reduced pressure, and purified via flash column chromatography (silica gel, EtOAc/Hex + 1% AcOH: 0%→10→%20%) to yield **53** (3.3 g, 67%

yield) as a red oil. The spectra of the isolated product was a mixture of at least 2 tautomeric species. Signals of the major tautomer are given: **^{1}H-NMR** (500 MHz, $CDCl_3$): δ 7.36-7.28 (m, 5 H), 4.73 (d, *J* = 7.3 Hz, 1 H), 4.54 (d, *J* = 5.5 Hz, 1 H), 4.48 (d, *J* = 3.8 Hz, 1 H), 3.68 (q, *J* = 6.9 Hz, 1 H), 2.98 (s, 3 H), 2.15-2.03 (m, 1 H), 1.35 (d, *J* = 7.3 Hz, 3 H), 1.05 (d, *J* = 6.9 Hz, 3H), 0.94 (d, *J* = 6.9 Hz, 3 H); **^{13}C-NMR** (125 MHz, $CDCl_3$): d = 194.4, 185.7, 172.3, 137.9, 128.4, 128.9, 128.2, 102.1, 80.5, 72.7, 62.7, 31.9, 26.9, 18.9, 18.6, 14.8; **HRMS** (ESI) m/ calculated for $C_{18}H_{23}N_2O_4$ $[M+H]^+$: 318.170, found 318.1702.

(*S*)-4-hydroxy-3-((*S*)-2-hydroxy-3-methylbutanoyl)-1,5-dimethyl-1,5-dihydro-2*H*-pyrrol-2-one (**6**)

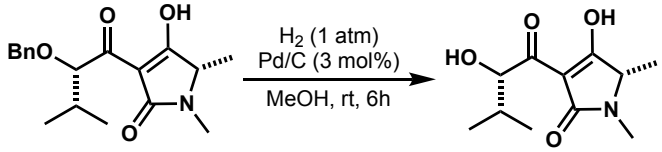

53 **6**

To a 100 mL round-bottom flask (equipped with a stir bar) was added **53** (870 mg, 2.7 mmol, 1.0 eq.) and Pd/C (10 wt. % Pd) (87 mg, 0.08 mmol, 3 mol%) followed by MeOH (55 mL). Once done, the reaction flask was evacuated of air and backfilled with H_2 after which, the reaction mixture was left to stir at rt under an atmosphere of H_2 gas for 6 h. After this time, the reaction mixture was purged with argon gas and the reaction mixture filtered through a plug of Celite®. The isolated filtrate was then concentrated under reduced pressure to yield **6** (617 mg, 99%) as a red oil. The spectra of the isolated product was a mixture of at least 2 tautomeric species. Signals of the major tautomer are given: **^{1}H-NMR** (methanol-d4, 500 MHz): δ 4.61 (d, *J* = 6.4 Hz, 1H), 3.91 (q, *J* = 6.4 Hz, 1H), 2.98 (s, 3H), 2.09-1.97 (m, 1H), 1.35 (d, *J* = 7.0 Hz, 3 H), 0.98 (t, *J* = 7.0 Hz, 6H); **^{13}C-NMR** (methanol-d4, 125 MHz): δ196.0, 195.2, 174.0, 98.6, 78.3, 60.8, 31.8, 25.1, 18.9, 15.1, 14.2; **HRMS** (ESI) m/ calculated for $C_{11}H_{17}NO_4$ $[M+H]^+$: 228.1230, found 228.1225.

(*S*)-5-(2-(benzyloxy)-1-hydroxy-3-methylbutylidene)-2,2-dimethyl-1,3-dioxane-4,6-dione (**54**)

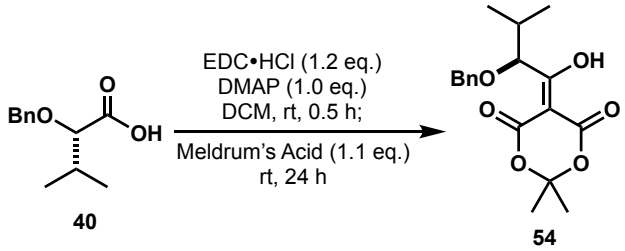

To a 1000 mL round-bottom flask (equipped with a stir bar) was added **40** (10.0 g, 48.0 mmol, 1.0 eq.) and EDC•HCl (11.6 g, 57.6 mmol, 1.2 eq., 95%) followed by DCM (480 mL). To the resulting stirred solution was then added DMAP (5.9 g, 48.0 mmol, 1.0 eq.) after which, the resulting reaction mixture was left to stir at rt under an atmosphere of argon gas for 0.5 h. After this time, Meldrum's acid (7.6 g, 52.8 mmol, 1.1 eq.) was added to the reaction mixture. Once done, the resulting reaction mixture was left to stir at rt under an atmosphere of argon gas for 24 h. After this time, the reaction mixture was directly concentrated under reduced pressure, and the resulting isolated material dissolved in ethyl acetate and then washed with 1M $HCl_{(aq)}$ followed by brine. The isolated organic layer was then dried over Na_2SO_4, filtered, and concentrated under reduced pressure to yield **54** (16.0g, 100% yield) as an organize oil which solidified into a yellow solid when stored in the freezer. Because **54** was found to be unstable to purification via flash column chromatography, crude **54** was carried forward to the next reaction without purification. **^{1}H-NMR** ($CDCl_3$, 500 MHz): δ 15.45 (s, 1H), 7.41-7.27 (m ,5H), 5.28 (d, J = 5.9 Hz, 1H), 4.55 (s, 2H), 2.17-2.07 (m ,1H), 1.71 (d, J = 11.0 Hz, 6H), 1.03 (dd, J = 15.9 Hz, 6.9 Hz, 6H); **HRMS** (ESI) m/ calculated for $C_{18}H_{22}NO_6[M+H]^+$: 335.1489, found 355.1492.

Ethyl *N*-((*S*)-4-(benzyloxy)-5-methyl-3-oxohexanoyl)-*N*-methyl-*L*-alaninate (**56**)

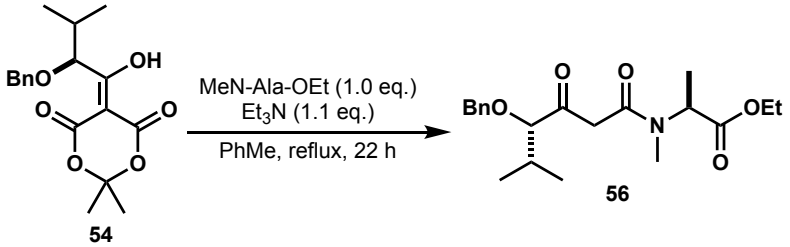

To a 500 mL round-bottom flask (equipped with a stir bar) was added N-methyl-L-alanine ethyl ester hydrochloride (**43**) (4.4 g, 26.2 mmol, 1.0 eq.) and **54** (10.5 g, 31.5 mmol, 1.2 eq.) followed by PhMe (218 mL). To the resulting stirred solution was then added Et_3N (4.0 mL, 28.9 mmol, 1.1 eq.) after which, the resulting reaction mixture was heated to reflux and left to stir under an atmosphere of argon gas for 22 h. After this time, the reaction was cooled to rt, directly concentrated under reduced pressure, and purified via flash column chromatography (silica gel, EtOAc/Hex: 0% 10% 20%) to yield **56** (7.0 g, 73%) as a yellow oil. The spectra of the isolated product was a mixture of at least 3 tautomeric species. Signals of the major tautomer are given: **^{1}H-NMR** (DMSO-d6, 500 MHz): δ 14.70 (s, 1H), 7.41-7.09 (m, 5H), 5.55 (s, 1H), 4.93 (q, J = 6.2 Hz, 1H), 4.65-4.52 (m, 1H), 4.43-4.30 (m, 1H), 4.17-4.01 (m, 2H), 2.91 (s, 3H), 2.15-1.90 (m, 1H), 1.35 (d, J = 6.2 Hz, 3H), 1.17 (t, J = 6.9 Hz, 3H), 0.94-0.80 (m, 6H); **^{13}C-NMR** (DMSO-d6, 125 MHz): δ 206.7, 176.2, 172.1, 171.5, 138.7, 128.7, 128.1, 89.0, 87.9, 72.6, 61.1, 52.6, 32.4, 31.3, 19.4, 18.2, 14.7, 14.5; **HRMS** (ESI) m/ calculated for $C_{20}H_{29}NO_5$ $[M+H]^+$: 364.2119, found 364.2122.

Ethyl *N*-((*S*)-4-hydroxy-5-methyl-3-oxohexanoyl)-*N*-methyl-*L*-alaninate (**6'**)

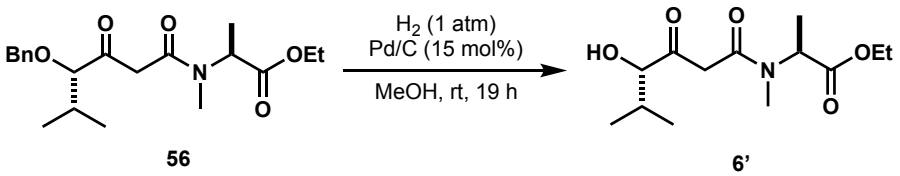

56 **6'**

To a 500 mL round bottom flask (equipped with a stir bar) was added **56** (8.9 g, 24.5 mmol, 1.0 eq.) and Pd/C (10 wt. % Pd) (3.9 g, 3.7 mmol, 15 mol%) followed MeOH (244 mL). Once done, the reaction flask was evacuated of air and backfilled with H_2 after which, the reaction mixture was left to stir at rt under an atmosphere of H_2 gas for 19 h. After this time, the reaction mixture was purged with argon gas and the reaction mixture filtered through a plug of Celite®. The isolated filtrate was then concentrated under reduced pressure to yield **6'** (6.1 g, 91%) as a red oil. The spectra of the isolated product was a mixture of at least 3 tautomeric species. Signals of the major tautomer are given: **^{1}H-NMR** (DMSO-d6, 500 MHz): δ 5.42 (d, J = 5.5 Hz, 1H) 4.85 (q, J = 7.3 Hz, 1H), 4.17-3.98 (m, 2H), 3.85-3.50 (m, 2H), 2.85 (s, 3H), 2.04-1.86 (m, 1H), 1.28 (d, J = 6.9 Hz, 3H), 1.18 (t, J = 7.3 Hz, 3H), 0.88 (d, J = 6.9, 3H), 0.79 (d, J = 7.7 Hz, 3H); **^{13}C-NMR** (DMSO-d6, 125 MHz): δ 208.5, 171.6, 167.9, 81.0, 60.9, 52.9, 45.4, 32.9, 30.9, 19.7, 17.1, 14.6, 14.5; **HRMS** (ESI) m/ calculated for $C_{20}H_{29}NO_5$ $[M+H]^+$: 364.2119, found 364.2122.

Tert-butyl (4*S*,5*R*)-4-allyl-5-(1-(((*S*)-6-(((*S*)-1-ethoxy-1-oxopropan-2-yl) (methyl) amino)-2-methyl-4,6-dioxohexan-3-yl)oxy)-2-methyl-1-oxopropan-2-yl)-2,2-dimethyloxazolidine-3-carboxylate (**57**)

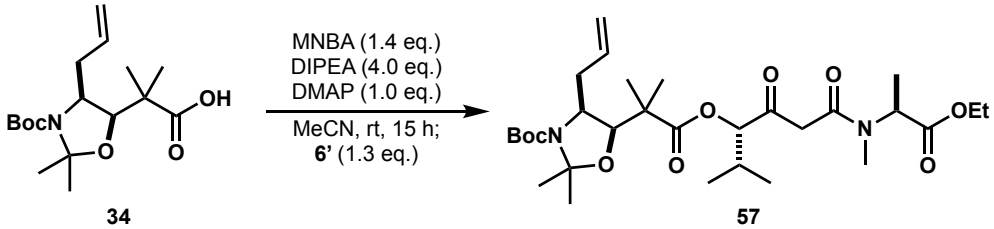

34 **57**

To a 25 mL round bottom flask (equipped with a stir bar) was added **34** (1.0 g, 3.0 mmol, 1.0 eq.) and 2-methyl-6-nitrobenzoic anhydride (MNBA) (1.5 g, 4.3 mmol, 1.4 eq.) followed by MeCN

(6.4 mL). To the resulting stirred solution was then added DMAP (373 mg, 3.0 mmol, 1.0 eq.) followed by DIPEA (2.1 mL, 12.2 mmol, 4.0 eq.) dropwise after which, the resulting reaction mixture was left to stir at rt under an atmosphere of argon gas for 0.5 h. After this time, **6'** (1.1 g, 4.0 mmol, 1.3 eq.) was added to the reaction mixture. Once done, the resulting was left to stir at rt under an atmosphere of argon gas for 15 h. After this time, the reaction was diluted with EtOAc, washed with sat. $NaHCO_{3(aq)}$ followed by brine, dried over Na_2SO_4, filtered, concentrated under reduced pressure, and purified via flash column chromatography (silica gel, 0%→5%→10% 20%) to yield 57 (1.0 g, 58% yield) as a yellow oil. The spectra of the isolated product was a mixture of at least 3 tautomeric species. Signals of the major tautomer are given: ^{1}H-NMR ($CDCl_3$, 500 MHz): δ 5.81-5.67 (m, 1H), 5.33-4.79 (m, 4H), 4.38-4.09 (m, 3H), 4.00-3.84 (m, 1H), 3.70 (s, 1H), 2.89 (d, J = 16.6 Hz, 2H), 2.83-2.58 (m, 1H), 2.41-2.21 (m, 2H), 1.55 (d, 16.6 Hz, 3H), 1.47 (s, 9H), 1.28-1.22 (m, 6H), 1.20 (d, J = 5.9 Hz, 3H), 1.05-0.93 (m, 6H); ^{13}C-NMR (CDCl3, 125 MHz): δ 200.1, 175.7, 171.5, 166.9, 151.6, 151.3, 133.7, 118.7, 118.6, 94.8, 93.9, 86.5, 86.3, 82.5, 80.1, 61.5, 61.2, 52.5, 46.8, 32.3, 31.4, 30.2, 28.4, 27.4, 27.2, 22.9, 22.7, 19.3, 19.0, 16.9, 14.3, 14.2; **HRMS** (ESI) m/ calculated for $C_{30}H_{50}N_2O_9$ $[M+H]^+$: 583.3589, found 583.3591.

(*S*)-6-(((*S*)-1-ethoxy-1-oxopropan-2-yl)(methyl)amino)-2-methyl-4,6-dioxohexan-3-yl (3*R*,4*S*)-4-amino-3-hydroxy-2,2-dimethylhept-6-enoate (**58**)

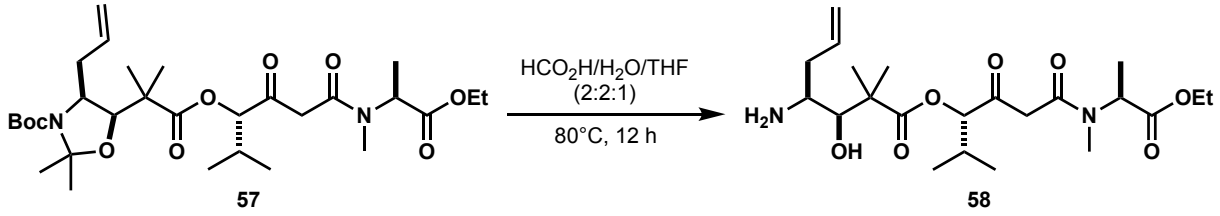

To a 10 mL round-bottom flask (equipped with a stir bar) was added **57** (264 mg, 0.5 mmol, 1.0) followed by a formic acid/H_2O/THF solution (2:2:1) (5.5 mL) after which, the resulting reaction mixture was heated to 80°C and left to stir under an atmosphere of argon gas for 12 h. After this

time, the reaction was diluted with EtOAc, washed with sat. $NaHCO_{3(aq)}$ followed by brine, dried over Na_2SO_4, filtered and, concentrated under reduced pressure to yield **58** (228 mg, 100% yield) as an off-white solid. Do the complex nature of the obtained NMR spectra, this product was characterized based on mass with its purity assessed via HPLC chromatograph readout.

HRMS (ESI) m/ calculated for $C_{22}H_{38}N_2O_7$ $[M+H]^+$: 443.2752, found 443.2756.

NMR Spectra

Spectrum 3.8.1 1H-NMR spectrum of compound **15** (methanol-d4, 400 MHz)

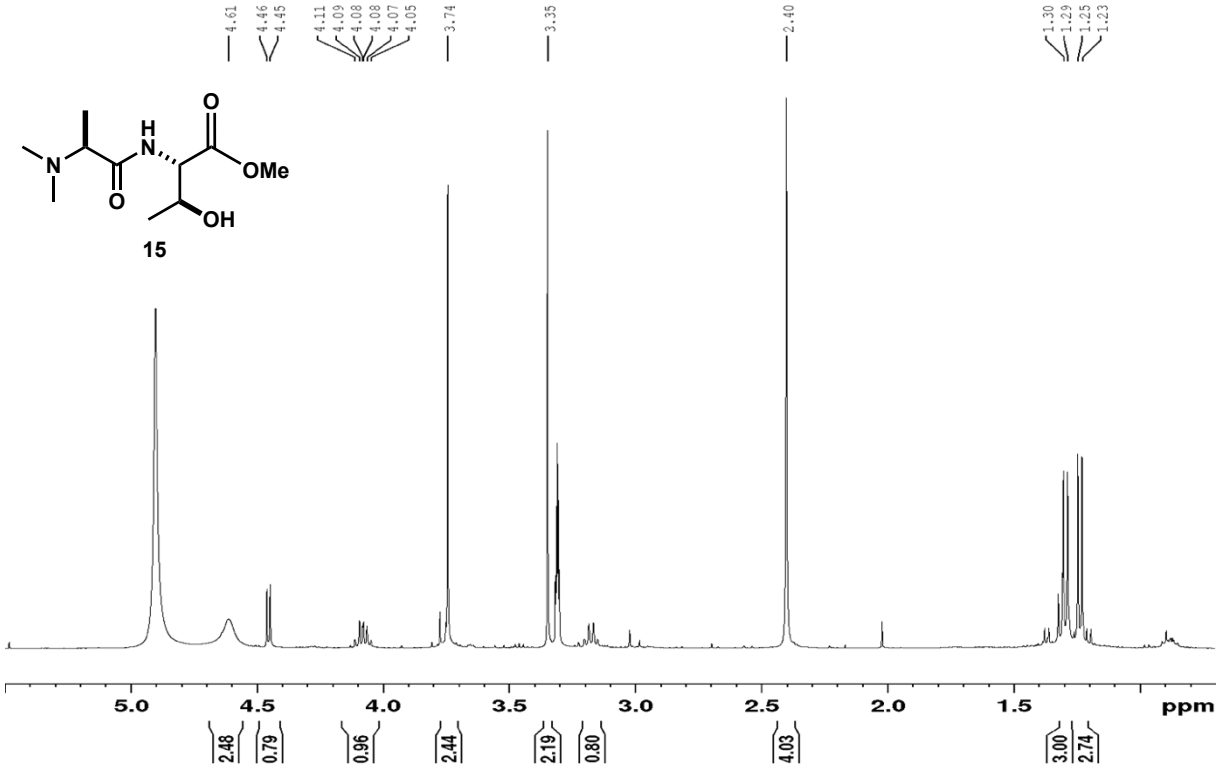

Spectrum 3.8.2 [1]H-NMR spectrum of compound **17** (methanol-d4, 500 MHz)

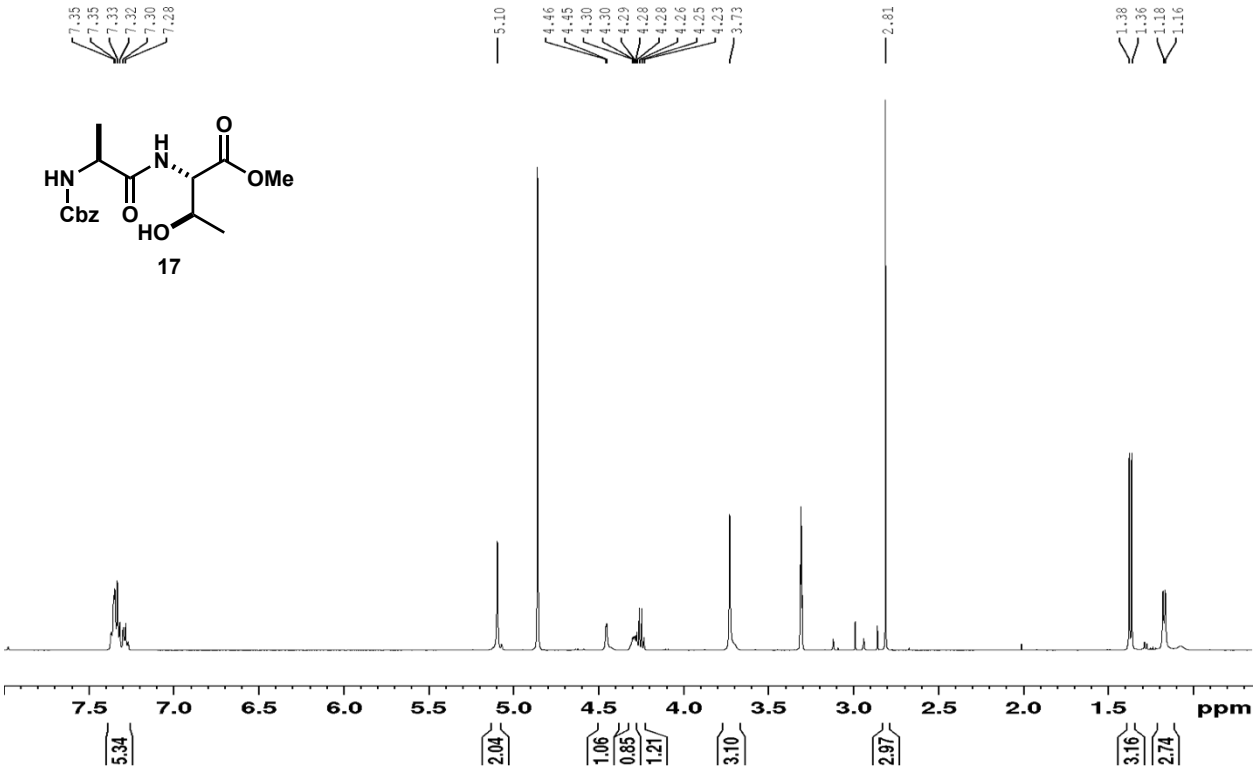

Spectrum 3.8.3 ^{1}H-NMR spectrum of compound **18** ($CDCl_3$, 500 MHz)

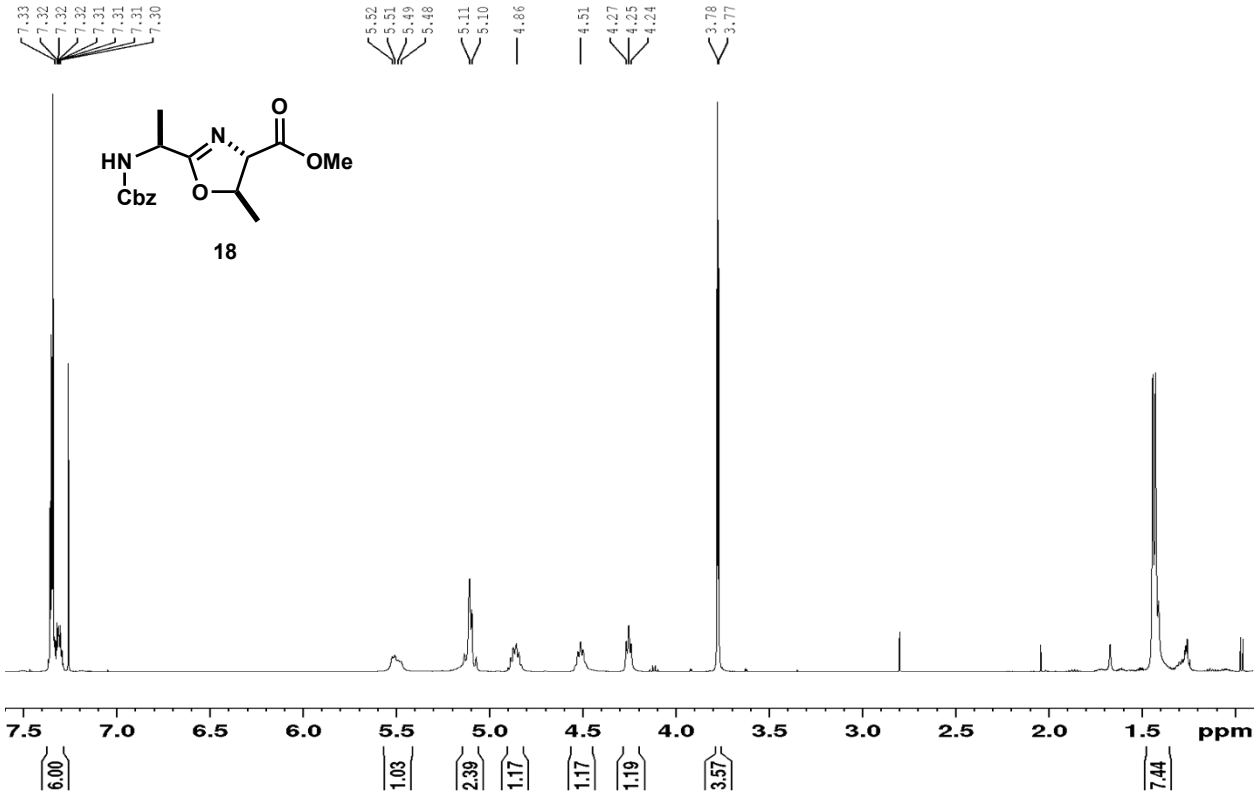

Spectrum 3.8.4 ^{13}C-NMR of compound **18** ($CDCl_3$, 125 MHz)

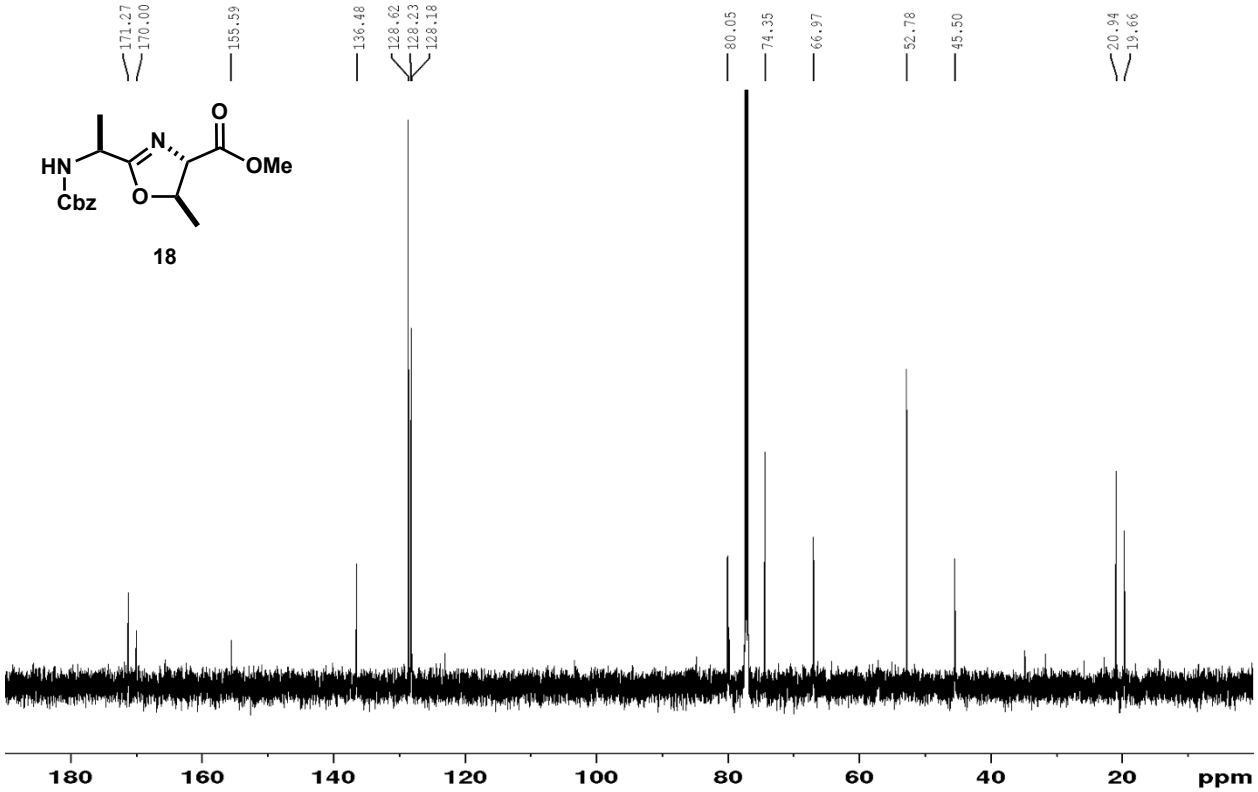

Spectrum 3.8.5 ^{1}H-NMR spectrum of compound **14** ($CDCl_3$, 500 MHz)

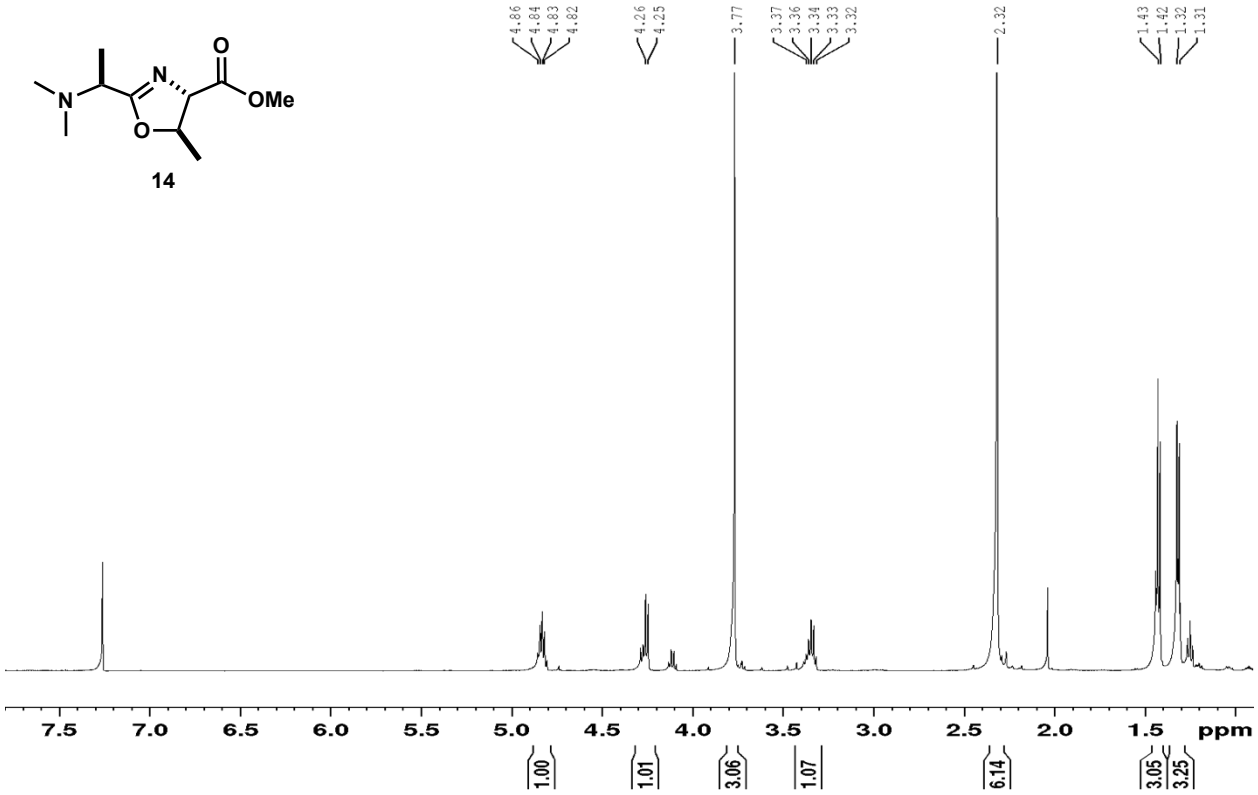

Spectrum 3.8 6 ^{1}H-NMR spectrum of compound **9** (methanol-d4, 500 MHz)

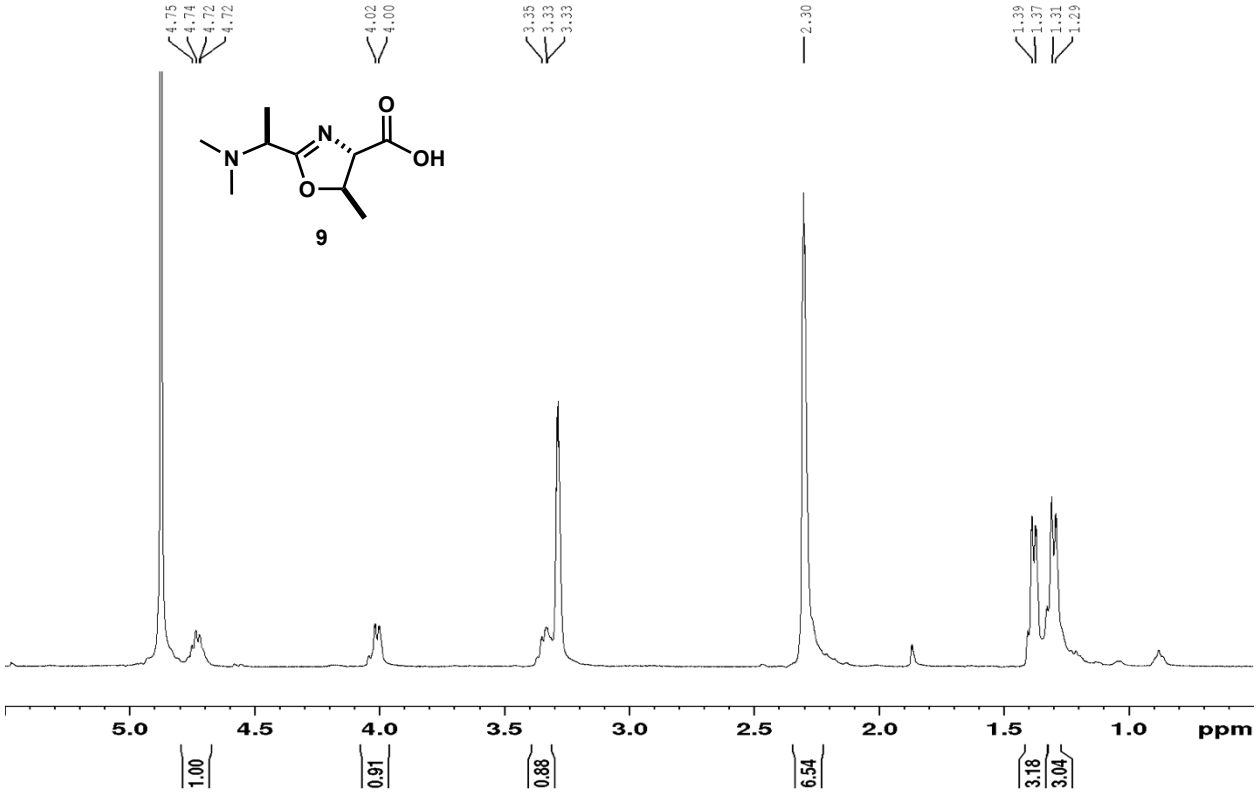

Spectrum 3.8.7 ^{1}H-NMR spectrum for compound **26** ($CDCl_3$, 400 MHz)

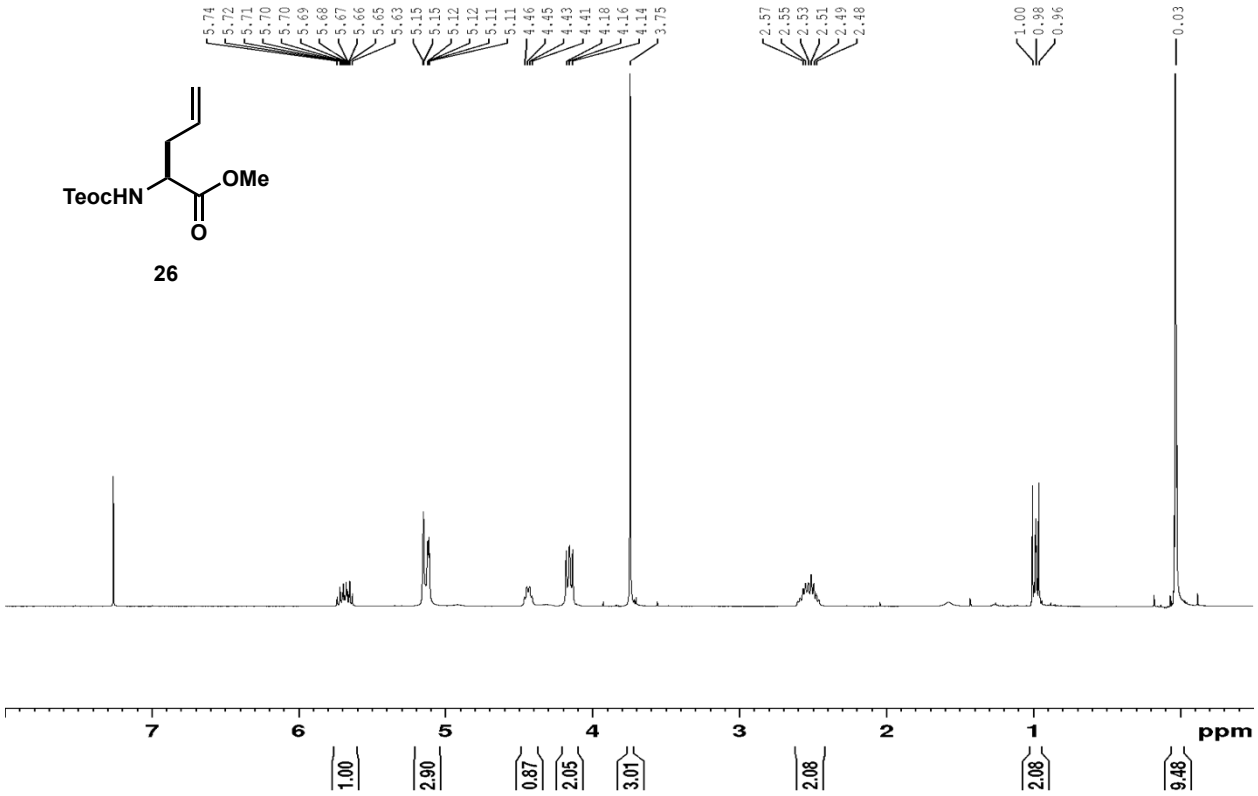

Spectrum 3.8.8 ^{1}H-NMR spectrum of compound **27** ($CDCl_3$, 400 MHz)

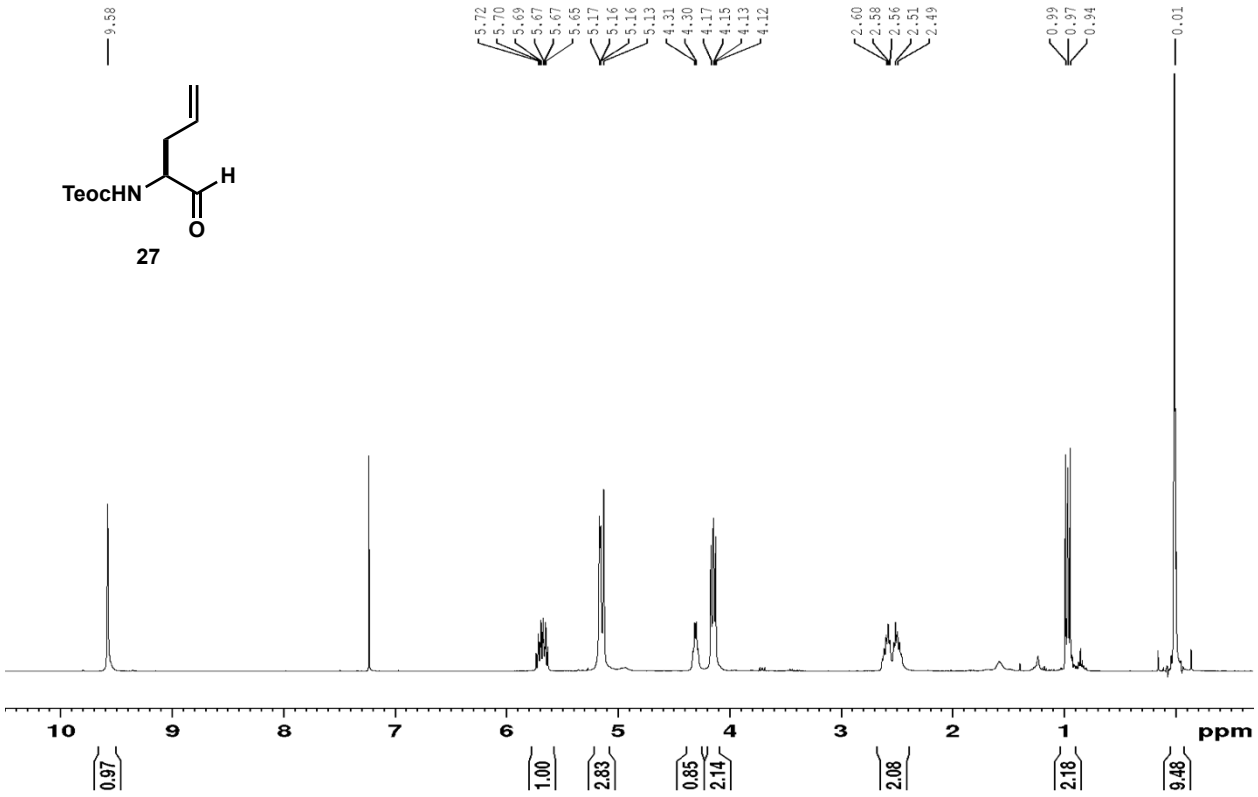

Spectrum 3.8.9 ^{1}H-NMR spectrum of compound **10** ($CDCl_3$, 400 MHz)

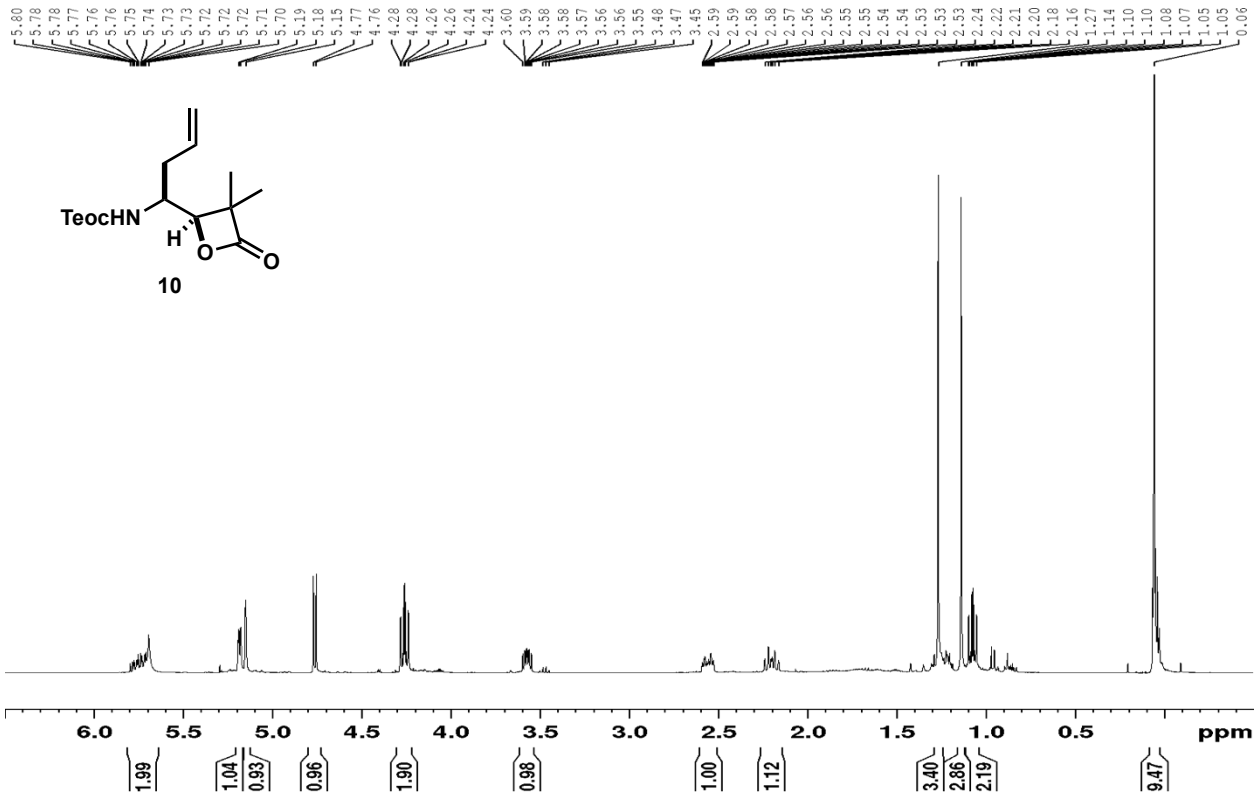

Spectrum 3.8.10 ^{13}C-NMr spectrum of compounds **10** ($CDCl_3$, 125 MHz)

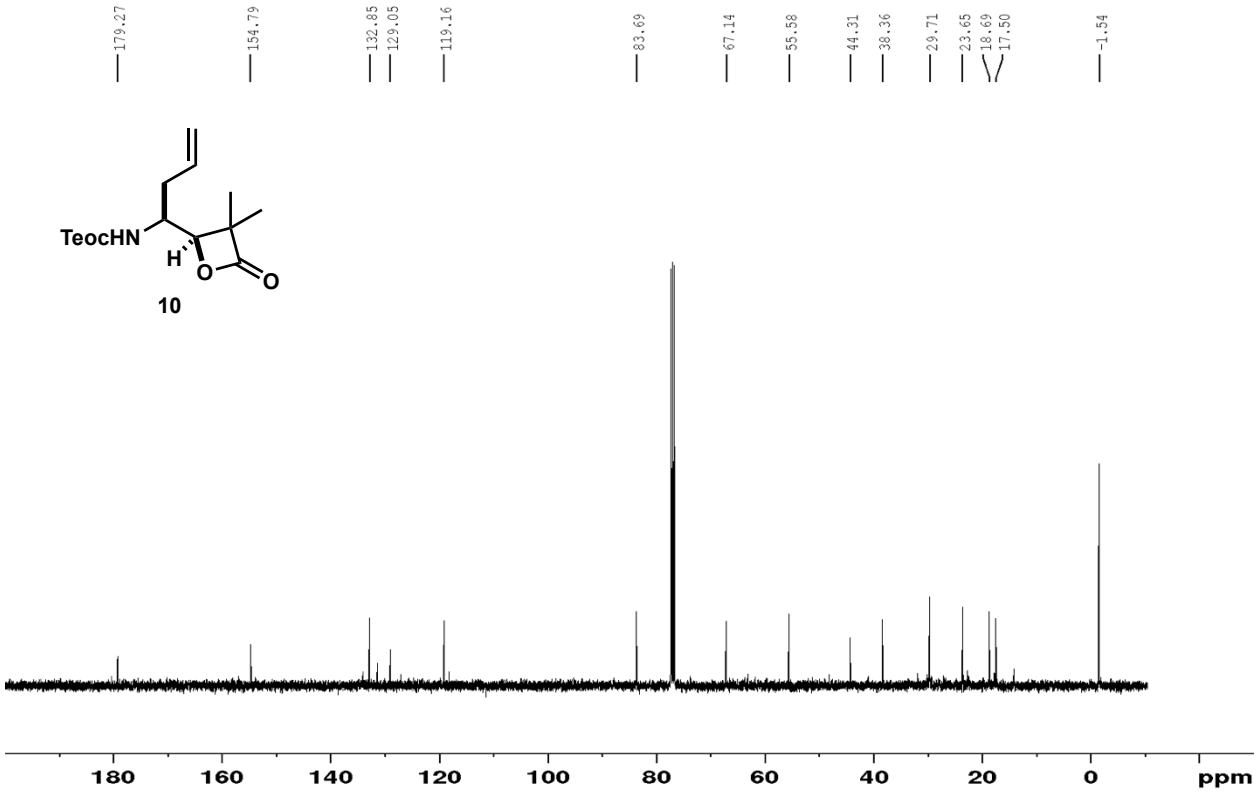

Spectrum 3.8.11 ^{1}H-NMR spectrum of compound **10'** ($CDCl_3$, 400 MHz)

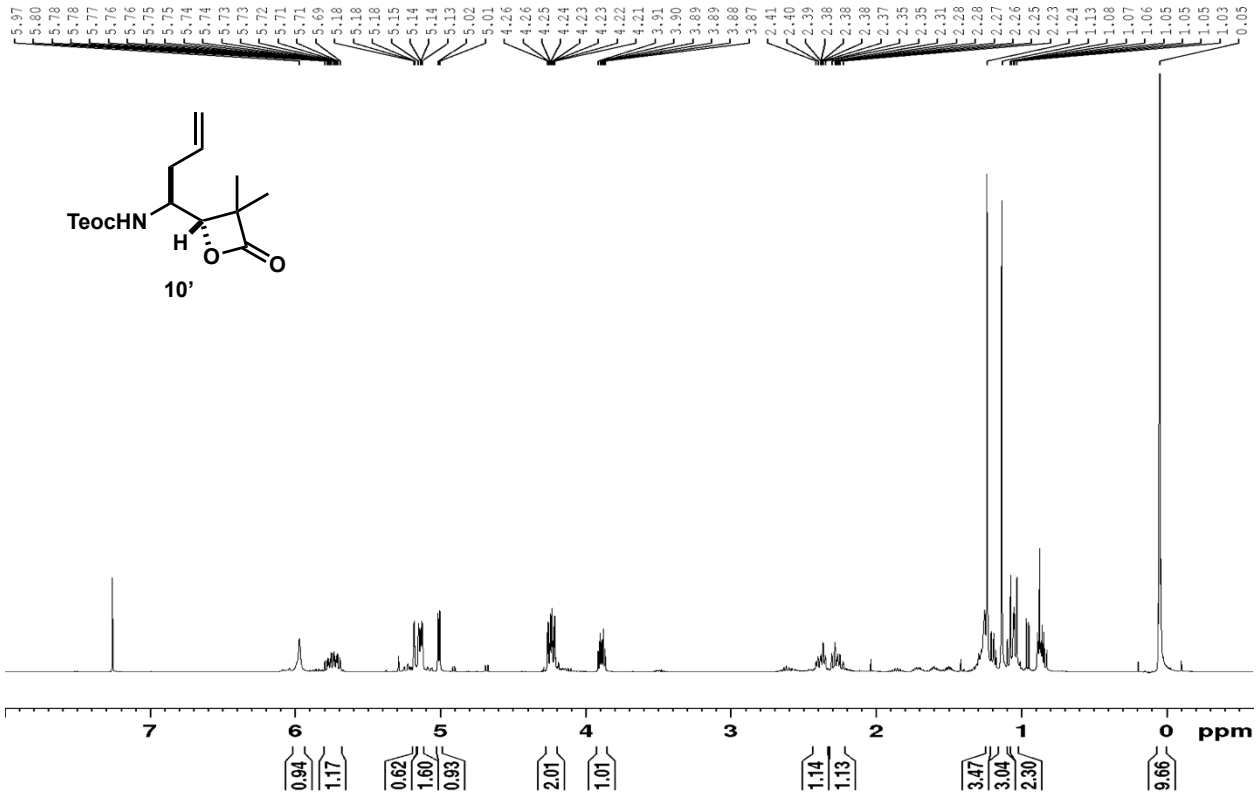

Spectrum 3.8.12 ^{13}C-NMR spectrum of compounds **10'** ($CDCl_3$, 125 MHz*)*

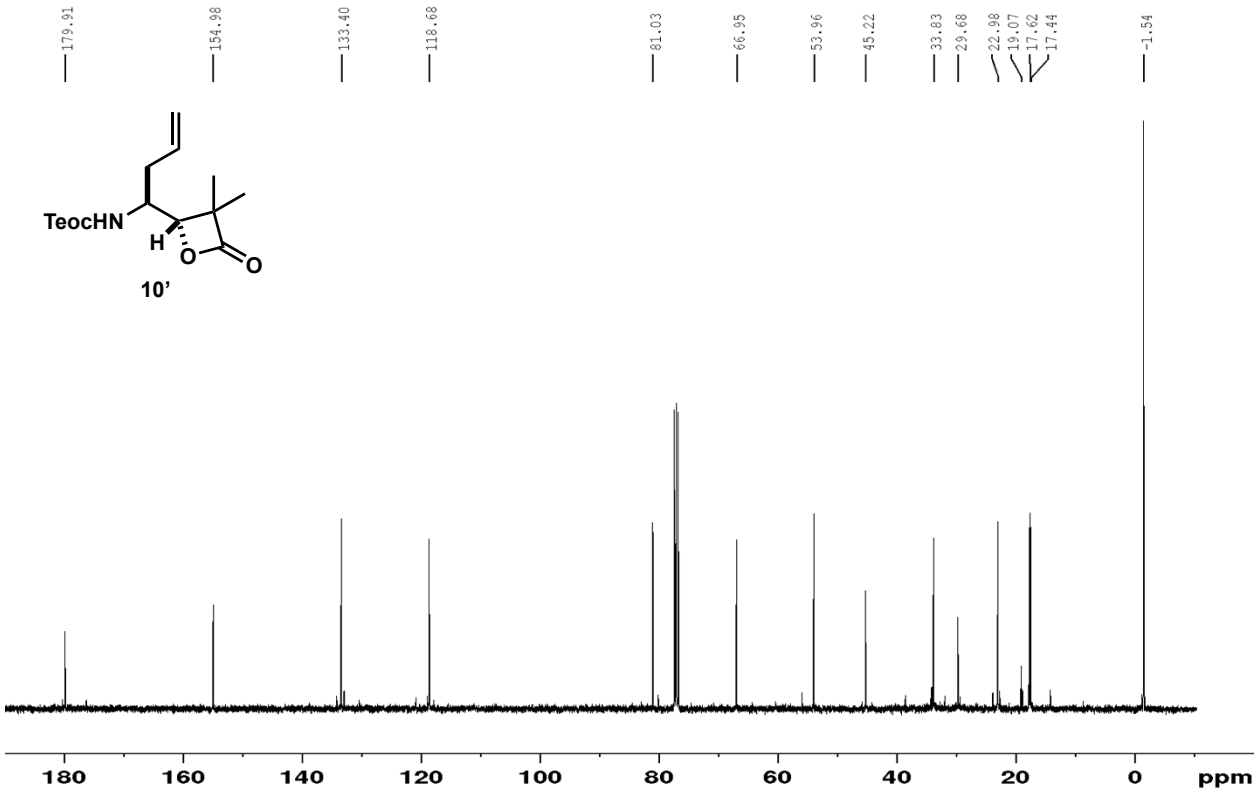

Spectrum 3.8.13 ^{1}H-NMR spectrum of compound **36** ($CDCl_3$, 500 MHz)

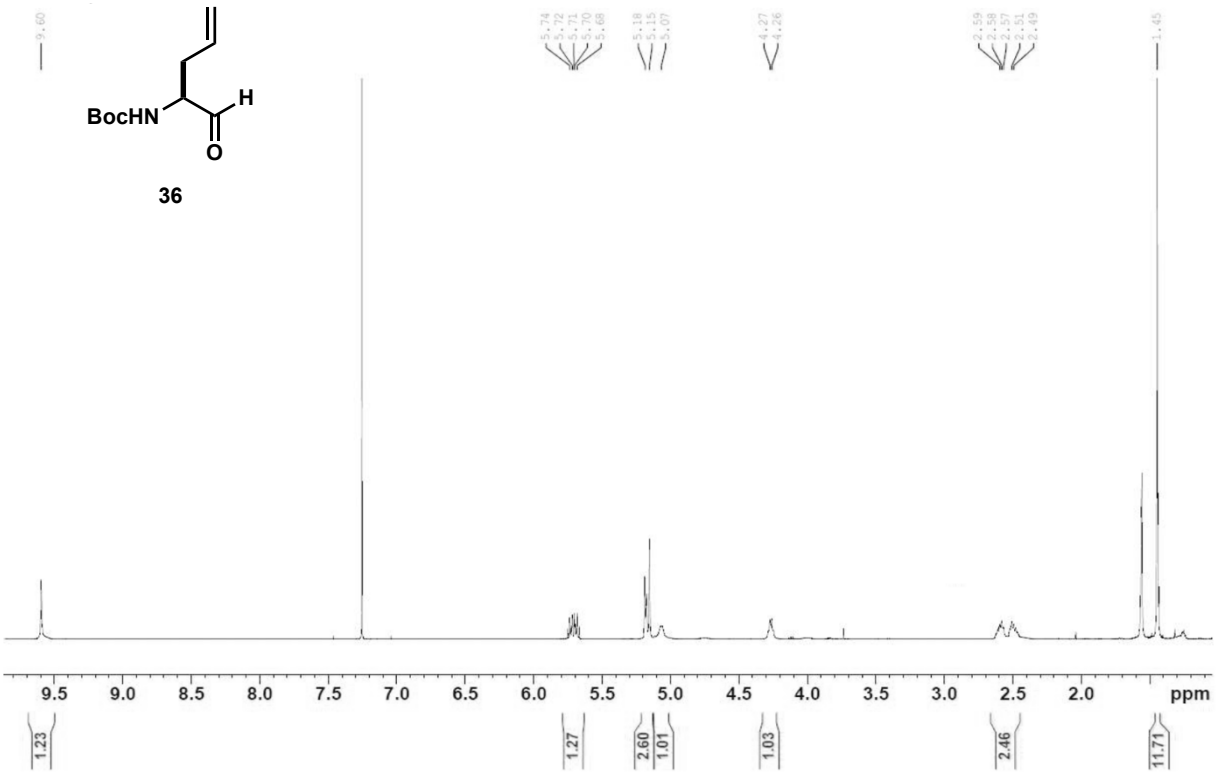

Spectrum 3.8.14 ^{1}H-NMR spectrum of compound **37** ($CDCl_3$, 500 MHz)

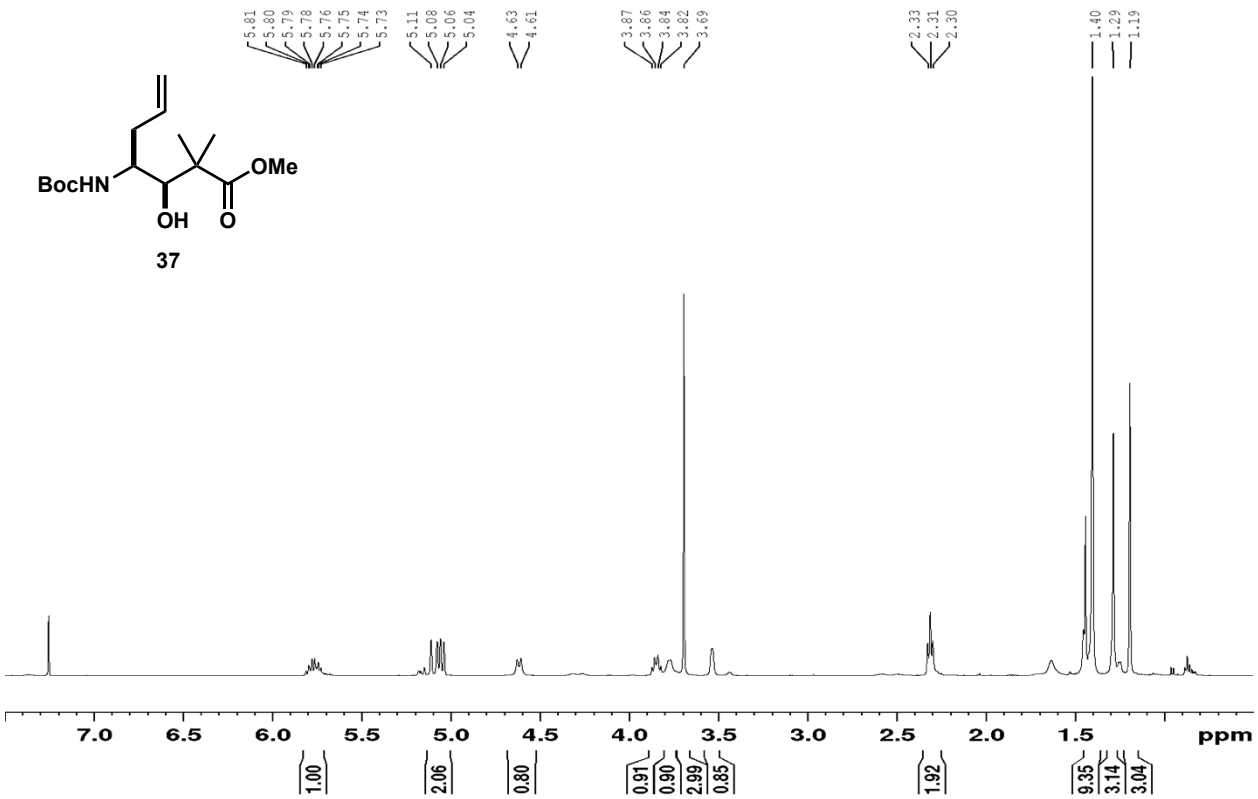

Spectrum 3.8.15 ^{13}C-NMR spectrum of compound **37** ($CDCl_3$, 125 MHz)

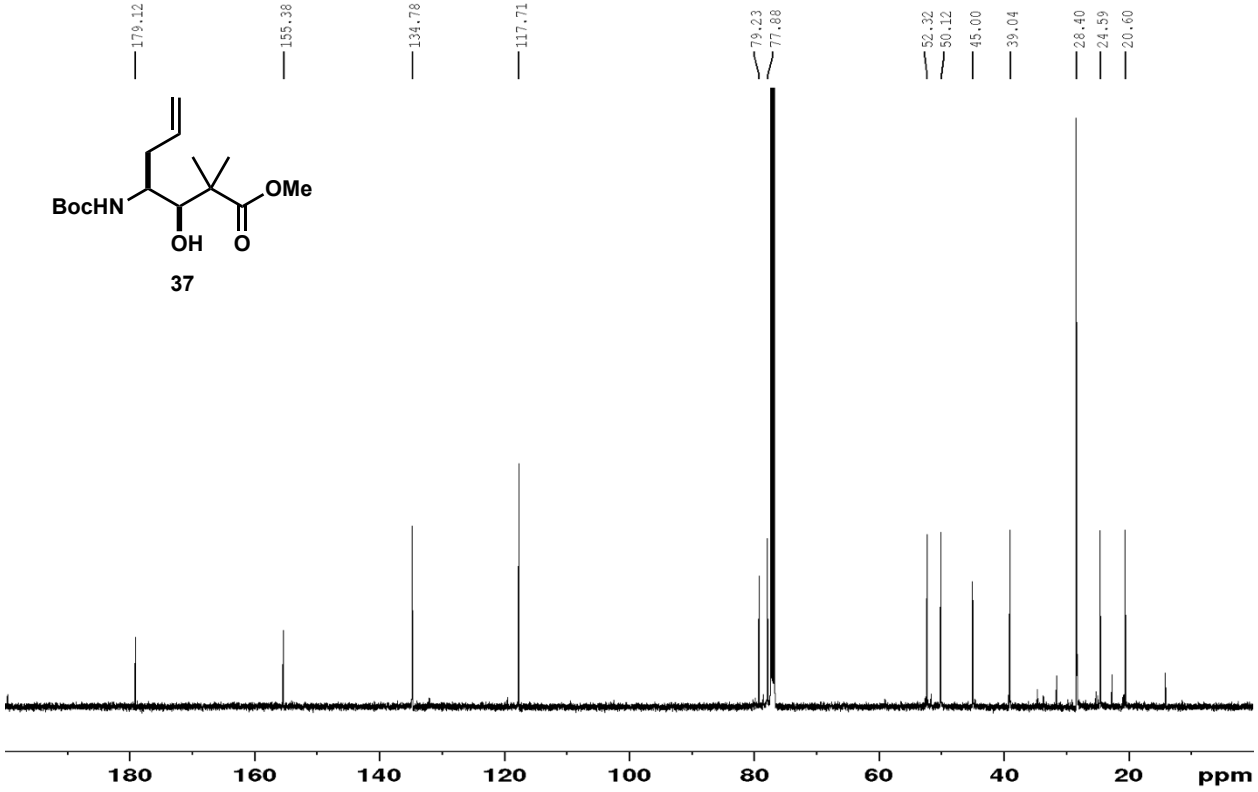

Spectrum 3.8.16 ^{1}H-NMR spectrum of compound **37'** ($CDCl_3$, 500 MHz)

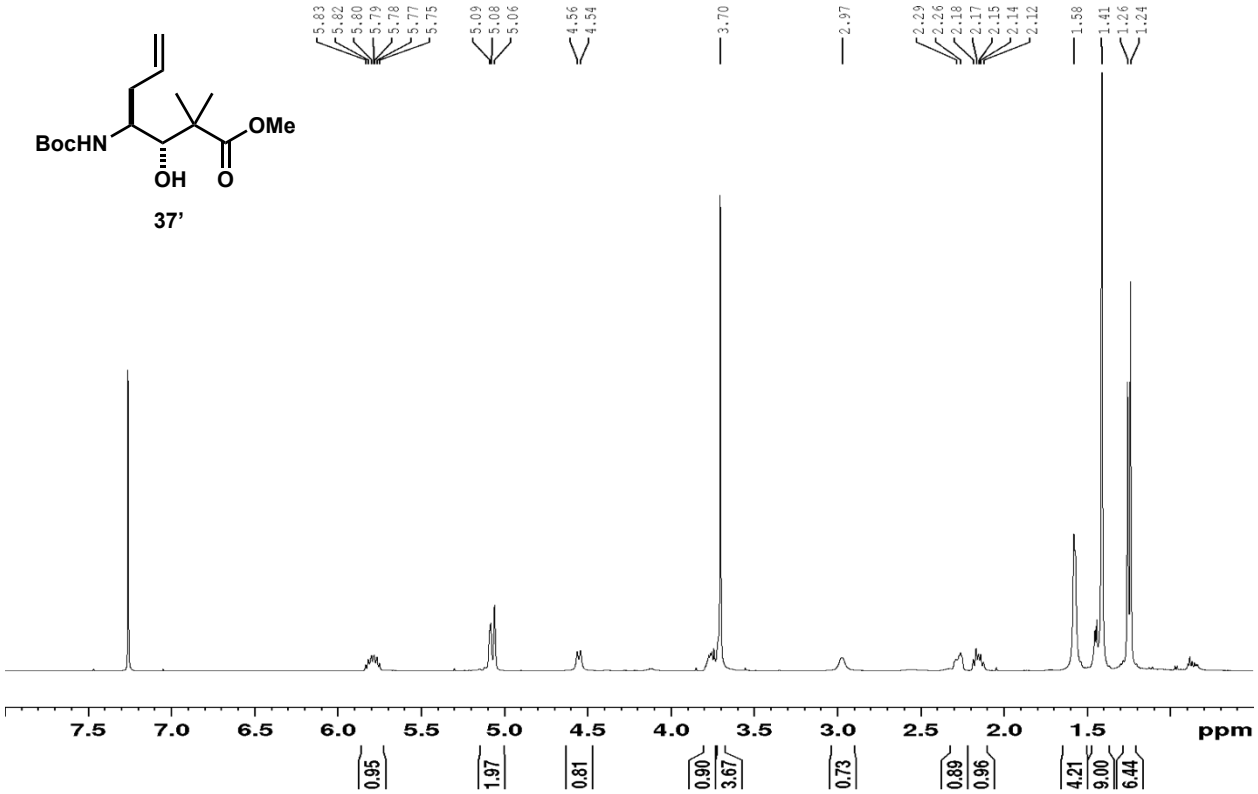

Spectrum 3.8.17 ^{13}C-NMR spectrum of compound **37** ($CDCl_3$, 125 MHz)

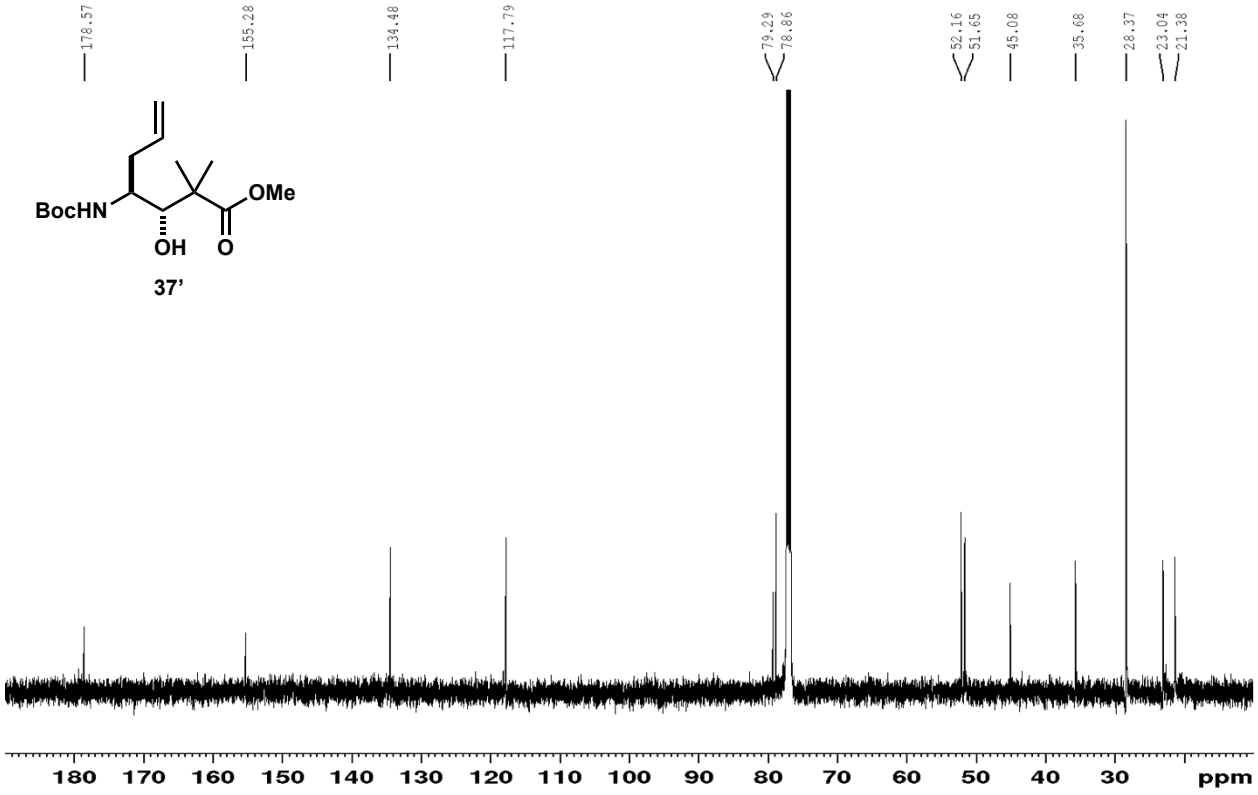

Spectrum 3.8.18 ^{1}H-NMR spectrum of compound **38** (methanol-d4, 500 MHz)

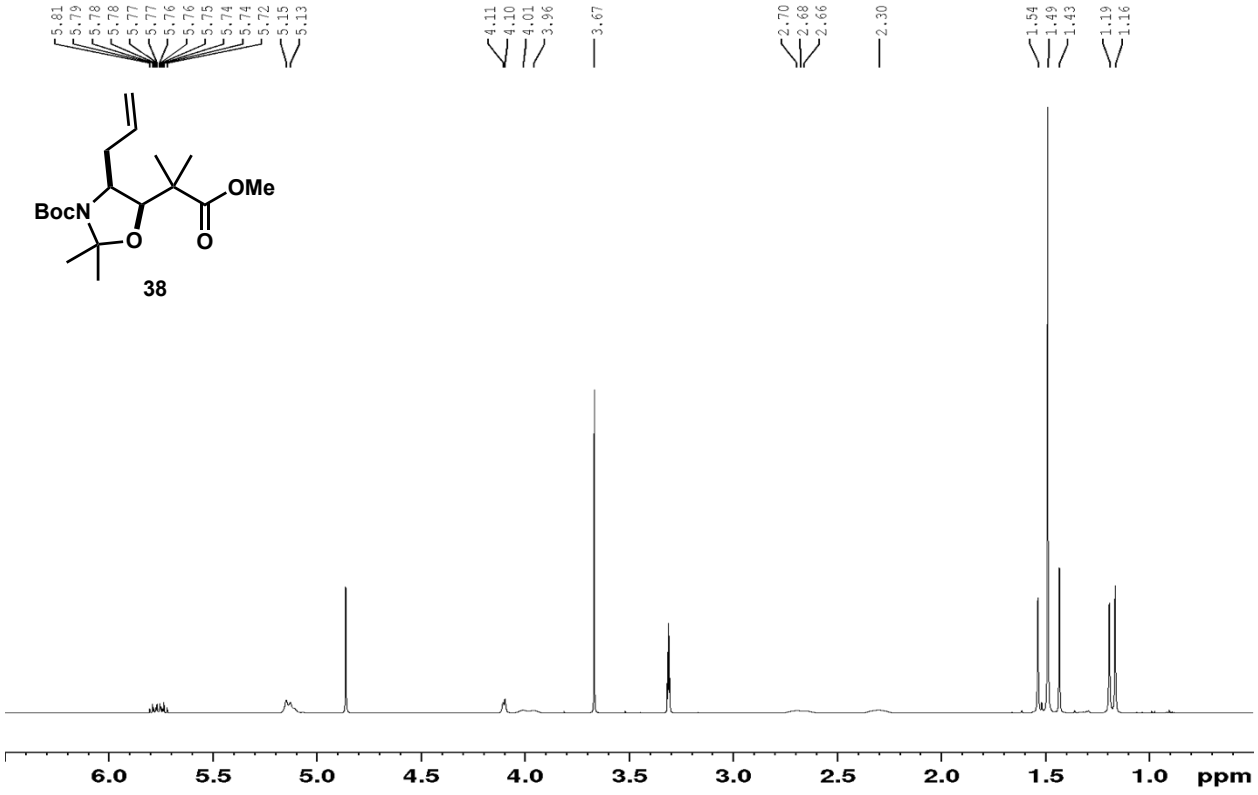

Spectrum 3.8.19 13C-NMR of compound **38** (methanol-d4, 125 MHz)

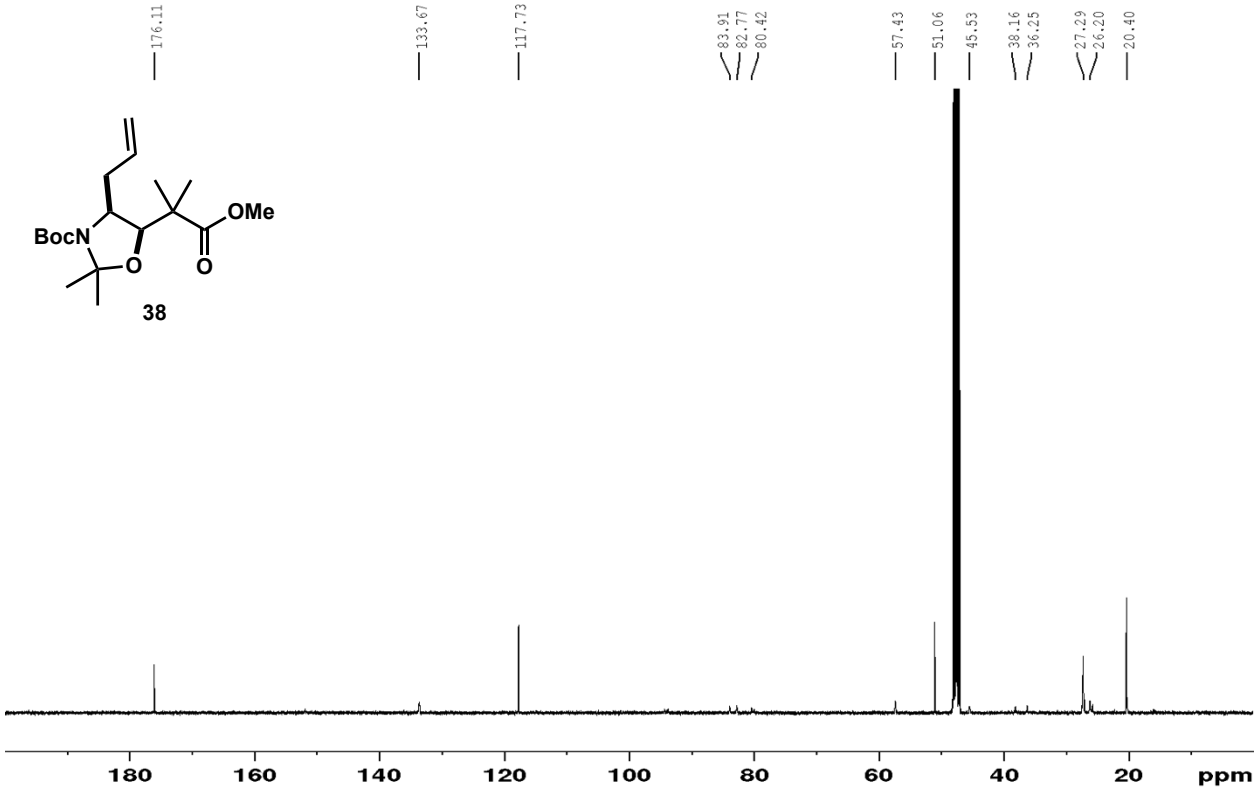

Spectrum 3.8.20 ^{1}H-NMR spectrum of compound **34** (DMSO-d6, 500 MHz)

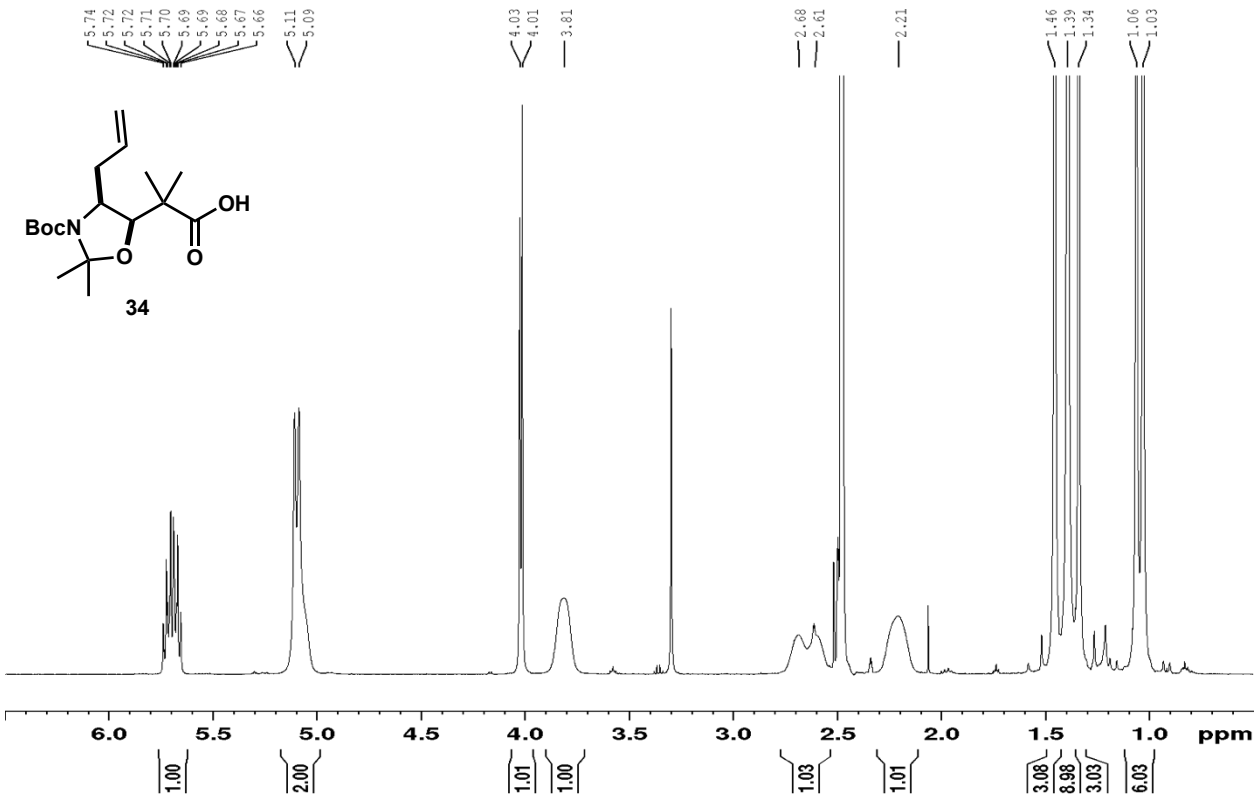

Spectrum 3.8.21 ^{13}C-NMR spectrum of compound **34** (DMSO-d6, 125 MHz)

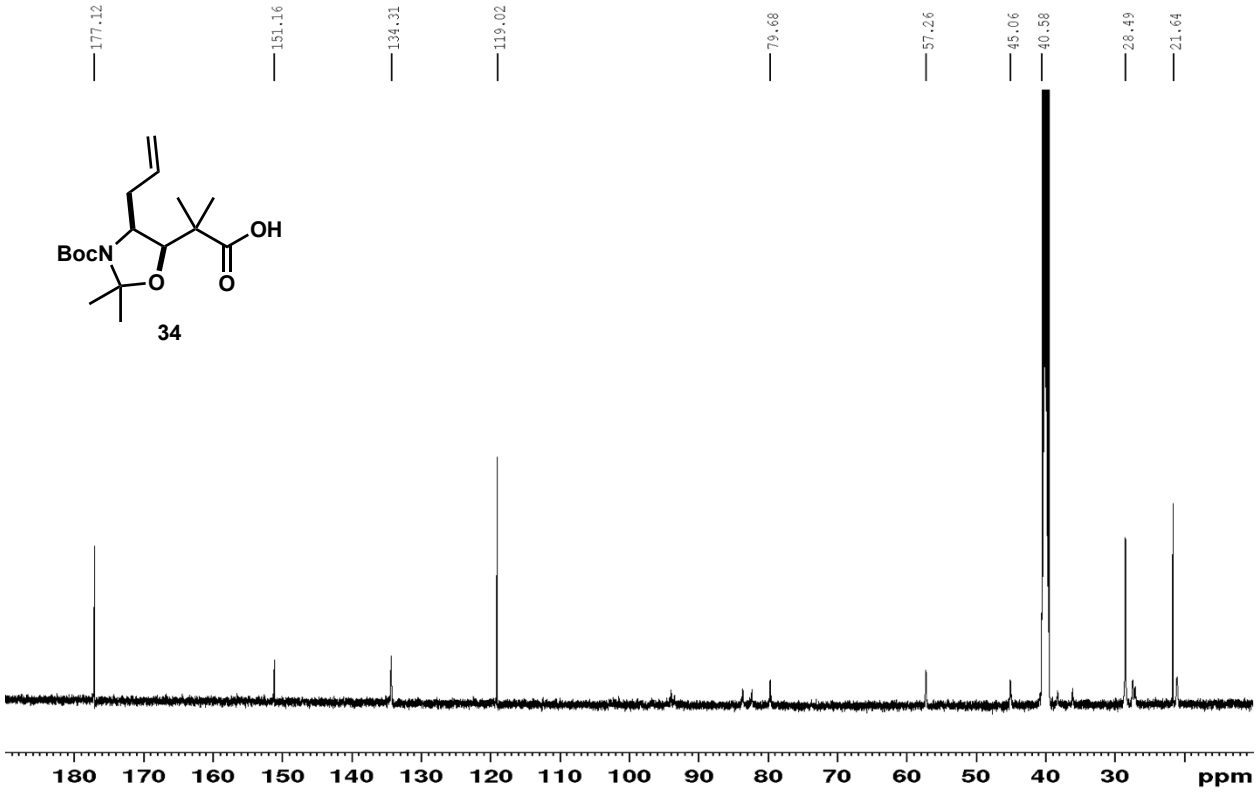

Spectrum 3.8.22 ^{1}H-NMR spectrum of compound **44** ($CDCl_3$, 400 MHz)

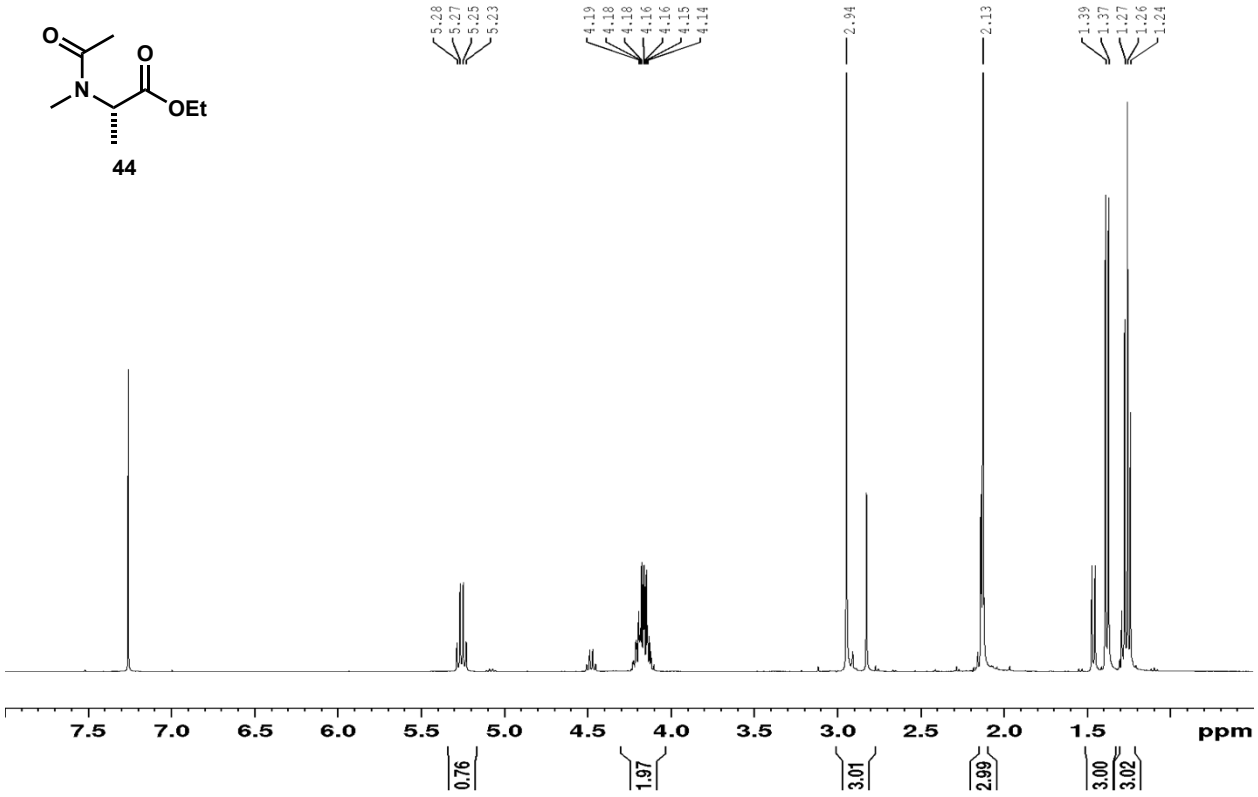

Spectrum 3.8.23 ^{1}H-NMR spectrum of compound **39** ($CDCl_3$, 500 MHz)

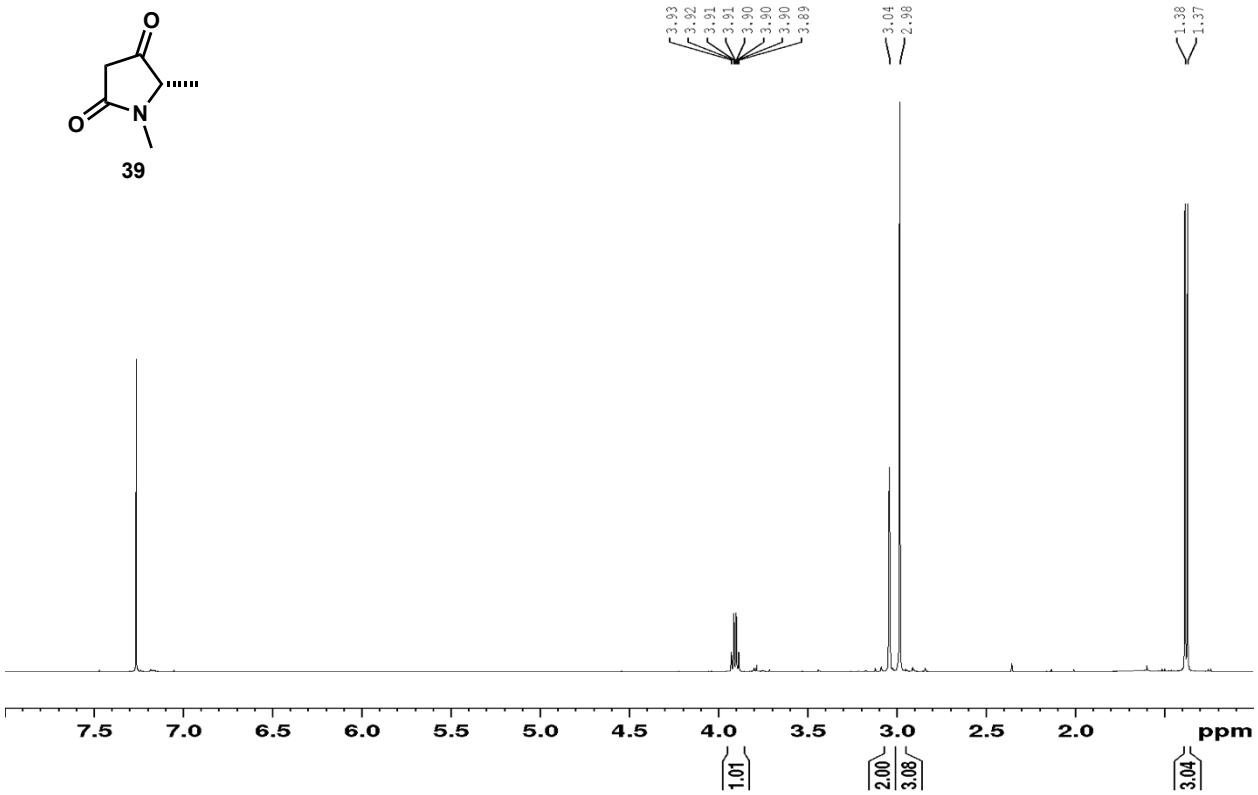

Spectrum 3.8.24 ^{13}C-NMR spectrum of compound **39** ($CDCl_3$, 125 MHz)

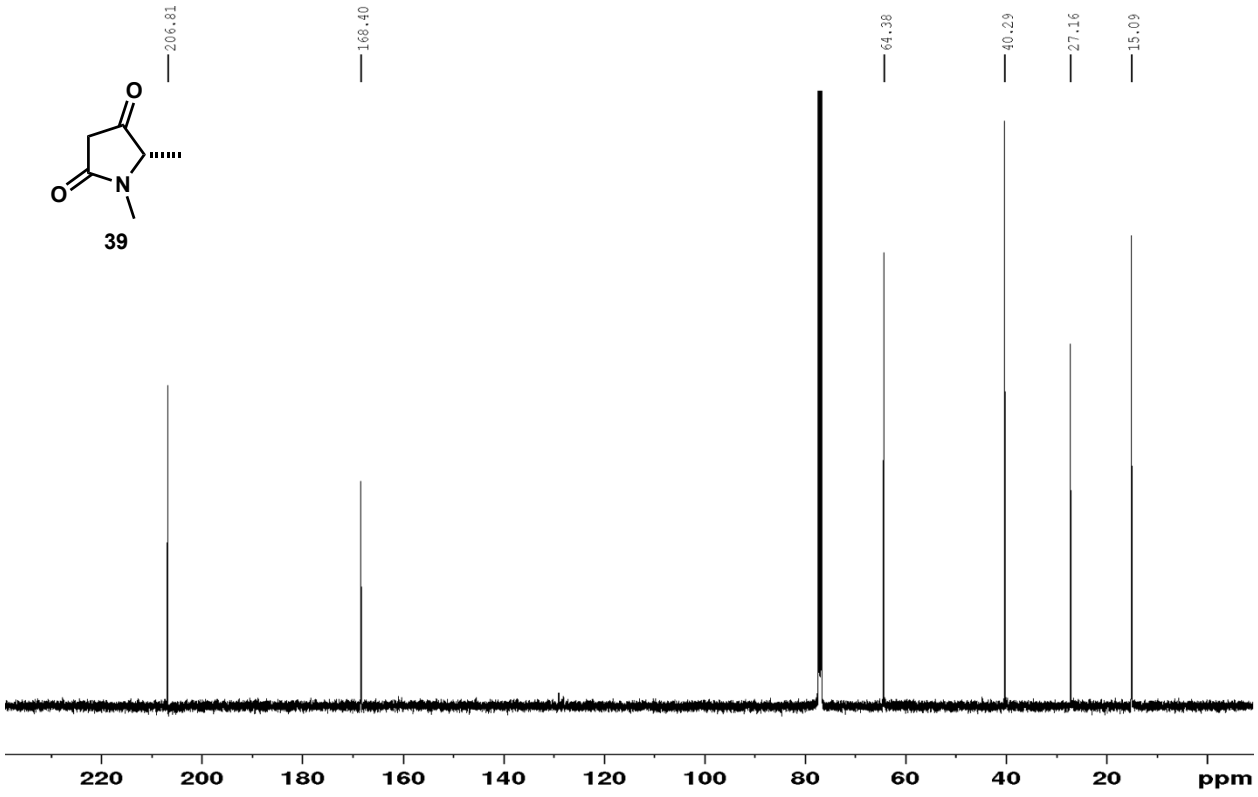

Spectrum 3.8.25 ^{1}H-NMR of compound **46** (CDCl3, 500 MHz)

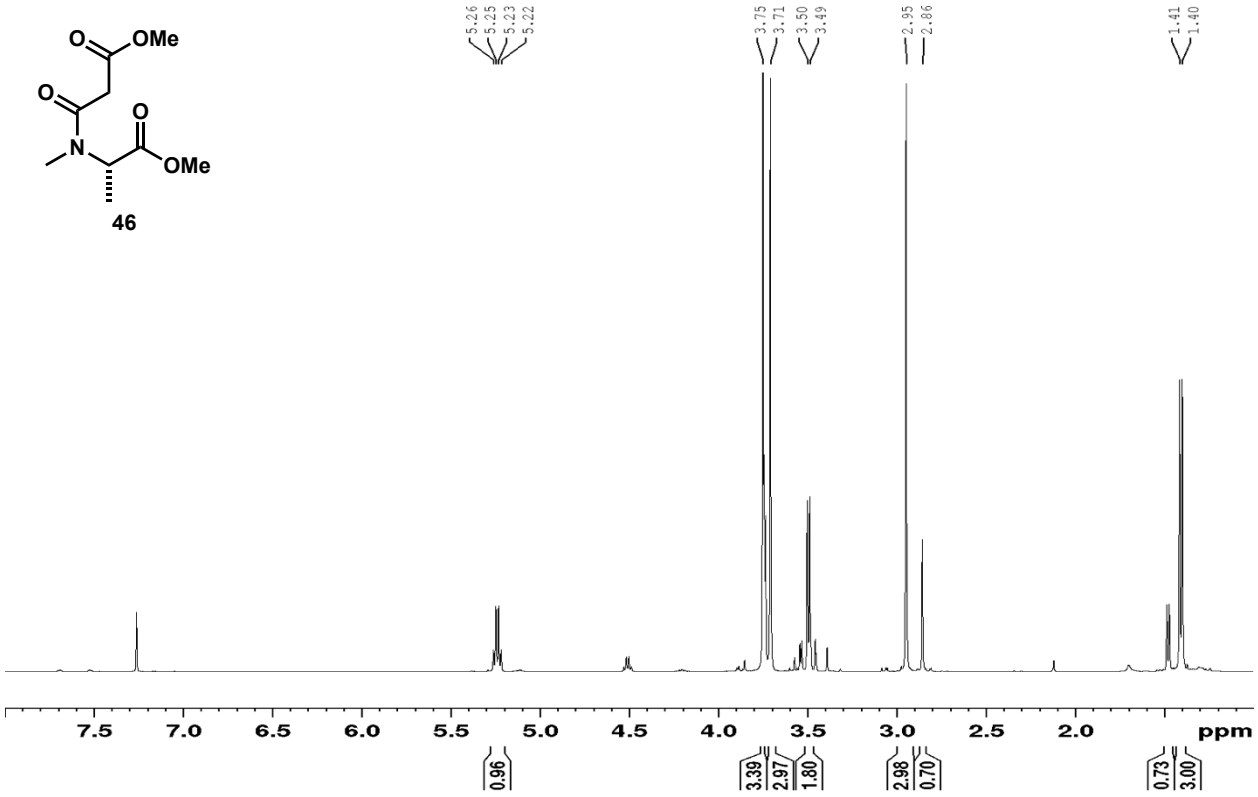

Spectrum 3.8.26 ^{13}C-NMR of compound **46** ($CDCl_3$, 125 MHz)

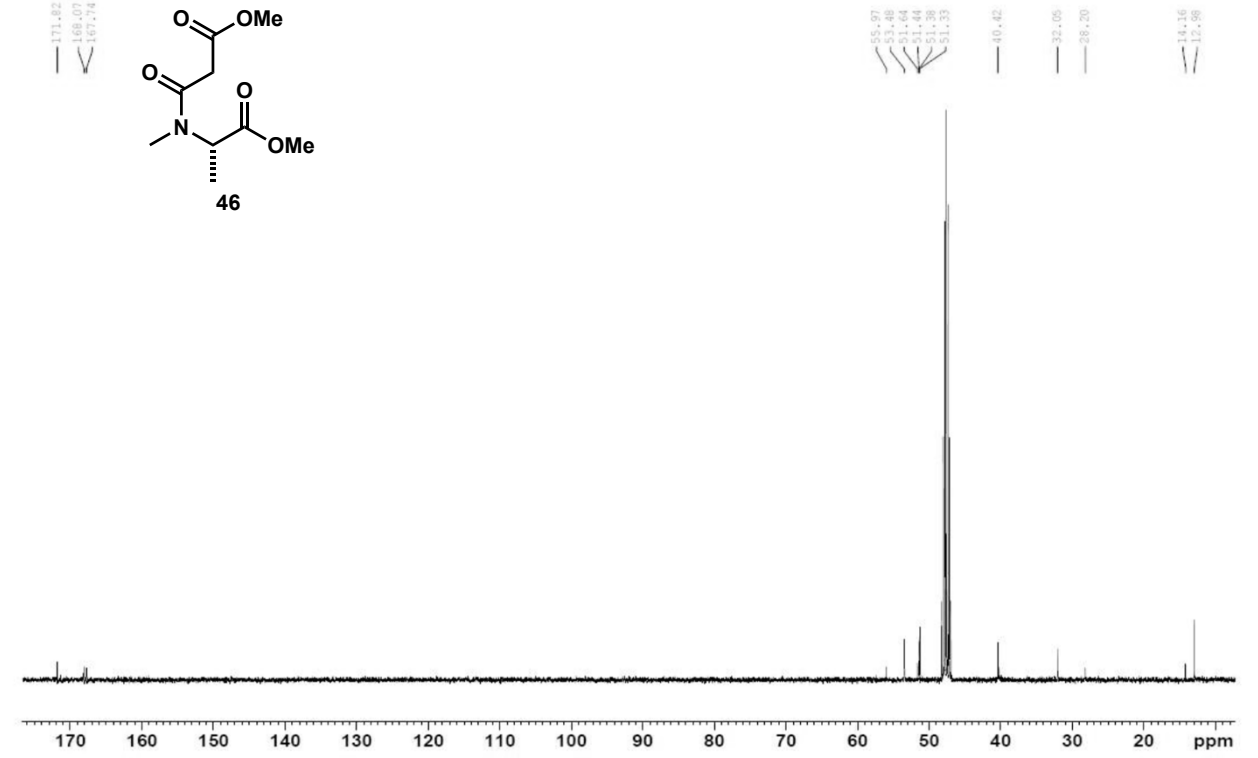

Spectrum 3.8.27 ^{1}H-NMR spectrum of compound **47** (CDCl4, 500 MHz)

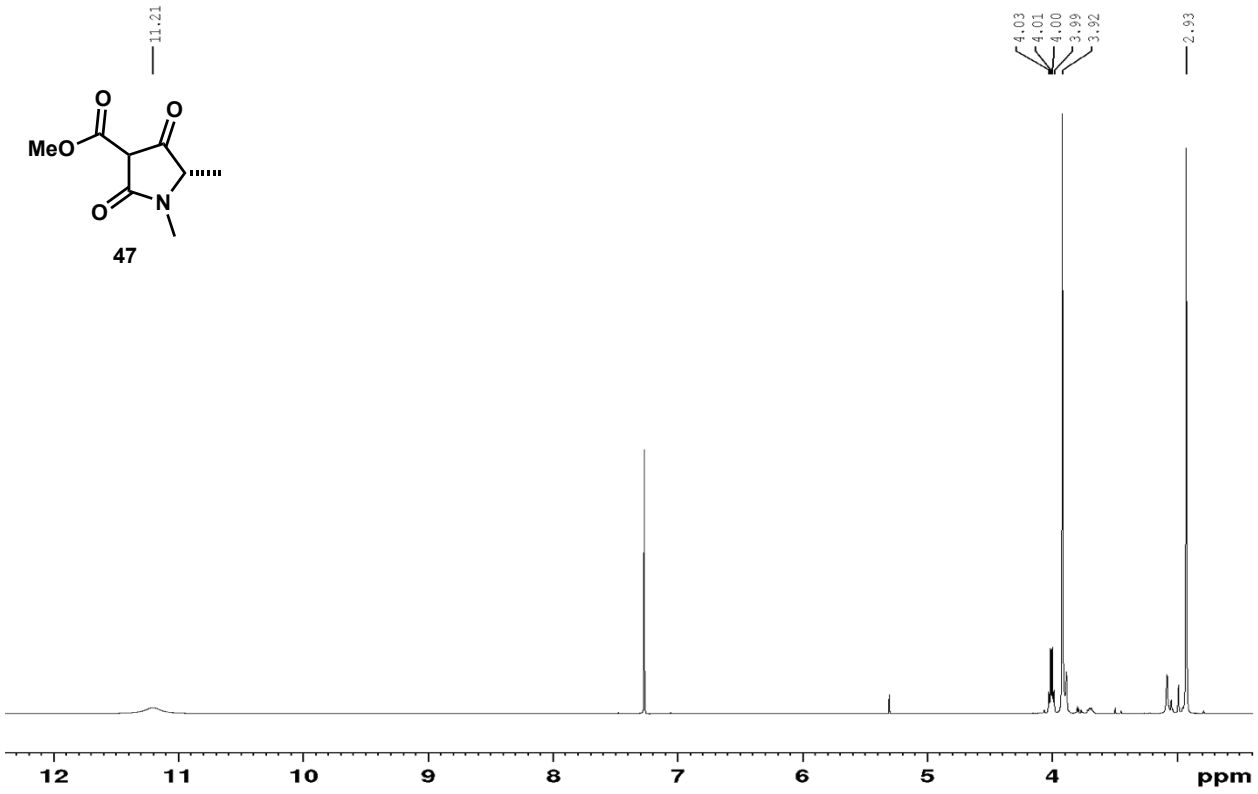

Spectrum 3.8.28 ^{1}H-NMR spectrum of compound **53** ($CDCl_3$, 500 MHz)

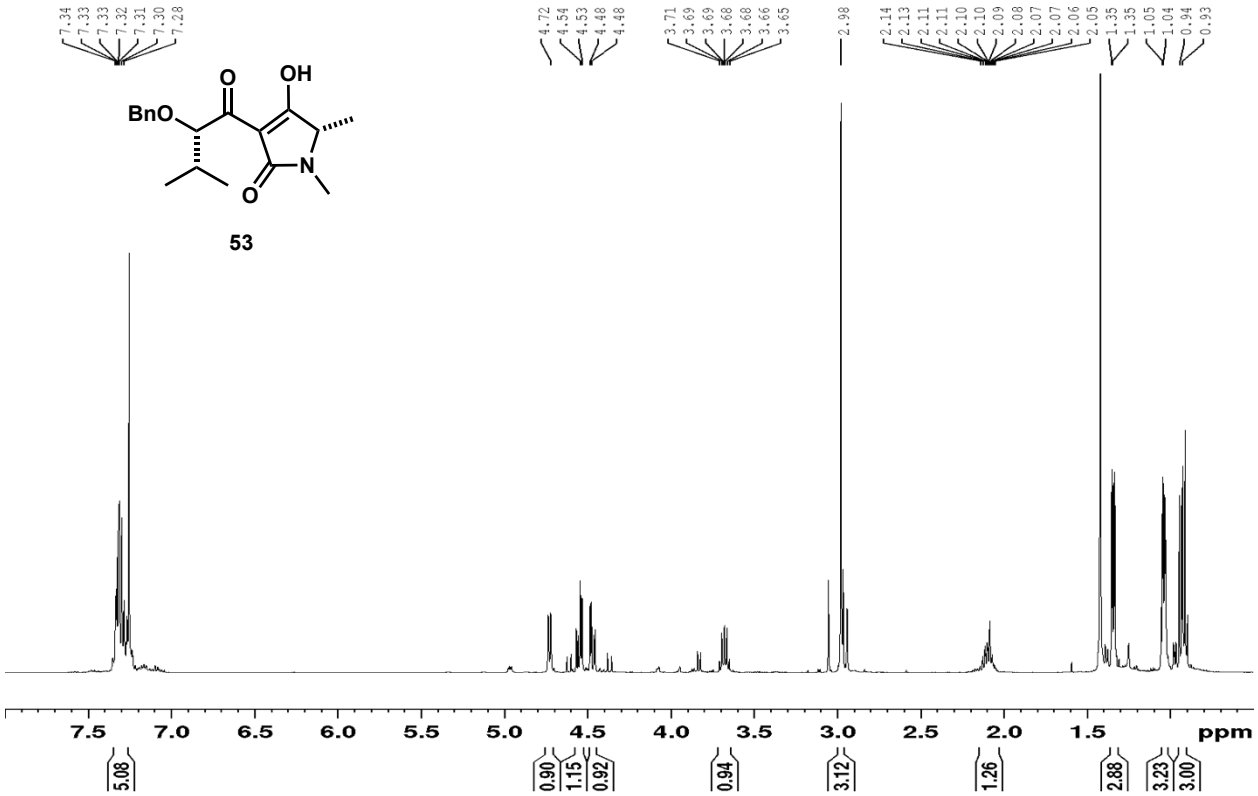

Spectrum 3.8.29 ^{13}C-NMR spectrum of compound **53** ($CDCl_3$, 125 MHz)

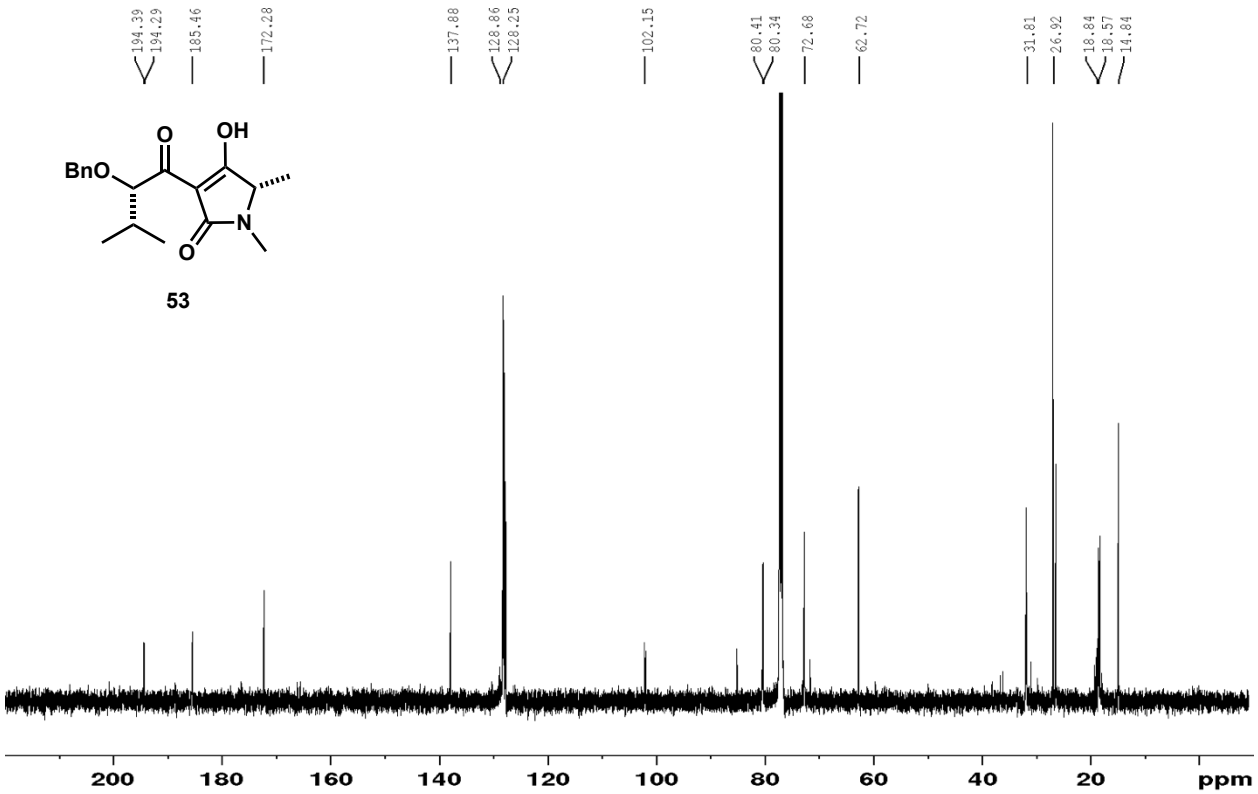

Spectrum 3.8.30 ^{1}H-NMR spectrum of compound **6** (methanol-d4, 500 MHz)

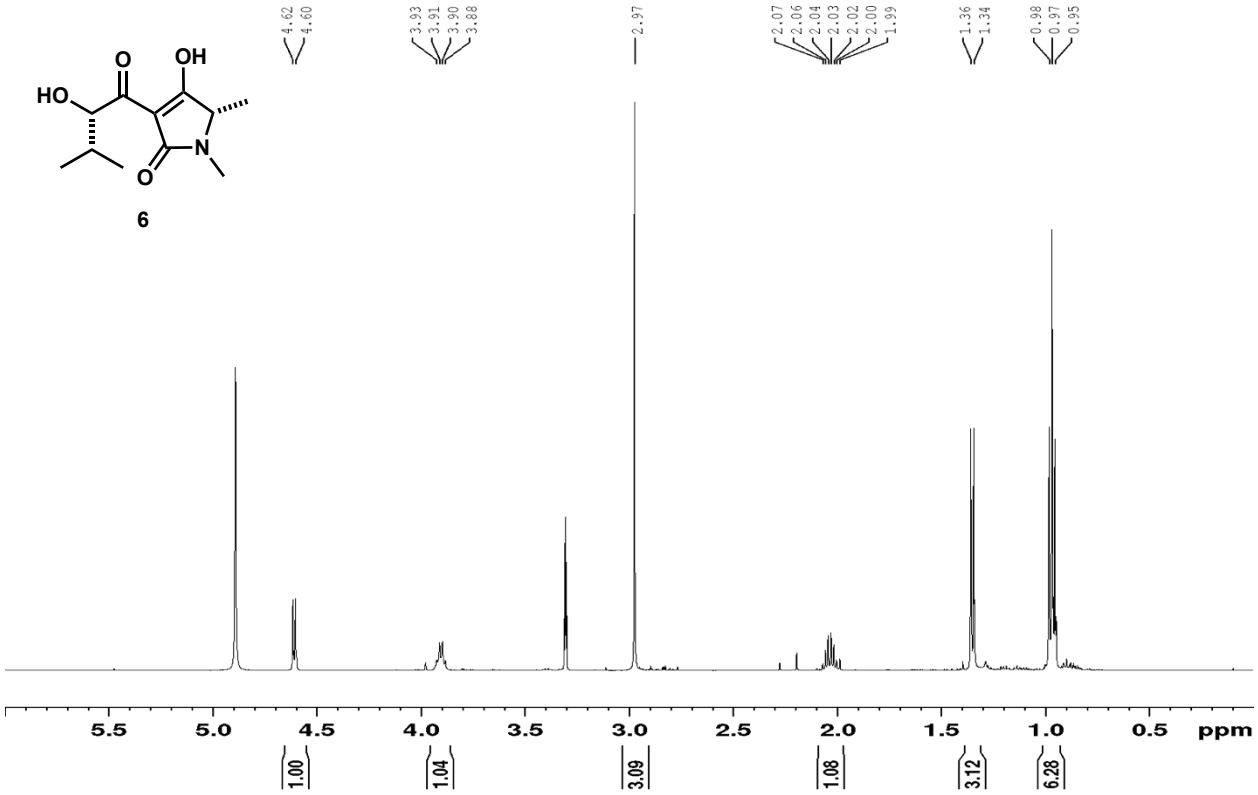

Spectrum 3.8.31 ^{13}C-NMR spectrum of compound **6** (methanol-d4, 125 MHz)

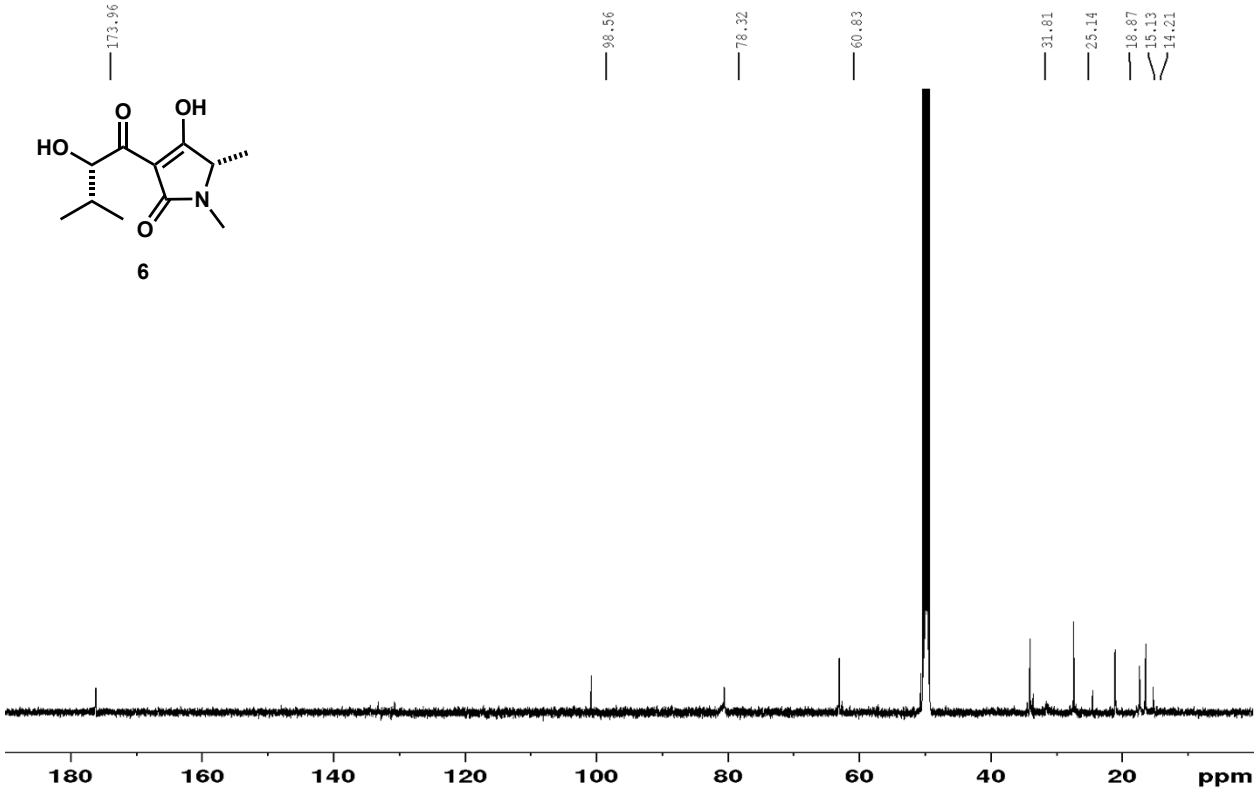

Spectrum 3.8.32 ^{1}H-NMR spectrum of compound **54** ($CDCl_3$, 500 MH)

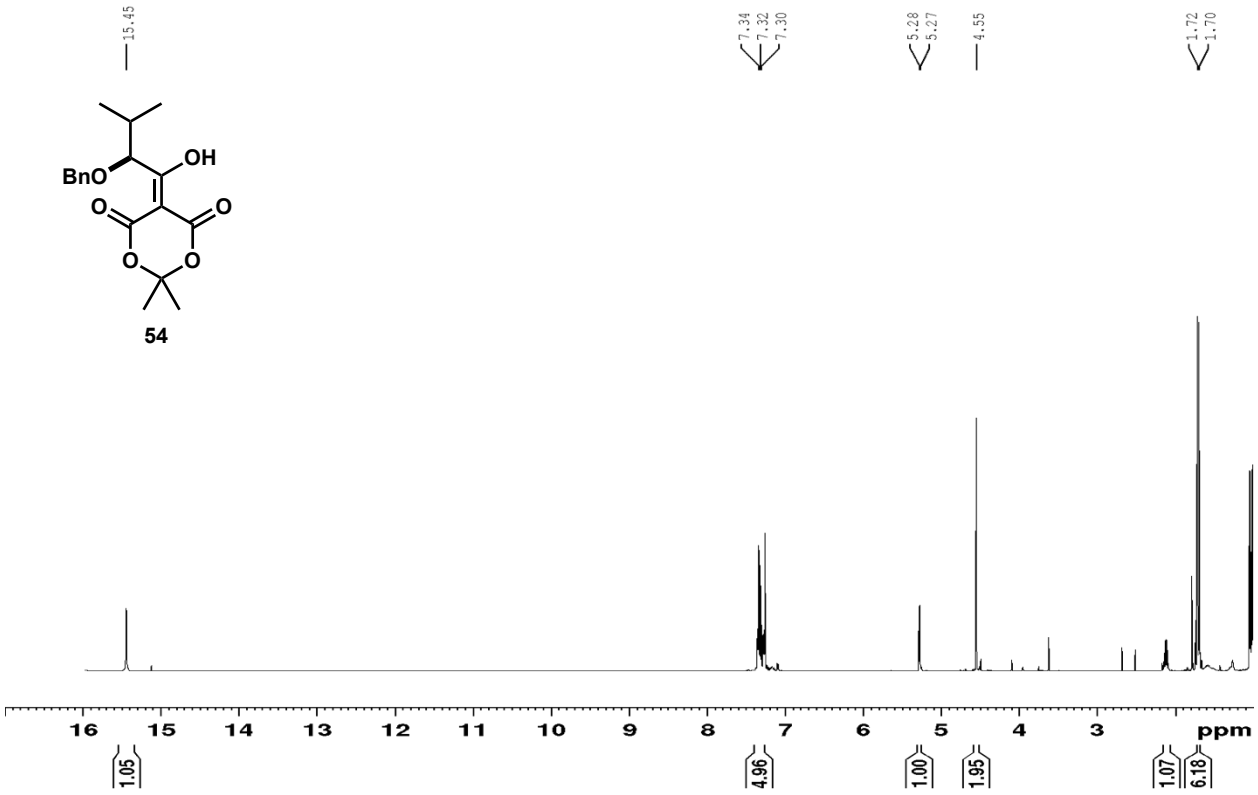

Spectrum 3.8.33 ^{1}H-NMR of compound **56** (DMSO-d6, 500 MHz)

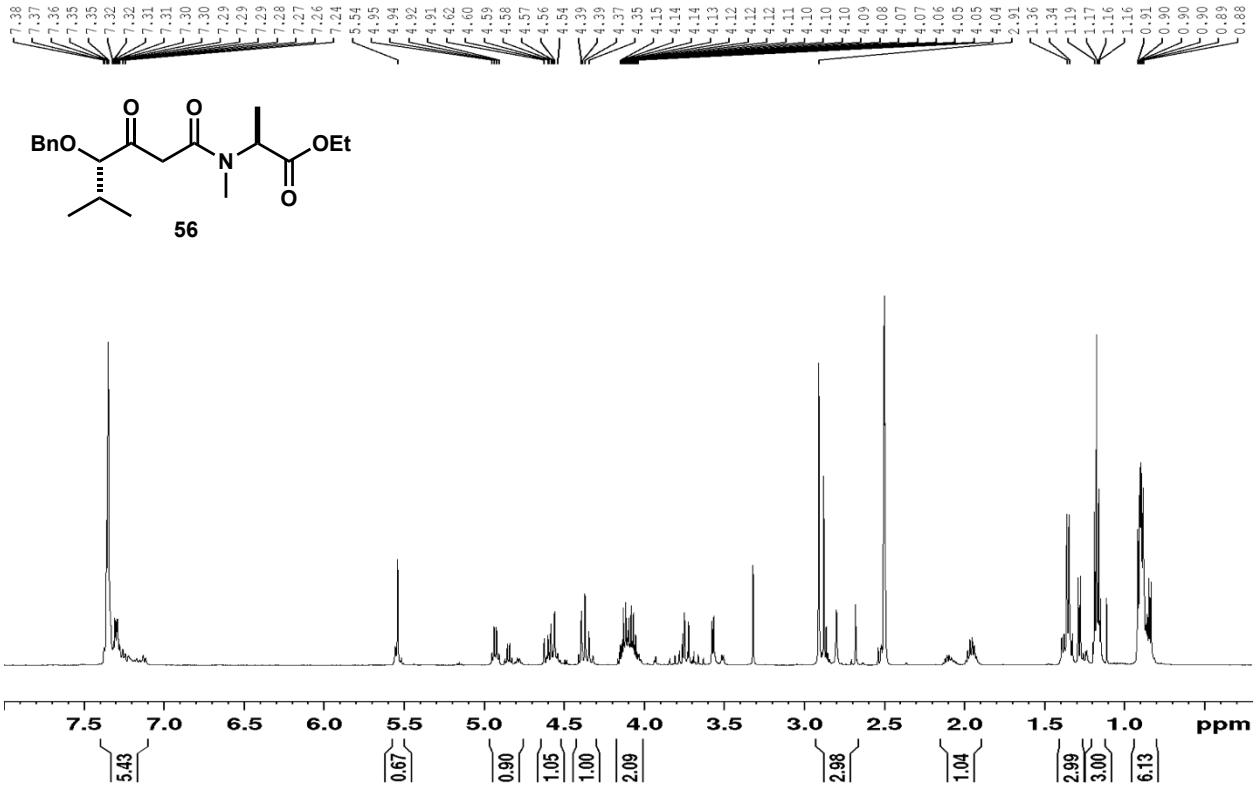

Spectrum 3.8.34 ^{13}C-NMR spectrum of compound **56** (DMSO-d6, 125 MHz)

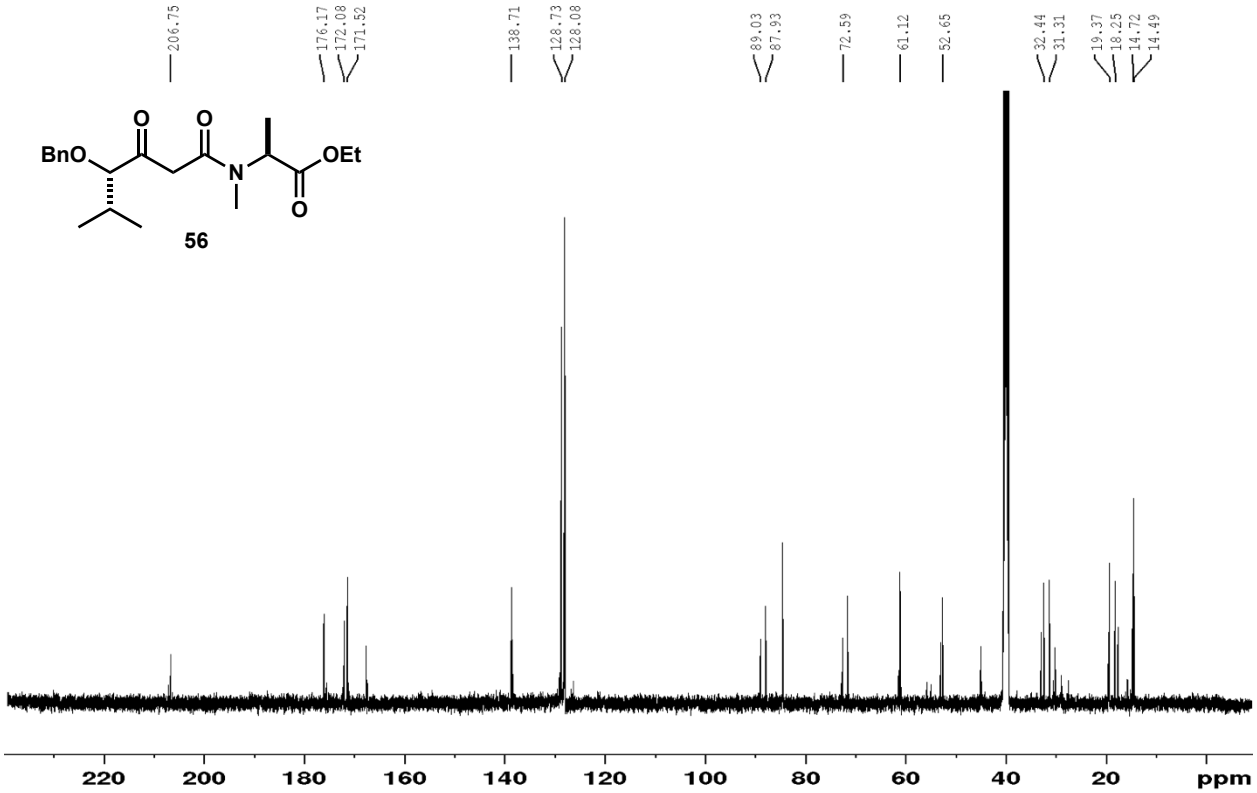

Spectrum 3.8.35 ^{1}H-NMR of compound **6'** (DMSO-d6, 500 MHz)

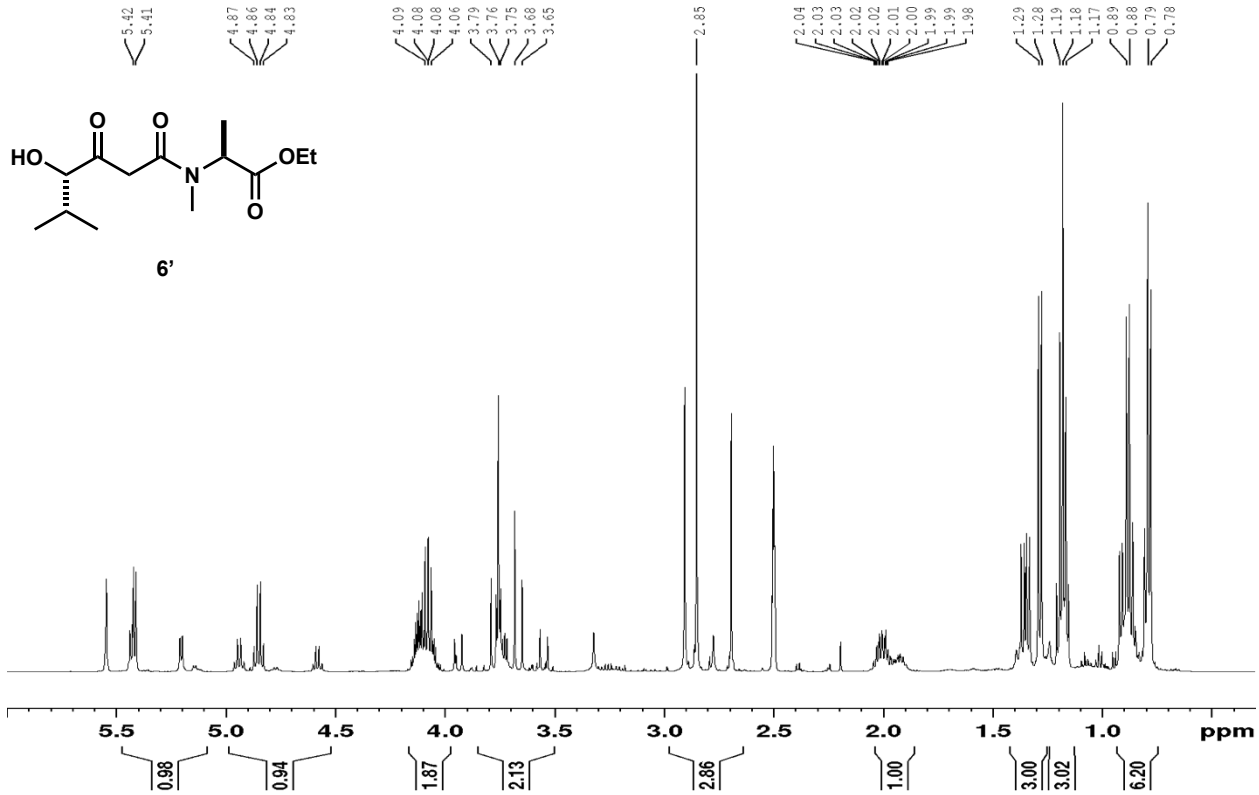

Spectrum 3.8.36 ^{13}C-NMR of compound **6'** (DMSO-d6, 125 MHz)

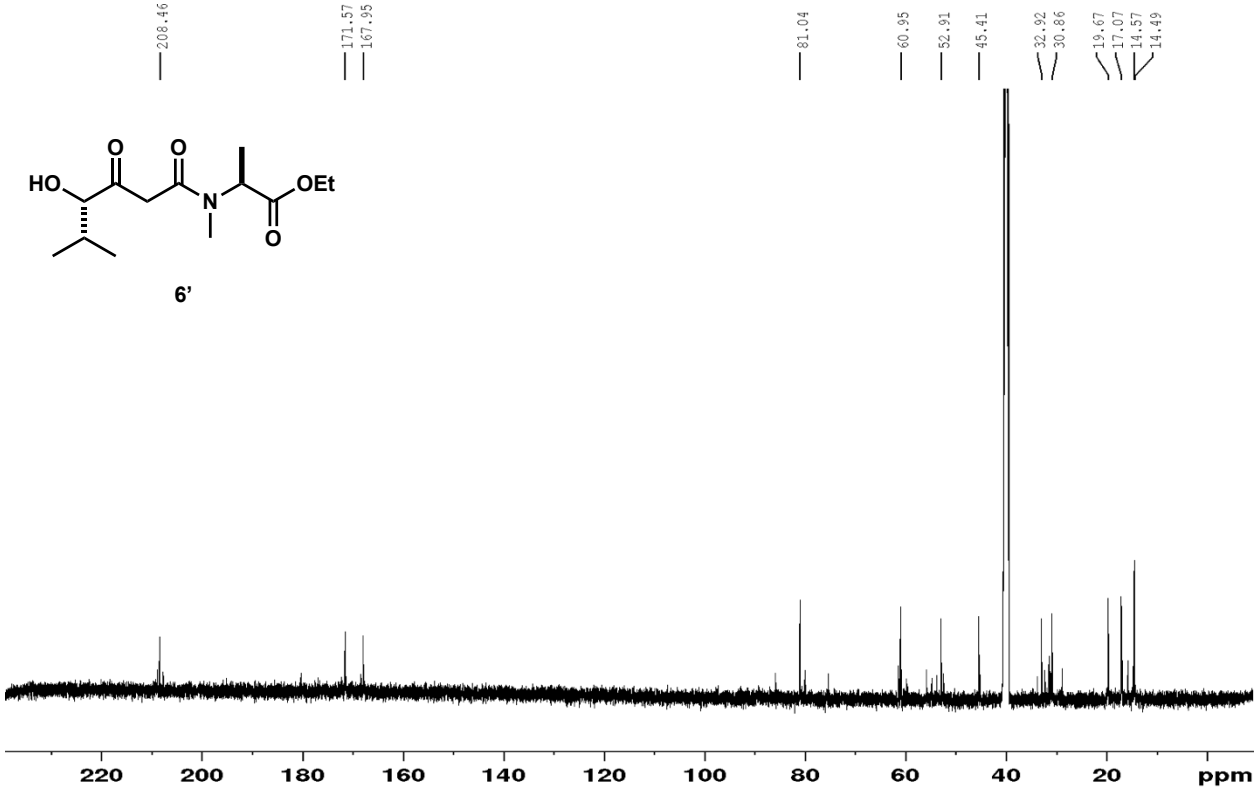

Spectrum 3.8.37 ^{1}H-NMR spectrum of compound **57** ($CDCl_3$, 500 MHz)

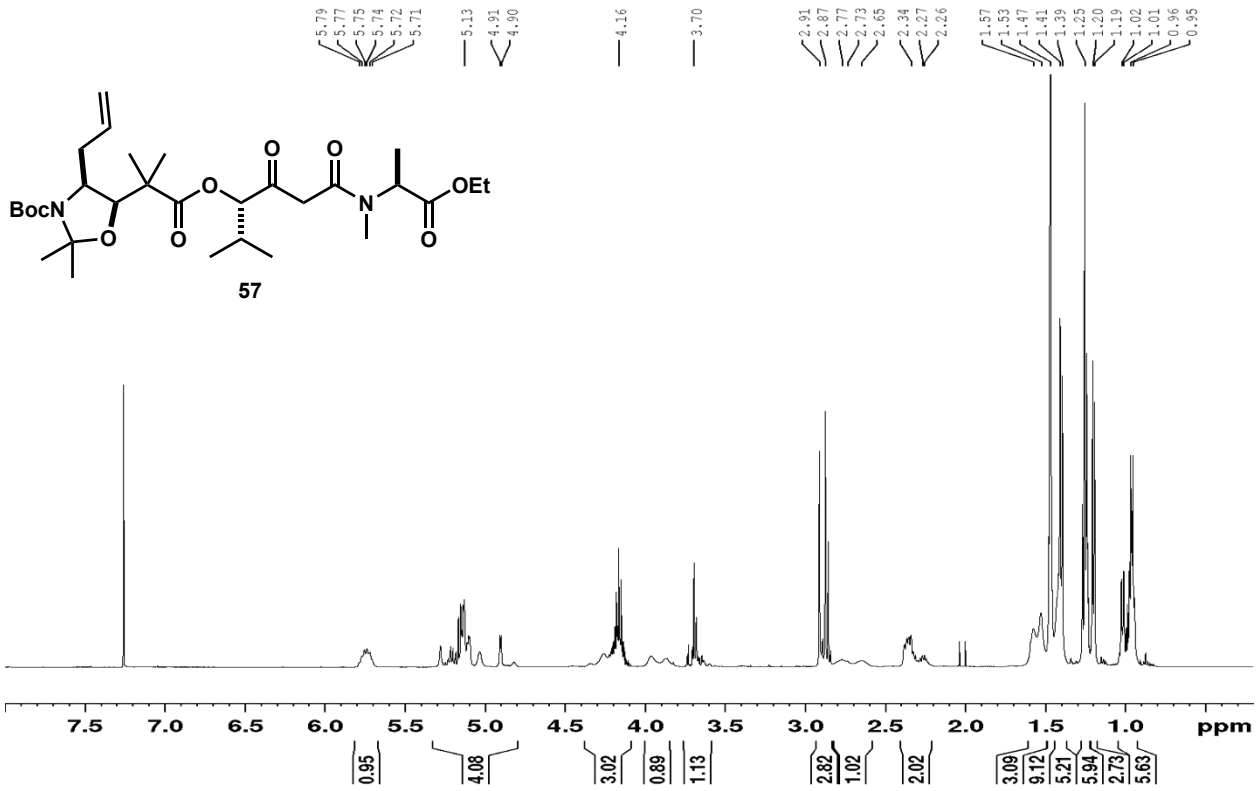

Spectrum 3.8.38 ^{13}H-NMR spectrum of compound **57** ($CDCl_3$, 125 MHz)

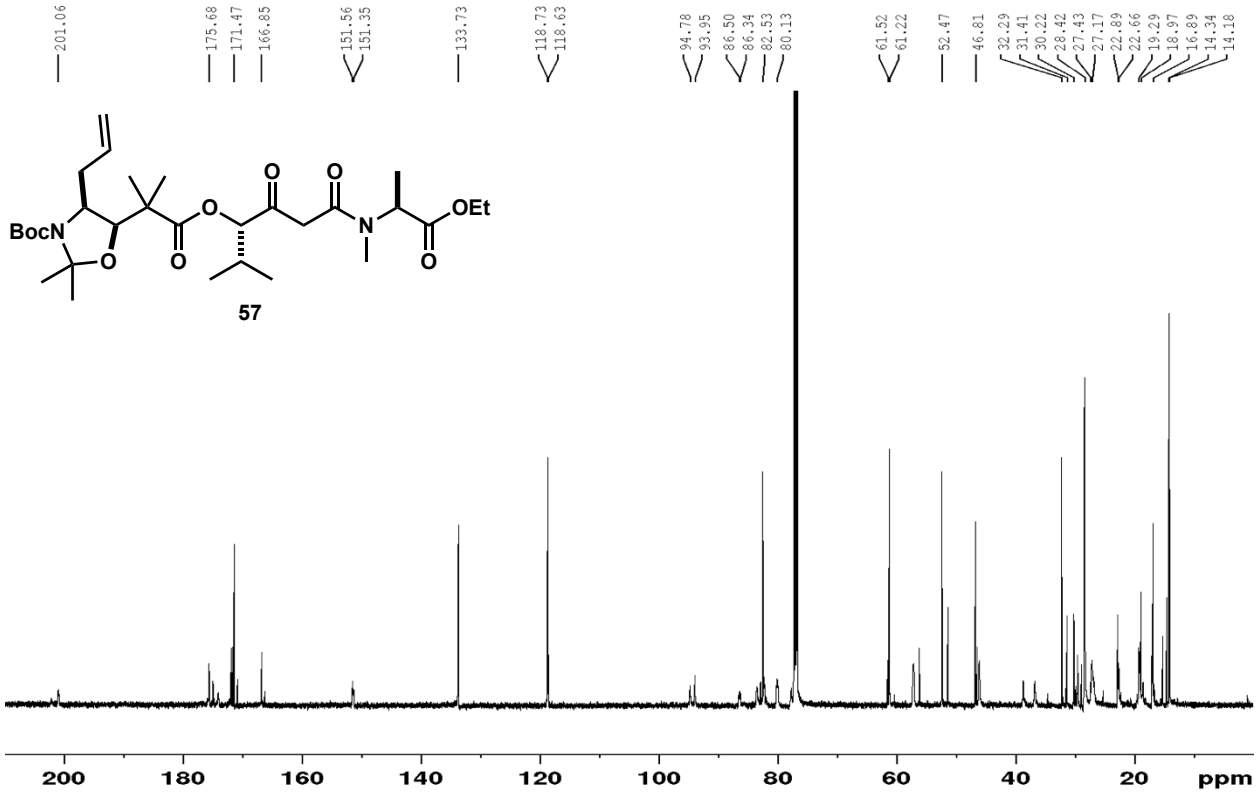

3.9 References

1. Vishnoi, K.; Viswakarma, N.; Rana, A.; Rana, B. Transcription Factors in Cancer Development and Therapy. *Cancers* **2020**, *12 (8)*, 2296–2327.

2. Henley, M. J.; Koehler, A. N., Advances in targeting 'undruggable' transcription factors with small molecules. *Nat. Rev. Drug Discov.* **2021,** *20* (9), 669–688.

3. Wang, F.; Marshall, C. B.; Yamamoto, K.; Li, G. Y.; Gasmi-Seabrook, G. M. C.; Okada, H.; Mak, T. W.; Ikura, M., Structures of KIX domain of CBP in complex with two FOXO3a transactivation domains reveal promiscuity and plasticity in coactivator recruitment. *Proc. Natl. Acad. Sci.* **2012,** *109* (16), 6078–6083.

4. Tenbaum, S. P.; Ordóñez-Morán, P.; Puig, I.; Chicote, I.; Arqués, O.; Landolfi, S.; Fernández, Y.; Herance, J. R.; Gispert, J. D.; Mendizabal, L.; Aguilar, S.; Ramón y Cajal, S.; Schwartz, S., Jr.; Vivancos, A.; Espín, E.; Rojas, S.; Baselga, J.; Tabernero, J.; Muñoz, A.; Palmer, H. G., β-catenin confers resistance to PI3K and AKT inhibitors and subverts FOXO3a to promote metastasis in colon cancer. *Nat. Med.* **2012,** *18* (6), 892–901.

5. Chen, J.; Gomes, A. R.; Monteiro, L. J.; Wong, S. Y.; Wu, L. H.; Ng, T.T.; Karadedou, C. T.; Millour, J.; Ip, Y.C.; Cheung, Y. N.; Sunters, A.; Chan, K. Y. K.; Lam, E. W. F.; Khoo, U.S., Constitutively nuclear FOXO3a localization predicts poor survival and promotes Akt phosphorylation in breast cancer. *PLoS One.* **2010,** *5* (8), 12293–12309.

6. Storz, P.; Döppler, H.; Copland, J. A.; Simpson, K. J.; Toker, A., FOXO3a promotes tumor cell invasion through the induction of matrix metalloproteinases. *Mol. Cel. Biol.* **2009,** *29* (18), 4906–4917.

7. Coomans de Brachène, A.; Demoulin, J. B., FOXO transcription factors in cancer development and therapy. *Cell. Mol. Life Sci.* **2016,** *73* (6), 1159–1172.

8. Santamaría, C. M.; Chillón, M. C.; García-Sanz, R.; Pérez, C.; Caballero, M. D.; Ramos, F.; de Coca, A. G.; Alonso, J. M.; Giraldo, P.; Bernal, T.; Queizán, J. A.; Rodriguez, J. N.; Fernández-Abellán, P.; Bárez, A.; Peñarrubia, M. J.; Vidriales, M. B.; Balanzategui, A.; Sarasquete, M. E.; Alcoceba, M.; Díaz-Mediavilla, J.; San Miguel, J. F.; Gonzalez, M., High FOXO3a expression is associated with a poorer prognosis in AML with normal cytogenetics. *Leuk. Res.* **2009,** *33* (12), 1706–1709.

9. Carter, M. E.; Brunet, A., FOXO transcription factors. *Curr. Biol.* **2007,** *17* (4), 113–114.

10. Ross, T. S.; Mgbemena, V. E., Re-evaluating the role of BCR/ABL in chronic myelogenous leukemia. *Mol. Cell. Oncol.* **2014,** *1* (3), 963450–963457.

11. Iqbal N.; Iqbal N., Imatinib: a breakthrough of targeted therapy in cancer. Chemother. Res. Pract. **2014**, *2014* (1), 1–9.

12. Naka, K.; Hoshii, T.; Hirao, A., Novel therapeutic approach to eradicate tyrosine kinase inhibitor resistant chronic myeloid leukemia stem cells. *Cancer Sci.* **2010,** *101* (7), 1577–1581.

13. Miyamoto, K.; Araki, K. Y.; Naka, K.; Arai, F.; Takubo, K.; Yamazaki, S.; Matsuoka, S.; Miyamoto, T.; Ito, K.; Ohmura, M.; Chen, C.; Hosokawa, K.; Nakauchi, H.; Nakayama, K.; Nakayama, K. I.; Harada, M.; Motoyama, N.; Suda, T.; Hirao, A., Foxo3a is essential for maintenance of the hematopoietic stem cell pool. *Cell.. Stem Cell.* **2007,** *1* (1), 101–112.

14. Naka, K.; Hoshii, T.; Muraguchi, T.; Tadokoro, Y.; Ooshio, T.; Kondo, Y.; Nakao, S.; Motoyama, N.; Hirao, A., TGF-β–FOXO signalling maintains leukaemia-initiating cells in chronic myeloid leukaemia. *Nature* **2010,** *463* (7281), 676–680.

15. Sykes, S. M.; Lane, S. W.; Bullinger, L.; Kalaitzidis, D.; Yusuf, R.; Saez, B.; Ferraro, F.; Mercier, F.; Singh, H.; Brumme, K. M.; Acharya, S. S.; Scholl, C.; Tothova, Z.; Attar, E. C.; Fröhling, S.; DePinho, R. A.; Armstrong, S. A.; Gilliland, D. G.; Scadden, D. T., AKT/FOXO signaling enforces reversible differentiation blockade in myeloid leukemias. *Cell.* **2011,** *146* (5), 697–708.

16. Kawahara, T.; Hwang, J.H.; Izumikawa, M.; Hashimoto, J.; Takagi, M.; Shin-Ya, K. *J.,* JBIR-129 and -139, cytotoxic 34-membered polyol macrolides of microbial origin. *J. Nat. Prod.* **2012**, *75* (10)*,* 1814–1818.

17. Kawahara, T.; Kagaya, N.; Masuda, Y.; Doi, T.; Izumikawa, M.; Ohta, K.; Hirao, A.; Shin-ya, K., Foxo3a Inhibitors of Microbial Origin, JBIR-141 and JBIR-142. *Org. Lett.* **2015,** *17* (21), 5476–5479.

18. Furihata, K.; Seto, H., Constant time HMBC (CT-HMBC), a new HMBC technique useful for improving separation of cross peaks. *Tetrahedron Lett.* **1998**, *39* (40), 7337–7340.

19. Ikeda, H.; Matsumori, N.; Ono, M.; Suzuki, A.; Isogai, A.; Nagasawa, H.; Sakuda, S., Absolute Configuration of Aflastatin A, a Specific Inhibitor of Aflatoxin Production by *Aspergillus parasiticus*. *J. Org. Chem.* **2000**, *65* (2), 438–444.

20. Sawa, R.; Takahashi, Y.; Hashizume, H.; Sasaki, K.; Ishizaki, Y.; Umekita, M.; Hatano, M.; Abe, H.; Watanabe, T.; Kinoshita, N.; Homma, Y.; Hayashi, C.; Inoue, K.; Ohba, S.; Masuda, T.; Arakawa, M.; Kobayashi, Y.; Hamada, M.; Igarashi, M.; Adachi, H.; Nishimura, Y.; Akamatsu, Y., Amycolamicin: a novel broad-spectrum antibiotic inhibiting bacterial topoisomerase. *Chem. Eur. J.* **2012**, *18* (49), 15772−15781.

21. Marfey, P., Determination of D-amino acids. II. Use of a bifunctional reagent, 1,5-difluoro-2,4-dinitrobenzene. *Carlsberg Res. Commun.* **1984**, *49* (6), 591−596.

22. Fu, P.; Jamison, M.; La, S.; MacMillan, J. B., Inducamides A–C, Chlorinated Alkaloids from an RNA Polymerase Mutant Strain of *Streptomyces* sp. *Org. Lett.* 2014, *16* (21), 5656−5659.

23. Nurse, P.; Lewis, R. A.; Hayles, J.; Ellis, N. E.; Errington, A. J., inventor; Demuris Limited, UK; The Francis Crick Institute Limited assignee. JBIR-141 zinc complex; zinc complexes and their uses. United States **2022**.

24. Gong, B.; Bai, E.; Feng, X.; Yi, L.; Wang, Y.; Chen, X.; Zhu, X.; Duan, Y.; Huang, Y., Characterization of Chalkophomycin, a Copper(II) Metallophore with an Unprecedented Molecular Architecture. *J. Am. Chem. Soc.* **2021,** *143* (49), 20579−20584.

25. Pracht, P.; Bohle, F.; Grimme, S., Automated exploration of the low-energy chemical space with fast quantum chemical methods. *Phys. Chem. Chem. Phys.* **2020,** *22* (14), 7169–7192.

26. Lee, C.; Yang, W.; Parr, R. G., Development of the Colle-Salvetti correlation-energy formula into a functional of the electron density. *Phys. Rev. B Condens. Matter* **1988,** *37* (2), 785–789.

27. Becke, A. D., Density-functional thermochemistry. III. The role of exact exchange. *J. Chem. Phys.* **1993,** *98* (7), 5648–5652.

28. Weigend, F.; Ahlrichs, R., Balanced basis sets of split valence, triple zeta valence and quadruple zeta valence quality for H to Rn: Design and assessment of accuracy. *Phys. Chem. Chem. Phys.* **2005,** *7* (18), 3297–3305.

29. Keefer, K. K., Fifty Years of Diazeniumdiolate Research. From Laboratory Curiosity to Broad-Spectrum Biomedical Advances. *ACS Chem. Biol.* **2011**, *6* (11), 1147–1155.

30. Christodoulou, D.; George, C.; Keefer, L. K., An unusual bi-tri-binuclear sandwich complex formed in the reaction of $CuCl_2$ with the $Et_2N\text{-}N_2O_2^-$ ion. *J. Chem. Soc. Chem. Commun*. **1993**, 937–939.

31. Walter P. L.; Kampotter, A.; Eckers, A.; Barthel, A.; Schmoll, D.; Sies, H.; Klotz L. O., Modulation of FoxO signaling in human hepatoma cells by exposure to copper or zinc ions. *Arch. Biochem. Biophys.* **2006**, *454* (2): 107–113.

32. Cameron A. R.; Anil, S.; Sutherland, E.; Harthill, J.; Rena, G., Zinc-dependent effects of small molecules on the insulin-sensitive transcription factor FOXOla and gluconeogenic genes. *Metallomics* **2010**, *2* (3): 195–203.

33. Borniquel, S.; García-Quintáns, N.; Valle, I.; Olmos, Y.; Wild, B.; Martínez-Granero, F.; Soria, E.; Lamas, S.; Monsalve, M., Inactivation of Foxo3a and subsequent downregulation of PGC-1 alpha mediate nitric oxide-induced endothelial cell migration. *Mo.l Cell. Biol.* **2010**, *30* (16), 4035–4044.

34. Huang, Z.; Fu, J.; Zhang, Y., Nitric Oxide Donor-Based Cancer Therapy: Advances and Prospects. *J. Med. Chem.* **2017**, *60* (18), 7617–7635.

35. Alston, T. A.; Porter, D. J.; Bright, H. J., Generation of nitric oxide by enzymatic oxidation of N-hydroxy-N-nitrosamines. *J. Bio. Chem.* **1985**, *260* (7), 4069–4074.

36. Leung, D.; Abbenante, G.; Fairlie, D. P., Protease inhibitors: current status and future prospects. *J. Med. Chem.* **2000,** *43* (3), 305–341.

37. Yasoshima, K.; Yoshida, M.; Doi, T., The Concise Synthesis of a tert-Butoxycarbonyl Derivative of (3R,4S)-4-Amino-3-hydroxy-7-(N-nitrosohydroxyamino)-2,2-dimethylheptanoate, a Component of JBIR-141. *Bull. Chem. Soc. Jpn.* **2022,** *95* (5), 830–832.

38. Yasoshima, K.; Yoshida, M.; Kawahara, T.; Shin-ya, K.; Doi, T., Synthetic study for novel Foxo3a inhibitor JBIR-141. The 59th Japanese Peptide Symposium, Minoh, Japan, Peptide Science: Minoh, Japan, **2019**, 11–12.

39. Wittman, L.; Wachter, A. C.; Hedda, S.; Schobert, R., A Synthetic Approach to the Natural *N*-Nitrosohydroxylamino Tetramic Acid JBIR-141. Org. Lett. **2022**, *24* (28), 5171−5175.

40. Schobert, R.; Schlenk, A. Tetramic and tetronic acids: an update on new derivatives and biological aspects. *Bioorg. Med. Chem.* **2008**, *16* (8), 4203−4221.

41. Mo, X.; Li, Q.; Ju, J. Naturally occurring tetramic acid products: isolation, structure elucidation and biological activity. *RSC Adv.* **2014**, *4*, 50566−50593.

42. Jiang, M.; Chen, S.; Li, J.; Liu, L.; The Biological and Chemical Diversity of Tetramic Acid Compounds from Marine-Derived Microorganisms. *Mar Drugs*. **2020**, *18* (2):114−156.

43. Frump, J. A., Oxazolines. Their preparation, reactions, and applications. *Chem. Rev.* 1971, *71* (5) 483−50543.

44. Royles B. J. L., Naturally Occurring Tetramic Acids: Structure, Isolation, and Synthesis. *Chem Rev.* 1995, *95* (6), 1981−2001.

45. Hrabie, J. R.; Keefer, L. K. Chemistry of the nitric oxide-releasing diazeniumdiolate ("nitrosohydroxylamine") functional group and its oxygen-substituted derivatives. *Chem. Rev.* **2002**, *102* (4), 1135−1154.

46. Hermenau, R.; Ishida, K.; Gama, S.; Hoffmann, B.; Pfeifer-Leeg, M.; Plass, W.; Mohr, J. F.; Wichard, T.; Saluz, H. P.; Hertweck, C. Gramibactin is a bacterial siderophore with a diazeniumdiolate ligand system. *Nat. Chem. Biol.* **2018**, *14* (9), 841−843.

47. Tilvi, S.; Keisham, S. S., Synthesis of Oxazole, Oxazoline and Isoxazoline Derived Marine Natural Products: A Review. *Curr. Org. Chem.* 2016, *20* (8), 898−929.

48. Davyt, D.; Serra G., Thiazole and oxazole alkaloids: isolation and synthesis. *Mar. Drugs.* **2010**, *8* (11), 2755−2780.

49. Connon, R.; Roche, B.; Rokade, B. V.; Guiry, P. J., Further Developments and Applications of Oxazoline-Containing Ligands in Asymmetric Catalysis. *Che. Rev.* **2021,** *121* (11), 6373−6521.

50. Roy, R. S.; Gehring, A. M.; Milne J. C.; Belshaw, P. J.; Walsh C. T., Thiazole and oxazole peptides: biosynthesis and molecular machinery. *Nat. Prod. Rep.* **1999,** *16* (2), 249−263.

51. Wong, G. S. K.; Wu, W., *In Oxazoles: Synthesis, Reactions, and Spectroscopy, Part B*; Palmer, D. C., Ed.; John Wiley & Sons, Inc.: Hoboken, **2004**, 331–528.

52. Kangani, C.O.; Kelley D. E., One pot direct synthesis of amides or oxazolines from carboxylic acids using Deoxo-Fluor reagent. *Tetrahedron Lett.* **2005**, *46* (51), 8917–8920.

53. Kangani, C. O.; Kelley, D. E.; Day, B. W., One pot direct synthesis of oxazolines, benzoxazoles, and oxadiazoles from carboxylic acids using the Deoxo-Fluor reagent. *Tetrahedron Let.* **2006,** *47* (37), 6497–6499.

54. Burrell, G.; Evans, J. M.; Jones, G. E.; Stemp, G. The action of diethylaminosulphur trifluoride (DAST) on trans-4-amido- 3-Chromanols: Preparation of cis-amidoalcohols via oxazolines. *Tetrahedron Lett.* **1990**, *31* (25), 3649–3652.

55. Paterson, I.; Fink, S. J.; Lee, L. Y. W.; Atkinson, S. J.; Blakey, S. B., Total Synthesis of Aplyronine C. *Org. Lett.* **2013,** *15* (12), 3118–3121.

56. Lall, M. S.; Ramtohul, Y. K.; James, M. N. G.; Vederas, J. C., Serine and Threonine β-Lactones: A New Class of Hepatitis A Virus 3C Cysteine Proteinase Inhibitors. *J. Org. Chem.* **2002,** *67* (5), 1536–1547.

57. Liang, X.; Lee, C.J.; Chen, X.; Chung, H.S.; Zeng, D.; Raetz, C. R.; Li, Y.; Zhou, P.; Toone, E. J.; Syntheses, structures and antibiotic activities of LpxC inhibitors based on the diacetylene scaffold. *Bioorg. Med Chem.* **2011**, *19* (2), 852–860.

58. White, J. M.; Tunoori, A. R.; Turunen, B. J., Georg G. I., [Bis(2-methoxyethyl)amino] sulfur Trifluoride, the Deoxo-Fluor Reagent: Application toward One-Flask Transformations of Carboxylic Acids to Amides. *J. Org. Chem.* **2004,** *69* (7), 2573–2576.

59. Pouliot, M. F.; Angers, L.; Hamel, J.D.; Paquin, J. F., Synthesis of 2-oxazolines and related N-containing heterocycles using $[Et_2NSF_2]BF_4$ as a cyclodehydration agent. *Tetrahedron Lett.* **2012,** *53* (32), 4121–4123.

60. Yokokawa, F.; Hamada, Y.; Shioiri, T., Synthesis of 2,4-Disubstituted Oxazoles, *Synlett.* **1992**, *2*, 153–155.

61. Yokokawa, F.; Shioiri, T., **Novel stereospecific dehydration of β-hydroxy-α-amino acids using Martin's sulfurane.** ***Tetrahedron Lett.*** 2002**,** ***43*** **(48), 8679–8682.**

62. Wipf, P.; Miller, C. P., Stereospecific synthesis of peptide analogs with allo-threonine and D-allo-threonine residues. *J. Org. Chem.* **1993,** *58* (6), 1575**–**1578.

63. Wipf, P.; Miller C. P., **An investigation of the mitsunobu reaction in the preparation of peptide oxazolines, thiazolines, and aziridines.** ***Tetrahedron Lett.*** 1992**,** ***33*** **(42), 6267–6270.**

64. Sakakura, A.; Kondo, R.; Ishihara, K., Molybdenum Oxides as Highly Effective Dehydrative Cyclization Catalysts for the Synthesis of Oxazolines and Thiazolines. *Org. Lett.* **2005,** *7* (10), 1971–1974.

65. Sakakura, A.; Kondo, R.; Umemura, S.; Ishihara, K., Catalytic Synthesis of Peptide-Derived Thiazolines and Oxazolines using Bis(quinolinolato)dioxomolybdenum(VI) Complexes. *Adv. Syn. Cat.* **2007,** *349* (10), 1641–1646.

66. Sakakura, A.; Kondo, R.; Umemura, S.; Ishihara, K., Dehydrative cyclization of serine, threonine, and cysteine residues catalyzed by molybdenum(VI) oxo compounds. *Tetrahedron* **2009,** *65* (10), 2102–2109.

67. Beresford, K. J. M.; Church, N. J.; Young, D. W., Synthesis of *α*-amino acids by reaction of aziridine-2-carboxylic acids with carbon nucleophiles. *Org. Biomol. Chem.* **2006**, *4*, 2888–2897.

68. Nicolaou, K. C.; Estrada, A. A.; Zak, M.; Lee, S. H.; Safina, B. S., A Mild and Selective Method for the Hydrolysis of Esters with Trimethyltin Hydroxide. *Angew. Chem., Int. Ed.* **2005,** *44* (9), 1378–1382.

69. Berthet, M.; Davanier, F.; Dujardin, G.; Martinez, J.; Parrot, I., MgI_2-Mediated Chemoselective Cleavage of Protecting Groups: An Alternative to Conventional Deprotection Methodologies. *Che. Eur. J.* **2015,** *21* (31), 11014–11016.

70. Fukuzumi, T.; Bode, J. W., A reagent for the convenient, solid-phase synthesis of N-terminal peptide hydroxylamines for chemoselective ligations. *J. Am. Chem. Soc.* **2009,** *131* (11), 3864–3865.

71. Fukuzumi, T.; Ju, L.; Bode, J. W., Chemoselective cyclization of unprotected linear peptides by α-ketoacid–hydroxylamine amide-ligation. *Org. Biomol. Chem.* **2012**, *10* (30), 5837–5844.

72. Boyle, T. P.; Bremner, J. B.; Coates, J.; Deadman, J.; Keller, P. A.; Pyne, S. G.; Rhodes, D. I., New cyclic peptides via ring-closing metathesis reactions and their anti-bacterial activities. *Tetrahedron* **2008,** *64* (49), 11270–11290.

73. Shute, R. E.; Rich, D. H., Synthesis and Evaluation of Novel Activated Mixed Carbonate Reagents for the Introduction of the 2-(Trimethylsilyl)ethoxycarbonyl(Teoc)-Protecting Group. *Synthesis*. 1987, *1987* (4), 346–349.

74. Arrastia, I.; Lecea, B. a.; Cossío, F. P., Highly stereocontrolled synthesis of substituted propiolactones and butyrolactones from achiral lithium enolates and homociral aldehydes. *Tetrahedron Lett.* **1996,** *37* (2), 245–248.

75. Danheiser, R. L.; Nowick, J. S., A Practical and Efficient Method for the Synthesis of β-Lactones. *J. Org. Chem.* **1991**, *56* (3), 1176–1185.

76. Danheiser, R. L.; Choi, Y. M.; Menichincheri, M.; Stoner, E. J., Synthesis of Allenes via Thermal Cycloreversion of α-alkylidene-β-lactones. *J. Org. Chem.* **1993**, *58* (2), 322–327.

77. Chérest, M.; Felkin, H.; Prudent, N., Torsional strain involving partial bonds. The stereochemistry of the lithium aluminium hydride reduction of some simple open-chain ketones. *Tetrahedron Let.*. **1968,** *9* (18), 2199–2204.

78. Anh, N.T.; Eisenstein, O., *Nouv. J. Chim.* **1977**, *1*, 61–70.

79. Cerda, M. M.; Newton, T. D.; Zhao, Y.; Collins, B. K.; Hendon, C. H.; Pluth, M. D., Dithioesters: simple, tunable, cysteine-selective H2S donors. *Chem. Sci.* **2019,** *10* (6), 1773–1779.

80. Evans, D. A.; Britton, T. C.; Ellman, J. A., Contrasteric carboximide hydrolysis with lithium hydroperoxide. *Tetrahedron Lett.* **1987,** *28* (49), 6141–6144.

81. Beesley, R. M.; Ingold, C. K.; Thorpe, J. F., CXIX.—The formation and stability of spiro-compounds. Part I. spiro-Compounds from cyclohexane. *J. Chem. Soc., Trans.* **1915,** *107*, 1080–1106.

82. Shaw, B. L., Formation of large rings, internal metalation reactions, and internal entropy effects. *J. Am. Chem. Soc.* **1975,** *97* (13), 3856–3857.

83. Kiyooka, S. I.; Suzuki, K.; Shirouchi, M.; Kaneko, Y.; Tanimori, S., Lewis acid-mediated reaction with silyl ketene acetals and allylstannane of the aluminum acetals generated by DIBAL-H reduction of α-amino acid esters. *Tetrahedron Lett.* **1993,** *34* (36), 5729–5732.

84. Guindon, Y.; Houde, K.; Prévost, M.; Cardinal-David, B.; Landry, S. R.; Daoust, B.; Bencheqroun, M.; Guérin, B., Synthesis of Propionate Motifs: Diastereoselective Tandem Reactions Involving Anionic and Free Radical Based Processes. *J. Am. Che, Soc.* **2001,** *123* (35), 8496–8501.

85. Jouin, P.; Castro, B.; Nisato, D., Stereospecific synthesis of N-protected statine and its analogues via chiral tetramic acid. *J. Chem. Soc., Perkin Trans. 1*, **1987**, 1177–1182.

86. Ripperger, H., The "normalizing factor" for the tomato mutant *chloronerva*. XXX. Synthesis of 3,4-Seconicotianamine. *J. Prakt. Chem.*, **1988**, *330*, 470–472.

87. Lambert, K. M.; Medley, A. W.; Jackson, A. C.; Markham, L. E., Wood, J. L., Synthesis of Chiral Tetramic Acids: Preparation of (S)-5-Benzylpyrrolidine-2,4-dione from L-Phenylalanine Methyl Ester Hydrochlorides. *Org. Synth.* **2019,** *96*, 528–585.

88. Xue, F.; Seto, C. T., Fluorogenic Peptide Substrates for Serine and Threonine Phosphatases. *Org. Lett.* **2010,** *12* (9), 1936–1939.

89. Royles, B. J. L., Naturally Occurring Tetramic Acids: Structure, Isolation, and Synthesis. *Chem. Rev.* **1995,** *95* (6), 1981–2001.

90. Li, W. R.; Ewing, W. R.; Harris, B. D.; Joullie, M. M., Total synthesis and structural investigations of didemnins A, B, and C. *J. Am. Chem. Soc.* **1990,** *112* (21), 7659–7672.

91. Hasuoka, A.; Nishikimi, Y.; Nakatama, Y.; Kamiyama, K.; Nakao, M.; Miyagawa, K. I.; Nishimura, O.; Fujino, M., Synthesis and Anti-*Helicobacter pylori* Activity of Pyloricidin Derivatives, *J. Antibiot.* **2002**, *55* (3), 322–336.

92. Ikeuchi, K.; Murasawa, K.; Yamada, H., A Simple Method for the Preparation of Stainless and Highly Pure Trichloroacetimidates Synlett., 2019, *30* (11), 1308–1312.

93. Hori, K.; Arai, M.; Nomura, K.; Yoshii, E., An Efficient 3(C)-Acylation of Tetramic Acids Involving Acyl Migration of 4(O)-Acylates. Chem Pharm. Bull. **1987,** *35* (10), 4368–4371.

94. Sengoku, T.; Wierzejska, J.; Takahashi, M.; Yoda, H., First stereoselective synthesis of penicillenol A1 via novel O-to C-acyl rearrangement of O-acyltetramic acid. *Synlett.* **2010,** *2010* (19), 2944–2946.

95. Sengoku, T.; Nagae, Y.; Ujihara, Y.; Takahashi, M.; Yoda, H., A Synthetic Approach to Diverse 3-Acyltetramic Acids via O- to C-Acyl Rearrangement and Application to the Total Synthesis of Penicillenol Series. *J. Org. Chem.* **2012,** *77* (9), 4391–4401.

96. Yang, S.; Chen, C.; Chen, J.; Li, C., Total Synthesis of the Potent and Broad-Spectrum Antibiotics Amycolamicin and Kibdelomycin. *J. Am. Chem. Soc.* **2021,** *143* (50),

21258–21263.

97. Jeong, Y. C.; Moloney, M. G., Tetramic Acids as Scaffolds: Synthesis, Tautomeric and Antibacterial Behaviour. *Synlett*. 2009, *15*, 2487–2491.

98. Broughton, H. B.; Woodward, P. R. *J.,* A semiempirical SCF-MO study of the tautomeric forms of 3-acetyl tetronic- and tetramic acids. *Comput. Aided Mol. Des.* 1990, *4* (2), 147–153.

99. Zaghouani, M.; Nay, B., 3-Acylated tetramic and tetronic acids as natural metal binders: myth or reality?. *Nat. Prod. Rep.* **2016,** *33* (4), 540–548.

100. Lebrun,M. H.; Duvert, P.; Gaudemer, F.; Gaudemer, A.; Deballon, C.; Boucly, P., Complexation of the fungal metabolite tenuazonic acid with copper (II), iron (III), nickel (II), and magnesium (II) ions *Inorg. Biochem.* 1985, *24* (3), 167–181.

101. Hansen, K. B.; Hsiao, Y.; Xu, F.; Rivera, N.; Clausen, A.; Kubryk, M.; Krska, S.; Rosner, T.; Simmons, B.; Balsells, J.; Ikemoto, N.; Sun, Y.; Spindler, F.; Malan, C.; Grabowski, E. J. J.; Armstrong, J. D., III, Highly Efficient Asymmetric Synthesis of Sitagliptin. *J. Am. Chem. Soc.* **2009,** *131* (25), 8798–8804.

102. Xu, F.; Armstrong, J. D.; Zhou, G. X.; Simmons, B.; Hughes, D.; Ge, Z.; Grabowski, E. J. J., Mechanistic Evidence for an α-Oxoketene Pathway in the Formation of β-Ketoamides/Esters via Meldrum's Acid Adducts. *J. Am. Chem. Soc.* **2004,** *126* (40), 13002–13009.

103. *Shiina, I.; Ibuka, R.; Kubota, M., A New Condensation Reaction for the Synthesis of Carboxylic Esters from Nearly Equimolar Amounts of Carboxylic Acids and Alcohols Using 2-Methyl-6-nitrobenzoic Anhydride. Chem. Lett.* ***2022****, 31 (3), 286–287.*

104. Wickens, Z. K.; Skakuj, K.; Morandi, B.; Grubbs, R. H., Catalyst-Controlled Wacker-Type Oxidation: Facile Access to Functionalized Aldehydes. *J. am. Chem. Soc.* **2014,** *136* (3), 890–893.

105. Kim, K. E.; Li, J.; Grubbs, R. H.; Stoltz, B. M., Catalytic Anti-Markovnikov Transformations of Hindered Terminal Alkenes Enabled by Aldehyde-Selective Wacker-Type Oxidation. *J. Am. Chem Soc.* **2016,** *138* (40), 13179–13182.

106. Morimoto, Y.; Kitao, S.; Okita, T.; Shoji, T., Total Synthesis and Assignment of the Double-Bond Position and Absolute Configuration of (−)-Pyrinodemin A. *Org. Lett.* **2003,** *5* (15), 2611–2614.

107. Chaudhary, P.; Gupta, S.; Muniyappan, N.; Sabiah, S.; Kandasamy, J., An efficient synthesis of N-nitrosamines under solvent, metal and acid free conditions using tert-butyl nitrite. *Green Chem.* **2016,** *18* (8), 2323–2330.

108. Brown, H. C.; Rathke, M. W.; Rogic, M. M., A fast reaction of organoboranes with iodine under the influence of base. A convenient procedure for the conversion of terminal olefins into primary iodides via hydroboration-iodination. *J. am. Chem. Soc.* **1968,** *90* (18), 5038–5040.

109. Kornblum, N.; Powers, J., Notes - Synthesis of Aliphatic Nitro Compounds. *J. Org. Chem.* **1957,** *22* (4), 455–456.

110. Tishkov, A. A.; Schmidhammer, U.; Roth, S.; Riedle, E.; Mayr, H., Ambident Reactivity of the Nitrite Ion Revisited. *Agnew. Chem. Int. Ed.* **2005,** *44* (29), 4623–4626.

111. Xun, S. Q.; Wen, L. R.; Kun, J.; Xia, Z. Z.; Feng, Z. D., Ultrasound-promoted Highly Chemoselective Reduction of Aromatic Nitro Compounds to the Corresponding N-Arylhydroxylamines Using Zinc and $HCOONH_4$ in CH_3CN. *Chem. Lett.* **2006,** *35* (2), 226–227.

112. Ley, S. V.; Smith S. C.; Woodward, P. R., Further reactions of t-butyl 3-oxobutanthioate and t-butyl 4-diethyl-phosphono-3-oxobutanthioate : Carbonyl coupling reactions, amination, use in the preparation of 3-acyltetramic acids and application to the total synthesis of fuligorubin A. *Tetrahedron*. 1992, *48* (6), 1145–1174.

113. Kou, Q.; Wang, T.; Zou, F.; Zhang, S.; Chen, Q.; Yang, Y., Design, synthesis and biological evaluation of C(4) substituted monobactams as antibacterial agents against multidrug-resistant Gram-negative bacteria. *Eur. J. Med. Chem.* 2018, *151*, 98-109.

Chapter Four: Synthesis of OFCP-Derived Macrobicycles and Evaluation of their Biological Utility

4.1 Introduction

Reaction processes that form multiple covalent bonds while creating new rings and stereocenters are inherently valuable in organic synthesis. They advance an overarching goal of the field, which is to enable syntheses of value-added products from abundant raw materials in the most direct manner possible. Reaction cascades have been used effectively for the synthesis of diverse carbocyclic and heterocyclic ring systems, using both catalytic and stoichiometric methods.[1,2] The typical objective is to streamline the assembly of molecules. However, multi bond-forming processes can also manipulate the form and properties of pre-assembled structures. For example, we have developed reagents that can engage small peptides in successive ring forming reactions to afford polycyclic derivatives.[3-11] In the example shown in **Scheme 4.1.1B**, three consecutive operations imbed the core of synthetic reagent **1** into unprotected tripeptide WWY. Four new bonds (red) are formed between the oligomer and the scaffolding reagent, resulting in four new rings and three new stereocenters.[8] Other methods to cyclize unprotected peptides using native functional groups (e.g. **Scheme 4.1.1A**) achieve less bonding with the scaffold and install fewer conformational constraints.[12-16] Using **1** and related reagents, it is possible to convert machine made oligomers systematically into stable composite macrocycles having diverse shapes and improved pharmacological properties.[17]

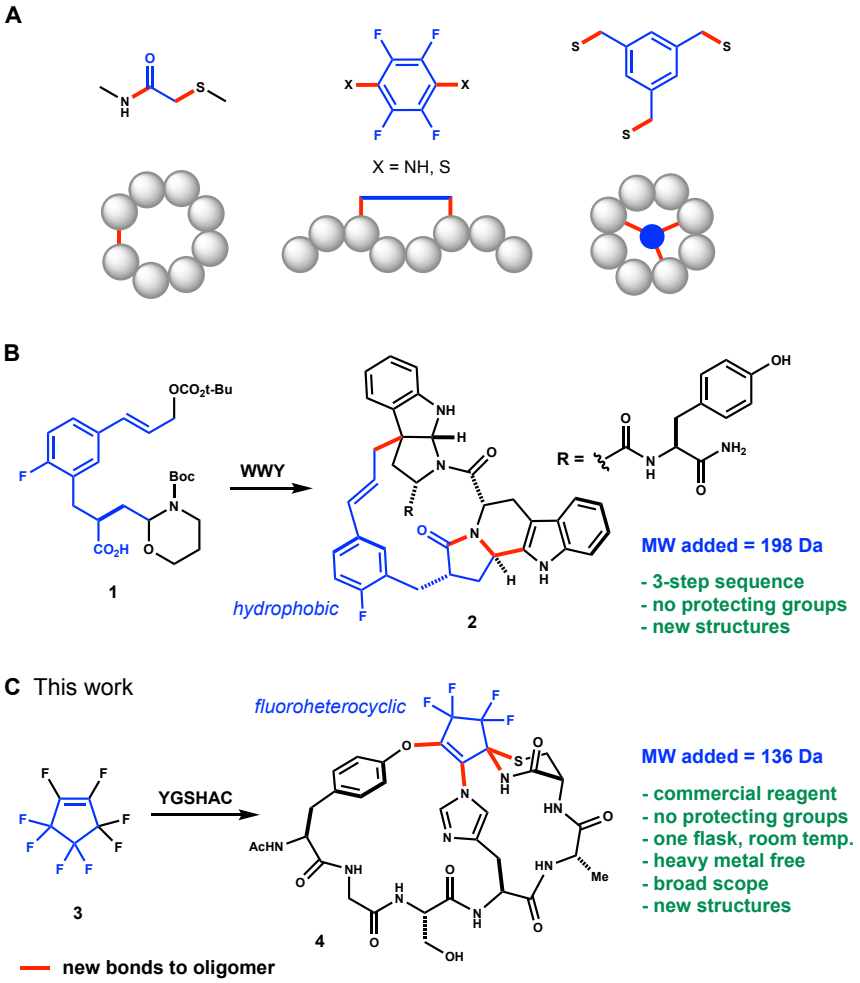

Scheme 4.1.1 Established methods for the cyclization of linear, unprotected peptides. (**A**) Common side chain engagements using native functional groups (*refs. 12-15*). (**B**) Our previous work - sequenced main chain and side chain reactions using multi-contact scaffolding. (**C**) This work - relative rate controlled polysubstitution cascades using perfluoro-cyclopentene.

The scaffolding imparted by residual **1** (colored blue in **2**) is hydrophobic. It was of interest to develop methods that could install scaffolding having polar elements and the potential for transannular hydrogen bonding. Here we describe new relative rate-controlled polysubstitution cascades that achieve this outcome (**Scheme 4.1.1C**). The reactions modify linear, unprotected peptides in a single flask at room temperature. They require no catalysts or heavy metals, and they generate a wealth of previously unknown heterocyclic ring systems with tunable properties.

Electron deficient aryl fluorides participate in nucleophilic ipso substitution (S_NAr) reactions. Sanger's method for N-terminal peptide sequencing is a seminal example.[18] More heavily fluorinated aromatics such as hexafluorobenzene can engage two nucleophiles successively at ring positions 1 and 4. The reaction is efficient with sulfur nucleophiles and has been used to generate macrocyclic peptides via cysteine 'stapling'.[13] Polysubstitutions become possible when using perfluorinated cycloalkenes. For example, commercial octafluorocyclopentene (OFCP) reacts with simple nucleophiles at both its vinyl positions, and subsequently at its allylic positions to afford adducts having up to six fluorine atoms replaced.[19] We have discovered how to translate this incremental electrophilicity of OFCP into relative rate-controlled substitution cascades. Using peptides as polynucleophilic partners, OFCP generates multicyclic products from linear precursors in a sequence dependent manner. We show how fluorinated thiazaspirodecenone intermediates can be intercepted to generate novel glycoconjugates, functionalization products and macrobicyclic composites using molecular inserts. We study the molecular properties of end products and computationally probe how fluorospirocyclic scaffolding can generate new structural mimics of major loop types observed at protein contact surfaces in the Protein Data Bank.

4.2: Direct OFCP Macrobicyclization of Unprotected Linear Peptides

Linear peptides having three proximal nucleophilic residues react with OFCP (1.5 eq, 25˚C, Et_3N, DMF) according to the progression shown in **Scheme 4.2.1A**. Two successive vinylic substitutions occur rapidly (k_{rel} for Ser:Tyr:His:Cys ~ 1:30:45:1000) to afford macrocycles **6**.[20] DFT calculations have been performed to elaborate details of this mechanism. The potent electrophilicity of OFCP is related to the high stabilization of anionic intermediates by negative

hyperconjugation. This is reflected, for example, in the highly delocalized HOMO calculated for the intermediate formed in the model reaction of ethyl mercaptide with OFCP (**Scheme 4.2.1B**). Fluoride loss from this intermediate is calculated to have a very low barrier (see Experimental Section for details). Excess OFCP (b.p. = 27˚C @ 1 atm) is removed from **6** in vacuo and the residue is redissolved in a DMF/THF solution containing excess Cs_2CO_3 or $KOSiMe_3$. This initiates spirocyclization via Sn2' displacement of a third fluorine atom (when Nu^3 is a C-terminal carboxamide) to afford a new vinyl fluoride that is captured by a fourth competent nucleophile to give polycycles **8**. Compounds **8** are stable, soluble and purified using standard chromatographic techniques. Linear peptide Ac-YNCTFC-NH_2 reacts with OFCP at its two cysteine residues within minutes at 25˚C. Subsequent treatment with Cs_2CO_3 installs the thiazaspirodecenone motif while forming a new vinyl fluoride that then captures the N-terminal tyrosine residue to afford **9** in 41% isolated yield (**Scheme 4.2.1C**). By initiating reaction cascades at a C-terminal cysteine amide, it is possible to synthesize a range of macrobicyclic structures that are bridged by sulfide and imidazole linkages. There is flexibility in ring size on either side of the bridging residue and, in the case of histidine derivative **4**, bridge position epimer **13** can be prepared readily. Diastereoselectivity at the newly formed spiro center is high (>10:1) across the series. Products show sharp, well resolved ^1H NMR spectra at ambient temperature. By repositioning the cysteinyl amide off of a glutamate or aspartate side chain, it is possible to initiate alternate macrobicyclization cascades. For example, branched peptide Ac-YGAE(C)H-NMe_2 affords the striking, double looped polycycle **16** when reacted successively with OFCP and $KOSiMe_3$. To our knowledge, each of the ring systems shown in **Scheme 4.2.1C** are without precedent in the literature.

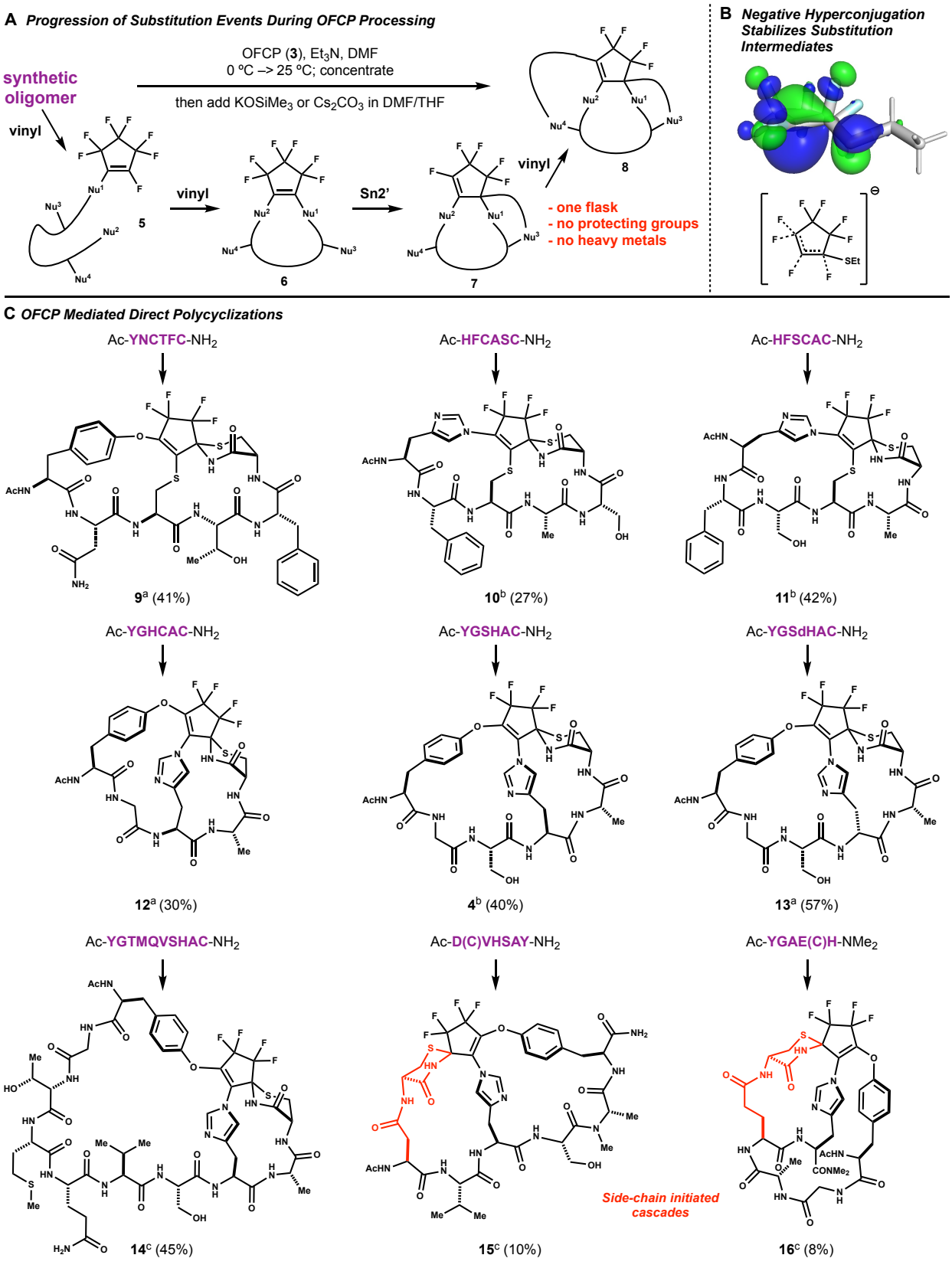
A Progression of Substitution Events During OFCP Processing
synthetic oligomer
vinyl
OFCP (3), Et3N, DMF
0 °C –> 25 °C; concentrate
then add KOSiMe3 or Cs2CO3 in DMF/THF
vinyl
Sn2'
vinyl
- one flask
- no protecting groups
- no heavy metals
5
6
7
8
B Negative Hyperconjugation Stabilizes Substitution Intermediates
C OFCP Mediated Direct Polycyclizations
Ac-YNCTFC-NH2
9a (41%)
Ac-HFCASC-NH2
10b (27%)
Ac-HFSCAC-NH2
11b (42%)
Ac-YGHCAC-NH2
12a (30%)
Ac-YGSHAC-NH2
4b (40%)
Ac-YGSdHAC-NH2
13a (57%)
Ac-YGTMQVSHAC-NH2
14c (45%)
Ac-D(C)VHSAY-NH2
15c (10%)
Side-chain initiated cascades
Ac-YGAE(C)H-NMe2
16c (8%)

Scheme 4.2.1 Direct macrobicyclization of linear unprotected peptides. (**A**) Progression of substitution events during OFCP processing. (**B**) Computational rendering of delocalized HOMO present in intermediate formed by model reaction of OFCP and ethyl mercaptide. Demonstrates negative hyperconjugation stabilization of substitution intermediates. See Experimental Section for computational details. (**C**) Products resulting from OFCP mediated direct polycyclizations. Linear peptides were synthesized on solid phase as N-terminal acetamides and cleaved as primary C-terminal carboxamides. Yields reflect preparative HPLC isolation wherein all histidine derived products were isolated as TFA salts. Reagent and Conditions: a) OFCP (1.5 equiv.), Et_3N (2.5 equiv.), DMF (5.0 mM), 0°C, 30 min; conc. then Cs_2CO_3 (6.0 equiv.), 1:4 DMF/THF (5.0 mM), 0°C –> RT, 3 h, (>10:1 d.r.). b) OFCP (1.5 equiv.), Et_3N (2.5 equiv.), DMF (5 mM), 0 °C, 30 min; conc. then $KOSiMe_3$ (4.0 equiv.), 1:4 DMF/THF (5.0 mM), 0°C –> RT, 3 h, (>10:1 d.r.). c) same as b) except using solely DMF as solvent.

It is possible to isolate and characterize vinyl fluorides **7** (**Scheme 4.2.1A**). As shown in **Scheme 4.2.2A**, treatment of linear peptide Ac-CWSC-NH_2 with OFCP followed by $KOSiMe_3$ affords spiro tricyclic compound **17** (35%, >10:1 d.r.). Under identical conditions, the same sequence containing D-cysteine affords epimeric macrocycle **25** (**Scheme 4.2.2B**), while its homo cysteine variant affords spiro thiazepinone **26** in good yield and diastereoselectivity (>10:1 d.r.). Smaller ring analogs are also accessible. Omitting the tryptophan residue results in the formation of spiro tricyclic substance **24**.

The vinyl fluoride in **17** can be intercepted in bimolecular reactions to give a variety of substituted and homologated derivatives. It reacts with commercial β-D-thioglucose sodium salt within minutes at 25˚C to afford unprotected glycoconjugate **19** in near quantitative yield. By varying the peptide sequence and the thioglycoside used, amalgamations with OFCP could generate a new class of glycosylated cyclic peptidomimetics. Compound **17** also reacts with a coniferyl alcohol derivative to afford **20**. The cinnamyl carbonate in **20** provides means to form an additional large ring via electrophilic capture of amines, carboxylates, imidazoles and pi basic aromatic residues (e.g. see **Scheme 4.1.1B**).[3-11] Azidation of **17** with NaN_3 in DMF provides vinyl azide **21** in >95% yield. This molecule participates in Sharpless/Huisgen ‘click’ cycloadditions

with terminal alkynes. Stirring **21** with 1.0 equiv. of propargyl alcohol in the presence of a phenylenediamine ligated Cu^{II} catalyst affords triazole **23** in 75% yield.[21] Alternatively, azide **21** can be hydrogenolyzed to afford β-thio enamine **22**. This molecule can be purified without hydrolysis. Its amino group strongly resists acylation, even with Ac_2O / DMAP. Proximal fluorination attenuates its nucleophilicity. In fact, inductive deactivation appears to have an impact on the stability of these structures in general. For example, **13** and **24** are stable (<5% loss by HPLC analysis) in aqueous buffer of varying pH for extended periods of time (72h at pH 4.5, 7.0 and 10.0, 25°C). In addition, both compounds were stable to superstoichiometric amounts of N-chlorosuccinimide (NCS) and 30% aq. H_2O_2 (2.0 eq. oxidant, pH 4.5 buffer / CH_3CN, 25˚C) over 72h. The alkene, the thioaminoketal, the imidazole and the sulfur atoms were unaffected in these experiments. For comparison, the disulfide derived from hexapeptide HFCASC (**S30**, the linear precursor to **10**) decomposed at pH 10.0 and reacted readily with NCS (see Experimental Section for details).

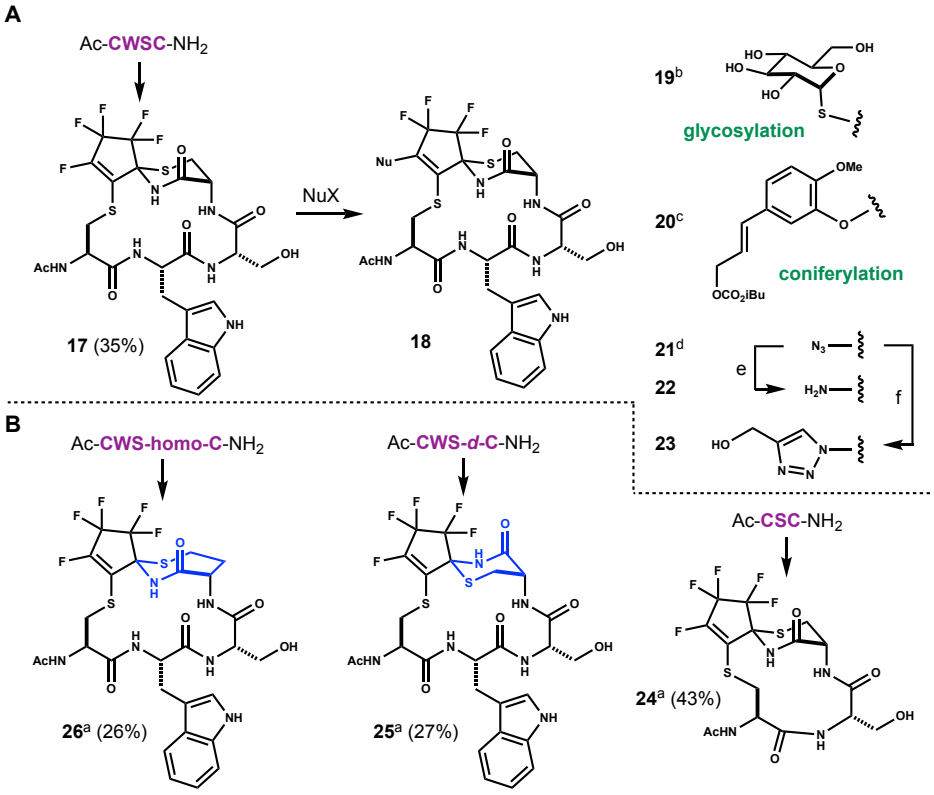

Scheme 4.2.2 Intermediate spirocyclic vinyl fluoride derivatization with exogenous nucleophiles. (**A**) Bimolecular substitution reactions using compound **17**. (**B**) Linear peptides were synthesized on solid phase as N-terminal acetamides and cleaved as primary C-terminal carboxamides. Yields reflect preparative HPLC isolation. Reagents and conditions: a) OFCP (1.5 equiv.), Et_3N (2.5 equiv.), DMF (5.0 mM), 0°C, 30 min; conc. then $KOSiMe_3$ (2.0 equiv.), 1:4 DMF/THF (5.0 mM), 0°C –> RT, 1 h, (>10:1 d.r.). b) beta-D-Thioglucose sodium salt (1.0 equiv.), DMF (50 mM), 0°C, 1 h, >95%. c) Coniferyl Carbonate **33** (2.0 equiv.), $KOSiMe_3$ (4.0 equiv.), DMF (50 mM), 0°C –> RT, 12 h, 53%. d) NaN_3 (1.0 equiv.), DMF (50 mM), 0°C, 1 h, >95%. e) H_2, Pd/C (10 wt %), EtOH, 35°C, 12 h, 87%. f) Propargyl Alcohol (1.0 equiv.), Phenylenediamine (15 mol %), Sodium ascorbate (10 mol%), $CuSO_4 \cdot 5H_2O$ (5 mol%), 2:3 H_2O:tBuOH (0.2 M), 12 h, 75%.

4.3: OFCP Macrobicyclization using Small-Molecule Inserts

The reactivity of intermediate vinyl fluorides **7** (**Scheme 4.2.1A**) provides options to form a second large ring using molecular inserts. This markedly expands the diversity of possible outcomes. In these experiments (**Scheme 4.3.1A**), initial OFCP mediated macrocyclizations and base-induced spirocyclizations occur in one flask as before. The incipient spirocyclic vinyl fluorides are then captured in situ with a nucleophile that can be subsequently activated as an electrophile. For example, treating linear peptide Ac-YACFAC-NH_2 with 1.5 eq. OFCP (Et_3N, DMF) forms a macrocycle at 0˚C (**Scheme 4.3.1B**). Subsequent exposure to $KOSiMe_3$ generates a spirocyclic vinyl fluoride that is intercepted in situ with hydroxymethylated thiazole thione **29** to afford **30** in good yield.[22] The strong nucleophilicity of the exocyclic sulfur atom in **29** permits biomolecular substitution to outcompete internal macrocyclization of the tyrosyl phenol in this system. Warming a $MeNO_2$ solution of **30** containing 7.5 vol % TFA ionizes the primary hydroxyl group and the incipient methyldene thiazolium cation captures the tethered phenol via C-C bonding to generate macrobicyclic structure **31** in good yield.

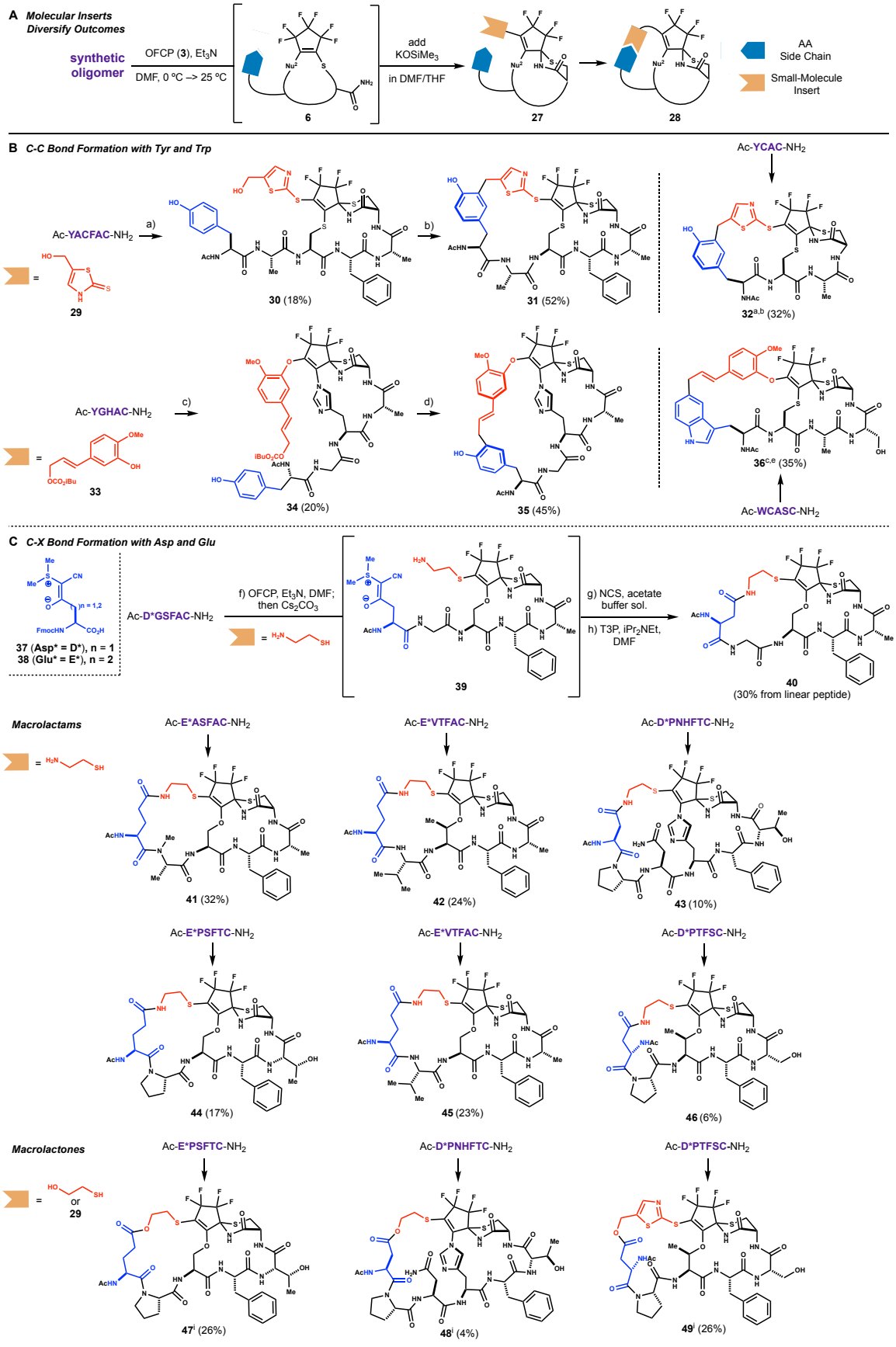
A Molecular Inserts Diversify Outcomes
synthetic oligomer
OFCP (3), Et3N
DMF, 0 °C –> 25 °C
6
add KOSiMe3
in DMF/THF
27
28
AA Side Chain
Small-Molecule Insert
B C-C Bond Formation with Tyr and Trp
Ac-YACFAC-NH2
a)
30 (18%)
b)
31 (52%)
29
Ac-YCAC-NH2
32a,b (32%)
Ac-YGHAC-NH2
c)
34 (20%)
d)
35 (45%)
33
36c,e (35%)
Ac-WCASC-NH2
C C-X Bond Formation with Asp and Glu
37 (Asp* = D*), n = 1
38 (Glu* = E*), n = 2
Ac-D*GSFAC-NH2
f) OFCP, Et3N, DMF; then Cs2CO3
39
g) NCS, acetate buffer sol.
h) T3P, iPr2NEt, DMF
40
(30% from linear peptide)
Macrolactams
Ac-E*ASFAC-NH2
41 (32%)
Ac-E*VTFAC-NH2
42 (24%)
Ac-D*PNHFTC-NH2
43 (10%)
Ac-E*PSFTC-NH2
44 (17%)
Ac-E*VTFAC-NH2
45 (23%)
Ac-D*PTFSC-NH2
46 (6%)
Macrolactones
Ac-E*PSFTC-NH2
47i (26%)
Ac-D*PNHFTC-NH2
48i (4%)
Ac-D*PTFSC-NH2
49i (26%)

Scheme 4.3.1 Synthesis of OFCP scaffolded macrobicyclic structures using small-molecule inserts. (**A**) Depict general use of small molecules inserts to diversify macrobicyclic products. (**B**) C-C bond formation with Tyr and Trp. (**C**) C-X bond formation with Asp and Glu. Linear peptides were synthesized on solid phase as N-terminal acetamides and cleaved as primary C-terminal carboxamides. Yields reflect preparative HPLC isolation wherein all histidine derived products were isolated as TFA salts. Yields shown for **40**–**49** refer to isolated yields from their respective linear oligomers. Reagents and conditions: a) OFCP (1.5 equiv.), Et_3N (2.5 equiv.), DMF (10 mM), 0°C, 30 min; conc. then $KOSiMe_3$ (3.5 equiv.), thiazole **29** (1.2 equiv.), 1:4 DMF/THF (30 mM), 0°C –> RT, 3 h. b) 7.5% TFA, $MeNO_2$ (5.0 mM), 80°C, 12 h. c) OFCP (1.5 equiv.), Et_3N (2.5 equiv.), DMF (10 mM), 0ºC, 30 min; conc. then Cs_2CO_3 **(**6.0 equiv.) 1:4 DMF/THF (30 mM) 0ºC, 1 h; then **33** (2.0 equiv.) 0ºC –> RT, 48 h. d) Tf_2NH (5.0 equiv.), $MeNO_2$ (2.5 mM), RT, 1 h. e) $Sc(OTf)_3$ **(**1.0 equiv.), $MeNO_2$ (5.0 mM), RT, 1 h. f) OFCP (1.5 equiv.), Et_3N (2.5 equiv.), DMF (10 mM), 0ºC, 30 min; conc. then Cs_2CO_3 (5.0 equiv.), 1:4 DMF/THF (30 mM), 0ºC, 1 h; then cysteamine, 2-mercaptoethanol, or **29** (1.2 equiv.), 0ºC, 1 h. g). N-Chlorosuccinimide (1.5–3.0 equiv.), 2:8 MeCN:NaOAc/AcOH (acetate buffer, pH 4.5) (1.0 mM), RT, 1 h. h) propanephosphonic acid anhydride (T3P) (1.5 equiv.), iPr_2NEt **(**3.5 equiv.), DMF (5.0 mM), 0ºC, 1 h. i) Macrolactonization done using EDC•HCl (3.0 equiv.), HOBt (2.0 equiv.), Et_3N (5.0 equiv.), DMF (5.0 mM), 0ºC –> RT, 44–64 h.

This alkylative macrocyclization is tolerant of varying ring sizes and substitution patterns. Reacting the 4-mer Ac-YCAC-NH_2 with OFCP and **29** in the same process as above affords macrobicycle **32** wherein each large ring contains one less amino acid residue. Replacing **29** with coniferyl alcohol derivative **33** provides for further options. For example, treating linear peptide Ac-YGHAC-NH_2 with OFCP (Et_3N, DMF) followed by an excess of Cs_2CO_3 generates a macrocyclic vinyl fluoride that reacts with added **33** (2.0 equiv.) to provide phenolic ether **34**. Relative to **29**, the capture rate by **33** is slower but the product is stable under the extended reaction conditions and is easily purified. When **34** is treated with Tf_2NH in $MeNO_2$ at 25˚C for 1 h, preparative HPLC provides imidazolium bridged macro-bicyclic structure **35** in good yield. As we have shown previously, the cinnamyl cation, generated either as a solvated ion pair or in metal stabilized form, is adept at large ring formations. When liner peptide Ac-WCASC-NH_2 is treated successively with OFCP and **33** as before and the resultant product is ionized with $Sc(OTf)_3$ in

$MeNO_2$, novel indole-linked macrobicycle **36** is produced. Internal cinnamylation engages the otherwise unreactive (towards OFCP) tryptophan side chain in C-C bond formation.

The side chains of Asp and Glu were also potential sites for ring closures (**Scheme 4.3.1C**). However, free carboxylate groups caused OFCP reactions to be chaotic and low yielding. Bode had developed a cyanosulfurylide masked form of Asp (D*) to avoid aspartimide forming truncations during SPPS.[23] We synthesized monomer **37** and its new one carbon homolog **38**. Each proved to be an excellent surrogate for Asp and Glu, respectively, during peptide synthesis and OFCP processing. For example, linear peptide Ac-D*GSFAC-NH_2 reacts successively with OFCP and Cs_2CO_3 to give a spirocyclic vinyl fluoride that is captured in situ with commercial cysteamine to form adduct **39** (>10:1 d.r.). It is not necessary to isolate this species. Rather, mild oxidative hydrolysis of the cyanosulfurylide (NCS, CH_3CN /pH 4.5 acetate buffer, 25˚C) provides the corresponding carboxylic acid in high yield. Lactamization of the incipient amino acid then affords macrobicyclic compound **40** in 30% overall yield from the starting peptide. Product **40** contains a bridging serine residue. Identical OFCP processing of cyanosulfurylide residue containing peptides tolerates variations in peripheral functionality (see **41**, **44**, **45**) as well as threonine bridging (**42** and **46**). The synthesis of imidazolium salt bridged macrobicycle **43** directly from linear peptide Ac-D*PNHFTC-NH_2 highlights the complexity forming potential of the methods. Replacing cysteamine with 2-mercaptoethanol or thiazole thione **29** permits the EDC mediated synthesis of macrolactones **47**–**49**. Structures of this kind are prototypes for a new class of hybrid cyclodepsipeptides.

4.4: Computational Evaluation of Loop Mimicry Potential

Inhibiting protein-protein interactions (PPIs) with synthetic molecules remains a frontier of chemical biology and is a growing field in drug discovery.[24] Recent work shows cyclic peptides and peptidomimetics are particularly adept at inhibiting PPIs due to their ability to serve as potent and selective ligands for PPI mediating surfaces.[25-26] While many PPIs have been successfully targeted by mimicking α-helices at protein-protein interfaces, the majority of characterized PPIs are mediated by non-helical, non-strand surface loops.[27] In 2014, Kritzer and coworkers sought to comprehensively identify and analyze these loop-mediated PPIs by writing and implementing LoopFinder; a customizable program that could identify loop-mediated PPIs within all of the protein-protein complexes deposited into the Protein Data Bank.[28] Analysis of this entire set of 25,005 interface loops revealed common structural motifs and features that distinguish loop-mediated PPIs from other PPIs. Furthermore, the data showed that the large majority of these PPI mediating loops cluster into just 11 general structural types based on backbone torsional angles and hydrogen bonding patterns. These 'Hot loops', which Kritzer named in analogy to protein hot spots, were identified as loops with favorable properties for mimicry using synthetic molecules. Because spectroscopic data indicated the thiazaspirodecenone scaffolded double looped structures in **Scheme 4.2.1C** to be conformationally well defined, we hypothesized that selective mimics of Kritzer's 'hot' loops might be devised by varying ring sizes on either side of the bridging residue.[29]

To probe this idea, we started by creating an in silico library of hypothetical macrobicycles resultant from OFCP processing of linear peptides derived from the sequence Ac-X–$(Ala)_m$–Y–$(Ala)_n$–Cys-NH_2 sequences: where X = Cys, His and Tyr, Y = Cys and His and m, n = 1–5. **Figure 4.4.1** shows a visual schematic of how this library was generated. As indicated shown, library members were given five-digit alphanumeric codes for labelling and reference purposes, with

letters corresponding to 1 letter amino acid abbreviations and numbers representing the number of intervening L-alanine residues between nucleophilic amino acids. For this hypothetical library, L-alanine was chosen as the generic amino acid with which to compose the macrocyclic rings due to its ability to capture key *Cα-Cβ* vectors which represents preferred projections of many amino acid combinations.[30] In this way, we reasoned that the use of L-alanine would reveal conformational biases of the core structure, unperturbed by sidechain-to-sidechain interactions, allowing for a conformational search landscape which would necessarily encompass all conformations that could be accessed with more conformationally restrictive side chains.

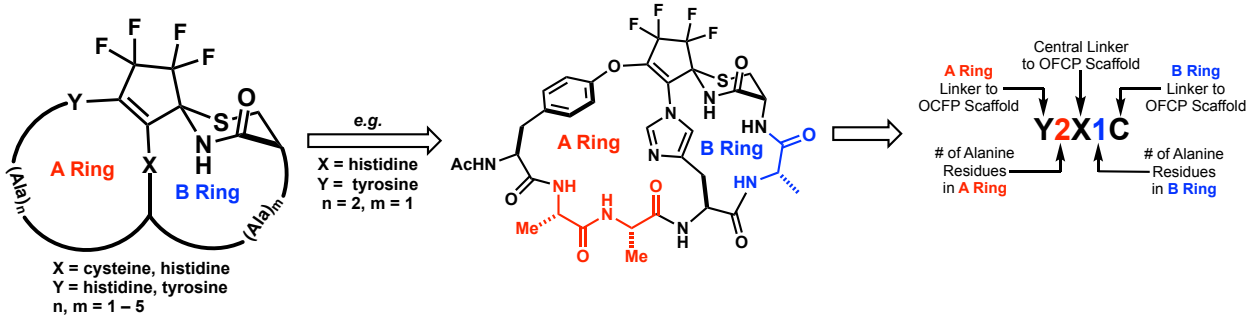

Figure 4.4.1 Creation of a hypothetical OFCP-derived macrobicycle library. General structure of OFCP-derived poly-alanine macrobicycles (left), a select example of an OFCP-derived poly-alanine macrobicycle (center) and an explanation of library naming convention (right). OFCP processed macrobicycles are named based on the amino acid sequence of the peptide from which they are derived with letters corresponding to 1 letter amino acid abbreviations and numbers representing the number of intervening L-alanine residues between nucleophilic amino acids.

Figure 4.4.2 shows the computational workflow we used to assess the mimicry potential of these hypothetical library members. As shown, the developed workflow begins with the geometry optimization of our 150 hypothetical library members. This was done using the AMBER* forcefield in a high dielectric solvent meant to simulate aqueous conditions. From the resulting 150 energy minimized structures, low energy conformations for each were identified using a Monte Carlo search algorithm using a search window of 5 kcal/mol from the lowest energy calculated structure (see Experimental Section for details). This resulted in a conformational

library composed of just over 5,700 members. With this conformational library in hand, we then selected a single loop from each of the 11 loop types identified by Krtizer to serve as a representative for it respective loop type. This was done by analyzing the average backbone torsional angles for each group and then selecting the member whose torsional angles were closest to the average for its respective group. While we understood that this method of representative selection did not account for the varied torsional angles that might exist within a given group, we concluded this simplification necessary to minimize computational run-time in future steps.

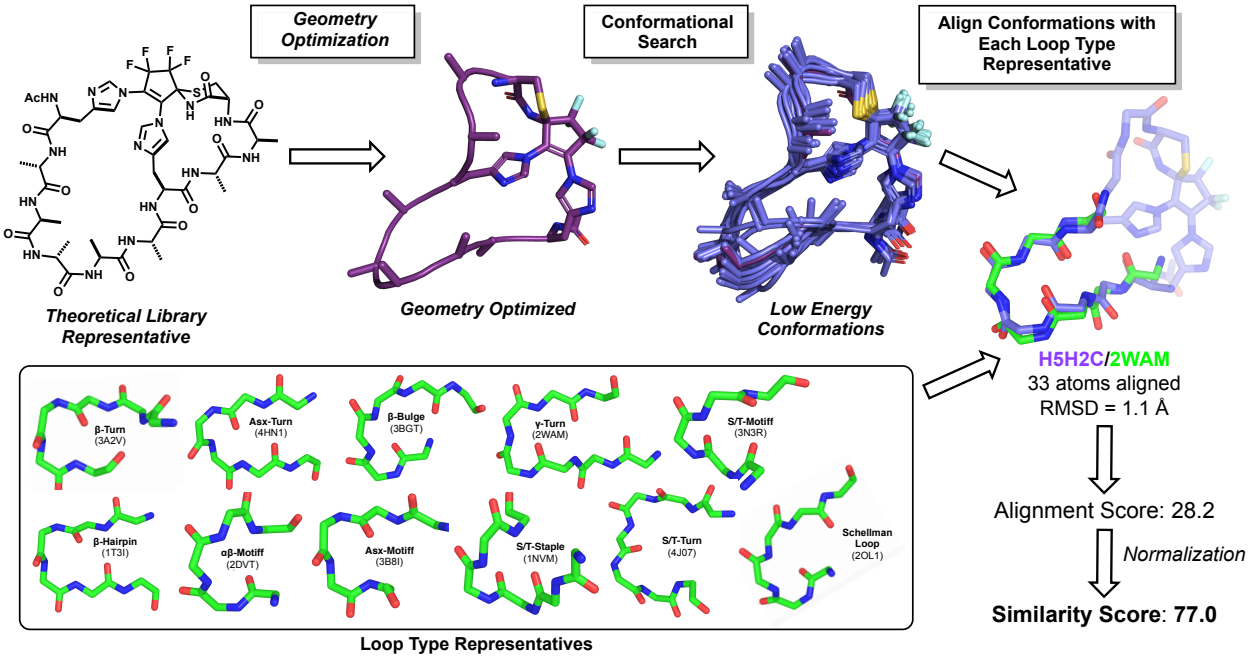

Figure 4.4 2 Computational workflow for determination of loop mimicry potential**.** Each of the 150 hypothetical OFCP-derived macrobicycles used in this study were geometry optimized using molecular force fields and low energy conformations were identified using a Monte Carlo search algorithm. Low energy conformers of each library member were overlaid onto a representative of the 11 Kritzer loop types using the PyMOL® superposition function. The resulting generated MatchAlign scores were normalized relative to loop self-superimposed maximal values to yield 'similarity scores'.

With all of the components needed for this analysis assembled, mimicry potential was assessed by systematically overlaying each member from the conformational library onto each of the selective loop type representatives. This was done using the PyMOL® superposition function[31]

in conjunction with a custom Python script written by Dr. Declan Evans of the Houk Group. For this particular application, the superposition function was used, as opposed to the align or cealign function, as it has been found to be preferable when comparing proteins with relatively low sequence identity. This systematic alignment resulted in the generation of MatchAlign scores for each conformers/loop pair which is a non-linear function of the number of atoms used in the superposition as well as the root-mean-square deviation (RMSD) of those aligned atoms. Because these MatchAlign scores do not allow for appropriate comparison between various conformer/loop pairs for which the loops are of different size and composition, these MatchAlign scores were normalized relative to representative loop self-superimposed maximal values. In this way, obtained MatchAligned scores were normalized to yield 'percent similarity' scores which range from 0, indicating the conformer and representative loop share no structural similarity, to 100, indicating that the conformer and representative loop bear perfect structure similarity. This method to evaluate structural mimicry permits meaningful comparisons across macrobicycle and representative loop size variations.

The percent similarity scores obtained from this systematic alignment was used to construct the heat map shown in **Figure 4.4.3** with library members that best mimic each representative loop type plotted along the diagonal (top right to bottom left). This core data set identifies close mimics (percent similarity > 75%) for six of the eleven major PPI mediating loop types. Of these six, three appear quite selective, despite the analysis lacking side chain annotations. Visualization of these optimal overlays shows mimicry is calculated to occur at both the N-terminal loop (see 2WAM/H5H2C overlay) and the C-terminal loop (see 2OL1/H1H5C overlay) as well as the composite surface created at the double loop junction (see 3N3R/Y4C1C overlay). This finding was not at all unexpected as we hypothesized that the dual-looped nature of these macrobicycles

would allow for multiple potential modes of mimicry. Visual overlays depicting the best mimic of each representative loop type are shown in see **Figure 4.7.18.**

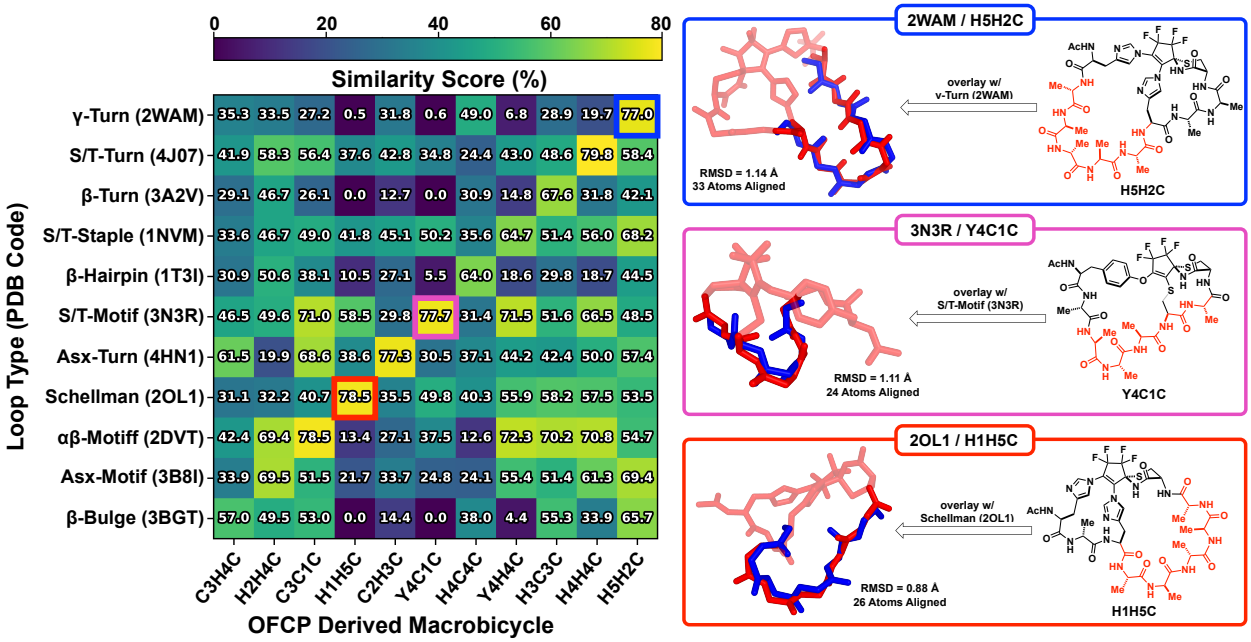

Figure 4.4.3 Results of determination of OFCP-derived macrobicycle loop mimicry potential. Heat map shows percent similarity scores between select OFCP-derived macrobicycles (x-axis) and select lop type representatives (y-axis). Data along the diagonal (top right to bottom left) shows those macrobicycles which best structurally mimics each loop type. See **Figure 4.1.1** for library member naming convention. Reaction schemes to synthesize CXCXC and HXHXC derived macrobicycles are described in the Experimental Section. As shown, OFCP-derived macrobicycles demonstrate good loop mimicry utilizing their N-terminal loop (2WAM/H5H2C), C-terminal loop (2OL1/H1H5C) as well as the composite surface created at the double loop junction (3N3R/Y4C1C) of the macrobicycle.

Analysis of the data generated from this systematic overlay shows that the size of the non-mimicking loop has a marked effect on the conformational preference of the mimicking ring. This is well demonstrated in **Figure 4.4.4**.For example, the 4J07/H4H4C overlay has a similarity score of 79.8 while the closely related 4J07/H4H5C overlay, which differs by only a single alanine residue in the N-terminal ring, has a similarity score of 8.6. This suggests the ability to conformationally fine tune the mimicking ring by making small structural perturbations to the non-

mimicking ring, just one of the many advantages afforded by the dual-turn surface nature of these compounds.

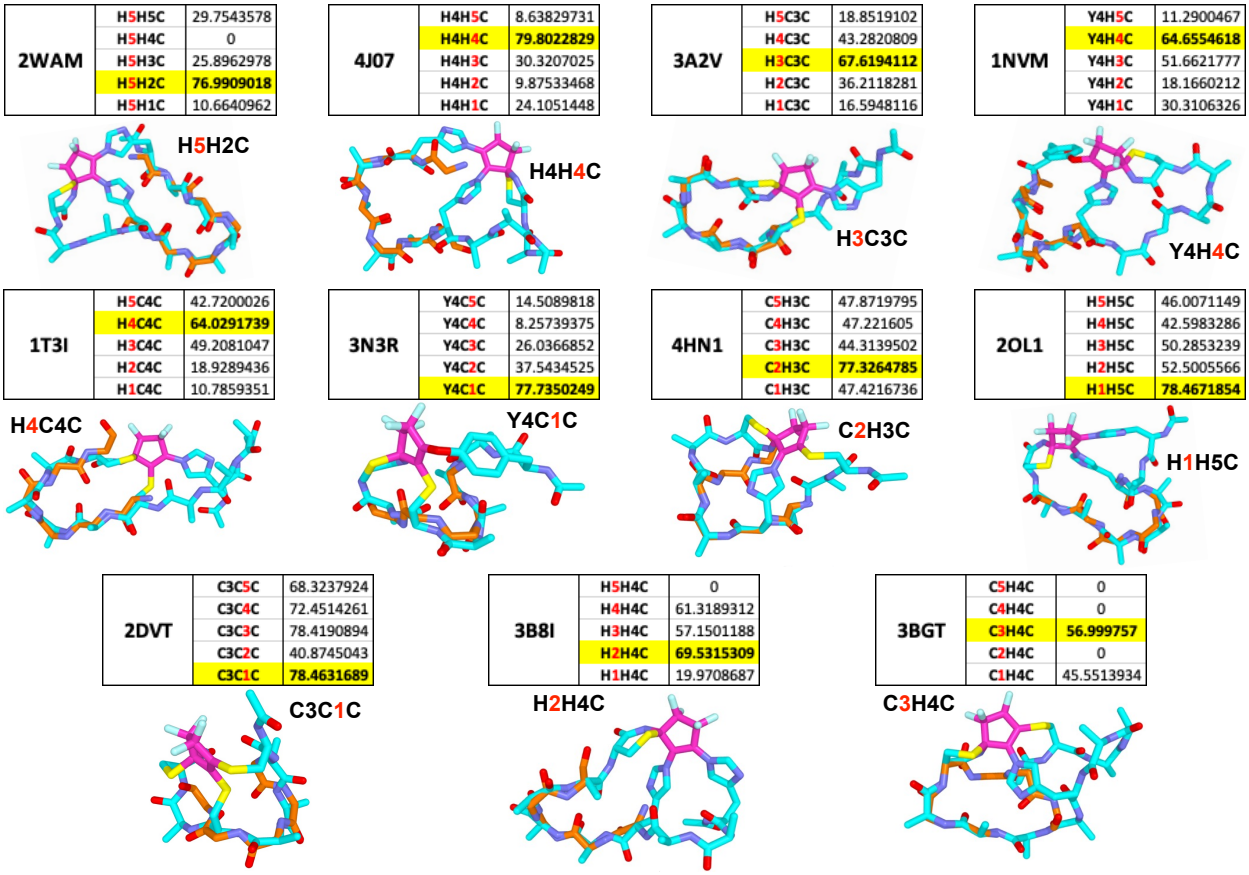

Figure 4.4.4 Analysis of loop mimicry potential with non-mimicking ring size variation. Figure shows the library members that best mimic each representative loop type (similarity score highlighted in yellow) along with the similarity scores of related library members that differ only in the size of the non-mimicking ring.

While this computational study greatly suggests that these OFCP-derived macrobicycles can serve as selective mimics for a majority of Kritzer's loop types, we are eager to prove this hypothesis. Towards this goal, we plan to use the use the data outlined in **Figure 4.4.3** to create medicinally relevant PPI mediating loop mimics for each of the loop types identified by Kritzer. We feel that this method of experimental validation is the most straight forward towards proving

our hypothesis and will demonstrate the ability of our OFCP-derived macrobicycles to serve as selective and potent mimics of a wide variety of biologically relevant PPIs.

4.5: OFCP-Derived Macrocycle and Macrobicycle Passive Membrane Permeability

Computed backbone overlays generate hypotheses that can be validated in future experiments. The utility of those experiments will be broader if the macrocyclic compounds are membrane permeant. Intracellular PPIs are particularly challenging to target with peptidic structures. Cyclic peptides having mw > 1 kDa are rarely taken up passively into cells.[32] Below 1 kDa, numerous factors must be considered. The fluorinated polycycles generated in this study are new chemotypes that have not been evaluated for permeability in any format. OFCP derived macrocycles were analyzed in parallel artificial membrane permeability assays. Averaged data is plotted in **Figure 4.5.1**. Nearly 30% of the molecules tested showed $P_{app} > 1.0 \times 10^{-6}$cm/sec, a 'significant' permeability benchmark recently advocated by Baker et al. in studies of computationally designed peptidyl macrocycles.[33] Notably, P_{app} measured for several compounds approached that of diclofenac and chloramphenicol – low molecular weight, orally bioavailable drugs used as permeability standards. Both mono and bimacrocyclic structures were among the most permeable (see **Figure 4.5.1**).

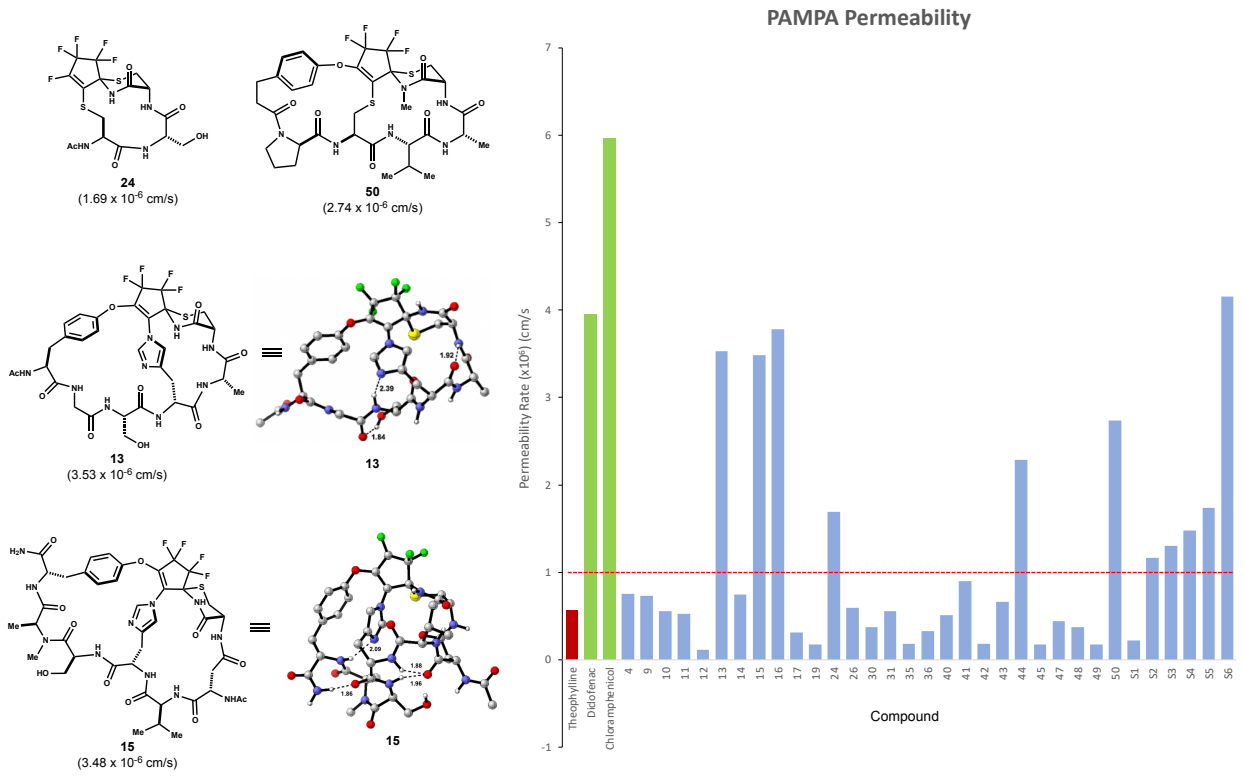

Figure 4.5.1 Evaluation of passive membrane permeability in vitro using PAMPA. Bar graph shows averaged data from two independent experiments, each performed in technical replicate in a 96-well format via UV-vis detection (see Experimental Section for details and data). Theophylline, diclofenac and chloramphenicol were used as low, medium and high permeability standards respectively. See Experimental Section for a complete list of all molecules tested. PAMPA analyses of linear peptide precursors was complicated by their insolubility in assay buffer. Calculated low energy conformers of **13** and **15** were calculated using Schrodinger Maestro Macromodel® and rendered using CylView®. Annotated intramolecular hydrogen bonds were identified using Schrodinger Maestro Macromodel® with bond length given in angstroms (see Experimental Section for details).

In general, macrobicyclic products from **Scheme 4.3.1C** show greater passive membrane permeability than their seco precursors. Imidazole bridged macrobicycle **13** has mass = 804 Da, 8 H-bond donors and a calculated tPSA = 249 A^2, yet it is one of the most permeable compounds tested. Calculated low energy conformations of **13** (free base) in a low dielectric field appear to be stabilized by transannular hydrogen bonding in both large rings (shown in **Figure 4.5.1**). Low energy conformers of doubled looped structure **15** are also calculated to be structured by internal

hydrogen bonding, involving both the bridging imidazole and peripheral functional groups. 'Chameleonic' conformational behavior that can transiently shield polar surface area is thought a contributing factor for passive permeability observed in other 'beyond rule of 5' macrocycles.[34] However, experimental studies on larger compound sets will be needed to define parameters, including internal hydrogen bonding and peripheral fluorination, most correlated with passive membrane permeability in these systems.

4.6 Conclusion

Relative rate controlled polysubstitution cascades using perflurorocycloalkenes is new methodology to rapidly generate complex fluorinated composite macrocycles. OFCP can directly polycyclize linear peptide sequences using native functionality, or fluorospirohetero-cyclic intermediates can be intercepted with exogenous nucleophiles. The latter tactic can generate a range of molecular hybrids composed of peptides, sugars, lipids and heterocyclic components. The platform can create both single and double looped macrocycles in multiple stereoisomeric forms. Subsets of these molecules will have low energy conformers that shield polar surface area through intramolecular hydrogen bonding, a behavior that may correlate with passive membrane permeability. Ongoing studies are focused on OFCP mediated polycyclizations that generate fluorinated molecular probes for chemical biology research, new classes of glycopeptide conjugates, novel fluorinated antimicrobials and molecular 'glues', as well as stable shape mimics of diverse loop structures mediating intracellular PPIs.[35]

4.7 Experimental Section

General Methods and Materials

Unless otherwise specified, reactions were performed in flame-dried glassware under an atmosphere of argon using anhydrous solvents. Reagents were purchased from commercial vendors and used as received unless otherwise stated. Tetrahydrofuran (THF), diethyl ether (Et_2O), acetonitrile (MeCN) and toluene (PhMe) were passed through a Glass Contour solvent drying system. Anhydrous N,N dimethylformamide (DMF) was purchased from Supelco, Inc – Sigma Aldrich. Yields refer to chromatographically and spectroscopically (^{1}H-NMR) homogeneous materials, unless otherwise stated. Thin-layer chromatography (TLC) was conducted on precoated plates (Sorbent Technologies, silica gel 60 PF254, 0.25 mm) visualized with UV 254 nm. Column chromatography was performed on silica gel 60 (SiliCycle, 240−400 mesh). Purification of peptides was performed using an Agilent 1200 HPLC system equipped with G1361A preparative pumps, a G1314A auto sampler, a G1314A VWD, a G1364B automated fraction collector, and a Waters Sunfire C18 column (5 μm, 19 mm × 250 mm), unless otherwise noted. 0.1% TFA in MeCN/H_2O solvent system. Analytical HPLC was performed using the same system, but with a G1312A binary pump. 0.1% TFA in MeCN/H_2O solvent system. Mass spectra were recorded using an Agilent 6130 LC/MS system equipped with an ESI source. High-resolution mass spectra were recorded on Thermo Scientific Exactive® Mass Spectrometer with DART ID-CUBE Waters GST Premier, Waters LCT Premier, and Agilent 6545 LC-QTOF. NMR spectra were recorded on Bruker Avance spectrometers (400/100 MHz, 500/125 MHz, and 600/150 MHz). NMR spectra were recorded on Bruker Advance (300, 400, 500, or 600 MHz) spectrometers. HSQC, HMBC,

and COSY NMR experiments were used to aid assignment of NMR peaks when required. All ^{19}F NMR spectrums used $CFCl_3$ as a calibration standard.

General Experimental Procedures

Peptide Synthesis for primary C-terminal carboxamides:

C-terminal carboxamide peptides were synthesized manually using standard Fmoc solid phase synthesis protocols on Rink Amide MBHA resin (200-400 mesh, 0.73 mmol/g, 1% DVB) on 0.37–0.50 mmol scale using a fritted glass reaction vessel. Fmoc-deprotection was achieved with 2%/5% DBU/piperazine in DMF (1 x 15 min). The reaction vessel was washed with DMF (2x), CH_2Cl_2 (2x), and DMF (2x). The vessel was then charged with the appropriate Fmoc-amino acid (3.0 equiv.) and HBTU (3.0 equiv.) followed by DMF (10–20 mL) and iPr_2NEt (10.0 equiv.). The resin was shaken for 45 minutes, drained, and washed with DMF (2x), CH_2Cl_2 (2x), and DMF (2x). Couplings involving secondary amines such as Pro or Asp*/Glu* were left to shake for 90 minutes. After all couplings were completed, the resin was cleaved by shaking with a solution of 90:5:5 TFA/H_2O/TIPS (27 mL of TFA, 1.5 mL of H_2O and TIPS) for 90 minutes. The cleaved resin was filtered and rinsed with Et_2O until ~200 mL of volume. The peptide was then triturated, and this process repeated with Et_2O (2x) to afford crude peptide. This crude peptide was then stripped with anhydrous PhMe (3x) to afford the desired linear peptide. If necessary, the resulting rude peptide was then purified via preparative HPLC.

Peptide synthesis for secondary C-terminal carboxamides:

C-terminal carboxamide peptides were synthesized manually using standard Fmoc solid phase synthesis protocols on 2-chlorotrityl chloride resin (100–200 mesh, 1.02 mmol/g, 1% DVB)

on 1.02 mmol scale using a fritted glass reaction vessel. Fmoc-deprotection was achieved with 2%/5% DBU/piperazine in DMF (1 x 15 min). The reaction vessel was washed with DMF (2x), CH_2Cl_2 (2x), and DMF (2x). The vessel was then charged with the appropriate Fmoc-amino acid (3.0 equiv.) and HBTU (3.0 equiv.) followed by DMF (10–20 mL) and iPr_2NEt (10.0 equiv.). The resin was shaken for 45 minutes, drained, and washed with DMF (2x), CH_2Cl_2 (2x), and DMF (2x). Couplings involving secondary amines such as Pro or Asp*/Glu* were left to shake for 90 minutes. After all couplings were completed, the resin was cleaved by shaking with a solution of 1:99 TFA:CH_2Cl_2 (3 x 33 mL, total of 100 mL). Filtered onto a solution filled with 1:9 pyridine:MeOH (100 mL). Concentration under reduced pressure afforded desired crude peptide. This crude peptide was then capped with $MeNH_2$. C-terminus capping was achieved following general EDC•HCl/HOBt coupling protocol. After capping, the crude peptide was purified via preparative HPLC.

Scheme 4.2.1 General Procedure A: Direct Macrobicyclization

To a flame-dried round bottom flask equipped with a stir bar was charged with linear peptide (1.0 equiv.), diluted with anhydrous DMF (5.0 mM), and then allowed to stir at 0ºC. Then OFCP (1.5 equiv., 1.0 M in MeCN) was added followed by NEt_3 (2.5 equiv.). The reaction mixture was allowed to stir at 0 ºC for 30 min. When HPLC indicated macrocycle intermediate formation, the reaction mixture was concentrated under reduced pressure to dryness. The reaction residue was then diluted with 1:4 DMF/THF (5.0 mM) and stirred at 0 ºC. Then Cs_2CO_3 (6.0 equiv.) was added, and the reaction mixture allowed to gradually warm up to 23ºC for 3 h. When HPLC indicated reaction completion, the reaction mixture was quenched with AcOH (10.0 equiv.) and then

concentrated under reduced pressure to afford crude product. The crude product was then purified via preparative HPLC – see details for specific examples below.

Scheme 4.2.1 General Procedure B: Direct Macrobicyclization

To a flame-dried round bottom flask equipped with a stir bar was charged with linear peptide (1.0 equiv.), diluted with anhydrous DMF (5.0 mM), and then allowed to stir at 0ºC. Then OFCP (1.5 equiv., 1.0 M in MeCN) was added followed by NEt_3 (2.5 equiv.). The reaction mixture was allowed to stir at 0ºC for 30 min. When HPLC indicated macrocycle intermediate formation, the reaction mixture was concentrated under reduced pressure to dryness. The reaction residue was then diluted with 1:4 DMF/THF (5.0 mM) and stirred at 0ºC. Then KOTMS (4.0 equiv.) was added, and the reaction mixture allowed to gradually warm up to 23ºC for 3 h. When HPLC indicated reaction completion, the reaction mixture was quenched with AcOH (10.0 equiv.) and then concentrated under reduced pressure to afford crude product. The crude product was then purified via preparative HPLC – see details for specific examples below.

Scheme 4.2.1 General Procedure C: Direct Macrobicyclization

To a flame-dried round bottom flask equipped with a stir bar was charged with linear peptide (1.0 equiv.), diluted with anhydrous DMF (5.0 mM), and then allowed to stir at 0ºC. Then OFCP (1.5 equiv., 1.0 M in MeCN) was added followed by NEt_3 (2.5 equiv.). The reaction mixture was allowed to stir at 0ºC for 30 min. When HPLC indicated macrocycle intermediate formation, the reaction mixture was concentrated under reduced pressure to dryness. The reaction residue was then diluted with DMF (5.0 mM) and stirred at 0ºC. Then KOTMS (4.0 equiv.) was added, and the reaction mixture allowed to gradually warm up to 23ºC for 3 h. When HPLC indicated reaction

completion, the reaction mixture was quenched with AcOH (10.0 equiv.) and then concentrated under reduced pressure to afford crude product. The crude product was then purified via preparative HPLC – see details for specific examples below.

Scheme 4.2.2 General Procedure A

To a flame-dried round bottom flask equipped with a stir bar was charged with linear peptide (1.0 equiv.), diluted with anhydrous DMF (5.0 mM), and then allowed to stir at 0ºC. Then OFCP (1.5 equiv., 1.0 M in MeCN) was added followed by NEt_3 (2.5 equiv.). The reaction mixture was allowed to stir at 0ºC for 30 min. When HPLC indicated macrocycle intermediate formation, the reaction mixture was concentrated under reduced pressure to dryness. The reaction residue was then diluted with 1:4 DMF/THF (5.0 mM) and stirred at 0ºC. Then KOTMS (2.0 equiv.) was added, and the reaction mixture allowed to gradually warm up to 23ºC for 1 h. When HPLC indicated reaction completion, the reaction mixture was quenched with AcOH (10.0 equiv.) and then concentrated under reduced pressure to afford crude product. The crude product was then purified via preparative HPLC – see details for specific examples below.

Scheme 4.3.1 General Procedure F: Macrobicyclization via bond formations with Asp and Glu

To a flame-dried round bottom flask equipped with a stir bar was charged with linear peptide (1.0 equiv), diluted with anhydrous DMF (10.0 mM), and then allowed to stir at 0ºC. Then OFCP (1.5 equiv., 1.0 M in MeCN) was added followed by NEt_3 (2.5 equiv.). The reaction mixture was allowed to stir at 0ºC for 30 min. When HPLC indicated macrocycle intermediate formation, the reaction mixture was concentrated under reduced pressure to dryness. The reaction residue was then added 1:4 DMF:THF (30 mM) and cooled to 0ºC. Then Cs_2CO_3 (5.0 equiv.) was added, and

the reaction mixture allowed to stir at 0ºC for 1 h. When HPLC indicated full conversion to the desired vinyl fluoride then cysteamine, 2-mercaptoethanol, or **29** were added and the reaction mixture allowed to stir at 0ºC for 1 h. When HPLC indicated reaction completion, the reaction mixture was quenched with AcOH (10.0 equiv.) and then concentrated under reduced pressure to afford crude product. The crude product was then telescoped to the next step.

Scheme 4.3.1 General Procedure G: Macrobicyclization via bond formations with Asp and Glu

A 50% yield from General Procedure F was assumed when calculating stoichiometry for this general procedure. To the same round bottom flask used in General Procedure F, the crude product was diluted with a solution 2:8 MeCN:aqueous buffer pH 4.5 (NaOAc/AcOH, 0.1 M). The reaction mixture was then allowed to stir at 23ºC and then was added NCS in MeCN (1.0 M) portionwise (0.5 equiv.). Total NCS varied from 1.5–3.0 equiv. depending on substrate. When HPLC indicated full conversion to the desired free acid, the reaction mixture was quenched with $Na_2S_2O_3$•$5H_2O$ (6.0 equiv.). The reaction mixture was concentrated under reduced pressure to afford crude product. The crude product was then purified via preparative HPLC – see details for specific examples below. Yields shown refer to yields from their linear peptides.

Scheme 4.3.1: General Procedure H: Macrobicyclization via bond formations with Asp and Glu

To a flame-dried round bottom flask equipped with a stir bar was charged with the seco-acid intermediate (1.0 equiv.) and diluted with anhydrous DMF (5.0 mM). The solution was added $iPrNEt_2$ (3.5 equiv.) and the reaction mixture allowed to cool to 0ºC. Then propanephosphonic acid anhydride in EtOAc (1.5 equiv., 50% wt.) was added and the reaction mixture allowed to stir at 0ºC for 1 h. After HPLC indicated reaction completion, the reaction mixture was quenched with

AcOH (5 equiv.) and then concentrated under reduced pressure to afford crude product. The crude product was then purified via preparative HPLC – see details for specific examples below.

Scheme 4.3.1: General Procedure I: Macrobicyclization via bond formations with Asp and Glu

To a flame-dried round bottom flask equipped with a stir bar was charged with the seco-acid intermediate (1.0 equiv.), EDC•HCl (2.5 equiv.), HOBt (1.5 equiv.), and then diluted with DMF (5.0 mM). The reaction mixture was then allowed to stir at 0ºC and then added NEt_3 (5.0 equiv.). The reaction mixture was then allowed to warm up to 23ºC and stirred for 44–64 h. After HPLC indicated reaction completion, the reaction mixture was quenched with AcOH (5.0 equiv.) and then concentrated under reduced pressure to afford crude product. The crude product was then purified via preparative HPLC – see details for specific examples below.

Experimental Procedures and Product Characterization

Scheme 4.7.1 Synthesis of Thiazole Thione Linker (**29**)

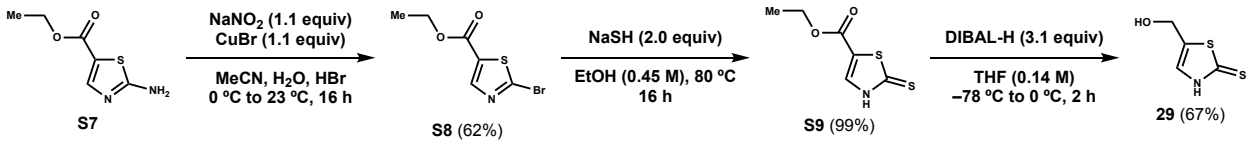

Ethyl 2-bromothiazole-5-carboxylate (**S8)**:

To a flame-dried 500 mL round bottom flask equipped with a stir bar was charged with **S7** (10.00 g, 56.91 mmol, 1.0 equiv.), $NaNO_2$ (4.32 g, 62.60 mmol, 1.1 equiv.), diluted with MeCN (58.68 mL, 0.97 M), H_2O (30.76 mL, 1.85 M), and the reaction mixture allowed to cool to 0ºC. Then CuBr (8.98 g, 62.60 mmol, 1.1 equiv.) was added portion-wise followed by dropwise addition of HBr (46.27 mL, 1.23 M) at 0ºC. The reaction mixture was then allowed to warm up to

23ºC and stirred for 16 h. After 16 h, the reaction mixture was diluted with ice water, CH_2Cl_2, and transferred to an Erlenmeyer flask. The solution was kept cool and gradually quenched with solid $NaHCO_3$ and then transferred to a separatory funnel. The aqueous layer was extracted with CH_2Cl_2 (3x), organic layers combined, washed with brine, dried over Na_2SO_4, filtered, and concentrated to afford crude product. The crude product was purified via flash SiO_2 chromatography (gradient Hex → 2.5% EtOAc/Hex) afforded title compound as a faint-yellow oil (8.26 g, 62% isolated yield), R_f = 0.28 at 5% EtOAc/Hex. ^{1}H NMR (DMSO-d_6, 500 MHz) δ8.31 (s, 1H), 4.32 (q, 2H), 1.29 (t, 3H) ^{13}C-NMR (500 MHz, DMSO-d_6) δ 159.47, 148.17, 142.19, 132.75, 61.94, 14.04 HRMS m/z calc'd for $[C_6H_6BrNO_2S+H]^+$ 236.9375; found 236.9375; 0 ppm mass defect.

Ethyl 2-thioxo-2,3-dihydrothiazole-5-carboxylate (**S9)**:

To a 100-mL round bottom flask equipped with a stir bar and a reflux condenser was charged with **S8** (2.86 g, 12.11 mmol, 1.0 equiv,), NaSH (2.26 g, 24.23 mmol, 2.0 equiv., 60% wt.), and then diluted with anhydrous EtOH (26.92 mL, 0.45 M). The reaction mixture was then heated to 80ºC and stirred for 16 h. After 16 h, the reaction mixture was allowed to cool to 23ºC and then poured onto an iced solution of aqueous 1 N HCl. The mixture was then transferred to a separatory funnel and the aqueous layer extracted with CH_2Cl_2 (4x). The organic layers were combined, dried over $MgSO_4$, filtered, and concentrated to afford title compound as a white-solid (2.26 g, 99% isolated yield) as a white-solid. HRMS m/z calc'd for $[C_6H_7NO_2S_2+H]^+$ 188.991823; found 188.991208; 3.3 ppm mass defect. ^{1}H-NMR (500 MHz, DMSO-d_6) δ 13.80 (s, 1H), 8.08 (s, 1H), 4.24 (q, 2H), 1.25 (t, 3H). ^{13}C-NMR (500 MHz, DMSO-d_6) δ 190.93, 158.87, 136.83, 118.59, 61.43, 14.08.

5-(hydroxymethyl)thiazole-2(3H)-thione (**29**):

To a flame-dried 250-mL round bottom flask equipped with a stir bar was charged with **S9** (2.26 g, 11.9 mmol, 1.0 equiv.) and diluted with anhydrous THF (85.3 mL, 0.14 M). The reaction solution was then allowed to cool down to –78ºC and stirred. Then at –78ºC was added dropwise DIBAL-H (37.0 mL, 37.0 mmol, 3.1 equiv., 1.0 M in hexanes). The reaction mixture was then allowed to stir at –78ºC for 30 min. Then after 30 min, the reaction mixture was allowed to warm up to 0ºC and stirred for 1.5 h. After 1.5 h, the reaction mixture was cooled to 0ºC and was added dropwise 1 N HCl and the mixture stirred. The reaction mixture was then transferred to a separatory funnel and the aqueous layer extracted with EtOAc (4x). The organic layers were combined (NOT washed with brine), dried over Na_2SO_4, filtered, and concentrated to afford crude product as a yellow-powder. The crude product was purified via flash SiO_2 chromatography (gradient 35% EtOAc/Hex → 75% EtOAc/Hex) afforded title compound as a white-powder (1.18 g, 67% isolated yield), HRMS m/z calc'd for $[C_4H_5NOS_2+H]^+$ 147.9890; found 147.9895; 3.1 ppm mass defect. ^{1}H-NMR (500 MHz, DMSO-d_6) δ 12.97 (s, 1H), 7.16 (s, 1H), 5.46 (s, 1H), 4.37 (s, 2H) ^{13}C-NMR (500 MHz, DMSO-d_6) δ 188.59, 132.59, 125.19, 55.88. HRMS [M+1] calc'd for $C_4H_5NOS_2H$ 147.9891, found 147.9894.

Scheme 4.7.2 Synthesis of Cinnamyl Phenol (**33**)

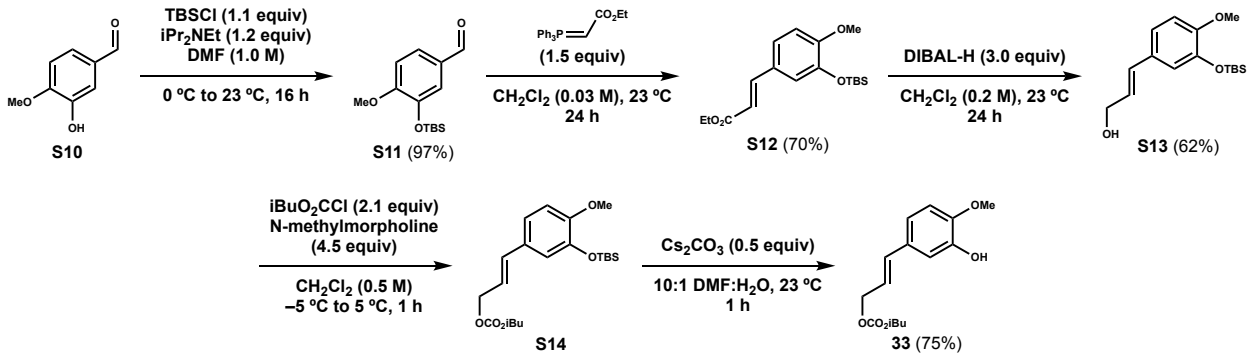

3-((tert-butyldimethylsilyl)oxy)-4-methoxybenzaldehyde **(S11)**:

To a flame-dried round bottom flask equipped with a stir bar was charged with 3-hydroxy-4-methoxybenzaldehyde (10.00 g, 65.77 mmol, 1.0 equiv., **S10**) and diluted with anhydrous DMF (6.58 mL, 1.0 M) and added iPr_2NEt (13.7 mL, 78.92 mmol, 1.2 equiv.). The reaction was cooled to 0°C and added TBSCl (10.86 g, 72.3 mmol, 1.1 equiv.) slowly then stirred for 16 h at 23ºC. The reaction was diluted with H_2O then extracted with EtOAc (3x). The combined organic phases were washed with brine (3x), dried over Na_2SO_4, filtered, and concentrated under reduced pressure to afford crude product. The residue was purified by flash SiO_2 column chromatography (gradient Hex → 15% EtOAc/Hexanes) to give **S11** (16.98 g, 97%) as a clear oil. ^{1}H NMR ($CDCl_3$, 300 MHz) δ9.81 (s, 1H), 7.47 (dd, J – 8.3, 2.0 Hz, 1H), 7.36 (d, J = 2.0 Hz, 1H), 6.94 (d, J = 8.3 Hz, 1H), 3.88 (s, 3H), 1.00 (s, 9H), 0.16 (s, 6H). ^{13}C NMR ($CDCl_3$, 126 MHz) δ191.0, 156.7, 145.7, 130.3, 126.4, 120.1, 111.3, 55.6, 25.7, 18.5, -4.6 HRMS m/z calc'd for $[C_{14}H_{22}O_3Si+H]^+$ 267.1416; found 267.1424; 3.0 ppm mass defect.

Ethyl (E)-3-(3-((tert-butyldimethylsilyl)oxy)-4-methoxyphenyl)acrylate **(S12)**:

To flame-dried round bottom flask equipped with a stir bar was charged with **S11** (10.00 g, 37.58 mmol, 1.0 equiv.) and diluted with anhydrous CH_2Cl_2 (1252 mL, 0.03 M). Then to this stirred solution was added ethyl 2-(triphenyl-l5- phosphaneylidene)acetate (19.62 g, 56.37 mmol, 1.5 equiv.) at 23ºC under inert atmosphere. The reaction mixture was stirred at 23ºC for 24 h. Solvent was removed under reduced pressure to afford crude product. The residue was purified by flash SiO_2 column chromatography (gradient Hex → 15% EtOAc/Hexanes) to give **S12** (8.84 g, 70% isolated yield). ^{1}H NMR ($CDCl_3$, 500 MHz) δ7.58 (d, J = 15.9 Hz, 1H), 7.09 (dd, J = 8.2, 2.1 Hz, 1H), 7.05 (d, J – 2.1 Hz, 1H), 6.83 (d, J = 8.2 Hz, 1H), 6.25 (d, J = 15.9 Hz, 1H), 4.25 (q, J =

7.12 Hz, 2H), 3.83 (s, 1H), 1.33 (t, J = 7.00 Hz, 3H), 1.00 (s, 3H), 0.16 (s, 6H). ^{13}C NMR ($CDCl_3$, 126 MHz) δ167.5, 153.2, 145.3, 144.6, 127.6, 123.2, 119.8, 115.9, 111.8, 60.5, 55.6, 25.8, 18.6, 14.5, -4.5. HRMS m/z calc'd for $[C_{18}H_{28}O_4Si+H]^+$ 337.1835; found 337.1836; 0.3 ppm mass defect.

(E)-3-(3-((tert-butyldimethylsilyl)oxy)-4-methoxyphenyl)prop-2-en-1-ol **(S13)**:

To a flame-dried round bottom flask equipped with a stir bar was charged with **S12** (5.00 g, 14.87 mmol, 1.0 equiv.) and diluted with anhydrous CH_2Cl_2 (74.36 mL, 0.2 M). To this stirred solution was added DIBAL-H (46.1 mL, 46.1 mmol, 3.1 equiv., 1.0 M in hexanes) dropwise at 23ºC under inert atmosphere. The reaction mixture was stirred at 23ºC for 24 h. After completion the reaction was concentrated under reduced pressure to afford crude product. The resulting residue was purified by flash SiO_2 column chromatography (gradient Hex → 20% EtOAc/Hex) to give **S13** (2.71 g, 62% isolated yield). ^{1}H NMR ($CDCl_3$, 500 MHz) δ6.95–6.90 (m, 2H), 6.79 (d, J = 8.9 Hz, 1H), 6.49 (d, J = 15.9 Hz, 1H), 6.20 (dt, J = 15.6, 5.9 Hz, 1H), 4.29 (dd, J = 6.1, 1.4 Hz, 2H), 3.80 (s, 1H), 1.00 (s, 9H), 0.16 (s, 6H). ^{13}C NMR ($CDCl_3$, 126 MHz) δ151.0, 145.2, 131.3, 129.9, 126.4, 120.6, 118.8, 112.0, 64.1, 55.6, 25.9, 18.6, -4.5. HRMS m/z calc'd for $[C_{16}H_{27}O_3Si+H]^+$ 295.1729; found 295.1735; 2.0 ppm mass defect.

(E)-3-(3-((tert-butyldimethylsilyl)oxy)-4-methoxyphenyl)allyl isobutyl carbonate **(S14)**:

To a flame-dried round bottom flask equipped with a stir bar was charged with **S13** (2.50 g, 1.0 equiv., 8.50 mmol), diluted with anhydrous CH_2Cl_2 (17.0 mL, 0.5 M), and N-methylmorpholine (4.21 mL, 38.25 mmol, 4.5 equiv.). The reaction mixture was then cooled to 5ºC under argon. Isobutyl chloroformate (2.44g, 17.85 mmol, 2.1 equiv.) was added dropwise and continued to stir at -5°C until completion. After completion as observed by TLC (1 h), the reaction

was quenched with $NaHCO_3$, extracted with EtOAc (3x), washed with $NaHCO_3$ (2x), brine, dried over Na_2SO_4, filtered, and concentrated under reduced pressure to afford crude product. The crude product was pushed through a plug of silica (50% EtOAc/Hex) and pushed forward without further purification.

(E)-3-(3-hydroxy-4-methoxyphenyl)allyl isobutyl carbonate **(33)**:

To a flame-dried round bottom flask equipped with a stir bar was charged with **S14** and diluted with 10:1 DMF:H_2O and added Cs_2CO_3 (1.38 g, 4.25 mmol, 0.5 equiv.). The reaction mixture was then allowed to stir at 23ºC until complete by TLC. The reaction mixture was then diluted with EtOAc, washed with brine (2 x), dried over Na_2SO_4, concentrated under reduced pressure to afford crude product. The crude product was purified by flash SiO_2 column chromatography (gradient Hex → 30% EtOAc/Hex) to give **33** as a clear oil (1.79 g, 75% isolated yield). ^{1}H NMR ($CDCl_3$, 500 MHz) δ7.01 (d, J = 2.0 Hz, 1H), 6.86 (dd, J = 8.3, 1.8, 1H), 6.79 (d, J = 8.4, 1H), 6.58 (d, J = 15.7 Hz, 1H), 6.15 (dt, J =15.8, 6.6 Hz, 1H), 5.62 (s, 1H), 4.75 (d, J = 6.6 Hz, 2H), 3.94 (d, J = 6.7 Hz, 2H), 3.88 (s, 1H), 1.98 (sept, J = 6.7 Hz, 1H), 0.95 (d, J = 6.7 Hz, 6H). ^{13}C NMR ($CDCl_3$, 126 MHz) δ 155.4, 146.9, 145.8, 134.7, 129.9, 120.9, 119.5, 112.3, 110.6, 74.3, 68.6, 56.1, 27.9, 19.0. HRMS m/z calc'd for $[C_{15}H_{20}O_5+H]^+$ 281.1389; found 281.1394; 1.8 ppm mass defect.

Scheme 4.7.3 Synthesis of Fmoc-Glu*-OH **(38)**

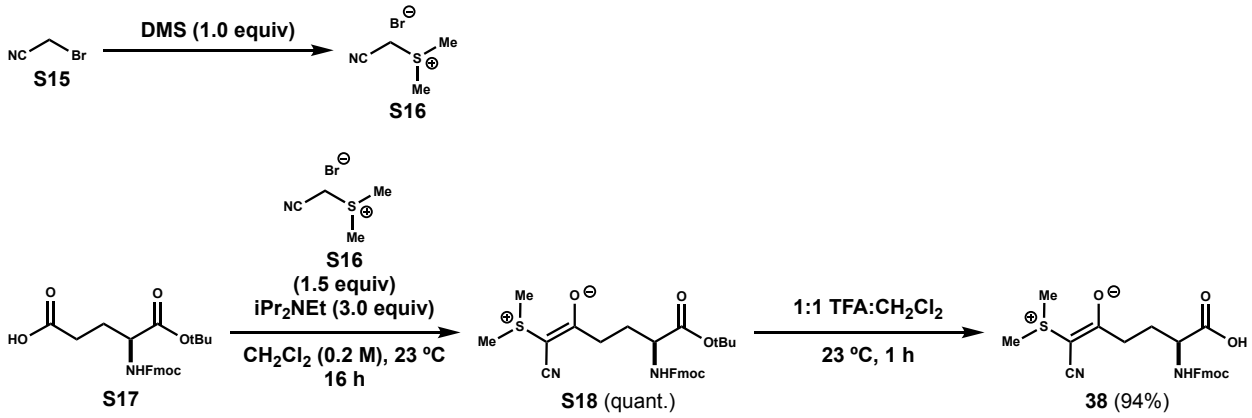

Compounds **37** and **S16** were synthesized following manuscript reference 23.

Fmoc-Glu*-OtBu (**S18**):

To a flame-dried 250-mL round bottom flask equipped with a stir bar was charged with Fmoc-Glu-OtBu (15.0 g, 1.0 equiv.), 35.3 mmol) and then dissolved in CH_2Cl_2 (176 mL, 0.2 M) until homogeneous. The solution was then added HBTU (16.2 g, 1.21 equiv., 42.7 mmol), **S16** (9.63 g, 1.5 equiv., 52.9 mmol), and iPr_2NEt (18.4 mL, 3.0 equiv., 106 mmol). The reaction mixture was then allowed to stir at 23ºC for 16 h. The reaction mixture was then added sat. $NaHCO_3$ (aq.) and then transferred to a separatory funnel. The aqueous layer was extracted with EtOAc (3x) and the organic layers combined. The organic layers were then washed with brine, dried over Na_2SO_4, filtered, and concentrated to afford crude product. The crude product was purified by flash SiO_2 column chromatography (gradient 50% EtOAc/Hex → 80% EtOAc/Hex → EtOAc) to give **S18** as a hydroscopic orange oil (17.9 g, quantitative yield).

Fmoc-Glu*-OH (**38**):

To a 100-mL round bottom flask equipped with a stir bar was charged with **S18** (17.9 g, 35.3 mmol) and added 1:1 TFA:CH_2Cl_2 (20:20 mL). The reaction mixture was then allowed to stir at 23ºC for 1 h. After HPLC indicated reaction completion; the reaction mixture was concentrated under reduced pressure to afford a crude oil which was solubilized with a minimal amount of CH_2Cl_2. Then MeOH was added and evaporated several times, to afford crude product as a yellow solid. Then the crude product was subjected to a trituration with Et_2O (3x) to afford **38** (15.0 g, 94% isolated yield) as a white solid. 1H NMR (DMSO-d_6, 600 MHz) δ 12.57 (s, 1H), 7.89 (d, J = 7.50 Hz, 2H), 7.73 (dd, J = 7.38 Hz, J = 3.06 Hz, 2H), 7.66 (d, J = 8.04 Hz, 1H), 7.42 (t, J = 7.32 Hz, 2H), 7.37-7.31 (m, 2H), 4.28-4.22 (m, 2H), 3.98-3.93 (m, 1H), 2.78 (s, 6H), 2.47-2.36 (m, 2H), 2.04-1.99 (m, 1H), 1.82-1.73 (m, 1H), 1.29-1.21 (m, 1H) 13C NMR (DMSO-d_6, 151 MHz) δ 188.56, 173.74, 156.11, 143.85, 140.70, 127.64, 127.10, 125.29, 120.11, 119.57, 65.7, 54.7, 53.4, 46.6, 34.4, 27.6, 26.2, 16.7 HRMS m/z calculated for $[C_{24}H_{24}N_2O_5S+H]^+$ = 453.1484; found 453.1487; 0.7 ppm mass defect.

Synthesis and Characterization of **Scheme 4.2.1** Products

Polycycle **9**:

Polycycle **9** was synthesized according to **Scheme 4.2.1** General Procedure A (outlined above) using crude linear peptide Ac-YNCTFC-NH_2 (60.0 mg, 1.0 equiv., 75.9 μmol). Purification by preparative-reverse phase HPLC (gradient 40% MeCN/H_2O → 55% MeCN/H_2O) afforded the title compound (29.1 mg, 41% isolated yield) as an off-white solid. ^{1}H NMR (DMSO-d_6, 500 MHz) δ 9.51 (s, 1H), 8.33 (d, J = 9.5 Hz, 1H), 8.12 (d, J = 6.9 Hz, 1H), 8.05 (d, J = 8.2 Hz, 1H),

7.98 (d, J = 6.8 Hz, 1H), 7.69 (d, J = 7.7 Hz, 1H), 7.42 (s, 1H), 7.36 (d, J = 8.6 Hz, 1H), 7.30-7.17 (m, 6H), 7.06-6.84 (m, 3H), 7.03 (s, 1H), 4.98 (brs, 1H), 4.84-4.79 (m, 1H), 4.72 (dd, J = 14.2, 6.8 Hz, 1H), 4.60-4.55 (m, 1H), 4.55-4.48 (m, 1H), 4.41-1.34 (m, 1H), 3.74 (t, J = 6.9 Hz, 1H), 3.61 (d, J = 14.0 Hz, 1H), 3.48-3.41 (m, 2H), 3.22 (dd, J = 14.0, 3.7 Hz, 1H), 2.97 (dd, J = 13.2, 5.1 Hz, 1H), 2.89-2.82 (m, 3H), 2.70 (dd, J = 13.2, 10.1 Hz, 1H), 2.38 (dd, J = 15.6, 8.5 Hz, 1H), 2.32 (dd, J = 15.6, 5.0 Hz, 1H), 1.87 (s, 3H), 0.51 (d, J = 6.0 Hz, 3H). ^{13}C NMR (DMSO-d_6, 126 MHz) δ 171.7, 170.8, 170.3, 169.5, 169.1, 168.8, 168.5, 168.0, 152.4, 139.2-138.8 (m, 1C), 137.8, 135.2-134.9 (m, 1C), 32.1, 130.5, 129.1, 128.2, 126.4, 118.7-111.5 (m, 2C), 114.9, 68.6-68.1 (m, 1C) 65.9, 62.1, 54.8, 53.6, 50.4, 48.4, 46.5, 38.4, 37.3, 37.2, 30.6, 22.4, 20.0 ^{19}F NMR (DMSO-d_6, 282 MHz) δ -103.2 and -119.2 (AB quartet, J = 252.2 Hz, 2F), -113.8 and -127.0 (AB quartet, J = 223.0 Hz, 2F). HRMS m/z calculated for $[C_{39}H_{42}F_4N_8O_{10}S_2+Na]^+$ = 945.2299, found 945.2327, 3.0 ppm mass defect.

Polycycle **10**:

Polycycle **10** was synthesized according to **Scheme 4.2.1** General Procedure B (outlined above) using crude linear peptide Ac-HFCASC-NH_2 (50.0 mg, 1.0 equiv., 53.43 μmol). Purification by preparative-reverse phase HPLC – (gradient 10% MeCN/H_2O → 50% MeCN/H_2O) afforded title compound (13.76 mg, 27% isolated yield) as an off-white solid. ^{1}H NMR (DMSO-d_6, 500 MHz) δ 9.38 (s, 1H), 8.42 (d, J = 8.9 Hz, 1H), 8.36 – 8.28 (m, 3H), 7.93 (t, J = 8.2, 1H), 7.31 (d, J = 9.2 Hz, 2H), 7.28 – 7.20 (m, 7H), 7.20 – 7.16 (m, 1H), 4.85 – 4.80 (m, 1H), 4.63 – 4.53 (m, 3H), 4.31 (quint, J = 4.5 Hz, 1H), 4.20 (quint, J = 7.4 Hz, 1H), 3.82 (dd, J = 10.85, 5.1 Hz, 1H), 3.52 (dd, J = 10.85, 3.80 Hz, 1H), 3.34 (dd, J = 12.6, 6.7 Hz, 1H), 2.92 – 2.86 (m, 2H), 2.85 – 2.79 (m, 1H), 2.79 – 2.74 (m, 1H) 1.82 (s, 3H), 1.24 (d, J = 7.2 Hz, 3H). ^{13}C (DMSO-d_6,

126 MHz) δ 172.9, 171.4, 169.7, 169.6, 168.8, 167.8, 167.7, 137.3, 133.8, 129.2, 128.0, 126.3, 61.2, 55.3, 53.5, 51.1, 51.0, 50.3, 48.6, 48.4, 46.4, 36.8, 33.7, 30.5, 30.1, 22.5, 17.6. ^{19}F (DMSO-d_6, 282 MHz) δ -103.2 – (-104.7) (m, 1F), -114.0 – (-116.4) (m, 2F), -136 – (-125.2) (m, 2F). HRMS m/z calculated for $[C_{34}H_{37}F_4N_9O_8S_2+H]^+$ = 840.2221; found 840.2233; 1.4 ppm mass defect.

Polycycle **11**:

Polycycle **11** was synthesized according to **Scheme 4.2.1** General Procedure B (outlined above) using crude linear peptide Ac-HFSCAC-NH_2 (50.0 mg, 1.0 equiv., 53.43 μmol). Purification by preparative-reverse phase HPLC (gradient 10% MeCN/H_2O → 55% MeCN/H_2O) afforded title compound (21.4 mg, 42% isolated yield) as an off-white solid. ^{1}H NMR (DMSO-d_6, 500 MHz) δ 9.10 (d, J = 7.7, 1H), 8.84 (s, 1H), 8.41 (d, J = 8.7 Hz, 1H), 8.07 - 8.01 (m, 2H), 7.63 (d, J = 8.1 Hz, 1H), 7.54 (d, J = 7.65 Hz, 1H), 7.38 (s, 1H), 7.28 - 7.17 (m, 6H), 4.75 - 4.70 (m, 1H), 4.68 - 4.62 (m, 1H), 4.62 - 4.56 (m, 2H) 4.52 (quint, J = 7.2, 1H), 4.43 - 4.36 (m, 1H), 3.80 - 3.73 (m, 1H), 3.57 - 3.39 (m, 3H), 3.47 - 3.41 (m, 1H), 3.16 - 3.05 (m, 2H), 3.03 - 2.94 (m, 2H), 2.94 - 2.81 (m, 3H), 1.77 (s, 3H), 1.31 (d, J = 7.3 Hz, 3H). ^{13}C NMR (DMSO-d_6, 126 MHz) δ 170.6, 170.3, 170.1, 170.0, 168.9, 167.9, 167.5, 141.3 - 140.9 (m, 1C), 139.0, 137.5, 135.6, 132.8 - 132.6 (m, 1C), 129.0, 128.2, 126.4, 117.6 - 115.8 (m, 2C), 117.6 - 115.8 (m, 2C), 114.5, 70.4 - 69.7 (m, 1C), 61.3, 55.1, 53.8, 51.6, 51.1, 48.5, 47.1, 38.6, 37.8, 30.8, 29.8, 22.5, 16.0. ^{19}F NMR (DMSO-d_6, 282 MHz) δ -98.8 and -120.7 (AB quartet, J = 254.1 Hz, 2F), -117.2 and -127.3 (AB quartet, J = 222.4 Hz, 2F). HRMS m/z calculated for $[C_{44}H_{37}F_4N_9O_8S_2+H]^+$ = 840.2221; found 840.2213; 1.0 ppm mass defect.

Polycycle **12**:

Polycycle **12** was synthesized according to **Scheme 4.2.1** General Procedure A (outlined above) using crude linear peptide Ac-YGHCAC-NH_2 (100. mg, 1.0 equiv., 142 μmol). Reaction completion took 24 h. Purification by preparative-reverse phase HPLC – (10% MeCN/H_2O → 57.5% MeCN/H_2O → 62.5% MeCN/H_2O) afforded desired product. Desired product was then repurified via pTLC; 10% MeOH/$CHCl_3$ solvent system; afforded title compound (35.7 mg, 30% isolated yield) as an off-white powder. ^{1}H NMR (DMSO-d_6, 600 MHz) δ 9.33 (s, 1H), 8.55 (d, J = 6.5 Hz, 1H), 8.26 (t, J = 5.5 Hz, 1H), 8.10 (d, J = 8.2 Hz, 1H), 8.04 (d, J = 7.7 Hz, 1H), 7.51 (s, 1H), 7.10 (d, J = 8.6 Hz, 2H), 6.97 (d, J = 8.6 Hz, 2H), 6.91 (s, 1H), 6.64–6.60 (m, 1H), 4.64 (d, J = 8.8 Hz, 1H), 4.60–4.54 (m, 1H), 4.40–4.32 (m, 1H), 4.08 (m, 1H), 3.72–3.64 (m, 2H), 3.00–2.91 (m, 2H), 2.88–2.78 (m, 2H), 2.66–2.58 (m, 2H), 1.72 (m, 3H), 1.18 (d, J = 7.4 Hz, 3H) ^{13}C NMR (DMSO-d_6, 126 MHz) δ 171.6, 170.9, 170.6, 169.5, 168.1, 167.2, 139.5, 138.8–138.7 (m, 1C), 138.6, 135.2, 130.2, 130.0–129.9 (m, 1C), 122.3–122.2 (m, 2C), 116.0, 114.9, 113.5, 67.8–67.7 (m, 1C), 53.9, 52.0, 49.6, 45.5, 42.1, 36.1, 30.2, 25.1, 22.5, 17.3 ^{19}F NMR (DMSO-d_6, 565 MHz) δ -105.9 and -120.1 (AB quartet, J = 254.0 Hz, 2F), -114.1 and -126.1 (AB quartet, J = 225.8 Hz, 2F) HRMS calculated for $[C_{33}H_{35}F_4N_9O_9S+H]^+$ = 810.2293; found 810.2329; 4.4 ppm mass defect.

Polycycle **4**:

Polycycle **4** was synthesized according to **Scheme 4.2.1** General Procedure B (outlined above) using crude linear peptide Ac-YGSHAC-NH_2 (50.0 mg, 1.0 equiv., 63.15 μmol). Purification by preparative-reverse phase HPLC (gradient 10% MeCN/H_2O → 60% MeCN/H_2O) afforded title compound (23.3 mg, 40% isolated yield). ^{1}H NMR (DMSO-d_6, 500 MHz) δ 8.93 (s, 1H), 8.58 (d, J = 7.0 Hz, 1H), 8.42 (d, J = 6.6 Hz, 2H), 8.34 (s, 1H), 7.78 (d, J = 7.8 Hz, 1H), 7.54

(s, 1H), 7.19 (s, 1H), 7.15 - 7.10 (m, 2H), 7.10 - 7.00 (m, 2H), 6.67 - 6.58 (m, 1H), 4.71 - 4.64 (m, 1H), 4.58 - 4.51 (m, 1H), 4.27 (q, J = 6.4 Hz, 1H), 4.17 (q, J = 7.0 Hz, 1H), 4.09 (quint, J = 7.1 Hz, 1H), 3.95 - 3.87 (m, 1H); 3.72 - 3.56 (m, 3H),, 3.45 (d, J = 13.1 Hz, 1H), 2.90 - 2.83 (m, 2H); 2.82 - 2.73 (m, 1H), 2.68 - 2.58 (m, 2H), 1.79 (s, 1H), 1.24 (d, J = 7.2 Hz, 3H). ^{13}C NMR (DMSO-d_6, 126 MHz) δ171.6, 171.0, 169.7, 169.7, 169.3, 169.0, 167.2, 151.0, 143.1 - 142.5 (m, 1C), 139.4, 136.8, 135.7, 130.8, 128.2 - 127.8 (m, 1C), 119.7 - 113.0 (m, 2C), 119.7 - 113.0 (m, 2C), 119.2, 118.09, 67.3 - 66.4 (m, 1C), 60.9, 55.8, 54.7, 50.8, 49.3, 46.3, 42.8, 36.7, 30.1, 29.8, 22.3, 17.3. ^{19}F NMR (DMSO-d_6, 282 MHz) δ -105.9 and -123.8 (AB quartet, J = 257.6 Hz, 2F), -117.1 and -127.2 (AB quartet, J = 223.6 Hz, 2F). HRMS m/z calculated for $[C_{33}H_{35}F_4N_9O_9S+H]^+$ = 810.2293; found 810.2294; 1.0 ppm mass defect; 0.1 ppm mass defect.

Polycycle **13**:

Polycycle **13** was synthesized according to **Scheme 4.2.1** General Procedure A (outlined above) using crude linear peptide Ac-YGSdHAc-NH_2 (100. mg, 1.0 equiv., 126 μmol). Purification by preparative-reverse phase HPLC (gradient 10% MeCN/H_2O → 55% MeCN/H_2O → 60% MeCN/H_2O) afforded title compound (66.0 mg, 57% isolated yield) as a yellow-powder. ^{1}H NMR (DMSO-d_6, 500 MHz) δ 9.25 (s, 1H), 8.75 (d, J = 6.6 Hz, 1H), 8.44 (d, J = 6.8 Hz, 1H), 8.23 (t, J = 5.1 Hz, 1H), 7.33 – 7.28 (m, 1H), 7.26 (d, J = 5.76 Hz, 1H), 7.09 – 7.05 (m, 2H), 7.93 – 6.98 (m, 4H), 6.19 (d, J = 8.6 Hz, 1H), 4.66 – 4.61 (m, 1H), 4.58 – 4.53 (m, 1H), 4.41 – 4.36 (m, 1H), 4.08 (quint, J = 3.3 Hz, 1H), 4.0 (quint, J = 6.9 Hz, 1H), 3.91 (dd, J = 16.2, 5.2 Hz, 1H), 3.85 (dd, J = 10.5, 3.8 Hz, 1H), 3.71 – 3.66 (m, 1H), 3.56 (d, J = 5.2 Hz, 1H), 3.54 – 3.48 (m, 1H), 3.06 (dd, J = 15.4, 3.5 Hz, 1H), 2.96 (dd, J = 13.4, 3.78 Hz, 1H), 2.81 – 2.75 (m, 4H), 1.93 (s, 3H), 1.13 (d, J = 7.3 Hz, 3H). ^{13}C NMR (DMSO-d_6, 126 MHz) 171.2, 170.7, 170.6, 170.1, 169.4, 168.9, 167.0, 153.8, 139.6, 138.1–138.0 (m, 1C), 134.0, 131.2, 128.3, 127.6, 123.2–120.0 (m, 1C), 116.8,

115.3, 114.7–114.4 (m, 2C), 67.3– 67.0 (m, 1C), 61.5, 56.3, 52.9, 52.5, 50.0, 46.0, 43.0, 37.8, 30.2, 28.1, 22.7, 16.7. ^{19}F NMR (DMSO-d_6, 565 MHz) -105.1 and -120.2 (AB quartet, J = 257.2 Hz, 2F), -114.7 and -125.8 (AB quartet, J = 227.3 Hz, 2F) HRMS m/z calculated for $[C_{33}H_{35}F_4N_9O_9+H]^+$ = 810.2293; found 810.2293; 0 ppm mass defect.

Polycycle **14**:

Polycycle **14** was synthesized according to **Scheme 4.2.1** General Procedure C (outlined above) using crude linear peptide Ac-YGTMQVSHAC-NH_2 (50.0 mg, 40.0 μmol, 1.0 equiv.). Purification by preparative-reverse phase HPLC (gradient 10% MeCN/H_2O → 55% MeCN/H_2O → 60% MeCN/H_2O) afforded title compound (24.6 mg, 45% isolated yield) as a yellow-crystalline powder. NMR of **14** contained complex mixture of rotational isomers; ratio ~ 1 : 8.5 . Major rotational isomer was characterized. ^{1}H NMR (DMSO-d_6, 600 MHz) δ 9.19 (s, 1H), 8.44 (t, J = 5.6 Hz, 1H), 8.38 (d, J = 7.0 Hz, 1H), 8.15–8.11 (m, 2H), 7.99 (d, J = 7.1 Hz, 1H), 7.91–7.85 (m, 3H), 7.79 (d, J = 7.4 Hz, 1H), 7.32 (d, J = 7.3 Hz, 1H), 7.13 (d, J = 8.6 Hz, 2H), 7.02–6.99 (m, 2H), 6.84 (s, 1H), 6.65–6.60 (m, 1H), 4.62 (dt, J = 9.1, 2.9 Hz, 1H), 4.53–4.48 (m, 1H), 4.40–4.34 (m, 3H), 4.27–4.21 (m, 2H), 4.17 (dd, J = 7.6, 3.5 Hz, 1H), 4.16–4.10 (m, 3H), 4.10–4.05 (m, 1H), 3.86 (dd, J = 16.4, 5.3 Hz, 1H), 3.80–3.74 (m, 1H), 3.61–3.55 (m, 2H), 3.55–3.50 (m, 2H), 3.13–3.08 (m, 1H), 2.97–2.91 (m, 2H), 2.85–2.80 (m, 1H), 2.70–2.62 (m, 1H), 2.45–2.40 (m, 1H), 2.13–2.09 (m, 2H), 2.01 (s, 3H), 1.90–1.79 (m, 2H), 1.74 (m, 3H), 1.18 (d, J = 2.6 Hz, 3H), 1.16 (d, J = 2.8 Hz, 1H), 1.06 (d, J = 6.3 Hz, 3H), 0.87 (d, J = 6.8 Hz, 3H), 0.82 (d, J = 6.8 Hz, 3H) ^{13}C NMR (DMSO-d_6, 126 MHz) δ 174.0, 172.0, 171.5, 171.2, 170.7, 170.5, 170.1, 170.1, 169.8, 169.8, 169.4, 167.2, 151.3, 139.1, 136.5–136.3 (m, 1C) 135.6, 130.4, 130.0, 128.1–128.0 (m, 1C), 116.8, 115.8–115.5 (m, 2C), 114.9, 67.3–67.2 (m, 1C), 67.0, 66.1, 58.6, 57.6, 55.3, 54.2, 53.0, 52.3, 52.0, 52.0, 49.3, 45.7, 45.6, 42.5, 35.8, 31.5, 30.8, 30.7, 29.7, 22.3, 19.8, 19.2, 17.7, 17.3, 14.5 ^{19}F NMR

(DMSO-d_6, 565 MHz) δ -106.8 and -120.8 (AB quartet, J = 254.9 Hz, 2F), -114.9 and -126.0 (AB quartet, J = 227.3 Hz, 2F). HRMS m/z calculated for $[C_{52}H_{68}F_4N_{14}O_{15}S_2+H]^+$ = 1269.4444; found 1269.4449; 0.4 ppm mass defect.

Polycycle **15**:

Polycycle **15** was synthesized according to **Scheme 4.2.1** General Procedure C (outlined above) using crude linear peptide Ac-D(C)VHSAY-NH_2 (90.0 mg, 1.0 equiv., 94.9 μmol). Purification by preparative-reverse phase HPLC – (10% MeCN/H_2O → 50% MeCN/H_2O → 55% MeCN/H_2O) afforded desired product. Desired product was repurified via SiO_2 pTLC; 10% MeOH/$CHCl_3$ solvent system (plate run up twice) afforded (10.6 mg, 10% isolated yield) as an off-white film. ^{1}H NMR (DMSO-d_6, 600 MHz) δ 9.42 (s, 1H), 8.79 (d, J = 6.0 Hz, 1H), 8.57 (d, J = 8.8 Hz, 1H), 8.30 (d, J = 5.7 Hz, 1H), 8.07 (d, J = 7.9 Hz, 1H), 7.89 (s, 2H), 7.64 (d, J = 5.9 Hz, 1H), 7.54 (s, 1H), 7.83 (s, 1H), 7.14 (d, J = 8.6 Hz, 2H), 6.96 (d, J = 8.6 Hz, 2H), 6.90 (s, 1H), 4.86 (t, J = 5.4 Hz, 1H), 4.74 (td, J = 7.5, 3.3 Hz, 1H), 4.67–4.63 (m, 1H), 4.53–4.48 (m, 1H), 4.39–4.33 (m, 1H), 4.26–4.22 (m, 1H), 4.18–4.11 (m, 2H), 3.65–3.59 (m, 2H), 3.51 (s, 1H), 3.47–3.41 (m, 2H), 3.17–3.13 (m, 1H), 3.03–2.98 (m, 1H), 2.98–2.91 (m, 2H), 2.87–2.77 (m, 2H), 2.66–2.62 (m, 1H), 2.02–1.97 (m, 1H), 1.97–1.90 (m, 1H), 1.83 (s, 3H), 1.23 (d, J = 6.6 Hz, 3H), 0.83 (d, J = 6.8 Hz, 3H), 0.80 (d, J = 6.8 Hz, 3H) ^{13}C NMR (DMSO-d_6, 126 MHz) δ 172.8, 171.1, 170.5, 170.1, 169.8, 169.6, 169.3, 169.1, 168.9, 153.8–153.6 (m, 1C), 138.1, 136.6, 135.4–135.3 (m, 1C), 130.8, 129.7, 121.0, 116.5, 116.4–116.3 (m, 2C), 113.8, 69.8, 67.0, 61.3, 58.4, 56.0, 54.6, 53.9, 51.5, 49.2, 48.4, 30.7, 29.0, 25.1, 22.5, 22.1, 19.0, 19.0, 17.5 HRMS m/z calculated for $[C_{40}H_{47}F_4N_{11}O_{11}S+H]^+$ = 966.3192; found 966.3155; 3.8 ppm mass defect.

Polycycle **16**:

Polycycle **16** was synthesized according to **Scheme 4.2.1** General Procedure C (outlined above) using crude linear peptide Ac-YGAE(C)H-NMe_2 (50.0 mg, 1.0 equiv., 59.0 μmol). Linear peptide was prepared via general solution phase protocols. Purification by preparative-reverse phase HPLC – (gradient 10% MeCN/H_2O → 65% MeCN/H_2O) afforded desired product. Desired product was repurified via pTLC; 10% MeOH/$CHCl_3$ solvent system afforded title compound (4.7 mg, 8% isolated yield) as a white-powder. ^{1}H NMR (DMSO-d_6, 500 MHz) δ 9.26 (s, 1H), 8.60 (s, 1H), 8.49 (d, J = 8.1 Hz, 1H), 8.37 (d, J = 7.7, 1H), 7.7 (s, 1H), 7.65 (d, J = 10.1 Hz, 1H), 7.18 (s, 1H), 6.99 (d, J = 8.7 Hz, 2H); 6.91 (d, J = 8.7, 2H), 6.70 (d, J = 6.2, 1H), 6.62 (s, 1H), 5.24 (quint, J = 7.1 Hz, 1H), 4.82 - 4.73 (m, 1H), 4.79 - 4.72 (m, 1H), 4.36 - 4.26 (m, 1H), 4.15 (dd, J = 17.3, 7.4, 1H), 4.03 - 3.97 (m, 1H), 3.53 (dd, J = 17.3, 3.4, 1H), 3.16 (s, 3H), 3.12 - 2.98 (m, 1H), 3.04 - 2.99 (m, 1H), 2.90 - 2.82 (m, 1H), 2.85 - 2.79 (m, 2H), 2.77 (s, 3H), 2.53 - 2.47 (m, 1H), 2.02 - 1.96 (m, 1H), 1.72 - 1.66 (m, 1H), 1.96 - 1.91 (m, 1H), 1.71 - 1.67 (m, 1H), 1.84 (s, 3H), 1.22 (d, J = 6.70, 3H). ^{13}C NMR (DMSO-d_6, 126 MHz) δ 173.8, 171.2, 171.0, 170.8, 170.0, 169.7, 168.9, 167.4, 153.2, 146.5 - 144.6 (m, 1C), 137.6, 136.9, 135.1, 130.2, 129.5 - 128.2 (m, 1C), 118.4, 118.4, 118.1 - 117.0 (m, 2C), 118.1 - 117.0 (m, 2C). ^{19}F NMR (DMSO-d_6, 282 MHz) δ -111.1 –(-112.2) (m, 1F), -115.8 – (-119.6) (m, 3F). HRMS m/z calculated for $[C_{37}H_{42}F_4N_{10}O_9S+H]^+$ = 879.2871; found 879.2868; 0.3 ppm mass defect.

Synthesis and Characterization of **Scheme 4.2.2** Products

Macrocycle **17**:

Macrocycle **17** was synthesized according to **Scheme 4.2.2** General Procedure A (outlined above) using crude linear peptide Ac-CWSC-NH_2 (300. mg, 1.0 equiv., 0.557 mmol). Purification by preparative-reverse phase HPLC afforded title compound (134.6 mg, 35% isolated yield). ^{1}H NMR (DMSO-d_6, 500 MHz) δ 10.88 (s, 1H), 8.61 (s, 1H), 7.82 (s, 1H), 7.64 – 7.54 (m, 1H), 7.54 – 7.47 (m, 1H), 7.46 – 7.38 (m, 1H), 7.38 – 7.28 (m, 1H), 7.26 – 7.16 (m, 1H),7.11 – 7.02 (m, 1H), 7.02 – 6.93 (m, 1H), 6.75 (bs, 1H), 5.22 – 5.11 (m, 1H), 5.07 – 4.99 (m, 1H), 4.55 – 4.45 (m, 1H), 4.37 – 4.25 (m, 1H), 4.15 – 4.00 (m, 1H), 3.95 – 3.87 (m, 1H), 3.72 – 3.55 (m, 2H), 3.52 – 3.43 (m, 1H), 3.26 – 3.13 (m, 3H), 2.74 – 2.65 (m, 1H), 2.02 – 1.93 (m, 1H). ^{13}C NMR (DMSO-d_6, 126 MHz) δ 173.2, 171.1, 170.8, 169.8, 169. 4, 136.1, 127.2, 123.5, 121.0, 118.4, 118.0, 111.4, 109.4, 64.9, 60.3, 57.4, 56.8, 51.7, 36.5, 34.4, 26.4, 24.3. HRMS m/z calculated for $[C_{27}H_{28}F_5N_6O_6S_2+H]^+$ = 691.1432; found 691.1431; 0.1 ppm mass defect.

Macrocycle **19**:

To a flame-dried 5-mL round bottom flask equipped with a stir bar was charged with Macrocycle **17** (20.0 mg, 1.0 equiv., 29.0 μmol), diluted with anhydrous DMF (0.58 mL, 50 mM), and cooled to 0ºC. To the flask was added beta-D-thioglucose sodium salt (1.0 equiv.) and stirred for 1 h. After completion the reaction was concentrated under reduced pressured and purified by reverse-phase to give Macrocycle **19** (25.1 mg, >95%).^{1}H NMR (DMSO-d_6, 500 MHz) δ 10.89 (s, 1H), 9.19 (bs, 1H), 9.11 – 8.84 (m, 2H), 8.26 (d, J = 8.6 Hz, 1H), 7.50 (d, J = 7.8 Hz, 1H), 7.33 (d, J = 8.1 Hz, 1H), 7.19 (d, J = 9.3 Hz, 1H), 7.06 (t, J = 7.26 Hz, 1H), 6.98 (t, J = 7.2 Hz, 1H), 4.79 (d, J = 9.2 Hz, 1H), 4.74 (d, J = 9.6 Hz, 1H), 4.66 (q, J = 7.6 Hz, 1H), 4.48 (q, J = 7.6 Hz, 1H),

4.38 – 4.31 (m, 1H), 3.85 – 3.77 (m, 1H), 3.64 – 3.54 (m, 3H), 3.53 – 3.43 (m, 3H), 3.30 – 3.21 (m, 3H), 3.11 – 2.98 (m, 3H), 1.83 (s, 3H). ^{13}C NMR (DMSO-d_6, 126 MHz) 172.1, 169.9, 169.5, 168.8, 167.6, 136.1, 127.1, 123.8, 120.9, 118.4, 118.0, 111.4, 109.3, 84.6, 81.3, 78.0, 73.5, 69.4, 61.9, 60.7, 55.7, 55.3, 51.5, 46.1, 33.4, 30.7, 27.8, 22.5. ^{19}F NMR (DMSO-d_6, 282 MHz) δ -98.6 and -112.7 (AB quartet, J = 248.8 Hz, 2F), -111.3 and -127.0 (AB quartet, J = 223.6 Hz, 2F). HRMS m/z calculated for $[C_{33}H_{38}F_4N_6O_{11}S_3+H]^+$ = 867.1775; found 867.1776; 0.1 ppm mass defect.

Macrocycle **20**:

To a flame-dried 5-mL round bottom flask equipped with a stir bar was charged with Macrocycle **17** (20.0 mg, 1.0 equiv., 29.0 μmol), diluted with DMF (0.58 mL, 50 mM), and cooled to 0°C. To the flask was added coniferyl carbonate **33** (2.0 equiv.), $KOSiMe_3$ (2.0 equiv.), and stirred until completion observed by HPLC. After completion the reaction was quenched with AcOH (5 equiv.) and concentrated under reduced pressured and purified by reverse-phase HPLC to give Macrocycle **20** (14.6 mg, 53%). ^{1}H NMR (DMSO-d_6, 500 MHz) δ10.87 (s, 1H), 9.30 (s, 1H), 8.62 (d, J = 9.3 Hz, 1H), 8.32 (t, J = 9.6 Hz, 2H), 7.49 (1H, J = 7.9 Hz, 1H), 7.33 (d, J = 7.9 Hz, 2H), 7.27 (d, J = 1.8 Hz, 1H), 7.16 (J = 9.9 Hz, 1H), 7.11 (1H, J = 8.7Hz, 1H), 7.08 – 7.03 (m, 2H), 6.98 (t, J = 7.1 Hz, 1H) 6.62 (1H, J = 15.9 Hz, 1H), 6.31 (dt, J = 15.9, 6.3 Hz, 1H), 4.87 (dt, J = 9.9, 2.6 Hz, 1H), 4.73 (d, J = 5.7 Hz, 2H), 4.66 – 4.53 (m, 2H), 4.46 – 4.44 (m, 1H), 3.89 (d, J = 6.6 Hz, 2H), 3.77 (s, 3H), 3.63 (d, J = 12.1 Hz, 1H), 3.55 – 3.49 (m, 1H), 3.38 (bs, 1H), 3.12 – 2.98 (m, 3H), 2.93 (t, J = 12.2, 1H), 2.75 – 2.68 (m, 1H), 1.95 – 1.85 (m, 2H), 1.73 (s, 3H), 1.46 – 1.41 (m, 1H), 0.89 (d, J = 6.6 Hz, 6H). ^{13}C NMR (DMSO-d_6, 126 MHz) 172.7, 169.7, 169.5, 169.1, 168.5, 155.0, 150.3, 142.2, 136.6, 132.9, 129.3, 127.4, 125.4, 124.1, 122.8, 121.4, 118.9, 118.3, 117.8, 113.6, 111.8, 109.6, 73.8, 68.2, 61.9, 61.2, 56.2, 56.0, 54.9, 52.5, 46.3, 30.5, 29.7, 28.4,

27.7, 22.7, 19.2. ^{19}F NMR (DMSO-d_6, 282 MHz) δ -103.1 and -119.0 (AB quartet, J = 252.3 Hz, 2F), -114.2 and -127.7 (AB quartet, J = 222.7 Hz, 2F). HRMS m/z calculated for $[C_{42}H_{46}F_4N_6O_{11}S_2+H]^+$ = 951.2680; found 951.2686; 0.6 ppm mass defect.

Macrocycle **21**:

To a flame-dried 5-mL round bottom flask equipped with a stir bar was charged with Macrocycle **17** (40.0 mg, 1.0 equiv., 58.0 µmol), diluted with DMF (0.58 mL, 50 mM), and cooled to 0°C. To the flask was added NaN_3 (1.0 equiv.) and stirred for 1 h. After completion the reaction was concentrated under reduced pressured and purified by reverse-phase HPLC to give Macrocycle **21** (41.4 mg, >95%). ^{1}H NMR (DMSO-d_6, 500 MHz) δ 10.88 (s, 1H), 9.16 (s, 1H), 8.52 (d, 1H), 8.35 (t, J = 10.0, 2H), 7.49 (d, J = 7.8 Hz, 1H), 7.33 (d, J = 8.1 Hz, 1H), 7.12 (d, J = 9.5 Hz, 1H), 7.10 – 7.03 (m, 2H), 6.98 (t, J = 7.4 Hz, 1H), 4.97 (bs, 1H), 4.81 (d, J = 9.2 Hz, 1H), 4.64 – 4.53 (m, 2H), 4.38 – 4.30 (m, 1H), 3.89 – 3.80 (m, 1H), 3.59 (d, J = 13.2 Hz, 1H), 3.54 – 3.46 (m, 1H), 3.23 – 3.13 (m, 2H), 3.09 – 3.02 (m, 2H), 1.79 (s, 3H). ^{13}C NMR (DMSO-d_6, 126 MHz) 172.1, 169.4, 169.1, 168.6, 167.8, 136.1, 127.1, 123.7, 120.9, 118.4, 117.9, 111.4, 109.2, 61.3, 55.3, 54.8, 51.9, 45.9, 32.1, 27.8, 22.4, 21.1. ^{19}F NMR (DMSO-d_6, 282 MHz) δ -102.8 and -115.7 (AB quartet, J = 250.6 Hz, 2F), -113.5 and -126.5 (AB quartet, J = 224.7 Hz, 2F). HRMS m/z calculated for $[C_{27}H_{27}F_4N_9O_6S_2+H]^+$ = 714.1540; found 714.1542; 0.3 ppm mass defect.

Macrocycle **22**:

To a flame-dried 5-mL round bottom flask equipped with a stir bar was charged with Macrocycle **21** (15.0 mg, 1.0 equiv., 21.0 µmol), diluted with EtOH (0.420 mL, 50 mM) and flushed with argon. Pd/C (10 wt. %) was then added, flushed with hydrogen gas, and warmed to 35°C. The reaction mixture was then stirred at 35ºC for 16 h. After completion the reaction was

filtered with celite and concentrated under reduced pressure. Purification by reverse-phase HPLC gave Macrocycle **22** (12.6 mg, 87%) as a solid. ^{1}H NMR (DMSO-d_6, 500 MHz) δ 10.88 (s, 1H), 8.63 (s, 1H), 8.54 (d, J = 8.6 Hz, 1H), 8.41 (d, J = 9.2 Hz, 1H), 8.25 (d, J = 7.7 Hz, 1H), 7.50 (d, J = 7.5 Hz, 1H), 7.33 (d, J = 7.75 Hz, 1H), 7.16 – 7.03 (m, 3H), 6.98 (t, J = 7.0 Hz, 1H), 6.55 (s, 2H), 4.74 (d, J = 9.2 Hz, 1H), 4.70 – 4.58 (m, 2H), 4.41 – 4.32 (m, 1H), 3.51 – 3.42 (m, 2H), 3.17 (s, 1H), 3.06 (bs, 2H), 2.70 – 2.64 (m, 1H), 2.62 – 2.55 (m, 1H), 1.80 (s, 3H). ^{13}C NMR (DMSO-d_6, 126 MHz) 172.2, 169.1, 168.9, 168.6, 168.0, 136.1, 127.2, 123.7, 120.9, 118.4, 118.0, 111.4, 109.1, 61.4, 55.1, 54.7, 51.9, 45.7, 34.4, 31.3, 30.4, 29.8, 28.3, 22.4, 20.7. ^{19}F NMR (DMSO-d_6, 282 MHz) δ –104.3 – (-106.0) (m, 2F), -111.5 – (-113.7) (m, 2F), -120.6 – (-122.5) (m, 2F), -126.7 – (-128.6) (m, 2F). HRMS m/z calculated for $[C_{27}H_{29}F_4N_7O_6S_2+H]^+$ = 688.1635; found 688.1637; 0.3 ppm mass defect.

Macrocycle **23**:

To a flame-dried 5-mL round bottom flask equipped with a stir bar was charged with Macrocycle **21** (15.0 mg, 1.0 equiv., 21.0 μmol), propargyl alcohol (1.0 equiv.), phenylenediamine (15 mol %), sodium ascorbate (10 mol%), $CuSO_4$•$5H_2O$ (5 mol%) in 2:3 H_2O:tBuOH (0.2 M). The reaction was let stir at 23ºC for 12 h until observed completion by HPLC. After completion the reaction was concentrated under reduced pressure and purified by reverse-phase HPLC gave Macrocycle **23** (12.1 mg, 75% isolated yield) as a solid. ^{1}H NMR (DMSO-d_6, 500 MHz) δ 10.89 (s, 1H), 9.48 (s, 1H), 8.44 (d, J = 9.1 Hz, 1H), 8.32 (d, J = 8.32 Hz, 2H), 8.27 (d, J = 8.6 Hz, 1H), 7.49 (d, J = 7.9 Hz, 1H), 7.32 (d, J = 8.1 Hz, 1H), 7.22 (d, J = 9.3 Hz, 1H), 7.10 (d, J = 2.2 Hz, 1H), 7.06 (t, J = 7.3 Hz, 1H), 6.97 (t, J = 7.4 Hz, 1H), 4.87 (dt, J = 9.3, 2.5 Hz, 1H), 4.61 (s, 2H), 4.47 (q, J = 7.7 Hz, 2H), 4.37 (quint, J = 4.2 Hz, 2H), 3.84 (dd, J = 10.8, 4.4 Hz, 1H), 3.72 – 3.65 (m, 1H), 3.47 (dd, J = 10.8, 3.5 Hz, 1H), 3.26 (dd, J = 12.5, 8.1 Hz, 1H), 3.11 – 2.98 (m, 2H), 2.87

– 3.83 (m, 1H), 2.36 (dd, J = 12.5, 7.0 Hz, 1H), 1.74 (s, 3H). ^{13}C NMR (DMSO-d_6, 126 MHz) 171.9, 169.6, 169.3, 168.6, 167.6, 149.1, 136.1, 127.1, 123.8, 123.1, 121.0, 118.4, 118.0, 111.4, 109.0, 61.4, 55.6, 55.0, 54.5, 51.6, 46.1, 32.6, 30.8, 27.6, 22.3. ^{19}F NMR (DMSO-d_6, 282 MHz) δ -101.7 – (-103.2) (m, 1F), -113.1 – (-118.0) (m, 2F), -124.0 – (-125.3) (m, 1F). HRMS m/z calculated for $[C_{30}H_{31}F_4N_9O_7S_2+H]^+$ = 770.1802; found 770.1806; 0.5 ppm mass defect.

Macrocycle **24**:

Macrocycle **24** was synthesized according to **Scheme 4.2.2** General Procedure A (outlined above) using crude linear peptide Ac-CSC-NH_2 (100. mg, 1.0 equiv., 0.297 mmol). Purification by reverse-phase preparative HPLC gave Macrocycle **24** (62.0 mg, 43% isolated yield). ^{1}H NMR (DMSO-d_6, 500 MHz) δ 9.09 (d, J = 8.0 Hz, 1H), 8.90 (bs, 1H), 8.29 (d, J = 7.2 Hz, 1H), 7.76 (d, J = 9.8 Hz, 1H), 5.09 – 5.02 (m, 1H), 4.71 – 4.63 (m, 1H), 4.45 – 4.37 (m, 1H), 3.83 (dd, J = 11.2, 5.6 Hz, 1H), 3.68 (dd, J = 11.1, 3.0 Hz, 1H), 3.64 – 3.57 (m, 1H), 3.53 (dd, J = 11.2, 4.0 Hz, 1H), 3.48 (d, J = 13.7 Hz, 1H), 3.43 – 3.36 (m, 1H), 2.87 (dd, J = 13.9, 3.4 Hz, 1H), 1.92 (s, 3H). ^{13}C NMR (DMSO-d_6, 126 MHz) 169.5, 168.7, 168.0, 167.5, 150.6 – 150.1 (m, 1C), 127.5 – 125.8 (m, 3C), 68.8 - 68.6 (m, 1C), 60.7, 60.3, 55.5, 51.1, 46.6, 31.3, 29.2, 22.4. ^{19}F NMR (DMSO-d_6, 282 MHz) δ -105.7 (dt, J = 255.1, 15.9 Hz, 1F), -120.2 (dd, J = 221.5, 6.99 Hz, 1F), -123.9 (dt, J = 255.4, 11.1 Hz, 1F), -125.0 (dd, J = 220.6, 13.3 Hz, 1F), -131.8 – (-132.1) (m, 1F). HRMS m/z calculated for $[C_{16}H_{17}F_5N_4O_5S_2+H]^+$ = 505.0639; found 505.0640; 0.2 ppm mass defect.

Macrocycle **25**:

Macrocycle **25** was synthesized according to **Scheme 4.2.2** General Procedure A (outlined above) using crude linear peptide Ac-CWS-*d*-C-NH_2 (100. mg, 1.0 equiv., 0.186 mmol). Purification by reverse-phase HPLC gave Macrocycle **25** (34.7 mg, 27% isolated yield). ^{1}H NMR

(DMSO-d_6, 500 MHz) δ 10.87 (s, 1H), 9.25 (s, 1H), 8.49 (d, J = 8.49 Hz, 1H), 8.40 (d, J = 8.4 Hz, 1H), 8.29 (d, J = 7.2 Hz, 1H), 7.45 (d, J = 7.9 Hz, 1H), 7.32 (d, J = 8.1 Hz, 1H), 7.29 (d, J = 9.0 Hz, 1H), 7.10 – 7.03 (m, 2H), 6.96 (t, J = 7.6 Hz, 1H), 5.07 (t, J = 5.3 Hz, 1H), 4.67 – 4.59 (m, 2H), 4.53 – 4.45 (m, 1H), 4.23 – 4.18 (m, 1H), 3.72 (quint, J = 5.7 Hz, 1H), 3.55 – 3.49 (m, 1H), 3.42 – 3.37 (m, 1H), 3.27 (dd, J = 11.0 Hz,, 4.5 Hz, 1H), 3.17 (d, J = 5.15 Hz, 1H), 3.12 – 3.05 (m, 1H), 3.04 – 2.96 (m, 1H), 2.75 – 2.67 (m, 1H), 1.81 (s, 1H). ^{13}C NMR (DMSO-d_6, 126 MHz) δ 172.5, 169.5, 169.0, 168.0, 167.4, 136.1, 127.1, 123.7, 120.9, 118.4, 117.9, 111.3, 109.1, 60.8, 57.0, 54.8, 51.1, 46.4, 32.2, 30.5, 28.7, 22.2. ^{19}F NMR (DMSO-d_6, 282 MHz) δ -106.4 (dt, J = 250.8, 14.7 Hz, 1F), -114.9 (dd, J = 222.0, 10.2 Hz, 1F), -121.5 (dt, J = 250.2, 11.7 Hz, 1F), -125.6 – (-126.6) (m, 1F), -142.4 (t, J = 14.3 Hz, 1F). HRMS m/z calculated for $[C_{27}H_{27}F_5N_6O_6S_2+H]^+$ = 691.1432; found 691.1432; 0 ppm mass defect.

Macrocycle **26**:

Macrocycle **26** was synthesized according to **Scheme 4.2.2** General Procedure A (outlined above) using crude linear peptide Ac-CWS-homo-C-NH_2 (100. mg, 1.0 equiv., 0.181 mmol). Purification by reverse-phase HPLC gave Macrocycle **26** (33.2 mg, 26% isolated yield) as a solid. ^{1}H NMR (DMSO-d_6, 500 MHz) δ 10.89 (s, 1H), 9.47 (s, 1H), 8.58 (s, 1H), 7.51 (d, J = 8.6 Hz, 1H), 7.32 (t, J = 8.55 Hz, 2H), 7.26 (s, 1H), 7.17 (s, 1H), 7.06 (t, J = 7.4 Hz, 1H), 6.84 (s, 1H), 6.88 (d, J = 5.2 Hz, 1H), 5.02 (s, 1H), 4.33 – 4.26 (m, 2H), 4.12 – 4.07 (m, 1H), 3.83 – 3.78 (m, 1H), 3.74 – 3.61 (m, 3H), 1.95 (s, 3H), 1.83 (s, 1H). ^{19}F NMR (DMSO-d_6, 282 MHz) δ -108.8 (dt, J = 252.1, 14.8 Hz, 1F), -112.6 (d, J = 218.1 Hz, 1F), -116.2 (d, J = 219.0 Hz, 1F), -120.1 – (-121.2) (m, 1F), -136.4 (d, J = 14.8 Hz, 1F). HRMS m/z calculated for $[C_{28}H_{29}F_5N_6O_6S_2+H]^+$ = 705.1588; found 705.1590; 0.3 ppm mass defect.

Synthesis and Characterization of **Scheme 4.3.1** Products

Macrocycle **30**:

To a flame-dried round bottom flask equipped with a stir bar was charged with crude linear Ac-YACFAC-NH_2 (219.9 mg, 1.0 equiv., 0.3063 mmol), diluted with anhydrous DMF (30.63 mL, 10.0 mM), and then allowed to stir at 0ºC. Then OFCP (229.7 mL, 1.5 equiv., 1.0 M in MeCN) was added followed by NEt_3 (107 µL, 2.5 equiv., 0.7658 mmol). The reaction mixture was allowed to stir at 0ºC for 30 min. When HPLC indicated macrocycle intermediate formation, the reaction mixture was concentrated under reduced pressure to dryness. The reaction residue was added thiazole **29**, diluted with 1:4 DMF/THF (30 mM), and then stirred at 0ºC. The reaction solution was then added KOTMS (3.5 equiv.) and the reaction mixture allowed to gradually warm up to 23ºC for 3 h. When HPLC indicated reaction completion, the reaction mixture was added AcOH (10 equiv.) and then concentrated under reduced pressure to afford crude product. The crude product was then purified via flash SiO_2 chromatography (gradient $CHCl_3$ → 5% MeOH/$CHCl_3$ → 10% MeOH/$CHCl_3$) afforded title compound (54.8 mg, 18% isolated yield) as a yellow-powder; R_f = 0.33 at 15% MeOH/$CHCl_3$.

Polycycle **31**:

To a flame-dried scintillation vial equipped with a stir bar was charged with **30** (22.8 mg, 1.0 equiv., 22.9 µmol), diluted with anhydrous $MeNO_2$ (4.57 mL, 5.0 mM), and then added TFA (344 µL, 7.5 vol %). The solution was then then purged with argon and added a screwtop cap. The reaction was then allowed to stir at 80ºC for 12 h. After HPLC indicated reaction completion, the reaction mixture was concentrated under reduced pressure to afford crude product. The crude product was then purified via reverse-phase preparative HPLC – (gradient 10% MeCN/H_2O →

60% MeCN/H_2O) to afford title compound (11.7 mg, 52% isolated yield) as an orange-powder. ^{1}H NMR (DMSO-d_6, 600 MHz) δ 9.49 (s, 1H), 8.46 (d, J = 7.5 Hz, 1H), 8.39 (d, J = 8.3 Hz, 1H), 8.26 (s, 1H), 8.15 (d, J = 7.7 Hz, 1H), 8.07 (d, J = 7.5 Hz, 1H), 7.65 (d, J = 8.0 Hz, 1H), 7.30–7.25 (m, 2H), 7.23–7.18 (m, 2H), 7.18–7.15 (m, 2H), 6.86 (d, J = 7.3 Hz, 1H) 6.68 (d, J = 7.9 Hz, 1 H), 4.70 (d, J = 8.2 Hz), 4.61–4.56 (m, 1H), 4.56–4.51 (m, 1H), 4.44 (dd, J = 14.1, 7.2 Hz, 1H), 4.25–4.19 (m, 1H), 4.19–4.11 (m, 1H), 4.03 (d, J = 15.6 Hz, 1H), 3.90 (d, J = 15.6 Hz, 1H), 3.74–3.67 (dd, J = 12.2, 7.1 Hz, 1H), 3.57 (d, J = 13.1 Hz, 1H), 3.53 (dd, J = 12.4, 8.1 Hz, 1H), 2.94–2.81 (m, 4H), 2.74–2.61 (m, 1H), 1.86 (s, 3H), 1.18 (d, J = 6.6 Hz, 3H), 1.00 (d, J = 6.5 Hz, 3H). ^{13}C NMR (DMSO-d_6, 126 MHz) δ 171.6, 171,3, 171.0, 169.3, 169.0, 168.8, 167.6, 153.2, 152.8, 143.3, 141.3, 137.9–137.9 (m, 1C), 136.6, 130.6, 129.5, 129.0, 128.3, 127.8, 126.6, 125.6–125.5 (m, 1C), 124.4, 119.4–119.3 (m, 1C), 117.1–117.0 (m, 1C), 114.8, 70.1–70.0 (m, 1C), 55.4, 53.6, 52.1, 48.5, 47.4, 46.5, 37.2, 36.1, 32.2, 30.4, 26.9, 22.5, 19.1, 17.3 ^{19}F NMR (DMSO-d_6, 565 MHz) ^{19}F (DMSO-d_6, 565 MHz) δ -98.3 and -112.2 (AB quartet, J = 248.8 Hz, 2F), -113.0 and -128.2 (AB quarter, J = 223.8 Hz, 2F) HRMS m/z calculated for $[C_{41}H_{42}F_4N_8O_8S_4+H]^+$ = 979.2023; found 979.2048; found 2.6 ppm mass defect.

Polycycle **32**:

Synthesized in same sequential procedure to make **30** and **31** using crude linear peptide Ac-YCAC-NH_2. Acyclic macrocycle intermediate (36.9 mg, 1.0 equiv., 47.4 μmol) afforded crude product which was then purified via reverse-phase preparative HPLC (gradient 10% MeCN/H_2O → 65% MeCN/H_2O → 70% MeCN/H_2O) to afford desired product. Desired product was repurified via pTLC; 10% MeOH/$CHCl_3$ solvent system to afford title compound (11.6 mg, 32% isolated yield) as a white-powder. ^{1}H NMR (DMSO-d_6, 600 MHz) δ 9.48 (s, 1H), 9.11 (s, 1H),

8.77 (d, J = 9.2 Hz, 1H), 7.96 (d, J = 7.3 Hz, 1H), 7.65 (s, 1H), 7.58 (d, J = 8.9 Hz, 1H), 7.53 (d, J = 9.6 Hz, 1H), 6.79–6.74 (m, 2H), 6.69 (d, J = 8.0 Hz, 1H), 4.73–4.67 (m, 1H), 4.58–4.52 (m, 2H), 4.50–4.46 (m, 1H), 4.26 (d, J = 15.6 Hz, 1H), 3.83 (dd, J = 14.0, 4.8 Hz, 1H), 3.70 (d, J = 15.5 Hz, 1H), 3.65–3.58 (m, 1H), 3.44–3.40 (m, 1H), 3.24 (dd, J = 13.1, 3.2 Hz, 1H), 2.91 (dd, J = 13.6, 3.7 Hz, 1H), 2.42 (dd, J = 13.1, 7.9 Hz, 1H), 1.87 (s, 3H), 1.23 (d, J = 5.2 Hz, 3H). ^{13}C NMR (DMSO-d_6, 126 MHz) δ 170.8, 170.6, 169.5, 168.5, 167.2, 154.2, 153.2, 143.9, 141.3, 136.9 (m, 1C), 135.5 (m, 1C), 129.9, 129.8, 127.0, 125.6, 114.9, 67.0 (m, 1C), 53.8, 53.5, 48.0, 47.3, 35.7, 32.7, 31.0, 26.7, 22.9, 15.5. ^{19}F NMR (DMSO-d_6, 565 MHz) -96.3, -114.0 (AB quartet, J = 250.6 Hz, 2F) -119.1, -127.7 (AB quartet, J = 219.4 Hz, 2F) HRMS m/z calculated for $[C_{29}H_{28}F_4N_6O_6S_4+H]^+$ = 761.0968; found 761.1005; 4.9 ppm mass defect.

Polycycle **34**:

To a flame-dried 50-mL round bottom flask equipped with a stir bar was charged with crude Ac-YGHAC-NH_2 (135.0 mg, 1.0 equiv., 192 μmol), diluted with anhydrous DMF (19.2 mL, 10.0 mM), and then allowed to stir at 0ºC. Then OFCP (287 μL, 1.5 equiv., 287 μmol, 1M in MeCN) followed by NEt_3 (134 μmol, 2.5 equiv., 958 μmol) were added and the reaction mixture allowed to stir at 0ºC for 30 min. After HPLC indicated full conversion to macrocycle intermediate, the reaction mixture was concentrated to dryness under reduced pressure to remove excess OFCP, NEt_3, and DMF. The reaction mixture was then dissolved in 1:4 DMF:THF (7.66 mL, 30 mM) and cooled to 0ºC. Then Cs_2CO_3 (375 mg, 6.0 equiv., 1.15 mmol) was added and the reaction mixture stirred at 0ºC for 1 h until full conversion to spirocycle intermediate was observed. The reaction mixture was then added phenol **33** (107.9 mg, 2.0 equiv., 129 μmol) and then allowed to stir at 23ºC for 48 h. After HPLC indicated reaction completion, the reaction mixture was quenched with

AcOH (165 μL, 15.0 equiv., 2.87 mmol), and then concentrated under reduced pressure to afford crude product. The crude product was then purified via flash SiO_2 chromatography (gradient $CHCl_3$ → 5% MeOH/$CHCl_3$ → 10% MeOH/$CHCl_3$) to afford **34** (37.8 mg, 20% isolated yield) as a yellow-powder, R_f = 0.32 at 15% MeOH/$CHCl_3$. HRMS m/z calculated for $[C_{45}H_{50}F_4N_8O_{12}S+Na]^+$ = 1025.3103; found 1025.3121; 1.8 ppm mass defect.

Polycycle **35**:

To a flame-dried 15-mL round bottom flask equipped with a stir bar was charged with Polycycle **34** (18.0 mg, 1.0 equiv., 17.9 μmol) and diluted with anhydrous $MeNO_2$ (3.59 mL, 5.0 mM). The mixture was then added Tf_2NH (25.2 mg, 5.0 equiv., 89.7 μmol) in dry $MeNO_2$ (3.59 mL, 5.0 mM) (total volume of 2.5 mM). The reaction mixture was then allowed to stir at 23 ºC for 1 h. After HPLC indicated reaction completion, the reaction mixture was quenched with iPr_2NEt (31.3 μL, 10.0 equiv., 379 μmol) and concentrated under reduced pressure to afford crude product. The crude product was then purified via preparative HPLC – (gradient 5% MeCN/H_2O → 60% MeCN/H_2O → 70% MeCN/H_2O) to afford desired product. Desired product was then repurified via flash SiO_2 chromatography (gradient $CHCl_3$ → 5% MeOH/$CHCl_3$ → 10% MeOH/$CHCl_3$) to afford title compound (8.0 mg, 45% isolated yield) as a colorless-film. ^{1}H NMR (DMSO-d_6, 600 MHz) δ 9.15 (s, 1H), 9.03 (s, 1H), 8.65 (d, J = 7.6 Hz, 1H), 8.39 (t, J = 5.6 Hz, 1H), 8.05 (d, J = 7.6 Hz, 1H), 7.89 (m, 1H), 7.39 (m, 1H), 7.04–7.01 (m, 2H), 6.96 (s, 1H), 6.88 (m, 1H), 6.87 (m, 1H), 6.85 (m, 1H), 6.70 (d, J = 8.3 Hz, 1H), 6.54 (m, 1H), 6.18 (dt, J = 15.9, 6.4 Hz, 1H), 6.07 (d, J = 15.9 Hz, 1H), 4.58 (m, 2H), 4.35 (q, J = 6.9 Hz, 1H), 4.14 (m, 1H), 4.01 (dd, J = 15.8, 7.0 Hz, 1H), 3.80 (s, 3H), 3.47 (m, 2H), 3.42–3.34 (m, 4H), 2.91 (m, 1H), 2.77–2.71 (m, 2H), 1.84 (s, 3H), 1.21 (d, J = 7.4 Hz, 3H) ^{13}C (DMSO-d_6, 126 MHz) δ 171.7, 170.7, 169.8, 169.0, 168.7, 167.2,

153.5, 147.9, 140.7, 138.4, 137.1–136.9 (m, 1C), 130.8, 130.5, 130.1, 129.7, 129.0, 127.9, 127.9, 127.6, 125.4, 124.4, 117.3–117.1 (m, 1C), 117.0, 116.3–116.2 (m, 2C), 114.6, 112.9, 67.0–66.7 (m, 1C), 55.9, 54.1, 51.3, 48.9, 45.8, 42.6, 37.3, 32.2, 29.8, 29.0, 22.6, 17.7 ^{19}F (DMSO-d_6, 565 MHz) δ -106.0 and -121.6 (AB quartet, J = 248.4 Hz, 2F), -116.0 and -126.1 (AB quartet, J = 215.6 Hz, 2F) HRMS m/z calculated for $[C_{40}H_{40}F_4N_8O_9S+H]^+$ = 885.2653; found 885.2694; 3.1 ppm mass defect.

Polycycle **36**:

A flame-dried round bottom flask equipped with a stir bar was charged with compound crude peptide Ac-WCASC-NH_2, diluted with DMF (10 mM), added Et_3N (2.5 equiv.), and cooled to 0°C. To the flask was added OFCP (3.0 equiv.) dropwise and let stir for 30 min. Then the flask was concentrated under reduced pressure. The crude intermediate macrocycle was then diluted with a DMF/THF mixture (1:4, 30 mM) a cooled to 0°C. To the flask was added **33** (2.0 equiv.), Cs_2CO_3 (6.0 equiv.), and let stir until completion observed by HPLC. After completion the reaction was quenched with AcOH (15.0 equiv.), concentrated under reduced pressured and purified by RP-HPLC. The acyclic intermediate (34.0 mg, 1.0 equiv., 33.3 μmol) was then diluted with dry $MeNO_2$ (6.65 mL, 5 mM). To the flask was added $ScOTf_3$ (32.7 mg, 2.0 equiv., 66.5 μmol) and let stir until completion observed by HPLC. Upon completion, the mixture was concentrated under reduced pressure and purified by reverse-phase HPLC – (gradient 10% MeCN/H_2O → 65% MeCN/H_2O) to obtain **36** (12.0 mg, 35% isolated yield) and two other regioisomeric products for a 70% combined yield. Only one of the regioisomeric products were characterized for NMR. ^{1}H NMR (DMSO-d_6, 500 MHz) δ 10.9 (s, 1H), 9.22 (s, 1H), 8.24 (d, J = 7.2 Hz, 2H), 7.94 (d, J = 8.8 Hz, 1H), 7.60 (d, J = 7.6 Hz, 1H), 7.50 (s, 1H), 7.26 – 7.07 (m, 6H), 6.96 (dt, J = 29.7, 7.3 Hz,

2H), 6.64 – 6.45 (m, 2H), 4.86 (d, J = 5.7 Hz, 1H), 4.80 (d, J = 9.6 Hz, 1H), 4.64 – 4.54 (m, 2H), 4.38 – 4.33 (m, 1H), 4.30 (t, J = 7.8 Hz, 1H), 3.82 (s, 3H), 2.44 – 2.16 (m, 2H), 3.13 – 3.06 (m, 4H), 2.90 – 2.80 (m, 1H), 2.79 – 2.70 (m, 1H), 2.67 (d, J = 13.9 Hz, 1H), 1.70 (s, 3H), 1.24 (d, J = 7.2 Hz, 3H). ^{13}C-NMR (500 MHz, DMSO-d_6) δ 173.2, 172.0, 169.3, 169.2, 168.1, 168.0, 148.9, 141.8, 137.4, 134.7, 133.1, 130.2, 130.0, 129.2, 128.9, 128.2, 126.8, 125.3, 124.6, 120.2, 118.3, 118.0, 117.2, 113.2, 110.6, 108.4, 74.2, 61.3, 55.9, 54.6, 54.2,52.7, 50.3, 32.9, 31.1, 30.7, 26.8, 22.8, 17.9. HRMS [M+1] calculated for $[C_{40}H_{41}F_4N_7O_9S+H]^+$ = 904.2422, found 904.2423; 0.1 ppm mass defect.

Polycycle **40**:

Polycycle **40** was synthesized according to **Scheme 4.3.1** General Procedure F,G and H (outlined above). To a flame-dried round bottom flask equipped with a stir bar was charged with crude Ac-D*GSFAC-NH_2 (339.3mg, 1.0 equiv., 469.4 µmol), diluted with anhydrous DMF (46.94 mL, 10.0 mM), and then allowed to stir at 0 ºC. Then OFCP (704.1 µL, 1.5 equiv., 1.0 M in MeCN) was added followed by NEt_3 (196 µL, 2.5 equiv., 1.41 mmol). The reaction mixture was allowed to stir at 0ºC for 30 min. When HPLC indicated macrocycle intermediate formation, the reaction mixture was concentrated under reduced pressure to dryness. The reaction residue was then added 1:4 DMF:THF (15.65 mL, 30 mM) and cooled to 0ºC. Then Cs_2CO_3 (917.6 mg, 6.0 equiv., 2.82 mmol) was added, and the reaction mixture allowed to stir at 0 ºC for 1 h. When HPLC indicated full conversion to the desired vinyl fluoride then cysteamine (64.0 mg, 1.2 equiv., 563.3 µmol) was added and the reaction mixture allowed to stir at 0ºC for 1 h. When HPLC indicated reaction completion, the reaction mixture was quenched with AcOH (268.7 µL, 10.0 equiv., 4.694 mmol)

and then concentrated under reduced pressure to afford crude product. The crude product was then telescoped to the next step.

Assumed a 50% yield from General Procedure F when calculating stoichiometry. To the same round bottom flask used for General Procedure F, the crude product was diluted with a solution 2:8 MeCN:aqueous buffer pH 4.5 (NaOAc/AcOH, 0.2 M). The reaction mixture was then allowed to stir at 23 ºC and then was added NCS in MeCN (1.0 M) portionwise (0.5 equiv.). Total NCS varied from 1.5–3.0 equiv. (1.5 equiv. for precursor that led to **40**) depending on substrate. When HPLC indicated full conversion to the desired free acid, the reaction mixture was quenched with $Na_2S_2O_3$•$5H_2O$ (6.0 equiv.). The reaction mixture was concentrated under reduced pressure to afford crude product. The crude product was then purified via preparative HPLC – (gradient 10% MeCN/H_2O → 55% MeCN/H_2O) afforded the acyclic amino acid (161.5 mg, 41% isolated yield) as a white-powder.

To a flame-dried round bottom flask equipped with a stir bar was charged with the acyclic amino acid (10.0 mg, 1.0 equiv., 10.4 μmol) and diluted with anhydrous DMF (2.08 mL, 5.0 mM). The solution was added iPr_2NEt (6.3 μL, 3.5 equiv., 36.4 μmol) and the reaction mixture allowed to cool to 0 ºC. Then propanephosphonic acid anhydride in EtOAc (9.3 μL, 1.5 equiv., 50% wt.) was added and the reaction mixture allowed to stir at 0ºC for 1 h. After HPLC indicated reaction completion, the reaction mixture was quenched with AcOH (2.98 μL, 5.0 equiv., 52 μmol) and then concentrated under reduced pressure to afford crude product. The crude product was then purified via reverse-phase preparative HPLC – (gradient 10% MeCN/H_2O → 65% MeCN/H_2O) afforded title compound (6.4 mg, 74% isolated yield, 30% from linear peptide) as a white-powder. ^{1}H NMR (DMSO-d_6, 500 MHz) δ 8.61 (d, J = 4.1 Hz, 1H), 8.07 (d, J = 7.5 Hz, 1H), 7.92 (d, J = 7.7 Hz, 1H), 7.80–7.74 (m, 1H), 7.56–7.51 (m, 1H), 7.50 (d, J = 7.6 Hz, 1H), 7.41 (s, 1H), 7.32–

7.24 (m, 2H), 7.26–7.21 (m, 3H), 4.97–4.91 (m, 1H), 4.86–4.80 (m, 1H), 4.55–4.49 (m, 1H), 4.26–4.21 (m, 1H), 4.20–4.14 (m, 2H), 4.09–4.04 (m, 1H), 3.58–3.50 (m, 2H), 3.37–3.25 (m, 2H), 3.18–3.06 (m, 3H), 3.03–2.95 (m, 2H), 2.87–2.83 (m, 1H), 2.47–2.40 (m, 1H), 2.32–2.26 (m, 1H), 1.80 (s, 3H), 1.16 (d, J = 6.8 Hz, 3H) ^{13}C NMR (DMSO-d_6, 126 MHz) δ 171.4, 171.2, 170.9, 168.9, 168.6, 168.3, 167.8, 162.3, 140.9–140.2 (m, 1C), 136.9, 129.0, 128.3, 126.6, 120.6–120.3 (m, 1C), 118.5–118.1 (m, 1C), 116.1–115.7 (m, 1C), 71.3, 69.0–68.9 (m, 1C) 57.3, 56.4, 52.6, 50.4, 48.5, 41.6, 41.1, 36.1, 35.8, 32.0, 30.3, 22.5, 16.0 ^{19}F NMR (DMSO-d_6, 282 MHz) δ -103.5, -107.6 (AB quartet, J = 247.0 Hz, 2F), -115.3, -120.2 (AB quartet, J = 229.0 Hz, 2F). HRMS [M+1] calculated for $[C_{33}H_{38}F_4N_8O_9S_2+H]^+$ = 831.2218; found 831.2225; 0.8 ppm mass defect.

Polycycle **41**:

Polycycle **41** was synthesized according to **Scheme 4.3.1** General Procedure F,G and H (outlined above). Following **Scheme 4.3.1** General Procedure F and G using crude linear peptide Ac-E*ASFAC-NH_2 (126. mg, 1.0 equiv., 165 μmol) afforded crude seco-acid intermediate. Crude product was purified via reverse-phase HPLC – (gradient 5% MeCN/H_2O → 45% MeCN/H_2O) to afford macrocyclic intermediate (65.5 mg, 40% isolated yield) as a yellow-film. HRMS calculated for $[C_{36}H_{46}F_4N_8O_{10}S_2+H]^+$ = 890.2715; found 890.2734; 2.1 ppm mass defect. Followed **Scheme 4.3.1** General Procedure H to obtain macrolactam from seco-acid intermediate (40.0 mg, 1.0 equiv., 39.8 μmol) afforded crude product. Crude product was purified via reverse-phase HPLC – (gradient 5% → 70% MeCN/H_2O → 85% MeCN/H_2O) to afford title compound (27.8 mg, 80% isolated yield, 32% from linear peptide) as an off-white powder. NMR of **41** contained complex mixture of rotational isomers; ratio ~ 2:3 + minor isomers. All rotational isomers were characterized. ^{1}H NMR (DMSO-d_6, 500 MHz) δ 9.21 (d, J = 6.45 Hz, 0.62H), 8.78 (d, J = 5.75

Hz, 1H), 8.39 (d, J = 8.10 Hz, 1H), 8.29 (d, J = 8.45 Hz, 1H), 8.23 (d, J = 7.20 Hz, 1H), 8.07 (d, J = 8.65 Hz, 1H), 7.95 (s, 1.7H), 7.71 (d, J = 7.60 Hz, 1H), 7.62 (d, J = 6.45 Hz, 1H), 7.42 (s, 1.7H), 7.32 (d, J = 17.55 H, 2H), 7.25-7.18 (m, 6H), 7.15-7.07 (m, 5H), 6.23 (d, J = 3.95 Hz, 1H), 4.98-4.82 (m , 1H), 4.81-4.71 (m, 2H), 4.67-4.59 (m, 2H), 4.41-4.30 (m, 1H), 4.24-4.08 (m, 6H), 3.60-3.42 (m, 4H), 3.38-3.28 (m, 2H), 3.28-3.16 (m, 3H) 3.16-3.04 (m, 4H), 3.03 (s, 3H), 2.99 (s, 3H), 2.97-2.90 (m, 3H), 1.96 (s, 2H), 1.90 (s, 3H), 1.86-1.79 (m, 3H), 1.78-1.65 (m, 4H), 1.56-1.46 (m, 2H), 1.23 (d, J = 6.55 Hz, 3H), 1.17 (d, J = 2.33 Hz, 3H) ^{13}C NMR (DMSO-d_6, 126 MHz) δ 173.7, 172.3, 172.5, 171.8, 171.3, 171.3, 171.3, 171.3, 171.2, 171.1, 170.7, 170.6, 169.5, 169.3, 168.9, 168.6, 147.0–146.9 (m, 1C), 141.1–141.0 (m, 1C), 137.3, 137.0, 128.9, 128.9, 128.2, 128.0, 126.3, 118.9–118.8 (m, 1C), 116.6, 114.3, 112.0–111.9 (m, 1C), 71.3–71.1 (m, 2C), 59.3, 58.6, 58.4, 53.5, 53.4, 53.2, 52.9, 48.3, 48.2, 47.5, 42.4, 35.8, 35.6, 34.8, 34.7, 34.0, 31.1, 30.3, 30.0, 29.9, 29.3, 29.2, 28.5, 27.7, 26.6 HRMS calculated for $[C_{36}H_{44}F_4N_8O_9S_2+H]^+$ = 873.2687; found 873.2691; 0.5 ppm mass defect.

Polycycle **42**:

Polycycle **42** was synthesized according to **Scheme 4.3.1** General Procedure F,G and H (outlined above). Following **Scheme 4.3.1** General Procedure F and G using crude peptide Ac-E*VTFAC-NH_2 (100. mg, 1.0 equiv., 126 μmol) afforded crude seco-acid intermediate. Crude product was purified via reverse-phase HPLC – (gradient 5% MeCN/H_2O → 55% MeCN/H_2O) to afford seco-acid intermediate (42.5 mg, 33% isolated yield) as a yellow-film. HRMS calculated for $[C_{38}H_{50}F_4N_8O_{10}S_2+H]^+$ = 919.3106; found 918.3110; 0.4 ppm mass defect. Followed **Scheme 4.3.1** General Procedure H to obtain macrolactam seco-acid intermediate (31.5 mg, 1.0 equiv., 30.5 μmol) afforded crude product. Crude product was purified via reverse-phase HPLC –

(gradient 5% → 65% MeCN/H_2O → 80% MeCN/H_2O) to afford title compound (19.8 mg, 72% isolated yield, 24% from linear peptide) as an off-yellow powder. NMR of **42** contained complex mixture of rotational isomers; ratio ~ 2:3 + minor isomers. All rotational isomers were characterized. See VT NMR experiment. ^{1}H NMR (DMSO-d_6, 500 MHz) δ 8.36–8.30 (m, 1.5 H), 8.09 (d, J = 7.8 Hz, 1H), 8.00 (d, J = 7.9 Hz, 0.5 H), 7.50 (s, 0.5H), 7.92–7.87 (m, 1.5H), 7.83 (d, J = 7.8 Hz, 1H), 7.79 (d, J = 7.9 Hz, 1H), 7.63 (d, J = 8.3 Hz, 0.5H), 7.40 (s, 1H), 7.34 (s, 1H), 7.30–7.24 (m, 4H), 7.24–7.17 (m, 5H), 6.47 (t, J = 4.8 Hz, 1H), 5.12–5.04 (m, 1H), 4.61–4.50 (m, 2H), 4.44–4.27 (m, 2H), 4.19–4.11 (m, 2H), 4.11–4.04 (m, 1H), 3.61–3.52 (m, 0.5H), 3.52–3.47 (m, 1H), 3.45–3.32 (m, 1H), 3.30–3.18 (m, 1.5 H), 3.18–3.09 (m, 2H), 3.07–3.00 (m, 1.5 H), 2.99–2.90 (m, 1H), 2.33–2.21 (m, 1H), 2.07–2.00 (m, 1H), 1.98–1.87 (m, 1.5H), 1.83 (s, 3H), 1.80 (s, 2H), 1.44–1.39 (m, 4H), 1.25–1.22 (m, 1H), 1.20 (d, J = 6.7 Hz, 2H), 1.15 (d, J = 6.8 Hz, 3H), 0.98–0.92 (m, 1.5H), 0.89 (d, J = 6.7 Hz, 3H), 0.86–0.82 (m, 4H), 0.81 (d, J = 6.7 Hz, 3H) ^{13}C NMR (DMSO-d_6, 126 MHz) δ 172.8, 172.4, 171.9, 171.8, 171.7, 171.7, 171.1, 171.7, 171.4, 170.9, 170.7, 170.4, 168.7, 168.4, 167.7, 167.3, 147.2–147.1 (m, 1C), 145.8–145.7 (m, 1C), 140.1–140.0 (m, 1C), 137.0, 136.8, 128.7, 128.5, 128.3, 128.3, 126.5, 126.4, 119.0–118.9 (m, 1C), 116.8–116.7 (m, 1C), 114.5–114.2 (m, 1C), 112.2–112.0 (m, 1C), 64.3, 50.1, 56.3, 55.8, 53.3, 53.3, 51.8, 50.7, 48.5, 48.3, 41.5, 41.3, 30.8, 35.5, 34.4, 33.6, 30.6, 30.3, 30.0, 29.9, 29.3, 29.2, 29.0, 28.7, 28.4, 27.9, 26.8, 22.5, 21.0, 20.9, 19.8, 19.6, 17.0, 16.5, 16.4, 16.3, 16.2, 16.0 HRMS calculated for $[C_{38}H_{48}F_4N_8O_9S_2+H]^+$ = 901.3000; found 901.3004; 0.4 ppm mass defect.

Polycycle **43**:

Polycycle **43** was synthesized according to **Scheme 4.3.1** General Procedure F,G and H (outlined above). Following **Scheme 4.3.1** General Procedure F and G using crude peptide Ac-

D*PTFSC-NH_2 (194.3 mg, 1.0 equiv., 181 μmol) afforded crude seco-acid intermediate. Crude product was purified via reverse-phase HPLC – (gradient 5% MeCN/H_2O → 45% MeCN/H_2O) to afford seco-acid intermediate (80.2 mg, 34% isolated yield) as a yellow-film. HRMS calculated for $[C_{44}H_{54}F_4N_{12}O_{12}S_2+H]^+$ = 1083.3440; found 1083.3448; 0.7 ppm mass defect. Followed **Scheme 4.3.1** General Procedure H to obtain macrolactam from seco-acid intermediate (40.0 mg, 1.0 equiv., 30.5 μmol) afforded crude product. Crude product was purified via reverse-phase HPLC – (gradient 5% → 45% MeCN/H_2O → 50% MeCN/H_2O) to afford title compound (10.8 mg, 30% isolated yield, 10% from linear peptide) as a yellow-powder. NMR of **43** contained complex mixture of rotational isomers; ratio ~ 1:10:35. Major rotational isomer was characterized. ^{1}H NMR (DMSO-d_6, 500 MHz) δ 9.31 (s, 1H), 8.25–8.21 (m, 2H), 8.05 (d, J = 7.2 Hz, 1H), 7.84 (d, J = 8.3 Hz, 1H), 7.74 (d, J = 6.4 Hz, 1H), 7.61 (t, J = 4.8 Hz, 1H), 7.57 (s, 1H), 7.39 (s, 1H), 7.31–7.24 (m, 5H), 7.22–7.19 (m, 2H), 6.97 (s, 1H), 4.85–4.74 (m, 3H), 4.58–4.49 (m, 1H), 4.44–4.32 (m, 2H), 4.29 (dd, J = 9.3, 2.1 Hz, 1H), 4.21 (dd, J = 8.5, 4.4 Hz, 1H), 4.18–4.12 (m, 1H), 3.71–3.63 (m, 1H), 3.62–3.55 (m, 2H), 3.24–3.08 (m, 4H), 3.07–2.99 (m, 3H), 2.86–2.78 (m, 3H), 2.71–2.67 (m, 1H), 2.28 (dd, J = 15.2, 8.9 Hz, 1H), 2.12–2.04 (m, 1H), 1.83 (s, 3H), 1.82–1.79 (m, 2H), 1.77–1.74 (m, 2H), 0.96 (d, J = 6.3 Hz, 3H) ^{13}C NMR (DMSO-d_6, 126 MHz) δ 171.8, 171.3, 171.2, 171.1, 170.9, 170.4, 170.2, 169.5, 168.9, 168.4, 131.4–131.3 (m, 1C), 129.3–129.2 (m, 1C), 129.0, 128.3, 126.5, 117.1, 115.8–115.7 (m, 1C), 114.7, 112.5–112.4 (m, 1C), 67.5–67.3 (m, 1C), 67.0, 66.5, 60.5, 58.8, 56.2, 53.6, 52.4, 49.7, 47.8, 47.1, 37.3, 36.3, 35.8, 33.0, 30.8, 29.0, 25.1, 24.3, 22.3, 20.1 ^{19}F NMR (DMSO-d_6, 565 MHz) δ -94.3 and -114.1 (AB quartet, J = 251.4 Hz, 2F), -114.1 and -127.0 (AB quartet, J = 230.0 Hz, 2F) HRMS calculated for $[C_{44}H_{51}F_4N_{12}O_{11}S_2+H]^+$ = 1065.3334; found 1065.3350; 1.5 ppm mass defect.

Polycycle **44**:

Polycycle **44** was synthesized according to **Scheme 4.3.1** General Procedure F,G and H (outlined above). Following **Scheme 4.3.1** General Procedure F and G using crude peptide Ac-E*PSFTC-NH_2 (126. mg, 1.0 equiv, 165 μmol) afforded crude seco-acid intermediate. Crude product was purified via reverse-phase HPLC – (gradient 5% MeCN/H_2O → 55% MeCN/H_2O) to afford seco-acid intermediate (64.3 mg, 33% isolated yield) as a yellow-film. Followed **Scheme 4.3.1** General Procedure H to obtain macrolactam from seco-acid intermediate (20.0 mg, 1.0 equiv., 19.1 μmol) afforded crude product. Crude product was purified via reverse-phase HPLC – (gradient 5% MeCN/H_2O → 65% MeCN/H_2O → 75% MeCN/H_2O) followed by a repurification via flash column chromatography SiO_2 – (gradient $CHCl_3$ → 5% MeOH/$CHCl_3$ → 10% MeOH/$CHCl_3$) afforded title compound (8.7 mg, 50% isolated yield, 17% isolated yield from linear peptide) as a white-film. NMR of **44** contained complex mixture of rotational isomers. Major rotational isomer was characterized. ^{1}H NMR (DMSO-d_6, 500 MHz) δ 8.13 (d, J = 7.5 Hz, 1H), 8.06 (d, J = 8.4 Hz, 1H), 7.97 (t, J = 5.6 Hz, 1H), 7.94 (d, J = 8.2 Hz, 1H), 7.47 (d, J = 9.3 Hz, 1H), 7.28–7.22 (m, 4H), 7.21–7.17 (m, 2H), 7.06 (s, 1H), 4.90 (dd, J = 6.3, 3.2 Hz, 1H), 4.85 (t, J = 5.5 Hz, 1H), 4.61 (dd, J = 9.4, 3.1 Hz, 1H), 4.54 (td, J = 8.8, 3.3 Hz, 1H), 4.45 (q, J = 7.3 Hz, 1H), 4.38 (dd, J = 8.2, 3.4 Hz, 1H), 4.35–4.29 (m, 1H), 3.73–3.66 (m, 2H), 3.60 (m, 1H), 3.50–3.41 (m, 4H), 3.26–3.22 (m, 1H), 3.15–3.00 (m, 3H), 3.00–2.90 (m, 2H), 1.92–1.89 (m, 1H), 1.89–1.84 (m, 2H), 1.81 (s, 3H), 1.77–1.69 (m, 4H), 1.04 (d, J = 6.4 Hz, 3H) ^{13}C NMR (DMSO-d_6, 126 MHz) δ 171.8, 171.5, 171.1, 170.4, 169.9, 169.1, 168.0, 167.9, 138.0, 134.8–134.6 (m, 1C), 134.6–134.4 (m, 1C), 129.1, 128.2, 126.3, 119.1–118.9 (m, 2C), 71.0, 71.0–70.9 (m, 1C), 61.6, 59.0, 55.9, 54.7, 54.3, 51.7, 49.8, 46.9, 45.6, 35.9, 30.7, 29.0, 28.9, 28.6, 25.1, 24.3, 22.2, 15.4 ^{19}F NMR (DMSO-d_6, 282 MHz) δ -99.6, -118.1 (AB quartet, J = 252 Hz, 2F), -120.3, -133.0 (AB quartet, J = 232

Hz, 2F). HRMS m/z calculated for $[C_{38}H_{46}F_4N_8O_{10}S_2+H]^+$ = 915.2783; found 915.2799; 1.8 ppm mass defect.

Polycycle **45**:

Polycycle **45** was synthesized according to **Scheme 4.3.1** General Procedure F,G and H (outlined above). Following **Scheme 4.3.1** General Procedure F and G using crude peptide Ac-E*VTFAC-NH_2 (123. mg, 1.0 equiv., 158 μmol) afforded crude seco-acid intermediate. Crude product was purified via reverse-phase preparative HPLC – (gradient 10% MeCN/H_2O → 55% MeCN/H_2O) to afford seco-acid intermediate (50.3 mg, 31% isolated yield) as a yellow-film. HRMS calculated for $[C_{37}H_{46}F_4N_8O_{11}S_2+H]^+$ = 905.2949; found 905.2978; 3.2 ppm mass defect. Followed **Scheme 4.3.1** General Procedure H to obtain macrolactam **45**. Seco-acid intermediate (40.0 mg, 1.0 equiv., 39.3 μmol) afforded crude product. Crude product was purified via reverse-phase preparative HPLC – (gradient 10% MeCN/H_2O → 70% MeCN/H_2O → 85% MeCN/H_2O) to afford title compound (25.2 mg, 72% isolated yield, 23% yield from peptide). NMR of **46** contained complex mixture of rotational isomers; ratio ~ 2:1 + minor isomers. Both rotational isomers were characterized. See VT NMR experiment. ^{1}H NMR (DMSO-d_6, 500 MHz) δ 8.65 (d, J = 6.2 Hz, 0.5 H), 8.37 (d, J = 7.4 Hz, 1H), 8.31 (s, 0.5H), 8.24 (d, J = 5.7 Hz, 1H), 8.11 (d, J = 6.0 Hz, 1H), 8.03 (dd, J = 11.8, 6.7 Hz, 1.4H), 7.93–7.88 (m, 1.5H), 7.86 (s, 0.5H), 7.82 (d, J = 7.9 Hz, 1H), 7.50–7.44 (m, 1.5 H), 7.33 (s, 1H), 7.30–7.21 (m, 4H), 7.20–7.15 (m, 5H), 6.31 (t, J = 4.0 Hz, 1H), 4.83 (d, J = 7.0 Hz, 1H), 4.74 (d, J = 6.8 Hz, 1H), 4.72–4.66 (m, 1.5H), 4.59–4.48 (m, 2H), 4.38–4.31 (2H), 4.30–4.21 (m, 2.5H), 4.14–4.09 (m, 1H), 4.08–4.01 (m, 1H), 3.98–3.92 (m, 2H), 3.89–3.84 (m, 1H), 3.75–3.71 (m, 0.5H), 3.60 (t, J = 6.5 Hz, 1H), 3.54–3.48 (m, 1H), 3.48–3.32 (m, 4H), 3.31–3.14 (m, 4H), 3.13–3.05 (m, 2H), 3.04–2.98 (m, 2H), 2.90–2.83 (m, 1.5H),

2.24–2.16 (m, 1H), 2.14 (m, 1H), 1.85 (s, 1.5 H), 1.83 (s, 3H), 1.19 (d, J = 6.6 Hz, 1.5H), 1.09 (d, J = 6.8 Hz, 3H), 0.91 (d, J = 6.8 Hz, 3H), 0.86 (d, J = 6.8 Hz, 3H), 0.80 (d, J = 6.7 Hz, 1.5H) ^{13}C NMR (DMSO-d_6, 126 MHz) δ 173.4, 173.4, 172.8, 172.4, 172.2, 172.1, 171.8, 171.8, 171.4, 171.2, 170.5, 170.4, 170.2, 169.2, 169.0, 168.9, 148.6–148.5 (m, 1C), 145.7–145.6 (m, 1C), 139.6–139.5 (m, 1C), 137.5, 137.4, 129.3, 129.0, 128.7, 126.9, 119.9, 118.5, 117.4–117.1 (m, 1C), 115.1–114.9 (m, 1C), 112.6–112.5 (m, 1C), 70.3–70.2 (m, 1C), 58.7, 58.2, 57.5, 57.0, 53.6, 53.5, 51.3, 51.1, 49.8, 49.0, 48.8, 46.2, 42.1, 36.4, 35.5, 34.5, 33.0, 31.0, 30.3, 30.2, 29.5, 28.8, 28.6, 27.9, 27.7, 26.4, 25.6, 25.0, 24.2, 22.9, 20.3, 20.1, 16.7, 16.6, 16.1, 16.1 ^{19}F NMR (DMSO-d_6, 282 MHz) δ -103.7 and -106.0 (AB quartet, J = 251.1 Hz, 2F), -116.6 and -122.0 (AB quartet, J = 229.2 Hz, 2F), -106.2 and -120.8 (AB quartet, J = 250.5 Hz, 2F minor)-106.4 and -115.7 (AB quartet, J = 227.4 Hz, 2F minor) HRMS calculated for $[C_{37}H_{46}F_4N_8O_9S_2+H]^+$ = 887.2844; found 887.2851; 0.8 ppm mass defect.

Polycycle **46**:

Polycycle **46** was synthesized according to **Scheme 4.3.1** General Procedure F,G and H (outlined above). Following **Scheme 4.3.1** General Procedure F and G using crude peptide Ac-D*PTFSC-NH_2 (130. mg, 1.0 equiv., 164 μmol) afforded crude seco-acid intermediate. Crude product was purified via reverse-phase preparative HPLC – (gradient 10% MeCN/H_2O → 55% MeCN/H_2O) to afford seco-acid intermediate (44.1 mg, 26% isolated yield) as a red-foam. HRMS calculated for $[C_{37}H_{46}F_4N_8O_{11}S_2+H]^+$ = 919.2742; found 919.2754; 1.3 ppm mass defect. Followed **Scheme 4.3.1** General Procedure H to obtain macrolactam **46**. Seco-acid intermediate (35.0 mg, 1.0 equiv, 33.9 μmol) afforded crude product. Crude product was purified via reverse-phase preparative HPLC – (gradient 10% MeCN/H_2O → 55% MeCN/H_2O → 65% MeCN/H_2O)

to afford desired product. Desired product was then repurified via pTLC; 10% MeOH/$CHCl_3$ solvent system to afford title compound (7.2 mg, 24% isolated yield, 6% yield from linear peptide) as a colorless-film. NMR of **46** contained complex mixture of rotational isomers; ratio ~ 1:1 + minor isomers. Both rotational isomers were characterized. ^{1}H NMR (DMSO-d_6, 600 MHz) δ 8.61 (d, J = 6.8 Hz, 1H), 8.37 (d, J = 8.9 Hz, 1H), 8.30–8.26 (m, 1H), 8.15 (t, J = 5.0 Hz, 1H), 8.03 (d, J = 7.6 Hz, 1H), 7.95 (t, J = 5.3 Hz, 1H), 7.73–7.65 (m, 4H), 7.44–7.41 (m, 1H), 7.26–7.21 (m, 9H), 7.20–7.16 (m, 2H), 7.08–7.02 (m, 2H), 5.32 (t, J = 4.7 Hz, 1H), 4.91–4.87 (m, 1H), 4.80–4.76 (m, 1H), 4.76–4.67 (m, 4H), 4.62–4.55 (m, 2H), 4.51 (m, 1H), 4.42–4.36 (m, 2H), 4.03 (dd, J = 11.4, 5.5 Hz, 1H), 3.91 (dd, J = 12.2, 6.1 Hz, 1H), 3.78–3.74 (m, 3H), 3.73–3.69 (m, 3H), 3.65–3.62 (m, 1H), 3.61–3.59 (m, 1H), 3.51–3.57 (m, 1H), 3.45–3.42 (m, 1H), 3.42–3.39 (m, 2H), 3.34–3.31 (m, 2H), 3.17–3.11 (m, 4H), 3.10–3.06 (m, 3H), 3.05–2.98 (m, 2H), 2.95–2.90 (m, 2H), 2.77 (dd, J = 14.0, 11.3 Hz, 1H), 2.46–2.42 (m, 2H), 2.34 (dd, J = 16.8, 5.4 Hz, 1H), 2.26 (dd, J = 15.7, 8.8 Hz, 1H), 2.04–1.96 (m, 3H), 1.94–1.90 (m, 1H), 1.86–1.80 (m, 4H), 1.76 (s, 6H), 0.85 (d, J = 6.3 Hz, 3H), 0.63 (d, J = 6.1 Hz, 3H) ^{13}C NMR (DMSO-d_6, 126 MHz) δ 174.3, 173.5, 172.2, 171.6, 170.7, 169.9, 169.9, 169.5, 169.4, 169.1, 169.0, 168.0, 167.7, 167.7, 167.6, 167.4, 138.4, 138.0, 129.7, 129.1, 128.2, 128.0, 126.3, 126.1, 67.0, 66.7–66.6 (m, 2C), 66.3, 65.9, 65.7, 64.9, 59.1, 55.3, 53.4, 53.0, 48.4, 47.7, 46.8, 46.7, 46.5, 37.4, 37.1, 36.5, 35.1, 33.1, 31.6, 31.3, 31.3, 30.7, 29.1, 29.0, 28.8, 28.7, 28.6, 25.1, 25.1, 22.3, 22.3, 22.1, 19.8, 19.7, 14.0 HRMS m/z ratio calculated for $[C_{37}H_{44}F_4N_8O_{10}S_2+H]^+$ = 901.2636; found 901.2702; 4.1 ppm mass defect.

Polycycle **47**:

Polycycle **47** was synthesized according to **Scheme 4.3.1** General Procedure F,G and I (outlined above). Following **Scheme 4.3.1** General Procedure F and G using crude peptide Ac-

E*PSFTC-NH_2 (150. mg, 1.0 equiv., 186 μmol) afforded crude seco-acid intermediate. Crude product was purified via reverse-phase preparative HPLC – (gradient 5% MeCN/H_2O → 55% MeCN/H_2O → 65% MeCN/H_2O) afforded acyclic seco-acid (108.2 mg, 62% isolated yield) as a light-yellow foam. HRMS calculated for $[C_{38}H_{47}F_4N_7O_{12}S_2+H]^+$ = 934.2739; found 934.2773; 3.6 ppm mass defect. Followed **Scheme 4.3.1** General Procedure I to obtain macrolactone **47**. Seco-acid intermediate (40.0 mg, 1.0 equiv., 42.8 μmol) afforded crude product after 44 h. Crude product was purified via reverse-phase preparative HPLC – (gradient 10% MeCN/H_2O → 60% MeCN/H_2O → 65% MeCN/H_2O) afforded title compound (16.4 mg, 42% isolated yield, 26% yield from linear peptide). NMR of **47** contained complex mixture of rotational isomers. Major rotational isomer was characterized. ^{1}H NMR (DMSO-d_6, 600 MHz) δ 8.52 (t, J = 7.6 Hz, 1H), 8.29 (d, J = 8.5 Hz, 1H), 8.22 (dd, J = 7.3, 2.3 Hz, 1H), 8.02 (d, J = 8.4 Hz, 1H), 7.32–7.22 (m, 5H), 7.19 (t, J = 7.0 Hz, 1H), 7.12 (s, 1H), 4.93–4.83 (m, 3H), 4.77–4.70 (m, 1H), 4.62–4.56 (m, 2H), 4.54 (t, J = 6.0 Hz, 1H), 4.44–4.40 (m, 1H), 3.88–3.77 (m, 2H), 3.60–3.56 (m, 1H), 3.55–3.47 (m, 2H), 3.41–3.35 (m, 1H), 3.35–3.29 (m, 2H), 3.10–3.04 (m, 1H), 3.04–2.99 (m, 1H), 2.82 (dd, J = 13.8, 10.4 Hz, 1H), 2.48–2.44 (m, 1H), 2.34–2.27 (m, 2H), 2.23–2.17 (m, 1H), 1.94–1.88 (m, 2H), 1.84 (s, 3H), 1.82–1.79 (m, 1H), 1.66–1.58 (m, 1H), 1.08 (dd, J = 6.0, 1.4 Hz, 3H) ^{13}C NMR (DMSO-d_6, 126 MHz) δ 172.7, 170.1, 168.9, 168,8, 168.3, 167.5, 167.4, 167.3, 148.3–148.2 (m, 1C), 144.5–144.4 (m, 1C), 137.6, 129.3, 128.1, 126.4, 117.1–116.9 (m, 1C), 116.1–115.9 (m, 1C), 72.0–71.7 (m, 1C), 66.4, 61.2, 60.3, 58.2, 53.7, 51.4, 50.5, 49.4, 46.0, 37.4, 34.9, 30.5, 28.8, 28.1, 25.1, 24.7, 24.3, 22.3, 16.2 ^{19}F NMR (DMSO-d_6, 565 MHz) δ -98.53 and -118.6 (AB quartet, J = 251.1 Hz, 2F), -117.0 and -131.7 (AB quartet, J = -223.8 Hz, 2F) HRMS calculated for $[C_{38}H_{45}F_4N_7O_{11}S_2+H]^+$ = 916.2633; found 916.2654; 2.3 ppm mass defect.

Polycycle **48**:

Polycycle **48** was synthesized according to **Scheme 4.3.1** General Procedure F,G and I (outlined above). Following **Scheme 4.3.1** General Procedure F and G using crude peptide Ac-D*PNHFTC-NH_2 (150. mg, 1.0 equiv., 157 μmol) afforded crude seco-acid intermediate. Crude product was purified via reverse-phase preparative HPLC – (gradient 10% MeCN/H_2O → 50% MeCN/H_2O) afforded seco-acid intermediate (73.1 mg, 43% isolated yield) as a yellow-powder. HRMS m/z calculated for $[C_{44}H_{53}F_4N_{11}O_{13}S_2+H]^+$ = 1084.3281; found 1084.3295; 1.3 ppm mass defect. Followed **Scheme 4.3.1** General Procedure I to obtain macrolactone **48**. Seco-acid intermediate (40.0 mg, 1.0 equiv., 33.4 μmol) afforded crude product after 64 h. Crude product was purified via reverse-phase preparative HPLC – (gradient 10% MeCN/H_2O → 55% MeCN/H_2O → 60% MeCN/H_2O) afforded desired product. Desired product was repurified via pTLC; 10% MeOH/$CHCl_3$ solvent system (plate was run up twice) to afford title compound (5.0 mg, 13% isolated yield, 6% yield from linear peptide) as an opaque-film. NMR of **48** contained complex mixture of rotational isomers. Major rotational isomer was characterized. ^{1}H NMR (DMSO-d_6, 600 MHz) δ 9.41 (s, 1H), 8.15 (d, J = 7.6 Hz, 1H), 8.12 (d, J = 7.6 Hz, 1H), 8.07 (d, J = 8.3 Hz, 1H), 7.94 (d, J = 8.9 Hz, 1H), 7.84 (d, J = 1.1 Hz, 1H), 7.60–7.52 (m, 2H), 7.44 (s, 1H), 7.42 (s, 1H), 7.30–7.26 (m, 2H), 7.22–7.17 (m, 3H), 5.16 (d, J = 5.2 Hz, 1H), 4.87–4.81 (m, 2H), 4.76–4.71 (m, 1H), 4.38–4.32 (m, 1H), 4.28 (dd, J = 12.8, 7.4 Hz, 1H), 4.24 (dd, J = 9.1, 2.4 Hz, 1H), 4.21–4.16 (m, 2H), 4.15–4.10 (m, 1H), 3.76–3.69 (m, 1H), 3.65–3.58 (m, 2H), 3.58–3.51 (m, 1H), 3.19–3.13 (m, 1H), 3.05–2.97 (m, 2H), 2.92–2.82 (m, 3H), 2.72–2.69 (m, 1H), 2.44 (dd, J = 15.4, 7.8 Hz, 1H), 2.24 (dd, J = 15.4, 10.4, 1H), 2.07–2.01 (m, 1H), 2.01–1.96 (m, 1H), 1.96–1.83 (m, 3H), 1.81 (s, 3H), 0.97 (d, J = 6.4 Hz, 3H) ^{13}C NMR (DMSO-d_6, 126 MHz) 172.2, 171.5, 171.2, 170.7, 170.5, 169.7, 169.2, 168.9, 168.0, 140.8, 138.9, 137.4, 131.3–131.1 (m, 1C), 129.8–

129.6 (m, 1C), 129.0, 128.3, 126.4, 115.2, 112.2–112.1 (m, 2C), 67.7–67.4 (m, 1C), 60.6, 60.3, 59.0, 56.0, 51.5, 49.7, 47.0, 46.9, 46.6, 38.1, 35.9, 35.4, 32.1, 30.4. 29.7, 29.0, 28.8, 24.3, 22.3. 20.2 ^{19}F NMR (DMSO-d_6, 565 MHz) δ -99.9 and -113.3 (AB quartet, J = 248.3 Hz, 2F), -114.5 and -127.2 (AB quartet, J = 225.8 Hz, 2F) HRMS calculated for $[C_{44}H_{51}F_4N_{11}O_{12}S_2+H]^+$ = 1066.3175; found 1066.3180; 0.5 ppm mass defect.

Polycycle **49**:

Polycycle **49** was synthesized according to **Scheme 4.3.1** General Procedure F,G and I (outlined above). Following **Scheme 4.3.1** General Procedure F and G using crude peptide Ac-D*PTFSC-NH_2 (150. mg, 1.0 equiv., 189 μmol) afforded crude seco-acid intermediate. Crude product was purified via reverse-phase preparative HPLC – (gradient 10% → 60% MeCN/H_2O → 65% MeCN/H_2O) afforded seco-acid intermediate (67.2 mg, 36% isolated yield) as a yellow-foam. HRMS m/z calculated for $[C_{39}H_{44}F_4N_8O_{12}S_3+H]^+$ = 989.2255; found 989.2239; 3.7 ppm mass defect. Followed **Scheme 4.3.1** General Procedure I to obtain macrolactone **49**. To a flame-dried 25-mL round bottom flask equipped with a stir bar was charged with the seco-acid intermediate (24.5 mg, 1.0 equiv., 24.8 μmol), EDC•HCl (12.1 mg, 2.5 equiv., 61.9 μmol), HOBt (7.11 mg, 1.5 equiv., 37.2 μmol, 80%), and then diluted with DMF (4.95 mL, 5.0 mM). The reaction mixture was then allowed to stir at 0ºC and then added NEt_3 (17.3 μL, 5.0 equiv., 124 μmol). The reaction mixture was then allowed to warm up to 23ºC and stirred for 48 h. After HPLC indicated reaction completion, the reaction mixture was quenched with AcOH (14.2 μL, 10.0 equiv., 248 μmol) and then concentrated under reduced pressure to afford crude product. The crude product was then purified via preparative HPLC – (gradient 10% MeCN/H_2O → 70% MeCN/H_2O → 75% MeCN/H_2O) afforded title compound (17.4 mg, 72% isolated yield, 26% from linear peptide) as a

white-powder. NMR of **49** contained complex mixture of rotational isomers. Major rotational isomer was characterized. ^{1}H NMR (DMSO-d_6, 600 MHz) δ 8.78 (d, J = 6.9 Hz, 1H), 8.29 (d, J = 8.0 Hz, 1H), 7.84 (m, 1H), 7.85 (m, 1H), 7.84 (s, 1H), 7.38 (d, J = 7.8 Hz, 1H), 7.27–7.23 (m, 3H), 7.22–7.19 (m, 2H), 7.09 (s, 1H), 5.31 (d, J = 13.0 Hz, 1H), 5.16 (d, J = 13.0 Hz, 1H), 4.87 (m, 1H), 4.70–4.66 (m, 1H), 4.66–4.62 (m, 1H), 4.53–4.50 (m, 1H), 4.29–4.26 (m, 1H), 4.06 (dd, J = 7.9, 4.2 Hz, 1H), 3.98 (dd, J = 11.3, 2.7 Hz, 1H), 3.91–3.88 (m, 1H), 3.85 (dd, J = 12.0, 3.1 Hz, 1H), 3.65–3.62 (m, 2H), 3.51–3.46 (m, 1H), 3.35–3.32 (m, 1H), 2.94 (dd, J = 13.8 Hz, 5.5 Hz, 1H), 2.84–2.75 (m, 3H), 2.54 (m, 1H), 2.06–2.02 (m, 1H), 1.81–1.79 (m, 1H), 1.79 (s, 3H), 0.94 (d, J = 6.4 Hz, 3H) ^{13}C NMR (DMSO-d_6, 126 MHz) δ 171.4, 171.1, 169.9, 169.3, 169.1, 167.3, 166.8, 161.3, 144.5, 137.6, 137.3–137.2 (m, 1C), 135.3, 135.2–135.1 (m, 1C), 129.1, 128.2, 126.4, 116.7–116.6 (m, 2C), 114.3, 67.5–67.4 (m, 1C), 66.7, 59.9, 58.3, 58.1, 57.0, 55.8, 53.6, 48.8, 47.0, 46.9, 37.0, 36.0, 35.8, 30.8, 29.2, 22.2, 19.7 ^{19}F NMR (DMSO-d_6, 565 MHz) δ -99.5 and -118.5 (AB quartet, J = 255.5 Hz, 2F), -119.0 and -132.0 (AB quartet, J = 218.0 Hz, 2F) HRMS m/z calculated for $[C_{39}H_{42}F_4N_8O_{11}S_3+H]^+$ = 971.2150; 971.2174; 2.5 ppm mass defect.

Synthesis and Characterization of **Figure 4.5.1** Compounds

Polycycle **50**:

Polycycle **50** was synthesized according to **Scheme 4.2.1** General Procedure A (outlined above) using crude linear peptide Ac-Dat-PCVAC-NHMe (50.0 mg, 1.0 equiv., 76.6 μmol) (where Dat = des-amino tyrosine). Purification via reverse-phase preparative HPLC – (gradient 10% MeCN/H_2O → 75% MeCN/H_2O) afforded title compound (15.7 mg, 26% isolated yield) as an opaque-film. NMR of **50** contained complex mixture of rotational isomers; ratio 1:1:4. Major rotational isomer was characterized. ^{1}H NMR (DMSO-d_6, 500 MHz) δ 8.31 (d, J = 9.4 Hz, 1H),

7.90 (d, J = 7.7 Hz, 1H), 7.70 (d, J = 6.9 Hz, 1H), 7.56 (d, J = 8.9 Hz, 1H), 7.30 (d, J = 8.2 Hz, 2H), 7.19 (dd, J = 8.2, 2.2 Hz, 2H), 4.71 (d, J = 6.6 Hz, 1H), 4.40 (d, J = 6.6 Hz, 1H), 4.34–4.29 (m, 1H), 4.25–4.18 (m, 1H), 3.96 (s, 3H), 3.94–3.88 (m, 1H), 3.63 (m, 1H), 3.49–3.41 (m, 2H), 3.20–3.16 (m, 1H), 3.06–2.99 (m, 1H), 2.97–2.90 (m, 1H), 2.82 (m, 1H), 2.44–2.37 (m, 2H), 2.21–2.17 (m, 1H), 2.08–2.02 (m, 1H), 2.02–1.92 (m, 2H), 1.89–1.82 (m, 1H), 1.70–1.65 (m, 1H), 1.31 (d, J = 7.4 Hz, 3H), 0.81 (d, J = 6.4 Hz, 3H), 0.78 (d, J = 6.4 Hz, 3H) ^{13}C NMR (DMSO-d_6, 126 MHz) δ 172.2, 171.9, 171.4, 170.4, 168.5, 167.6, 148.3–148.1 (m, 1C), 137.8, 131.5, 129.3–129.2 (m, 1C), 118.6, 117.2–116.9 (m, 1C), 115.6, 114.9–114.6 (m, 1C), 74.7–74.5 (m, 1C), 60.1, 58.8, 55.1, 52.1, 49.5, 48.4, 47.3, 35.5, 35.3, 33.8, 30.4, 29.5, 25.9, 24.3, 19.0, 18.5, 17.9 ^{19}F NMR (DMSO-d_6, 282 MHz) δ -106.8 and -119.7 (AB quartet, J = 257.6 Hz, 2F), -113.5 and -120.3 (AB quartet, J = 229.7 Hz, 2F) HRMS m/z calculated for $[C_{33}H_{40}F_4N_6O_7S_2+H]^+$ = 785.2414; found 785.2419; 0.6 ppm mass defect.

Compound **S1**

To a stirred solution of Macrocycle **17** in DMF (50 mM) was added Et_3N (2.2 equiv.) and 1,4-benzenedithiol (0.5 equiv.) at 0°C and let stir and warm to rt. Upon completion as observed by HPLC, the reaction was quenched with AcOH (5.0 equiv.) and concentrated under reduced pressure. Purification by RP-HPLC afforded the dimerized product **S1** (20%). ^{1}H NMR (DMSO-d_6, 500 MHz) δ 10.91 (s, 2H), 9.51 (s, 2H), 8.50 (d, J = 9.1 Hz, 2H), 8.39 (d, J = 8.0 Hz, 2H), 8.31 (d, J = 8.5 Hz, 2H), 7.69 (d, J = 19.5 Hz, 2H), 7.50 (d, J = 7.7 Hz, 2H), 7.38 – 7.29 (m, 6H), 7.22 (d, J = 9.0 Hz, 2H), 7.13 (s, 2H), 7.07 (t, J = 7.3 Hz, 2H), 6.98 (t, J = 7.3 Hz, 2H), 5.02 (s, 2H), 4.83 (d, J = 8.9 Hz, 2H), 4.66 (q, J = 7.7 Hz, 2H), 4.47 (q, J = 7.4 Hz, 2H), 4.42 – 4.33 (m, 2H), 4.26 – 4.17 (m, 2H), 3.88 – 3.76 (m, 2H), 3.66 (d, 2H), 3.55 – 3.42 (m, 5H), 3.11 – 3.03 (m, 6H),

2.82 (d, J = 14.0 Hz, 2H), 1.79 (s, 6H). ^{13}C-NMR (500 MHz, DMSO-d_6) δ 171.8, 169.8, 169.5, 168.7, 167.6, 167.0, 136.1, 131.6, 130.4, 129.7, 128.7, 127.1, 123.7, 121.0, 118.5, 118.0, 111.4, 109.1, 79.2, 65.7, 61.6, 55.7, 55.0, 51.5, 46.1, 45.6, 36.0, 35.9, 35.8, 33.7, 33.0, 32.6, 31.9, 31.3, 30.7, 29.0, 28.9, 28.7, 28.7, 28.7, 28.0, 27.6, 26.2, 25.8, 25.5, 25.4, 25.3, 22.5, 22.4, 22.3, 22.1, 19.4, 19.1, 14.0, 14.0, 12.0, 11.2, 8.5. ^{19}F NMR (DMSO-d_6, 282 MHz) δ -96.8 – (-98.8) (m, 2F), -111.3 – (-113.8) (m, 4F), -127.0 – (-128.7) (m, 2F).

Compound **S5**

To a stirred solution of crude peptide Cbz-Glu(Cys)-Ala-Histamine in DMF (5 mM) was added Et_3N (2.5 equiv.), and OFCP (1.5 equiv.) at 0°C and let stir for 30 min. After initial macrocyclization was complete, the mixture was concentrated under reduced pressure to remove excess Et_3N, OFCP, and MeCN. The reaction mixture was then cooled once again to 0°C and added Me_3SiOK (4.0 equiv.) and let stir at rt. After reaction completion as observed by HPLC the mixture was quenched with AcOH (10.0 equiv.) and concentrated under reduced pressure. Purification by FCC (0 - 10% MeOH/$CHCl_3$) afforded **S5** (41%). ^{1}H NMR (DMSO-d_6, 500 MHz) δ 9.96 (bs, 1H), 9.88 (bs, 1H), 8.48 (s, 1H), 8.01 (s, 1H), 7.67 (s, 1H), 7.46 (s, 1H), 7.42 - 7.24 (m, 5H), 7.07 (s, 1H), 5.07 - 4.92 (m, 2H), 4.89 (s, 1H), 4.4 - 4.25 (m, 1H), 4.04 (q, J = 12.3 Hz 1H); 3.09 (d, J = 13.0 Hz, 1H), 3.8 - 3.64 (m, 1H), 2.98 (d, J = 15.0 Hz, 1H), 2.85 - 2.63 (m, 2H), 2.29 - 2.16 (m, 1H); 2.13 - 1.98 (m, 1H), 1.97 - 1.72 (m, 2H), 1.18 - 1.02 (m, 3H). ^{13}C-NMR (500 MHz, DMSO-d_6) δ 174.2, 171.3, 170.6, 170, 155.3, 140.6, 139.8 - 139.1 (m, 1C), 138.4, 137, 128.4, 127.9, 127.8, 123.3 - 122.9 (m, 1C), 115.5 - 109.5 (m, 2C), 113.4, 65.4, 53.5, 47.5, 46, 35.5, 31.4, 30.9, 29.9, 28.2, 17.9. ^{19}F NMR (DMSO-d_6, 282 MHz) δ -110.7 (dt, J = 251.3, 13.5 hz, 1F), -112.2

(dd, J = 223.7, 8.9 Hz, 1F), -116.9 (dt, J = 251.5, 12.5 Hz, 1F), -119.8 (dd, J = 224.0, 10.5 Hz, 1F), -146.4 (t, J = 13.9 Hz, 1F). HRMS [M+1] calc'd for $C_{29}H_{30}F_5N_7O_6SH$ 700.1977, found 700.1998.

Compound **S6**

TFA (10 ml) was added to a solution of SM (1.75 g, 3.84 mmol) in DCM (20 ml) and stirred for 1h at rt. The reaction mixture was concentrated by rotary evaporation to give a crude solid 12 (1.80 g, 3.84 mmol). The residue **12** (62 mg, 0.131 mmol, analytical) was dissolved in DMF (1.3 ml) and added **7** (43 mg, 0.144 mmol), cooled to 0°C, and then added iPr_2EtN (34 ul, 0.197 mmol). The reaction mixture was stirred for 2 h at rt, then added H_2O, extracted with EtOAc, washed with 1N HCl, sat. $NaHCO_3$ and brine. The organic layer was dried over Na_2SO_4, filtered and the solvent was removed by rotary evaporation to give crude **15**. The residue **15** was dissolved in DMF (13 ml) and added Cs_2CO_3 (64 mg, 0.196 mmol) at 0°C, stirred for 1 h at rt,. The reaction mixture was added H_2O, extracted with EtOAc. The combined extract was washed with brine (x5), dried over Na_2SO_4 and concentrated. Purification by column chromatography (SiO_2, gradient 1-5% MeOH/$CHCl_3$) afforded the title compound (38 mg, 0.0619 mmol, 47% from SM) as a white-solid. ^{1}H NMR (DMSO-d_6, 500 MHz) δ 8.14 (d, J = 4.4 Hz, 1H), 7.53 (d, J = 8.1 Hz, 1H), 7.32 (t, J = 5.4 Hz, 1H), 7.26–7.24 (m, 2H), 7.18–7.14 (m, 5H), 7.02 (d, J = 8.6 Hz, 2H), 4.31–4.27 (m, 1H), 4.17–4.11 (t, J = 6.8 Hz, 2H), 3.73–3.71 (m, 1H), 3.60–3.57 (m, 1H), 3.19 (dd, J = 14.3, 4.0 Hz, 1H), 3.05–2.96 (m, 1H), 2.99 (dd, J = 14.3, 10.0 Hz, 1H), 2.80–2.75 (m, 1H), 2.68–2.63 (m, 1H), 2.02–1.89 (m, 2H), 1.43–1.28 (m, 2H), 1.00 (d, J = 7.2 Hz, 3H). ^{13}C NMR (DMSO-d_6, 126 MHz) δ 172.6, 172.3, 171.0, 153.2, 138.8–138.3 (m, 1C), 138.3, 136.7, 130.6, 129.6–129.1 (m, 1C), 128.8, 128.1, 126.2, 116.2, 116.2, 116.2, 115.6–105.7 (m, 3C), 72.9, 53.7, 50.5, 40.6, 35.8, 33.7, 30.5, 24.5, 16.9 ^{19}F NMR (DMSO-d_6, 282 MHz) δ -111.8 (d, J = 54.6 Hz, 2F), -112.5 (d, J

= 71.9 Hz, 2F), -128.6-(-128.8) (m, 2F). HRMS m/z calculated for $[C_{28}H_{30}F_6N_3O_5+H]^+$ = 614.2084; found 614.2062; 3.6 ppm mass defect.

Compound **S30**

Crude peptide Ac-HFCASC-NH_2 (50.0 mg, 1.0 equiv., 60.8 μmol) was diluted with H_2O (1.0 mM, 60.8 mL). The solution was allowed to stir until the peptide was homogenous and then 30% aqueous H_2O_2 (31.1 μL, 5.0 equiv., 304 μmol) was added. The reaction mixture was then allowed to stir at 23 ºC over 16 h. When HPLC indicated reaction completion, the reaction mixture was concentrated under reduced pressure to afford product. Crude product was then purified via reverse-phase preparative HPLC – (gradient 10% MeCN/H_2O → 32.5% MeCN/H_2O → 37.5% MeCN/H_2O) afforded title compound (10.8 mg, 22% isolated yield) as a white-film. ^{1}H NMR (DMSO-d_6, 500 MHz) δ 8.96–8.90 (s, 2H), 8.54 (d, J = 6.0 Hz, 1H), 8.52 (d, J = 7.5 Hz, 1H), 8.13 (d, J = 8.3 Hz, 1H), 8.07 (d, J = 7.6 Hz, 1H), 7.81 (d, J = 7.6 Hz, 1H), 7.38 (d, J = 7.6 Hz, 1H), 7.28–7.23 (m, 1H), 7.22–7.18 (m, 3H), 7.07–7.03 (m, 1H), 4.59–4.54 (m, 2H), 4.53–4.47 (m, 2H), 4.35–4.30 (m, 1H), 4.22–4.18 (m, 1H), 4.10 (q, J = 6.8 Hz, 1H), 3.74 (dd, J = 10.8, 5.4 Hz, 1H), 3.63 (dd, J = 6.7, 4.2 Hz, 1H), 3.22–3.15 (m, 1H), 3.09–3.03 (m, 2H), 3.02–2.96 (m, 2H), 2.87–2.80 (m, 3H), 1.80 (s, 3H), 1.30 (d, J = 7.3 Hz, 3H) ^{13}C NMR (DMSO-d_6, 126 MHz) δ 173.2, 171.3, 170.6, 170.0, 170.0, 169.5, 169.4, 137.2, 133.8, 129.4, 129.2, 128.1, 126.4, 116.7, 60.1, 55.9, 55.2, 53.8, 51.3, 51.1, 51.1, 45.7, 43.0, 26.9, 22.5, 20.4, 17.0 HRMS m/z calculated for $[C_{29}H_{39}N_9O_8S_2+H]^+$ = 706.2441; found 706.2472; 4.4 ppm mass defect.

Stability Tests

Stability Studies on Macrobicycle 13

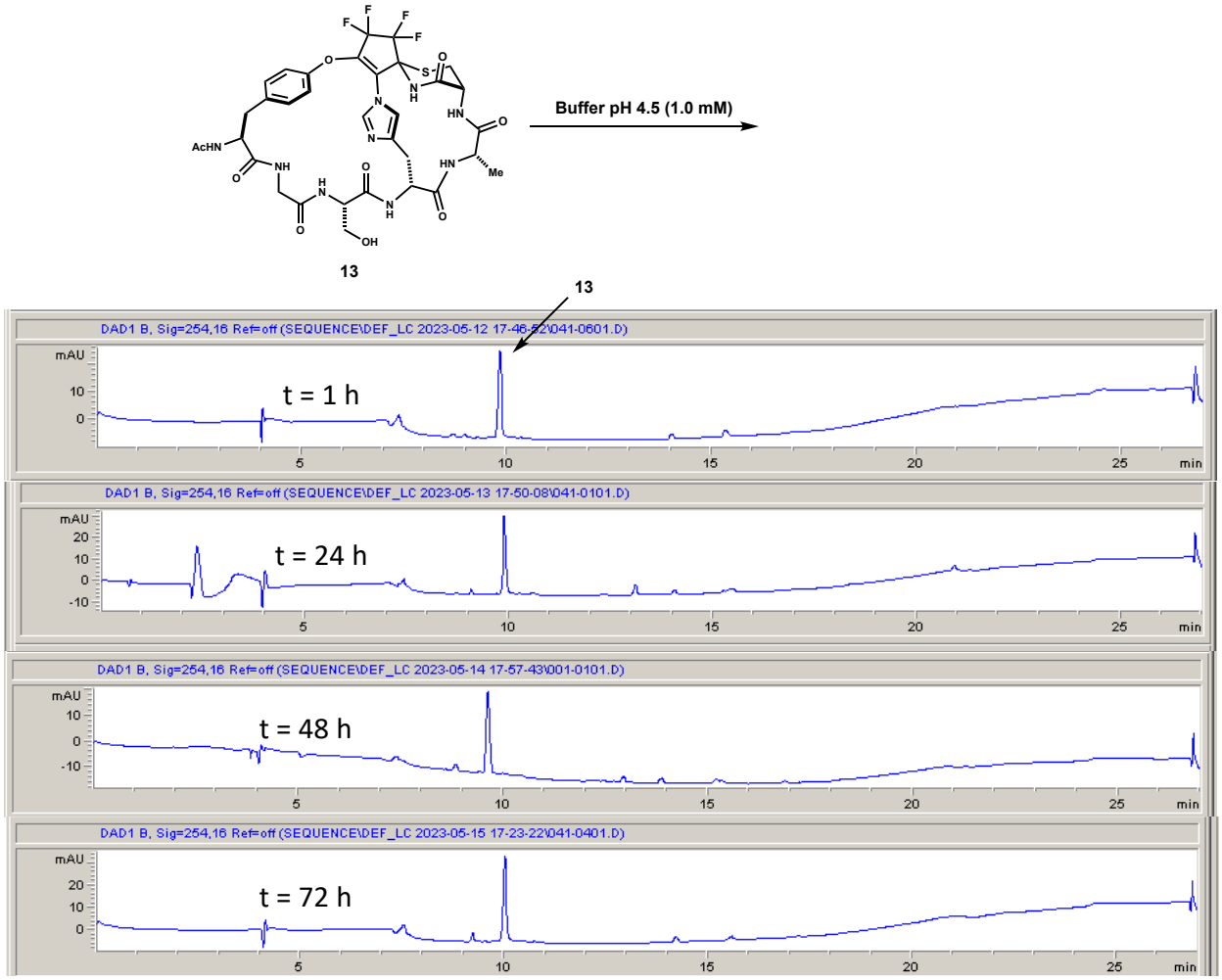

Figure 4.7.1 Degradation Experiment of Marcobicycle **13** at pH 4.5. Compound **13** was subjected to a degradation experiment at pH 4.5 over a 72 h time course. No noticeable decomposition of **13** was observed. **13** (1.0 mg, 1.0 equiv., 1.2 µmol) was diluted with NaOAc/AcOH (0.2 M) buffer pH 4.5 (1.0 mM, 1.2 mL). The solution was then allowed to stir at 25ºC for 72 h. Time points were taken at 1 h, 24 h, 48 h, and 72 h. Monitored via analytical HPLC (254 nm). The reaction was monitored by taking 10 µL aliquots at of the reaction mixture at the stated time points and diluting into 130 µL of 1% AcOH in MeCN.

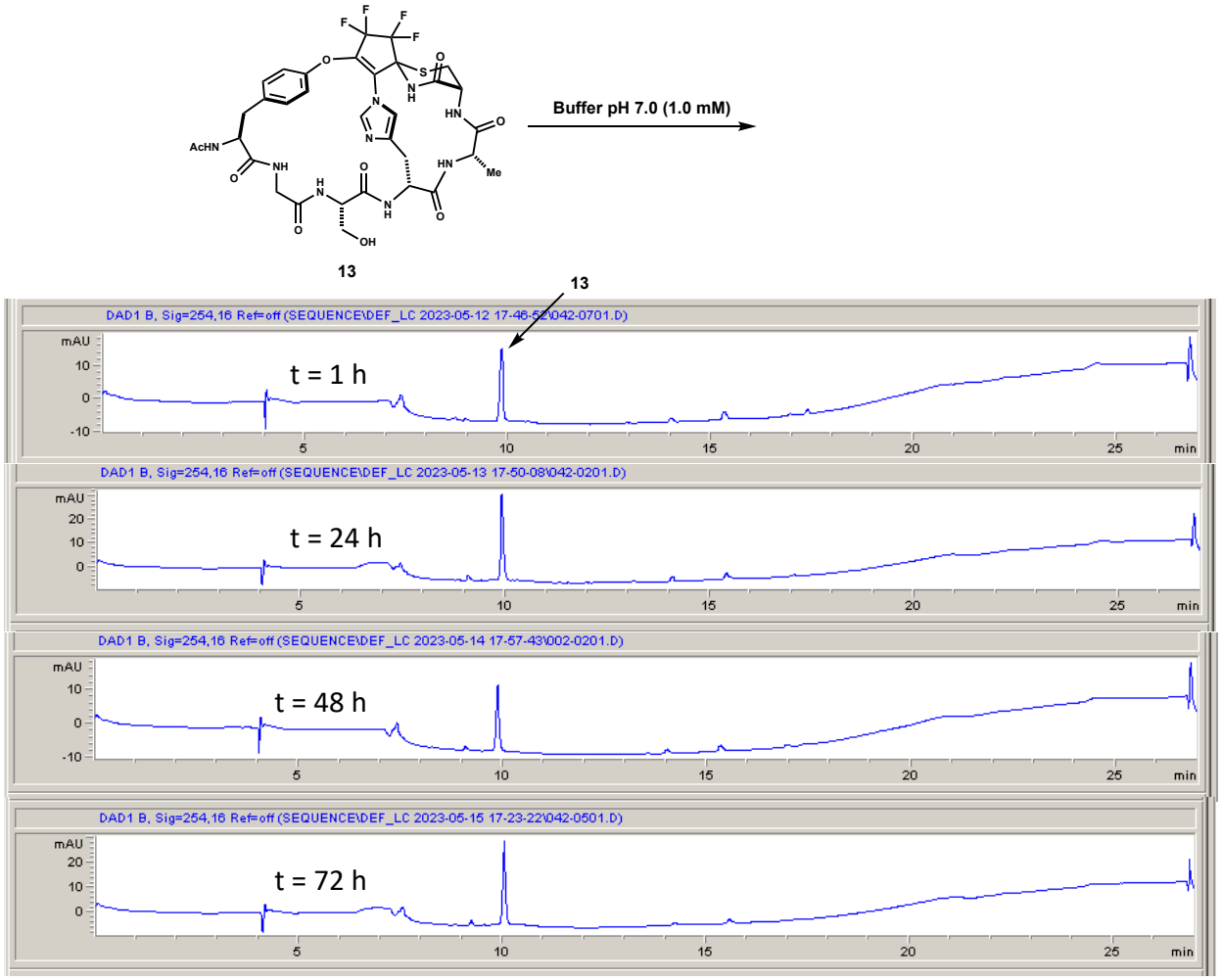

Figure 4.7.2 Degradation Experiment of Macrobicycle **13** at pH 7.0. Compound **13** was subjected to a degradation experiment at pH 7.0 over a 72 h time course. No noticeable decomposition of **13** was observed. **13** (1.0 mg, 1.0 equiv., 1.2 µmol) was diluted with KH_2PO_4/Na_2HPO_4 (0.05 M) buffer pH 7.0 (1.0 mM, 1.2 mL). The solution was then allowed to stir at 25ºC for 72 h. Time points were taken at 1 h, 24 h, 48 h, and 72 h. Monitored via analytical HPLC (254 nm). The reaction was monitored by taking 10 µL aliquots at of the reaction mixture at the stated time points and diluting into 130 µL of 1% AcOH in MeCN.

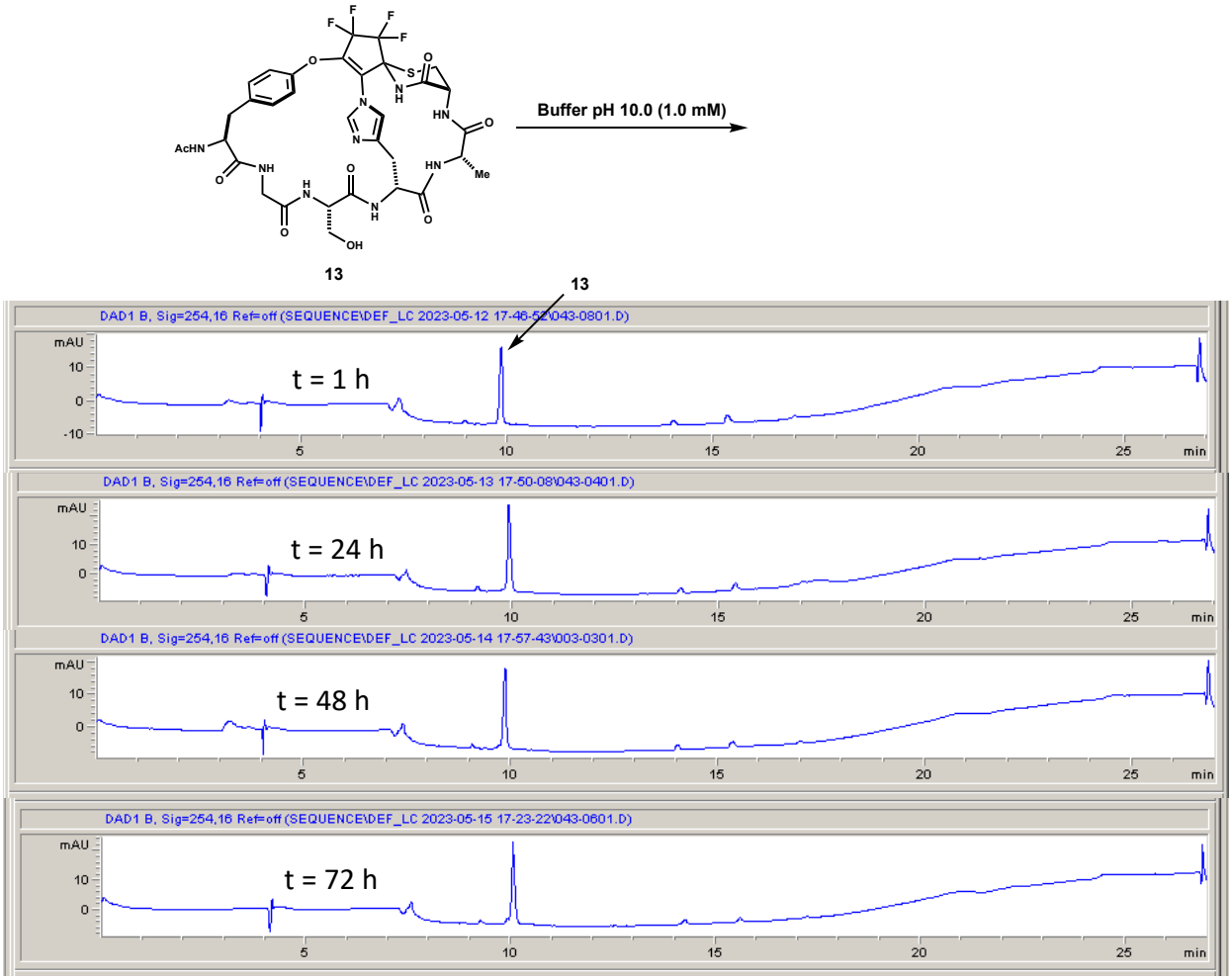

Figure 4.7.3 Degradation Experiment of Macrobicycle **13** at pH 10.0. Compound **13** was subjected to a degradation experiment at pH 10.0 over a 72 h time course. No noticeable decomposition of **13** was observed. **13** (1.0 mg, 1.0 equiv., 1.2 µmol) was diluted with $K_2CO_3/BK_3O_3/KOH$ (0.05 M) buffer pH 10.0 (1.0 mM, 1.2 mL). The solution was then allowed to stir at 25ºC for 72 h. Time points were taken at 1 h, 24 h, 48 h, and 72 h. Monitored via analytical HPLC (254 nm). The reaction was monitored by taking 10 µL aliquots at of the reaction mixture at the stated time points and diluting into 130 µL of 1% AcOH in MeCN.

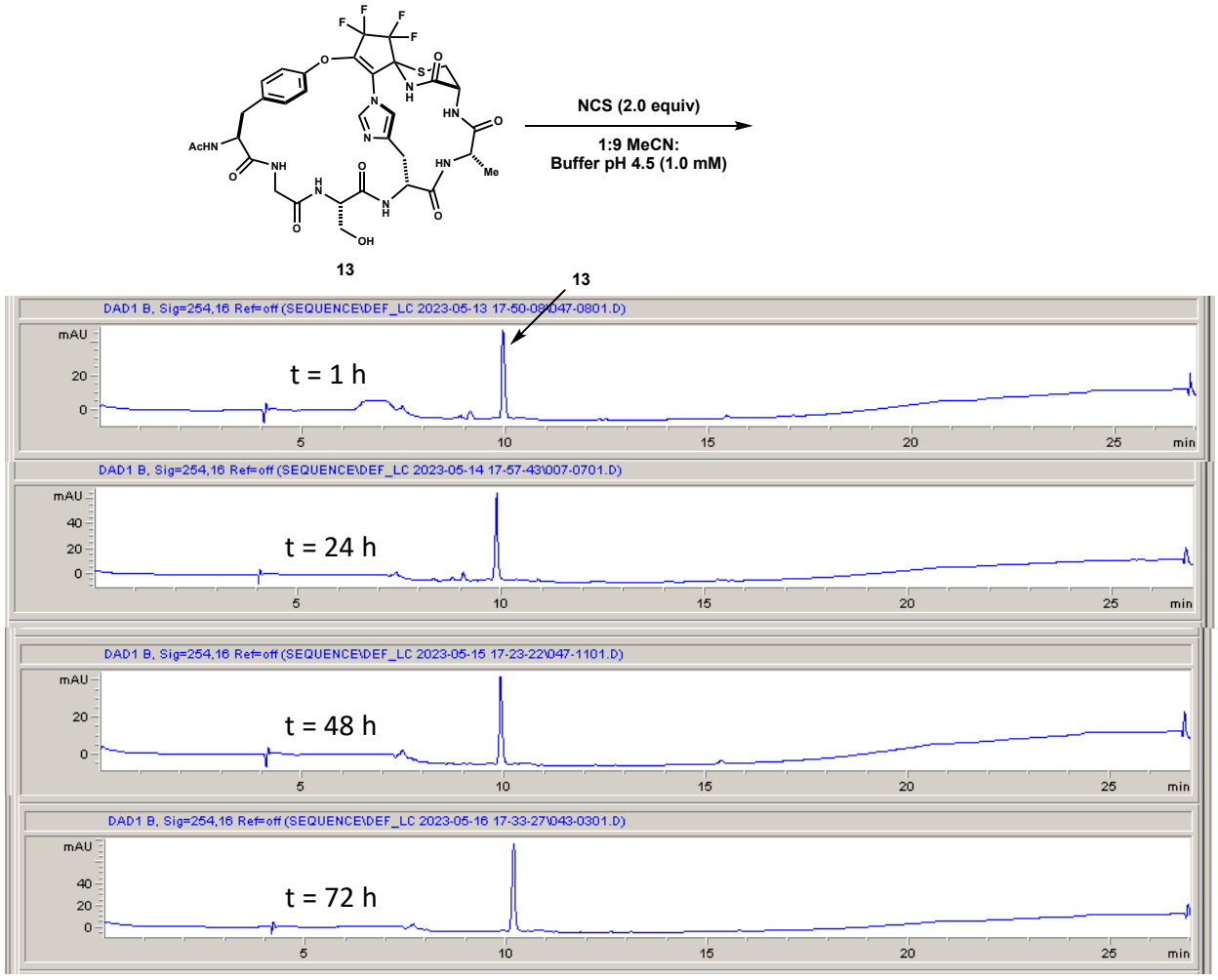

Figure 4.7.4 Degradation Experiment of Macrobicycle **13** with NCS. Compound **13** was subjected to a degradation experiment with NCS over a 72 h time course. No noticeable decomposition of **13** was observed. **13** (1.0 mg, 1.0 equiv., 1.2 µmol) was diluted with 1:9 MeCN : NaOAc/AcOH (0.2 M) buffer pH 4.5 (1.0 mM, 1.2 mL). The solution was then added NCS (25 µL, 2.0 equiv., 2.5 µmol, 0.1 M in MeCN) and the reaction mixture allowed to stir at 25ºC for 72 h. Time points were taken at 1 h, 24 h, 48 h, and 72 h. Monitored via analytical HPLC (254 nm). The reaction was monitored by taking 10 µL aliquots at of the reaction mixture at the stated time points and diluting into 130 µL of 1% AcOH in MeCN.

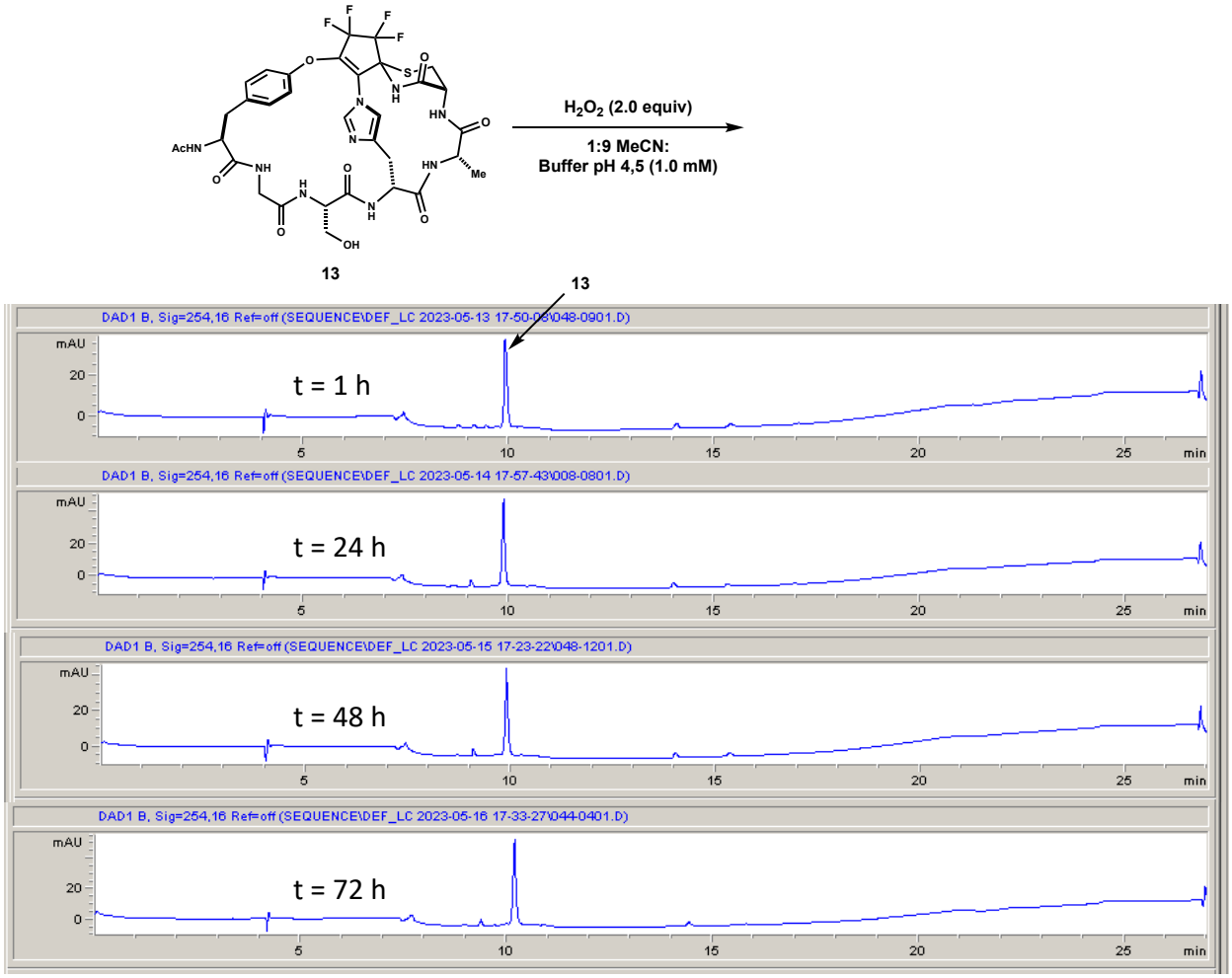

Figure 4.7.5 Degradation Experiment of Macrobicycle **13** with H_2O_2. Compound **13** was subjected to a degradation experiment with H_2O_2 over a 72 h time course. No noticeable decomposition of **13** was observed. **13** (1.0 mg, 1.0 equiv., 1.2 µmol) was diluted with 1:9 MeCN : NaOAc/AcOH (0.2 M) buffer pH 4.5 (1.0 mM, 1.2 mL). The solution was then added H_2O_2 (25 µL, 2.0 equiv., 2.5 µmol, 0.1 M in MeCN) and the reaction mixture allowed to stir at 25ºC for 72 h. H_2O_2 solution prepared from 30% aqueous H_2O_2. Time points were taken at 1 h, 24 h, 48 h, and 72 h. Monitored via analytical HPLC (254 nm). The reaction was monitored by taking 10 µL aliquots at of the reaction mixture at the stated time points and diluting into 130 µL of 1% AcOH in MeCN.

Stability Studies on Macrocycle 24

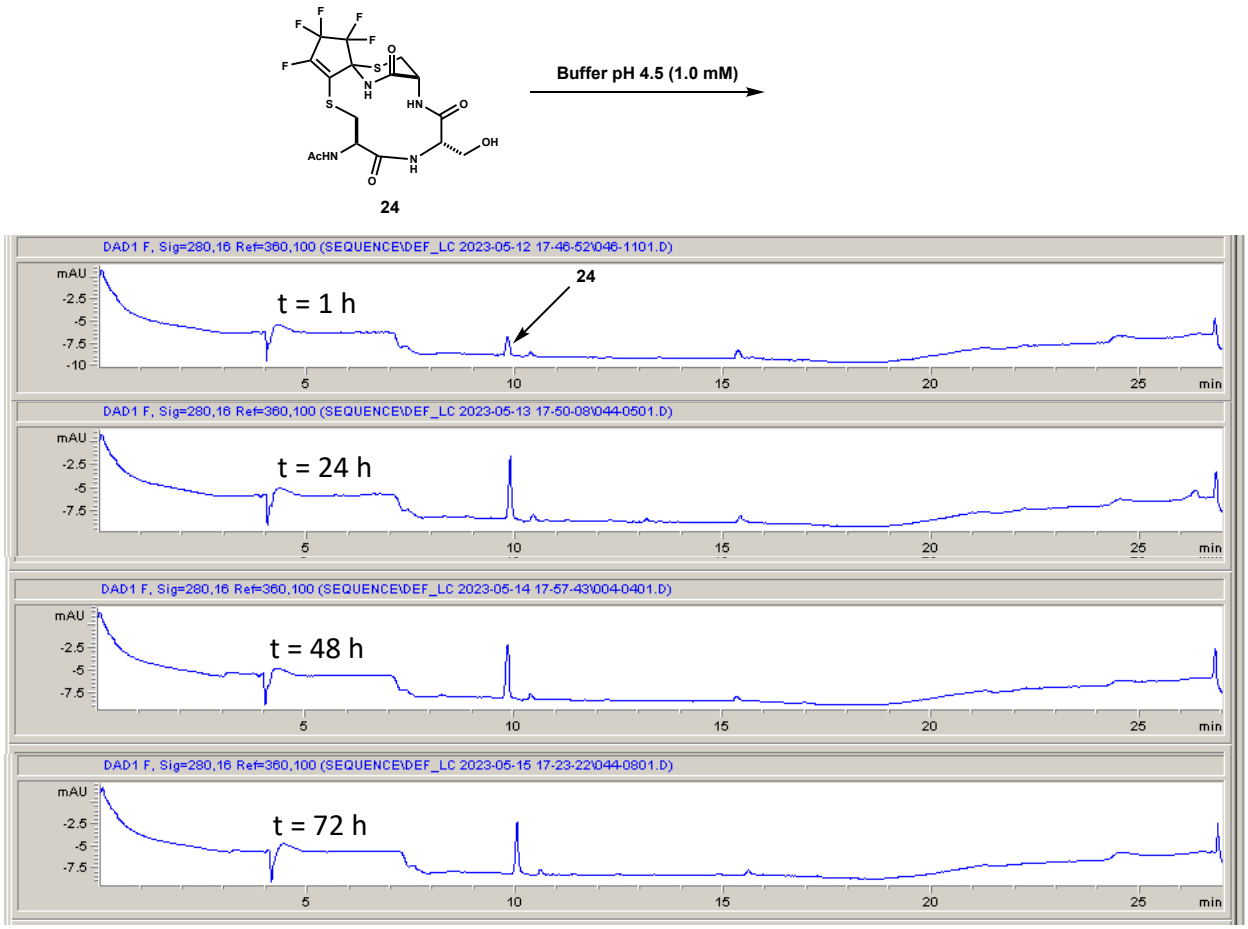

Figure 4.7.6 Degradation Experiment of Macrocycle **24** at pH 4.5. Compound **24** was subjected to a degradation experiment at pH 4.5 over a 72 h time course. No noticeable decomposition of **24** was observed. **24** (1.0 mg, 1.0 equiv., 2.0 µmol) was diluted with NaOAc/AcOH (0.2 M) buffer pH 4.5 (1.0 mM, 2.0 mL). The solution was then allowed to stir at 25ºC for 72 h. Time points were taken at 1 h, 24 h, 48 h, and 72 h. Monitored via analytical HPLC (280 nm). The reaction was monitored by taking 10 µL aliquots at of the reaction mixture at the stated time points and diluting into 130 µL of 1% AcOH in MeCN.

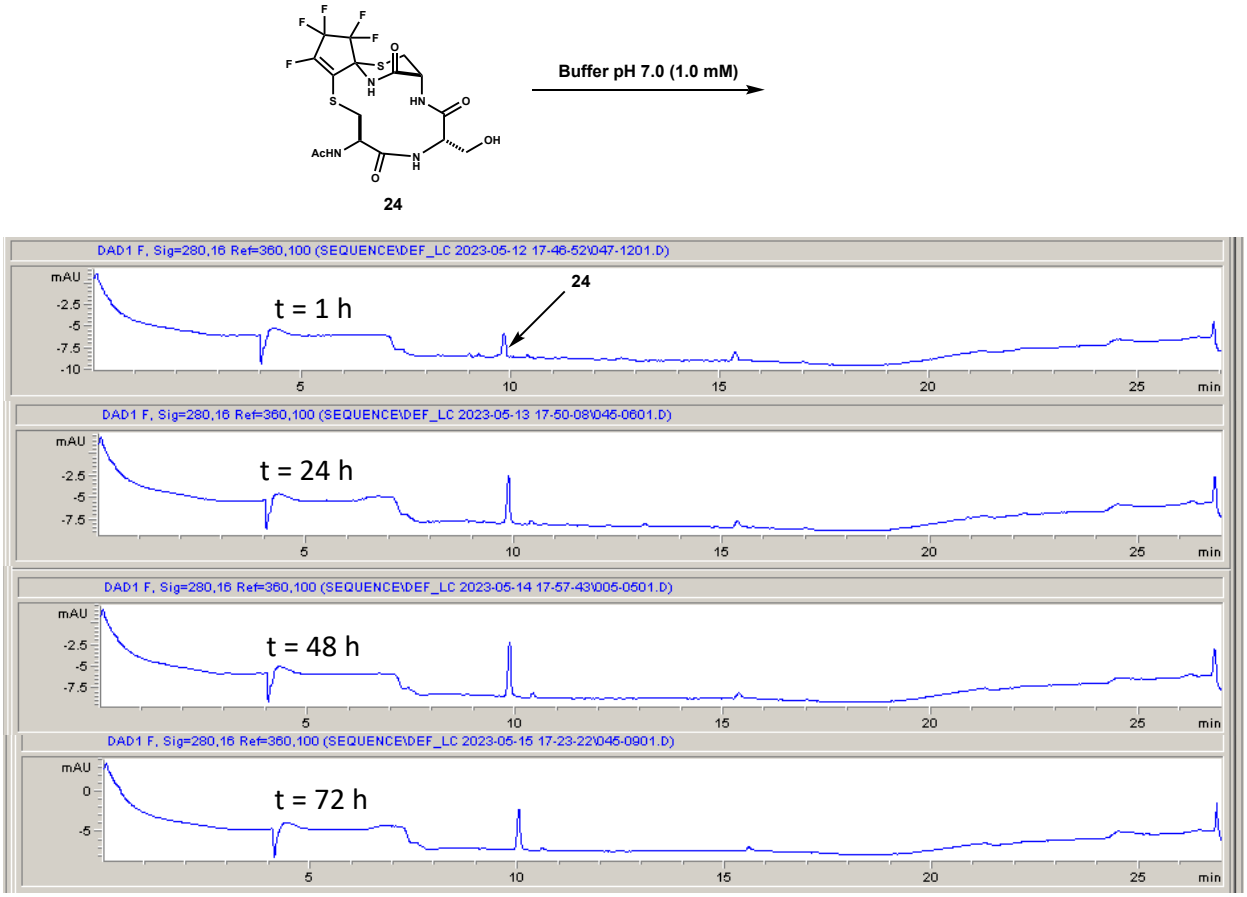

Figure 4.7.7 Degradation Experiment of Macrocycle **24** at pH 7.0. Compound **24** was subjected to a degradation experiment at pH 7.0 over a 72 h time course. No noticeable decomposition of **24** was observed. **24** (1.0 mg, 1.0 equiv., 2.0 µmol) was diluted with KH_2PO_4/Na_2HPO_4 (0.05 M) buffer pH 7.0 (1.0 mM, 2.0 mL). The solution was then allowed to stir at 25ºC for 72 h. Time points were taken at 1 h, 24 h, 48 h, and 72 h. Monitored via analytical HPLC (280 nm). The reaction was monitored by taking 10 µL aliquots at of the reaction mixture at the stated time points and diluting into 130 µL of 1% AcOH in MeCN.

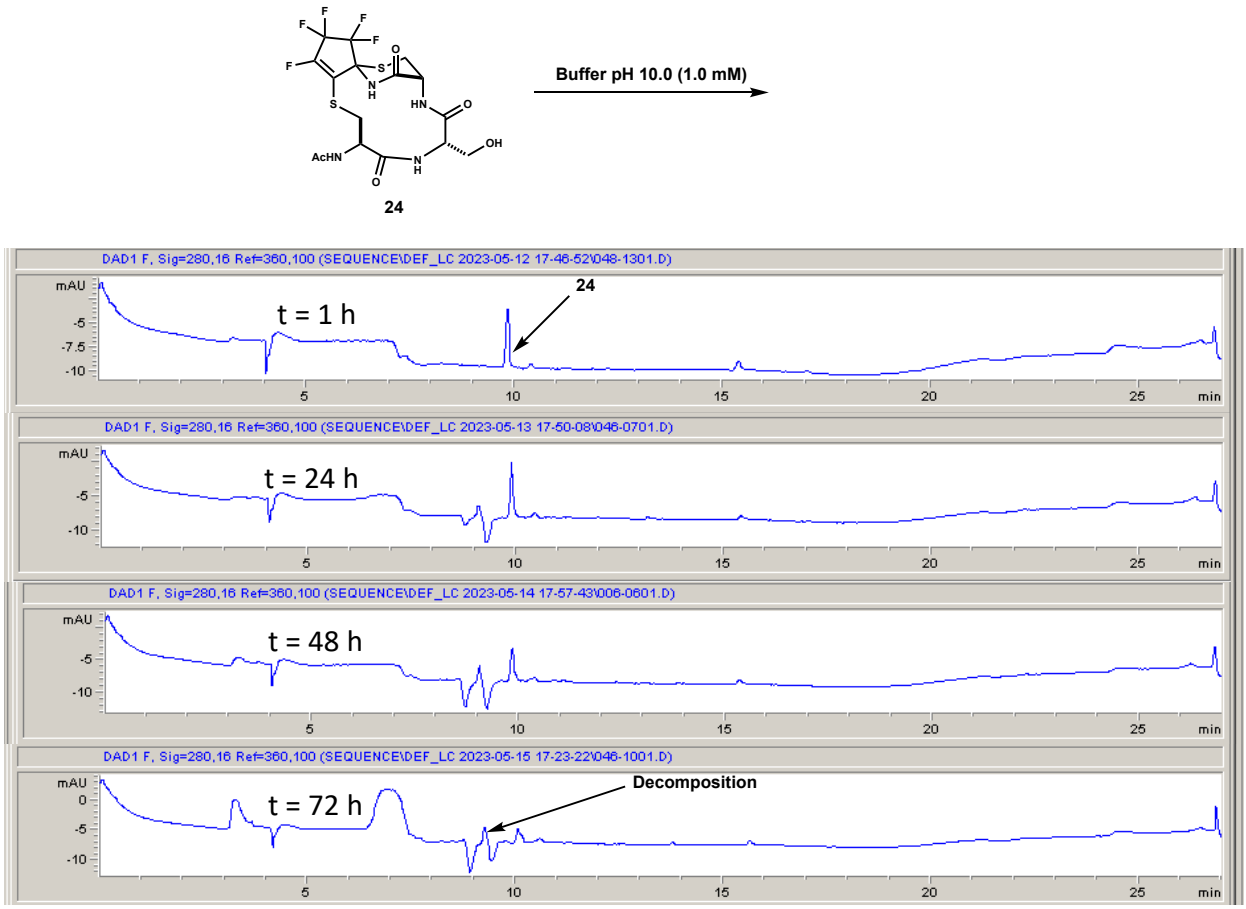

Figure 4.7.8 Degradation Experiment of Macrocycle **24** at pH 10.0. Compound **24** was subjected to a degradation experiment at pH 10.0 over a 72 h time course. Noticeable decomposition of **24** was observed starting at 24 h. **24** (1.0 mg, 1.0 equiv., 2.0 µmol) was diluted with $K_2CO_3/BK_3O_3/KOH$ (0.05 M) buffer pH 10.0 (1.0 mM, 2.0 mL). The solution was then allowed to stir at 25ºC for 72 h. Time points were taken at 1 h, 24 h, 48 h, and 72 h. Monitored via analytical HPLC (280 nm). The reaction was monitored by taking 10 µL aliquots at of the reaction mixture at the stated time points and diluting into 130 µL of 1% AcOH in MeCN.

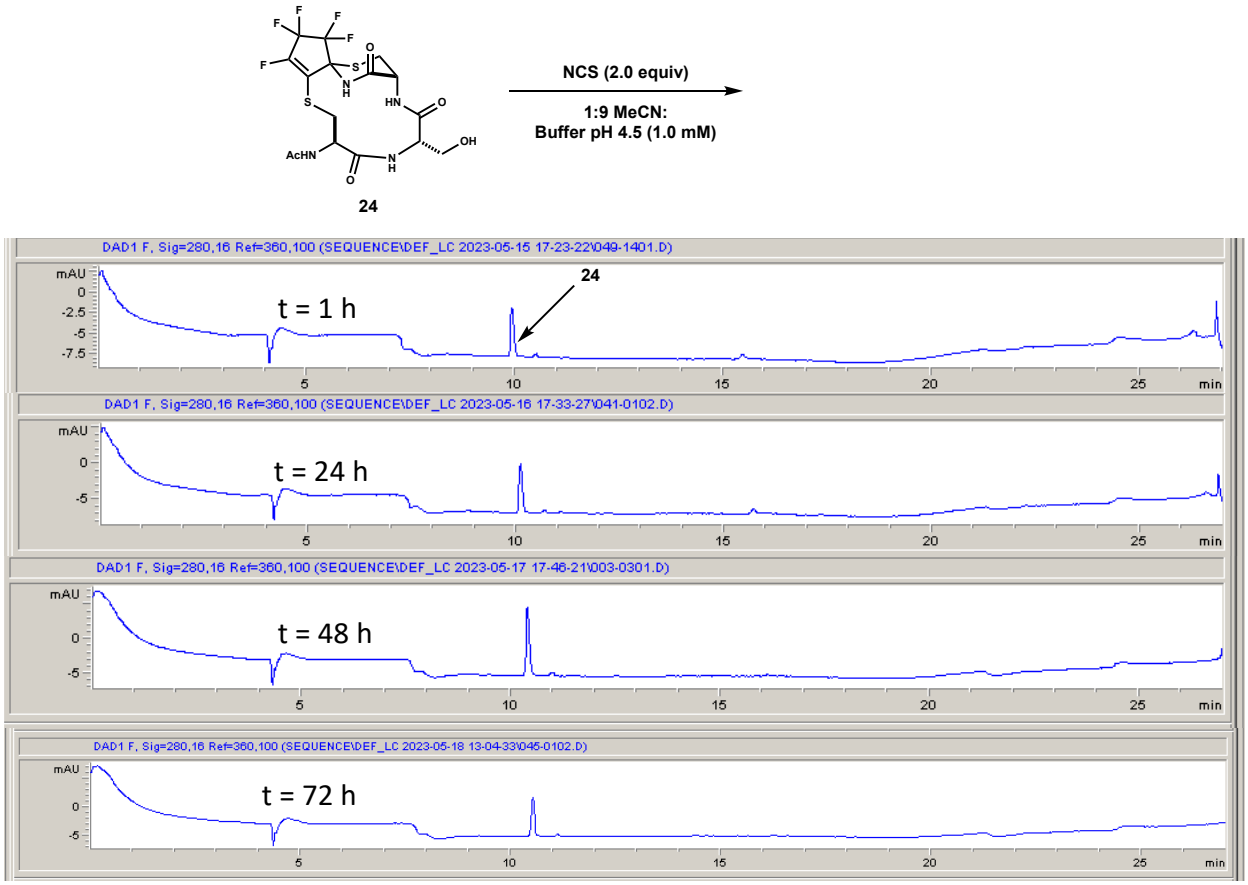

Figure 4.7.9 Degradation Experiment of Macrocycle **24** with NCS. Compound **24** was subjected to a degradation experiment with NCS over a 72 h time course. No noticeable decomposition of **24** was observed. **24** (1.0 mg, 1.0 equiv., 2.0 µmol) was diluted with 1:9 MeCN : NaOAc/AcOH (0.2 M) buffer pH 4.5 (1.0 mM, 2.0 mL). The solution was then added NCS (40 µL, 2.0 equiv., 4.0 µmol, 0.1 M in MeCN) and the reaction mixture allowed to stir at 25ºC for 72 h. Time points were taken at 1 h, 24 h, 48 h, and 72 h. Monitored via analytical HPLC (280 nm). The reaction was monitored by taking 10 µL aliquots at of the reaction mixture at the stated time points and diluting into 130 µL of 1% AcOH in MeCN.

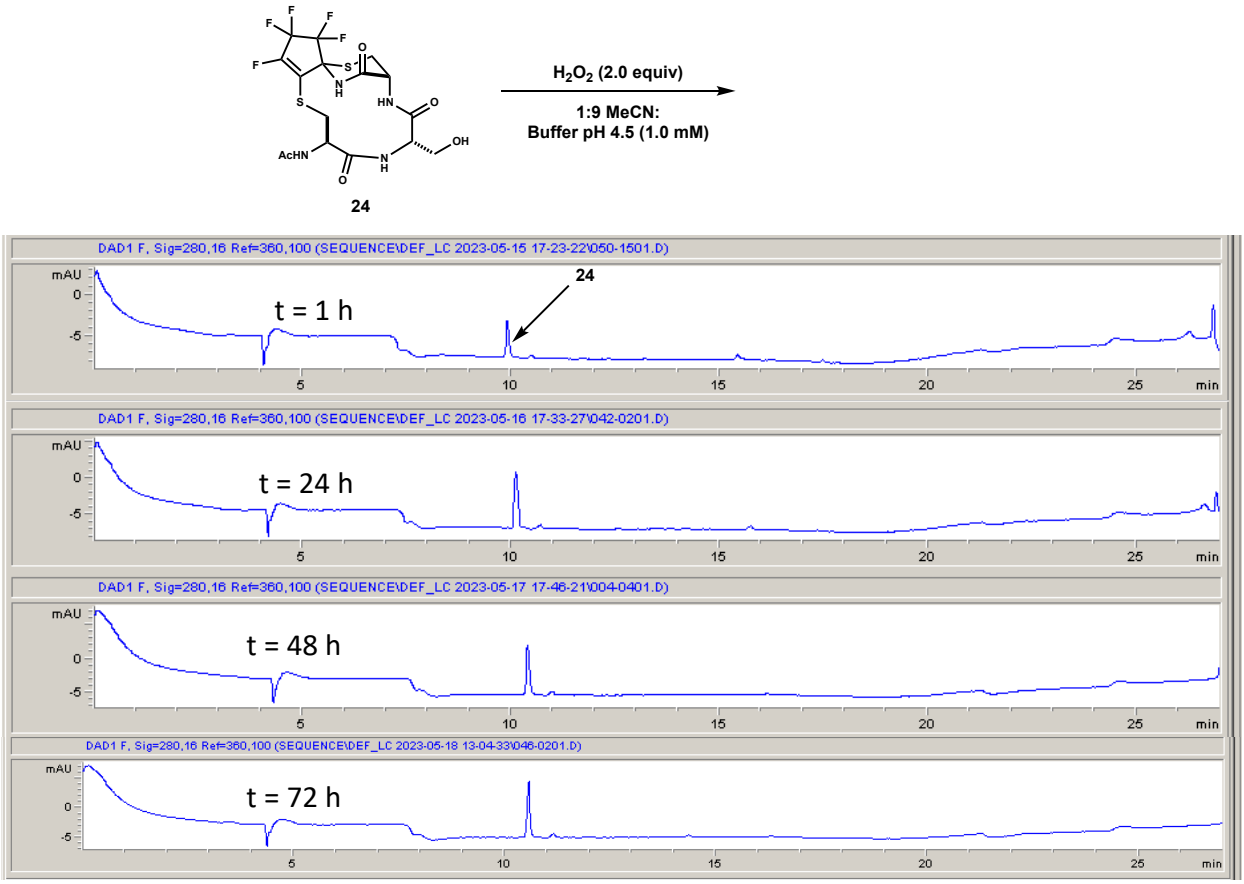

Figure 4.7.10 Degradation Experiment of Macrocycle **24** with H_2O_2. Compound **24** was subjected to a degradation experiment with H_2O_2 over a 72 h time course. No noticeable decomposition of **24** was observed. **24** (1.0 mg, 1.0 equiv., 2.0 µmol) was diluted with 1:9 MeCN : NaOAc/AcOH (0.2 M) buffer pH 4.5 (1.0 mM, 2.0 mL). The solution was then added H_2O_2 (40 µL, 2.0 equiv., 4.0 µmol, 0.1 M in MeCN) and the reaction mixture allowed to stir at 25ºC for 72 h. H_2O_2 solution prepared from 30% aqueous H_2O_2. Time points were taken at 1 h, 24 h, 48 h, and 72 h. Monitored via analytical HPLC (280 nm). The reaction was monitored by taking 10 µL aliquots at of the reaction mixture at the stated time points and diluting into 130 µL of 1% AcOH in MeCN.

Stability Studies on Disulfide S30

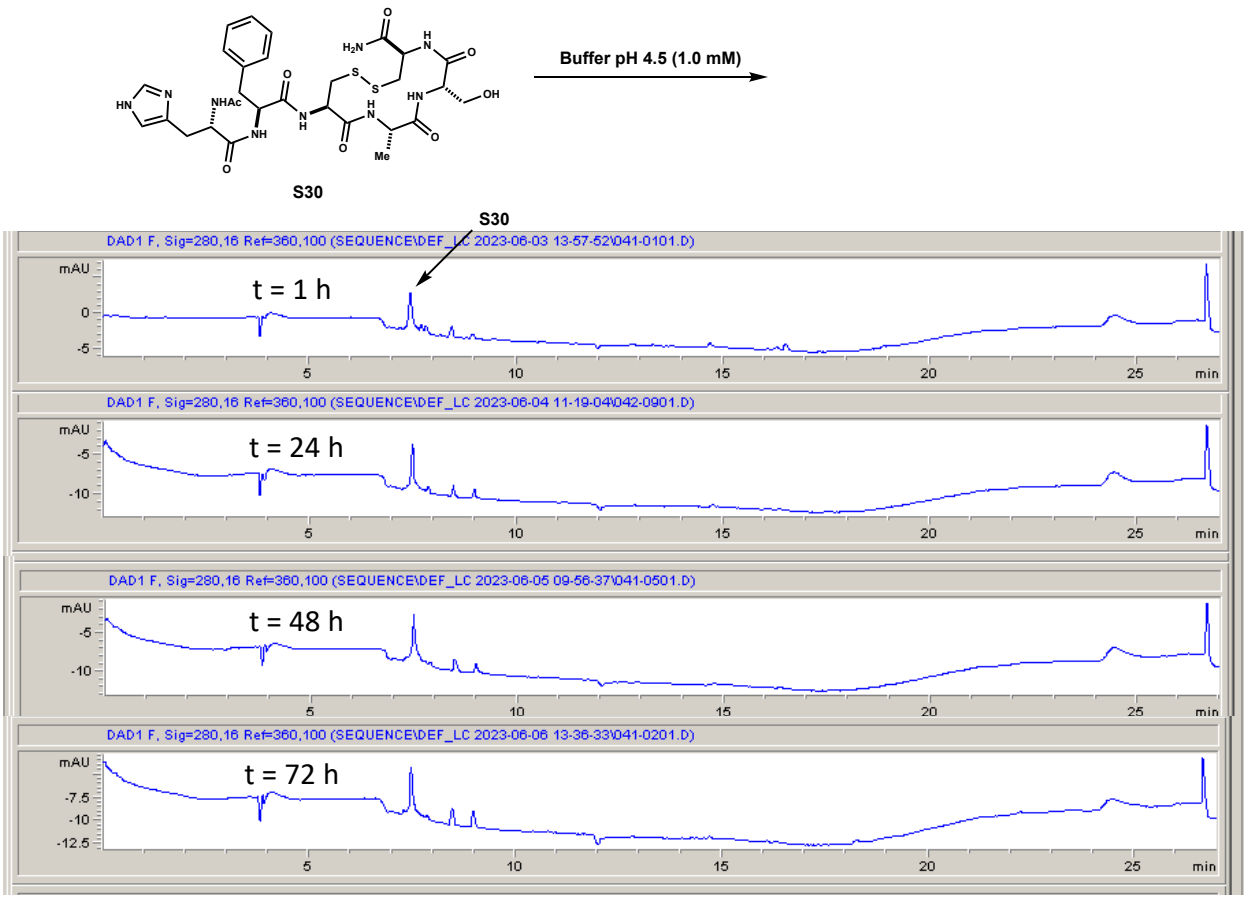

Figure 4.7.11 Degradation Experiment of Macrocycle **S30** at pH 4.5. Compound **S30** was subjected to a degradation experiment at **pH** 4.5 over a 72 h time course. Noticeable decomposition of **S30** was observed starting at 1 h. **S30** (1.0 mg, 1.0 equiv., 1.2 µmol) was diluted with NaOAc/AcOH (0.2 M) buffer pH 4.5 (1.0 mM, 1.2 mL). The solution was then allowed to stir at 25ºC for 72 h. Time points were taken at 1 h, 24 h, 48 h, and 72 h. Monitored via analytical HPLC (280 nm). The reaction was monitored by taking 10 µL aliquots at of the reaction mixture at the stated time points and diluting into 130 µL of 1% AcOH in MeCN.

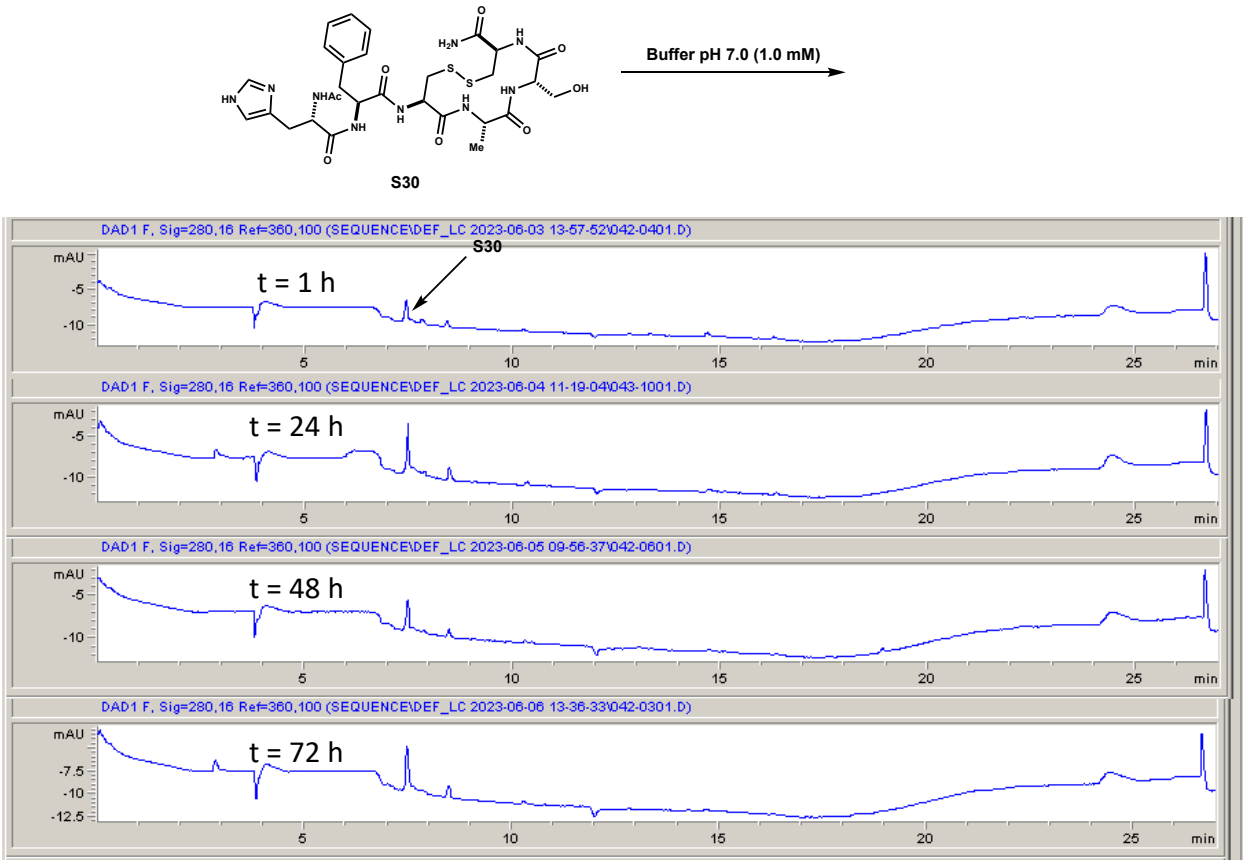

Figure 4.7.12 Degradation Experiment of Macrocycle **S30** at pH 7.0. Compound **S30** was subjected to a degradation experiment at pH 7.0 over a 72 h time course. No noticeable decomposition of **S30** was observed. **S30** (1.0 mg, 1.0 equiv., 1.2 µmol) was diluted with KH_2PO_4/Na_2HPO_4 (0.05 M) buffer pH 7.0 (1.0 mM, 1.2 mL). The solution was then allowed to stir at 25ºC for 72 h. Time points were taken at 1 h, 24 h, 48 h, and 72 h. Monitored via analytical HPLC (280 nm). The reaction was monitored by taking 10 µL aliquots at of the reaction mixture at the stated time points and diluting into 130 µL of 1% AcOH in MeCN.

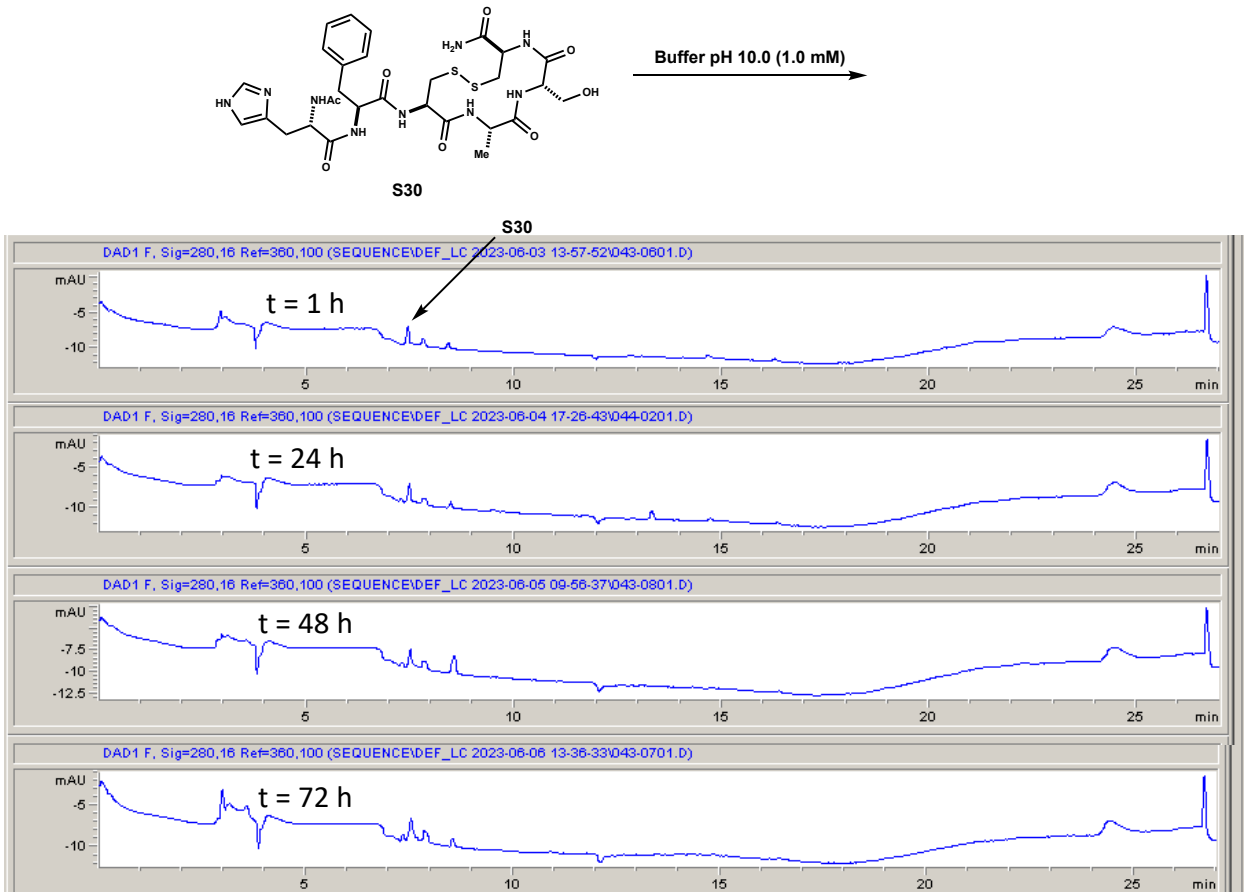

Figure 4.7.13 Degradation Experiment of Macrocycle **S30** at pH 10.0. Compound **S30** was subjected to a degradation experiment at pH 10.0 over a 72 h time course. Noticeable decomposition of **S30** was observed starting at 1 h. **S30** (1.0 mg, 1.0 equiv., 1.2 µmol) was diluted with K_2CO_3/BK_3O_3/KOH (0.05 M) buffer pH 10.0 (1.0 mM, 1.2 mL). The solution was then allowed to stir at 25ºC for 72 h. Time points were taken at 1 h, 24 h, 48 h, and 72 h. Monitored via analytical HPLC (280 nm). The reaction was monitored by taking 10 µL aliquots at of the reaction mixture at the stated time points and diluting into 130 µL of 1% AcOH in MeCN.

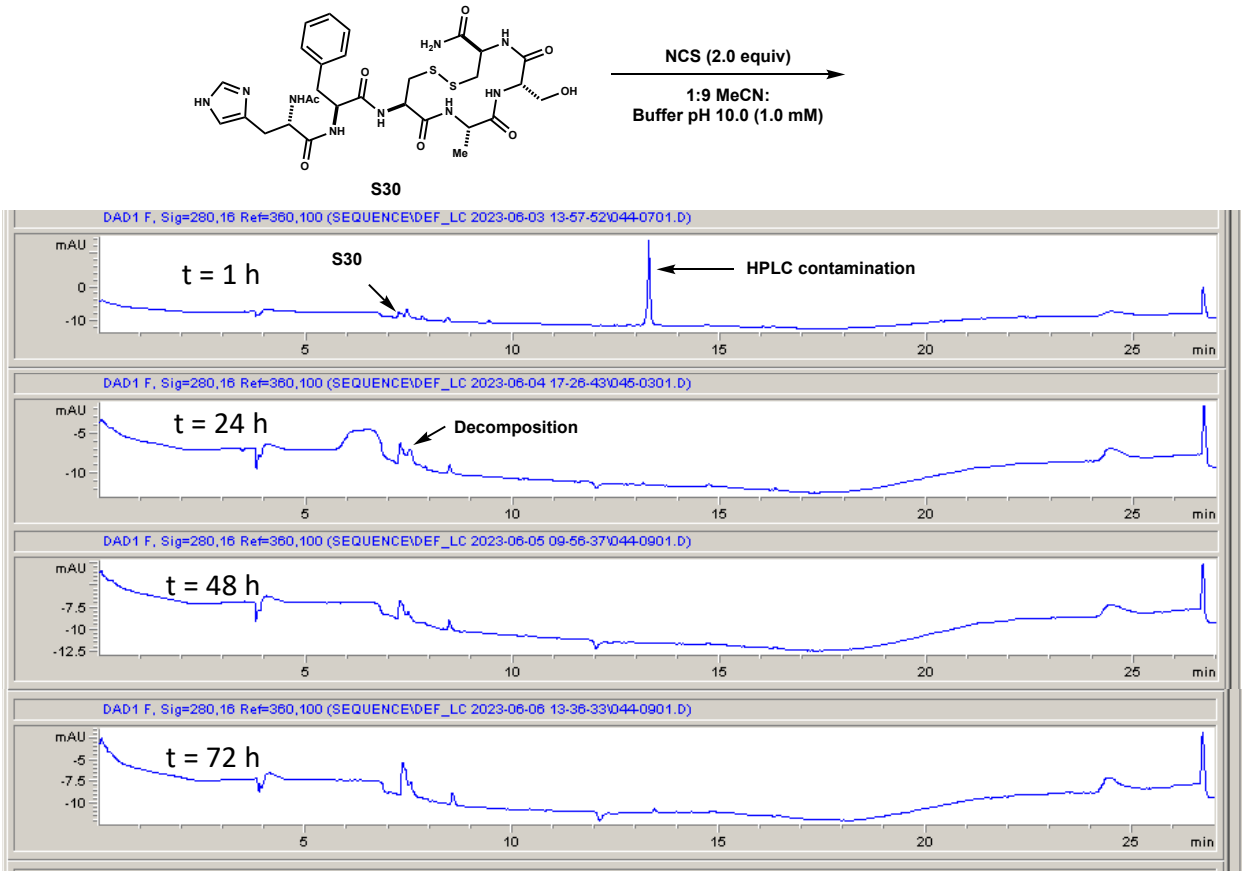

Figure 4.7.14 Degradation Experiment of Macrocycle **S30** with NCS. Compound **S30** was subjected to a degradation experiment with NCS over a 72 h time course. Noticeable decomposition of **S30** was observed after 1 h and complete decomposition observed after 24 h. **S30** (1.0 mg, 1.0 equiv, 1.2 µmol) was diluted with 1:9 MeCN : NaOAc/AcOH (0.2 M) buffer pH 4.5 (1.0 mM, 1.2 mL). The solution was then added NCS (25 µL, 2.0 equiv., 2.5 µmol, 0.1 M in MeCN) and the reaction mixture allowed to stir at 25ºC for 72 h. Time points were taken at 1 h, 24 h, 48 h, and 72 h. Monitored via analytical HPLC (280 nm). The reaction was monitored by taking 10 µL aliquots at of the reaction mixture at the stated time points and diluting into 130 µL of 1% AcOH in MeCN.

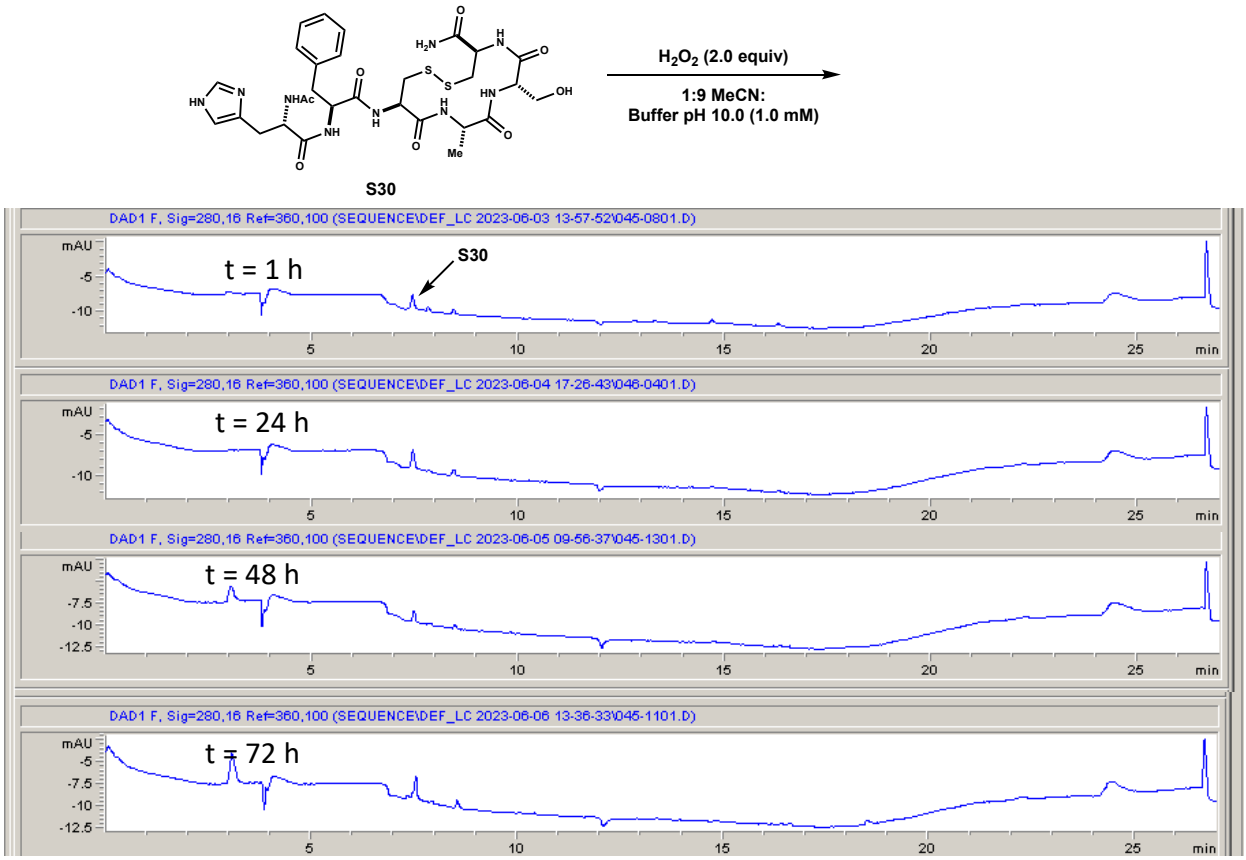

Figure 4.7.15 Degradation Experiment of Macrocycle **S30** with H_2O_2. Compound **S30** was subjected to a degradation experiment with H_2O_2 over a 72 h time course. No noticeable decomposition of **S30** was observed. **S30** (1.0 mg, 1.0 equiv., 1.2 µmol) was diluted with 1:9 MeCN : NaOAc/AcOH (0.2 M) buffer pH 4.5 (1.0 mM, 1.2 mL). The solution was then added H_2O_2 (25 µL, 2.0 equiv., 4.0 µmol, 0.1 M in MeCN) and the reaction mixture allowed to stir at 25ºC for 72 h. H_2O_2 solution prepared from 30% aqueous H_2O_2. Time points were taken at 1 h, 24 h, 48 h, and 72 h. Monitored via analytical HPLC (280 nm). The reaction was monitored by taking 10 µL aliquots at of the reaction mixture at the stated time points and diluting into 130 µL of 1% AcOH in MeCN.

Computational Evaluation of Loop Mimicry

Computational Methods

Computational models of macrocycles and macrobicycle as well as all calculations performed on them (geometry optimization and conformational searches) were generated and carried out using Schrödinger's Maestro Macromodel®.[36.37] Geometry optimizations were carried out using the AMBER* force field minimization in water with default settings (Method: PRGC, Maximum iterations: 2500, Convergence threshold: 0.05). Low energy conformations of each geometry optimized structure were identified using a Monte Carlo search algorithm using the AMBER* force field in water with default settings (Method: PRGC, Maximum iteration: 2500, Convergence threshold: 0.05, Maximum number of steps: 1000, 21.0 kJ/mol energy window for saving structures). Low energy conformers of each library member were overlaid onto each of the 11 Kritzer loop type representatives using the PyMOL® superposition[31] function; generating MatchAlign scores for each confirmation-loop type pair. The generated MatchAlign scores, which are a function of root-mean-square deviation (RMSD) and the number of atoms used in the superposition, were normalized relative to loop self-superimposed maximal values to yield 'similarity scores (%)'. Normalizing each MatchAlign score in this way allows for appropriate comparison of confirmation-loop type pair overlays regardless of the length of the loop and/or macrobicycle. Determination of intramolecular hydrogen bonding (shown in **Figure 4.5.1**) was done using Schrödinger's Maestro MacroModel® and verified using PyMOL®.

Supplemental Figures and Tables

Loop Type	PDB Code	Chain	Length	First AA	Last AA	Sequence	Max Align. Score
β-Turn	3A2V	A	6	S207	F212	SLDWWF	30.7
β-Hairpin	1T3I	A	6	V264	F269	VFFDHF	30.7
β-Bulge	3BGT	A	6	H174	P179	HVDGSP	20.8
Schellman Loop	2OL1	B	6	S73	D78	SLKGID	20.8
αβ-Motiff	2DVT	D	5	I274	G278	ILEIG	19.8
γ-Turn	2WAM	A	7	T89	F95	TFKTDHF	36.7
Asx-Turn	4HN1	A	6	S18	R23	SDHRGR	20.8
Asx-Motif	3B8I	C	5	G94	N98	GNALN	19.8
S/T-Turn	4J07	A	7	R84	F90	RGDTPHF	26.7
S/T-Motif	3N3R	A	5	R40	P44	RDWWP	24.8
S/T-Staple	1NVM	A	6	V278	L283	VDRETL	30.7

Table 4.7.1 Loop type representative information. The table above shows selected representatives for each of the 11 loop types identified by Kritzer. Representatives were chosen on the basis that they have backbone torsional angles closest to that of the average for each loop type.

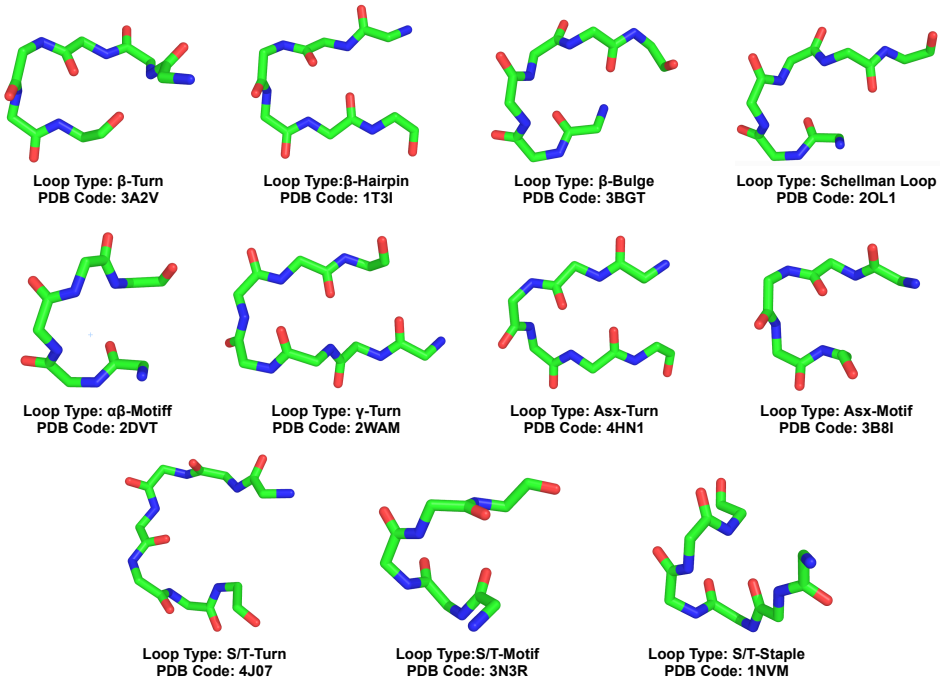

Figure 4.7.16 Images of loop type representatives. Depicted loops were extracted from protein crystal structures obtained from the Protein Data Bank (PDB) and are rendered using PyMOL®.

Entry #	Group	Family	Code	Conformations
1	X#X1X	X1X1X	C1C1C	6
2			H1C1C	7
3			Y1C1C	5
4			C1H1C	5
5			H1H1C	8
6			Y1H1C	7
7		X2X1X	C2C1C	85
8			H2C1C	10
9			Y2C1C	11
10			C2H1C	18
11			H2H1C	11
12			Y2H1C	5
13		X3X1X	C3C1C	34
14			H3C1C	15
15			Y3C1C	20
16			C3H1C	8
17			H3H1C	28
18			Y3H1C	25
19		X4X1X	C4C1C	99
20			H4C1C	65
21			Y4C1C	35
22			C4H1C	6
23			H4H1C	43
24			Y4H1C	22
25		X5X1X	C5C1C	52
26			H5C1C	54
27			Y5C1C	29
28			C5H1C	5
29			H5H1C	51
30			Y5H1C	44

Entry #	Group	Family	Code	Conformations
31	X#X2X	X1X2X	C1C2C	25
32			H1C2C	10
33			Y1C2C	13
34			C1H2C	18
35			H1H2C	10
36			Y1H2C	9
37		X2X2X	C2C2C	29
38			H2C2C	25
39			Y2C2C	58
40			C2H2C	10
41			H2H2C	23
42			Y2H2C	27
43		X3X2X	C3C2C	106
44			H3C2C	30
45			Y3C2C	29
46			C3H2C	31
47			H3H2C	33
48			Y3H2C	56
49		X4X2X	C4C2C	23
50			H4C2C	55
51			Y4C2C	44
52			C4H2C	48
53			H4H2C	27
54			Y4H2C	43
55		X5X2X	C5C2C	19
56			H5C2C	97
57			Y5C2C	55
58			C5H2C	39
59			H5H2C	54
60			Y5H2C	19

Entry #	Group	Family	Code	Conformations
61	X#X3X	X1X3X	C1C3C	35
62			H1C3C	13
63			Y1C3C	50
64			C1H3C	55
65			H1H3C	22
66			Y1H3C	10
67		X2X3X	C2C3C	6
68			H2C3C	64
69			Y2C3C	88
70			C2H3C	65
71			H2H3C	24
72			Y2H3C	36
73		X3X3X	C3C3C	60
74			H3C3C	42
75			Y3C3C	36
76			C3H3C	22
77			H3H3C	31
78			Y3H3C	25
79		X4X3X	C4C3C	34
80			H4C3C	68
81			Y4C3C	20
82			C4H3C	81
83			H4H3C	63
84			Y4H3C	20
85		X5X3X	C5C3C	6
86			H5C3C	70
87			Y5C3C	44
88			C5H3C	33
89			H5H3C	46
90			Y5H3C	6

Entry #	Group	Family	Code	Conformations
91	X#X4X	X1X4X	C1C4C	65
92			H1C4C	27
93			Y1C4C	41
94			C1H4C	88
95			H1H4C	30
96			Y1H4C	15
97		X2X4X	C2C4C	24
98			H2C4C	44
99			Y2C4C	23
100			C2H4C	48
101			H2H4C	10
102			Y2H4C	24
103		X3X4X	C3C4C	130
104			H3C4C	56
105			Y3C4C	21
106			C3H4C	38
107			H3H4C	21
108			Y3H4C	37
109		X4X4X	C4C4C	24
110			H4C4C	86
111			Y4C4C	21
112			C4H4C	34
113			H4H4C	78
114			Y4H4C	95
115		X5X4X	C5C4C	25
116			H5C4C	79
117			Y5C4C	74
118			C5H4C	7
119			H5H4C	4
120			Y5H4C	104

Entry #	Group	Family	Code	Conformations
121	X#X5X	X1X5X	C1C5C	35
122			H1C5C	19
123			Y1C5C	27
124			C1H5C	7
125			H1H5C	54
126			Y1H5C	36
127		X2X5X	C2C5C	36
128			H2C5C	23
129			Y2C5C	21
130			C2H5C	64
131			H2H5C	64
132			Y2H5C	45
133		X3X5X	C3C5C	123
134			H3C5C	57
135			Y3C5C	39
136			C3H5C	33
137			H3H5C	48
138			Y3H5C	53
139		X4X5X	C4C5C	16
140			H4C5C	19
141			Y4C5C	57
142			C4H5C	60
143			H4H5C	52
144			Y4H5C	33
145		X5X5X	C5C5C	93
146			H5C5C	13
147			Y5C5C	73
148			C5H5C	15
149			H5H5C	39
150			Y5H5C	51

Table 4.7.2 Complete OFCP-derived poly-alanine macrobicycle library. OFCP derived poly-alanine macrobicycles were categorized into groups based on the number of intervening L-alanine residues composing the B Ring and then into families based on the number of intervening L-alanine residues composing the A Ring. Also, shown are the number of low-energy conformations identified for each of the 150 OFCP-derived poly-alanine macrobicycles.

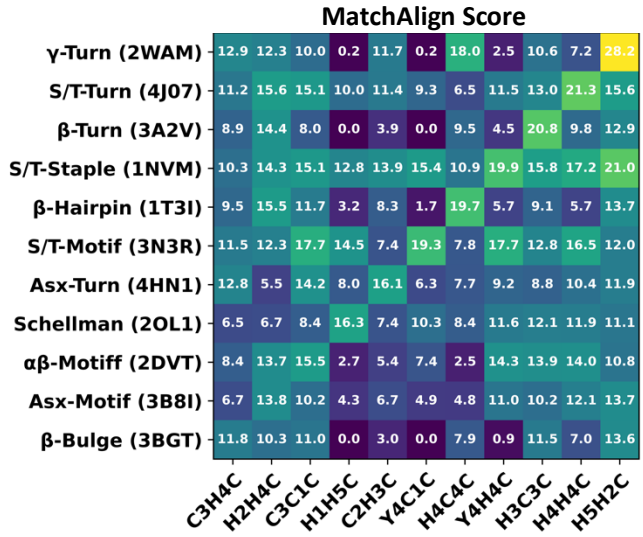

Figure 4.7.17 Non-normalized version of heat map shown in **Figure 4.4.1**. Heatmap above shows non-normalized MatchAlign scores calculated using the PyMOL superposition function.

Loop	Macrobicycle	Conf. #	RMSD	# of Atoms	Align. Score	Max Align.	% Similarity
γ-Turn	H5H2C	4	1.14	33	28.2	36.7	77.0
S/T-Turn	H4H4C	77	0.72	25	21.3	26.7	79.8
β-Turn	H3C3C	23	0.36	24	20.8	30.7	67.6
S/T-Staple	Y4H4C	70	0.89	28	19.9	30.7	64.7
β-Hairpin	H4C4C	33	0.79	24	19.7	30.7	64.0
S/T-Motif	Y4C1C	22	1.11	24	19.3	24.8	77.7
Asx-Turn	C2H3C	9	0.27	16	16.1	20.8	77.3
Schellman	H1H5C	25	0.88	26	16.3	20.8	78.5
αβ-Motiff	C3C1C	2	1.39	23	15.5	19.8	78.5
Asx-Motif	H2H4C	3	0.77	18	13.8	19.8	69.5
β-Bulge	C3H4C	29	0.24	12	11.8	20.8	57.0

Table 4.7.3 Data for best mimics of each loop type representative. Data in the table above correspond to the OFCP-derived poly-alanine macrobicycles/representative loop type overlays displayed along the diagonal (top right to bottom left) in **Figure 4.4.1**.

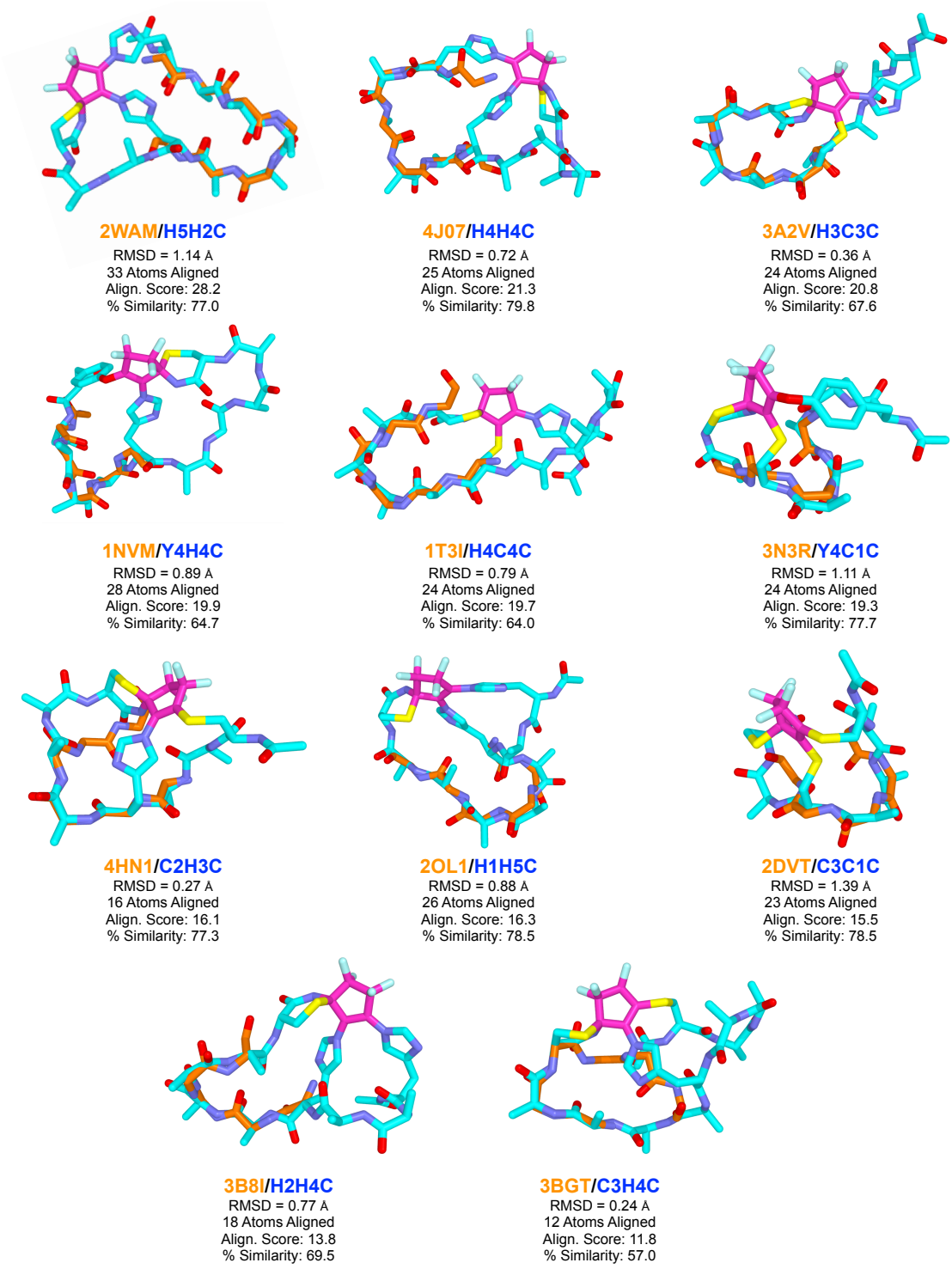

Figure 4.7.18 Visualized overlays of best conformer/loop type pairs. Depicted are the 11 loop type representatives super imposed onto their optimal OFCP-derived poly-alanine macrobicycle mimic. Overlays were performed using the PyMOL® super position function.

Schellman Loop vs. H1H5C							
Scaffold	Peptide	Conformer #	RMSD	# of Atoms	Align Score	Max Align. Score	% Similarity
2OL1_Schellman	H1H5C	25	0.88421607	26	16.29135513	20.762	78.46717625
3P9A_Schellman	H1H5C	25	1.401694179	28	19.56832886	25.742	76.01712710
2W31_Schellman	H1H5C	25	1.658171535	30	22.90710068	30.721	74.56495777
1ZMD_Schellman	H1H5C	25	1.10956645	28	15.14722252	20.762	72.95647105
2HV2_Schellman	H1H5C	25	1.476985216	29	22.27397156	30.721	72.50405767
1I3C_Schellman	H1H5C	25	1.246664882	28	17.8298645	24.771	71.97878367
3NOQ_Schellman	H1H5C	25	0.900729239	24	21.19808769	30.721	69.00194555
2Q01_Schellman	H1H5C	25	1.489648342	29	20.80150032	30.721	67.71101305
1GDH_Schellman	H1H5C	25	0.92443943	23	20.41290665	30.721	66.44610086
2HCY_Schellman	H1H5C	25	1.831531405	30	20.14535332	30.721	65.57518739
2ZBL_Schellman	H1H5C	25	1.357090116	31	20.02081871	30.721	65.16981449
1LDN_Schellman	H1H5C	25	1.242733955	26	19.14774895	30.721	62.32788303
2AR7_Schellman	H1H5C	25	1.400835514	30	18.95789528	30.721	61.70988991
2AFH_Schellman	H1H5C	25	1.137803555	29	12.54950619	20.762	60.44459198
1LEH_Schellman	H1H5C	25	1.675282598	30	17.93689156	30.721	58.38641827
2YFD_Schellman	H1H5C	25	0.516484976	29	11.73530388	20.762	56.52299335
1T06_Schellman	H1H5C	25	0.786531866	25	11.50237751	20.762	55.40110543
2P6P_Schellman	H1H5C	25	0.961323798	28	11.39608002	20.762	54.88912444
2WU9_Schellman	H1H5C	25	0.888848305	29	11.35975933	20.762	54.71418616
2NTX_Schellman	H1H5C	25	0.579154968	20	11.16182518	20.762	53.76083797
1L5X_Schellman	H1H5C	25	0.180126742	14	7.959266663	14.812	53.73525967
4BFZ_Schellman	H1H5C	25	0.51499027	19	11.06298447	20.762	53.28477250
3ISP_Schellman	H1H5C	25	0.757302523	21	10.77571869	20.762	51.90115928
3V8D_Schellman	H1H5C	25	0.183440045	13	7.685449123	14.812	51.88664004
1BWN_Schellman	H1H5C	42	0.809048951	15	10.74102688	20.762	51.73406646
1F8M_Schellman	H1H5C	25	0.854737818	22	7.58887291	14.812	51.23462672

Table 4.7.4 Similarity scores of all the Schellman loops identified by Krtizer and coworkers in the Protein Data Bank (PDB) against theoretical OFCP-derived macrobicycle H1H5C having a score > 50%.

β-Bulge vs. C3H4C							
Scaffold	Peptide	Conformer #	RMSD	# of Atoms	Align Score	Max Align. Score	% Similarity
1VFJ_Bbulge	C3H4C	14	0.353249192	16	14.55334568	20.762	70.09606820
4AFX_Bbulge	C3H4C	14	0.567602515	18	14.1434145	20.762	68.12163809
1UL3_Bbulge	C3H4C	14	0.37648499	16	13.79792881	20.762	66.45760914
4EGX_Bbulge	C3H4C	31	0.303482413	12	9.360966682	14.812	63.19853282
2D5F_Bbulge	C3H4C	32	0.818367779	32	20.62849426	32.662	63.15747431
3BGT_Bbulge	C3H4C	29	0.243290663	12	11.83428955	20.762	56.99975701
3VTO_Bbulge	C3H4C	30	0.511535347	13	11.80018234	20.762	56.83547992
1GK9_Bbulge	C3H4C	29	0.243508384	13	10.4375	19.792	52.73595392
1L8L_Bbulge	C3H4C	31	1.241113424	16	10.607234	20.762	51.08965418
3AJV_Bbulge	C3H4C	12	0.448780864	13	9.799287796	20.762	47.19818802
1BWN_Bbulge	C3H4C	14	1.191673279	16	9.794635773	20.762	47.17578159
2FPF_Bbulge	C3H4C	11	1.496762276	25	17.19746017	36.671	46.89662177
3MMZ_Bbulge	C3H4C	3	0.871813476	14	9.613739014	20.762	46.30449385
2DG5_Bbulge	C3H4C	38	0.656006515	19	15.01911449	32.662	45.98345016
1CP9_Bbulge	C3H4C	12	0.379625946	12	8.97013092	19.792	45.32200344
1V0Z_Bbulge	C3H4C	38	0.755455673	14	7.042289734	15.783	44.61946229
1IM9_Bbulge	C3H4C	11	1.014074802	18	13.66701889	32.662	41.84379061
2A5H_Bbulge	C3H4C	36	0.640851617	20	15.33636951	36.671	41.82151976
2I8D_Bbulge	C3H4C	11	0.824626386	18	10.96436405	26.712	41.04658599
2FHQ_Bbulge	C3H4C	36	0.484371603	13	10.83055019	26.712	40.54563563
1MTP_Bbulge	C3H4C	34	1.390290022	28	10.76965523	26.712	40.31766708

Table 4.7. 5 Similarity scores of all the β-Bulges identified by Krtizer and coworkers in the Protein Data Bank (PDB) against theoretical OFCP-derived macrobicycle C3H4C having a score > 40%.

ab-Motif vs. C3C1C							
Scaffold	Peptide	Conformer #	RMSD	# of Atoms	Align Score	Max Align. Score	% Similarity
2PBZ_ABmotif	C3C1C	1	0.581512988	22	17.0686245	20.762	82.21088766
3VLJ_ABmotif	C3C1C	1	0.938679039	23	19.91806412	24.771	80.40880109
3A1G_ABmotif	C3C1C	1	0.978260696	23	19.76910782	24.771	79.80746768
4F3L_ABmotif	C3C1C	1	1.041450024	21	15.69570923	19.792	79.30330047
2NP9_ABmotif	C3C1C	1	0.508054554	18	18.75664139	23.771	78.90556303
2JB0_ABmotif	C3C1C	27	1.114786148	21	19.51566696	24.771	78.78433233
4H1Z_ABmotif	C3C1C	4	0.571699321	18	12.41984081	15.783	78.69125523
1TT5_ABmotif	C3C1C	1	1.090606332	21	15.51529694	19.792	78.39175897
3UZO_ABmotif	C3C1C	27	1.102343082	21	19.39369583	24.771	78.29193747
3I4E_ABmotif	C3C1C	1	1.186784387	22	19.3266468	24.771	78.02126198
3JZ6_ABmotif	C3C1C	1	1.145448565	22	15.43157959	19.792	77.96877319
2DVT_ABmotif	C3C1C	2	1.387537599	23	15.52943039	19.972	77.75601036
3EUP_ABmotif	C3C1C	27	1.068169951	21	19.12299538	24.771	77.19912550
2NVU_ABmotif	C3C1C	1	1.228185177	22	15.14432812	19.792	76.51742177
1QHH_ABmotif	C3C1C	1	1.111777306	23	18.9410038	24.771	76.46442937
1WLS_ABmotif	C3C1C	2	0.91927886	24	20.4146843	26.712	76.42514336
3OIS_ABmotif	C3C1C	1	1.185916901	22	15.0853796	19.792	76.21958165
2Q4D_ABmotif	C3C1C	27	1.848179936	28	15.57083511	20.762	74.99679758
3JYG_ABmotif	C3C1C	29	1.291326046	23	18.36027527	24.771	74.12004065
1T98_ABmotif	C3C1C	27	1.072797418	22	18.31200218	24.771	73.92516322
2UVB_ABmotif	C3C1C	29	1.237036824	29	27.06902313	36.671	73.81588485
1UGP_ABmotif	C3C1C	1	1.003030062	22	18.16857529	24.771	73.34615190
1A05_ABmotif	C3C1C	4	1.211265206	29	26.38762665	36.671	71.95775040
2AFH_ABmotif	C3C1C	1	0.993402779	23	14.72633648	20.762	70.92927694
3BEO_ABmotif	C3C1C	25	1.082759738	28	21.60921288	30.721	70.34020011
3FZ3_ABmotif	C3C1C	1	1.387328863	28	25.70983315	36.671	70.10944110
3P5J_ABmotif	C3C1C	27	0.957629502	17	17.29448128	24.771	69.81745298
1FNG_ABmotif	C3C1C	27	0.997924149	21	17.14268875	24.771	69.20466978
1F6D_ABmotif	C3C1C	1	1.026213288	28	21.22824669	30.721	69.10011617
1UMD_ABmotif	C3C1C	1	0.851346672	27	14.25194931	20.762	68.64439510
3GG2_ABmotif	C3C1C	11	0.546100855	20	17.59423447	25.742	68.34835858
2Y0C_ABmotif	C3C1C	11	0.614321351	20	17.53938866	25.742	68.13529895
3IK5_ABmotif	C3C1C	25	1.168270826	28	20.86926079	30.721	67.93158031
3EUH_ABmotif	C3C1C	25	0.911467493	18	16.5407486	24.771	66.77465018
1LDN_ABmotif	C3C1C	1	0.923798501	26	20.38579559	30.721	66.35785161
2IX5_ABmotif	C3C1C	2	1.037609696	22	16.30278206	24.771	65.81398433
3BRC_ABmotif	C3C1C	1	1.073004484	24	16.13868141	24.771	65.15151351
4DH2_ABmotif	C3C1C	11	1.535759926	50	19.7825737	30.721	64.39430259
3E4V_ABmotif	C3C1C	25	0.96004802	18	15.59446144	24.771	62.95450907
1FXZ_ABmotif	C3C1C	29	0.668985248	18	15.26769161	24.771	61.63534622
1DOF_ABmotif	C3C1C	11	0.561134994	20	18.87925911	30.721	61.45392113
3HVD_ABmotif	C3C1C	25	0.947651982	23	22.50969315	36.671	61.38281788
3LVY_ABmotif	C3C1C	1	1.113957405	27	22.42508316	36.671	61.15209064
4IDO_ABmotif	C3C1C	2	1.280631661	24	15.10272312	24.771	60.96937193
3GBX_ABmotif	C3C1C	29	1.939512014	30	25.57317352	42.621	60.00134563

Table 4.7.6 Similarity scores of all the α,β-Motifs identified by Krtizer and coworkers in the Protein Data Bank (PDB) against theoretical OFCP-derived macrobicycle C3C1C having a score > 60%.

Asx-turns vs. C2H3C							
Scaffold	Peptide	Conformer #	RMSD	# of Atoms	Align Score	Max Align. Score	% Similarity
4HN1_AsxTurn	C2H3C	9	0.26757583	16	16.05452728	20.762	77.32649687
3CEA_AsxTurn	C2H3C	9	0.40757513	19	15.24367046	20.762	73.42101175
3OQP_AsxTurn	C2H3C	9	0.402321368	19	13.9856596	20.762	67.36181293
3IP3_AsxTurn	C2H3C	9	0.476385385	19	13.36727047	20.762	64.38334684
3UNC_AsxTurn	C2H3C	50	1.691823244	25	16.99975014	26.712	63.64087354
3HMU_AsxTurn	C2H3C	39	0.794880629	22	19.02816772	30.721	61.93863390
4JOI_AsxTurn	C2H3C	37	0.808450341	13	12.5046587	20.762	60.22858443
2YV9_AsxTurn	C2H3C	12	1.203696251	26	17.35415268	30.721	56.48954357
4KKM_AsxTurn	C2H3C	40	0.301968783	16	16.04253197	30.721	52.22008388
1X0R_AsxTurn	C2H3C	58	1.07335794	19	13.73476601	26.712	51.41796200
4IXO_AsxTurn	C2H3C	9	0.482471973	17	13.16745758	25.742	51.15164937
3R4E_AsxTurn	C2H3C	12	1.854942203	25	15.41523361	30.721	50.17816350
1BOU_AsxTurn	C2H3C	14	0.888552904	13	2.798203707	5.583	50.12007356

Table 4.7.7 Similarity scores of all the Asx-Turns identified by Krtizer and coworkers in the Protein Data Bank (PDB) against theoretical OFCP-derived macrobicycle C2H3C having a score > 50%.

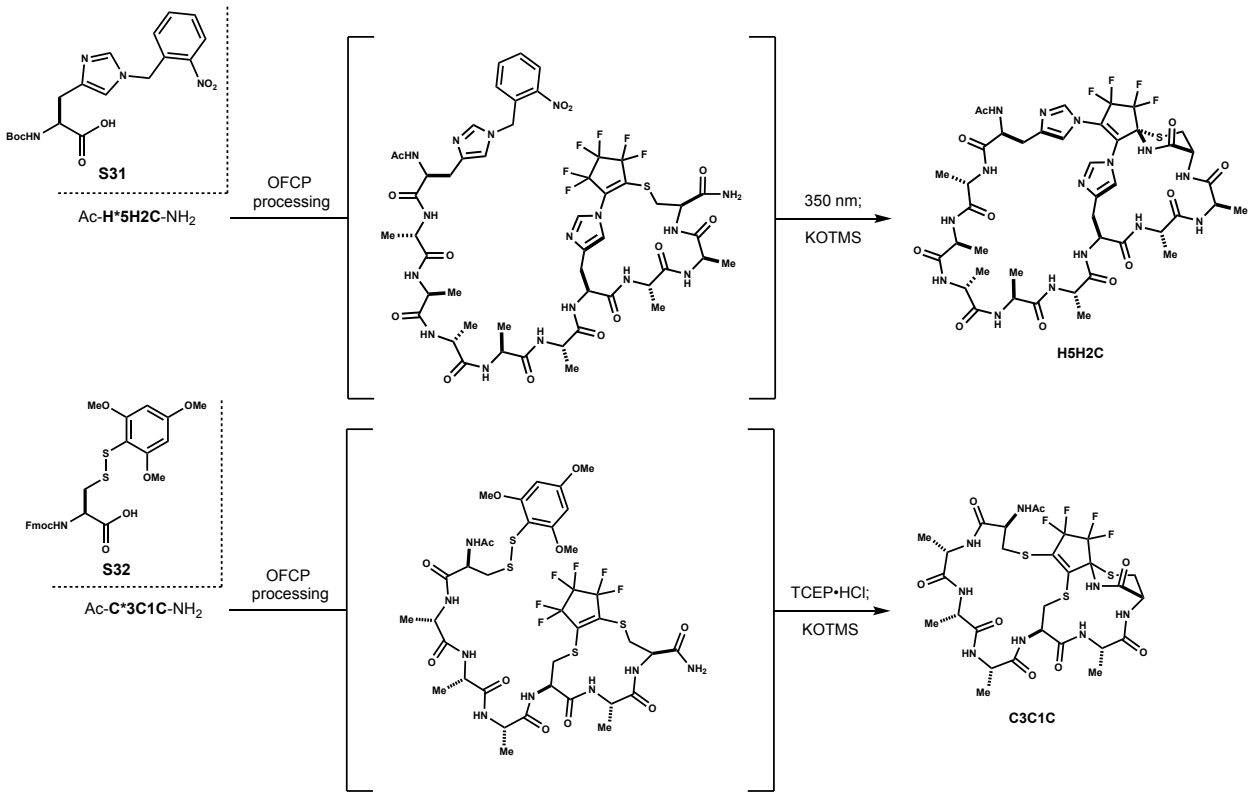

Scheme 4.7.4 Differential protecting group schemes to access macrobicycles derived from sequences of type HXHXC and CXCXC. Macrobicycles derived from linear peptides such as Ac-H5H2C-NH_2 can be accessed from differential protection of the histidine residue proximal to the N-terminus. Differential protection via known monomer **S31**.[38] Macrobicycles derived from linear peptides such as Ac-C3C1C-NH_2 can be accessed from differential protection of the cysteine residue proximal to the N-terminus. Differential protection via known monomer **S32**.[39]

Computations Related to Reactivity of OFCP

Computational Methods

All computations related to the calculations of the delocalized HOMO present in the intermediate formed by model reaction of ethyl mercaptide with OFCP (shown in **Figure 4.2.1B**) were carried out using the Gaussian 16 program[40] and performed at the level of M062X-D3/def2TZVP/SMD.[41-47] Homo cube file was obtained using Multiwfn[48] with picture rendering being done in PyMOL®. After detailed calculations of different nucleophiles, it can be shown that negative charge will always be delocalized which reflects the importance of negative hyperconjugation in lowering the activation energy of the reaction.

Parallel Artificial Membrane Permeability Assay (PAMPA) Data

This assay was performed as outlined in the protocol of the parallel artificial permeability assay kit (BioAssay Systems Cat. # PAMPA-096). Incubation was performed at rt for 18 h. Data analysis was performed using a Tecan M1000 plate reader and 96-well UV plates purchased from BioAssay Systems (Cat. # P96 UV). UV absorbance was measured from 230 to 500 nm in 10 nm intervals to determine peak absorbance of test compounds and controls. The following equation used to determined Permeability Rate (P_e):

$$P_e = C \times -\ln\left(1 - \frac{OD_A}{OD_E}\right) \text{ cm/s}$$

Where OD_A is the absorbance of Acceptor Solution minus Blank, OD_e is the absorbance of Equilibrium Standard minus Blank, and, using an 18 h incubation, C = 7.72 x 10^{-6}. Two PAMPA assays were run each in respective technical replicates.

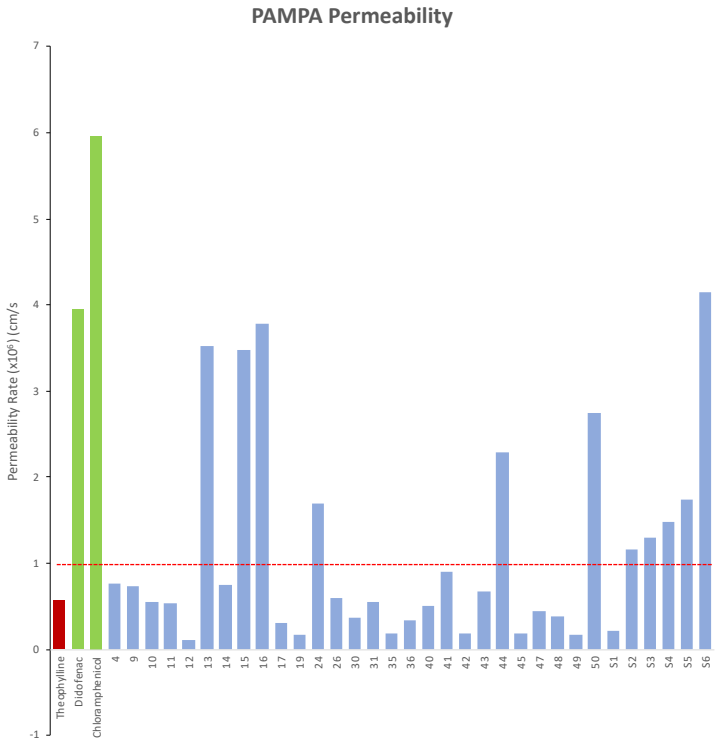

Figure 4.7.19 PAMPA average data set of select structures from two PAMPA assays.

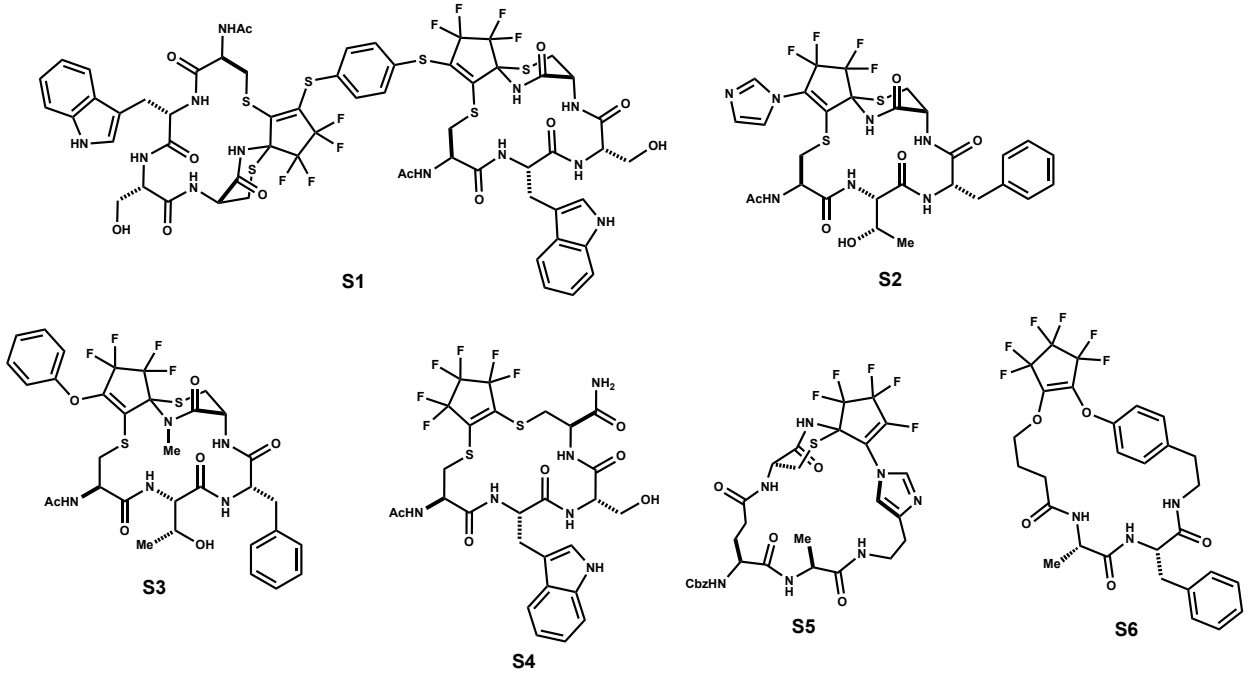

Figure 4.7.20 Figure depicting structures of PAMPA tested compounds **S1**–**S6**.

Compound #	Average Permeability
Theophylline	5.62389E-07
Diclofenac	3.94501E-06
Chloramphenicol	5.96548E-06
4	7.56292E-07
9	7.32926E-07
10	5.54279E-07
11	5.28474E-07
12	1.12019E-07
13	3.52671E-06
14	7.44164E-07
15	3.48058E-06
16	3.78308E-06
17	3.10102E-07
19	1.74545E-07
24	1.68976E-06
26	5.97371E-07
30	3.73806E-07
31	5.53492E-07
35	1.82988E-07
36	3.28936E-07
40	5.11253E-07
41	8.978E-07
42	1.81437E-07
43	6.65527E-07
44	2.28393E-06
45	1.77868E-07
47	4.39143E-07
48	3.76608E-07
49	1.74244E-07
50	2.73852E-06
S1	2.20475E-07
S2	1.16524E-06
S3	1.30106E-06
S4	1.48167E-06
S5	1.73852E-06
S6	4.15331E-06

Table 4.7.8 Mean permeability rates (cm/sec) of select structures from two PAMPA assays. For more detailed breakdown see **Table 4.7.4**.

Compound #	Value 1 (1st Assay)	Value 2 (1st Assay)	Value 3 (2nd Assay)	Value 4 (2nd Assay)	Mean Permeability	standard deviation
Theophylline	5.50506E-07	4.83665E-07	5.966E-07	6.18784E-07	5.62389E-07	5.96921E-08
Diclofenac	3.42111E-06	3.00558E-06	4.0553E-06	5.29804E-06	3.94501E-06	9.99975E-07
Chloramphenicol	4.4116E-06	3.77755E-06	9.6062E-06	6.06656E-06	5.96548E-06	2.61194E-06
24	1.21507E-06	1.12784E-06	9.09285E-07	3.50685E-06	1.68976E-06	1.2182E-06
26	1.03955E-06	5.67439E-07	4.78383E-07	3.04109E-07	5.97371E-07	2.72296E-07
S5	2.13268E-06	2.67784E-06	6.91806E-07	1.45176E-06	1.73852E-06	8.59366E-07
17	4.83377E-07	4.12442E-07	1.05394E-07	2.39193E-07	3.10102E-07	1.70715E-07
S1	9.67674E-08	2.31138E-08	3.5097E-07	4.11048E-07	2.20475E-07	1.89387E-07
16	7.37655E-06	2.83884E-06	2.45846E-06	2.45846E-06	3.78308E-06	2.40235E-06
4	1.19846E-06	1.02366E-06	4.28999E-07	3.74052E-07	7.56292E-07	4.16422E-07
11	4.60269E-07	4.86662E-07	8.92448E-07	2.74518E-07	5.28474E-07	2.60366E-07
10	8.1878E-07	7.11556E-07	4.01875E-07	2.84903E-07	5.54279E-07	2.51983E-07
13	6.70897E-06	6.13686E-06	7.24281E-07	5.36741E-07	3.52671E-06	3.35327E-06
36	3.83341E-07	2.30465E-07	3.5097E-07	3.5097E-07	3.28936E-07	6.73979E-08
S20	2.50116E-07	1.70253E-07	2.6509E-07	1.6248E-07	2.11985E-07	5.31241E-08
50	3.21103E-06	2.66217E-06	2.36361E-06	2.71726E-06	2.73852E-06	3.51238E-07
40	7.72644E-07	6.71728E-07	3.16438E-07	2.84204E-07	5.11253E-07	2.47374E-07
41	6.23807E-07	5.47747E-07	1.07896E-06	1.34068E-06	8.978E-07	3.77082E-07
S19	7.79745E-07	7.4254E-07	2.74762E-07	8.14067E-08	4.69613E-07	3.46093E-07
S27	1.01154E-06	1.1675E-06	9.66259E-07	6.30554E-07	9.43964E-07	2.26023E-07
9	8.3408E-07	7.82441E-07	1.09354E-06	2.21642E-07	7.32926E-07	3.67033E-07
S2	6.01863E-07	5.32625E-07	1.57178E-06	1.95467E-06	1.16524E-06	7.08538E-07
S3	1.37509E-06	1.13606E-06	1.43846E-06	1.25465E-06	1.30106E-06	1.33841E-07
S4	3.13019E-06	2.54358E-06	1.12293E-07	1.40623E-07	1.48167E-06	1.58313E-06
S28	6.58694E-07	4.42951E-07	1.05919E-06	1.52721E-06	9.22013E-07	4.77467E-07
S6	7.74549E-06	7.07376E-06	1.01577E-06	7.78212E-07	4.15331E-06	3.77131E-06
S29	9.88791E-07	8.93482E-07	1.47417E-05	1.23785E-06	4.46545E-06	5.93431E-06
30	Not Tested	Not Tested	3.5365E-07	3.93963E-07	3.73806E-07	2.85059E-08
49	Not Tested	Not Tested	2.05331E-07	1.43156E-07	1.74244E-07	4.39642E-08
14	Not Tested	Not Tested	6.57418E-07	8.30909E-07	7.44164E-07	1.22677E-07
31	Not Tested	Not Tested	7.63816E-07	3.43168E-07	5.53492E-07	2.97444E-07
44	Not Tested	Not Tested	2.28393E-06	2.28393E-06	2.28393E-06	0
48	Not Tested	Not Tested	2.61088E-07	4.92127E-07	3.76608E-07	1.6337E-07
47	Not Tested	Not Tested	5.03657E-07	3.74629E-07	4.39143E-07	9.12366E-08
S22	Not Tested	Not Tested	2.55718E-07	3.15952E-07	2.85835E-07	4.25921E-08
S24	Not Tested	Not Tested	3.35705E-07	3.93103E-07	3.64404E-07	4.05865E-08
15	Not Tested	Not Tested	1.84053E-06	5.12063E-06	3.48058E-06	2.31938E-06
43	Not Tested	Not Tested	1.07582E-06	2.5523E-07	6.65527E-07	5.80248E-07
S23	Not Tested	Not Tested	4.05224E-07	1.77479E-07	2.91352E-07	1.6104E-07
S21	Not Tested	Not Tested	4.18909E-07	5.45585E-08	2.36734E-07	2.57635E-07
42	Not Tested	Not Tested	1.71775E-07	1.91099E-07	1.81437E-07	1.36642E-08
45	Not Tested	Not Tested	1.94224E-07	1.61512E-07	1.77868E-07	2.31308E-08
35	Not Tested	Not Tested	7.75886E-08	2.88387E-07	1.82988E-07	1.49057E-07
S26	Not Tested	Not Tested	1.03086E-06	3.87156E-07	7.09009E-07	4.55169E-07
S25	Not Tested	Not Tested	5.14857E-07	5.91294E-07	5.53076E-07	5.40486E-08
12	Not Tested	Not Tested	1.28136E-07	9.59019E-08	1.12019E-07	2.27928E-08
19	3.73191E-07	3.47748E-08	1.66028E-07	1.24185E-07	1.74545E-07	1.433E-07

Table 4.7.9 Mean permeability rates (cm/sec) of all compounds from 2nd PAMPA assay averaged out with permeability values from 1st PAMPA assay. Value 1 and 2 reflect first independent PAMPA assay. Value 3 and 4 reflect 2nd independent PAMPA assay.

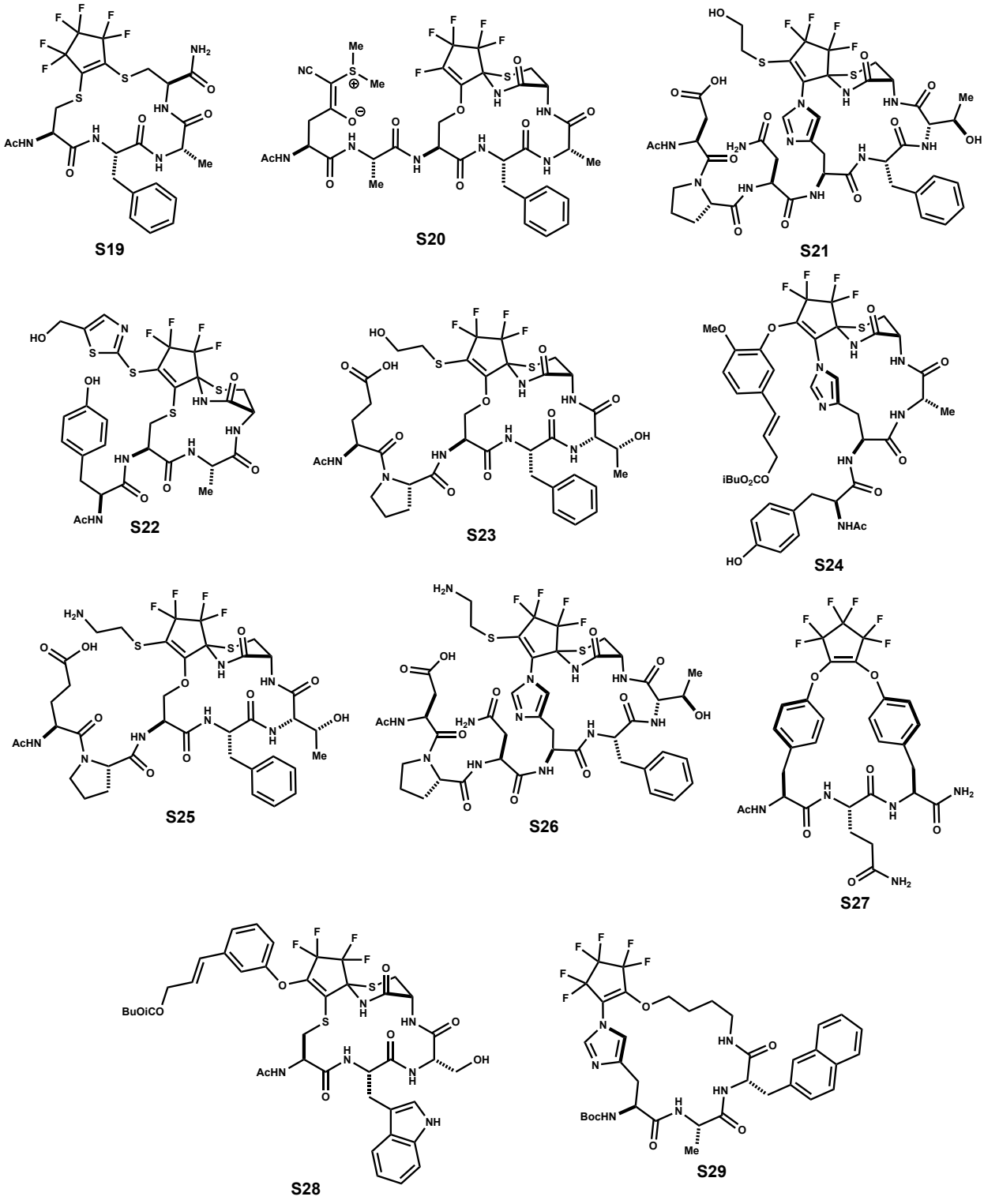

Figure 4.7.21 Figure depicting structures of PAMPA tested compounds **S19**–**S29**.

Compound #	Value 1	Value 2	Mean Permeability	standard deviation
Theophylline	5.966E-07	6.18784E-07	6.07692E-07	1.56864E-08
Diclofenac	4.0553E-06	5.29804E-06	4.67667E-06	8.7875E-07
Chloramphenicol	9.60618E-06	6.06656E-06	7.83637E-06	2.50289E-06
12	1.28136E-07	9.59019E-08	1.12019E-07	2.27928E-08
S4	1.12293E-07	1.40623E-07	1.26458E-07	2.00326E-08
19	1.66028E-07	1.24185E-07	1.45106E-07	2.95874E-08
17	1.05394E-07	2.39193E-07	1.72294E-07	9.46101E-08
49	2.05331E-07	1.43156E-07	1.74244E-07	4.39642E-08
45	1.94224E-07	1.61512E-07	1.77868E-07	2.31308E-08
S19	2.74762E-07	8.14067E-08	1.78084E-07	1.36723E-07
42	1.71775E-07	1.91099E-07	1.81437E-07	1.36642E-08
35	7.75886E-08	2.88387E-07	1.82988E-07	1.49057E-07
S20	2.6509E-07	1.6248E-07	2.13785E-07	7.25569E-08
S21	4.18909E-07	5.45585E-08	2.36734E-07	2.57635E-07
S22	2.55718E-07	3.15952E-07	2.85835E-07	4.25921E-08
S23	4.05224E-07	1.77479E-07	2.91352E-07	1.6104E-07
40	3.16438E-07	2.84204E-07	3.00321E-07	2.27928E-08
10	4.01875E-07	2.84903E-07	3.43389E-07	8.27116E-08
36	3.5097E-07	3.5097E-07	3.5097E-07	0
S24	3.35705E-07	3.93103E-07	3.64404E-07	4.05865E-08
30	3.5365E-07	3.93963E-07	3.73806E-07	2.85059E-08
48	2.61088E-07	4.92127E-07	3.76608E-07	1.6337E-07
S1	3.5097E-07	4.11048E-07	3.81009E-07	4.24816E-08
26	4.78383E-07	3.04109E-07	3.91246E-07	1.2323E-07
4	4.28999E-07	3.74052E-07	4.01526E-07	3.88533E-08
47	5.03657E-07	3.74629E-07	4.39143E-07	9.12366E-08
S25	5.14857E-07	5.91294E-07	5.53076E-07	5.40486E-08
31	7.63816E-07	3.43168E-07	5.53492E-07	2.97444E-07
11	8.92448E-07	2.74518E-07	5.83483E-07	4.36942E-07
13	7.24281E-07	5.36741E-07	6.30511E-07	1.32611E-07
9	1.09354E-06	2.21642E-07	6.57592E-07	6.16526E-07
43	1.07582E-06	2.5523E-07	6.65527E-07	5.80248E-07
S26	1.03086E-06	3.87156E-07	7.09009E-07	4.55169E-07
14	6.57418E-07	8.30909E-07	7.44164E-07	1.22677E-07
S27	9.66259E-07	6.30554E-07	7.98407E-07	2.37379E-07
S6	1.01577E-06	7.78212E-07	8.96991E-07	1.67978E-07
S5	6.91806E-07	1.45176E-06	1.07178E-06	5.37371E-07
41	1.07896E-06	1.34068E-06	1.20982E-06	1.85064E-07
S28	1.05919E-06	1.52721E-06	1.2932E-06	3.30942E-07
S3	1.43846E-06	1.25465E-06	1.34656E-06	1.29979E-07
S2	1.57178E-06	1.95467E-06	1.76323E-06	2.70743E-07
24	9.09285E-07	3.50685E-06	2.20807E-06	1.83676E-06
44	2.28393E-06	2.28393E-06	2.28393E-06	0
24	2.45846E-06	2.45846E-06	2.45846E-06	0
50	2.36361E-06	2.71726E-06	2.54043E-06	2.50068E-07
15	1.84053E-06	5.12063E-06	3.48058E-06	2.31938E-06
S29	1.47417E-05	1.23785E-06	7.98976E-06	9.54864E-06

Table 4.7.10 Permeability rates (cm/sec) of full library for 2nd PAMPA assay (including technical duplicates, permeability average, and standard deviations).

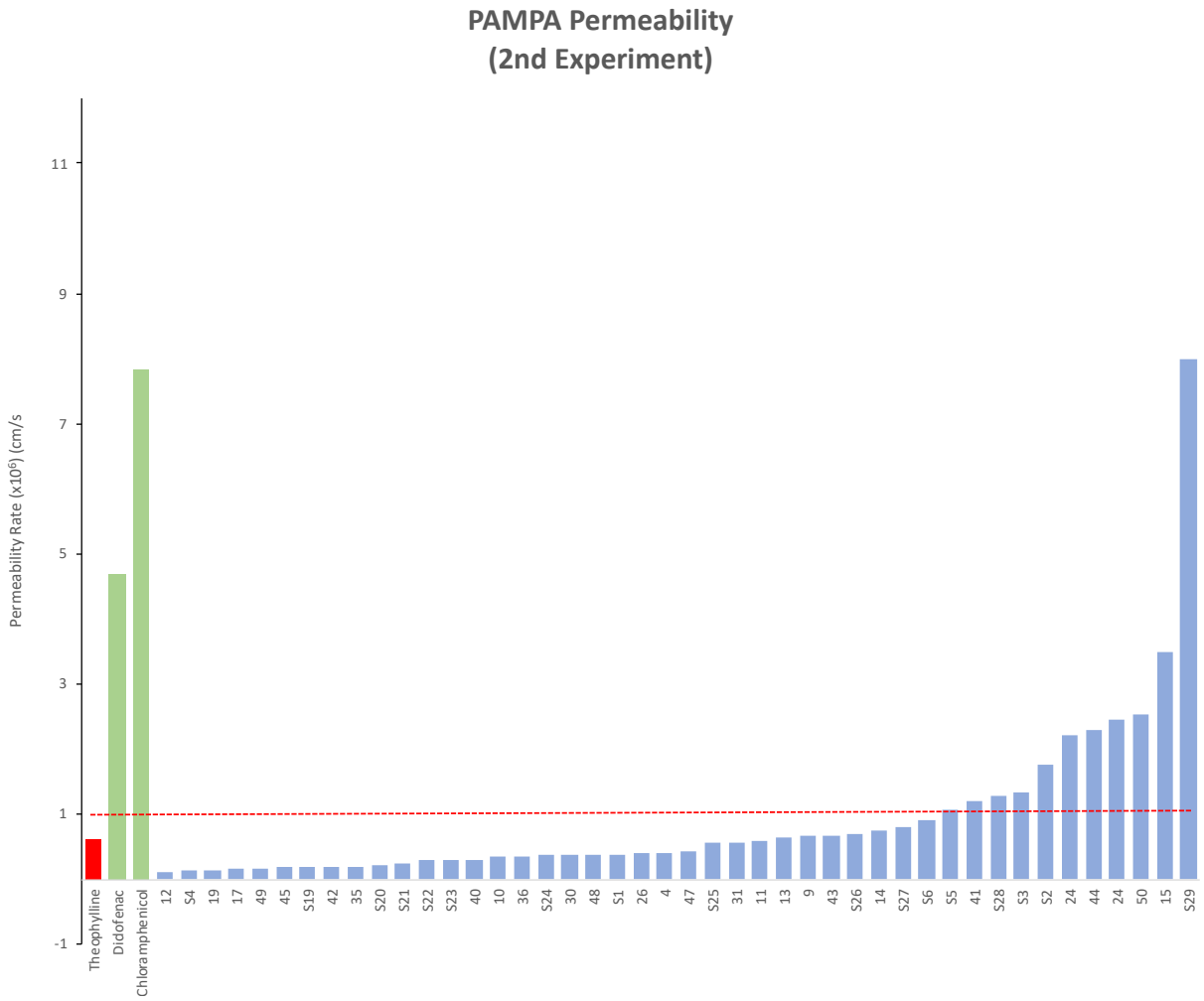

Figure 4.7.22 Graph represents mean permeability values (cm/sec). See **Table 4.7.6** above for a complete list of all compounds tested in 2nd PAMPA assay.

.

Raw Absorbance Data for 1st PAMPA Assay

Wavelength/Well	A1	A2	A3	A4	A5	A6	A7	A8
230	0.11	0.097	0.096	0.104	0.139	0.107	0.106	0.103
240	0.084	0.074	0.076	0.08	0.1	0.082	0.08	0.08
250	0.071	0.063	0.067	0.068	0.084	0.072	0.07	0.07
260	0.061	0.053	0.057	0.058	0.071	0.061	0.06	0.061
270	0.053	0.045	0.051	0.05	0.064	0.054	0.053	0.054
280	0.048	0.041	0.046	0.045	0.058	0.049	0.048	0.05
290	0.044	0.038	0.041	0.041	0.054	0.044	0.044	0.047
300	0.041	0.035	0.038	0.038	0.048	0.041	0.04	0.043
310	0.039	0.033	0.037	0.036	0.044	0.039	0.037	0.04
320	0.038	0.032	0.036	0.034	0.042	0.037	0.034	0.038
330	0.036	0.03	0.034	0.033	0.039	0.036	0.032	0.036
340	0.035	0.029	0.033	0.032	0.038	0.034	0.031	0.034
350	0.034	0.028	0.032	0.03	0.036	0.033	0.03	0.033
360	0.032	0.026	0.031	0.029	0.034	0.031	0.028	0.031
370	0.032	0.026	0.031	0.029	0.034	0.031	0.028	0.032
380	0.042	0.036	0.041	0.038	0.043	0.041	0.038	0.041
390	0.031	0.025	0.03	0.028	0.032	0.03	0.027	0.03
400	0.031	0.026	0.03	0.028	0.032	0.03	0.027	0.03
410	0.03	0.025	0.029	0.028	0.031	0.03	0.027	0.03
420	0.03	0.025	0.029	0.027	0.031	0.03	0.027	0.03
430	0.03	0.025	0.029	0.027	0.031	0.03	0.027	0.03
440	0.03	0.025	0.029	0.027	0.03	0.029	0.027	0.029
450	0.029	0.025	0.028	0.027	0.03	0.029	0.026	0.029
460	0.029	0.025	0.028	0.027	0.03	0.029	0.026	0.029
470	0.029	0.025	0.028	0.027	0.029	0.029	0.026	0.029
480	0.029	0.025	0.028	0.027	0.029	0.028	0.026	0.028
490	0.029	0.025	0.028	0.026	0.029	0.028	0.026	0.029
500	0.028	0.025	0.028	0.026	0.029	0.028	0.026	0.028

Wavelength/Well	**A9**	**A10**	**A11**	**A12**	**B1**	**B2**	**B3**	**B4**
230	0.097	0.103	0.109	0.095	0.103	0.095	0.096	0.097
240	0.074	0.08	0.084	0.074	0.08	0.075	0.076	0.076
250	0.065	0.07	0.074	0.066	0.071	0.067	0.068	0.068
260	0.054	0.06	0.065	0.055	0.061	0.058	0.058	0.058
270	0.047	0.053	0.058	0.048	0.054	0.051	0.051	0.052
280	0.042	0.047	0.053	0.044	0.049	0.046	0.047	0.047
290	0.04	0.042	0.047	0.039	0.045	0.042	0.042	0.043
300	0.037	0.04	0.043	0.037	0.042	0.039	0.04	0.04
310	0.036	0.038	0.041	0.035	0.04	0.037	0.038	0.038
320	0.035	0.036	0.039	0.034	0.038	0.036	0.036	0.036
330	0.033	0.035	0.037	0.032	0.037	0.034	0.034	0.034
340	0.032	0.034	0.035	0.031	0.036	0.033	0.033	0.033
350	0.03	0.032	0.033	0.03	0.034	0.032	0.032	0.032
360	0.028	0.031	0.031	0.029	0.033	0.03	0.03	0.031
370	0.028	0.031	0.031	0.029	0.033	0.031	0.031	0.031
380	0.038	0.04	0.041	0.039	0.042	0.04	0.04	0.04
390	0.027	0.03	0.03	0.028	0.032	0.03	0.03	0.03
400	0.027	0.03	0.03	0.028	0.032	0.03	0.029	0.03
410	0.027	0.029	0.03	0.028	0.031	0.03	0.029	0.029
420	0.027	0.029	0.029	0.028	0.031	0.029	0.029	0.029
430	0.027	0.029	0.029	0.028	0.031	0.029	0.029	0.029
440	0.027	0.029	0.029	0.028	0.03	0.029	0.028	0.029
450	0.027	0.029	0.029	0.028	0.03	0.028	0.028	0.028
460	0.027	0.029	0.029	0.028	0.03	0.028	0.028	0.028
470	0.027	0.028	0.028	0.027	0.03	0.028	0.028	0.028
480	0.026	0.028	0.028	0.027	0.029	0.028	0.028	0.028
490	0.026	0.028	0.028	0.027	0.029	0.028	0.028	0.028
500	0.026	0.028	0.028	0.027	0.029	0.028	0.027	0.028

Wavelength/Well	B5	B6	B7	B8	B9	B10	B11	B12
230	0.094	0.097	0.108	0.103	0.101	0.142	0.094	0.096
240	0.075	0.077	0.084	0.084	0.08	0.099	0.075	0.074
250	0.067	0.071	0.076	0.076	0.071	0.091	0.067	0.065
260	0.057	0.058	0.067	0.067	0.061	0.087	0.058	0.056
270	0.05	0.046	0.06	0.06	0.053	0.081	0.051	0.049
280	0.046	0.038	0.054	0.055	0.048	0.068	0.047	0.045
290	0.042	0.033	0.047	0.049	0.043	0.054	0.042	0.041
300	0.039	0.032	0.044	0.047	0.04	0.046	0.04	0.038
310	0.037	0.031	0.04	0.045	0.038	0.038	0.037	0.036
320	0.035	0.029	0.039	0.043	0.036	0.036	0.036	0.034
330	0.034	0.027	0.037	0.041	0.034	0.034	0.034	0.032
340	0.033	0.026	0.036	0.04	0.034	0.033	0.033	0.031
350	0.031	0.024	0.034	0.039	0.032	0.032	0.032	0.03
360	0.03	0.022	0.032	0.039	0.031	0.03	0.03	0.029
370	0.03	0.021	0.032	0.038	0.031	0.03	0.031	0.029
380	0.04	0.031	0.042	0.047	0.04	0.04	0.04	0.038
390	0.029	0.021	0.031	0.037	0.03	0.029	0.03	0.028
400	0.029	0.021	0.031	0.037	0.03	0.029	0.03	0.028
410	0.028	0.021	0.031	0.036	0.029	0.029	0.029	0.027
420	0.028	0.021	0.03	0.036	0.029	0.028	0.029	0.027
430	0.028	0.021	0.031	0.036	0.029	0.029	0.029	0.027
440	0.028	0.021	0.03	0.036	0.029	0.028	0.029	0.027
450	0.028	0.021	0.03	0.035	0.029	0.028	0.028	0.027
460	0.028	0.021	0.03	0.035	0.029	0.028	0.028	0.027
470	0.027	0.021	0.03	0.035	0.028	0.028	0.028	0.026
480	0.027	0.021	0.029	0.035	0.028	0.027	0.028	0.026
490	0.027	0.021	0.029	0.034	0.028	0.028	0.028	0.026
500	0.027	0.021	0.029	0.034	0.028	0.027	0.028	0.026

Wavelength/Well	C1	C2	C3	C4	C5	C6	C7	C8
230	0.111	0.097	0.102	0.122	0.098	0.095	0.095	0.076
240	0.086	0.077	0.076	0.088	0.077	0.072	0.075	0.062
250	0.075	0.07	0.065	0.075	0.069	0.064	0.068	0.053
260	0.065	0.06	0.055	0.063	0.059	0.054	0.059	0.043
270	0.058	0.053	0.046	0.054	0.051	0.046	0.052	0.034
280	0.053	0.048	0.04	0.05	0.047	0.041	0.047	0.029
290	0.048	0.044	0.034	0.045	0.042	0.037	0.042	0.026
300	0.044	0.041	0.032	0.041	0.039	0.035	0.039	0.025
310	0.042	0.039	0.031	0.037	0.037	0.033	0.037	0.024
320	0.04	0.038	0.03	0.036	0.036	0.032	0.036	0.024
330	0.038	0.036	0.029	0.033	0.034	0.031	0.034	0.022
340	0.037	0.035	0.028	0.032	0.033	0.03	0.034	0.021
350	0.035	0.034	0.026	0.031	0.032	0.029	0.032	0.02
360	0.033	0.032	0.024	0.03	0.03	0.027	0.031	0.019
370	0.034	0.032	0.024	0.03	0.03	0.028	0.032	0.019
380	0.043	0.042	0.035	0.04	0.04	0.037	0.041	0.029
390	0.032	0.031	0.024	0.029	0.03	0.026	0.03	0.019
400	0.032	0.031	0.025	0.029	0.03	0.026	0.031	0.02
410	0.031	0.031	0.024	0.029	0.029	0.026	0.03	0.02
420	0.031	0.03	0.025	0.028	0.029	0.026	0.03	0.02
430	0.031	0.03	0.025	0.028	0.029	0.026	0.03	0.02
440	0.03	0.03	0.025	0.028	0.028	0.026	0.03	0.02
450	0.03	0.03	0.025	0.028	0.028	0.026	0.03	0.02
460	0.03	0.029	0.025	0.028	0.028	0.026	0.029	0.02
470	0.03	0.029	0.025	0.028	0.028	0.026	0.029	0.02
480	0.03	0.029	0.025	0.027	0.028	0.026	0.029	0.02
490	0.03	0.029	0.025	0.027	0.028	0.026	0.029	0.02
500	0.029	0.029	0.025	0.027	0.027	0.025	0.029	0.02

Wavelength/Well	C9	C10	C11	C12	D1	D2	D3	D4
230	0.098	0.094	0.129	0.102	0.115	0.096	0.133	0.136
240	0.07	0.074	0.092	0.081	0.091	0.076	0.082	0.1
250	0.06	0.066	0.081	0.07	0.083	0.068	0.073	0.097
260	0.049	0.057	0.071	0.06	0.073	0.058	0.063	0.089
270	0.041	0.05	0.063	0.052	0.063	0.051	0.055	0.074
280	0.035	0.046	0.054	0.047	0.054	0.047	0.05	0.059
290	0.03	0.041	0.045	0.041	0.048	0.042	0.044	0.051
300	0.028	0.039	0.039	0.039	0.043	0.04	0.04	0.043
310	0.027	0.037	0.036	0.037	0.04	0.038	0.038	0.039
320	0.026	0.036	0.035	0.036	0.038	0.037	0.037	0.038
330	0.025	0.034	0.033	0.035	0.036	0.035	0.035	0.036
340	0.024	0.033	0.032	0.034	0.035	0.034	0.034	0.034
350	0.023	0.032	0.031	0.032	0.034	0.032	0.033	0.033
360	0.022	0.03	0.03	0.031	0.032	0.031	0.031	0.031
370	0.022	0.031	0.03	0.031	0.032	0.031	0.032	0.031
380	0.032	0.04	0.039	0.04	0.042	0.041	0.041	0.041
390	0.022	0.03	0.029	0.03	0.031	0.03	0.03	0.03
400	0.022	0.03	0.029	0.03	0.031	0.03	0.03	0.03
410	0.022	0.029	0.029	0.03	0.03	0.03	0.03	0.029
420	0.022	0.029	0.028	0.03	0.03	0.029	0.03	0.029
430	0.022	0.029	0.028	0.031	0.03	0.029	0.03	0.029
440	0.022	0.029	0.028	0.03	0.029	0.029	0.029	0.028
450	0.022	0.029	0.028	0.03	0.029	0.029	0.029	0.028
460	0.023	0.028	0.028	0.031	0.029	0.028	0.029	0.028
470	0.022	0.028	0.028	0.03	0.029	0.028	0.029	0.028
480	0.022	0.028	0.027	0.03	0.029	0.028	0.029	0.028
490	0.022	0.028	0.027	0.03	0.029	0.028	0.029	0.028
500	0.022	0.028	0.027	0.03	0.028	0.028	0.028	0.028

Wavelength/Well	D5	D6	D7	D8	D9	D10	D11	D12
230	0.292	0.164	0.123	0.358	0.219	0.094	0.093	0.094
240	0.201	0.127	0.097	0.232	0.175	0.073	0.073	0.073
250	0.231	0.133	0.087	0.187	0.194	0.066	0.066	0.065
260	0.221	0.126	0.083	0.222	0.252	0.056	0.056	0.056
270	0.148	0.092	0.083	0.266	0.31	0.049	0.049	0.049
280	0.082	0.068	0.078	0.27	0.327	0.046	0.045	0.045
290	0.059	0.055	0.06	0.213	0.285	0.04	0.041	0.04
300	0.047	0.045	0.054	0.138	0.219	0.038	0.038	0.037
310	0.039	0.04	0.056	0.084	0.155	0.037	0.037	0.036
320	0.037	0.037	0.048	0.056	0.1	0.036	0.035	0.035
330	0.034	0.036	0.039	0.041	0.067	0.035	0.034	0.033
340	0.033	0.034	0.033	0.034	0.051	0.034	0.033	0.032
350	0.032	0.034	0.03	0.031	0.044	0.032	0.032	0.031
360	0.03	0.032	0.029	0.03	0.038	0.031	0.031	0.03
370	0.03	0.032	0.029	0.03	0.036	0.031	0.031	0.03
380	0.04	0.041	0.038	0.039	0.043	0.041	0.04	0.04
390	0.029	0.031	0.028	0.029	0.032	0.03	0.03	0.029
400	0.029	0.031	0.028	0.028	0.031	0.03	0.03	0.029
410	0.029	0.03	0.028	0.028	0.03	0.03	0.03	0.029
420	0.029	0.03	0.027	0.028	0.03	0.03	0.029	0.028
430	0.029	0.03	0.028	0.028	0.03	0.03	0.029	0.028
440	0.028	0.03	0.027	0.028	0.03	0.029	0.029	0.028
450	0.028	0.03	0.027	0.028	0.03	0.029	0.029	0.028
460	0.028	0.029	0.027	0.028	0.03	0.029	0.029	0.028
470	0.028	0.029	0.027	0.027	0.029	0.029	0.029	0.028
480	0.028	0.029	0.027	0.027	0.029	0.028	0.028	0.027
490	0.028	0.029	0.027	0.027	0.029	0.029	0.028	0.027
500	0.028	0.029	0.026	0.027	0.029	0.028	0.028	0.027

Wavelength/Well	E1	E2	E3	E4	E5	E6	E7	E8
230	0.089	0.108	0.084	0.097	0.096	0.094	0.096	0.089
240	0.068	0.078	0.062	0.073	0.075	0.073	0.074	0.067
250	0.058	0.068	0.054	0.066	0.066	0.066	0.066	0.058
260	0.047	0.057	0.043	0.057	0.057	0.056	0.057	0.047
270	0.04	0.05	0.034	0.049	0.05	0.05	0.05	0.039
280	0.035	0.045	0.03	0.044	0.044	0.045	0.046	0.034
290	0.032	0.042	0.026	0.039	0.041	0.041	0.041	0.03
300	0.031	0.039	0.026	0.037	0.038	0.039	0.039	0.029
310	0.029	0.037	0.025	0.035	0.036	0.037	0.037	0.028
320	0.028	0.036	0.024	0.033	0.035	0.036	0.036	0.026
330	0.027	0.034	0.022	0.031	0.033	0.034	0.034	0.025
340	0.026	0.033	0.021	0.03	0.032	0.033	0.033	0.024
350	0.025	0.032	0.02	0.029	0.031	0.032	0.032	0.023
360	0.023	0.03	0.019	0.028	0.03	0.03	0.03	0.021
370	0.023	0.031	0.019	0.028	0.03	0.03	0.03	0.021
380	0.033	0.04	0.028	0.037	0.039	0.04	0.04	0.031
390	0.023	0.03	0.019	0.027	0.029	0.03	0.03	0.021
400	0.023	0.03	0.019	0.027	0.029	0.03	0.03	0.021
410	0.023	0.029	0.019	0.027	0.029	0.03	0.029	0.021
420	0.023	0.029	0.019	0.026	0.029	0.029	0.029	0.021
430	0.023	0.029	0.02	0.026	0.029	0.029	0.029	0.021
440	0.023	0.029	0.02	0.026	0.028	0.029	0.029	0.022
450	0.023	0.028	0.02	0.026	0.028	0.029	0.029	0.021
460	0.023	0.028	0.02	0.026	0.028	0.029	0.028	0.022
470	0.023	0.028	0.02	0.026	0.028	0.029	0.028	0.021
480	0.023	0.028	0.02	0.026	0.028	0.028	0.028	0.021
490	0.023	0.028	0.02	0.026	0.028	0.028	0.028	0.022
500	0.023	0.028	0.02	0.025	0.028	0.028	0.028	0.022

Wavelength/Well	E9	E10	E11	E12	F1	F2	F3	F4
230	0.086	0.096	0.096	0.094	0.091	0.089	0.094	0.096
240	0.067	0.075	0.075	0.074	0.072	0.073	0.077	0.073
250	0.059	0.067	0.067	0.065	0.065	0.066	0.072	0.065
260	0.048	0.057	0.058	0.056	0.056	0.056	0.061	0.057
270	0.041	0.051	0.051	0.049	0.049	0.049	0.05	0.049
280	0.036	0.046	0.047	0.045	0.044	0.045	0.045	0.042
290	0.033	0.041	0.042	0.04	0.04	0.04	0.041	0.038
300	0.031	0.039	0.04	0.038	0.038	0.039	0.039	0.036
310	0.03	0.037	0.038	0.036	0.036	0.037	0.037	0.034
320	0.029	0.035	0.037	0.035	0.034	0.037	0.036	0.032
330	0.027	0.034	0.035	0.033	0.033	0.035	0.034	0.031
340	0.026	0.033	0.034	0.032	0.032	0.034	0.033	0.029
350	0.025	0.032	0.033	0.031	0.031	0.033	0.031	0.028
360	0.024	0.03	0.031	0.03	0.03	0.032	0.029	0.027
370	0.024	0.03	0.032	0.03	0.03	0.032	0.028	0.026
380	0.034	0.04	0.041	0.039	0.04	0.042	0.038	0.036
390	0.023	0.03	0.031	0.029	0.029	0.031	0.028	0.025
400	0.024	0.03	0.031	0.029	0.029	0.031	0.028	0.025
410	0.023	0.03	0.03	0.029	0.029	0.031	0.027	0.025
420	0.023	0.029	0.03	0.028	0.028	0.031	0.027	0.025
430	0.024	0.029	0.03	0.028	0.028	0.031	0.027	0.025
440	0.023	0.029	0.03	0.028	0.028	0.03	0.027	0.025
450	0.023	0.029	0.03	0.028	0.028	0.03	0.026	0.025
460	0.023	0.028	0.029	0.028	0.028	0.03	0.026	0.025
470	0.023	0.028	0.029	0.028	0.028	0.03	0.026	0.024
480	0.023	0.028	0.029	0.027	0.027	0.029	0.026	0.024
490	0.023	0.028	0.029	0.028	0.028	0.03	0.026	0.024
500	0.023	0.028	0.029	0.027	0.027	0.029	0.026	0.024

Wavelength/Well	F5	F6	F7	F8	F9	F10	F11	F12
230	0.09	0.089	0.128	0.088	0.088	0.105	0.09	0.097
240	0.072	0.071	0.092	0.071	0.071	0.081	0.07	0.072
250	0.065	0.064	0.085	0.064	0.063	0.071	0.062	0.061
260	0.055	0.055	0.08	0.055	0.054	0.061	0.052	0.05
270	0.049	0.048	0.074	0.049	0.048	0.054	0.045	0.043
280	0.044	0.044	0.063	0.044	0.043	0.049	0.04	0.038
290	0.04	0.04	0.05	0.04	0.04	0.045	0.036	0.034
300	0.038	0.038	0.044	0.037	0.037	0.042	0.034	0.032
310	0.036	0.036	0.038	0.036	0.035	0.04	0.032	0.031
320	0.035	0.034	0.035	0.034	0.034	0.038	0.031	0.03
330	0.033	0.033	0.033	0.033	0.033	0.036	0.03	0.028
340	0.032	0.032	0.032	0.032	0.032	0.035	0.029	0.027
350	0.031	0.031	0.031	0.031	0.03	0.034	0.028	0.026
360	0.03	0.029	0.03	0.029	0.029	0.032	0.027	0.025
370	0.03	0.03	0.03	0.03	0.029	0.032	0.027	0.025
380	0.039	0.039	0.039	0.039	0.039	0.042	0.036	0.034
390	0.029	0.029	0.029	0.028	0.028	0.031	0.026	0.024
400	0.029	0.028	0.029	0.028	0.028	0.031	0.026	0.024
410	0.028	0.028	0.028	0.028	0.028	0.031	0.026	0.024
420	0.028	0.028	0.028	0.028	0.028	0.03	0.026	0.024
430	0.028	0.028	0.028	0.028	0.028	0.031	0.026	0.024
440	0.028	0.028	0.028	0.028	0.028	0.03	0.025	0.024
450	0.028	0.027	0.028	0.027	0.027	0.03	0.025	0.024
460	0.028	0.028	0.028	0.027	0.027	0.03	0.025	0.024
470	0.027	0.027	0.027	0.027	0.027	0.03	0.025	0.024
480	0.027	0.027	0.027	0.027	0.027	0.03	0.025	0.024
490	0.027	0.027	0.027	0.027	0.027	0.03	0.025	0.024
500	0.027	0.027	0.027	0.027	0.027	0.029	0.025	0.024

Wavelength/Well	G1	G2	G3	G4	G5	G6	G7	G8
230	0.12	0.097	0.093	0.097	0.089	0.095	0.092	0.118
240	0.088	0.077	0.072	0.077	0.072	0.074	0.072	0.087
250	0.074	0.068	0.065	0.068	0.064	0.065	0.064	0.076
260	0.062	0.058	0.056	0.058	0.055	0.056	0.055	0.066
270	0.053	0.05	0.048	0.052	0.049	0.049	0.048	0.058
280	0.048	0.045	0.044	0.046	0.044	0.045	0.044	0.051
290	0.043	0.041	0.04	0.042	0.04	0.04	0.04	0.043
300	0.039	0.038	0.038	0.039	0.038	0.037	0.037	0.038
310	0.037	0.036	0.036	0.037	0.036	0.036	0.036	0.036
320	0.035	0.035	0.035	0.036	0.034	0.034	0.034	0.034
330	0.034	0.033	0.033	0.034	0.033	0.033	0.033	0.033
340	0.033	0.032	0.032	0.033	0.032	0.032	0.032	0.032
350	0.032	0.031	0.031	0.032	0.031	0.031	0.031	0.031
360	0.03	0.03	0.03	0.031	0.03	0.03	0.03	0.03
370	0.03	0.03	0.03	0.031	0.03	0.03	0.03	0.03
380	0.04	0.039	0.039	0.04	0.039	0.039	0.039	0.039
390	0.029	0.029	0.029	0.03	0.029	0.029	0.029	0.029
400	0.029	0.029	0.029	0.03	0.029	0.029	0.029	0.029
410	0.029	0.029	0.028	0.029	0.029	0.029	0.028	0.028
420	0.028	0.029	0.028	0.029	0.028	0.028	0.028	0.028
430	0.029	0.028	0.028	0.029	0.028	0.028	0.028	0.028
440	0.028	0.028	0.028	0.028	0.028	0.028	0.028	0.028
450	0.028	0.028	0.028	0.028	0.028	0.028	0.028	0.028
460	0.028	0.028	0.027	0.028	0.028	0.028	0.028	0.028
470	0.028	0.028	0.027	0.028	0.028	0.028	0.028	0.028
480	0.028	0.028	0.027	0.028	0.028	0.028	0.027	0.027
490	0.028	0.027	0.027	0.028	0.028	0.027	0.027	0.027
500	0.027	0.027	0.027	0.028	0.027	0.027	0.027	0.027

Wavelength/Well	G9	G10	G11	G12	H1	H2	H3	H4	H5	H6
230	0.089	0.093	0.096	0.106	0.11	0.32	0.161	0.12	0.334	0.199
240	0.071	0.074	0.075	0.078	0.083	0.218	0.126	0.095	0.218	0.16
250	0.064	0.067	0.066	0.068	0.077	0.252	0.129	0.084	0.175	0.176
260	0.055	0.057	0.057	0.058	0.068	0.241	0.121	0.078	0.204	0.227
270	0.048	0.05	0.05	0.052	0.058	0.158	0.09	0.077	0.243	0.279
280	0.044	0.046	0.046	0.048	0.05	0.081	0.069	0.072	0.246	0.295
290	0.039	0.041	0.042	0.042	0.044	0.055	0.056	0.056	0.196	0.257
300	0.037	0.038	0.039	0.039	0.039	0.042	0.046	0.051	0.128	0.198
310	0.035	0.036	0.037	0.038	0.037	0.033	0.041	0.053	0.08	0.141
320	0.034	0.035	0.035	0.036	0.035	0.031	0.039	0.047	0.054	0.091
330	0.033	0.033	0.034	0.035	0.034	0.029	0.038	0.038	0.041	0.06
340	0.032	0.032	0.033	0.034	0.032	0.028	0.036	0.032	0.034	0.046
350	0.031	0.031	0.032	0.033	0.032	0.027	0.035	0.03	0.032	0.039
360	0.029	0.03	0.03	0.032	0.03	0.025	0.034	0.029	0.03	0.034
370	0.029	0.03	0.03	0.032	0.03	0.025	0.034	0.029	0.03	0.032
380	0.039	0.039	0.04	0.041	0.04	0.034	0.043	0.038	0.04	0.039
390	0.029	0.029	0.03	0.031	0.029	0.024	0.032	0.028	0.029	0.028
400	0.028	0.029	0.029	0.031	0.029	0.024	0.032	0.028	0.029	0.027
410	0.028	0.028	0.029	0.031	0.029	0.024	0.032	0.027	0.029	0.027
420	0.028	0.028	0.029	0.03	0.028	0.024	0.031	0.027	0.028	0.027
430	0.028	0.028	0.029	0.03	0.028	0.024	0.031	0.027	0.028	0.027
440	0.028	0.028	0.028	0.03	0.028	0.024	0.031	0.027	0.028	0.026
450	0.028	0.028	0.028	0.03	0.028	0.024	0.031	0.027	0.028	0.026
460	0.028	0.028	0.028	0.03	0.028	0.024	0.03	0.027	0.028	0.026
470	0.028	0.028	0.028	0.03	0.028	0.024	0.03	0.027	0.028	0.026
480	0.027	0.028	0.028	0.029	0.027	0.024	0.03	0.026	0.028	0.026
490	0.027	0.028	0.028	0.029	0.028	0.024	0.03	0.026	0.027	0.026
500	0.027	0.028	0.028	0.029	0.027	0.024	0.03	0.026	0.027	0.026

Raw Equilibrium Solutions for 1st PAMPA Assay

Wavelength/Well	A1	A2	A3	A4	A5	A6	A7	A8
230	1.934	1.313	1.648	1.488	1.529	1.92	1.656	1.487
240	0.62	0.2	0.22	0.302	0.339	0.39	0.389	0.327
250	0.527	0.196	0.155	0.232	0.266	0.313	0.329	0.293
260	0.531	0.265	0.145	0.238	0.274	0.368	0.351	0.31
270	0.521	0.363	0.124	0.248	0.286	0.437	0.414	0.341
280	0.478	0.443	0.085	0.232	0.274	0.473	0.478	0.389
290	0.374	0.412	0.052	0.175	0.217	0.43	0.467	0.392
300	0.241	0.248	0.039	0.08	0.12	0.283	0.37	0.332
310	0.199	0.098	0.035	0.056	0.092	0.198	0.239	0.238
320	0.176	0.051	0.033	0.05	0.082	0.119	0.158	0.163
330	0.169	0.043	0.031	0.048	0.075	0.07	0.127	0.12
340	0.158	0.042	0.03	0.047	0.07	0.054	0.11	0.105
350	0.156	0.042	0.029	0.045	0.067	0.049	0.102	0.102
360	0.154	0.041	0.027	0.041	0.063	0.046	0.096	0.097
370	0.143	0.04	0.025	0.038	0.06	0.043	0.089	0.086
380	0.139	0.048	0.033	0.045	0.067	0.05	0.091	0.084
390	0.123	0.034	0.022	0.033	0.054	0.037	0.078	0.064
400	0.114	0.033	0.022	0.032	0.051	0.036	0.074	0.059
410	0.108	0.033	0.022	0.032	0.049	0.034	0.071	0.055
420	0.103	0.032	0.022	0.031	0.047	0.034	0.069	0.052
430	0.096	0.032	0.022	0.03	0.046	0.033	0.066	0.051
440	0.092	0.031	0.022	0.03	0.044	0.032	0.064	0.049
450	0.088	0.03	0.022	0.029	0.043	0.031	0.062	0.047
460	0.085	0.03	0.022	0.029	0.041	0.031	0.06	0.045
470	0.081	0.03	0.022	0.029	0.041	0.03	0.058	0.044
480	0.078	0.029	0.022	0.029	0.04	0.03	0.057	0.043
490	0.075	0.029	0.021	0.028	0.039	0.03	0.055	0.042
500	0.073	0.029	0.022	0.028	0.038	0.03	0.055	0.042

Wavelength/Well	A9	A10	A11	A12	B1	B2	B3	B4
230	1.354	1.777	3.416	1.436	1.641	1.612	1.456	1.354
240	0.248	0.351	2.159	0.201	0.371	0.554	0.297	0.246
250	0.191	0.288	1.947	0.137	0.243	0.475	0.202	0.208
260	0.167	0.342	1.948	0.104	0.198	0.398	0.178	0.219
270	0.125	0.378	2.028	0.075	0.185	0.355	0.169	0.236
280	0.086	0.346	2.035	0.054	0.16	0.339	0.177	0.226
290	0.06	0.24	1.778	0.043	0.12	0.307	0.185	0.177
300	0.047	0.091	1.713	0.039	0.091	0.242	0.163	0.128
310	0.041	0.06	1.662	0.036	0.067	0.16	0.118	0.082
320	0.038	0.055	1.56	0.035	0.054	0.101	0.075	0.055
330	0.036	0.051	1.464	0.034	0.047	0.075	0.054	0.044
340	0.035	0.047	1.303	0.032	0.044	0.065	0.046	0.04
350	0.033	0.043	1.17	0.03	0.041	0.06	0.042	0.038
360	0.031	0.04	1.058	0.028	0.039	0.055	0.04	0.036
370	0.031	0.039	0.942	0.027	0.038	0.05	0.038	0.035
380	0.04	0.048	0.867	0.037	0.046	0.055	0.046	0.043
390	0.029	0.036	0.816	0.026	0.035	0.04	0.034	0.031
400	0.029	0.035	0.762	0.026	0.035	0.038	0.033	0.031
410	0.029	0.034	0.723	0.025	0.034	0.037	0.032	0.03
420	0.028	0.032	0.689	0.025	0.034	0.036	0.031	0.029
430	0.028	0.032	0.65	0.025	0.034	0.035	0.031	0.03
440	0.028	0.032	0.622	0.025	0.033	0.034	0.03	0.029
450	0.028	0.031	0.595	0.025	0.032	0.033	0.03	0.029
460	0.028	0.03	0.57	0.025	0.032	0.032	0.029	0.028
470	0.027	0.03	0.545	0.025	0.032	0.032	0.029	0.028
480	0.027	0.03	0.524	0.024	0.032	0.032	0.029	0.028
490	0.027	0.03	0.501	0.024	0.032	0.031	0.029	0.028
500	0.027	0.03	0.484	0.024	0.032	0.031	0.028	0.027

Wavelength/Well	B5	B6	B7	B8	B9	B10	B11	B12
230	1.01	1.414	2.041	1.666	1.544	1.188	1.206	1.15
240	0.136	0.274	0.748	0.364	0.517	0.222	0.189	0.217
250	0.089	0.292	0.605	0.278	0.627	0.177	0.132	0.167
260	0.072	0.352	0.618	0.277	0.638	0.18	0.137	0.194
270	0.063	0.318	0.61	0.289	0.492	0.176	0.159	0.231
280	0.053	0.225	0.552	0.285	0.278	0.145	0.181	0.247
290	0.041	0.167	0.464	0.239	0.116	0.102	0.194	0.228
300	0.037	0.14	0.369	0.147	0.075	0.078	0.175	0.187
310	0.035	0.114	0.283	0.108	0.063	0.055	0.129	0.136
320	0.033	0.094	0.214	0.081	0.057	0.047	0.082	0.092
330	0.031	0.083	0.166	0.061	0.053	0.043	0.059	0.075
340	0.03	0.077	0.133	0.05	0.05	0.04	0.048	0.066
350	0.028	0.067	0.109	0.043	0.047	0.039	0.044	0.064
360	0.027	0.051	0.094	0.038	0.043	0.037	0.042	0.064
370	0.027	0.039	0.085	0.036	0.041	0.037	0.041	0.061
380	0.036	0.043	0.087	0.043	0.048	0.046	0.049	0.066
390	0.026	0.03	0.071	0.031	0.036	0.035	0.039	0.056
400	0.026	0.029	0.066	0.03	0.034	0.034	0.038	0.055
410	0.026	0.028	0.06	0.029	0.033	0.034	0.038	0.055
420	0.025	0.027	0.056	0.028	0.032	0.033	0.038	0.054
430	0.025	0.026	0.052	0.028	0.032	0.033	0.037	0.052
440	0.025	0.026	0.049	0.028	0.031	0.032	0.036	0.052
450	0.025	0.025	0.046	0.027	0.03	0.032	0.036	0.051
460	0.025	0.025	0.044	0.027	0.03	0.032	0.036	0.05
470	0.025	0.024	0.042	0.027	0.029	0.031	0.035	0.05
480	0.025	0.024	0.04	0.026	0.029	0.031	0.035	0.049
490	0.024	0.024	0.039	0.026	0.029	0.031	0.034	0.048
500	0.025	0.024	0.038	0.026	0.029	0.031	0.035	0.049

Wavelength/Well	C1	C2	C3	C4	C5	C6	C7	C8
230	2.807	1.697	1.716	1.306	1.499	1.33	1.327	1.399
240	1.324	0.618	0.498	0.325	0.342	0.292	0.232	0.232
250	1.16	0.61	0.41	0.272	0.314	0.208	0.196	0.194
260	1.161	0.566	0.45	0.266	0.35	0.167	0.208	0.207
270	1.246	0.426	0.466	0.261	0.295	0.146	0.197	0.179
280	1.251	0.256	0.416	0.247	0.191	0.114	0.148	0.118
290	1.017	0.11	0.313	0.227	0.1	0.098	0.085	0.069
300	0.7	0.062	0.165	0.205	0.064	0.089	0.054	0.049
310	0.544	0.048	0.112	0.175	0.049	0.082	0.043	0.044
320	0.475	0.042	0.096	0.125	0.042	0.073	0.039	0.04
330	0.446	0.04	0.085	0.108	0.038	0.07	0.037	0.038
340	0.414	0.039	0.077	0.096	0.036	0.066	0.037	0.036
350	0.39	0.038	0.069	0.096	0.034	0.065	0.036	0.035
360	0.369	0.036	0.062	0.095	0.032	0.063	0.035	0.035
370	0.326	0.036	0.059	0.09	0.032	0.061	0.033	0.033
380	0.301	0.045	0.067	0.092	0.041	0.066	0.041	0.041
390	0.268	0.034	0.054	0.084	0.03	0.056	0.03	0.031
400	0.24	0.034	0.052	0.082	0.03	0.055	0.029	0.031
410	0.219	0.034	0.05	0.082	0.029	0.054	0.029	0.031
420	0.202	0.033	0.048	0.083	0.029	0.052	0.028	0.031
430	0.186	0.033	0.047	0.078	0.029	0.05	0.028	0.031
440	0.172	0.033	0.046	0.079	0.028	0.049	0.028	0.031
450	0.158	0.032	0.044	0.078	0.028	0.048	0.028	0.031
460	0.147	0.032	0.044	0.078	0.028	0.047	0.027	0.031
470	0.135	0.032	0.042	0.076	0.028	0.046	0.027	0.031
480	0.126	0.031	0.041	0.079	0.027	0.046	0.027	0.031
490	0.118	0.031	0.041	0.073	0.027	0.044	0.027	0.03
500	0.111	0.031	0.04	0.075	0.027	0.045	0.027	0.031

Wavelength/Well	C9	C10	C11	C12	D1	D2	D3	D4
230	1.413	1.837	1.418	1.349	1.628	1.572	1.637	2.542
240	0.334	0.481	0.299	0.15	0.481	0.144	0.332	1.433
250	0.28	0.331	0.241	0.095	0.418	0.077	0.26	1.386
260	0.292	0.285	0.236	0.085	0.412	0.064	0.24	1.417
270	0.287	0.264	0.222	0.085	0.364	0.062	0.229	1.384
280	0.217	0.268	0.173	0.085	0.288	0.053	0.211	1.289
290	0.118	0.261	0.112	0.078	0.295	0.038	0.158	1.037
300	0.065	0.211	0.073	0.06	0.223	0.034	0.124	0.85
310	0.049	0.13	0.059	0.047	0.17	0.031	0.108	0.66
320	0.044	0.065	0.052	0.04	0.125	0.027	0.093	0.567
330	0.042	0.04	0.051	0.037	0.12	0.025	0.086	0.522
340	0.04	0.034	0.051	0.034	0.108	0.024	0.08	0.475
350	0.038	0.031	0.053	0.033	0.11	0.023	0.078	0.447
360	0.037	0.029	0.053	0.031	0.11	0.022	0.075	0.424
370	0.036	0.029	0.05	0.031	0.1	0.021	0.071	0.389
380	0.045	0.039	0.054	0.04	0.093	0.031	0.076	0.37
390	0.034	0.028	0.042	0.029	0.083	0.021	0.065	0.342
400	0.033	0.028	0.041	0.029	0.077	0.021	0.062	0.317
410	0.032	0.027	0.04	0.029	0.075	0.021	0.059	0.298
420	0.032	0.027	0.039	0.029	0.072	0.021	0.058	0.282
430	0.032	0.027	0.038	0.028	0.066	0.021	0.055	0.265
440	0.031	0.027	0.037	0.028	0.064	0.022	0.054	0.252
450	0.031	0.027	0.036	0.028	0.062	0.021	0.052	0.238
460	0.03	0.026	0.036	0.028	0.059	0.021	0.05	0.227
470	0.03	0.026	0.035	0.028	0.058	0.021	0.049	0.214
480	0.03	0.026	0.035	0.028	0.057	0.021	0.047	0.204
490	0.03	0.026	0.034	0.027	0.053	0.021	0.046	0.195
500	0.03	0.026	0.034	0.028	0.054	0.021	0.045	0.186

Wavelength/Well	D5	D6	D7	D8	D9	D10
230	1.603	1.828	1.936	2.232	1.801	1.493
240	0.393	0.713	0.361	0.586	0.368	0.122
250	0.42	0.715	0.343	0.411	0.373	0.06
260	0.402	0.732	0.568	0.525	0.519	0.042
270	0.26	0.639	0.773	0.676	0.668	0.032
280	0.135	0.467	0.649	0.704	0.718	0.028
290	0.09	0.392	0.221	0.548	0.621	0.026
300	0.068	0.341	0.074	0.327	0.462	0.025
310	0.05	0.3	0.071	0.162	0.31	0.024
320	0.044	0.247	0.057	0.079	0.178	0.023
330	0.038	0.247	0.04	0.046	0.103	0.022
340	0.034	0.221	0.029	0.032	0.068	0.021
350	0.032	0.225	0.026	0.029	0.052	0.02
360	0.03	0.228	0.024	0.027	0.041	0.018
370	0.03	0.203	0.024	0.026	0.033	0.018
380	0.04	0.184	0.033	0.035	0.038	0.028
390	0.029	0.179	0.023	0.025	0.025	0.018
400	0.029	0.165	0.024	0.025	0.024	0.019
410	0.028	0.161	0.024	0.025	0.023	0.019
420	0.028	0.154	0.024	0.025	0.023	0.019
430	0.028	0.141	0.024	0.025	0.023	0.019
440	0.028	0.136	0.024	0.025	0.023	0.019
450	0.027	0.13	0.024	0.025	0.023	0.019
460	0.028	0.125	0.024	0.025	0.023	0.019
470	0.027	0.12	0.024	0.025	0.023	0.019
480	0.027	0.116	0.023	0.025	0.023	0.019
490	0.027	0.108	0.023	0.024	0.023	0.019
500	0.027	0.108	0.023	0.024	0.023	0.02

Raw Absorbance Data for 2nd PAMPA Assay

Wavelength	A1	A2	A3	A4	A5	A6	A7	A8
230	0.106	0.097	0.093	0.094	0.145	0.238	0.093	0.085
240	0.077	0.07	0.068	0.074	0.093	0.094	0.076	0.067
250	0.068	0.061	0.06	0.065	0.077	0.074	0.068	0.059
260	0.059	0.052	0.049	0.056	0.064	0.057	0.059	0.049
270	0.051	0.044	0.042	0.048	0.056	0.048	0.053	0.041
280	0.048	0.04	0.038	0.043	0.05	0.044	0.05	0.037
290	0.044	0.037	0.036	0.041	0.044	0.04	0.044	0.036
300	0.042	0.035	0.034	0.038	0.041	0.037	0.042	0.034
310	0.04	0.033	0.033	0.036	0.038	0.035	0.04	0.032
320	0.039	0.031	0.032	0.034	0.036	0.034	0.038	0.031
330	0.037	0.029	0.03	0.033	0.034	0.032	0.036	0.03
340	0.035	0.028	0.029	0.031	0.032	0.031	0.036	0.029
350	0.034	0.027	0.028	0.03	0.031	0.029	0.034	0.027
360	0.032	0.026	0.026	0.029	0.029	0.028	0.033	0.026
370	0.032	0.026	0.026	0.029	0.029	0.028	0.033	0.026
380	0.042	0.035	0.036	0.038	0.038	0.038	0.042	0.036
390	0.03	0.024	0.025	0.027	0.027	0.027	0.032	0.025
400	0.03	0.024	0.025	0.027	0.027	0.027	0.032	0.025
410	0.03	0.024	0.025	0.027	0.027	0.027	0.031	0.025
420	0.03	0.024	0.025	0.027	0.027	0.027	0.031	0.025
430	0.03	0.025	0.025	0.027	0.027	0.027	0.031	0.025
440	0.03	0.025	0.025	0.027	0.027	0.027	0.031	0.025
450	0.029	0.024	0.025	0.026	0.026	0.026	0.03	0.025
460	0.029	0.024	0.025	0.026	0.026	0.026	0.03	0.025
470	0.029	0.024	0.025	0.026	0.026	0.026	0.03	0.025
480	0.029	0.024	0.025	0.026	0.026	0.026	0.03	0.024
490	0.029	0.024	0.025	0.026	0.026	0.026	0.03	0.025
500	0.029	0.024	0.025	0.026	0.026	0.026	0.03	0.024

A9	A10	A11	A12	B1	B2	B3	B4	B5	B6
0.096	0.087	0.131	0.244	0.102	0.094	0.104	0.092	0.096	0.095
0.07	0.069	0.087	0.112	0.074	0.071	0.077	0.069	0.07	0.07
0.061	0.06	0.073	0.09	0.065	0.062	0.066	0.059	0.061	0.061
0.051	0.049	0.062	0.073	0.055	0.053	0.054	0.048	0.051	0.049
0.044	0.042	0.056	0.062	0.047	0.046	0.046	0.041	0.043	0.041
0.04	0.037	0.051	0.056	0.042	0.042	0.043	0.036	0.039	0.037
0.038	0.034	0.048	0.052	0.04	0.038	0.04	0.033	0.036	0.033
0.036	0.033	0.045	0.049	0.038	0.036	0.038	0.032	0.034	0.031
0.034	0.031	0.042	0.046	0.036	0.034	0.036	0.03	0.032	0.03
0.033	0.029	0.041	0.043	0.034	0.033	0.034	0.029	0.031	0.029
0.032	0.028	0.038	0.041	0.033	0.031	0.031	0.027	0.03	0.027
0.031	0.026	0.037	0.039	0.032	0.03	0.03	0.026	0.029	0.026
0.029	0.025	0.035	0.037	0.03	0.029	0.028	0.025	0.027	0.025
0.028	0.024	0.033	0.036	0.029	0.027	0.027	0.024	0.026	0.024
0.028	0.024	0.033	0.035	0.029	0.027	0.026	0.024	0.026	0.024
0.038	0.033	0.043	0.044	0.038	0.037	0.036	0.033	0.036	0.033
0.027	0.023	0.031	0.033	0.028	0.026	0.025	0.023	0.025	0.023
0.026	0.022	0.031	0.032	0.028	0.026	0.025	0.023	0.024	0.023
0.027	0.023	0.031	0.032	0.028	0.026	0.025	0.023	0.025	0.024
0.026	0.023	0.03	0.032	0.028	0.026	0.025	0.023	0.025	0.023
0.027	0.023	0.031	0.032	0.027	0.026	0.025	0.023	0.025	0.024
0.027	0.023	0.03	0.031	0.027	0.026	0.025	0.023	0.025	0.024
0.027	0.023	0.03	0.031	0.027	0.026	0.025	0.023	0.025	0.024
0.026	0.023	0.029	0.031	0.027	0.026	0.025	0.023	0.025	0.024
0.026	0.023	0.029	0.03	0.027	0.026	0.025	0.023	0.025	0.024
0.026	0.023	0.029	0.03	0.027	0.026	0.025	0.023	0.025	0.024
0.027	0.023	0.029	0.03	0.027	0.026	0.025	0.023	0.025	0.024
0.026	0.023	0.029	0.03	0.027	0.026	0.024	0.023	0.025	0.024

B7	B8	B9	B10	B11	B12	C1	C2	C3
0.096	0.095	0.106	0.108	0.096	0.097	0.095	0.099	0.098
0.071	0.069	0.078	0.071	0.071	0.076	0.074	0.071	0.073
0.062	0.06	0.068	0.06	0.062	0.068	0.066	0.062	0.065
0.052	0.051	0.057	0.05	0.052	0.058	0.056	0.052	0.056
0.044	0.044	0.049	0.042	0.045	0.051	0.049	0.044	0.05
0.04	0.039	0.046	0.037	0.041	0.046	0.046	0.039	0.045
0.04	0.036	0.043	0.034	0.039	0.042	0.042	0.036	0.04
0.038	0.034	0.041	0.033	0.037	0.039	0.04	0.034	0.037
0.036	0.032	0.039	0.031	0.035	0.037	0.038	0.033	0.035
0.034	0.03	0.037	0.03	0.034	0.035	0.036	0.031	0.034
0.032	0.029	0.034	0.028	0.032	0.033	0.035	0.03	0.032
0.031	0.028	0.032	0.027	0.031	0.032	0.034	0.029	0.031
0.03	0.027	0.03	0.025	0.03	0.031	0.032	0.028	0.03
0.028	0.025	0.029	0.024	0.029	0.03	0.031	0.027	0.029
0.028	0.026	0.029	0.024	0.029	0.03	0.031	0.026	0.029
0.038	0.034	0.038	0.033	0.038	0.039	0.04	0.035	0.038
0.027	0.024	0.027	0.023	0.028	0.029	0.03	0.025	0.028
0.026	0.024	0.027	0.023	0.027	0.028	0.029	0.025	0.028
0.027	0.024	0.027	0.023	0.028	0.029	0.029	0.025	0.028
0.026	0.024	0.027	0.023	0.027	0.029	0.029	0.025	0.028
0.026	0.024	0.027	0.023	0.027	0.028	0.029	0.025	0.028
0.026	0.024	0.027	0.024	0.027	0.028	0.029	0.025	0.028
0.026	0.024	0.027	0.023	0.027	0.028	0.028	0.025	0.028
0.026	0.024	0.027	0.023	0.027	0.028	0.028	0.025	0.027
0.026	0.024	0.026	0.023	0.027	0.028	0.028	0.025	0.028
0.026	0.025	0.026	0.023	0.026	0.028	0.028	0.025	0.028
0.026	0.024	0.027	0.023	0.026	0.028	0.028	0.025	0.027
0.026	0.025	0.026	0.023	0.026	0.028	0.028	0.025	0.028

C4	C5	C6	C7	C8	C9	C10	C11	C12
0.1	0.106	0.08	0.083	0.092	0.084	0.1	0.106	0.136
0.07	0.074	0.063	0.064	0.066	0.063	0.071	0.072	0.073
0.061	0.064	0.055	0.056	0.057	0.055	0.062	0.063	0.062
0.05	0.053	0.045	0.045	0.047	0.044	0.052	0.052	0.052
0.042	0.046	0.037	0.038	0.039	0.036	0.044	0.044	0.045
0.039	0.042	0.033	0.034	0.035	0.032	0.04	0.04	0.041
0.036	0.039	0.029	0.032	0.032	0.03	0.038	0.037	0.038
0.034	0.036	0.028	0.03	0.031	0.028	0.036	0.035	0.036
0.032	0.034	0.027	0.029	0.029	0.027	0.034	0.033	0.034
0.03	0.033	0.026	0.027	0.028	0.026	0.033	0.031	0.032
0.029	0.031	0.025	0.026	0.027	0.025	0.031	0.03	0.031
0.028	0.03	0.024	0.025	0.026	0.024	0.03	0.028	0.03
0.026	0.028	0.023	0.024	0.024	0.023	0.029	0.027	0.028
0.025	0.027	0.022	0.023	0.023	0.022	0.027	0.026	0.026
0.025	0.027	0.022	0.022	0.023	0.022	0.027	0.026	0.026
0.034	0.036	0.031	0.032	0.032	0.031	0.036	0.035	0.036
0.024	0.025	0.022	0.022	0.022	0.021	0.026	0.024	0.025
0.024	0.025	0.021	0.022	0.022	0.021	0.026	0.024	0.025
0.024	0.025	0.022	0.022	0.023	0.021	0.026	0.025	0.025
0.024	0.025	0.022	0.022	0.023	0.022	0.026	0.025	0.025
0.024	0.025	0.022	0.022	0.023	0.022	0.026	0.025	0.025
0.024	0.025	0.022	0.022	0.023	0.022	0.026	0.025	0.025
0.024	0.025	0.022	0.022	0.023	0.022	0.025	0.024	0.025
0.024	0.025	0.022	0.022	0.023	0.022	0.025	0.024	0.025
0.024	0.025	0.022	0.022	0.023	0.022	0.025	0.024	0.025
0.024	0.025	0.022	0.022	0.023	0.022	0.025	0.025	0.025
0.024	0.025	0.022	0.022	0.023	0.022	0.025	0.024	0.025
0.024	0.025	0.022	0.022	0.023	0.022	0.025	0.025	0.025

D1	D2	D3	D4	D5	D6	D7	D8	D9
0.118	0.1	0.125	0.097	0.096	0.12	0.093	0.105	0.122
0.086	0.072	0.083	0.072	0.068	0.081	0.067	0.075	0.085
0.076	0.063	0.073	0.063	0.059	0.07	0.059	0.066	0.075
0.066	0.053	0.065	0.053	0.049	0.058	0.049	0.057	0.067
0.058	0.047	0.059	0.045	0.041	0.048	0.043	0.05	0.062
0.053	0.044	0.053	0.039	0.037	0.044	0.039	0.046	0.056
0.048	0.04	0.043	0.035	0.034	0.039	0.036	0.045	0.046
0.044	0.039	0.037	0.033	0.032	0.038	0.033	0.042	0.04
0.041	0.036	0.032	0.032	0.03	0.035	0.031	0.039	0.035
0.04	0.033	0.03	0.03	0.029	0.035	0.029	0.036	0.033
0.038	0.03	0.029	0.029	0.028	0.033	0.028	0.033	0.031
0.036	0.029	0.027	0.027	0.027	0.033	0.027	0.032	0.03
0.034	0.027	0.026	0.026	0.025	0.031	0.026	0.031	0.029
0.031	0.026	0.025	0.025	0.024	0.029	0.024	0.03	0.028
0.032	0.026	0.025	0.025	0.024	0.029	0.024	0.029	0.028
0.042	0.035	0.034	0.034	0.034	0.04	0.033	0.038	0.037
0.03	0.025	0.024	0.024	0.023	0.028	0.023	0.028	0.026
0.031	0.025	0.024	0.024	0.023	0.029	0.023	0.028	0.026
0.031	0.025	0.024	0.024	0.024	0.029	0.023	0.028	0.026
0.03	0.025	0.024	0.024	0.023	0.028	0.023	0.028	0.026
0.03	0.025	0.024	0.024	0.024	0.03	0.024	0.028	0.026
0.03	0.025	0.024	0.024	0.024	0.03	0.023	0.028	0.026
0.03	0.025	0.024	0.024	0.024	0.029	0.023	0.028	0.026
0.03	0.025	0.024	0.024	0.024	0.03	0.023	0.028	0.026
0.03	0.025	0.024	0.024	0.024	0.029	0.024	0.028	0.026
0.03	0.025	0.024	0.024	0.024	0.029	0.023	0.028	0.026
0.03	0.025	0.024	0.024	0.024	0.03	0.023	0.027	0.026
0.029	0.025	0.024	0.024	0.024	0.029	0.023	0.028	0.026

D10	D11	D12	E1	E2	E3	E4	E5	E6
0.096	0.12	0.122	0.098	0.096	0.098	0.091	0.1	0.095
0.07	0.085	0.076	0.069	0.068	0.068	0.067	0.068	0.067
0.061	0.076	0.062	0.06	0.058	0.059	0.058	0.058	0.059
0.051	0.066	0.05	0.049	0.048	0.049	0.047	0.047	0.051
0.044	0.059	0.042	0.041	0.04	0.042	0.04	0.039	0.043
0.039	0.053	0.039	0.036	0.036	0.038	0.036	0.034	0.038
0.036	0.049	0.037	0.033	0.033	0.034	0.034	0.033	0.035
0.034	0.046	0.035	0.032	0.032	0.032	0.032	0.032	0.033
0.033	0.043	0.033	0.03	0.03	0.031	0.031	0.03	0.031
0.031	0.041	0.031	0.029	0.029	0.029	0.03	0.029	0.03
0.029	0.04	0.03	0.027	0.028	0.028	0.028	0.027	0.028
0.028	0.038	0.029	0.026	0.027	0.027	0.027	0.026	0.027
0.027	0.037	0.027	0.025	0.026	0.026	0.026	0.024	0.026
0.026	0.035	0.026	0.024	0.024	0.024	0.025	0.023	0.025
0.026	0.035	0.026	0.024	0.025	0.025	0.025	0.023	0.025
0.035	0.044	0.035	0.033	0.034	0.034	0.034	0.032	0.034
0.024	0.033	0.024	0.023	0.024	0.024	0.024	0.022	0.024
0.024	0.033	0.024	0.023	0.024	0.023	0.024	0.022	0.024
0.025	0.033	0.024	0.023	0.024	0.024	0.024	0.022	0.024
0.025	0.033	0.024	0.023	0.024	0.024	0.024	0.022	0.024
0.025	0.032	0.024	0.023	0.024	0.024	0.024	0.022	0.024
0.025	0.032	0.024	0.024	0.024	0.024	0.024	0.022	0.024
0.025	0.032	0.024	0.023	0.024	0.024	0.024	0.022	0.024
0.025	0.031	0.024	0.023	0.024	0.024	0.024	0.022	0.024
0.025	0.031	0.024	0.024	0.024	0.024	0.024	0.022	0.024
0.025	0.031	0.024	0.023	0.024	0.024	0.024	0.022	0.024
0.025	0.031	0.024	0.023	0.024	0.024	0.024	0.022	0.024
0.025	0.03	0.024	0.024	0.024	0.024	0.024	0.022	0.024

E7	E8	E9	E10	E11	E12	F1	F2	F3
0.098	0.09	0.097	0.101	0.101	0.094	0.107	0.099	0.118
0.069	0.066	0.067	0.072	0.07	0.067	0.081	0.068	0.077
0.059	0.058	0.058	0.064	0.061	0.06	0.074	0.059	0.068
0.049	0.048	0.048	0.054	0.051	0.05	0.064	0.049	0.059
0.041	0.04	0.04	0.046	0.043	0.042	0.058	0.041	0.051
0.037	0.036	0.036	0.042	0.039	0.037	0.055	0.037	0.044
0.033	0.033	0.033	0.037	0.036	0.034	0.047	0.034	0.04
0.032	0.032	0.031	0.035	0.034	0.032	0.046	0.033	0.038
0.03	0.03	0.03	0.033	0.033	0.03	0.046	0.032	0.034
0.029	0.029	0.029	0.032	0.032	0.029	0.046	0.031	0.033
0.028	0.028	0.027	0.031	0.03	0.027	0.045	0.03	0.031
0.026	0.026	0.026	0.03	0.029	0.026	0.044	0.029	0.03
0.025	0.025	0.025	0.029	0.028	0.025	0.043	0.028	0.028
0.024	0.024	0.024	0.028	0.027	0.024	0.042	0.026	0.026
0.024	0.024	0.024	0.028	0.026	0.024	0.042	0.026	0.026
0.033	0.033	0.033	0.037	0.036	0.033	0.052	0.036	0.035
0.023	0.023	0.023	0.027	0.025	0.023	0.041	0.026	0.025
0.023	0.023	0.023	0.027	0.025	0.023	0.04	0.026	0.024
0.024	0.024	0.023	0.027	0.026	0.023	0.04	0.026	0.024
0.023	0.024	0.023	0.027	0.025	0.023	0.04	0.026	0.024
0.024	0.024	0.023	0.027	0.026	0.023	0.04	0.026	0.024
0.024	0.024	0.023	0.027	0.025	0.023	0.04	0.026	0.024
0.024	0.024	0.023	0.028	0.025	0.023	0.039	0.026	0.024
0.023	0.024	0.023	0.027	0.025	0.023	0.039	0.026	0.024
0.024	0.024	0.023	0.027	0.025	0.023	0.039	0.026	0.024
0.024	0.024	0.023	0.028	0.025	0.023	0.038	0.026	0.024
0.024	0.024	0.023	0.027	0.025	0.023	0.039	0.026	0.024
0.024	0.024	0.023	0.027	0.025	0.023	0.038	0.026	0.024

F4	F5	F6	F7	F8	F9	F10	F11	F12
0.123	0.094	0.091	0.094	0.099	0.11	0.126	0.096	0.093
0.069	0.068	0.065	0.068	0.069	0.076	0.071	0.068	0.066
0.06	0.059	0.056	0.06	0.059	0.068	0.062	0.06	0.057
0.052	0.049	0.046	0.05	0.048	0.059	0.055	0.05	0.046
0.048	0.04	0.038	0.043	0.04	0.051	0.05	0.041	0.039
0.044	0.035	0.034	0.038	0.035	0.044	0.047	0.037	0.035
0.034	0.033	0.031	0.035	0.03	0.039	0.036	0.034	0.035
0.031	0.031	0.03	0.033	0.029	0.037	0.034	0.032	0.033
0.03	0.03	0.028	0.031	0.027	0.034	0.032	0.03	0.032
0.028	0.028	0.028	0.03	0.026	0.032	0.031	0.029	0.032
0.027	0.027	0.026	0.029	0.025	0.03	0.029	0.028	0.029
0.026	0.026	0.025	0.027	0.024	0.029	0.028	0.026	0.029
0.025	0.024	0.024	0.026	0.023	0.027	0.027	0.025	0.026
0.024	0.023	0.023	0.025	0.022	0.026	0.026	0.024	0.023
0.024	0.023	0.023	0.025	0.022	0.026	0.026	0.024	0.024
0.033	0.032	0.032	0.034	0.031	0.034	0.035	0.033	0.033
0.023	0.022	0.022	0.024	0.021	0.024	0.025	0.023	0.023
0.023	0.022	0.022	0.024	0.021	0.024	0.025	0.023	0.023
0.023	0.023	0.022	0.024	0.021	0.024	0.025	0.023	0.022
0.023	0.022	0.022	0.024	0.021	0.024	0.025	0.023	0.022
0.023	0.022	0.022	0.024	0.022	0.024	0.025	0.023	0.023
0.023	0.023	0.022	0.024	0.022	0.024	0.025	0.023	0.023
0.023	0.023	0.022	0.024	0.022	0.024	0.025	0.023	0.023
0.023	0.023	0.022	0.024	0.022	0.024	0.025	0.024	0.023
0.023	0.023	0.022	0.024	0.022	0.024	0.025	0.024	0.023
0.023	0.022	0.022	0.024	0.022	0.024	0.025	0.024	0.023
0.023	0.023	0.022	0.024	0.022	0.024	0.025	0.024	0.023
0.023	0.023	0.022	0.024	0.022	0.024	0.025	0.024	0.023

G1	G2	G3	G4	G5	G6	G7	G8	G9
0.101	0.152	0.118	0.131	0.13	0.105	0.092	0.112	0.101
0.073	0.107	0.07	0.085	0.086	0.069	0.064	0.07	0.067
0.064	0.094	0.059	0.069	0.074	0.06	0.056	0.06	0.057
0.054	0.082	0.049	0.056	0.065	0.05	0.045	0.05	0.046
0.048	0.076	0.041	0.044	0.055	0.043	0.038	0.042	0.038
0.044	0.076	0.036	0.04	0.047	0.039	0.033	0.038	0.034
0.04	0.068	0.034	0.036	0.04	0.036	0.03	0.034	0.032
0.038	0.066	0.032	0.032	0.036	0.034	0.029	0.032	0.03
0.036	0.064	0.03	0.03	0.033	0.032	0.028	0.031	0.029
0.035	0.066	0.029	0.028	0.032	0.031	0.027	0.029	0.028
0.033	0.061	0.027	0.027	0.03	0.029	0.026	0.028	0.026
0.032	0.06	0.026	0.026	0.029	0.028	0.024	0.027	0.025
0.031	0.055	0.025	0.025	0.028	0.027	0.023	0.026	0.024
0.03	0.05	0.024	0.024	0.027	0.026	0.022	0.024	0.023
0.03	0.049	0.024	0.023	0.027	0.026	0.022	0.024	0.023
0.039	0.059	0.032	0.033	0.036	0.035	0.031	0.033	0.032
0.029	0.046	0.022	0.023	0.026	0.025	0.021	0.023	0.022
0.029	0.045	0.022	0.023	0.025	0.024	0.021	0.023	0.022
0.029	0.043	0.023	0.023	0.026	0.025	0.022	0.023	0.022
0.028	0.042	0.023	0.023	0.025	0.025	0.022	0.023	0.022
0.028	0.042	0.023	0.023	0.026	0.025	0.022	0.023	0.022
0.028	0.041	0.023	0.023	0.026	0.024	0.022	0.023	0.022
0.028	0.04	0.023	0.023	0.025	0.025	0.022	0.023	0.022
0.028	0.039	0.023	0.023	0.025	0.025	0.022	0.023	0.022
0.028	0.038	0.023	0.023	0.025	0.024	0.022	0.024	0.023
0.028	0.037	0.023	0.023	0.025	0.024	0.022	0.023	0.023
0.028	0.038	0.023	0.023	0.025	0.025	0.022	0.023	0.023
0.028	0.036	0.023	0.023	0.025	0.025	0.022	0.024	0.023

G10	G11	G12	H1	H2	H3	H4	H5	H6
0.098	0.121	0.097	0.098	0.093	0.248	0.367	0.138	0.098
0.073	0.083	0.067	0.069	0.066	0.188	0.226	0.093	0.066
0.06	0.071	0.058	0.06	0.057	0.218	0.178	0.082	0.057
0.049	0.061	0.048	0.05	0.046	0.302	0.215	0.084	0.047
0.038	0.052	0.041	0.042	0.039	0.384	0.262	0.091	0.04
0.033	0.045	0.037	0.038	0.034	0.408	0.267	0.081	0.035
0.03	0.038	0.035	0.035	0.031	0.356	0.211	0.054	0.032
0.028	0.034	0.033	0.033	0.03	0.269	0.133	0.046	0.03
0.027	0.032	0.031	0.031	0.028	0.18	0.074	0.047	0.029
0.026	0.031	0.03	0.03	0.027	0.109	0.047	0.04	0.027
0.025	0.029	0.028	0.028	0.026	0.07	0.038	0.032	0.026
0.024	0.028	0.027	0.027	0.025	0.052	0.034	0.026	0.025
0.023	0.027	0.026	0.026	0.023	0.042	0.033	0.025	0.024
0.021	0.026	0.025	0.025	0.022	0.036	0.031	0.023	0.022
0.022	0.026	0.025	0.025	0.022	0.031	0.031	0.023	0.022
0.031	0.035	0.034	0.034	0.031	0.038	0.04	0.032	0.031
0.021	0.025	0.024	0.023	0.021	0.026	0.03	0.022	0.021
0.021	0.025	0.024	0.023	0.021	0.025	0.029	0.022	0.021
0.021	0.025	0.024	0.024	0.022	0.025	0.029	0.022	0.022
0.021	0.025	0.024	0.023	0.022	0.025	0.029	0.022	0.022
0.022	0.025	0.024	0.024	0.022	0.025	0.029	0.022	0.022
0.022	0.025	0.024	0.024	0.022	0.025	0.029	0.023	0.022
0.022	0.025	0.024	0.024	0.022	0.025	0.029	0.023	0.022
0.022	0.025	0.024	0.024	0.022	0.024	0.028	0.022	0.022
0.022	0.025	0.024	0.024	0.022	0.025	0.028	0.022	0.022
0.022	0.025	0.024	0.024	0.022	0.024	0.028	0.023	0.022
0.022	0.025	0.024	0.024	0.022	0.024	0.028	0.022	0.022
0.022	0.025	0.024	0.023	0.022	0.024	0.028	0.022	0.022

H7	H8	H9	H10	H11	H12
0.092	0.204	0.43	0.138	0.073	0.073
0.065	0.157	0.258	0.091	0.063	0.063
0.056	0.178	0.2	0.08	0.054	0.055
0.046	0.24	0.25	0.084	0.044	0.044
0.038	0.302	0.312	0.093	0.036	0.037
0.033	0.319	0.318	0.082	0.032	0.033
0.031	0.28	0.249	0.051	0.028	0.029
0.029	0.213	0.15	0.042	0.027	0.028
0.028	0.146	0.074	0.044	0.026	0.027
0.027	0.09	0.04	0.038	0.025	0.026
0.026	0.059	0.029	0.029	0.024	0.025
0.024	0.044	0.025	0.024	0.023	0.024
0.023	0.037	0.023	0.022	0.022	0.022
0.022	0.031	0.022	0.021	0.021	0.021
0.022	0.028	0.022	0.021	0.021	0.021
0.031	0.035	0.031	0.03	0.03	0.031
0.021	0.023	0.021	0.02	0.02	0.021
0.021	0.023	0.021	0.02	0.02	0.021
0.022	0.023	0.022	0.021	0.021	0.022
0.022	0.023	0.022	0.021	0.021	0.022
0.022	0.023	0.022	0.021	0.021	0.022
0.022	0.023	0.022	0.021	0.021	0.022
0.022	0.023	0.022	0.021	0.021	0.022
0.022	0.023	0.022	0.021	0.021	0.022
0.022	0.023	0.022	0.021	0.021	0.022
0.022	0.023	0.022	0.021	0.022	0.022
0.022	0.023	0.022	0.021	0.021	0.022
0.022	0.023	0.022	0.021	0.022	0.022

Raw Equilibrium Solutions for 2nd PAMPA Assay

Wavelength	A1	A2	A3	A4	A5	A6
230	1.501	1.376	1.55	1.014	1.327	#SAT
240	0.389	0.346	0.418	0.21	0.202	0.745
250	0.323	0.298	0.31	0.163	0.143	0.447
260	0.353	0.341	0.248	0.161	0.127	0.431
270	0.404	0.396	0.209	0.173	0.117	0.451
280	0.432	0.411	0.173	0.181	0.125	0.451
290	0.403	0.392	0.126	0.166	0.134	0.391
300	0.346	0.327	0.095	0.142	0.131	0.291
310	0.292	0.26	0.071	0.121	0.11	0.208
320	0.226	0.195	0.058	0.098	0.082	0.162
330	0.158	0.138	0.052	0.075	0.058	0.142
340	0.111	0.101	0.052	0.06	0.048	0.13
350	0.086	0.081	0.052	0.051	0.044	0.12
360	0.072	0.066	0.051	0.045	0.041	0.11
370	0.063	0.057	0.047	0.042	0.04	0.102
380	0.066	0.06	0.052	0.05	0.048	0.104
390	0.051	0.046	0.038	0.038	0.037	0.089
400	0.048	0.044	0.037	0.036	0.036	0.086
410	0.046	0.042	0.035	0.035	0.035	0.083
420	0.044	0.041	0.034	0.034	0.034	0.081
430	0.042	0.04	0.034	0.034	0.034	0.079
440	0.041	0.039	0.033	0.033	0.033	0.077
450	0.039	0.038	0.033	0.032	0.033	0.075
460	0.038	0.037	0.032	0.032	0.032	0.074
470	0.037	0.036	0.032	0.031	0.032	0.072
480	0.036	0.036	0.032	0.031	0.032	0.072
490	0.035	0.035	0.031	0.031	0.031	0.07
500	0.035	0.035	0.031	0.03	0.031	0.07

B1	B2	B3	B4	B5	B6
1.505	1.566	1.834	1.451	1.201	1.84
0.292	0.361	0.496	0.332	0.138	0.186
0.22	0.263	0.394	0.271	0.089	0.106
0.204	0.217	0.393	0.265	0.088	0.083
0.225	0.194	0.425	0.235	0.096	0.071
0.289	0.164	0.429	0.171	0.099	0.063
0.326	0.119	0.367	0.125	0.09	0.056
0.277	0.085	0.311	0.105	0.075	0.052
0.191	0.064	0.262	0.087	0.057	0.048
0.112	0.054	0.21	0.065	0.042	0.046
0.061	0.052	0.151	0.056	0.036	0.044
0.045	0.053	0.106	0.052	0.032	0.041
0.042	0.054	0.086	0.049	0.03	0.039
0.04	0.05	0.075	0.046	0.029	0.037
0.04	0.043	0.07	0.045	0.029	0.037
0.048	0.047	0.076	0.052	0.038	0.046
0.036	0.033	0.061	0.04	0.028	0.035
0.035	0.032	0.054	0.039	0.027	0.035
0.034	0.031	0.048	0.038	0.027	0.034
0.034	0.03	0.045	0.037	0.027	0.033
0.033	0.03	0.043	0.037	0.027	0.033
0.033	0.03	0.04	0.036	0.026	0.032
0.032	0.029	0.039	0.035	0.026	0.032
0.032	0.029	0.038	0.034	0.026	0.032
0.032	0.028	0.036	0.034	0.026	0.031
0.032	0.028	0.035	0.033	0.026	0.031
0.031	0.028	0.035	0.033	0.026	0.031
0.031	0.028	0.034	0.032	0.026	0.03

C1	C2	C3	C4	C5	C6
0.952	1.425	1.495	1.61	1.829	3.523
0.2	0.262	0.359	0.325	0.382	0.558
0.152	0.211	0.302	0.26	0.3	0.448
0.15	0.2	0.315	0.325	0.356	0.52
0.155	0.211	0.328	0.407	0.443	0.461
0.153	0.256	0.314	0.439	0.513	0.33
0.134	0.282	0.258	0.403	0.52	0.202
0.104	0.242	0.181	0.348	0.456	0.136
0.079	0.171	0.115	0.264	0.324	0.107
0.065	0.105	0.08	0.177	0.192	0.076
0.059	0.062	0.066	0.116	0.114	0.064
0.054	0.047	0.059	0.087	0.076	0.06
0.05	0.041	0.056	0.072	0.06	0.058
0.046	0.037	0.052	0.063	0.052	0.055
0.044	0.035	0.049	0.062	0.05	0.054
0.052	0.043	0.055	0.07	0.057	0.062
0.04	0.031	0.042	0.057	0.045	0.051
0.039	0.031	0.039	0.054	0.043	0.05
0.038	0.03	0.038	0.05	0.042	0.049
0.037	0.029	0.036	0.048	0.039	0.048
0.037	0.03	0.035	0.048	0.039	0.048
0.036	0.029	0.034	0.046	0.038	0.047
0.035	0.028	0.033	0.045	0.036	0.046
0.035	0.028	0.033	0.045	0.036	0.046
0.034	0.028	0.032	0.044	0.036	0.045
0.034	0.028	0.032	0.043	0.035	0.045
0.033	0.028	0.031	0.044	0.035	0.044
0.033	0.028	0.031	0.042	0.034	0.044

D1	D2	D3	D4	D5	D6
1.439	1.442	1.041	1.294	1.554	1.607
0.274	0.264	0.177	0.224	0.214	0.327
0.223	0.205	0.133	0.184	0.153	0.255
0.233	0.198	0.127	0.232	0.145	0.263
0.235	0.213	0.126	0.284	0.128	0.276
0.214	0.247	0.111	0.252	0.093	0.263
0.171	0.256	0.082	0.196	0.064	0.209
0.126	0.213	0.059	0.17	0.052	0.114
0.096	0.157	0.044	0.125	0.046	0.087
0.083	0.107	0.038	0.082	0.043	0.076
0.076	0.074	0.035	0.057	0.041	0.069
0.069	0.061	0.033	0.046	0.04	0.065
0.061	0.054	0.032	0.042	0.039	0.062
0.053	0.046	0.031	0.038	0.034	0.059
0.049	0.041	0.031	0.038	0.03	0.056
0.055	0.047	0.04	0.047	0.036	0.062
0.042	0.035	0.029	0.036	0.024	0.047
0.041	0.034	0.03	0.035	0.024	0.044
0.039	0.033	0.03	0.034	0.024	0.043
0.037	0.031	0.029	0.034	0.023	0.041
0.036	0.03	0.029	0.033	0.023	0.04
0.035	0.029	0.029	0.033	0.023	0.039
0.034	0.028	0.028	0.032	0.023	0.038
0.033	0.028	0.028	0.032	0.023	0.037
0.032	0.028	0.028	0.031	0.023	0.036
0.032	0.027	0.028	0.031	0.023	0.036
0.031	0.027	0.028	0.031	0.023	0.035
0.031	0.027	0.028	0.03	0.023	0.035

E1	E2	E3	E4	E5	E6
1.396	1.4	1.857	1.412	1.853	1.634
0.25	0.19	0.371	0.253	0.336	0.31
0.184	0.127	0.293	0.193	0.27	0.212
0.175	0.097	0.329	0.171	0.321	0.192
0.172	0.071	0.38	0.135	0.356	0.196
0.165	0.052	0.406	0.1	0.325	0.178
0.155	0.043	0.372	0.074	0.229	0.13
0.137	0.039	0.253	0.059	0.081	0.093
0.126	0.036	0.185	0.05	0.05	0.061
0.115	0.035	0.116	0.047	0.046	0.044
0.101	0.034	0.07	0.045	0.042	0.037
0.086	0.033	0.054	0.043	0.038	0.034
0.073	0.031	0.049	0.039	0.035	0.032
0.063	0.028	0.043	0.035	0.032	0.03
0.057	0.028	0.04	0.034	0.032	0.029
0.062	0.036	0.046	0.043	0.04	0.038
0.049	0.026	0.034	0.032	0.029	0.027
0.047	0.026	0.032	0.032	0.028	0.026
0.045	0.026	0.031	0.031	0.027	0.026
0.043	0.025	0.03	0.03	0.026	0.026
0.042	0.025	0.03	0.03	0.026	0.026
0.041	0.025	0.029	0.03	0.026	0.026
0.04	0.025	0.029	0.03	0.026	0.025
0.039	0.025	0.028	0.029	0.025	0.025
0.038	0.024	0.028	0.029	0.025	0.025
0.037	0.024	0.028	0.029	0.025	0.025
0.037	0.024	0.027	0.029	0.025	0.025
0.036	0.024	0.027	0.029	0.025	0.025

F1	F2	F3	F4	F5	F6
1.299	1.437	1.789	1.65	1.3	1.525
0.401	0.284	0.502	0.147	0.166	0.363
0.35	0.195	0.405	0.083	0.113	0.298
0.312	0.171	0.408	0.087	0.097	0.298
0.286	0.164	0.395	0.107	0.082	0.306
0.259	0.168	0.355	0.106	0.069	0.307
0.221	0.17	0.307	0.044	0.062	0.348
0.173	0.149	0.242	0.033	0.049	0.305
0.117	0.11	0.19	0.031	0.042	0.254
0.076	0.074	0.152	0.029	0.039	0.205
0.058	0.055	0.12	0.028	0.038	0.186
0.051	0.048	0.098	0.027	0.037	0.169
0.047	0.045	0.081	0.026	0.037	0.164
0.044	0.042	0.071	0.024	0.035	0.158
0.041	0.041	0.066	0.024	0.034	0.151
0.047	0.049	0.071	0.034	0.041	0.15
0.035	0.037	0.056	0.024	0.029	0.139
0.034	0.036	0.052	0.024	0.028	0.135
0.033	0.035	0.048	0.024	0.027	0.132
0.032	0.034	0.044	0.023	0.026	0.129
0.032	0.034	0.042	0.024	0.026	0.122
0.031	0.033	0.039	0.024	0.026	0.119
0.031	0.032	0.037	0.024	0.026	0.117
0.03	0.032	0.036	0.023	0.026	0.114
0.03	0.032	0.034	0.023	0.025	0.112
0.03	0.031	0.033	0.023	0.025	0.11
0.03	0.031	0.033	0.023	0.025	0.104
0.03	0.031	0.032	0.023	0.025	0.107

G1	G2	G3	G4	G5	G6
1.289	1.443	1.28	1.664	1.302	1.523
0.218	0.186	0.28	0.419	0.242	0.18
0.18	0.122	0.193	0.343	0.186	0.109
0.188	0.104	0.149	0.337	0.178	0.108
0.178	0.094	0.129	0.329	0.166	0.118
0.136	0.084	0.1	0.316	0.13	0.103
0.08	0.073	0.079	0.286	0.083	0.065
0.054	0.06	0.073	0.254	0.054	0.054
0.044	0.053	0.07	0.21	0.044	0.046
0.041	0.049	0.066	0.146	0.04	0.041
0.039	0.045	0.064	0.125	0.04	0.037
0.038	0.042	0.061	0.11	0.04	0.036
0.038	0.04	0.06	0.109	0.041	0.035
0.037	0.038	0.058	0.11	0.04	0.034
0.036	0.037	0.057	0.104	0.039	0.034
0.043	0.046	0.065	0.105	0.045	0.043
0.032	0.035	0.055	0.096	0.032	0.032
0.032	0.034	0.054	0.092	0.031	0.033
0.032	0.034	0.053	0.091	0.03	0.033
0.031	0.033	0.052	0.09	0.03	0.033
0.031	0.033	0.052	0.086	0.03	0.033
0.03	0.032	0.051	0.085	0.029	0.032
0.03	0.031	0.05	0.083	0.029	0.032
0.03	0.031	0.05	0.081	0.028	0.032
0.03	0.03	0.049	0.079	0.028	0.032
0.03	0.03	0.048	0.078	0.028	0.032
0.03	0.03	0.048	0.075	0.028	0.032
0.029	0.03	0.047	0.075	0.028	0.032

					DMSO-blank
H1	H2	H3	H4	H5	H6
1.626	1.831	1.644	2.043	2.018	1.565
0.494	0.683	0.302	0.508	0.371	0.128
0.587	0.538	0.296	0.35	0.346	0.061
0.599	0.434	0.409	0.451	0.575	0.044
0.466	0.35	0.524	0.586	0.788	0.035
0.267	0.273	0.561	0.61	0.665	0.03
0.111	0.193	0.49	0.475	0.234	0.028
0.071	0.14	0.367	0.279	0.078	0.027
0.059	0.1	0.244	0.126	0.071	0.026
0.053	0.079	0.144	0.057	0.058	0.025
0.049	0.071	0.087	0.036	0.041	0.024
0.046	0.065	0.061	0.029	0.031	0.022
0.044	0.06	0.048	0.027	0.028	0.022
0.04	0.054	0.039	0.026	0.026	0.02
0.038	0.048	0.033	0.026	0.026	0.02
0.046	0.053	0.038	0.035	0.034	0.03
0.034	0.04	0.026	0.024	0.025	0.02
0.032	0.038	0.025	0.024	0.024	0.02
0.031	0.037	0.024	0.025	0.024	0.02
0.03	0.036	0.024	0.024	0.024	0.02
0.03	0.035	0.024	0.025	0.024	0.02
0.03	0.034	0.024	0.025	0.024	0.02
0.03	0.034	0.024	0.024	0.024	0.021
0.029	0.033	0.024	0.024	0.024	0.021
0.029	0.032	0.024	0.024	0.024	0.021
0.029	0.032	0.024	0.024	0.024	0.02
0.029	0.032	0.024	0.024	0.023	0.021
0.028	0.031	0.024	0.024	0.024	0.021

Crystallographic Data

The diffraction data were measured 100K (2) on a Bruker Smart Apex2 CCD-based X-ray diffractometer system equipped with a Mo-Kα radiation (λ = 0.71073 Å). The frames were integrated with the Bruker Saint software package using a narrow-frame integration algorithm. The structure was solved and refined using the Bruker SHELXTL Software Package. All atoms were refined anisotropically, and hydrogen atoms were removed for clarity.

Deposition Number 1946197 contains the supplementary crystallographic data for this paper. These data are provided free of charge by the joint Cambridge Crystallographic Data Centre and Fachinformationszentrum Karlsruhe Access Structures service www.ccdc.cam.ac.uk/structures.

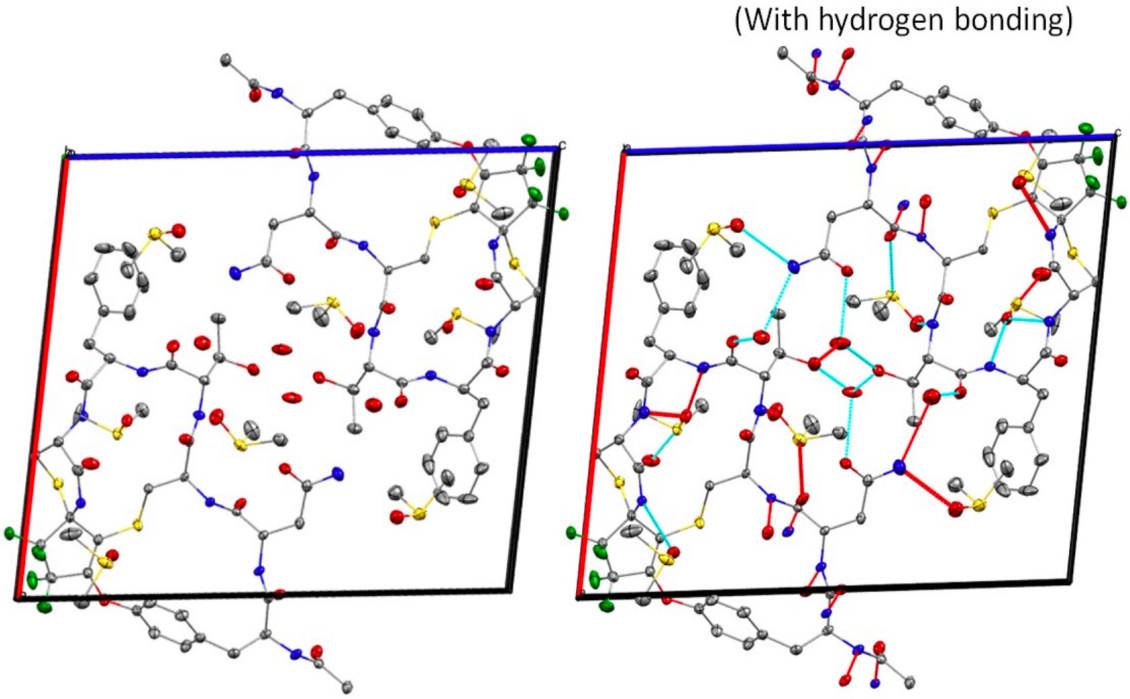

Figure 4.7.23 Crystal structure of polycycle **9**. Structure was solved in space group P2 with ORTEP showing 50% probability. Both residual DMSO and water molecules can be observed within the unit cell. Water atoms can be seen localized between the two asymmetric units of the unit cell and may be providing additional stabilization effects through hydrogen bonding.

NMR Spectra

Spectrum 4.7.1 ^{1}H-NMR of compound **S8** (DMSO-d_6, 500 MHz)

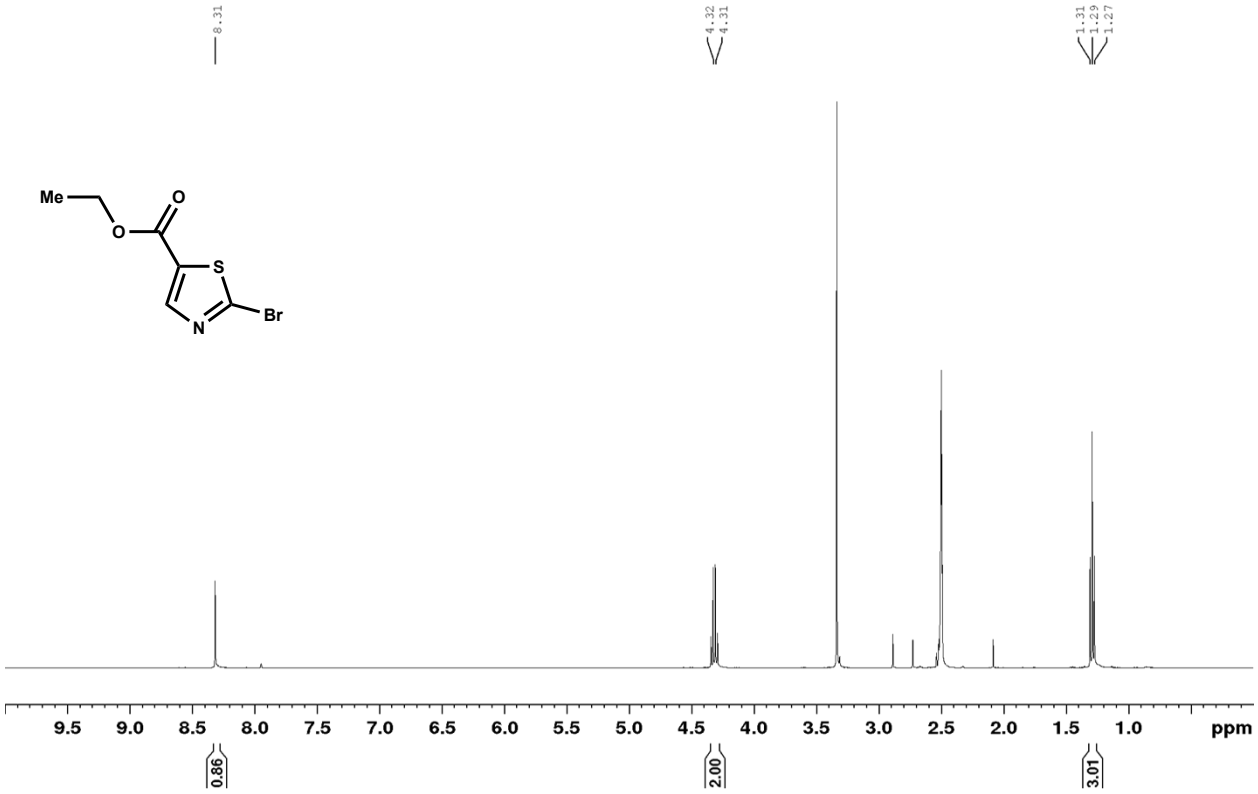

Spectrum 4.7.2 ^{13}C-NMR of compound **S8** (DMSO-d_6, 126 MHz)

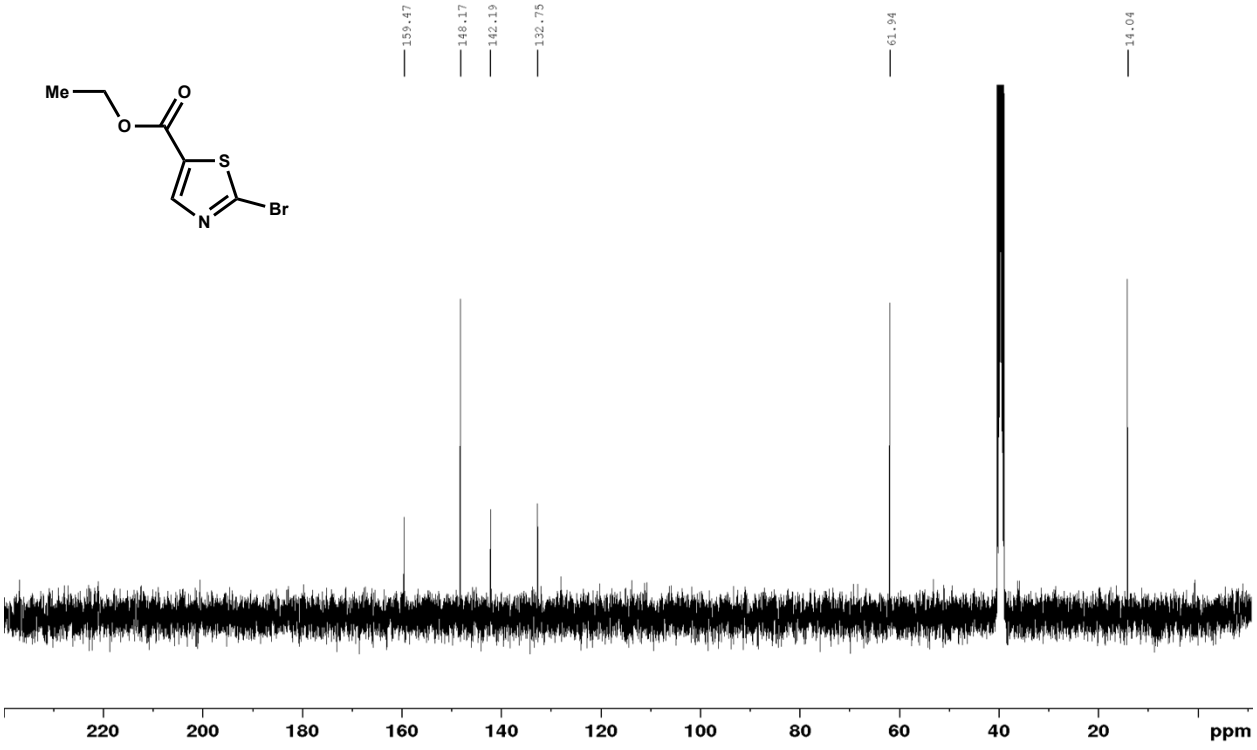

Spectrum 4.7.3 ^{1}H-NMR of compound **S9** (DMSO-d_6, 500 MHz)

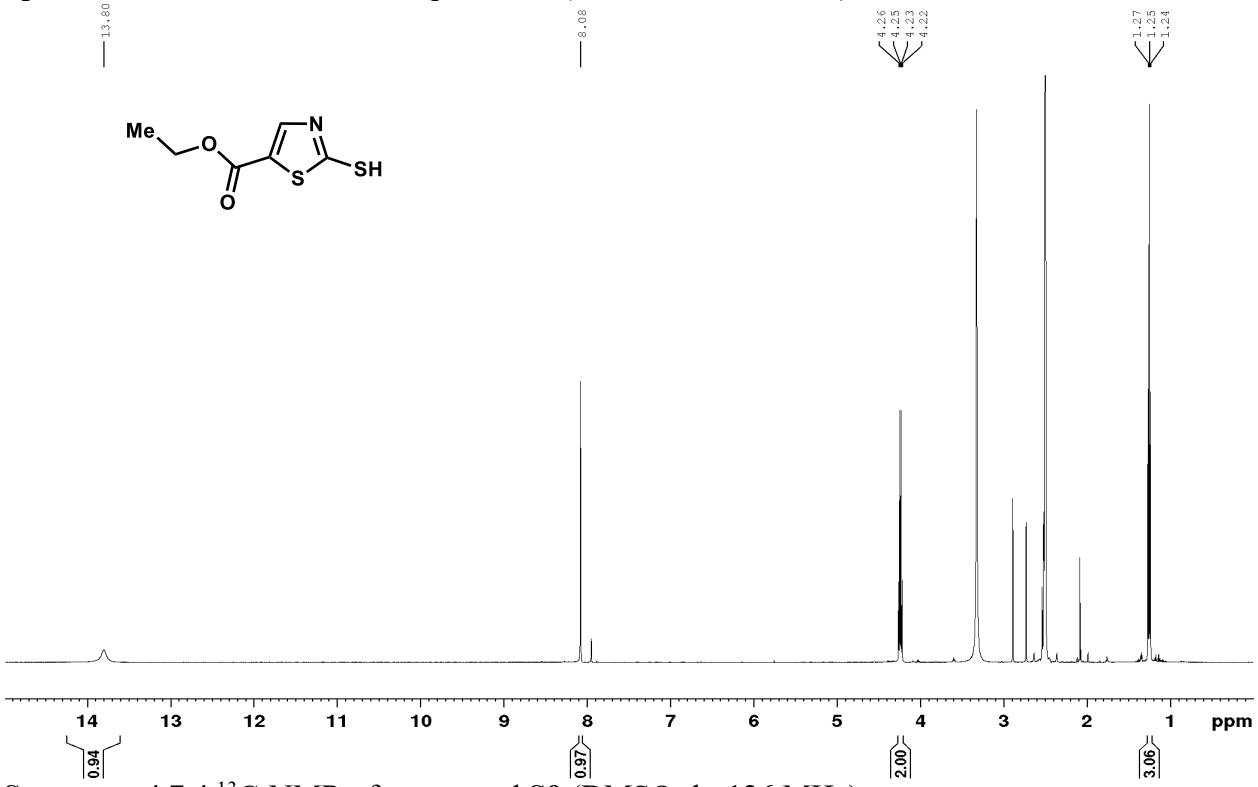

Spectrum 4.7.4 ^{13}C-NMR of compound **S9** (DMSO-d_6, 126 MHz)

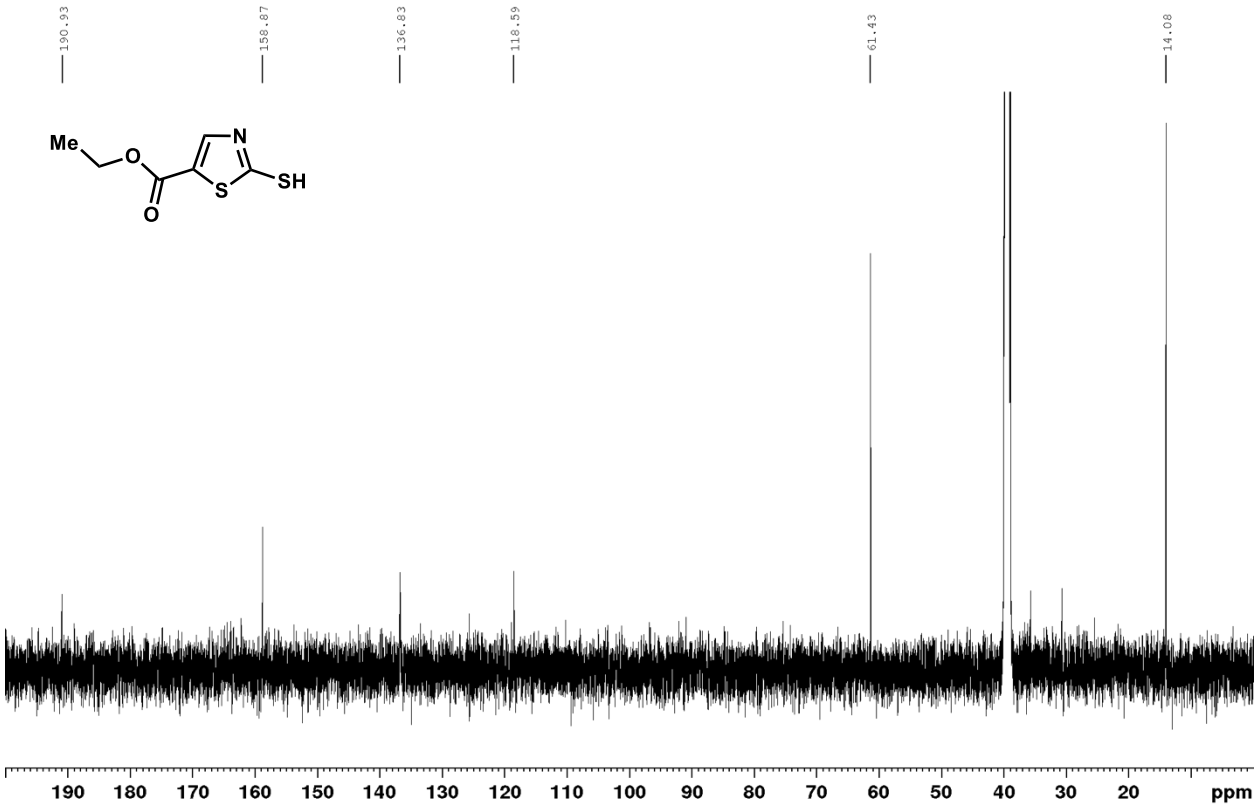

Spectrum 4.7.5 ^{1}H-NMR of compound **29** (DMSO-d_6, 500 MHz)

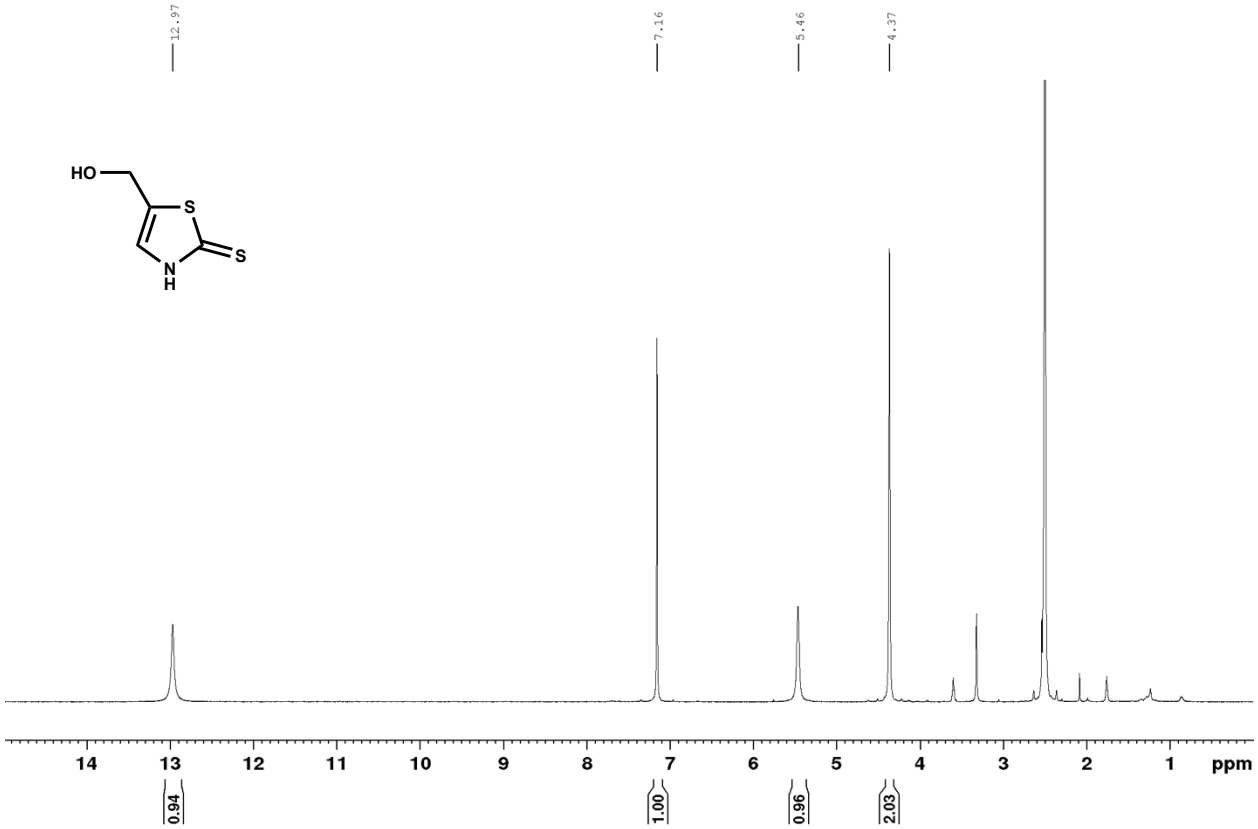

Spectrum 4.7.6 ^{13}C-NMR of compound **29** (DMSO-d_6, 126 MHz)

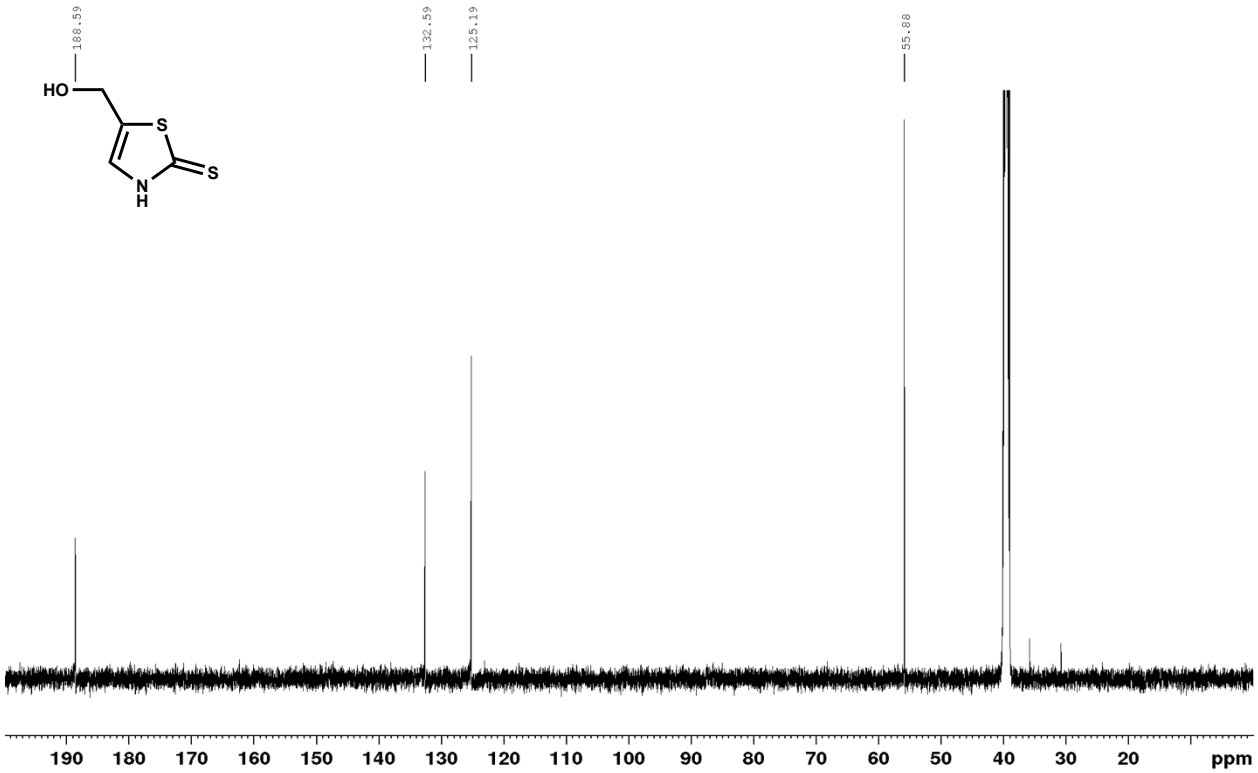

Spectrum 4.7.7 ^{1}H-NMR of compound **S11** ($CDCl_3$, 300 MHz)

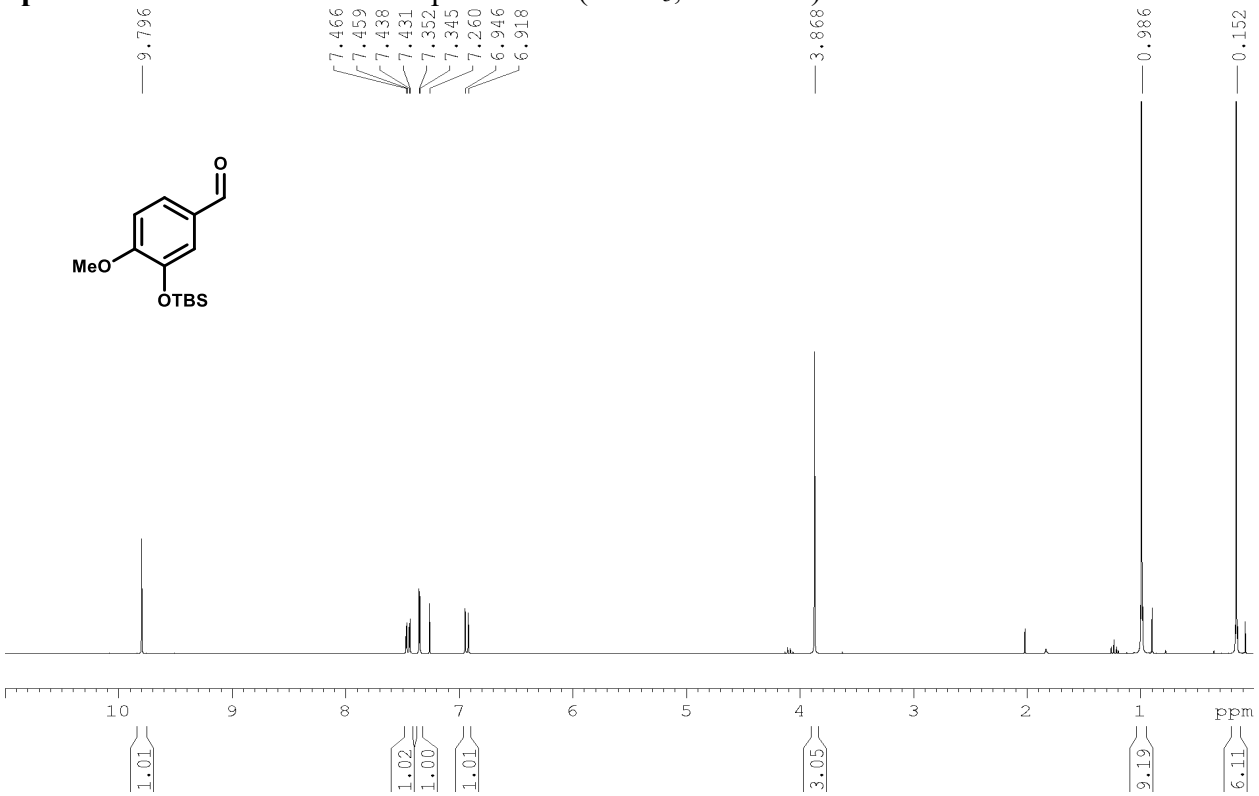

Spectrum 4.7.8 ^{13}C-NMR of compound **S11** ($CDCl_3$, 126 MHz)

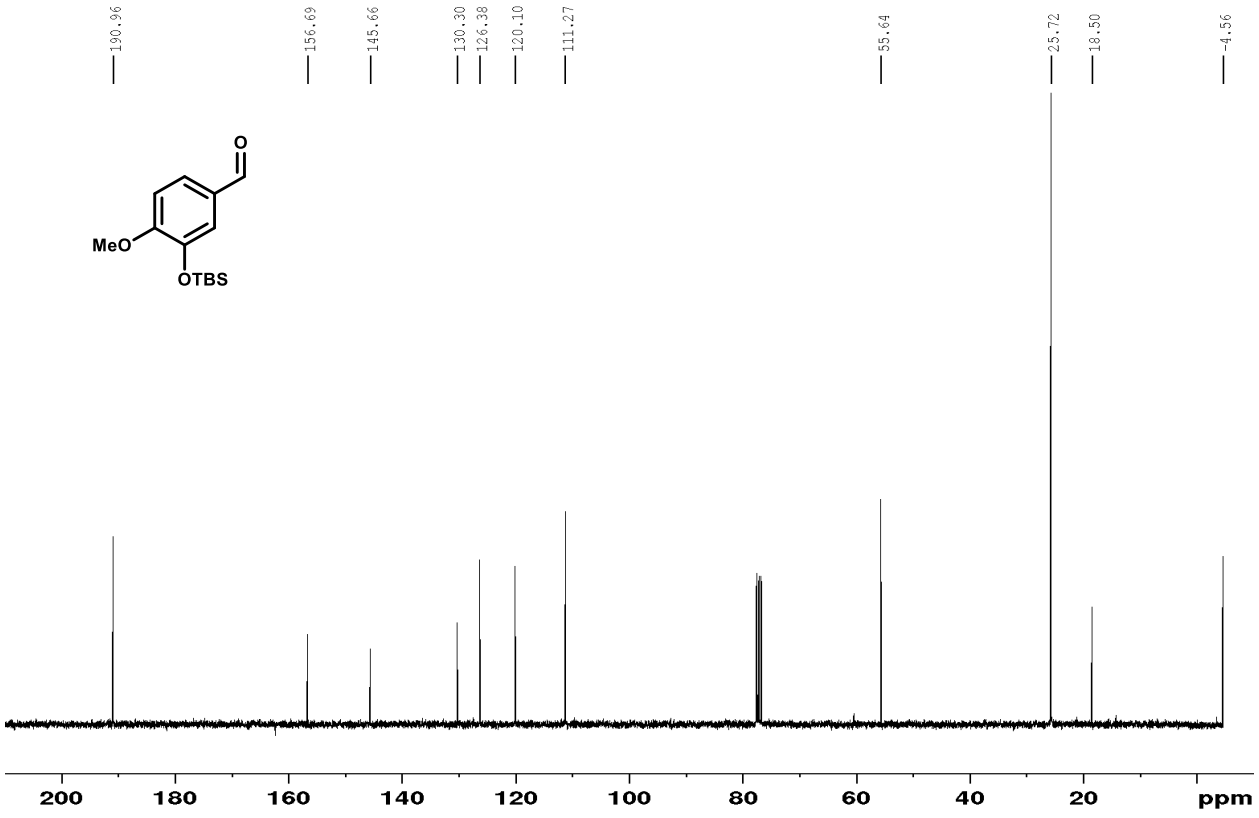

Spectrum 4.7.9 ^{1}H-NMR of compound **S12** ($CDCl_3$, 500 MHz)

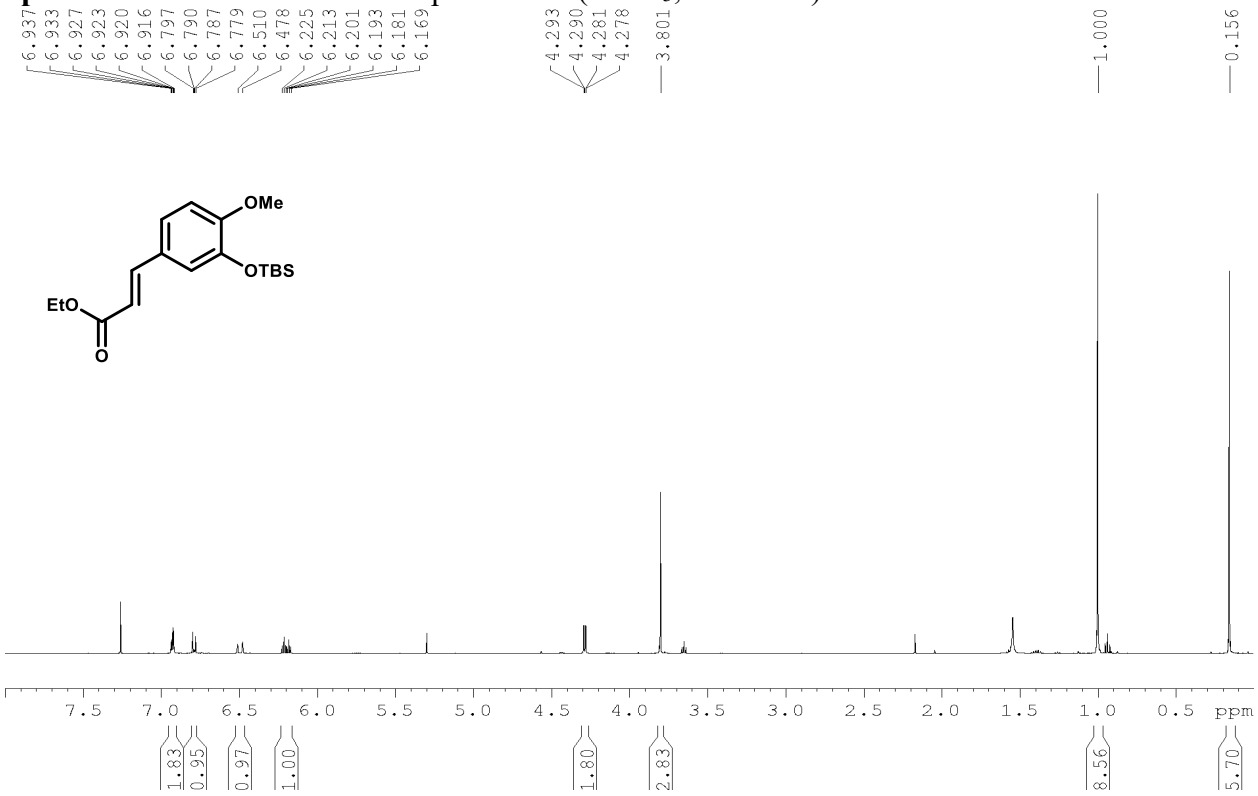

Spectrum 4.7.10 ^{13}C-NMR of compound **S12** ($CDCl_3$, 126 MHz)

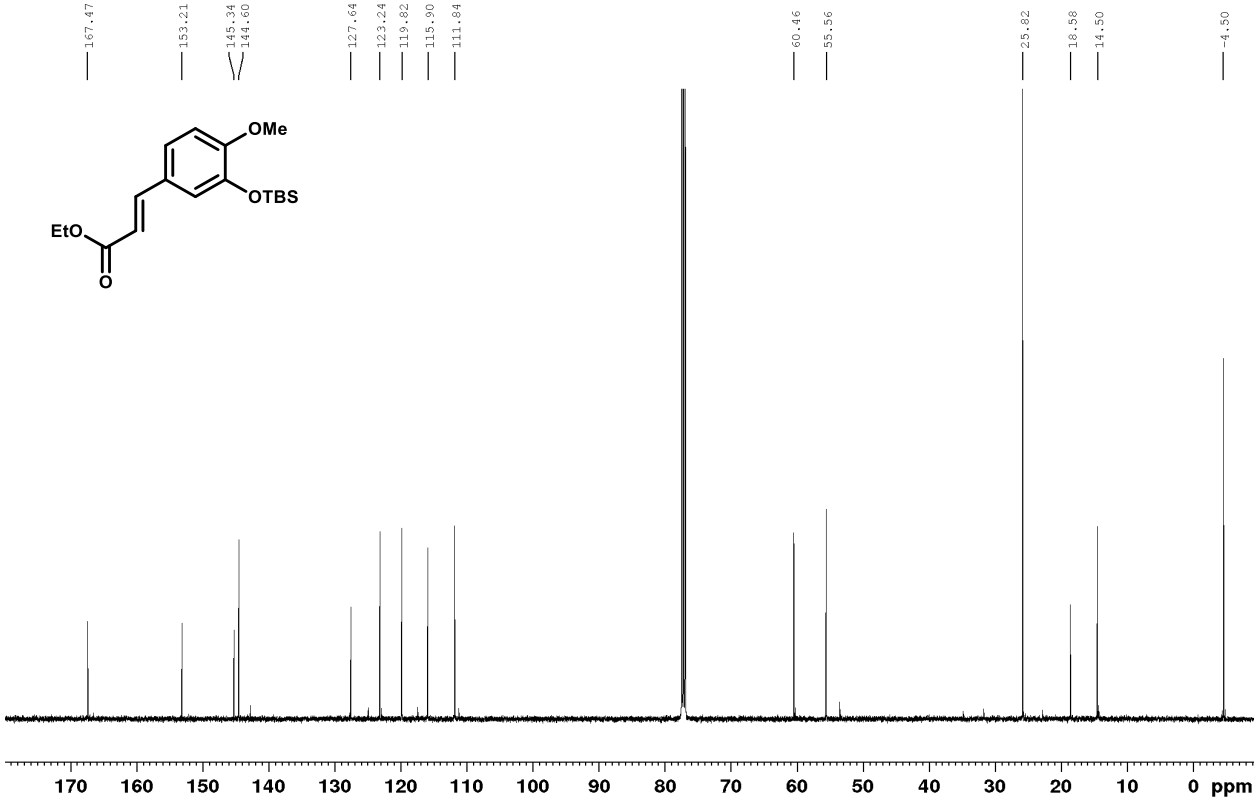

Spectrum 4.7.11 ^{1}H-NMR of compound **S13** ($CDCl_3$, 500 MHz)

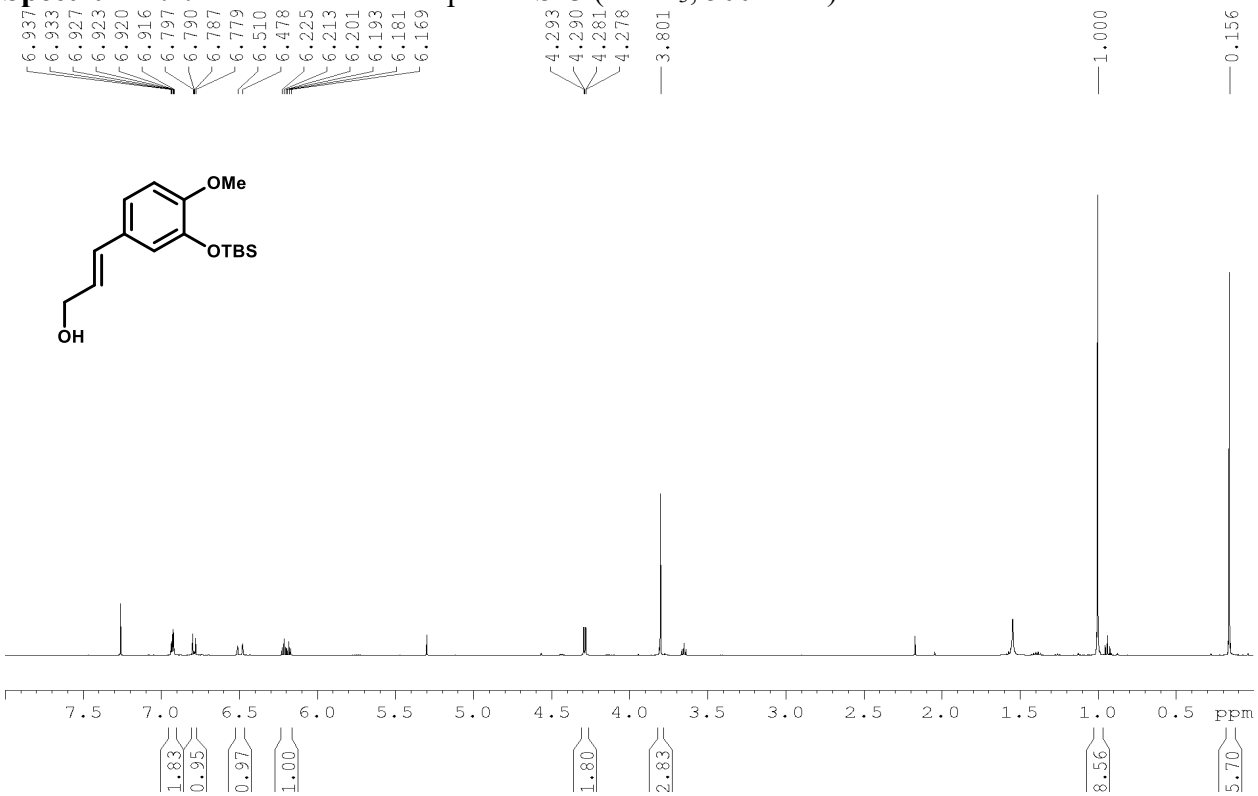

Spectrum 4.7.12 ^{13}C-NMR of compound **S13** ($CDCl_3$, 126 MHz)

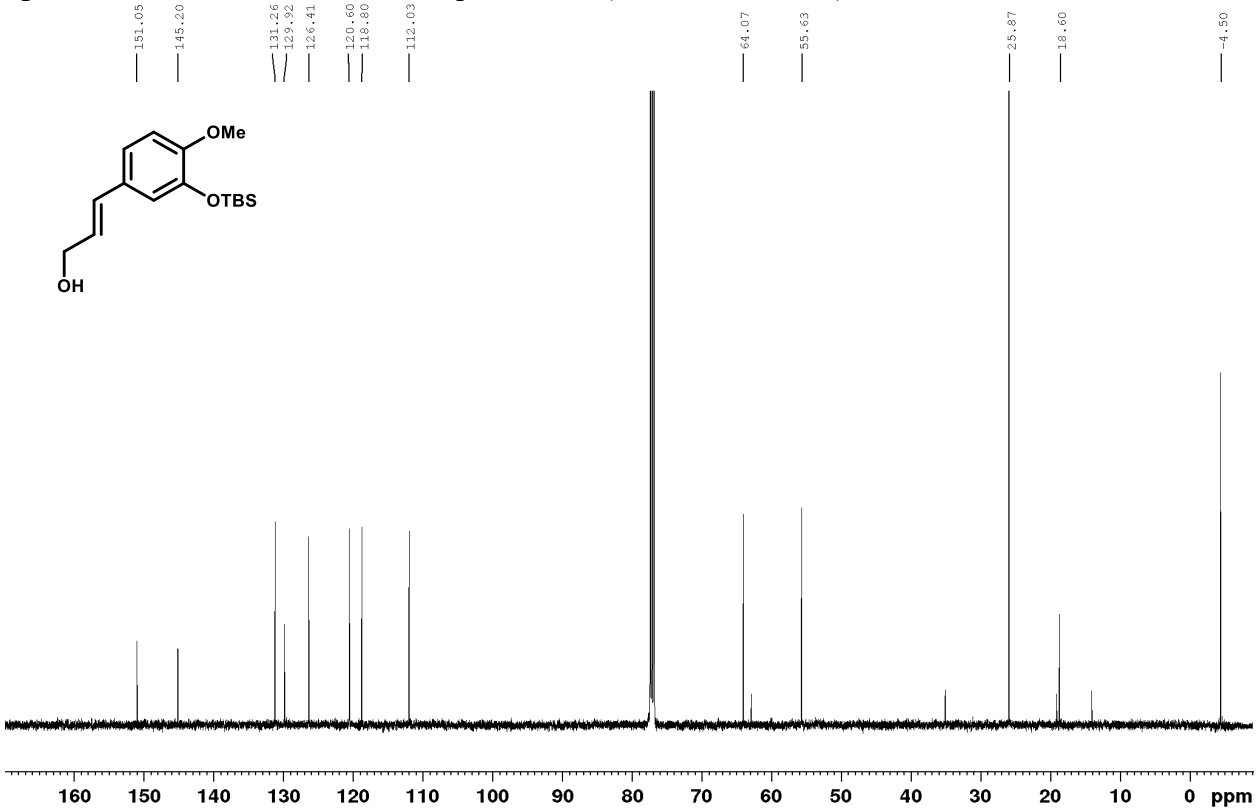

Spectrum 4.7.13 ^{1}H-NMR of compound **33** ($CDCl_3$, 500 MHz)

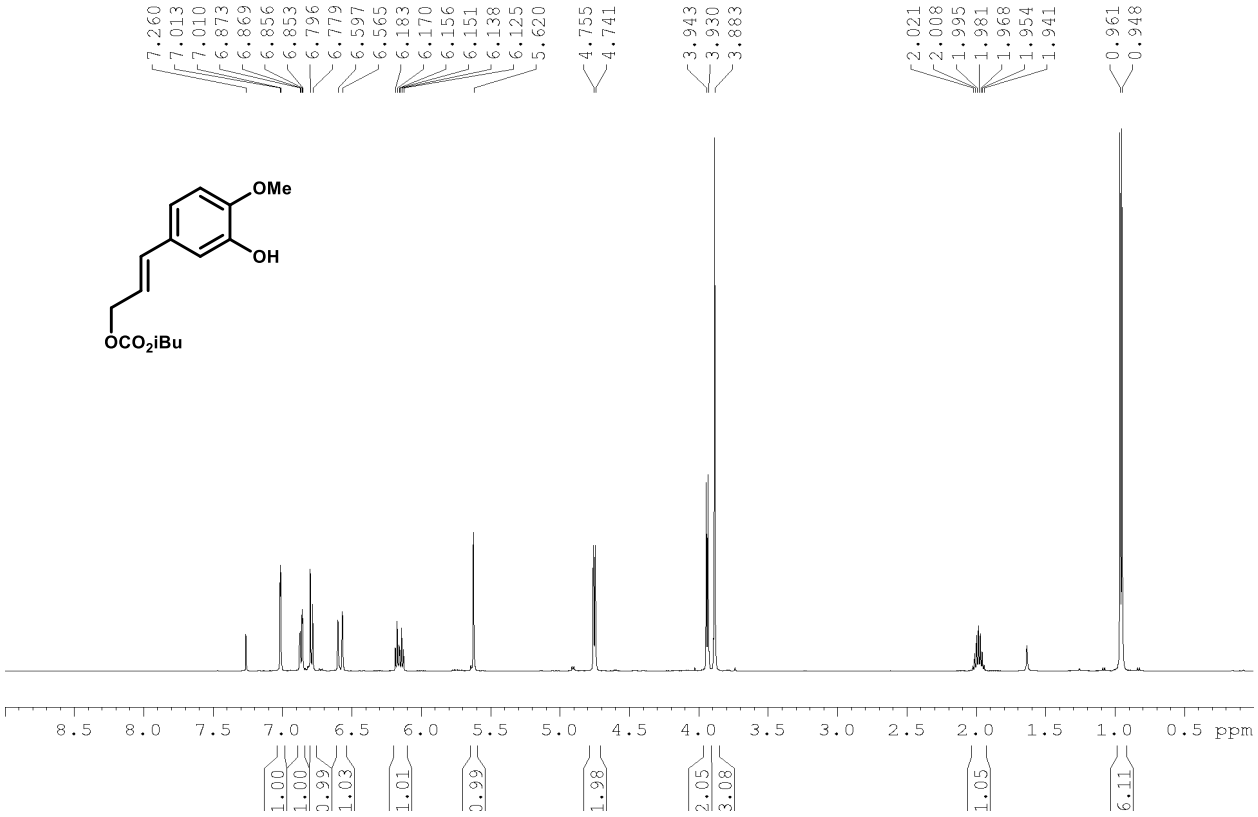

Spectrum 4.7.14 ^{13}C-NMR of compound **33** ($CDCl_3$, 126 MHz)

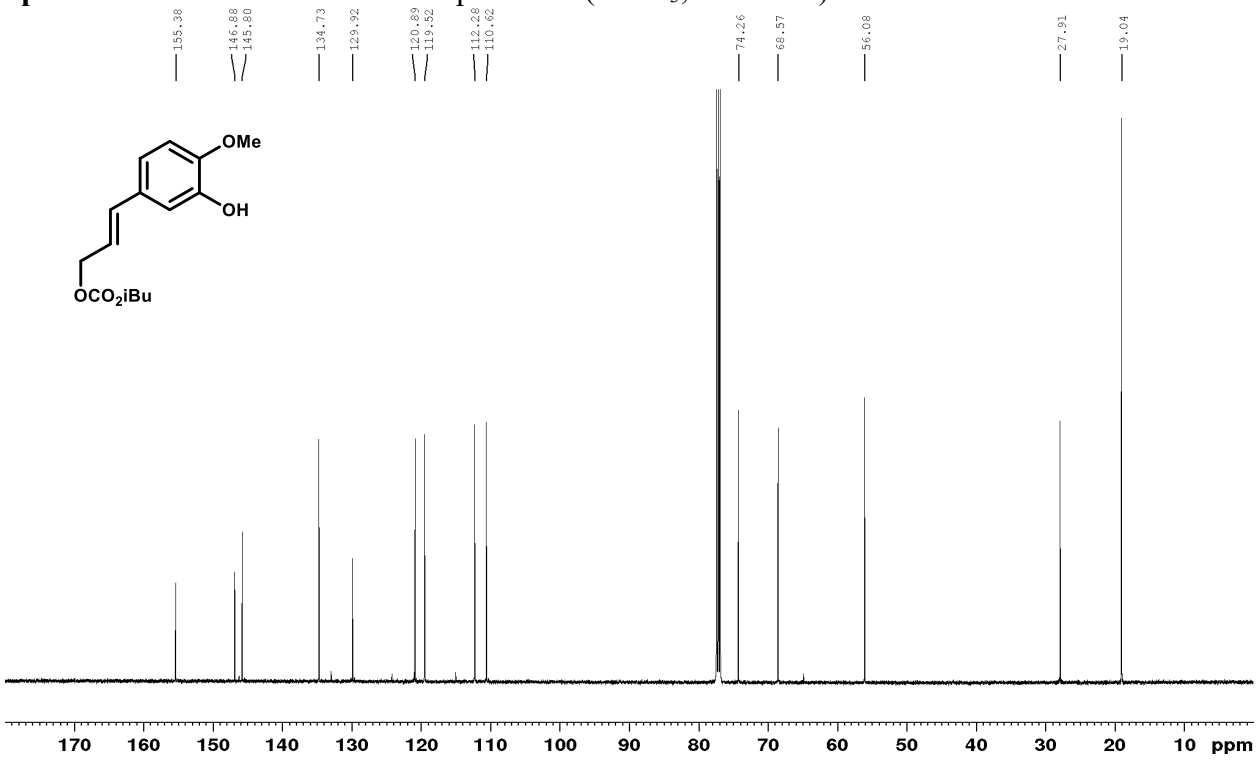

Spectrum 4.7.15 ^{1}H-NMR of compound **38** (DMSO-d_6, 600 MHz)

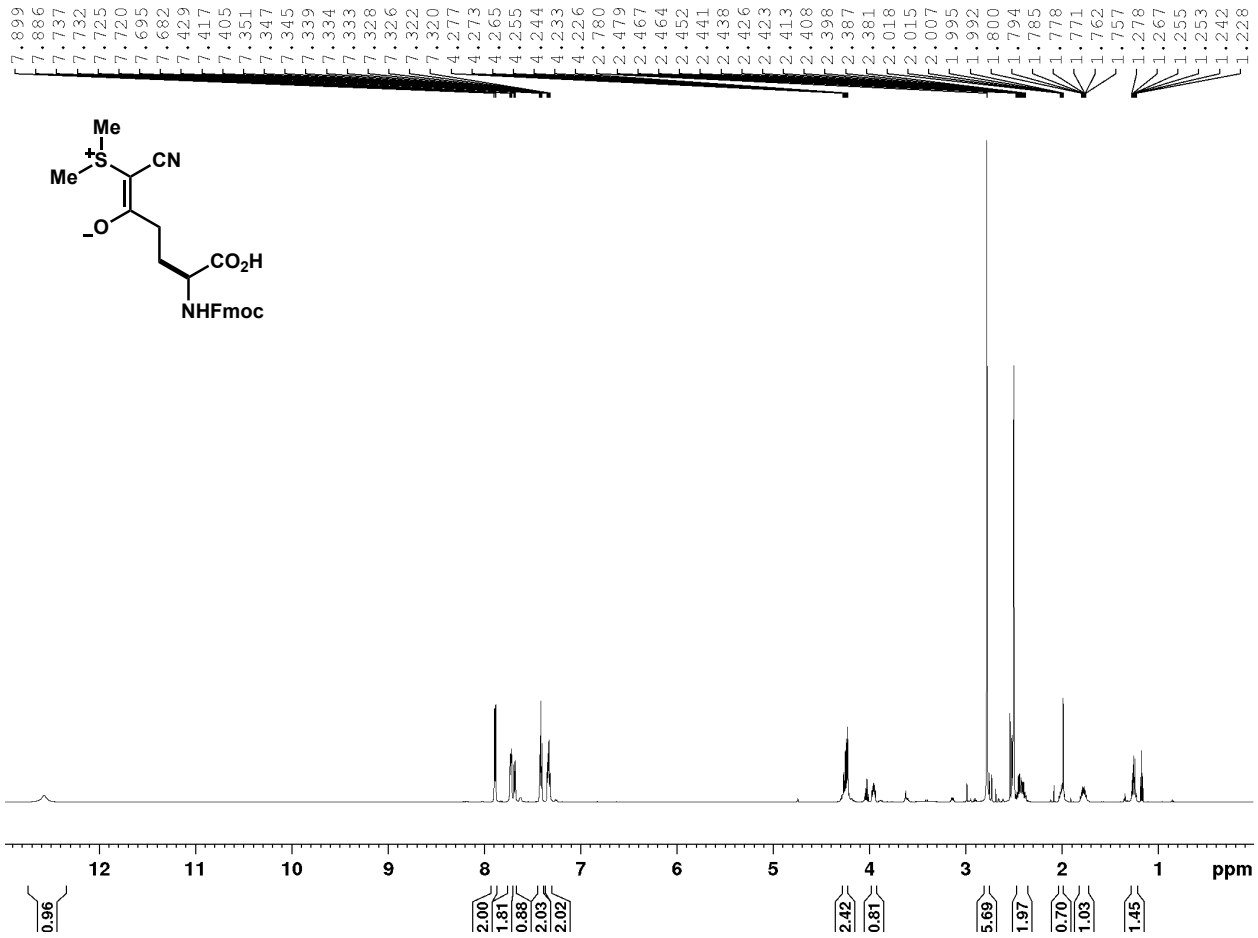

Spectrum 4.7.16 ^{13}C-NMR of compound **38** (DMSO-d_6, 151 MHz)

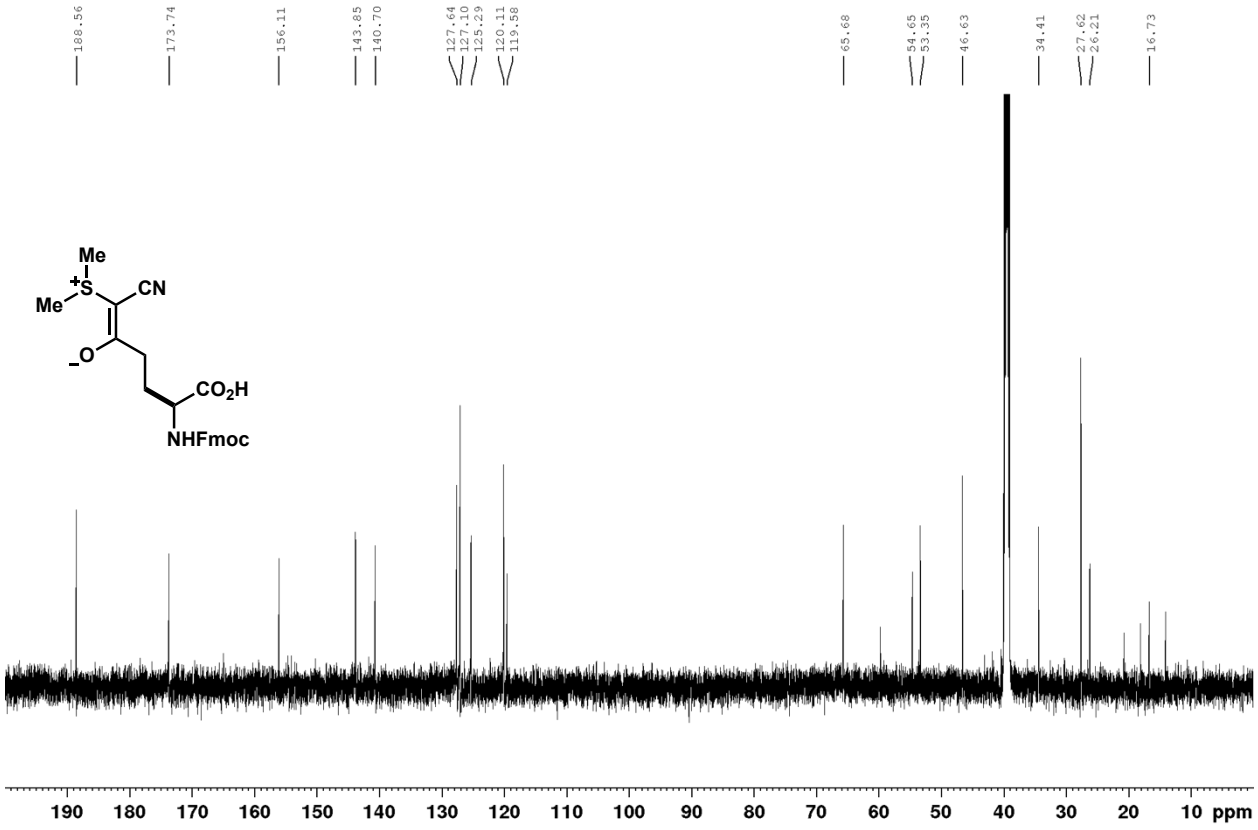

Spectrum 4.7.17 ^{1}H-NMR of Polycycle **9** (DMSO-d_6, 500 MHz)

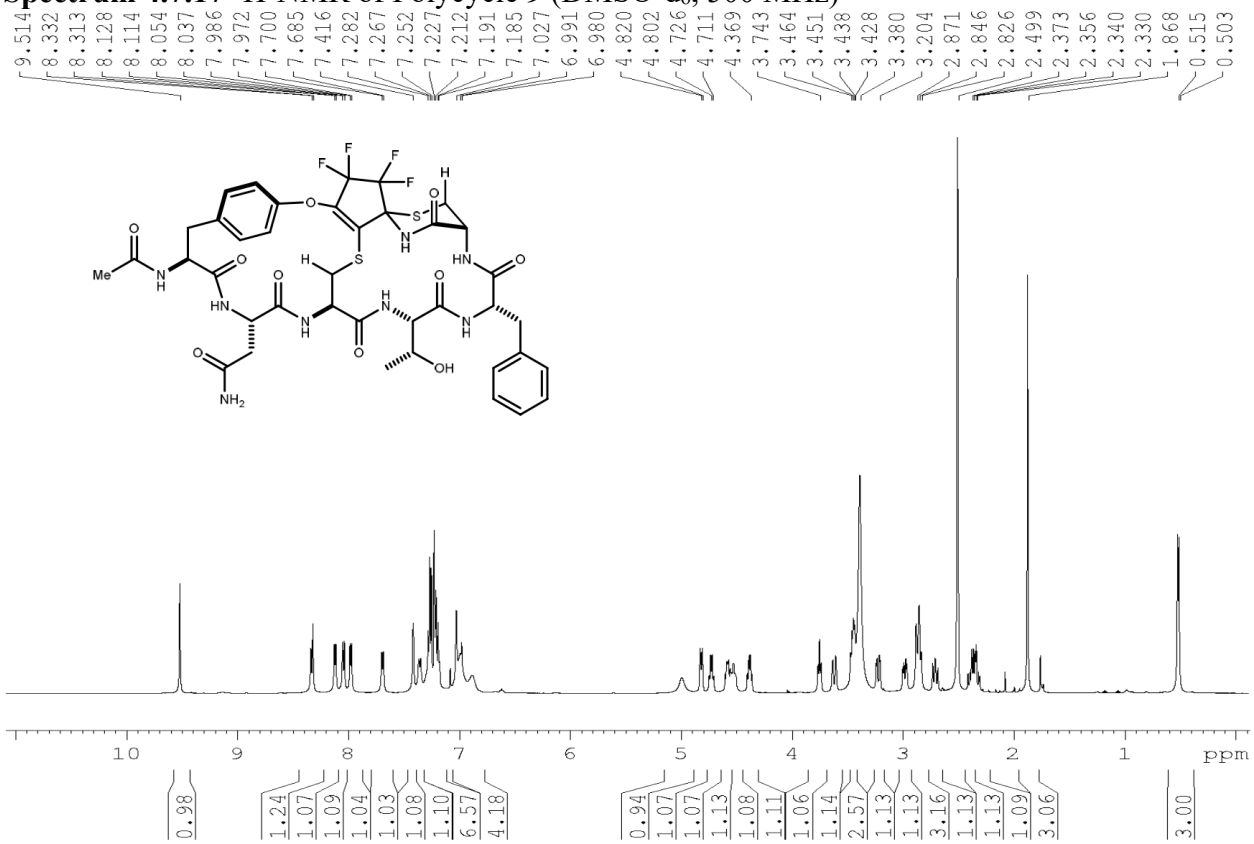

Spectrum 4.7.18 ^{13}C-NMR of Polycycle **9** (DMSO-d_6, 126 MHz)

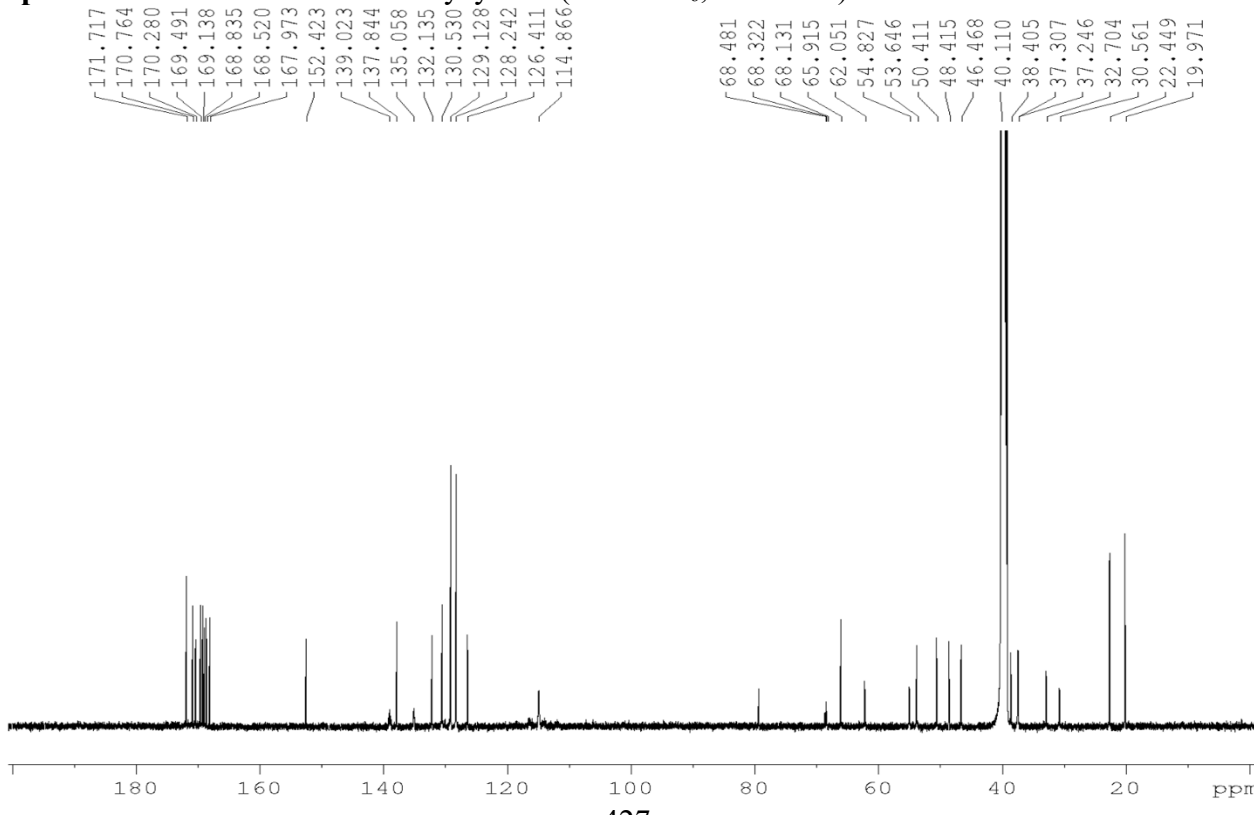

Spectrum 4.7.19 ^{19}F-NMR of Polycycle **9** (DMSO-d_6, 282 MHz)

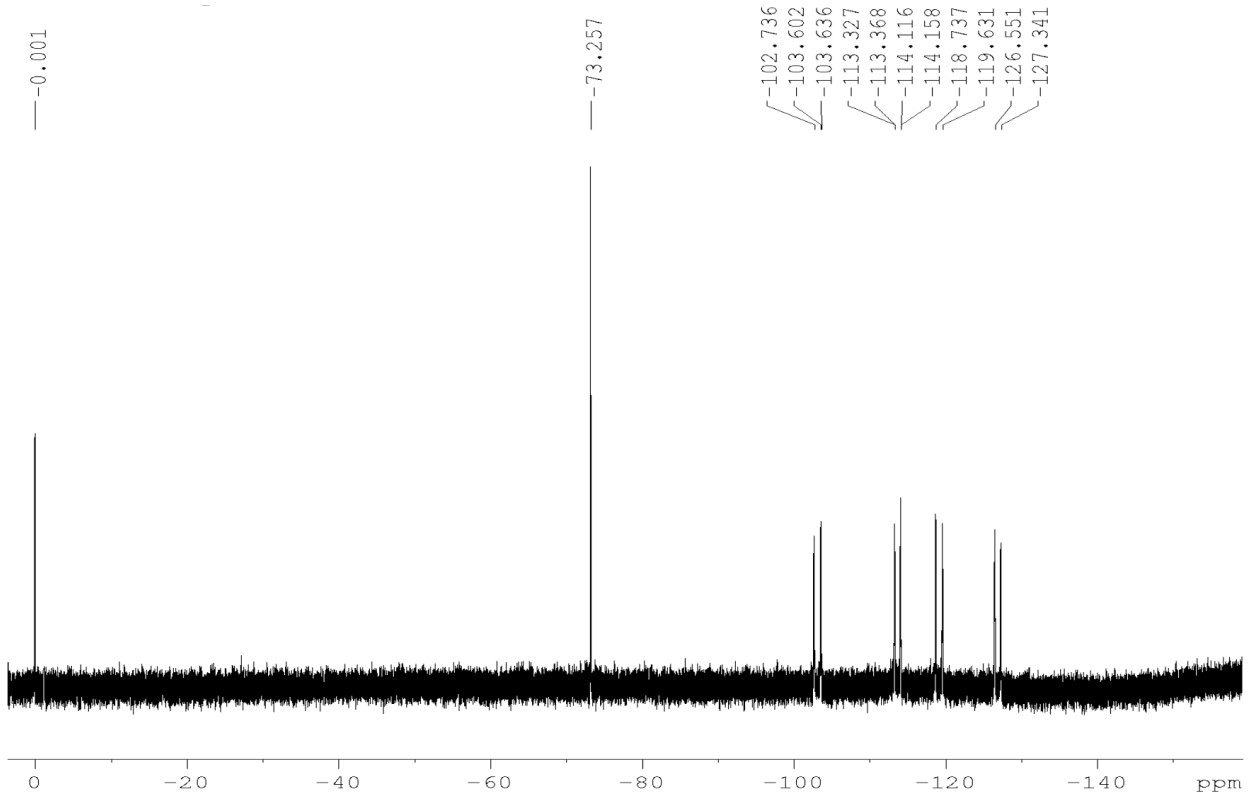

Spectrum 4.7.20 HMBC spectrum of Polycycle **9** (DMSO-d_6)

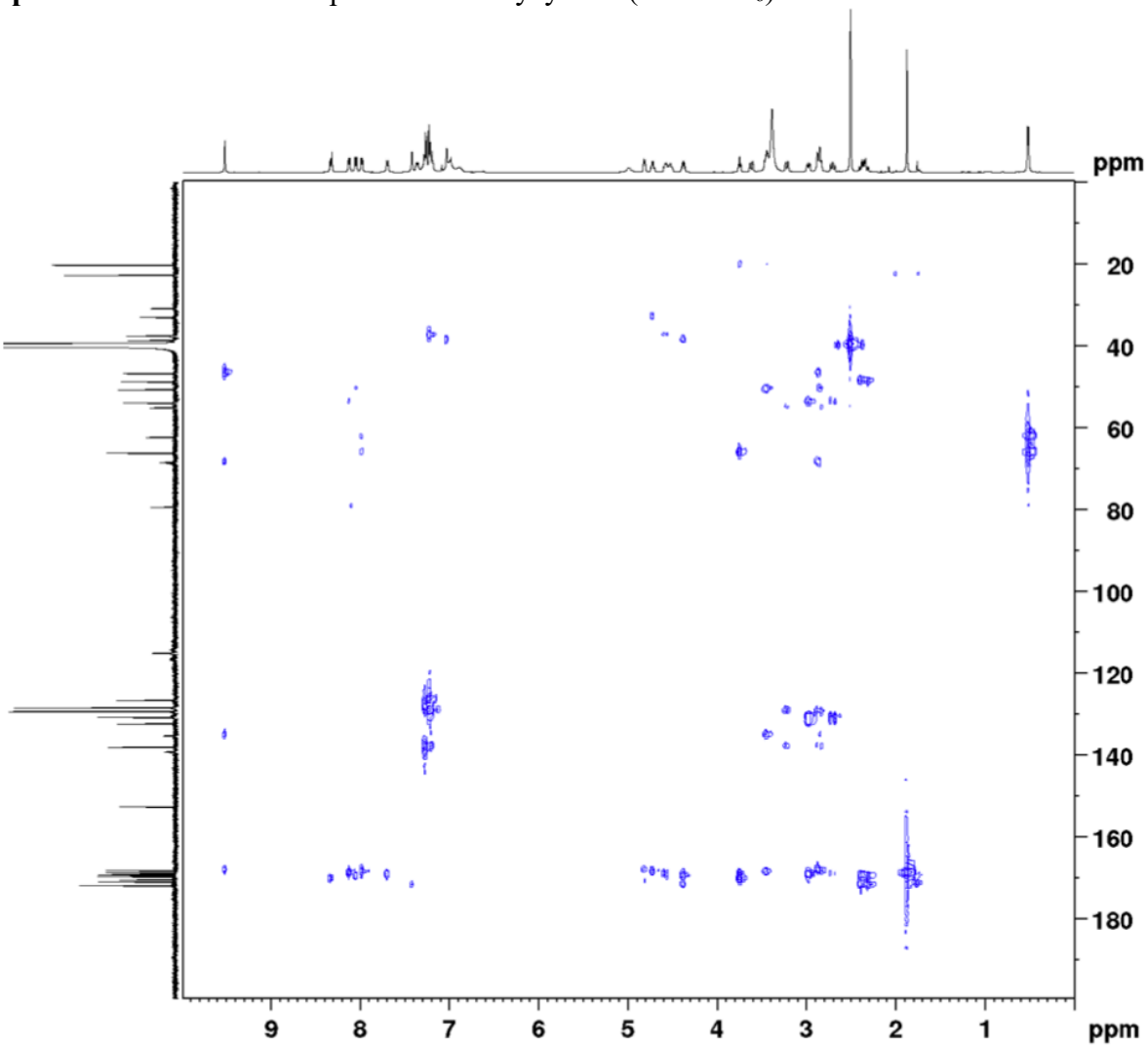

Spectrum 4.7.21 HSQC spectrum of Polycycle **9** (DMSO-d_6)

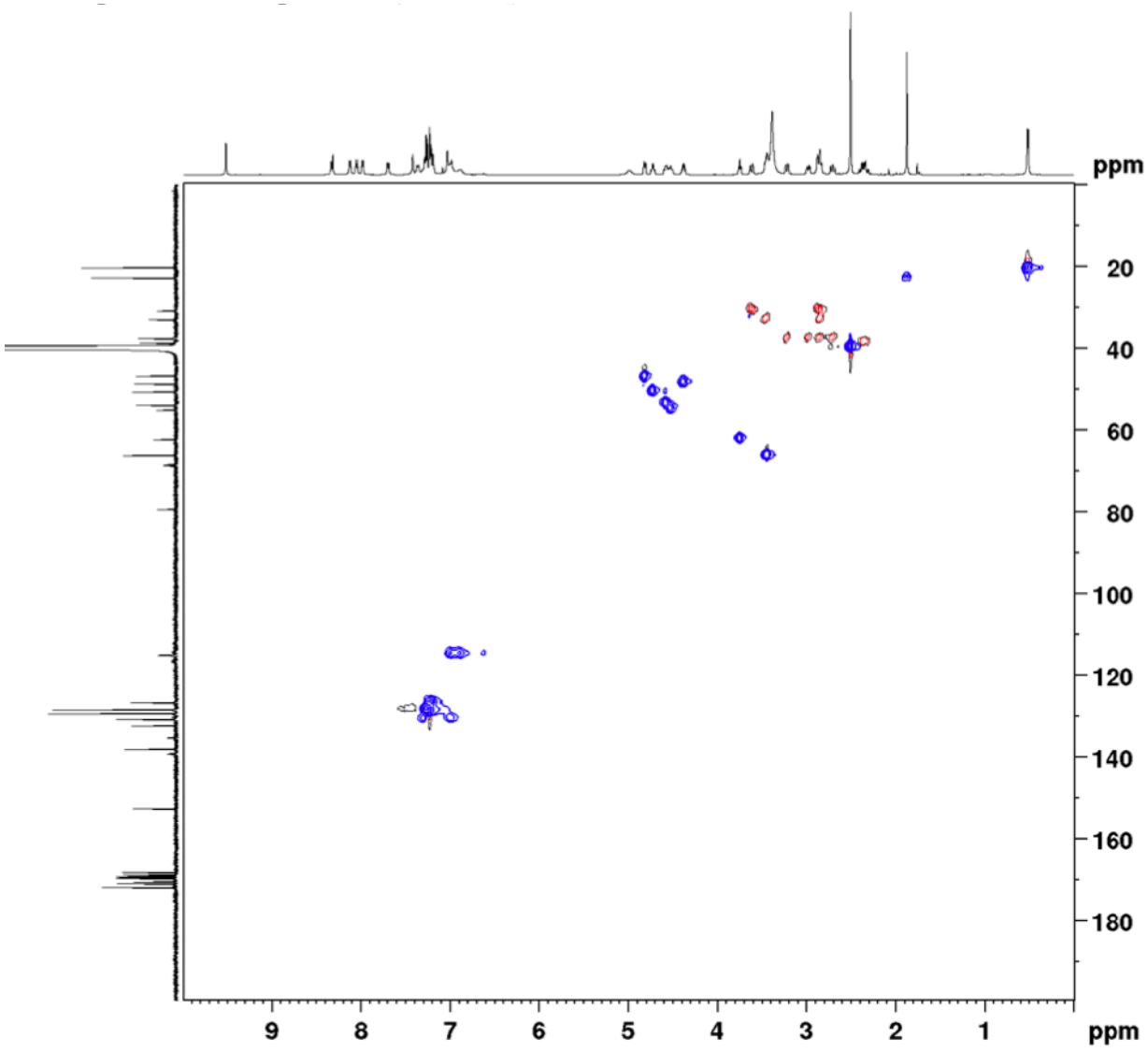

Table 4.7.11 Signal Assignment for Polycycle **9** (DMSO-d_6)

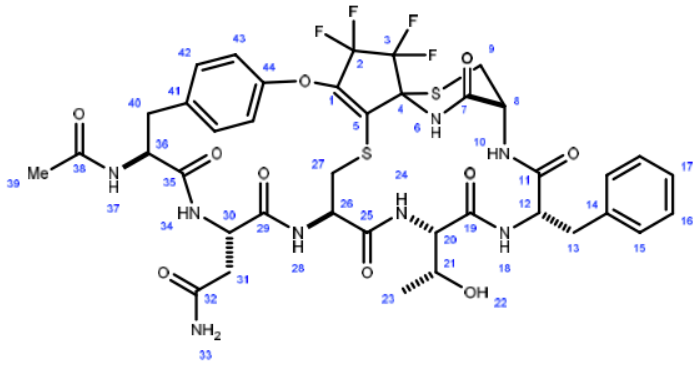

	13C	1H	Key Correlation
1	139.2–138.8 (m, 1C)	–	
2	118.7–111.5 (m, 2C)	–	
3	118.7–111.5 (m, 2C)	–	
4	68.6–68.1 (m, 1C)	–	HMBC 6, 9 –> 4
5	135.2–134.9 (m, 1C)	–	HMBC 6, 9, 27 –> 5
6	–	9.51 (s, 1H)	HMBC 6 –> 7
7	168.0	–	HMBC 6 –> 7
8	46.5	4.84–4.79 (m, 1H)	HMBC 8 –> 7, HSQC
9	30.6	3.61 (d, J = 14.0 Hz, 1H), 2.89–2.82 (m, 1H) overlap	HMBC 9 –> 4, 8, HSQC
10	–	7.36 (d, J = 8.6 Hz, 1H)	HMBC 10 –> 11
11	170.8	–	HMBC 12 –> 11
12	54.8	4.55–4.48 (m, 1H)	HMBC 13 –> 12
13	37.3 or 37.2	3.22 (dd, J = 14.0, 3.7 Hz, 1H)	HMBC 12 –> 13, HSQC
14	137.8	–	HMBC 13 –> 14
15	128.2	7.30–7.17 (m, 2H) overlap	HMBC 15 –> 14, HSQC
16	129.1	7.30–7.17 (m, 2H) overlap	HMBC 15 –> 16, HSQC
17	126.4	7.30–7.17 (m, 1H) overlap	HMBC 17 –> 16, HSQC
18	–	8.33 (d, J = 9.5 Hz, 1H)	HMBC 18 –> 19
19	170.3	–	HMBC 18, 20 –> 19
20	62.1	3.74 (t, J = 6.9 Hz, 1H)	HMBC 20 –> 19, 24, HSQC
21	65.9	3.48–3.41 (m, 1H) overlap	HMBC 20, 23 –> 21, HSQC
22	–	4.98 (brs, 1H)	
23	20.0	0.51 (d, J = 6.0 Hz, 3H)	HMBC 21 –> 23, HSQC
24	–	7.98 (d, J = 6.8 Hz, 1H)	HMBC 24 –> 20, 25
25	168.5	–	HMBC 24, 26 –> 25
26	50.4	4.72 (dd, J = 14.2, 6.8 Hz, 1H)	HMBC 26 –> 25, 27, HSQC
27	32.7	3.48–3.41 (m, 1H) overlap	HMBC 27 –> 5, HSQC
28	–	8.05 (d, J = 8.2 Hz, 1H)	HMBC 28 –> 26, 29
29	169.5	–	HMBC 28, 30 –> 29
30	48.4	4.41–1.34 (m, 1H)	HMBC 30 –> 29, 31, HSQC
31	38.4	2.38 (dd, J = 15.6, 8.5 Hz, 1H), 2.32 (dd, J = 15.6, 5.0 Hz,	HMBC 31 –> 32, HSQC
32	171.7	–	HMBC 31, 33 –> 32
33	–	7.42 (s, 1H), 7.03 (s, 1H)	HMBC 33 –> 32
34	–	7.69 (d, J = 7.7 Hz, 1H)	HMBC 34 –> 30, 35
35	169.1	–	HMBC 34, 36 –> 35
36	53.6	4.60–4.55 (m, 1H)	HMBC 37, 40 –> 36, HSQC
37	–	8.12 (d, J = 6.9 Hz, 1H)	HMBC 37 –> 36, 38, HSQC
38	168.8	–	HMBC 37, 39 –> 38
39	22.4	1.87 (s, 3H)	HMBC 39 –> 38, HSQC
40	37.3 or 37.2	2.97 (dd, J = 13.2, 5.1 Hz, 1H), 2.70 (dd, J = 13.2, 10.1 Hz	HMBC 40 –> 36, 41
41	132.1	–	HMBC 42 –> 41
42	130.5	7.30–7.17 (m, 1H) overlap, 7.06–6.84 (m, 1H) overlap	HMBC 42 –> 41, HSQC
43	114.9	7.06–6.84 (m, 2H) overlap	HMBC 43 –> 42, 44, HSQC
44	152.4	–	HMBC 43 –> 44, HSQC

Spectrum 4.7.22 ^{1}H-NMR of Polycycle **10** (DMSO-d_6, 500 MHz)

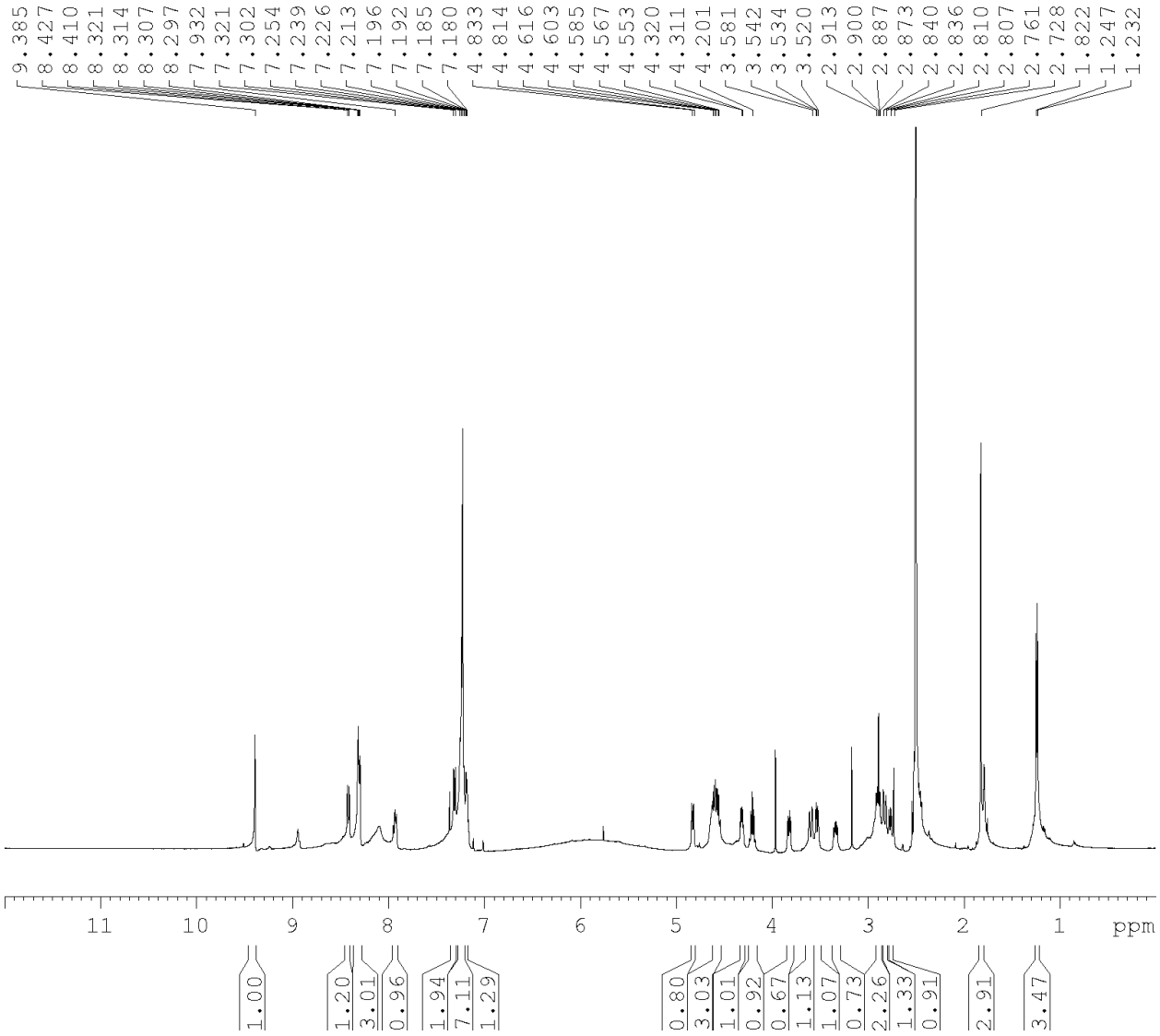

Spectrum 4.7.23 ^{13}C-NMR of Polycycle **10** (DMSO-d_6, 126 MHz)

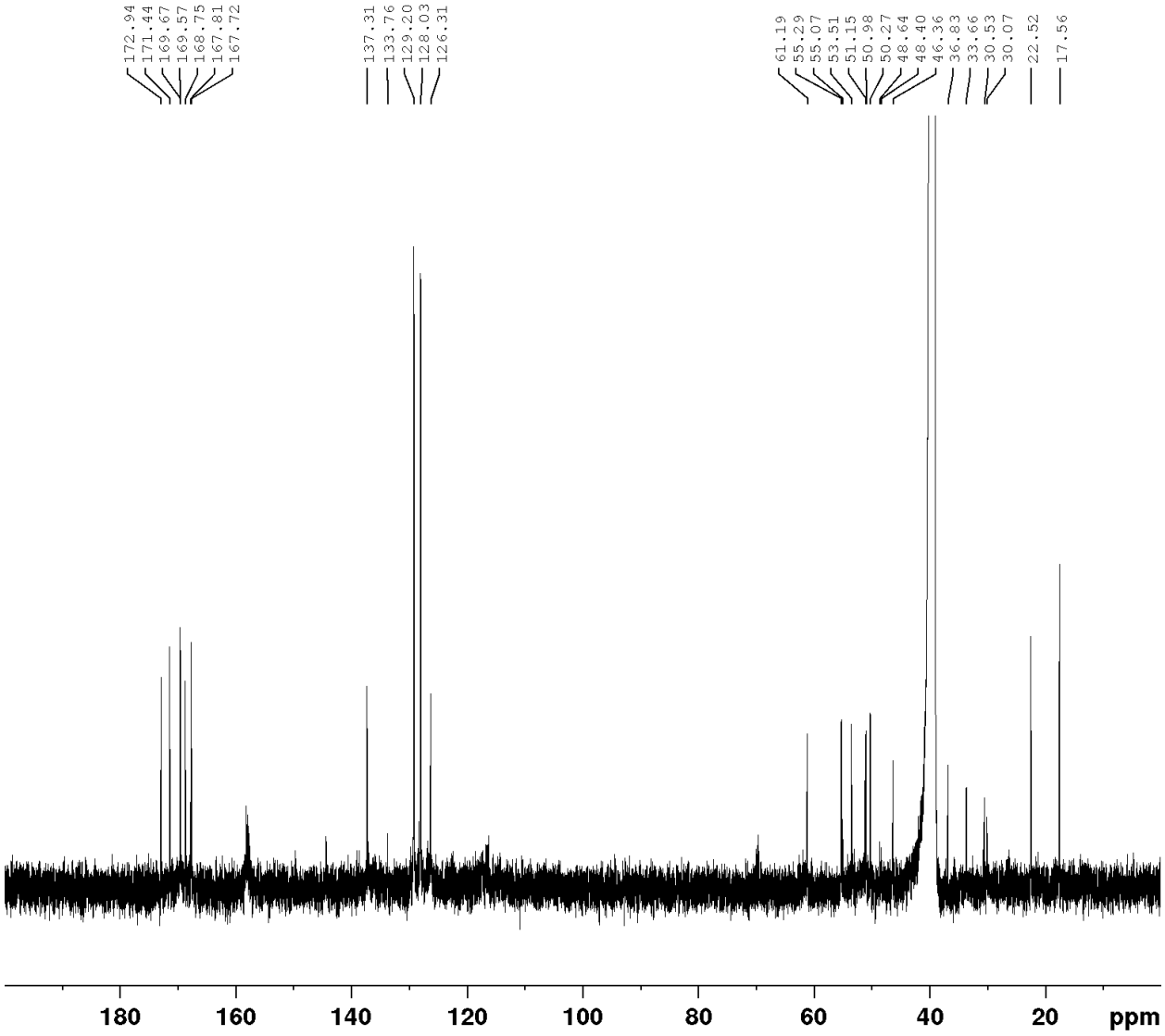

Spectrum 4.7.24 ^{19}F-NMR of Polycycle **10** (DMSO-d_6, 282 MHz)

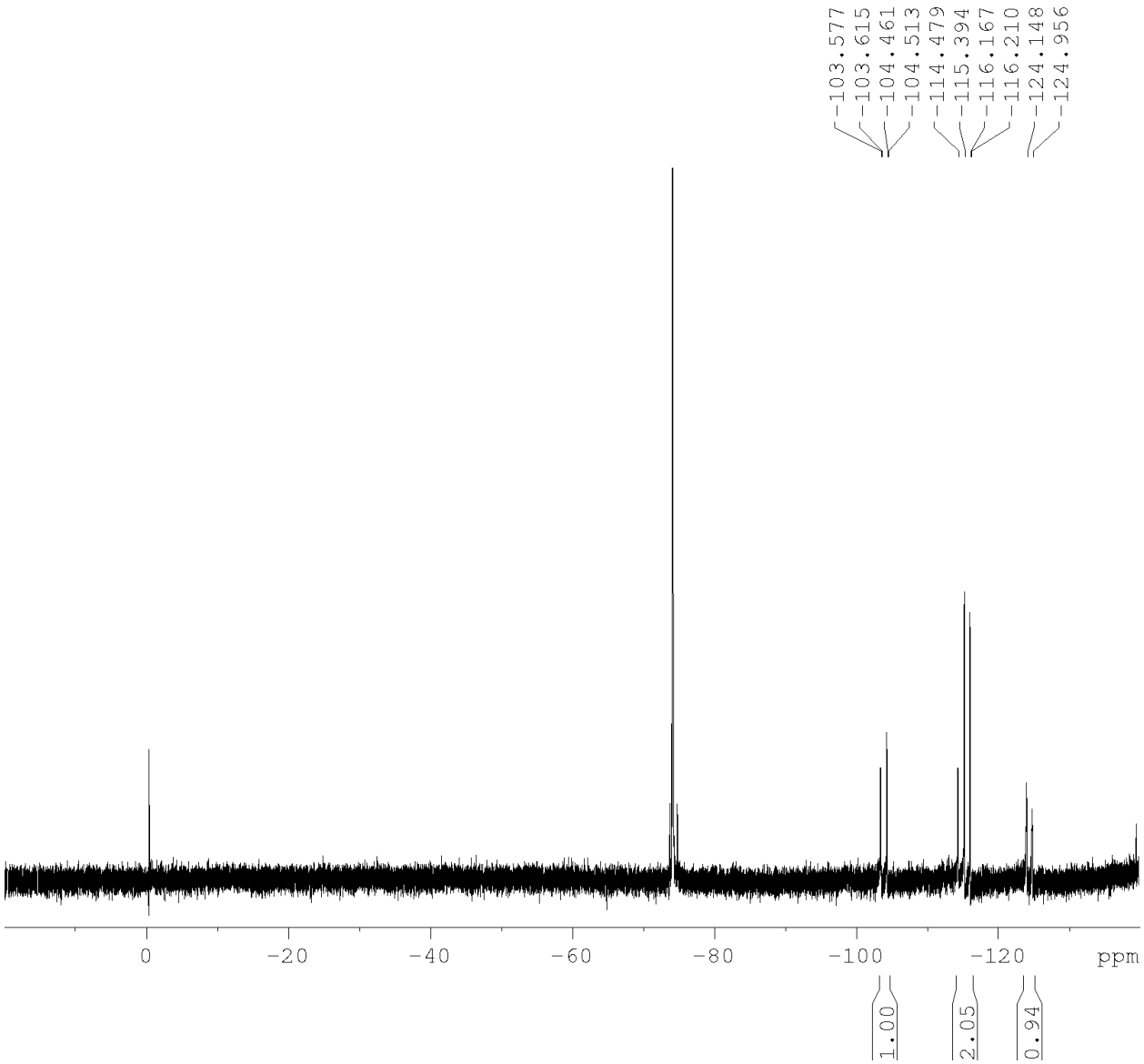

Spectrum 4.7.25 HMBC spectrum of Polycycle **10** (DMSO-d_6)

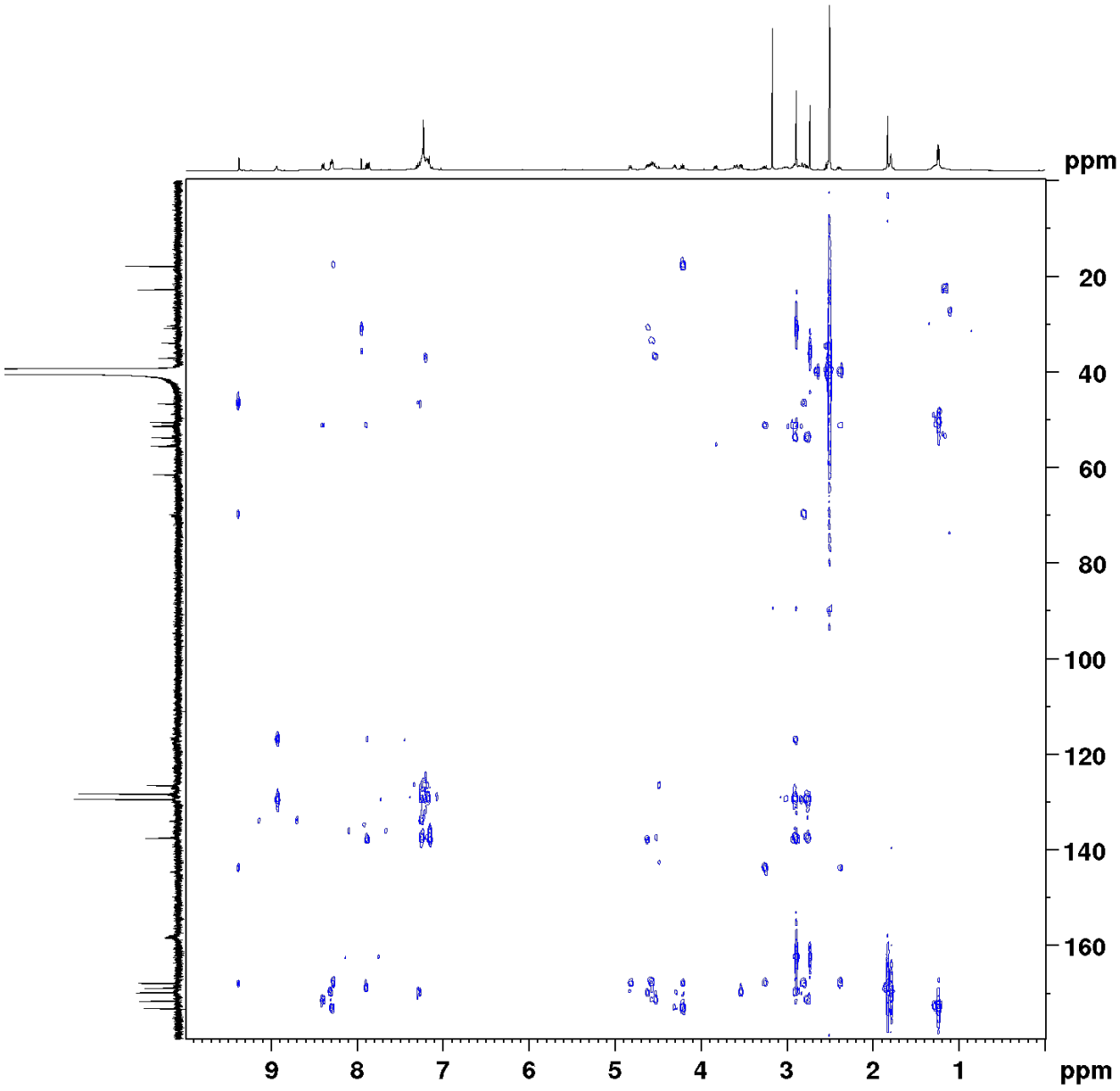

Spectrum 4.7.26 HSQC spectrum of Polycycle **10** (DMSO-d_6)

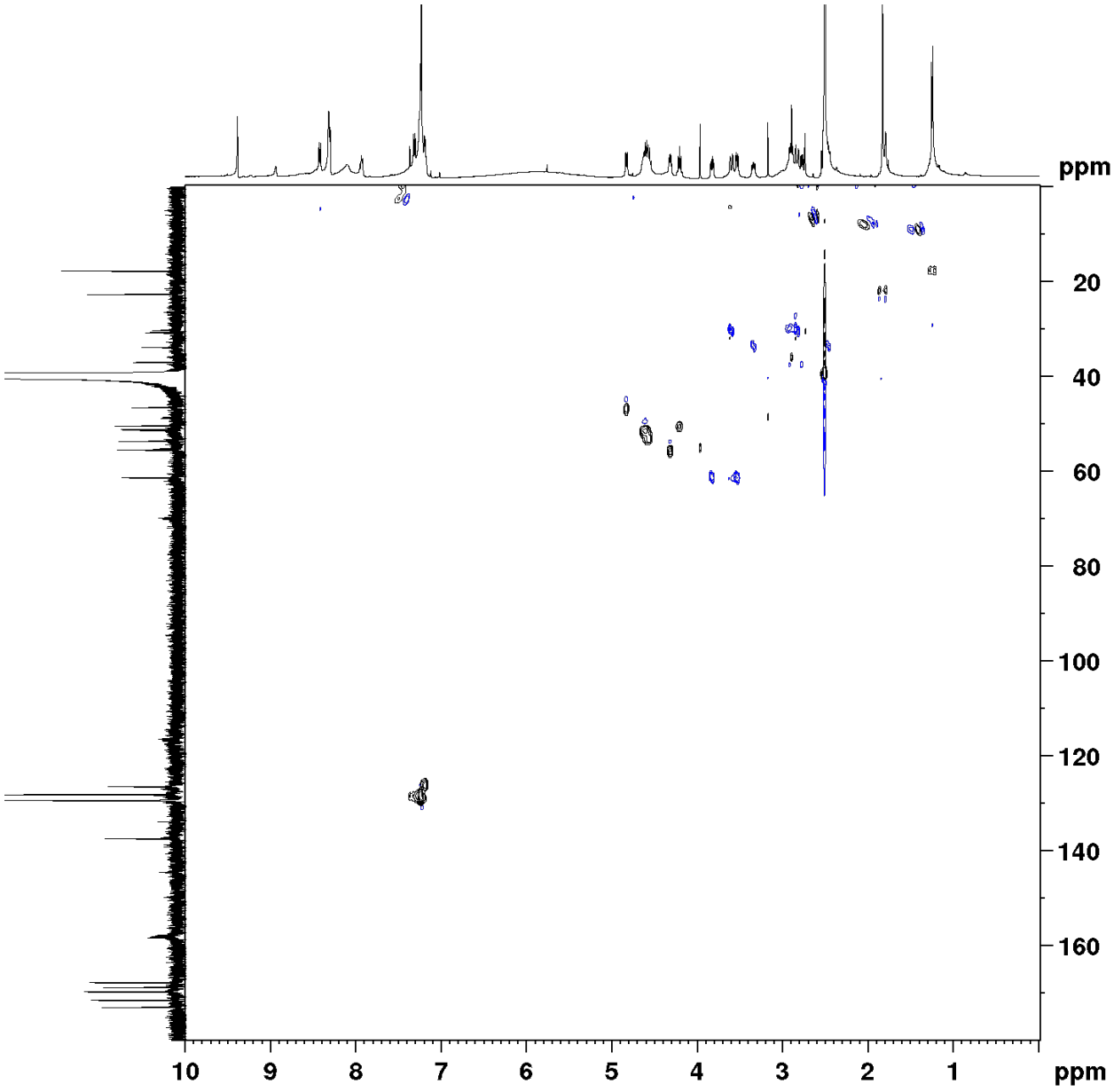

Table 4.7.12 Signal Assignment for Polycycle **10** (DMSO-d_6, 298K)

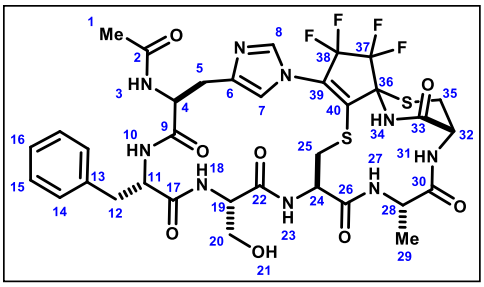

	13C	1H	Key Correlation
1	22.5	1.77 (s, 3H)	1 -> 2 HMBC
2	168.9	-	1 -> 2 HMBC
3	-	7.63 (d, J = 8.1 Hz, 1H)	3 -> 2, 4 HMBC
4	51.1	4.68 - 4.62 (m, 1H)	3 -> 4 HMBC
5	29.8	3.16 - 3.05 (m, 2H); 2.94 - 2.81 (m, 3H)	4 -> 5 HMBC
6	139.0	-	4, 5 -> 6 HMBC
7	114.5	7.38 (s, 1H)	8 -> 7 HMBC
8	135.6	8.07 - 8.01 (m, 2H)	8 -> 7 HMBC
9	170.0	-	4 -> 9 HMBC
10	-	8.41 (d, J = 8.7 Hz, 1H)	10 -> 9 HMBC
11	55.1	4.43 - 4.36 (m, 1H)	10 -> 11 HMBC
12	37.8	3.03 - 2.94 (m, 2H); 2.90 - 2.81 (m, 3H)	11 -> 12 HMBC
13	137.5	-	12 -> 13 HMBC
14	129.0	7.28 - 7.17 (m, 6H)	12 -> 14 HMBC
15	128.2	7.28 - 7.17 (m, 6H)	14 -> 15 HMBC
16	126.4	7.28 - 7.17 (m, 6H)	15 -> 16 HMBC
17	170.1	-	11, 19 -> 17 HMBC
18	-	7.28 - 7.17 (m, 6H)	-
19	53.8	4.62 - 4.56 (m, 2H)	20 -> 19 HMBC
20	61.3	3.57 - 3.39 (m, 3H)	19 -> 20 HMBC
21	-	-	-
22	170.3	-	19, 23 -> 22 HMBC
23	-	8.07 - 8.01 (m, 2H)	23 -> 24 COSY
24	51.6	4.75 - 4.70 (m, 1H)	23 -> 24 COSY
25	38.6	3.80 - 3.73 (m, 1H); 3.16 - 3.05 (m, 2H)	24 -> 25 HMBC
26	167.9	-	27 -> 26 HMBC
27	-	9.10 (d, J = 7.7, 1H)	27 -> 28 HMBC
28	48.5	4.52 (quint, J = 7.2, 1H)	29 -> 28 HMBC
29	16.0	1.31 (d, J = 7.3 Hz, 3H)	28 -> 29 HMBC
30	170.6	-	31 -> 30 HMBC
31	-	7.54 (d, J = 7.65 Hz, 1H)	32 -> 32, 35 HMBC
32	47.1	4.62 - 4.56 (m, 2H)	HMBC 34 -> 32 HMBC
33	167.5	-	34 -> 35 HMBC
34	-	8.84 (s, 1H)	34 -> 36 HMBC
35	30.8	3.47 - 3.41 (m, 1H) 3.03 - 2.94 (m, 2H)	35 -> 36 HMBC
36	70.4 - 69.7 (m, 1C)	-	35 -> 36 HMBC
37	117.6 - 115.8 (m, 2C)	-	
38	117.6 - 115.8 (m, 2C)	-	
39	141.3 - 140.9 (m, 1C)	-	
40	132.8 - 132.6 (m, 1C)	-	

Spectrum 4.7.27 ^{1}H-NMR of Polycycle **11** (DMSO-d_6, 500 MHz)

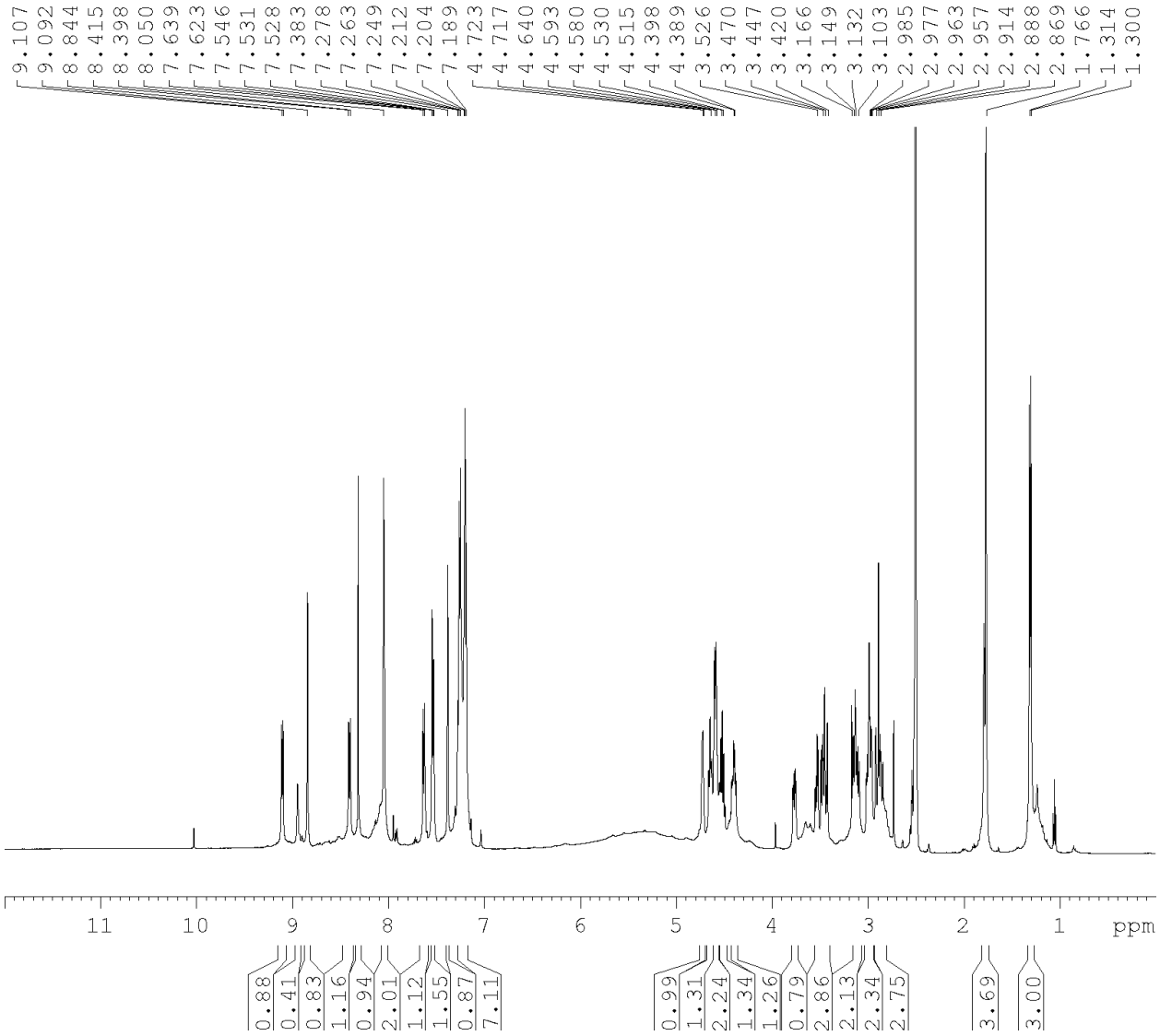

Spectrum 4.7.28 ^{13}C-NMR of Polycycle **11** (DMSO-d_6, 126 MHz)

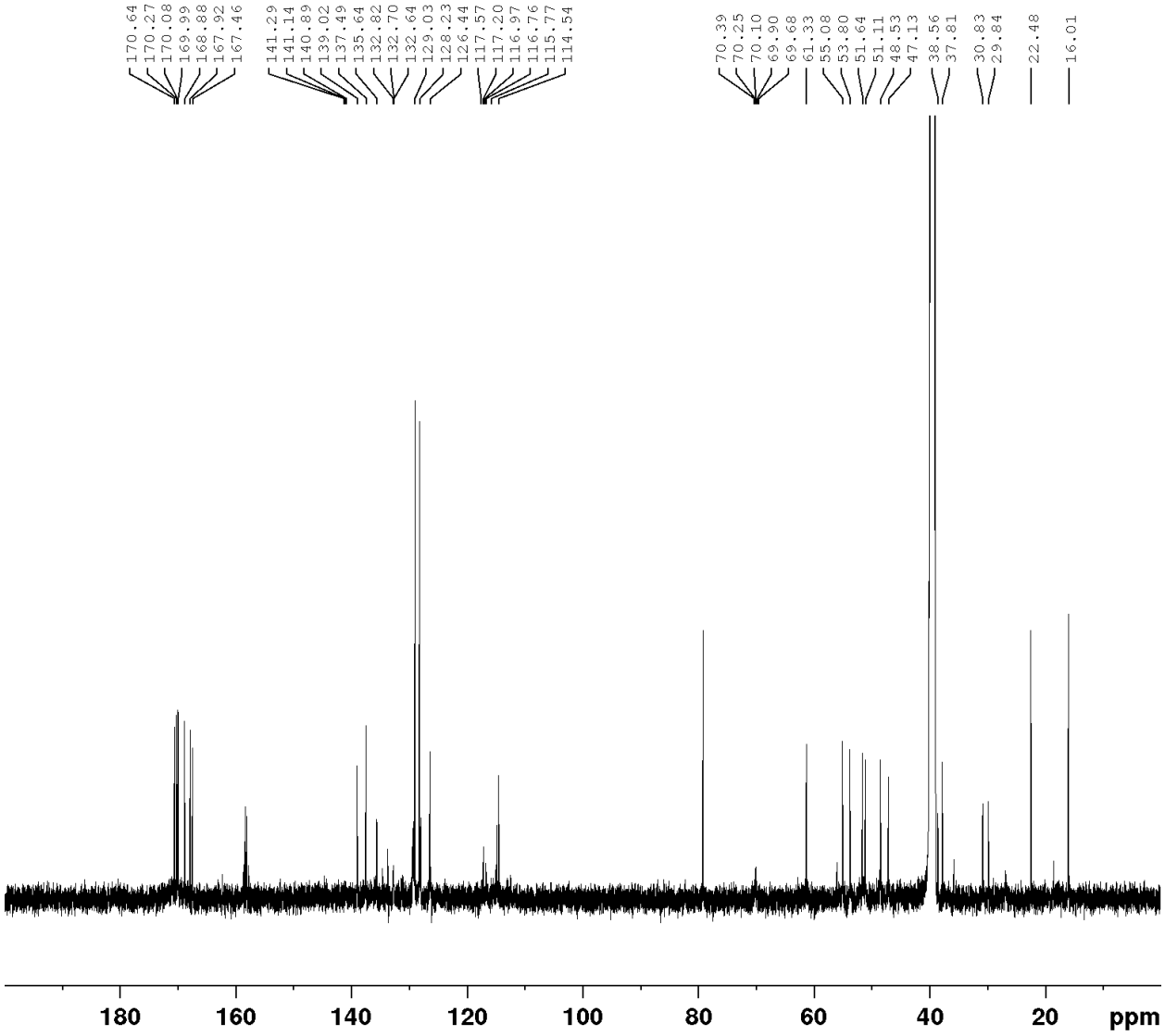

Spectrum 4.7.29 ^{19}F-NMR of Polycycle **11** (DMSO-d_6, 282 MHz)

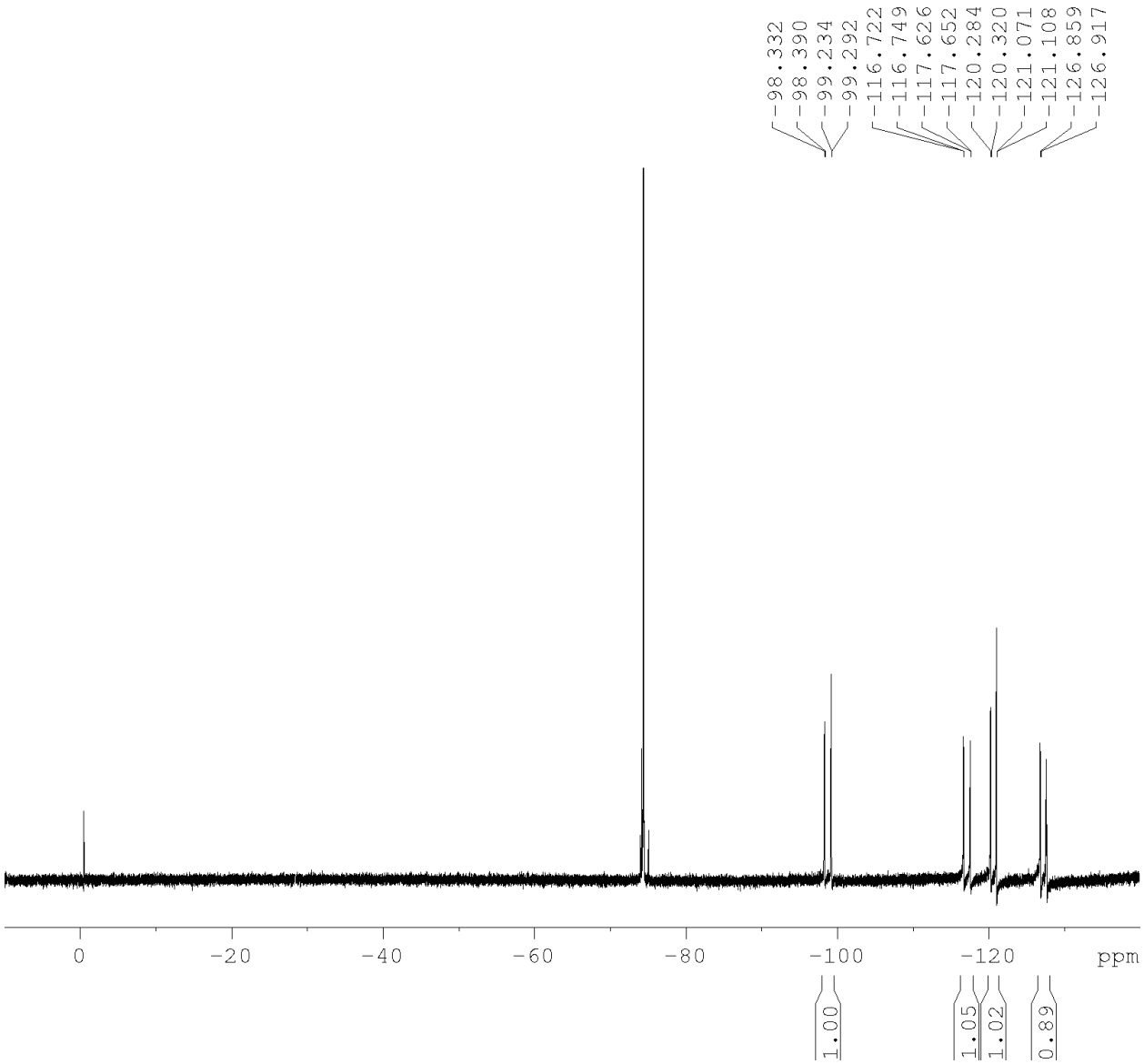

Spectrum 4.7.30 HMBC spectrum of polycycle **11** (DMSO-d_6)

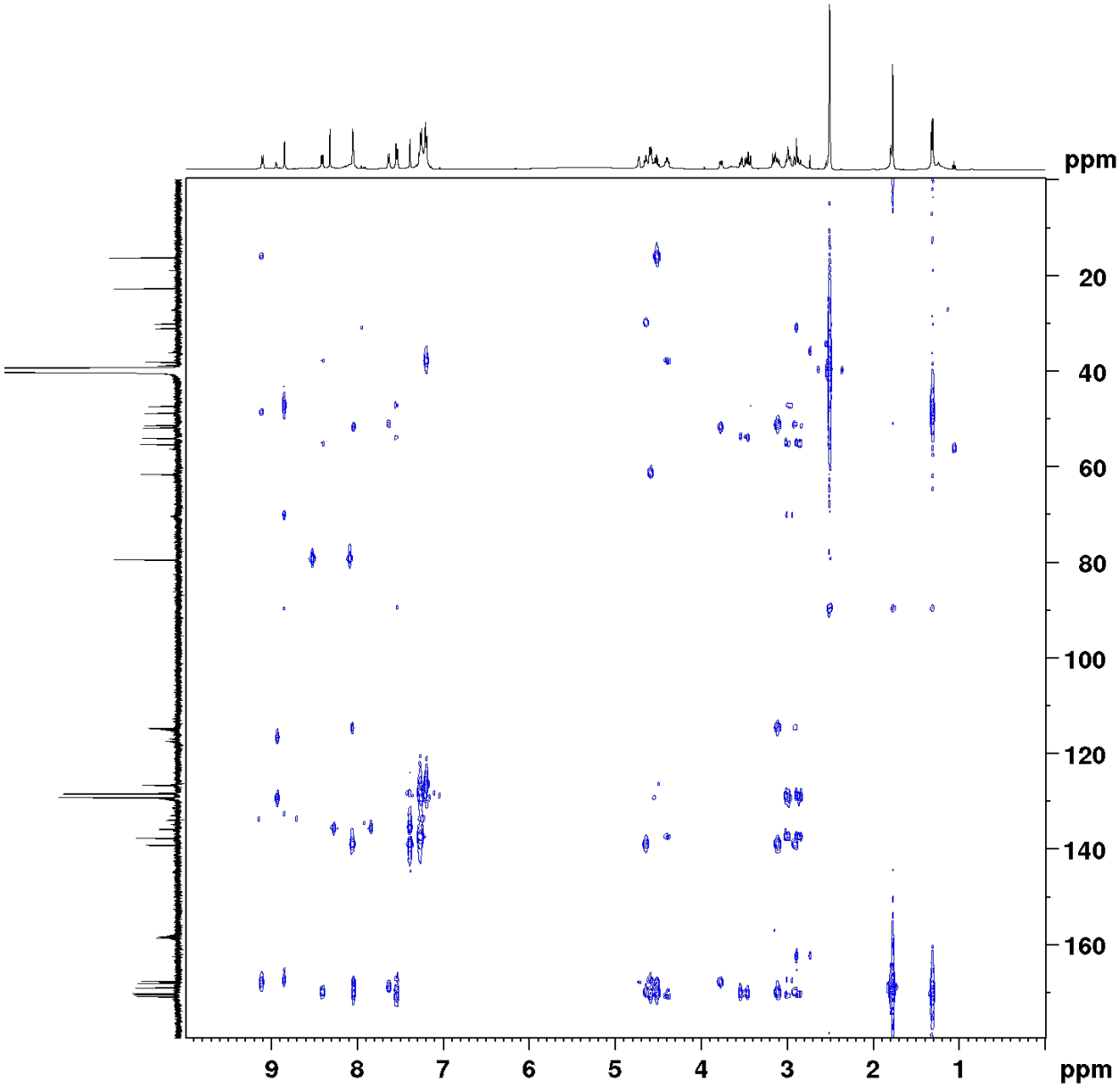

Spectrum 4.7.31 HSQC spectrum of polycycle **11** (DMSO-d_6)

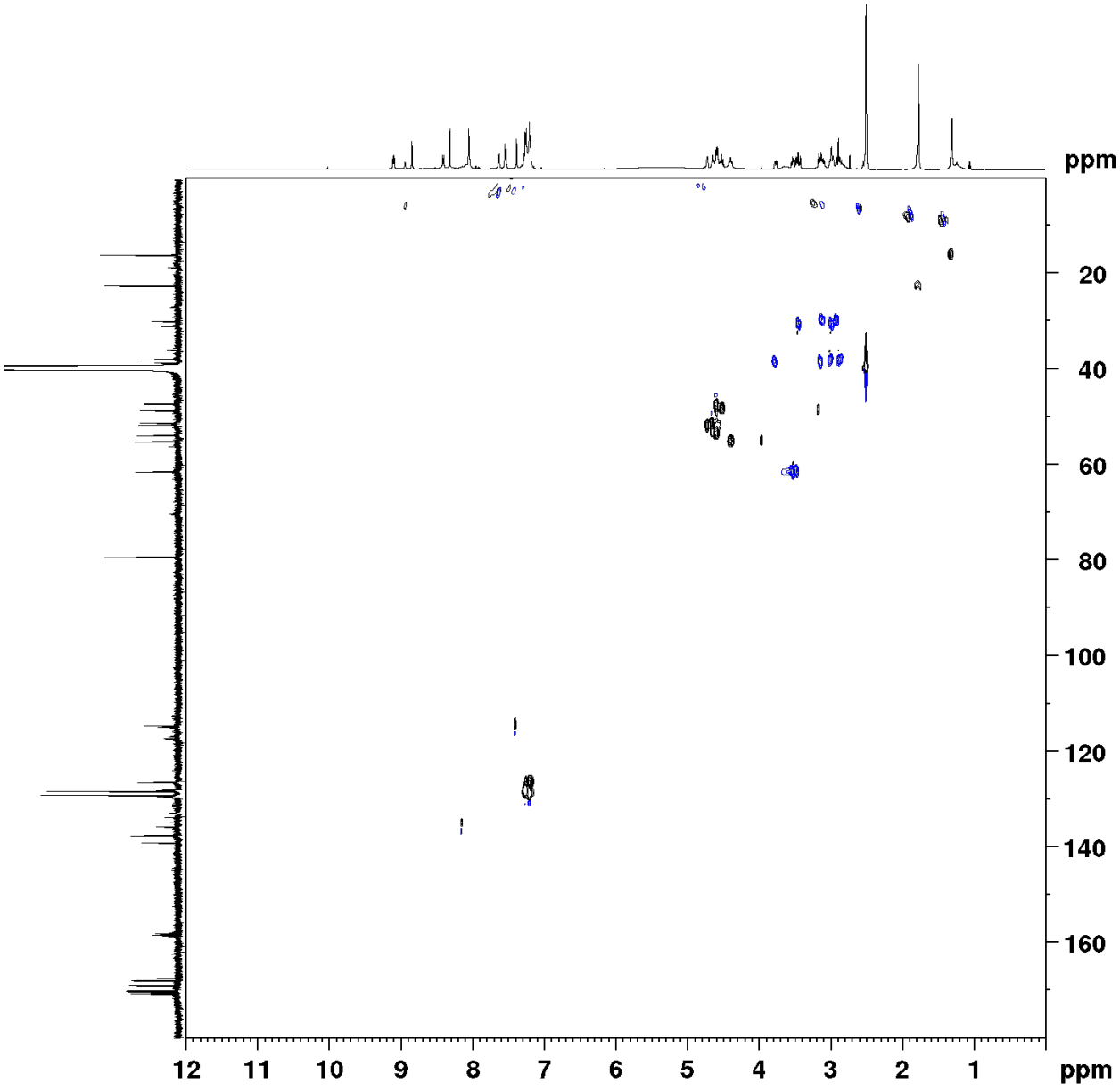

Spectrum 4.7.32 COSY spectrum of polycycle **11** (DMSO-d_6)

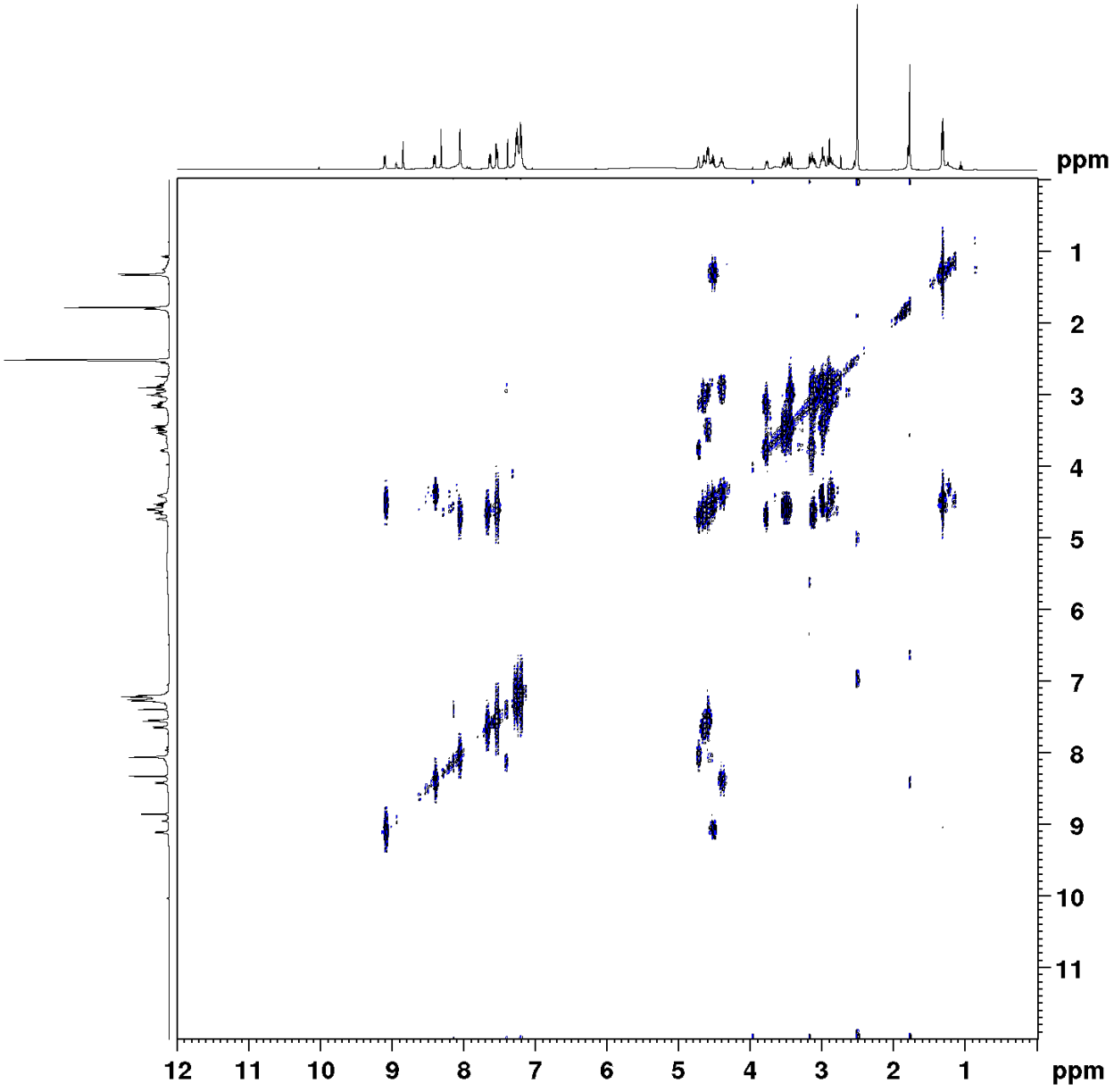

Table 4.7.13 Signal Assignment for Polycycle **11** (DMSO-d_6, 298K)

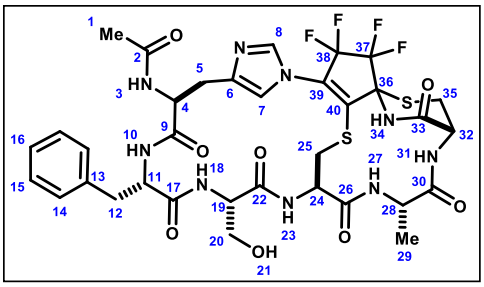

	13C	1H	Key Correlation
1	22.5	1.77 (s, 3H)	1 -> 2 HMBC
2	168.9	-	1 -> 2 HMBC
3	-	7.63 (d, J = 8.1 Hz, 1H)	3 -> 2, 4 HMBC
4	51.1	4.68 - 4.62 (m, 1H)	3 -> 4 HMBC
5	29.8	3.16 - 3.05 (m, 2H); 2.94 - 2.81 (m, 3H)	4 -> 5 HMBC
6	139.0	-	4, 5 -> 6 HMBC
7	114.5	7.38 (s, 1H)	8 -> 7 HMBC
8	135.6	8.07 - 8.01 (m, 2H)	8 -> 7 HMBC
9	170.0	-	4 -> 9 HMBC
10	-	8.41 (d, J = 8.7 Hz, 1H)	10 -> 9 HMBC
11	55.1	4.43 - 4.36 (m, 1H)	10 -> 11 HMBC
12	37.8	3.03 - 2.94 (m, 2H); 2.90 - 2.81 (m, 3H)	11 -> 12 HMBC
13	137.5	-	12 -> 13 HMBC
14	129.0	7.28 - 7.17 (m, 6H)	12 -> 14 HMBC
15	128.2	7.28 - 7.17 (m, 6H)	14 -> 15 HMBC
16	126.4	7.28 - 7.17 (m, 6H)	15 -> 16 HMBC
17	170.1	-	11, 19 -> 17 HMBC
18	-	7.28 - 7.17 (m, 6H)	-
19	53.8	4.62 - 4.56 (m, 2H)	20 -> 19 HMBC
20	61.3	3.57 - 3.39 (m, 3H)	19 -> 20 HMBC
21	-	-	-
22	170.3	-	19, 23 -> 22 HMBC
23	-	8.07 - 8.01 (m, 2H)	23 -> 24 COSY
24	51.6	4.75 - 4.70 (m, 1H)	23 -> 24 COSY
25	38.6	3.80 - 3.73 (m, 1H); 3.16 - 3.05 (m, 2H)	24 -> 25 HMBC
26	167.9	-	27 -> 26 HMBC
27	-	9.10 (d, J = 7.7, 1H)	27 -> 28 HMBC
28	48.5	4.52 (quint, J = 7.2, 1H)	29 -> 28 HMBC
29	16.0	1.31 (d, J = 7.3 Hz, 3H)	28 -> 29 HMBC
30	170.6	-	31 -> 30 HMBC
31	-	7.54 (d, J = 7.65 Hz, 1H)	32 -> 32, 35 HMBC
32	47.1	4.62 - 4.56 (m, 2H)	HMBC 34 -> 32 HMBC
33	167.5	-	34 -> 35 HMBC
34	-	8.84 (s, 1H)	34 -> 36 HMBC
35	30.8	3.47 - 3.41 (m, 1H) 3.03 - 2.94 (m, 2H)	35 -> 36 HMBC
36	70.4 - 69.7 (m, 1C)	-	35 -> 36 HMBC
37	117.6 - 115.8 (m, 2C)	-	
38	117.6 - 115.8 (m, 2C)	-	
39	141.3 - 140.9 (m, 1C)	-	
40	132.8 - 132.6 (m, 1C)	-	

Spectrum 4.7.33 ^{1}H-NMR of Polycycle **12** (DMSO-d_6, 600 MHz)

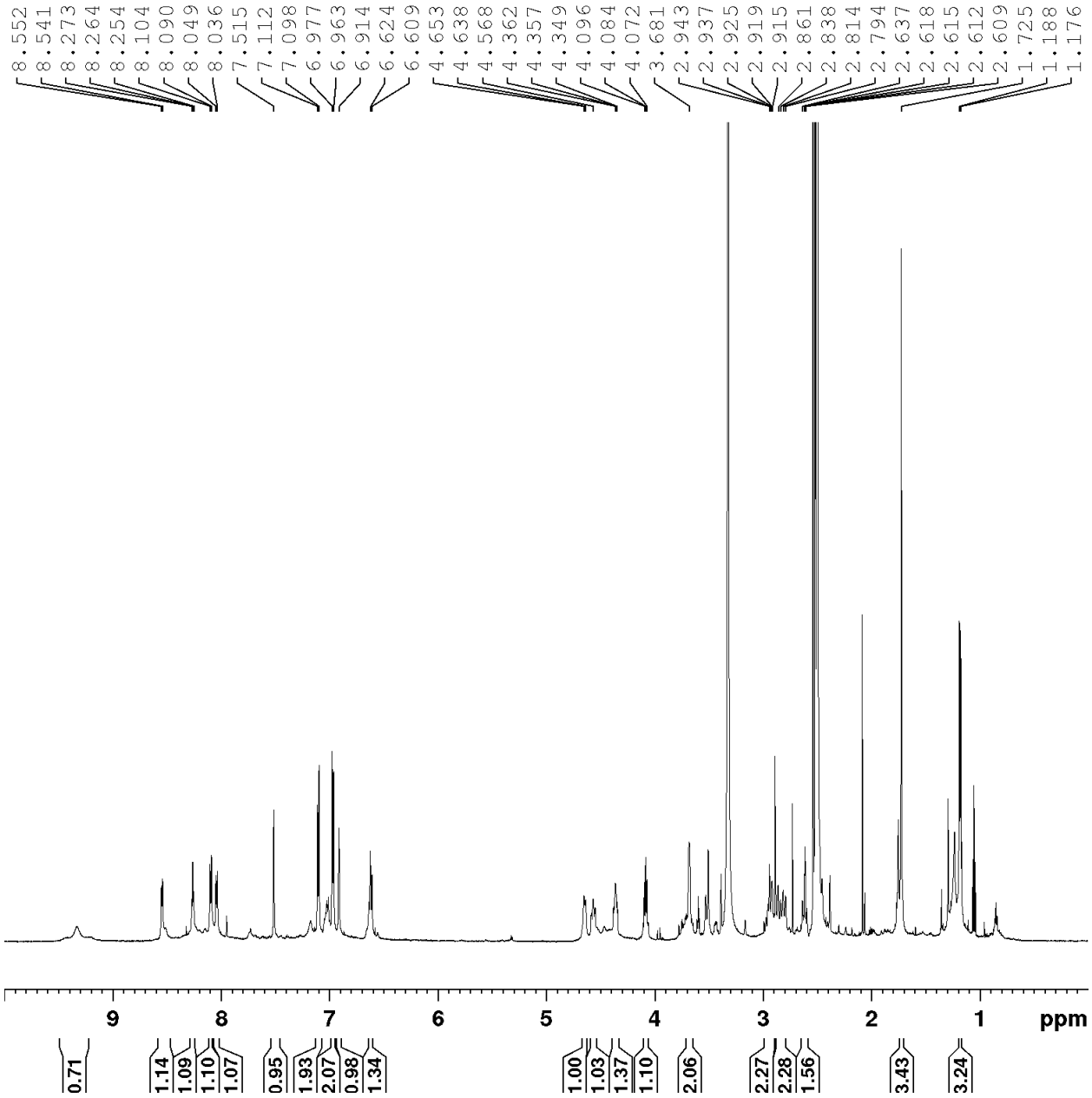

Spectrum 4.7.34 ^{13}C-NMR of Polycycle **12** (DMSO-d_6, 126 MHz)

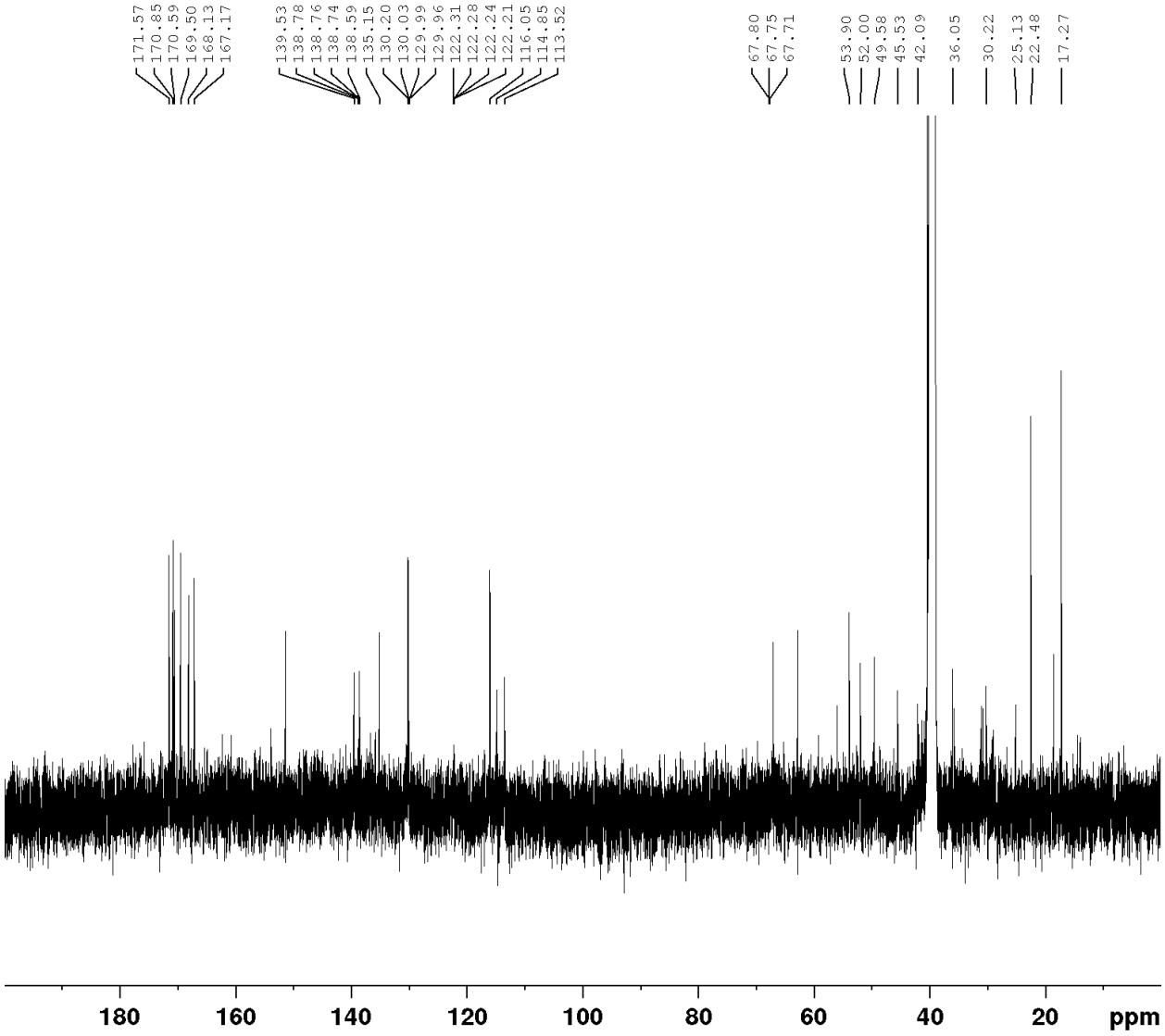

Spectrum 4.7.35 ^{19}F-NMR of Polycycle **12** (DMSO-d_6, 565 MHz)

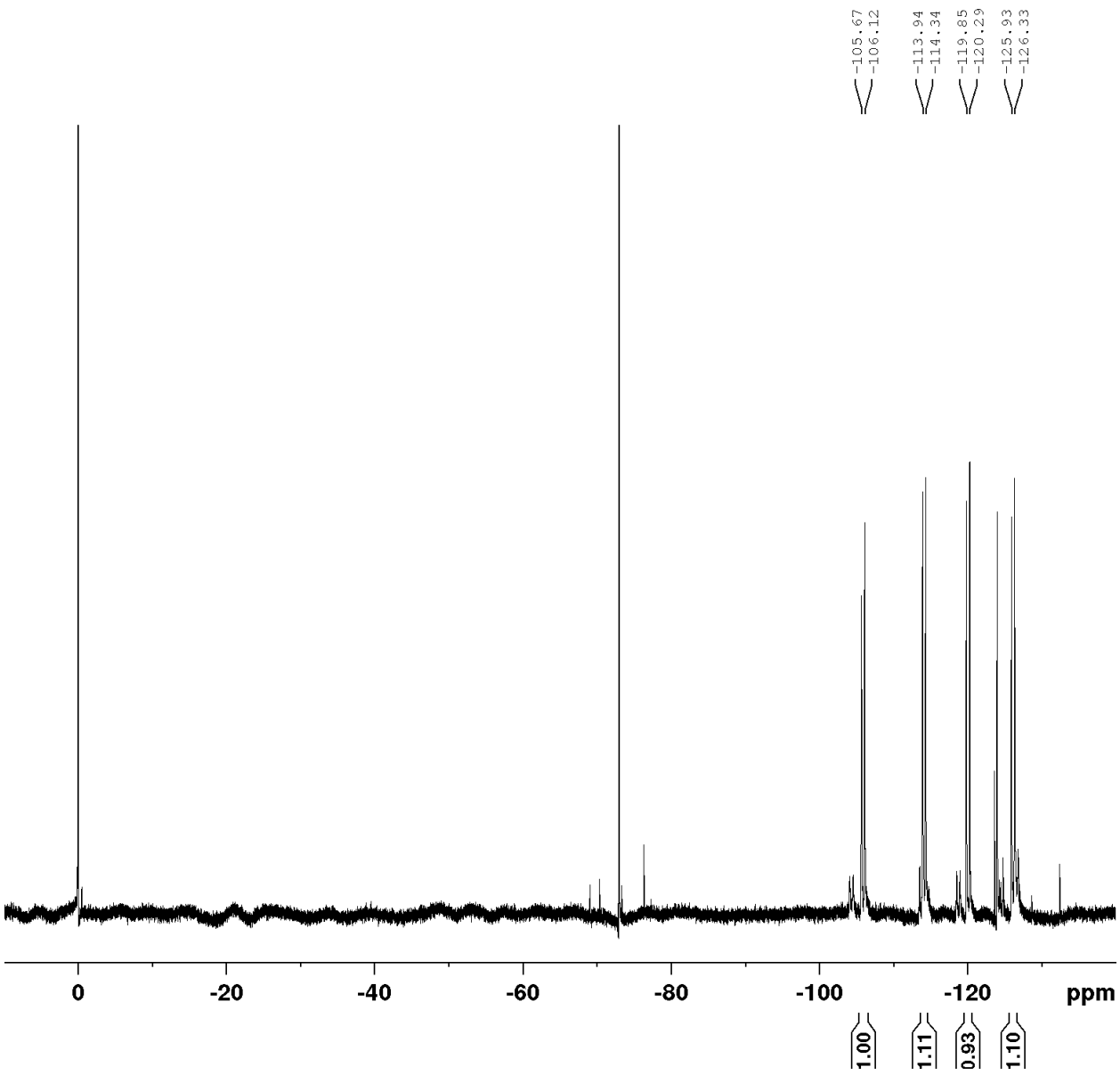

Spectrum 4.7.36 HMBC Spectrum of Polycycle **12** (DMSO-d_6)

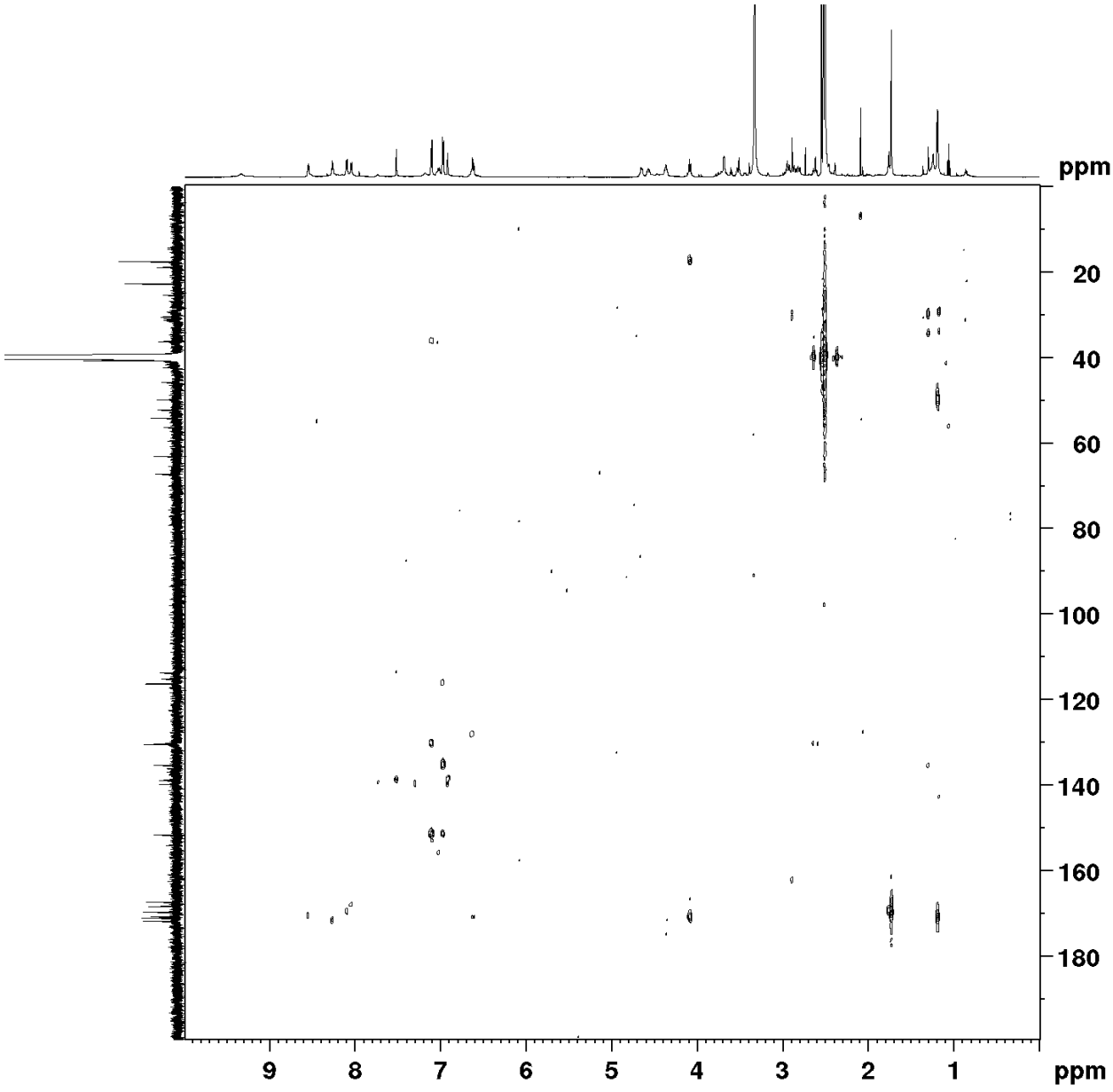

Spectrum 4.7.37 HSQC Spectrum of Polycycle **12** (DMSO-d_6)

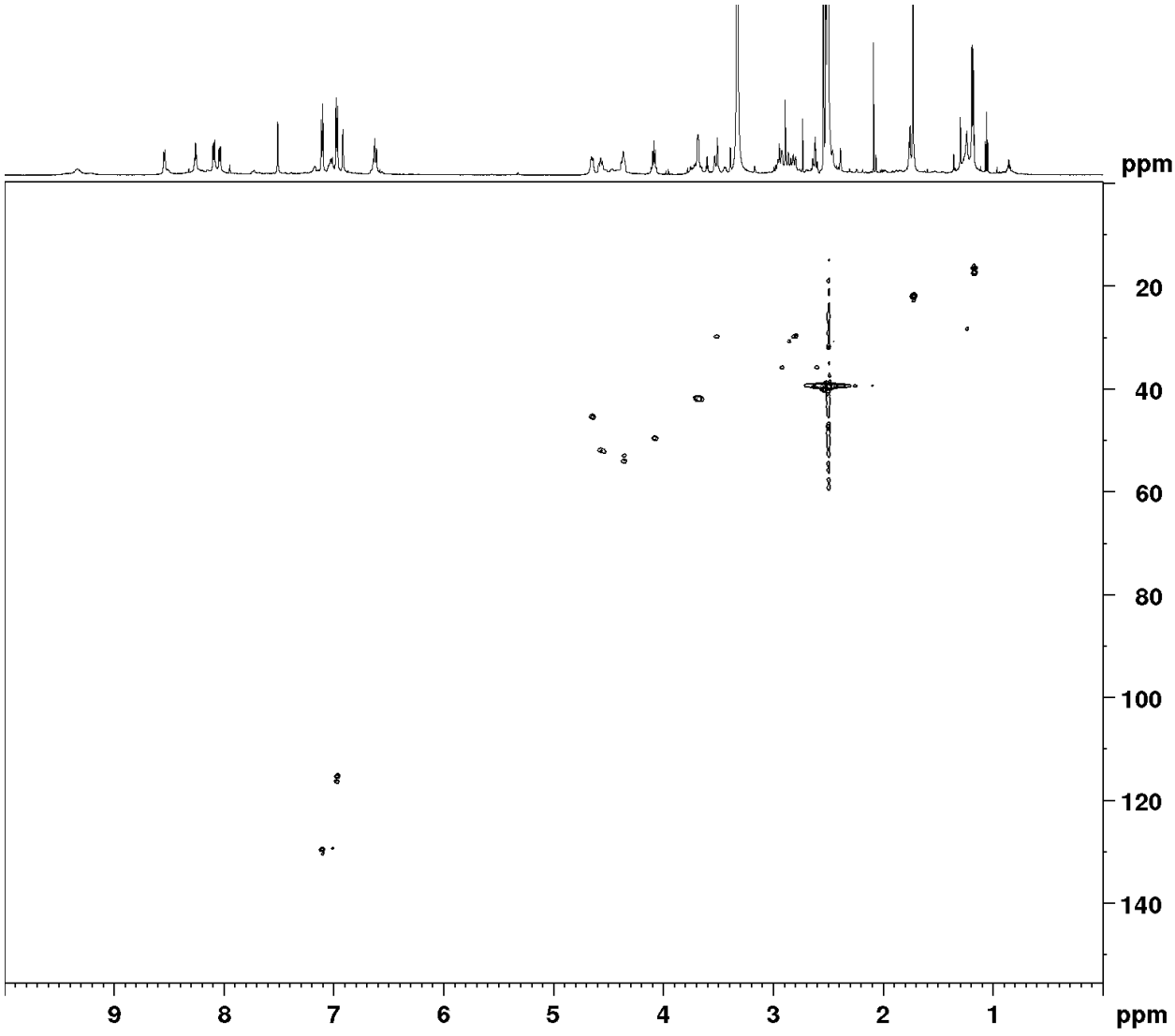

Spectrum 4.7.38 COSY Spectrum of Polycycle **12** (DMSO-d_6)

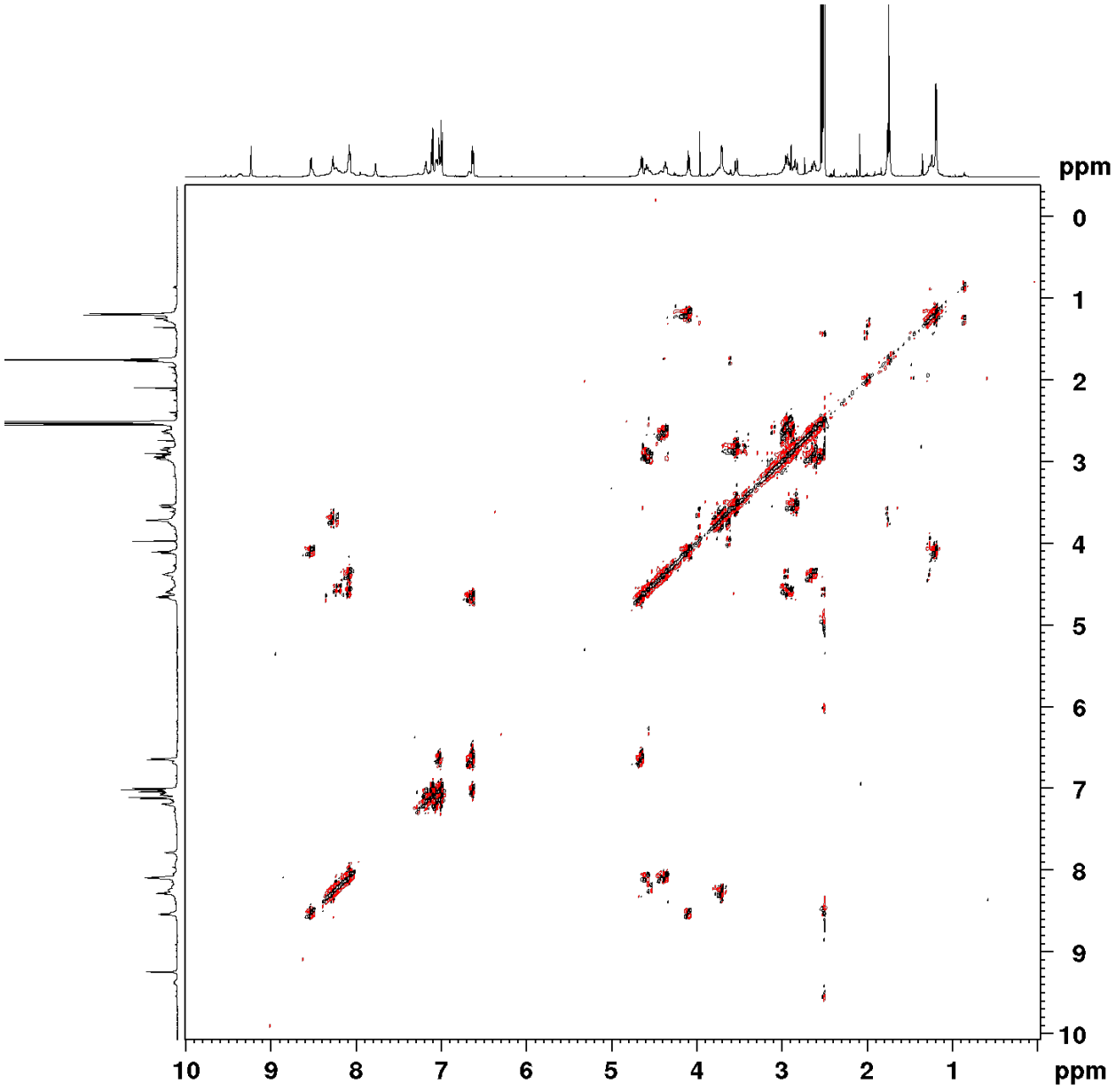

Table 4.7.14 Signal Assignment for Polycycle **12** (DMSO-d_6, 298K)

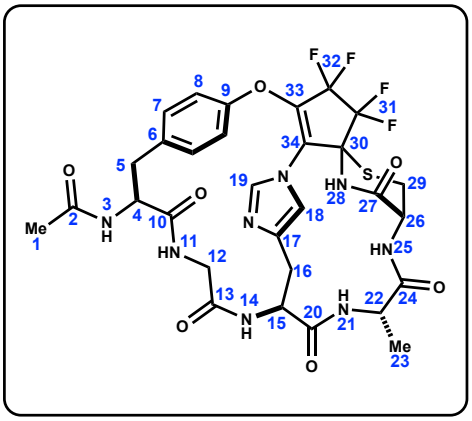

	13C	1H	Key Correlation
1	22.48	1.72 (s, 1H)	HSQC
2	169.50	–	1->2 HMBC
3	–	8.10 (d, J = 8.16 Hz, 1H)	3 ->2 HMBC
4	53.90	4.40-4.32 (m, 1H)	3 ->4 COSY, HSQC
5	36.05	2.66-2.58 (m, 2H)	4->5 COSY, HSQC
6	135.15	–	5 ->6 HMBC
7	130.20	7.10 (d, J = 8.58 Hz, 1H)	7->6 HMBC, HSQC
8	116.04	6.97 (d, J = 8.58 Hz, 1H)	7 ->8 HMBC, 7-> 8 COSY, HSQC
9	151.37	–	8 ->9 HMBC
10	171.57	–	11 ->10, 4->10HMBC
11	–	8.26 (t, J = 5.46 Hz, 1H)	11->10 HMBC, 11->12 COSY
12	42.10	3.72-3.64 (m, 2H)	11->12 HMBC, HSQC
13	168.13	–	14->13, 12->13 HMBC
14	–	8.04 (d, J = 7.74 Hz, 1H)	14->13 HMBC
15	52.00	4.60-4.54 (m, 1H)	15->16 HMBC, 15>16 COSY, HSQC
16	25.13	3.00-2.91 (m, 2H)	16->15 HMBC, 15->16 COSY, HSQC
17	138.59	–	16->17, 18->17 HMBC
18	113.52	6.91 (s, 1H)	18->17 HMBC, HSQC
19	139.53	7.51 (s, 1H)	HSQC
20	170.85	–	21->20, 15->20 HMBC
21	–	6.64-6.60 (m, 1H)	21 ->20 HMBC
22	49.58	4.08 (m, 1H)	22->23 COSY, HSQC
23	17.26	1.18 (d, J = 7.38 Hz, 1H)	HSQC
24	170.59	–	22->24 HMBC
25	–	8.55 (d, J = 6.54 Hz, 1H)	25->24 HMBC
26	45.53	4.64 (d, J = 8.82 Hz, 1H)	25 ->27 HMBC, HSQC
27	167.17	–	28->27, 26->27 HMBC
28	–	9.33 (s, 1H)	–
29	30.22	2.88-2.78 (m, 2H)	26->29 HMBC, 26->29 COSY, HSQC
30	67.8-67.7 (m, 1C)	–	28->30 HMBC
31	122.20-122.30 (m, 1C)	–	–
32	122.20-122.30 (m, 1C)	–	–
33	138.74-138.77 (m, 1C)	–	–
34	129.96-130.03 (m, 1C)	–	–

Spectrum 4.7.39 ^{1}H-NMR of Polycycle **4** (DMSO-d_6, 500 MHz)

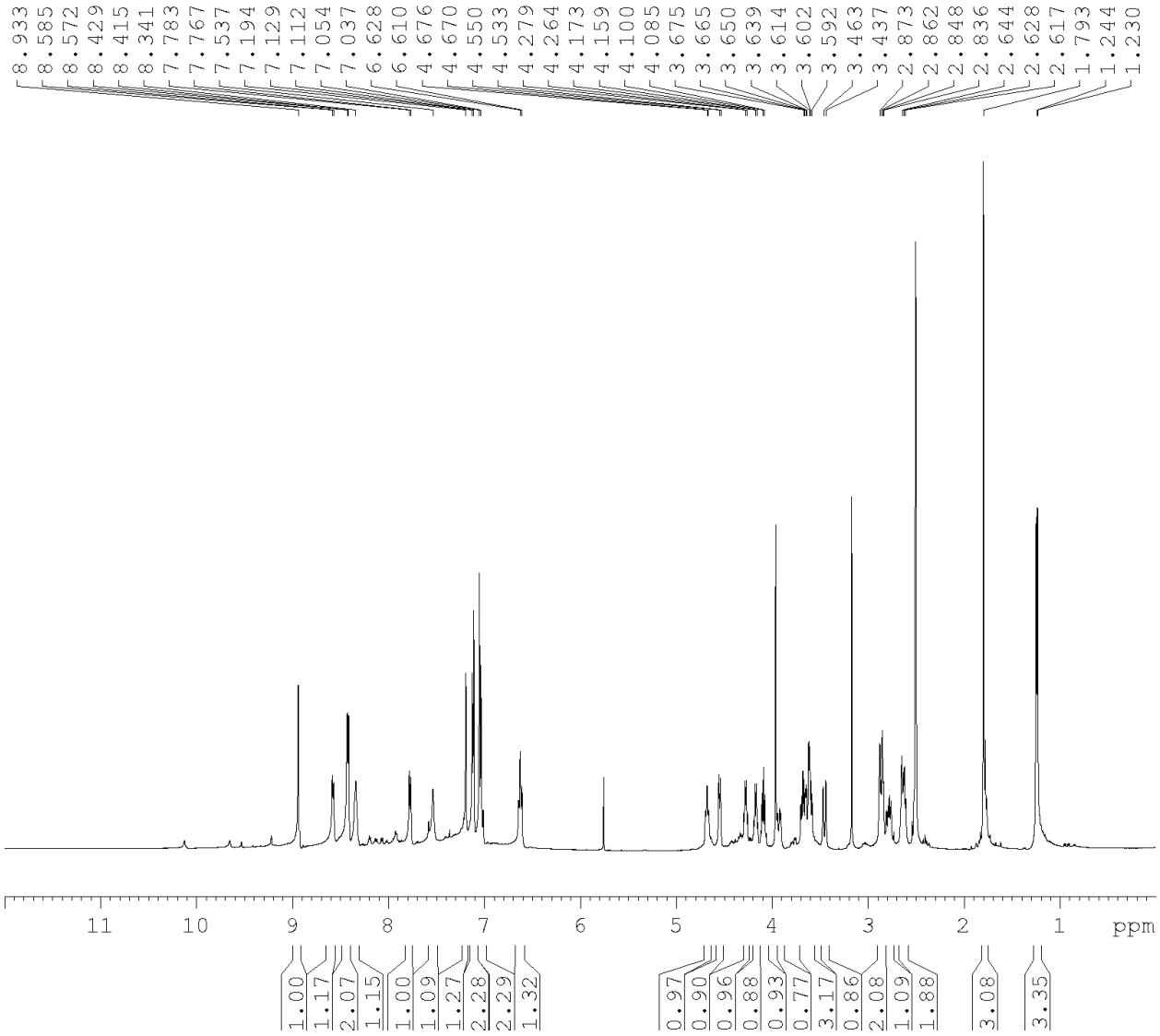

Spectrum 4.7.40 ^{13}C-NMR of Polycycle **4** (DMSO-d_6, 126 MHz)

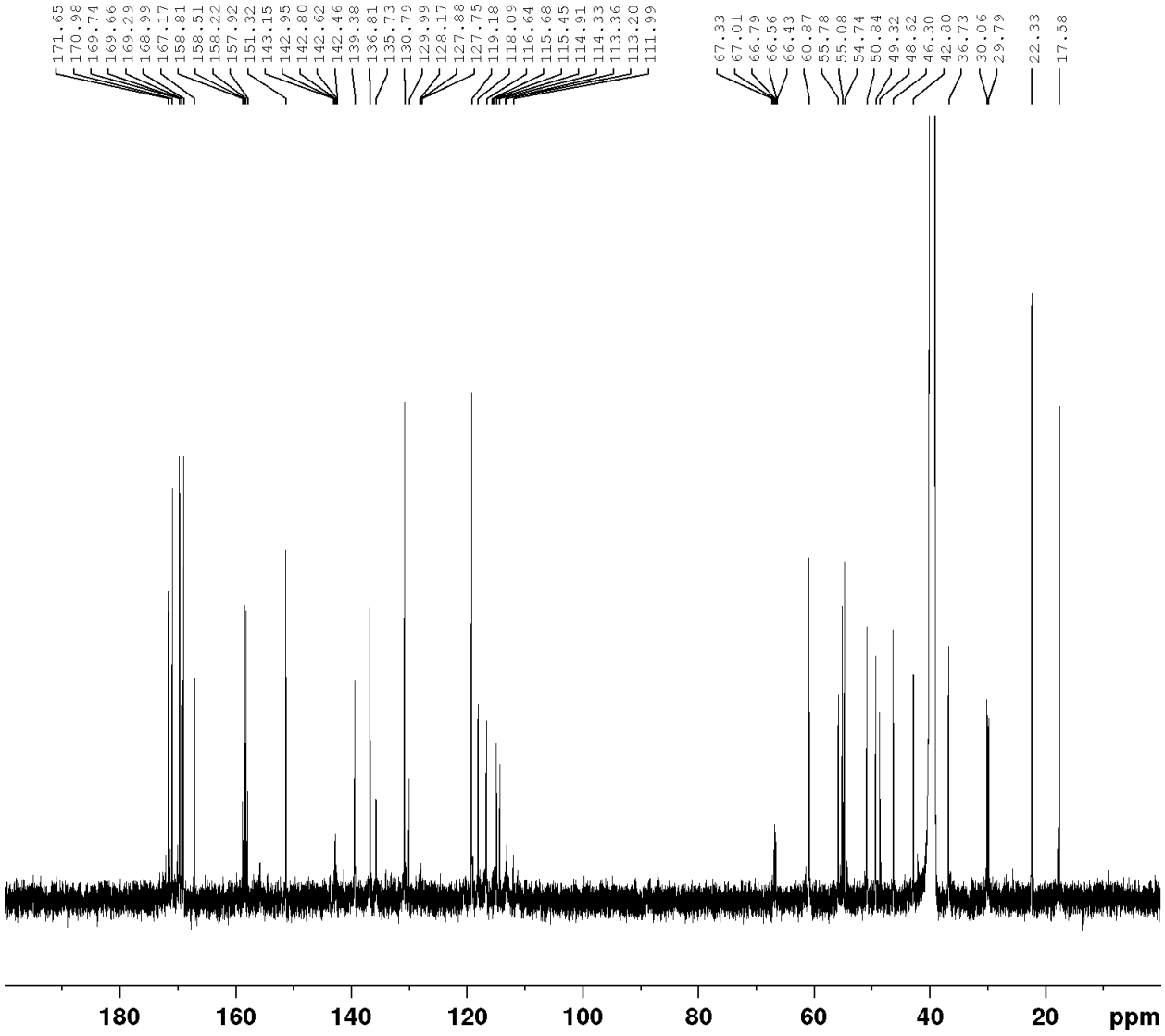

Spectrum 4.7.41 ^{19}F-NMR of Polycycle **4** (DMSO-d_6, 282 MHz)

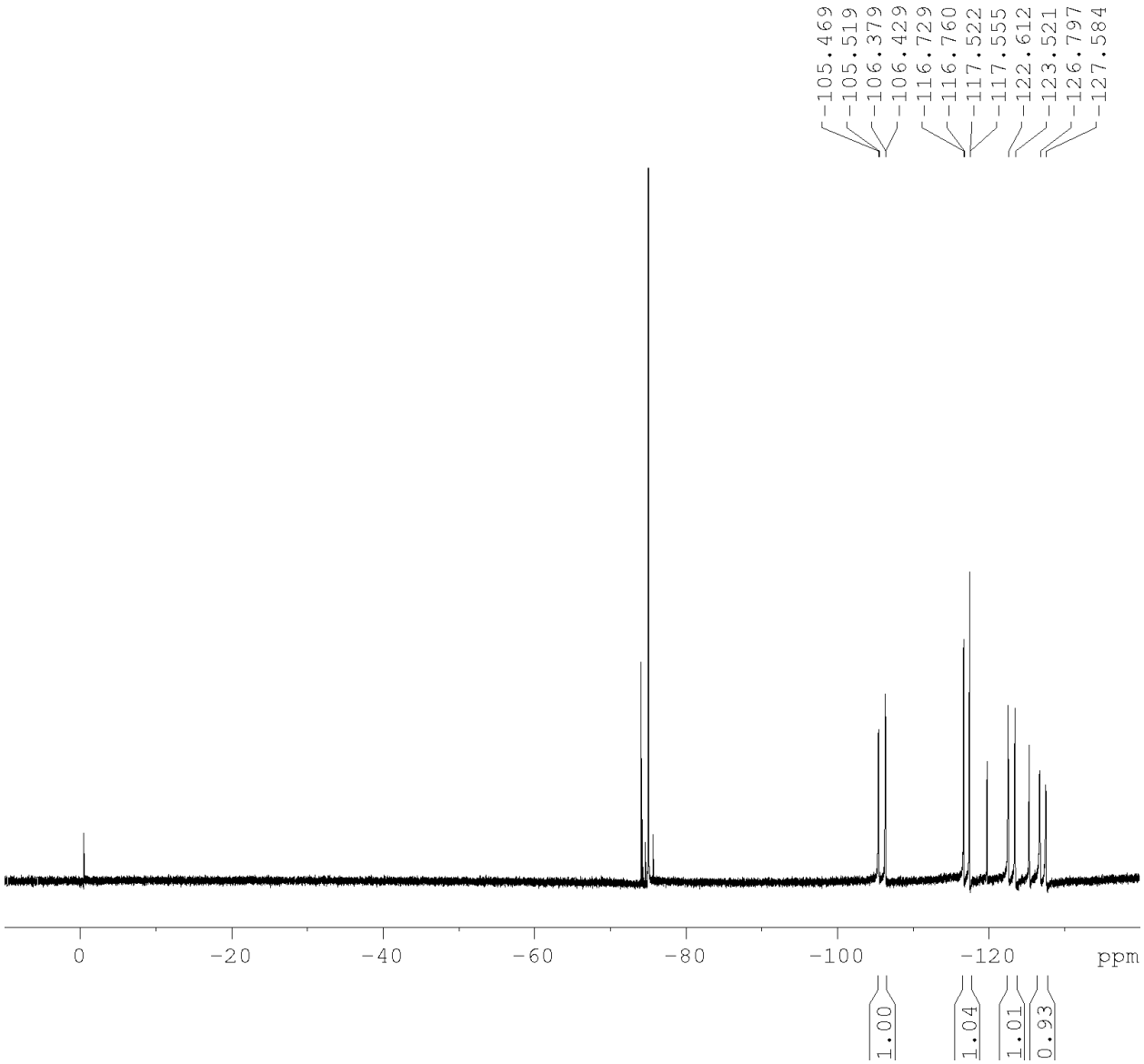

Spectrum 4.7.42 HMBC of Polycycle **4** (DMSO-d_6)

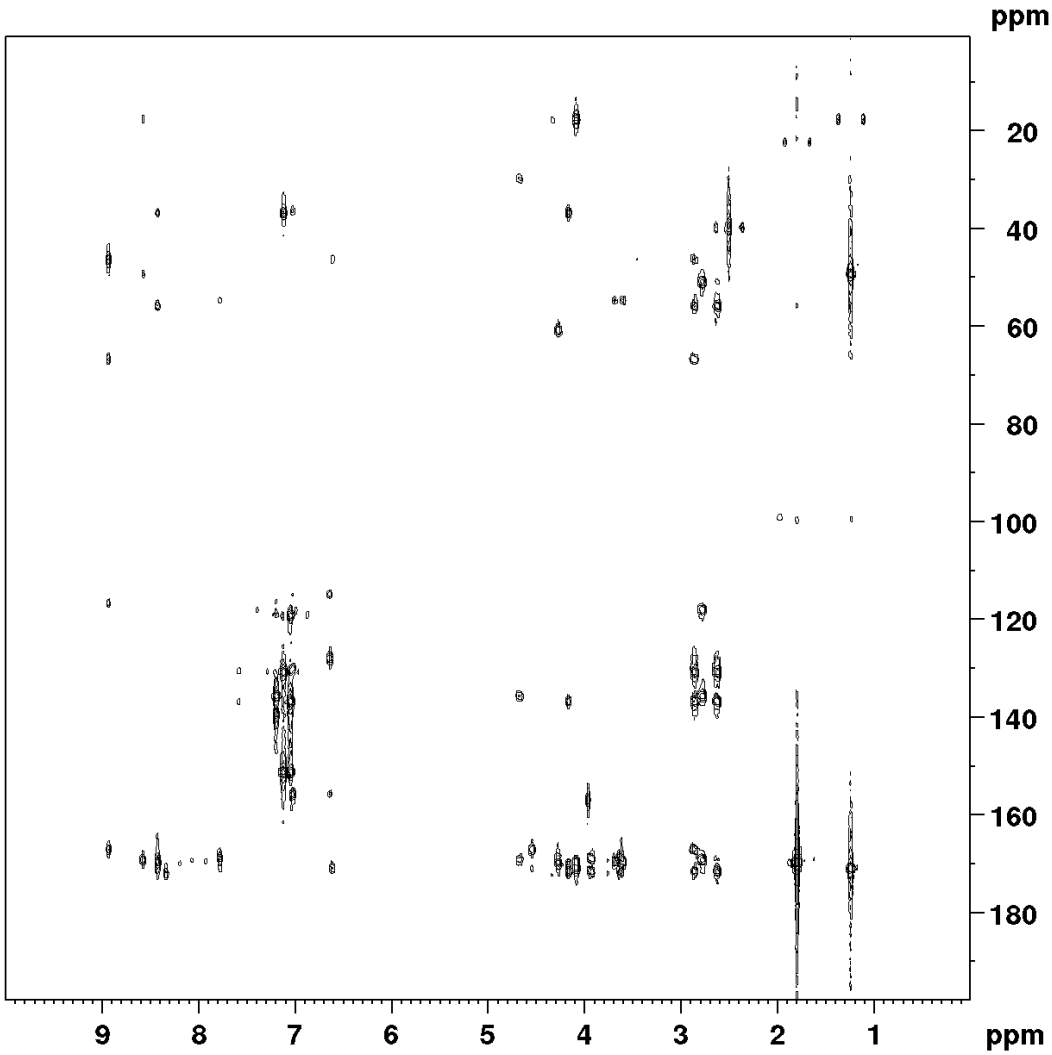

Spectrum 4.7.43 HSQC spectrum of Polycycle **4** (DMSO-d_6)

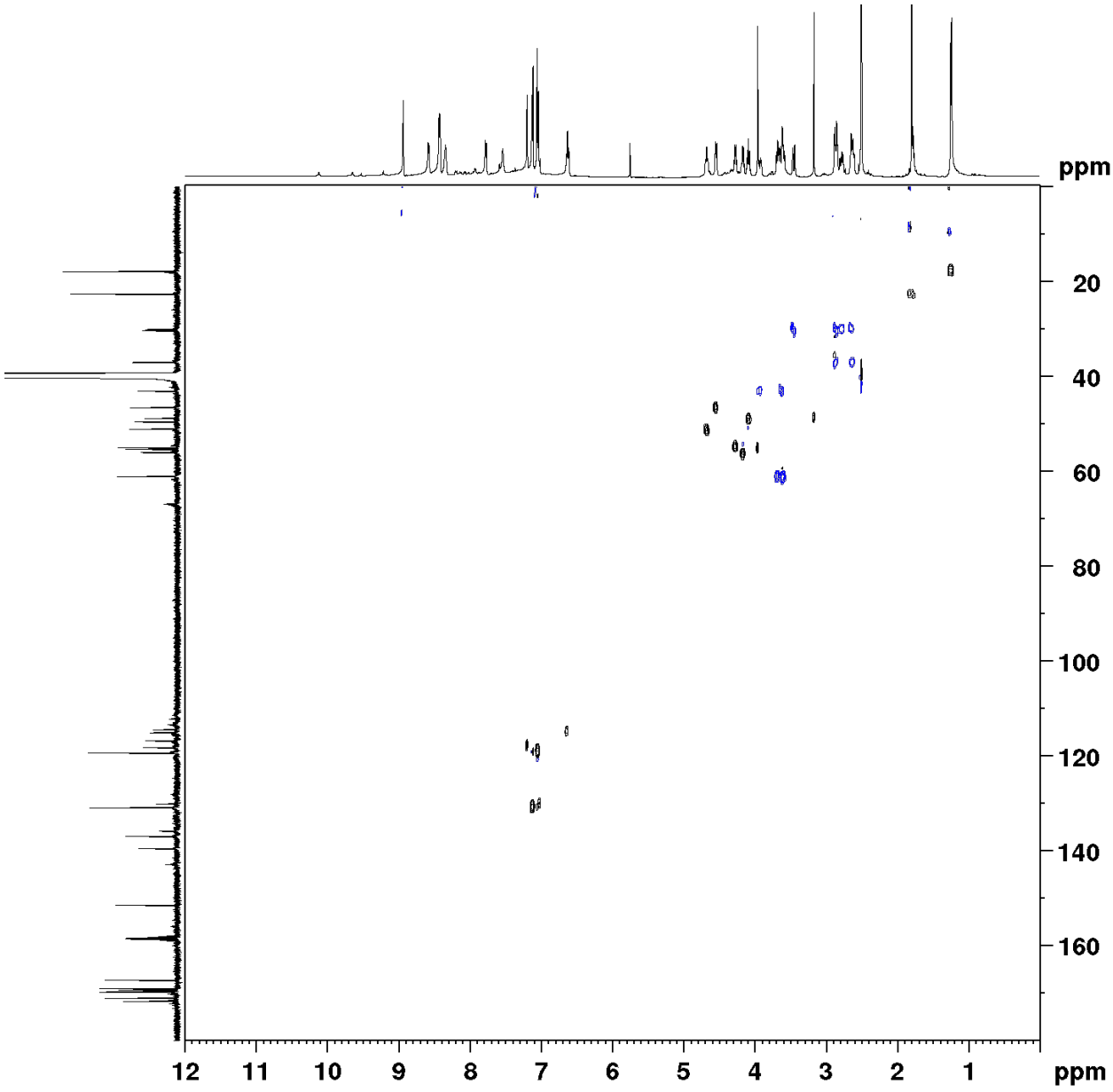

Spectrum 4.7.44 COSY spectrum of Polycycle **4** (DMSO-d_6)

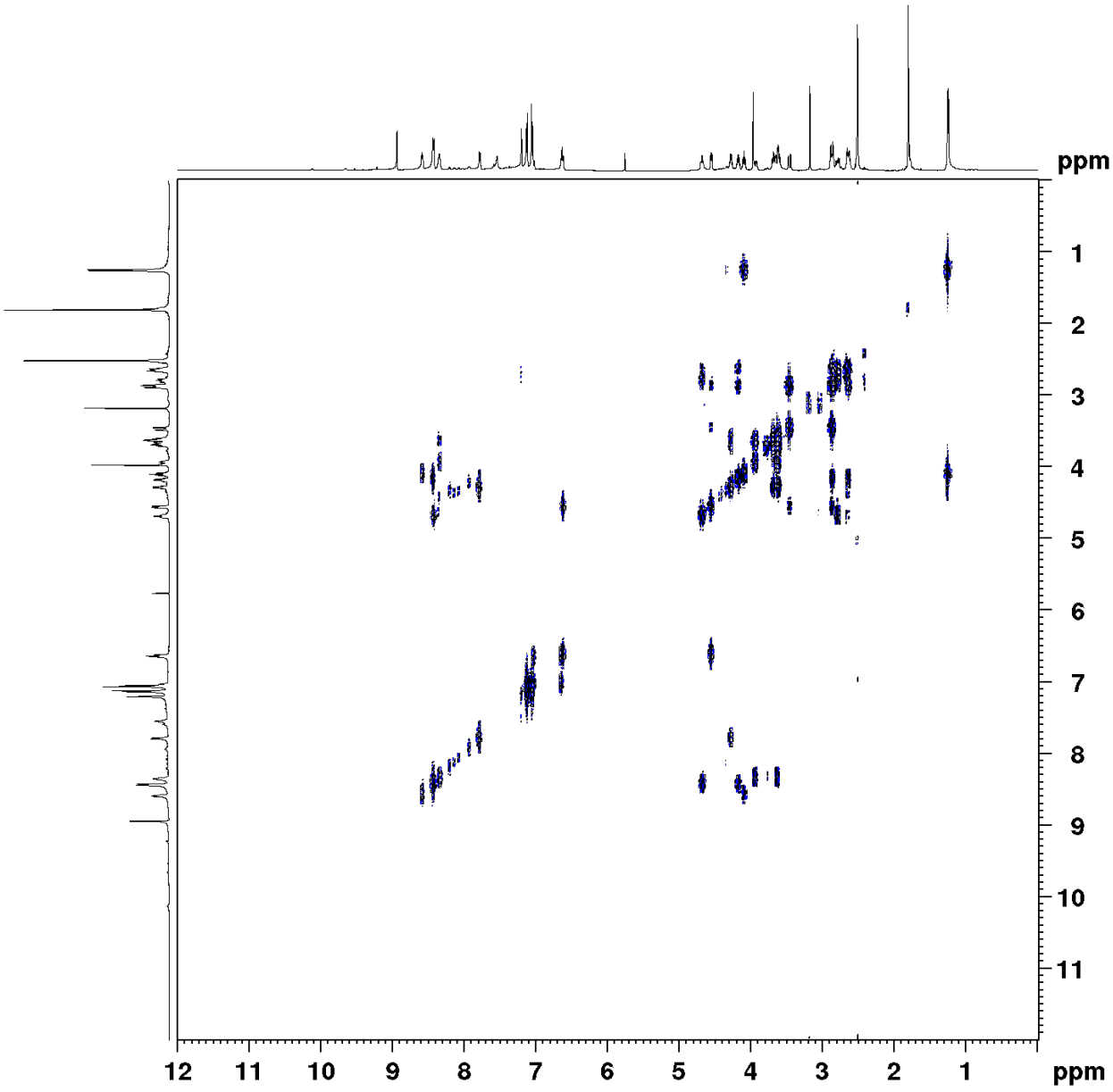

Table 4.7.15 Polycycle **4** (DMSO-d_6, 298K)

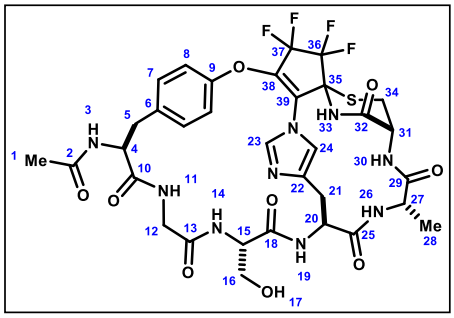

	13C	1H	Key Correlation
1	22.3	1.79 (s, 1H)	1 -> 2 HMBC
2	169.7	-	1, 3 -> 2 HMBC
3	-	8.42 (d, J = 6.6 Hz, 2H)	3 -> 2, 4, 5 HMBC
4	55.8	4.17 (q, J = 7.0 Hz, 1H)	3, 5 -> 4
5	36.7	2.90 - 2.83 (m, 2H); 2.68 - 2.58 (m, 2H)	5 -> 4, 6 HMBC
6	136.8	-	4, 5 -> 6 HMBC
7	130.8	7.15 - 7.10 (m, 2H)	5 -> 7 HMBC
8	119.2	7.10 - 7.00 (m, 2H)	7 -> 8 HMBC
9	151.0	-	7 -> 9 HMBC
10	171.6	-	4 -> 10 HMBC
11	-	8.34 (s, 1H)	11 -> 10 HMBC
12	42.8	3.95 - 3.87 (m, 1H); 3.72 - 3.56 (m, 3H)	11 -> 12 HMBC
13	169.0	-	12 -> 13 HMBC
14	-	7.78 (d, J = 7.8 Hz, 1H)	14 -> 13 HMBC
15	54.7	4.27 (q, J = 6.4 Hz, 1H)	14 -> 15 HMBC
16	60.9	3.72 - 3.56 (m, 3H)	15 -> 16 HMBC
17	-	-	-
18	169.7	-	15, 16 -> HMBC
19	-	8.42 (d, J = 6.6 Hz, 2H)	19 -> 20 HMBC
20	50.8	4.71 - 4.64 (m, 1H)	19 -> 20 HMBC
21	29.8	2.82 - 2.73 (m, 1H); 2.68 - 2.58 (m, 2H)	20 -> 21 HMBC
22	135.7	-	21 -> 22 HMBC
23	139.4	7.54 (s, 1H)	24 -> 23 HMBC
24	118.09	7.19 (s, 1H)	23 -> 24 HMBC
25	169.3	-	26 -> 25 HMBC
26	-	8.58 (d, J = 7.0 Hz, 1H)	26 -> 25 HMBC
27	49.3	4.09 (quint, J = 7.1 Hz, 1H)	28 -> 27 HMBC
28	17.6	1.24 (d, J = 7.2 Hz, 3H)	27 -> 28 HMBC
29	171.0	-	28 -> 29 HMBC
30	-	6.67 - 6.58 (m, 1H)	30 -> 31, 32 HMBC
31	46.3	4.58 - 4.51 (m, 1H)	32 -> 32, 34 HMBC
32	167.2	-	33 -> 32 HMBC
33	-	8.93 (s, 1H)	33 -> 35 HMBC
34	30.1	3.45 (d, J = 13.1 Hz, 1H) ; 2.90 - 2.83 (m, 2H)	31 -> 34 HMBC
35	67.3 - 66.4 (m, 1C)	-	34 -> 35 HMBC
36	119.7 - 113.0 (m, 2C)	-	33 -> 36 HMBC
37	119.7 - 113.0 (m, 2C)	-	
38	143.1 - 142.5 (m, 1C)	-	
39	128.2 - 127.8 (m, 1C)	-	

Spectrum 4.7.45 ^{1}H-NMR of Polycycle **13** (DMSO-d_6, 500 MHz)

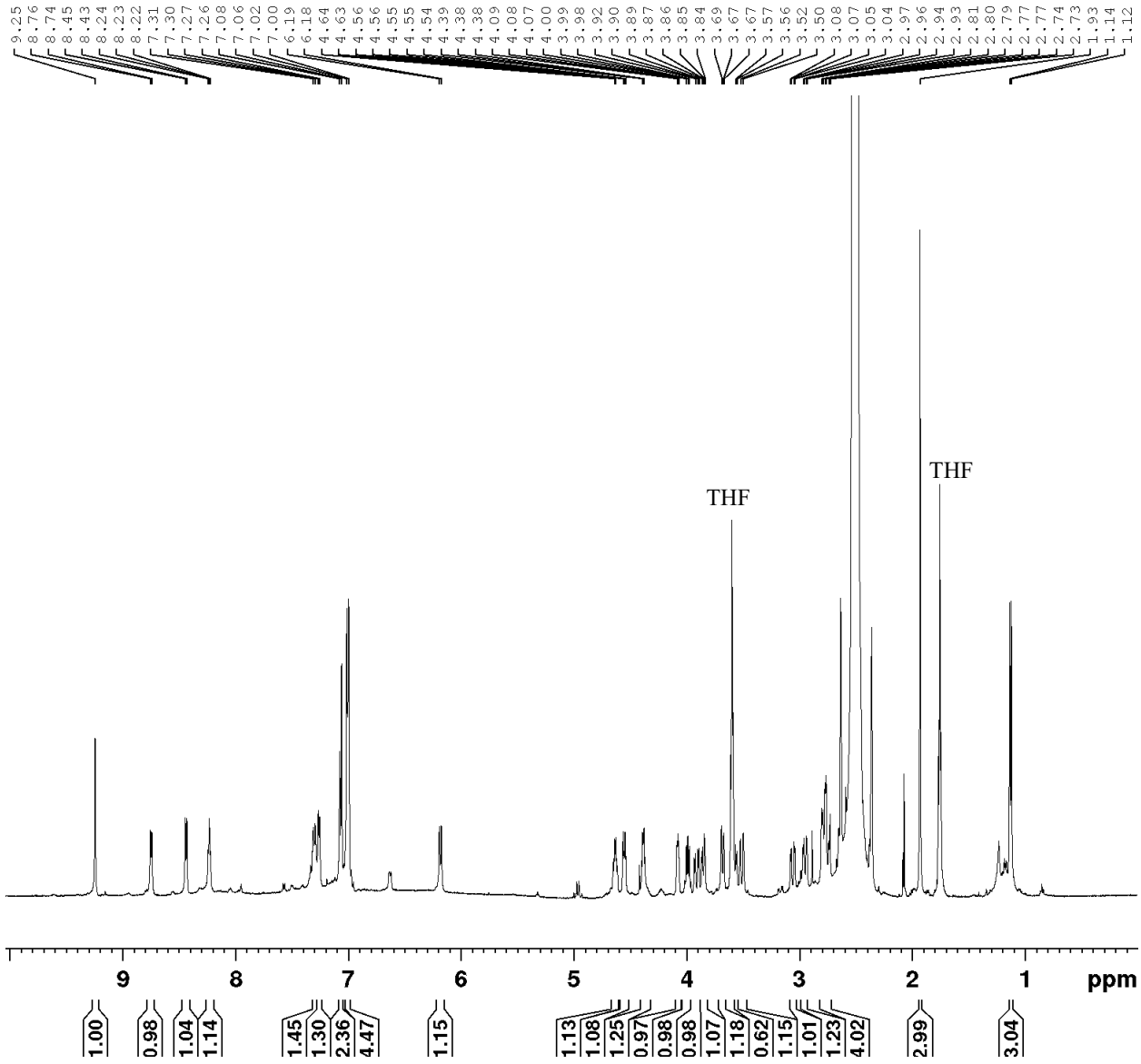

Spectrum 4.7.46 ^{13}C-NMR of Polycycle **13** (DMSO-d_6, 126 MHz)

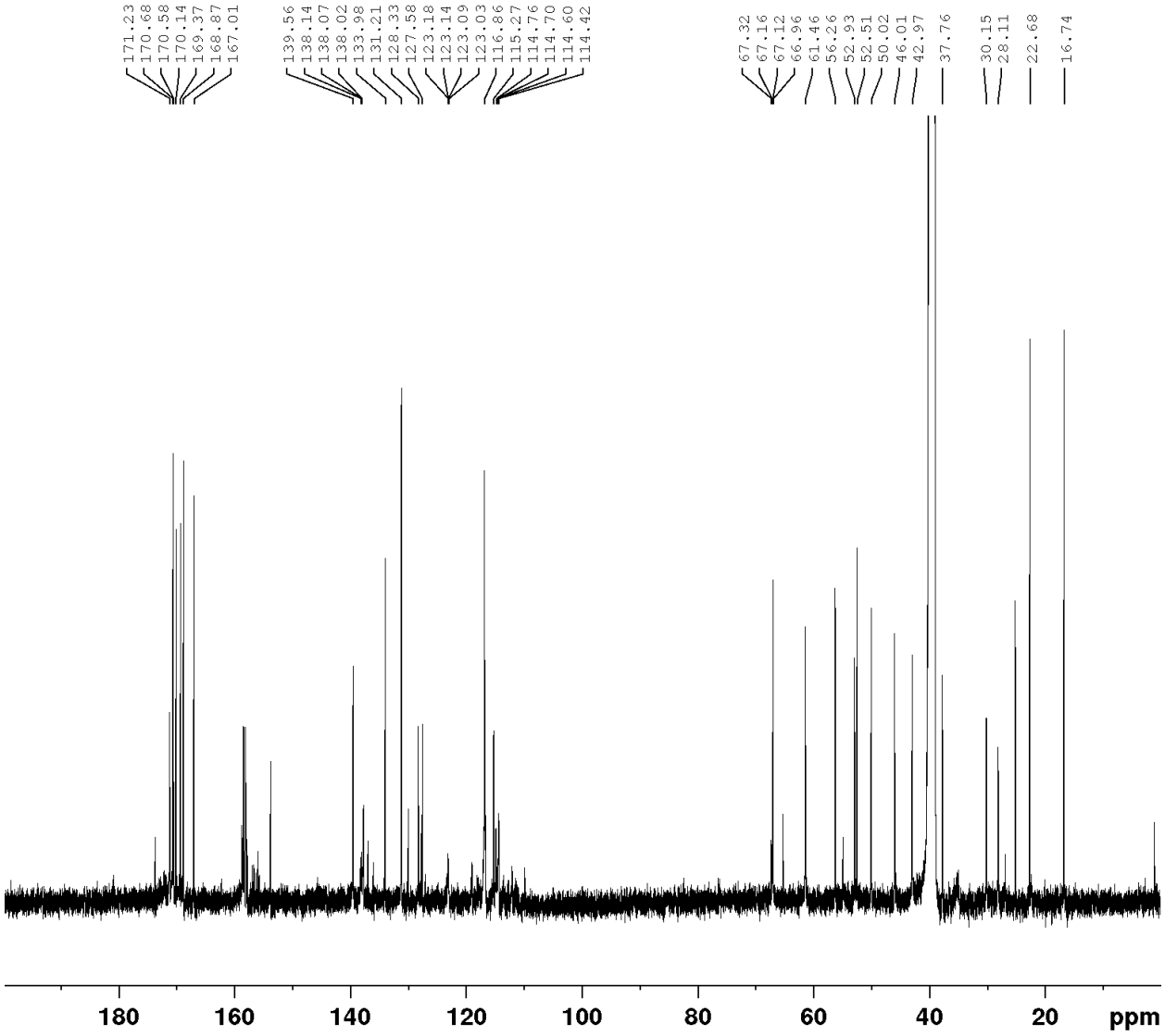

Spectrum 4.7.47 ^{19}F-NMR of Polycycle **13** (DMSO-d_6, 565 MHz)

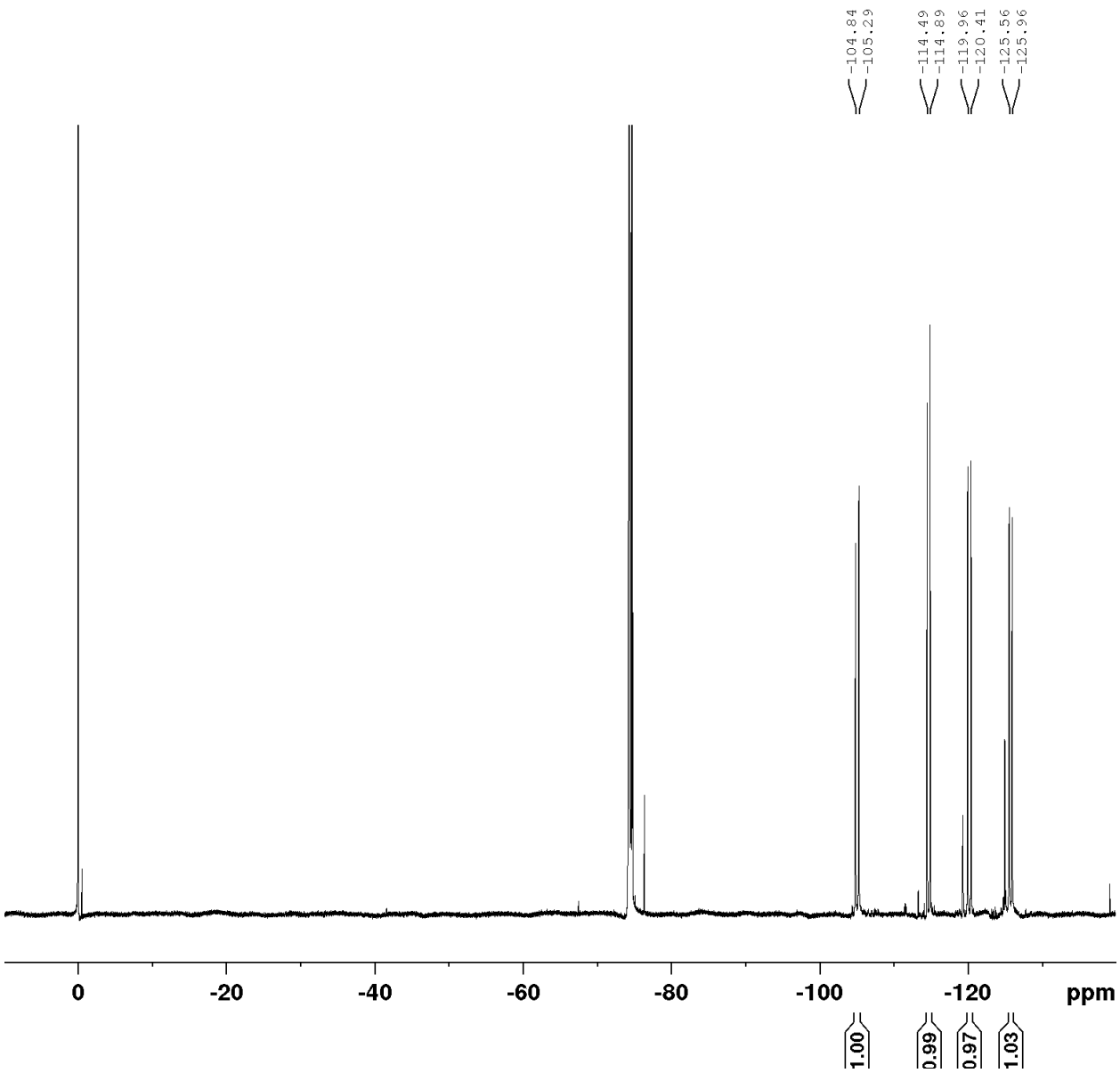

Spectrum 4.7.48 HMBC Spectrum of Polycycle **13** (DMSO-d_6)

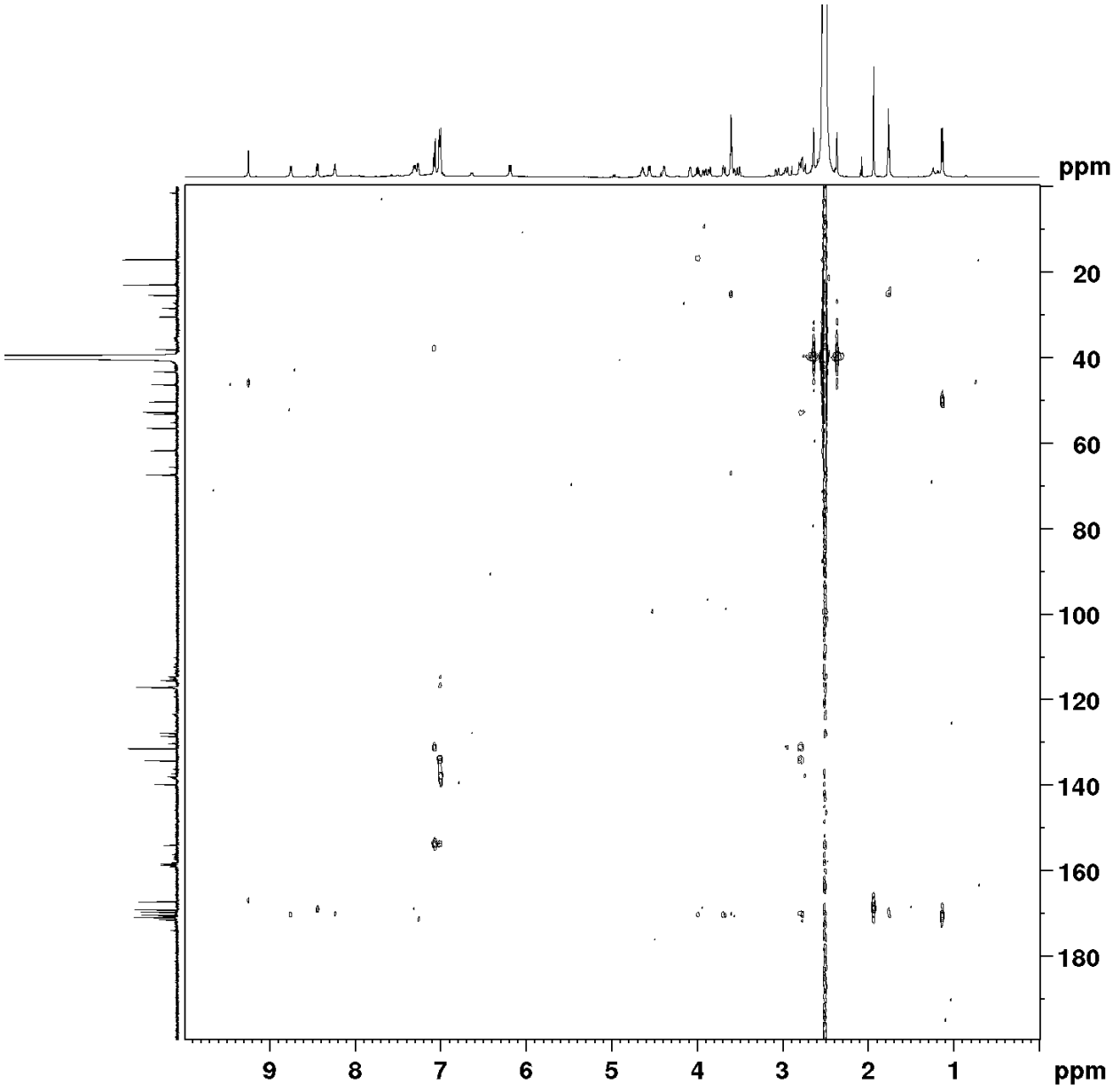

Spectrum 4.7.49 HSQC Spectrum of Polycycle **13** (DMSO-d_6)

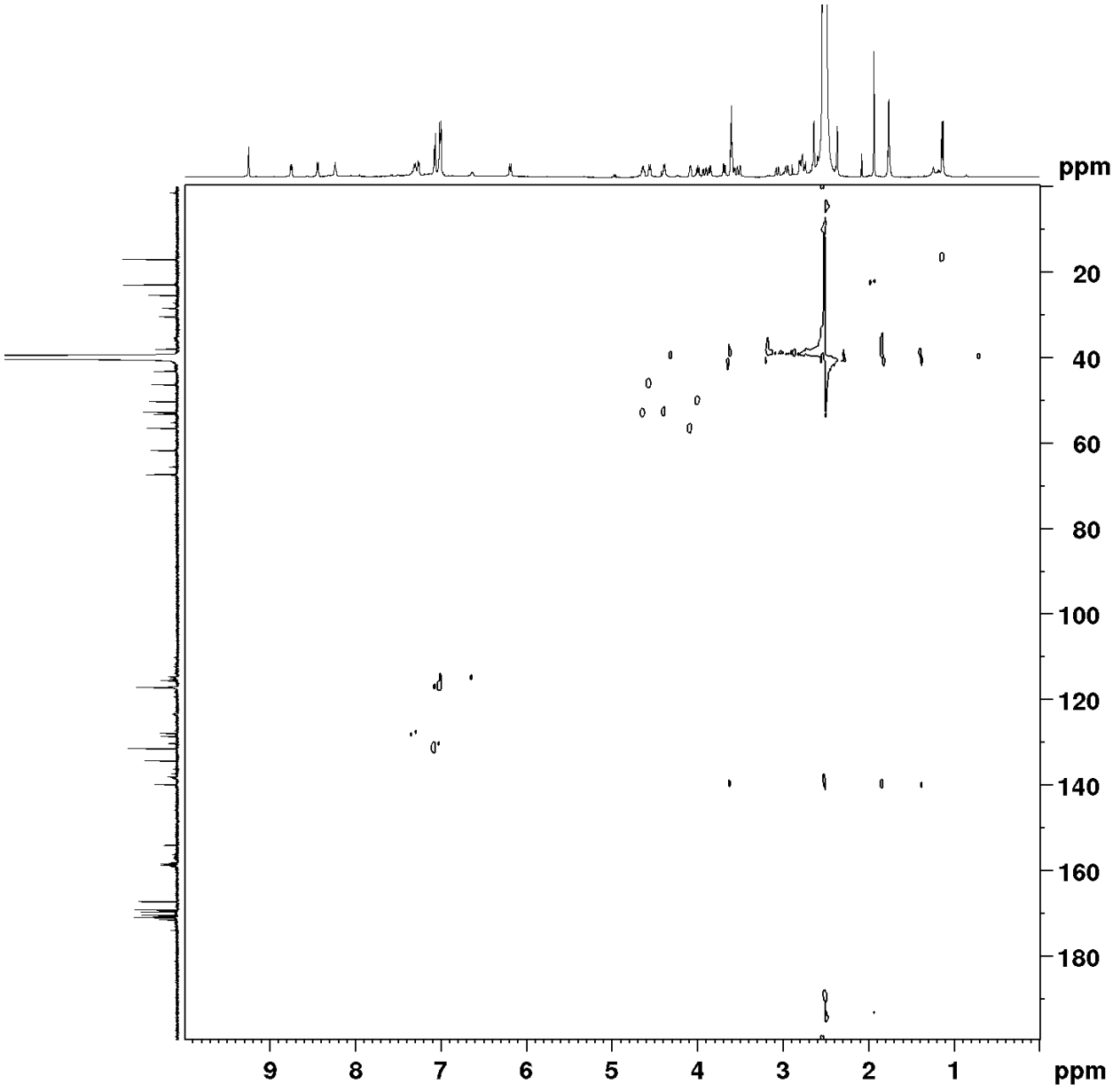

Spectrum 4.7.50 COSY Spectrum of Polycycle **13** (DMSO-d_6)

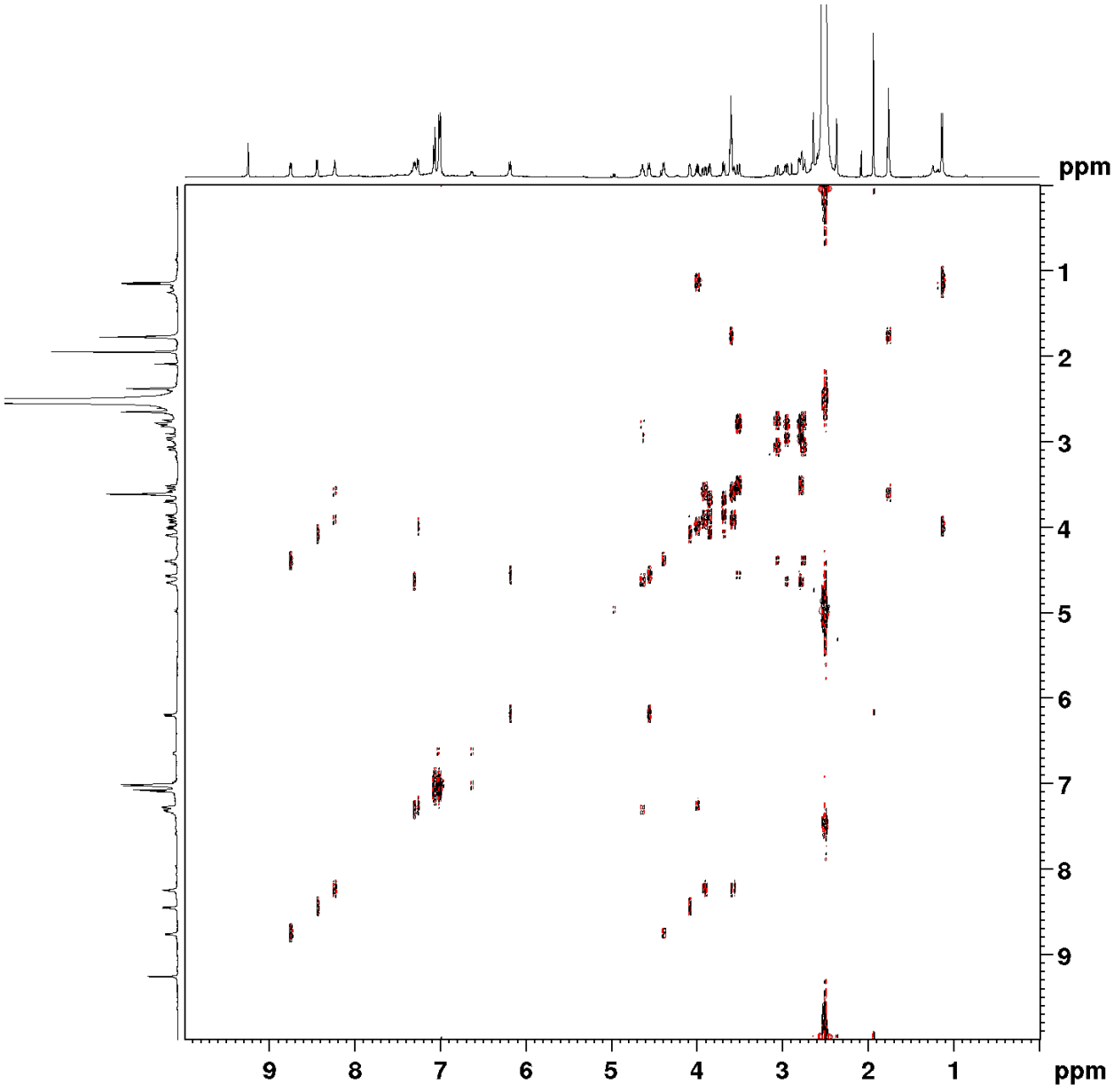

Spectrum 4.7.51 ^{1}H-NMR of Polycycle **14** (DMSO-d_6, 600 MHz)

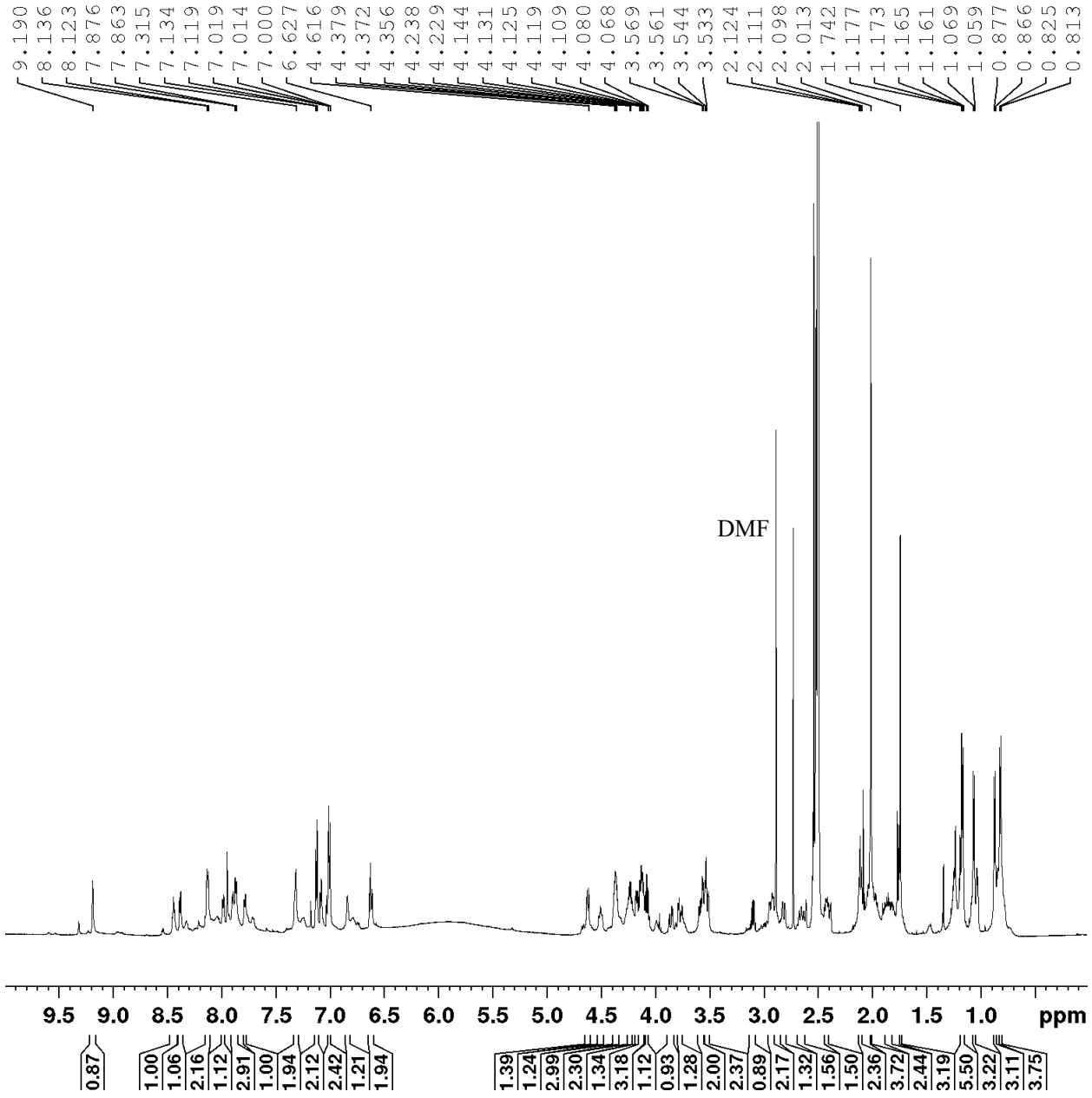

Spectrum 4.7.52 ^{13}C-NMR of Polycycle **14** (DMSO-d_6, 126 MHz)

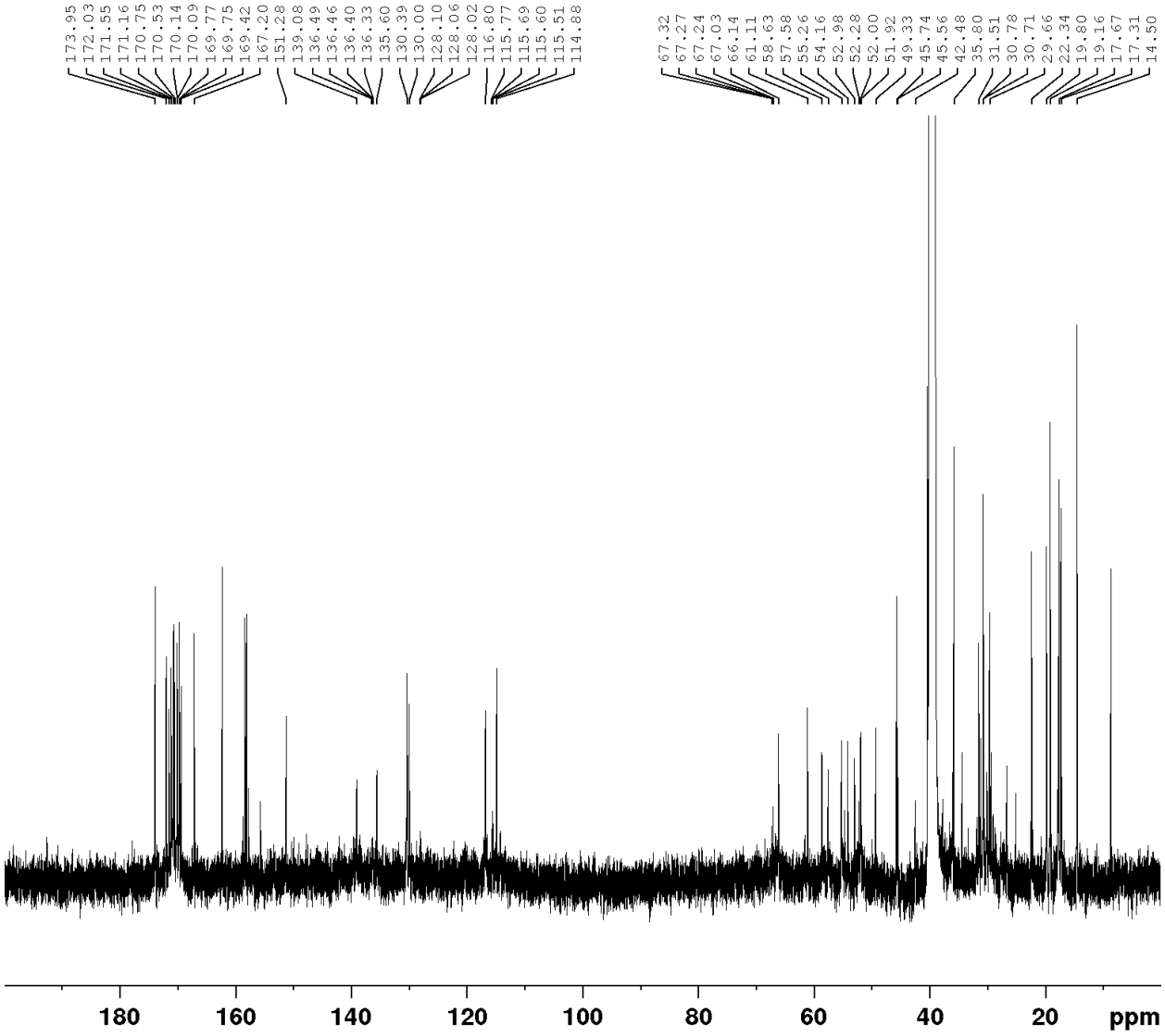

Spectrum 4.7.53 ^{19}F-NMR of Polycycle **14** (DMSO-d_6, 565 MHz)

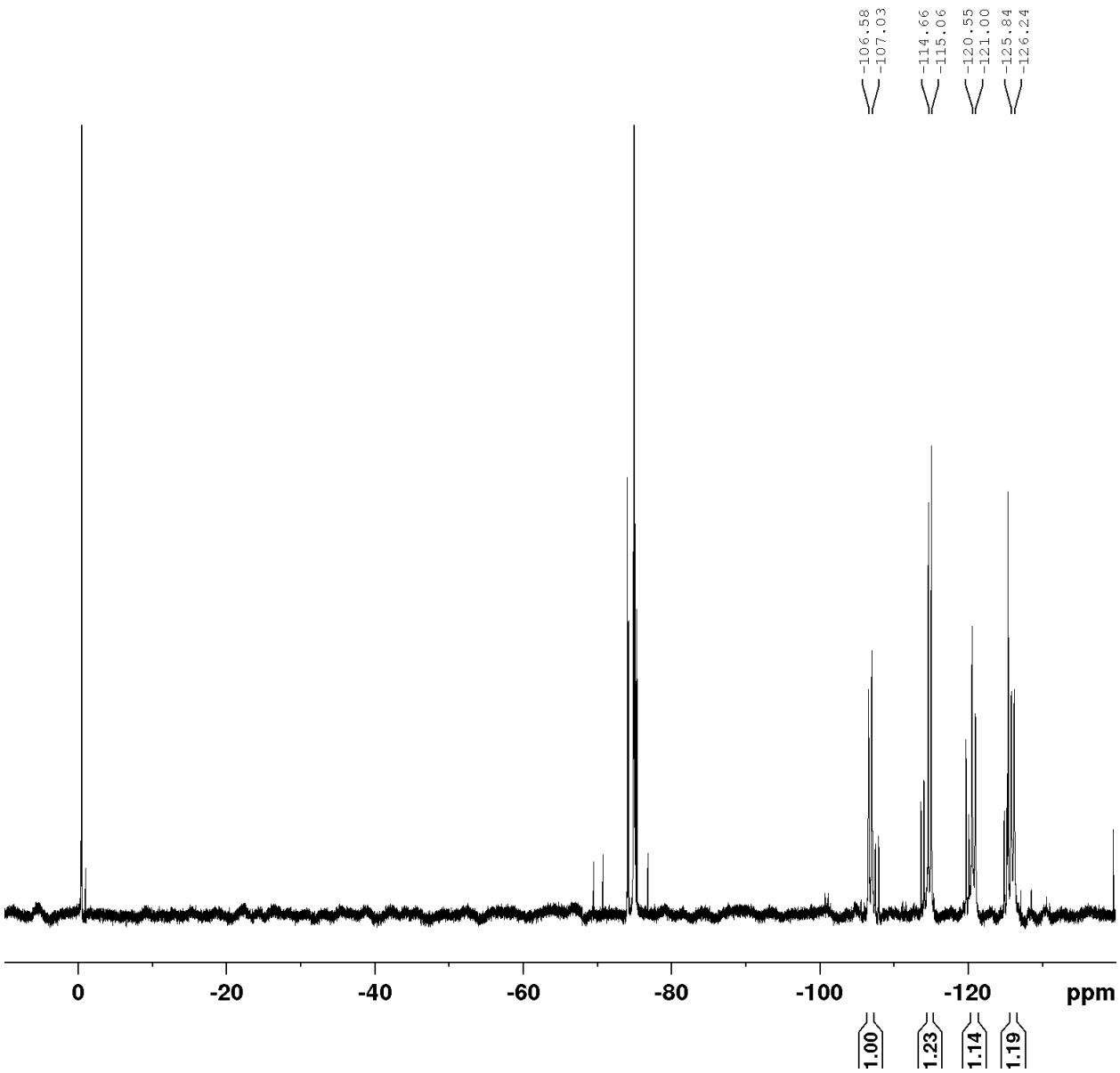

Spectrum 4.7.54 HMBC spectrum of Polycycle **14** (DMSO-d_6)

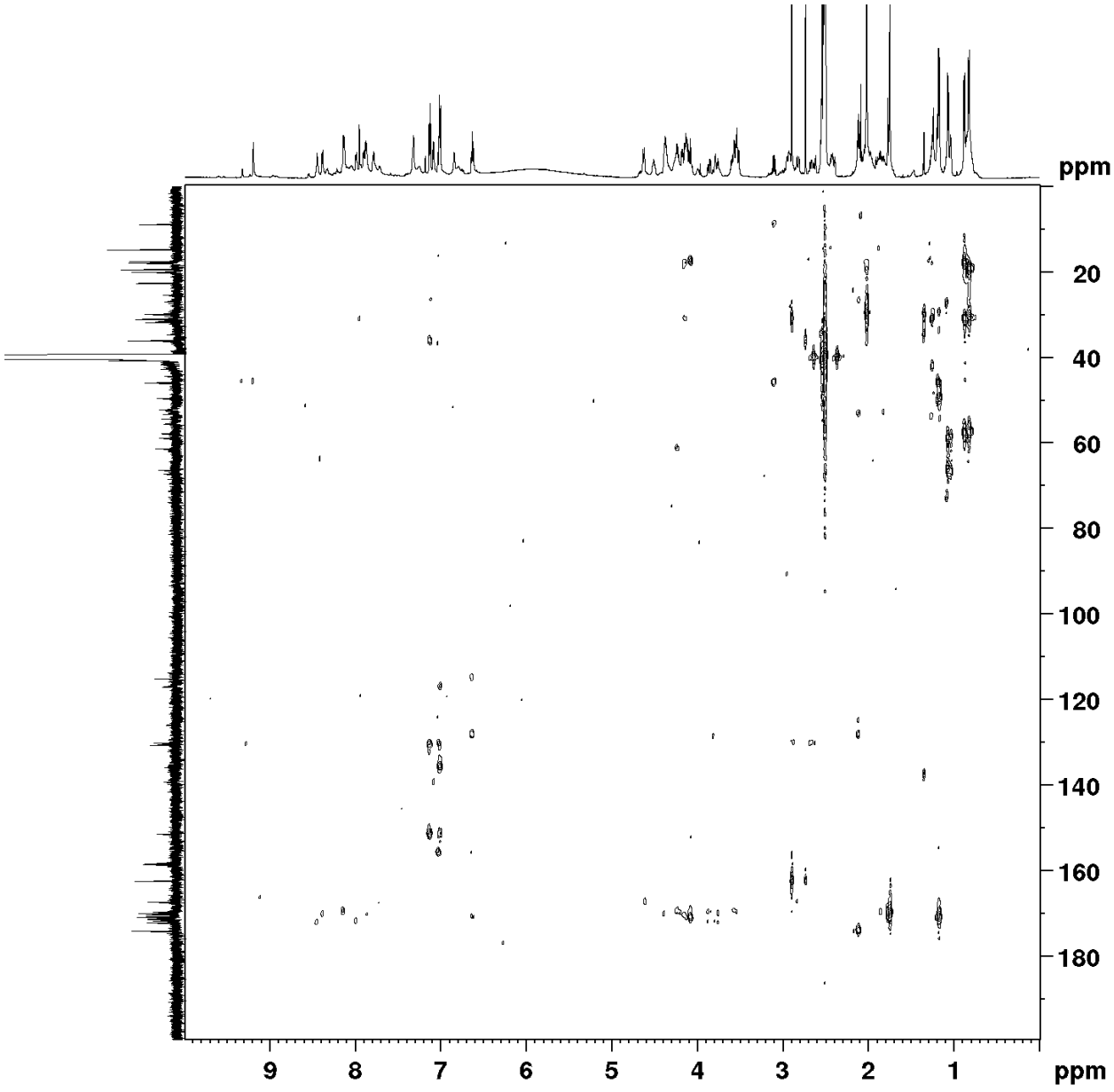

Spectrum 4.7.55 HSQC spectrum of Polycycle **14** (DMSO-d_6)

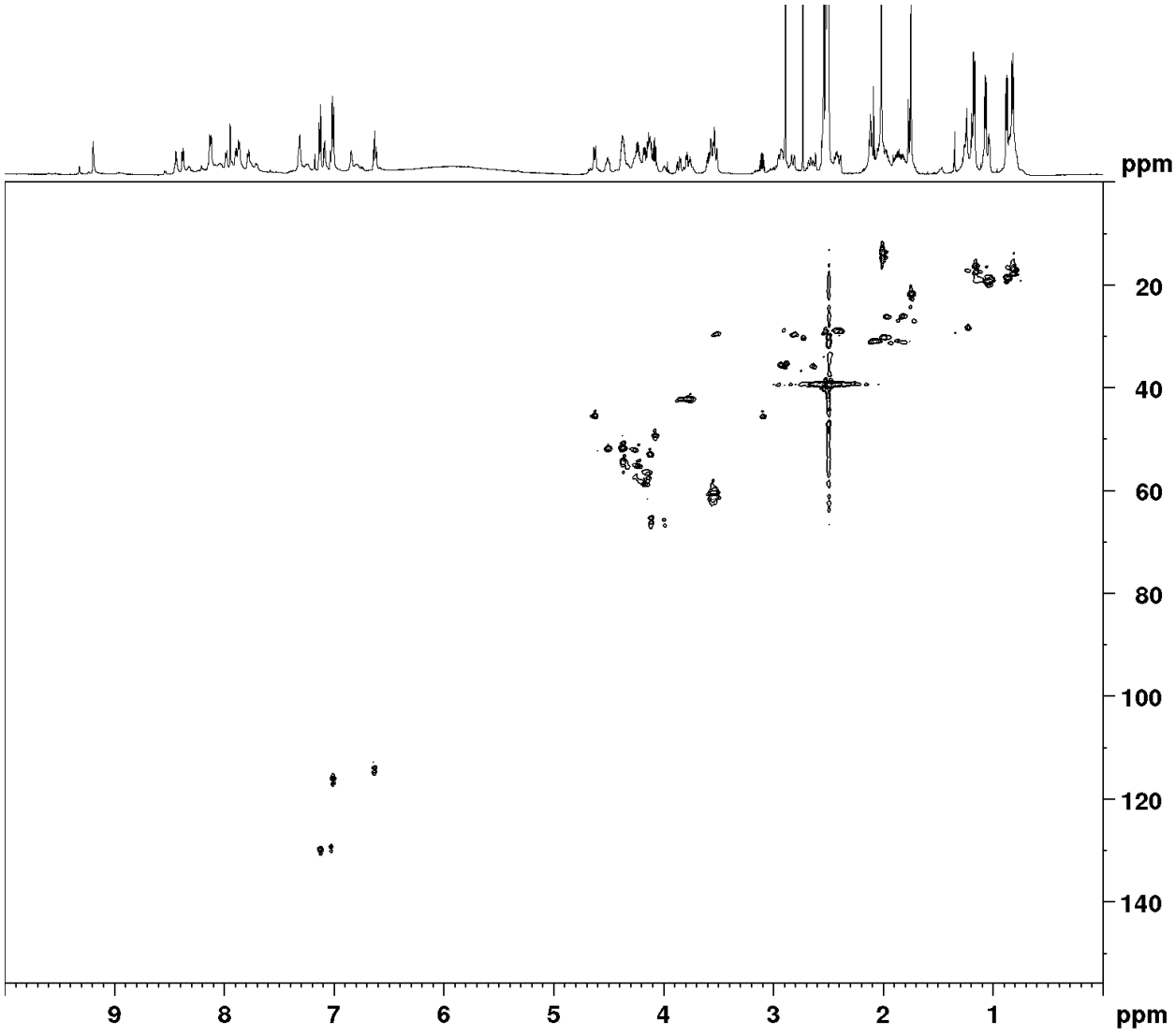

Spectrum 4.7.56 COSY spectrum of Polycycle **14** (DMSO-d_6)

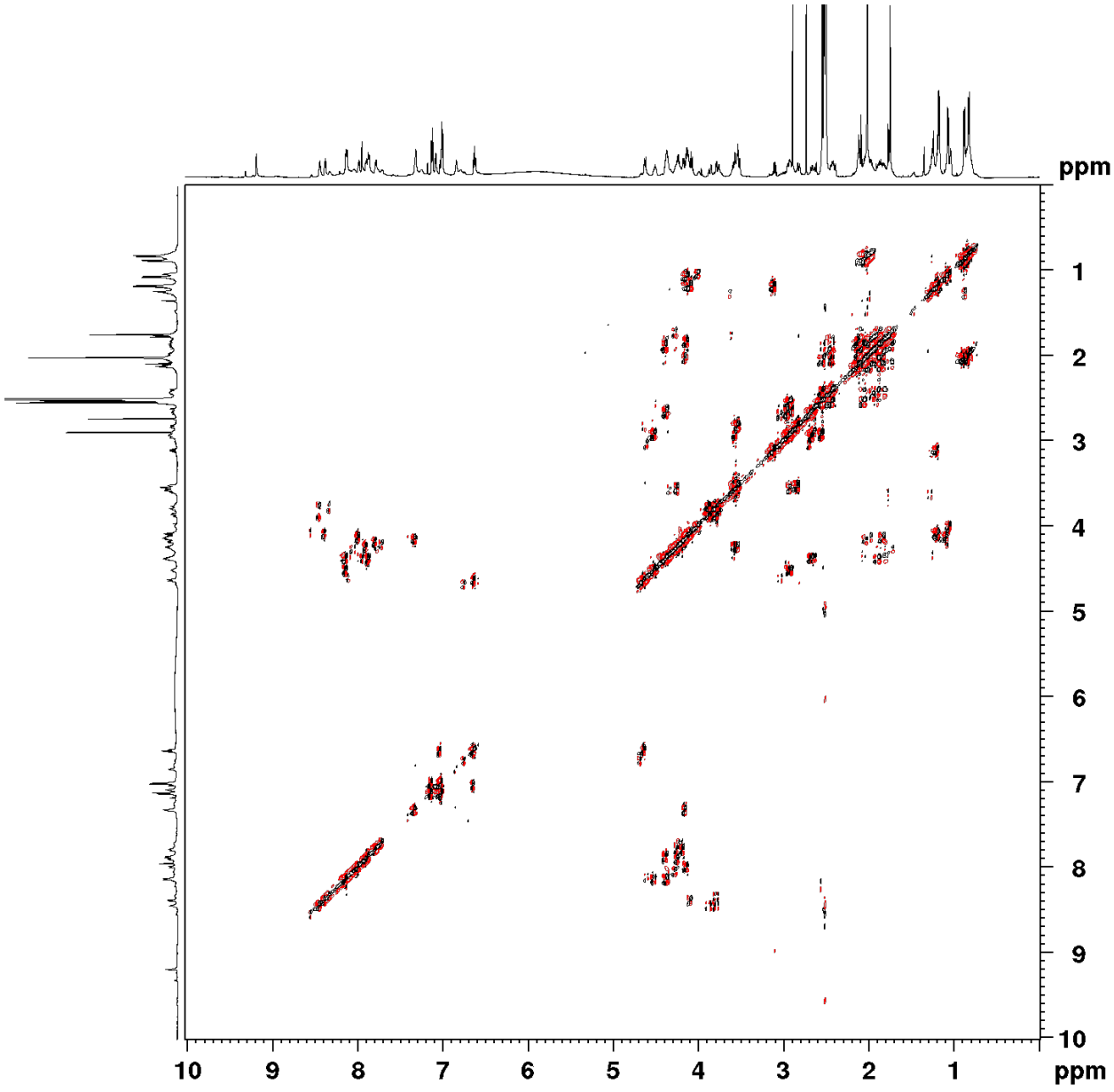

Spectrum 4.7.57 ^{1}H-NMR of Polycycle **15** (DMSO-d_6, 600 MHz)

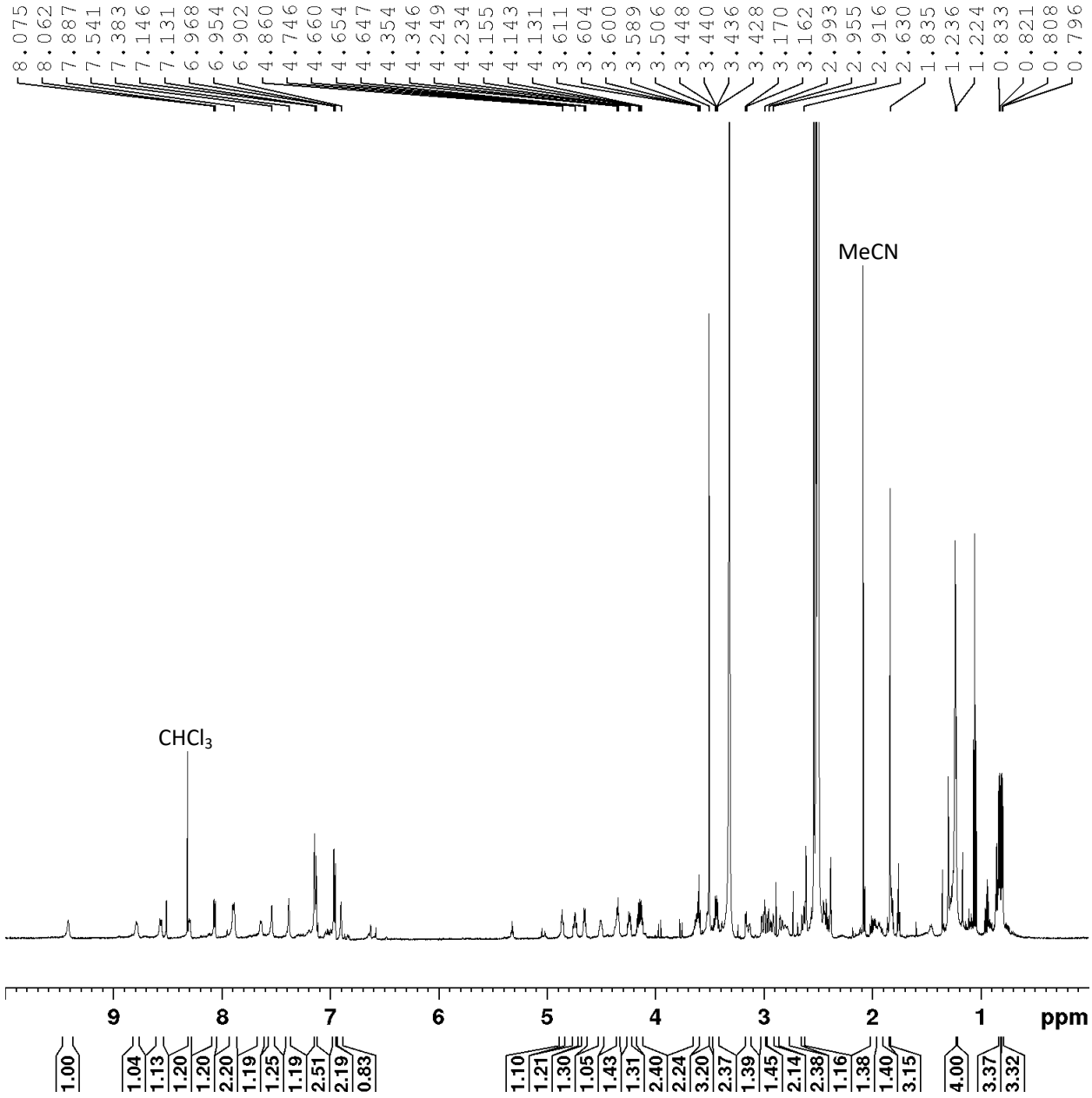

Spectrum 4.7.58 ^{13}C-NMR of Polycycle **15** (DMSO-d_6, 126 MHz)

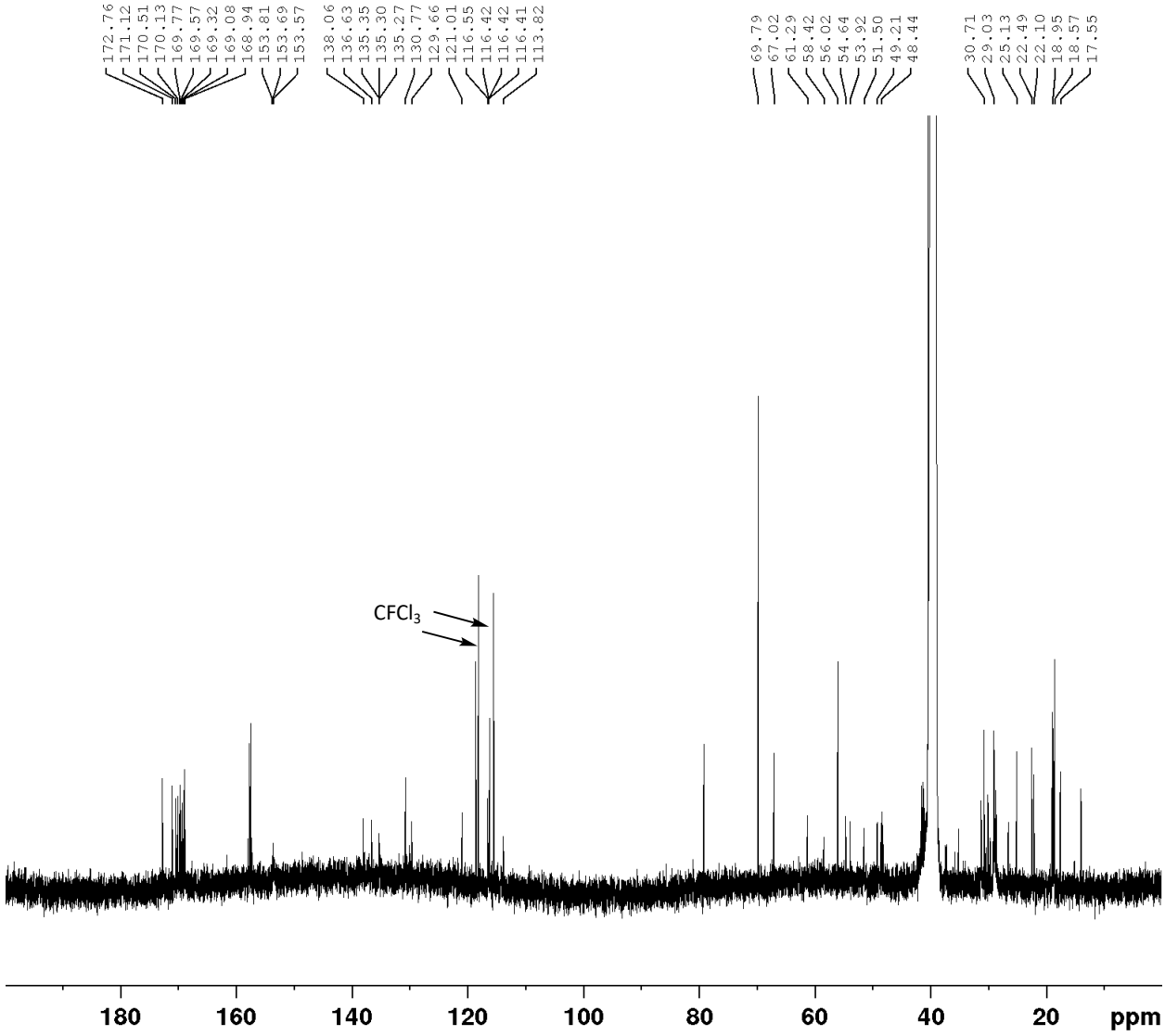

Spectrum 4.7.59 HSQC Spectrum of Polycycle **15** (DMSO-d_6)

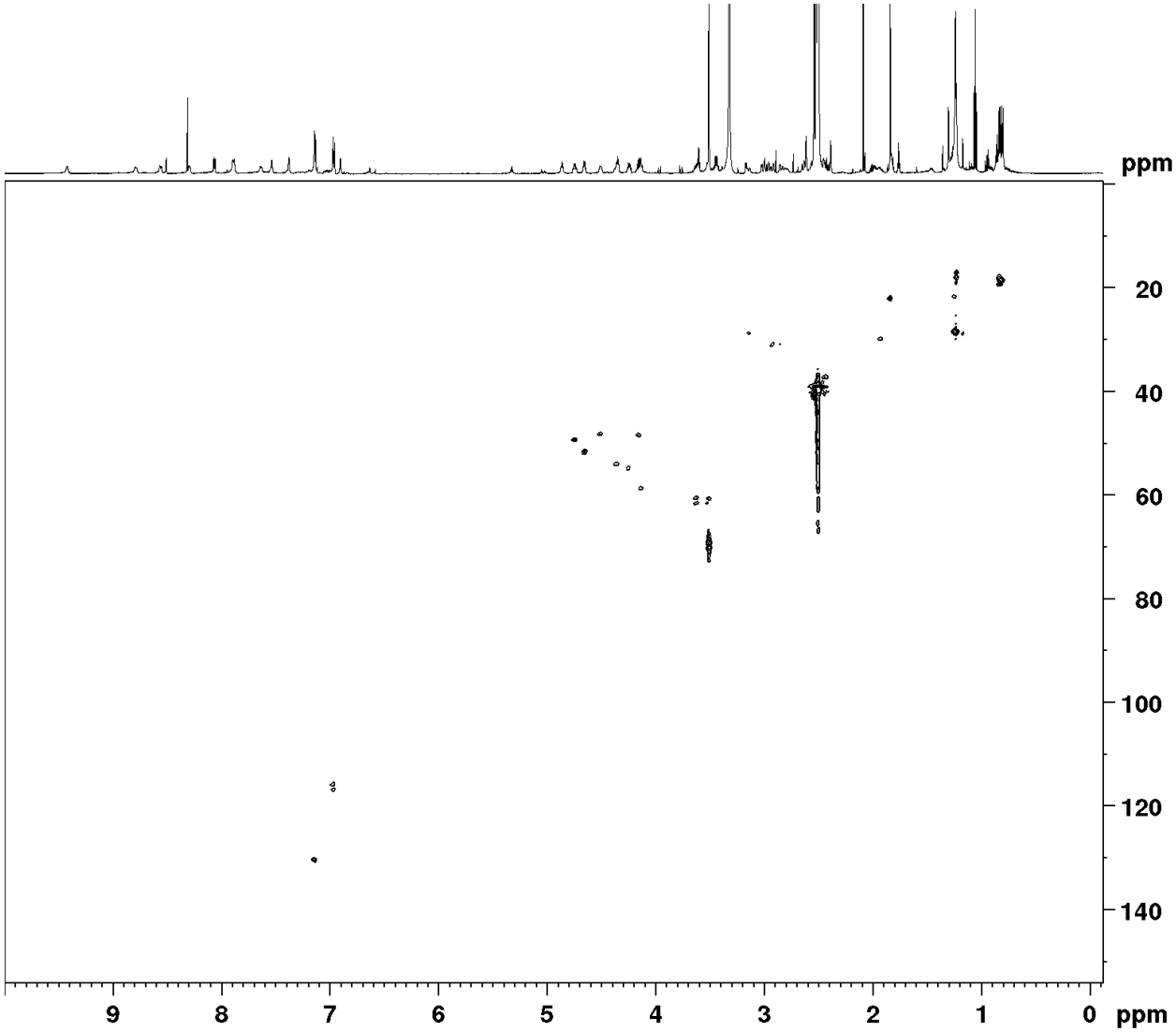

Spectrum 4.7.60 COSY Spectrum of Polycycle **15** (DMSO-d_6)

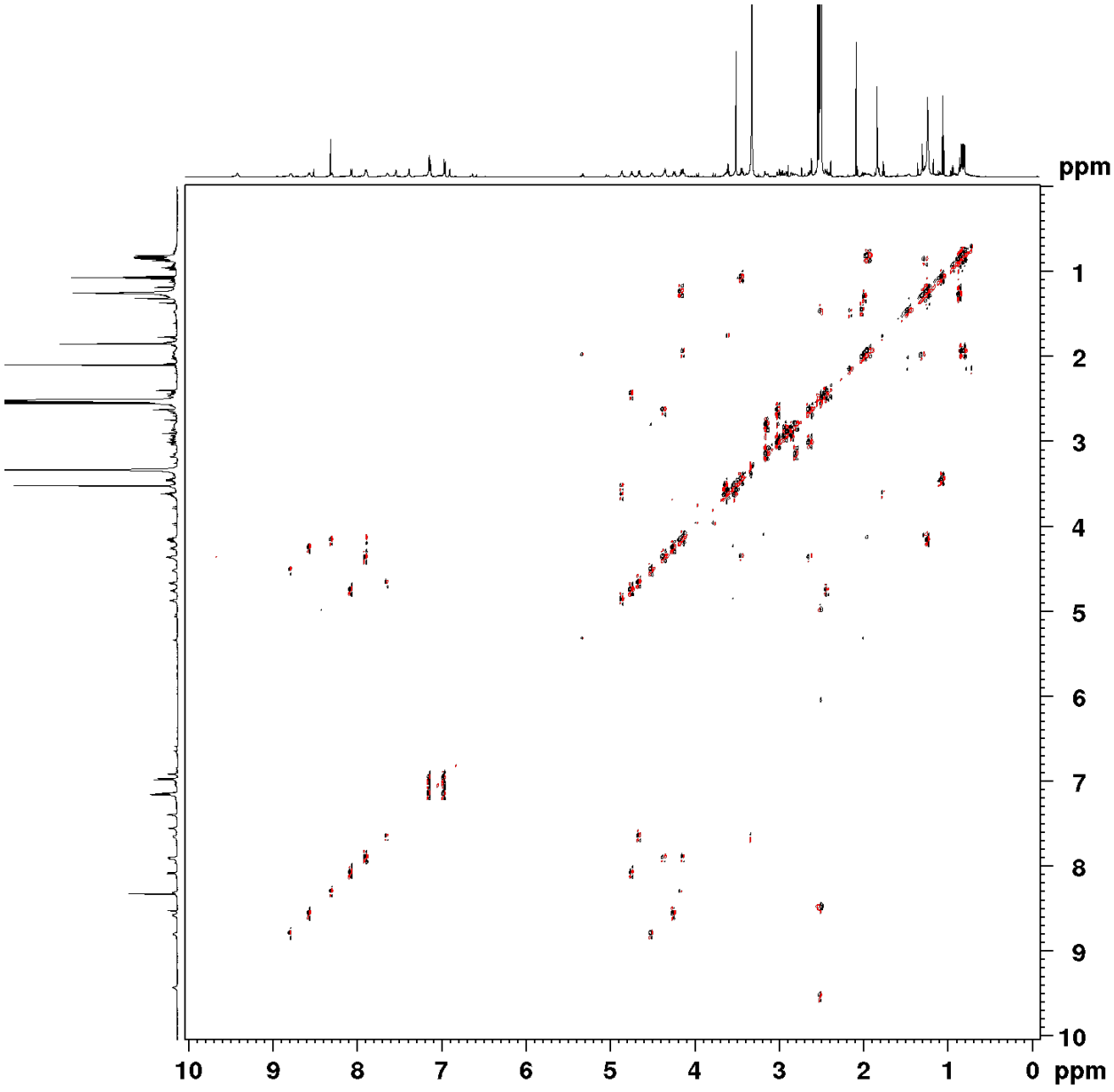

Spectrum 4.7.61 ^{1}H-NMR of Polycycle **16** (DMSO-d_6, 500 MHz)

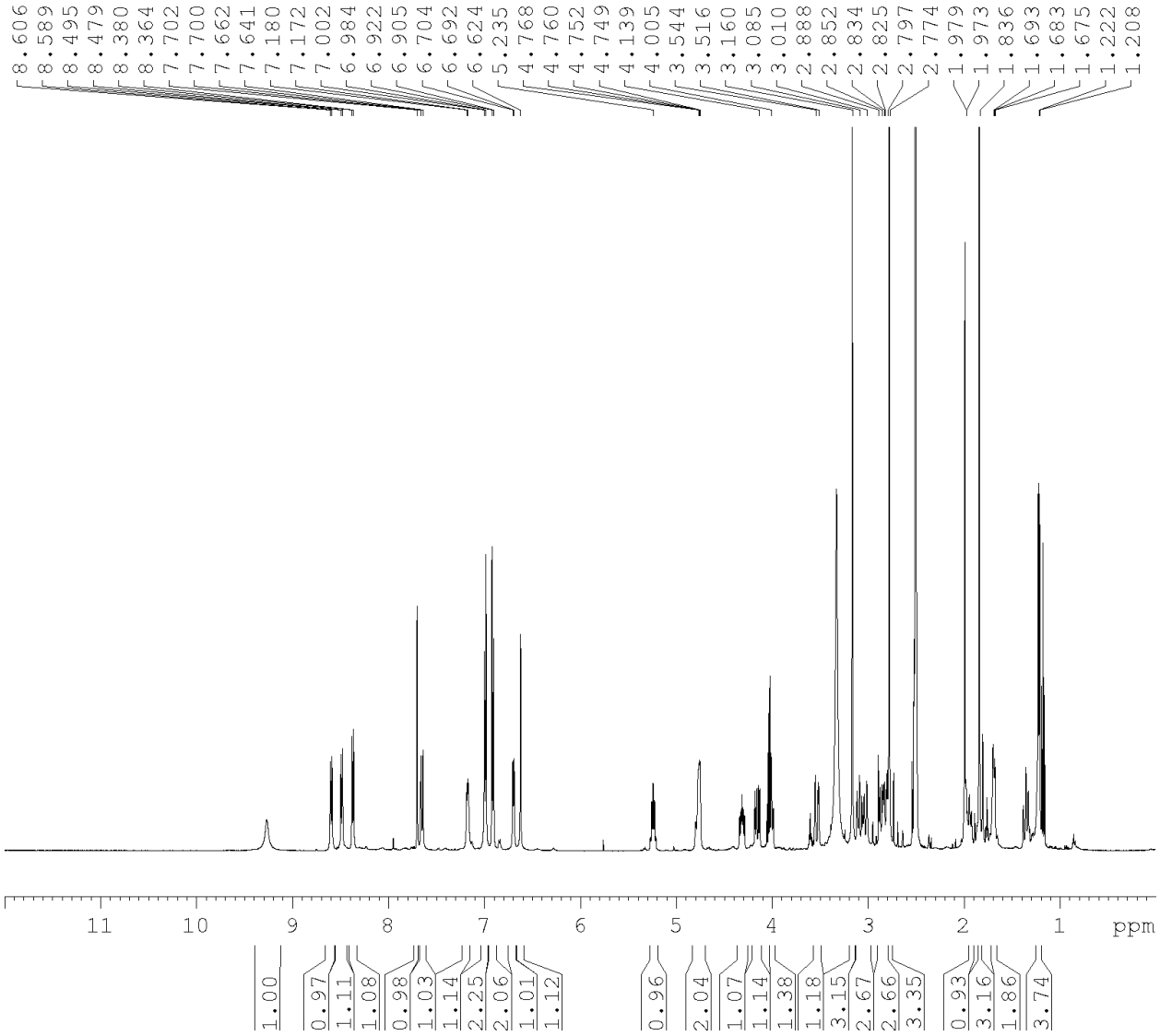

Spectrum 4.7.62 ^{13}C-NMR of Polycycle **16** (DMSO-d_6, 126 MHz)

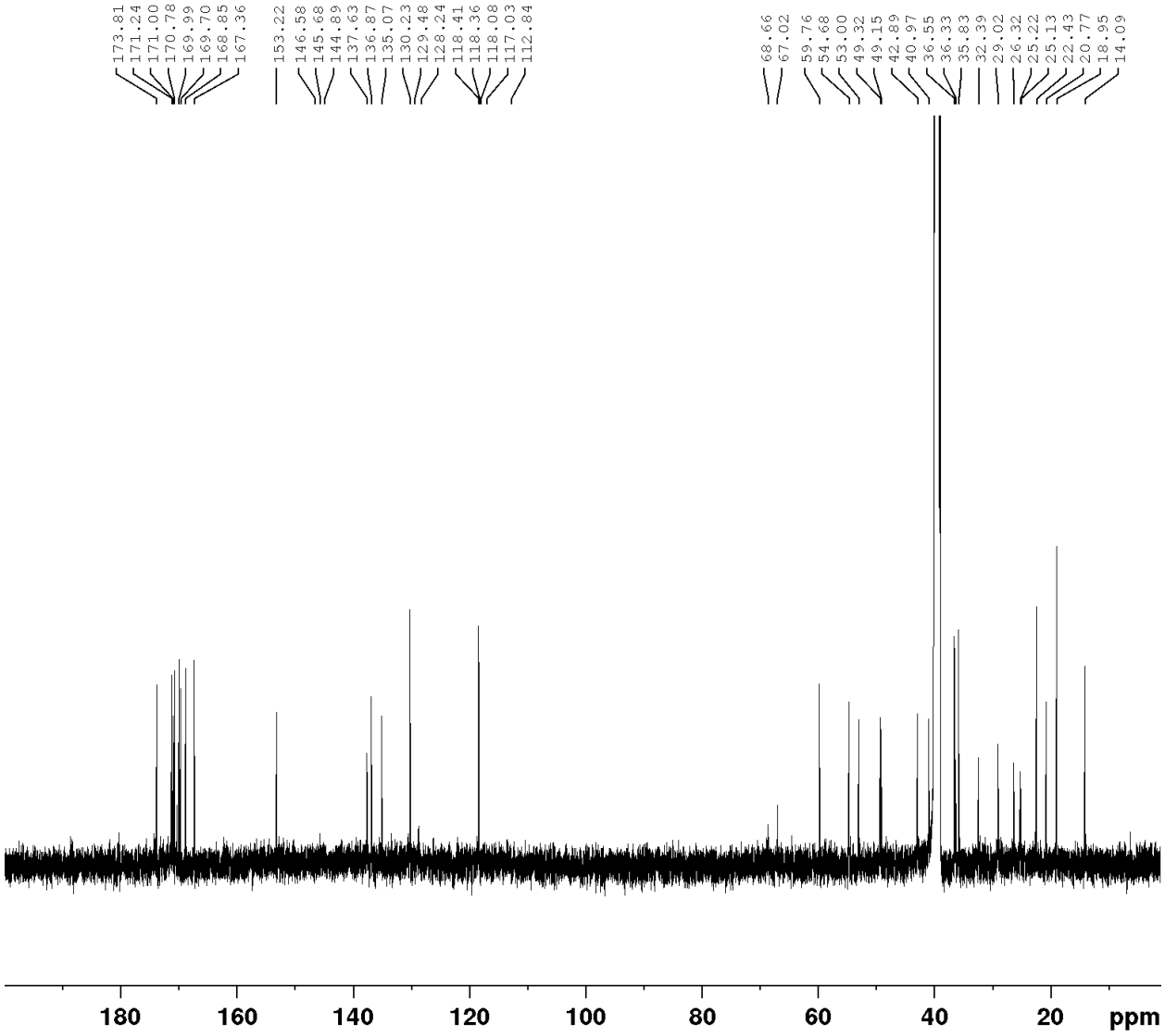

Spectrum 4.7.63 ^{19}F-NMR of Polycycle **16** (DMSO-d_6, 282 MHz)

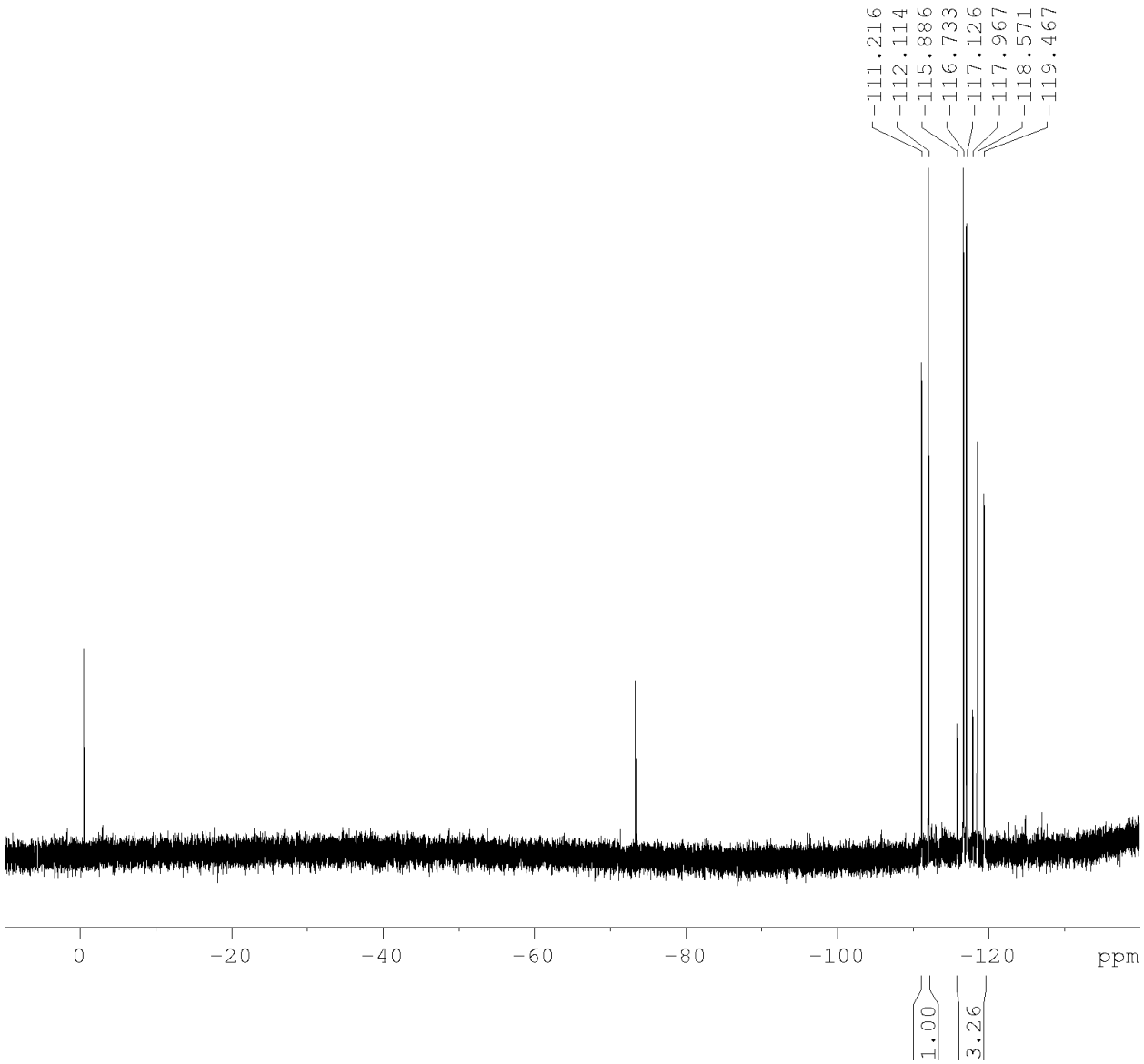

Spectrum 4.7.64 HMBC spectrum of Polycycle **16** (DMSO-d_6)

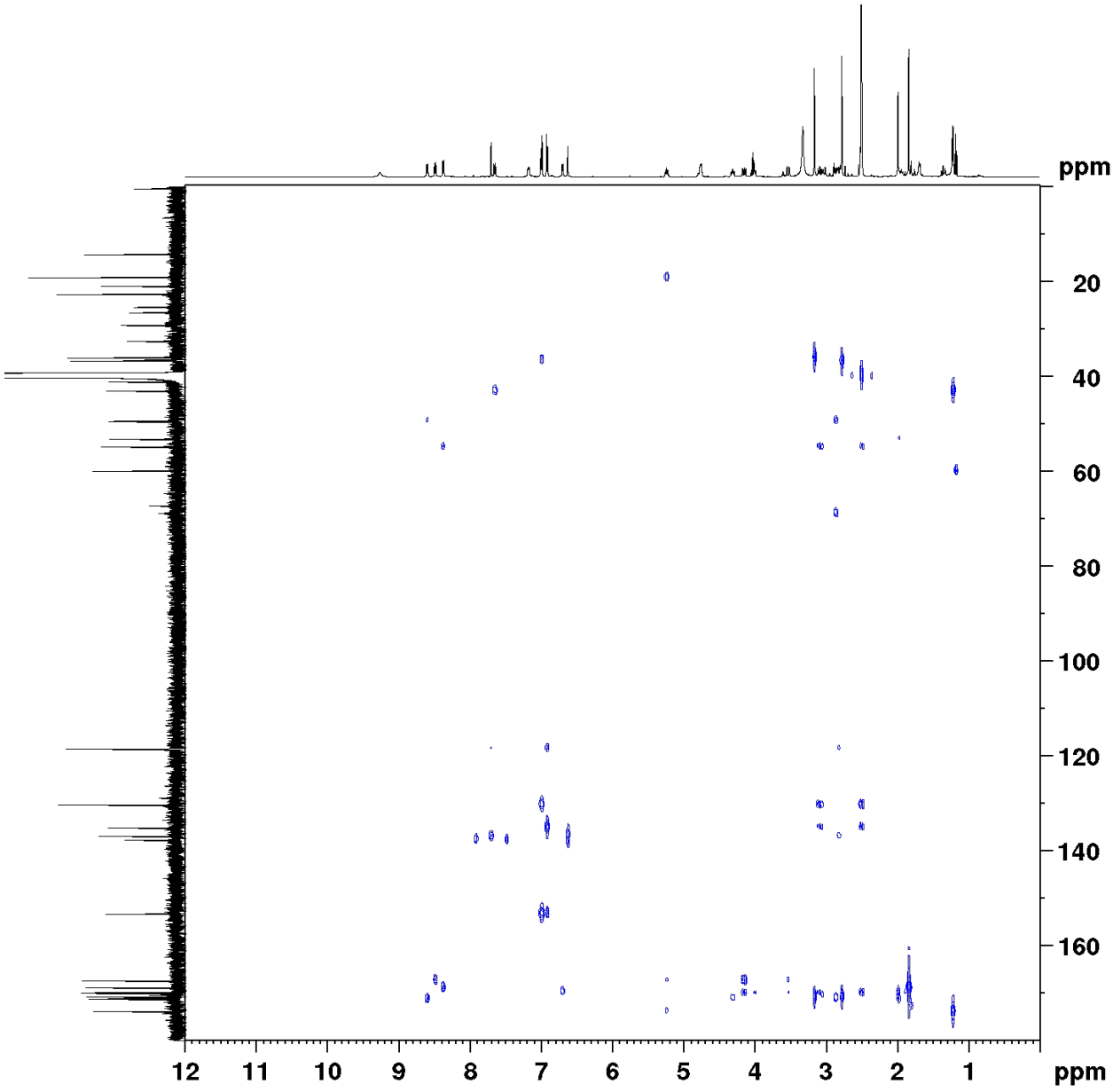

Spectrum 4.7.65 HSQC spectrum of Polycycle **16** (DMSO-d_6)

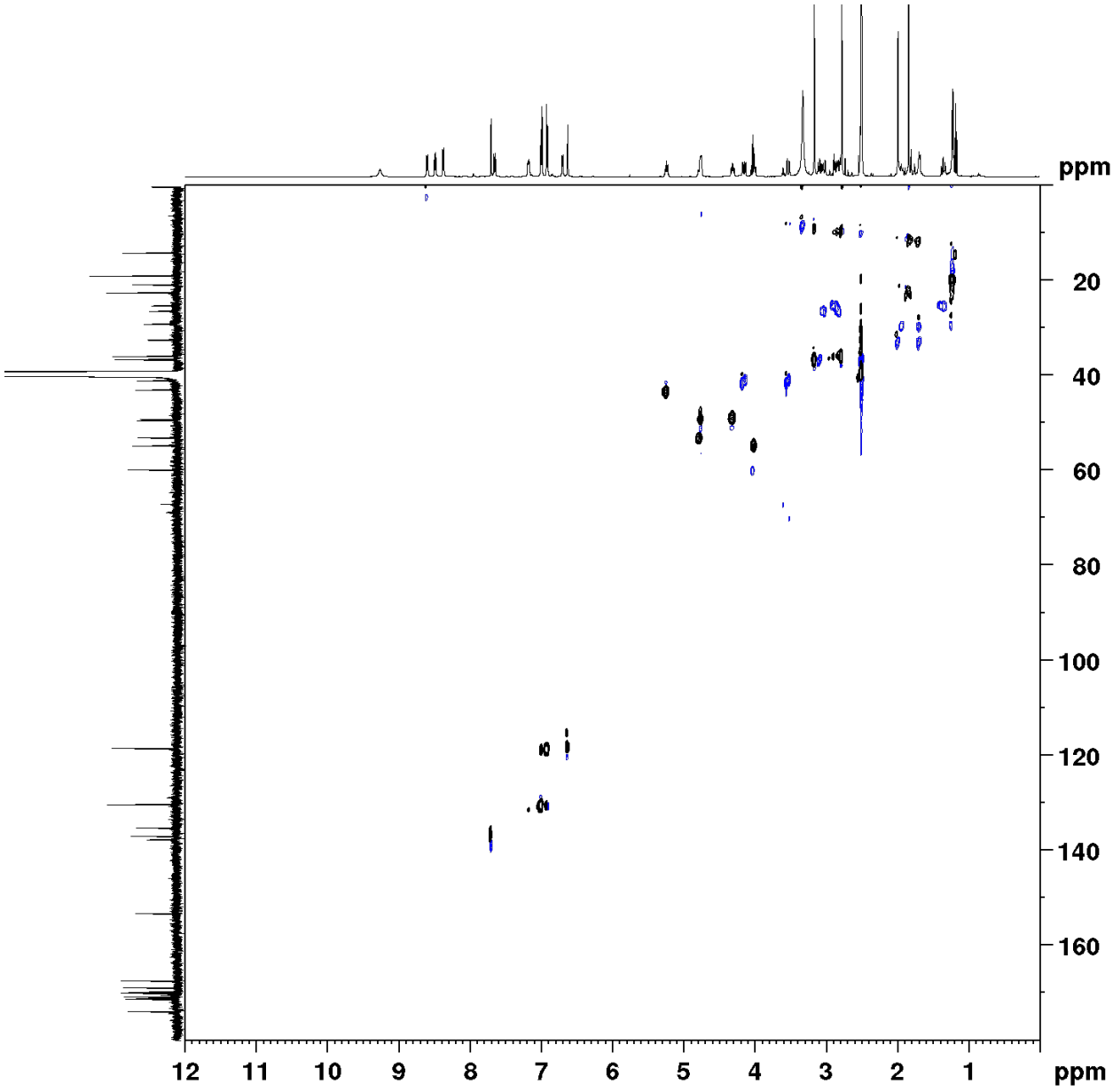

Spectrum 4.7.66 COSY spectrum of Polycycle **16** (DMSO-d_6)

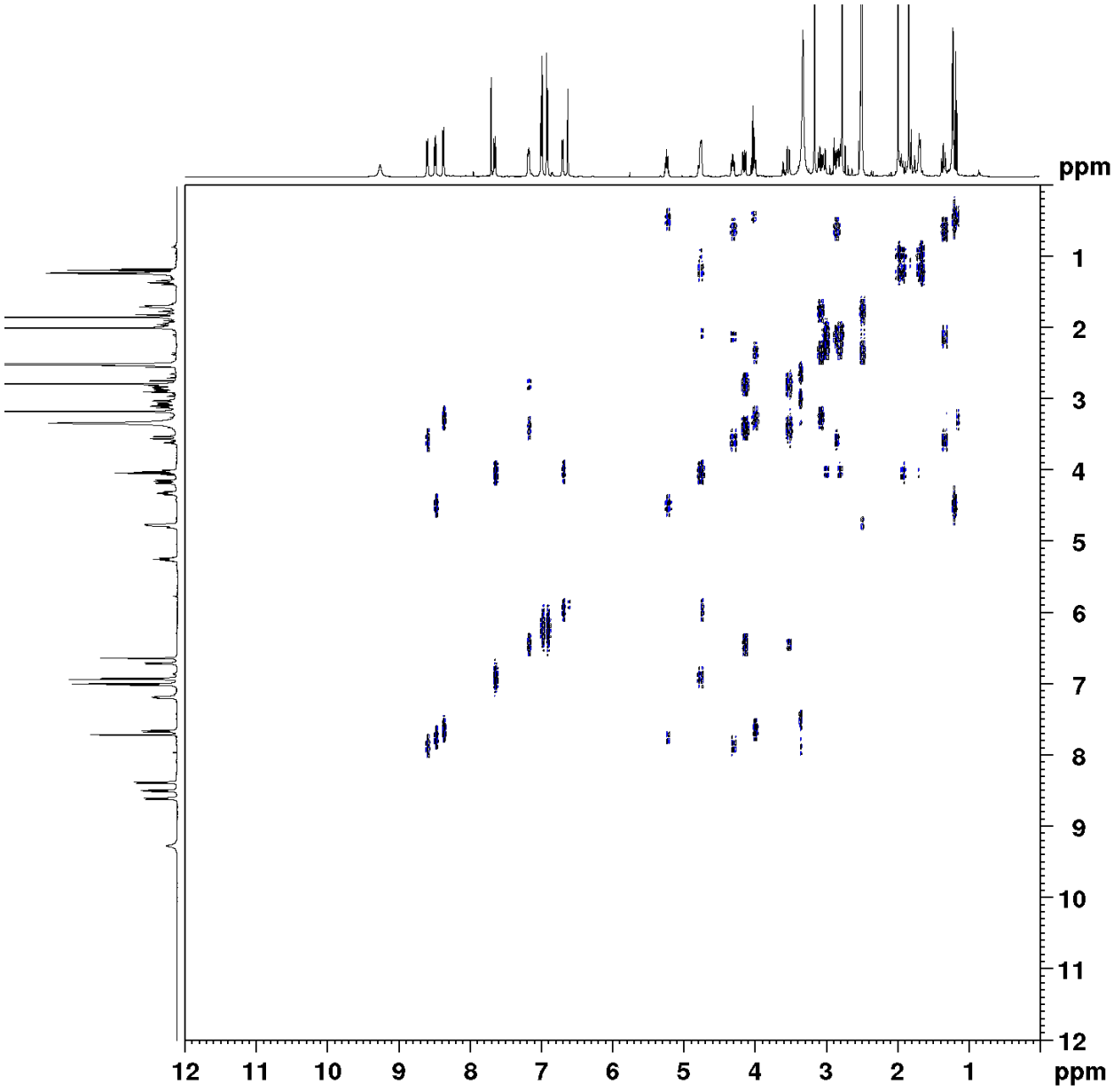

Table 4.7.16 Polycycle **16** (DMSO-d_6, 298K)

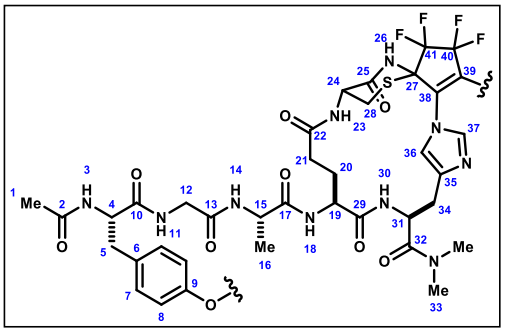

	13C	1H	Key Correlation
1	22.4	1.84 (s, 3H)	1 -> 2 HMBC
2	168.9	-	1 -> 2 HMBC
3	-	8.37 (d, J = 7.7, 1H)	3 -> 2 HMBC
4	54.7	4.03 - 3.97 (m, 1H)	3 -> 4 HMBC
5	36.4	3.12 - 2.98 (m, 1H); 2.53 - 2.47 (m, 1H)	4, 7 -> 5 HMBC
6	135.1	-	4 -> 6 HMBC
7	130.2	6.99 (d, J = 8.7 Hz, 2H); 6.91 (d, J = 8.7, 2H)	8 -> 7 HMBC
8	118.4	6.99 (d, J = 8.7 Hz, 2H); 6.91 (d, J = 8.7, 2H)	7 -> 8 HMBC
9	153.2	-	8 -> 9 HMBC
10	170.0	-	4 -> 10 HMBC
11	-	8.49 (d, J = 8.1 Hz, 1H)	11 -> 12, 13 HMBC
12	41.0	4.15 (dd, J = 17.3, 7.4, 1H); 3.53 (dd, J = 17.3, 3.4, 1H)	12 -> 13, 10 HMBC
13	167.4	-	15 -> 13 HMBC
14	-	7.65 (d, J = 10.1 Hz, 1H)	14 -> 15 HMBC
15	42.9	5.24 (quint, J = 7.1 Hz, 1H)	15 -> 16 HMBC
16	19.0	1.22 (d, J = 6.70, 3H)	16 -> 17 HMBC
17	173.8	-	15, 16 -> 17 HMBC
18	-	7.18 (s, 1H)	18 -> 17 HMBC
19	53.0	4.82 - 4.73 (m, 1H)	18 -> 19 HMBC
20	29.0	1.96 - 1.91 (m, 1H), 1.71 - 1.67 (m, 1H)	20 -> 19, 29 HMBC
21	32.4	2.02 - 1.96 (m, 1H), 1.72 - 1.66 (m, 1H)	21 -> 22, 20 HMBC
22	169.7	-	21 -> 22 HMBC
23	-	6.70 (d, J = 6.2, 1H)	23 -> 22, 24 HMBC
24	49.3	4.36 - 4.26 (m, 1H)	24 -> 28, 25 HMBC
25	171.0	-	24, 28 -> 25 HMBC
26	-	9.26 (s, 1H)	
27	69.5 - 67.8 (m, 1C)	-	28 -> 27 HMBC
28	25.2	3.04 - 2.99 (m, 1H), 2.90 - 2.82 (m, 1H)	28 -> 27 HMBC
29	171.2	-	30 -> 29 HMBC
30	-	8.60 (s, 1H)	30 -> 29 HMBC
31	49.2	4.79 - 4.72 (m, 1H)	31 -> 34 HMBC
32	170.8	-	33 -> 32 HMBC
33	36.5, 35.8	3.16 (s, 3H); 2.77 (s, 3H)	33 -> 32 HMBC
34	26.3	2.85 - 2.79 (m, 2H)	34 -> 35, 36 HMBC
35	136.9	-	36, 37 -> 35 HMBC
36	118.4	6.62 (s, 1H)	36, 37 -> 35 HMBC
37	137.6	7.7 (s, 1H)	36 -> 37 HMBC
38	129.5 - 128.2 (m, 1C)	-	
39	146.5 - 144.6 (m, 1C)	-	
40	118.1 - 117.0 (m, 2C)	-	
41	118.1 - 117.0 (m, 2C)	-	

Spectrum 4.7.67 ^{1}H-NMR of Macrocycle **17** (DMSO-d_6, 500 MHz)

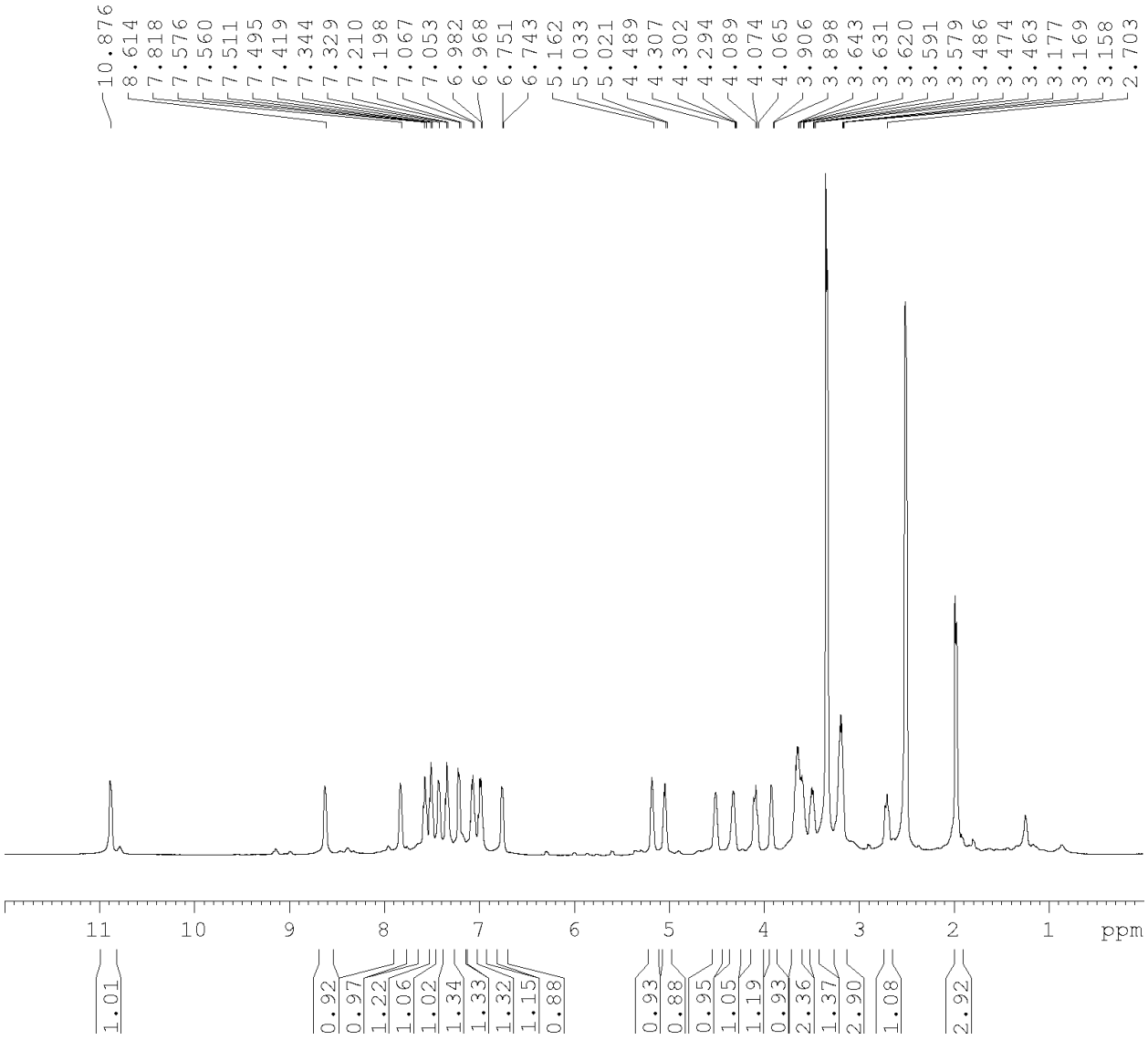

Spectrum 4.7.68 ^{13}C-NMR of Macrocycle **17** (DMSO-d_6, 126 MHz)

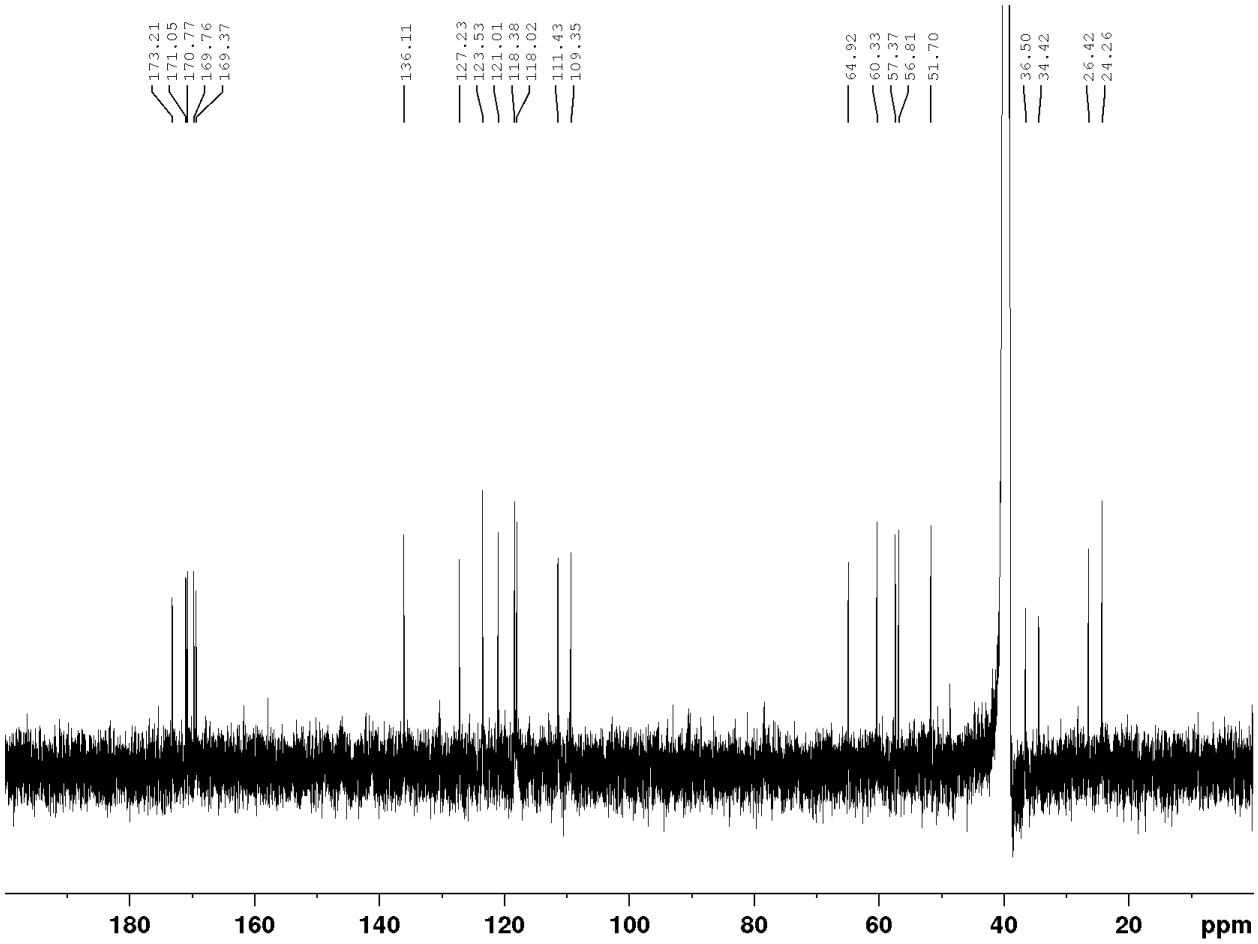

Spectrum 4.7.69 ^{1}H-NMR of Macrocycle **19** (DMSO-d_6, 500 MHz)

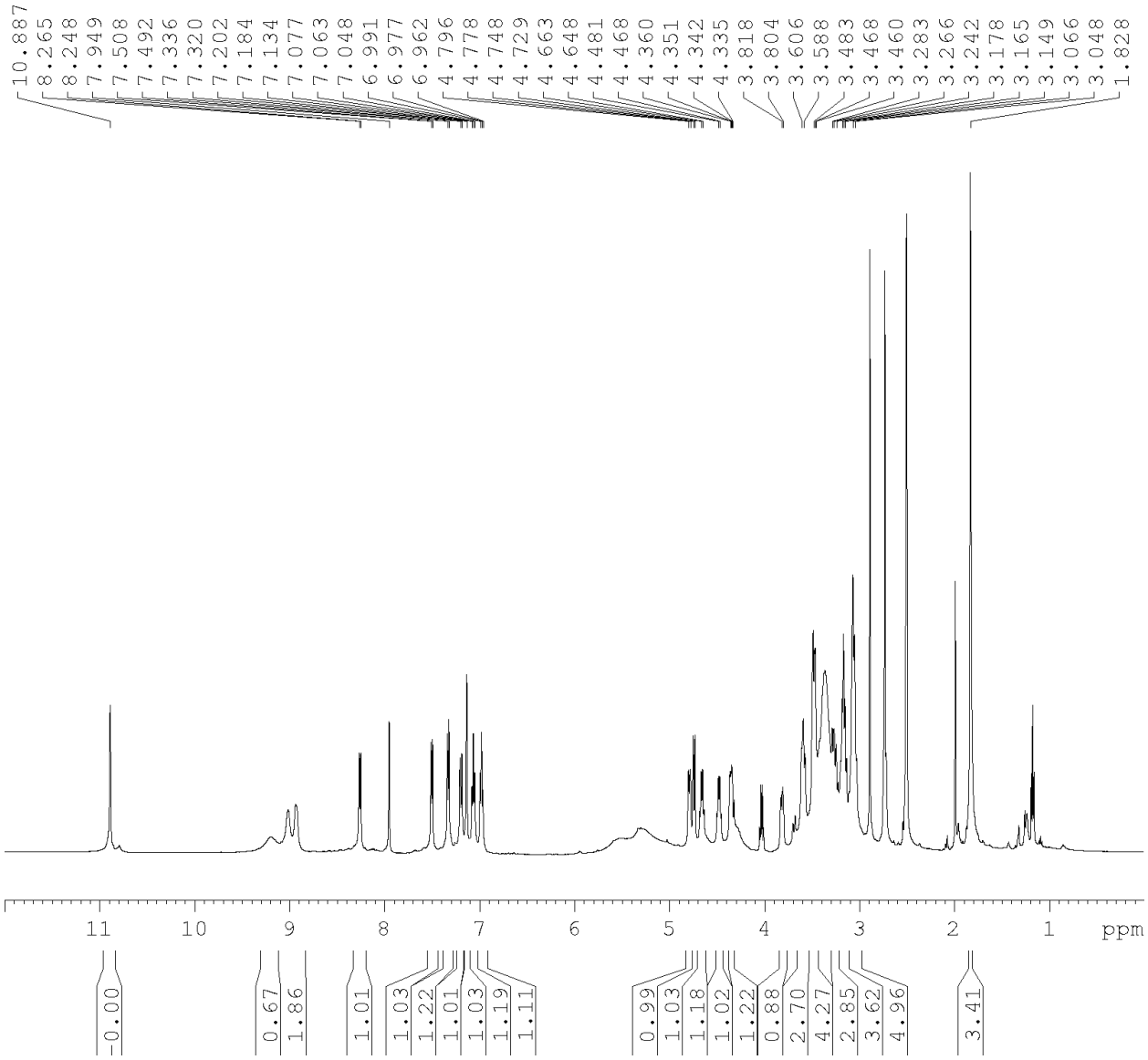

Spectrum 4.7.70 ^{13}C-NMR of Macrocycle **19** (DMSO-d_6, 500 MHz)

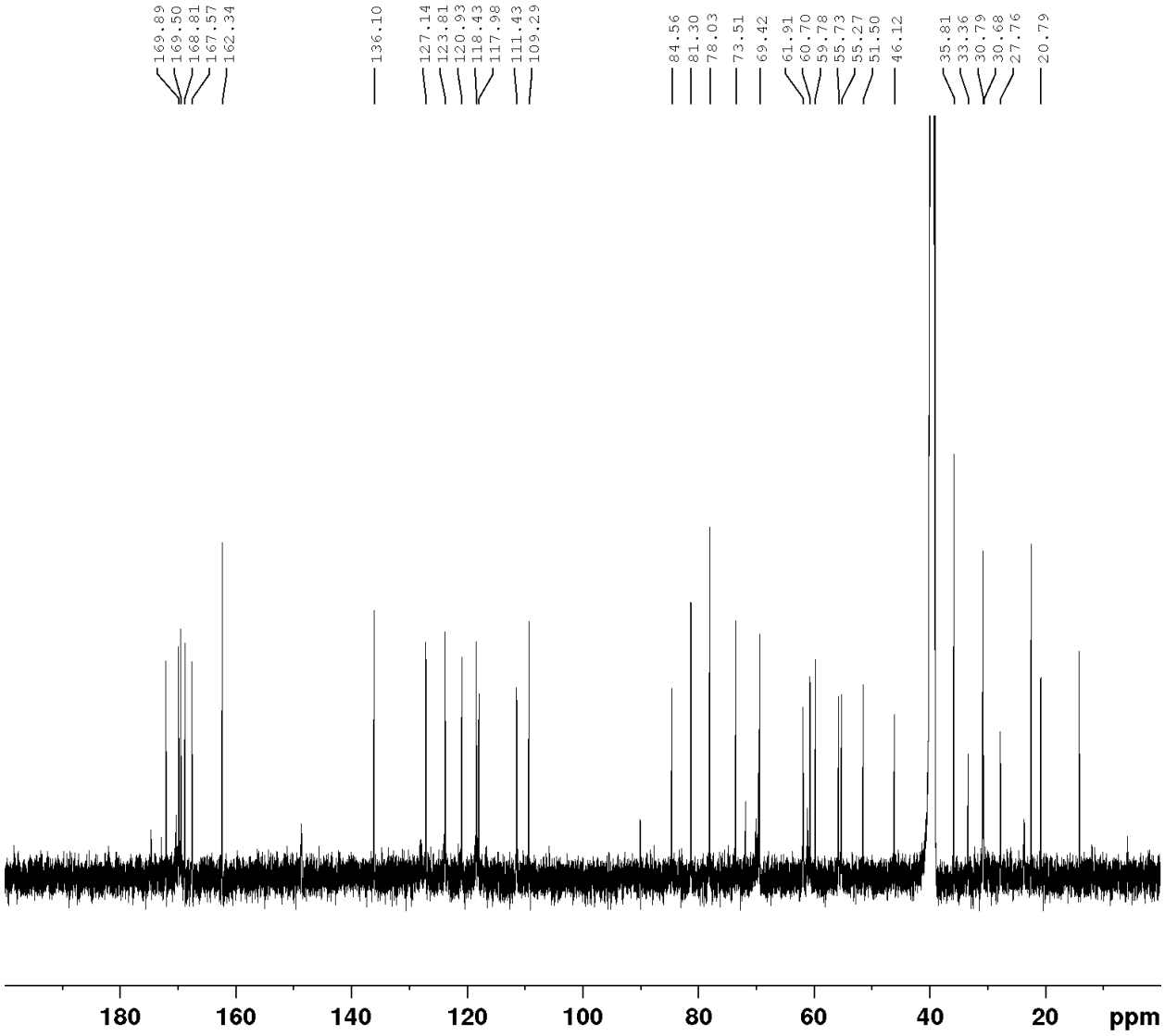

Spectrum 4.7.71 ^{19}F-NMR of Macrocycle **19** (DMSO-d_6, 282 MHz)

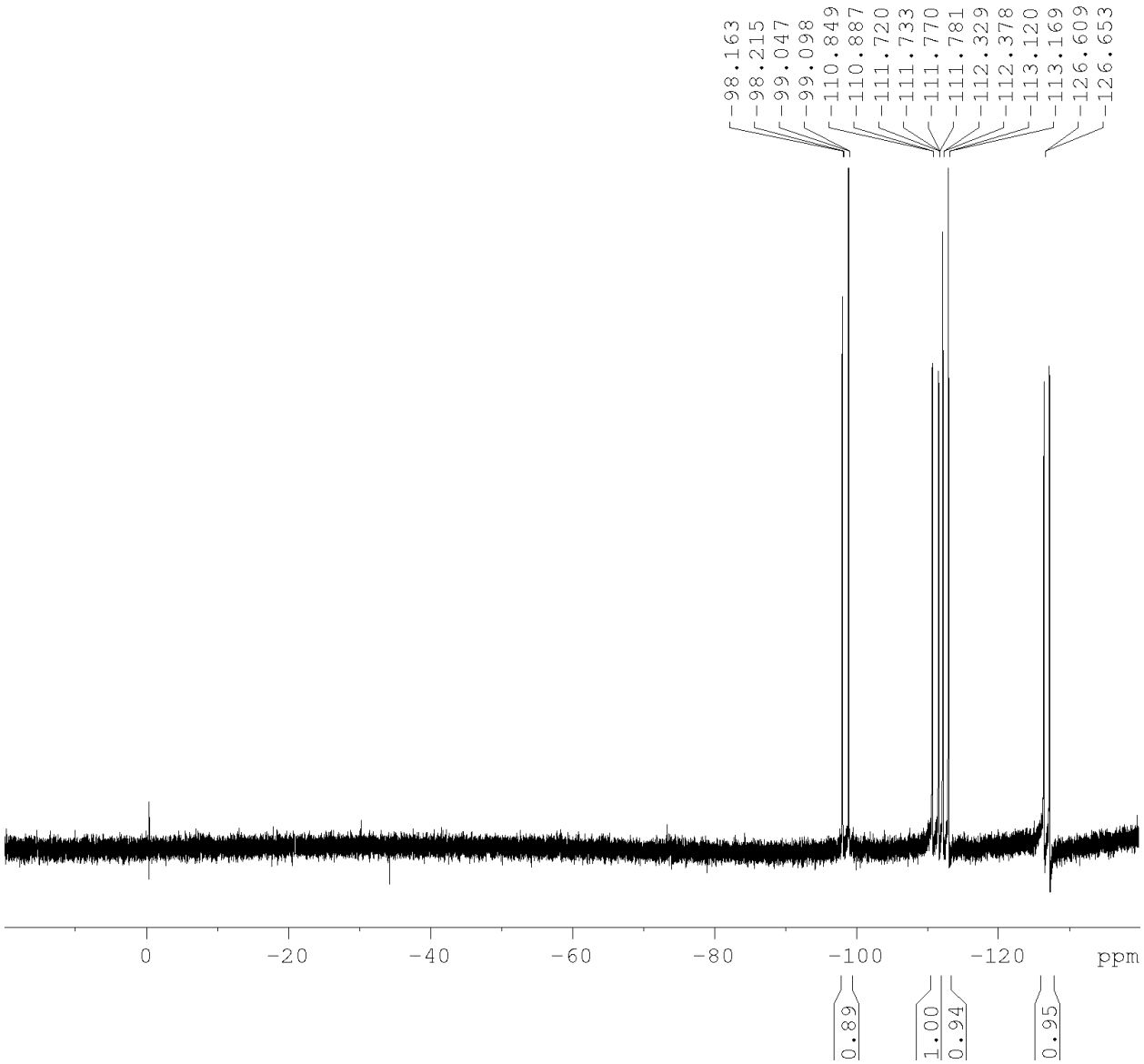

Spectrum 4.7.72 ^{1}H-NMR of Macrocycle **20** (DMSO-d_6, 500 MHz)

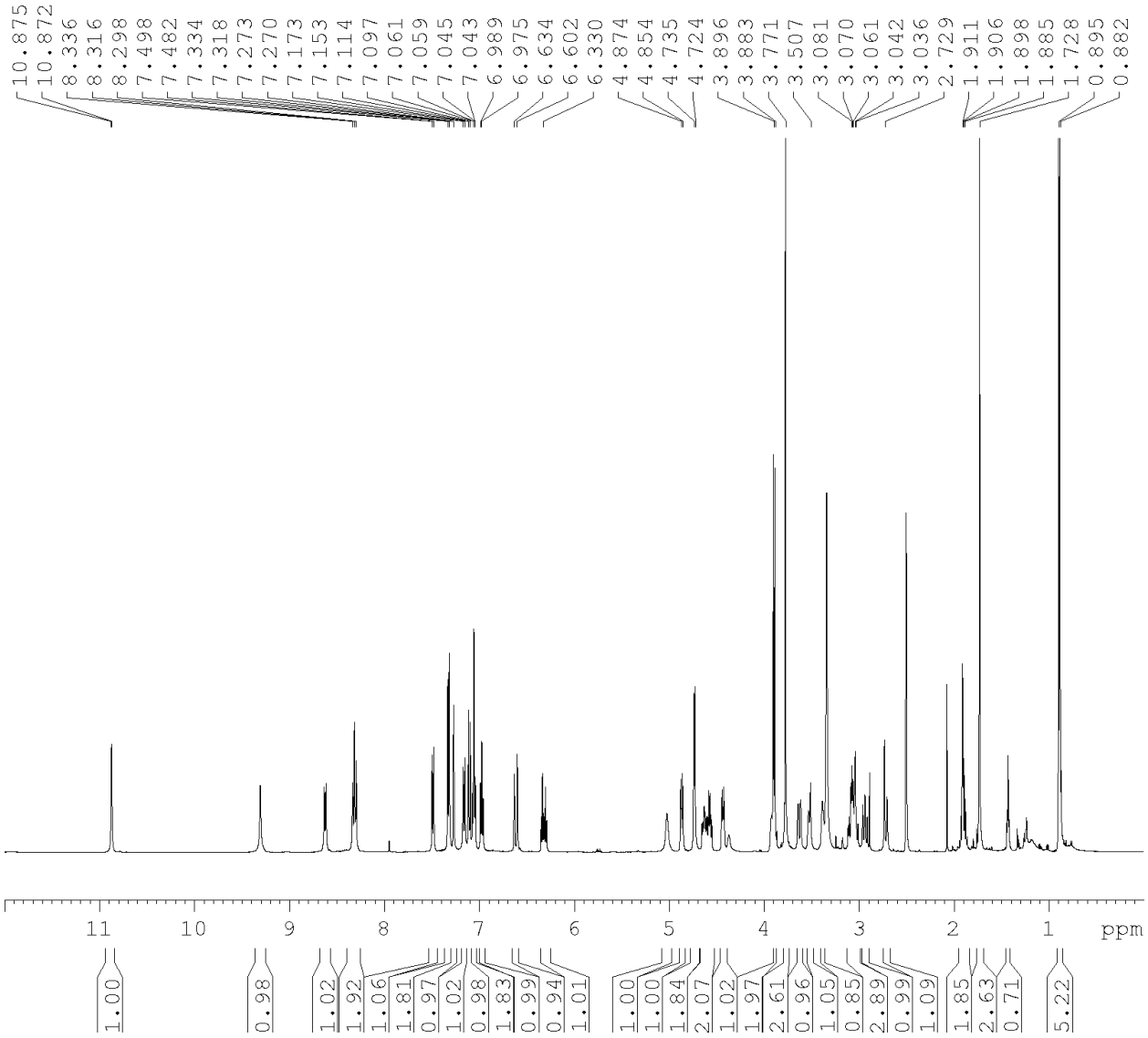

Spectrum 4.7.73 ^{13}C-NMR of Macrocycle **20** (DMSO-d_6, 126 MHz)

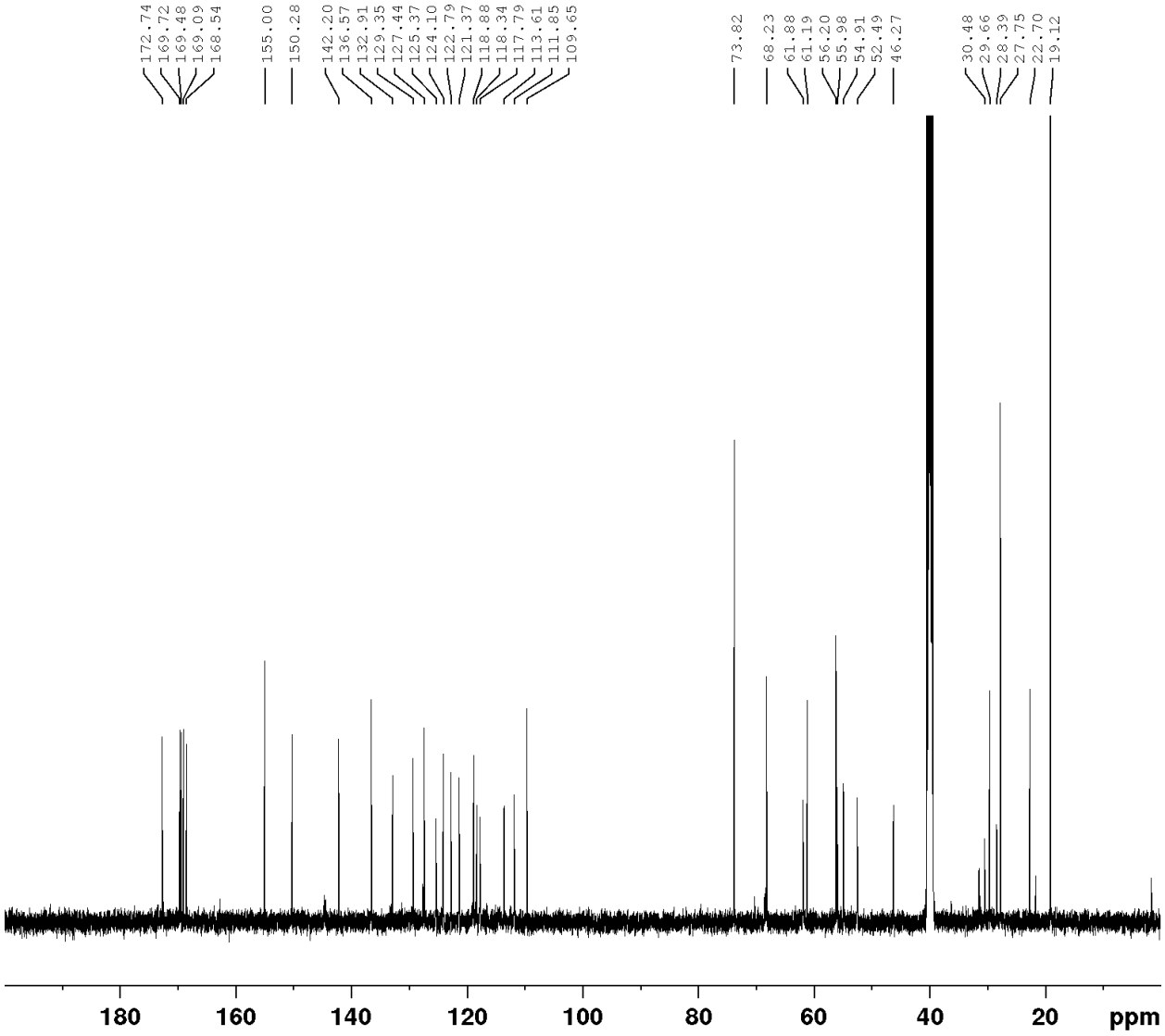

Spectrum 4.7.74 ^{19}F-NMR of Macrocycle **20** (DMSO-d_6, 282 MHz)

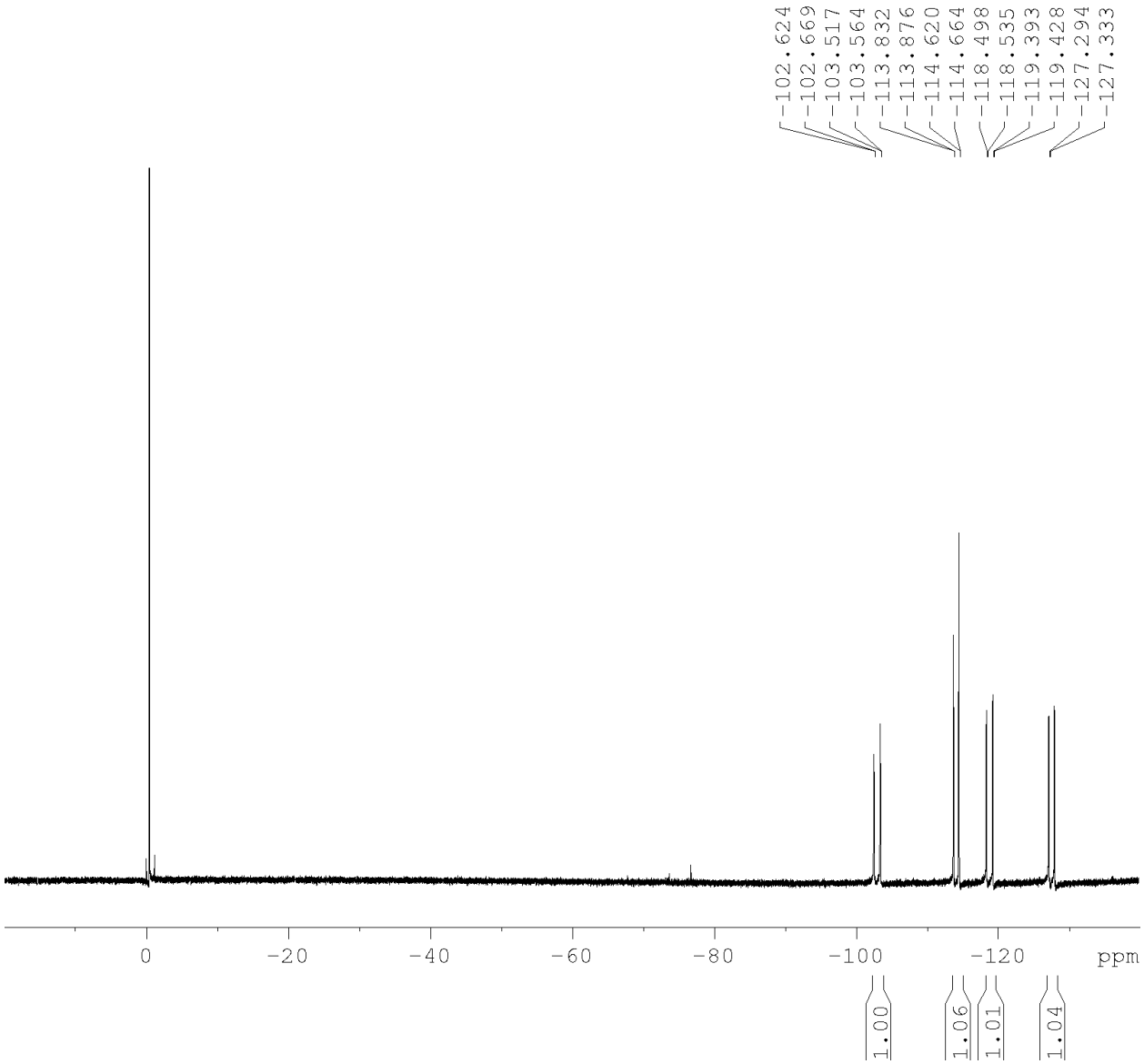

Spectrum 4.7.75 ^{1}H-NMR of Macrocycle **21** (DMSO-d_6, 500 MHz)

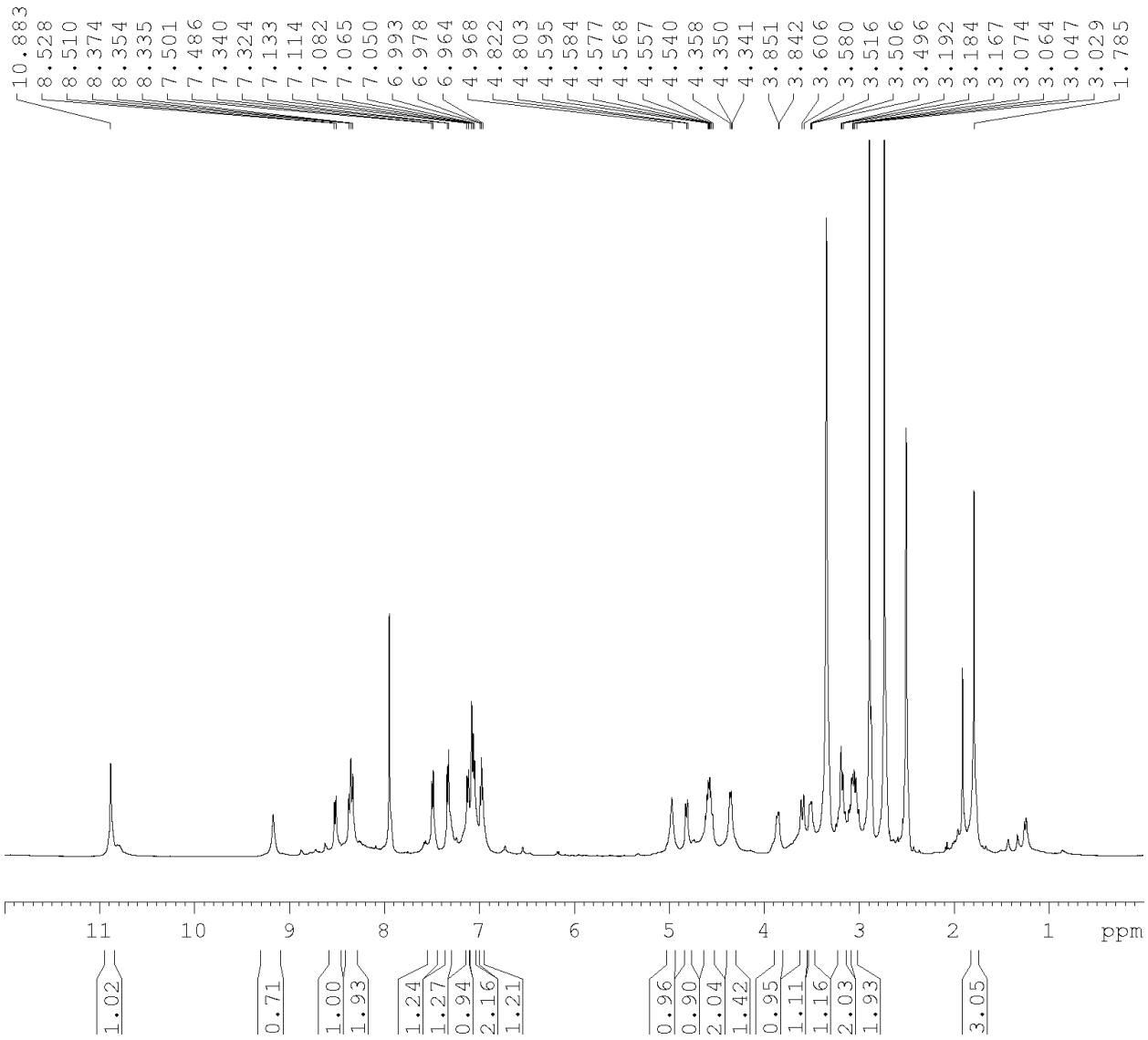

Spectrum 4.7.76 ^{13}C-NMR of Macrocycle **21** (DMSO-d_6, 126 MHz)

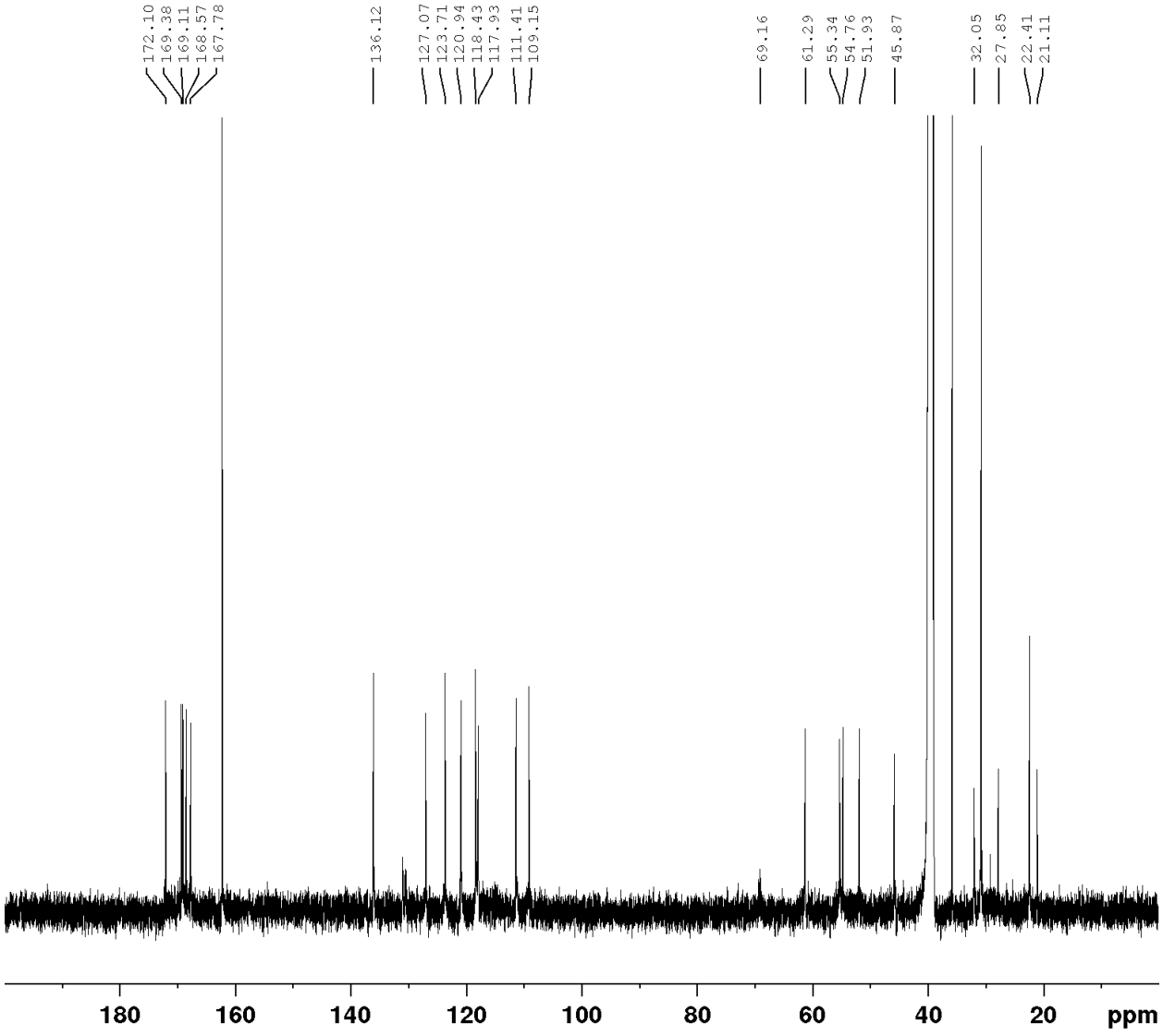

Spectrum 4.7.77 ^{19}F-NMR of Macrocycle **21** (DMSO-d_6, 282 MHz)

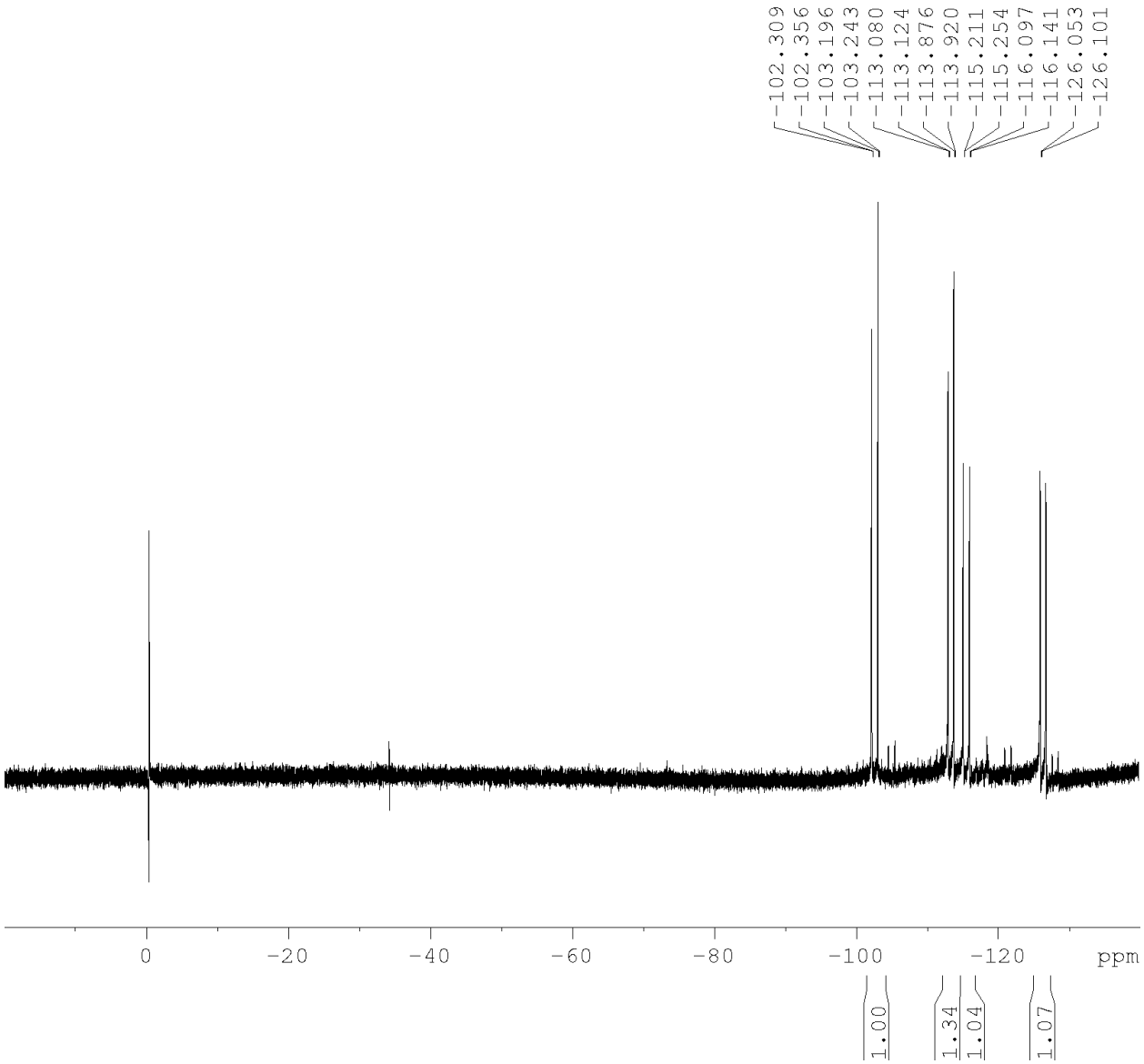

Spectrum 4.7.78 ^{1}H-NMR of Macrocycle **22** (DMSO-d_6, 500 MHz)

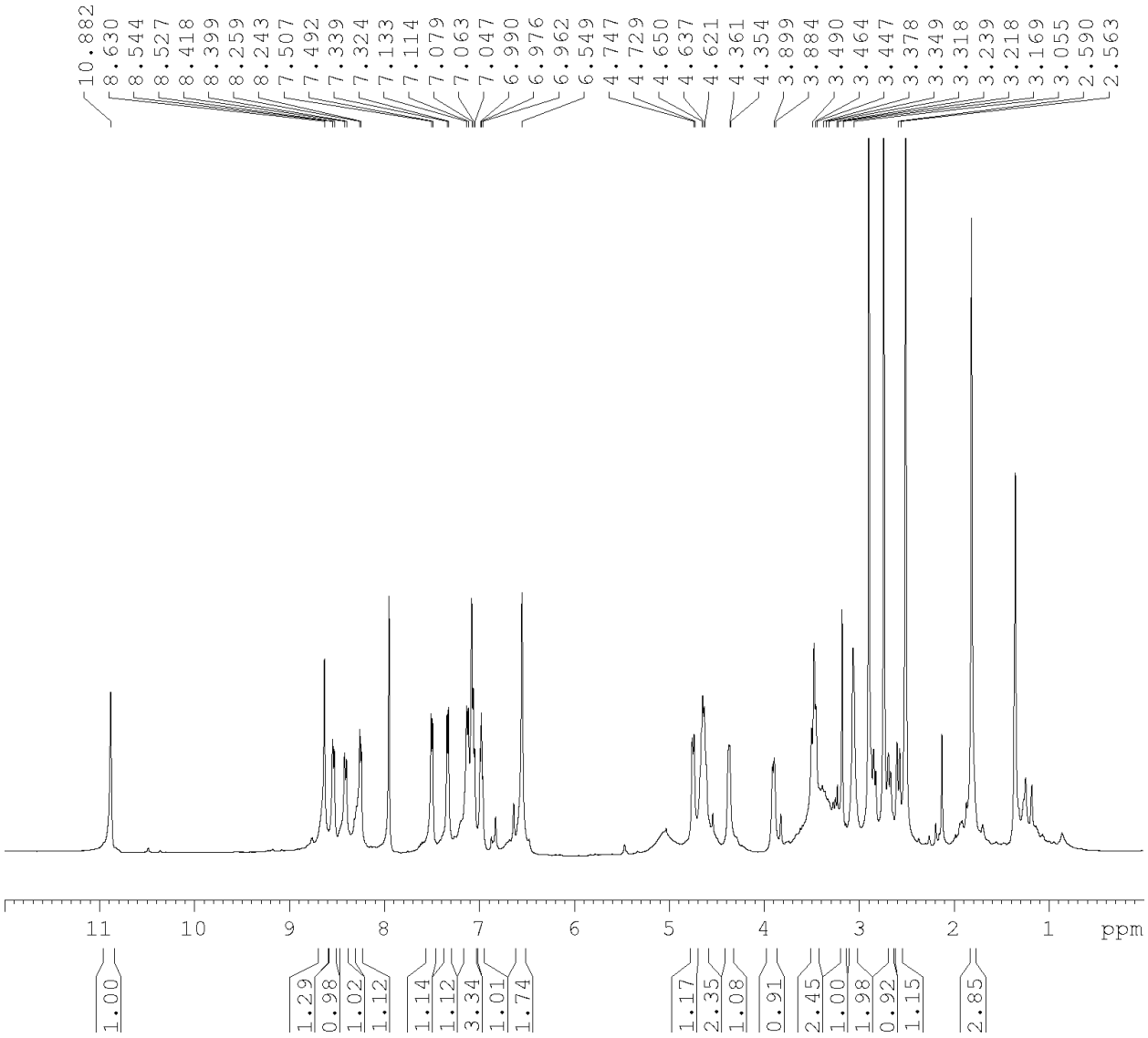

Spectrum 4.7.79 ^{13}C-NMR of Macrocycle **22** (DMSO-d_6, 126 MHz)

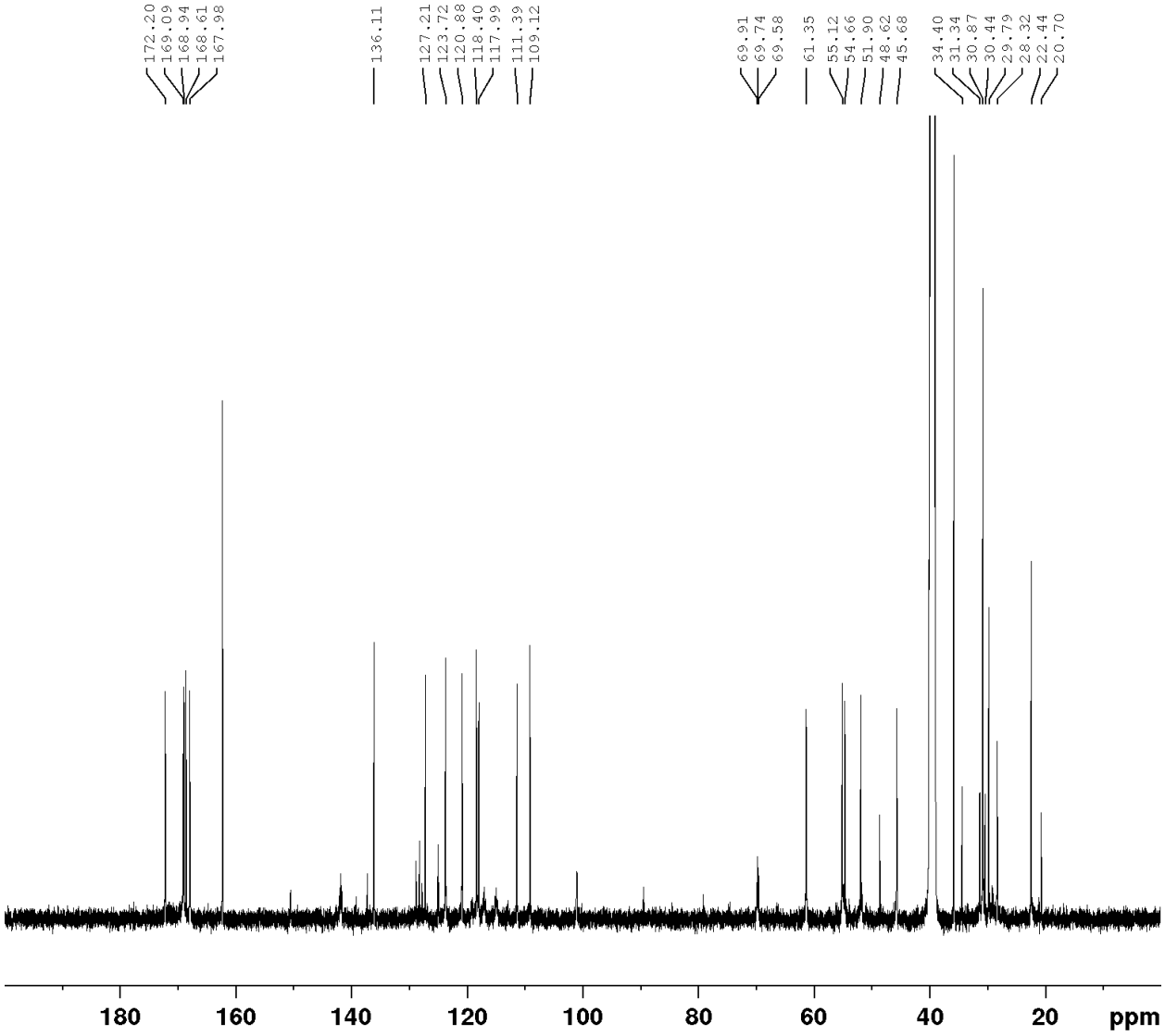

Spectrum 4.7.80 ^{19}F-NMR of Macrocycle **22** (DMSO-d_6, 282 MHz)

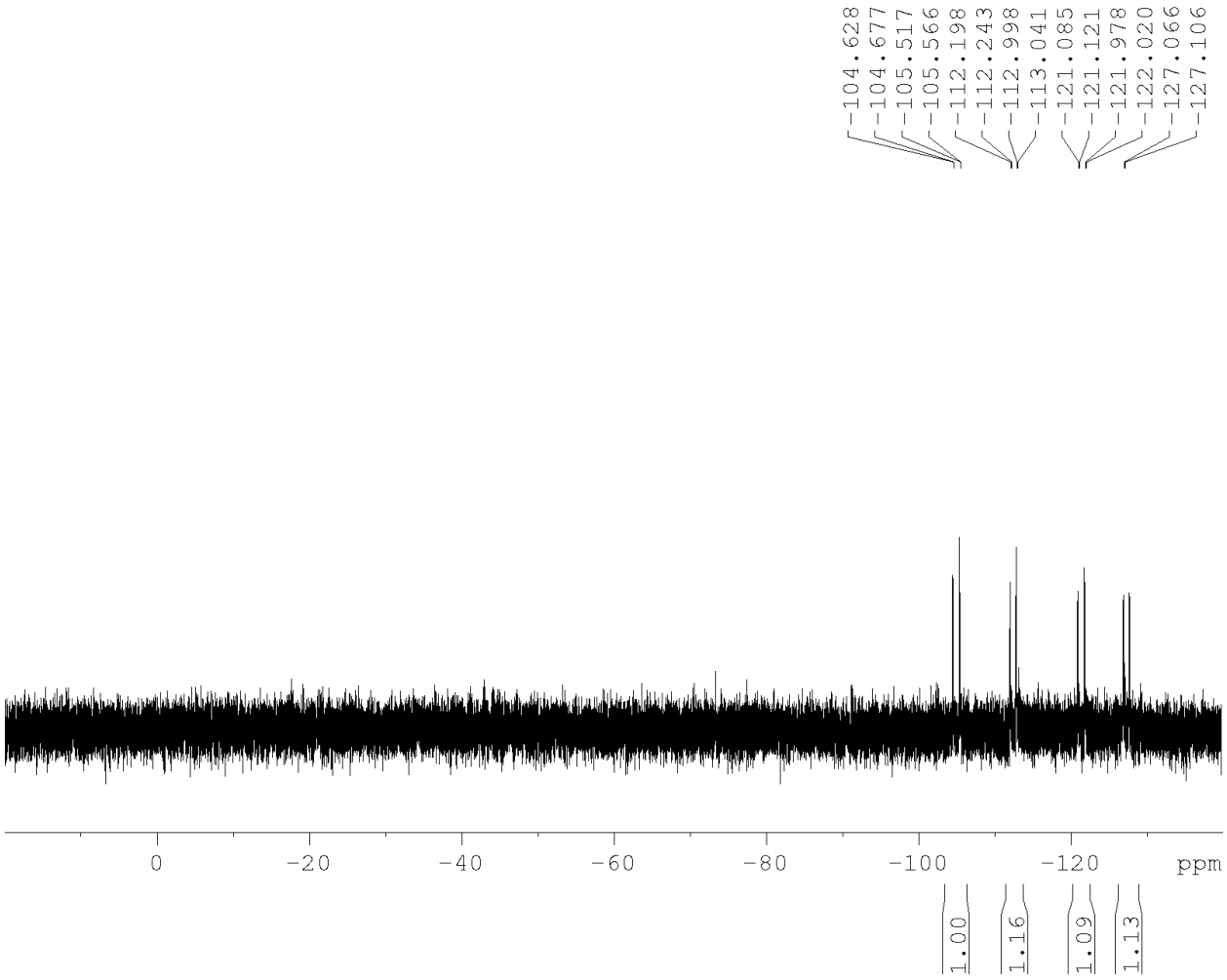

Spectrum 4.7.81 ^{1}H-NMR of Macrocycle **23** (DMSO-d_6, 500 MHz)

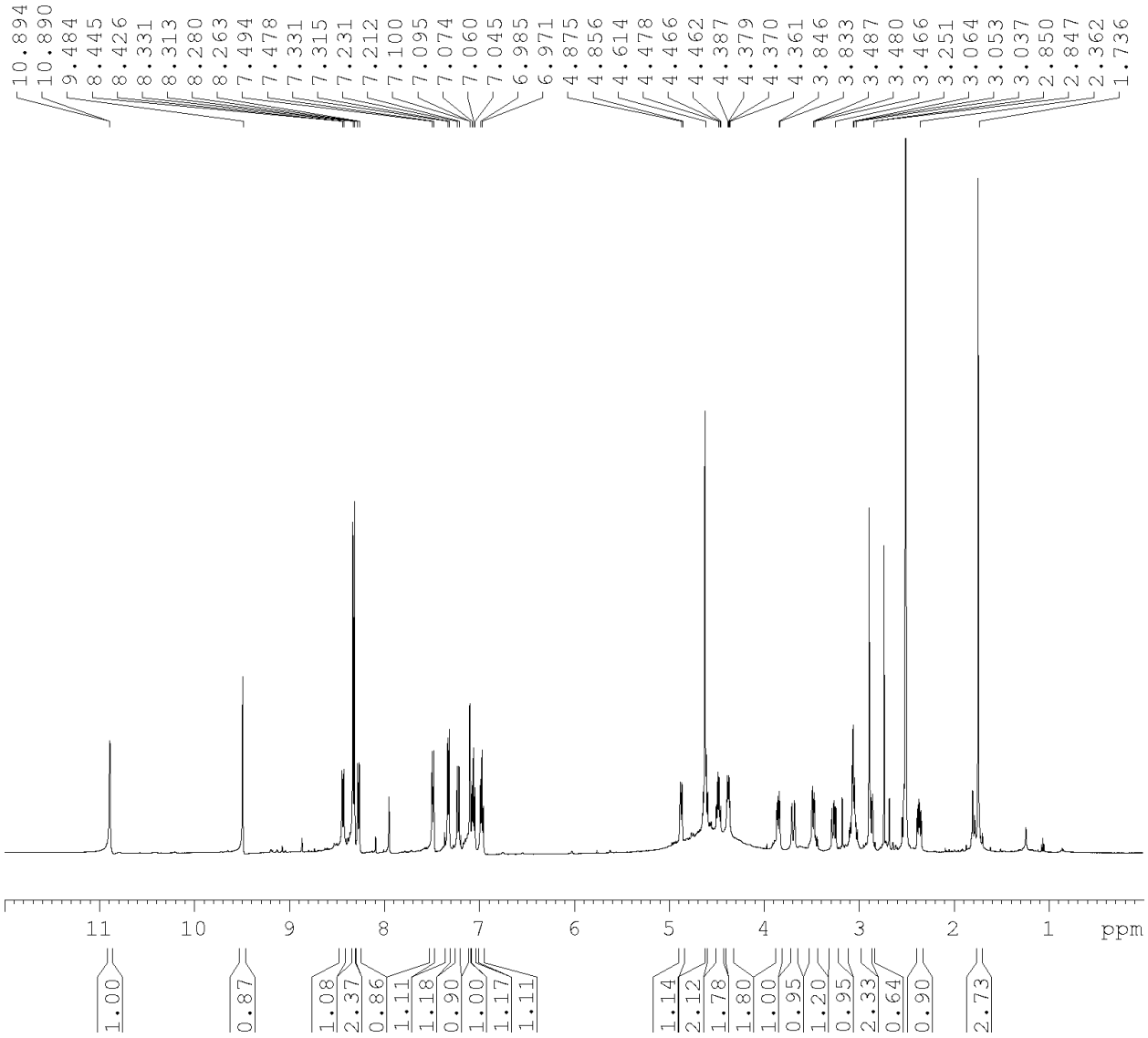

Spectrum 4.7.82 ^{13}C-NMR of Macrocycle **23** (DMSO-d_6, 126 MHz)

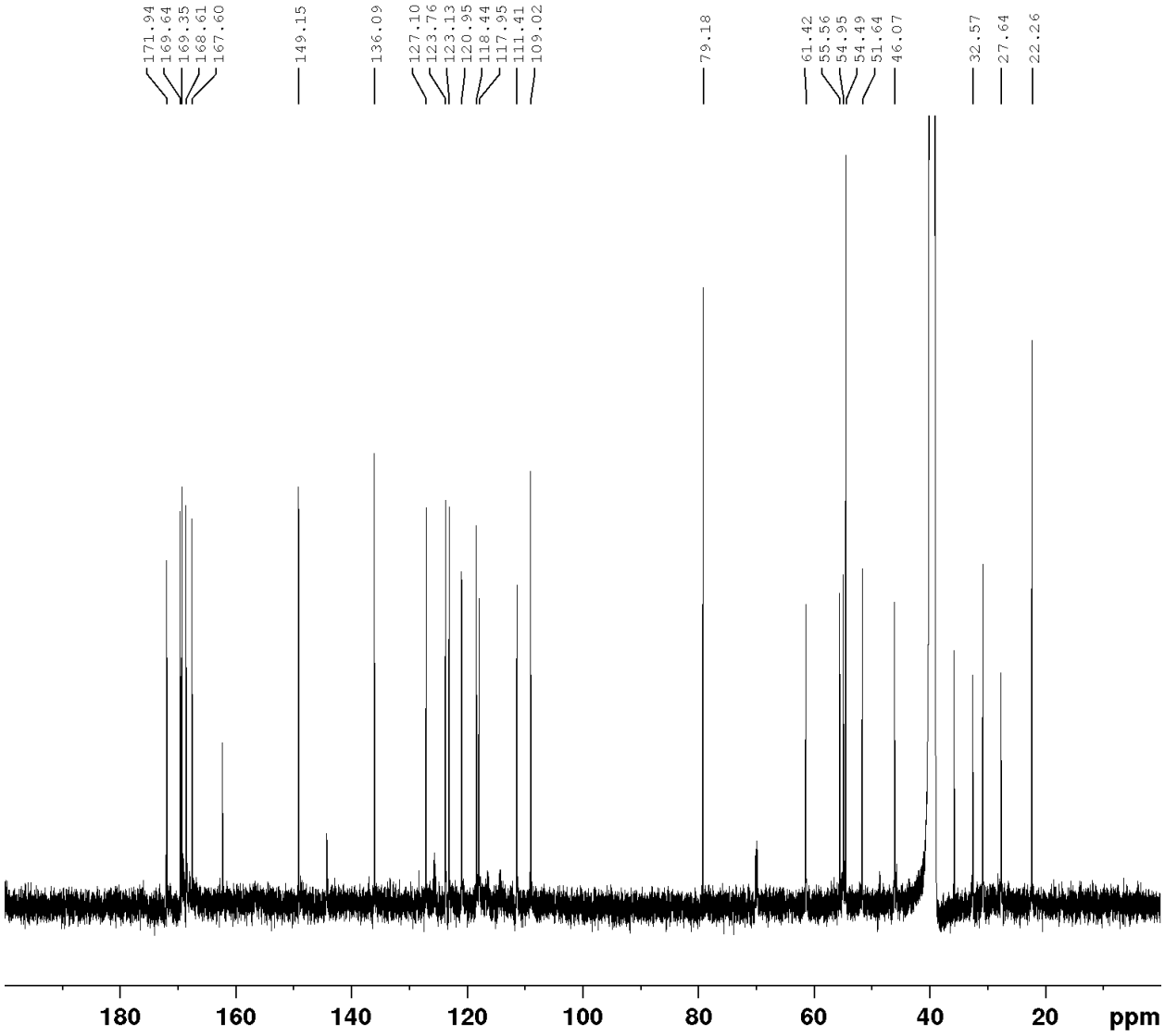

Spectrum 4.7.83 ^{19}F-NMR of Macrocycle **23** (DMSO-d_6, 282 MHz)

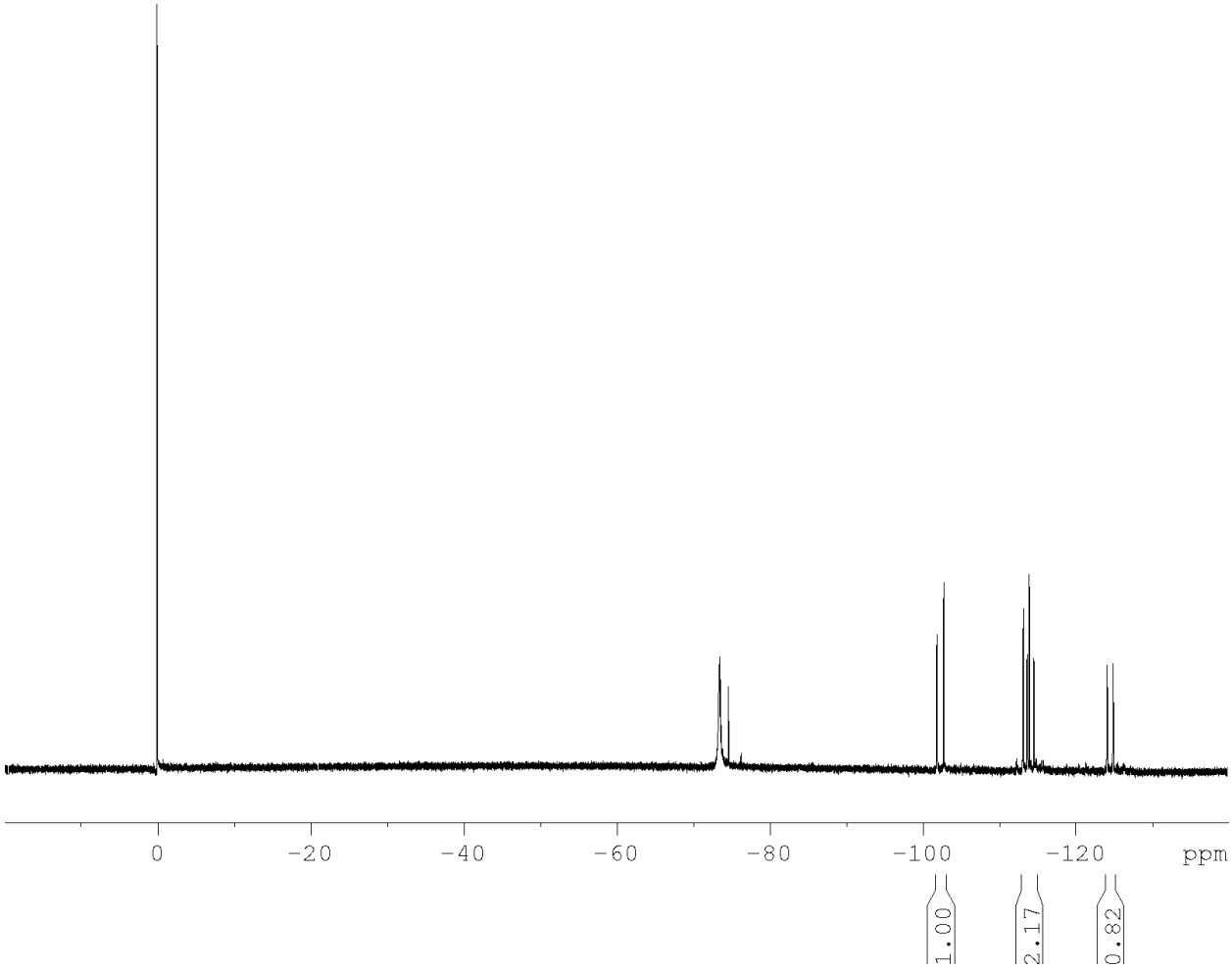

Spectrum 4.7.84 ^{1}H-NMR of Macrocycle **24** (DMSO-d_6, 500 MHz)

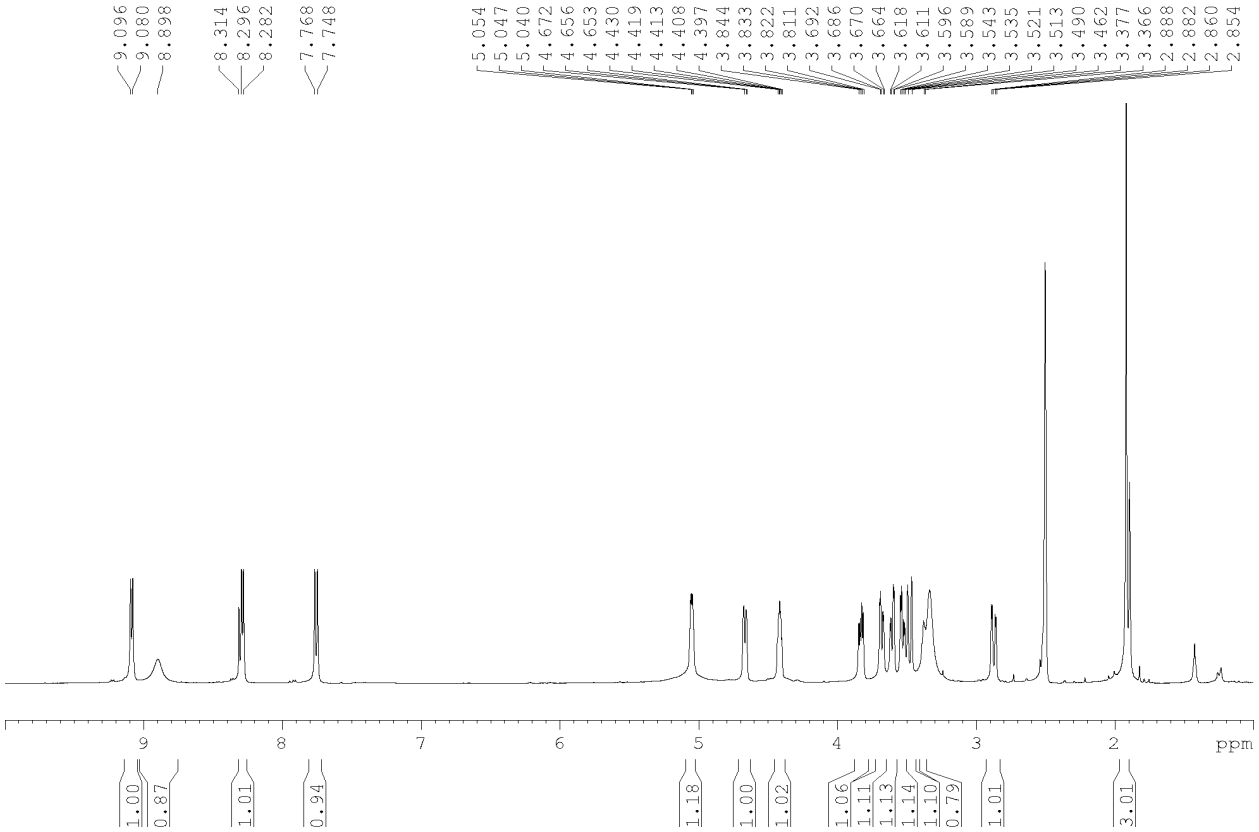

Spectrum 4.7.85 ^{13}C-NMR of Macrocycle **24** (DMSO-d_6, 126 MHz)

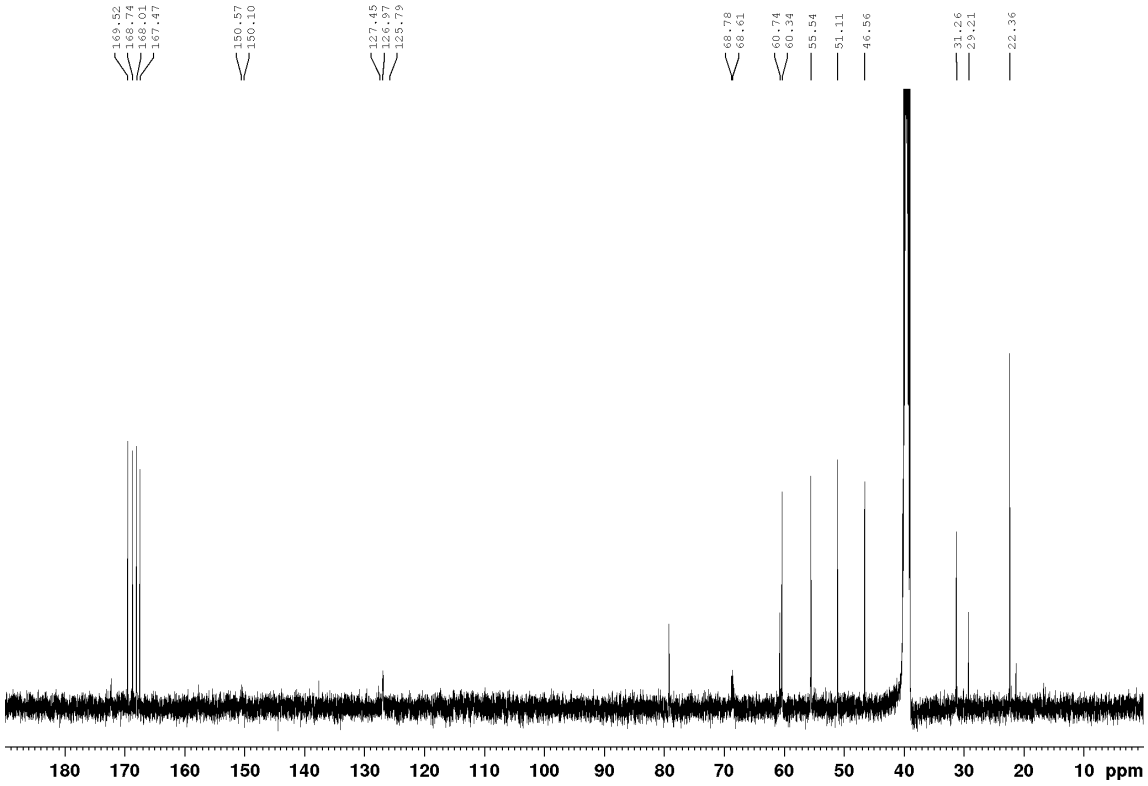

Spectrum 4.7.86 ^{19}F-NMR of Macrocycle **24** (DMSO-d_6, 282 MHz)

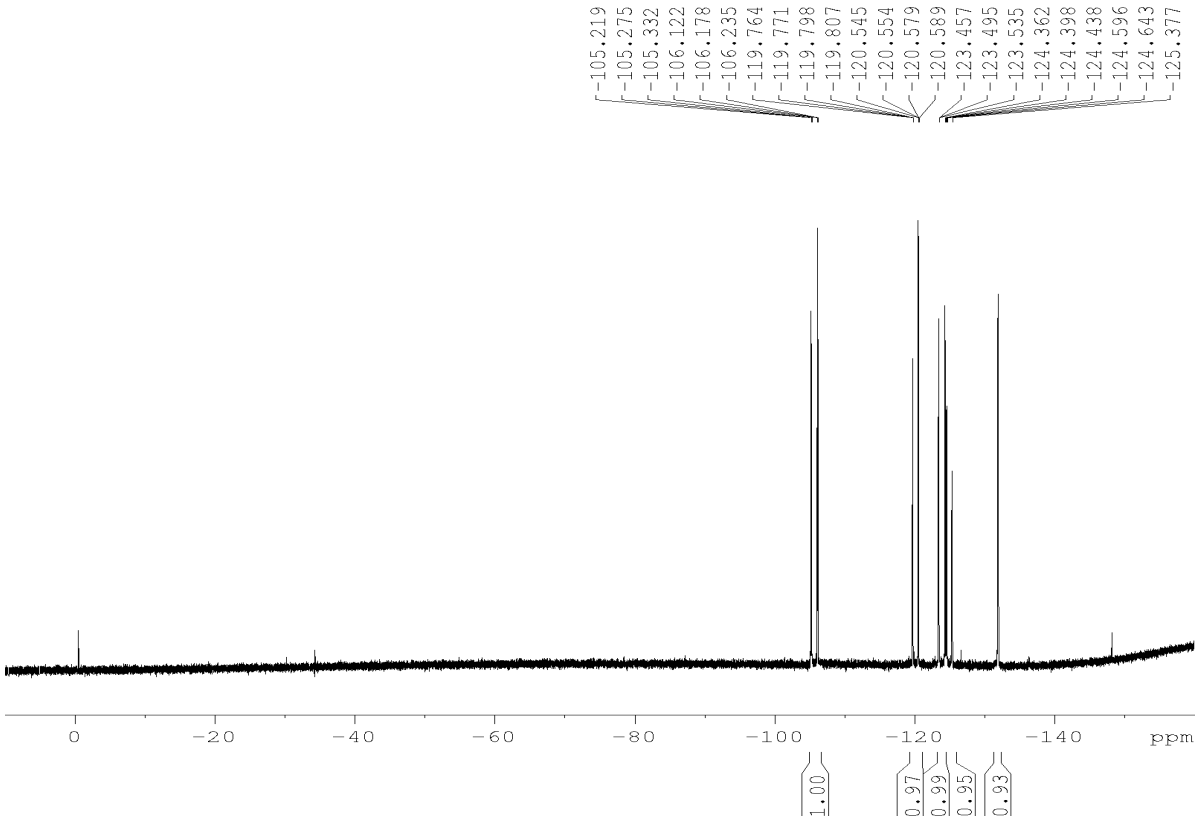

Spectrum 4.7.87 ^{1}H-NMR of Macrocycle **25** (DMSO-d_6, 500 MHz)

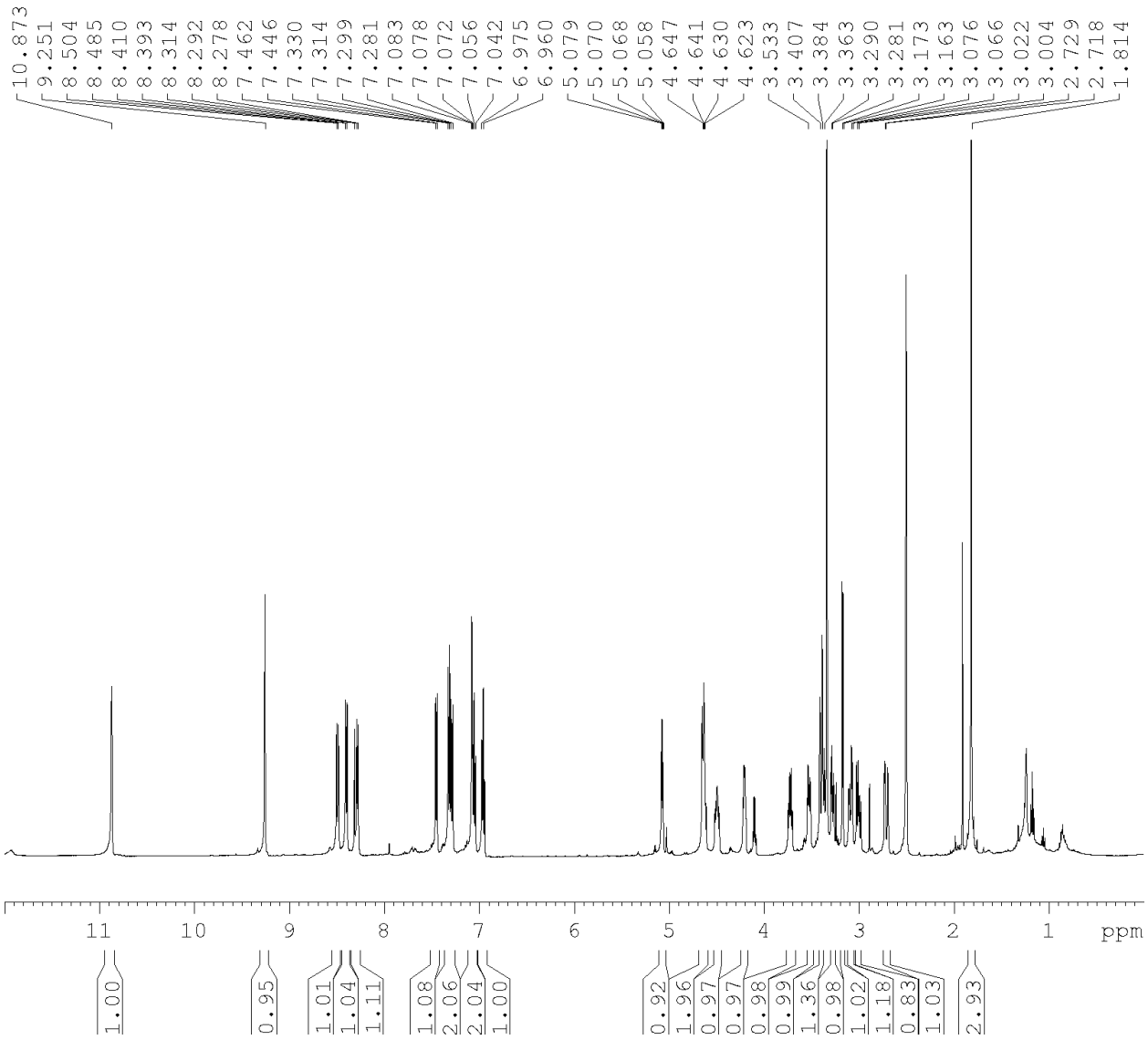

Spectrum 4.7.88 ^{19}F-NMR of Macrocycle **25** (DMSO-d_6, 282 MHz)

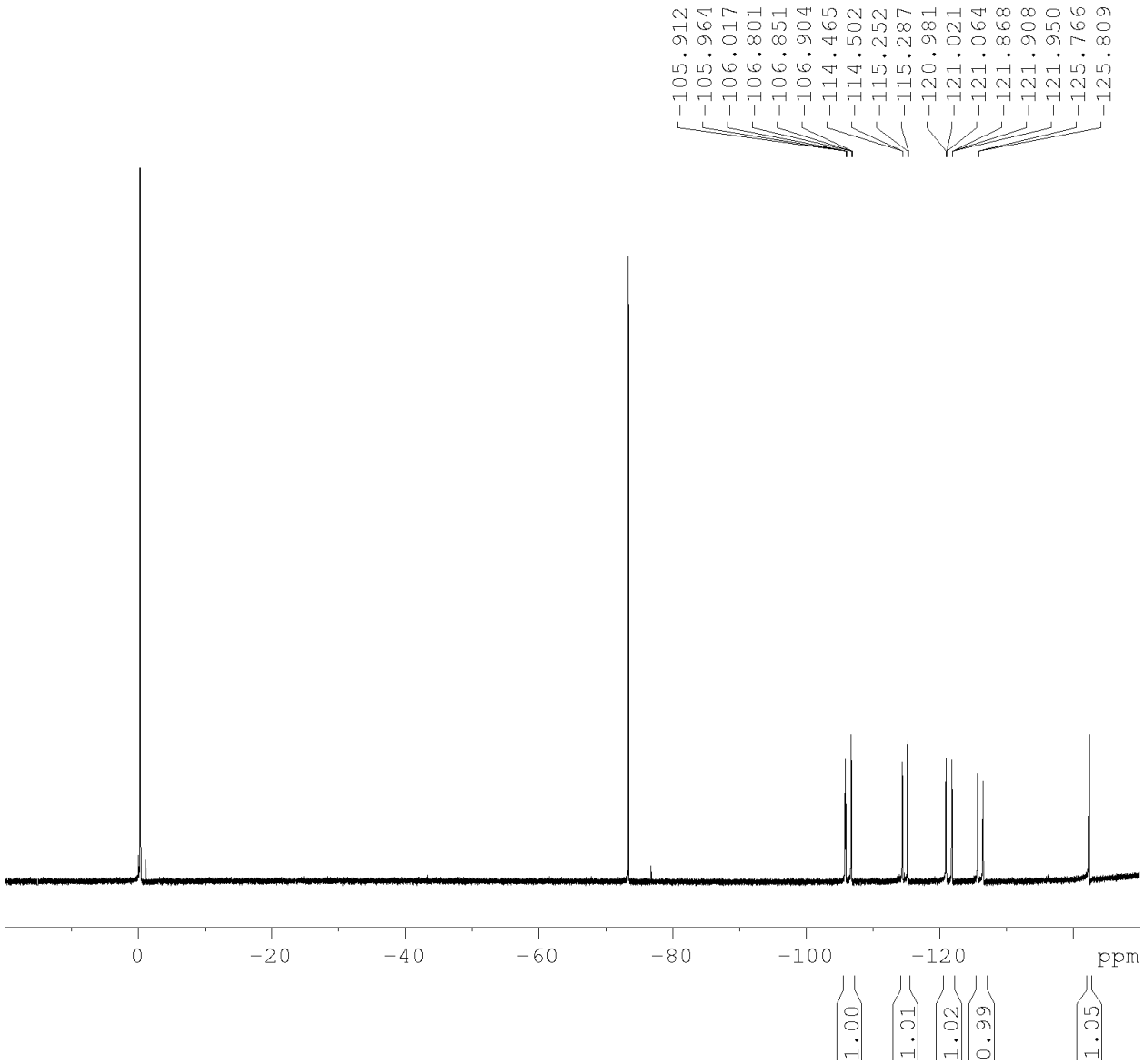

Spectrum 4.7.89 HMBC spectrum of Macrocycle **25** (DMSO-d_6)

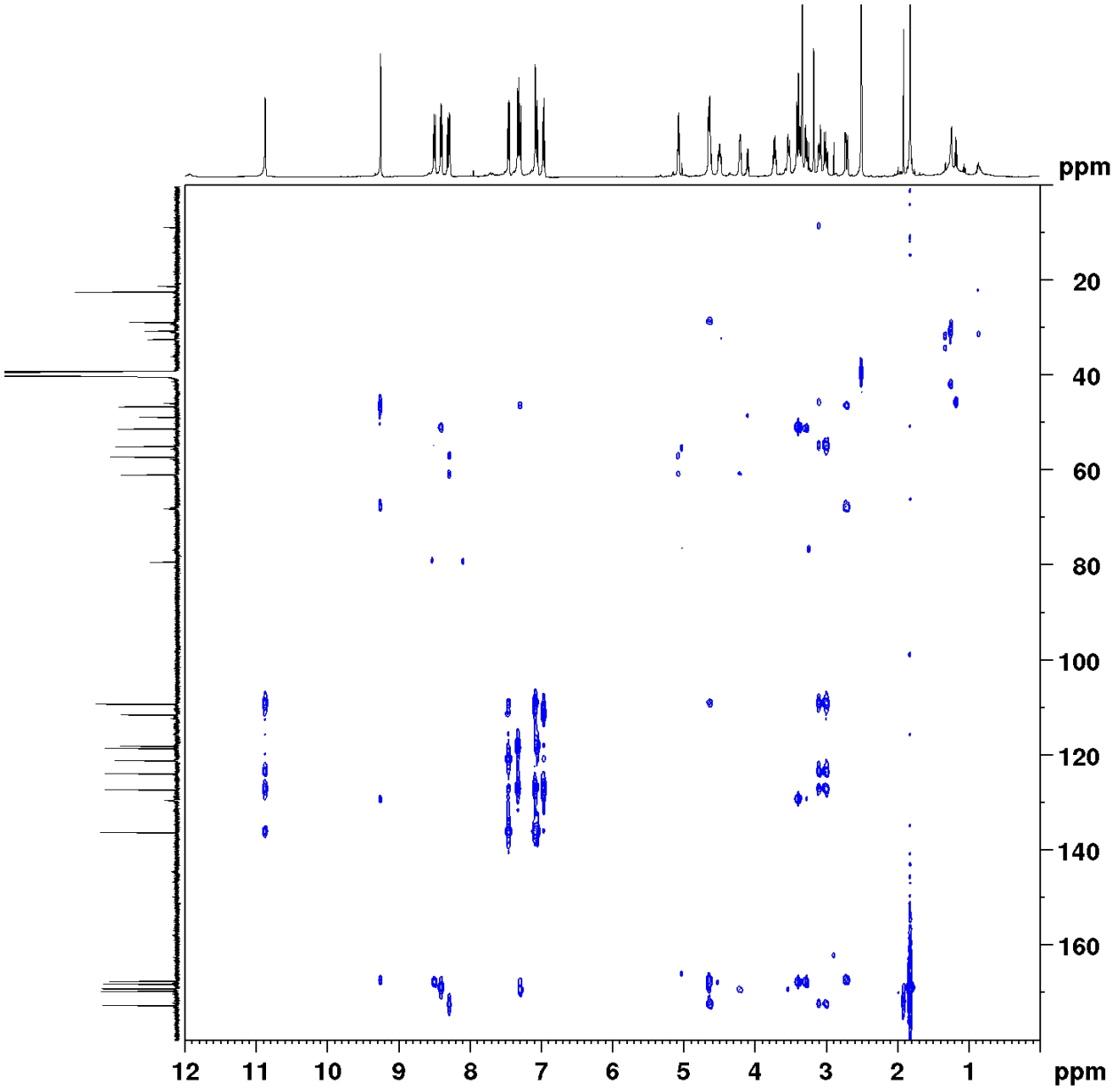

Spectrum 4.7.90 HSQC spectrum of Macrocycle **25** (DMSO-d_6)

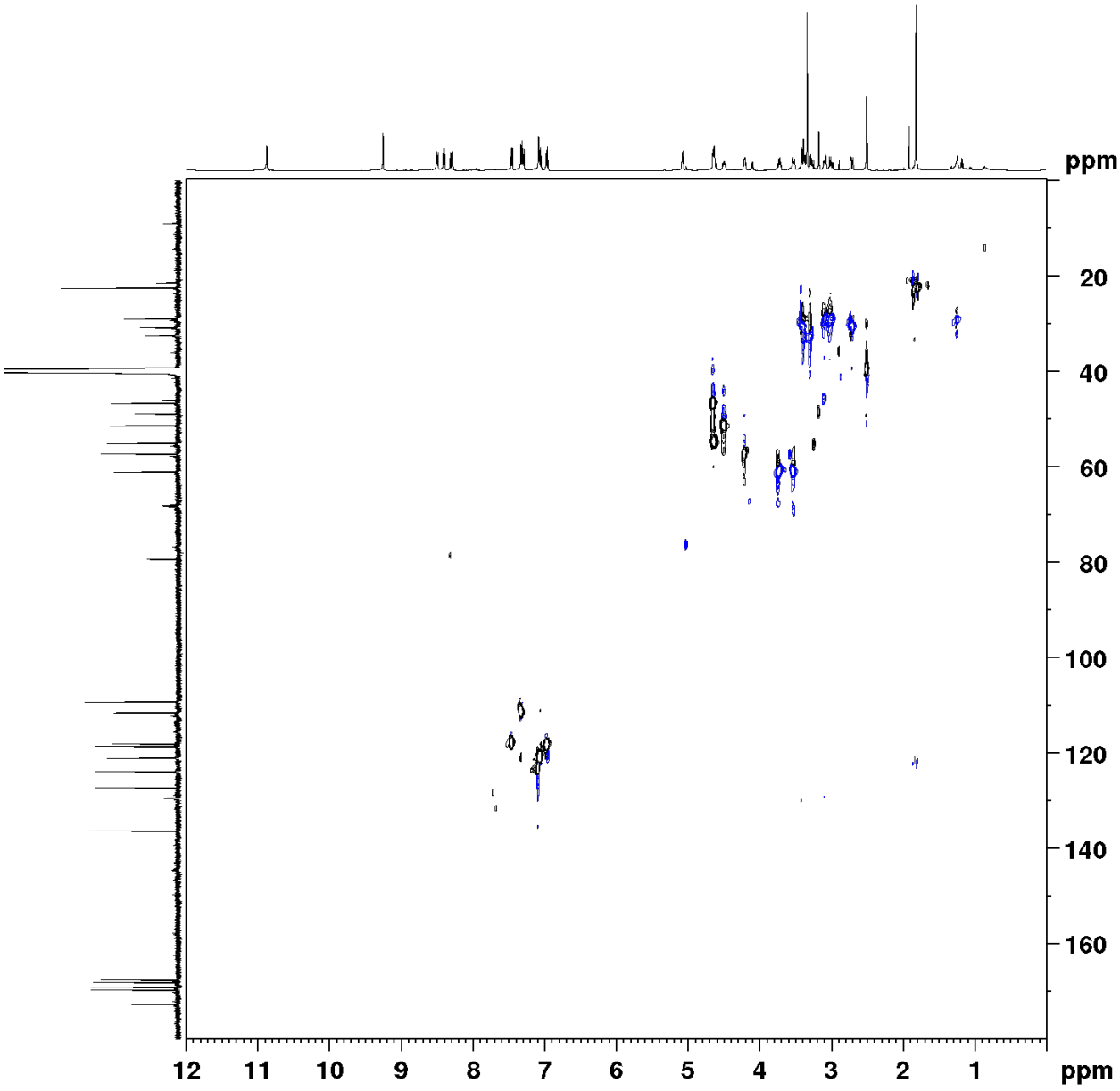

Spectrum 4.7.91 COSY spectrum of Macrocycle **25** (DMSO-d_6)

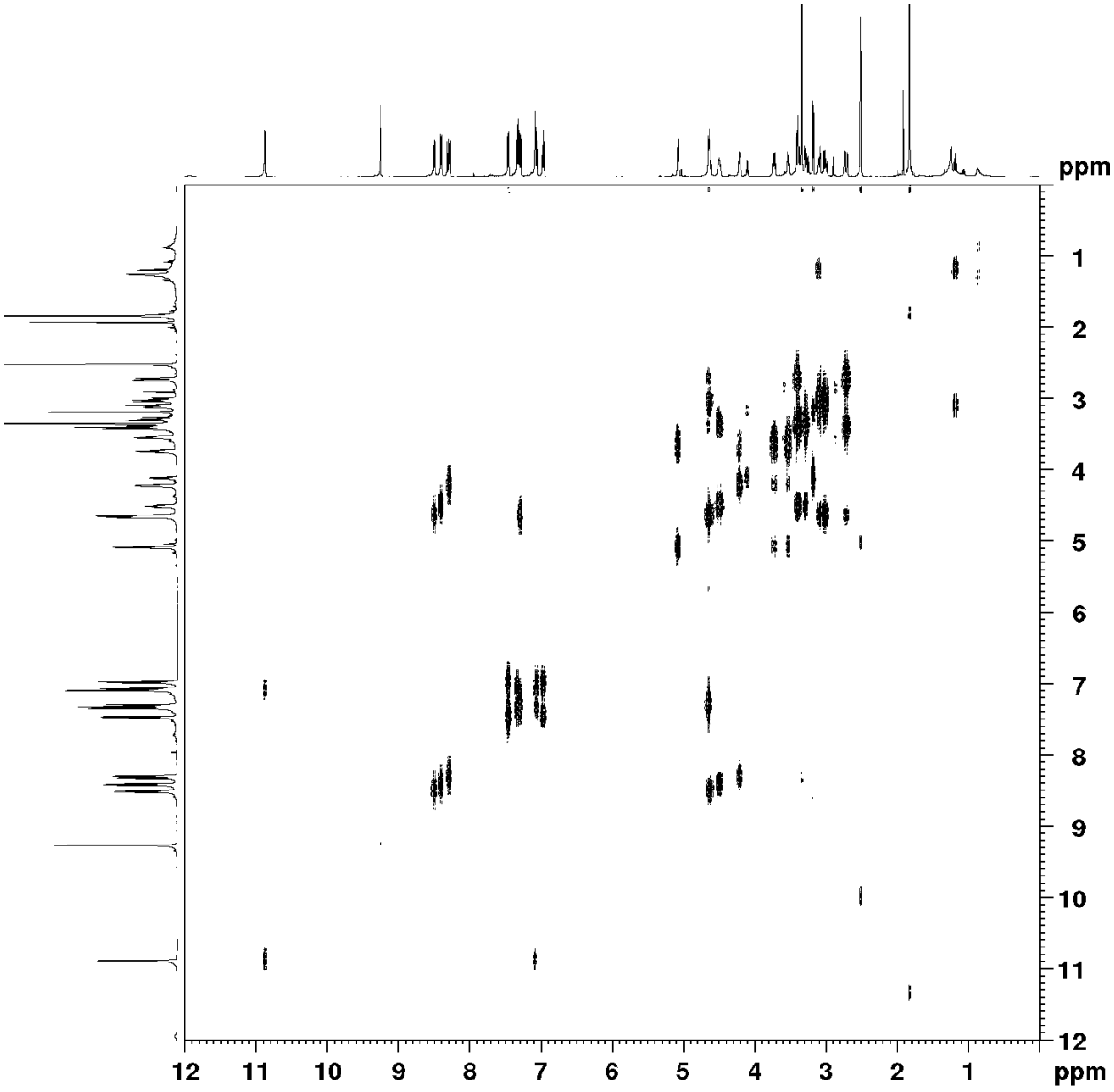

Spectrum 4.7.92 ^{1}H-NMR of Macrocycle **26** (DMSO-d_6, 500 MHz)

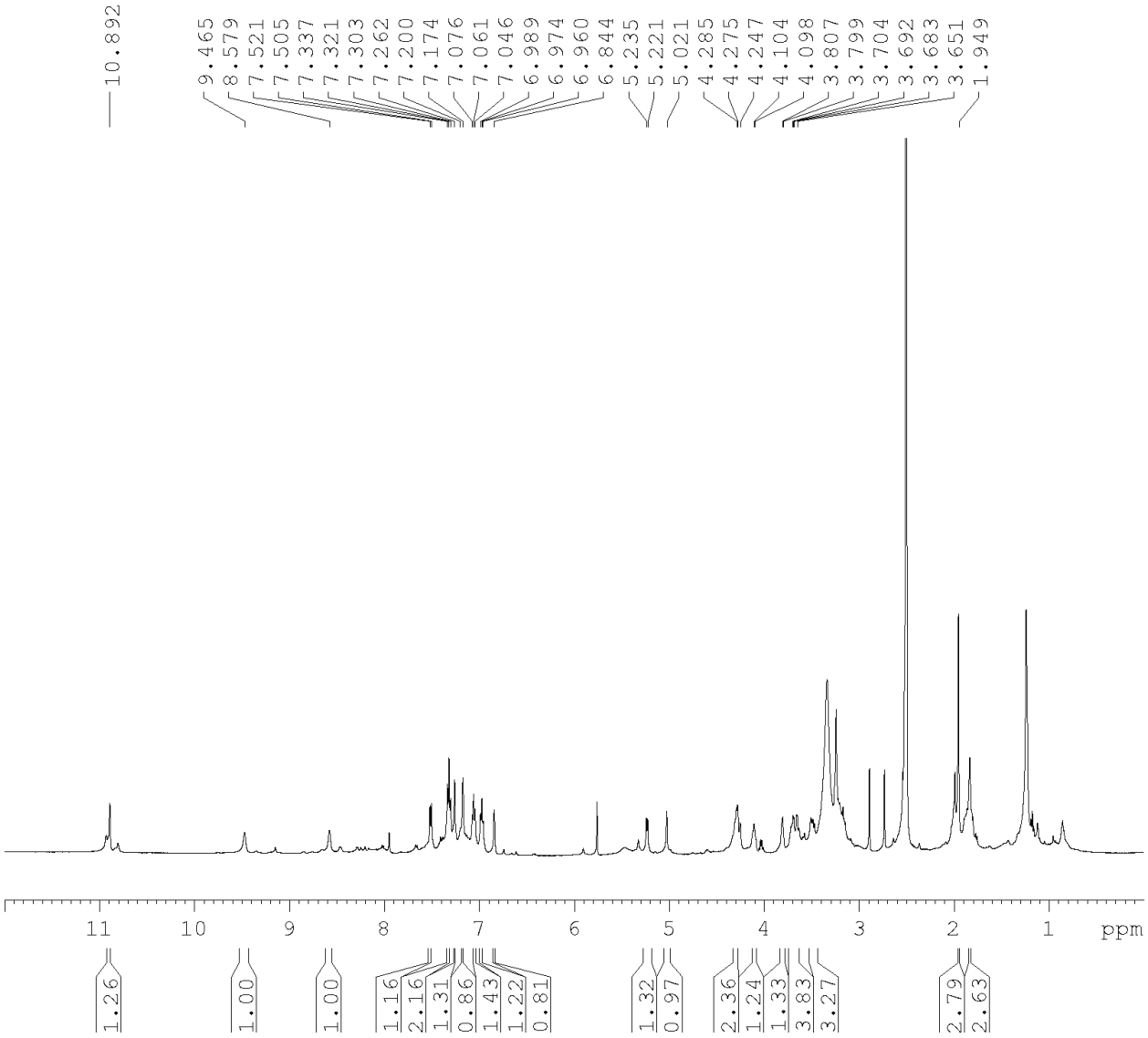

Spectrum 4.7.93 ^{19}F-NMR of Macrocycle **26** (DMSO-d_6, 282 MHz)

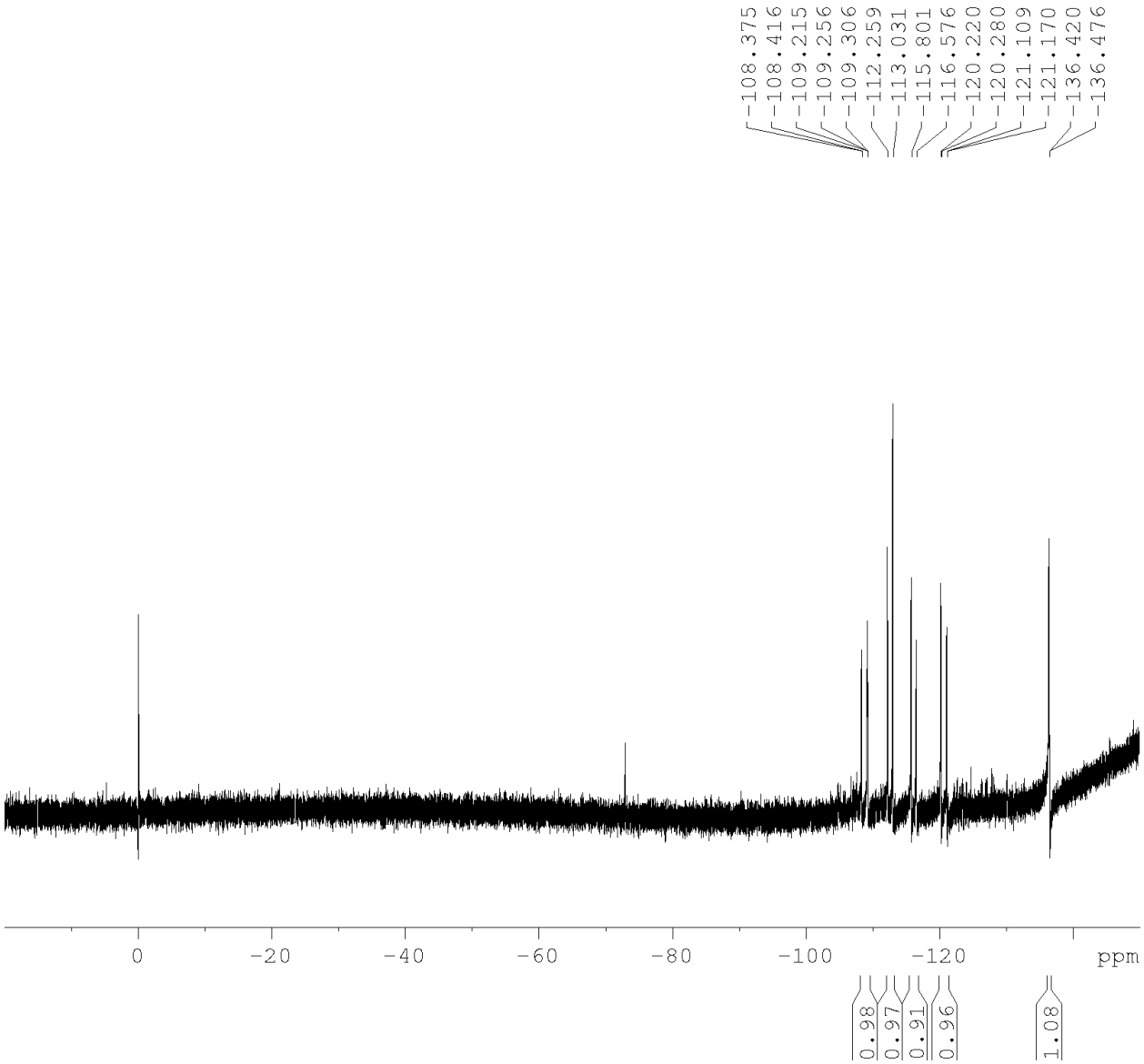

Spectrum 4.7.94 ^{1}H-NMR of Polycycle **31** (DMSO-d_6, 600 MHz)

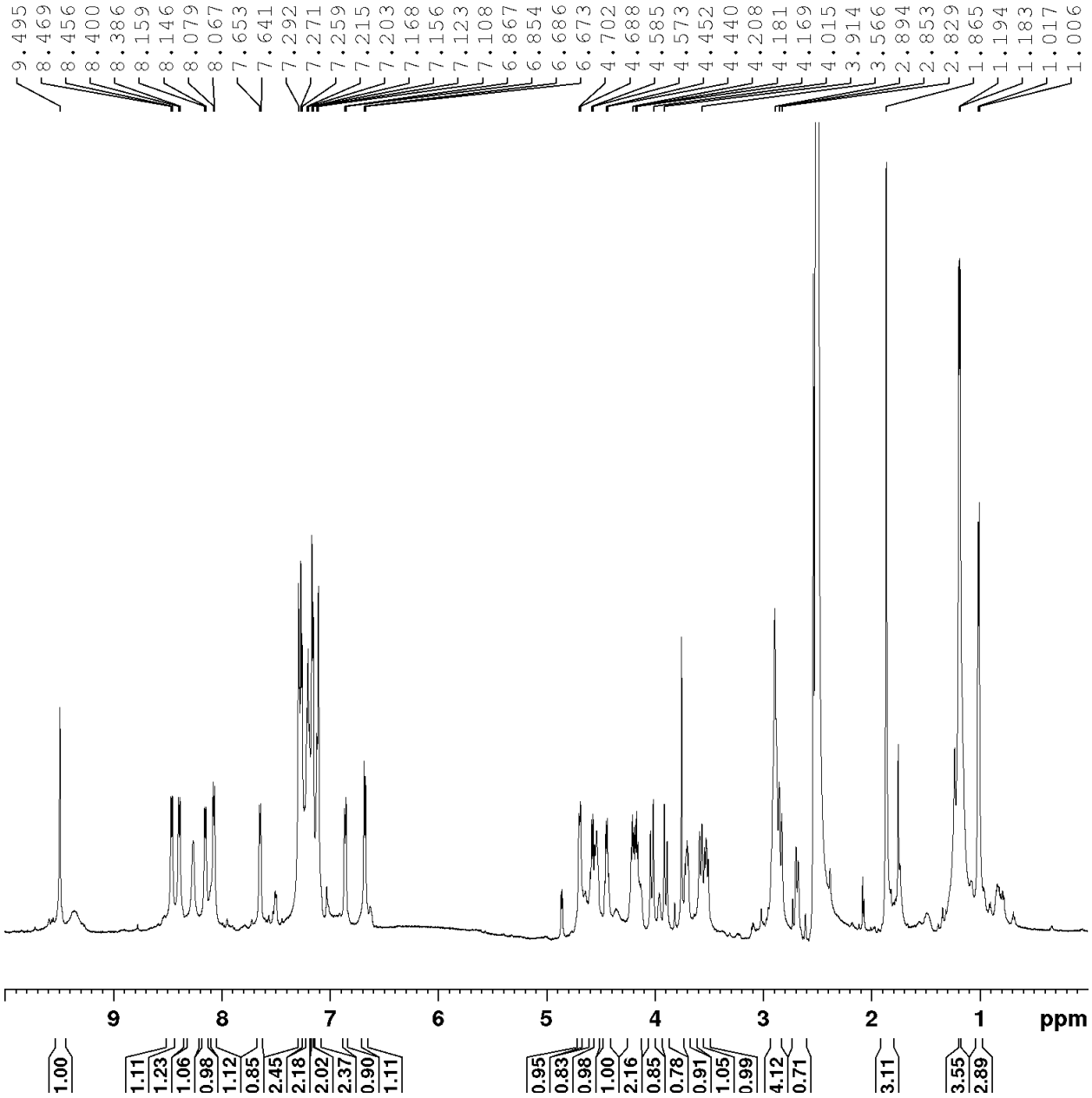

Spectrum 4.7.95 ^{13}C-NMR of Polycycle **31** (DMSO-d_6, 126 MHz)

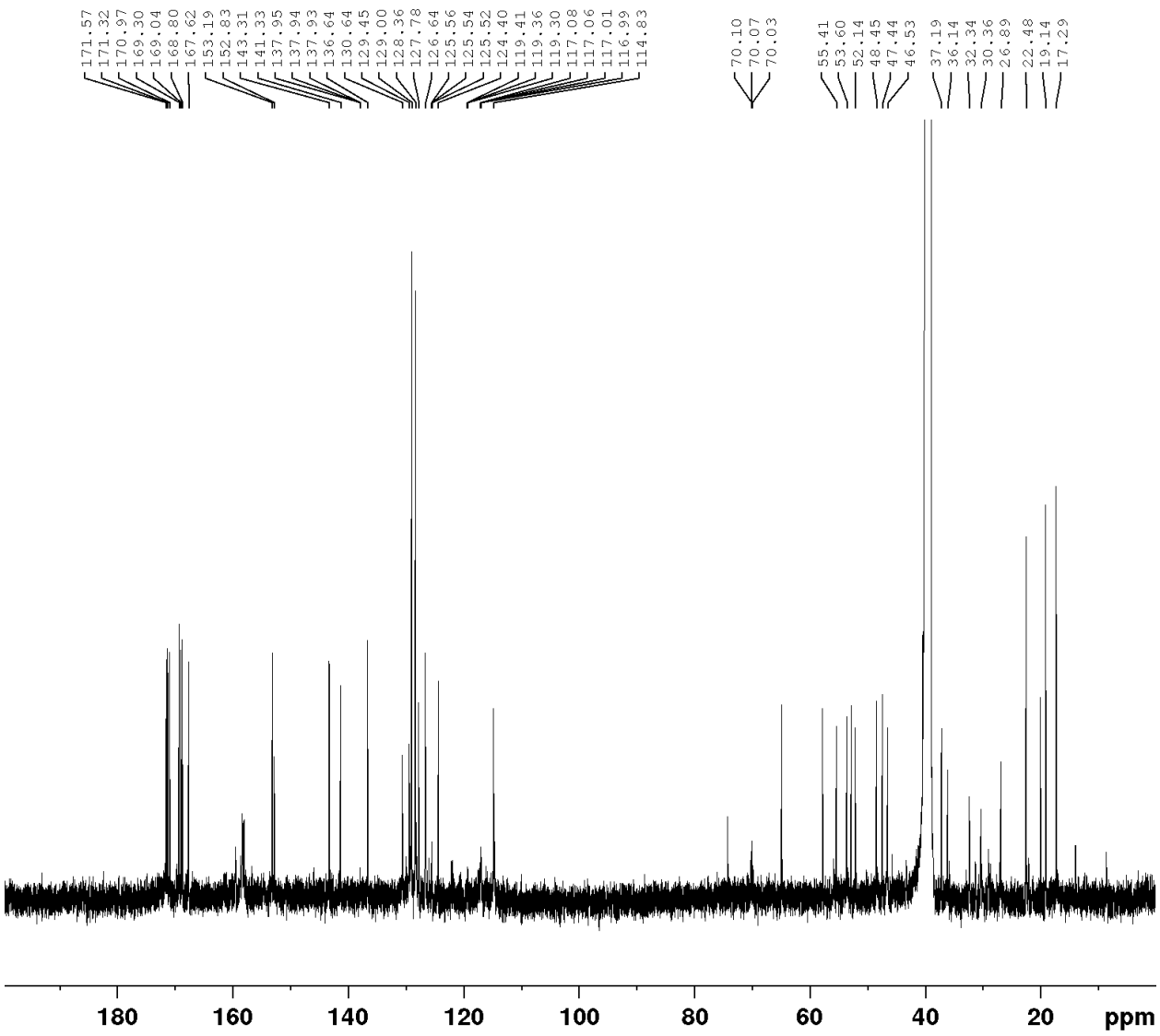

Spectrum 4.7.96 ^{19}F-NMR of Polycycle **31** (DMSO-d_6, 565 MHz)

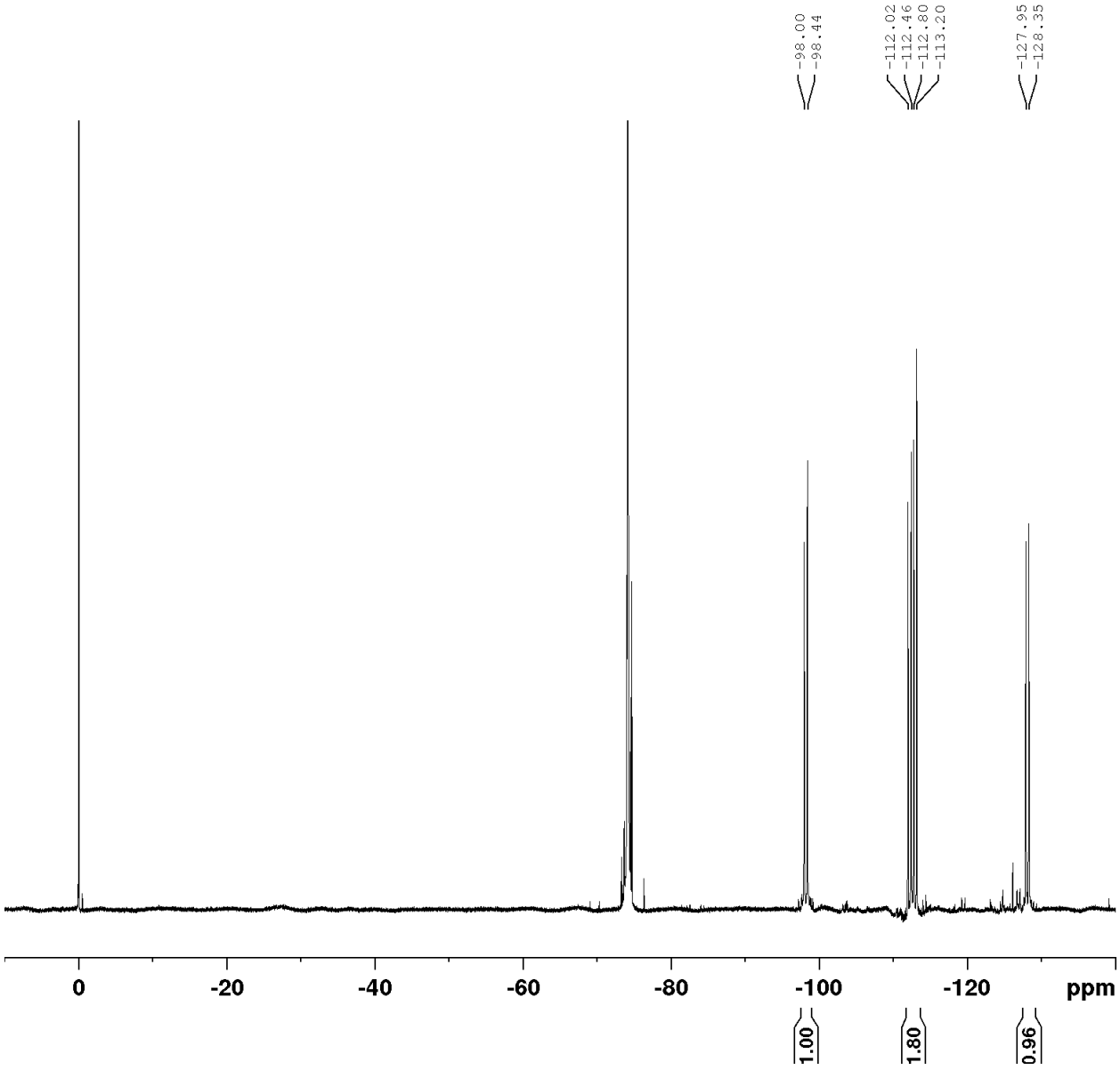

Spectrum 4.7.97 HMBC spectrum of Polycycle **31** (DMSO-d_6)

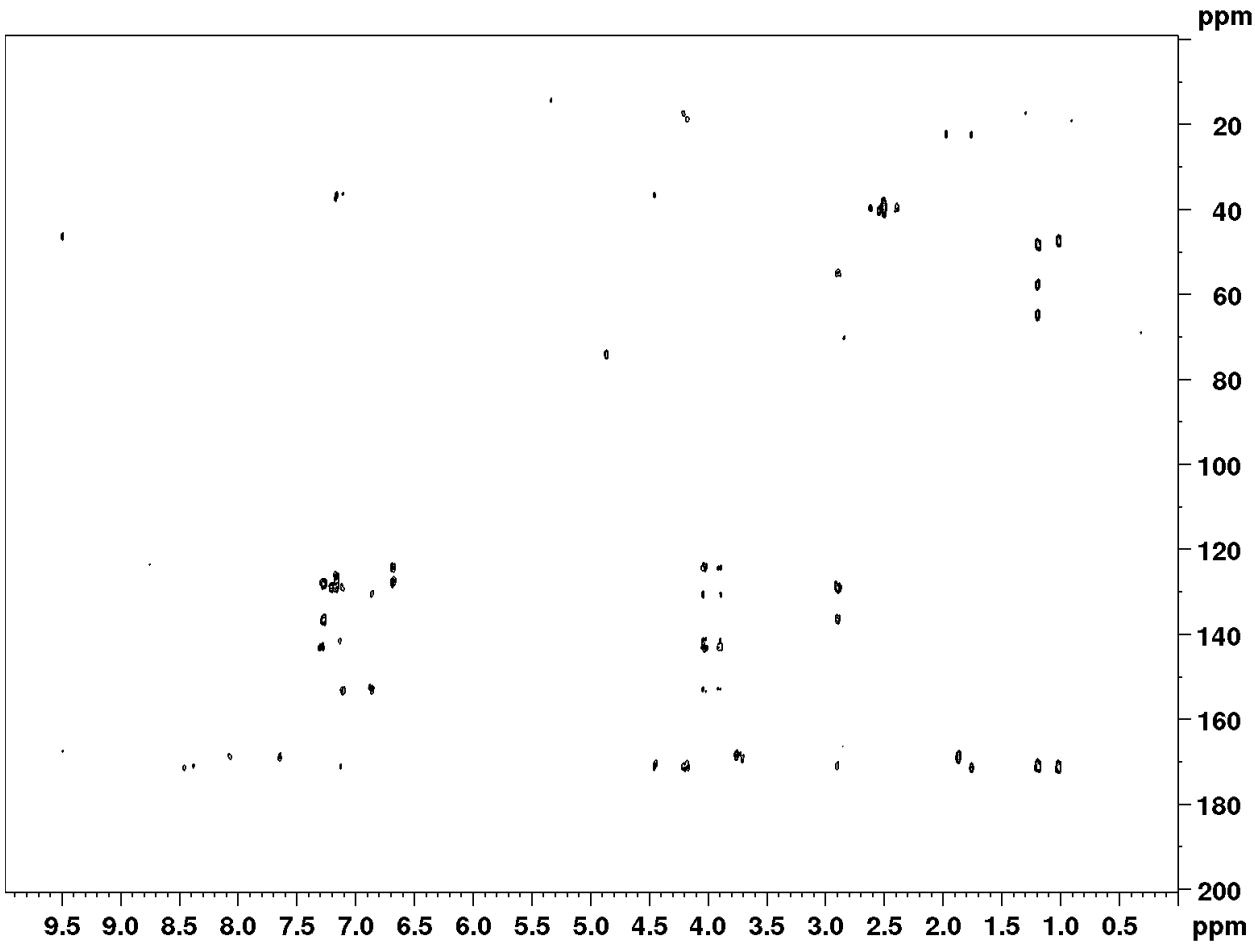

Spectrum 4.7.98 HSQC spectrum of Polycycle **31** (DMSO-d_6)

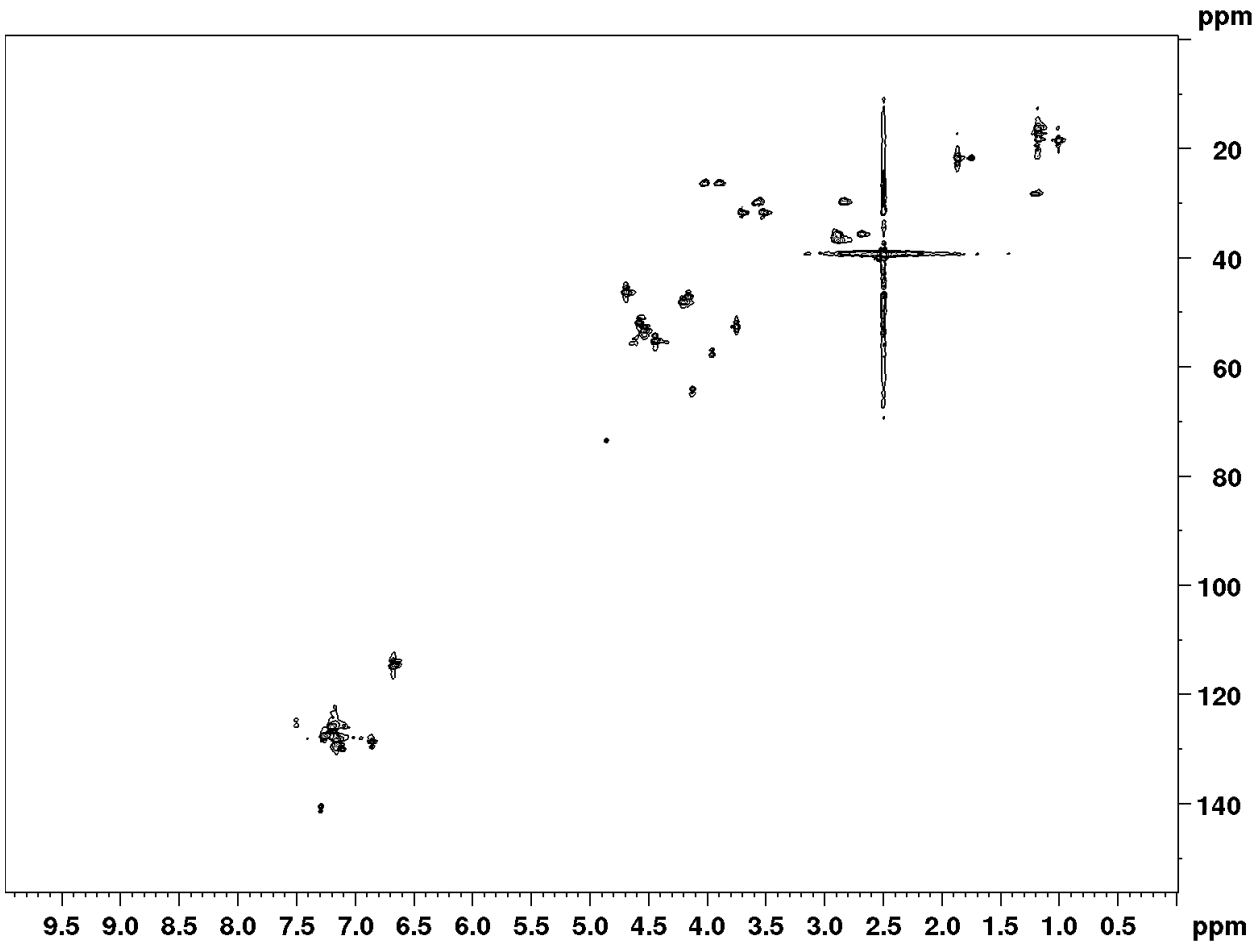

Spectrum 4.7.99 COSY spectrum of Polycycle **31** (DMSO-d_6)

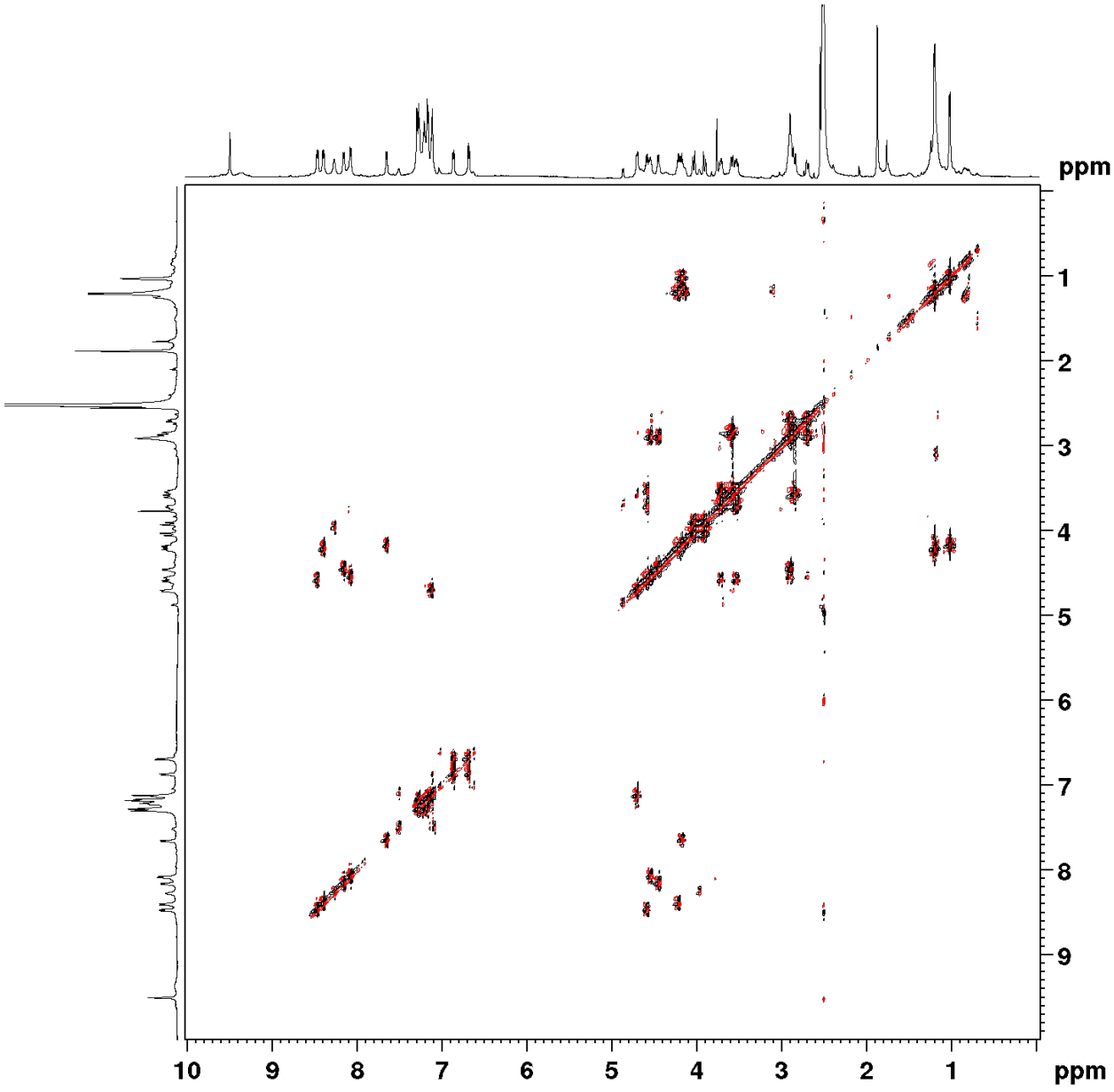

Table 4.7.17 Polycycle **31** (DMSO-d_6)

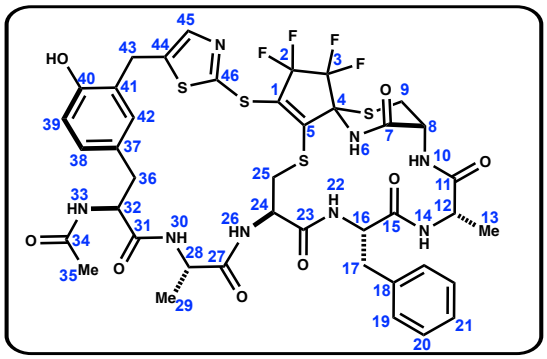

	13C	1H	Key Correlation
1	137.95-137.93 (m, 1C)	–	–
2	117.08-117.00 (m ,1C)	–	–
3	119.41-119.30 (m, 1C)	–	–
4	70.10-70.03 (m, 1C)	–	9->4 HMBC
5	125.56-125.52 (m, 1C)	–	25->5 HMBC
6	–	9.49 (s,1H)	6->7 HMBC
7	167.62	–	6->7 HMBC
8	46.53	4.70 (d, J = 8.2 Hz, 1H)	8->7 HMBC, HSQC
9	30.35	3.72-3.69 (dd, J = 12.2, 7.1 Hz, 1H) 3.53 (dd, J = 12.4, 8.1 Hz, 1H)	9->8 HMBC, HSQC
10	–	7.11 (d, 1H)	10->11 HMBC
11	171.57	–	10->11 HMBC
12	48.45	4.26-4.15 (m, 1H) overlap	12->13 HMBC, 12->13 COSY, HSQC
13	17.29	1.18 (d, J = 6.6 Hz, 3H)	12->13 HMBC, 12->13 COSY, HSQC
14	–	8.46 (d, J = 7.5 Hz, 1H)	14->12 HMBC
15	171.32	–	14->15 HMBC
16	53.59	4.56-4.50 (m, 1H)	16->15 HMBC, HSQC
17	37.19	2.95-2.85 (m, 2H) overlap	16->17 HMBC, HSQC
18	136.64	–	17->18 HMBC
19	129.00	7.15 (m, 2H)	19->20 HMBC, HSQC
20	128.35	7.20 (m, 2H)	20->19 HMBC, HSQC
21	126.64	7.30-7.25 (m, 1H)	20->21 HMBC, HSQC
22	–	8.39 (d, J = 8.3 Hz, 1H)	16->22 HMBC
23	168.70	–	22->23, 24->23 HMBC
24	52.14	4.44 (dd, J = 14.1, 7.2 Hz, 1H)	24->23 HMBC
25	32.34	3.57 (d, J = 13.1 Hz, 1H), 2.72–2.61 (m, 1H)	24->25, 25->27 HMBC, HSQC
26	–	8.07 (d, J = 7.5 Hz, 1H)	26->24 HMBC
27	168.80	–	26->27 HMBC
28	47.44	4.19 (m, 1H) overlap	29->28 HMBC, HSQC
29	19.14	1.00 (d, J = 6.5 Hz, 3H)	28->29 HMBC, HSQC
30	–	8.15 (d, J = 7.7 Hz, 1H)	30->28 HMBC
31	169.30	–	30->31 HMBC
32	55.41	4.61-4.56 (m, 1H) overlap	33->32 HMBC, HSQC
33	–	7.65 (d, J = 8.0 Hz, 1H)	34->33 HMBC
34	169.04	–	35-> 34 HMBC
35	22.48	1.86 (s, 3H)	HSQC
36	36.14	2.97-2.83 (m, 2H) overlap	32->36 HMBC, HSQC
37	130.63	–	36->37 HMBC
38	129.45	6.86 (d, J = 7.3 Hz, 1H)	38->37, 39->38 HMBC
39	114.83	6.68 (d, J = 7.9 Hz, 1H)	38->39 HMBC
40	127.78	–	39->40 HMBC
41	124.40	–	43->41 HMBC
42	129.45	7.16 (d, 1H)	42->41 HMBC
43	26.88	4.03 (d, J = 15.6 Hz, 1H), 3.90 (d, J = 15.6 Hz, 1H)	43->44, 43->41 HMBC
44	143.31	–	45->44 HMBC
45	141.33	7.29 (s, 1H)	45->44 HMBC
46	153.19	–	45->46 HMBC

Spectrum 4.7.100 ^{1}H-NMR of Polycycle **32** (DMSO-d_6, 600 MHz)

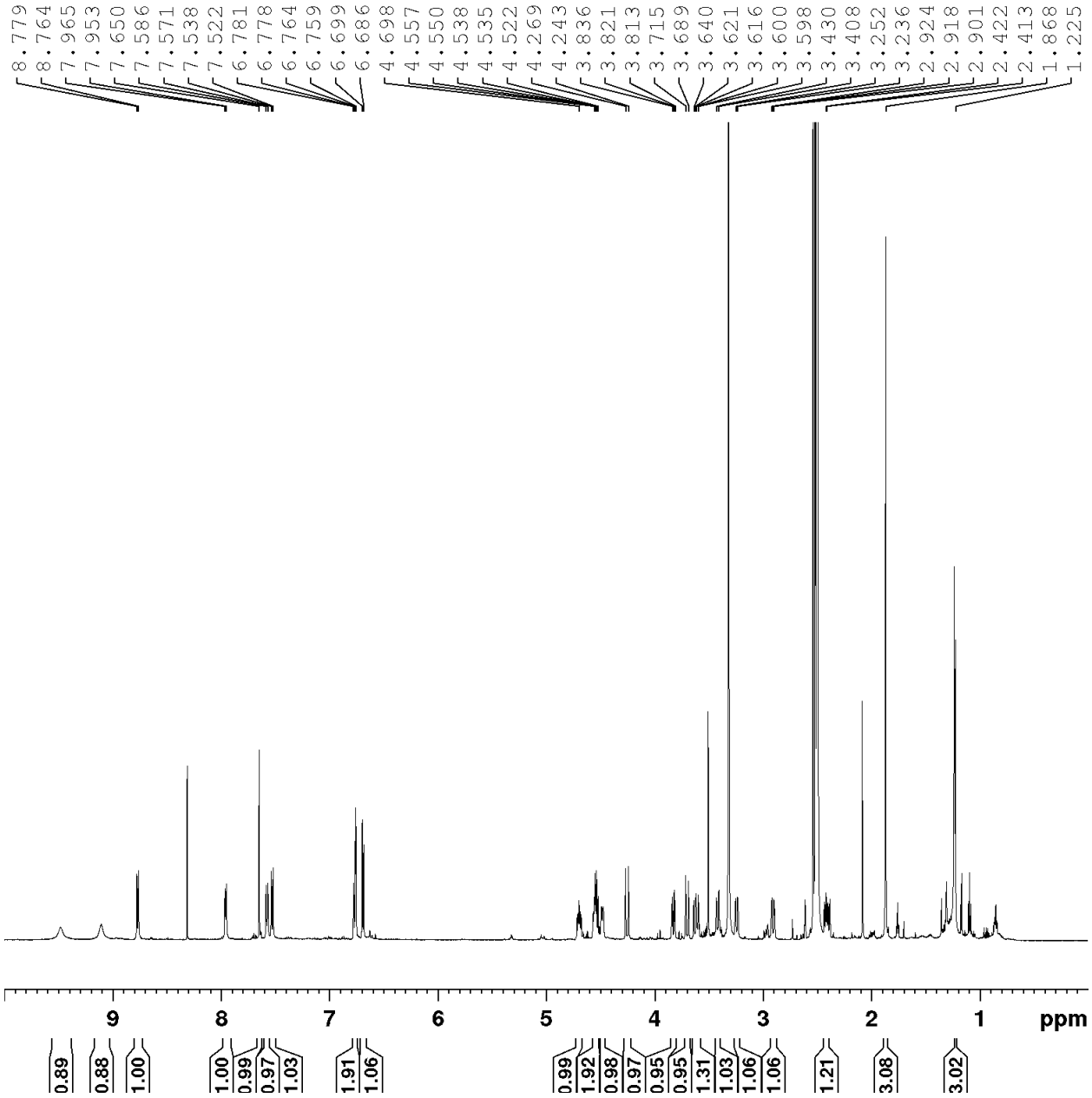

Spectrum 4.7.101 ^{13}C-NMR of Polycycle **32** (DMSO-d_6, 126 MHz)

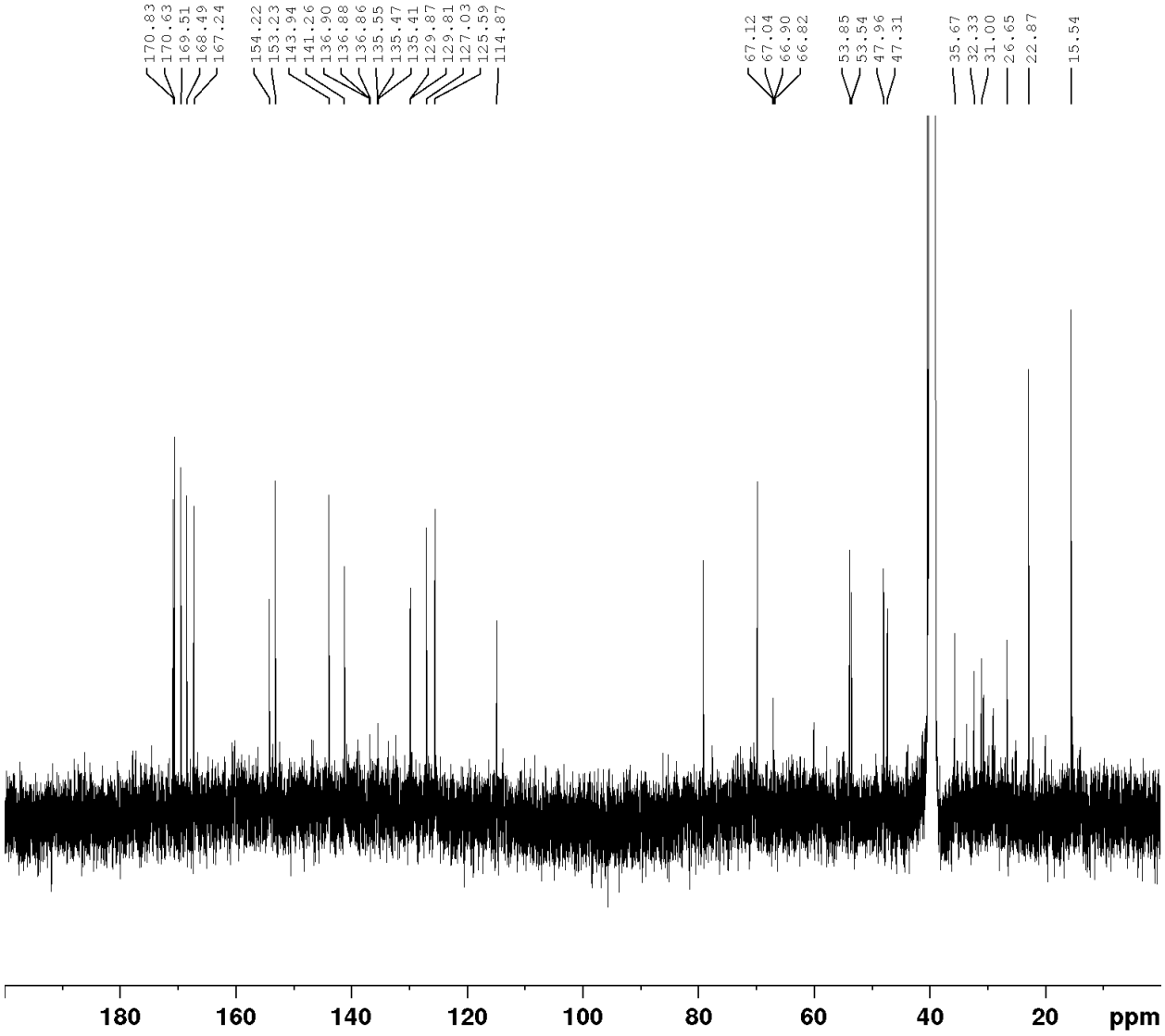

Spectrum 4.7.102 ^{19}F-NMR of Polycycle **32** (DMSO-d_6, 565 MHz)

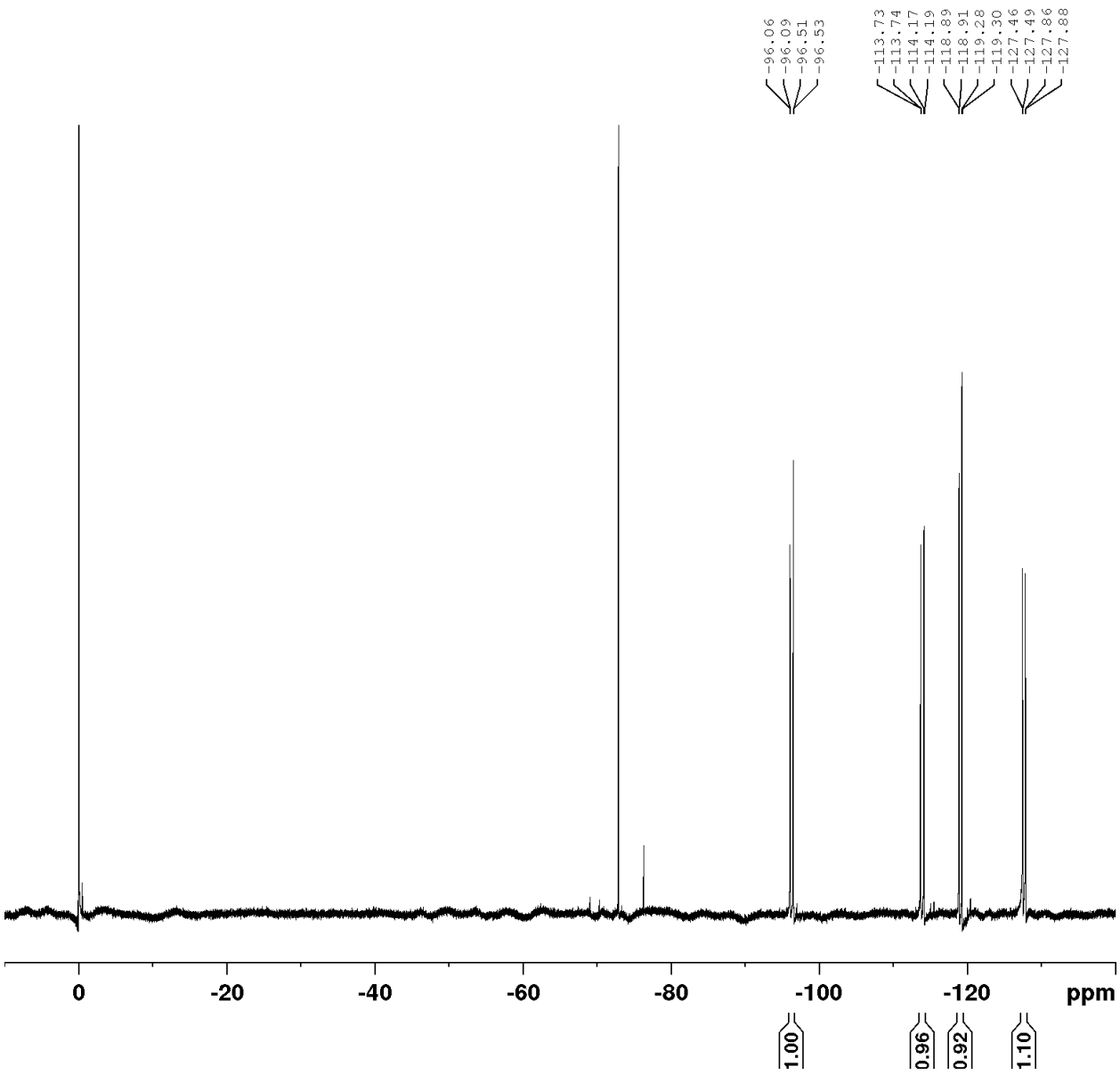

Spectrum 4.7.103 HMBC spectrum of Polycycle **32** (DMSO-d_6)

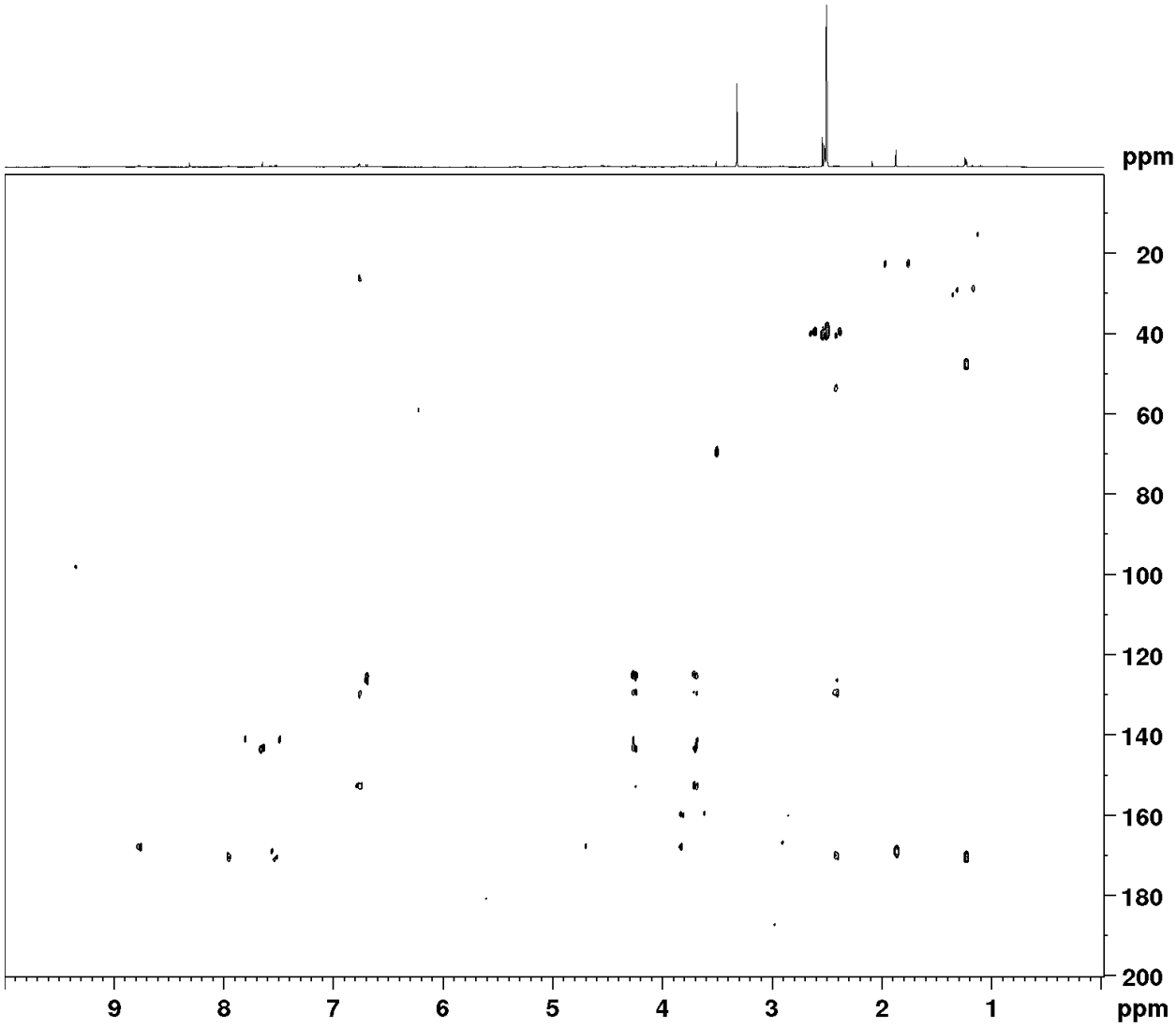

Spectrum 4.7.104 HSQC spectrum of Polycycle **32** (DMSO-d_6)

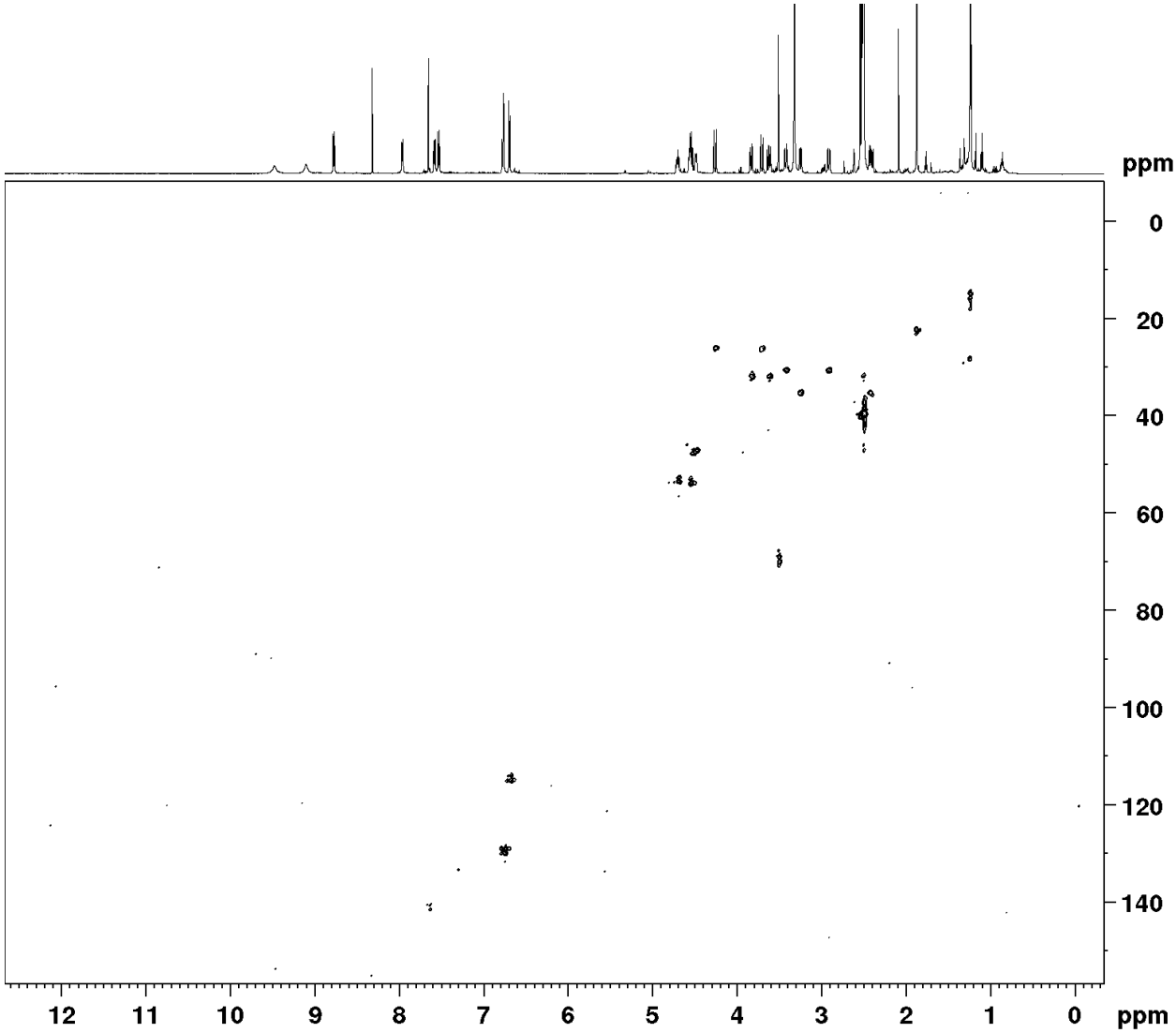

Spectrum 4.7.105 COSY spectrum of Polycycle **32** (DMSO-d_6)

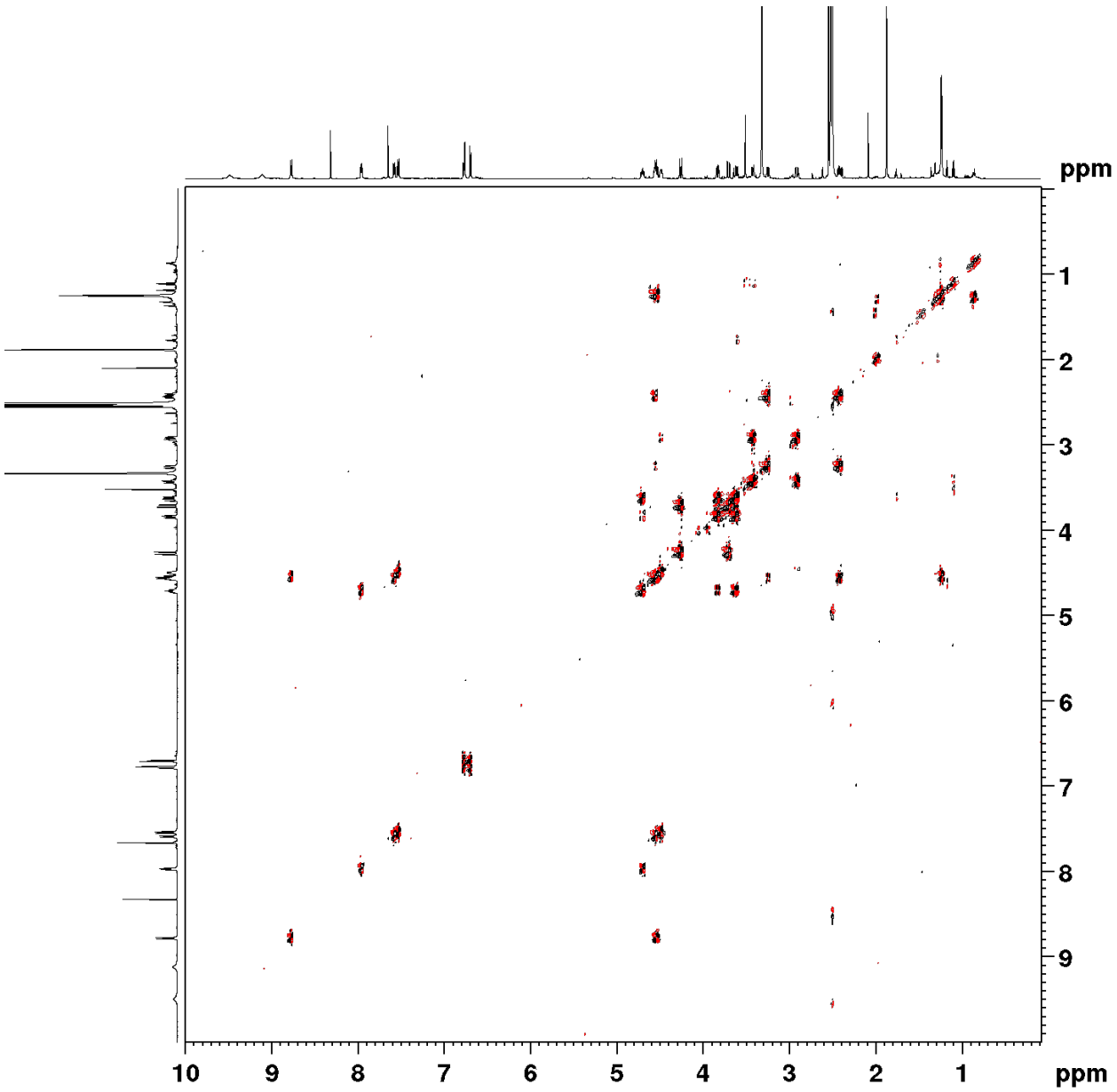

Table 4.7.18 Polycycle **32** (DMSO-d_6, 298K)

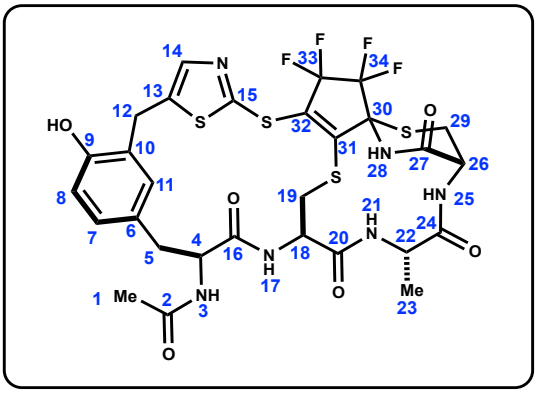

	13C	1H	Key Correlation
1	22.87	1.87 (s, 3H)	HMBC, HSQC
2	169.51	-	1->2 HMBC
3	-	7.58 (d, 1H)	2->3 HMBC
4	53.86	4.55 (m, 1H) overlap	3->4 COSY, HSQC
5	35.67	3.24 (dd, J = 13.1, 3.2 Hz, 1H), 2.42 (dd, J = 13.1, 7.9 Hz, 1H)	HSQC
6	125.59	-	5->4 HMBC
7	127.03	6.76 (m, 1H) overlap	8->7 HMBC
8	114.9	6.69 (d, J = 8.0 Hz, 1H)	HSQC
9	153.22	-	8->7 HMBC
10	129.82	-	12->10 HMBC
11	129.89	6.76 (m, 1H) overlap	10->11 HMBC, HSQC
12	26.65	4.26 (d, J = 15.6 Hz, 1H), 3.70 (d, J = 15.5 Hz, 1H)	13->12 HMBC, HSQC
13	143.94	-	13->12 HMBC, HSQC
14	141.26	7.65 (s, 1H)	HSQC
15	154.22	-	-
16	170.83	-	17->16 HMBC
17	-	7.96 (d, J = 7.3 Hz, 1H)	18->17 COSY
18	53.54	4.70 (m, 1H)	20->18 HMBC, HSQC
19	32.33	3.83 (dd, J = 14.0, 4.8 Hz, 1H), 3.62 (m, 1H)	18->19 COSY, HSQC
20	168.49	-	21->20 HMBC
21	-	8.77 (d, J = 9.2 Hz, 1H)	22->21 COSY
22	47.96	4.54 (m, 1H) overlap	23->22 COSY, HSQC
23	15.54	1.23 (d, J = 5.3 Hz, 1 H)	HSQC
24	170.63	-	22->24 HMBC
25	-	7.53 (d, J = 9.6 Hz, 1H)	
26	47.31	4.49 (m, 1H)	25->26 COSY, HSQC
27	167.24	-	26->27 HMBC
28	-	9.11 or 9.48	-
29	31.00	3.41 (m, 1H), 2.91 (m, 1H)	26->29 HMBC, HSQC
30	66.98 (m, 1C)	-	-
31	135.47 (m, 1C)	-	-
32	136.88 (m, 1C)	-	-
33	-	-	-
34	-	-	-

Spectrum 4.7.106 ^{1}H-NMR of Polycycle **35** (DMSO-d_6, 500 MHz)

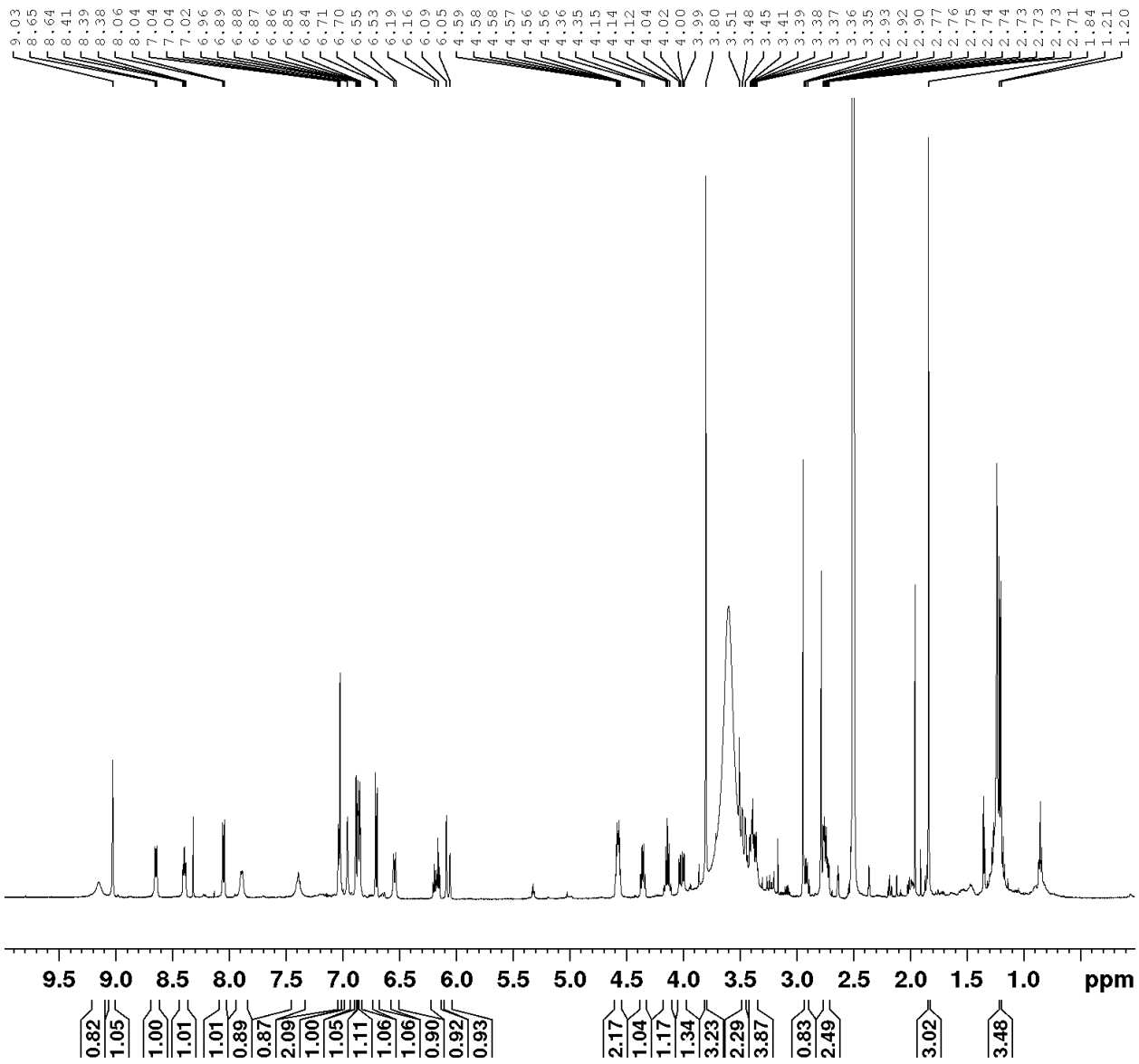

Spectrum 4.7.107 ^{13}C-NMR of Polycycle **35** (DMSO-d_6, 126 MHz)

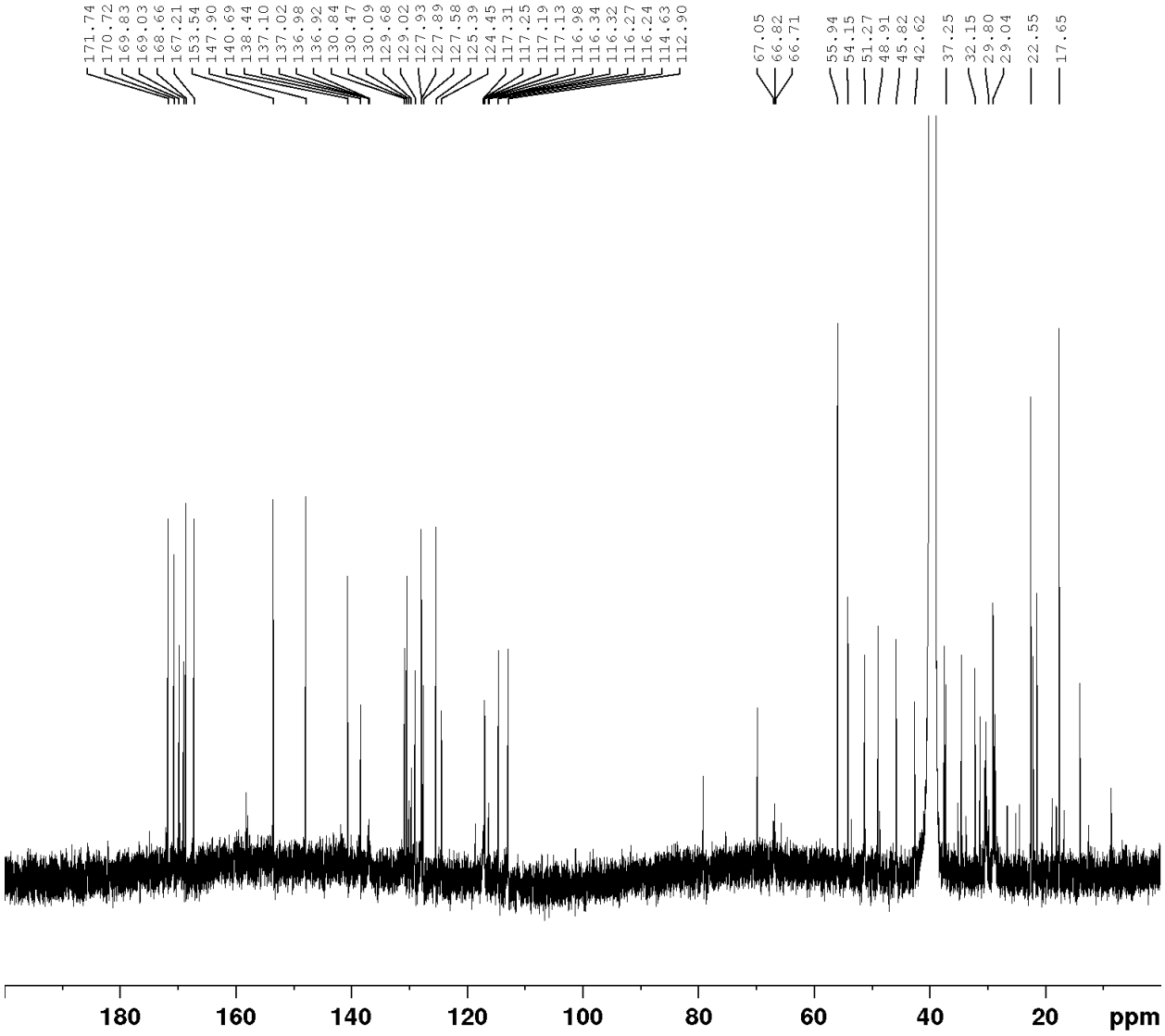

Spectrum 4.7.108 ^{19}F-NMR of Polycycle **35** (DMSO-d_6, 565 MHz)

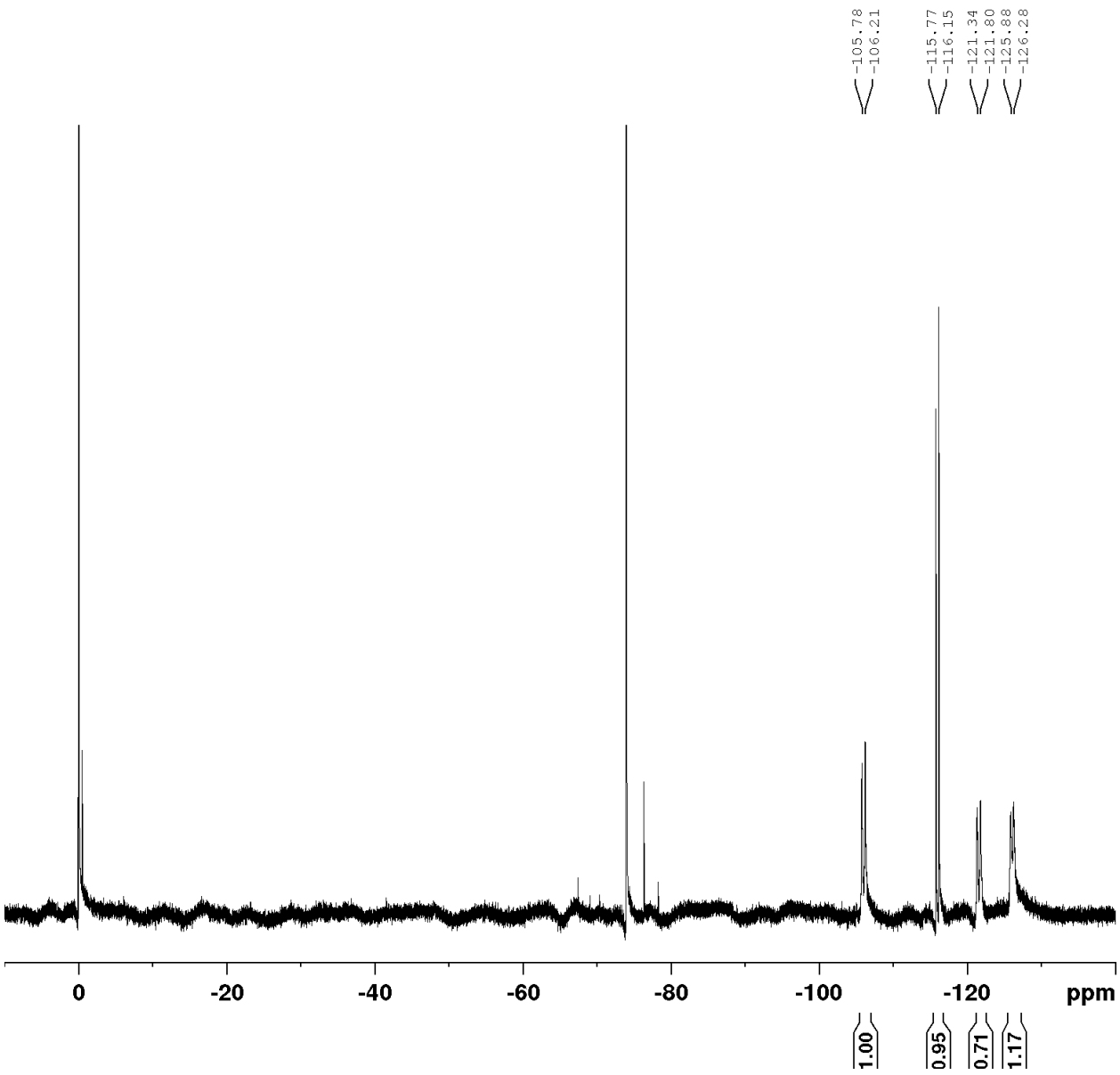

Spectrum 4.7.109 HMBC spectrum of Polycycle **35** (DMSO-d_6)

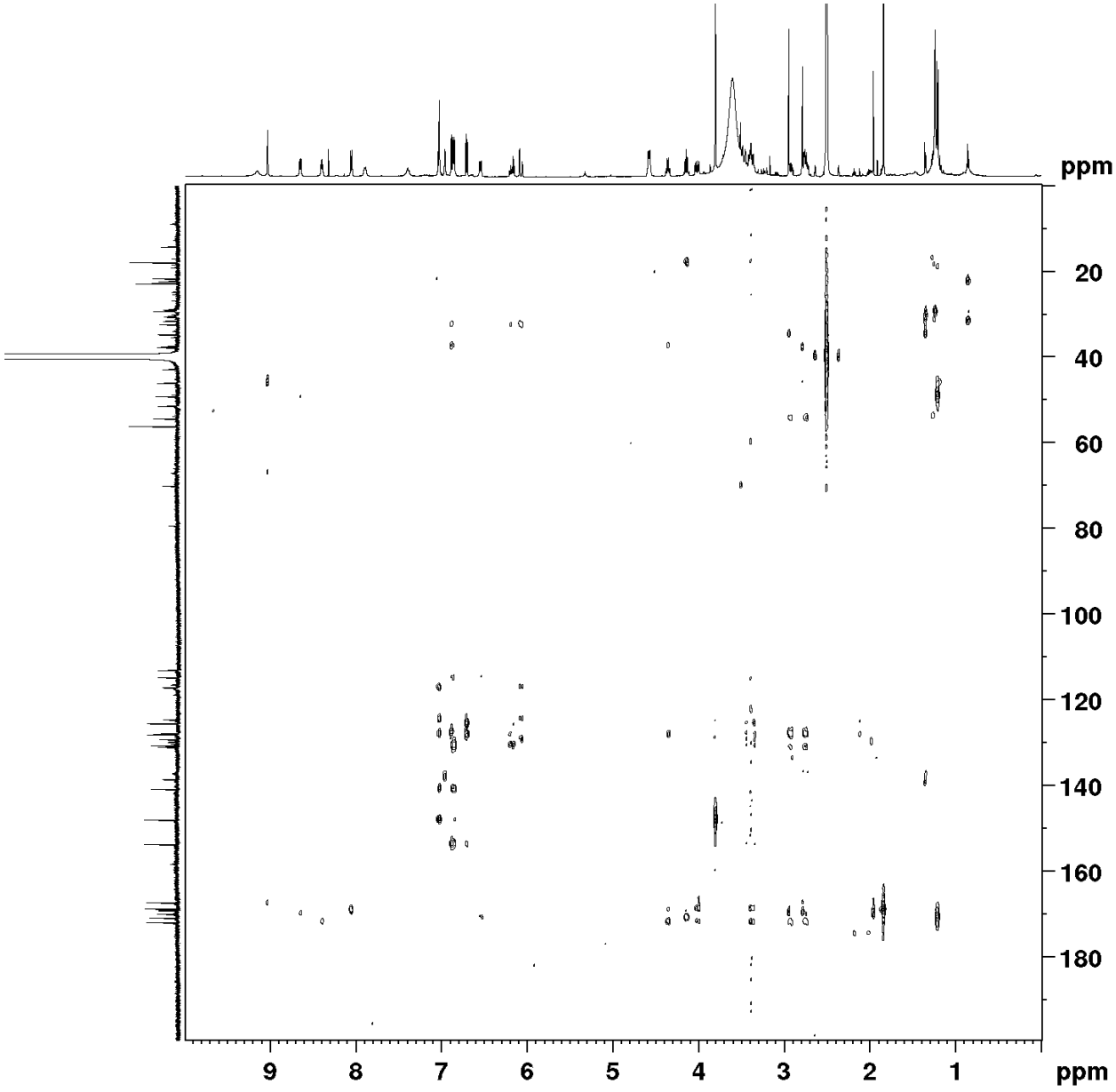

Spectrum 4.7.110 HSQC spectrum of Polycycle **35** (DMSO-d_6)

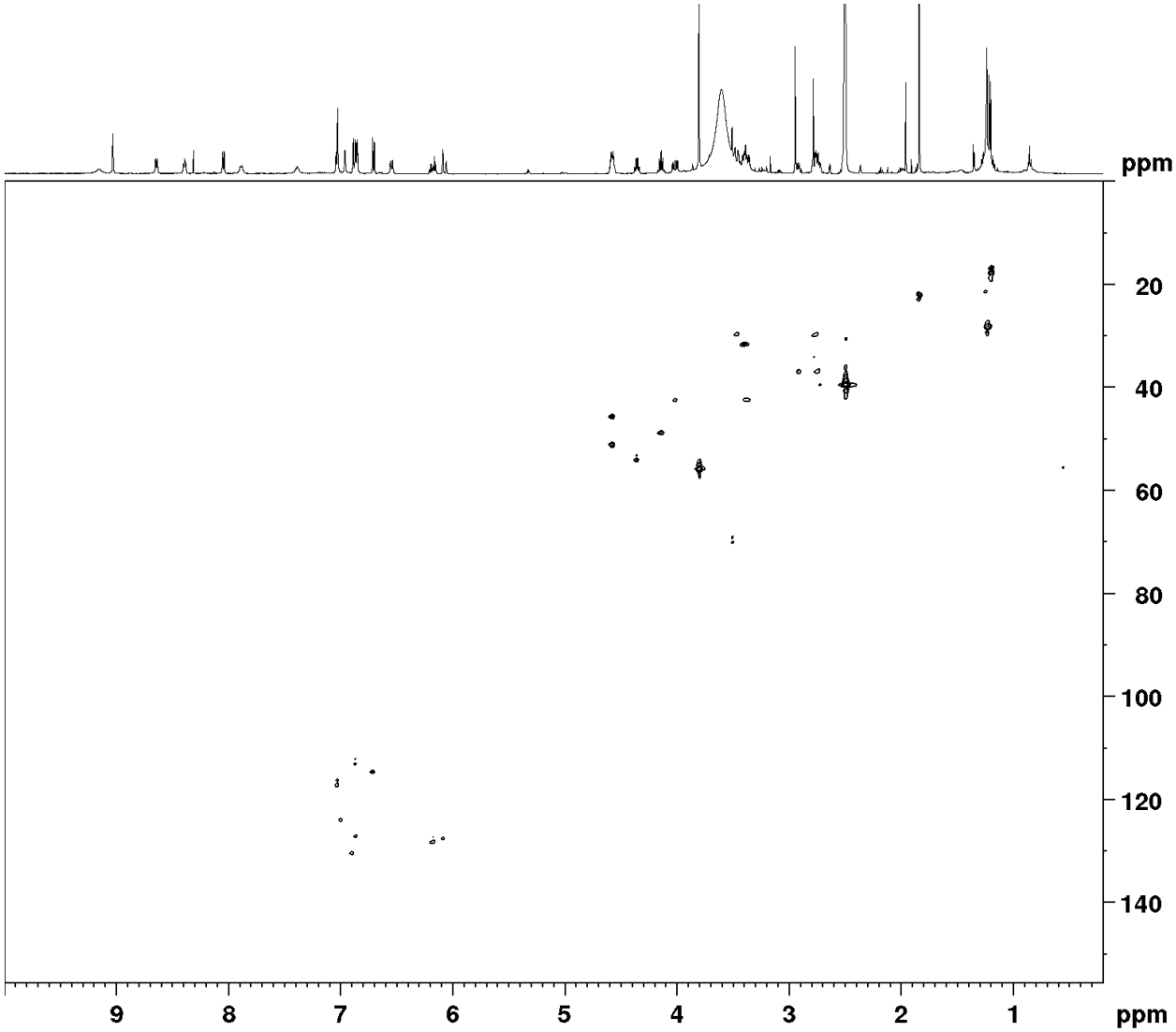

Spectrum 4.7.111 COSY spectrum of Polycycle **35** (DMSO-d_6)

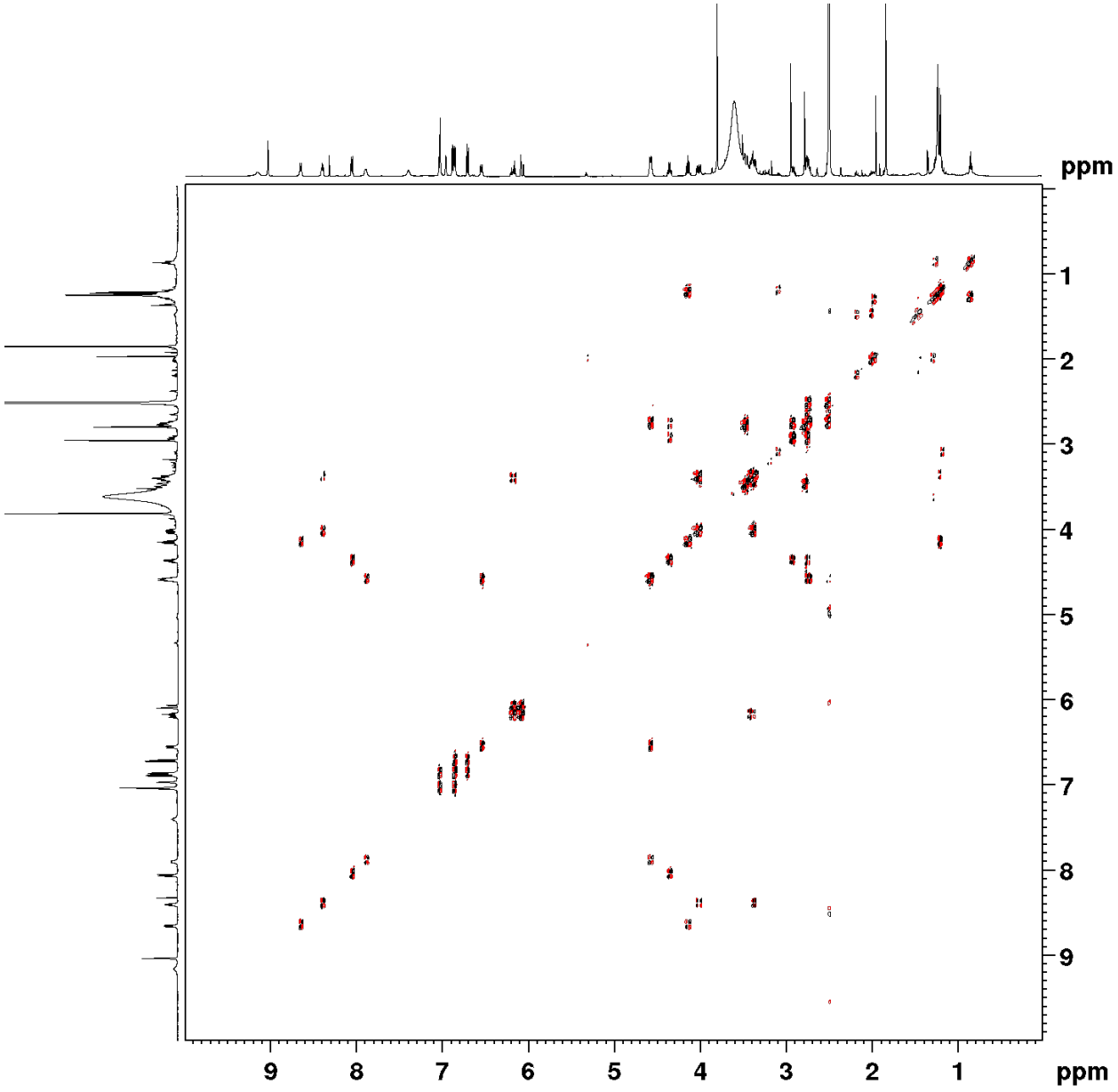

Table 4.7.19 Polycycle **35** (DMSO-d_6, 298K)

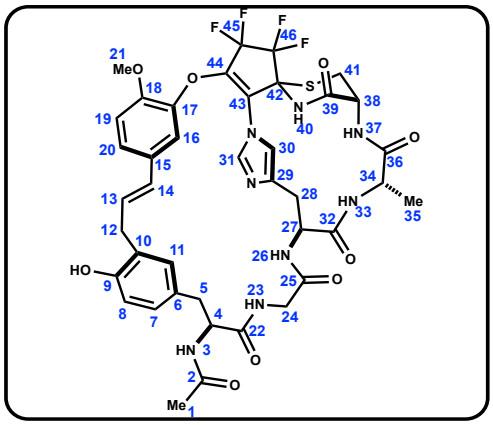

	13C	1H	Key Correlation
1	22.55	1.84 (s, 3H)	2->1 HMBC, HSQC
2	169.03	-	1->2 HMBC
3	-	8.05 (d, 2H)	2->3 HMBC
4	54.15	4.35 (q, 1H)	3->4 COSY, HSQC
5	37.25	2.94–2.89 (m, 1H), 2.77–2.71 (m, 1H)	4->5 COSY, HSQC
6	130.02	-	5->4 HMBC
7	127.58	6.87–6.85 (m, 1H)	8->7 COSY, HSQC
8	114.63	6.70 (d, 1 H) J = 8.2 Hz	7->8 COSY, HSQC, HMBC
9	153.54	-	8->7 COSY, HSQC, HMBC
10	129.02	-	12->10 HMBC
11	124.48	7.02 (m, 1H) overlap	6->11 HMBC, HSQC
12	32.15	3.42–3.35 (m, 2H)	13->12 COSY, HSQC
13	127.9	6.20–6.14 (dt, 1H) J = 15.9, 6.2 Hz	15->14 HMBC, HSQC
14	127.59	6.07 (d, 1H) J = 15.9 Hz	14->13 COSY, HSQC
15	116.98	-	14->15 HMBC, HSQC
16	130.49	6.89 (overlap, 1H)	15->16 HMBC, HSQC
17	147.89	-	16->17 HMBC
18	140.69	-	19->18 HMBC
19	112.94	6.84 (m, 1H)	20->19 COSY, HMBC, HSQC
20	125.41	7.04–7.02 (m, 1H) overlap	19->20 COSY, HMBC, HSQC
21	55.94	3.80 (s, 3H)	2->1 HMBC, HSQC
22	171.76	-	4->22 HMBC
23	-	8.39 (t, 1H)	22->23 HMBC
24	42.62	4.01 (dd, 1H) J = 15.9, 7.0 Hz 3.37–3.33 (m, 1H) overlap	23–>24 COSY, HSQC
25	168.67	-	24->25 HMBC
26	-	7.89 (d, 1H)	27->27 HMBC
27	45.82	4.57 (m, 1H) overlap	32->27 HMBC, HSQC
28	29.48	3.39 (m, 2H)	26->28 COSY, HSQC
29	138.44	-	30->29 HMBC, HSQC
30	116.98	6.52 (m, 1H)	29->30 HMBC, HSQC
31	130.83	6.96 (s, 1H)	HSQC
32	169.64	-	33->32 HMBC
33	-	8.65 (d, 1H)	34->33 COSY
34	48.91	4.14 (m, 1H)	35->34 COSY
35	17.65	1.20 (d, 3 H) J = 7.39 Hz	34->35 COSY, HSQC
36	170.73	-	34->36 HMBC
37	-	7.39 (m, 1H)	36->37 HMBC
38	51.27	4.57 (m, 1H) overlap	37->38 COSY, HMBC, HSQC
39	167.22	-	40->39 HMBC
40	-	9.03 (s, 1H)	39->40 HMBC
41	29.04	3.47 (m, 1H), 2.75 (m, 1H)	38->41 COSY, HMBC, HSQC
42	66.82 (m, 1C)	-	40->42 HMBC
43	117.18 (m, 1C)	-	-
44	137.02 (m, 1C)	-	-
45	116.29 (m, 1C)	-	-
46	116.29 (m, 1C)	-	-

Spectrum 4.7.112 ^{1}H-NMR of Polycycle **36** (DMSO-d_6, 500 MHz)

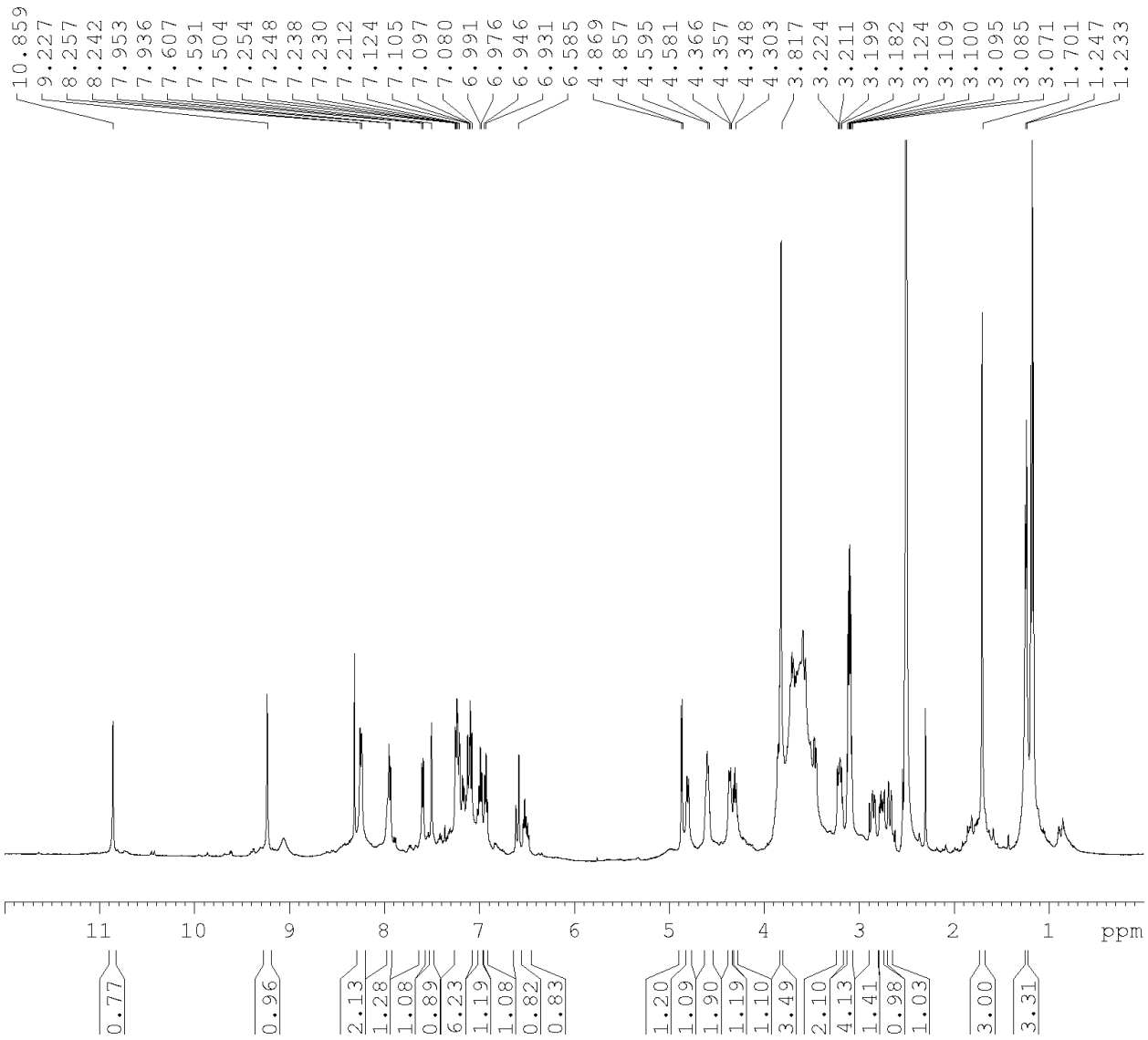

Spectrum 4.7.113 ^{13}C-NMR of Polycycle **36** (DMSO-d_6, 126 MHz)

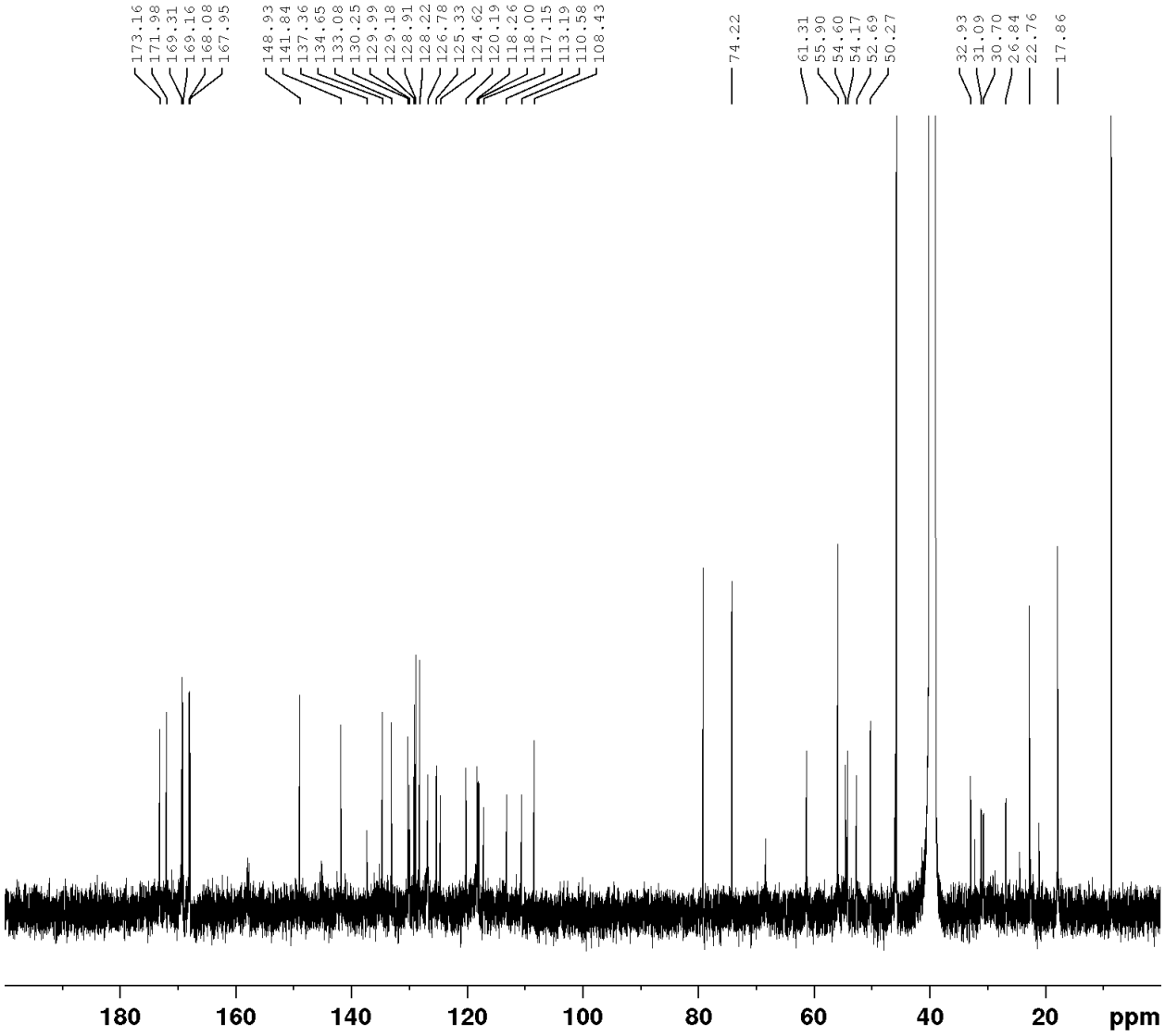

Spectrum 4.7.114 HMBC spectrum of Polycycle **36** (DMSO-d_6)

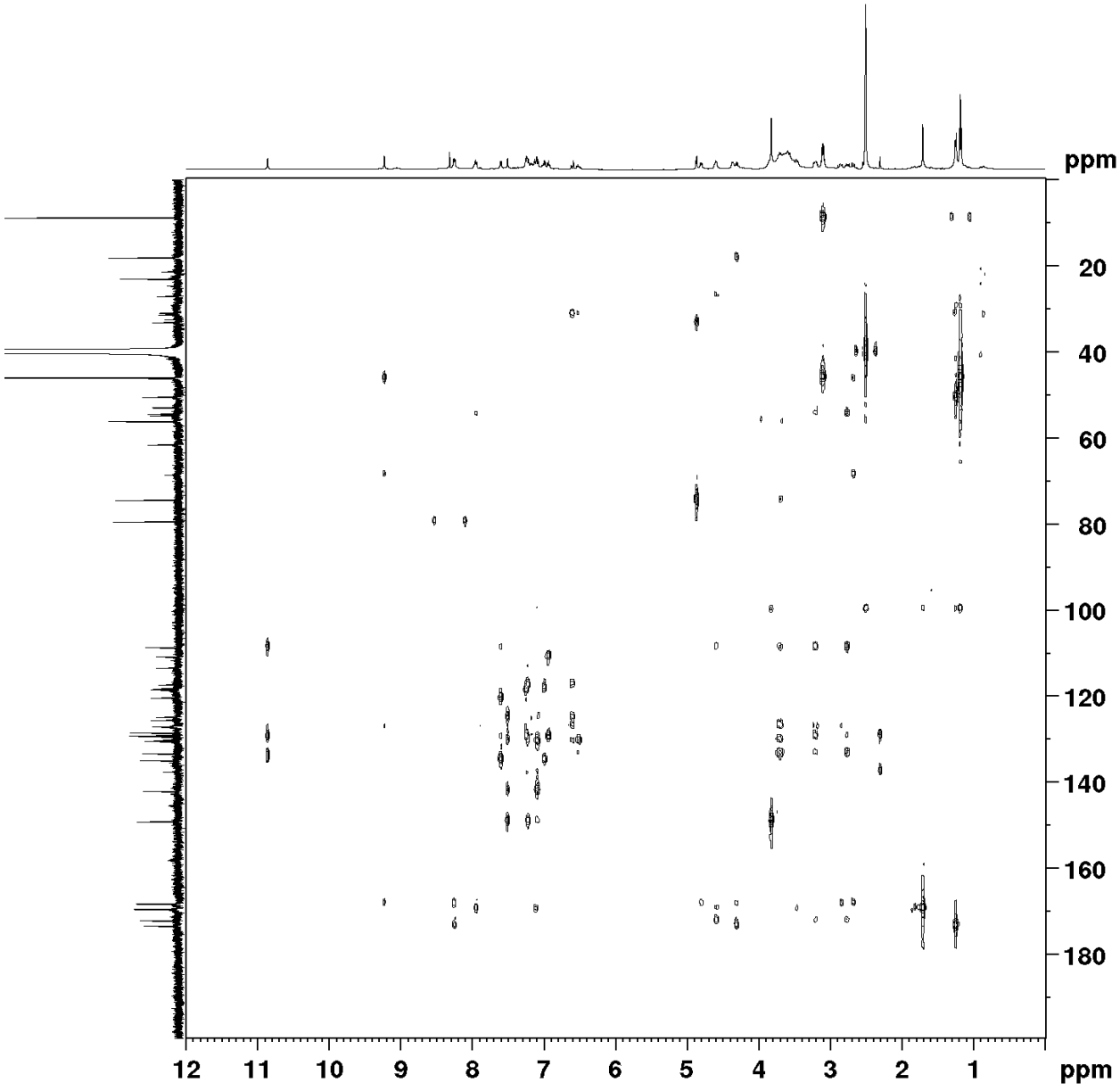

Spectrum 4.7.115 HSQC spectrum of Polycycle **36** (DMSO-d_6)

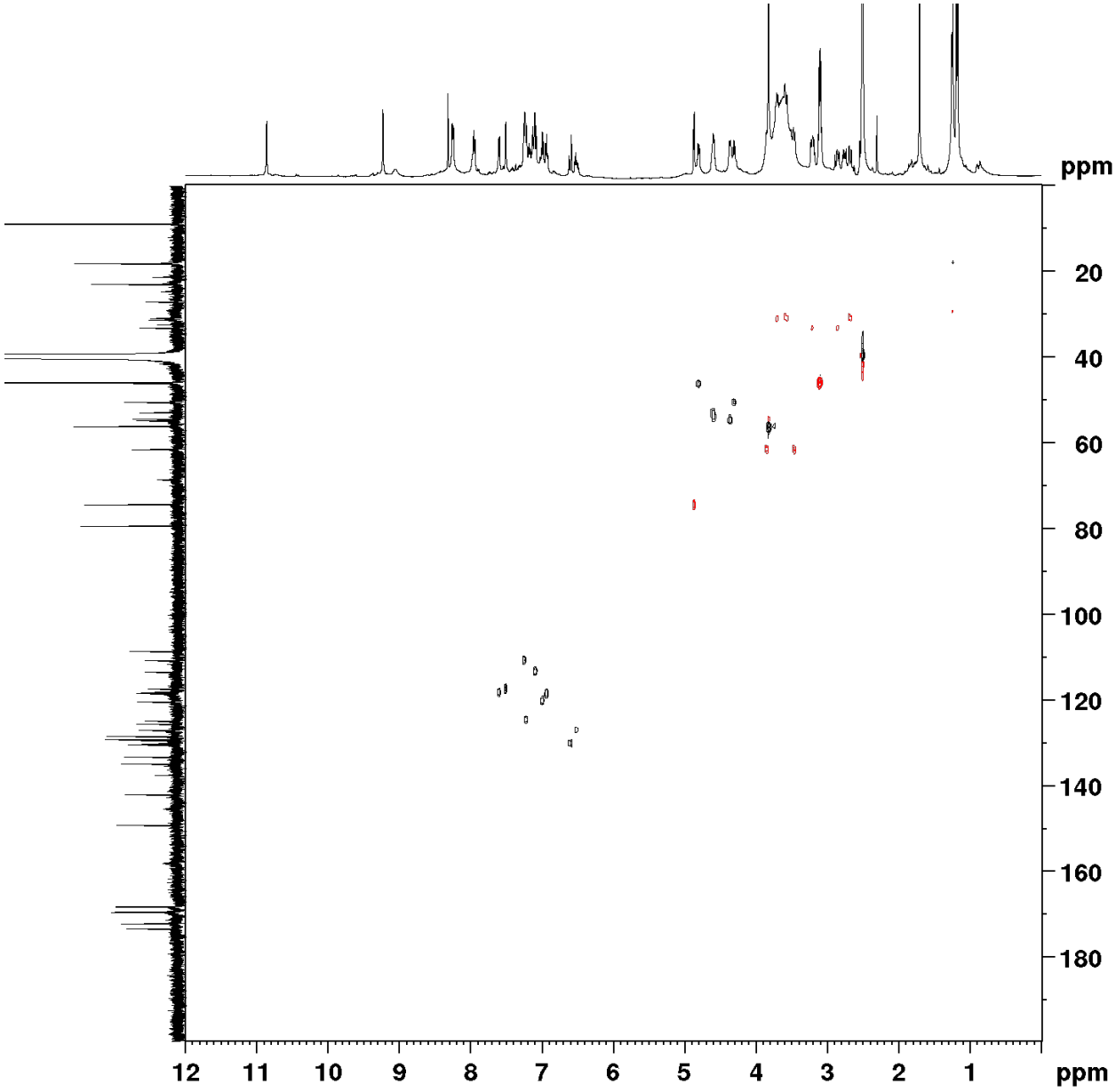

Spectrum 4.7.116 COSY spectrum of Polycycle **36** (DMSO-d_6)

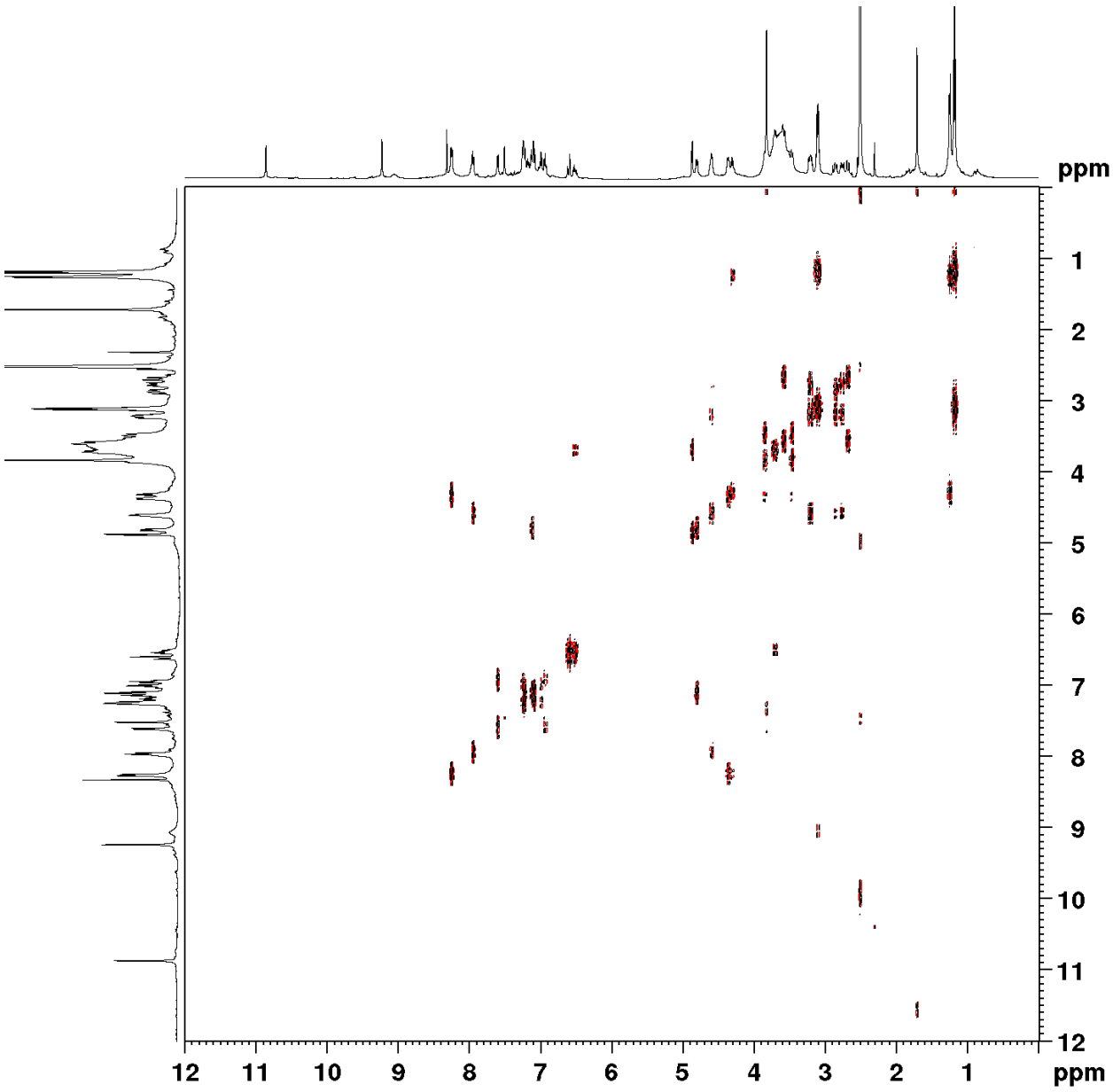

Spectrum 4.7.117 ^{1}H-NMR of Polycycle **40** (DMSO-d_6, 500 MHz)

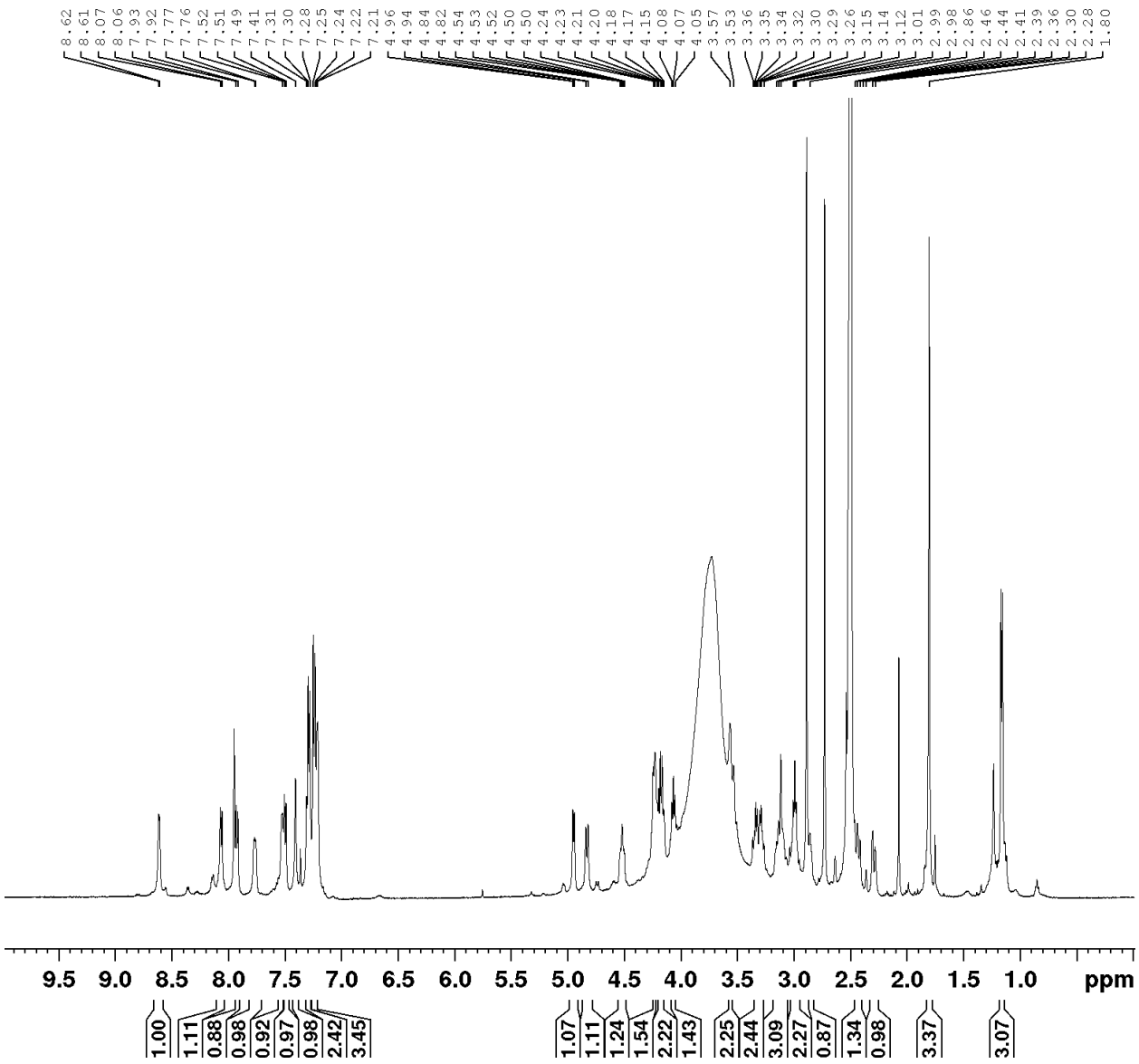

Spectrum 4.7.118 ^{13}C-NMR of Polycycle **40** (DMSO-d_6, 126 MHz)

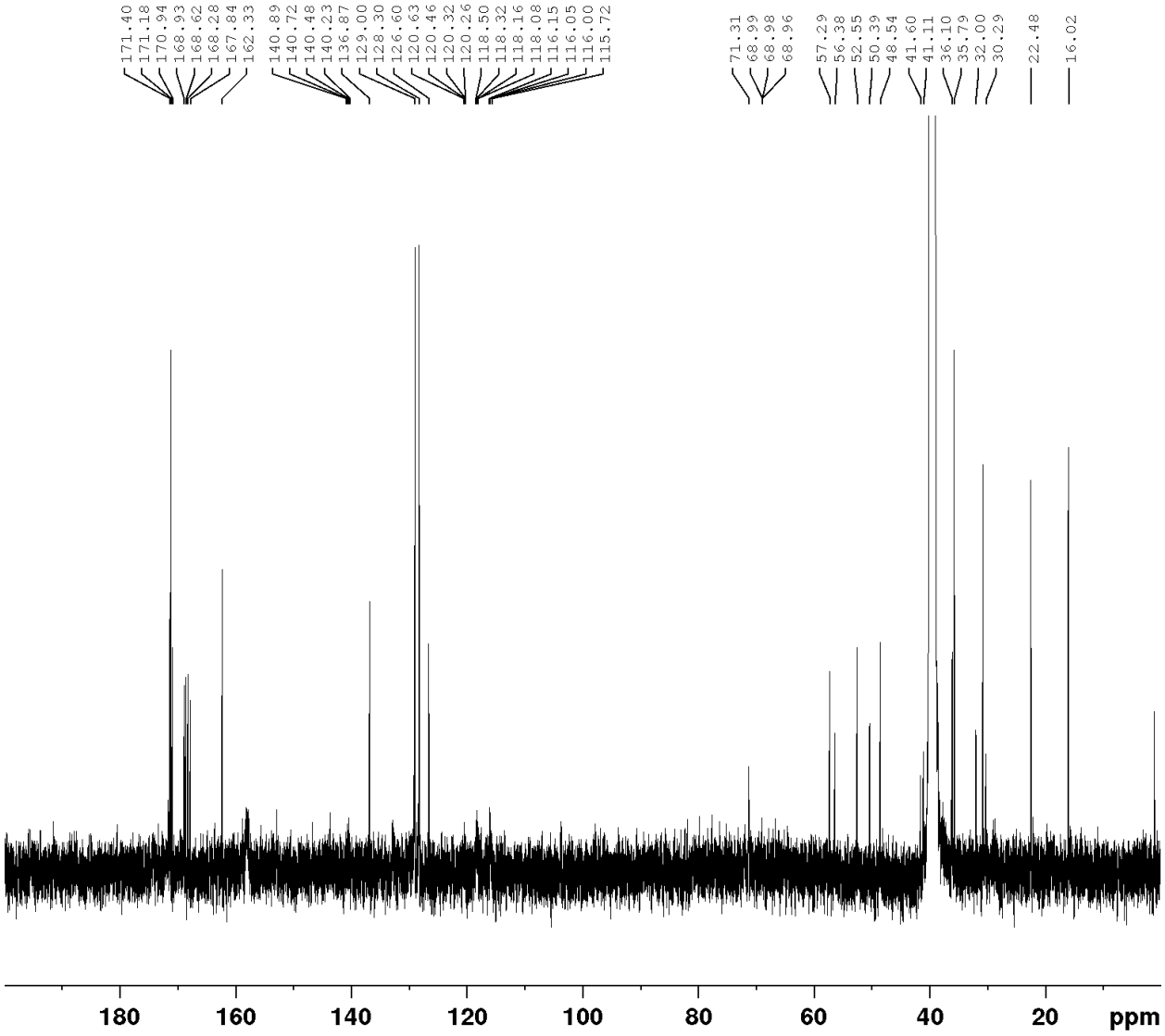

Spectrum 4.7.119 ^{19}F-NMR of Polycycle **40** (DMSO-d_6, 282 MHz)

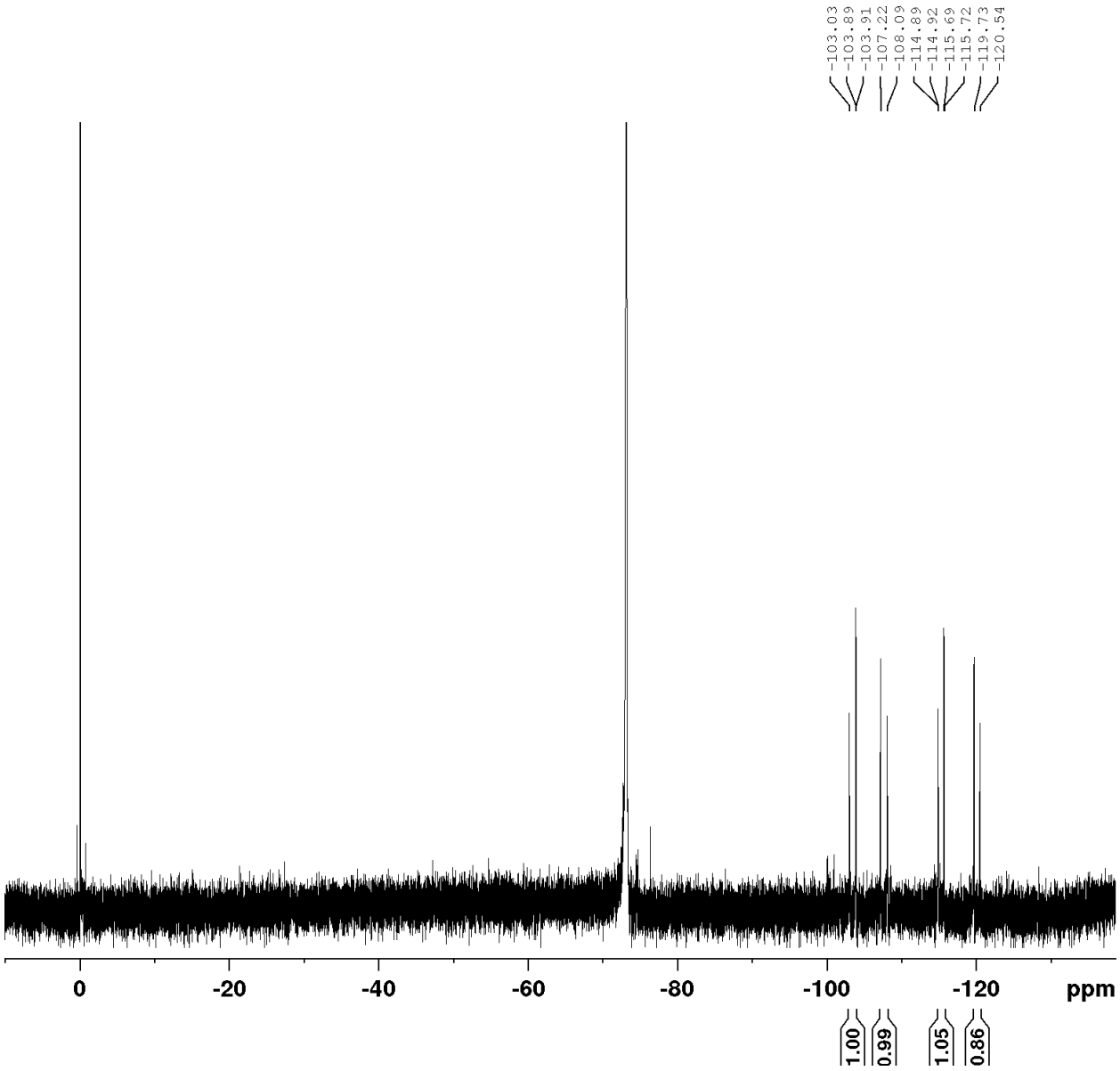

Spectrum 4.7.120 HMBC spectrum of Polycycle **40** (DMSO-d_6)

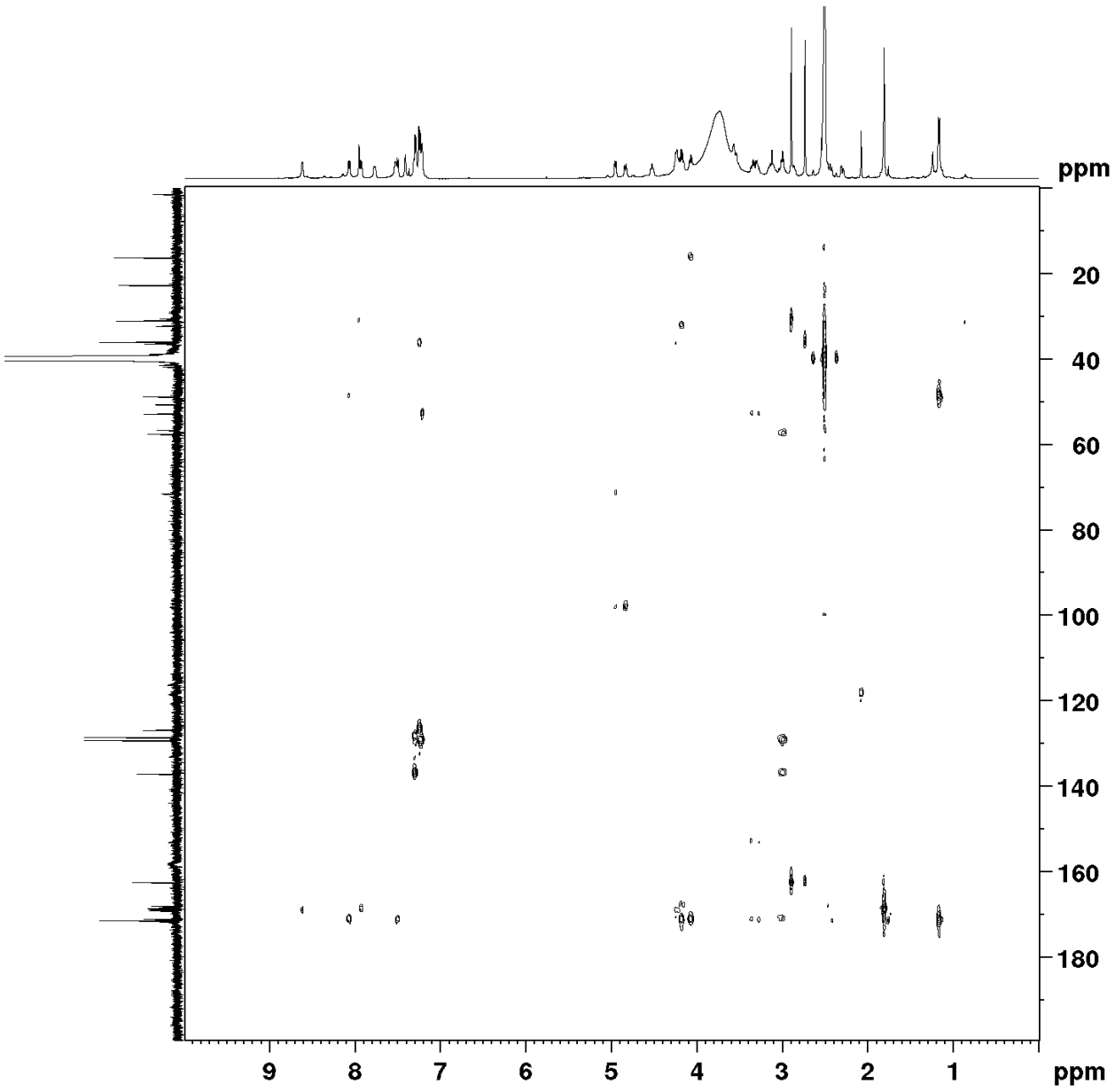

Spectrum 4.7.121 HSQC spectrum of Polycycle **40** (DMSO-d_6)

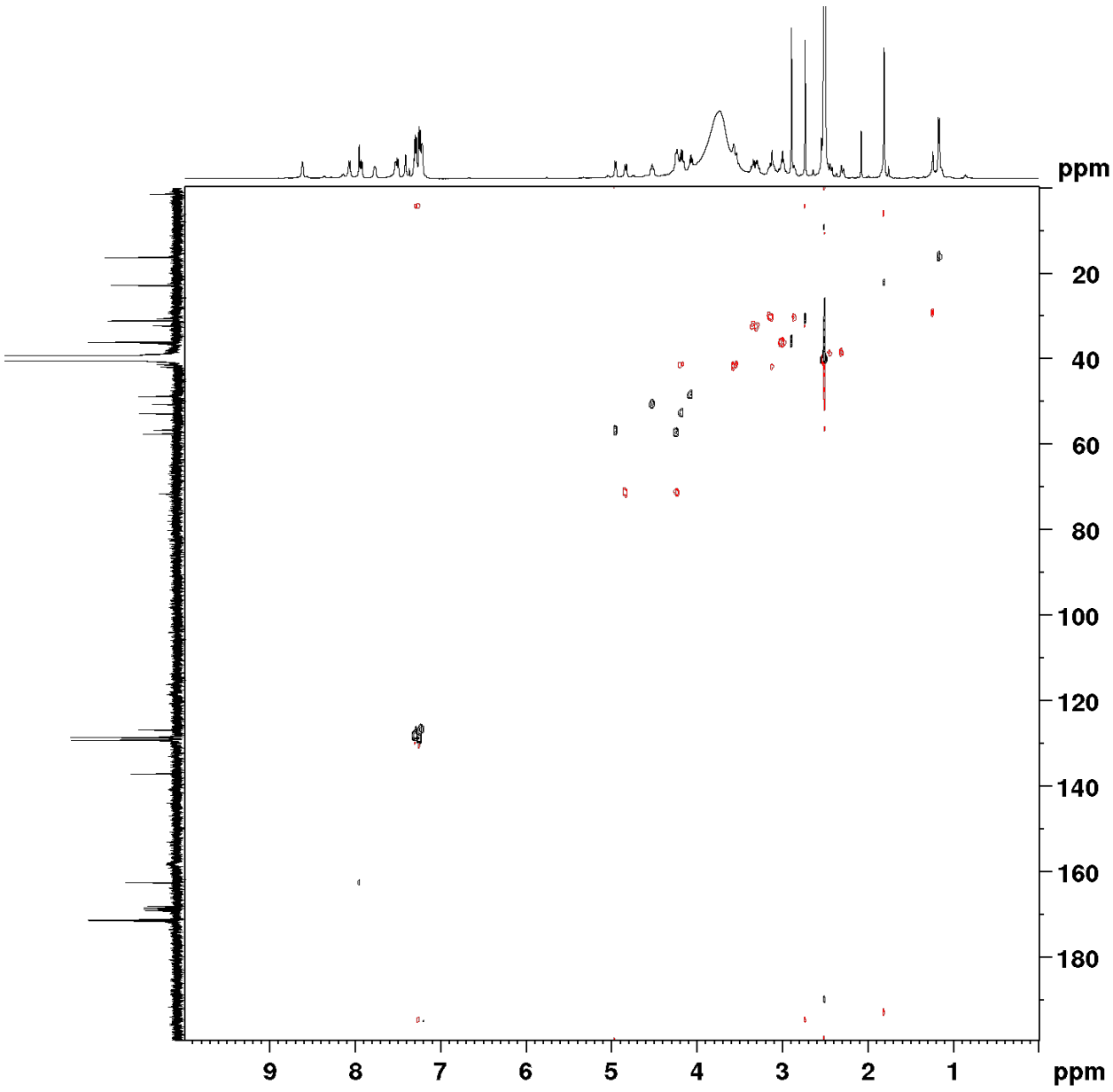

Spectrum 4.7.122 COSY spectrum of Polycycle **40** (DMSO-d_6)

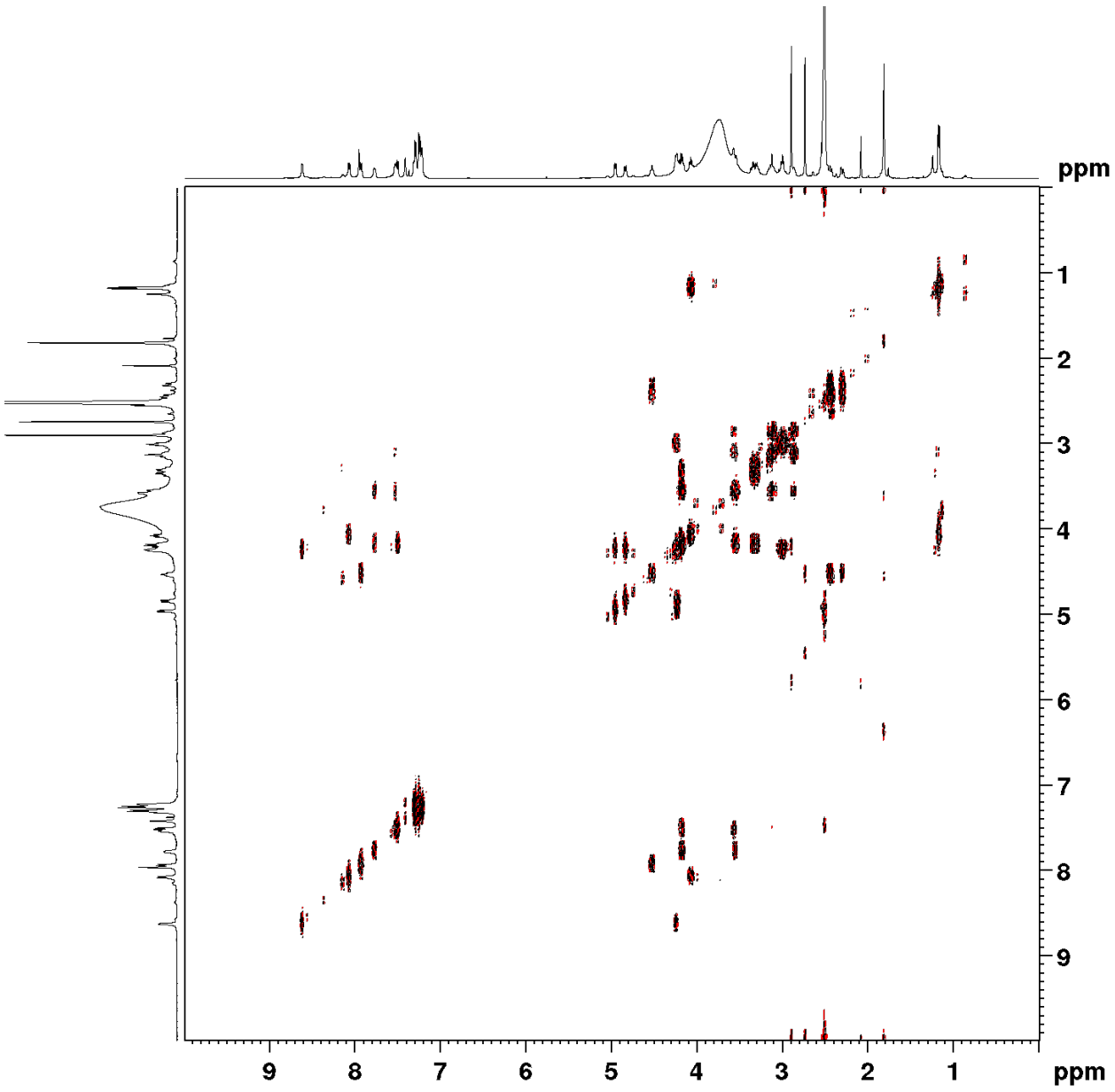

Table 4.7.20 Polycycle **40** (DMSO-d_6, 298K)

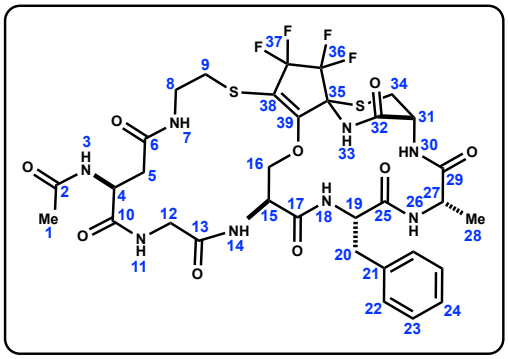

	13C	1H	Key Correlation
1	22.48	1.80 (s, 3H)	27->28 COSY, HMBC, HSQC
2	168.62	-	1->2 HMBC
3	-	7.92 (d, J = 7.7 Hz, 1H)	2->3 HMBC
4	50.39	4.52 (m, 1H)	3->4 COSY, HMBC, HSQC
5	35.79	2.42 (m, 1H), 2.29 (m, 1H)	4->5 COSY, HSQC
6	171.40	-	5->6 HMBC, COSY, HMBC
7	-	7.77 (m, 1H)	6->7 HMBC
8	41.11	4.17 (m, 1H), 3.55 (m, 1H) overlap	7->8 COSY, HSQC
9	52.58	3.14 (m, 2H) overlap	8->9 COSY, HSQC
10	167.23	-	11->10 HMBC
11	-	7.53 (m, 1H)	10->11 HMBC
12	41.59	4.16 (m, 1H) overlap, 3.55 (m, 1H)	11->12 COSY, HSQC
13	162.33	-	12->13 HMBC
14	-	7.50 (d, J = 7.6 Hz, 1H)	15->14 COSY
15	71.32	4.83 (m, 1H)	17->15 HMBC, HSQC
16	32.00	3.31 (m,2H)	15->16 COSY, HSQC
17	168.94	-	18->17 HMBC
18	-	8.61 (d, J = 4.1 Hz, 1H)	19->20 COSY
19	57.29	4.24 (m, 1H)	20->19 COSY
20	36.01	2.99 (m, 2H)	21->20 HMBC, HSQC
21	136.87	-	20->21 HMBC
22	129.00	7.32–7.21 (m, 2H)	COSY, HMBC, HSQC
23	128.30	7.32-7.21 (m, 2H)	COSY, HMBC, HSQC
24	126.60	7.32–7.21 (m,1H)	COSY, HMBC, HSQC
25	168.23	-	19->25 HMBC
26	-	8.07 (d, J = 7.5 Hz, 1H)	27->26 COSY, HSQC
27	48.54	4.07 (m, 1H)	28->27 COSY
28	16.02	1.16 (d, J = , 3H)	27->28 HMBC, COSY, HSQC
29	170.94	-	27->29 HMBC
30	-	-	-
31	56.38	4.95 (m 1H)	32->31 HMBC, HSQC
32	171.19	-	33->32 HMBC
33	-	7.40 (s, 1H)	-
34	30.29	3.11 (m, 1H), 2.86 (m, 1H) overlap	31->34 HMBC, COSY, HSQC
35	69.0–68.9 (m, 1C)	-	-
36	114.7–116.1 (m, 1C)	-	-
37	118.1–118.5 (m, 1C)	-	-
38	120.3–120.6 (m, 1C)	-	-
39	140.2–140.9(m, 1C)	-	-

Spectrum 4.7.123 ^{1}H-NMR of Polycycle **41** (DMSO-d_6, 500 MHz)

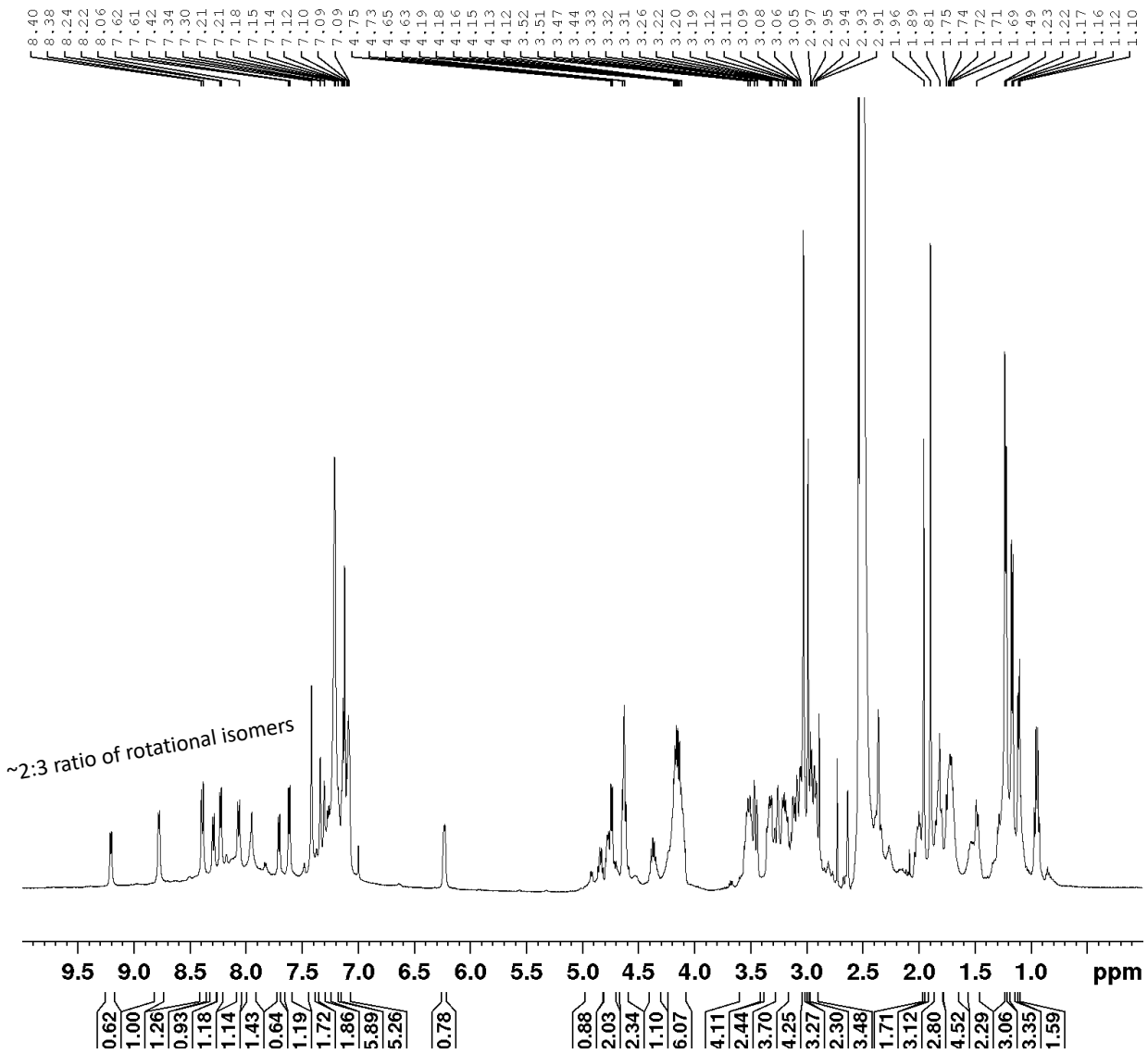

Spectrum 4.7.124 ^{13}C-NMR of Polycycle **41** (DMSO-d_6, 126 MHz)

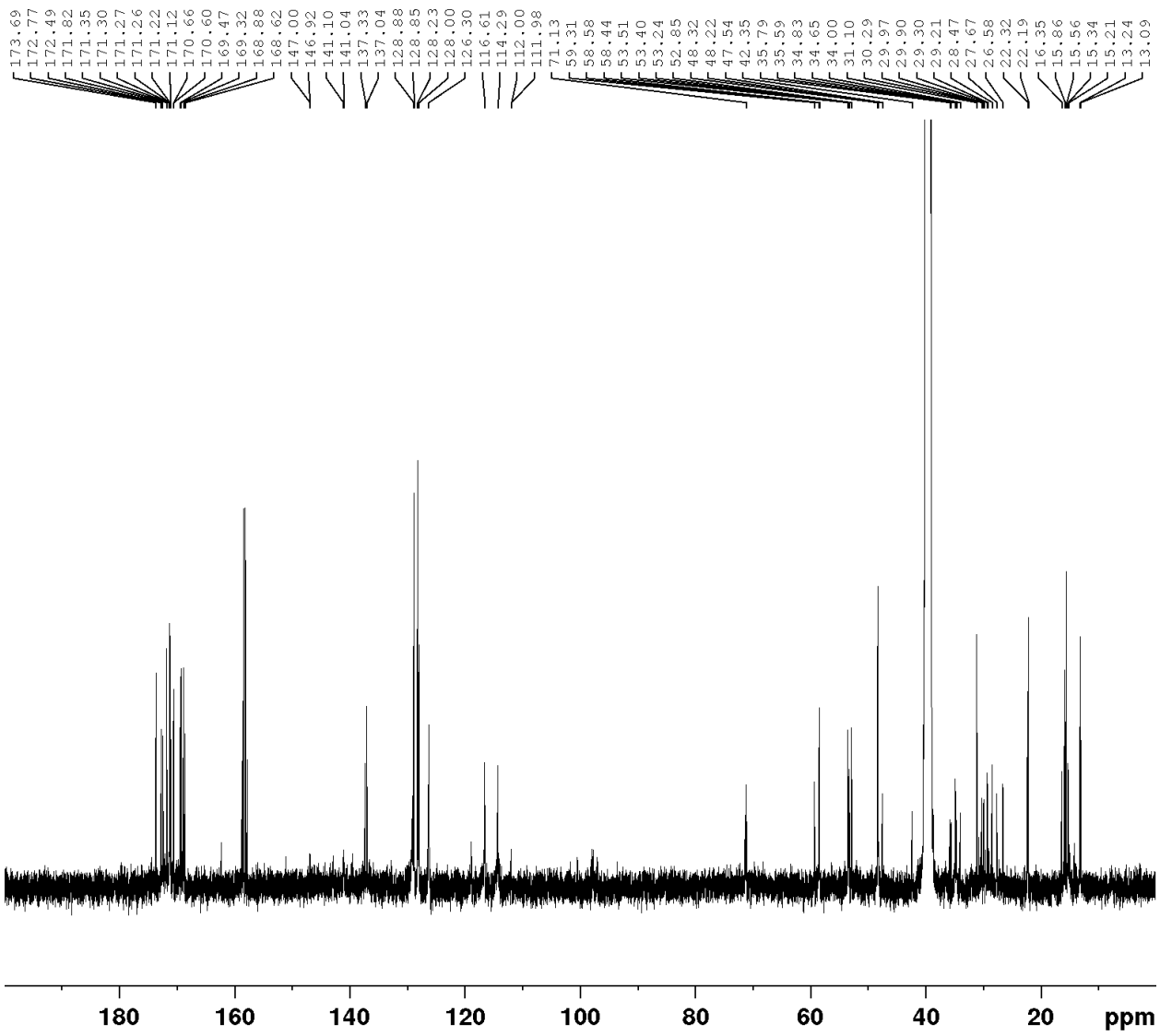

Spectrum 4.7.125 HMBC Spectrum of Polycycle **41** (DMSO-d_6)

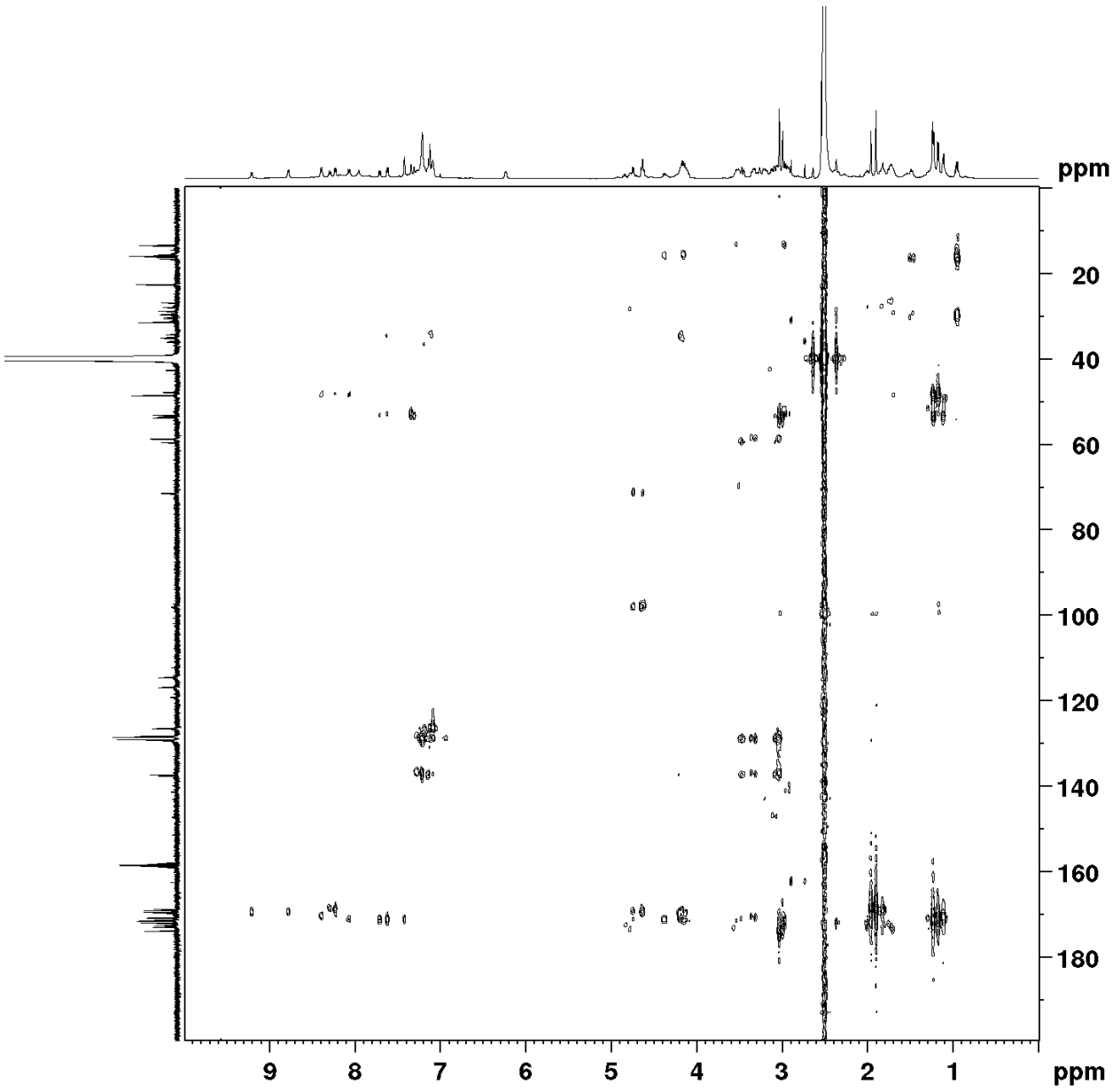

Spectrum 4.7.126 HSQC Spectrum of Polycycle **41** (DMSO-d_6)

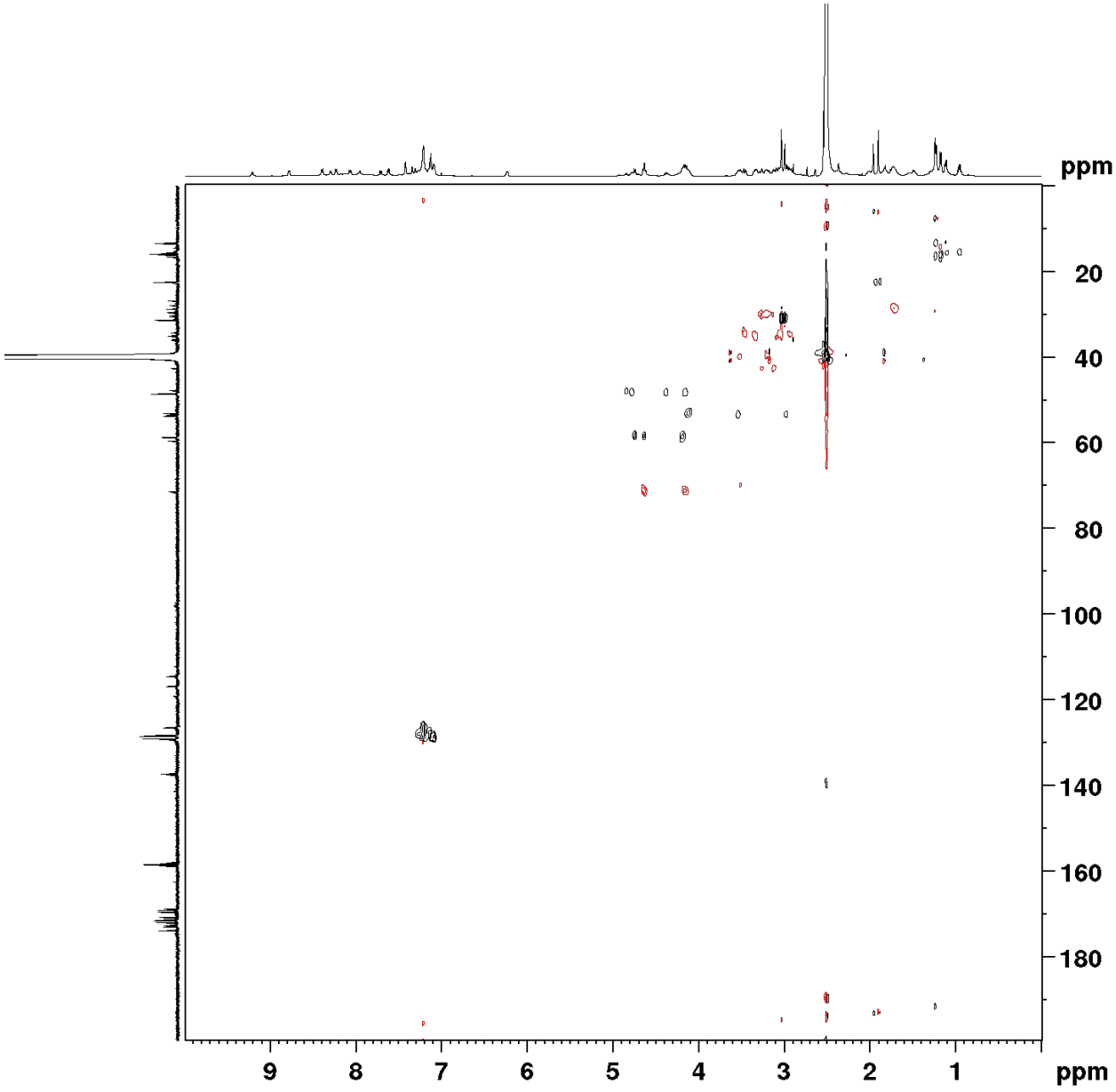

Spectrum 4.7.127 COSY Spectrum of Polycycle **41** (DMSO-d_6)

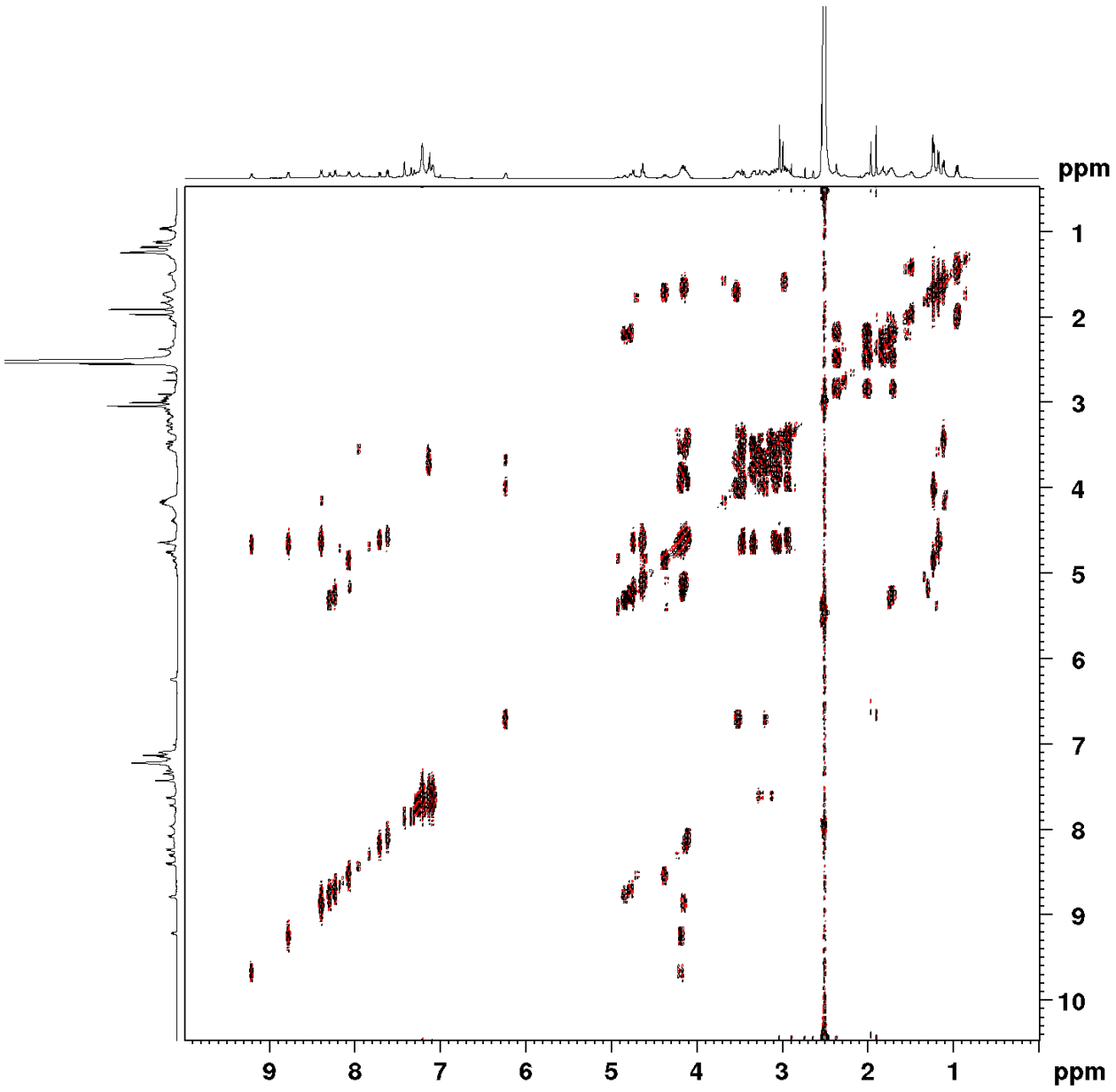

Spectrum 4.7.128 ^{1}H-NMR of Polycycle **42** (DMSO-d_6, 500 MHz)

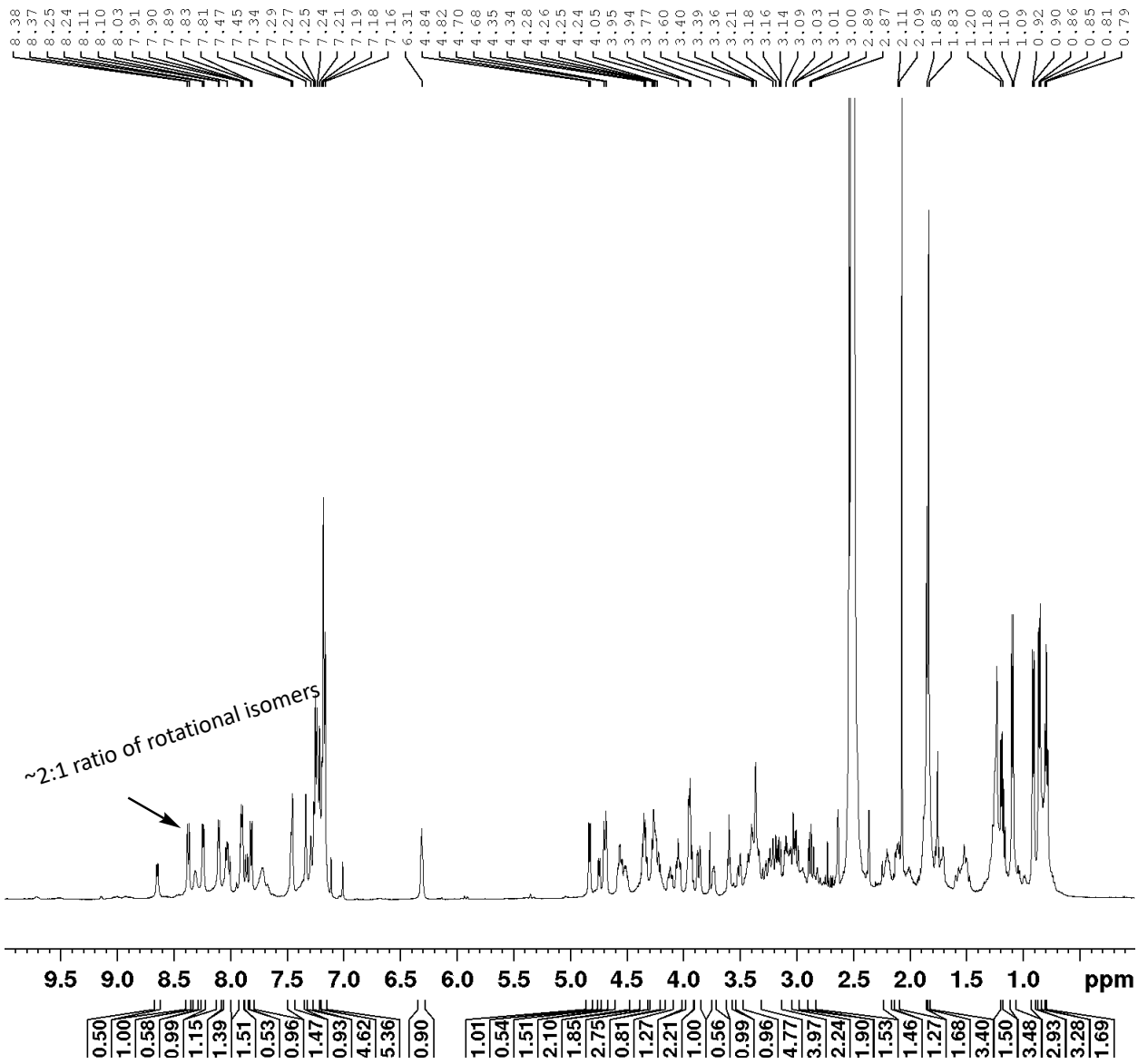

Spectrum 4.7.129 ^{13}C-NMR of Polycycle **42** (DMSO-d_6, 126 MHz)

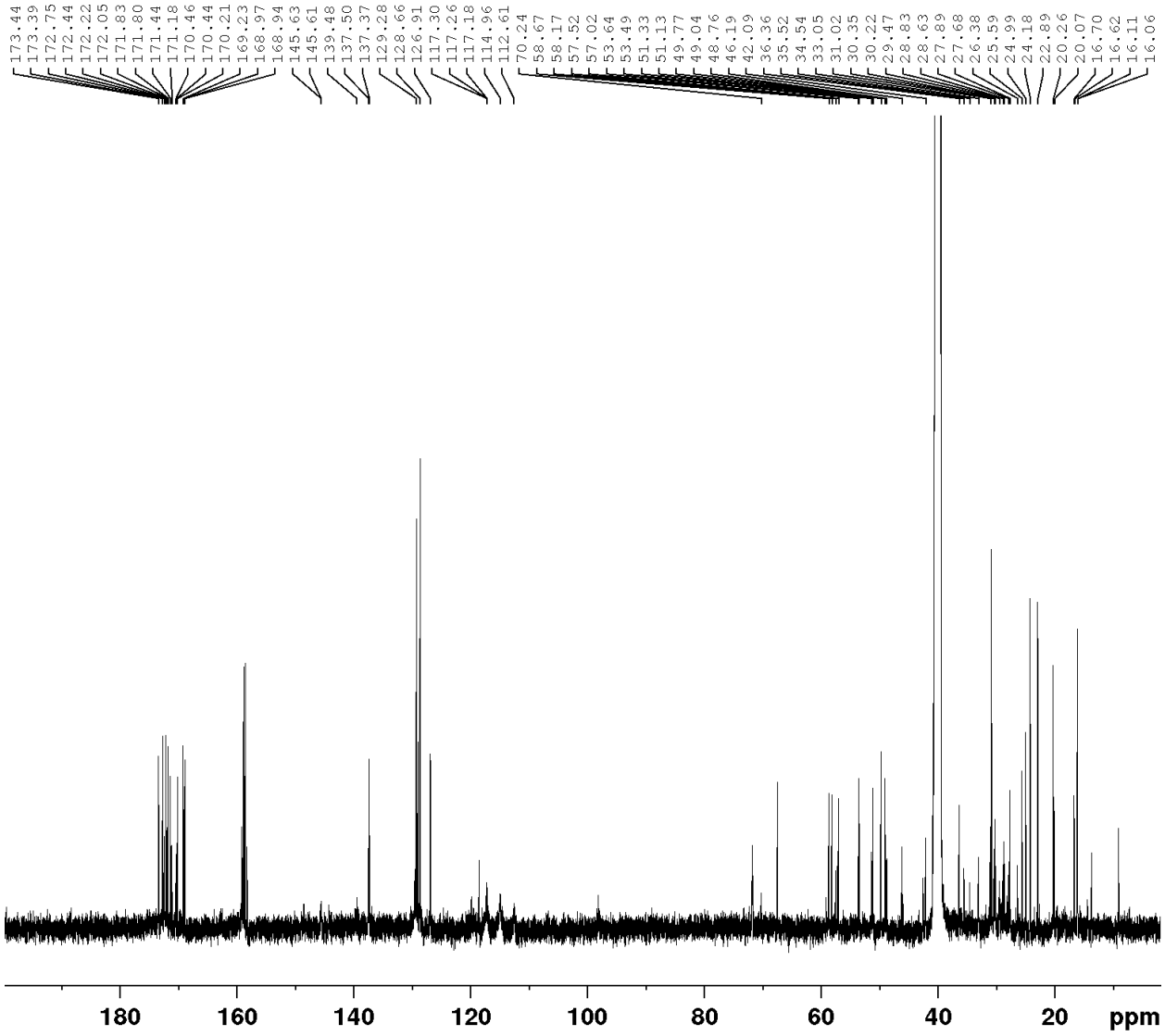

Spectrum 4.7.130 ^{19}F-NMR of Polycycle **42** (DMSO-d_6, 565 MHz)

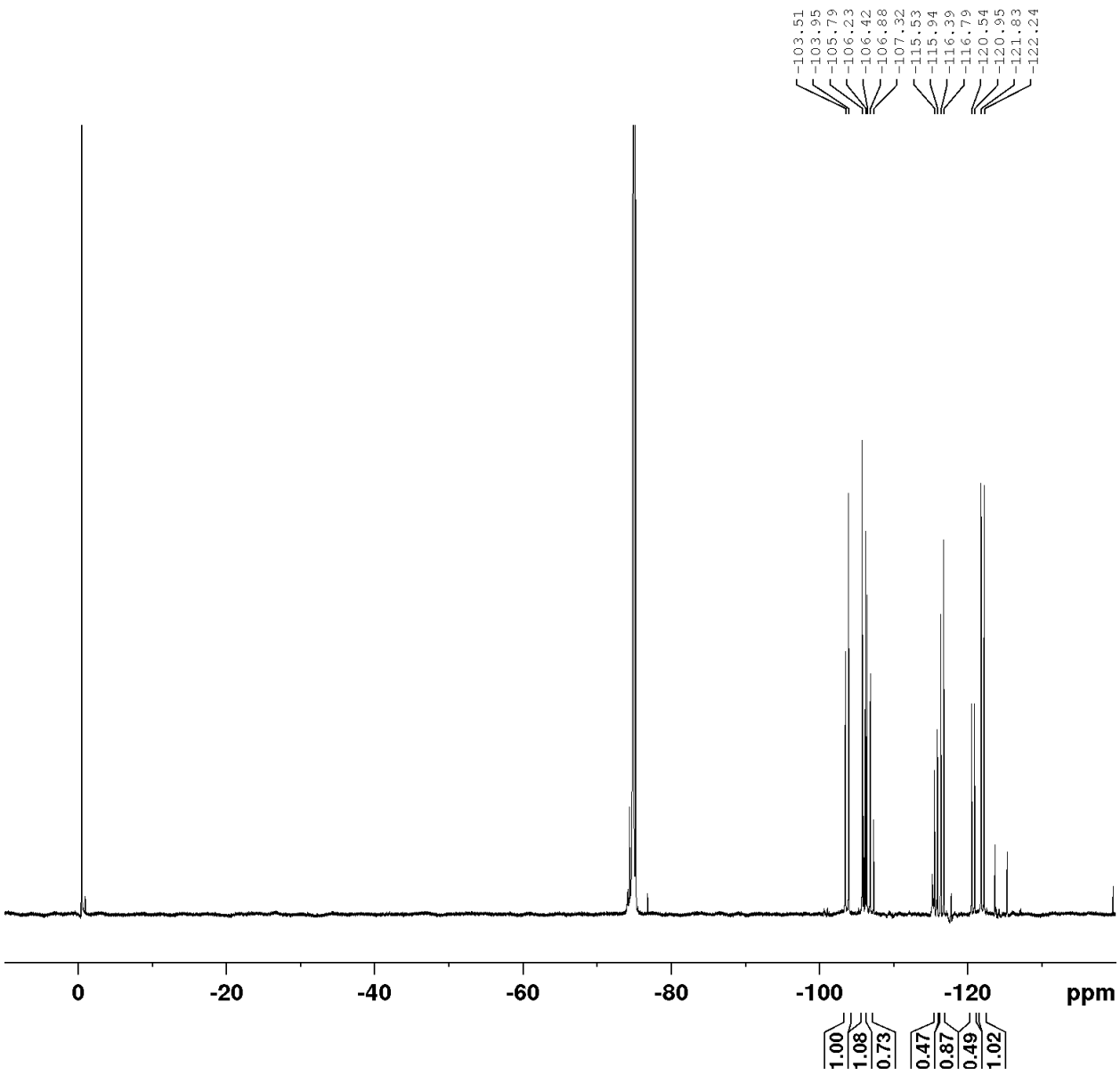

Spectrum 4.7.131 HMBC Spectrum of Polycycle **42** (DMSO-d_6)

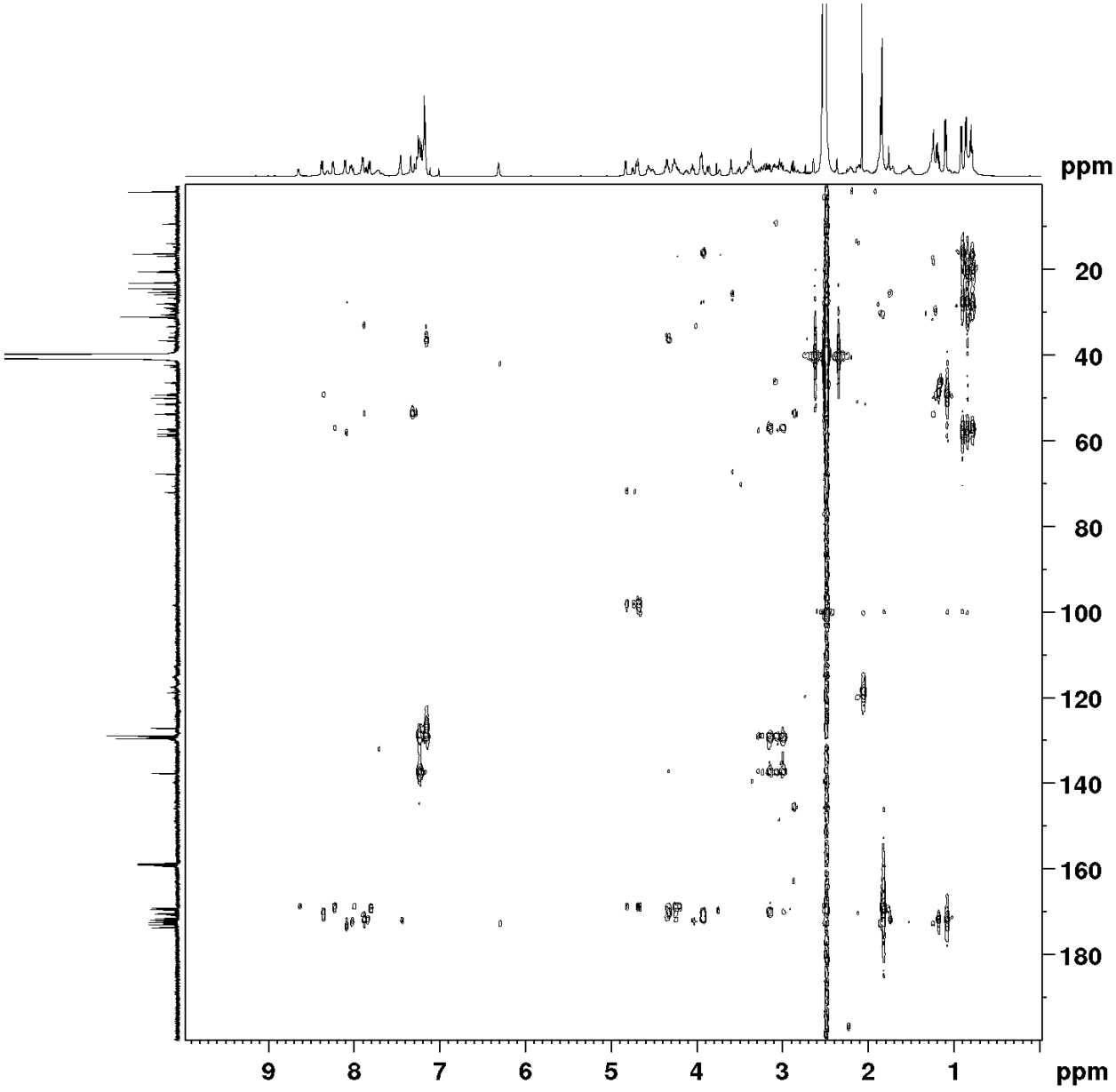

Spectrum 4.7.132 HSQC Spectrum of Polycycle **42** (DMSO-d_6)

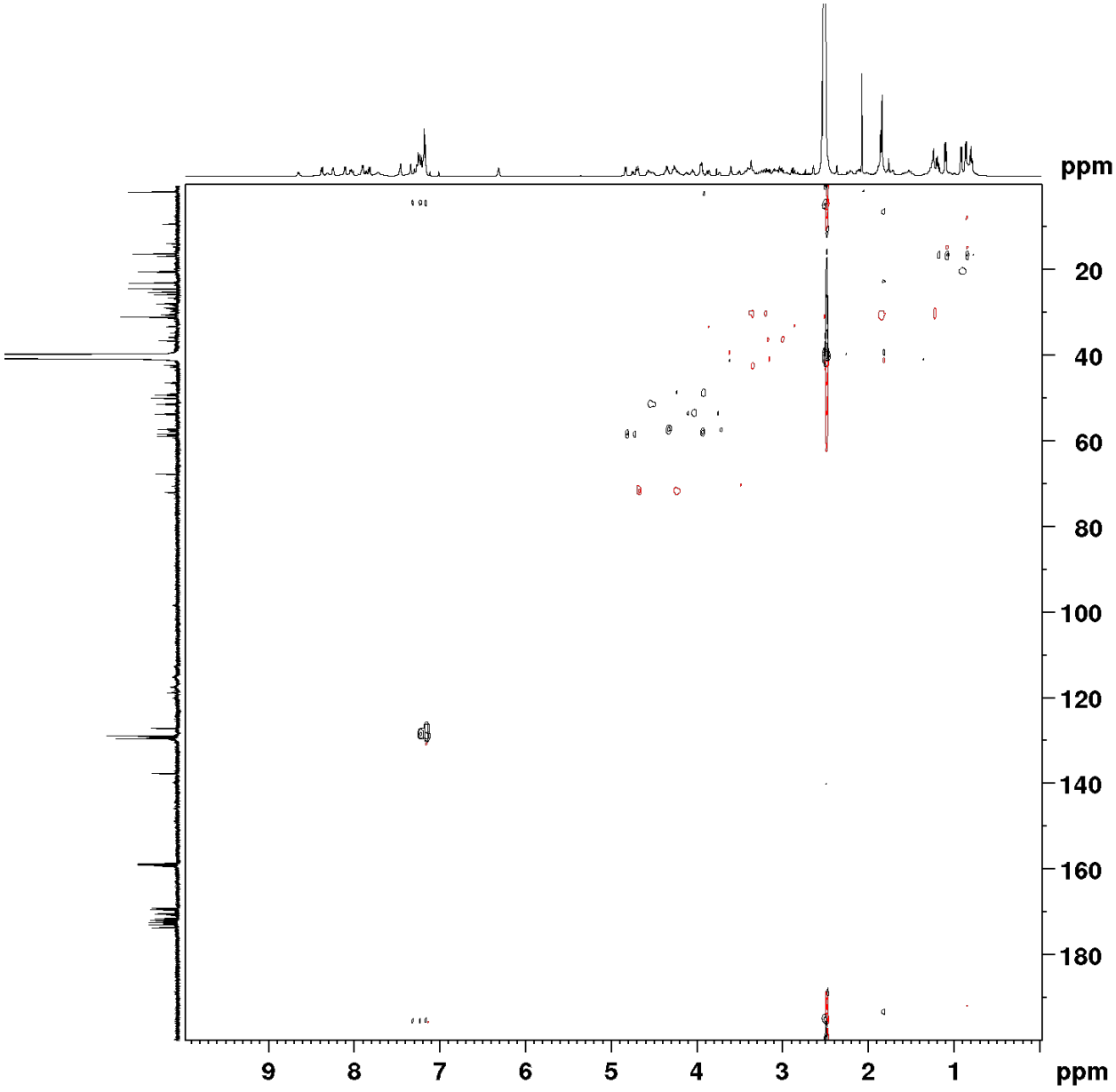

Spectrum 4.7.133 COSY Spectrum of Polycycle **42** (DMSO-d_6)

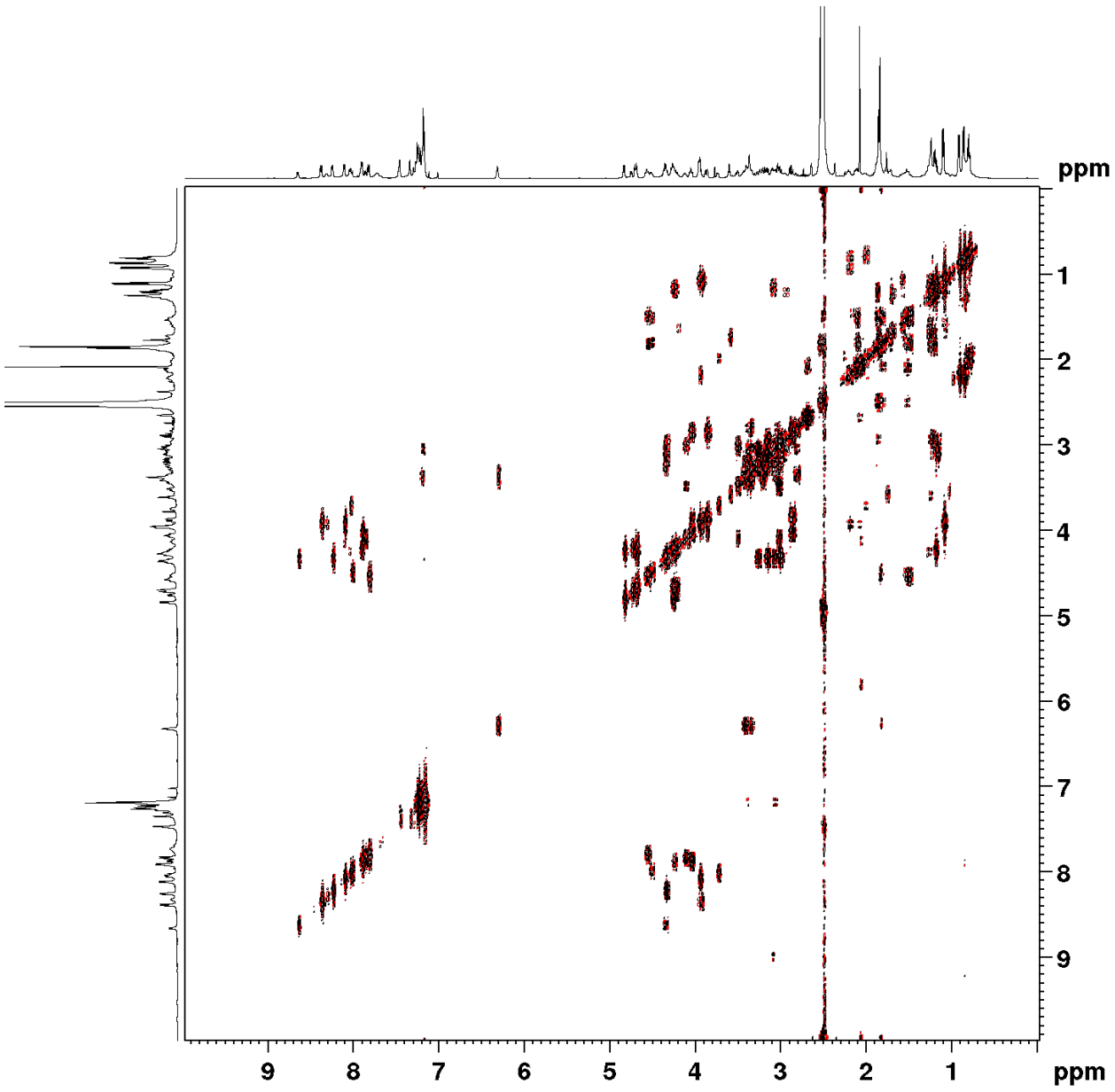

Spectrum 4.7.134 ^{1}H-NMR of Polycycle **43** (DMSO-d_6, 500 MHz)

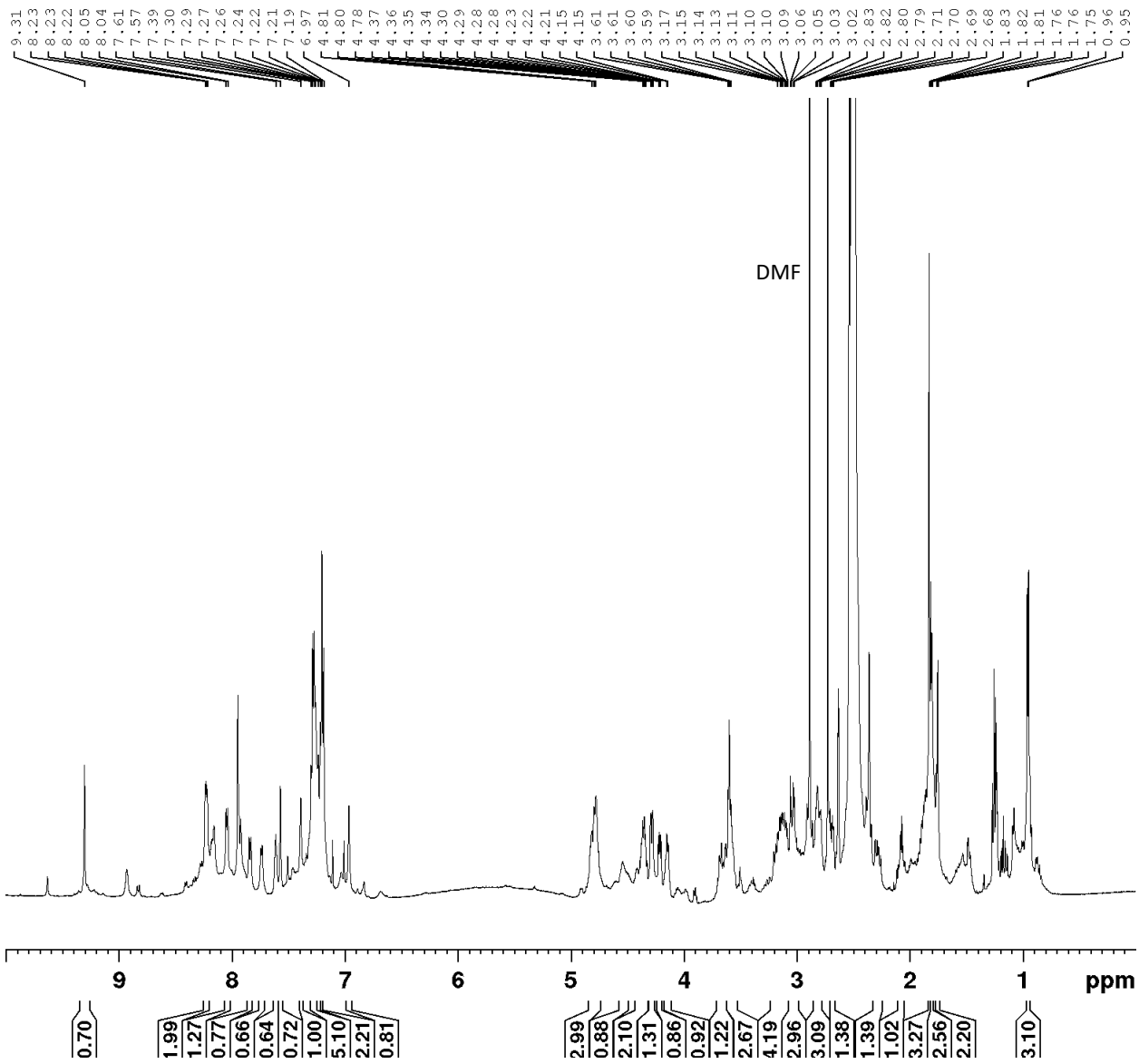

Spectrum 4.7.135 ^{13}C-NMR of Polycycle **43** (DMSO-d_6, 126 MHz)

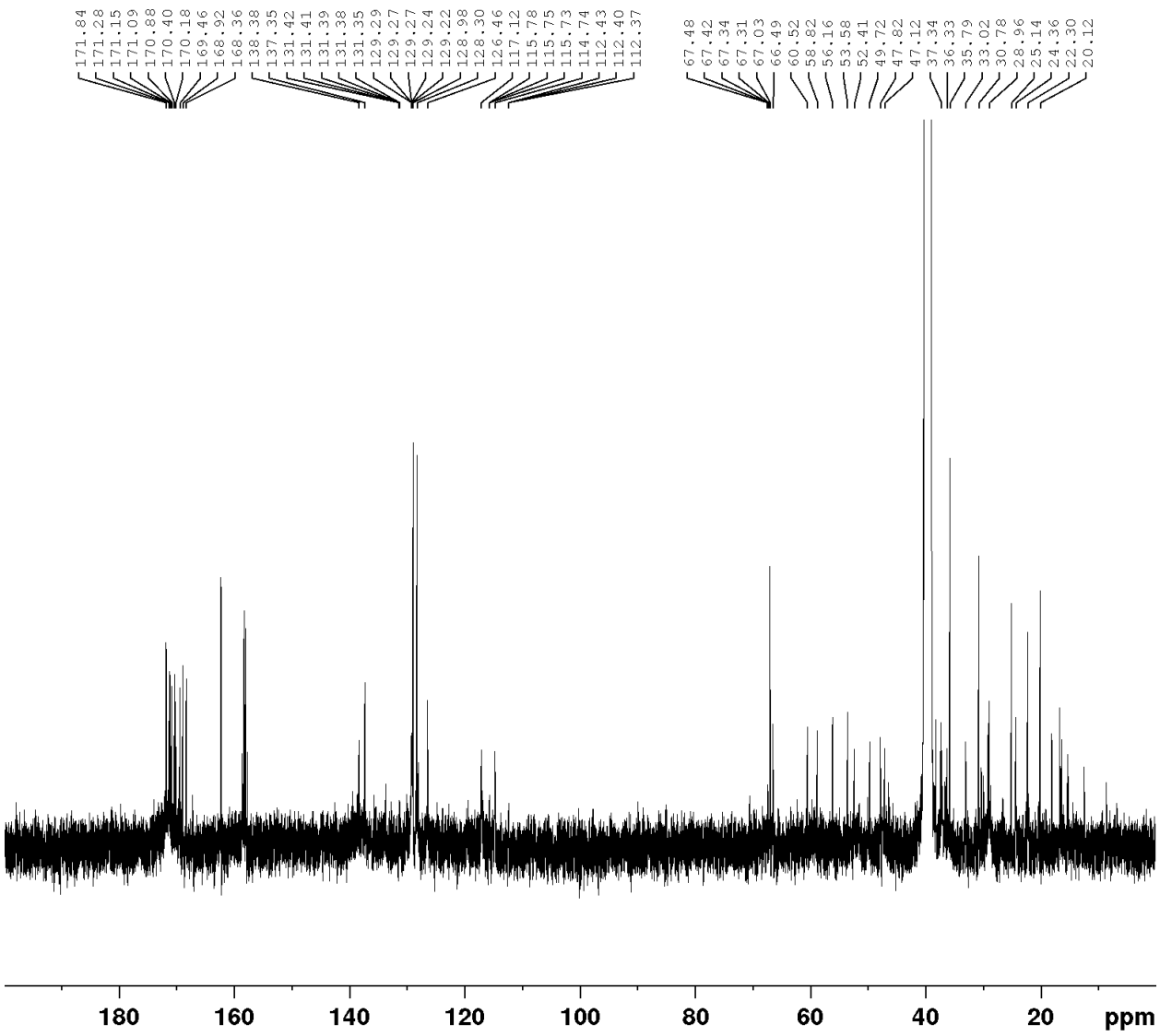

Spectrum 4.7.136 ^{19}F-NMR of Polycycle **43** (DMSO-d_6, 282 MHz)

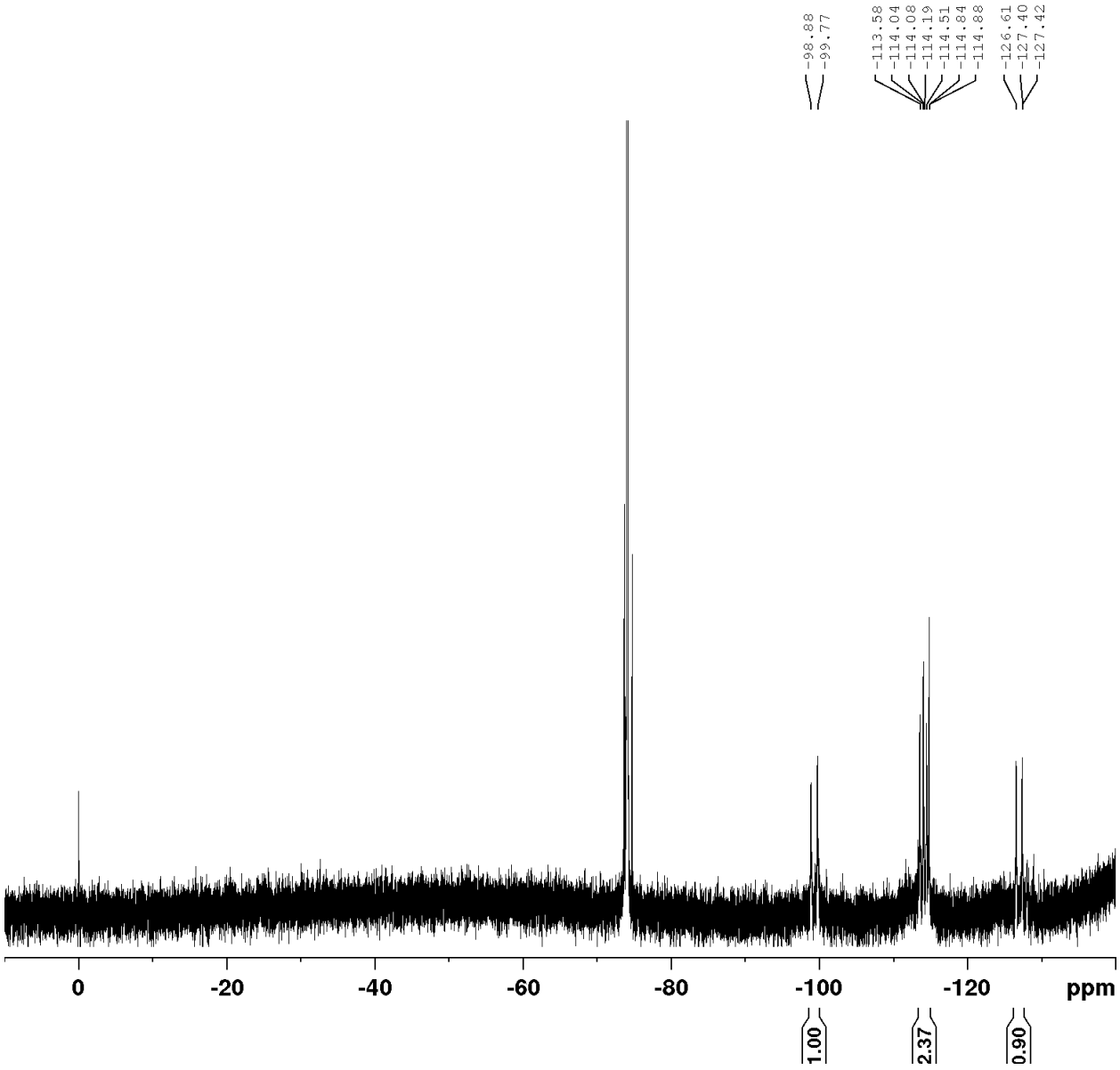

Spectrum 4.7.137 HMBC Spectrum of Polycycle **43** (DMSO-d_6)

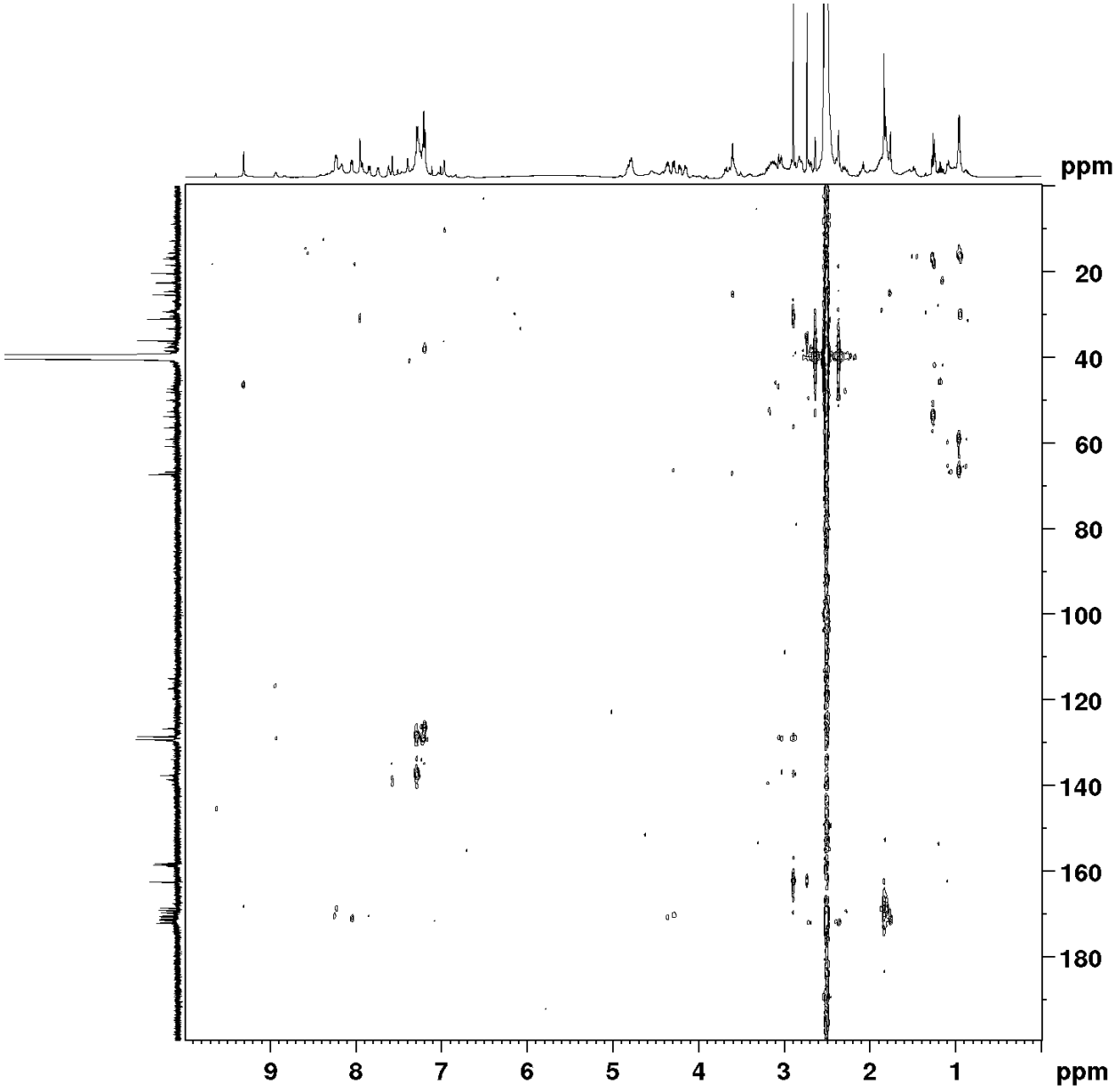

Spectrum 4.7.138 HSQC Spectrum of Polycycle **43** (DMSO-d_6)

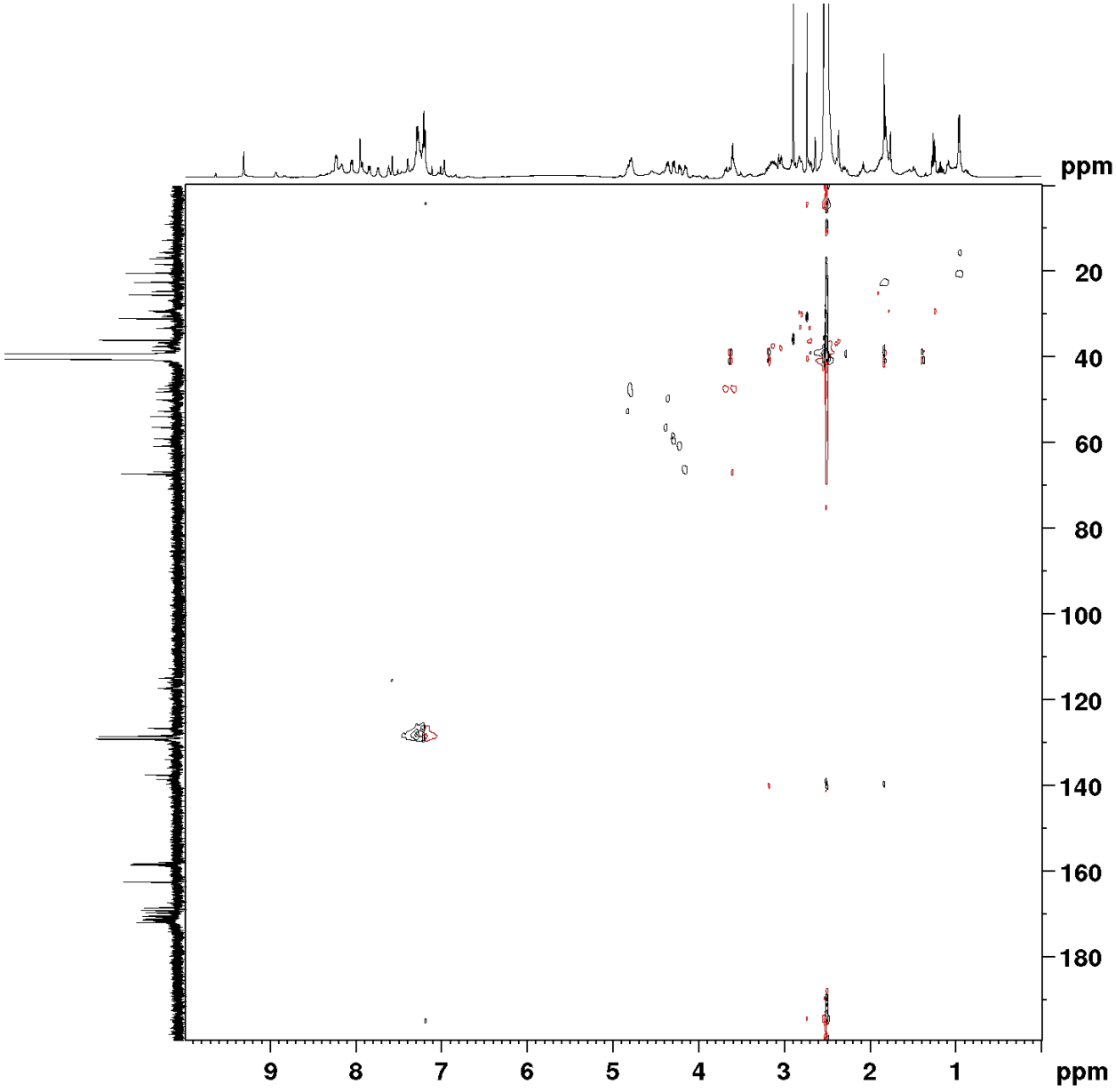

Spectrum 4.7.139 COSY Spectrum of Polycycle **43** (DMSO-d_6)

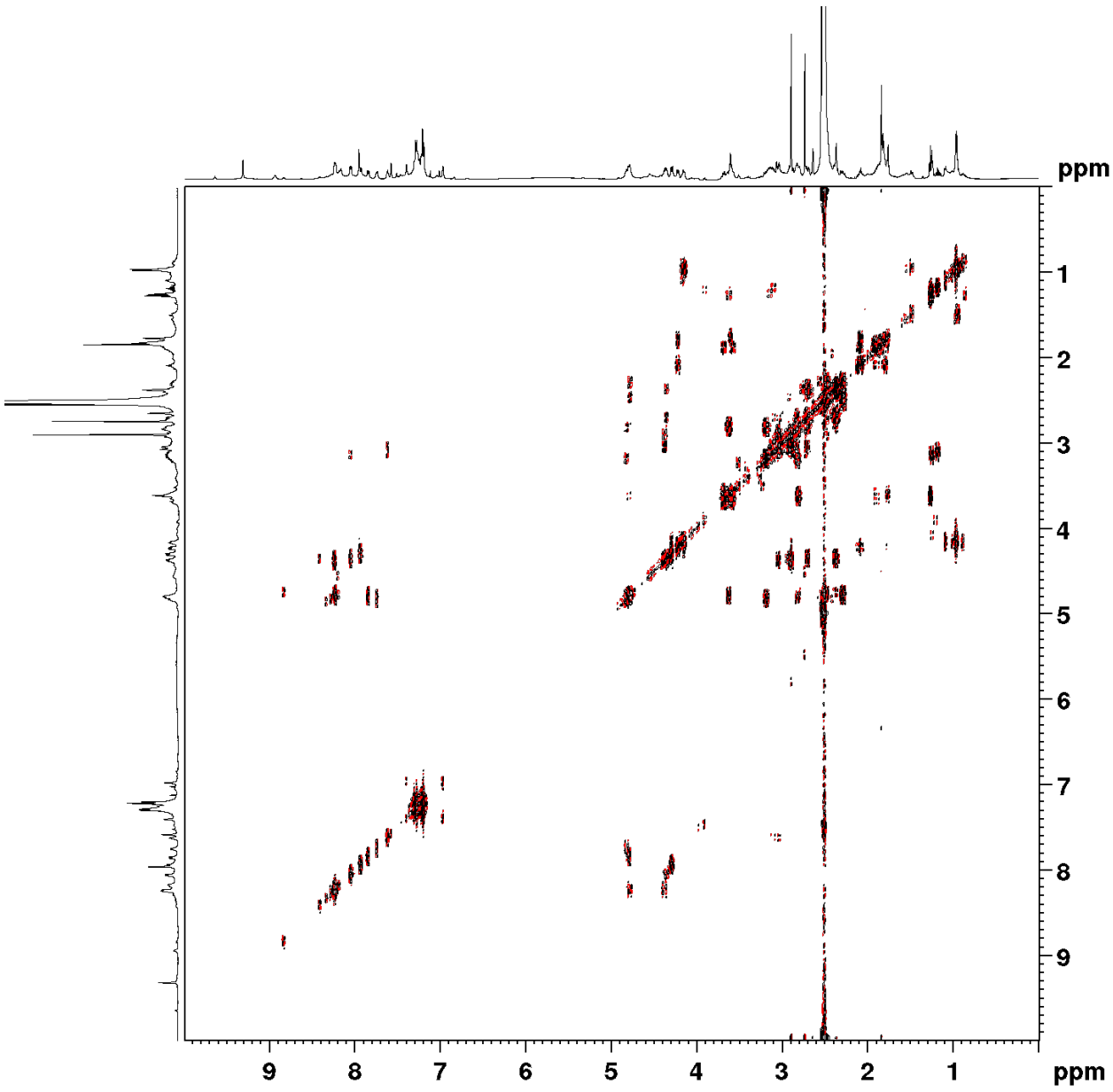

Table 4.7.21 Polycycle **43** (DMSO-d_6)

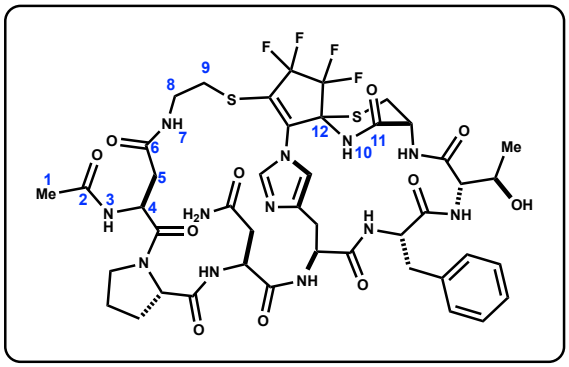

	13C	1H	Key Correlation
1		1.83 (s, 3H)	HSQC
2	168.93	-	1->2 HMBC
3	-	8.22 (m, 1H) overlap	2->3 HMBC
4	47.82	4.78 (m, 1H) overlap	3->4 COSY, HSQC
5	38.24	2.69 (dd, J = 10.3, 4.6 Hz, 1H), 2.29 (dd, J = 15.2, 9.0 Hz, 1H)	4->5 COSY, HSQC
6	171.85	-	5->6 HMBC
7	-	7.61 (t, J = 4.8 Hz, 1H)	6->7 HMBC
8	37.35	3.10 (m, 1H), 3.04 (m, 1H) overlap	7->8 COSY, HSQC
9	28.97	2.07 (m, 1H), 1.77 (m, 1H) overlap	8->9 HMBC, HSQC
10	-	9.31 (s, 1H)	11->10 HMBC
11	168.36	-	10->11 HMBC
12	67.3–67.5 (m, 1C)	-	10->12 HMBC

Spectrum 4.7.140 ^{1}H-NMR of Polycycle **44** (DMSO-d_6, 500 MHz)

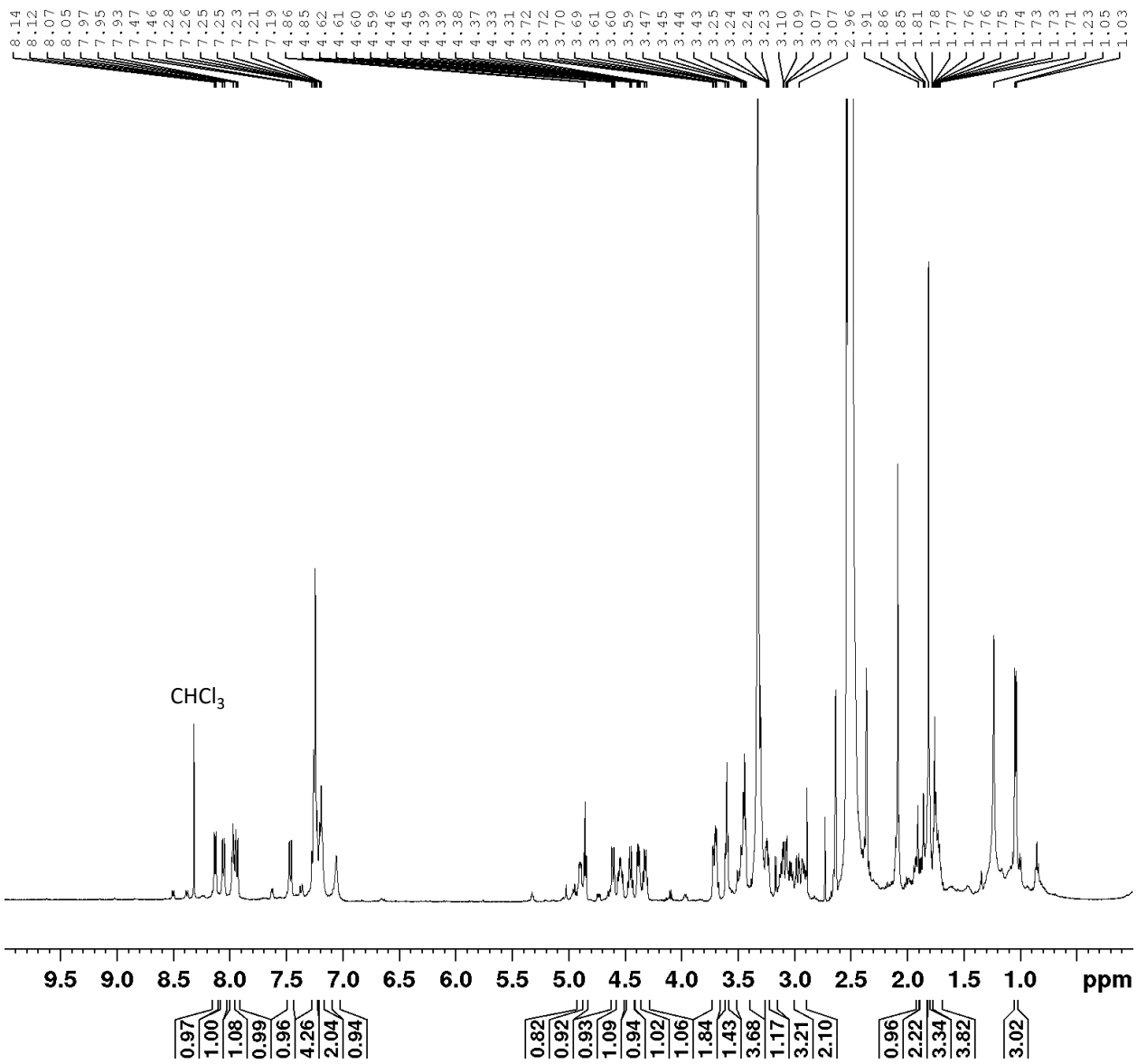

Spectrum 4.7.141 ^{13}C-NMR of Polycycle **44** (DMSO-d_6, 126 MHz)

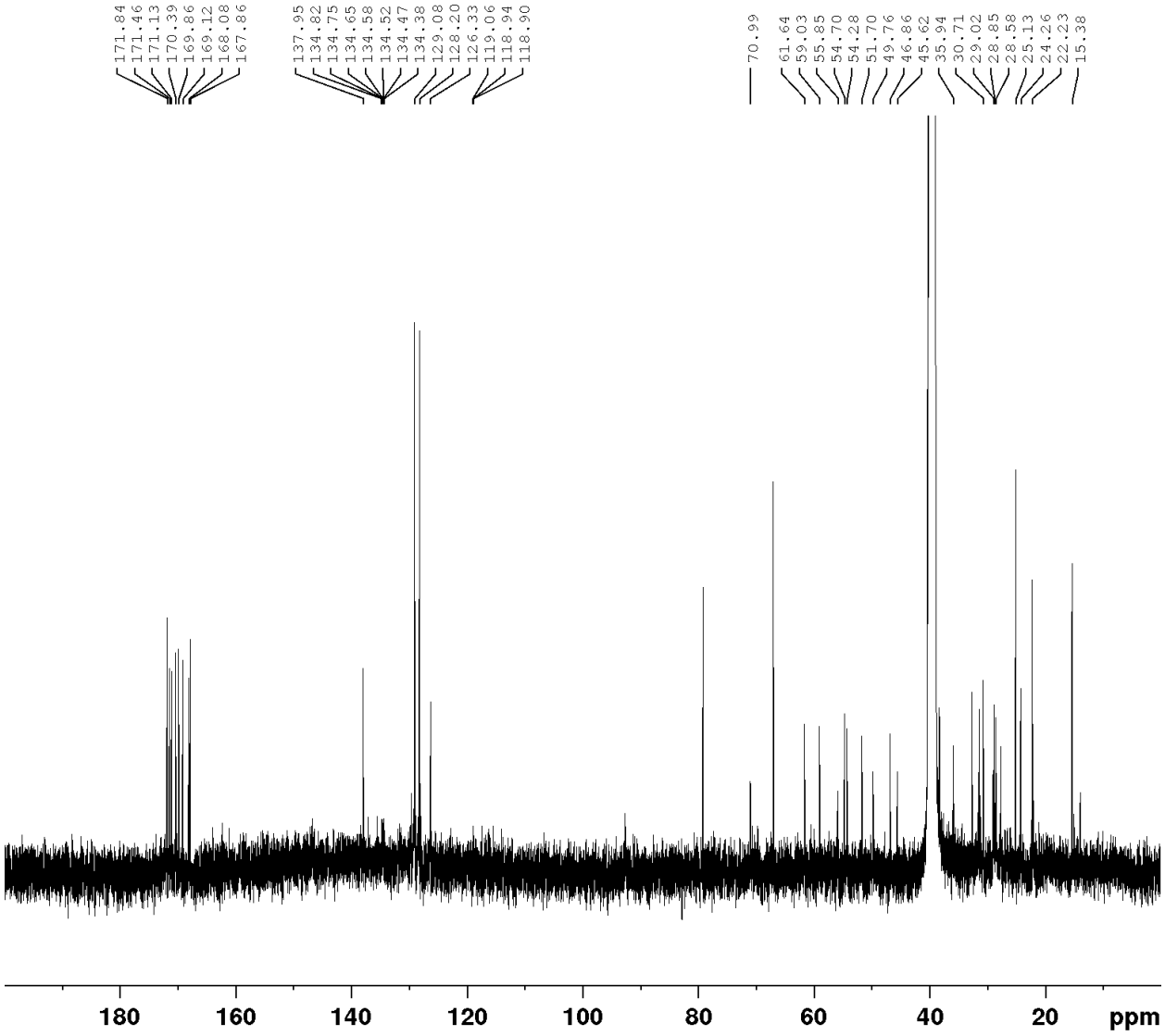

Spectrum 4.7.142 ^{19}F-NMR of Polycycle **44** (DMSO-d_6, 282 MHz)

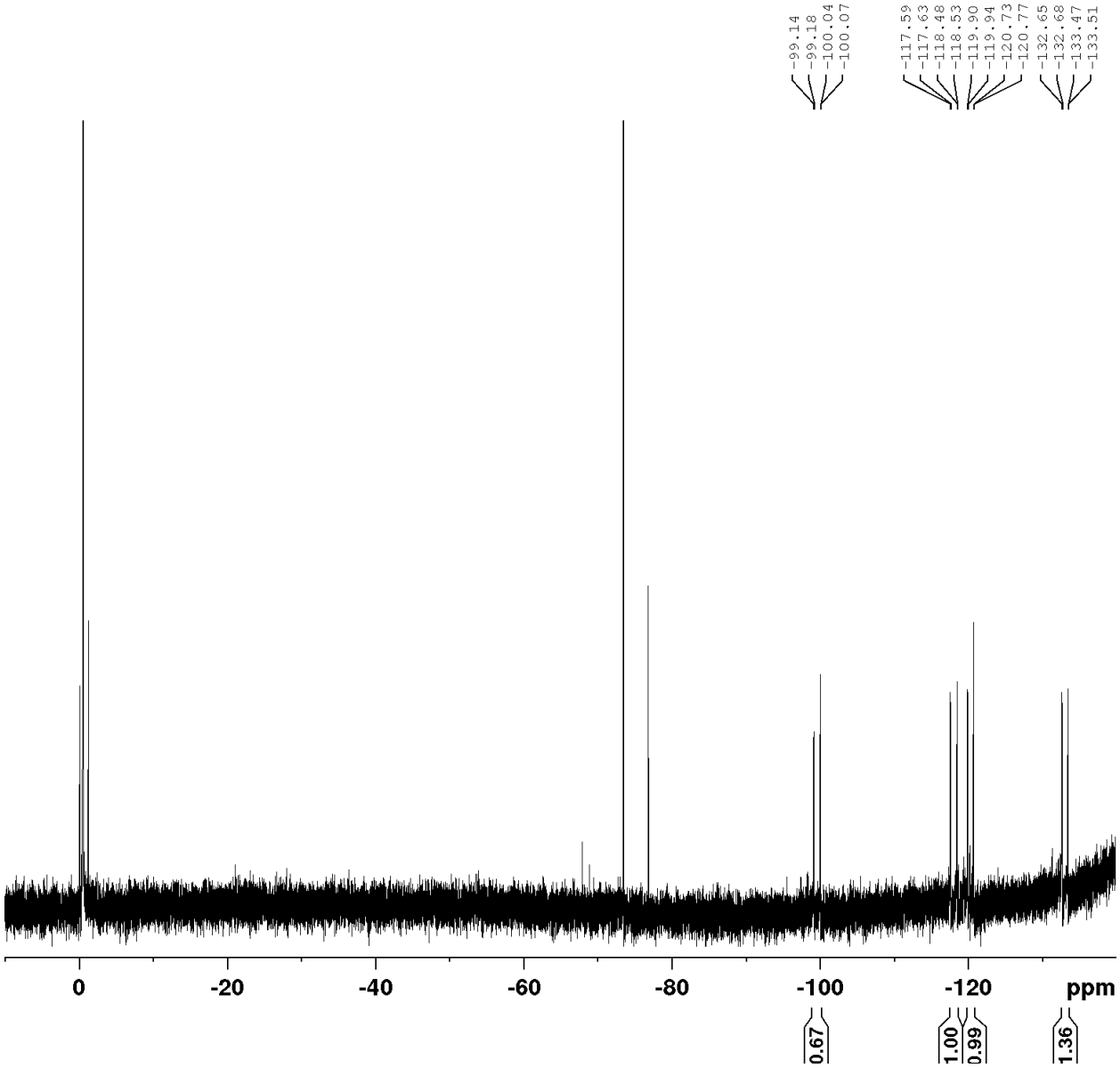

Spectrum 4.7.143 HMBC Spectrum of Polycycle **44** (DMSO-d_6)

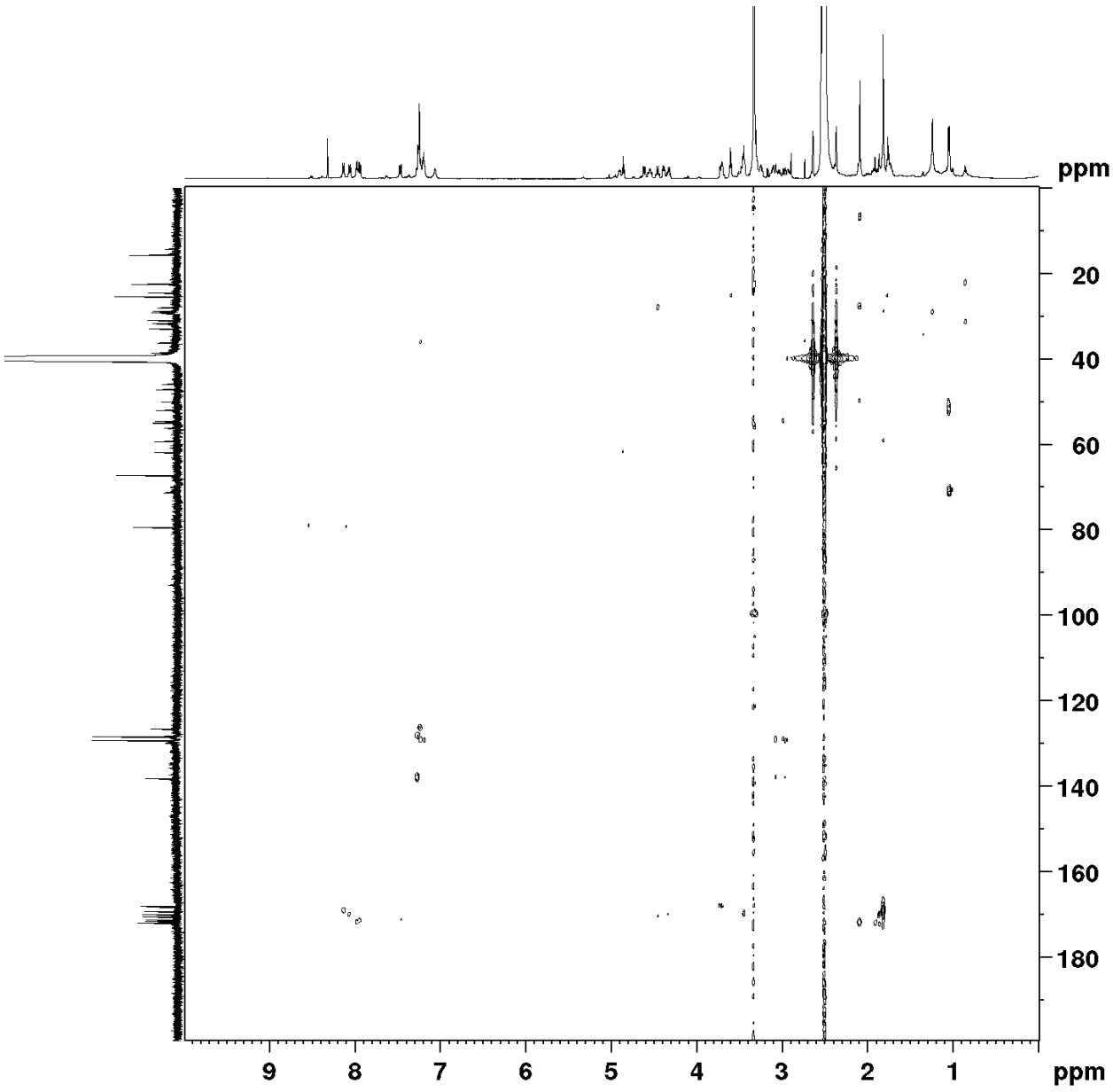

Spectrum 4.7.144 HSQC Spectrum of Polycycle **44** (DMSO-d_6)

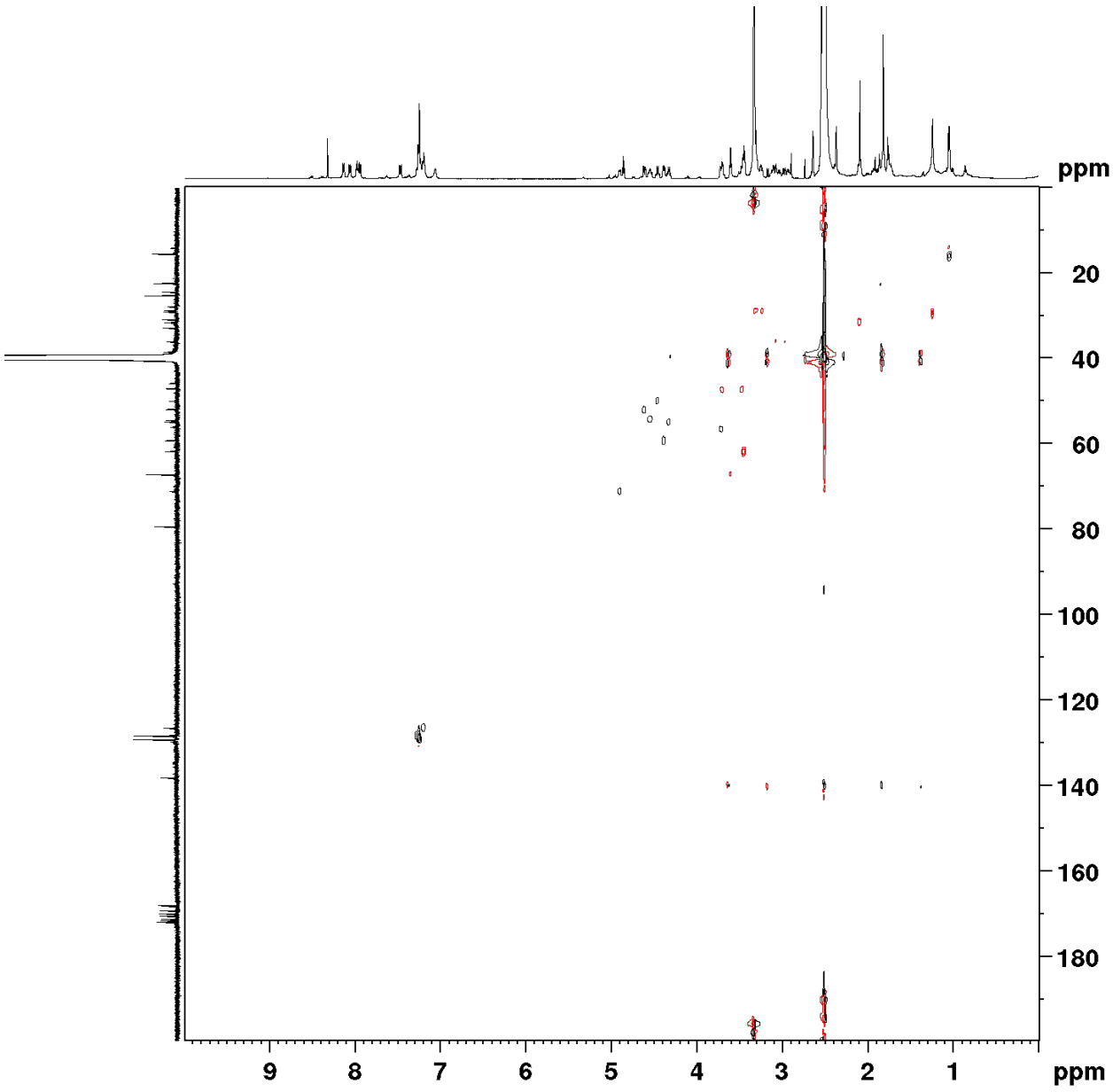

Spectrum 4.7.145 COSY Spectrum of Polycycle **44** (DMSO-d_6)

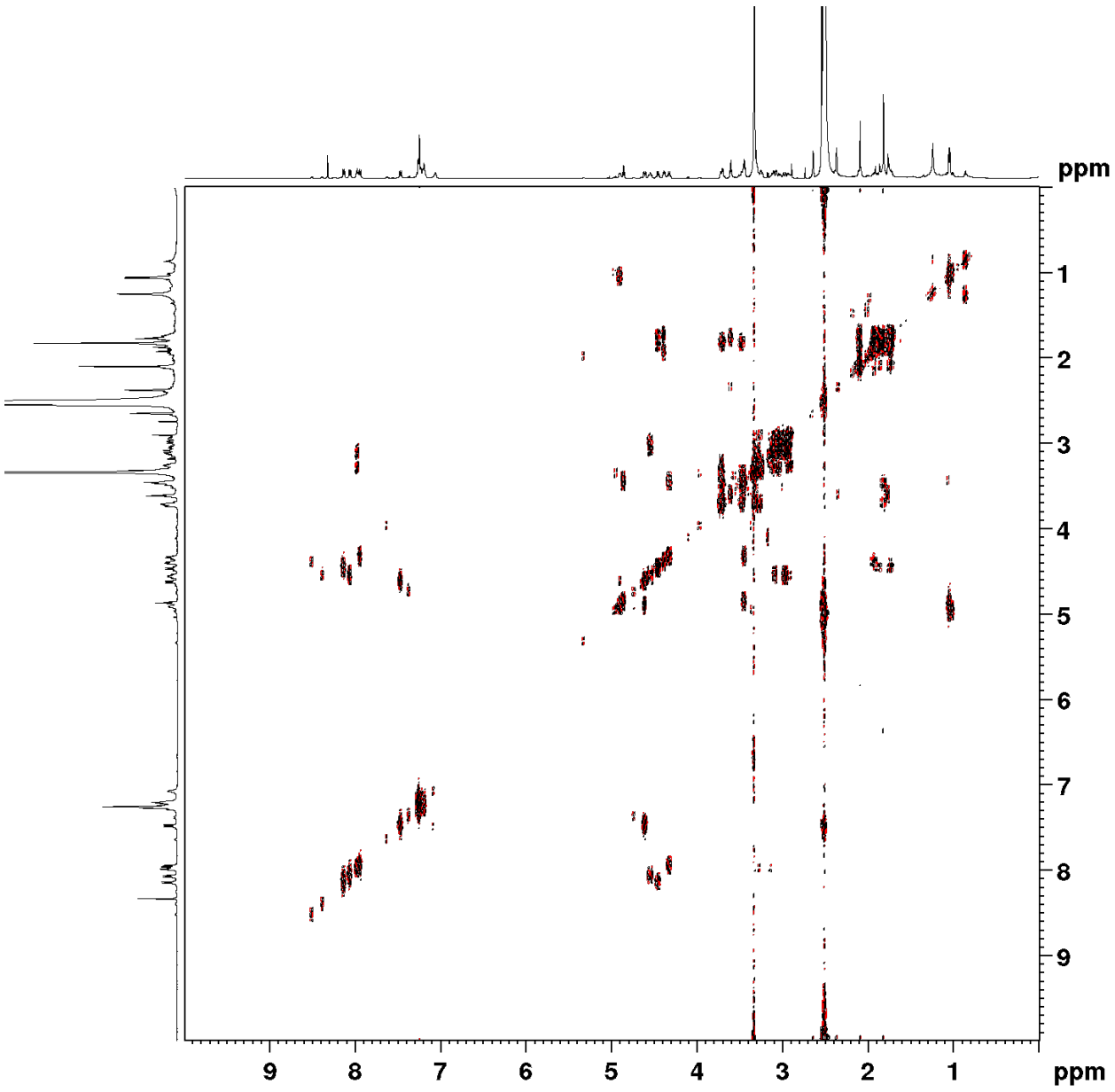

Table 4.7.22 Polycycle **44** (DMSO-d_6)

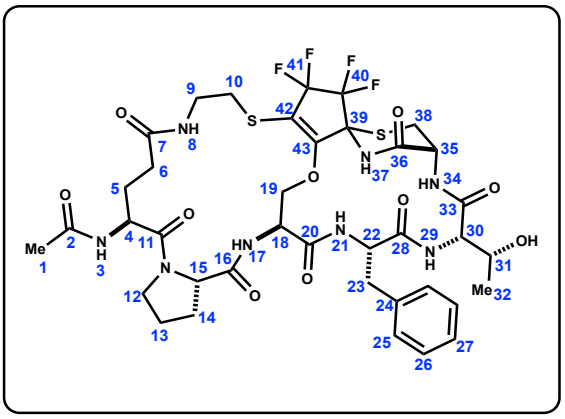

	13C	1H	Key Correlation
1	25.13	1.81 (s, 3H)	HSQC
2	169.13	-	1->2 HMBC
3	-	8.13 (d, J = 7.5 Hz, 1H)	2->3 HMBC
4	49.77	4.45 (q, J = 7.3 Hz , 1H)	3->4 COSY, HSQC
5	29.02	1.86 (m, 1H), 1.72 (overlap, 1H), overlap	4->5 COSY, HSQC
6	30.71	3.09 (m, 1H), 2.97 (m, 1H) overlap	7->6 HMBC, HSQC
7	171.86	-	8->7 HMBC
8	-	7.93 (t, J = 5.6 Hz, 1H)	7->8 HMBC
9	28.58	3.10 (m, 1H), 3.25 (m, 1H) overlap	8->9 COSY, HSQC
10	28.86	1.86 (m, 1H), 1.71 (m, 1H) overlap	8->9 HMBC, HSQC
11	170.39	-	4->11 HMBC
12	46.86	3.69 (m, 1H), 3.47 (m, 1H) overlap	14->12 HMBC, HSQC
13	22.23	1.84 (m, 1H), 1.76 (m, 1H) overlap	14->13 COSY, HSQC
14	45.61	3.70 (m, 1H), 3.45 (m, 1H) overlap	15->14 HMBC, HSQC
15	55.86	4.85 (t, J = 5.5 Hz, 1H)	16->15 HMBC, HSQC
16	171.47	-	17->16 HMBC
17	-	7.94 (d, J = 8.2 Hz,1H)	18->17 HMBC
18	54.70	4.32 (m, 1H)	20->18 HMBC
19	61.64	3.44 (m, 2H)	18->19 COSY, HSQC
20	169.87	-	21->20 HMBC
21	-	8.06 (d, J = 8.4 Hz, 1H)	22->21 COSY
22	54.28	4.54 (td, J = 8.8, 3.3 Hz, 1H)	23->22 COSY, HSQC
23	35.94	3.08 (m, 1H), 2.96 (m, 1H)	24->23 HMBC, HSQC
24	137.96	-	25, 26 ->24 HMBC
25	129.08	7.28–7.23 (m, 2H)	HSQC
26	128.20	7.28–7.23(m, 2H)	HSQC
27	126.33	7.21–7.19 (m, 1H)	HSQC
28	171.13	-	22->28 HMBC
29	-	7.47 (d, J = 9.3 Hz, 1H)	30->31 COSY
30	51.70	4.61 (dd, J = 9.4, 3.1 Hz, 1H)	31->30 COSY, HSQC
31	70.99	4.90 (dd, J = 6.3, 3.2 Hz, 1H)	32->31 COSY, HSQC
32	15.36	1.04 (d, J = 6.4 Hz, 3H)	HSQC
33	168.08	-	30->33 HMBC
34	-	-	-
35	59.03	4.38 (dd, J = 8.2, 3.4 Hz, 1H)	36->35 COSY, HSQC
36	167.08	-	35->36 HMBC
37	-	7.06 (s, 1H)	-
38	24.26	1.90 (overlap, 1H), 1.73 (overlap, 1H)	35->38 COSY, HMBC, HSQC
39	70.7–70.6 (m, 1C)	-	-
40	119.1–118.9 (m, 1C)	-	-
41	119.1–118.9 (m, 1C)	-	-
42	134.9–134.6 (m, 1C)	-	-
43	134.6–131.4 (m, 1C)	-	-

Spectrum 4.7.146 ^{1}H-NMR of Polycycle **45** (DMSO-d_6, 500 MHz)

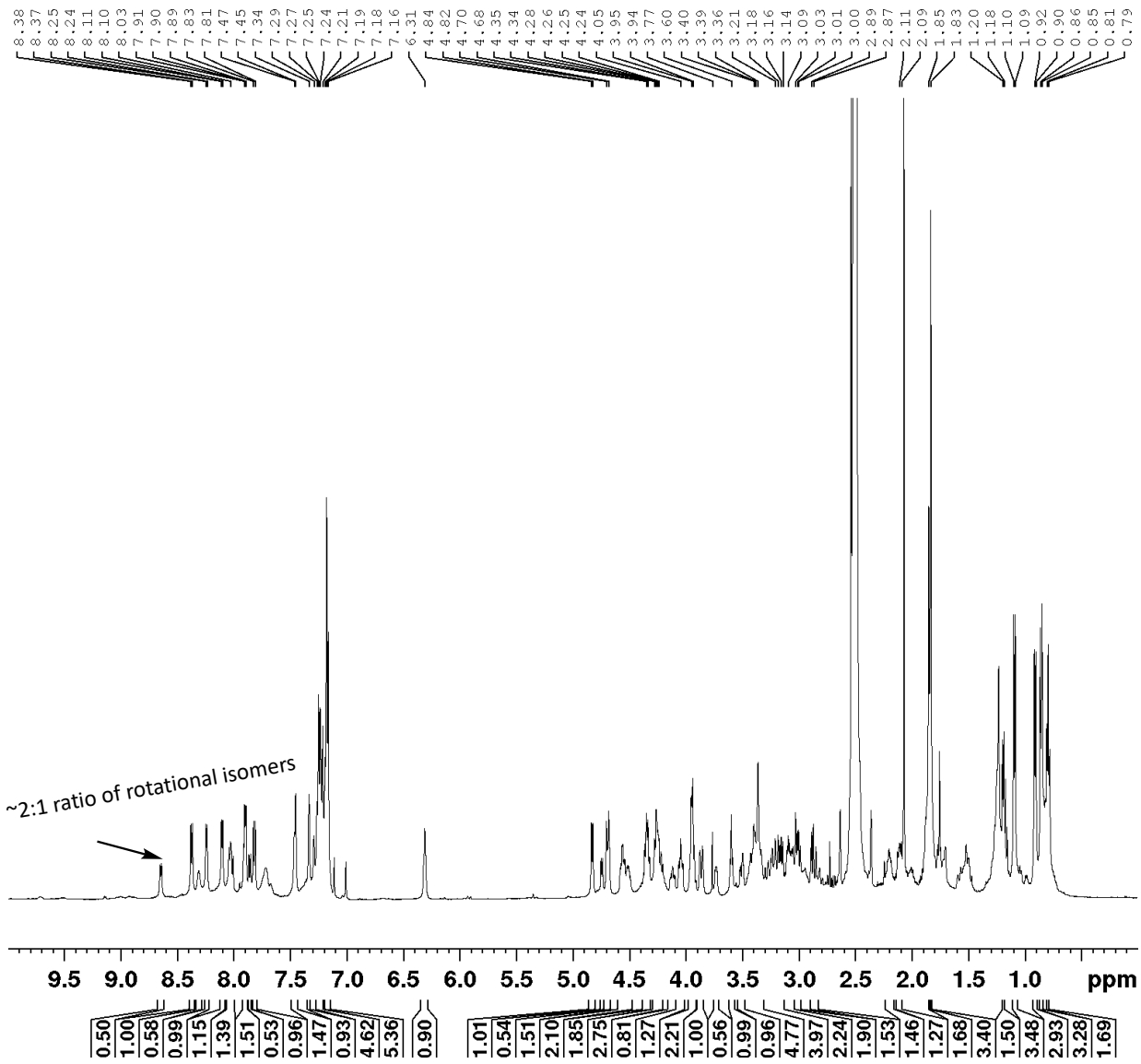

Spectrum 4.7.147 ^{13}C-NMR of Polycycle **45** (DMSO-d_6, 126 MHz)

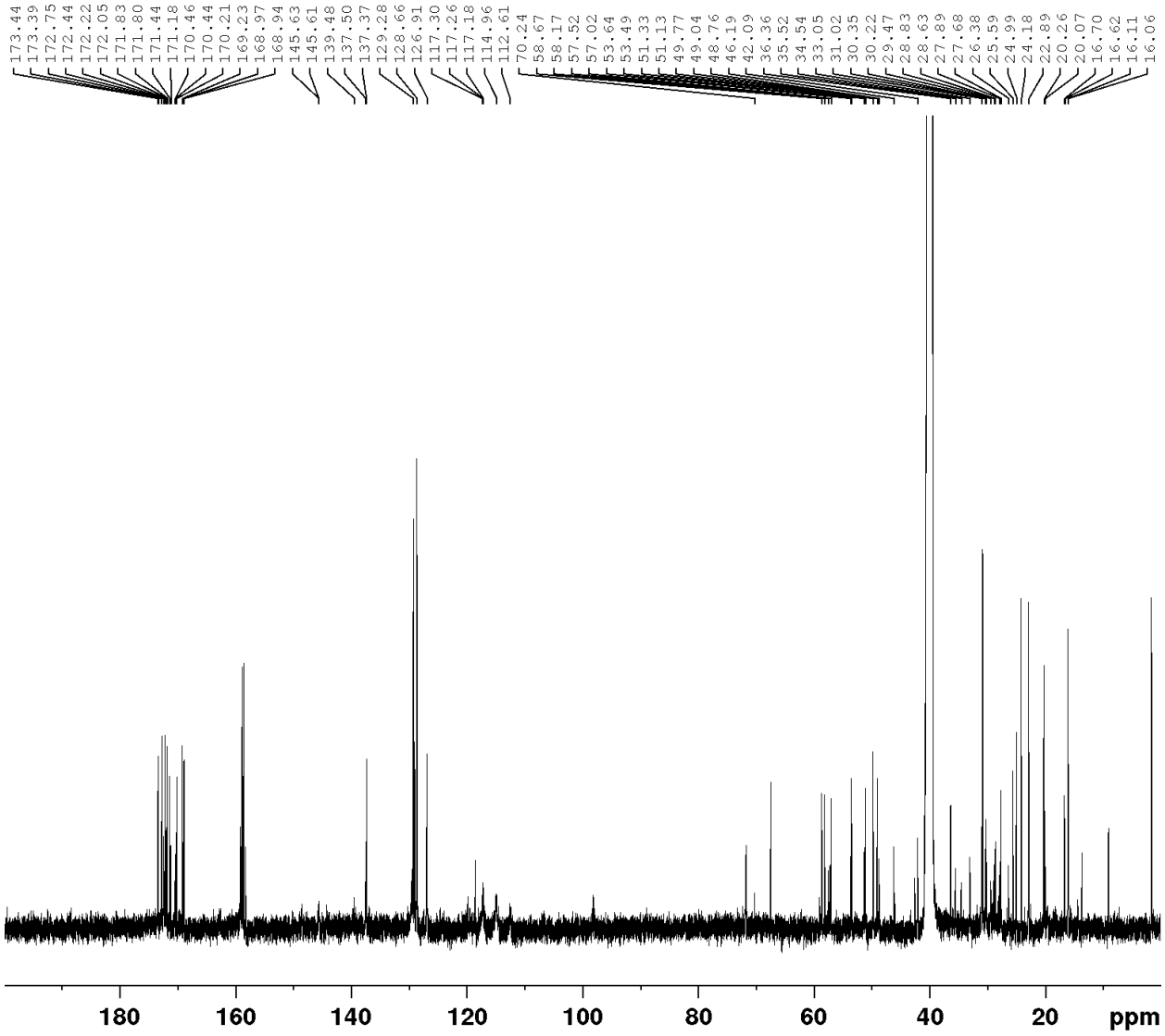

Spectrum 4.7.148 ^{19}F-NMR of Polycycle **45** (DMSO-d_6, 565 MHz)

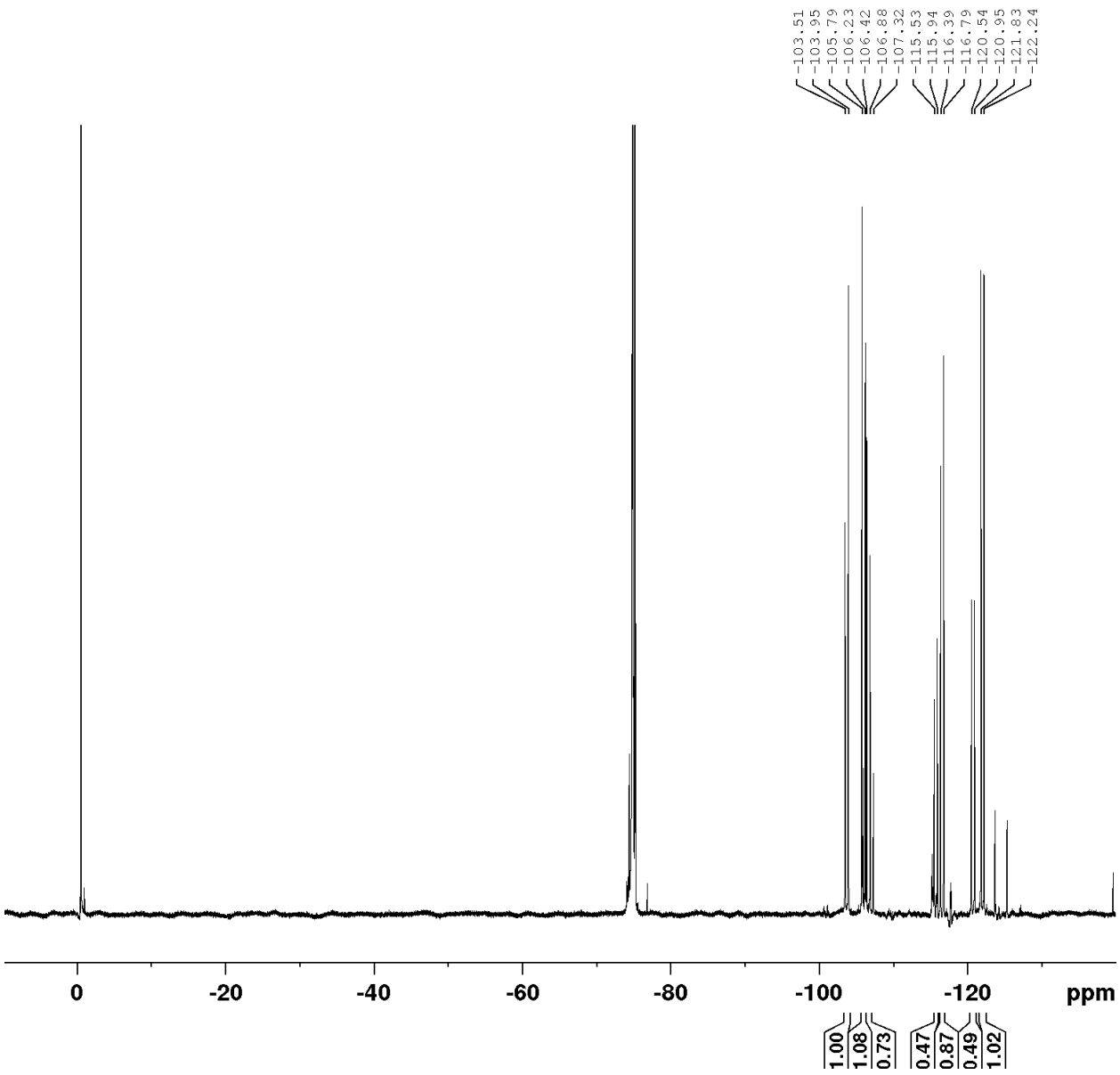

Spectrum 4.7.149 HMBC of Polycycle **45** (DMSO-d_6)

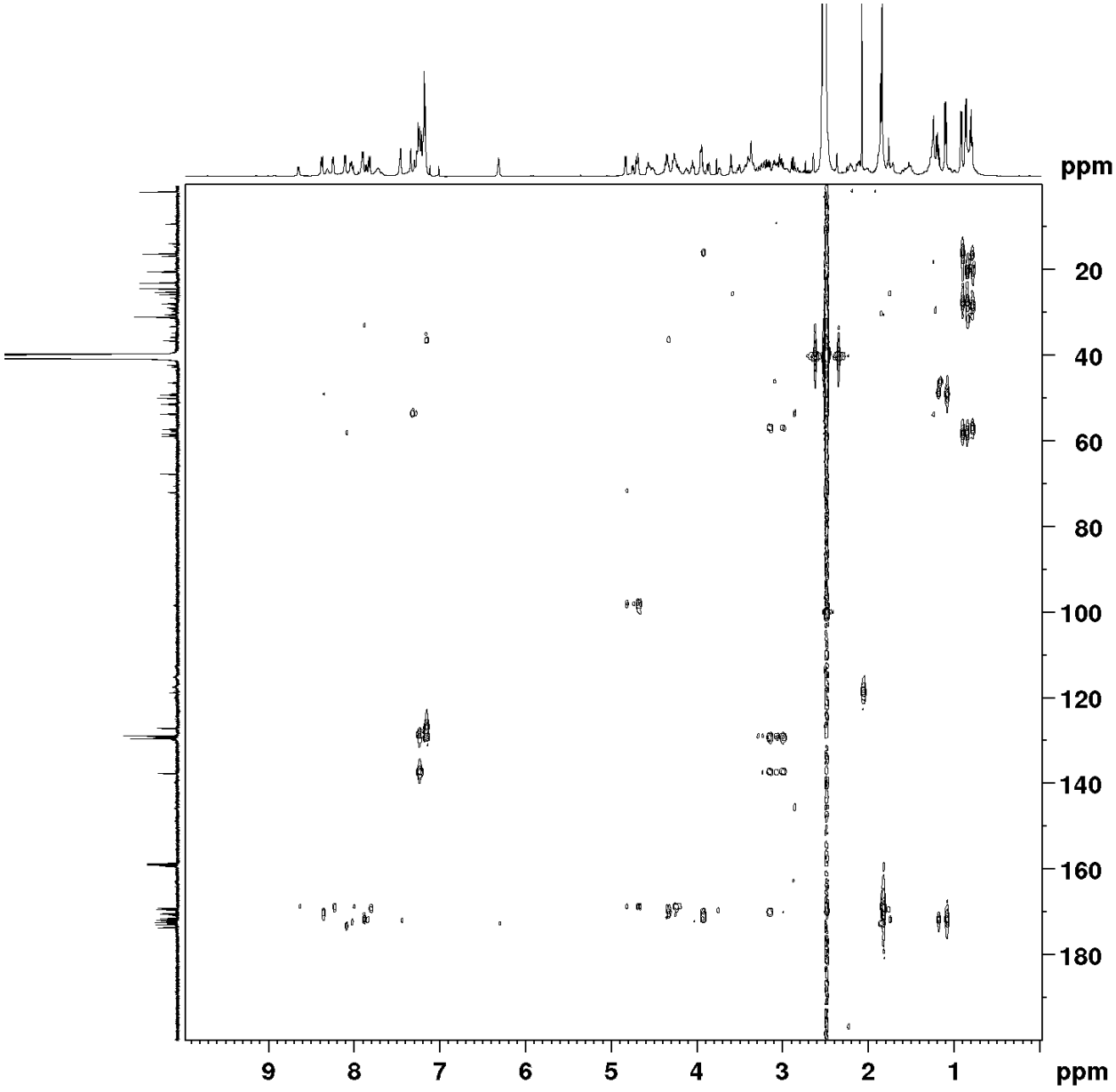

Spectrum 4.7.150 HSQC of Polycycle **45** (DMSO-d_6)

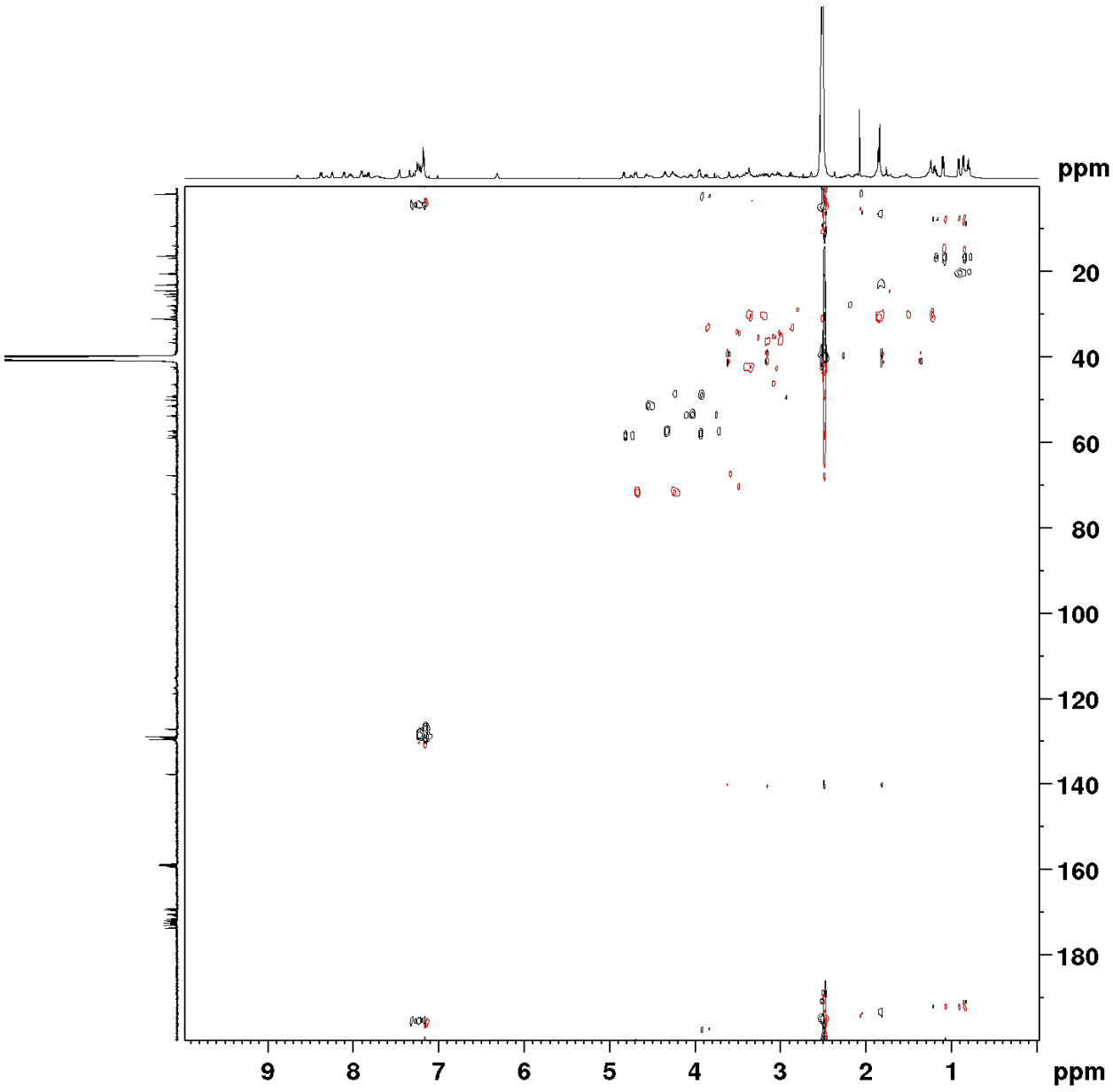

Spectrum 4.7.151 COSY of Polycycle **45** (DMSO-d_6)

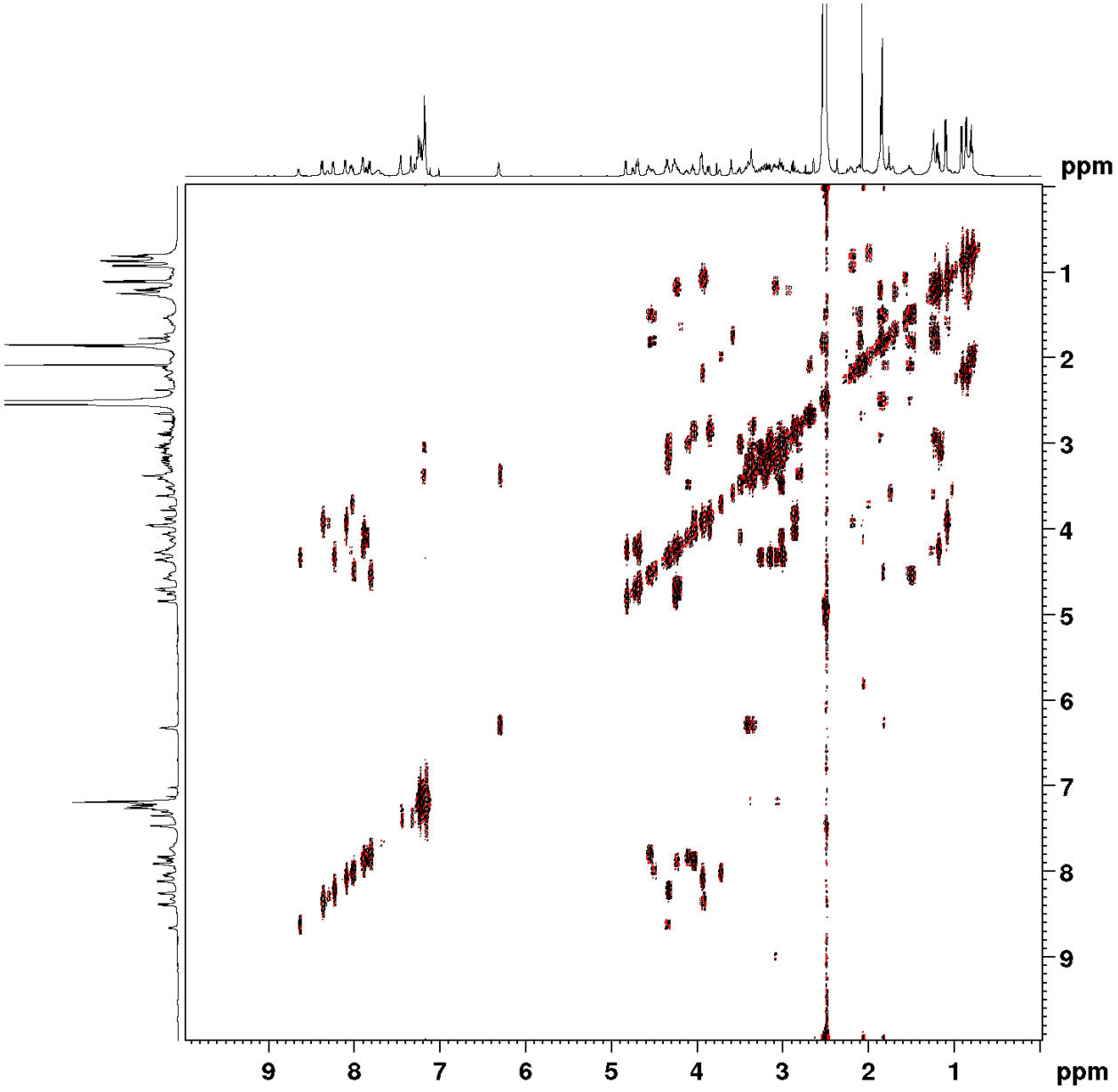

Spectrum 4.7.152 ^{1}H-NMR of Polycycle **46** (DMSO-d_6, 600 MHz)

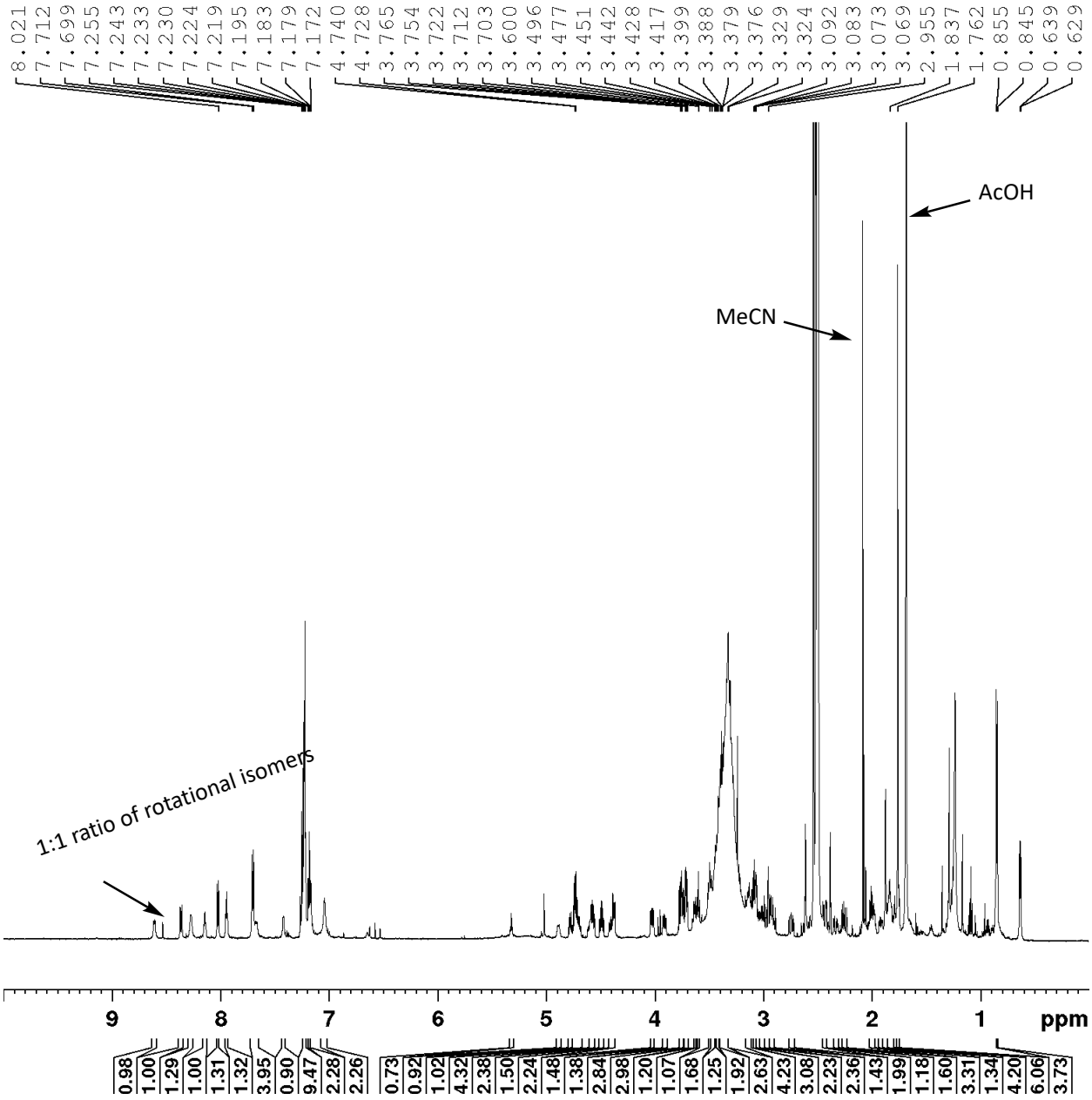

Spectrum 4.7.153 ^{13}C-NMR of Polycycle **46** (DMSO-d_6, 126 MHz)

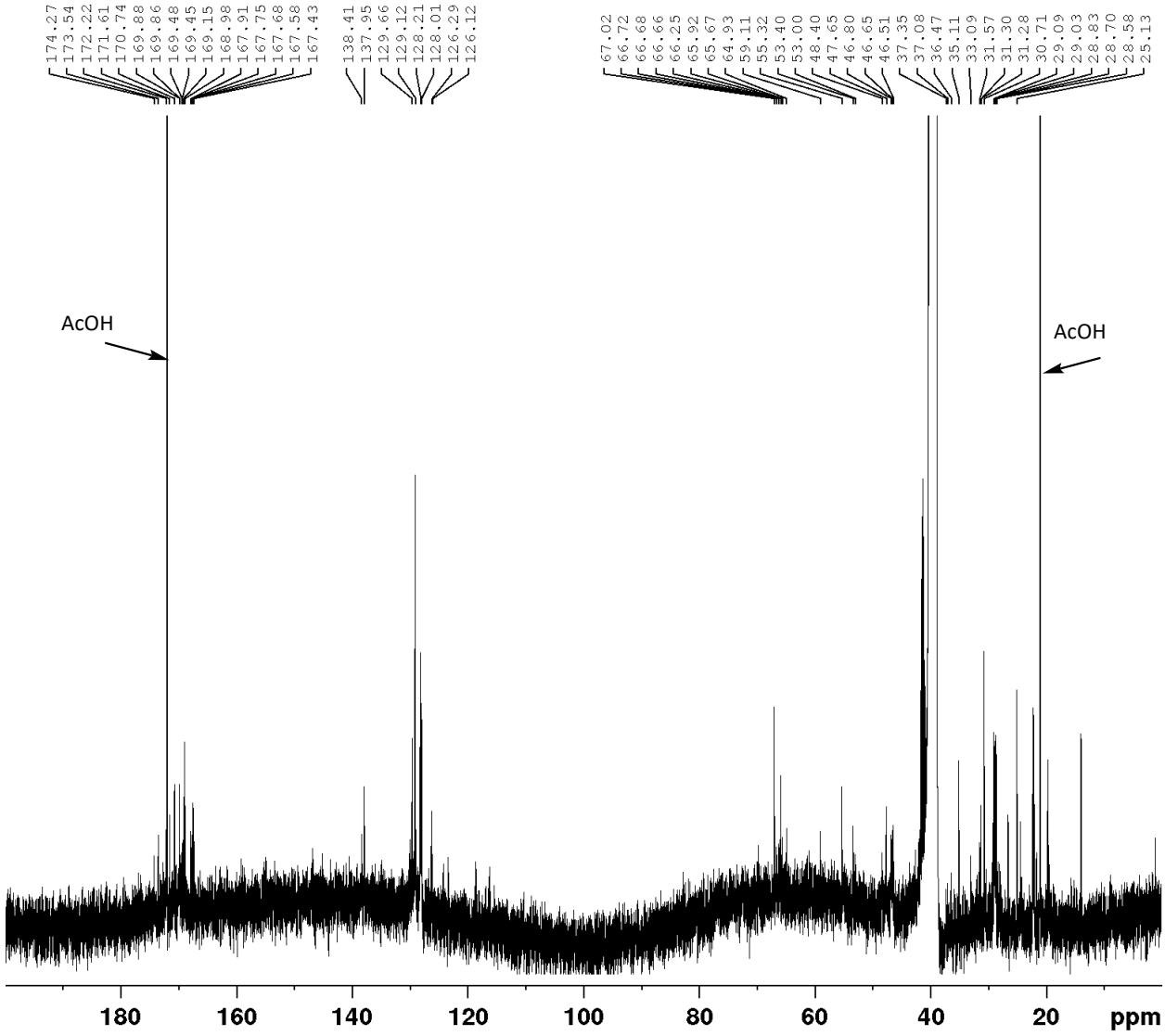

Spectrum 4.7.154 HSQC Spectrum of Polycycle **46** (DMSO-d_6)

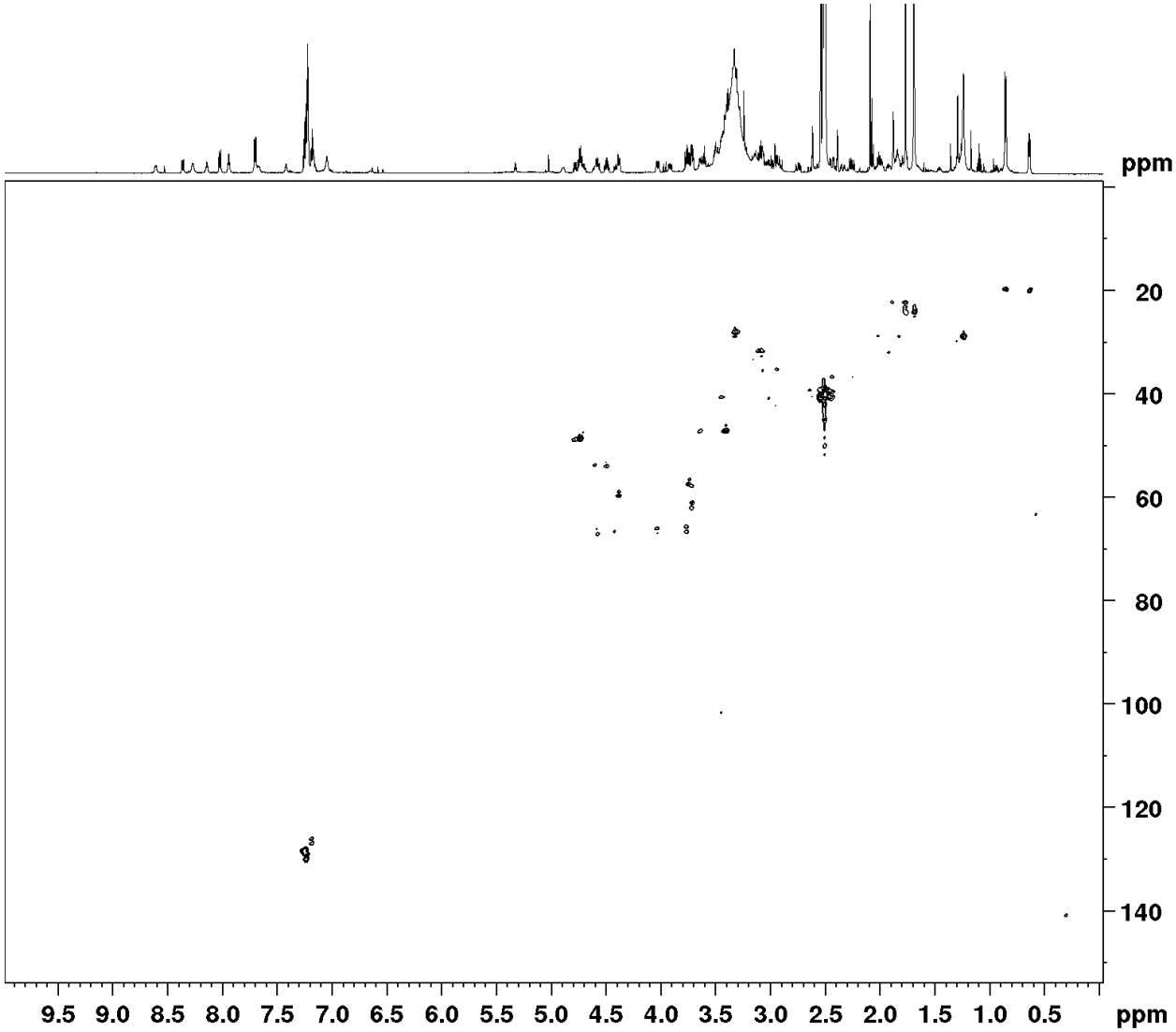

Spectrum 4.7.155 ^{1}H-NMR of Polycycle **47** (DMSO-d_6, 600 MHz)

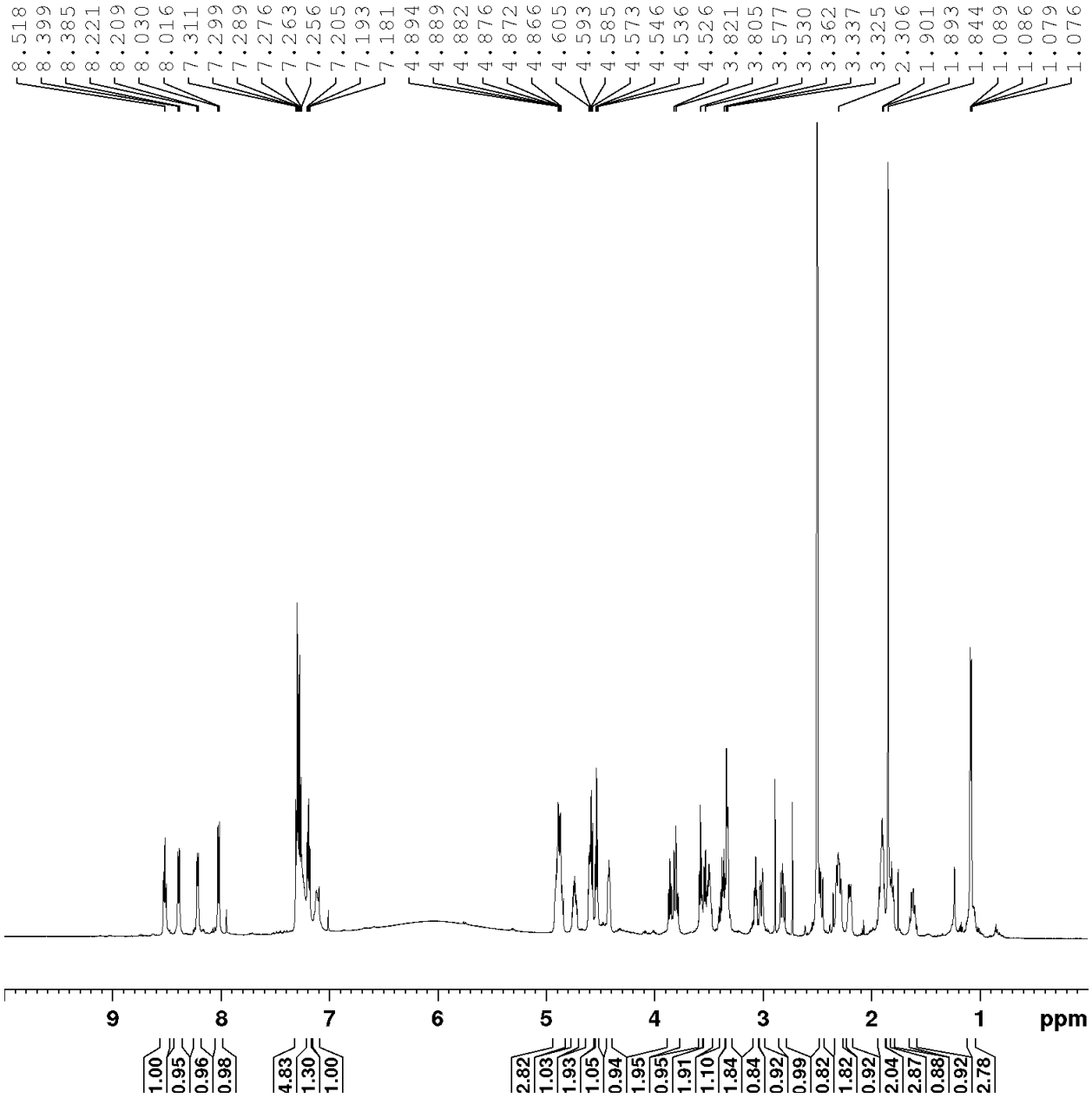

Spectrum 4.7.156 ^{13}C-NMR of Polycycle **47** (DMSO-d_6, 600 MHz)

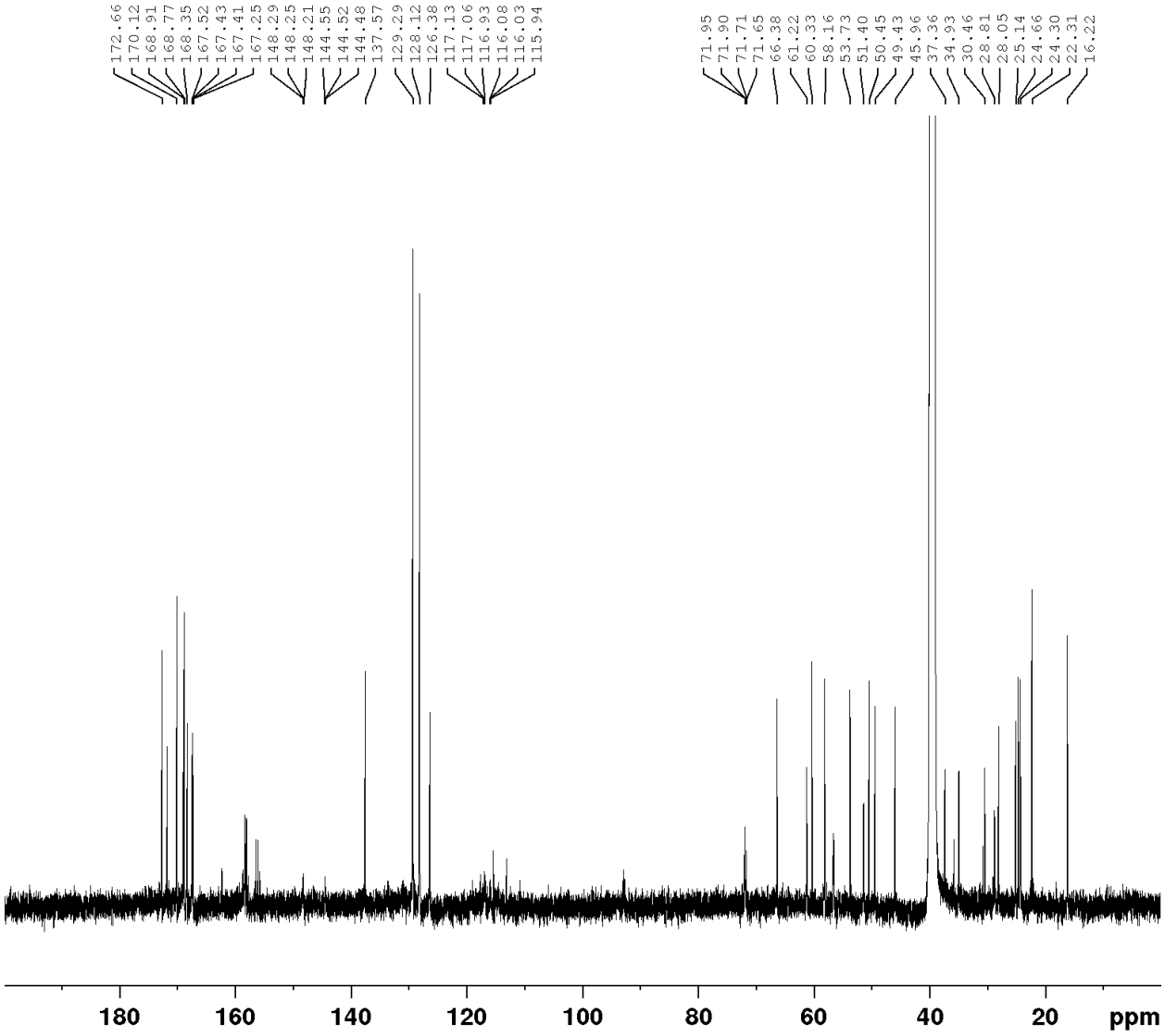

Spectrum 4.7.157 ^{19}F-NMR of Polycycle **47** (DMSO-d_6, 565 MHz)

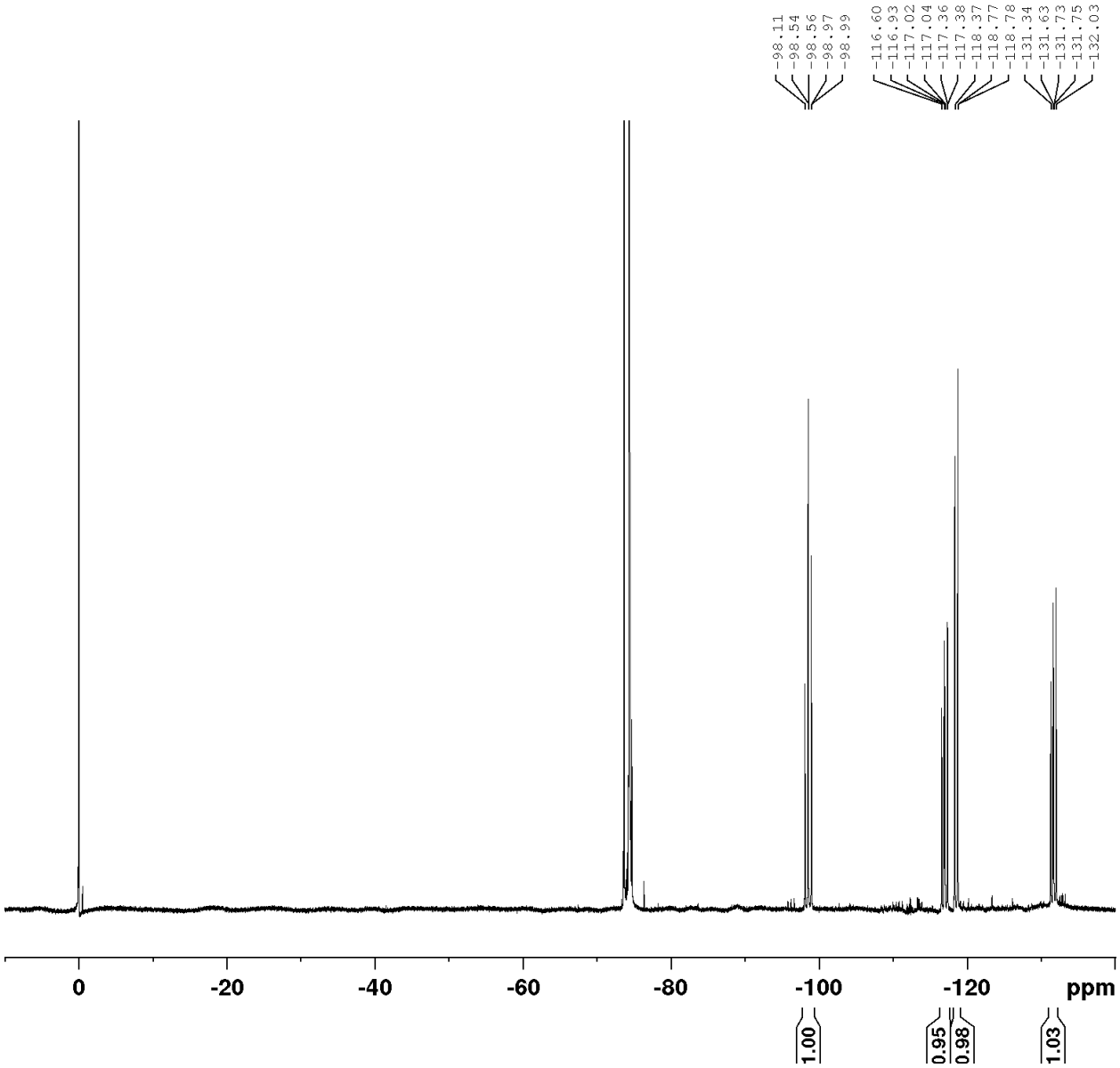

Spectrum 4.7.158 HMBC Spectrum of Polycycle **47** (DMSO-d_6)

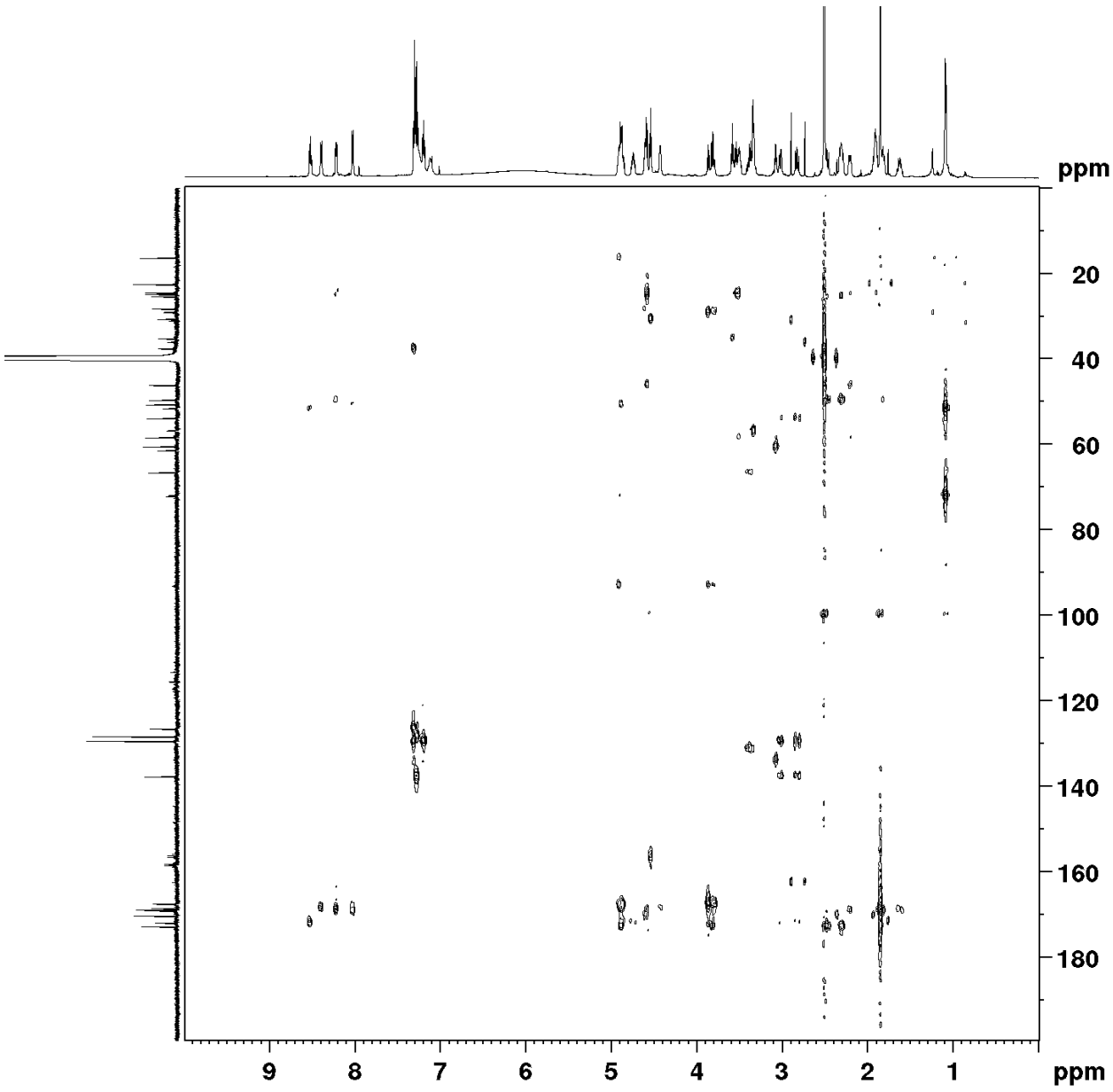

Spectrum 4.7.159 HSQC Spectrum of Polycycle **47** (DMSO-d_6)

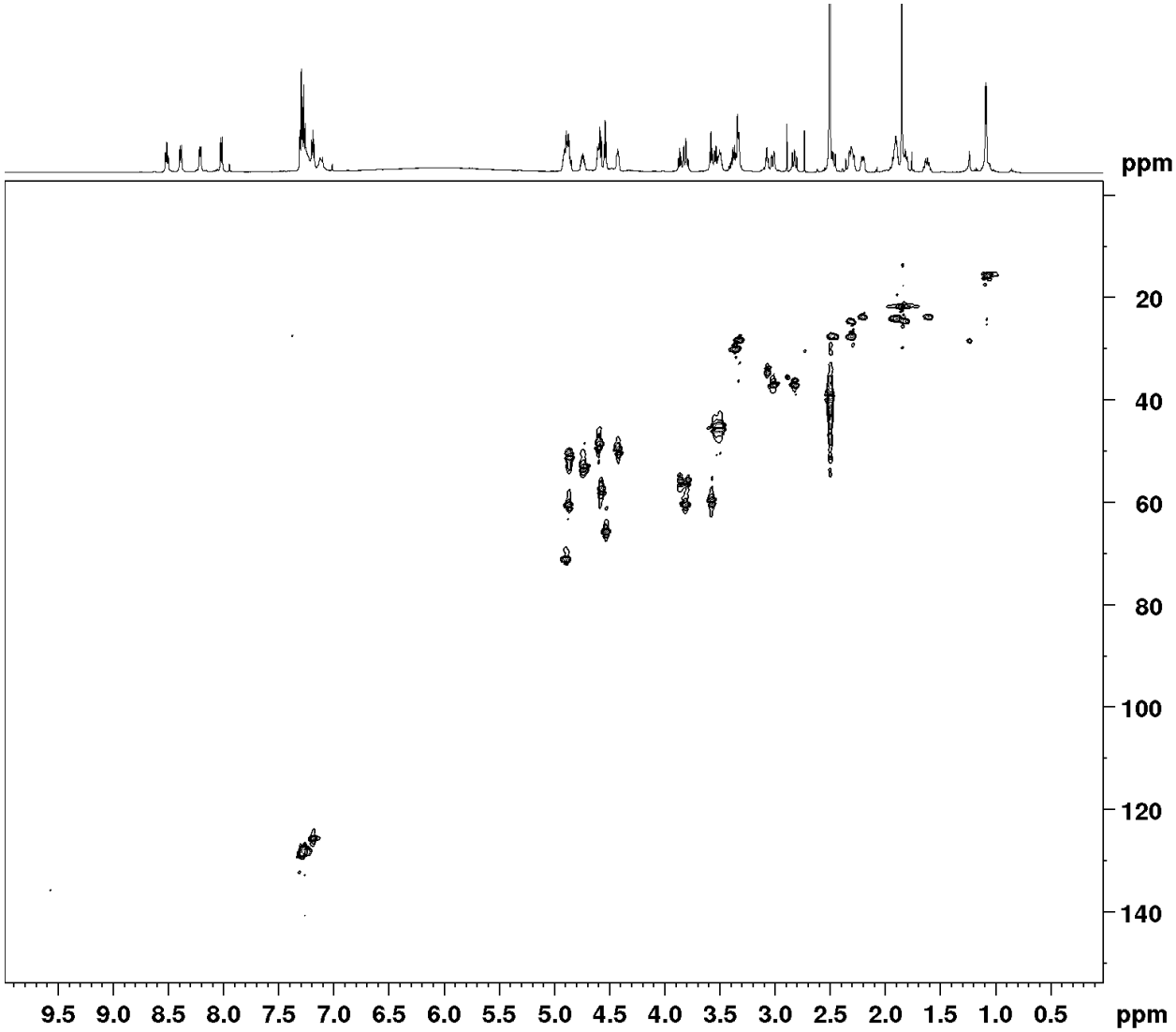

Spectrum 4.7.160 COSY Spectrum of Polycycle **47** (DMSO-d_6)

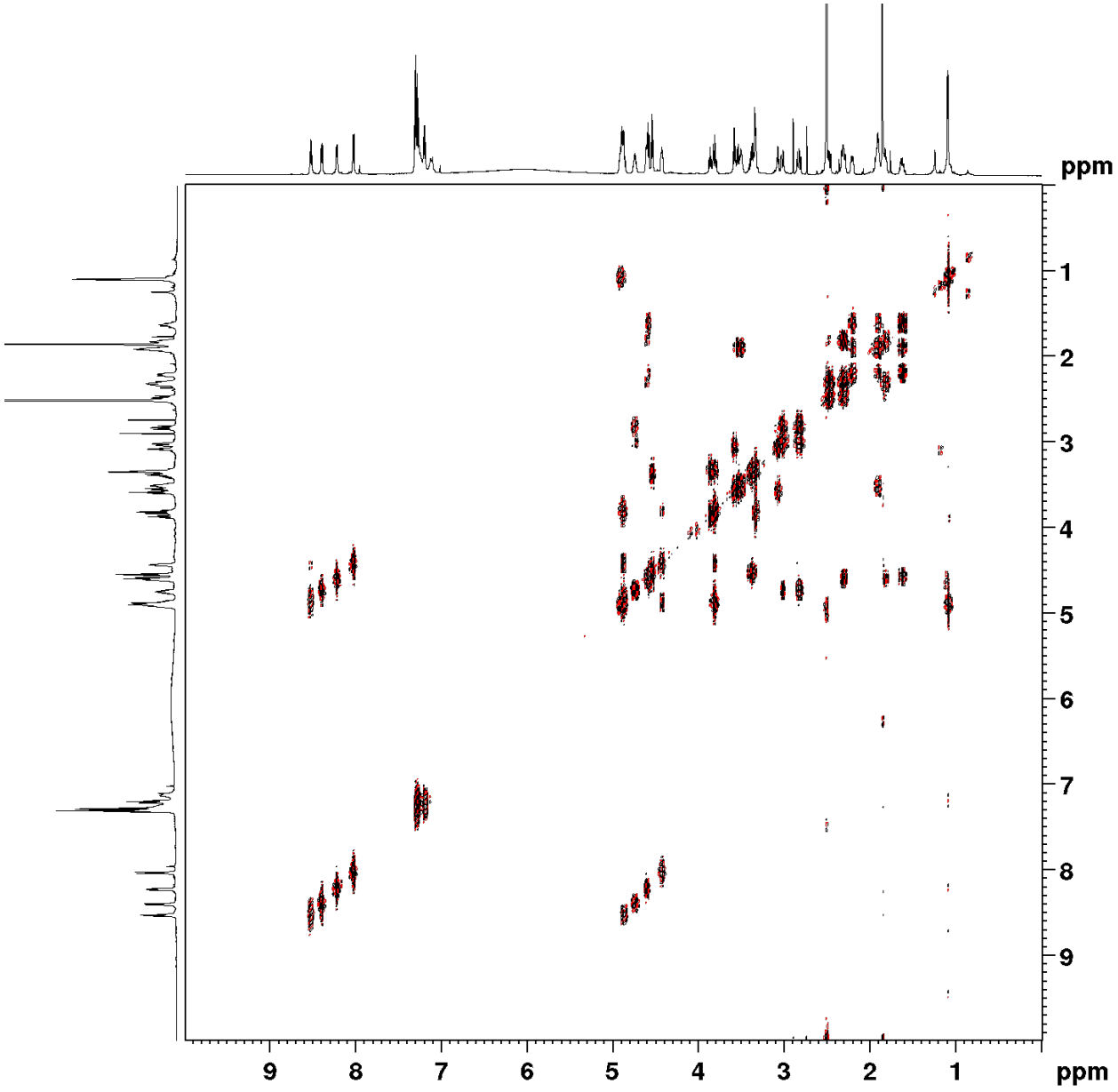

Spectrum 4.7.161 ^{1}H-NMR of Polycycle **48** (DMSO-d_6, 600 MHz)

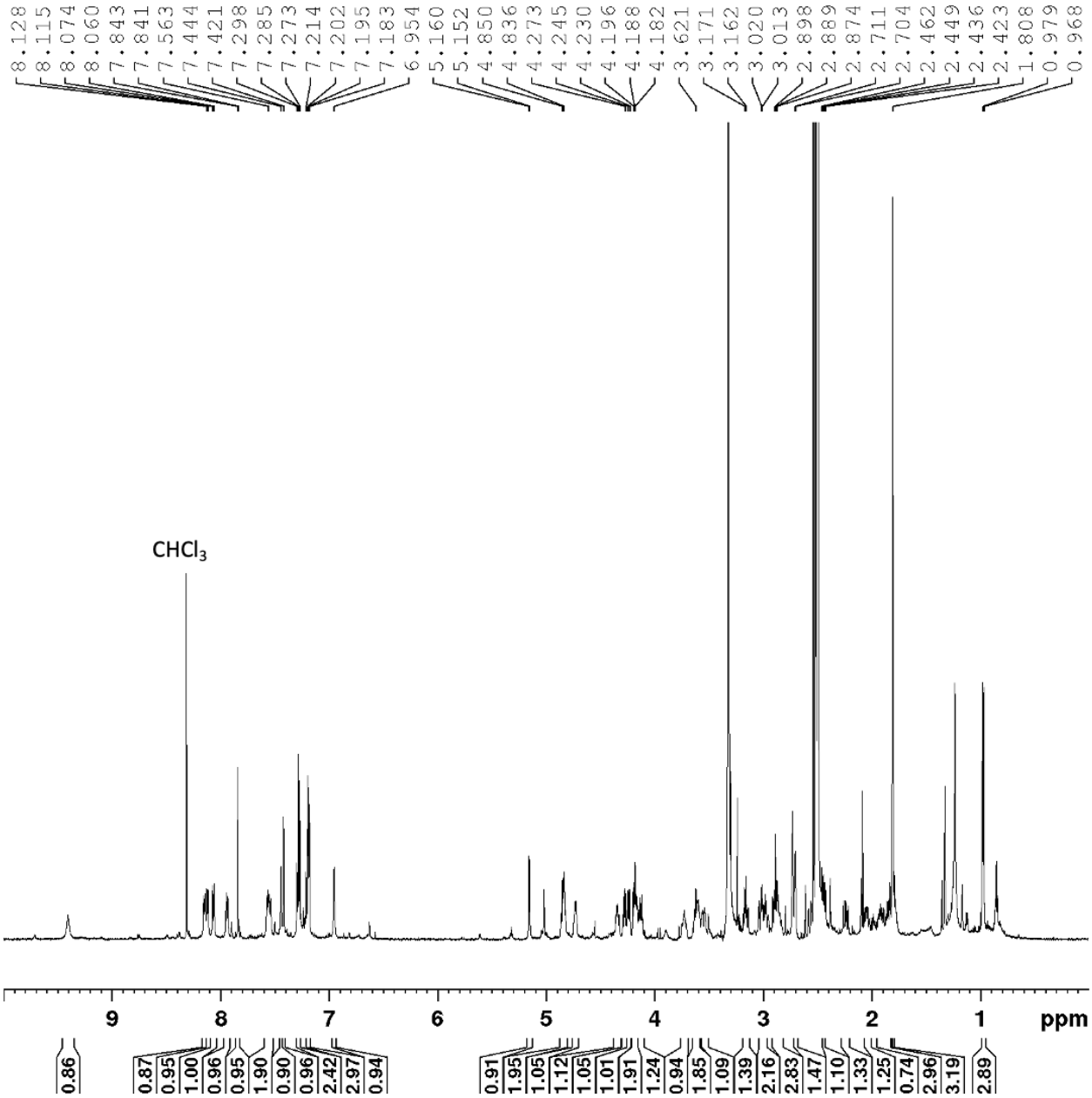

Spectrum 4.7.162 ^{13}C-NMR of Polycycle **48** (DMSO-d_6, 126 MHz)

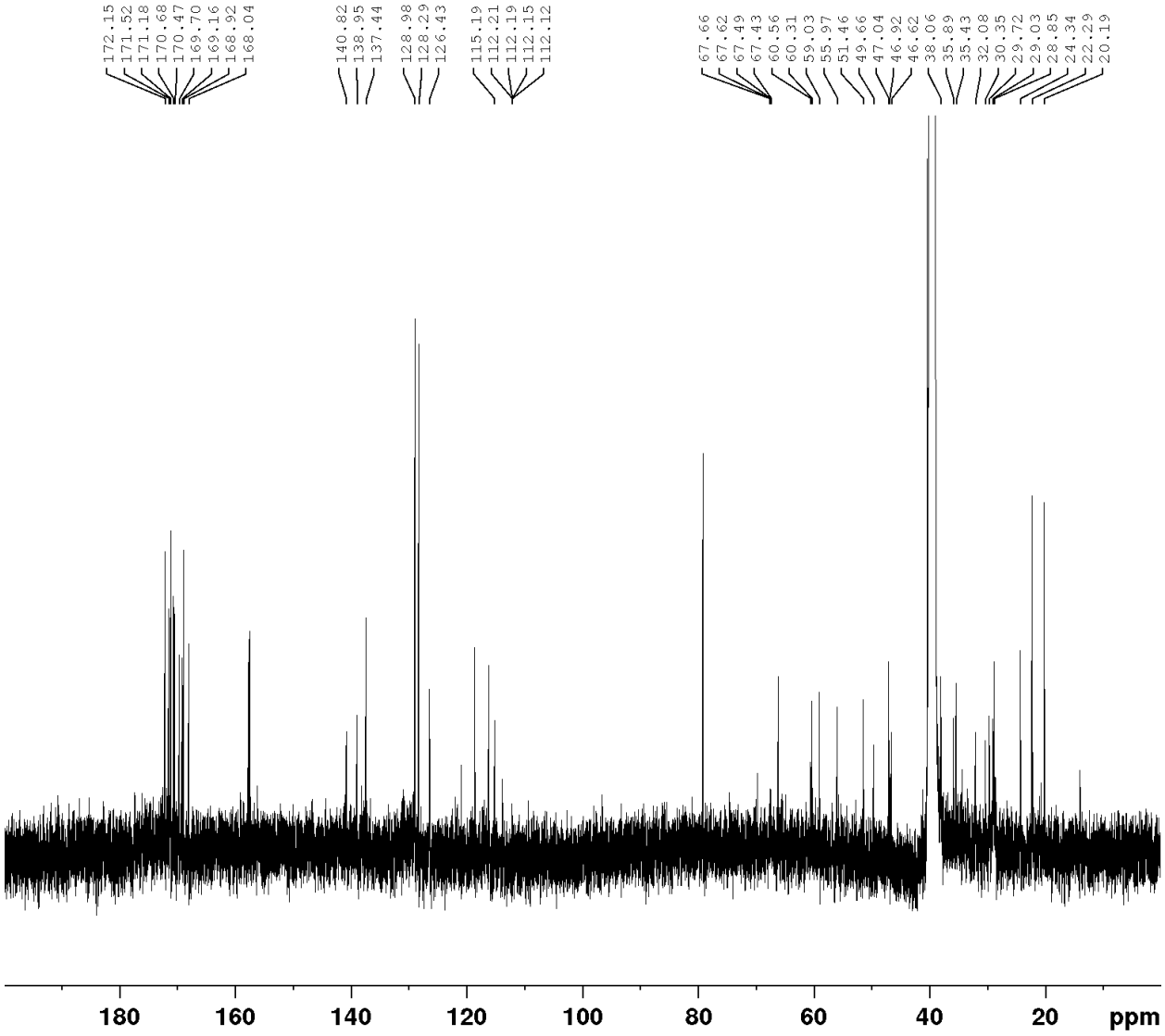

Spectrum 4.7.163 ^{19}F-NMR of Polycycle **48** (DMSO-d_6, 565 MHz)

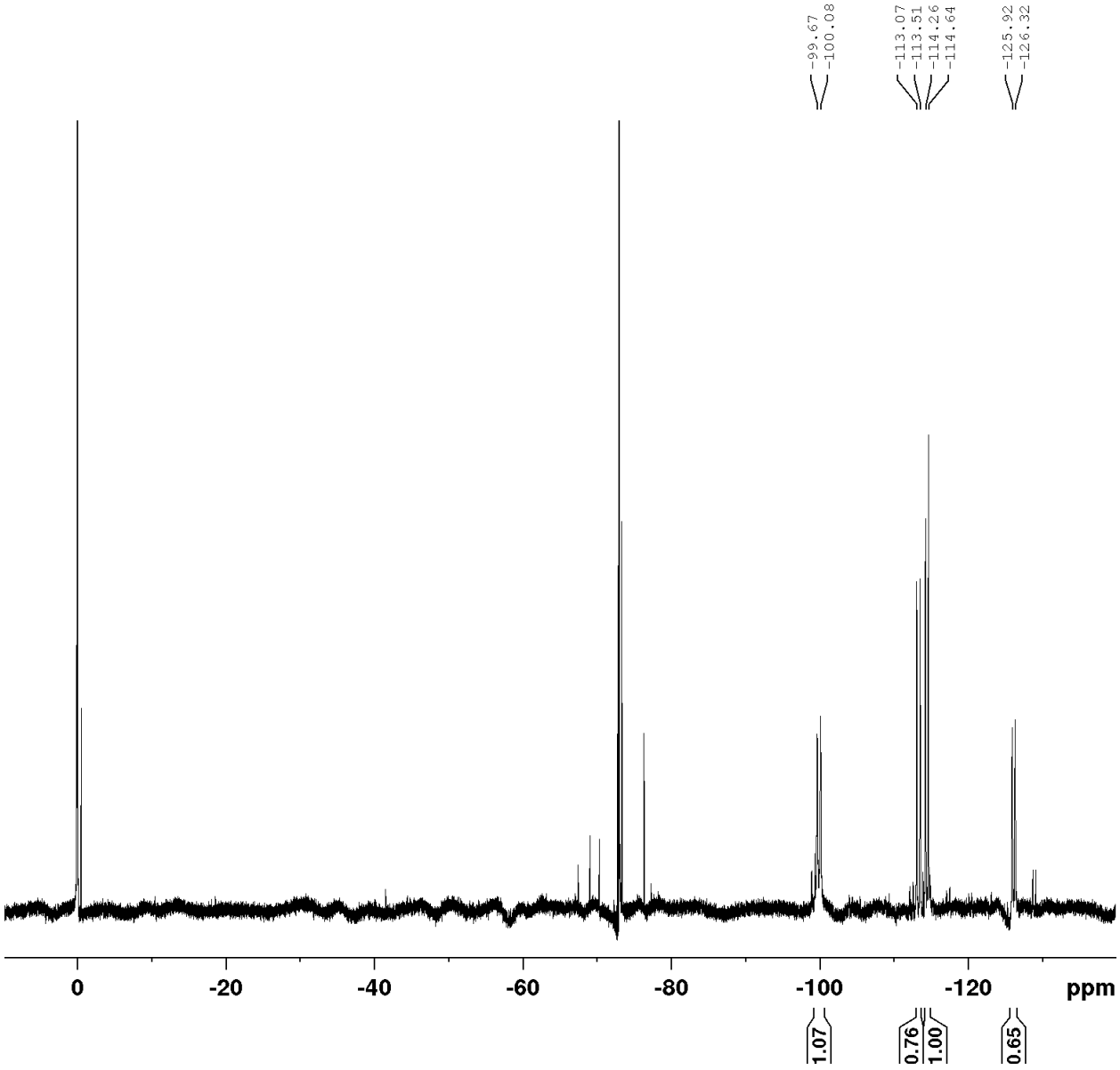

Spectrum 4.7.164 HMBC Spectrum of Polycycle **48** (DMSO-d_6)

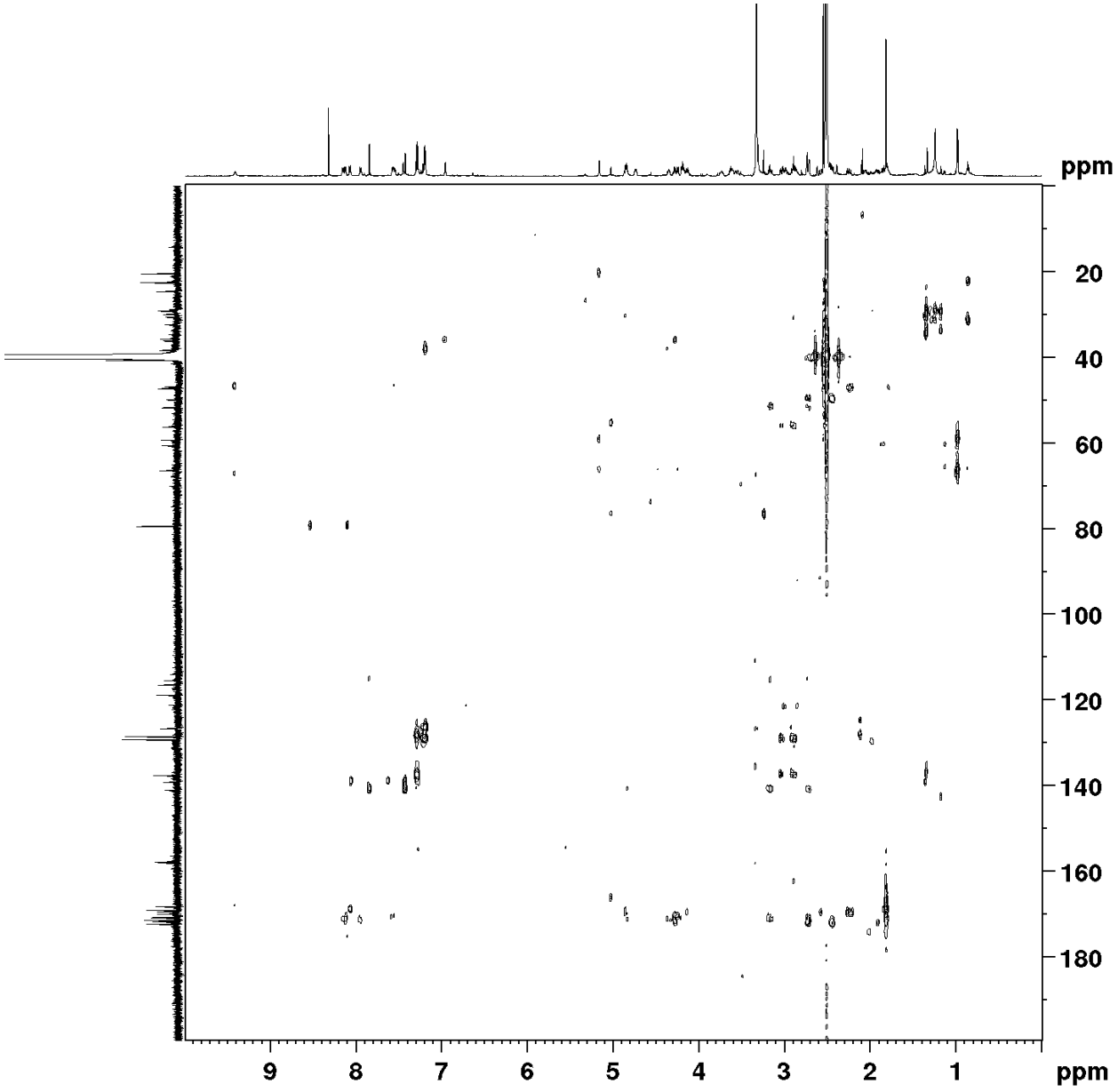

Spectrum 4.7.165 HSQC Spectrum of Polycycle **48** (DMSO-d_6)

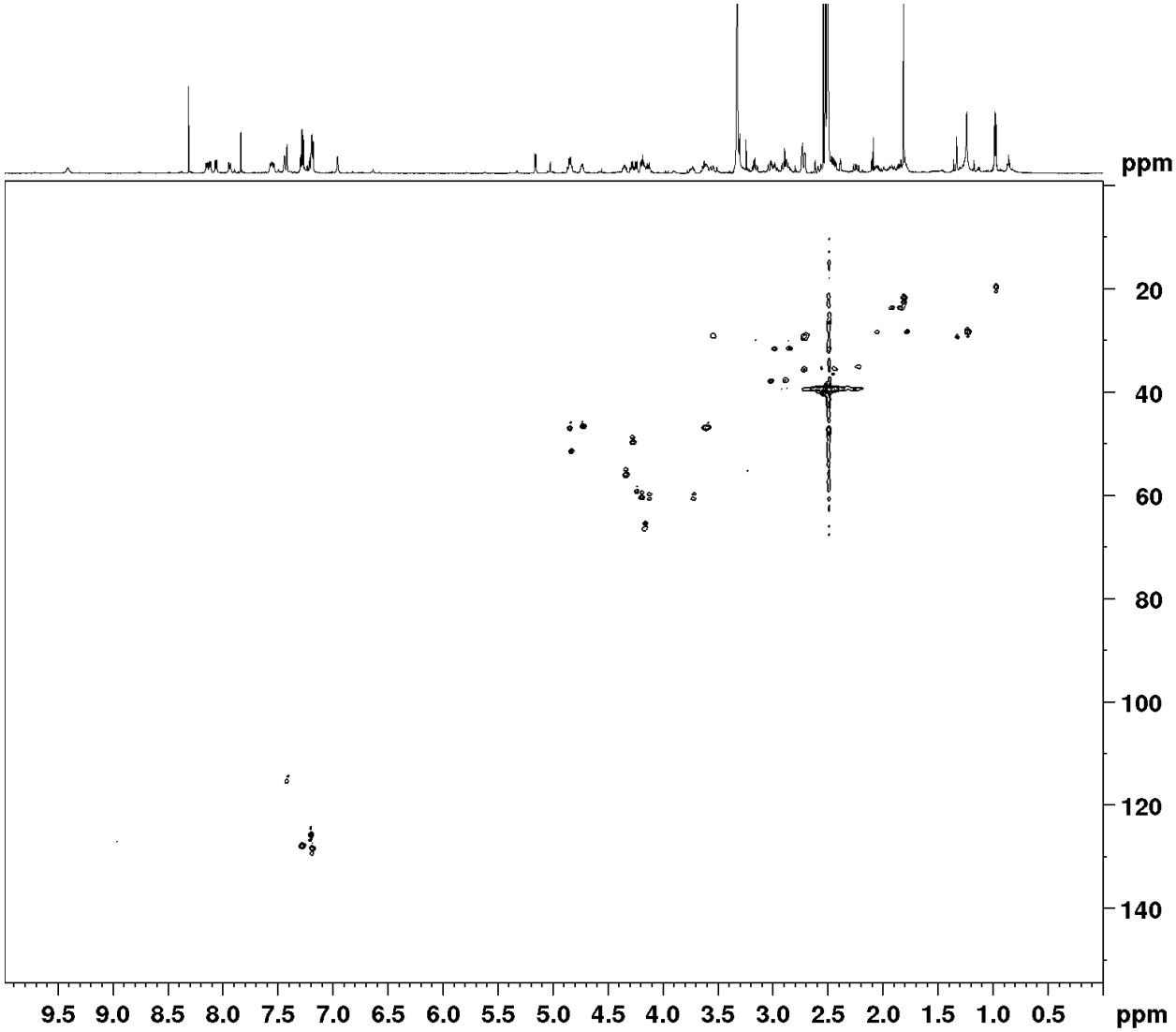

Spectrum 4.7.166 COSY Spectrum of Polycycle **48** (DMSO-d_6)

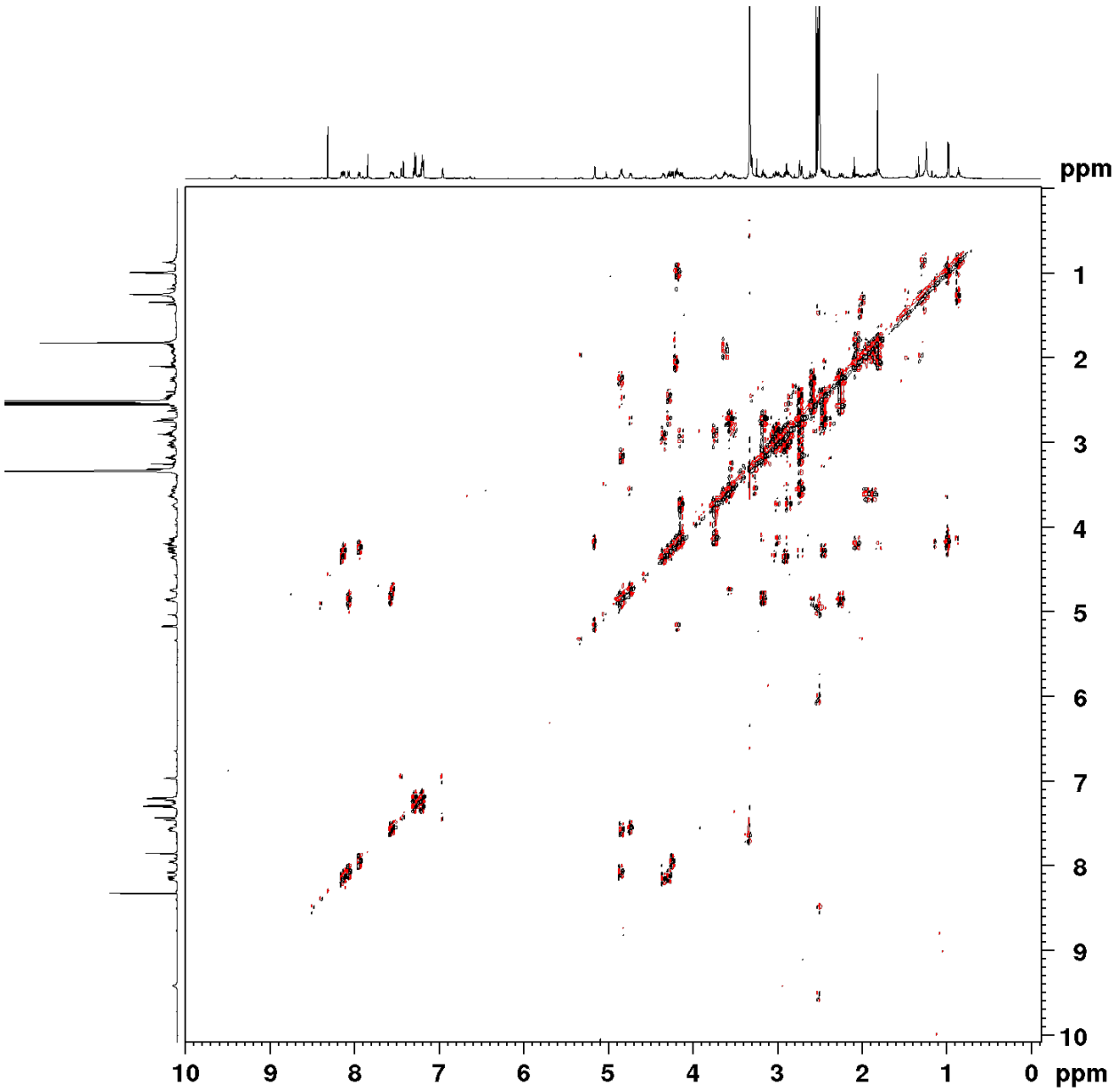

Table 4.7.23 Polycycle **48** (DMSO-d_6)

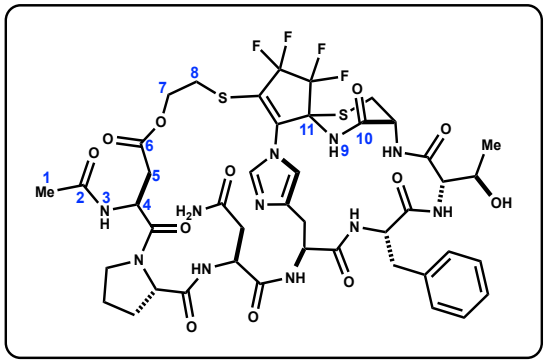

	13C	1H	Key Correlation
1	22.29	1.81 (s, 3H)	HSQC
2	168.93	-	1->2 HMBC
3	-	8.07 (d, J = 8.3 Hz, 1H)	2->3 HMBC
4	46.62	4.87-4.81 (m, 1H) overlap	3->4 COSY, HSQC
5	35.43	2.24 (dd, J = 15.4, 10.4 Hz, 1H), 2.44 (dd, J = 15.4, 7.8 Hz, 1H)	4->5 COSY, HSQC
6	169.71	-	5->6 HMBC
7	60.31	4.15–4.10 (m, 1H), 3.76–3.69 (m, 1H)	7->6 HMBC, HSQC
8	38.06	2.89 (m, 2H) overlap	7->8 COSY, HMBC, HSQC
9	-	9.41 (s, 1H)	11->9 HMBC
10	168.05	-	9->10 HMBC
11	67.7–66.4 (m, 1C)	-	9->11 HMBC

Spectrum 4.7.167 ^{1}H-NMR of Polycycle **49** (DMSO-d_6, 600 MHz)

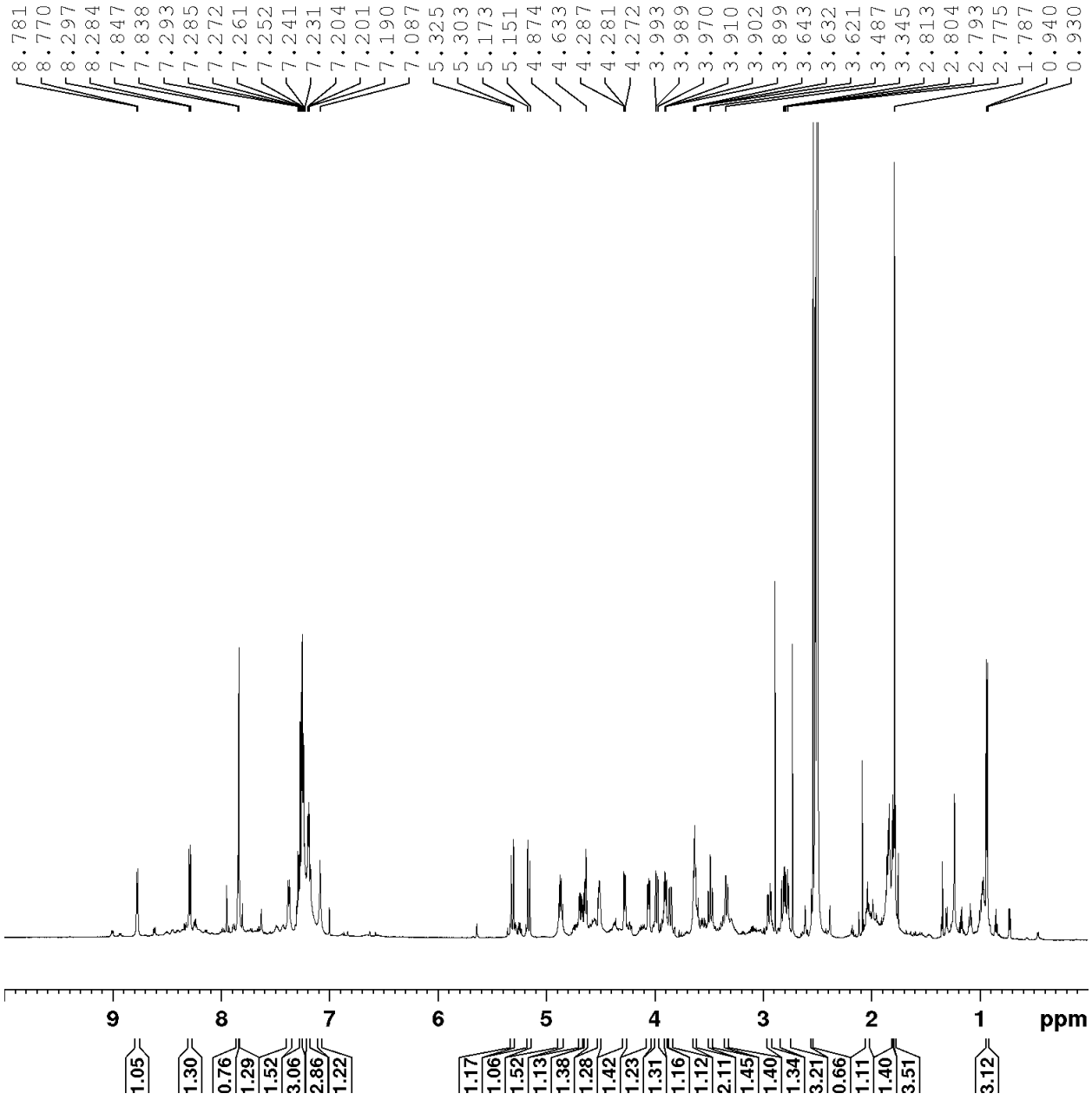

Spectrum 4.7.168 ^{13}C-NMR of Polycycle **49** (DMSO-d_6, 126 MHz)

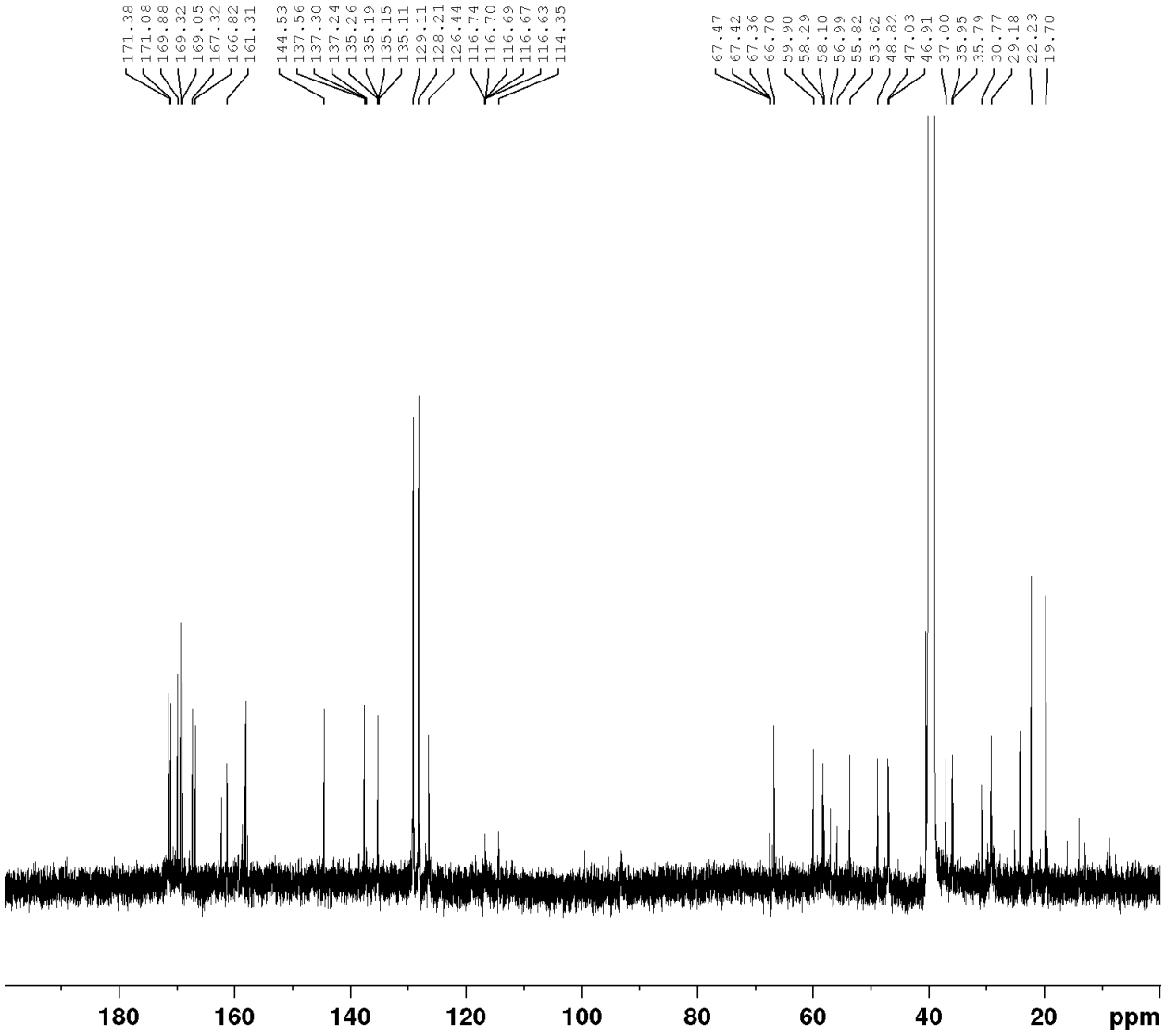

Spectrum 4.7.169 ^{19}F-NMR of Polycycle **49** (DMSO-d_6, 565 MHz)

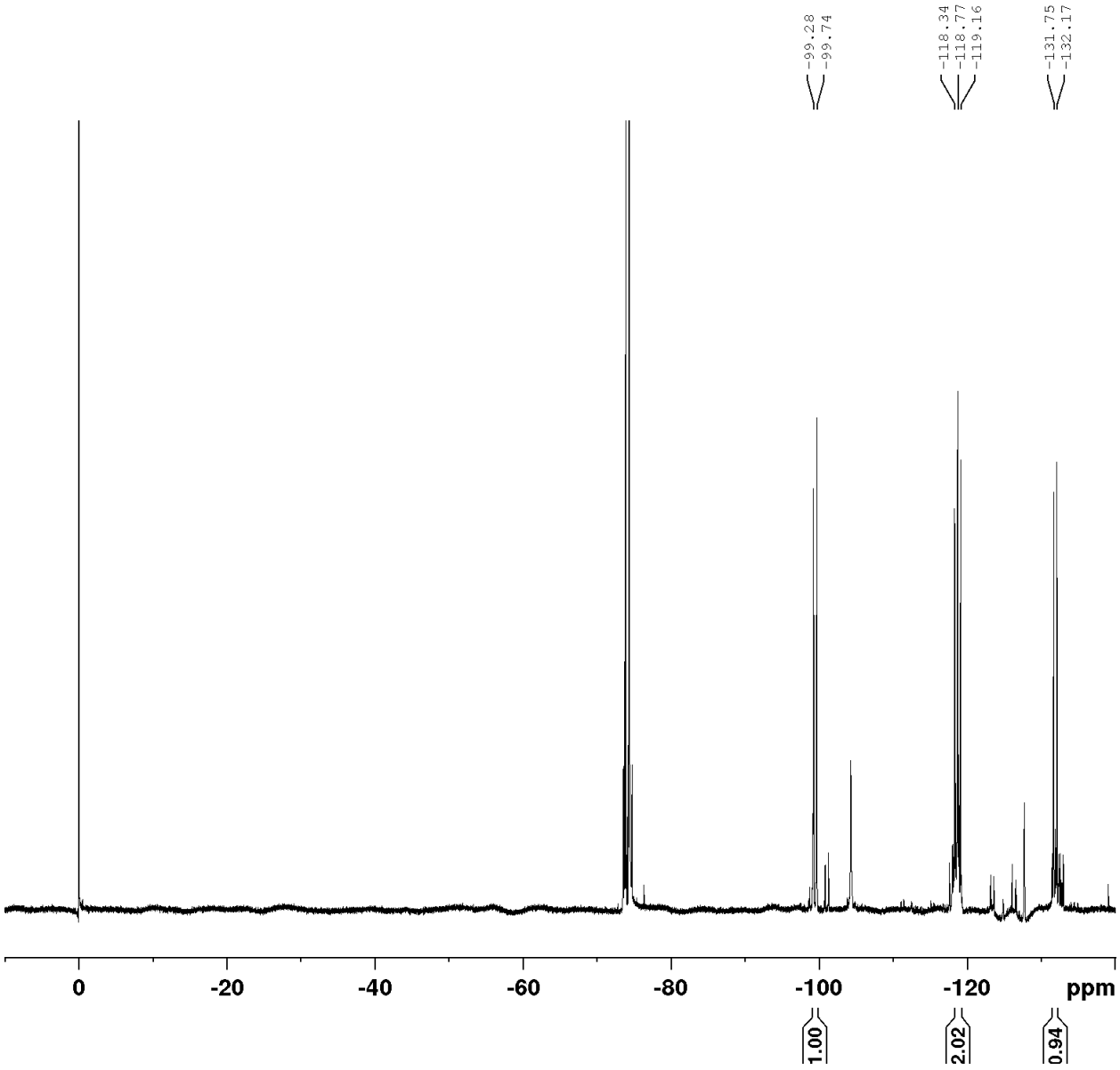

Spectrum 4.7.170 HMBC Spectrum of Polycycle **49** (DMSO-d_6)

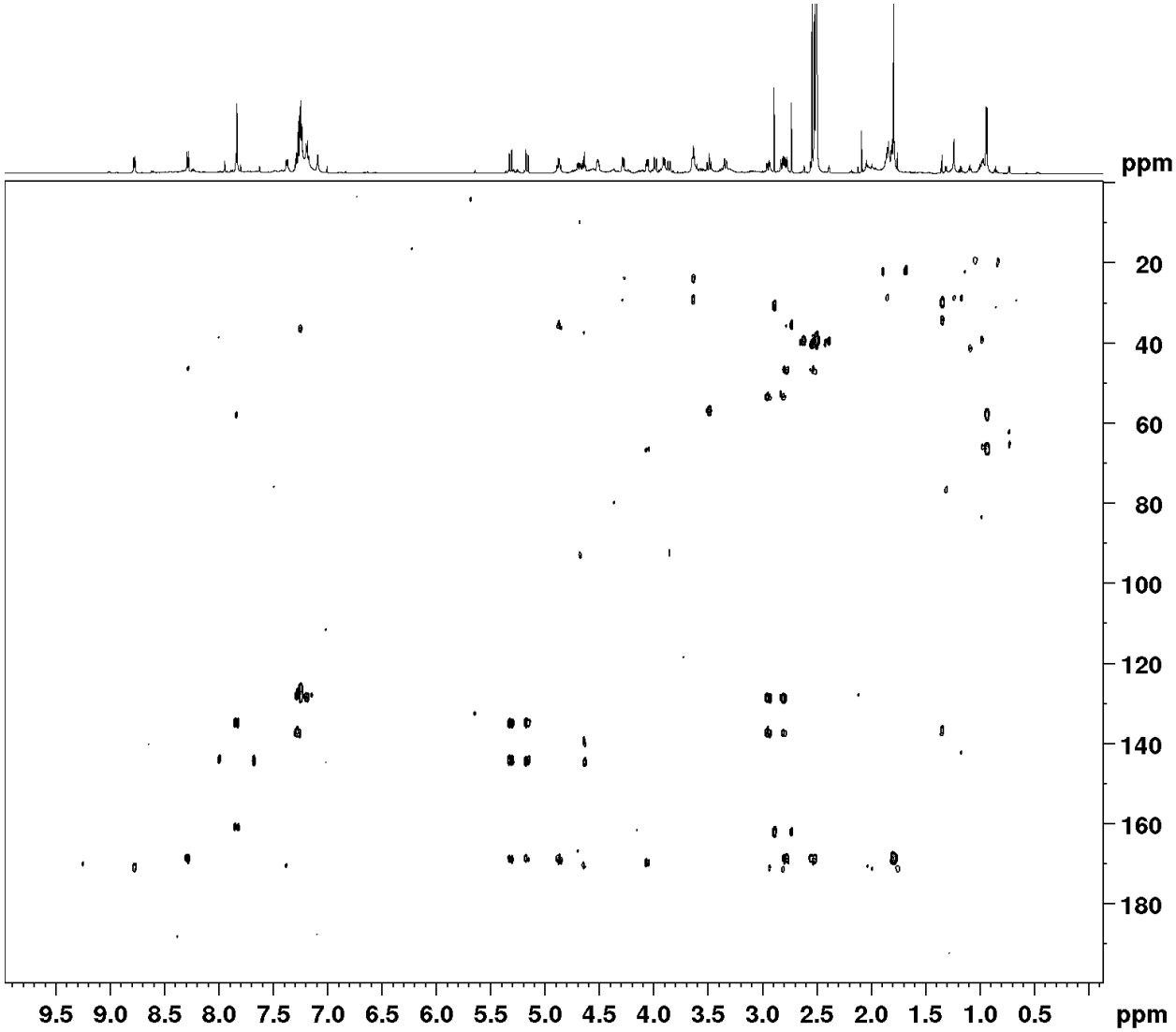

Spectrum 4.7.171 HSQC Spectrum of Polycycle **49** (DMSO-d_6)

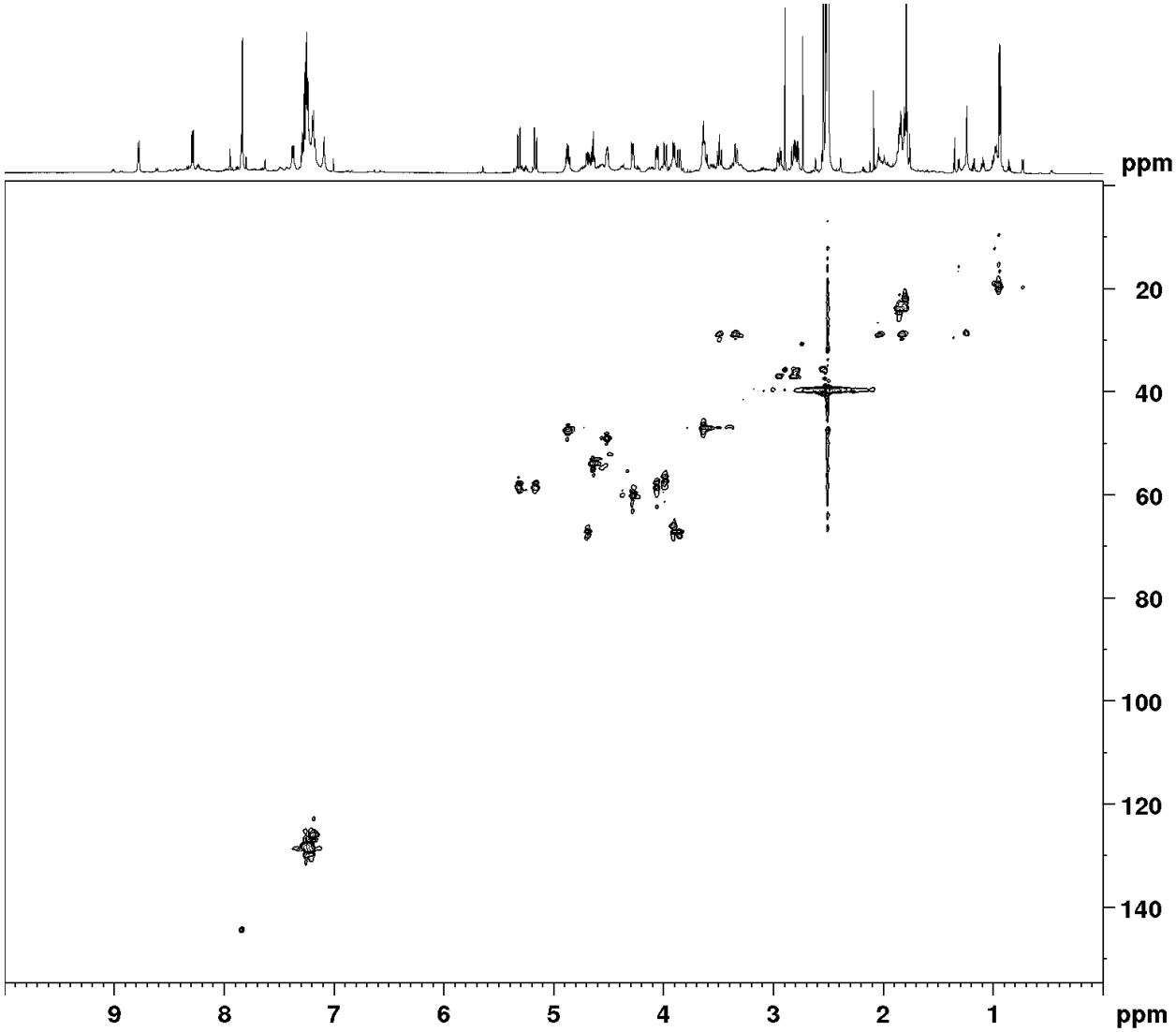

Spectrum 4.7.172 COSY Spectrum of Polycycle **49** (DMSO-d_6)

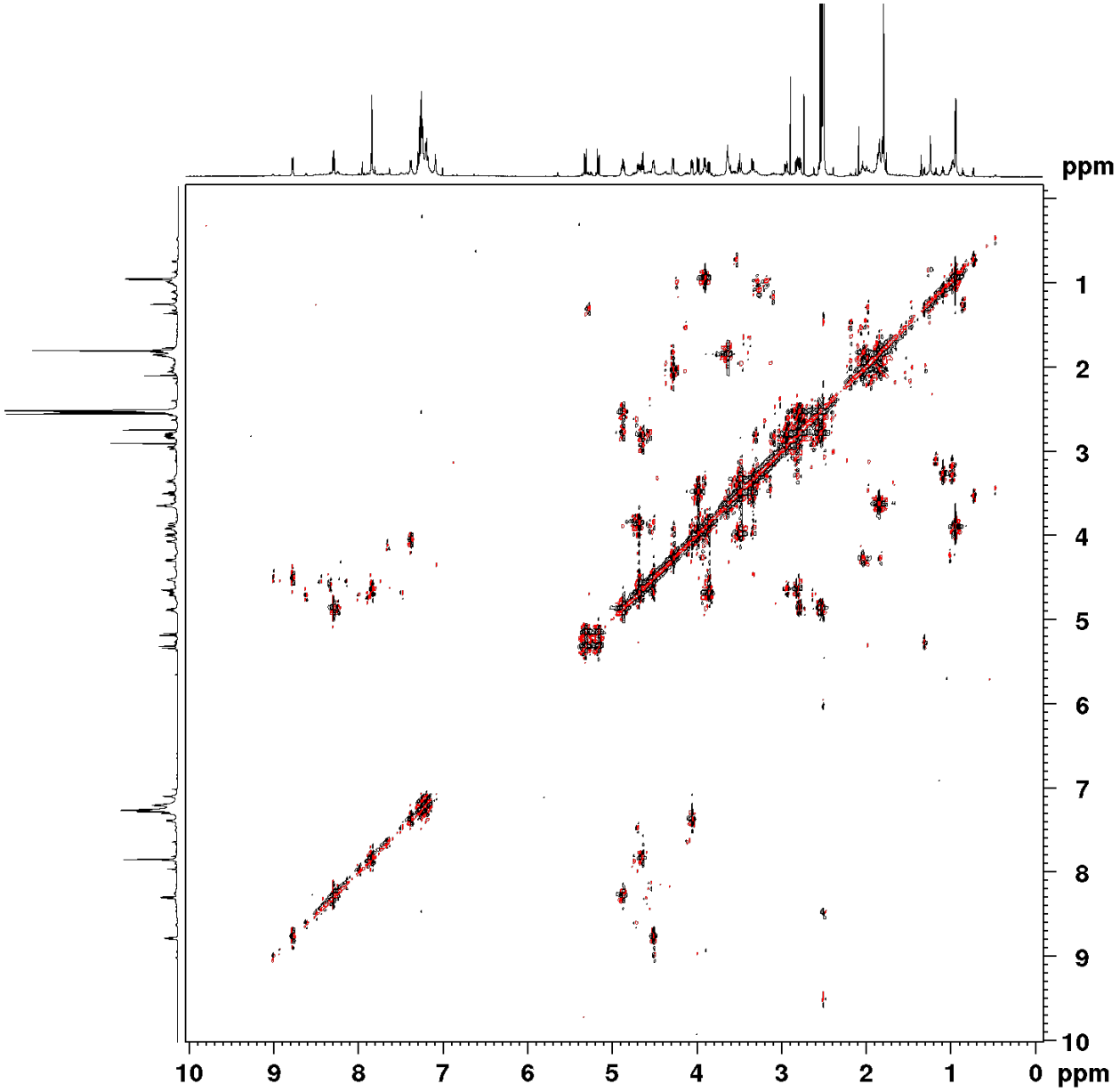

Table 4.7.24 Polycycle **49** (DMSO-d_6)

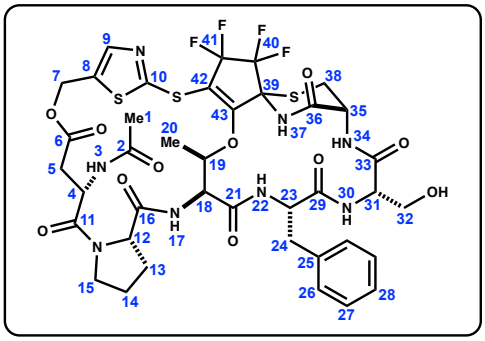

	13C	1H	Key Correlation
1	22.23	1.79 (s, 3H)	HSQC
2	169.05	-	1->2 HMBC
3	-	8.29 (d, J = 8.0 Hz, 1H)	2->3 HMBC
4	47.03	4.87 (q, J = 5.9 Hz, 1H)	2->3 HMBC, HSQC
5	35.79	2.78 (m, 1H), 2.52 (m, 1H)	4->5 COSY, HSQC
6	169.32	-	5->6 HMBC and 7->6 HMBC
7	58.29	5.31 (d, J = 13.0 Hz, 1H), 5.16 (d, J = 13.0 Hz, 1H)	6->7, 8-7, 9->7 HMBC, HSQC
8	135.26	-	9->8 HMBC
9	144.53	7.74 (s, 1H)	HSQC, 7->9 HMBC, HSQC
10	114.44	-	-
11	169.88	-	4->11 HMBC
12	55.82	4.68 (m, 1H) overlap	16->12 HMBC
13	35.95	2.80 (overlap, 1H), 2.53 (overlap, 1H)	12->13 HMBC, HSQC
14	29.18	2.03 (m, 1H), 1.84 (m, 1H) overlap	13->14 HMBC, HSQC
15	46.92	3.64 (m, 2H)	14->15 HMBC, HSQC
16	171.38	-	17->16 HMBC
17	-	7.38 (d, J = 7.8 Hz, 1H)	18->17 COSY
18	58.10	4.06 (dd, J = 7.9, 4.2 Hz , 1H)	20->18 HMBC, HSQC
19	66.74	3.90 (m, 1H)	20->19 COSY
20	19.71	0.94 (d, J = 6.3 Hz, 3H)	HSQC
21	161.32	-	22->21 HMBC
22	-	7.85 (m, 1H) overlap	23->22 COSY
23	53.62	4.63 (m, 1H) overlap	24->23 COSY, HSQC
24	37.00	2.94 (dd, J = , 1H), 2.80 (overlap, 1H)	25->24 HMBC, 26->24 HMBC, HSQC
25	137.56	-	24->25 HMBC
26	129.12	7.27–7.23, 7.21–7.17 (m, 2)	HSQC
27	128.22	7.27–7.23, 7.21–7.17 (m, 2)	HSQC
28	126.45	7.27–7.23, 7.21–7.17 (m, 1)	HSQC
29	171.08	-	23->29 HMBC
30	-	8.77 (d, J = 7.0 Hz, 1H)	31->30 HMBC, HSQC
31	48.82	4.51 (m, 1H)	30->31 COSY, HSQC
32	56.99	3.98 (dd, J =, 1H), 3.86 (dd, J=, 1H)	31->32 HMBC, HSQC
33	167.32	-	31->30 HMBC
34	-	-	-
35	59.90	4.28 (m, 1H)	38->35 HMBC, HSQC
36	166.82	-	35->36 HMBC
37	-	7.09	-
38	30.77	3.49 (m, 1H), 3.33 (m, 1H)	38->35 HMBC
39	67.3–67.5 (m, 1C)	-	-
40	116.6–116.7 (m, 1C)	-	-
41	116.6–116.7 (m, 1C)	-	-
42	137.2–137.3 (m, 1C)	-	-
43	135.1–135.2 (m, 1C)	-	-

Spectrum 4.7.173 ^{1}H-NMR of Polycycle **50** (DMSO-d_6, 500 MHz)

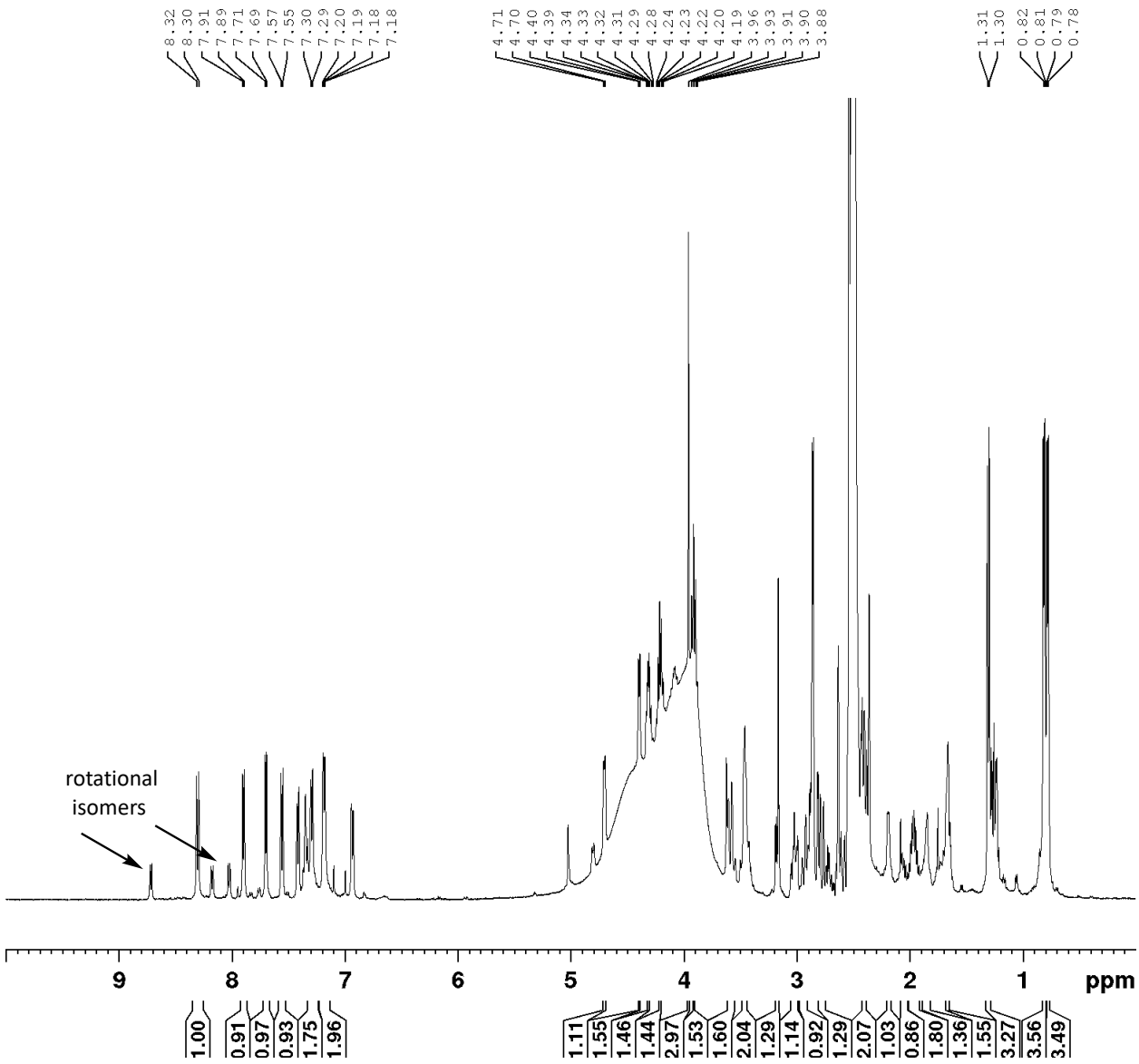

Spectrum 4.7.174 ^{13}C-NMR of Polycycle **50** (DMSO-d_6, 126 MHz)

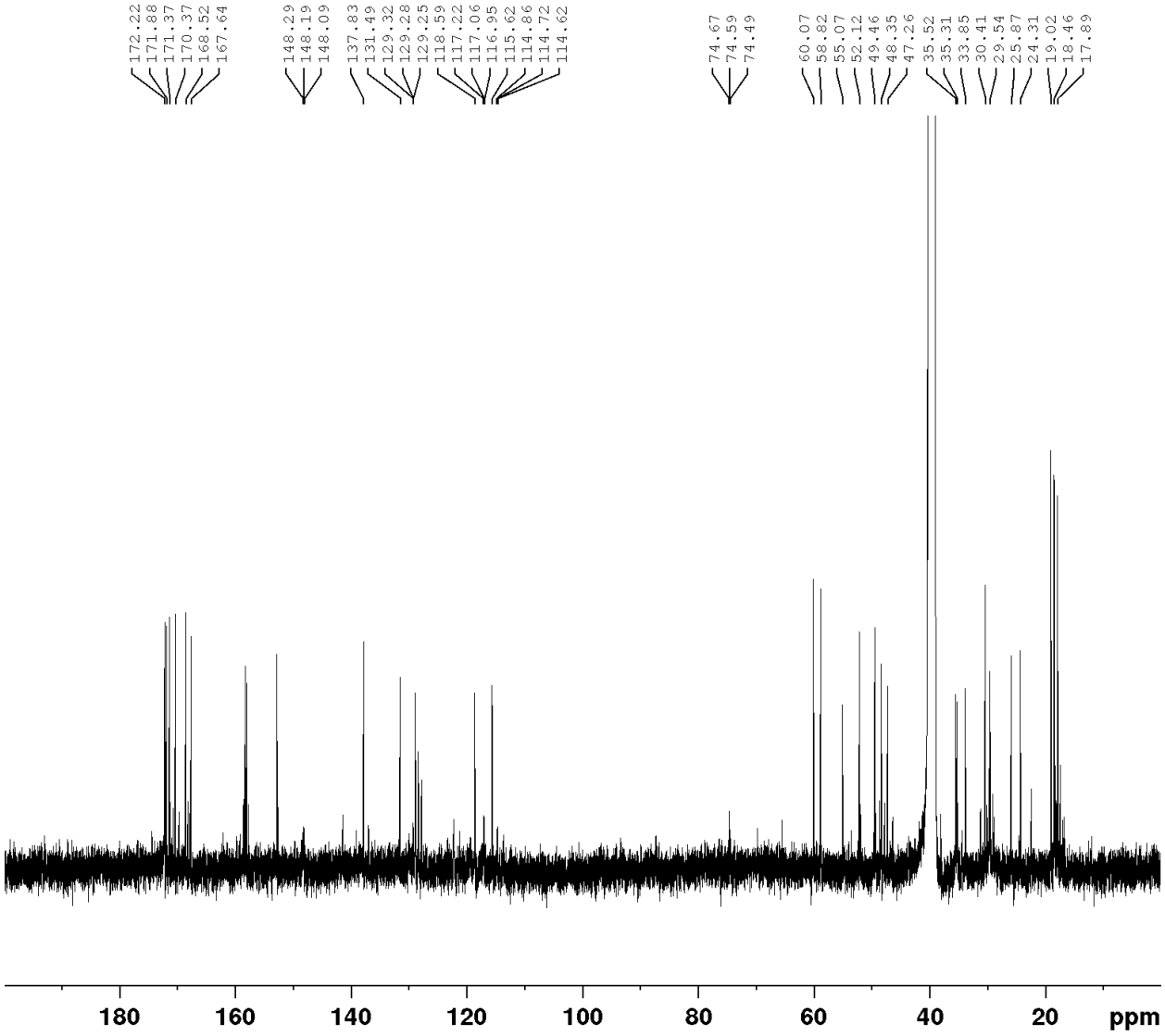

Spectrum 4.7.175 ^{19}F-NMR of Polycycle **50** (DMSO-d_6, 282 MHz)

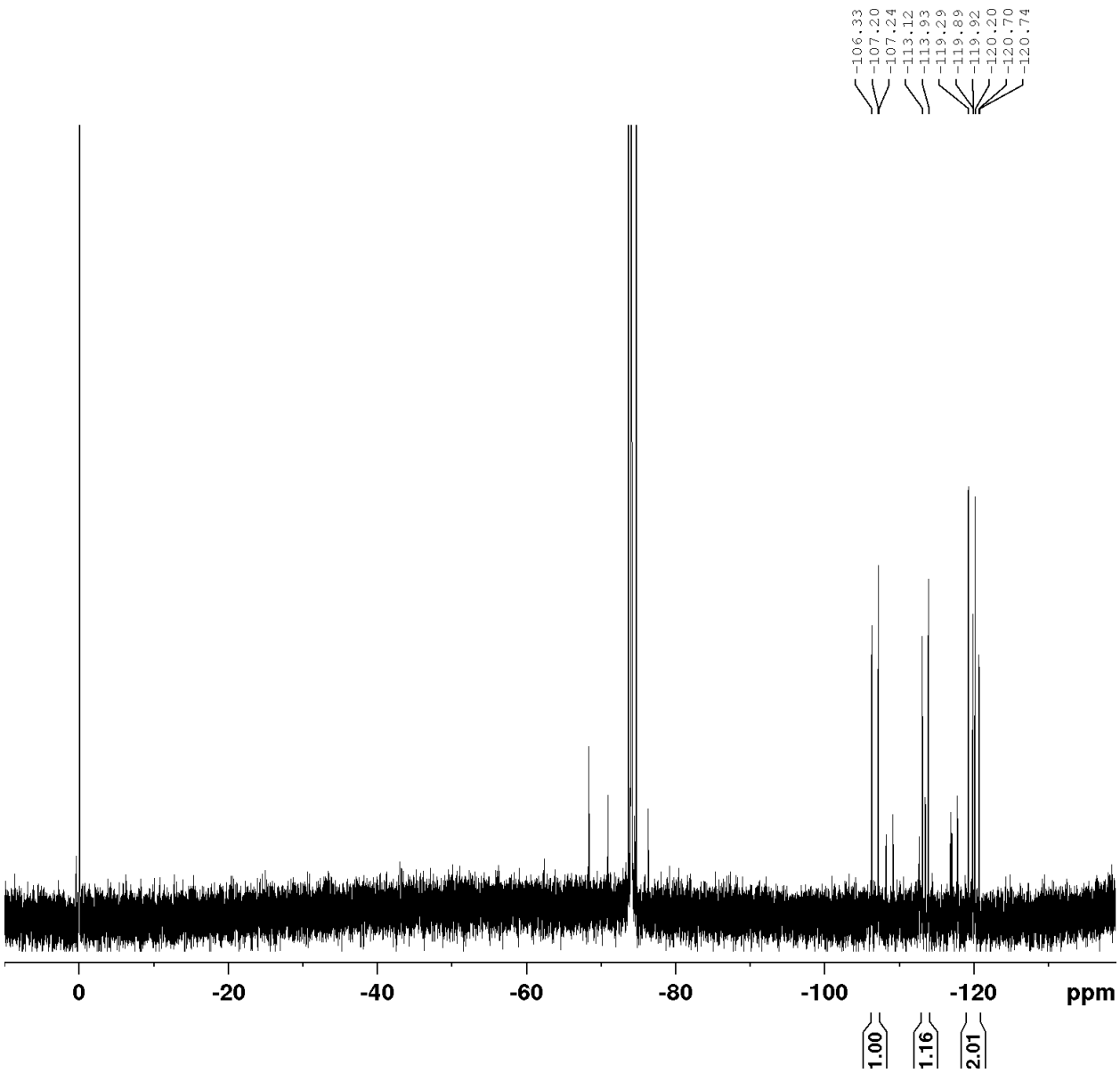

Spectrum 4.7.176 HMBC of Polycycle **50** (DMSO-d_6)

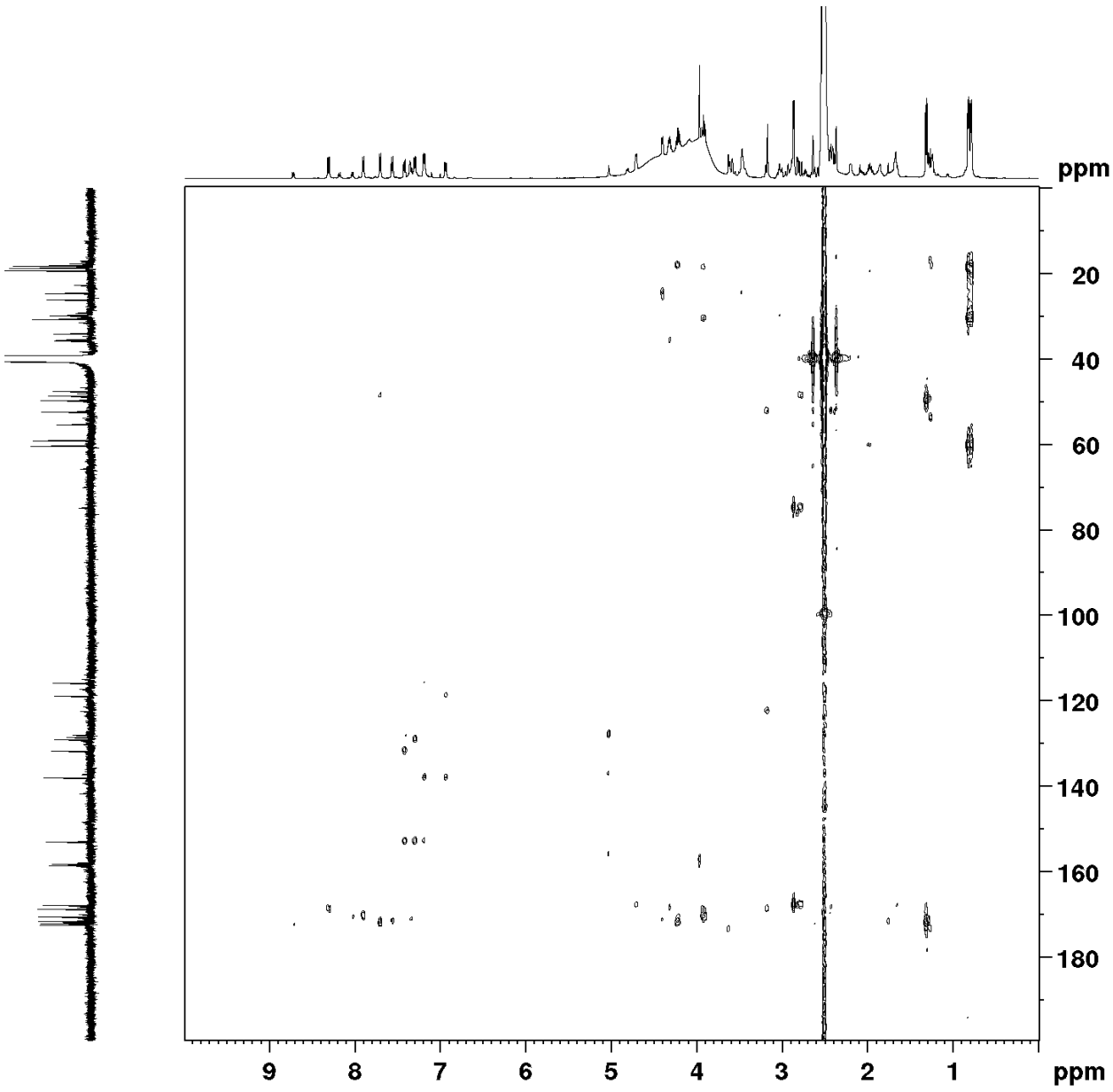

Spectrum 4.7.177 HSQC of Polycycle **50** (DMSO-d_6)

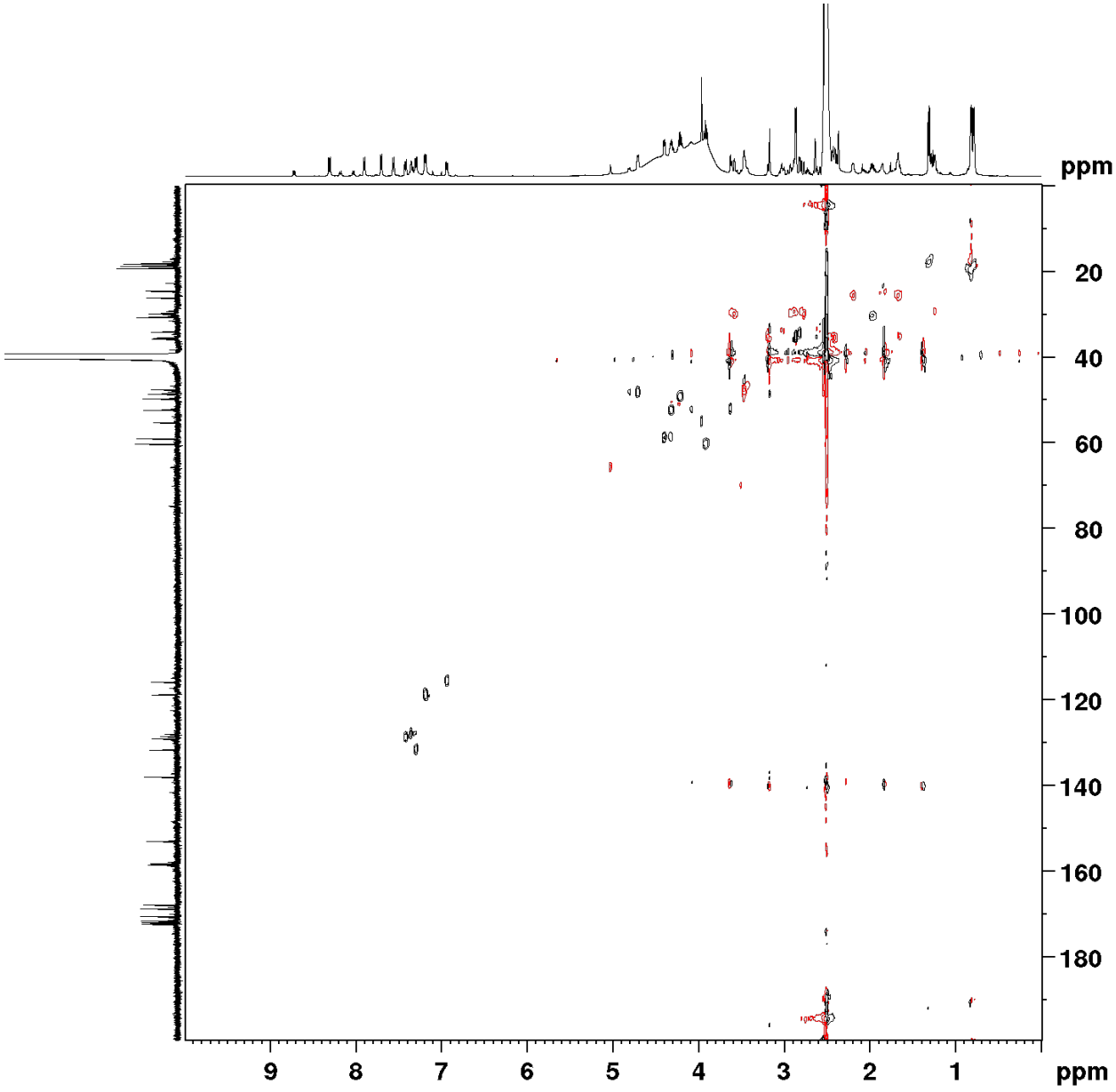

Spectrum 4.7.178 COSY of Polycycle **50** (DMSO-d_6)

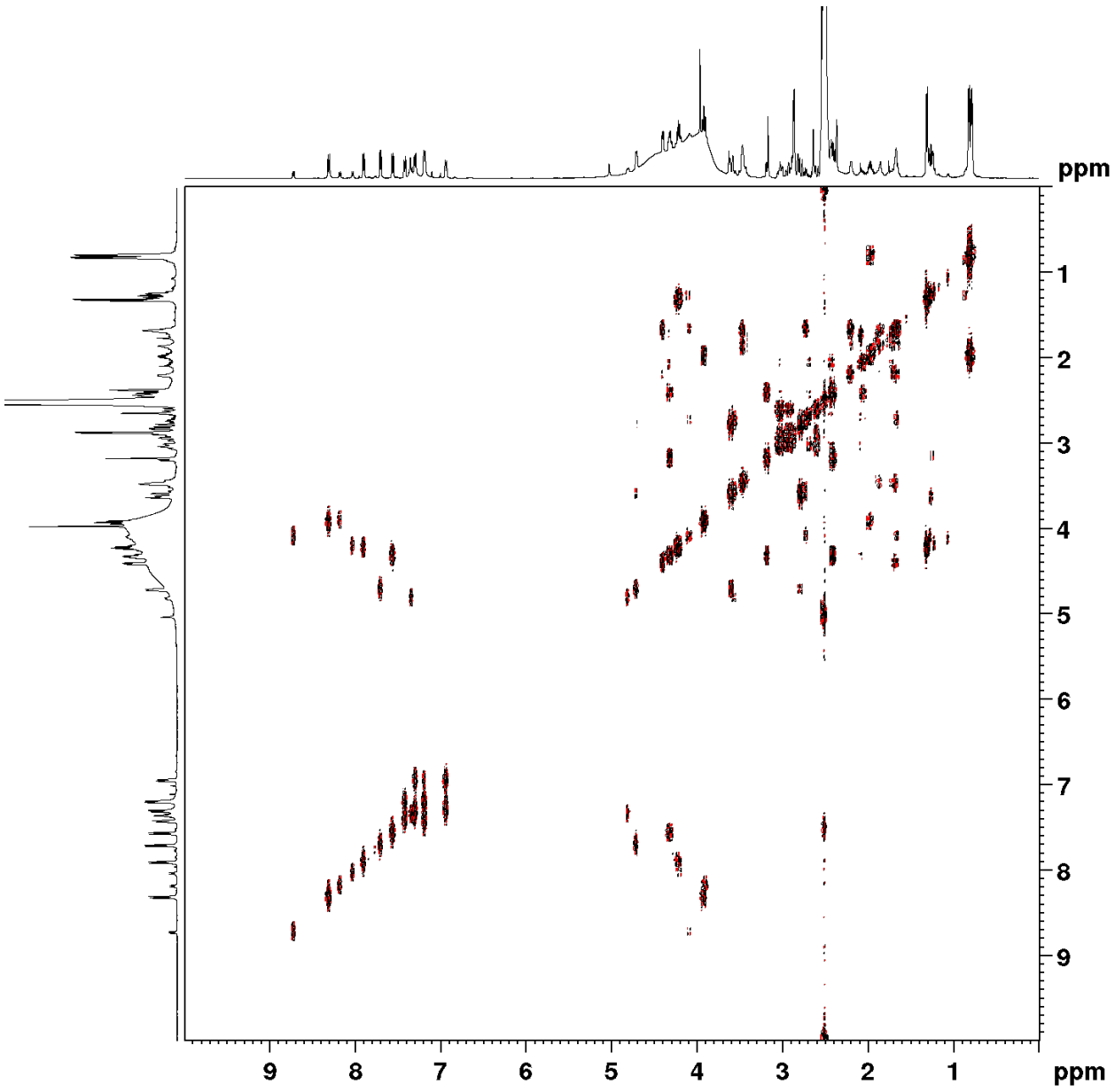

Spectrum 4.7.179 ^{1}H-NMR of Polycycle **S1** (DMSO-d_6, 500 MHz)

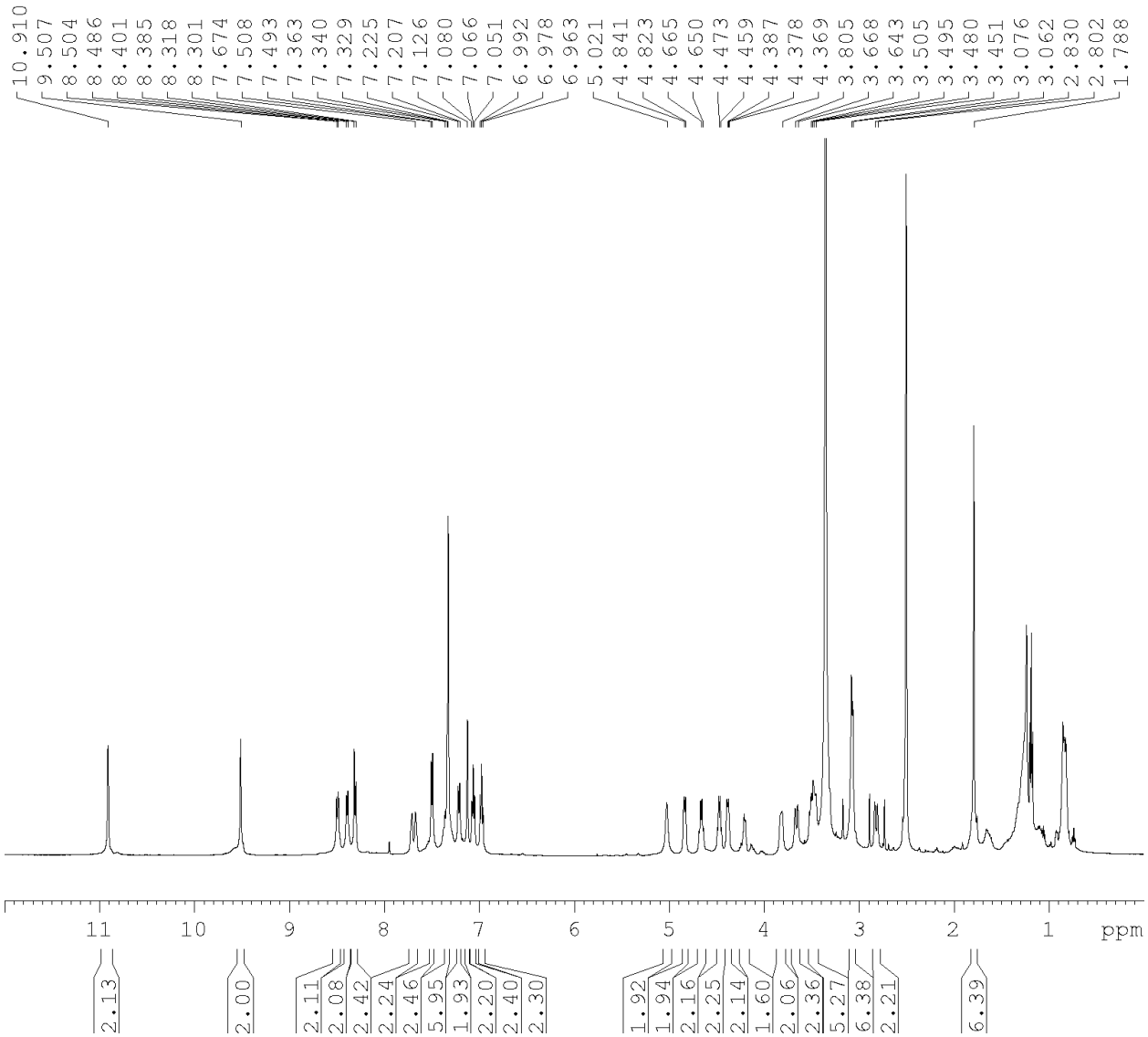

Spectrum 4.7.180 ^{13}C-NMR of Polycycle **S1** (DMSO-d_6, 126 MHz)

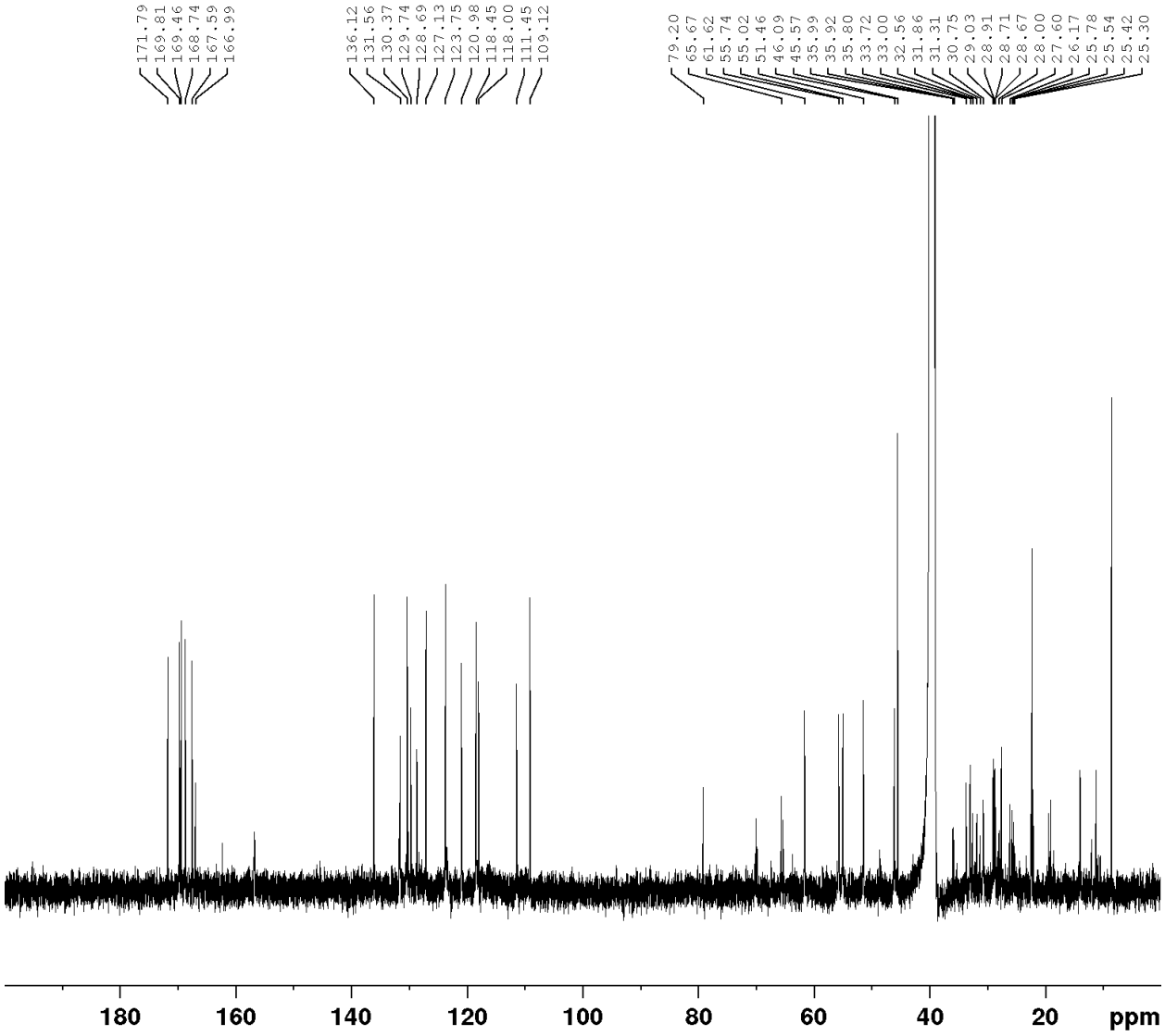

Spectrum 4.7.181 ^{19}F-NMR of Polycycle **S1** (DMSO-d_6, 282 MHz)

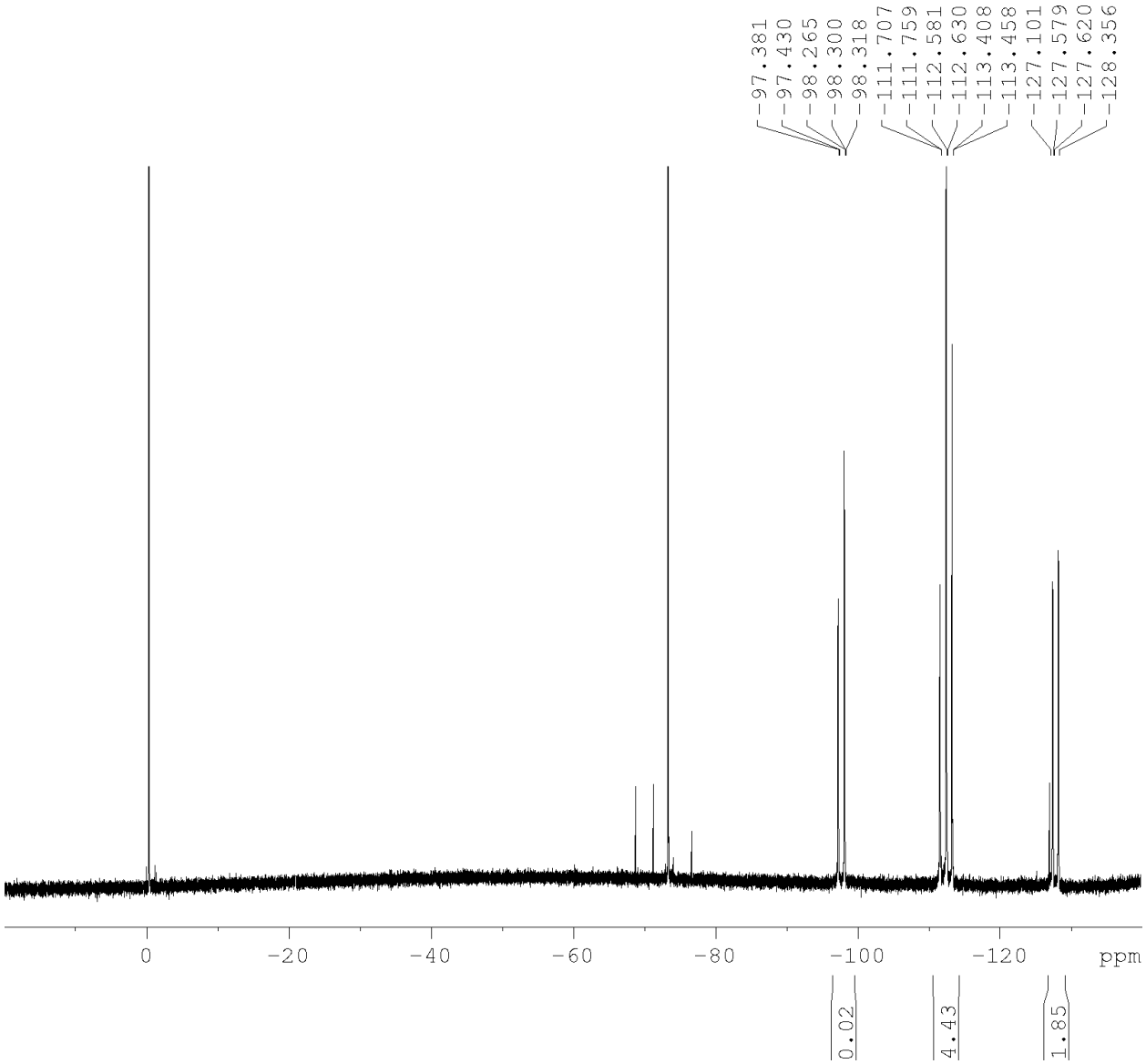

Spectrum 4.7.182 ^{1}H-NMR of Macrocycle **S5** (DMSO-d_6, 500 MHz)

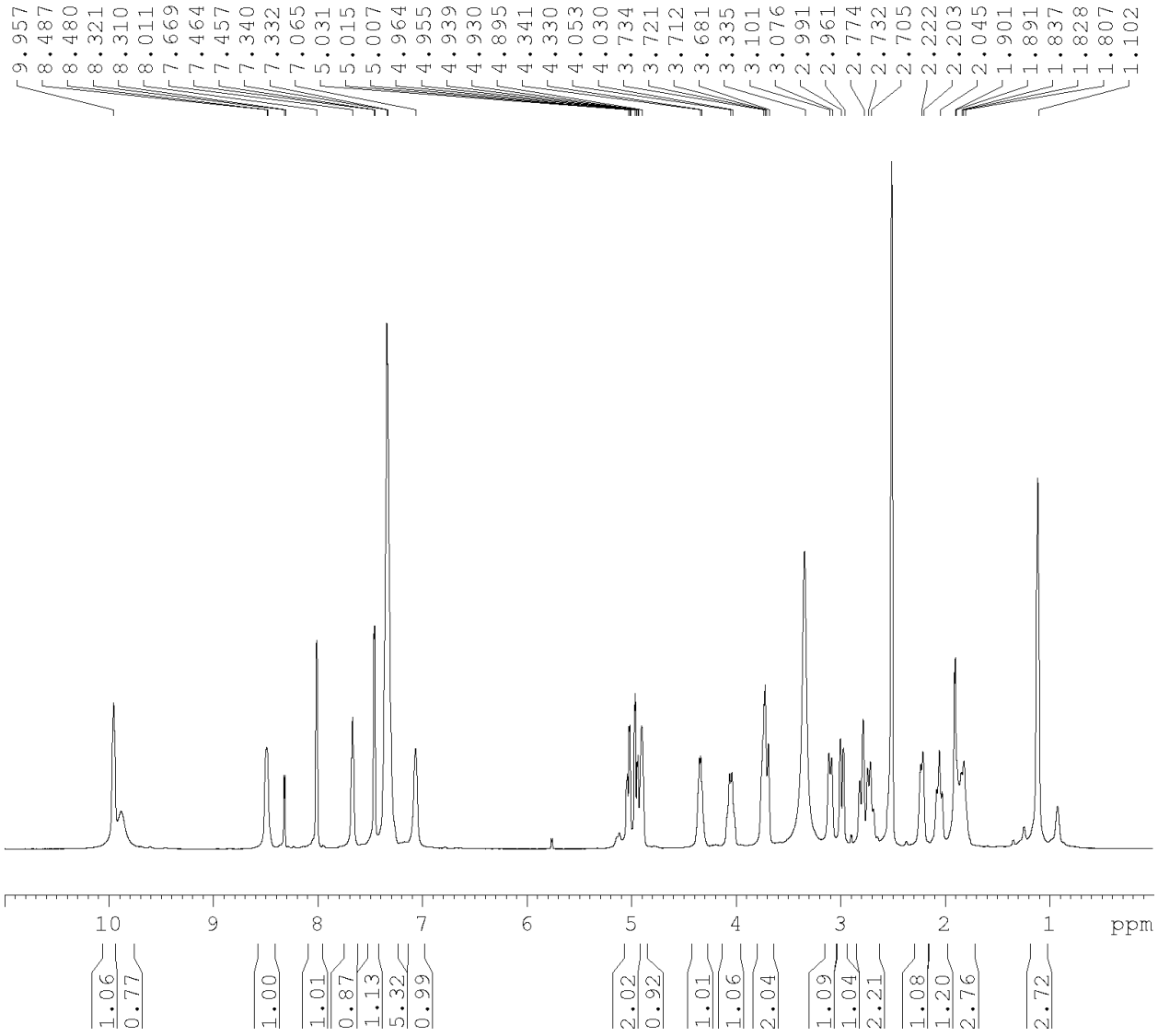

Spectrum 4.7.183 ^{13}C-NMR of Macrocycle **S5** (DMSO-d_6, 500 MHz)

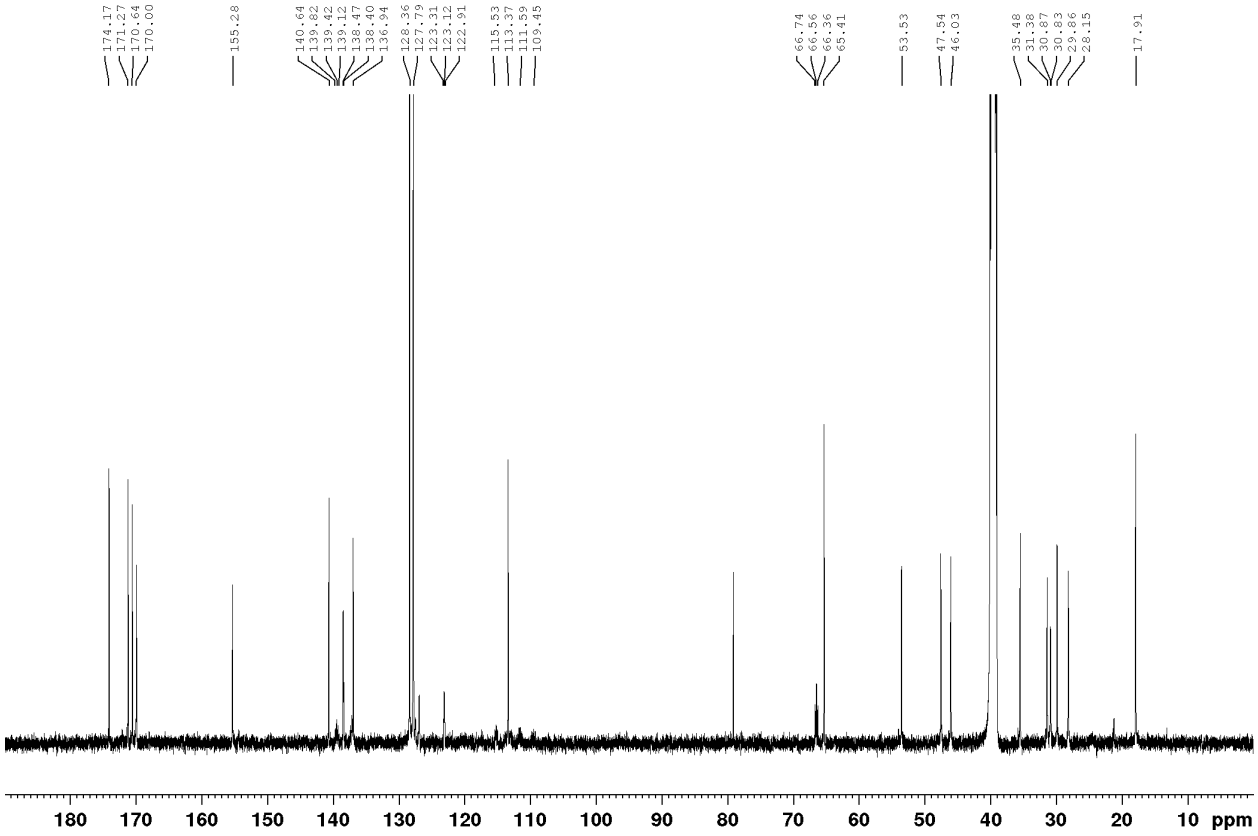

Spectrum 4.7.184 ^{19}F-NMR of Macrocycle **S5** (DMSO-d_6, 282 MHz)

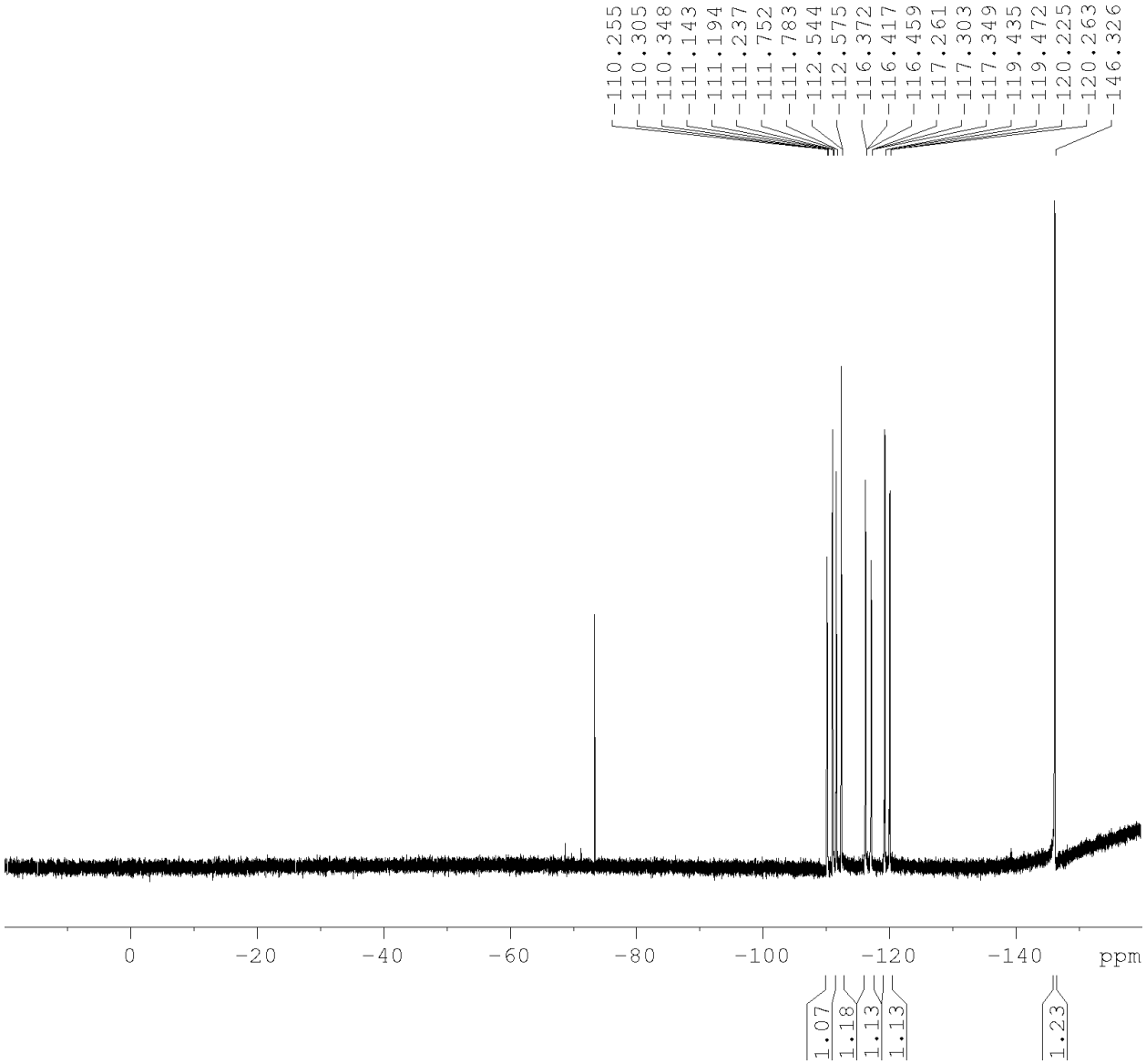

Spectrum 4.7.185 HMBC Spectrum of Macrocycle **S5** (DMSO-d_6)

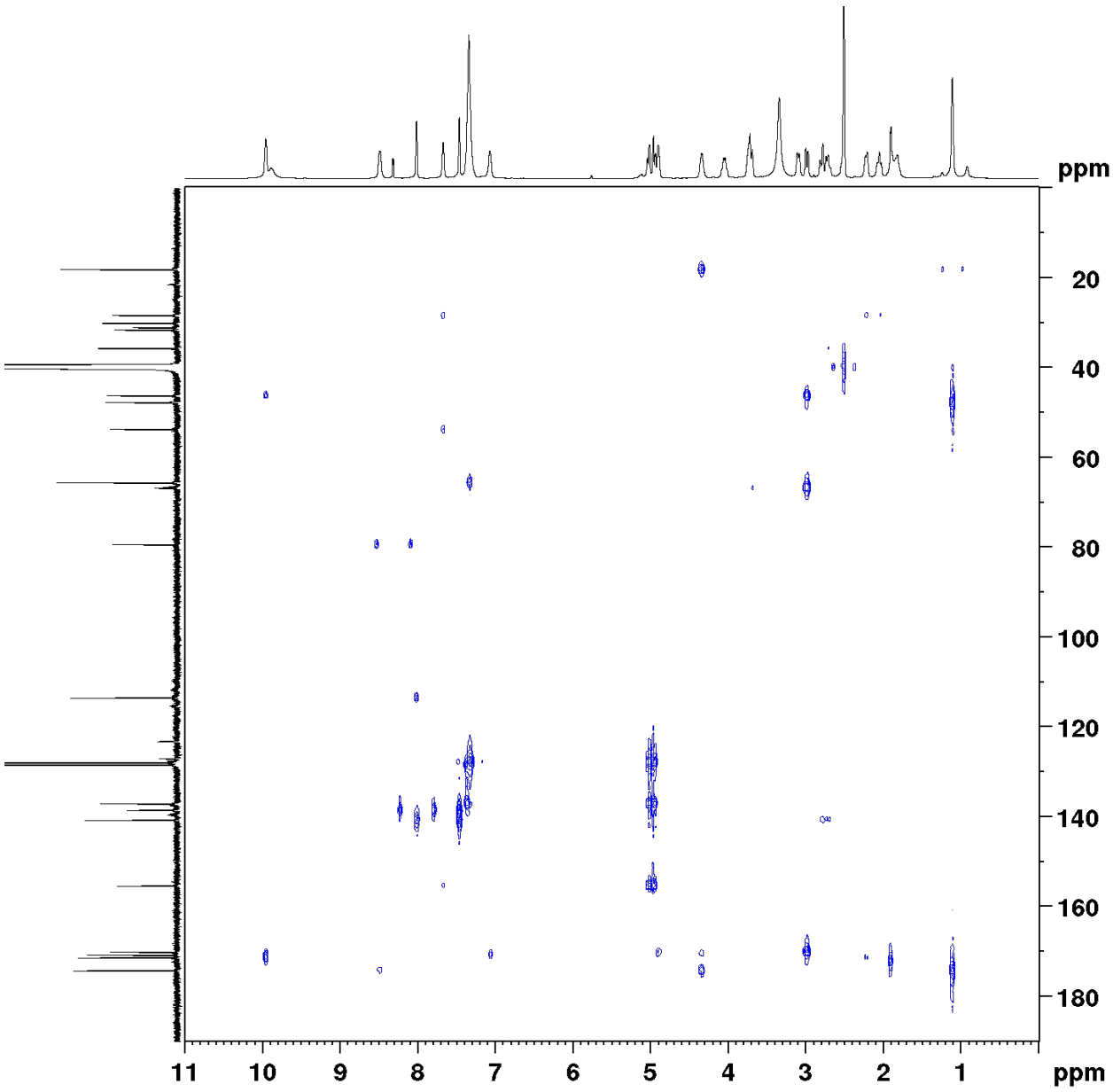

Spectrum 4.7.186 HSQC Spectrum of Macrocycle **S5** (DMSO-d_6)

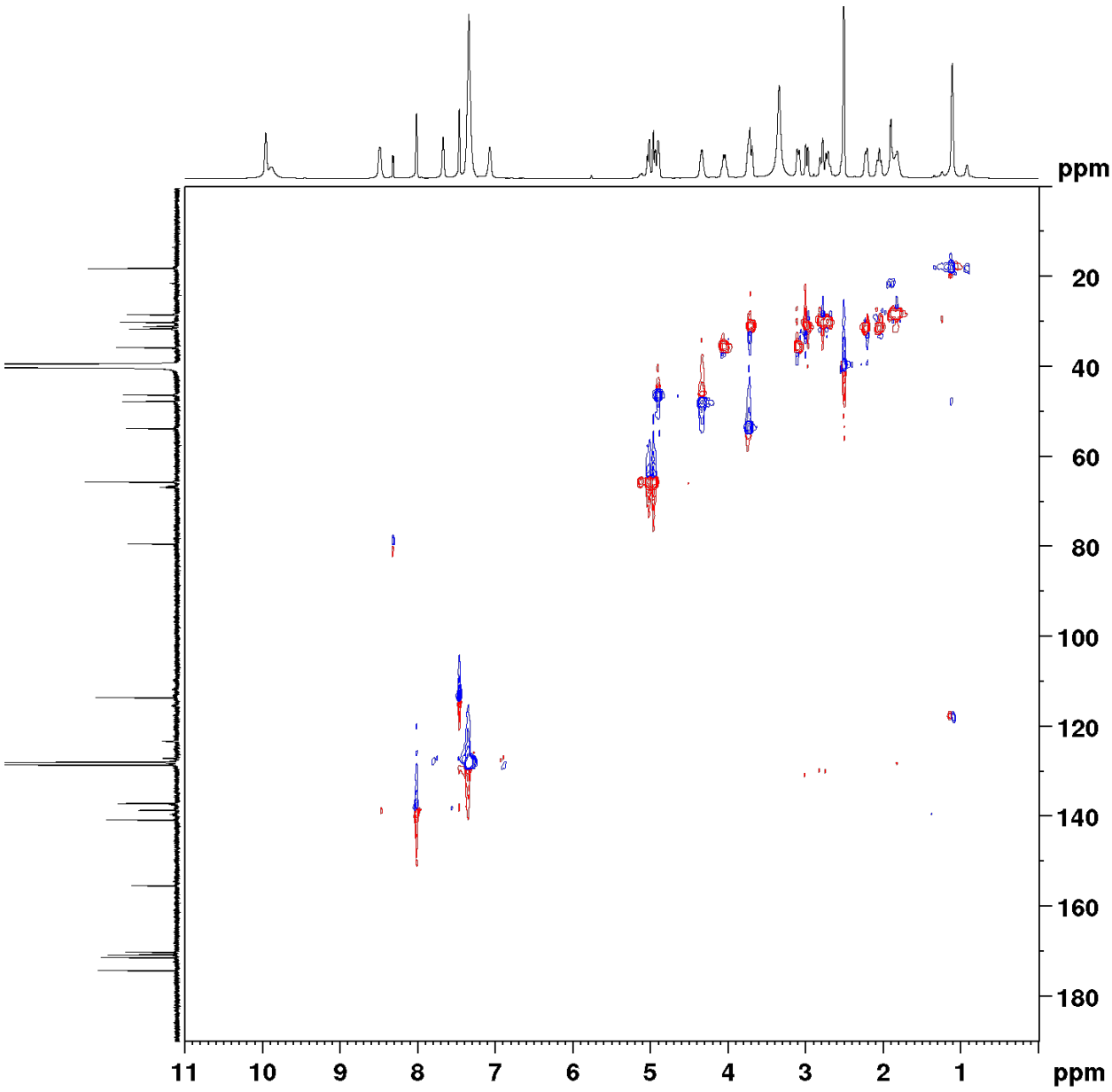

Spectrum 4.7.187 COSY Spectrum of Macrocycle **S5** (DMSO-d_6)

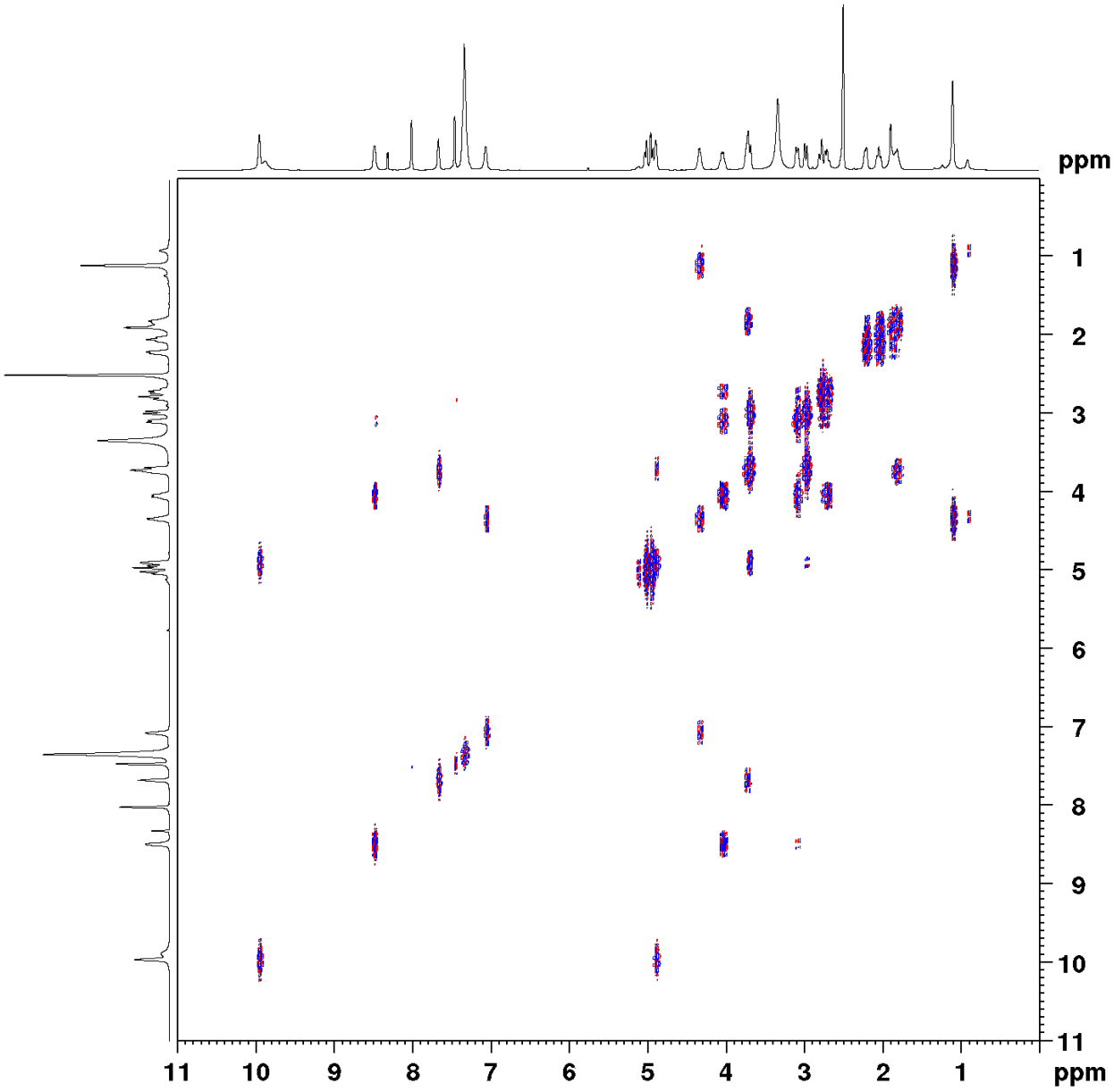

Table 4.7.25 Macrocycle **S5** (DMSO-d_6)

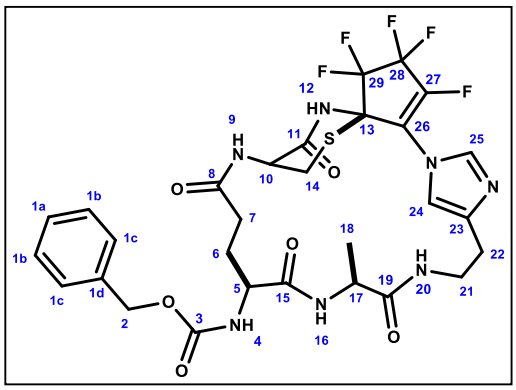

	13C	1H	Key Correlation
1a	127.8	7.42 - 7.24 (m, 5H)	HMBC 2 -> 1d, 1c, 3
1b	128.4	7.42 - 7.24 (m, 5H)	HMBC 1b -> 1c, 1d
1c	127.9	7.42 - 7.24 (m, 5H)	HMBC 1c -> 2
1d	137	-	HMBC 1d -> 2
2	65.4	5.07 - 4.92 (m, 2H)	HMBC 2 -> 1d, 1c, 3
3	155.3	-	HMBC 2,4 -> 3
4	-	7.67 (s, 1H)	HMBC 4 -> 3,5
5	53.5	3.8 - 3.64 (m, 1H)	HMBC 5 -> 6, 15
6	28.2	1.97 - 1.72 (m, 2H)	HMBC 6 -> 5,7
7	31.4	2.29 - 2.16 (m, 1H); 2.13 - 1.98 (m, 1H)	HMBC 7 -> 6,8
8	171.3	-	HMBC 7 -> 8
9	-	9.96 (bs, 1H)	COSY 9 -> 10
10	46	4.89 (s, 1H)	HMBC 10 -> 14, 11
11	170	-	HMBC 12, 14 -> 11
12	-	9.88 (bs, 1H)	HMBC 12 -> 10
13	66.6 (m, 1C)	-	HMBC 14 -> 13
14	30.9	2.98 (d, J = 15.0 Hz, 1H); 3.8 - 3.65 (m) (1H)	HMBC 14 -> 13, 10
15	170.6	-	HMBC 5, 6 -> 15
16	-	7.07 (s, 1H)	HMBC 16 -> 15, 17
17	47.5	4.4 - 4.25 (m, 1H)	HMBC 17 -> 18
18	17.9	1.18 - 1.02 (m, 3H)	HMBC 18 -> 17
19	174.2	-	HMBC 17, 20 -> 19
20	-	8.48 (s, 1H)	HMBC 20 -> 19
21	35.5	4.04 (q, J = 12.3 Hz 1H); 3.09 (d, J = 13.0 Hz, 1H)	HMBC 21 -> 22
22	29.9	2.85 - 2.63 (m, 2H)	HMBC 22 -> 23
23	140.6	-	HMBC 22, 24 -> 23
24	113.4	7.46 (s, 1H)	HMBC 24 -> 23, 26
25	138.4	8.01 (s, 1H)	HMBC 24 -> 25
26	123.3 - 122.9 (m, 1C)	-	HMBC 24 -> 26
27	139.8 - 139.1 (m, 1C)	-	
28	115.5 - 109.5 (m, 2C)	-	
29	115.5 - 109.5 (m, 2C)	-	

Spectrum 4.7.188 ^{1}H-NMR of Macrocycle **S6** (DMSO-d_6, 500 MHz)

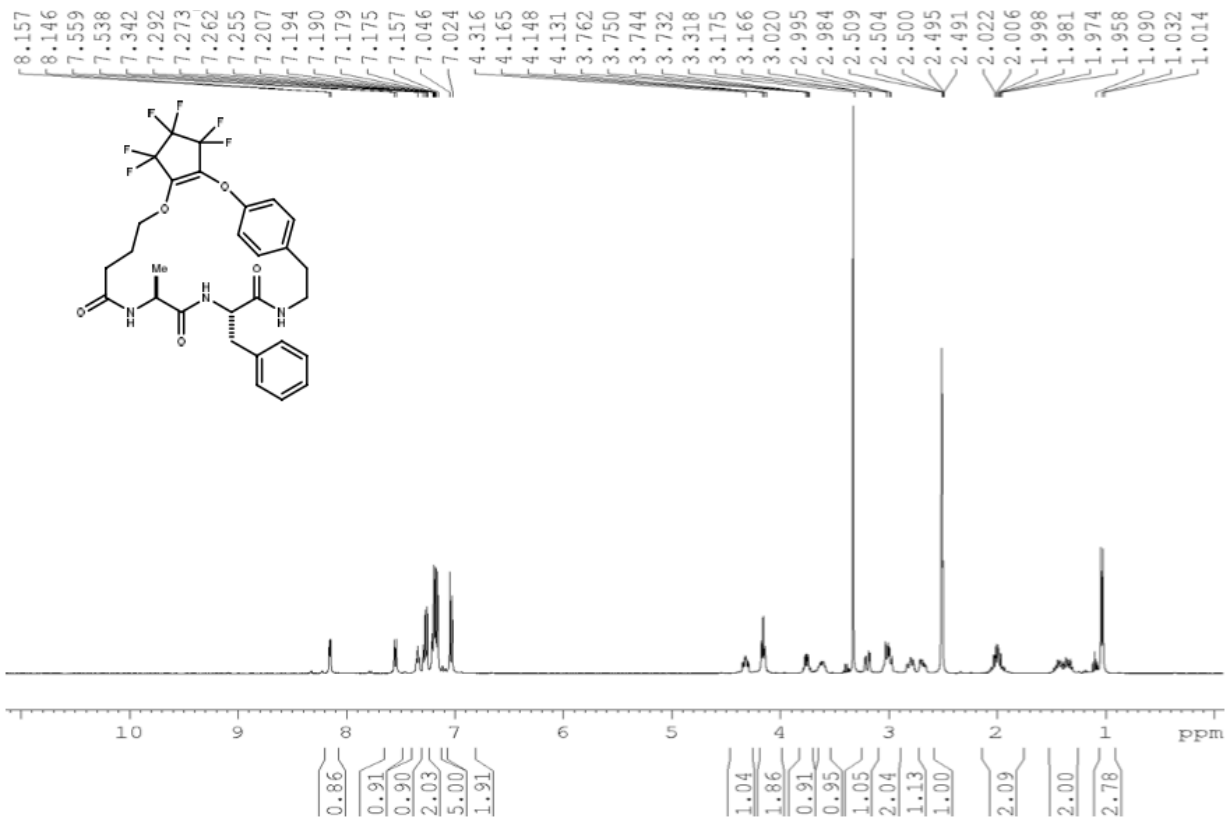

Spectrum 4.7.189 ^{13}C-NMR of Macrocycle **S6** (DMSO-d_6, 126 MHz)

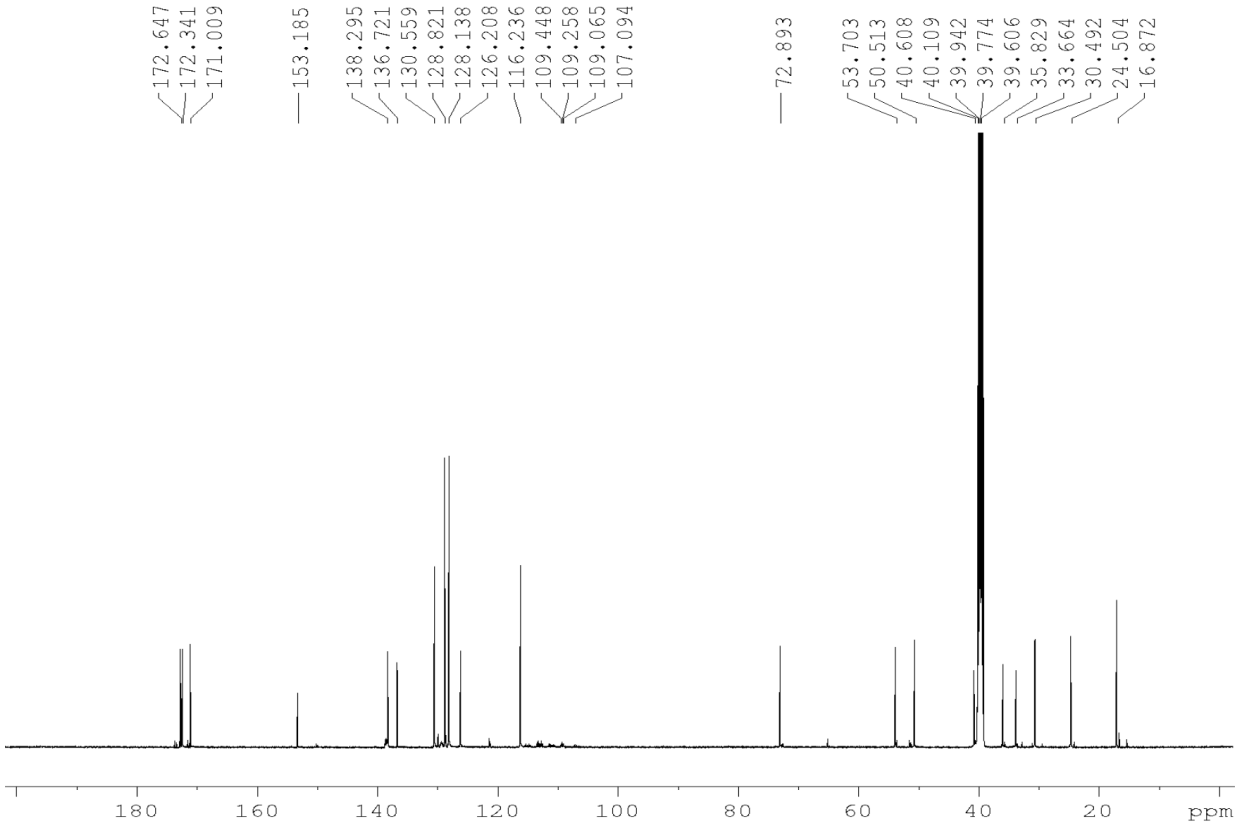

Spectrum 4.7.190 ^{19}F-NMR of Macrocycle **S6** (DMSO-d_6, 500 MHz)

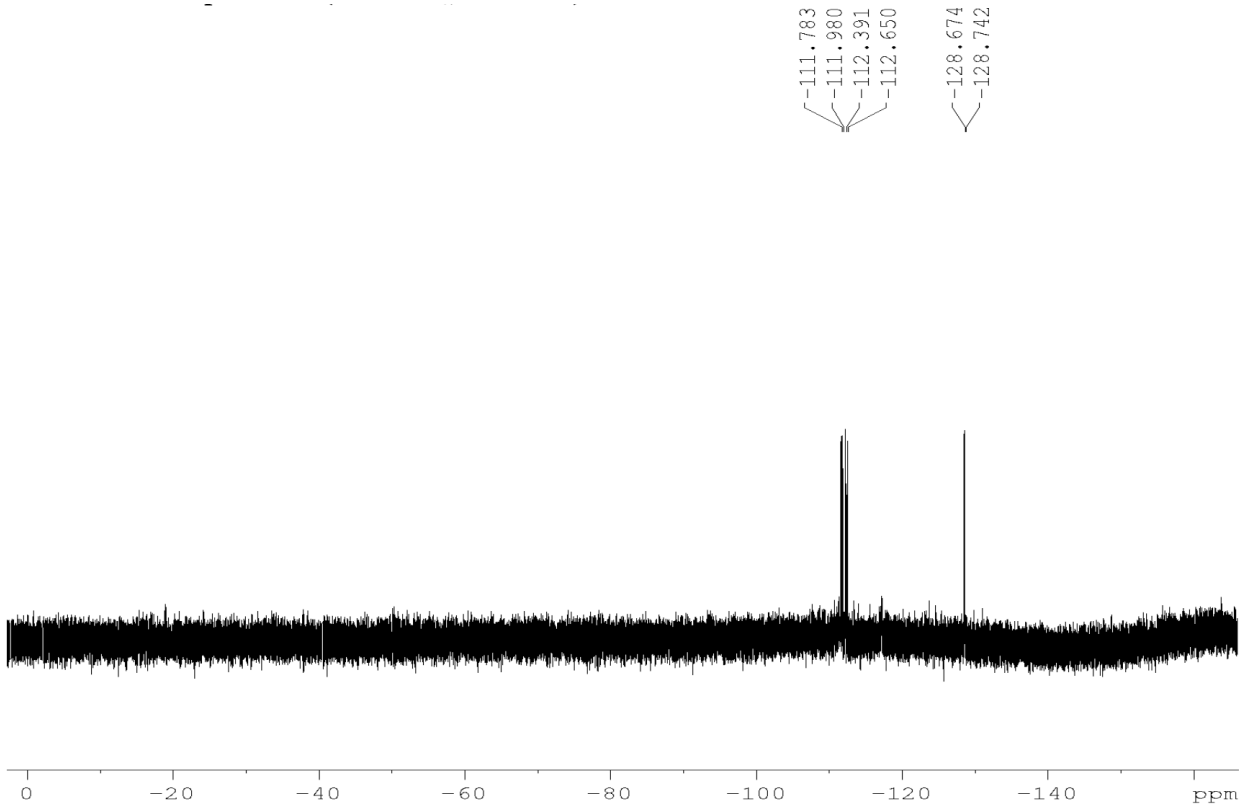

Spectrum 4.7.191 ^{1}H-NMR of Macrocycle **S30** (DMSO-d_6, 500 MHz)

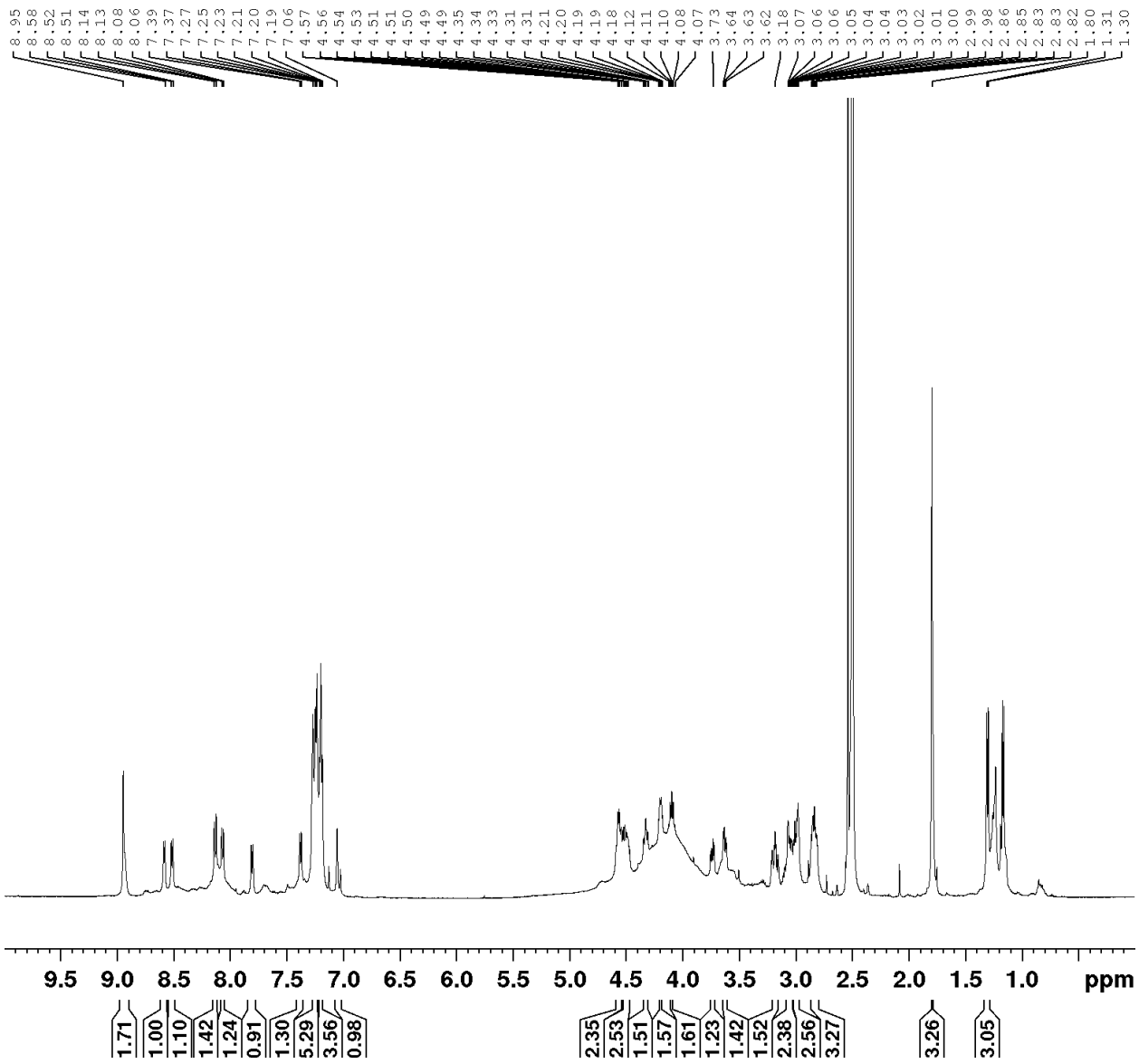

Spectrum 4.7.192 ^{13}C-NMR of Macrocycle **S30** (DMSO-d_6, 126 MHz)

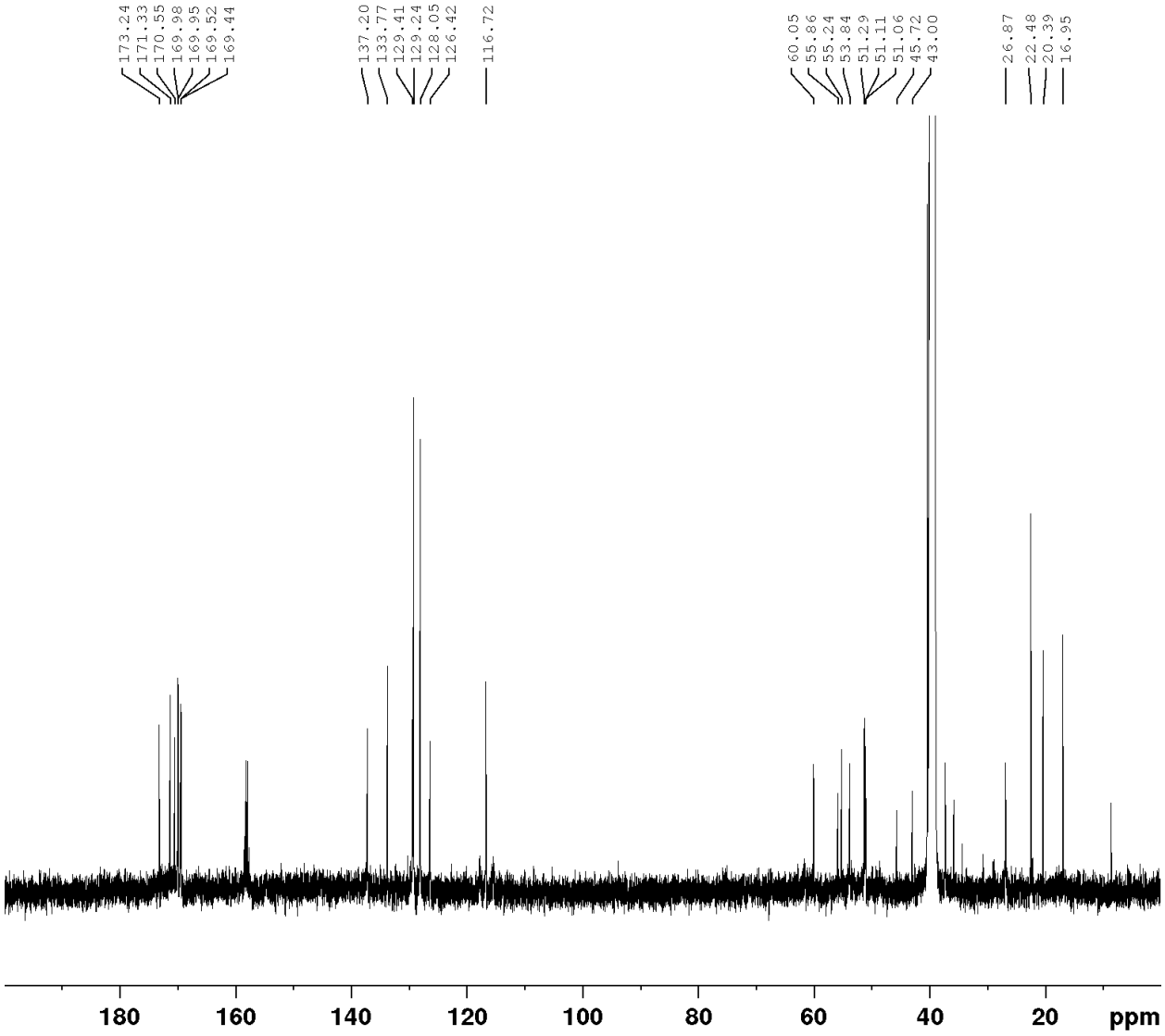

Variable Temperature NMR Experiments

Spectrum 4.7.193 ^{1}H-NMR of Polycycle **42** (DMSO-d_6, 500 MHz)

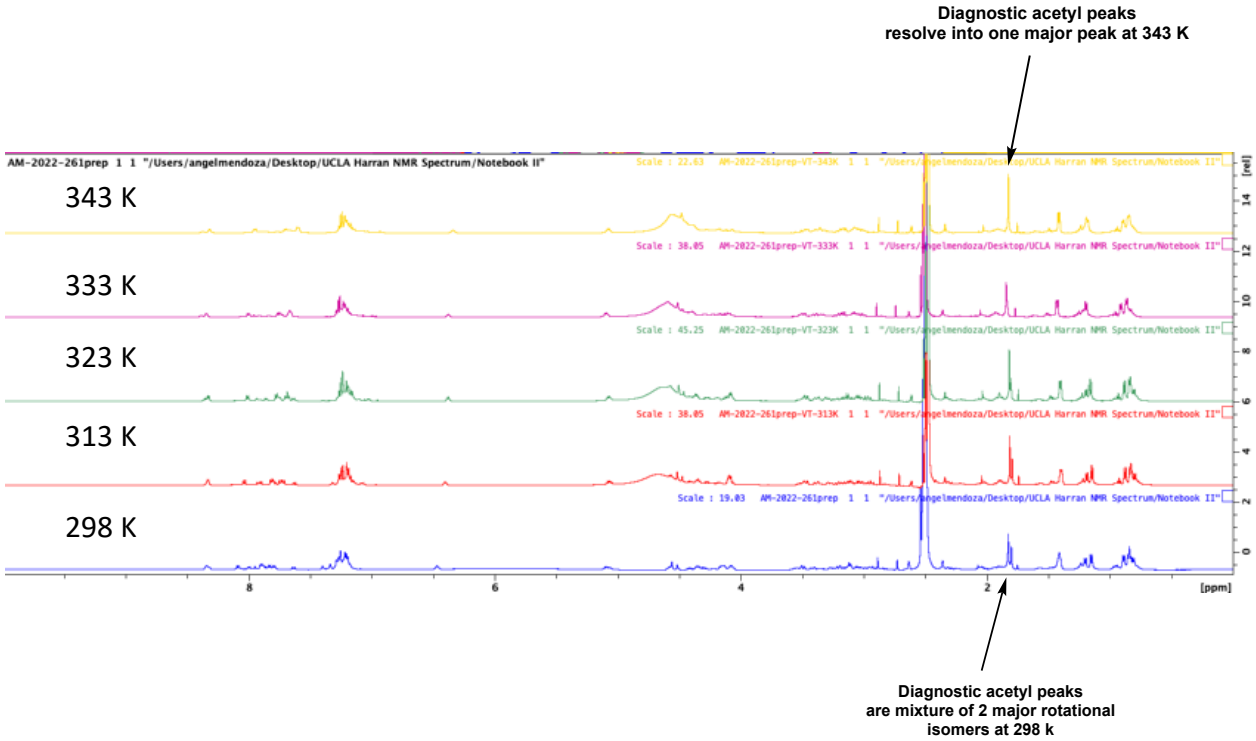

Variable temperature NMR experiment of polycycle 42. Temperature range from 298 K – 343 K. At 298 K, diagnostic acetyl peaks are at a ratio of ~3:2 due to rotational isomers. Acetyl peak resolves into one major peak at 343 K. ~4.5 ppm is water hump. NMR sample was stored in the freezer from between taking of 298 K spectrum and 313 K – 343 K VT NMR experiment. 298 K proton spectrum was taken 2 weeks before VT NMR experiment.

Spectrum 4.7.194 ^{1}H-NMR of Polycycle **45** (DMSO-d_6, 500 MHz)

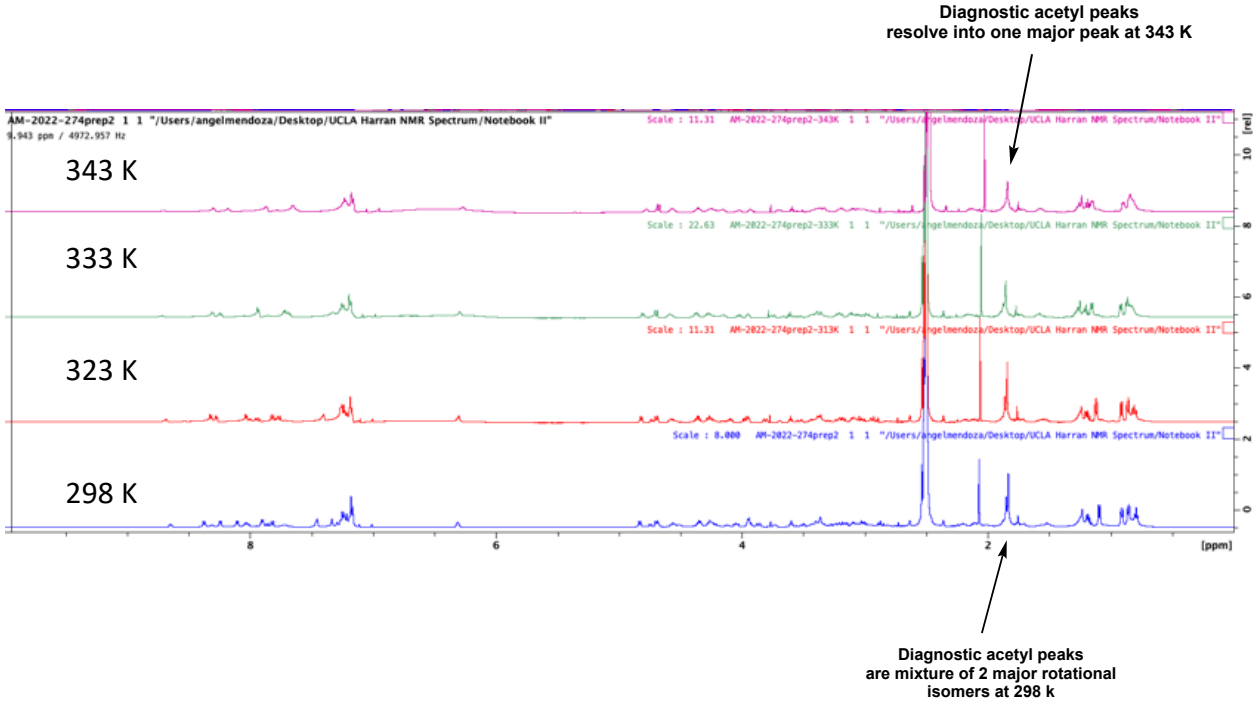

Variable temperature NMR experiment of polycycle 45. Temperature range from 298 K – 343 K. At 298 K, diagnostic acetyl peaks are at a ratio of ~2:1 due to rotational isomers. Acetyl peak resolves into one major peak at 343 K.

4.8 References

1. Nicolaou, K.C.; Chen, J. S. The art of total synthesis through cascade reactions. Chem. Soc. Rev. 2009, 38 (11), 2993–3009.

2. Tietze, L. F. Domino Reactions in Organic Synthesis. Chem. Rev. 1996, 96 (1), 115–136.

3. Zhao, H.; Negash, L.; Wei, Q.; LaCour, T. G.; Estill, S. J.; Capota, E.; Pieper, A. A.; Harran, P. G. Acid promoted cinnamyl ion mobility within peptide derived macrocycles. J. Am. Chem Soc. 2008, 130 (42), 13864–13866.

4. Lawson, K. V.; Rose, T. E.; Harran, P. G. Synthesis of a designed sesquiterpenoid that forms useful composites with peptides and related oligomers. Tetrahedron Lett. 2011, 52 (6), 653–654.

5. Lawson, K. V.; Rose, T. E.; Harran, P. G. Template-induced macrocycle diversity through large ring-forming alkylations of tryptophan. Tetrahedron 2013, 69 (36), 7683–7691.

6. Lawson, K. V.; Rose, T. E.; Harran, P. G. Template-constrained macrocyclic peptides prepared from native, unprotected precursors. Natl. Acad. Sci. U. S. A. 2013, 110 (40), 3753–3760.

7. Rose, T. E.; Lawson, K. V.; Harran, P. G. Large ring-forming alkylations provide facile access to composite macrocycles. Chem. Sci. 2015, 6, 2219–2223.

8. Rose, T. E.; Curtin, B. C.; Lawson, K. V.; Simon, A.; Houk, K. N.; Harran, P. G. On the prevalence of bridged macrocyclic pyrroloindolines formed in regiodivergent alkylations of tryptophan. Chem. Sci. 2016, 7, 4158–4166.

9. Curtin, B. H.; Manoni, F.; Park, J.; Sisto, L. J.; Lam, Y-h.; Gravel, M.; Roulston, A.; Harran, P. G. Assembly of Complex Macrocycles by Incrementally Amalgamating Unprotected Peptides with a Designed Four-Armed Insert. J. Org. Chem. 2018, 83 (6), 3090–3108.

10. Sisto, L. J.; Harran, P. G. Sulfane transalkylations and metal catalyzed allylic substitutions for the synthesis of composite macrobicyclic peptides. Tetrahedron Lett. 2020, 61 (24), 151986.

11. Sisto, L. J.; Harran, P. G. Syntheses of hybrid cyclopeptidyl [n]sulfanes by internal alkyl group exchange. Tetrahedron Lett. 2020, 61 (24), 151985.

12. Goto, Y.; Suga, H. The RaPID Platform for the Discovery of Pseudo-Natural Macrocyclic Peptides. Acc. Chem. Res. 2021, 54 (18), 3604–3617.

13. Spokoyny, A. M.; Zou, Y.; Ling, J. J.; Yu, H.; Lin, Y-S.; Pentelute, B. L. A Perfluoroaryl-Cysteine SNAr Chemistry Approach to Unprotected Peptide Stapling. J. Am. Chem. Soc. 2013, 135 (16), 5946–5949.

14. Zou, Y.; Spokoyny, A. M.; Zhang, C.; Simon, M. D.; Yu, H.; Lin, Y-S.; Pentelute, B. L. Convergent diversity-oriented side-chain macrocyclization scan for unprotected polypeptides. Org. Biol. Chem. 2014, 12 (4), 566–573.

15. Heinis, C.; Rutherford, T.; Freund, S.; Winter, G. Phage-encoded combinatorial chemical libraries based on bicyclic peptides. Nat. Chem. Biol. 2009, 5 (7), 502–507.

16. Li, B.; Wan, Z.; Zheng, H.; Cai, S.; Tian, H.W.; Tang, H.; Chu, X.; He, G.; Guo, D.S.; Xue, X.S.; Chen, G. Construction of Complex Macromulticyclic Peptides via Stitching with Formaldehyde and Guanidine. J. Am. Chem. Soc. 2022, 144 (22), 10080–10090.

17. Saha, I.; Dang, E. K.; Svatunek, D.; Houk, K. N.; Harran, P. G. Computational generation of an annotated gigalibrary of synthesizable, composite peptidic macrocycles. Proc. Natl. Acad. Sci. U. S. A. 2020, 117 (40), 24679–24690.

18. Sanger, F. The free amino groups of insulin. Biochem. J. 1945, 39 (5), 507–515.

19. Garg, S.; Twamley, B.; Zeng, Z.; Shreeve, J.M. Azoles as Reactive Nucleophiles with Cyclic Perfluoroalkenes. Eur. J. Chem. 2009, 15 (40), 10554–10562.

20. Tsunemi, T.; Bernardino, S. J.; Mendoza, A.; Jones, C. G.; Harran, P. G. Syntheses of Atypically Fluorinated Peptidyl Macrocycles through Sequential Vinylic Substitutions. Angew. Chem. Int. Ed. 2020, 59 (2), 674–678.

21. Baron, A.; Blériot, Y.; Sollogoub, M.; Vauzeilles, B. Phenylenediamine catalysis of “click glycosylations” in water: practical and direct access to unprotected neoglycoconjugates. Org. Biomol. Chem. 2008, 6 (11), 1898–1901.

22. Saulnier, M. G.; Dodier, M.; Frennesson, D. B.; Langley, D. R.; Vyas, D. M. Nucleophilic Capture of the Imino-Quinone Methide Type Intermediates Generated from 2-Aminothiazol-5-yl Carbinols. Org. Lett. 2009, 11 (22), 5154–5157.

23. Neumann, K.; Farnung, J.; Baldauf, S.; Bode, J. W. Prevention of aspartimide formation during peptide synthesis using cyanosulfurylides as carboxylic acid-protecting groups. Nat. Commun. 2020, 11, 982.

24. Wells, J. A.; McClendon, C. L. Reaching for high-hanging fruit in drug discovery at protein–protein interfaces. Nature 2007, 450, 1001–1009.

25. Marsault, E.; Peterson, M. L. Macrocycles are great cycles: applications, opportunities, and challenges of synthetic macrocycles in drug discovery. J. Med. Chem. 2011, 54 (7), 1961–2004.

26. Qian, Z.; Dougherty, P. G.; Pei, D. Targeting intracellular protein-protein interactions with cell-permeable cyclic peptides. Curr. Opin. Chem. Biol. 2017, 38, 80–86.

27. Guharoy, M.; Chakrabarti, P. Secondary structure based analysis and classification of biological interfaces: identification of binding motifs in protein-protein interactions. Bioinformatics 2007, 23 (15), 1909–1918.

28. Gavenonis, J.; Sheneman, B. A.; Siegert, T. R.; Eshelman, M. R.; Kritzer, J. A. Comprehensive analysis of loops at protein-protein interfaces for macrocycle design. Nat. Chem. Biol. 2014, 10 (9), 716–722.

29. Guéret, S. M.; Thavam, S.; Carbajo, R. J.; Potowski, M.; Larsson, N.; Dahl, G.; Dellsén, A.; Grossmann, T. N.; Plowright, A. T.; Valeur, E.; Lemurrell, M.; Waldmann, H. Macrocyclic Modalities Combining Peptide Epitopes and Natural Product Fragments. J. Am. Chem. Soc. 2020, 142 (10), 4904–4915.

30. Mi, T.; Nguyen, D,; Burgess, K. Bicyclic Schellman Loop Mimics (BSMs): Rigid Synthetic C-Caps for Enforcing Peptide Helicity. ACS Cent. Sci. 2023, 9 (2), 300–306

31. The PyMOL Molecular Graphics System, Version 2.5.2; Schrödinger, LLC: New York, NY, 2015.

32. Matsson, P.; Kihlberg, J. How Big Is Too Big for Cell Permeability? J. Med. Chem. 2017, 60 (5), 1662–1664.

33. Bhardwaj, G.; O'Connor, J.; Rettie, S.; Huang, Y-H.; Ramelot, T. A.; Mulligan, V. K.; Alpkilic, G. G.; Palmer, J.; Bera, A. K.; Bick, M. J.; Piazza, M. D.; Li, X.; Hosseinzadeh, P.; Craven, T. W.; Tejero, R.; Lauko, A.; Choi, R.; Glynn, C.; Dong, L.; Griffin, R.; van Voorhis, W. C.; Rodriguez, J.; Stewart, L.; Montelione, G. T.; Craik, D.; Baker, D. Accurate de novo design of membrane-traversing macrocycles. Cell 2022, 185 (19), 3520–3532.

34. Rossi Sebastiano, M.; Doak, B. C.; Backlund, M.; Poongavanam, V.; Over, B.; Ermondi, G.; Caron, G.; Matsson, P.; Kihlberg, J. Impact of Dynamically Exposed Polarity on Permeability and Solubility of Chameleonic Drugs Beyond the Rule of 5. J. Med. Chem. 2018, 61 (9), 4189–4202.

35. Schreiber, S. L. The Rise of Molecular Glues. Cell 2021, 184 (1), 3–9.

36. Schrödinger Release 2023-3: Maestro, Schrödinger, LLC, New York, NY, 2023.

37. Schrödinger Release 2023-3: MacroModel, Schrödinger, LLC, New York, NY, 2023.

38. Kalbag, S. M.; Roeske, R. W. A Photolabile Protecting Group for Histidine. J. Am. Chem. Soc. 1975, 97 (2), 440–441.

39. Posta, T. B.; Giraud, M.; Albericio, F. Trimethoxyphenylthio as a highly labile replacement for tert-butylthio cysteine protection in Fmoc solid phase synthesis. Org. Lett., 2012, 14 (21), 5468–5471.

40. M. J. Frisch et al., Gaussian 16, Revision C.01; Gaussian, Inc.: Wallingford CT, 2016.

41. Zhao Y.; Truhlar, D. G. A new local density functional for main-group thermochemistry, transition metal bonding, thermochemical kinetics, and noncovalent interactions. J. Chem. Phys. 2006, 125 (19), 194101–194120.

42. Grimme, S.; Ehrlich, S.; Goerigk L. Effect of the damping function in dispersion corrected density functional theory. J. Comput. Chem. 2011, 32 (7), 1456-1465.

43. Mochida, S.; Shimizu, M.; Hirano, K.; Satoh, T.; Miura, M. Synthesis of Naphtho[1,8-bc]pyran Derivatives and Related Compounds through Hydroxy Group Directed C-H Bond Cleavage under Rhodium Catalysis. Chemistry – An Asian Journal 2010, 5 (4), 847–851.

44. Thirunavukkarasu, V. S.; Donati, M.; Ackermann, L. Hydroxyl-Directed Ruthenium-Catalyzed C–H Bond Functionalization: Versatile Access to Fluorescent Pyrans. Org. Lett. 2012, 14 (13), 3416–3419.

45. Weigend, F.; Ahlrichs, R. Balanced basis sets of split valence, triple zeta valence and quadruple zeta valence quality for H to Rn: Design and assessment of accuracy. Physical Chemistry Chemical Physics 2005, 7 (18), 3297–3305.

46. Schäfer, A.; Horn, H.; Ahlrichs, R. Fully optimized contracted Gaussian basis sets for atoms Li to Kr. The Journal of Chemical Physics 1992, 97, 2571–2577.

47. Marenich, A. V.; Cramer, C. J. ; Truhlar, D. G. Universal Solvation Model Based on Solute Electron Density and on a Continuum Model of the Solvent Defined by the Bulk Dielectric Constant and Atomic Surface Tensions. The Journal of Physical Chemistry B 2009, 113 (18), 6378–6396.

48. Lu, T.; Chen, F. Multiwfn: A multifunctional wavefunction analyzer. J. Comput. Chem. 2012, 33 (5), 580–592.